Economic Geology

Economic Geology Principles and Practice
Metals, Minerals, Coal and Hydrocarbons – Introduction to Formation and Sustainable Exploitation of Mineral Deposits, Walter L. Pohl
© 2011 Walter L. Pohl. Published 2011 by Blackwell Publishing Ltd.

To the Memory of Walther E. Petrascheck
(1906–1991)

Inspiring Geologist and Academic Teacher

COMPANION WEBSITE
This book has a companion website:
www.wiley.com/go/pohl/geology
with Figures and Tables from the book for downloading

Economic Geology Principles and Practice

Metals, Minerals, Coal and Hydrocarbons – Introduction to Formation and Sustainable Exploitation of Mineral Deposits

Walter L. Pohl

WILEY-BLACKWELL
A John Wiley & Sons, Ltd., Publication

This edition first published 2011, © 2011 by Walter L. Pohl

Blackwell Publishing was acquired by John Wiley & Sons in February 2007. Blackwell's publishing program has been merged with Wiley's global Scientific, Technical and Medical business to form Wiley-Blackwell.

Registered office: John Wiley & Sons Ltd, The Atrium, Southern Gate, Chichester, West Sussex, PO19 8SQ, UK

Editorial offices: 9600 Garsington Road, Oxford, OX4 2DQ, UK
The Atrium, Southern Gate, Chichester, West Sussex, PO19 8SQ, UK
111 River Street, Hoboken, NJ 07030-5774, USA

For details of our global editorial offices, for customer services and for information about how to apply for permission to reuse the copyright material in this book please see our website at www.wiley.com/wiley-blackwell

The right of the author to be identified as the author of this work has been asserted in accordance with the Copyright, Designs and Patents Act 1988.

All rights reserved. No part of this publication may be reproduced, stored in a retrieval system, or transmitted, in any form or by any means, electronic, mechanical, photocopying, recording or otherwise, except as permitted by the UK Copyright, Designs and Patents Act 1988, without the prior permission of the publisher.

Wiley also publishes its books in a variety of electronic formats. Some content that appears in print may not be available in electronic books.

Designations used by companies to distinguish their products are often claimed as trademarks. All brand names and product names used in this book are trade names, service marks, trademarks or registered trademarks of their respective owners. The publisher is not associated with any product or vendor mentioned in this book. This publication is designed to provide accurate and authoritative information in regard to the subject matter covered. It is sold on the understanding that the publisher is not engaged in rendering professional services. If professional advice or other expert assistance is required, the services of a competent professional should be sought.

Library of Congress Cataloguing-in-Publication Data

Pohl, Walter, 1941-
Economic geology : principles and practice : metals, minerals, coal and hydrocarbons introduction to formation and sustainable exploitation of mineral deposits / Walter L. Pohl.
p. cm.
Includes bibliographical references and index.
ISBN 978-1-4443-3662-7 (hardback) – ISBN 978-1-4443-3663-4 (pbk.) 1. Geology, Economic. I. Title.
TN260.P64 2011
553—dc22
2010047192

A catalogue record for this book is available from the British Library.

This book is published in the following electronic formats: ePDF 9781444394863;
Wiley Online Library 9781444394870; ePub 9781444394856

Set in 9/11.5pt, TrumpMediaeval by Thomson Digital, Noida, India

1 2011

Contents

Preface xiii

Introduction 1

- What are ore deposits? 1
- Mining in the stress field between society and environment 2
- The mineral resources conundrum 4

Part I Metalliferous Ore Deposits 5

1 Geological ore formation process systems (metallogenesis) 7

Synopsis 7

- 1.1 Magmatic Ore Formation Systems 8
  - 1.1.1 Orthomagmatic ore formation 11
  - 1.1.2 Ore deposits at mid-ocean ridges and in ophiolites 18
  - 1.1.3 Ore formation related to alkaline magmatic rocks, carbonatites and kimberlites 23
  - 1.1.4 Granitoids and ore formation processes 25
  - 1.1.5 Ore deposits in pegmatites 32
  - 1.1.6 Hydrothermal ore formation 35
  - 1.1.7 Skarn- and contact-metasomatic ore deposits 54
  - 1.1.8 Porphyry copper (Mo-Au-Sn-W) deposits 56
  - 1.1.9 Hydrothermal-metasomatic ore deposits 59
  - 1.1.10 Hydrothermal vein deposits 62
  - 1.1.11 Volcanogenic ore deposits 68

- 1.2 Supergene Ore Formation Systems 76
  - 1.2.1 Residual (eluvial) ore deposits 80
  - 1.2.2 Supergene enrichment by descending (vadose) solutions 82
  - 1.2.3 Infiltration as an agent of ore formation 88

- 1.3 Sedimentary Ore Formation Systems 92
  - 1.3.1 Black shales in metallogenesis 93
  - 1.3.2 Placer deposits 94
  - 1.3.3 Autochthonous iron and manganese deposits 100
  - 1.3.4 Sediment-hosted, submarine-exhalative (sedex) base metal deposits 107

1.4 Diagenetic Ore Formation Systems 110
  1.4.1 The European Copper Shale 114
  1.4.2 Diagenetic-hydrothermal carbonate-hosted Pb-Zn (F-Ba) deposits 116
  1.4.3 Diagenetic-hydrothermal ore formation related to salt diapirs 119

1.5 Metamorphic and Metamorphosed Ore Deposits 121

1.6 Metamorphogenic Ore Formation Systems 125

1.7 Metallogeny – Ore Deposit Formation in Space and Time 132
  1.7.1 Metallogenetic epochs and provinces 133
  1.7.2 Metallogeny and plate tectonics 134

1.8 Genetic Classification of Ore and Mineral Deposits 139

1.9 Summary and Further Reading 146

2 Economic geology of metals 149

Synopsis 149

2.1 The Iron and Steel Metals 149
  2.1.1 Iron 149
  2.1.2 Manganese 159
  2.1.3 Chromium 163
  2.1.4 Nickel 168
  2.1.5 Cobalt 173
  2.1.6 Molybdenum 175
  2.1.7 Tungsten (Wolfram) 179
  2.1.8 Vanadium 183

2.2 Base Metals 185
  2.2.1 Copper 185
  2.2.2 Lead and zinc 195
  2.2.3 Tin 202

2.3 Precious Metals 207
  2.3.1 Gold 207
  2.3.2 Silver 221
  2.3.3 Platinum and Platinum Group Metals 228

2.4 Light Metals 233
  2.4.1 Aluminium 233
  2.4.2 Magnesium 238

2.5 Minor and Speciality Metals 239
  2.5.1 Mercury 239
  2.5.2 Antimony 243

2.5.3 Arsenic 245
2.5.4 By-product electronic metals (selenium, tellurium, gallium, germanium, indium, cadmium) and silicon 247
2.5.5 Bismuth 250
2.5.6 Zirconium and hafnium 251
2.5.7 Titanium 254
2.5.8 Rare earth elements (REE, lanthanides) 257
2.5.9 Niobium and tantalum 261
2.5.10 Lithium 265
2.5.11 Beryllium 268
2.5.12 Uranium (and thorium) 270

2.6 Summary and Further Reading 283

Part II Non-Metallic Minerals and Rocks 285

3 Industrial minerals, earths and rocks 287

Synopsis 287

3.1 Andalusite, Kyanite and Sillimanite 288
3.1.1 Andalusite 289
3.1.2 Kyanite 290
3.1.3 Sillimanite 291

3.2 Asbestos 291
3.2.1 Asbestos mineralization types 292

3.3 Barite and Celestite 293
3.3.1 Geochemistry 294
3.3.2 Barite deposit types 296

3.4 Bentonite (Smectite Rocks) 299
3.4.1 Bentonite deposit types 301

3.5 Boron 302
3.5.1 Geochemistry 303
3.5.2 Boron deposit types 303

3.6 Carbonate Rocks: Limestone, Calcite Marble, Marlstone, Dolomite 305
3.6.1 Limestone 306
3.6.2 Metamorphic calcite (and occasionally dolomite) marbles 306
3.6.3 Marlstone 306
3.6.4 Dolomite 307

3.7 Clay and Clay Rocks 308
3.7.1 Clay deposit types 308

3.8 Diamond 310
  3.8.1 Source and formation of diamonds 311
  3.8.2 Diamond deposit types 312

3.9 Diatomite and Tripoli 317
  3.9.1 Diatomite deposit types 318
  3.9.2 Tripoli 319

3.10 Feldspar 319

3.11 Fluorite 320
  3.11.1 Geochemistry 321
  3.11.2 Fluorite deposit types 322

3.12 Graphite 325
  3.12.1 Graphite deposit types 326

3.13 Gypsum and Anhydrite 327
  3.13.1 Deposits of gypsum and anhydrite 328

3.14 Kaolin 330
  3.14.1 Kaolin deposit types 331

3.15 Magnesite 333
  3.15.1 Magnesite deposit types 334

3.16 Mica (Muscovite, Phlogopite, Vermiculite) 339
  3.16.1 Muscovite and phlogopite 339
  3.16.2 Vermiculite 340

3.17 Olivine 342
  3.17.1 Olivine deposits 342

3.18 Phosphates 342
  3.18.1 Geochemistry 345
  3.18.2 Phosphate deposit types 345

3.19 Quartz and Silicon 347
  3.19.1 Quartz deposit types 348

3.20 Quartzite 349
  3.20.1 Metamorphic quartzite deposits 350
  3.20.2 Sedimentary quartzite 350

3.21 Quartz Sand and Gravel 350
  3.21.1 Industrial sand and gravel 351
  3.21.2 Building sand and gravel 352

3.22 Sodium Carbonate, Sulfate and Alum 354
  3.22.1 Sodium sulphate 355
  3.22.2 Alum salts 355

3.23 Sulphur 355
  3.23.1 Geochemistry 356
  3.23.2 Deposit types of elementary sulphur 356

3.24 Talc and Pyrophyllite 358
  3.24.1 Talc deposit types 359
  3.24.2 Pyrophyllite 361

3.25 Volcaniclastic Rocks 362
  3.25.1 Pumice 362
  3.25.2 Perlite 363
  3.25.3 Trass 363

3.26 Wollastonite 364
  3.26.1 Wollastonite deposit formation 364

3.27 Zeolites 365
  3.27.1 Zeolite deposit types 366

3.28 Summary and Further Reading 367

4 Salt deposits (evaporites) 369

Synopsis 369

4.1 Salt Minerals and Salt Rocks 371
  4.1.1 Salt minerals 371
  4.1.2 Salt rocks 371

4.2 The Formation of Salt Deposits 376
  4.2.1 Salt formation today 376
  4.2.2 Salt formation in the geological past 384

4.3 Post-Depositional Fate of Salt Rocks 394
  4.3.1 Diagenesis and metamorphism of evaporites 394
  4.3.2 Deformation of salt rocks 397
  4.3.3 Forms and structures of salt deposits 398
  4.3.4 Supergene alteration of salt deposits 403

4.4 From Exploration to Salt Mining 405
  4.4.1 Exploration and development of salt deposits 405
  4.4.2 Geological practice of salt mining 406

4.5 Summary and Further Reading 409

Part III The Practice of Economic Geology 411

5 Geological concepts and methods in the mining cycle: exploration, exploitation and closure of mines 413

Synopsis 413

5.1 Economic Considerations 414

5.2 The Search for Mineral Deposits (Exploration) 416
  5.2.1 The pre-exploration stage 416
  5.2.2 Geological exploration 417
  5.2.3 Geological remote sensing 420
  5.2.4 Geochemical exploration 422
  5.2.5 Geophysical exploration 428
  5.2.6 Trenching and drilling 432

5.3 Development and Valuation of Mineral Deposits 437
  5.3.1 Geological mapping and sampling 439
  5.3.2 Ore reserve estimation and determination of grade 440
  5.3.3 Valuation of mineral deposits 447

5.4 Mining and the Environment 448
  5.4.1 Potential environmental problems related to mining and mine-site processing plants 450

5.5 Deep Geological Disposal of Dangerous Waste 458

5.6 Summary and Further Reading 462

Part IV Fossil Energy Raw Materials – Coal, Oil and Gas 465

6 Coal 467

Synopsis 467

6.1 The Substance of Coal 471
  6.1.1 Coal types 471
  6.1.2 Petrography of coal 474
  6.1.3 The chemical composition of coal 479

6.2 Peat Formation and Coal Deposits 487
  6.2.1 Types and dimensions of coal seams 487
  6.2.2 Concordant and discordant clastic sediments in coal seams 488
  6.2.3 Peat formation environments 491
  6.2.4 Host rocks of coal 495
  6.2.5 Marker beds in coal formations 497
  6.2.6 Coal formation in geological space and time 498

6.3 The Coalification Process 499
- 6.3.1 Biochemical peatification 499
- 6.3.2 Geochemical coalification 500
- 6.3.3 Measuring the degree of coalification 500
- 6.3.4 Causes of coalification 501
- 6.3.5 Coal maturity and diagenesis of country rocks 505

6.4 Post-Depositional Changes of Coal Seams 505
- 6.4.1 Tectonic deformation 505
- 6.4.2 Epigenetic mineralization of coal seams 506
- 6.4.3 Exogenic alteration of coal 506

6.5 Applications of Coal Geology 507
- 6.5.1 Exploration 507
- 6.5.2 Reserve estimation 510
- 6.5.3 Coal mining geology 512
- 6.5.4 Environmental aspects of coal mining 513

6.6 Summary and Further Reading 518

7 Petroleum and natural gas deposits 521

Synopsis 521

7.1 Species of Natural Bitumens, Gas and Kerogen, and their Properties 524
- 7.1.1 Crude oil, or petroleum 524
- 7.1.2 Natural gas 527
- 7.1.3 Natural gas hydrates (clathrates) 530
- 7.1.4 Tar 530
- 7.1.5 Earth wax (ozocerite) 531
- 7.1.6 Pyrobitumens 531
- 7.1.7 Natural asphalt 531
- 7.1.8 Kerogen 531

7.2 The Origin of Petroleum and Natural Gas 533
- 7.2.1 Petroleum source rocks 533
- 7.2.2 Dry gas source rocks 536
- 7.2.3 Eogenesis and catagenesis of kerogen 537
- 7.2.4 The oil window 539

7.3 Formation of Petroleum and Natural Gas Deposits 540
- 7.3.1 Migration 540
- 7.3.2 Reservoir rocks 543
- 7.3.3 Petroleum and gas traps 545
- 7.3.4 Formation and reservoir waters 551
- 7.3.5 Alteration of petroleum in reservoirs (degradation) 551
- 7.3.6 Tectonic environments and age of hydrocarbon provinces 552

7.4 Exploring for Petroleum and Natural Gas Deposits 553
  7.4.1 Geophysical methods 555
  7.4.2 Geochemical methods of hydrocarbon exploration 556
  7.4.3 Exploration drilling 557
  7.4.4 Geophysical borehole measurements 558

7.5 The Exploitation of Petroleum and Natural Gas Deposits 561
  7.5.1 Reservoir conditions 561
  7.5.2 Oil or gasfield development 563
  7.5.3 Oil and gas production 565
  7.5.4 Petroleum mining 568
  7.5.5 Reserve and resource estimation 568
  7.5.6 Post-production uses of oil and gas fields 570

7.6 Tar Sand, Asphalt, Pyrobitumen and Shungite 570
  7.6.1 Tar sand 570
  7.6.2 Asphalt 572
  7.6.3 Pyrobitumens 572
  7.6.4 Shungite 573

7.7 Oil Shales 573

7.8 Environmental Aspects of Oil and Gas Production 575
  7.8.1 Water resources protection 577
  7.8.2 Induced seismic activity 577
  7.8.3 Tar sand mining 577
  7.8.4 Hydrocarbons and climate 578

7.9 Summary and Further Reading 579

Epilogue **583**

References **585**

Index **655**

This book has a companion website: www.wiley.com/go/pohl/geology

Preface

Wisely used, mineral resources create wealth, employment, a vital social and natural environment and peace. If the reverse of these conditions occurs only too often, illustrating the so-called "resource curse", this should be attributed to the true perpetrators, namely irresponsible, weak or selfish leaders. This book, however, does not intend to provide rules for good governance. I wrote it as a broad overview on geoscientific aspects of mineral deposits, including their origin and geological characteristics, the principles of the search for ores and minerals, and the investigation of newly found deposits. In addition, practical and environmental aspects are addressed that arise during the life-cycle of a mine and after its closure. I am convinced that in our time, economic geology cannot be taught, studied or practised without an understanding of environmental issues. The scientific core of the book is the attempt to present the extraordinary genetic variability of mineral deposits in the frame of fundamental geological process systems. The comprehensive approach – covering materials from metal ores to minerals and hydrocarbons – is both an advantage and a loss. The second concerns the sacrifice of much detail but I chose the first for its benefit of a panoramic view over the whole field of economic geology. Being aware that the specialist level of subjects presented in this book fills whole libraries, I do hope that even experienced practitioners, academic teachers and advanced students of particular subjects will find the synopsis useful.

Over more than 50 years, five editions of this book were published in German. Since the first edition (Wilhelm & Walther E. Petrascheck 1950), the book was intended to provide a concise introduction to the geology of mineral deposits, including its applications to exploration and mining. The target audience has changed, however. Originally, it was written for students of mining engineering. Today, it is mainly directed to aspiring and practising geologists. Each of the seven chapters of the book was developed with my own students as a university course and should be useful to fellow academic teachers. After initially working in industry I never lost contact with applications of economic geology, which is my motive for the constant interweaving of practical aspects in the text and for dedicating one of the chapters to the practice of economic geology. For professional reference purposes, practitioners in geology and mining should appreciate this melange of science and application. Frequent explanations and references to environmental and health aspects of extraction and processing of ores and minerals should assist users involved in environmental work. To those with no background in geology, I recommend they acquire an introductory geoscience text for looking up terms that are employed but cannot be explained in the available space.

Compared with the last German edition (Pohl 2005), this book has been rewritten for an international public. Although it retains a moderate European penchant by referring to examples from this region, important deposits worldwide are preferentially chosen to explain genetic types and practical aspects. I trust that this will be useful to both scholars and practitioners, wherever they work. Generally, it was my ambition to present the state of the art in economic geology, by referring to and citing recent publications as well as earlier fundamental concepts. This should assist and motivate students to pursue topics to greater depth.

Many people have supported me in my life-long pursuit of theory and practice of economic geology, and helped with this book, especially by donating photographs. I cannot name them all but in captions, donors are acknowledged. Here, just let me say thank you.

Walter L. Pohl

Plate 1.1 Bauxite extraction at Huntley mine, southwestern Australia. On the Darling Plateau, bauxite is part of a mature soil profile developed over Archaean gneiss and granite. The area is covered by woodland (the jarrah, or *Eucalyptus marginata* forest). Mining depends on the availability of land and its social acceptance on rapid re-establishment of the native ecosystem. Reproduced by permission of Alcoa Inc.

Plate 1.2 Rehabilitated jarrah forest covers former extraction panels of Huntley bauxite mine in front of the lake. Reproduced by permission of Alcoa Inc.

Economic Geology Principles and Practice
Metals, Minerals, Coal and Hydrocarbons – Introduction to Formation and Sustainable Exploitation of Mineral Deposits, Walter L. Pohl
© 2011 Walter L. Pohl. Published 2011 by Blackwell Publishing Ltd.

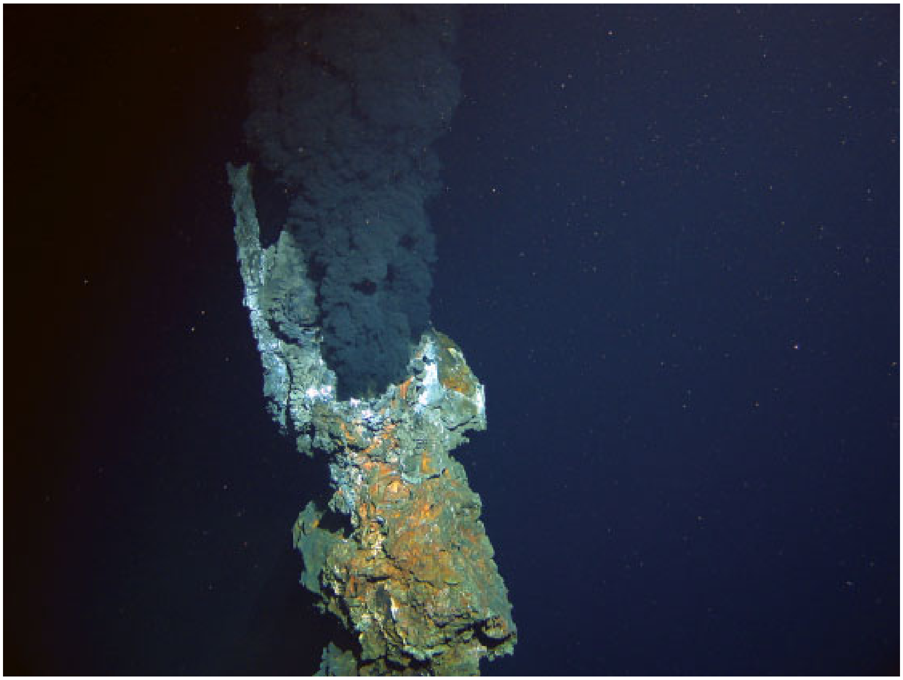

Plate 1.11 Black smoker in the Mid-Atlantic Ridge graben, 4°48 S, 12°37 W, at a water depth of ca. 3000 m. Courtesy P.M. Herzig, IFM-GEOMAR (ROV Kiel 6000, 2009).

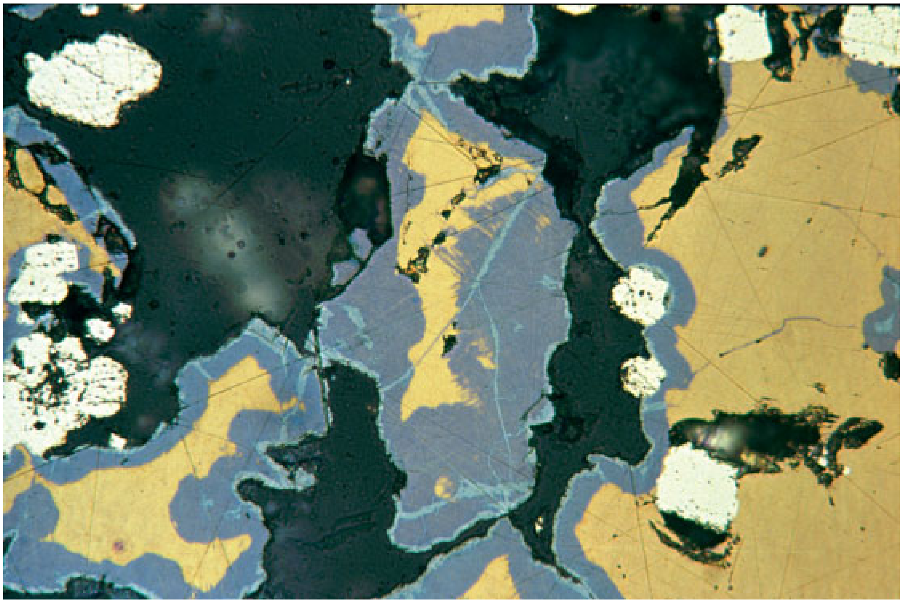

Plate 1.13 Mid-oceanic copper mineralization in chimney fragments from inactive Sonne Field in the Central Indian Ocean. Courtesy P. Halbach (©FU Berlin). The polished section shows pyrite (white) as the earliest sulphide phase, followed by chalcopyrite (yellow), and increasing hydrothermal depletion of iron in bornite (Cu_5FeS_4, blue-brown) and a thin rim of digenite (Cu_9S_5, pale blue). The long side of the image corresponds to 0.6 mm. Pore space filled by casting resin is variably dark.

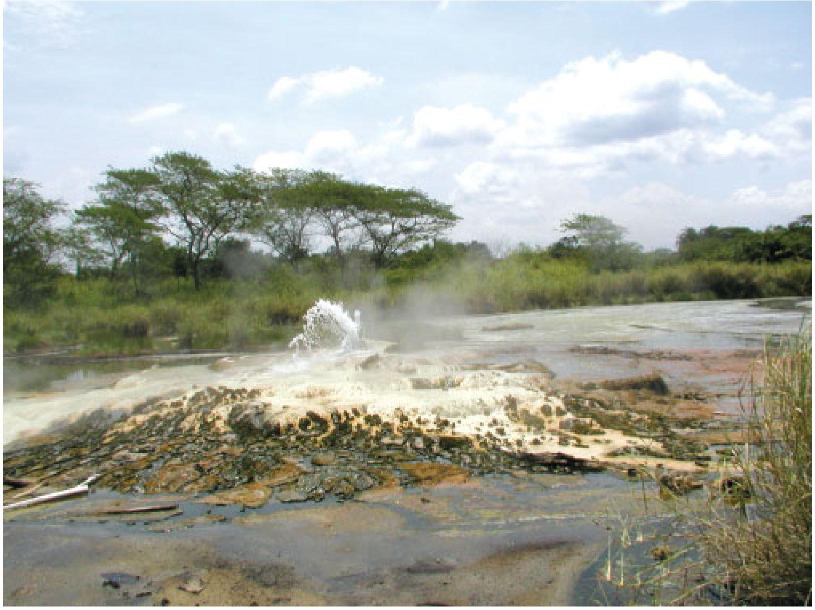

Plate 1.21 Geothermal hot springs and siliceous sinter mound at Sempaya in northwestern Uganda. The convective system is related to the large border fault of the Ruwenzori Mountains, with a vertical displacement of more than 10 km between the petroliferous Tertiary Albert Rift in the west and the Palaeoproterozoic crystalline horst in the east.

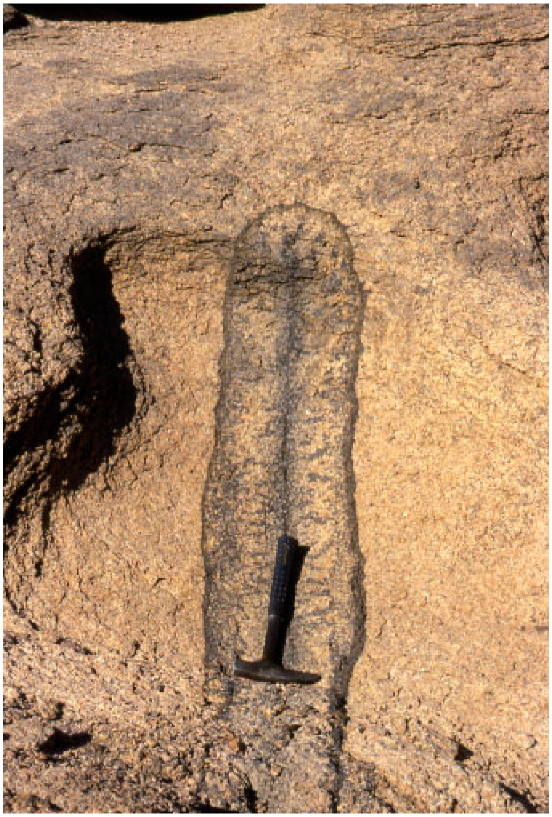

Plate 1.29 The essence of hydrothermal alteration visible at outcrop-scale, depicted by the halo centred on a small fissure branching off from formerly exploited wolframite-quartz veins in Panafrican granite at Gash Emir, Red Sea Hills, Sudan. Note the enhancement by later supergene oxidation.

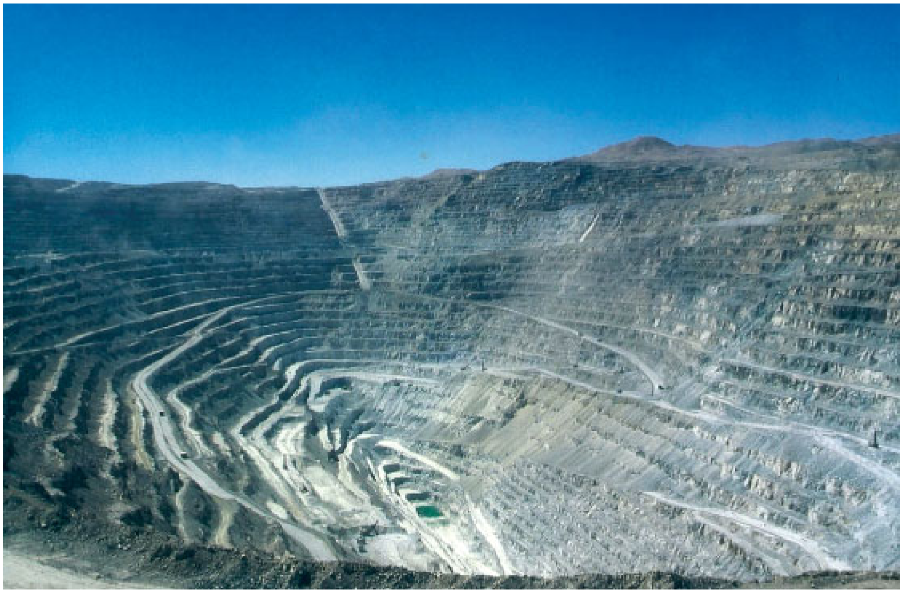

Plate 1.31 Chuquicamata open pit in Chile, one of the world's largest porphyry copper mines. Courtesy Bernd Lehmann, Clausthal.The pit measures 2 × 3 km and approaches a depth of 900 m. Total pre-mining resources were nearly 3000 Mt at 1% Cu and by-product Mo. Annual production is ~1.2 Mt copper and 20,000 t molybdenum plus rhenium.

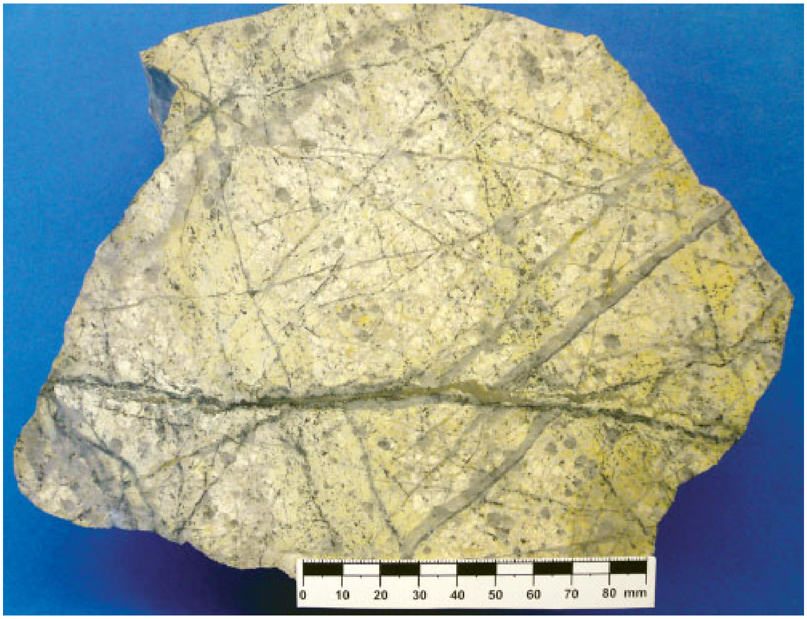

Plate 1.33 Typical copper porphyry ore from Chuquicamata, displaying brecciation and quartz veining, pervasive sericitic (greenish) and argillic alteration. Courtesy Bernd Lehmann, Clausthal.Grey ore in veinlets is largely chalcocite due to supergene enrichment, which reaches 800 m below surface.

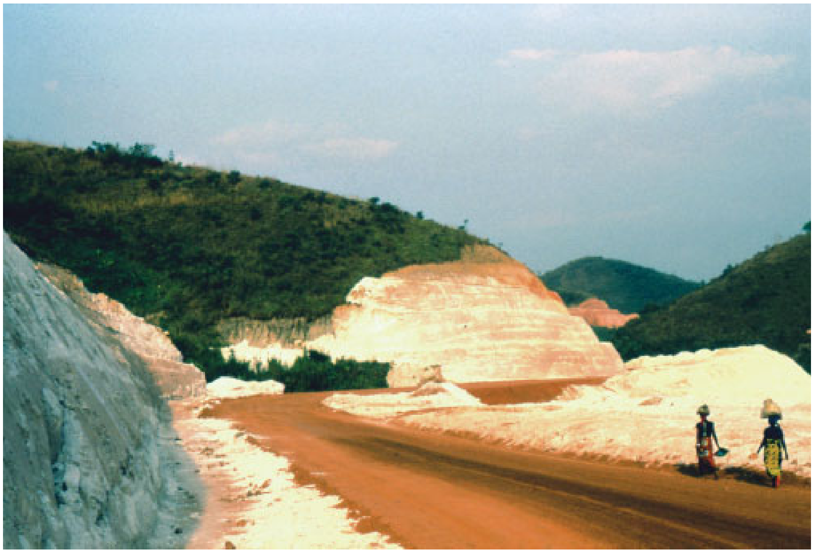

Plate 1.50 Brilliantly white supergene kaolin below red laterite in the rainforest of northern Burundi illustrates lateritic soil profiles which are shaped by tropical weathering.

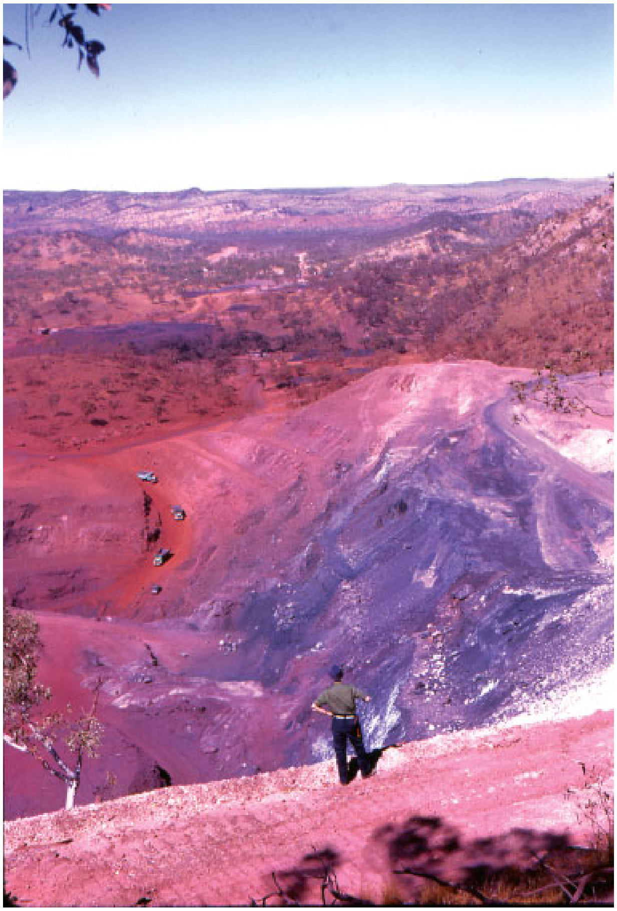

Plate 1.56 For over 100 years, the supergene, high-grade chalcocite ore of the black shale-hosted copper deposit at Mt Oxide in the Mt Isa district, Australia, was the symbolic example of fortune and destitution for investors and miners.Gossan (red) covered an accumulation zone of 55 m thickness which graded into subeconomic primary sulphides. A sizeable ore shoot of 15.9% Cu was extracted by underground methods. Later, the pit was excavated and overall, the deposit yielded 23,000 t of copper (J.H. Brooks in Glasson & Rattigan 1990).

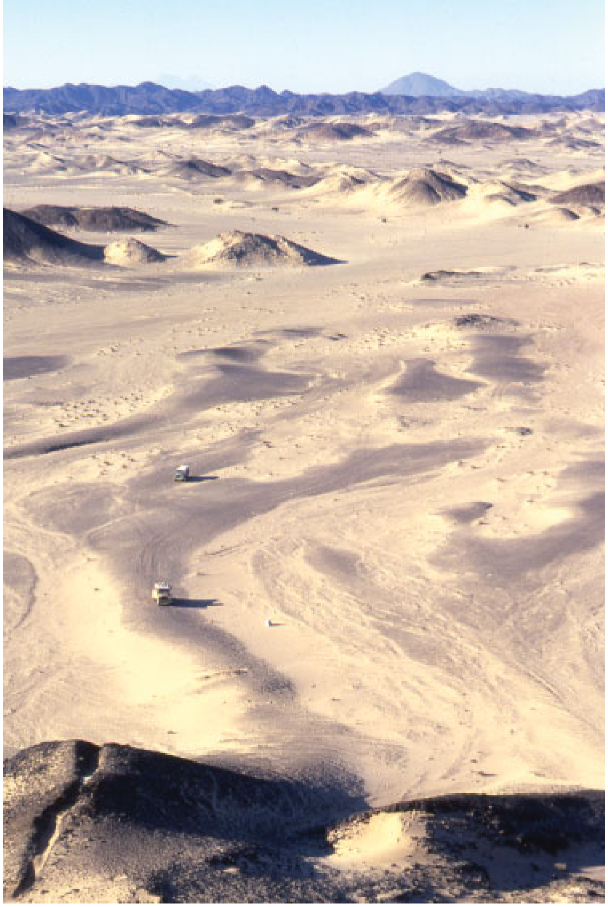

Plate 1.61 Aeolian lag enrichment of magnetite (dark sand patches) at An Kor, Red Sea Hills, Sudan. Note the exploration trench testing the Neoproterozoic primary mineralization in the foreground.

Plate 1.62 Panning cassiterite-columbite ore from Ngara pegmatite, eastern Rwanda. Note the small mass of black ore mineral sand which remains from washing the pan filled with ore.

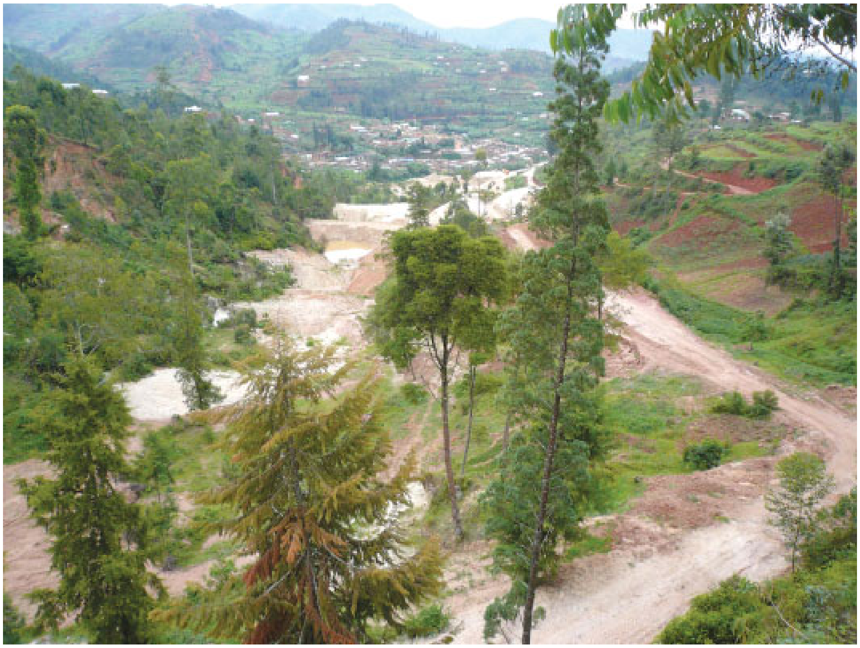

Plate 1.64 Alluvial placer mining near Ruhanga in the tin-tantalum district of Gatumba, Rwanda. After extraction, the devastated valley must be restored. Courtesy B. Lehmann, Clausthal.

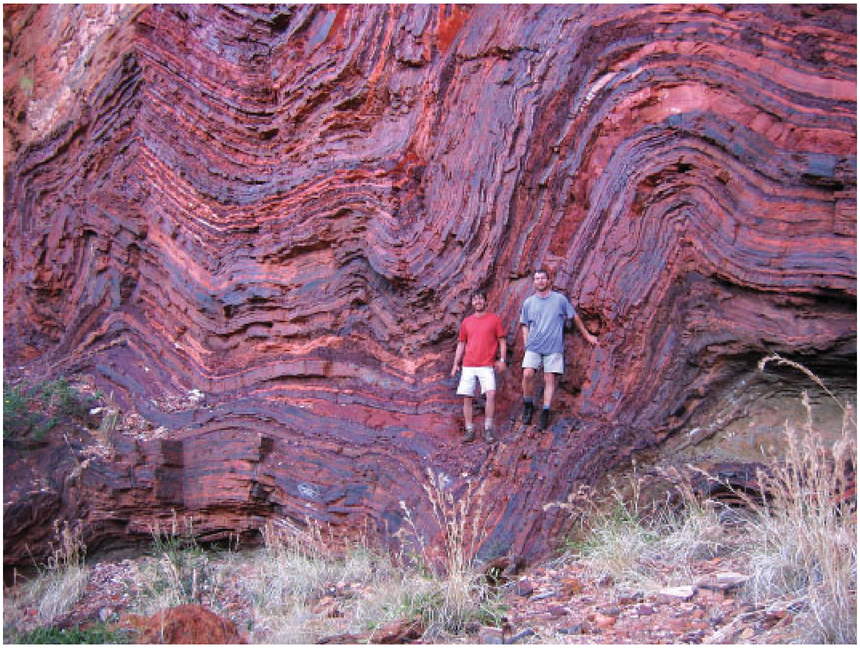

Plate 1.67 Folded and metamorphosed Superior type banded iron formation near Mt Tom Price mine in the Hamersley Gorge (Karijini National Park, Western Australia) with marine scientists Aivo Lepland and Mark van Zuilen kindly posing for scale. Iron-rich beds black, silica (jasper) red. Photograph by Aivo Lepland, courtesy Geological Survey of Western Australia.

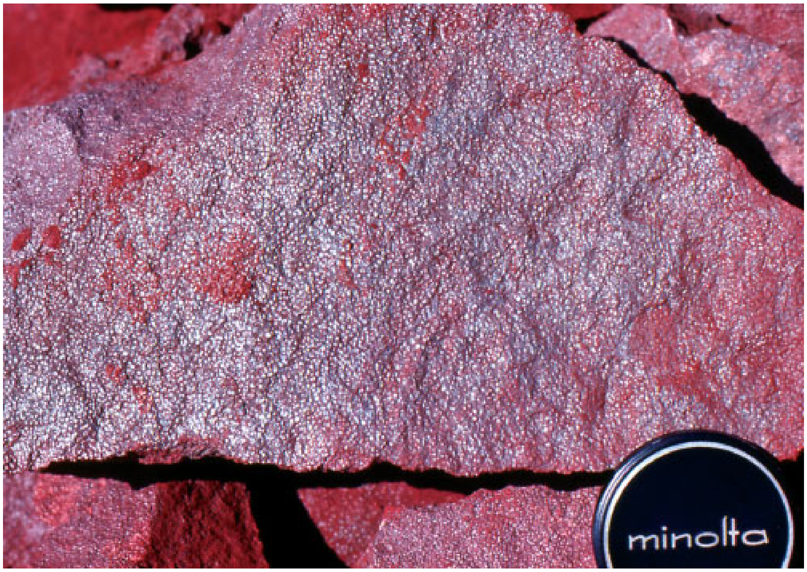

Plate 1.68 Haematitic iron oolite ore formed in a Late Cretaceous marine embayment at Aswan, Upper Egypt.

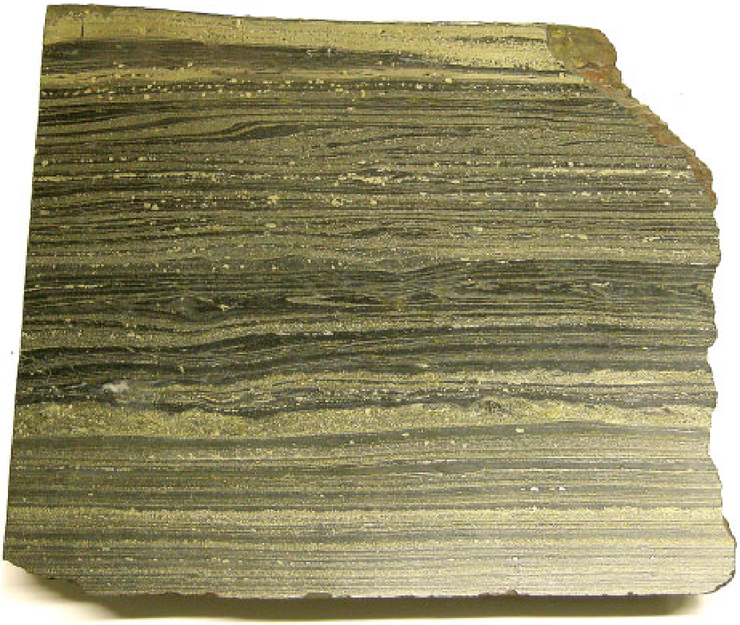

Plate 1.72 Undeformed shale-banded copper-zinc dominated sulphide ore from Rammelsberg sedex deposit (Germany) displays ductile soft-sediment deformation and cross-lamination. Width of image ~20 cm. Courtesy B. Lehmann, Clausthal.

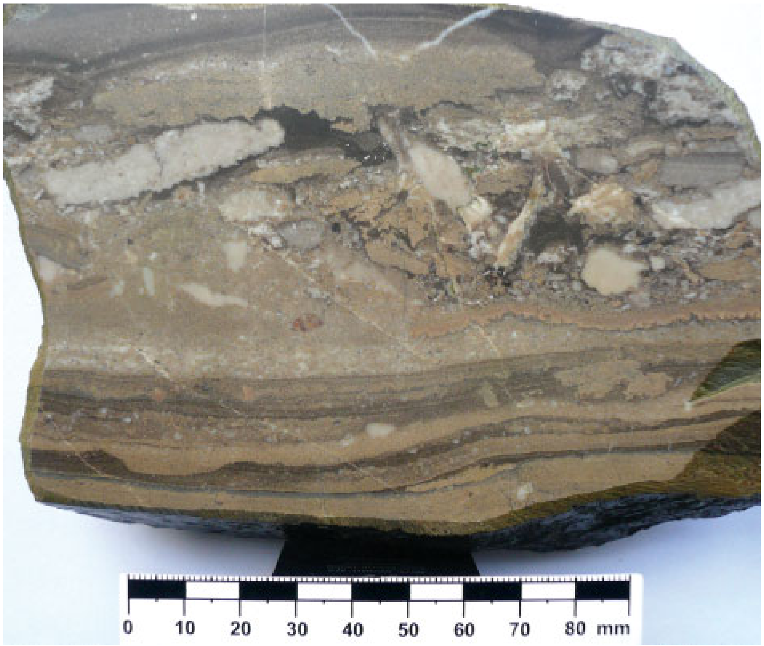

Plate 1.76 Banded and breccia cave ore of brown sphalerite in the historic Lafatsch mine, Karwendel, Tyrol. This is one of the outliers of the Triassic Alpine type carbonate-hosted Pb-Zn deposits. Courtesy B. Lehmann, Clausthal.

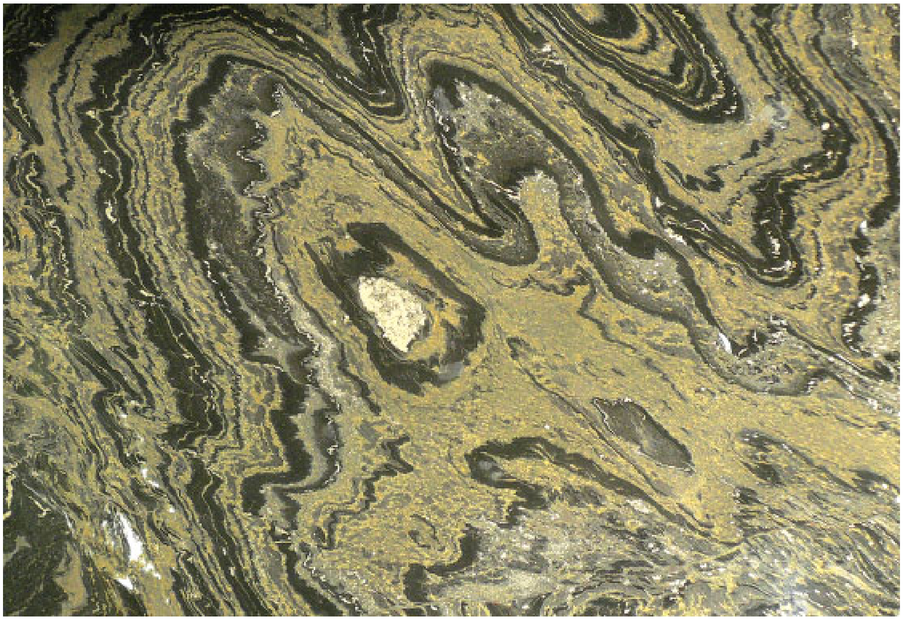

Plate 1.81 Ductilely folded sedimentary bedding in very-low-grade metamorphic shale-banded Fe-Cu-Zn sulphide ore with wispy white dolomite laminae. Note the diffuse axial plane cleavage. Sample from the closure of the orebody synform, Rammelsberg, Germany. Width of image ~20 cm. Courtesy B. Lehmann, Clausthal.

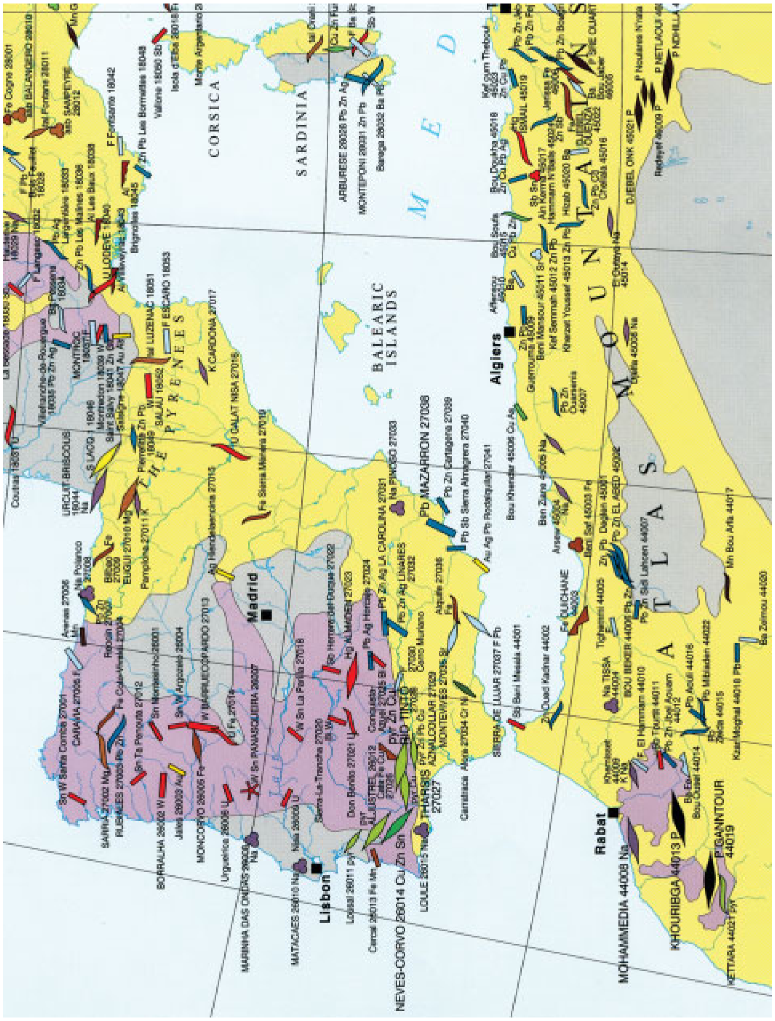
CORSICA
SARDINIA
BALEARIC ISLANDS
PYRENEES
Madrid
Lisbon
Algiers
Rabat
MED
ATLAS MOUNTAINS
RIO TINTO
NEVES-CORVO 26014 Cu Zn Sn
THARSIS
KHOURIBGA 44013 P
MOHAMMEDIA 44008 Na

Plate 1.89 Metallogenetic overview of Southwestern Europe and adjacent Africa (clipping from Juve & Storseth 1997). With kind permission of NGU, Trondheim. Text and symbols (cf. Plate 1.87) in four classes that indicate relative size of deposits. The geological background is simplified to Hercynian (purple, mainly Palaeozoic); Alpine (yellow, mainly Mesozoic) and cover sediments (light grey, mainly Tertiary). The distance between 5° latitude parallels is ~550 km.

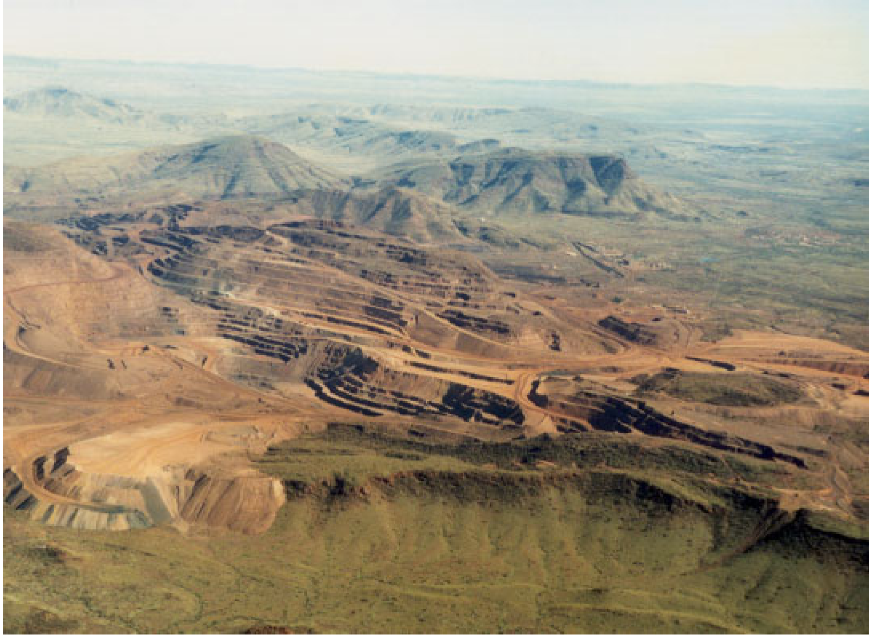

Plate 2.4 Birds-eye view of the high-grade haematite Mt Tom Price mine in the Hamersley Basin, looking to the northwest (cf. Plate 1.52). Southwest dipping Precambrian banded iron formations build the hills that rise above the plains. Courtesy of A.E. Harding, Rio Tinto Iron Ore, Perth, Western Australia.

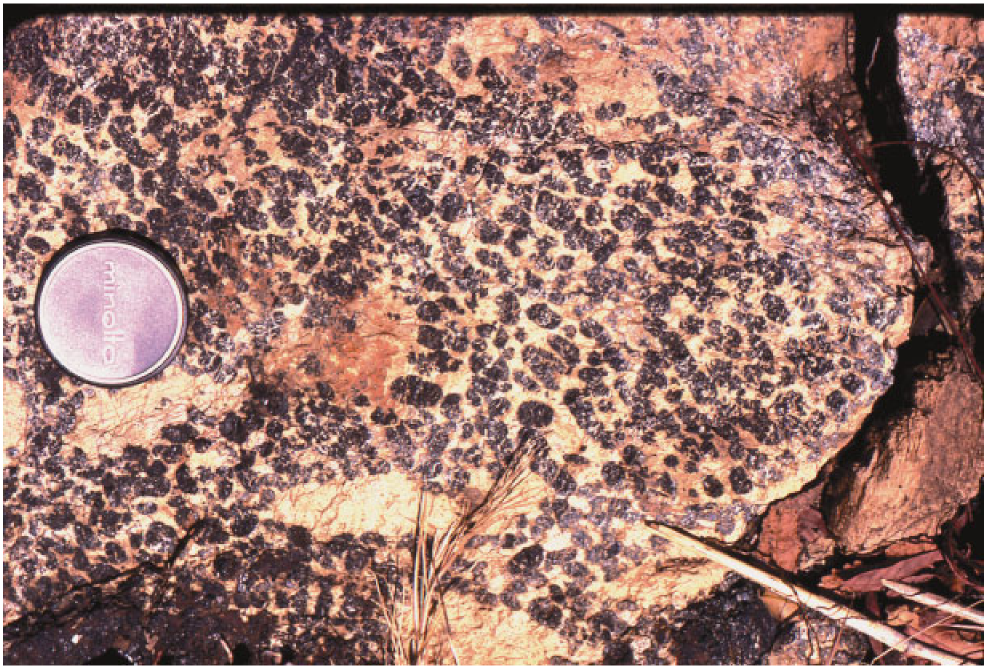

Plate 2.9 Dunite with nodular chromite in the Ingessana Hills, southern Sudan. The hills expose a large Neoproterozoic ophiolite and host several former chromite mines.

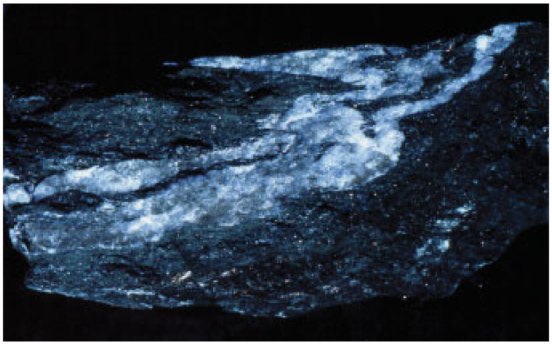

Plate 2.12a Folded scheelite-quartz veinlet cutting across foliation of host greenschist at Felbertal mine, Austria. Length of specimen 50 cm.

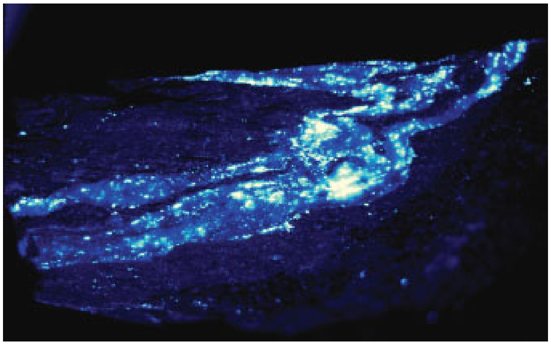

Plate 2.12b UV illumination reveals the distribution of scheelite (white).

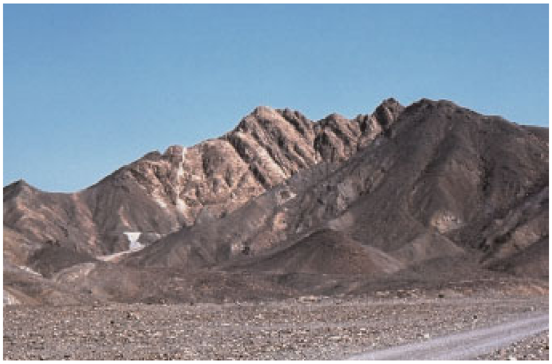

Plate 2.18 Among dark Neoproterozoic volcanic rocks, the white peak of Abu Dabbab leucogranite in the Eastern Desert, Egypt, is striking (although marred by desert varnish). The cupola is investigated for production of tantalum, cassiterite and ceramic-grade feldspar. An exploration adit produced the white waste rock dump on the left slope.

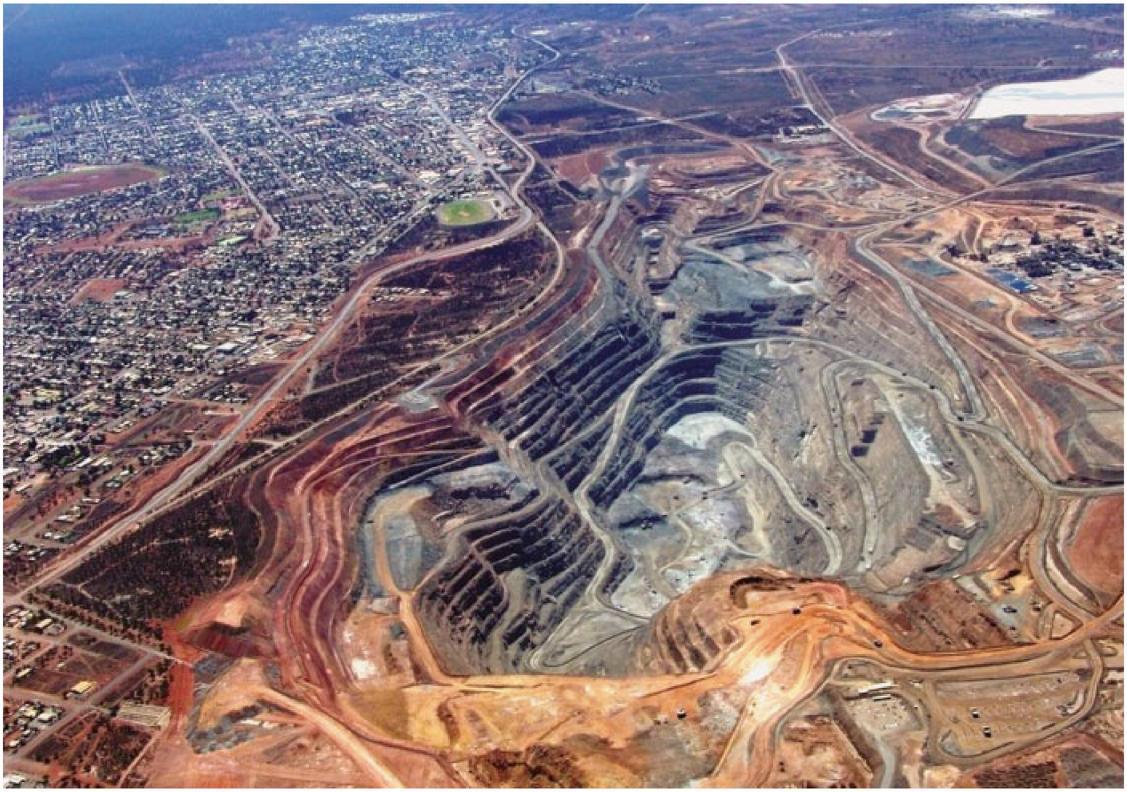

Plate 2.25 The Golden Mile Superpit at Kalgoorlie, Western Australia (2006). Note supergene oxidation in the foreground, the city of Kalgoorlie-Boulder on the left and tailings (white) in the right-hand background. Photo provided courtesy Kalgoorlie Consolidated Gold Mines (KCGM).

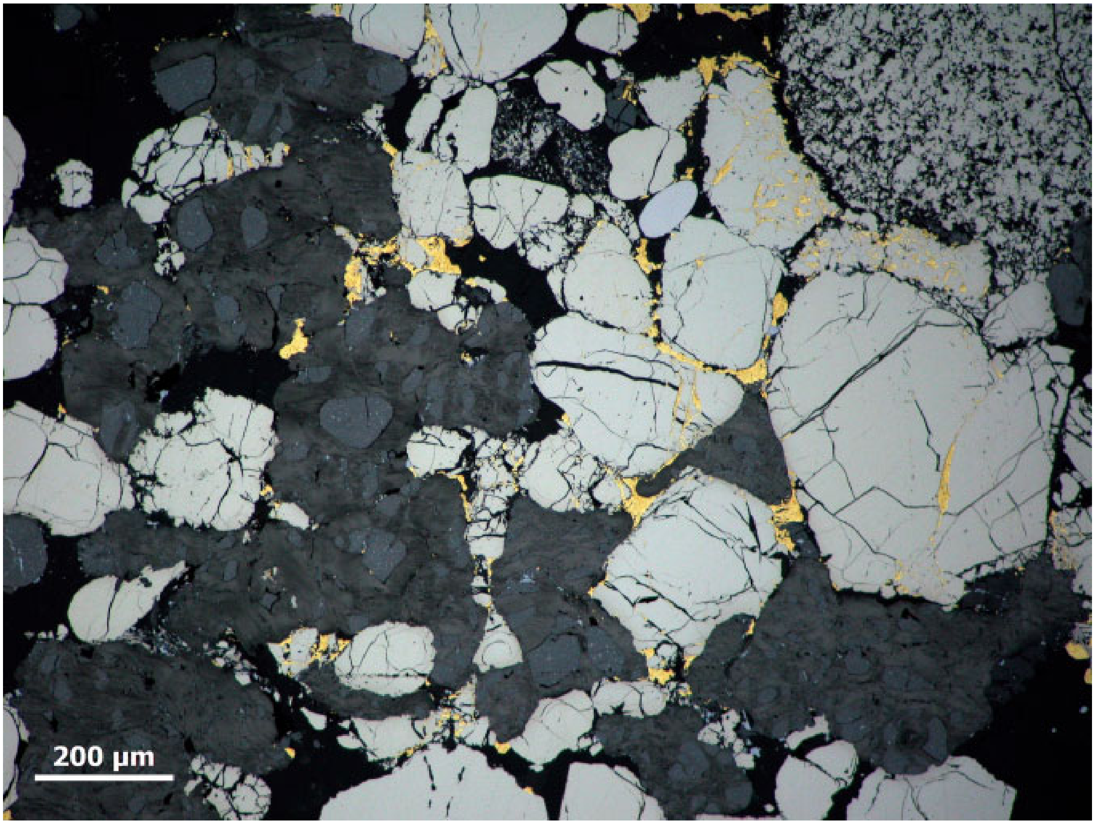

Plate 2.26 a Overview of high-grade gold ore in carbon-rich reef at Elsburg Mine, Witwatersrand, S.A. (plane-polarized reflected light). Courtesy B. Lehmann, Clausthal. The matrix between quartz pebbles (not visible) consists of clastic pyrite (light grey with fissures), pyritized claystone pebbles (top right margin) and clastic uraninite (medium grey with specks of radiogenic lead in galena, white) in thucholite matrix (pyrobitumen, wavy dark grey and black). Gold (yellow) in intragranular pore space is mostly remobilized.

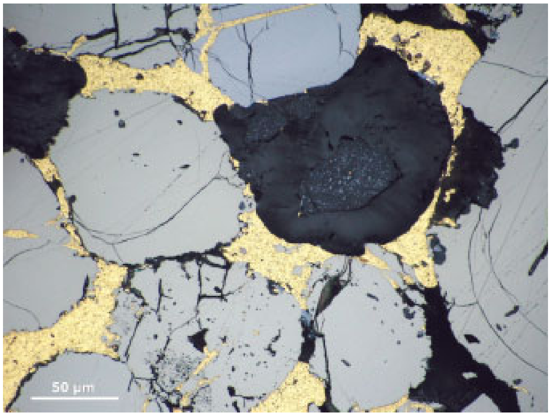

Plate 2.26b Detailed image of high-grade gold ore in carbon-rich reef at Elsburg Mine, Witwatersrand (polarized reflected light, oblique nicols, oil immersion). Courtesy B. Lehmann, Clausthal. Pyrite (light grey with fissures), gold (yellow, intergranular), uraninite (medium grey speckled with galena) in thucholite (pyrobitumen, wavy dark grey and black).

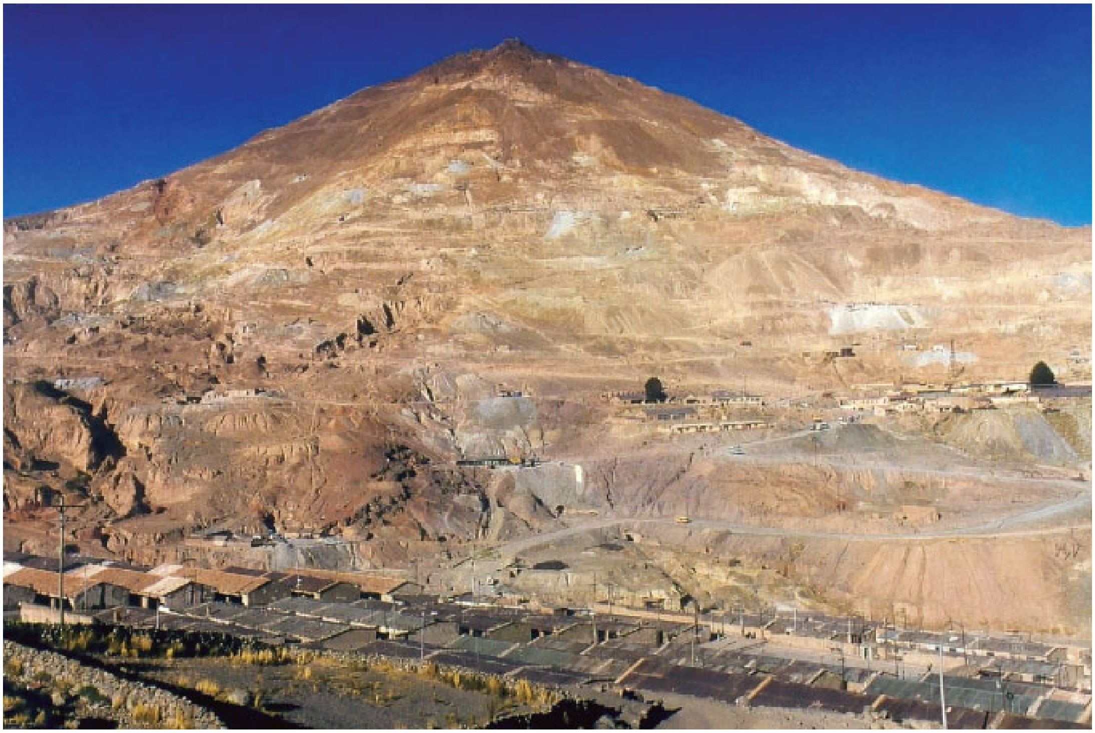

Plate 2.30 Cerro Rico de Potosí, Central Cordillera, Bolivia, contained the world's largest pre-mining silver concentration. Courtesy B. Lehmann, Clausthal. Visible are ubiquitous traces of vein mining on the slopes and the oxidized cap of the Miocene volcano. During the 17th century, Potosí was the principle source of fabulous wealth for Spain and of silver inflation in Europe.

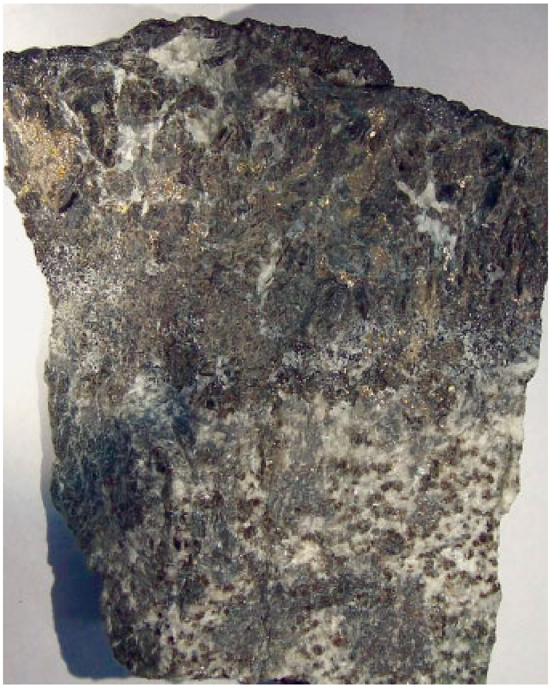

Plate 2.32 Merensky Reef at Impala mine, S.A., with footwall anorthosite (lower part), a thin chromitite band in the middle and the pegmatoid reef on top (orthopyroxene, plagioclase and the sulphides pentlandite-pyrrhotite- chalcopyrite). Height of sample is ~15 cm. Courtesy B. Lehmann, Clausthal.

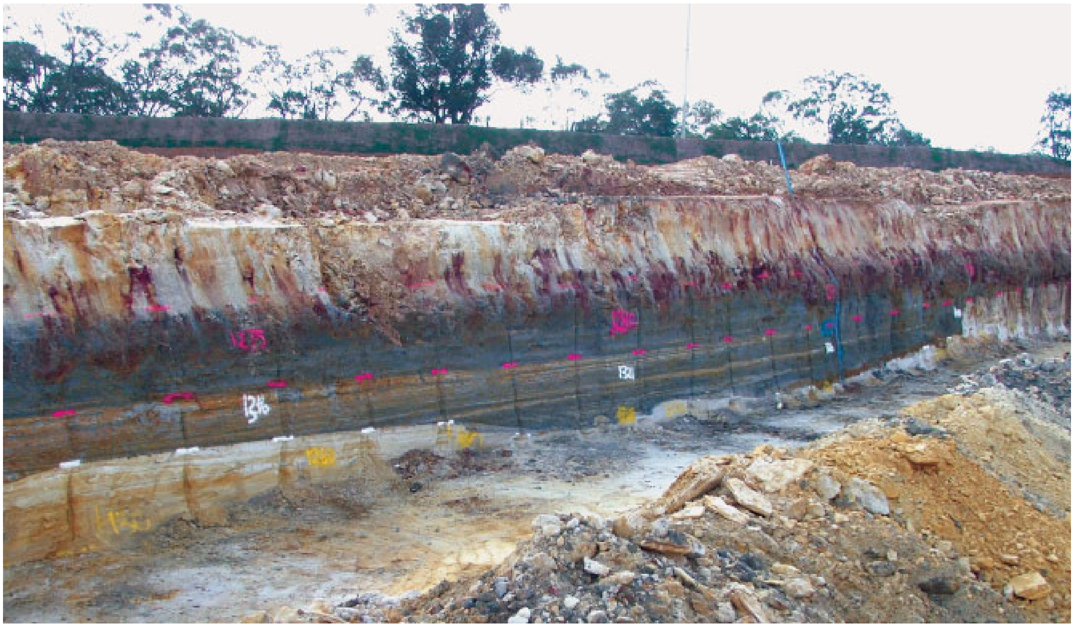

Plate 2.39 Bondi East heavy mineral deposit near the southeastern margin of the Murray Basin in Victoria, Australia, looking north at an active mine face, which has been cleaned up for channel sampling and detailed mapping. Courtesy David Whitworth (Iluka Resources). Barren overburden is removed; upper low-grade ore (ca. 10% HM) is white sand with 30% clay. Note the near-vertical incision of the high grade ilmenite-zircon-rutile sand (dark, 50–70% HM) at the right of the image. The footwall consists of barren massive silty sand (white). Patchy oxidation is ubiquitous.

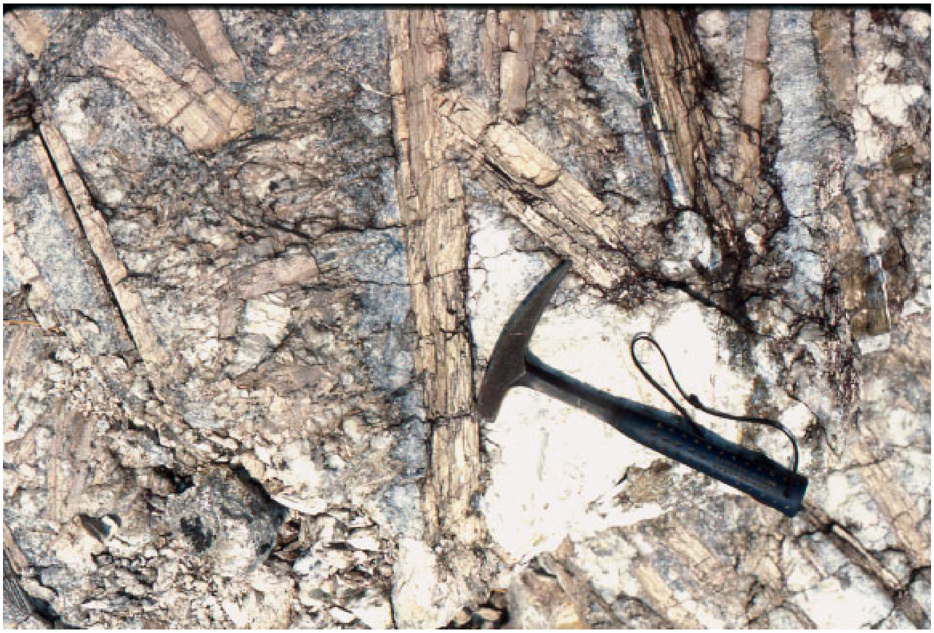

Plate 2.43 Giant Manono pegmatite in D.R. Congo is a sub-horizontal sheet and asymmetrically zoned. An upper marginal zone is made up of near-vertical palisades of spodumene (with microcline) and patches of stanniferous albitite (centre).

Plate 2.44 Artisanal salt production at Salar de Uyuni, at 3500 m altitude in the Altiplano of Bolivia: One of the largest salt lakes on Earth, the salar contains giant resources of lithium, potassium, boron and magnesium in brines below the surface. The background mountains are part of the Central Cordillera, which hosts Cerro Rico de Potosi. Courtesy B. Lehmann, Clausthal.

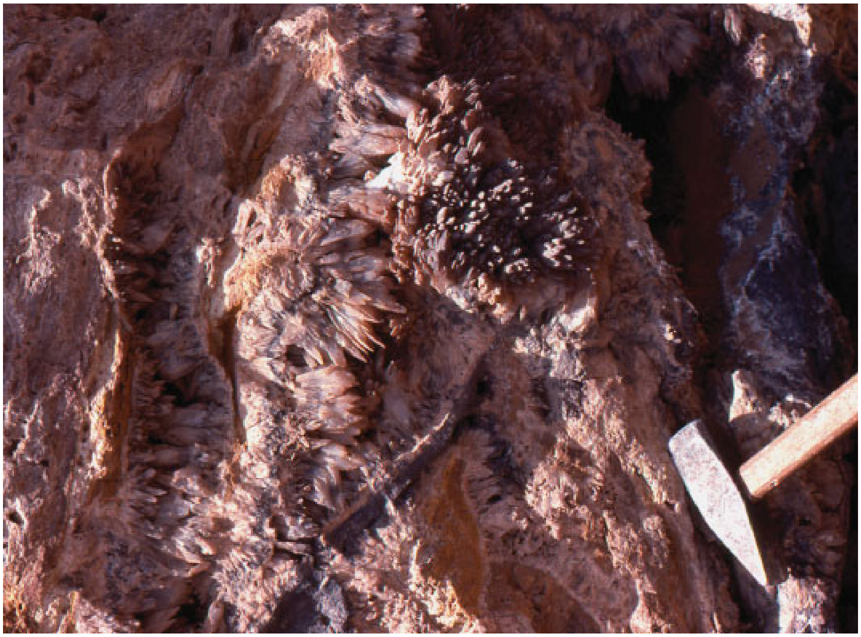

Plate 3.3 Celestite crystals in roughly bedding-parallel solution cavities of Neogene gypsum at Wadi Essel, Red Sea Coast, Egypt.

Plate 3.8 Bentonite sample from Moosburg mining district, Germany. Copyright © Süd-Chemie AG 2009.

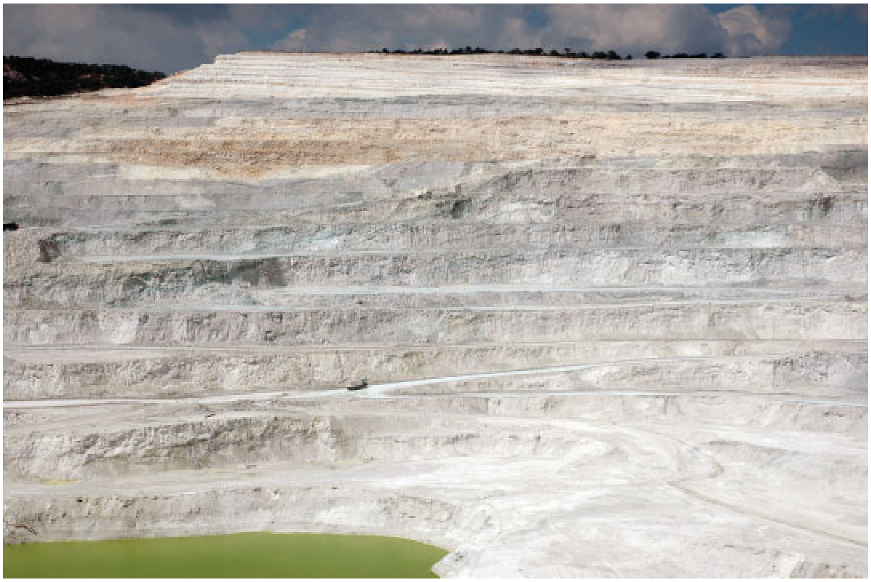

Plate 3.9 Borax mine Kirka in western Turkey is one of the world's largest boron producers. Courtesy Walter Prochaska, MU Leoben. Formed in a Miocene evaporitic lake (Helvaci & Orti 2004), the borax ore (lower part) is enveloped in limestone and overlain by claystone and banded limestone, tuff, marl and chert. Gangue of borates comprises realgar, orpiment, gypsum, celestite, calcite, dolomite and smectite clay. Ore thickness reaches 145 m, resources comprise >110 Mt of 45% B_2O_3.

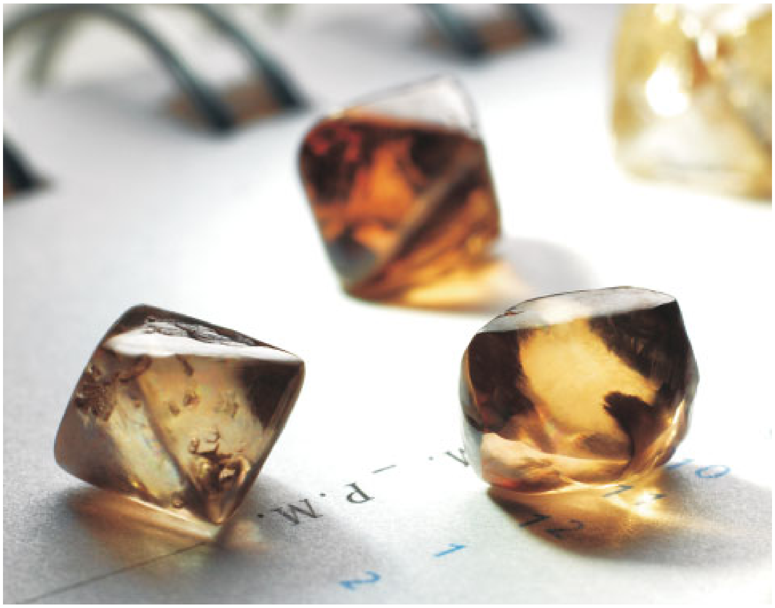

Plate 3.13 Champagne-coloured octahedral diamond crystals from Argyle, Australia. Note the macroscopic (eclogitic) inclusions. Courtesy Rio Tinto © Argyle Diamonds.

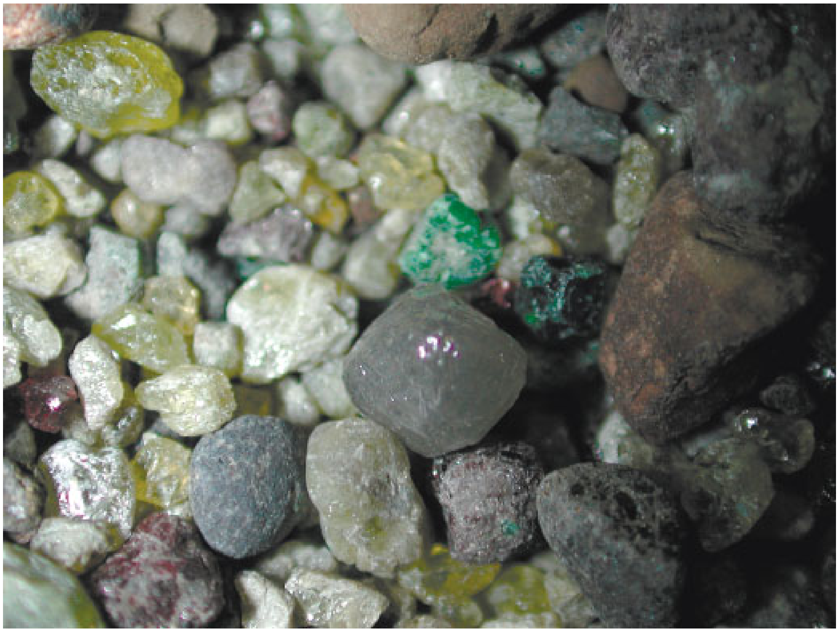

Plate 3.14 Heavy minerals concentrate from glacial till in the region around Ekati, N. T., Canada, where more than 150 kimberlite pipes have been found. Courtesy W. Prochaska, MU Leoben. Indicator minerals on display include dark green Cr-diopside, pale or transparent yellow eclogitic garnet (?), light grey picroilmenite, dark grey chromite, dark red Cr-pyrope, bright green olivine and one octahedral diamond (centre, diameter ~1.8 mm).

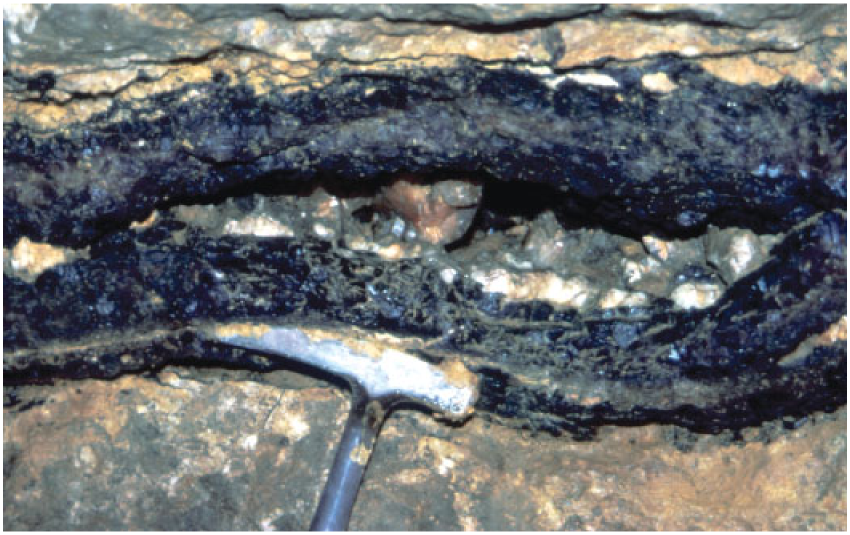

Plate 3.16 Banded dark blue, purple and yellow hydrothermal fluorite ("Blue John") filling karst pipes and replacement bodies in Carboniferous limestone, Derbyshire, England. Light crystals in the centre cavity are calcite. Courtesy Volker Lüders, GFZ Potsdam.

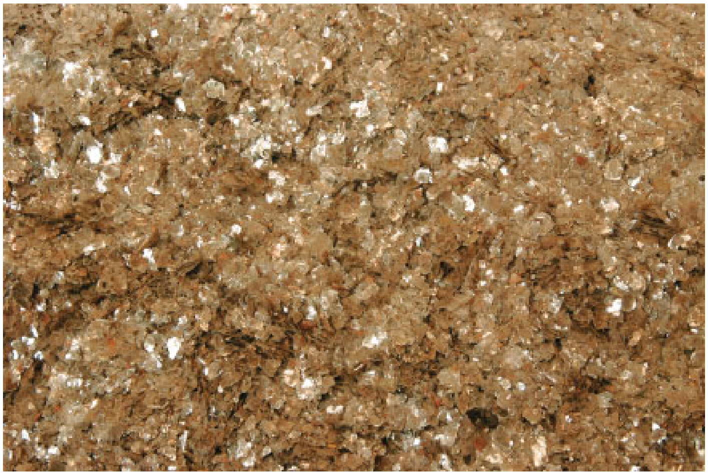

Plate 3.24 Concentrate of phlogopite flakes produced at Siilinjärvi, Finland, is processed for use in decorative paint, special plastics and fire protection coatings. Courtesy LKAB 2010.

Plate 3.26 Part of the Åheim (Almklovdalen) olivine quarry in southern Norway. Courtesy of Håvard Gautneb, Geological Survey of Norway, Trondheim.

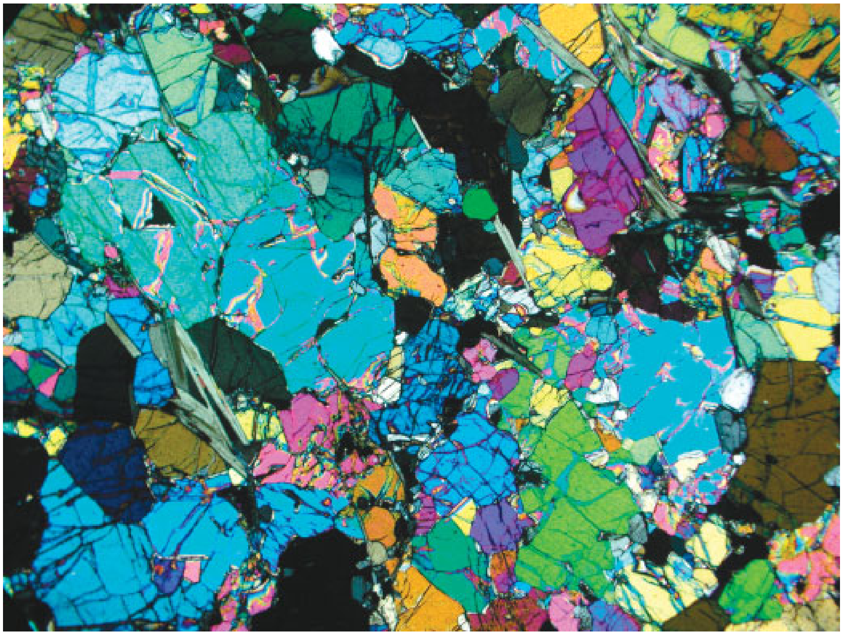

Plate 3.27 Åheim dunite in thin section (crossed nicols). Olivine grain diameter is 1–2 mm. Note the fractures with weak net-textured serpentinization. Courtesy of Håvard Gautneb, Geological Survey of Norway, Trondheim.

Plate 3.30 High-grade industrial sands at Uhry in northern Germany were deposited in a shallow bay of the Late Cretaceous sea north of the Harz Mountains and chemically upgraded when the sea retreated westwards and tropical forests covered the area.

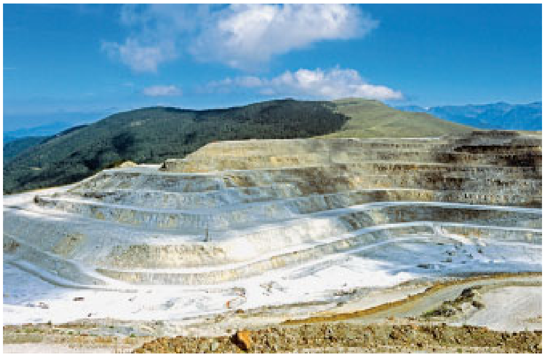

Plate 3.34 Eastward bird's eye view of the talc quarry at Luzenac in the French Pyrenees. White talc marks the working face. © Philippe Psaila/SPL/PictureDesk.com.

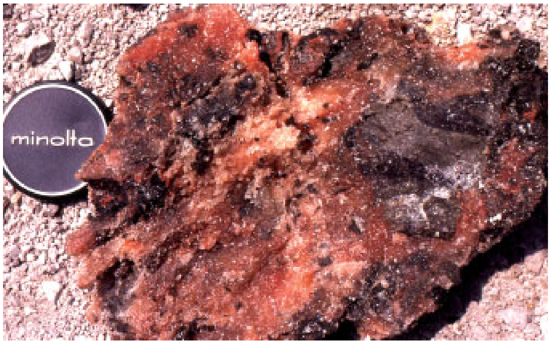

Plate 4.3 Haselgebirge sample from Bad Aussee mine near Salzburg, Austria. This variety displays a red halite matrix with dispersed angular fragments of black claystone.

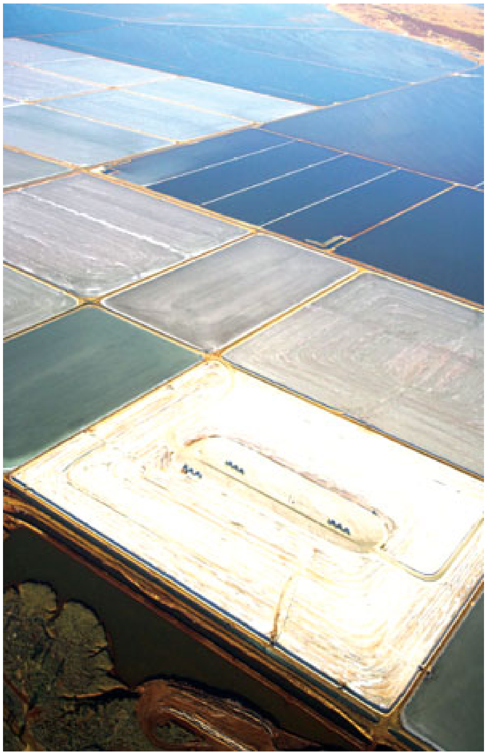

Plate 4.6 Solar seawater evaporation pans for industrial salt production on the West Australian coast. Courtesy Dampier Salt Ltd and Rio Tinto Minerals. Seawater is first concentrated to specific gravity 1.21 in order to precipitate carbonate and gypsum. Different grades of salt are crystallized between brine gravity 1.21 and 1.275. Harvesting is visible in the foreground. The remaining K-Mg brine ("bittern") may be processed or pumped back into the sea.

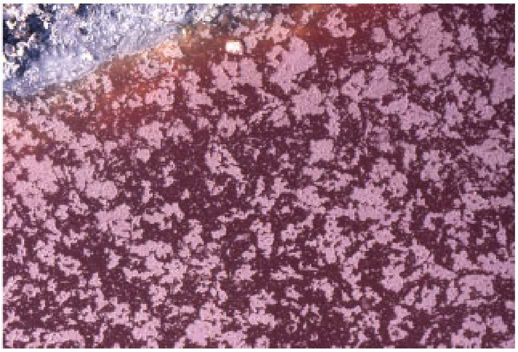

Plate 4.12a Salt rafts floating on brine at the shore of Lake Katwe, western Uganda. Katwe is a large maar lake due to Pleistocene volcanism. It draws seepage water from close-by fresh Lake Edward. The dark red colour of the brine is caused by teeming micro-organisms. Upper left corner is organic-rich mud.

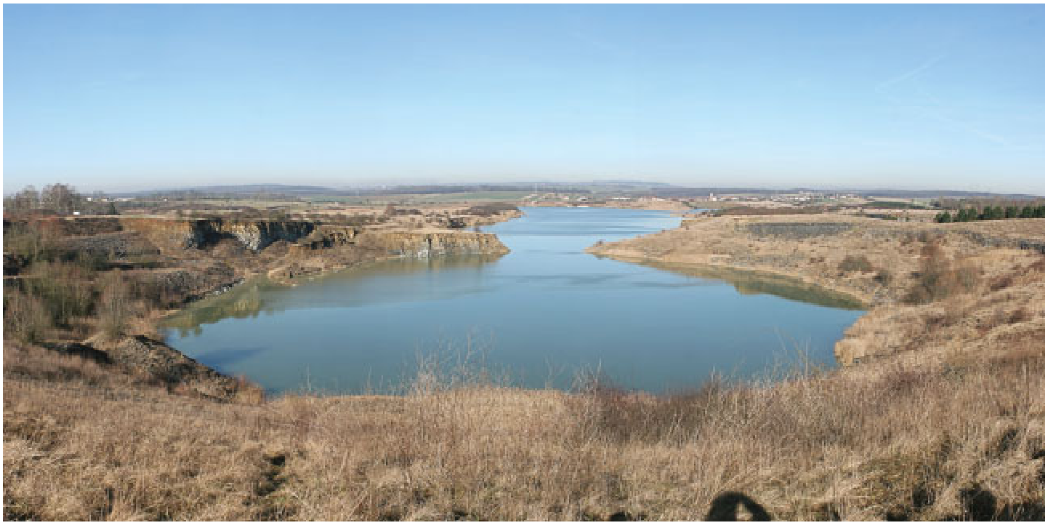

Plate 4.30 Historic salt exploitation by borehole solution at Haraucourt (Meurthe-et-Moselle, France) caused these flooded collapse craters. The deposits are subhorizontal Late Triassic (Keuper) salt beds at shallow depth. Courtesy Christian Wolkersdorfer, CBU, Sydney, Canada.

Plate 5.6 Environmental stream sediment and water sampling (including *in-situ* determination of pH, T and Eh) in the Gatumba tin-tantalum mining district, Rwanda.

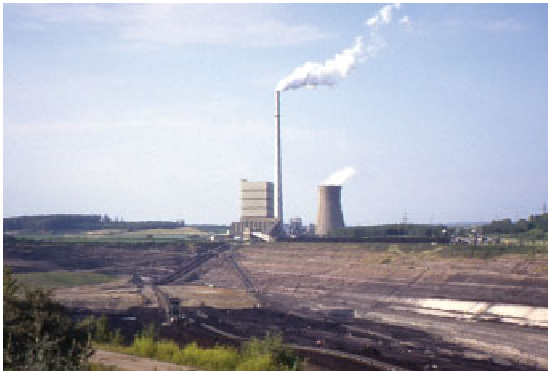

Plate 5.18 Lignite pit Schöningen in northern Germany with its captive power station. Coal extraction takes place at the pit bottom. Overburden and combustion residues are used to refill nearby exhausted pits. Flue gas cleaning yields by-product elementary sulphur. Note white sands on bench to the right. Strata are limnic and marine due to marine transgression during the Palaeocene-Eocene thermal maximum.

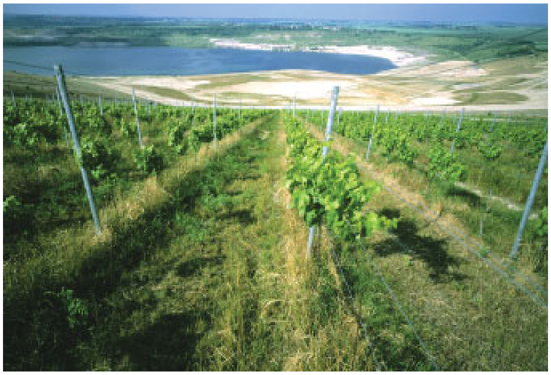

Plate 5.19 Recultivation of the lignite pit Geiseltal in northern Germany during the flooding operation in 2005. Photograph by Christian Bedeschinski 2005. © LMBV (Lausitzer und Mitteldeutsche Bergbau-Verwaltungsgesellschaft mbH). The sunny slope on footwall limestone in the foreground was planted with grapevines. The Eocene lignite seam attained a thickness of 100 m in a large salt subrosion depression within Triassic limestone measuring 5 × 15 km. Because of the induced alkalinity, the coal was famous for exceptional preservation of vertebrate fossils and of chlorophyll in green leaves. Exploited through nearly 300 years, original lignite resources were 1600 Mt.

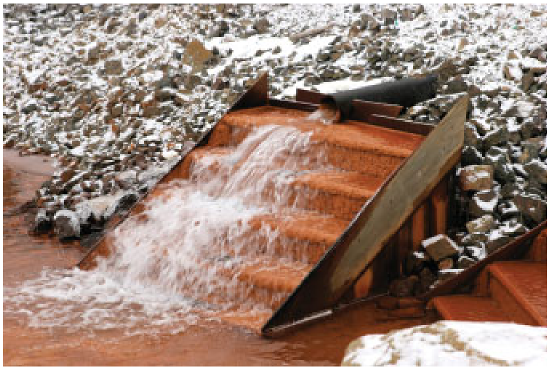

Plate 5.24 Cascades for aerating mine water from the abandoned Dominion number 25 coal mine on Cape Breton Island, Canada. Oxidation initiates precipitation of colloidal red oxyferrohydrate, which gradually matures into minerals such as goethite, ferrihydrite and jarosite. Courtesy Christian Wolkersdorfer, CBU, Sydney, Canada.

Plate 5.25 Polishing reed bed as the last element in a passive treatment system consisting of a combined reducing and alkalinity-producing (RAPS) wetland system for acid mine drainage from an abandoned coal mine (Bowden Close near Durham, County Durham, UK). Courtesy Christian Wolkersdorfer, CBU, Sydney, Canada.

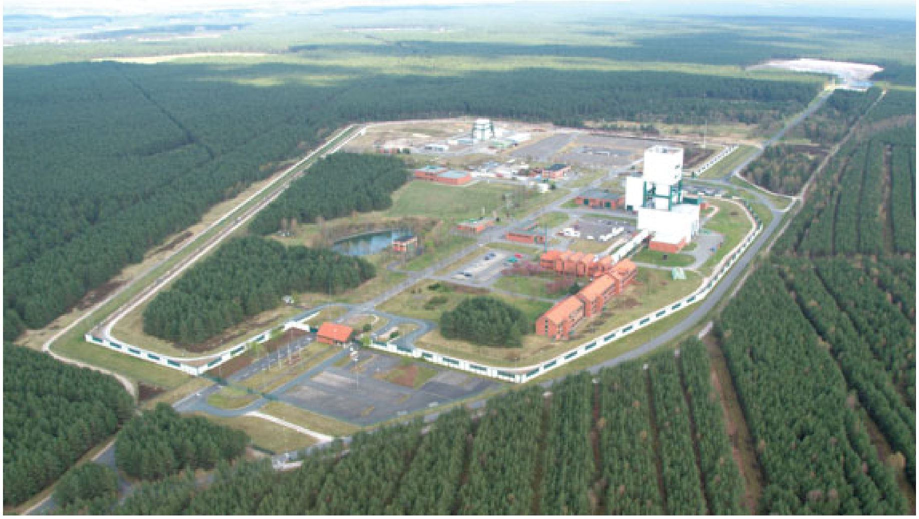

Plate 5.29 Gorleben mine in northern Germany is destined (although not yet licensed) to function as a repository for heat-producing radioactive waste in salt rock. The aerial view shows surface installations, the two shaft buildings, waste disposal and Elbe River in the far distance to the left. © Bundesamt für Strahlenschutz, Germany.

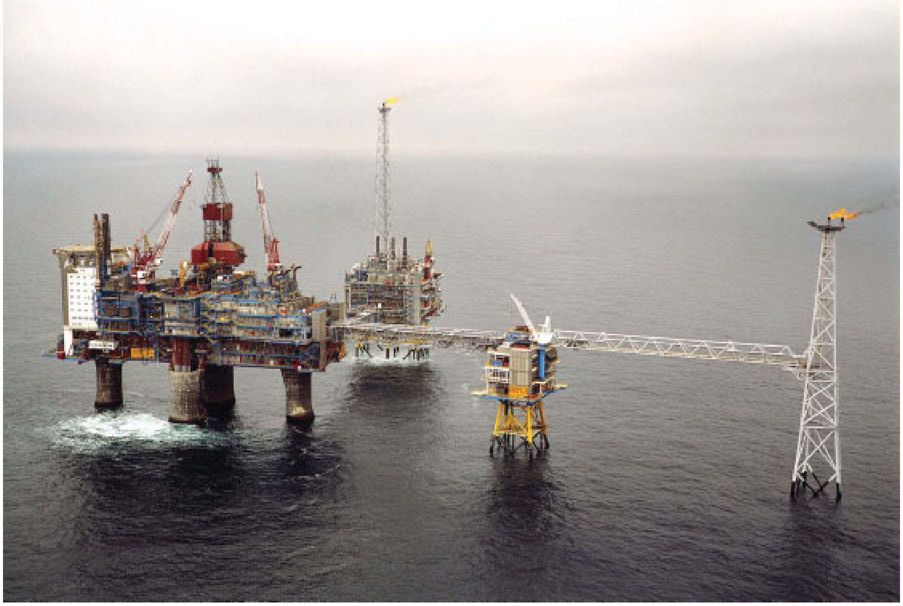

Plate 6.2 Sleipner platform in the North Sea offshore Norway is the world's first large-scale geological CO_2 sequestration operation. On the platform, carbon dioxide is separated from natural gas and pumped into a sub-seafloor aquifer. © Øyvind Hagen, Statoil.

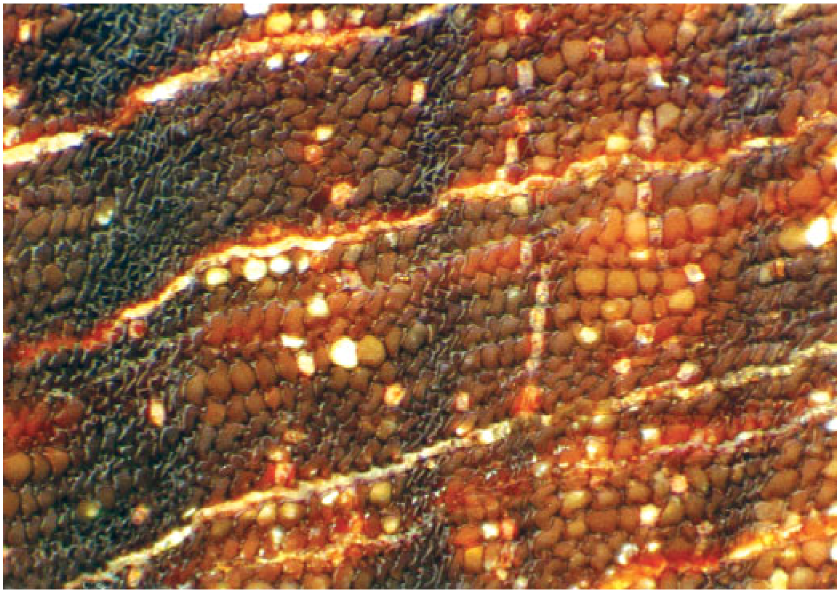

Plate 6.7 Microphotograph of the coal maceral textinite (a huminite; ungelified woody tissue with intact botanical cell structures) in Tertiary lignite, Poland. Reflected light, oil immersion; long side of image 0.5 mm. Courtesy of Maria Mastalerz and Indiana Geological Survey.

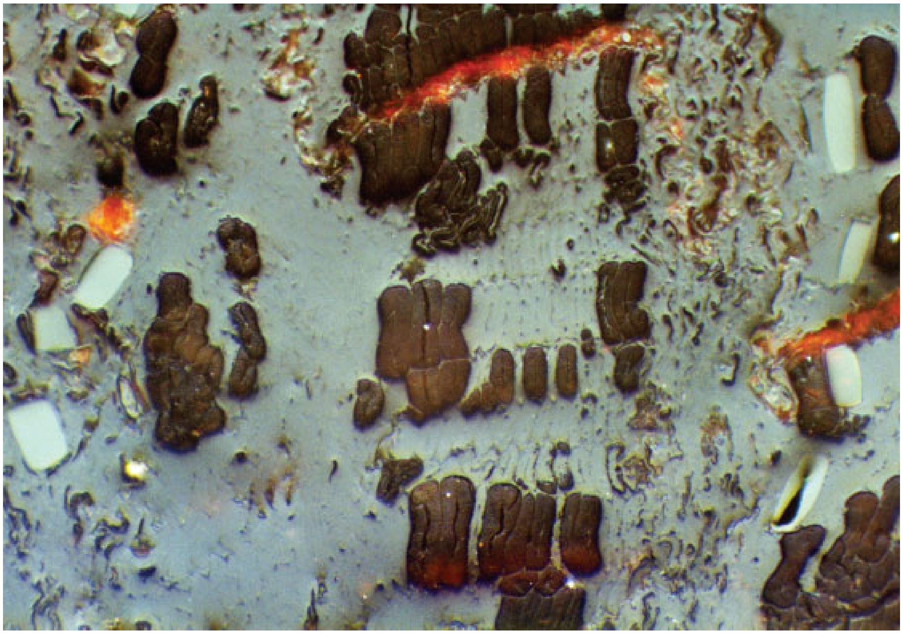

Plate 6.8 Microphotograph of the coal maceral ulminite (a huminite; more or less gelified woody tissue) in Tertiary lignite, Poland. Reflected light, oil immersion; long side of image 0.5 mm. Courtesy of Maria Mastalerz and Indiana Geological Survey.

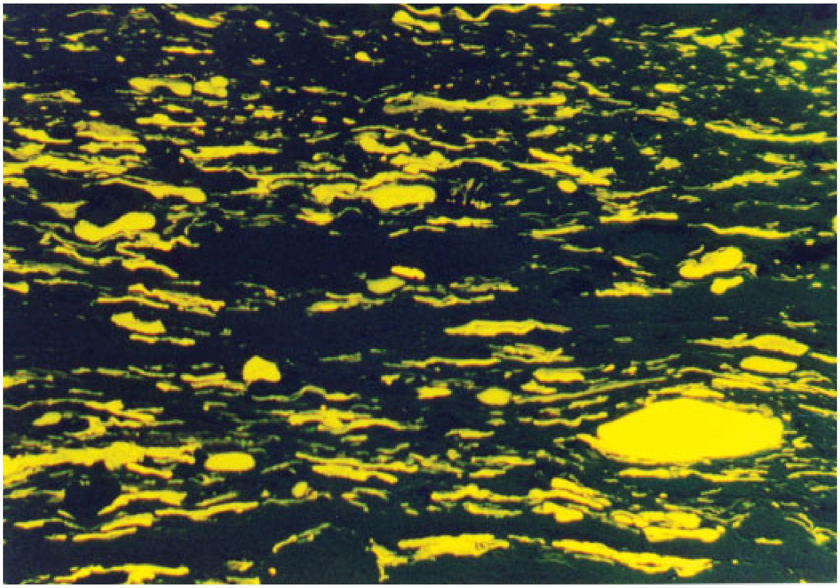

Plate 6.9 Microphotograph of the coal maceral sporinite (liptinite; wax-coated fossil spores and pollen) in Pennsylvanian bituminous coal, USA. Fluorescent light; long side of image 1.0 mm. Courtesy of Maria Mastalerz and Indiana Geological Survey.

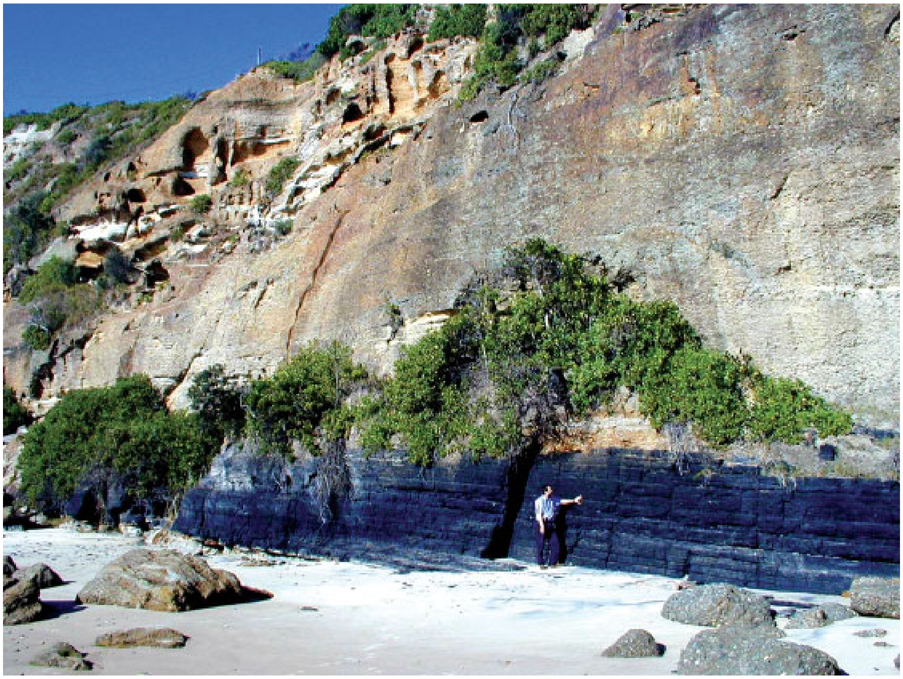

Plate 6.20 Outcrop of Permian Great Northern coal seam below fluvial conglomerate on the Pacific shore, Sydney basin, New South Wales, Australia. Note vertical joints and subdivision of seam into plies. Courtesy of Keith Bartlett, Minarco-Mineconsult, Tuggerah, NSW.

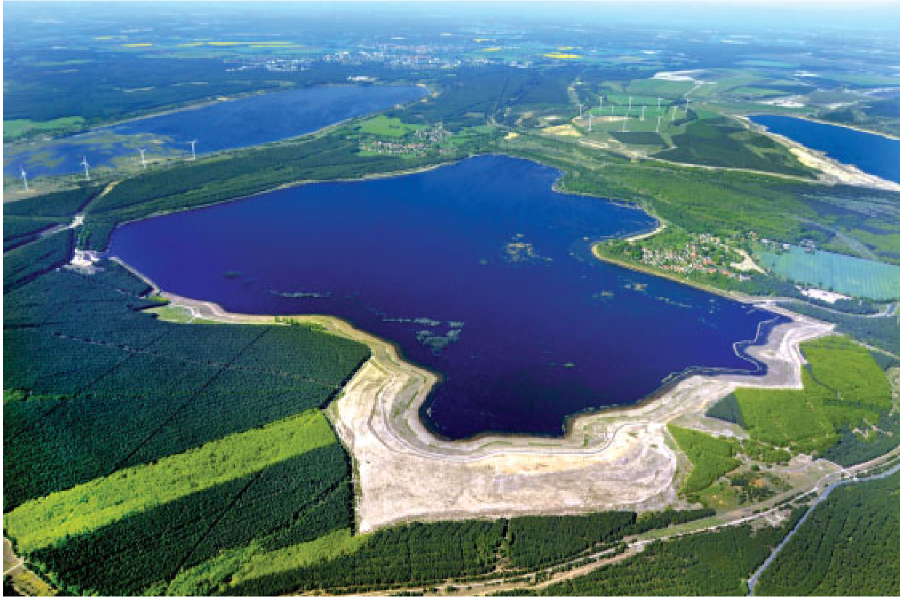

Plate 6.30 Post-mining lignite open pit lakes in the Lausitz region, Germany, in the last stages of filling and rehabilitation. Courtesy of P. Radke, © LMBV, Lausitzer und Mitteldeutsche Bergbau-Verwaltungsgesellschaft mbH.

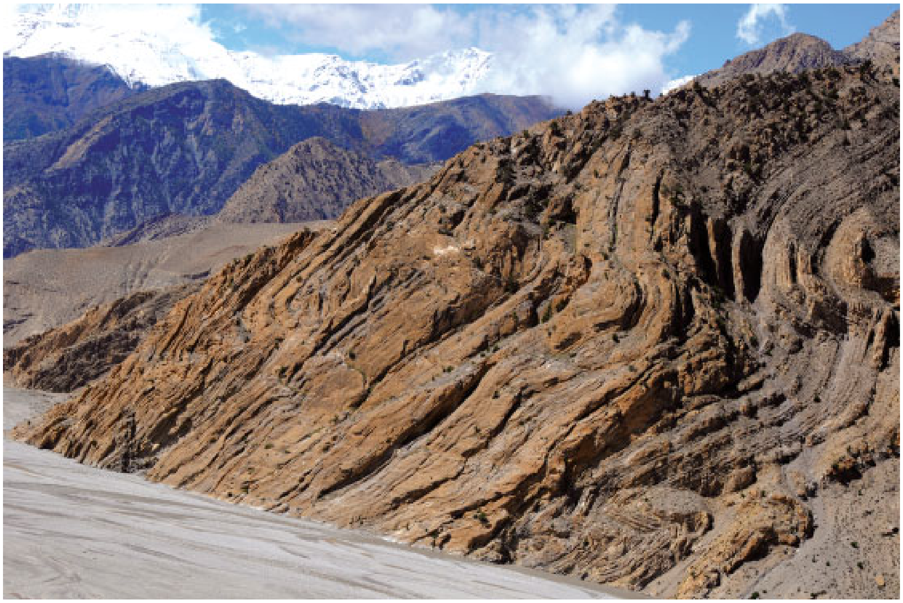

Plate 7.6 Early Mesozoic bituminous rocks in the upper Kali Gandaki valley of the Annapurna-Dhaulagiri zone, western Nepal. This is part of the unmetamorphosed sediments of the Tethyan zone above the crystalline Greater Himalayan Sequence. Courtesy Krishna Karki, © Travel-to-Nature Asia. The image serves as a paradigm for hydrocarbon source rocks. Further up in the mountains, natural methane seepage feeds eternal flames in Jwala Mai temple.

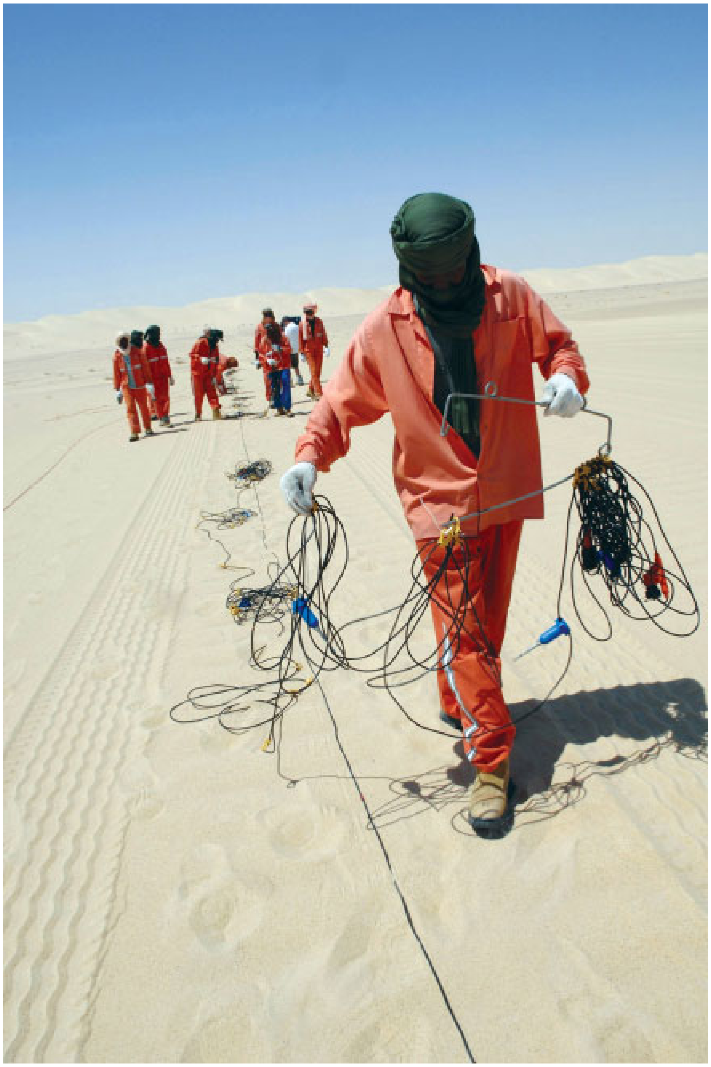

Plate 7.22 Laying out a seismic reflection survey line of geophones in the desert of Cyrenaica, Libya. © Øyvind Hagen, Statoil.

Plate 7.23 A fleet of heavy vibrator trucks waiting for the deployment order. Cyrenaica, Libya. © Øyvind Hagen, Statoil.

Plate 7.24 Drilling for CBM gas in the Rocky Mountains near Pinedale, Wyoming, USA (2008). Copyright Shell plc.

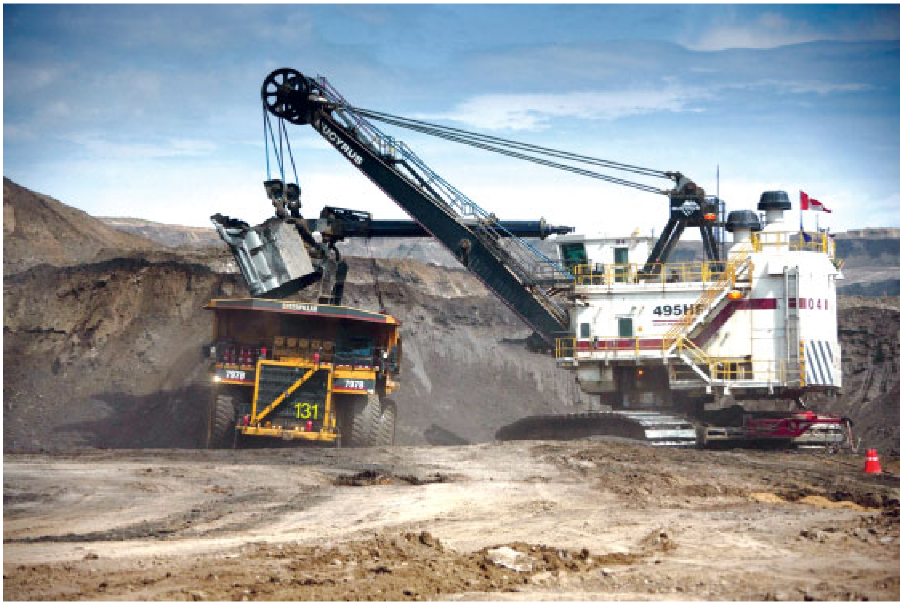

Plate 7.29 Oil sand mining at Muskeg mine, Athabasca, Canada (2009). Copyright Shell plc.

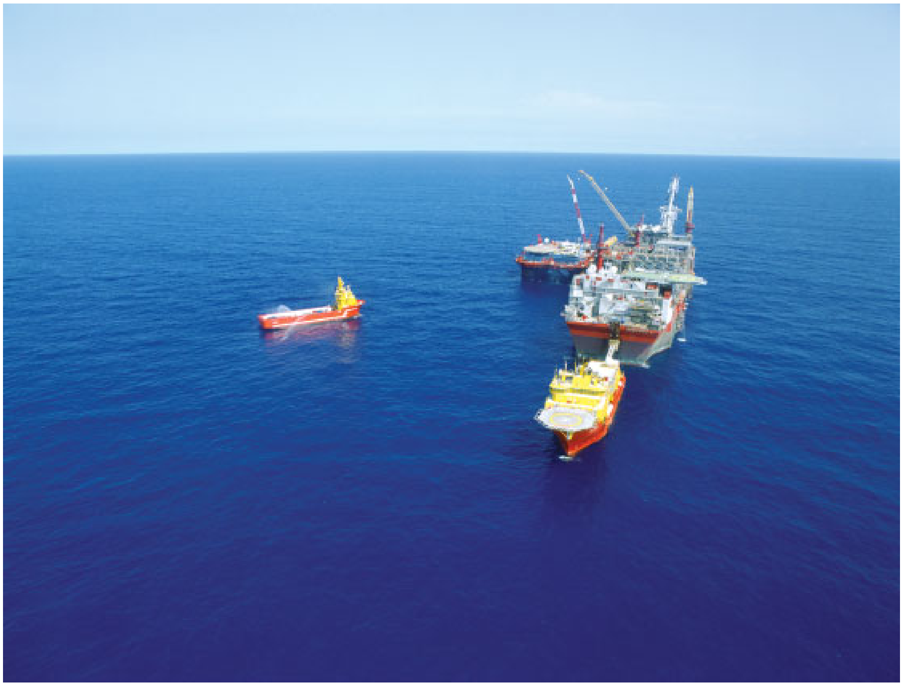

Plate 7.32 Floating production storage and loading vessel in the Bonga field offshore Nigeria. The field lies 120 km from the River Niger mouth in water more than 1000 m deep. Copyright Shell plc.

Introduction

Human societies need sufficient water, productive soil, energy in different forms, and organic and mineral raw materials as a base for their physical existence. An additional important requirement is a healthy natural and socio-economic environment.

Economic Geology is a subdiscipline of the geosciences. It devotes itself to the scientific study of the Earth's sources of mineral raw materials and to the practical application of the acquired knowledge. Considering the life-cycle of a mine, economic geology leads in the search for new mineral deposits and in their detailed investigation. It contributes to economic and technical evaluations, which confirm the feasibility of a project and end with the physical establishment of a mine. While mining goes on, economic geology provides many services that assist rational exploitation, foremost by continuously renewing mineable reserves and by limiting effects on the mine's environment to a minimum. Possible negative impacts of mining include surface subsidence, lowering of the water table, various emissions and mechanically unstable or environmentally doubtful waste rock dumps. In the phase of mine closure, economic geology helps to avoid insufficient or outright wrong measures of physical and chemical stabilization, recultivation and renaturalization.

In recent years, the economic evolution of industrial and of rapidly developing countries caused incisive changes in supply and consumption of mineral raw materials. China, rather than Europe or North America, provides world markets with essential metals and minerals, although at the same time importing large quantities of needed feedstock for its expanding population and industry. The future supply of petroleum appears to be unreliable, but its role as the main source of liquid fuels for transport is hardly dented by biofuels and other developments. Wind and geothermal energy are increasingly contributing to electricity production, yet without coal, nuclear power and natural gas, industrial economies would soon break down and developing nations would be locked in poverty. Ours is a time of transition but we cannot yet discern the outcome. Whatever it will be, metals, minerals and energy raw materials will remain a precondition of human welfare.

WHAT ARE ORE DEPOSITS?

Ore and mineral deposits are natural concentrations of useful metals, minerals or rocks, which can be economically exploited. Concentrations that are too small or too low-grade for mining are called occurrences or mineralizations. It is very important to understand the economic implications of the difference between these terms. Unfortunately, their wrong application is common and leads to fundamentally misleading deductions. Therefore, the denomination

Economic Geology Principles and Practice
Metals, Minerals, Coal and Hydrocarbons – Introduction to Formation and Sustainable Exploitation of Mineral Deposits, Walter L. Pohl
© 2011 Walter L. Pohl. Published 2011 by Blackwell Publishing Ltd.

"economic ore deposit" may be used when a clear attribution to this class is to be emphasized. Note that not all ores are strictly natural – it is very common that waste of a former miners' generation is today's profitable ore, such as tailings of earlier gold, copper and diamond mining.

Mineral deposits are basically just valuable rocks. Their formation is compared with processes that have produced ordinary rocks and is investigated with petrological methods (Robb 2005). Mineral deposits can also be thought of as a geochemical enrichment of elements or compounds in the Earth's crust, which is determined by their chemical properties (Railsback 2003; Lehmann *et al.* 2000b). The ratio between the content of a valued element in an ore deposit and its crustal average (Clarke values, Wedepohl 1995) is called the "concentration factor". Formation of iron ore, with today's typical grade of 60% Fe relative to an average crustal iron concentration of ~5%, requires 12-fold concentration. Copper ore that has 1% Cu compared to the crustal average of 0.007% Cu in the crust exhibits a 140-fold enrichment. Gold ore with 10 grams/tonne "distilled" from ordinary rocks with 0.002 g/t Au attests to a 5000-fold concentration.

Manifold are the processes and factors leading to the concentration of elements and minerals, including the formation of mineral deposits (Robb 2005). Final causes are the dynamic interactions between the Earth's core, mantle and crust, and of the hydro-, bio- and atmosphere. Cooling and devolatilization of the Earth and unmixing of the system in the geological-geochemical cycle and during the transfer of elements have important roles (Lehmann *et al.* 2000b). With reference to the origin, endogenous and exogenous process systems are distinguished. The first are those resulting from the dynamics of the Earth's interior that are ultimately driven by the Earth's heat flow. At present, the total heat flow at the Earth's surface is 46 ± 3 Terawatts (10^{12} J/s), resulting from heat entering the mantle from the core, of mantle cooling, radiogenic heating of mantle and crust by the decay of radioactive elements and of various minor processes (Lay *et al.* 2008). Exogenous processes take place at the Earth's surface and are mainly due to the flow of energy from the sun ($\sim 12.10^{18}$ J/s). In rare cases, extraterrestrial processes have contributed to the formation of mineral deposits by impact of meteorites and asteroids.

The origin of mineral deposits is often due to a complex combination of several processes, boundary conditions and modifying factors, collectively making up the metallogenetic, or minerogenetic system. Evidence for such systems that operated in the geological past is always fragmentary. Some questions can possibly be answered by studying presently active ore-forming systems (e.g. black smokers in the deep oceans), but this method ("actualism") has limitations. Because of the unknown factors, there is often room for different interpretations (hypotheses) of the scientific facts. Economic geology strives to improve continuously the genetic models of ore formation, i.e. complete schemes of these systems. This effort is assisted by progress in many other sciences (from biology to physics), but the reverse is also true. Economic geology provides a fascinating insight into geological systems that are extremely rare and can only be illuminated by studying mineral deposits. The practical mission of economic geology is the provision of metals and minerals that society requires. Of course, this implies cooperation with other scientific, technical and financial professionals.

MINING IN THE STRESS FIELD BETWEEN SOCIETY AND ENVIRONMENT

> *Cum semper fuerit inter homines de metallis dissensio, quod alii eis praeconium tribuerent, alii ea graviter vituperarent* (the original text in Latin by Georgius Agricola 1556).
>
> In English: "People were always divided in their opinion about mining, as some praised it highly while others condemned it fiercely."

Agricola reports that enemies of mining in his time deplored not only harmful effects on the immediate environs but even moral aspects – they accused mining of advancing greed. Today, this remains one motive of opposition to the industry, but fundamental rejection of any extraction of minerals is more common. The main reasons given are that mining visibly uses the land and often leaves a profound and enduring change.

Certainly there are often sound arguments against mining at a specific location. Compromises should be sought, however, because mineral deposits cannot be installed at arbitrary places. Their locations are predetermined by nature. Examples are sand and gravel deposits in river plains. Today, these raw materials are so scarce in many regions that they have to be protected against other claims (e.g. housing developments). Yet, everyone consumes minerals and mineral-derived products for homes, heating, transport, computers, medicinal use and numerous articles of daily life. Mining provides these minerals. Recycling replaces only part of primary production.

As a percentage of total area, land use by mining is very small and only locally visible. Biofuel agriculture, solar and wind energy plants require much more land. Indeed, they create additional demand for minerals (e.g. fertilizer, metals for machines and processing plants, transport). Toxic elements, such as arsenic and cadmium, are essential for sustainable energy production, for example in photovoltaics. In many cases, even low footprint technologies such as geothermal power plants have serious problems with waste, such as brines, salt, toxic and heavy metals (most notably arsenic, mercury and radionuclides). This demonstrates that there are no simple solutions for a sustainable economy without mining. On the contrary, it is undeniable that conservation of our quality of life and development for the major part of humans who still lack the most basic necessities for a life of dignity, require both mineral raw materials and an intact environment.

Mining without an impact on the environment is impossible (Figure 1.1), but the industry strives to minimize negative effects (Figure 1.2) and to improve the welfare of affected communities ("green mining"). Some mining operations create an enriched landscape of constructed ecosystems, which provide humans with a variety of services (e.g. food, flood and erosion control, areas for recreation and aesthetics, and clean water). Examples include lignite and clay pits, which bequeath beautiful new lakes. Hard rock mines and quarries may grow into rare islands of nature in a sea of human occupation. Many of these sites support rare and threatened species from archaea and bacteria to plants and animals, helping to preserve biodiversity (Batty 2005).

Reversing mineral extraction, mines also have an extremely important role as deep disposal sites for the safe storage of society's unavoidable toxic and radioactive waste. Chemically dangerous waste is usually stored in worked sections of suitable underground mines. For highly toxic and radioactive waste, the construction of dedicated underground disposal mines is the best solution for protecting the biosphere. Underground disposal takes lessons from nature that has preserved high concentrations of hazardous solid and gaseous substances in the form of mineral deposits over many millions of years (e.g. sulphide metal ore, natural gas, uranium and even the remains of natural nuclear reactors).

The World Commission on Environment and Development ("*Brundtland-Report*", Brundtland 1987) extended the concept of sustainable development to non-renewable resources. Clearly, few mineral resources fit into the concept of sustainability, as it was formulated 300 years ago for the management of forests, "that the amount of wood cut should not exceed the growth rate" (Carlowitz 1713). Such exceptions may be salt, magnesium and potassium harvested from seawater. Most metals and minerals are non-renewable and their use should be managed according to the following rules: i) Consume as little as possible; ii) optimize the recycling rate; and iii) increase the efficiency of using natural resources, especially of energy. The original concept of sustainability considered mainly the interests of later generations. In the Rio Declaration (UN Conference on Environment and Development 1992) the concept of intrageneration fairness was added, to allow for the interests of the living generation of mankind.

In fact, the world population's rapid growth and demands for a better life enforce a continuing expansion of raw materials production. Yet, every individual extractive operation must have the acceptance of public opinion. To reach that aim, all stakeholders must profit and the mine's social as well as the natural environment need to be improved. The radical call that sustainability requires immediate termination of mineral exploitation is, of course, social and economic nonsense (Gilpin 2000). Let us use needed resources in the interest of living humans, and let us trust in technical and economic inventiveness to provide for later generations.

THE MINERAL RESOURCES CONUNDRUM

But is there a sufficient mass of minerals for an ever-increasing consumption? Because of the limited size of our planet it is true that geological resources are principally finite, although very large indeed. The search for most minerals has hardly gone deeper than a few hundred metres below the surface, and only land, shallow seas and the margins of the vast oceans are fully explored for petroleum and gas deposits. Yet, even in the well-known Gulf of Mexico, the new giant Tiber oilfield was recently (2009) discovered. Metal mining on the sea floor has a large future potential. Giant unconventional gas resources promise to fundamentally alter geopolitics of global energy supply. In contrast to resources, reserves that can be exploited at present economic and technological conditions are only a small part of the total geological endowment, because searching and defining reserves is a capital investment that must be paid back with interests. Due to the rules of depreciation of a future income, reserves are typically defined for the next 10 to 30 years. The result is that at any time a division of total reserves by the yearly consumption (the R/C ratio or "life-index") will predict that in 10 (or 20, or 30) year's time, "the world will run out of" the respective minerals. This fundamental error was famously made by the Club of Rome when it predicted this dire fate for the years 1990–2000 (Meadows *et al.* 1974). However, predictions of impending catastrophes are always popular and this gave the Club of Rome's hypothesis a sweeping impact. Actually, the imminent scarcity of important minerals was announced many times in the past but never arrived. The term "life-index" is misleading, and the figure is rather an indication of specific conditions that dictate financing, production and marketing of individual metals and minerals. With few exceptions, individual R/C ratios change little over time-scales of several decades. In the future, just as in the past, science and technology will continue to provide the mineral raw materials needed by society, both by finding new deposits and by providing natural or synthetic replacement (Wellmer 2008). Temporary scarceness of certain critical raw materials is only possible if political constraints distort markets (European Commission 2010). Furthermore, exploiting lower-grade ores, producing functional replacements for certain minerals and metals, and recycling of materials, all need energy. Accordingly, energy is the most important natural resource of all.

It is undeniable that there are physical limits to the availability of certain quality classes of raw materials. Severe problems arising from this fact are not expected as long as the unlimited resource of human creativity is given the freedom to search for solutions. The continuously expanding reserve base for practically all minerals, roughly in parallel to increasing consumption, is the best proof of this principle in the mining industry.

PART I

Metalliferous Ore Deposits

Economic geology defines ore as a natural material (ore rock) from which metals or minerals can be profitably extracted. Mining professionals use the word in an identical connotation. Note that metals and minerals can also be recovered from quite exotic materials that are not ore *sensu stricto*, for example saline brines (lithium, magnesium), geothermal waters (zinc), metal-accumulating plants (nickel; "phytomining"), acid mine water (copper) and of course, recycled scrap (iron). The term ore is also applied to metalliferous minerals in a rock, for example chromite in dunite, or magnetite in gabbro ("ore minerals"). Ore rock, commonly just called ore, is typically an intergrowth of useless minerals ("gangue") with ore minerals. Massive ore consists of ore minerals only, with little gangue, for example high-grade haematite iron ore.

Ore deposits form by geological process systems that can be viewed as a large cycle of constructive (e.g. magmatism) and destructive sectors (e.g. weathering; Figure 1.3). Within this cycling of earth materials, individual metals have specific enrichment sites that depend on chemical and physical properties of the metal or its compounds. It is very important to remember that biogeochemical fluxes mediated by life (Falkowski *et al.* 2008) control many ore forming processes.

Part I of this book is divided into two chapters. In Chapter 1, general observations, characteristics and interpretations of ore deposit formation processes, process systems and associated outstanding deposit types are presented. In Chapter 2, the economic geology of metals is systematically presented and illustrated by reference to specific mining districts and deposits.

Economic Geology Principles and Practice
Metals, Minerals, Coal and Hydrocarbons – Introduction to Formation and Sustainable Exploitation of Mineral Deposits, Walter L. Pohl
© 2011 Walter L. Pohl. Published 2011 by Blackwell Publishing Ltd.

CHAPTER 1

Geological ore formation process systems (metallogenesis)

Synopsis

Energy flow from the Earth's interior and from the sun drives geological process systems. The concentration of ore and minerals is part of these systems, which comprise intrusive and extrusive magmatism, weathering, erosion, transport and sedimentation, followed by diagenesis and metamorphism. In this chapter, we aim to acquire an overview of these systems in respect of the principles which govern the generation of ore deposits. Finally, the inspection of the different major systems is brought together in a synthetic view of global dynamics and metallogeny (i.e. the science of ore deposit formation). This chapter lays the ground for the rest of the book.

For a long time in the past, processes associated with differentiation and cooling of magmatic bodies were thought to be the main agents of ore deposit formation. Starting with mafic melt, ore minerals can form upon cooling or metal-rich melts can segregate from the silicate liquid. Because mafic silicate minerals crystallize at higher temperature, intermediate and felsic residual melts are formed with their own suite of ore deposits. Late-stage magmatic fluids collect metals and produce hydrothermal mineralization. Lindgren (1933), Niggli (1948), Schneiderhöhn 1932, 1962), Stanton (1972), Guilbert & Park (1986) and many others developed this concept of igneous ore formation. In addition, the role of weathering, erosion and sedimentation in concentrating metals was recognized. Metamorphic processes were seen to transform previously existing ore but without appreciable mass transfer.

More recently, these earlier views (here very simplified) on ore deposit formation were fundamentally expanded (Robb 2005, Evans 1998). First, the discovery of plate tectonics caused a revolution in understanding the dynamic interaction of the Earth's crust and mantle. Plate tectonics determine the origin and distribution of many ore deposits. Present ore-forming processes were investigated. Outstanding impulses brought the exploration of ocean floor hydrothermal venting that produces metal concentrations, which closely resemble long-known ore deposits (e.g. copper on Cyprus Island).

The application of new technologies of the geosciences (e.g. trace element analysis, microprobe, isotope geochemistry, fluid inclusions investigations, mathematical modelling and simulation)

Economic Geology Principles and Practice
Metals, Minerals, Coal and Hydrocarbons – Introduction to Formation and Sustainable Exploitation of Mineral Deposits, Walter L. Pohl
© 2011 Walter L. Pohl. Published 2011 by Blackwell Publishing Ltd.

guided by old and new hypotheses, led to changes in metallogenetic thinking and to the recognition of additional ore formation systems. One example is the dehydration of sedimentary basins during diagenesis: Expelled fluids cause appreciable geochemical mass-transport and formation of numerous metallic and mineral concentrations, without involvement of igneous processes. Furthermore, the role of dissolved salt, hydrocarbons, reefs and karst cavities in diagenetic ore formation was illuminated. Long after the first hypothetical considerations, metamorphism was finally proved to cause migration of aqueous fluids that transport and precipitate metals.

The classification of ore deposits by major earth process systems is in principle quite simple. Complications arise mainly because of the extreme variability of individual deposits due to manifold combinations of different processes and factors. Therefore, some authors prefer to arrange deposits into associations and types, which are related by geological setting, paragenesis and form, but not necessarily by the same genetic process (Routhier 1963, Laznicka 1985, 1993). Other authors dispense with geological environs and concentrate mainly on processes (Robb 2005). In this book, fundamental geological cycles (Figure 1.3) and ore-forming systems are to guide the reader through metallogeny.

The genetic terms of Table 1.1 provide the basic vocabulary of metallogeny. The non-genetic descriptors stratiform (layer-shaped) and stratabound (restricted to certain strata) only denote shape and position of an orebody in relation to sedimentary features, not its origin. Comprehensive explanations of geological and mining terms can be found in the *Dictionary of Mining* (AGI 1999) and the *Glossary of Geology* by Neuendorf *et al.* (2005). Geological time nomenclature in this book follows Walker & Geissmann (2009).

1.1 MAGMATIC ORE FORMATION SYSTEMS

A very large and diverse group of ore deposits originates by various processes during formation,

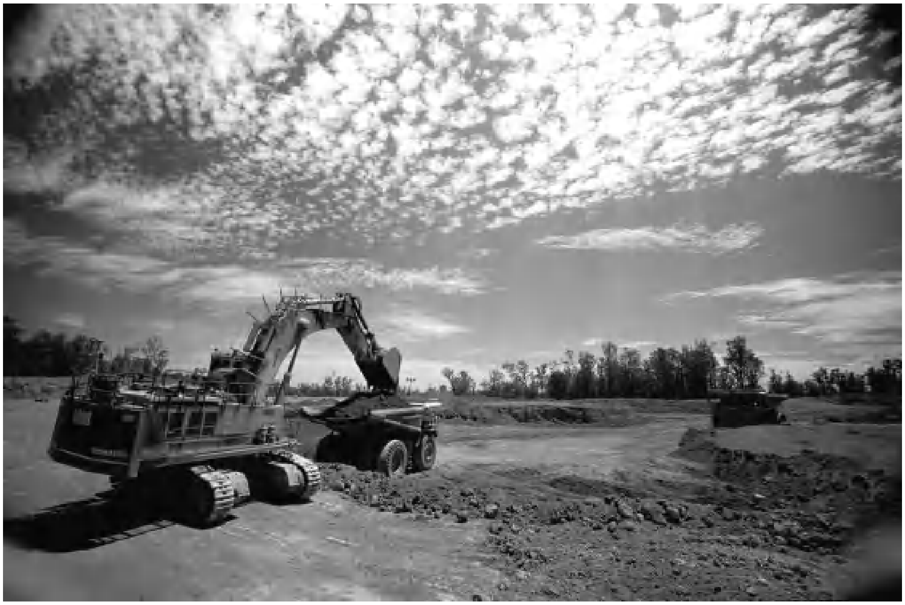

Figure 1.1 (Plate 1.1) Bauxite extraction at Huntley mine, southwestern Australia. On the Darling Plateau, bauxite is part of a mature soil profile developed over Archaean gneiss and granite. The area is covered by woodland (the jarrah, or *Eucalyptus marginata* forest). Mining depends on the availability of land and its social acceptance on rapid re-establishment of the native ecosystem. Reproduced by permission of Alcoa Inc.

Figure 1.2 (Plate 1.2) Rehabilitated jarrah forest covers former extraction panels of Huntley bauxite mine in front of the lake. Reproduced by permission of Alcoa Inc.

evolution, emplacement and crystallization of silicate melts (magmas) in the upper mantle and in the Earth's crust.

Most post-Archaean magmatic rocks can be classed according to their plate-tectonic environment. Rocks of the ophiolite association (basalt, gabbro, ultramafic rocks) are remnants of former mid-ocean ridges, back arc basins, and of early and primitive parts of immature oceanic island arcs. Mature island arcs and active continental margins are distinguished by profuse amounts of orogenic andesites and equivalent intrusive magmatic

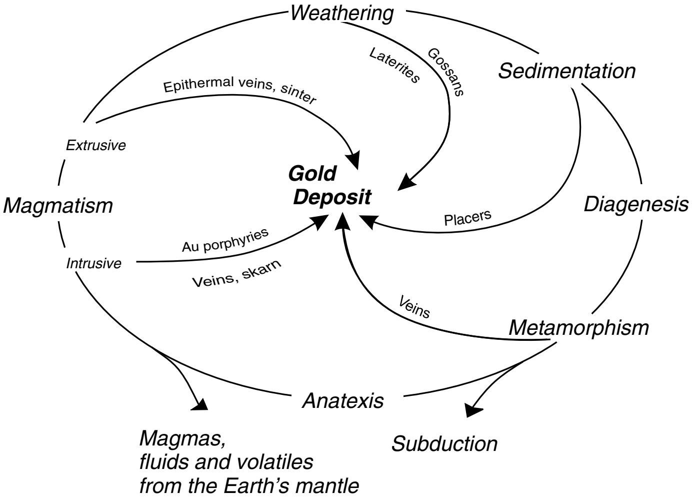
Weathering
Laterites
Gossans
Sedimentation
Epithermal veins, sinter
Extrusive
Gold Deposit
Magmatism
Placers
Diagenesis
Au porphyries
Intrusive
Veins, skarn
Veins
Metamorphism
Anatexis
Magmas, fluids and volatiles from the Earth's mantle
Subduction

Figure 1.3 The origin of gold deposits in relation to major geological process systems within the Earth's crust, demonstrating the variety of ore-forming systems.

Table 1.1 Common metallogenetic terms

- *Syngenetic* – denotes ores and minerals that formed at the same time as their host rocks (most often applied to sedimentary rocks and ore)
- *Epigenetic* – ores were emplaced into pre-existing rocks of any origin (e.g. veins, metasomatic ore)
- *Hypogene* – ores that were formed by ascending solutions (e.g. Mississippi Valley type lead-zinc)
- *Supergene* – ore formation by descending solutions (meteoric water interacting with rocks during surficial weathering processes)
- *Lateral secretion* – concentration of metals by abstraction from surrounding rock
- *Endogenetic* – concentration caused by processes in the Earth's interior (magmatism or metamorphism)
- *Exogenetic* – concentration caused by processes at the Earth's surface (sedimentation, weathering).

rocks. Continental collision causes melting of sialic crust and voluminous granitic magmatism. Continental rifts are associated with bimodal alkaline volcanism (basalt and rhyolite). Extensional deformation of continents and mantle melting result in emplacement of layered mafic intrusions, flood basalts and alkaline magmatic provinces. Most notable are subvolcanic ring complexes and kimberlite diatremes that transport diamond from 200 km depth to the surface.

The association of certain igneous rocks with specific metal ores was established long ago. Ultramafic rocks host ores of nickel, chromium and platinum, gabbro and norite copper, cobalt, nickel, iron, titanium and vanadium, andesite and intermediate intrusive rocks induce copper and gold ore, and granites are related to beryllium, lithium, tin and tungsten concentrations. Essentially, this distribution was understood as a result of the geochemical fate of different metals during fractional crystallization (solid-liquid fractionation) of silicate melt bodies (Goldschmidt 1958). Meanwhile, magmatic rocks can be further differentiated according to plate-tectonic setting, source rocks, degree of partial melting, role of volatiles and many other genetic variables. Examples are the various basalt types (N- and E-MORB, intraplate, island arc: Pearce *et al.* 1984; Pearce 1982; Winchester & Floyd 1977), or the S-, I- and A-granitoids. We shall see later in this chapter that some of these rock classes are related to specific ore deposits.

Impact magmas result from heat and high pressure caused by collision of extraterrestrial bodies with the Earth. Melting affects part of the crust and in rare cases even the upper mantle. Impact magmas differ chemically from other melts because whole volumes of crust are liquefied, whereas normally partial melting is the rule. In addition, the impacting body may induce geochemical anomalies, especially regarding siderophile elements (e.g. platinum, iridium, cobalt and nickel). Post-impact cooling can induce hydrothermal systems that are able to redistribute matter and provoke ore deposit formation.

In conclusion, the geodynamic environment controls the formation of ores from silicate melts in several ways. At the scale of ore-forming processes caused by single magmatic bodies, the following major genetic stages are differentiated:

- Orthomagmatic ore deposits are formed before the melt cools to complete solidification, or in other terms, in the liquid stage before solidus.
- Pegmatitic ore deposits are the result of segregation of small residual melt batches from a large crystallizing magma body approaching the solid state; fertile pegmatite melt is characterized by high amounts of volatiles and of incompatible and rare elements.
- Magmatic-hydrothermal ore deposits are produced by super- or sub-critical fluids, solutions and gases that are segregated by all magmas, which had more dissolved volatiles (H_2O, CO_2, S, B, F, Cl, etc.) than the amount that could be accommodated in silicates during crystallization; because of this connection, the time of fluid phase expulsion is commonly coeval with the formation of solid phases (minerals) from the melt; a significant part of the geochemical signature of magmatic-hydrothermal ore deposits is determined by processes at the magmatic stage (Audétat *et al.* 2008).

1.1.1 Orthomagmatic ore formation

Oxide (magnetite, ilmenite, chromite), base metal sulphide (Ni, Cu), and ore of precious metals (Pt, Pd, Au) is often found in ultramafic and mafic igneous rocks. More rarely, magnetite occurs in intermediate and felsic silicate melts. Textural (and many other) observations show that these ores were formed at magmatic temperatures, while the melt was essentially liquid and before total solidification (Naldrett 2004). Therefore, this class of ore deposits is called "orthomagmatic".

Numerous observations suggest that enrichment processes concentrate ("segregate") low metal traces from a large mass of silicate melt into small volumes. A common evolution is that the parent melt evolves towards saturation so that either a solid (e.g. chromite) or a liquid (e.g. sulphide melt) accumulates the metal in question. At some stage, residual fluids may intervene. Many parameters influence these processes, including the depth of intrusion, tectonic activities, the temperature gradient in space and time, fractional crystallization, dynamics of the melt body (e.g. convective flow), repeated injection of fresh melt, assimilation of country rocks, sulphur or external fluids, liquid immiscibility of ore and silicate melts and mixing or redissolution (Kerr & Leitch 2005). Because of their higher density compared to silicate liquids, ore melt droplets or solid ore phases typically accumulate above or within floor rocks, which may be cumulates below still liquid magma (gravitational accumulation; Sparks *et al.* 1993). Consolidation of cumulate minerals can lead to expulsion of intercumulus liquid ("filter pressing"). As the system cools, ore melts themselves may then separate into cumulates (e.g. Fe-sulphides) and residual liquids (Cu-rich sulphide melt).

Various mathematical models have been proposed that describe the orthomagmatic enrichment process. Concentration of metals such as PGM (platinum group metals), Au, Ni and Cu in sulphide melt is controlled by the Nernst partition coefficient (D) between sulphide and silicate liquids, and by kinetic factors. Disequilibrium is exposed by calculating the silicate/sulphide liquid mass ratio ("R-factor"; Robb 2005, Campbell & Naldrett 1979). A zone refining model is appropriate when, for example, sulphide droplets sink through a magma chamber and collect chalcophile metals. Limited base metal content but very high PGM enrichment can be explained by resorption of iron sulphide liquid in undersaturated magma (Kerr & Leitch 2005). In this process, the residual sulphide retains the precious metals, which it may bequeath to a later batch of undersaturated mafic melt.

Most orthomagmatic ore deposits are found in intrusive rocks. Eruptive equivalents are also notable, such as the Ni-Cu-Fe sulphides in komatiitic lava flows of Archaean greenstone belts, or the magnetite and haematite lavas and tuffs in andesitic-rhyolitic volcanoes in Chile, Mexico and Pakistan.

Basic shapes of orthomagmatic orebodies are layers in stratified magmatic rocks (often formed as cumulates), lenses or cross-cutting dykes and veins. This depends on the morphology of the segregation (sedimentation) surface and on dynamic factors. Massive ore is the product of highly efficient unmixing of ore particles or melt droplets and silicates, whereas disseminated mineralization reflects lower efficiency. Highly complex orebody shapes can be found in flow channels and pipes of mafic lavas and intrusions, for example when widening or curvature of flow tubes induce lower flow velocity of silicate melt that carries chromite crystals or sulphide melt droplets (Naldrett 1200, 1199; e.g. Voisey's Bay, Canada).

Textbook examples of orthomagmatic deposits are sulphide Fe-Ni-(Cu-PGE) ores hosted by Archaean komatiitic lavas of the Yilgarn Craton in Western Australia (Box 1.1; Barnes *et al.* 2007, Barnes 2004, Hoatson *et al.* 2006).

Gravitational settling can also explain many features of ore formation in layered mafic intrusions (Naldrett 2004, Cawthorn 1996, Irvine 1982). Other contributing processes include flowage differentiation and convective scavenging (Rice & Von Gruenewaldt 1994), *in-situ* crystallization on the floor of the melt body, mixing of two different melts, and uptake of material from outside (e.g. by melting siliceous or sulphur-rich host rocks). Often, the formation and segregation of a sulphide melt is the key to enrichment of exploitable metals (Barnes *et al.* 2009). Layered melt bodies (in respect of composition, temperature and density)

BOX 1.1 Orthomagmatic nickel sulphide ore in komatiites

Komatiites are ultramafic volcanic rocks with melting temperatures of ~1700°C containing >18 wt.% MgO (Arndt *et al.* 2008). Their formation is the consequence of mantle temperatures ~100°C higher than today (Naldrett 2010). Komatiitic melts originated by 30–50% partial melting of mantle. Normally, these melts remained sulphide-undersaturated from extraction through ascent and eruption to emplacement. Liquid komatiite lavas had a very high temperature and very low viscosity (similar to water), resulting in high flow velocities. Komatiite lavas are capable of eroding and melting most volcanic and sedimentary footwall rocks ("ground melting" or "thermochemical erosion"). The flows followed troughs on the seafloor and formed flow tubes similar to submarine basalts. Komatiites were typically charged with suspended olivine crystals. During cooling, cumulates and vesicular textures formed. Because of the extreme temperature difference between ocean water and Mg-rich melts, flow tops are characterized by skeletal growth of olivine and pyroxene ("spinifex textures"; Shore & Fowler 1999).

Elongate massive sulphide bodies, which were clearly formed from liquid sulphide melt, occur at the floor of flow tubes and grade upwards into disseminated (matrix or net-textured) ore (Figure 1.4). Ore textures reflect gravitational settling in the liquid phase. Sulphide melts can only form upon sulphur saturation, implying high sulphur content. The common association of sulphide mineralization with the presence of sulphur-rich interflow sediments and isotopic compositions of sulphur (Bekker *et al.* 2009) are strong arguments that admixture of crustal sulphur is the main difference between fertile and barren komatiites. The availability of nickel (and elements such as platinum) for partitioning into iron sulphide melt is favoured by low redox conditions. In that case, nickel is dissolved in the silicate liquid as uncharged Ni^0 and is not available for incorporation into olivine. Apart from the redox constraints, nickel content of magmatic sulphide liquids is largely controlled by partitioning equilibria and the mass balance between silicate and sulphide melt (the "R-factor"; Campbell & Naldrett 1979), including dynamic factors such as mixing and redissolution. The ore minerals of komatiite nickel deposits comprise pyrrhotite, pentlandite, chalcopyrite and pyrite, with nickel concentrations in ore reaching 20%. Prendergast (2003) describes the nickel-bearing komatiites of Zimbabwe as proximal and basal parts of submarine volcanoes that were quite flat and extended over hundreds of kilometres. The Neoarchaean komatiites of Western Australia (2.7–2.9 Ga) host the majority of the world's komatiite-associated Ni-Cu-PGE deposits. Palaeoarchaean komatiites are depleted in platinum group elements (PGE) because the metal source of the younger, metalliferous komatiites, i.e. cosmic matter bombarding the Earth during the period from 4.5 to 3.8 Ga, was only gradually mixed into the mantle (Maier *et al.* 2009). In contrast to Western Australia, the closely comparable Abitibi Greenstone Belt in Canada is richly endowed with volcanogenic massive sulphide deposits (e.g. Kidd Creek, Noranda). Both regions display abundant orogenic gold deposits. It is assumed that the disparity is due to a different lithospheric structure (Barnes *et al.* 2007).

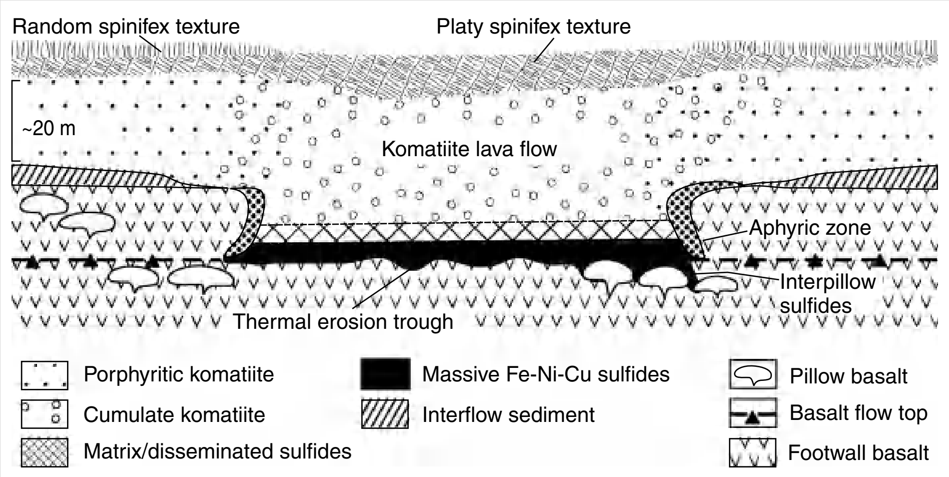

Figure 1.4 Massive and disseminated nickeliferous pyrrhotite orebodies (Lunnon shoot, Kambalda, Western Australia) at the base of an Archaean komatiite lava flow (adapted after Groves *et al.* 1986). By permission from Macmillan Publishers Ltd. *Nature* © 1986.

BOX 1.2 Orthomagmatic ore formation in the Bushveld Complex

The Bushveld Intrusive Complex comprises the Rustenburg Layered Suite and the Lebowa Granites. The first term designates the layered mafic-ultramafic intrusion, which was formed in the Palaeoproterozoic at ~2054 Ma, and which contains enormous metal resources. The granites have nearly the same age and host less important fluorite and tin deposits. The roof of the Bushveld Complex and the overlying granites consists of thick precursor basaltic andesites to rhyolites (the "Rooiberg Group" volcanics). Rooiberg volcanics and the intruding granites are the products of crustal melting caused by the giant mass of hot mafic melt. Country rocks of the Bushveld intrusion are Palaeoproterozoic sediments and volcanics of the Transvaal Supergroup and Archaean basement. The Rustenburg Layered Suite reaches a thickness of 9000 m. It is strongly layered at all scales. The major units from bottom to top comprise (Figure 1.5 and Figure 1.6):

- the Lower Zone with dunite, bronzitite, and harzburgite;
- the conspicuously banded Critical Zone with a lower part of orthopyroxenite, chromitite bands and some harzburgite, and a higher part marked by the first cumulus plagioclase and by cyclic layering of economically significant platiniferous chromitite, harzburgite, bronzitite, norite and anorthosite in this order (cyclic units); its upper boundary is marked by the Merensky Reef (Pt, Ni, Cu);
- the Main Zone with gabbronorite and minor layering;
- the Upper Zone with magnetite (ferro) gabbro and ferrodiorite, which contains numerous magnetite (V-Ti) layers.

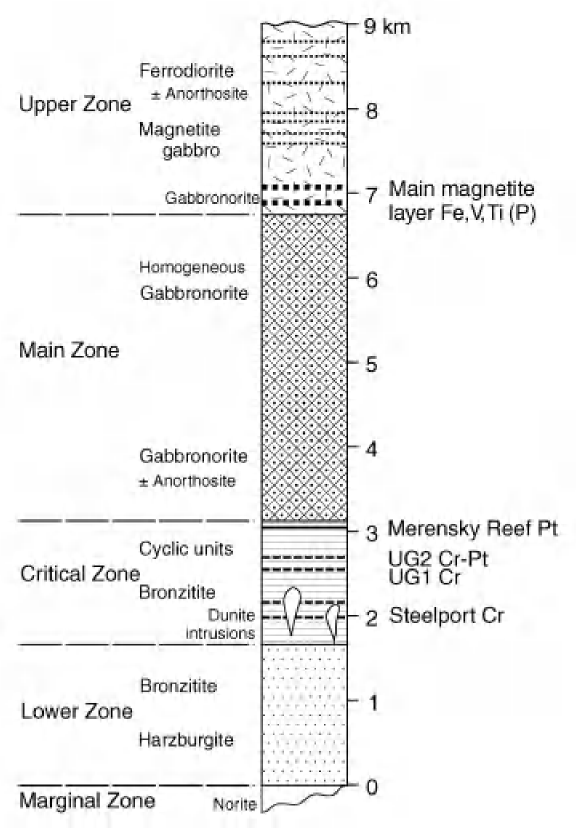
9 km
Upper Zone
Ferrodiorite
± Anorthosite
Magnetite gabbro
8
Gabbronorite
7
Main magnetite layer Fe,V,Ti (P)
Homogeneous Gabbronorite
6
Main Zone
5
Gabbronorite
± Anorthosite
4
3
Merensky Reef Pt
Cyclic units
UG2 Cr-Pt
UG1 Cr
Critical Zone
Bronzitite
Dunite intrusions
2
Steelport Cr
Bronzitite
1
Lower Zone
Harzburgite
0
Marginal Zone
Norite

Figure 1.5 Simplified lithostratigraphic column of the mafic Rustenburg Layered Suite in the Eastern Bushveld, South Africa, with major ore horizons.

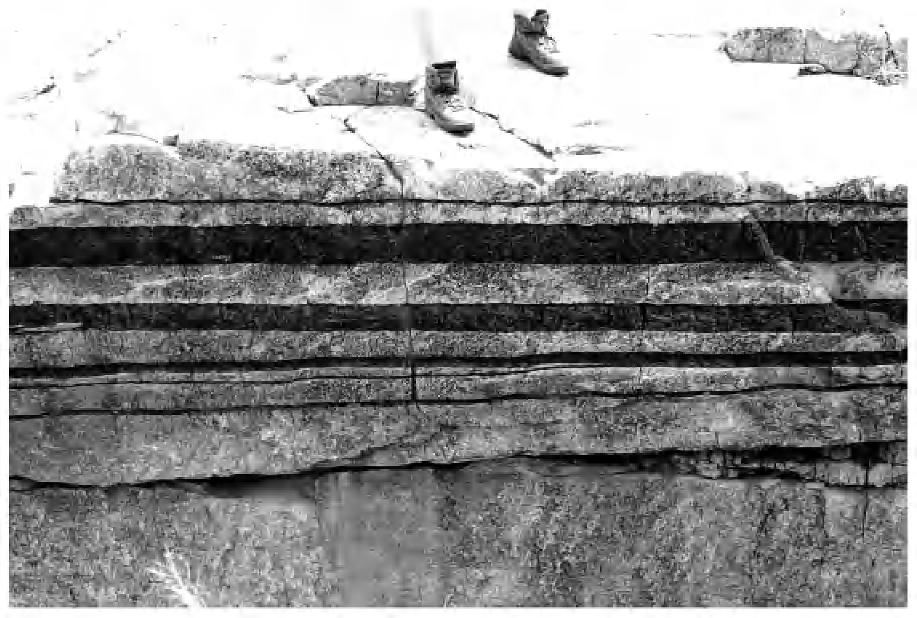

Figure 1.6 Bushveld Upper Group (UG1) chromite seam in anorthosite at Dwars River, S.A. Thin bands at the bottom display bifurcation, illustrating the complexity of cumulate ore formation in layered mafic intrusions. Courtesy Bernd Lehmann, Clausthal.

An extremely detailed lithostratigraphic scheme has been established for most parts ("lobes") of the intrusion (Vermaak & Gruenewaldt 1986, Eales & Cawthorn 1996). Strontium isotope stratigraphy reveals that the intrusion formed by numerous influxes of magma of contrasting isotopic composition with concomitant mixing, crystallization and deposition of cumulates. Locally, in all five lobes of the Complex, remarkable differences in thickness and facies of layers have been noted that point to proximity of magma inflow (Maier & Eales 1994). The cyclic units of the Critical Zone were formed by mixing or mingling of two different magmas, a resident magma of Main Zone type (or T-type) precipitating plagioclase, and fresh inflows of Critical Zone type (U-type) contributing orthopyroxene (Naldrett *et al.* 2009). Apart from chemical processes, pressure fluctuations are thought to have controlled rhythmic layering and ore deposition in the Bushveld melt chamber (Cawthorn 2005b). The Bushveld contains the world's largest exploitable resources of chromium, platinum metals and vanadium. For the future, large amounts of titaniferous magnetite and apatite are available that have at present no economic value.

undergo thermal and chemical diffusion that can concentrate ore metals. Although much less obvious than in many felsic intrusions, mafic melt bodies may also experience unmixing and expulsion of magmatic fluids that can form ore. The largest preserved layered intrusion in the world is the Bushveld Complex of South Africa, hosting an exceptional variety and mass of high-grade metal ores (Box 1.2; Vermaak & Von Gruenewaldt 1986, Eales & Cawthorn 1996).

Layered mafic intrusions occur in several geodynamic settings:

- Archaean greenstone belts;
- intracratonic regions (the Bushveld);
- at passive margins of continents; and
- in active orogenic belts.

Intracratonic regions that experienced tensional tectonics can also exhibit unstratified, very complex mafic-ultramafic intrusions with Cu-Ni-PGM ores. The most important district of this kind is Noril'sk-Talnakh in Siberia, which originated at the Permo-Triassic boundary as a feeder to the giant Siberian trap basalt province (Yakubchuk & Nikishin 2004, Li *et al.* 2009).

Impact magma bodies with orthomagmatic ore deposits

Mineralized impact structures are very rare. A giant example is the Sudbury Igneous Complex (SIC) of Ontario, Canada, the second-largest source of nickel (plus much copper and platinum metals) in the world, after Noril'sk in Russia. The SIC is the remnant of a voluminous melt body that has been produced by the impact of a meteorite into continental crust 1.85 Ga ago (Dietz 1964). The surrounding rocks comprise Archaean granites and gneisses, and metamorphic Palaeoproterozoic volcano-sedimentary suites. The elliptic outline of the intrusion is thought to be due to later orogenic deformation. Hydrothermally altered (Ames *et al.* 1998) suevitic breccias, shales and turbidites (Whitewater Group) cover part of the intrusive complex, forming a central basin. Ore deposits occur mainly in embayments of the footwall contact of the intrusion, in radiating dykes ("offsets", Figure 1.7) and within intensely brecciated footwall rocks up to 2 km from the contact. There is a lithologic zonation from the footwall upwards and towards the centre of the intrusion: Marginal norite, gabbro and quartz-diorite with dunite inclusions and the Ni-Cu-sulphides form the "Sublayer Norite" and the offsets, followed by norite of the "Lower Zone", quartz-gabbro of the transitional "Middle Zone" and granophyre of the "Upper Zone". The rocks are clearly the product of crustal melting (Therriault *et al.* 2002), but are very different from typical layered intrusions (e.g. there is no rhythmic banding). At Sudbury, lithologic zonation is interpreted to be due to gravity separation of mafic and felsic liquids that formed an emulsion immediately after the impact, and subsequent vigorous thermal convection within the norite and granophyre layers (Zieg & Marsh 2005). The ore-bearing sublayer displays typical features of mafic cumulates and gravity segregation of sulphide liquids. Offset dykes and footwall deposits host an important part

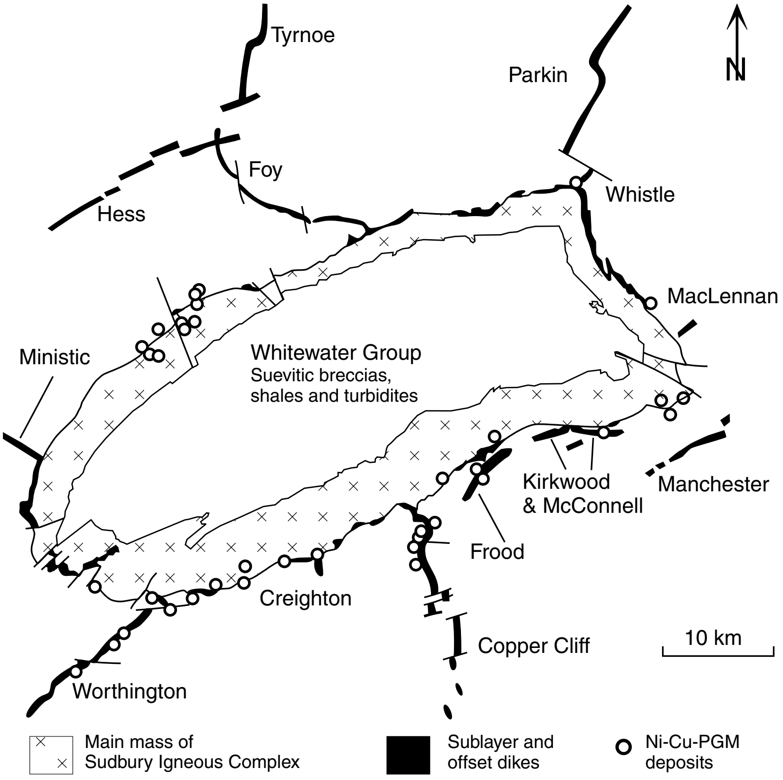
Tyrnoe
Parkin
N
Foy
Hess
Whistle
MacLennan
Ministic
Whitewater Group
Suevitic breccias, shales and turbidites
Kirkwood & McConnell
Manchester
Frood
Creighton
Copper Cliff
10 km
Worthington
Main mass of Sudbury Igneous Complex
Sublayer and offset dikes
Ni-Cu-PGM deposits

Figure 1.7 Overview map of the Sudbury impact structure, Canada, one of the giant nickel-copper mining districts of the world. Of close to 90 single deposits known (Ames *et al.* 2008), a selection is shown here.

of metal resources. Total past production and current reserves of the Sudbury District are estimated at >1700 Mt of Ni, Cu, Co, Pt, Pd, Au and Ag ore (Ames *et al.* 2008). Among approximately 90 known Ni-Cu-PGE deposits, 14 are currently worked.

Anorthosite-ferrodiorite complexes

Anorthosite-ferrodiorite complexes of Mesoproterozoic age have an outstanding role as sources of titanium (Ashwal 1993). Orebodies consist of ilmenite and/or rutile, magnetite or haematite, and a gangue of apatite and some graphite. Similar rocks of lesser economic importance occur as strata in the upper parts of layered mafic intrusions. The anorthosites are commonly coarsely crystalline, rather massive than layered and consist of >90% andesine to labradorite. Anorthosite plutons may be associated with coeval intrusions of troctolite, charnockite, rapakivi granite, ferrogabbro and ferrodiorite. The latter are often remnant melts after plagioclase crystallized to form anorthosite and are parental to the immiscible Ti-Fe-P melts. Because of their high density, the ore melts accumulate near the base of the magma chamber. Resulting orebodies are stratiform and either massive or disseminated (as at Lac Tio in Quebec, Canada). Some occur as thick dyke-like bodies in deeper parts of the intrusive suite or in country rocks. The origin of anorthosite-ferrodiorite complexes is not fully understood; one hypothesis presumes late to post-orogenic partial melting of tongues of lower crust in the mantle (Duchèsne *et al.* 1999). From these rocks, ~50% of the world's titanium supply is derived; they also contain about half of the total titanium resources. Since the high-grade Ni-Cu sulphides at Voisey's Bay in Canada were found in troctolites belonging to this family, these rare rocks have acquired a new prospective role.

Fe-rich melts segregated from intermediate to felsic magmas

The metallogenetic role of these melts is a more contentious case of orthomagmatic ore formation. While there is no doubt that under conditions of high fO_2 an immiscible FeO_x liquid is in equilibrium with melt of felsic composition (Naslund 1983), there is no general consensus that this is a path to the formation of large ore deposits. One objection is that the high viscosity of SiO_2-rich liquids should physically inhibit segregation by gravity. Arguments brought forward to support the concept include: i) shearing by slow convection of the melt so that low-viscosity FeO_x liquid may be concentrated; and ii) high content of sodium and phosphorous that act as fluxing agents for iron melt. The process should produce ore of magnetite and apatite in the proportion of about 2 : 1, as exploited in the Kiruna-Malmberget District (Sweden). High fluorine and chlorine content of the apatites, and the presence of minerals such as amphibole and scapolite, imply an eminent role of magmatic volatiles (H_2O, Cl, F, CO_2, etc.). Volatiles promote segregation and mobility of ore melt. High fluid and salt content of melt batches segregating from felsic magmas evoke a likeness to pegmatites and, similar to pegmatite systems, the transition to hydrothermal ore formation may be gradual and indistinctive (Borrok *et al.* 1998). The unusual chemical composition of parental magmas and fluids may be due to assimilation of evaporitic country rocks or of migrating saline brines (Barton & Johnson 1996). After the discovery and investigation, at the giant Olympic Dam in southern Australia, numerous iron oxide-rich deposits were subsumed in a new class, the **iron oxide-copper-gold (U-REE) deposits (IOCG)** (Groves *et al.* 2010, Cox & Singer 2007, Pollard 2006, Hitzman *et al.* 1992). Although a hydrothermal origin of IOCG mineralization is generally accepted, the broader group displays a considerable variety of geological setting, the ratio of orthomagmatic and magmatic-hydrothermal mineralization, the nature of hydrothermal alteration systems and mineralizing fluid compositions. In some cases, metamorphic fluids may have formed Cu-Au deposits resembling IOCG (Baker *et al.* 2008):

> Kiruna in northern Sweden (Figure 1.8), the largest iron ore district in Europe, is traditionally considered as the type-deposit of orthomagmatic iron ore formation in felsic intrusions (Harlov *et al.* 2002), because

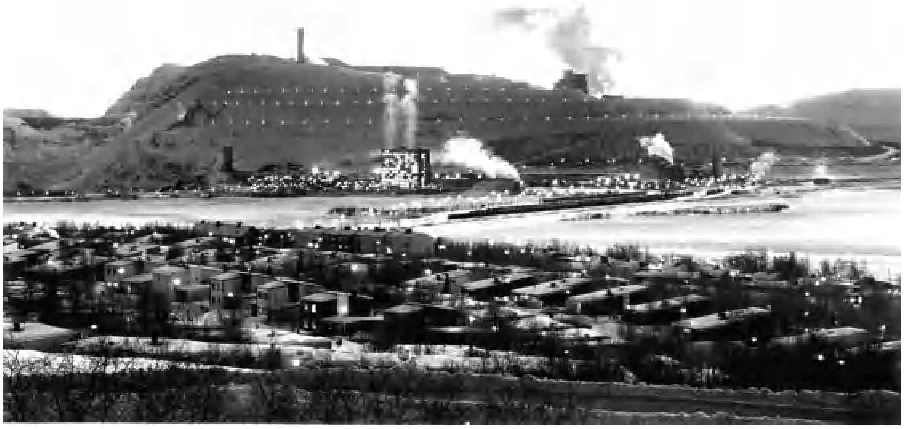

Figure 1.8 Kirunavaara iron ore mountain, northern Sweden. The steeply dipping magnetite orebody was originally mined in an open pit on the left side of the hill. Today, extraction is underground. Courtesy LKAB 2010.

the ore is cogenetic with Palaeoproterozoic magmatic host rocks (trachyandesite, rhyodacite). Lower Ti and V concentrations distinguish this type from massive iron oxides (e.g. nelsonite) segregated from mafic magmatic melts. Repeatedly, arguments have been put forward for a magmatic-extrusive ore formation (Nyström & Henriquez 1994). Still other authors invoke a magmatic-hydrothermal metasomatic origin related to IOCG deposits (Hitzman *et al.* 1992), but Kiruna is not part of this class because it lacks Cu and Au (Groves *et al.* 2010). An extrusive origin is also considered for Pliocene magnetite orebodies at El Laco, Chile (Nyström & Henriquez 1994; but note the contradiction by Sillitoe & Burrows 2003) and for 30 Ma old Cerro de Mercado (Durango, Mexico). Magnetite or haematite-apatite ores at both sites have been described as massive and vesicular lavas, veins, crystal tuffs and pyroclastic agglomerates deposited by volcanoes built of rhyolite and latite (Lyons 1988, Figure 1.9).

In conclusion, orthomagmatic deposits of iron oxides and apatite in intermediate to felsic igneous rocks (intrusive and extrusive types) share a number of features with IOCG deposits, but are different (Groves *et al.* 2010). However, both may

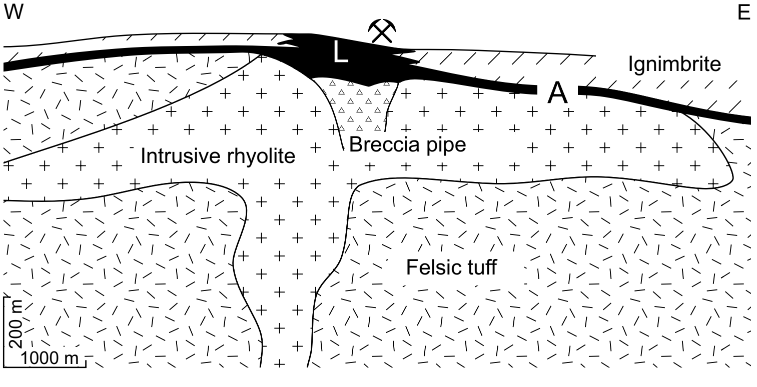

Figure 1.9 Schematic profile of the volcanogenic iron ore deposit at Cerro de Mercado, Mexico (modified from Swanson *et al.* 1978). Magnetite lavas (L) above an eruptive centre pass laterally into haematite tuff (A, both black).

originate by mixing and mingling of (ultra)mafic and silicic melt (Clark & Kontak 2004).

Lower sections of ophiolites also contain orthomagmatic ore deposits. This includes diapiric dunite bodies with streaky or lenticular disseminated and massive chromitite. The dunites occur mainly within deformed refractory harzburgite of tectonized mantle. Tabular chromitite seams may occur in the lowermost ultramafic cumulates of the mid-ocean gabbroic magma chamber. Both cases are considered to be a consequence of chromite segregation from the melts that rise from the mantle beneath mid-ocean spreading ridges. The metallogeny of ophiolites is considered in more detail below.

Ultramafic complexes of the Urals-Alaska type are concentrically zoned intrusions in orogenic and platform settings (Taylor 1967). In the central dunite of the ring complexes, important chromium and platinum ores can be concentrated (Urals: Garuti *et al.* 2003). Orthomagmatic concentrations of minerals and metals are also part of the economic significance of carbonatites.

1.1.2 Ore deposits at mid-ocean ridges and in ophiolites

Exploration of ocean floors resulted not only in the recognition of plate tectonics but also in the discovery of conspicuous signs of active ore forming systems – the "black smokers". Black smokers are points of discharge of hot metalliferous solutions from the ocean floor. Black smoker fields build accumulations of metal sulphides on the ocean floor, some of which may soon be economically exploitable. Comparative investigations revealed that ophiolites, an association of mafic and ultramafic rocks common in orogenic belts, are remnants of oceanic spreading processes that took place at mid-ocean ridges, in marginal basins in front of or behind island arcs (Dilek *et al.* 2001), or within intra-ocean primitive island arcs. Ophiolites host ore deposits that display features reminiscent of black smoker fields and sulphide mounds. However, fluid venting on the seafloor may also occur in other tectonic settings, including magmatic arcs above subduction zones (Stoffers *et al.* 2006), hotspot ocean island volcanoes and dewatering sediments of active and passive continental margins.

Ophiolites

Ophiolites are fragments of oceanic crust and mantle that have been transported (obducted) as thrust sheets (nappes) or schuppen towards continental masses. The tectonic emplacement was normally associated with dismemberment of the original succession. Yet there exist some exceptionally well preserved ophiolites (e.g. Cyprus, Oman, Dongwanzi, China). A complete ophiolite sequence comprises (Anon 1972):

- Extrusive basalts of typical chemical (MORB) characteristics at the top, often in the shape of pillow lavas; ocean floor metamorphism of basalt increases from the zeolite facies at the top to greenschist facies at the bottom; however, many ophiolites display volcanic rocks with supra-subduction zone signatures.
- The sheeted dyke complex, consisting of vertical basalt dykes that strike parallel to the former oceanic graben; greenschist facies metamorphism is dominant but may grade into amphibolite facies near the footwall; contact metamorphism resulting from underlying melt bodies may occur; many ophiolites, however, lack sheeted dykes.
- The plutonic complex, comprising higher intrusive homogeneous gabbro, diorite, tonalite and trondhjemite ("plagiogranite"), and deeper layered gabbro and peridotites, that display properties of cumulate rocks (the "cumulate sequence"); the magmatic rocks are normally not metamorphosed.
- The tectonized and depleted mantle, dominated by large masses of serpentinite (after harzburgite) and characteristic pods of dunite.

Various marine sediments may cover the igneous rocks, but most frequent are biogenic cherts and pelagic limestones. It is interesting to note that abiogenic exhalite cherts and jasper have only formed before the Middle Cretaceous; since that time, seawater is highly undersaturated with respect to silica because of the emergence of silica-consuming diatoms (Grenne & Slack 2005).

Formation of the ophiolite sequence can be modelled by partial melting of primitive mantle under mid-ocean ridges, due to mantle heat flow and the decompression caused by extension. The liquid rises in numerous melt batches and accumulates to fill large shallow magma chambers. These evolve by fractional crystallization and episodic volcanic processes. Mid-ocean ridges with low spreading rates are composed of sections with high magmatic activity that alternate with sections of tectonic rifting only. The first produces the typically layered ophiolite sequence ("Penrose Crust"); the second may lead to exposure of mantle rocks (serpentinites and peridotites: "Hess Crust"). The latter is quite inconspicuous because black smokers are very rare, and has received little attention. Superfast spreading rates produce thin crust and shallow melt bodies.

Economic interest focuses on deep ultramafic rock suites of the Penrose sequence (for chromite and platinum) and the near-surface volcanic hydrothermal system (for base metals). Tectonized (foliated) harzburgite and the lower cumulates host dunite bodies that may contain massive and disseminated chromite ore. Dunite in harzburgite can be understood as lag segregation from rising basaltic melt diapirs. Chromitites originate from dunite by liquid-liquid immiscibility. Because of ductile shearing in the oceanic mantle, both dunites and chromite orebodies are strongly deformed, resulting in lenticular pod-like shapes. Chromites in cumulates occur in seams that lack early deformation.

From the beginning of geological history, newly-formed ocean crust was cooled by convecting seawater. This is at the origin of ocean floor metamorphism and possibly, of earliest life on Earth (Russell *et al.* 2005). Processes taking place along the mid-ocean ridges are interconnected with the whole Earth System (Halbach *et al.* 2003). Rising branches of convection cells transport metals and reduced sulphur leached from mafic and ultramafic rocks towards the ocean floor (Figure 1.10). Some of the volatiles and metals may be derived from magmatic fluids. More than 100 active submarine venting sites have been discovered over the last 30 years along the 60,000 km-long worldwide network of mid-ocean ridges. Most vents are basalt-hosted and of the black smoker type (Herzig & Hannington 1995).

Black smokers

Submarine black smoker vents are hydrothermal cones or chimneys that may reach a height of about 20 m, built on outcrops of bare basalt (Figure 1.11). From an opening at the top, a high-speed jet of hot clear fluid is ejected. The vents are tubes with zoned walls, from pyrite and chalcopyrite inside through sphalerite, marcasite, barite, anhydrite and amorphous SiO_2 to the exterior (Figure 1.12 and Figure 1.13). Oxidation of

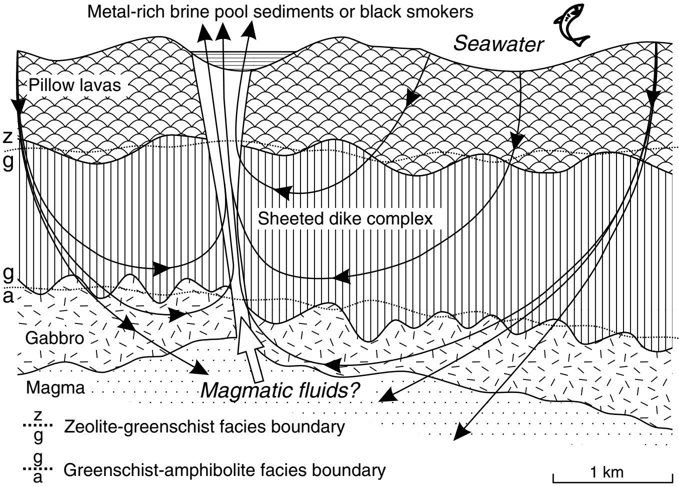
Metal-rich brine pool sediments or black smokers
Seawater
Pillow lavas
z
g
z
g
Sheeted dike complex
g
a
g
a
Gabbro
Magma
Magmatic fluids?
z g Zeolite-greenschist facies boundary
g a Greenschist-amphibolite facies boundary
1 km

Figure 1.10 Seawater convection, ocean floor metamorphism and focusing of rising hot fluids by apical parts of a mid-ocean magma chamber and by faulting (modified from Gass 1980). By kind permission of Geological Survey Department Cyprus.

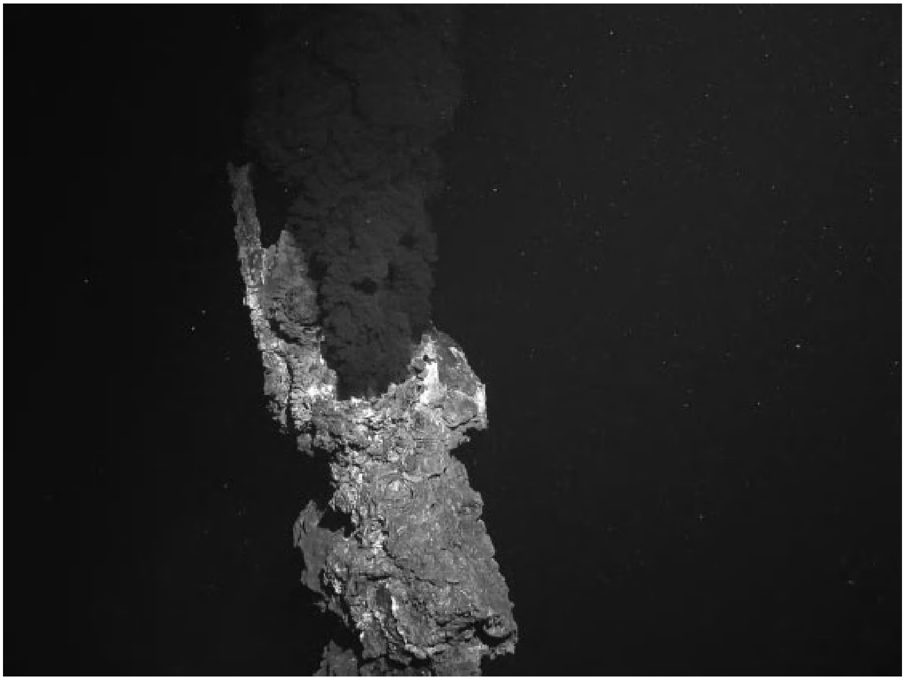

Figure 1.11 (Plate 1.11) Black smoker in the Mid-Atlantic Ridge graben, 4°48 S, 12°37 W, at a water depth of ca. 3000 m. Courtesy P.M. Herzig, IFM-GEOMAR (ROV Kiel 6000, 2009).

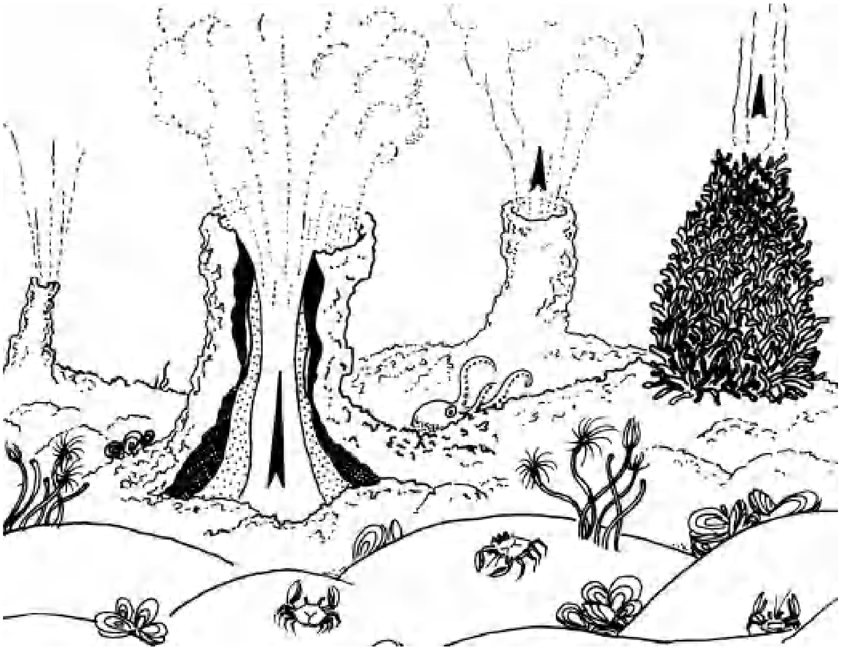

Figure 1.12 Hydrothermal vents on pillow basalt lava in a mid-ocean rift. Adapted from Haymon (1983). With permission from Macmillan Publishers Ltd. *Nature* © 1983. In the foreground "black smoker" vents, white smoker on the right. Section from interior to exterior: Dotted = Cu-Fe-sulphides; hatched = weathered sulphides; white = talc and sulphides; black = anhydrite and sulphides.

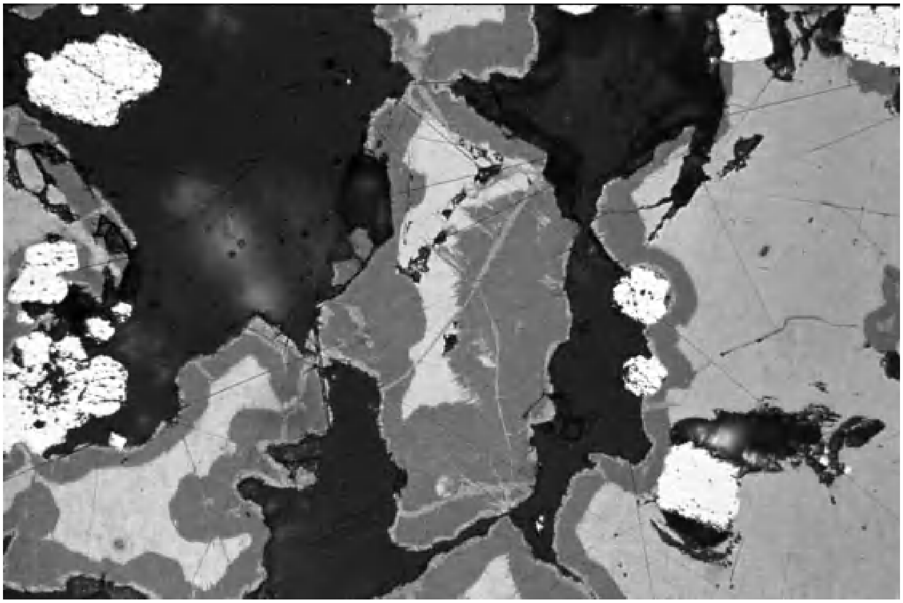

Figure 1.13 (Plate 1.13) Mid-oceanic copper mineralization in chimney fragments from inactive Sonne Field in the Central Indian Ocean. Courtesy P. Halbach (©FU Berlin). The polished section shows pyrite (white) as the earliest sulphide phase, followed by chalcopyrite (yellow), and increasing hydrothermal depletion of iron in bornite (Cu_5FeS_4, blue-brown) and a thin rim of digenite (Cu_9S_5, pale blue). The long side of the image corresponds to 0.6 mm. Pore space filled by casting resin is variably dark.

sulphides by seawater ("seafloor weathering") produces varicoloured ochreous alteration fragments, which mainly consist of iron oxy-hydroxides that assemble on the floor around the vents and build gossan-like mounds. Because the leaky vent tubes draw in cold seawater, an amazing macrofauna of large mussels, bright-red tube-worms, crabs and shrimp finds perfect ecological conditions (Van Dover 2000, Fisher & Girguis 2007). The base of the higher life forms are thermoacidophilic and hyperthermophilic chemotrophic microbes (bacteria and archaea, e.g. *Pyrolobus fumarii*) that inhabit the vent walls at temperatures up to 121°C (read more about archaea, the third domain of life, in Friend 2007). Macrofossils similar to some of the fauna living on active vents today were described from the Cretaceous sulphide ore deposits of the Troodos ophiolites on the Mediterranean island of Cyprus (Little *et al.* 1999). The expulsion temperature of the metalliferous solutions is most often at ~350°C. With 407°C (fluid) and 464°C (vapour), the highest temperatures were measured in the equatorial Atlantic (Koschinsky *et al.* 2008). Alkaline "white smokers" and diffuse discharges of warm water with little dissolved matter have lower temperatures.

The hot Na-Ca-Cl fluids of the black smokers are reducing and have pH from 2 to 5.5 (mostly 4–5), salinities from 0.1 to 3 times seawater, elevated iron, copper, zinc, barium and SiO_2, and traces of As, Cd, Li, Be, Cs, Mn, B, Cl, HCl, H_2S, and CH_4. Different solutes are derived from various protoliths, possibly from magma, and reflect also different conditions of water-rock reactions. For example, copper is enriched relative to iron under moderately oxidizing conditions, whereas a low fO_2 results in a high Fe/Cu ratio (Seyfried & Ding 1993). Deep unboiled fluids display higher metal concentrations than vent fluids (e.g. Cu 14–17 ppm, Zn 5–27 ppm: Hardardóttir *et al.* 2009). Fluid properties change by phase separation, boiling, alteration and mineral precipitation during rise to the seafloor. Manganese, iron and ^3He of the venting fluids disperse in ocean water and form a wide geochemical halo that is a guide to the search for submarine hydrothermal zones. Indications for supercritical unmixing of fluids before discharge into a depleted gas phase and a metal-rich brine were found at several spreading ridges. Supercritical unmixing and normal boiling followed by condensation of vapour and mixing of products are thought to explain the spread of salinities and unusual compositions of vent fluids (Cathles 1993). Only one site is known were fluids discharge at supercritical conditions (the critical point of seawater is at 298 bar and 407°C: Koschinsky *et al.* 2008).

Upon discharge at the ocean floor, hot acidic fluids mix with cold alkalic seawater, which results in immediate precipitation of solutes. If iron prevails, black or grey smoke-like plumes of amorphous iron sulphide and iron-manganese oxy-hydroxides rise several hundred metres upwards and disperse over a distance of many kilometres. Zinc forms bluish, SiO_2, barite and anhydrite white clouds (white smokers). So-called "snow-blower vents" emit dense clouds of white filaments of native sulphur that is produced from H_2S by sulphur-oxidizing bacteria (Taylor & Wirsen 1997). Particle chemistry and ^3He, CH_4 and H_2S content of seawater near vents allow predictions of temperature and composition of vent fluids (Feely *et al.* 1994).

White smokers

White smoker vents discharge fluids between ~100 and 300°C (Halbach *et al.* 2003). They form mainly: i) in the early stage of a newly established hydrothermal system; and ii) by subseafloor mixing of hot black smoker fluid with cooler waters. The second probably leads to precipitation of sulphides at depth. Therefore, white smokers may indicate the presence of hidden stockwork and vein deposits of copper and zinc. In Figure 1.12, the third vent from the left in the background is a "white smoker", consisting of barite, anhydrite and amorphous silica.

The activity of vents seems to be constant for a long time. Sudden large hydrothermal plumes are related to seismic seafloor spreading events, rapid injection of dykes and seafloor extrusion of basalt lavas (event plume, or megaplume; Palmer & Ernst 1998). In common vents, seismic strain causes changing temperature and discharge rate.

The origin of mid-ocean submarine hydrothermal systems is mainly seawater convection in hot young oceanic crust, on top or above the flanks (Cathles 1993) of shallow magma bodies 1 to 3 km below the seafloor (Figure 1.10). This setting explains the steep geothermal gradient (up to 500°C/km), that is deduced from several observations. The required high permeabilities are provided by intensive tensional fracturing in mid-ocean rifts and around calderas. In the periphery, seawater flows downwards to more than 3 km depth. Because of the retrograde solubility of calcium sulphate, anhydrite is precipitated at moderate temperature during down-flow. At higher temperature and deeper levels, seawater reacts with basalts causing ocean floor greenschist facies metamorphism. Oxygen is rapidly consumed by reaction with Fe(II). Newly formed hydrated minerals (e.g. chlorite, amphibole) incorporate OH^-, which increases H^+ concentration in the fluid. The reduced state and high acidity favour dissolution of metals and of sulphur.

Alteration of basalt at low water/rock mass ratios leads to a paragenesis of albite, epidote, chlorite and actinolite. The product is greenstone (note the absence of penetrative deformation such as schistosity). Extreme alteration produces epidosites (equigranular epidote-quartz-titanite rocks) and chlorite-quartz rocks (e.g. beneath the Bent Hill deposit: Teagle & Alt 2004). Similar alteration products are known from ophiolite-hosted sulphide deposits. Magmatic fluids may mix with altered seawater and do have a role in mineralization (Yang & Scott 1996, 2005), as indicated by high ^3He and CO_2 content, although stable isotopes imply mainly seawater. Part of the fluids could have a multi-stage history, for example dehydration of hydrated basalts by prograde thermal metamorphism induced by a new magma intrusion. Near transform faults, rocks of the deeper ophiolite sequence may be hydrothermally altered (e.g. formation of chlorine serpentinite from peridotite). Ultramafic-hosted hydrothermal systems produce highly reducing and high-pH vent fluids, such as the Lost City hydrothermal field at 30°N on the mid-Atlantic ridge (Seyfried *et al.* 2007). In these systems, the coexistence of dissolved CO_2 and H_2 favours the formation of methane (toukos & Seyfried 2004). High-energy, fast-spreading mid-ocean ridges are dotted by submarine volcanoes and intrusions extending to an off-axis distance of 25 km from the graben margin. Hydrothermal fields and large ocean floor orebodies display a similar range (Fouquet *et al.* 1996).

Although most of the emitted metals are diluted in ocean water and sediments, approximately 250 metalliferous bodies of economic mass and grade have meanwhile been discovered. One example is a low sulphide mound on the mid-Atlantic rise at 26°N with a diameter of 250 m and a height of 50 m, that contains about 10 Mt of metalliferous sediments, sulphide debris and anhydrite, covered by oxidized sulphides and active as well as inactive chimneys. It is underlain by a sub-seafloor stockwork (Petersen *et al.* 2000). This is comparable to ancient volcanic-hosted massive sulphide (VMS) deposits of obducted ophiolites (the Cyprus type). The Bent Hill deposit on the San Juan de Fuca ridge is remarkably copper-rich, very much like the ores on Cyprus (Ziehrenberg *et al.* 1998). In the shallow crust beneath vent fields, large Cu, Zn and Au accumulations are probably formed by precipitation because of boiling and vapour loss during depressurization (Hardardóttir *et al.* 2009). Metalliferous mud in several depressions of the Red Sea represents the largest known submarine base metal mineralization. Sulphides in the Atlantis II basin, for example, cover 60 km^2 and reach a thickness of 30 m. The deposit comprises nearly 100 Mt (dry) of sulphides (Halbach *et al.* 2003). In these locations, the causative hydrothermal activity is not spectacular because metal-bearing solutions do not vent but discharge into stratified brines (Blanc & Anschutz 1995).

Ore deposits in ophiolites include two major groups: i) Chromite of the "Alpine" type (so-called because of the numerous former mines in the Alpine chains of southeastern Europe), in rare cases with co-precipitated exploitable platinum (Lord & Prichard 1997); and ii) exhalative volcanic massive sulphide (VMS) deposits of iron, copper and zinc sulphides (± Ag and Au, but note the virtual absence of Pb), including possible underlying stockwork ore. Because the ophiolite-hosted VMS deposits have been historically of great significance on the Mediterranean island of Cyprus, they are also termed "Cyprus type sulphide deposits". However, most ophiolitic VMS sulphides are pyrite-rich and have low base metal grades. In the future, recently formed concentrations of this type that occur on the floors of the world's oceans may become viable sources of metals. Ophiolites host other important mineralizations that they have "acquired" during obduction, nappe transport, deformation, metamorphism and finally weathering. These include asbestos, magnesite, gold (in listvaenite), talc, and lateritic Ni-(Cr-Co-Fe) ore in deeply weathered soil profiles.

1.1.3 Ore formation related to alkaline magmatic rocks, carbonatites and kimberlites

Rocks of these families generally have low SiO_2 and high alkali element content, especially of sodium and potassium. They occur commonly in cratonic, consolidated portions of continents, rarely within oceanic plates. An anorogenic setting is affirmed by their clustering near continental rifts, in lithospheric distension zones and over heat anomalies of the mantle (hot spots, plumes, superplumes). Occurrences of the typically "continental" rocks, nephelinite and carbonatite in association with oceanic intraplate volcanism, are very rare. Most magmas of this group originate by a low degree of partial melting of enriched mantle material, but for some melts the reverse is true. The enrichment may stem from subducted oceanic crust, or more probably, from metasomatized lithospheric mantle (Pilet *et al.* 2008). Nephelinite magma is the most common mafic alkaline liquid that crystallizes to give a range of igneous rocks (termed the ijolite suite). They are typically associated with the much rarer carbonatites that have a more prominent metallogenetic role. However, complex intrusions displaying felsic rocks (e.g. A-type granite) in addition to the mafic ones are not rare. This is due to secondary melting and assimilation of deep continental crust.

Alkaline melts form in the subcontinental mantle lithosphere by rising temperature, falling pressure, or under the influence of volatile and incompatible substances (mantle metasomatism), the ultimate origin of which may be mantle plumes or subducted crust. "Shallow" carbonatitic and deep kimberlitic melts with high CO_2 and low H_2O content originate in lithospheric mantle at 120–260 km depth. The high gas content facilitates rapid rise of magma diapirs to the surface where eruption takes place. The present outcrop pattern depends on the depth of erosion. By erosion to subvolcanic levels, ring complexes or diatremes are exposed, whereas recent uneroded examples are simple stratovolcanoes (such as the active alkali-carbonatite volcano Oldoinyo Lengai in the East African rift, Tanzania: Bell & Keller 1995; Figure 1.14). Examples of erosion to deeper levels are (B) Napak, Uganda and (C) Chilwa Island, Malawi. Kimberlite volcanoes build maar-like circular depressions or maar lakes.

Carbonatites

Carbonatites are igneous rocks with more than 50% of carbonate minerals. They are further subdivided depending on the nature of the carbonates (calcite, dolomite, and ankerite) and the silicate phases (biotite, pyroxene, amphibole, etc.). The formation of carbonatite-alkali complexes is probably controlled by i) fractional crystallization and ii) unmixing of carbonate and silicate melts (ijolite, pyroxenite and nepheline syenite) in the crust. Experimental and petrologic investigations of African carbonatites have shown that primary carbonatite melt can also originate iii) by a very low degree of melting in the mantle at elevated pCO_2, temperatures of 930–1080°C and pressures of 21–30 kbar (Bailey 1993). Anomalous amounts of rare earth elements (REE) are remarkable features of carbonatites, especially of the light REE elements. Half of all known carbonatites occur in Africa, and of those, most are related to the East African Rift System.

Metals exploited from complex intrusions of carbonatite, alkali-pyroxenites and nepheline syenites include copper, rare earth elements, iron-titanium-vanadium, uranium-thorium and zirconium; non-metallic resources are the industrial minerals vermiculite, apatite, fluorite and barite, and limestone (Notholt *et al.* 1990). In southern Siberia, one mine produces nepheline syenite for Russia's aluminium industry. Three characteristic ore associations occur with carbonatites:

1 Magnetite-apatite carbonatite and nephelinite (e.g. Khibiny, Kola Peninsula) are sources of pyrochlore (a niobium ore), copper (Palabora, South Africa) and zirconium ± hafnium; at Bayan Obo, Mongolia, iron, rare earth elements and niobium are exploited. worldwide, apatite is the prevalent mineral extracted from carbonatites;

2 Rare earths, fluorine and uranium; characteristic ore minerals are bastnaesite (as at Mountain Pass, California), monazite, and strontianite.

3 A hydrothermal paragenesis of barite, fluorite, manganese and sulphides.

The first group is orthomagmatic, often concentrated in aplitic and pegmatitic segregations. The

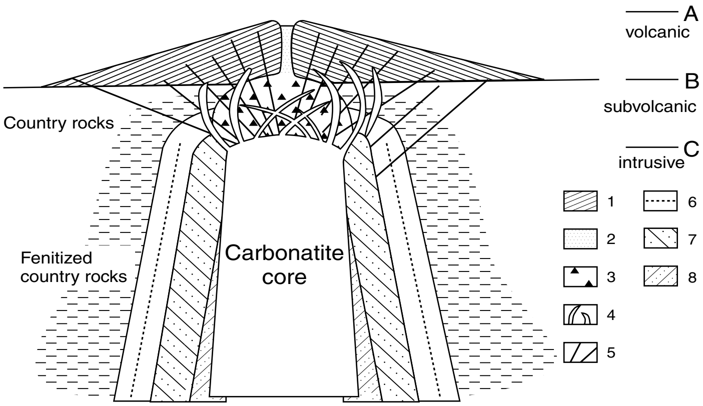

Figure 1.14 Hypothetical section of a carbonatite complex (modified from Kinnaird & Bowden 1991). With kind permission from Springer Science + Business Media. 1: Phonolitic and nephelinitic lava and tuff; 2: Natrocarbonatite; 3: Breccia; 4: Carbonatite ring dykes; 5: Carbonatite cone dykes; 6: Syenitic fenite; 7: Nepheline syenite; 8: Ijolite.

second is transitional, and the third occurs in hydrothermal-metasomatic or hydrothermal vein orebodies. Intruded silicate country rocks are fenitized. The term "fenitization" denotes alteration into a greenish rock consisting of alkali feldspar, aegirine and alkali hornblende. This alteration is a consequence of the high alkali element and volatiles content of carbonatite melt that are released during solidification (Bühn & Rankin 1999).

Kimberlites

Kimberlites are derived from the Earth's mantle at more than 140 km depth. They are petrographically variable rocks and almost always comprise strongly altered breccias and tuffs. Basically, they are porphyric, SiO_2-undersaturated, K-rich (1–3 wt.% K_2O) peridotites with xenoliths, and xenocrysts of diamond, olivine, Mg-ilmenite and chrome-rich pyrope in a carbonated and serpentinized groundmass with accessory phlogopite, perovskite, Cr-spinel and magnetite (Mitchell 1991, 1986; cf. Chapter 3 "Diamond"). Extremely rare are unaltered kimberlites, which in Siberia have been found to contain at least 8 wt.% of water-soluble alkali chlorides, alkali carbonates and sulphates (Kamenetsky *et al.* 2004). Close relatives of kimberlites are the K-Mg rich, ultramafic lamproites that are characterized by leucite, titanium-phlogopite, clinopyroxene, amphibole, olivine and sanidine. Lamproites received more attention when the great diamond deposit Argyle in Western Australia was found to be hosted in this rock. Kimberlites occur most frequently in subvolcanic pipes and occasionally in sills and dykes, whereas lamproite magmas with lower CO_2 content also form shallow intrusions. Kimberlites in old cratons are more often diamondiferous than others, possibly because of the prolonged and complex evolution of the subcontinental lithosphere. Age dating revealed that kimberlites and their diamonds may have same or widely differing ages. This implies that diamond formation is not directly connected with the phase of melting that produces kimberlite liquid. Diamonds are rather exotic xenocrystals that have been passively extracted from the mantle, in several cases long after their crystallization. It is important to remember that most kimberlites and lamproites contain no diamonds.

1.1.4 Granitoids and ore formation processes

Granitoids are felsic plutonic rocks with more than 20 mode % of quartz (Streckeisen 1976). The term is sometimes used in a wider sense to include more mafic rocks of an igneous suite.

Granitic rocks are commonly used as construction aggregates, building material and for the production of feldspar concentrates. Weathered granites are exploited for kaolin and quartz sand. Deep granite bodies are a potential source of geothermal energy extracted with the hot dry rock technology. In Sweden and in Finland, granites were chosen for the underground storage of heat-producing radioactive waste. In this chapter, however, the formation of magmatic and magmatic-hydrothermal ore deposits that are spatially and genetically related to granitoids will be discussed. Members of this diverse group include disseminated, stockwork and breccia ores of copper, molybdenum and gold (the porphyry deposits), highly differentiated small intrusions hosting tin and tantalum ("tin granites"), rare element pegmatites with ores of lithium, tin, tantalum and beryllium, skarn deposits of copper, lead and zinc, and hydrothermal vein and stockwork deposits of tin, tungsten and gold that occur in the roof of granite intrusions (Figure 1.15 and Figure 1.16). Apart from metals, many industrial minerals (e.g. fluorite, talc and wollastonite) can be enriched to exploitable grades in the magmatic and hydrothermal aureole of felsic intrusions.

The ore formation potential depends on origin and evolution of the parental granitoid. Important controls are the plate tectonic setting, the nature of source rocks, P/T-parameters of melting, content of water and other volatiles, the depth of intrusion, coeval tectonic deformation, partial pressure of oxygen (redox state) of the melt, assimilation of country rocks and the evolution of the magma by fractionation, cooling and crystallization including fluid segregation. Favourably coinciding factors account for the fertility of a granite intrusion. Understanding these controls and

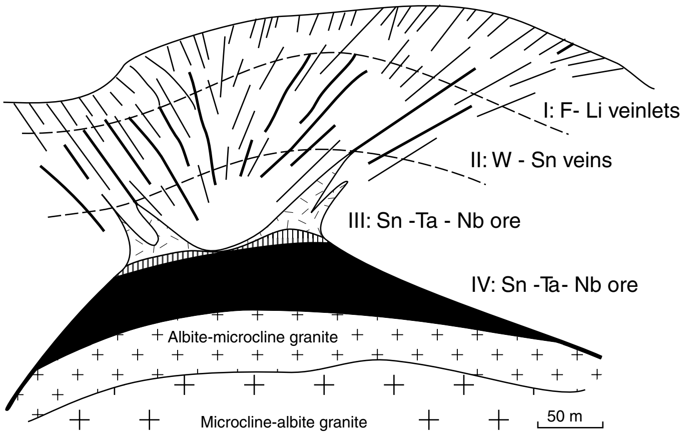
I: F- Li veinlets
II: W - Sn veins
III: Sn -Ta - Nb ore
IV: Sn -Ta- Nb ore
Albite-microcline granite
Microcline-albite granite
50 m

Figure 1.15 Schematic section of the granitic tantalum ore deposit Shuiximiao in southeastern China (modified from Zhu *et al.* 2001). With kind permission from Springer Science + Business Media.
I - Fluorite-lepidolite; II - Wolframite-cassiterite-quartz, III - Pegmatite-aplite and stockscheider pegmatite; IV - Albite-topaz-granite. Host rocks are Early Carboniferous limestones and slates.

constructing a holistic model are essential for the search for new deposits (exploration) and for rational exploitation of granite-related orebodies.

Geochemical analysis of trace elements and of isotope systems in granitoids provides valuable information on the source rocks. Fundamentally distinct sources of granitoids are:

1 peridotites of the Earth's upper mantle (asthenosphere, lithosphere);
2 magmatic and metamorphic rocks of the deep continental crust (infracrustal);
3 clastic metasediments and metamorphic equivalents (supracrustal);
4 restites of sediments and of magmatic rocks that have experienced earlier anatexis before a later melting event.

Ad 1: **M-type granitoids** are sourced in the mantle. Together with gabbro, they intrude the crustal rocks of ophiolites in the form of plagiogranite and quartz diorite, and the thick volcanic piles of primitive oceanic island arcs. Typical ore deposits associated with M-type granitoids are copper-gold porphyries and hydrothermal gold.

Ad 2: **I-type granitoids** are the most common intrusive magmatic rocks. They display an

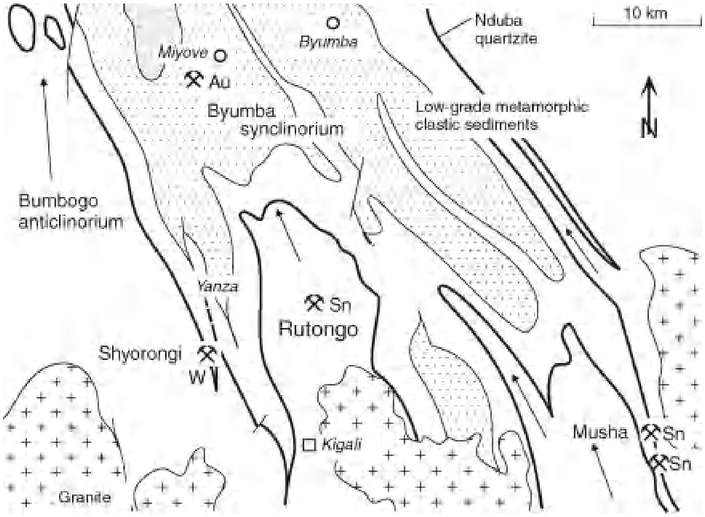
Nduba quartzite
10 km
Byumba
Miyove
Au
Byumba synclinorium
Low-grade metamorphic clastic sediments
N
Bumbogo anticlinorium
Yanza
Sn
Rutongo
Shyorongi
W
Kigali
Musha
Sn
Sn
Granite

Figure 1.16 Pegmatitic tin (Musha) and magmatic-hydrothermal vein deposits of tin, tungsten and gold in the sedimentary roof of Mesoproterozoic (950 Ma) granites in the Kibara orogen, Rwanda (Pohl 1994). Thick lines denote the distinctive Nduba quartzite marker band. Rutongo produced a total of about 30,000 t cassiterite, Shyorongi ca. 2500 t wolframite. Miyove is a small artisanal mine working a gold vein deposit.

abundance of hornblende and higher concentrations of Ca, Na and Sr compared with granites derived from sediments. Typically, large plutons consist of tonalites and granodiorites, but are often intimately associated with more basic rocks from gabbro to diorite. Some of these melts were undersaturated with water, which enabled them to rise to the surface, forming volcanic rocks (e.g. andesite and dacite). It is commonly accepted that I-type granitoids originated by melting of pre-existing infracrustal igneous rocks (Blevin & Chappell 1995). However, geochemical and isotopic I-type characteristics can also be explained by mixing of rising mantle magmas with anatectic lower as well as upper crustal melts (Kemp *et al.* 2007). Accessory minerals of I-type rocks are often magnetite and titanite, causing their attribution to the class of magnetite-series magmatic rocks (Ishihara 1981, Figure 1.17). This is due to a commonly higher oxidation degree of these magmas, although reduced I-type granitoids are known. Characteristic ore deposits related to oxidized granitoids are the iron oxide-copper-gold (U-REE) deposits (IOCG), copper-molybdenum porphyries, Mo-W-Cu skarn, hydrothermal lead-zinc and certain gold and silver ores.

Ad 3: **S-type granitoids** originate by continental collision and deep subduction of sediments to great depths and high temperatures, where the transition between metamorphism and significant melting is attained (Clemens 2003). Products of these partial melts are mainly leucocratic, SiO_2 rich rocks of a monzogranitic nature, often with muscovite besides biotite. Accessory minerals include cordierite, garnet, kyanite and ilmenite as the prevalent opaque mineral. This is why S- (and A-) granites are part of the ilmenite-series magmatic rocks (Ishihara 1981, Figure 1.17). The degree of oxidation of these magmas is low, due to organic carbon in the source sediments. The water of the melts is derived by dehydration of muscovite in the metasediments. The resulting melts are rather "wet" and crystallize at greater depth. Therefore, volcanic rocks are rare in this group. In the Palaeozoic Lachlan Fold Belt (Australia), both I- and S-type granites are common. Highly fractionated intrusions ("tin granites") of both suites are clearly associated with tin, tungsten and tantalum ore deposits (Blevin & Chappell 1995).

Ad 4: **A-type granitoids** are the product of repeated melt-extraction from the same source rocks (Eby 1992). Note that with every cycle of melting the source rocks acquire a more pronounced restite composition, marked by enrichment of less mobile substances. The "A" in the term may be translated into "abnormal, anhydrous, alkali rich, aluminous and anorogenic". Another possible source of A-type magma is lithospheric mantle (Turner *et al.* 1992) and not all A-granites are anorogenic (Whalen *et al.*

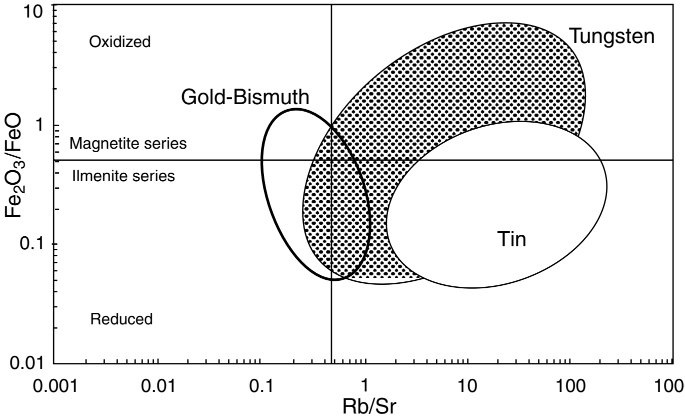

Figure 1.17 Typical fields of granites which are genetically associated with tungsten, tin and gold-bismuth deposits, in a plot of redox-state (vertical axis) versus increasing specialization (horizontal axis). Modified from Baker, T., Pollard, P. J., Mustard, R., Mark, G. and Graham, J. L. 2005, Society of Economic Geologists, *SEG Newsletter*, Figure 4, p. 12.

1987). Some granites that have A-type characteristics may be derived by extreme fractionation of I- and S-type magmas (Creaser *et al.* 1991; Taylor & Fallick 1997). Typical A-type granites are the alkali granites of continental rifts, for example the Jurassic tin-mineralized Younger Granites of Nigeria and the Mesoproterozoic Rapakivi granites in Finland, with their large red perthitic alkali feldspars mantled by green plagioclase. Volcanic equivalents include tin-rich topaz rhyolites in fields of crustal distension (Tertiary volcanics in Mexico). Two different ore associations occur with A-type granitoids: i) Sodium-rich granites, striking because of attached albitite bodies, contain concentrations of niobium, uranium, thorium, rare earth elements and some tin, whereas; ii) potassium-rich granites with profuse hydrothermal silicification, tourmalinization and acidity produce deposits of tin, tungsten, lead, zinc and fluorspar. The second association may occur within the granite body (endogranitic greisen, pegmatite, and porphyry stockwork ore) or in vein fields within intruded rocks (exogranitic).

HHP (high heat producing) granites

These granites are U-Th rich granitoids that attract attention because they seem parental to hydrothermal deposits, which formed much later than the granite:

> The Early Devonian Weardale granite in Northern England, for example, seems to have produced the hydrothermal Cu-Pb-Zn-fluorite-barite ore deposits of the North Pennines in the Permian. The explanation is its long-lasting heat production due to elevated amounts of K, U and Th (Plant *et al.* 1985), which produce heat by radioactive decay. Latent heat is one element of the HHP ore-forming systems. The second is sufficient permeability that allows deep circulation of down-flowing, usually meteoric water. Crustal permeability is commonly created by tensional tectonic fracturing. Heated water at depth can dissolve substances that are precipitated during ascent. Note that HHP-stocks must be quite large with a minimal diameter of 15 km and a considerable depth extension because the heat of small granites is rapidly dissipated. Typical HHP-granites include the post-orogenic Variscan tin granites of Cornwall, which are related to important polymetallic mineralization and are now explored for the production of geothermal energy.

Not all granites can be assigned to one of the source categories because of several reasons including complex mixtures of source rocks and extreme fractionation, which leads to increasing convergence of magma chemistry (Taylor & Fallick 1997). This is why the youngest granites in orogenic provinces geochemically approach those that occur in anorogenic settings such as continental rifts, zones of crustal extension and continental "hot spots" (Turner *et al.* 1992). These observations motivate classification of Phanerozoic (and older) granitoids according to tectonic setting: Island arc, active continental margin, post-orogenic uplift, continental collision and continental rifting granitoids (Pitcher 1997).

A time-dependent chemical evolution of intrusions has been noted in many granite-related ore provinces of the world: Early batholithic intrusions (i) are geochemically ordinary, whereas later and smaller precursor granites(ii) are transitional to small, geochemically specialized (iii) and to usually very small, mineralized granites (iv), which are intimately related to ore formation.

Compared with ordinary granites, precursor granites display higher content of K, SiO_2 and granophile trace elements, and less Fe, Ti, Ca, Sr and Mg. Precursor intrusions always predate specialized granites, although they are genetically related. Specialized and mineralized (parental) granites are distinguished by geochemically elevated content of metals, such as Sn, W, Nb, Ta, Mo, U, Th, REE, Rb, Cs, Li, Be, often F (the latter include "topaz granites") and P (Figure 1.17 and Figure 1.18). Petrographically, specialized and mineralized granites are mostly aplitic muscovite-biotite rocks, alaskites and leucogranites that intruded at shallow crustal levels. In specialized granites, rare elements are enriched in silicates and accessory minerals. Mineralized or parental granites, in contrast, stand out by their close relations to ore-grade concentration of rare elements. The geochemical changes from ordinary to mineralized granitoids are mainly caused by a process

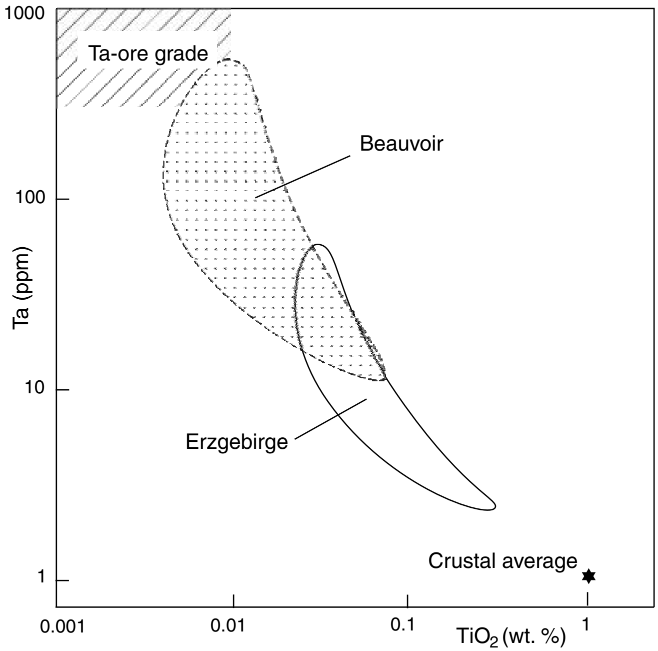

Figure 1.18 Ta/TiO$_2$ variation of granites from the northern French Massif Central (Beauvoir) and the Saxo-Bohemian Erzgebirge (modified from Lehmann 1990). With kind permission from Springer Science+Business Media.

system, which is generally termed "magmatic fractionation" (see below). The degree of fractionation may be measured by various indices. In metallogenetic research dealing with granitoids, increasing Cs concentration in melt, minerals and fluids is a particularly useful tracer of fractionation (Audétat *et al.* 2008).

Granites and related pegmatites with extreme chemical fractionation are the source (and often the hosts) of deposits of rare elements including Sn, Li and Be. They are enriched in large ion lithophile elements (LILE) such as Rb and Cs, and high field strength elements (HFSE) such as P, Y, Zr, Hf, Nb, Ta, Th and U (Linnen & Samson 2005). If ordinary and precursor granites are present, the enrichment may be traced back to common, geochemically not anomalous crustal rocks (Lehmann *et al.* 2000b, Cerny 1991). Figure 1.18 illustrates this principle and shows how tantalum (an incompatible element) is continuously enriched by increasing differentiation of successively more fractionated (and younger) granite melt batches and finally reaches exploitable grades. Concurrently, concentrations of the compatible element titanium decrease. Derivation of tantalum from geochemically ordinary crust appears possible.

The increasing differentiation of magmas is caused by fractional crystallization, early crystal settling and/or removal of liquid melt from a solid framework of phenocrysts (Weinberg 2006). Other explanations include a very low degree of partial melting (Robb 2005), or unmixing of melts because of fluid saturation. In some cases, melting of geochemically anomalous source rocks is considered to account for metal enrichment. An example are magmas with a high content of the chalcophile elements Au, Ag, Bi, Sb, Hg and Tl, which are supposedly inherited from a pre-enriched melt region (Tomkins & Mavrogenes 2003). Giant molybdenum porphyry deposits of the southwestern USA are thought to be extracted from an inherent large-scale Mo enrichment of the crust or lithospheric mantle (Klemm *et al.* 2008).

The petrological evolution of mineralized granites can be schematically subdivided into two phases: The first phase comprises the fractionation of elements between melt and early solid phases that crystallize during cooling, and is followed by a second phase of partitioning of trace elements between the small remaining melt fraction and exsolving fluids, which concentrate volatiles and metals:

> Elements that partition preferentially into the solid phase are referred to as compatible because they are included in nascent rock-forming silicate minerals, for example europium in plagioclase. Incompatible elements concentrate in the liquid (melt) phase. Lithophile or oxyphile elements are common in crustal silicates but are incompatible with minerals that have an important role in the formation of mantle magmas (e.g. olivine, pyroxene, spinel, garnet). Lithophile elements include Al, Si, O, alkalis, earth alkalis, rare earth elements and actinides, as well as metals such as Ti, Ta, Nb and W (Goldschmidt 1958). LIL elements (large ion lithophile) such as Rb, Sr, K, Ba, Zr, Th, U and light REE are preferentially enriched in late, highly differentiated melt derived from restites, because these elements are less prone to partition into early water-rich liquids. Cations with a high charge ($^{+}3$ to $^{+}6$) such as Mo, Nb, Zr, Sn, W, Ta, U, Th, Y and REE are normally abstracted from the melt by incorporation in crystallizing biotite, amphibole, apatite, zircon, monazite and magnetite. This process is inhibited by high activity of complexing volatile compounds, which cause these HFS (high field strength) elements to collect in late liquid and fluid phases. Because this is uncommon, elements such as Ti, Zr, Y, Ta, Nb, Hf, Th and REE are generally immobile and useful petrogenetic indicators (Pearce 1982, Pearce *et al.* 1984).

The fertility of granitoids is closely related to differentiation, fractionation and the formation of exsolved magmatic volatile phases. The composition of magmatic volatile phases is investigated by sampling volcanic exhalations, fluid inclusions in minerals (especially from miarolitic cavities) and volatiles included in volcanic glass. Miaroles are crystal-lined cavities in granitoids that are thought to have formed from fluid pockets during the solidification of magma. Fluid and melt inclusions preserved in miarolitic minerals reveal details about segregation, composition and evolution of mineralizing fluids (Audétat *et al.* 2008).

> Water is the most common substance in magmatic volatiles. In silicate melts, dissolved water reaches a maximum of 8 wt.% or 25 mole % (Ochs & Lange 1999). Arc magmas are more hydrous (and more oxidized) than those of other tectonic settings. Water is followed in decreasing order by CO_2, H_2S or SO_2, HCl and HF, and small amounts of N_2, H_2, CO, P, B, Br, CH_4 and O_2. Trace elements in volcanic emanations include the metals Pb, Bi, Cd, Cu, Zn, Hg, Sb, Te and As, and major rock-forming elements such as Al, Mg, Na and K. The annual exhalative emissions of Etna volcano, Sicily, include ~2.5 t lead and 250 t potassium. Metal fluxes in vapour from White Island volcano, New Zealand, are estimated to >106 t Cu and 100 t Au in 10,000 years of volcanic activity (Hedenquist *et al.* 1993). Different volcanoes have ratios of SO_2/HCl and SO_2/HF between 1 and >100. Ratios from 1 to 10 are typical for volcanoes above convergent plate boundaries, because they discharge more HCl. Gas released in explosive mode by Stromboli volcano (Italy), for example, consists of 64% H_2O, 33% CO_2, 1.8% SO_2 and 0.33% HCl (Burton *et al.* 2007). Note, however, that molecular HCl is only stable at very low pressure or in the absence of water. Above 200 bar, chlorine occurs as an ion or is dissolved in magmatic water as a complex with Na, K and Fe. In epizonal magmatic water, the average chlorine concentration in solution is 3.5%, or 6 wt.% (range 2–10) NaCl equivalent. The segregation of saturated or hypersaline solutions is only possible at pressures >1.3 kbar. In that case, a hypersaline solution (or should it better be called a hydrous saline melt?) at 700°C contains 84% NaCl.

Fertile granitoid magmas are distinguished by high content of volatiles. Volatiles collect the rare elements that form ore, and also lower density, viscosity and solidus temperature of a melt increasing its mobility (Baker & Vaillancourt 1995). Low magmatic temperatures and high salt concentrations favour the fractionation of metals into the fluid phase (Audétat & Pettke 2003). Oxygen fugacity in the melt is an important control (Figure 1.17). High oxygen in granitic magma causes depletion of tin and tungsten in the liquid and in late fluids, because the metals are abstracted in dispersed accessory minerals already during main-stage crystallization. Behaviour of copper and uranium is quite the reverse. Oxidized magmas (of the magnetite series) dissolve more sulphur (as an "anhydrite component", compare Streck & Dilles 1998) and derived fluids may produce large Cu-Au deposits. In "reduced" granitic magmas (ilmenite series), early sulphur saturation causes formation of dispersed sulphide droplets that collect copper and gold. Late fluids will be barren.

Formation of a volatile phase (degassing) during the ascent of silicate magmas through the crust is initiated by decreasing pressure, or in the case of roof fracturing, by sudden decompression ("first boiling"). The solubility of CO_2 in basaltic magmas can decrease rapidly at a depth of 70 km, but most basalts reach this stage at 10 to 15 km below the surface (Lowenstern 2001). Supersaturation leads first to formation of bubbles of liquid CO_2 that expand with further ascent until the density reaches that of gas. Water has a similar behaviour, although changes occur at shallower depths. As a function of the total water content in melt (commonly 3–5%, maximum 6–8 wt.%) and chlorine concentration, felsic magmas start to segregate an aqueous fluid phase at a pressure of $\sim$260 MPa (ca. 9 km, but more often around 4 km below the surface). Commonly at this stage, the melt body will freeze. Kinetic factors may, however, allow further ascent of the magma. In that case, expansion of fluid bubbles will produce a frothy liquid that is able to convect vigorously. Rare elements are effectively scavenged from the melt, and as the fluids move upwards, ore formation can take place either in the apex of the intrusion or in its roof. The remaining melt solidifies rapidly.

After final emplacement, when ascent is stopped and first boiling is finished, the intensive formation of solid phases from melt causes renewed concentration of volatiles. If the amount of volatiles is higher than the mass that can be included in minerals (e.g. OH^- in mica), a free volatile phase will form once more ("second boiling"). In the case of relatively shallow intrusions, fluid pressures may cause fracturing of the roof and sudden injection of mineralizing fluids. In this case, fluid-induced stress is larger than the sum of rock mass strength and the minimum natural principle stress (Brady and Brown 2004). Unmixing of a fluid phase from mesozonal intrusions (at pressures >2 kbar) is restricted to a narrow temperature interval. Often in this environment, volatiles form small batches of fluid-rich silicate melt that solidify to coarsely crystalline pegmatites. Shallow epizonal intrusions degas over a wide temperature interval (Fournier 1999), producing miarolitic and hydrothermally altered granites, but foremost the many variegated magmatic-hydrothermal ore deposits.

In Japan, granites related to magmatic-hydrothermal mineralization display a correlation between the main ore metals and the solidification pressure of the parent pluton. Total Al-content in biotite, the sphalerite and hornblende geobarometers and the petrology of surrounding rocks all suggest that Pb-Zn and Mo deposits formed at pressures of less than 1 kbar, Cu-Fe and Sn at 1 to 2 kbar and W deposits at 2 to 3 kbar (Uchida *et al.* 2007). Deeper intrusions are barren. The principle, although not the precise figures, may be of a wider significance.

In the past, a "pneumatogenic phase" of ore formation was distinguished between pegmatitic and hydrothermal conditions. The assumption was that certain ores were formed by precipitation from a magmatic gas phase of extreme mobility and with high concentrations of rare metals. Greisen orebodies of tin and many skarn ores were thus explained. More recently, the term is rarely used and often explicitly dismissed. Arguments include that water vapour (with a density below the critical density of 0.32 g/cm^3) cannot carry more than traces of dissolved matter, and supercritical fluids with densities that reach 2 g/cm^3 can hardly be called a gas (Roedder 1984; remember that pneuma in classical Greek is "air" or "breath"). Furthermore, the distinction is thought to be difficult, because supercritical fluids may pass into subcritical solutions or gases without any discontinuity (condensation). The limit between pneumatogenic and hydrothermal conditions had been assumed at the critical temperature of water, which occurs at 374°C and 225 bar, but rises as a function of solute concentration:

Even if there is no need for the old term, attention must be drawn to the fact that supercritical fluids do have properties that differ from solutions with the same composition: The density of supercritical fluids varies widely with changing pressure and temperature; they have higher pH (Ding & Seyfried 1996), are able to dissolve many organic substances, and exhibit extreme dissociation of water and diffusion coefficients. Geologically most important are probably the variable density (from dense fluid to gas), reaction rates and equilibrium constants that control transport and precipitation.

Of course, there is no doubt that magmatic gases and fluids of low density can transport metals (e.g. Etna volcano in Sicily) and precipitate ore. Cassiterite-quartz veins in the Mole granite, New South Wales (Australia), contain two types of inclusions: a saline brine (a solution) with elevated trace content of Mn, Fe, Zn, Pb and Sn, whereas the other is "gas" with ~1 % Cu. Observations suggest that both are cogenetic and unmixed from magma. Copper was concentrated into the gas phase (Heinrich *et al.* 1992). A broader investigation of magmatic-hydrothermal ore deposits revealed that boiling of magmatic fluids concentrates Cu, As, Au and B preferentially into the vapour phase, whereas Na, K, Fe, Mn, Zn, Rb, Cs, Ag, W, Sn, Pb and Tl are enriched in the residual saline brine (Heinrich *et al.* 1999, Williams-Jones & Heinrich 2005). The most important controls on this behaviour appear to be fluid density (Pokrovski *et al.* 2005) and sulphur content (Nagaseki & Hayashi 2008).

Exsolution of magmatic fluids and hydrothermal ore formation are an integral part of ascent and crystallization of an intrusion. Cooling down to environmental temperatures drives meteoric, convective hydrothermal systems that are often called "geothermal". In these systems, magmatic fluids and volatiles typically mix with meteoric water. Age determinations, model calculations and observation in nature reveal that an isolated single upper crustal intrusion may sustain a hydrothermal system for ~100,000 years (Cathles *et al.* 1997). Magmatic-hydrothermal processes can be prolonged to millions of years in the case of incremental growth of a pluton by multiple intrusions, regional deep magmatism and autonomous heating, due to radioactive decay that retard cooling.

1.1.5 Ore deposits in pegmatites

Pegmatites crystallize from highly fractionated hydrous residual melt batches of felsic magma bodies that are enriched in volatiles and incompatible trace elements. Pegmatites are characterized by coarsely crystalline textures, occasionally by giant crystals, miarolitic cavities and by minerals of rare elements. Most pegmatites are related to granites and have a paragenesis of orthoclase (perthite), microcline, albite, mica and quartz. Common minor minerals include tourmaline, topaz, beryl, cassiterite and lithium minerals. Felsic pegmatite melts intruding ultramafic rocks suffer desilication resulting in plumasites that are characterized by corundum, kyanite and anorthite. Gabbro pegmatites are derived from mafic magmas and are composed of anorthite, pyroxene, amphibole, biotite and titanomagnetite, occasionally including carbonates and sulphides (similar to the Merensky Reef "pegmatoid" of the Bushveld Complex). Iron-rich ultramafic pegmatites composed of olivine intrude the cumulates of the upper Critical Zone of the Bushveld Complex (Figure 1.5). Rare syenite pegmatites with microcline, nepheline, apatite, niobium and rare earth element minerals are related to alkaline intrusions. Certain diamonds are thought to have crystallized from kimberlitic pegmatite melt deep in the mantle (Moore 2009). Anatectic pegmatites (metamorphic segregations) that are formed in the upper amphibolite facies are rarely mineralized. Yet, some mineralized pegmatites may have originated by partial anatexis at great depth and not from large magma bodies (e.g. the uranium-molybdenum-rare earth pegmatites of the Grenville orogen: Lentz 1996). Most pegmatites crystallized at intermediate crustal levels, at fluid pressures of ~200 MPa (2 kbar). Therefore, they are commonly found in metamorphic country rocks. Volcanic equivalents of highly differentiated pegmatitic melts are extremely rare.

Classifying granitic pegmatites by their emplacement depth leads to differentiation of the following types:

- Abyssal pegmatites are anatectic stringers in migmatites of amphibolite and granulite facies metamorphic zones.
- Muscovite pegmatites occur in amphibolite facies kyanite-mica schists and are commonly related to granites, but exhibit little fractionation.

- Highly fractionated rare element pegmatites are derived from strongly differentiated fertile granites; host rocks typically contain cordierite and andalusite.
- Miarolitic pegmatites form at low pressure (1.5–2 kbar) and are proximal to granites. They may contain quartz of optical quality, various gemstones and valuable crystals of many rare minerals.

Granitic pegmatites occur in the form of dykes, oval and lenticular bodies. Most pegmatite bodies are relatively small with a thickness that rarely surpasses tens of metres and a length of a few hundred metres. Some pegmatites occur at the roof of granite cupolas and form a thin shell between the intrusion and the roof rock (stockscheider, i.e. "border pegmatite" in the German Erzgebirge). Giant pegmatites of this type are rare but economically significant (e.g. the tin-tantalum and spodumene pegmatite at Manono, D.R. Congo, which extends over ~12 km^2). Granitic pegmatites may be homogeneous (without a change of mineralogy or texture from wall to wall) and isotropic, or strikingly inhomogeneous and anisotropic ("zoned" or "complex" pegmatites). In contrast to the zonation of the interior of a pegmatite body, an external zonation can also be observed. This term designates the occurrence of different pegmatite types in one district, with a map-scale zonation, ideally around a central parental granite (Figure 1.19 provides pegmatite compositions of the field classification by Varlamoff 1972).

The internal zonation of complex pegmatites (Figure 1.20) reflects crystallization from the walls to the centre of a pegmatite body where the last melt solidified. The following zones are distinguished:

- *Border zone*: often fine-grained, aplitic, and very thin;
- *Wall zone*: coarsely crystalline, in some deposits with exploitable muscovite and beryl;
- *Intermediate zones*: which contain most of the valuable minerals (cassiterite, columbite, spodumene, beryl, etc.); the outer intermediate zones are often sugary albitites, followed by coarse albitite (cleavelandite) or microcline towards the core;
- *Core*: which is commonly a solid mass of barren grey or white quartz, but may also contain feldspar, tourmaline and spodumen.

Subhorizontal pegmatite sheets often have asymmetric zones, in contrast to the concentric zones that characterize most steeply-dipping bodies. Flat-lying pegmatites typically display bottom-to-top differentiation (e.g. Kenticha in Ethiopia: Küster 2009). Some cases of internal zonation are so complicated as to appear chaotic. Post-solidus cross-cutting fracture fillings, irregular metasomatic masses and hydrothermal quartz veins can further disarrange the internal structure. Because of crystallization from the wall to the centre, exsolving aqueous fluids will act from

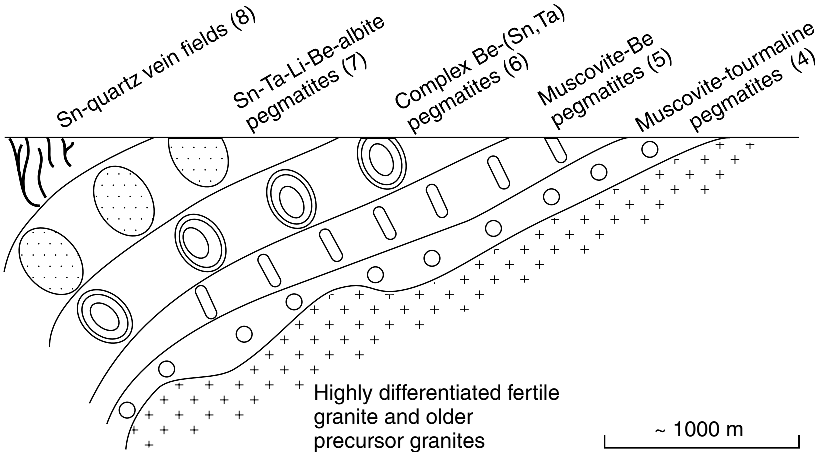
Sn-quartz vein fields (8)
Sn-Ta-Li-Be-albite pegmatites (7)
Complex Be-(Sn,Ta) pegmatites (6)
Muscovite-Be pegmatites (5)
Muscovite-tourmaline pegmatites (4)
Highly differentiated fertile granite and older precursor granites
~ 1000 m

Figure 1.19 External zonation of rare element pegmatites and cassiterite-quartz veins near fertile granites in Central Africa (adapted from Varlamoff 1972; cf. Figure 1.16). With kind permission from Springer Science+Business Media.

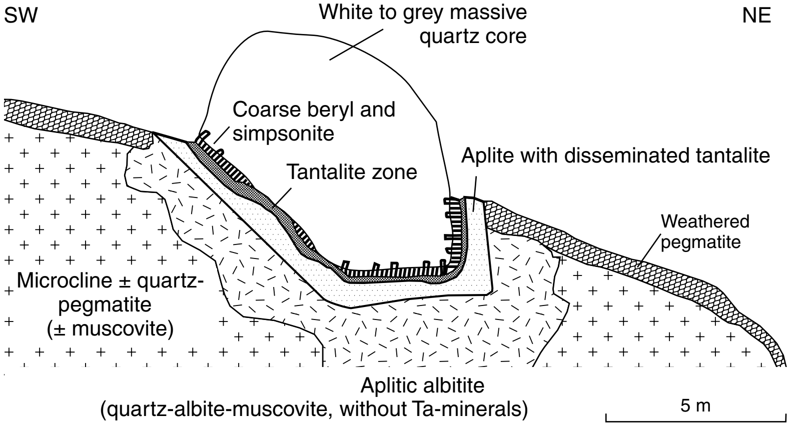
SW
White to grey massive quartz core
NE
Coarse beryl and simpsonite
Tantalite zone
Aplite with disseminated tantalite
Weathered pegmatite
Microcline ± quartz-pegmatite (± muscovite)
Aplitic albitite (quartz-albite-muscovite, without Ta-minerals)
5 m

Figure 1.20 Section of the Mesoarchaean tantalum-tin-beryllium pegmatite at Tabba Tabba near Port Hedland, northwestern Australia, with a well-developed internal zonation. After Sweetapple, M.T. & Collins, P.L.F. 2002, Society of Economic Geologists, *Economic Geology* 97, Figure 5, p. 882. Simpsonite is $Al_4(Ta,Nb)_3(O,OH,F)_{14}$ and indicates extreme fractionation.

the centre outwards. Therefore, post-solidification hydrothermal alteration of magmatic minerals is not rare (e.g. sericitization, kaolinization).

In contrast to granites, pegmatites frequently exhibit striking anisotropic textures. Most obvious examples are the giant crystals of amblygonite-montebrasite, beryl, topaz, tourmaline and other minerals that grow inwards from the cooling surface ("unidirectional solidification textures": Shannon *et al.* 1982). Related features are bands in sugary albitites, and graphic, skeletal or radial crystal growth.

Alteration of host rocks at the contact with pegmatite is often observed. However, the nature of this alteration is not of high-temperature contact-metamorphic type but hydrothermal, for example tourmalinization, silicification and propylitization (cf. "Hydrothermal Host Rock Alteration"). The alteration is due to expulsion of water and other volatiles from the pegmatite. A chemical exchange directed from enclosing rocks to the pegmatite is also possible, as shown by garnet appearing in the wall zone, the plumasite formation mentioned above, or the occurrence of a tourmaline border zone that is due to reaction of iron and magnesium mobilized from the host rocks with boron from the volatile phase of the pegmatite.

Cooling and crystallization of pegmatite melt bodies induces the segregation of immiscible liquid phases, which may include a peraluminous melt containing less water, and a water-rich peralkaline melt, as at Ehrenfriedersdorf in Germany, co-existing from 720–490°C (Rickers *et al.* 2006). Other phases, such as hydrosaline melt (a highly concentrated aqueous fluid), saline fluids and a vapour phase may appear at certain evolution stages. Inclusions of co-existing melts and hydrothermal fluids in quartz confirm this model (Rickers *et al.* 2006, Thomas & Webster 2000, Thomas *et al.* 2000). Ordinary unmineralized pegmatites crystallize at temperatures between 690 and 540°C, whereas fractionated melts with elevated content of boron, fluorine, phosphorous, chlorine, etc. finally solidify at ~450°C. Below the solidus, aqueous fluids dominate the system. Undercooling of the melt bodies injected into cooler host rocks may play an important role in the formation of zoned pegmatites (London 2008). The development of giant crystals seems to contradict the concept of undercooling, but a low density of nucleation sites, water-like viscosity of the peralkaline and hydrosaline melts, and high diffusion rates explain its feasibility.

The internal zonation in complex pegmatites might have two causes: i) fractional crystallization in a closed system; or ii) repeated injection of new melt batches in an open system. The worldwide similarity of zoned pegmatites (and many other data) argues for a closed system. Undercooling and back-reaction between remaining melt and earlier solids are the main factors supporting the "disequilibrium fractional crystallization through liquidus undercooling hypothesis" (London 2008). The unusual occurrence of nearly monomineralic rocks such as albitites and part of the enrichment of metals can probably be explained by zone refining. This concept assumes that pore liquids in outer zones, consisting of semi-solid crystal mush, take up solutes and move inwards.

The external zonation of different pegmatites around parent intrusions is explained by the increasing mobility of more fractionated melts, because increasing fractionation lowers solidus temperature, density and viscosity of melts (Cerny 1991). This explains why ordinary pegmatites occur near the parent intrusion, whereas specialized, complex pegmatites and hydrothermal ore deposits are found at a greater distance (Figure 1.16 and Figure 1.19). The degree of fractionation of pegmatites can be determined by trace element analyses of whole rock samples (Li, Rb, Cs, Ta), mica (Cs, Ta, Nb, Zn, Li, U, Be, Ba) and potassium feldspar (Cs, Rb, Na, Ba) (Wise 1995, Morteani *et al.* 2000). Some pegmatites display fractionation to less than 0.05% of the parental melt volume (Evensen & London 2002).

Little is known about details of the physical derivation of pegmatite melts from parent intrusions. The common implication is that pulses of increasingly specialized melt are ejected while the main magma body crystallizes. Rickers *et al.* (2006) report that melt inclusions in parent granites show a gradual transition to embryonic pegmatite melts, along with enrichment of water, B, F, P, Sn, Rb and other incompatible elements. Yet it is not impossible that small pegmatitic melt batches rise directly from the source region of the "parent" granite (Shearer *et al.* 1992).

Pegmatites may host many useful raw materials (Sweetapple & Collins 2002, Morteani *et al.* 2000, Martin & Cerny 1992). These include ores of Be, Li, Rb, Cs, Ta > Nb, U, Th, REE, Mo, Bi, Sn and W, the industrial minerals muscovite, feldspar, kaolin, quartz, spodumene, petalite and fluorite, and gemstones as well as rare mineral specimens (emerald, topaz, tourmaline, ruby, etc.). The derivation of pegmatites from I-, S- and A-type granites is probably the main control of the availability of specific elements for enrichment. The feasibility of pegmatite mining is often limited by a small tonnage and a heterogeneous distribution of economic minerals. The determination of mining reserves is notoriously difficult. Therefore, pegmatite mining is more common in countries with low labour costs.

1.1.6 Hydrothermal ore formation

Nearly each of the preceding sections contained a reference to the important role of aqueous fluids, although relations between igneous rocks and ore deposits were the main subject. In the following, important aspects of ore formation by hot aqueous fluids are presented.

The term "hydrothermal water" applies to subsurface water with a temperature that makes it an agent of geological processes, including hydrothermal ore formation. "Geothermal waters" are a subgroup of hydrothermal solutions that occur near the Earth's surface and are mainly used as an energy source, but also for balneology. Thermal springs (Figure 1.21) are common indicators of geothermal reservoirs at depth. Many hot springs and geysers currently display precipitation of minerals and ore. However, most hydrothermal ore deposits were formed at depth, at temperatures of ~700–50°C and pressures of a few hundred to >3000 bar. In the past, the term hydrothermal was mainly understood to imply condensed magmatic vapours below ca. 400°C, based on observations in volcanic geothermal districts. Meanwhile, isotopic investigations revealed that many geothermal and hydrothermal waters are not of magmatic but of meteoric derivation (i.e. from local precipitation). Similarly, hot water in mud volcanoes of oilfields is not magmatic but formation or connate water (diagenetically altered seawater enclosed in sediments). Many other observations confirm that "hydrothermal water" has no unique but many possible sources.

Much has been learnt by studying natural thermal springs and geothermal water tapped by drilling. Most hot waters are dilute solutions of chloride, carbonate and sulphate, but dissolved silica, boron and sulphide are also common (Gallup 1998). Examples of thoroughly investigated hydrothermal systems include the mid-oceanic black smokers, gold-rich hot waters of deep geothermal boreholes in New Zealand (Simmons

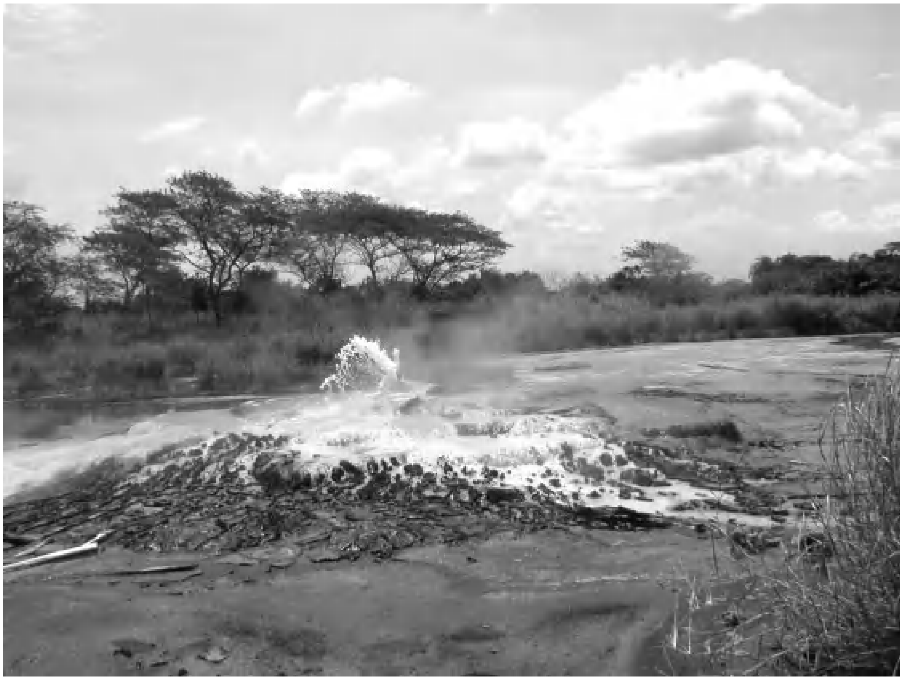

Figure 1.21 (Plate 1.21) Geothermal hot springs and siliceous sinter mound at Sempaya in northwestern Uganda. The convective system is related to the large border fault of the Ruwenzori Mountains, with a vertical displacement of more than 10 km between the petroliferous Tertiary Albert Rift in the west and the Palaeoproterozoic crystalline horst in the east.

& Brown 2000, 2007) and base metal-bearing brines of the geothermal field at Salton Sea in Southern California:

> Salton Sea is a playa lake in the Colorado River delta of the Imperial Valley graben. It occurs in a transtensional pull-apart basin formed atop the Pacific-North America plate boundary near the transition of the spreading Gulf of California to the San Andreas transform fault zone. The basin fill comprises Tertiary and Quaternary sediments and basaltic sills. Seeps of hot water and gas (CO_2, methane) are widespread (Svensen *et al.* 2007). Very high heat flow caused by shallow intrusions supports geothermal electricity production. Brine is produced from ~1.4 km depth with a temperature exceeding 350°C and content of 506 ppm Zn, 95 ppm Pb and 6 ppm Cu, as well as Na, K, Ca, Cl, S and many other elements. Total salinity reaches 27 wt.%. Zinc is precipitated from the brine after its passage through the turbines; production attains ~30,000 t/year. Isotope data reveal that the geothermal water is of meteoric origin and closely resembles Colorado River water. Apparently, river water infiltrates along faults down into the basin sediments, where it is heated and acquires solutes from the rocks. Metal-rich scales in the drill pipes substantiate the hypothesis that focused upflow of such waters is a way of ore deposit formation.

Fluids in the Rotokawa and Mokai geothermal fields of the Taupo Volcanic Zone in New Zealand have an exceptionally high content of precious metals (gold and silver) and of arsenic, antimony and mercury (Simmons & Brown 2006, 2007). Ore deposits, however, have not been found until recently and the systems are only used for the production of electric energy. More than 50 drillholes have been sunk to explore and develop the fields, some of them to >2600 m depth. Very few surface signs of the vast geothermal zone had existed before. One famous site is the Ohaaki pool with siliceous sinter and ochreous muds that contain 85 ppm gold, 500 ppm silver and 10% antimony as well as high trace content of As, Hg and Tl. This material would be gold ore if the total mass were not so tiny. The geothermal zone is an excellent natural laboratory for investigating hydrothermal ore formation of the epithermal low sulphidation type (Simmons & Brown 2000). Note that high content of solutes is rather a nuisance for geothermal energy production. The precious metals, for example, precipitate from the ascending fluids because of boiling and gas loss, so that tubes are clogged.

Hydrothermal convection

Hydrothermal convection cells, such as the ones at Salton Sea, are established where heat sources below the surface coincide with permeable flow paths, often provided by extensional tectonic deformation (Figure 1.10). Cold infiltrating surface and groundwater is drawn to the "heat exchanger" at depth. The lower density of hot compared to cold water causes ascent of hydrothermal solutions and establishes hydrothermal convection.

Chemical composition

The chemical composition of hydrothermal solutions is extremely variable. Generally, chlorine and sulphur are the most important anions. Salinity ranges from very low to more than 50% and the source of salinity (e.g. halite dissolution, evaporation of seawater, etc.) is detectable by determination of halogens and electrolytes (Botrell *et al.* 1988). Metals are to some extent dissolved as simple ions or ion pairs, but more commonly in the form of complex ions, which combine chlorine, dissociated OH^- groups and bisulphides, as well as NH_3, H_2S and CO_3^{2-}. The fraction of dissolved matter in hydrothermal solutions varies from less than 1 to over 50 wt.%. Metal concentrations range from less than 1 to several 1000 ppm (parts per million, equal to gram/tonne). Even higher concentrations in solution are possible when metals are part of complex ions. This reduces the mass of water needed to produce an ore deposit compared to transport in the form of simple ions. Hydrothermal solutions carry metals not only in dissolved form but also as colloidal particles. Colloids are tiny particles (1–1000 nm), which are quite common in many natural waters, usually at low concentrations (Ranville & Schmiermund 1999). High concentrations of dispersed colloids in water are called hydrosols. In many cases, hydrosols are the precursors of gels. Hydrosols and gels may form by local supersaturation of a substance, for example because of a sudden change of pH, T, P or Eh.

Essentially, the chemistry of hydrothermal solutions is the result of interaction between rocks and hot water, in space and time (Barnes 1998). Most important variables controlling these interactions are the initial state of rock and water, the water/rock mass ratio, temperature, chloride concentration, pressure and redox state (Yardley 2005). Geochemical thermodynamic modelling of hydrothermal systems is a tool that provides both a deeper scientific understanding (Moore *et al.* 2000) and solutions to very practical problems, especially in geothermal reservoir and production management.

Possible phase states of hydrothermal waters are liquid, gaseous (vapour) and fluid (supercritical "gas" or "liquid"). In fact, many hydrothermal deposits were formed by supercritical fluids. Water reaches its supercritical state at $T > 374°C$ and $P > 225$ bar (the critical point of pure water). Increasing salinity moves the critical point to higher T and P (Haas 1971), for example 298 bar and 407°C for seawater. Similar to gas, supercritical fluids are more compressible than subcritical aqueous solutions and have a smaller kinematic viscosity; they are highly mobile (Eckert *et al.* 1996). A fluid comprising CO_2 or CH_4 in addition to water has a high carrying capacity that depends on pressure and density variations. Very small variations cause either dissolution or precipitation of solids. Highly concentrated supercritical fluids have a texture similar to molten salt with polynuclear ion clusters such as $CuNa_2Cl_2^+$ or $FeNa_2Cl_3^+$. These clusters reach the size of megacomplexes with over six constituent ions that can transport metals efficiently at very low concentrations (Oelkers & Helgeson 1993). In contrast to subcritical solutions, which form a gas-rich vapour with low content of dissolved matter when pressure is released (true boiling), supercritical fluids segregate into a brine and a dense vapour, which is capable of effective metal transport (Pokrovski *et al.* 2005).

Hydrogen ion activity (pH) of hydrothermal solutions varies from moderately acidic to moderately alkalic. Exceptions occur, of course, and can be recognized by formation of indicative alteration minerals. Acidic conditions, for example, cause formation of kaolinite, alunite or topaz from feldspar. Deep hydrothermal water is normally reduced; oxygen content may increase near the surface by mixing with fresh meteoric water. Bituminous substances are a common accessory in hydrothermal deposits, for example pyrobitumen in the silver veins at Kongsberg, Norway, and oil in the Pb-Zn deposit at Pine Point, Canada. This can be a sign that the hydrothermal solutions were sourced in basinal sediments (e.g. diagenetic formation water mixed with hydrocarbon fluids). Present-day examples are submarine seeps of hot solutions in the Guaymas Basin (Gulf of California) that contain large drops of petroleum (1–2 cm diameter); the vents are mainly built of barite. Organic-chemical investigations (of biomarkers, etc.) allow a very detailed reconstruction of causative processes, covering both hydrotherms and hydrocarbon genesis (Jochum 2000, Svenson *et al.* 2007).

Biological processes

Biological processes at depth influence many hydrothermal solutions. Hyperthermophilic bacteria and archaea are known from hot springs at the Earth's surface to black smoker vents on the ocean floor. With descending branches of convection systems, microbes can be swept deep into crustal rocks. At ~100°C and in the presence of sulphate (from seawater) and organic matter (oil or gas, kerogen), the anaerobes reduce the SO_4 ion to H_2S. This has been observed in oil reservoirs where flooding with seawater was employed in order to boost production. High H_2S content favours dissolution and transport of a number of metals. At falling temperature, however, H_2S contributes to precipitation of metals.

Precipitation of ore and gangue minerals

Many causes may induce the precipitation of ore and gangue minerals from solutions. Their understanding is an important element of the search for ore. In the first place, decreasing temperature and pressure reduce solubility. Precipitation is a function of the relative stability of metal complexes and decreasing temperature often results in the common sulphide precipitation sequence from early Cu to Zn, Pb, Ag and finally Hg. Pressure drops may cause fluid immiscibility, such as the formation of two fluids (e.g. aqueous and carbonic) from an originally homogeneous fluid (aqueous-carbonic). This can drastically change pH, fO_2 and temperature, thus inducing mineral deposition. Note that rapid pressure fluctuations are typically caused by tectonic events ("seismic pumping" Sibson 1990). Falling pressure is especially effective if common boiling takes place in the two-phase field of liquid plus vapour. Boiling suddenly changes several chemical properties of a hydrothermal solution (concentration, pH, Eh, stability of complex ions), which reduce the solubility of dissolved matter. The term "effervescence" is preferably used in place of "boiling", when gas bubbles form that are not vapour of the host liquid (e.g. carbon dioxide gas bubbles in water). Yet like boiling, effervescence may also induce rapid precipitation of minerals.

Relatively simple systems of this type can be investigated in geothermal power plants where production wells are often affected by mineral precipitation on pipe walls. With time, this process diminishes the open diameter of the tubes ("scaling"). Corrosion, and the effects of re-injecting cooled and depressurized solutions into the reservoir, are also instructive (Czernichowski-Lauriol & Fouillac 1991).

Often, mixing of chemically different waters induces deposition of ores and minerals. A common example is the formation of barite. Barite ($BaSO_4$) is precipitated when ascending chloride solutions with dissolved barium ions encounter sulphate-ion bearing water (e.g. seawater). Furthermore, the reaction of hydrothermal solutions with host rocks or with previously deposited ore minerals is a very efficient means of immobilizing dissolved elements. When metal-bearing solutions encounter sulphide minerals, more noble metals are precipitated, whereas less noble elements pass into solution (eq. 1.1). This is a function of properties such as electronegativity, ionization potential, electron affinity, redox potential and the energy of chemical bond formation.

Selective precipitation of more noble metals from solution by exchange with less valuable elements:

$$CuFeS_2 + Cu^{2+}_{solution} \rightarrow 2CuS + Fe^{2+}_{solution} \quad (1.1)$$

Gold (electronegativity 2.4 Pauling's) is more noble than silver (1.9), which is followed by Cu (1.9) and Fe (1.8), explaining common replacement relations. Note that in physical terms, only copper, silver and gold are noble metals. In chemistry, the electric ionization potential of elements is used to define relative nobility. Host rocks exert a strong control on noble metal enrichment. Silver ore veins at Kongsberg (Norway) were fabulously rich in native silver and argentite (Figure 1.22), where they crossed pyrite-rich layers ("fahlband") in host rock gneisses. Gold ore veins of the Mother Lode system, USA are of higher grade where they intersect pyrite-bearing amphibolite. At the giant Golden Mile deposit, Kalgoorlie, Western Australia, deposition of gold is explained by reaction of sulphide solutions with reduced iron of doleritic host rocks, forming pyrite ("sulphidation"). This triggered a radical decrease of reduced sulphur in the hydrothermal solutions causing gold precipitation.

Organic substances (coal, kerogen, oil, gas) also provoke immobilization of many metals by adsorption or reduction. Gold ore veins at Ballarat, Australia and the metasomatic gold orebodies of Carlin, USA are enriched where host rocks contain kerogen-rich layers. Sulphide precipitation in Mississippi Valley deposits is often caused by reaction between solutions and the organic substance of host rock carbonates (Spirakis & Heyl 1995). Incompletely oxidized sulphur (e.g. thiosulphate, $S_2O_3^{2-}$, polysulphides, S_nS^{2-}, or colloidal sulphur, S^0) supports high metal content in solution. These compounds, however, are easily reduced by contact with organic matter so that metals are instantly immobilized as sulphides. An indirect consequence is the precipitation of gangue, such as barite and fluorite.

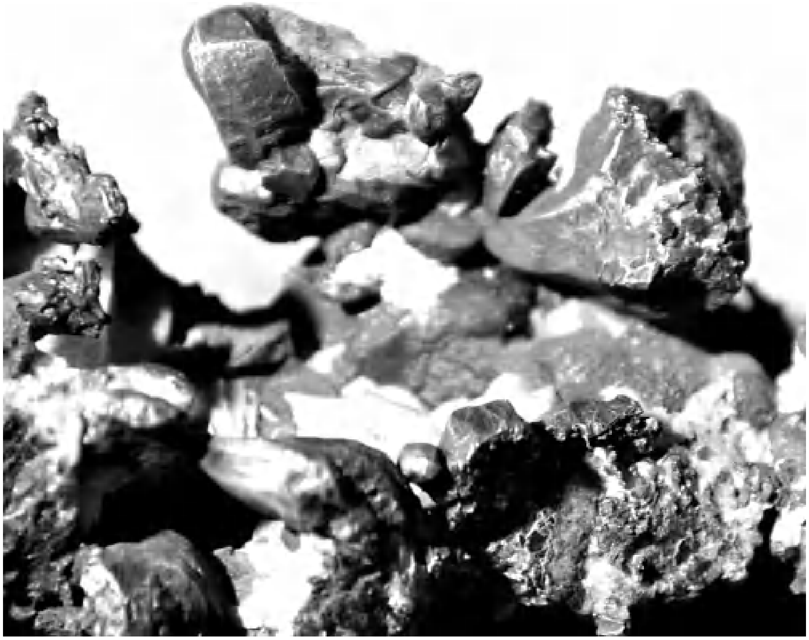

Figure 1.22 Hydrothermal native silver crystals (isometric, malformed) from Kongsberg in Norway. Gangue includes calcite, barite, zeolite, fluorite and quartz. Courtesy Wolfhart Pohl, Washington.

Although reduction is a frequent means of ore mineral deposition, oxidation can have a similar role, most often concerning iron and manganese. Hydrothermal solutions transport these metals in reduced form (Fe^{2+}, Mn^{2+}) and precipitation of haematite, magnetite or pyrolusite requires oxidation to Fe^{3+} or Mn^{4+}.

Contact of metal-bearing solutions with carbonate rocks is a frequent factor of precipitation. Individual agents include the "pH-shock" upon contact with alkaline rocks and formation fluids, a larger permeability compared with pelitic country rocks, a higher solubility of carbonates in acidic or CO_2-rich solutions (which may result in the formation of "hydrothermal karst"), and mixing with formation water in carbonate rocks. Orebodies in carbonates take the form of veins, breccia and karst pipes. They can also occur as stratiform orebodies with irregular outlines ("mantos") and as cross-cutting cloudy masses. When the replacing masses consist of sulphides, it is obvious that dissolution of the original carbonate rock and replacement ("metasomatism") by ore must have taken place. The same process term is used for cases where only cations are exchanged (e.g. siderite in limestone). Systems of delicately balanced dissolution of one component and precipitation of another are best investigated by geochemical modelling based on thermodynamic principles (Anderson 1996; Bethke 1996).

Source and origin of hydrothermal fluids and solutions

Source and origin of hydrothermal fluids and solutions may be related to quite different geological process systems:

- magmatism (exsolution of an aqueous fluid phase from silicate magma);
- heating of meteoric, oceanic or formation water by convection within or near cooling intrusions, in HHP granites and other heat anomalies, including large faults or uplifted hot metamorphic complexes;
- diagenesis (mainly physical dehydration of sediments by increasing pressure and temperature because of increasing overburden, thrust sheet superposition, or accretion on active continental margins);
- metamorphism (mainly chemical dehydration of minerals that include OH-groups in their crystal lattice, caused by prograde metamorphic reactions);
- mixing of two or more of the mentioned source systems.

"Juvenile water" is more a concept than reality. The term refers to water that originates from degassing of the mantle, and that has never before been at the Earth's surface. The second stipulation cannot be proved with present scientific methods. Casual usage of the word wrongly implies any magmatic water. Note that "geothermal water" does not refer to a specific origin but to any hot water that occurs near the surface. Usually the term is employed in the context with production of geothermal energy.

Differentiation of the various genetic possibilities is often difficult, as is shown by the persistent discussion concerning the precise origin of many mineral deposits. Geological and geochemical arguments are most decisive, especially based on isotope systems including noble gases that characterize major earth domains (e.g. ^{40}Ar the crust, ^{3}He the mantle: Kendrick *et al.* 2001, 2002). Halogens, such as Br and Cl, conserve source ratios and isotope compositions through subduction and magmatism (Nahnybida *et al.* 2009).

In the Earth's crust, aqueous solutions and fluids are ubiquitous (Yardley 2005, Fyfe *et al.* 1978) and therefore, hydrothermal ore deposits occur in a fascinating diversity. This includes veins (e.g. "orogenic gold"), metasomatic bodies in carbonates, breccia ores in magmatic rocks ("porphyry deposits"), ore stockworks and pipes, volcanogenic terrestrial and submarine exhalations, stratiform base metal ore beds in marine sediments (sedimentary-exhalative ore) and stratabound diagenetic Pb-Zn-Ba-F deposits in marine carbonates. More detailed information on these deposit types and their formation is provided in later sections. Here, it is essential to introduce first the most important methods, which provide data that constitute essential building blocks of genetic models.

Methods of genetic investigations (1)

Isotope Geochemistry – The Origin of Water and Minerals, and the Age Determination of Hydrothermal Mineral Deposits

The application of isotope geochemical methods provides a new dimension of metallogenetic research (Hoefs 2009, Allègre 2008, Faure & Mensing 2004, Valley & Cole 2001, Dickin 1995). Isotope systems indicate the source of water, gas, metals and other compounds in hydrothermal solutions, illuminate reactions between solutions and host rocks, reveal formation temperatures and expose mixing processes between solutions of different origin. In addition, isotopes are invaluable means of age determination of hydrothermal, magmatic and supergene ore deposits. Isotope geochemistry is an essential element in the quest for a full understanding of genetic processes. Too often, however, complex relations still limit reconstruction of past processes (Hoefs 2009).

Unstable (radioactive) isotopes are distinguished from stable (non-radioactive) isotopes. Radiogenic isotopes or daughter elements (nuclides) originate by radioactive decay of unstable parent elements. Isotopes of an element have an identical electron configuration but different mass. In physical, chemical and biological processes, this causes thermodynamic and kinetic effects. Isotopes of light elements that have a high mass difference display isotope fractionation. A simple example is evaporation: Lighter isotopes preferentially enter the vapour phase because of their higher vibration energy. Mass difference also affects reaction rate and bond strength, inducing fractionation between syngenetic minerals, and between a mineral and its parent solution. Because the fractionation is a function of temperature, several isotope systems (e.g. sulphur, oxygen, silicon) are very sensitive geothermometers, although only if full equilibrium was attained (Onasch & Vennemann 1995).

Isotopic compositions are measured relative to a standard, using mass spectrometers. Therefore, the fractionation of stable isotopes is commonly expressed as the deviation (**δ**, in ‰, *per mil*, of mass) from a standard (eq. 1.2).

Calculation of isotope fractionation as a deviation from a standard:

$$\delta(‰) = 10^3[(R_{\text{Sample}} - R_{\text{Standard}})/R_{\text{Standard}}] \qquad (1.2)$$

R is the ratio of an isotope pair, for example $^{18}O/^{16}O$, D/H, etc. Negative δ values indicate an enrichment of the light isotope relative to the standard, whereas the heavy isotope is enriched if the sign is positive.

Isotope age dating of minerals that originated as a consequence of ore formation processes is based on the time dependence of the genesis of a stable daughter nuclide (D) by radioactive decay of an unstable parent element (P). The age expressed in unit "annum" (a, ka, Ma) is calculated with the following equation 1.3.

Determination of geological ages by radioactive decay:

$$t = 1/\lambda \cdot \ln(1+D/P) \qquad (1.3)$$

Time (t) is the date before present, when radioactive decay started, D is the number of atoms of the daughter element, P the number of atoms of the parent element, and lambda (λ) the decay constant of the parent element ($\lambda = 0.693$ divided by its half-life). Resulting age data or model ages can only be considered as real ages if the analysed system was closed for both parent and daughter element during the whole time span (Dickin 1995).

Commonly, gangue silicates or alteration minerals, including K-feldspar, white mica (muscovite, sericite), biotite, apatite, monazite, rutile, titanite, xenotime and zircon, are used for the age determination of hydrothermal ore deposits. Several isotope systems can be studied, for example U-He, U-Pb, Pb-Pb, Rb-Sr, Sm-Nd, K-Ar and $^{40}Ar/^{39}Ar$. Also, ore minerals such as cassiterite, columbite, sphalerite, several sulphides and scheelite can be dated with these systems. U-He, U-Pb, Th-Pb and K-Ar systems, however, are subject to complications by α-recoil that will damage the "container" with time, allowing partial loss of parent and daughter. Moreover, very careful investigations revealed that many isotope systems are impaired by later thermal events or the passage of migrating fluids, even at relatively low temperature (Kerrich & Cassidy 1994, Selby *et al.* 2002). Clearly, the geological significance of age data and model ages must always be critically examined.

The age of most ore minerals (e.g. sulphides, oxides) cannot be determined precisely with the above mentioned methods, because they rarely host lithophile elements in their crystal lattice. One alternative is direct dating of sulphides, oxides and even gold using the chalcophile-siderophile element rhenium. The rhenium-osmium method is based on the β-decay of ^{187}Re to ^{187}Os with a half-life of 41.6 Ga. Thus, the age of molybdenite, arsenopyrite, sulphides and oxides can easily be established. This is especially useful for investigating gold deposits (Morelli *et al.* 2007). Similar to lead isotopes, the Re-Os system allows conclusions concerning the source of metals apart from dating (Stein *et al.* 2001).

Improvements of the precision of dating techniques allow increasing resolution of ages and with that, reliable measurement of the duration of ore deposit formation. Results show that many hydrothermal ore deposits have been formed in geologically very short time (several thousands to a few ten thousands of years), which is just about the error margin of present methods. Some data imply that other hydrothermal systems may have been surprisingly long-lived (hundred thousands to millions of years).

Stables isotopes of water

Stable isotopes of water, including ^{1}H (hydrogen) and ^{2}H (D, deuterium) as well as ^{16}O and ^{18}O, are exceptionally revealing keys for the comprehension of hydrothermal processes. Average ocean water is employed as a standard (SMOW = Standard Mean Ocean Water). Evaporation of ocean water is the starting point of precipitation/evaporation cycles that produce isotopically "lighter" water vapour (and derived precipitation), as the distance to the sea and to the equator increases. The isotopic composition of precipitation, surface and shallow groundwater forms a band that is termed the meteoric water line (Figure 1.23). "Meteoric water" is water that has been part of the meteorological cycle evaporation – condensation – precipitation (excluding seawater). The meteoric water line is in reality a band because of local deviations. Note that "formation water" is not a genetic term but simply designates water of unknown origin and age in sediments; formation waters generally show an increase of δ^{18}O with increasing burial depth. Brines that form by evaporation in semi-closed marine lagoons are isotopically heavy. Isotope exchange between rocks and ocean or meteoric water produces fluids that retain largely the original hydrogen isotopic composition. Oxygen isotope ratios, however, are considerably altered by partial exchange with oxygen contained in rocks. An equivalent effect is commonly observed in geothermal fields; while the fluids are increasingly enriched in heavy oxygen, the hydrothermally altered rocks are depleted in ^{18}O. The depletion zones allow mapping of fluid passage and can be vectors to ore (Hoefs 2009, Holk *et al.* 2008).

In the δD/δ^{18}O diagram, waters of magmatic, metamorphic and sedimentary origin occupy partly overlapping fields (Figure 1.23) so that they cannot always be clearly discerned. Water

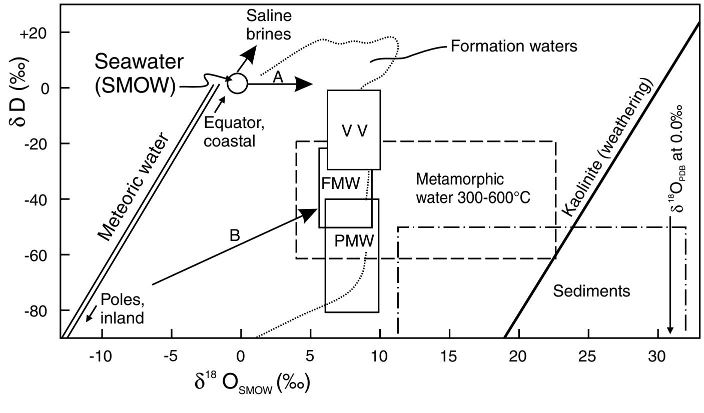

Figure 1.23 Isotopic composition of waters that participate in hydrothermal ore formation (adapted from Hoefs 2009). With kind permission from Springer Science+Business Media. PMW is primary magmatic water; FMW felsic magmatic water; VV is volcanic vapour. Path A shows evolution of ocean water to formation water. Path B suggests mixing of magmatic with meteoric water.

involved in fossil hydrothermal systems can be sampled from fluid inclusions in minerals, but this is fraught with various limitations (Faure 2003). The use of gangue minerals with hydroxyl (OH^-) groups is generally less error-prone. In that case, however, the mineral/fluid fractionation factor must be known. Later isotope exchange with passing fluids (e.g. the common flooding of cooling magmatic bodies and of hydrothermal systems by meteoric and formation waters) needs to be investigated. Ore formation systems involving high pressure fluctuations (e.g. Sibson's "seismic pumping") are characterized by wide variations in D/H fractionation between water and minerals (Horita *et al.* 1999). This is intensified at conditions above the critical temperature of water and generally with fluids of very low "gaseous" density (Driesner 1997).

Carbon isotopes

Carbon consists of the stable isotopes ^{12}C and ^{13}C. Because of its short half-life (5730 years), age dating with cosmogenic ^{14}C is limited to very recent geological processes. The origin of carbonate minerals and rocks is investigated by stable carbon and oxygen isotope fractionation relative to the PDB standard (belemnites found in the Cretaceous Peedee Formation, Carolina, USA). Consequently, marine carbonates have $\boldsymbol{\delta}_{PDB}$ values about zero, mantle carbon about −7‰ and kerogen between −20 and −30‰. Hydrothermal carbonate carbon varies from −6 to −9‰ indicating a deep origin of the CO_2. However, the source signal may be veiled by inorganic isotope fractionation of carbon, which is a function of oxygen partial pressure, temperature, pH, ionic strength and carbon concentration, complicating genetic interpretations. Comparative investigations of the large travertine deposits near Florence, Italy and warm (29–34°C) springs in the same area that deposit travertine (Guo *et al.* 1996), provide an instructive example. Recent calcite shows an increase of ^{13}C with higher distance to the spring orifice, due to two factors: i) simple degassing ($^{12}CO_2$ evaporates preferentially, whereas $^{13}CO_2$ is retained in the solution and collects in the travertine); and ii) bacterial fractionation. Bacteria predominantly abstract ^{12}C from the solution, so that $\boldsymbol{\delta}^{13}C_{Calcite}$ is increased compared to abiotic processes.

Sulphur isotopes

Sulphur isotopes provide genetic information on sulphides and sulphates of ore deposits. Standard is troilite (FeS) from the Cañon Diablo meteorite that has about the same $^{34}S/^{32}S$ ratio as the Earth's mantle. Therefore, basalts and other mantle magmas and sulphide ore deposits derived from them have $\boldsymbol{\delta}^{34}S$ near zero. Clearly different is sulphide sulphur produced by organic fractionation with $\boldsymbol{\delta}^{34}S$ from −20 to −30‰ (the so-called "bacteriogenic sulphur"; Canfield & Thamdrup 1994) and marine sulphates with +10 to +30‰. This is why the origin of sedimentary sulphur can often be determined with high precision. Magmatic and hydrothermal ore deposits may contain sulphur of mixed origin, veiled by inorganic fractionation. The isotope fractionation between cogenetic sulphide minerals, or sulphides and sulphates can be a useful geothermometer (Zheng 1991).

Strontium isotopes

Strontium isotopes also provide evidence of the derivation of ore solutions. The system comprises radiogenic ^{87}Sr, a decay nuclide from ^{87}Rb, and the stable ^{86}Sr. It is the base of a widely used method of age determination. In hydrothermal ore deposits, the ratio $^{87}Sr/^{86}Sr$ is a means of characterizing fluids that formed carbonates (Ca, Mg, Fe), sulphates (Ca, Ba, Sr), fluorite and apatite. Samples used should have extremely small rubidium content. The $^{87}Sr/^{86}Sr$ ratio of large source reservoirs such as the Earth's mantle, continental crust and seawater are quite different. Seawater displays systematic variations in geological time. On that basis, hydrothermal and marine-sedimentary carbonates can be distinguished. Analysis of time-dependent diagenetic processes is possible (Schreiber & Tabakh 2000).

Lead isotopes

Lead isotopes are an especially powerful tool to trace metal sources in mineral deposits, because their geochemical behaviour in aqueous fluids resembles that of many associated metals (e.g. Zn, Cu, and Ag). Also, traces of lead are ubiquitous in most rocks and in many ore minerals. Terrestrial lead consists of four stable isotopes:

- 1.0–1.6 wt.% ^{204}Pb, primordial (not radiogenic), used as a reference base;
- 20.8–27.4% ^{206}Pb, radiogenic decay product of ^{238}U;
- 17.6–23.6% ^{207}Pb, radiogenic decay product of ^{235}U;
- 51.2–56.2% ^{208}Pb, radiogenic decay product of ^{232}Th.

Because of the minimal mass difference between lead isotopes, fractionation by geological processes is very small. Their inherent useful information rests in formation and mixing of the radiogenic isotopes. Both are controlled by properties of the source rocks, including age, lithology (Chiaradia & Fontboté 2003) and geochemistry (uranium and thorium content). Uranium concentrations in the source are described by μ-values (the ratio ^{238}U/^{204}Pb). Because uranium and thorium are markedly lithophile elements, they are enriched in the continental crust (with high μ) relative to the mantle. The evolution of present-day lead started with the primordial or meteoritic composition ~4550 Ma BP (before present), which is derived from troilite in the Cañon Diablo meteorite (like sulphur isotopes). Since then, radiogenic lead increased because of uranium and thorium decay in the major geological reservoirs (mantle, lower and upper crust). Without any disturbance, ordinary lead is the result. When ordinary lead is separated from uranium and thorium, and concentrated in ore deposits (e.g. as galena), its isotopic composition reveals both the age of mineralization and the source reservoir of the lead ("plumbotectonics", Zartman & Doe 1981). "Single stage lead" is derived by single-phase extraction from a very large reservoir, probably continental lower crust or uppermost mantle and is present in a number of large ore deposits (e.g. Mt Isa, Broken Hill, Australia). Other ore deposits have lead of an anomalous composition, which originated by multi-stage processes. Typically, anomalous lead provides model ages that are clearly different from the geological age. Two extremes shall serve as an example:

> An unusually high radiogenic fraction was found in lead of the Tri-State mining district (USA). Its source is thought to lie in uraniferous Cambrian sandstones and Precambrian basement rocks that had a very low content of ordinary lead. Therefore, the migrating hydrothermal brines took up the easily soluble radiogenic lead from decayed U-Th phases. Lead model ages of the resulting galena plot in the geological future, whereas the mineralization took place in the Late Palaeozoic (Symons *et al.* 2005). In the mining district of Bleiberg, Austria, the lead model age is Mesopalaeozoic, but the ore deposits clearly formed much later, in Triassic time. It is assumed that the lead of Bleiberg is derived by leaching of feldspars in Palaeozoic gneisses that contain up to 50 ppm Pb, but very little uranium (<1 ppm U + Th). Therefore, hardly any radiogenic lead was available for extraction by the hydrothermal solutions.

Accordingly, lead model ages are very often not "dates", but nevertheless provide important information on ore genesis. Lead isotopes may indicate the source of the metal and this is an essential element of genetic modelling (cf. Everett *et al.* 2003).

Many other isotope systems provide deeper insight into ore forming processes. Examples include chlorine (Nahnybida *et al.* 2009, Banks *et al.* 2000), nitrogen (Jia *et al.* 2003), iron (Johnson *et al.* 2009, 2008, Staubwasser *et al.* 2006, Beard *et al.* 2003) and boron (Perez Xavier *et al.* 2008). Subrecent geological processes (younger than ~20 Ma), such as the age of supergene ore deposits, are investigated with cosmogenic nuclides (e.g. ^{10}Be, ^{14}C, ^{26}Al, ^{36}Cl and ^{129}I; Siame *et al.* 2006, Muzikar *et al.* 2003) and with the uranium-series disequilibrium method (Reich *et al.* 2009). Typically, results reveal extraordinarily long durations of supergene processes, although hardly at constant rates.

Methods of genetic investigations (2)

Temperature and pressure of hydrothermal ore formation

Apart from geochemical parameters, temperature and pressure of a hydrothermal system are essential determinants of solubility, transport and precipitation of elements and compounds. In order to understand such systems, formation temperature and pressure have to be measured. Unfortunately, there are relatively few methods that allow the precise determination of pressure, but the reverse can be said concerning temperature. Conventional petrologic geothermometers and geobarometers can rarely be applied to hydrothermal mineralizations.

Frequently employed "geothermometers" of economic geology include:

- microthermometry of fluid inclusions in minerals;
- cation-exchange geothermometers, indicating the temperature of the last equilibration of fluids with host rocks (e.g. silica: Fournier & Potter 1982; magnesium-lithium: Kharaka & Mariner 1990);
- trace element geothermometers (e.g. Ti-in-zircon for very high temperatures: Watson *et al.* 2006);
- different modifications of minerals (e.g. α- vs. β-quartz at 573–600°C);
- exsolution or unmixing of phases during cooling (e.g. cubanite lamellae in chalcopyrite that formed at >205°C);
- oxygen, silicon and sulphur isotope fractionation in cogenetic minerals (stable isotope geothermometry);
- the distribution of certain elements in cogenetic minerals (e.g. Fe-Zn-S or Au-Ag-S systems; As-contents, e.g. in arsenopyrite);
- chlorite and muscovite mineral geothermometers.

All of the above-mentioned geological thermometers are inaccurate due to factors that control the results but cannot be precisely determined. It is best practice in economic geology to combine several methods, for example microthermometry of fluid inclusions (Roedder 1984, Samson *et al.* 2003), the arsenopyrite geothermometer (Kretschmar & Scott 1976) and the fractionation of stable isotopes.

Fluid inclusions

During formation of minerals from fluids or solutions, irregularities on growth planes often cause inclusion of tiny droplets of the parent liquid (primary inclusions). Quite common are also inclusions that are hosted by microfractures in a mineral (secondary inclusions). Fluid inclusions are usually very small (below 100 μm), so that investigations are carried out on polished thin or thick sections using a microscope. At room temperature, many inclusions contain an aqueous liquid with a gas bubble that occupies ~10–40% of the volume (type 1 of Figure 1.24). Upon heating of the sample, the bubble disappears at a determinate temperature that is described as the homogenization temperature Th. In the simplest case, Th is equal to the formation, or trapping temperature Tt, because the bubble results from cooling and shrinking of the hot inclusion within a volume fixed by the surrounding host mineral. However, Th is only the minimum temperature of trapping since pressure at the time of formation controls size and density of the bubble. An accurate determination of the formation temperature is only possible if the formation pressure is known and the so-called pressure correction can be calculated (actually, this is a correction of temperature as a function of pressure: Roedder 1984). The density of the inclusion, its degree of fill (liquid vs. total volume), the salinity of the liquid (mostly due to dissolved NaCl, but Mg, Ca, K, etc. may be involved), the presence of daughter crystals (common are halite cubes: type 3 in Figure 1.24), of fluid hydrocarbons and contents of non-aqueous gases (frequently CO_2, followed by CH_4, N_2, etc.) are all needed for a full understanding. Investigations must also address the identification of groups of associated inclusions that were trapped from a fluid of the same composition at the same time, temperature and pressure (a "fluid inclusion assemblage" or FIA). Natural minerals

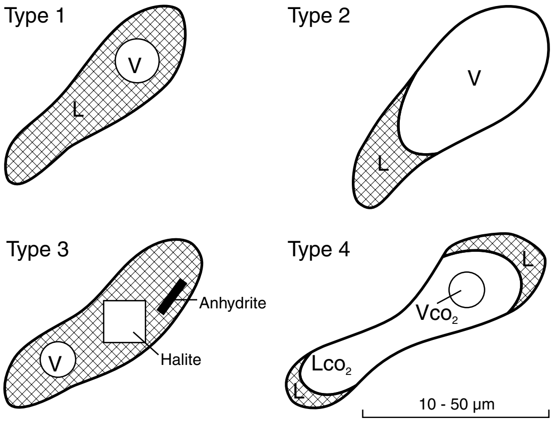

Figure 1.24 The four most common types of fluid inclusions as they appear under the microscope at room temperature.

typically contain many different FIAs, which reveal the evolution of a hydrothermal system.

Most fluid inclusions observed in hydrothermal ore deposits belong to one of four groups (Figure 1.24):

1 *Type 1*: Liquid (L) aqueous inclusions of low to moderate salinity (<26.5 wt.% NaCl, which marks saturation at room temperature), a water vapour bubble (V) and a density of $\sim$1 g/cm^3;

2 *Type 2*: Water vapour occupies >60% of the inclusion volume, the salinity is similar to type 1; the density is clearly <1 g/cm^3; if types 1 and 2 (or 2 and 3) are cogenetic in the same sample, true boiling (as opposed to effervescence of a dissolved gas like carbon dioxide or methane in water) of the solution below the critical point or at boiling curve conditions is indicated; this gives rise to the term "boiling assemblage" (Figure 1.25);

3 *Type 3*: Highly saline (26.4 to >50 wt.% salinity) aqueous inclusions with halite daughter crystals and with a high density; fluids of this nature can result from dissolution of evaporites, seawater evaporation, segregation of brines from melt at magmatic temperatures (Audétat *et al.* 2008), by formation of residual brines because of vigorous

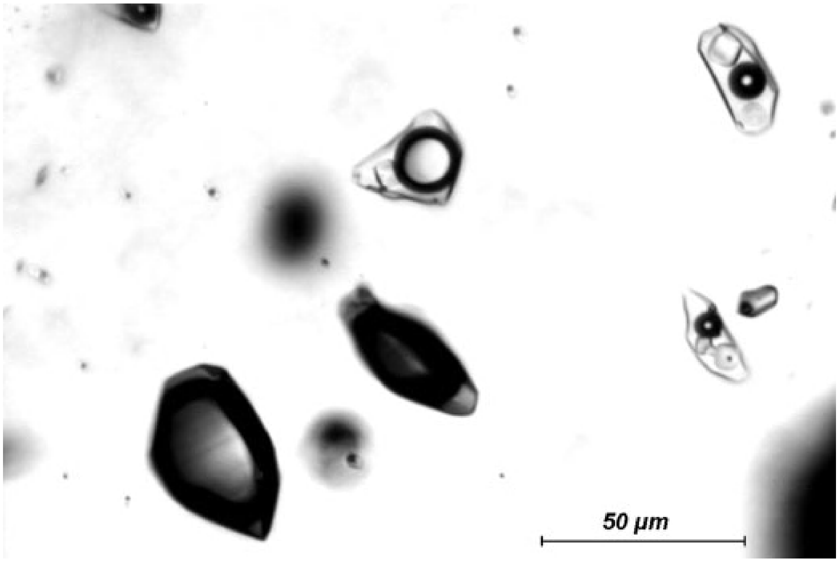

Figure 1.25 Fluid inclusion assemblage (FIA) formed by subcritical boiling in quartz from miarolic cavities in the barren Torres del Paine granite (Patagonia, Chile). Vapour (dark), concentrated Cu and As, whereas the brine inclusions marked by halite crystals are enriched in metals such as Mn, Fe and Zn (Lüders *et al.* 2005). Courtesy Volker Lüders, GFZ Potsdam.

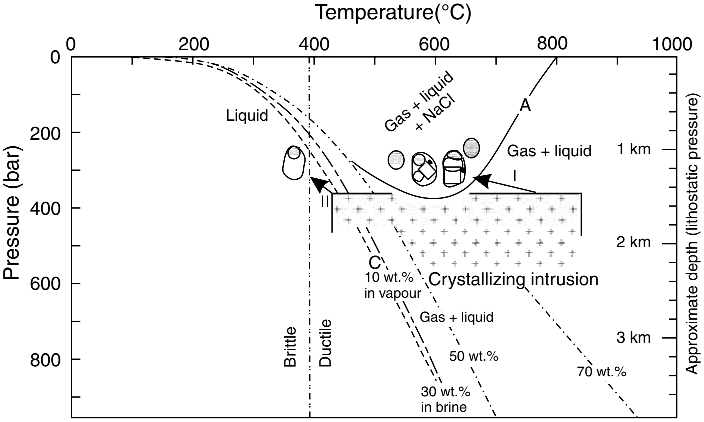

Figure 1.26 A crystallizing shallow intrusion may exsolve (I) early and very hot brines, or (II) later saline fluids of intermediate temperature, resulting in characteristic fluid inclusions (after Brathwaite *et al.* 2001). With kind permission from Springer Science + Business Media.

subcritical boiling (abstraction of vapour causes concentration of salt in the liquid phase and by supercritical phase separation;

4 *Type 4*: CO_2-rich inclusions, with little water; at room temperature carbon dioxide in the inclusions occurs in both liquid (L_{CO_2}) and gaseous phase (V_{CO_2}).

In Figure 1.26, path I is entered by very hot, hypersaline magmatic liquids (±vapour). Above the phase boundary A, cogenetic type 2 and type 3 fluid inclusions segregate. Path II illustrates the fate of late, less saline and much cooler fluids. Part of these may be derived from vapour that because of cooling contracts at higher pressure into the liquid phase. Inclusions trapping these fluids are type 1 with low to intermediate salinity (3–20 wt.% NaCl). Phase boundaries between liquid and gas+liquid are shown for different salt contents. Boiling assemblages must have formed at a point along such a phase boundary. C is the critical point for an aqueous solution with 10 wt.% NaCl.

The salinity of 26.4 wt.% separating type 1 and type 3 inclusions is the solubility of NaCl in water at room temperature (20°C). In practice, the presence of other salts, such as $CaCl_2$ lowers the NaCl saturation to ~23 wt.%. The salinity of fluid inclusions is determined by freezing with liquid nitrogen and remelting, i.e. the temperature is allowed to rise back to ambient conditions. Because dissolved salts depress the freezing point (Bodnar 1993, Potter *et al.* 1978), the melting temperature of ice (Tm ice) provides a precise measure of salinity. Results are expressed in the form of equivalent weight percent of NaCl (wt.% NaCl equiv.). The chemical determination of the composition of inclusions is complicated by the tiny mass of individuals. Yet, a number of methods are available; most advanced is the approach with laser ablation (LA) connected to ICP-MS (Sylvester 2008, Audétat *et al.* 1998). Merging the data with results from high-resolution investigations of the hydrothermal paragenesis (e.g. SEM-CL, Scanning Electron Microscope-Cathodoluminescence: Rusk & Reed 2002) allows a detailed unravelling of the chemical and physical evolution of a hydrothermal system.

The investigation of fluid inclusions is somewhat restricted by the need for samples that are transparent to visible light, thus excluding most ore minerals. Of the opaque oxides, sulphides and sulphosalts only few, such as wolframite, iron-rich sphalerite, and antimonite are transparent for infrared light and can be examined with the methods described above (Figure 1.27). The result is that most fluid inclusion investigations are based on gangue and not on ore minerals. This may introduce severe errors (Wilkinson *et al.* 2009), for example if ore and gangue formed from differing fluids (Lüders 1996). Other problems are connected with post-formation changes of the inclusions, for example by renewed equilibration at different P/T-conditions. Metamorphic shearing and recrystallization often destroy fluid inclusions. Even synmetamorphic inclusions in mobilizates are usually decrepitated because of pressure

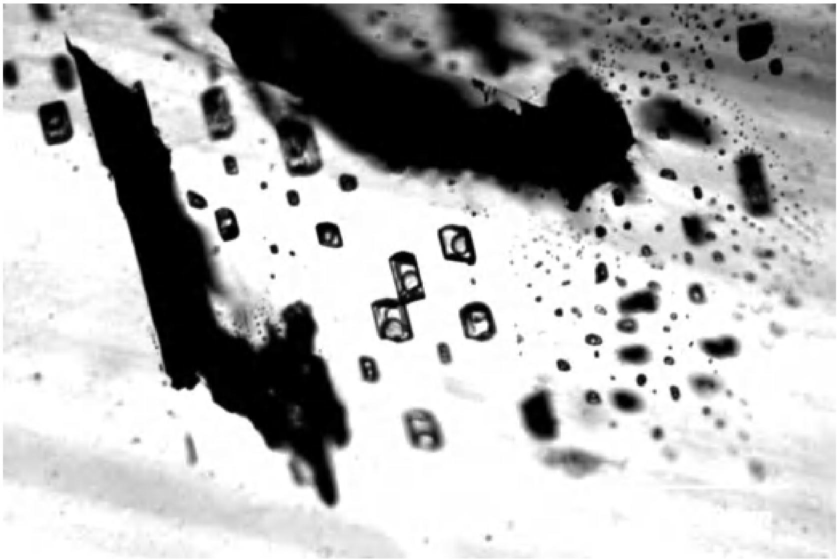

Figure 1.27 Aqueous fluid inclusions in wolframite of Panasqueira mine, Portugal, studied by near-infrared microscopy. The fluids homogenize between 320 and 325°C and have a salinity of ~12% NaCl (Lüders 1996). Note the large vapour bubbles in inclusions which resemble type 2 of Figure 1.24. Courtesy Volker Lüders, GFZ Potsdam.

release during uplift (e.g. Joma Mine, Norway: Giles & Marshall 1994). However, in spite of many obstacles, petrographic and microthermometric work on fluid inclusions brought great advances of understanding hydrothermal ore deposit formation. Even eminently practical questions can be solved, such as the differentiation between mineralized and barren veins.

The broad application of microthermometric methods suppressed the older decrepitation analysis. Its principle was to count acoustic emissions, while a mineral was submitted to stepped heating. Because each micro-acoustic signal is due to a bursting inclusion, maxima were taken to indicate roughly the temperature of formation. Of course, precise genetic data cannot be obtained with this method. But as decrepitation analysis is relatively simple and gives quick results, it may be a valuable tool in exploration. In the Cowra Gold District, New South Wales, Australia, auriferous veins can easily be distinguished from sterile quartz veins, because the first contain much more CO_2 and display a unique decrepitation pattern (Mavrogenes *et al.* 1995).

Traditionally, hydrothermal ore deposits were grouped according to assumed formation temperatures into hypo- or katathermal (500–300°C), mesothermal (300–200°C) and epithermal (below 200°C). This classification was quietly abandoned, while a wealth of data has been acquired on real temperatures of hydrothermal processes and resulting deposits. Temperatures vary widely, even during the lifetime of one single hydrothermal system. Accordingly, temperature is a poor criterion for classification, although, of course, an integral part of the description of the formation of mineral deposits. In many scientific reports, the terms named above are still used in a very wide sense, indicating rather depth than temperature. In this usage, epithermal deposits are those formed in the uppermost part of the crust (<1 km from the surface) and below 200°C (but note that the most important member of this class, the "epithermal gold deposits", typically originated at ~300°C). "Meso-" and "hypothermal" describe increasing depth and temperature. However, depth and temperature are not always correlated. Fluids in shallow porphyry copper deposits, for example, may originally have had a temperature approaching 800°C (Figure 1.26). Clearly, depth (or pressure) is a much more useful criterion to describe related groups of hydrothermal deposits. Therefore, Gebre-Mariam *et al.* (1995) suggested to adopt the terms "epi-, meso- and hypozonal" (Table 1.2), similar to the notations referring to metamorphism or the intrusion depths of granites. The

Table 1.2 Depth-zone classification of hydrothermal mineral deposits

Epizonal	150–300°C	0.5–1.5 kbar	<6 km depth
Mesozonal	300–475°C	1.5–3.5 kbar	6–12 km
Hypozonal	475–700°C	3–6 kbar	>12 km

Temperature is not a classification criterion. T-values given here apply to epigenetic Archaean gold deposits only (Gebre-Mariam *et al.* 1995).

proposal was aimed at epigenetic Archaean gold deposits, but could be advantageously used for all hydrothermal mineral deposits.

Formation pressures

Rarely, formation pressures of hydrothermal ore deposits can be precisely measured. Usually, geological estimates are derived from the assumed depth of formation and lithostatic or hydrostatic boundary conditions. Other approaches include modern methods of metamorphic petrology in combination with fluid inclusions data. If the minerals are present, methods such as the sphalerite-pyrite-pyrrhotite geobarometer can be applied (Lusk *et al.* 1993): Between 300 and 600°C, the FeS-content in sphalerite in contact with pyrite and pyrrhotite is only a function of pressure. Isochores of fluid inclusions (lines of constant volume and density in P-T space) can be intersected with independent data, such as the solidus temperature of the parental granite (Audétat *et al.* 2008). Some fluid systems allow pressure analysis based on experimental data of thermodynamic properties of synthetic fluids similar to natural inclusions; simple systems, such as H_2O-NaCl provide a good approximation, but high vapour and gas contents cause large error margins. Unambiguous evidence of boiling still provides the most accurate geobarometry data available (Roedder 1984).

Methods of genetic investigations (3)
Mineral succession, textures and structures of hydrothermal mineral deposits

The precipitation of minerals from hydrothermal solution is controlled by various boundary conditions, some of which have been discussed earlier. For a reconstruction of the conditions at a point in time and for the whole duration of hydrothermal activity, minerals that formed simultaneously (the paragenesis) must be strictly discerned from the sequential order of mineral assemblages (the paragenetic sequence). Macroscopic observations of mine exposures and hand specimen, ore microscopy and other mineralogical techniques are combined to resolve the evolution of hydrothermal systems.

Because most ore minerals are opaque, microscopic examination is usually based on polished specimen and reflected light. This allows resolution of the intergrowth of different minerals. The position of minerals in one paragenesis or in the whole paragenetic sequence is revealed by observations that include exsolution, replacement along grain boundaries or microfractures and many other textures and structures. Ore microscopy has attained a level of very high perfection (Craig & Vaughan 1994, Ramdohr 1980, Stanton 1972). Methods, such as electron probe microanalysis (EPMA), transmission electron microscopy (TEM), scanning electron microscopy – cathodoluminescence (SEM-CL) and other methods of mineralogical analysis (e.g. QEMSCAN, CSIRO, Australia), confirm and complement optical determination. Even greater resolving power is available with 100-nm-resolution secondary ionizing mass spectrometry (nanoSIMS; Barker *et al.* 2009).

Macroscopic features that assist in establishing the mineral succession include overgrowths and crusts, symmetric vein fillings and cross-cutting relations of veins. This is supplemented by colour, texture type and grain form or crystal habit of minerals, and by examination of fluorescence and luminescence. Because quartz is an important part of most hydrothermal parageneses, recording its structures and textures is most instructive (Dong *et al.* 1995). Combined with results of microthermometry, trace and isotope geochemistry and geological investigations, the evolution of an individual hydrothermal ore deposit can be resolved.

Open space filling is a characteristic feature of many hydrothermal ore deposits. The term implies that precipitation of minerals occurred in open fissures, pipes or caves, which acted as flow channels for hydrothermal solutions. Open space

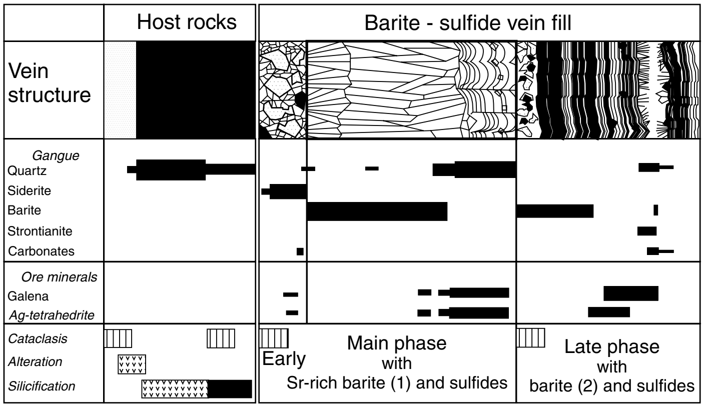

Figure 1.28 Parageneses and paragenetic sequence of Tertiary rift-related lead-silver-barite veins in the Caroline mine, near Freiburg, Germany (modified from Germann *et al.* 1994). With kind permission of R. Lang and LGRB Freiburg.

filling starts with nucleation of minerals on a solid surface of the flow channel walls. This explains the often observed younging of the mineral succession towards the centre. In Figure 1.28, different parageneses of a specific phase of vein formation can be read vertically, whereas the horizontal axis reflects evolution in time (from left to right; crystals in the open space on the right represent the youngest hydrothermal minerals and the vein's symmetry axis). Banding of hydrothermal precipitates results from variations of physical and chemical conditions in time. Tectonic movements during hydrothermal activity cause fracturing of earlier minerals and cementation by younger precipitates. Fibrous texture of minerals, such as quartz aligned vertically or obliquely to vein margins, indicates synchronized opening and mineral growth. In near-surface hydrothermal channels, clastic sediments have been observed that indicate high flow velocity of hydrothermal solutions. Hydrothermal sediments formed in this way include bedded rock flour, clay, sand, solid hydrothermal precipitates and even gravel (pebble dykes). Mainly epizonal features include hydrothermal breccias that may host fabulous orebodies. Many breccias were formed by self-sealing of flow paths and consequent phreatic explosions.

Sedimentary textures of material filling open spaces of hydrothermal veins are not rare (e.g. in the fluorite vein at Rossignol, France). This occurs when solid material is eroded, or when minerals and colloidal particles nucleate in suspension from ascending fluid. Sedimentation of these particles depends on the ratio of the upflow speed of the fluid to gravitational settling of the particles. Stoke's law can be used to calculate the settling velocity (V) of the particles, allowing an estimate of the fluids' upflow velocity (eq. 1.4). Suspended minerals nucleating and growing in fluids settle to produce "blocky" vein textures (Okamoto & Tsuchiya 2009).

Settling velocity of particles in a fluid:

$$V = \frac{1}{18} \cdot \frac{(\sigma - \rho) g . D^2}{\mu} \tag{1.4}$$

V = free-falling velocity (m/s), σ = density of the particle, ρ = density of the fluid, D = particle diameter (m), g = acceleration due to gravity (m/s^2), μ = viscosity of the fluid (m^2/s).

Hydrothermal open space deposits are usually coarsely crystalline. In certain deposits, minerals may occur in dense, reniform-botryoidal and banded crusts, often with fissures due to shrinkage. Such textures are described as "colloform" and are thought to imply formation from a gel (a hydrosol with a mechanical resistance). Such precipitates are amorphous and may gradually mature into crystalline phases (i.e. opal, wood tin and garnierite) or into proper minerals including chalcedony, reniform sphalerite and malachite. Often, but not necessarily always, the origin of colloform substances may be traced to colloids forming in the hydrothermal fluids. It is also possible that coagulated colloids are transported with the hydrothermal flow and deposited higher up as a gel. Colloidal particles in water typically have a free negative charge, which leads to electrostatic repulsion and dissipation (Ranville & Schmiermund 1999), similar to heat energy. While the formation of aggregates may be due to van der Waals forces, neutralization of the charge (by mixing with an electrolyte, pH-change, cooling, etc.) frequently effects aggregation and precipitation as a gel. Some hydrosols form "colloidal crystals". Apart from colloids, hydrosols and gels, botryoidal textures may be inherited from microbial mats (Labrenz *et al.* 2000). Obviously, different ways may lead to formation of a colloform mineralization.

The characteristic banding of many colloform precipitates may be due to external factors, but also to self-organization. Heany & Davis (1995) propose that the banding of agate, which is a rhythmic succession of chalcedony and quartz, is the product of a changing degree of polymerization of the solution on the tips of the growing chalcedony fibres. Polymerization decreases when chalcedony is rapidly deposited, so that the system flips to slow quartz precipitation from a monomeric solution. In this phase, diffusion slowly raises the concentration of the solution until the state of a concentrated polymeric solution is again reached. Colloform SiO_2 can also form from "silicothermal fluids" (Wilkinson *et al.* 1996). These are liquids with $\sim$90% SiO_2 that co-exist with an aqueous supercritical fluid in a wide temperature field ($\sim$400 to $>$750°C). Silicothermal fluids might be the explanation of the high frequency of amorphous silica phases in epizonal and especially in epithermal ore deposits.

Replacement of earlier solid phases is very common in hydrothermal ore deposits. As one mineral is dissolved, another forms in the same place, often without a change of volume and with conservation of very fine textures (pseudomorphism). Characteristic examples include cassiterite replacing orthoclase (Cornwall, England) or even crinoids (New South Wales, Australia), scheelite after wolframite, and from low-temperature solutions, the silicification and pyritization of whole tree trunks in coal seams. The term "replacement, or metasomatic ore deposit" is only used if the process produced most of the actual ore. Carbonates are frequently the subject of replacement because of their disposition for chemical reactions. Advection and evacuation of matter is usually enacted by physical flow but diffusion can also play a role.

The waning stages of hydrothermal systems typically display falling temperature, lower mass flow, pervasive fracturing and cataclasis, and often infiltration of oxidizing meteoric water. This leaves fractures and thin fissures of the hydrothermal vein mass covered by films of goethite, haematite or manganese oxides.

Methods of genetic investigations (4)

Hydrothermal host rock alteration

Host rocks influence hydrothermal solutions to the point of controlling the site of ore precipitation, but at the same time they are affected by alterations that emanate from the solutions. The resulting changes ("hydrothermal alteration") may extend from only centimetres off the flow channel (Figure 1.29) to very wide halos in the case of pervasive flow. Alteration zones are important clues for ore deposit exploration and for the prospectivity of an area (Lentz 1994). Some alteration halos can be mapped by remote sensing from space. Hydrothermally altered rocks are often so fine-grained that even the microscope may not suffice in revealing the constituent minerals. Portable SWIR (short-wave infrared) spectrometers are routinely used to determine alteration parageneses.

The changes concern colour, texture, mineralogical and chemical composition including stable isotope ratios in different combinations. The end product is a function of the nature of both the solutions (pH, Eh, T, pressure, dissolved matter) and of the affected rocks (mineralogy, permeability, porosity). Ion exchange is ubiquitous, implicating an open system with import and export of matter (Anthony & Titley 1994). Dissociated water plays an eminent role, because of reactions with silicate minerals that include incorporation of OH^- groups and exchange of cations with H^+ (hydrolysis). Frequently, altered rocks display a zebra-like pattern of rhythmic banding, which is

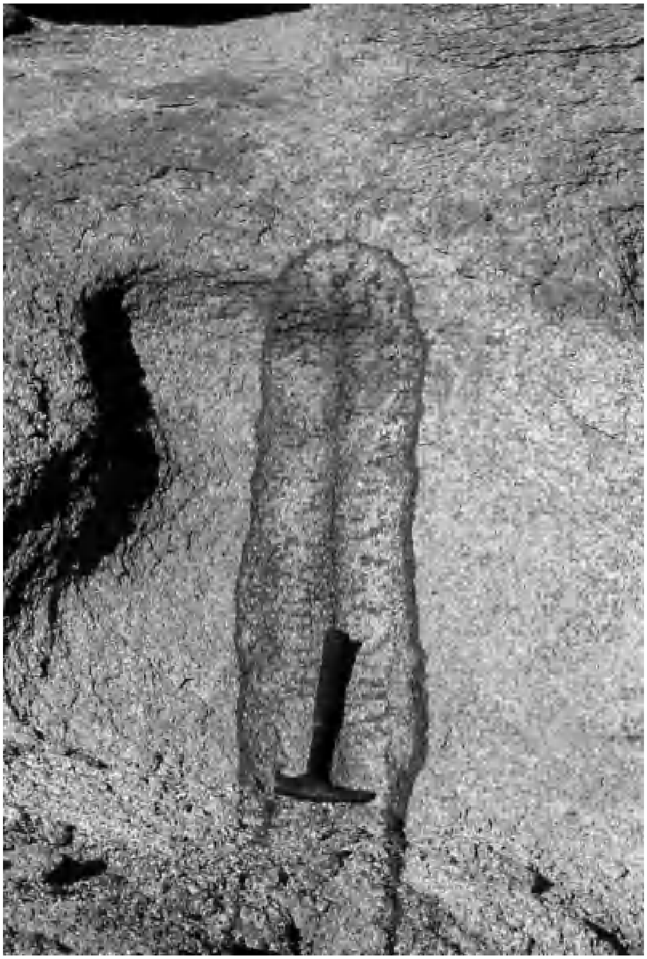

Figure 1.29 (Plate 1.29) The essence of hydrothermal alteration visible at outcrop-scale, depicted by the halo centred on a small fissure branching off from formerly exploited wolframite-quartz veins in Panafrican granite at Gash Emir, Red Sea Hills, Sudan. Note the enhancement by later supergene oxidation.

caused by coupling of diffusion with precipitation reactions (Kapral & Showater 1995). Hydrothermal alterations also affect mass and volume of the altered body, with the possibility of a positive or negative balance. Calculation of the balance relies on assumed immobility of specific elements (e.g. zirconium, titanium). By comparison of concentrations in unaltered rock and in its altered equivalent, enrichment or dilution can be calculated (Herrmann *et al.* 2009).

In many cases, hydrothermal solutions are weakly acidic because of fluorine or CO_2 contents and dissociation of water. In that case, carbonates, zeolites, feldspathoids and calcium-rich plagioclase are especially prone to alteration. Pyroxene, amphibole and biotite are somewhat more stable, whereas albite, K-feldspar and muscovite are relatively resistant. Quartz is rarely affected.

Alteration of pervaded rocks before the solutions reach the site of ore formation may extract trace metals that are then concentrated in the ore. It is quite possible that many ore deposits are a product of this process (e.g. cassiterite ore produced from aqueous solutions that have passed through tin granite bodies: Lehmann 1990). Examples of trace elements that are incorporated in minerals include copper and zinc in biotite, amphibole, pyroxene and magnetite, lead in K-feldspar and accessory uranium minerals, tin in mica and ilmenite, tungsten in biotite, fluorine in amphibole and mica, and barium in mica and feldspar. Based on appropriate data, genetic ore formation models incorporate such relations.

Not only ascending hypogene hydrothermal solutions may cause host rock alteration. Some alterations are the product of downward-percolating waters. Examples include solutions formed from magmatic-derived HCl, HF, H_2S and SO_2 steam condensating into, and heating shallow groundwater. Resulting strong acids cause acid-sulphate alteration, characterized by alunite (eq. 1.5), typically in near-surface epithermal gold ore-forming systems (Mutlu *et al.* 2005).

Alunite formation under extremely acidic hydrothermal conditions:

$$\underset{\text{K-feldspar}}{KAlSi_3O_8} + 2Al^{+3} + 2H_2SO_4 + 4H_2O \rightarrow \underset{\text{Alunite}}{KAl_3(SO_4)_2(OH)_6} + 3SiO_2 + 6H^+ \quad (1.5)$$

Hydrothermal host rock alterations include the less visible change of increased maturation of dispersed organic matter (kerogen) under the influence of heat imported by the solutions (Heroux *et al.* 1996). Along flow paths and around orebodies, the induced thermal anomaly can be mapped by appropriate methods, for example increased reflectance of organic particles (cf. Chapter "The Coalification Process").

Spatial zonation of alteration types

Spatial zonation of alteration types has an outstanding role in ore deposit investigations. Alteration zoning illustrates changing chemistry of the solutions by reactions with wall rocks, and different physico-chemical boundary conditions (temperature, pressure, etc.). Zoning is an extremely useful guide and spatial vector pointing to ore, as this is always connected with a certain type of alteration. Zonation is best illustrated by the classical alteration model of porphyry copper ore deposits.

There are many different hydrothermal alteration types (Thompson & Thompson 1997). Some characterize certain ore deposits, while others are linked to the presence of specific rocks. Propylitization, for example, typically affects andesite and diorite, listwaenitization ultramafic rocks and dolomitization limestone. The names given to alteration types are mainly derived from the most noticeable newly formed mineral, but some have their own traditional rock names (e.g. greisen, propylite). Important examples of hydrothermal wall rock alteration include:

- *Silicification* is the permeation of host rocks with dissolved silica, resulting in increased contents of opal, chalcedony or quartz. The rocks often obtain the aspect of quartzites. Silicification is very frequent around epithermal gold deposits.
- *Albitization* (or sodic alteration) often affects magmatic rocks by replacing more calcic with sodic plagioclase, but albite (± chlorite, epidote, etc.) may be introduced into most rock types. The source of the sodium may be seawater, evaporative brines, or dissolution of salt bodies and transport by basinal or metamorphic brines. Also, sodium is enriched in liquids and fluids segregating at high temperatures from crystallizing magmas.
- *Argillic alteration* is the conversion of rock-forming silicates into clay minerals. Two variants are distinguished, advanced and intermediate argillization. In the first case, the core of the altered rock body typically consists of alunite and quartz, and is surrounded by argillic zone minerals nacrite, dickite, kaolinite and pyrophyllite with variable contents of sericite, pyrite, tourmaline and topaz. The agents are strong acids, which impose a nearly total loss of alkali elements and aluminium enrichment. Advanced argillization is often found with gold or tin mineralization. Intermediate argillization is marked by conversion of feldspars to kaolinite (proximal to main flow channels) or montmorillonite (in a distal position). Extending into the distance, a propylitization halo is often developed.
- *Propylitization* may affect large rock masses in the wider vicinity of ore deposits, by imparting a greenish tinge. It is a complex alteration with neoformation of chlorite, epidote, albite and carbonates (calcite, dolomite, ankerite), which was first observed in diorite and andesite near gold deposits. If one of those minerals prevails, terms such chloritization can be applied and mapped as subzones.

- *Sericitization* is a common alteration of aluminium-rich felsic rocks (granite, gneiss, schists). The typical paragenesis comprises sericite and quartz (± pyrite). The involved solutions were acidic and leached part of alkali element contents (Ca, Na and part of K; eq. 1.6).

Sericitization of K-feldspar:

$$\underset{\text{K-feldspar}}{3KAlSi_3O_8} + 2H^+ \Rightarrow$$

$$\underset{\text{Sericite}}{KAl_2(AlSi_3O_{10})(OH)_2} + 2K^+ + 6SiO_2 \qquad (1.6)$$

- *Greisenization:* Acidic, fluorine-rich solutions reacting with felsic rocks convert feldspar to topaz. Medieval tin miners in the German Erzgebirge called the resulting grey rock *greisen*. Greisen is a massive or vuggy rock that consists of quartz, topaz and light mica (muscovite or lepidolite). Accessory tourmaline, fluorite, rutile, cassiterite and wolframite are common. Tin and tungsten enriched greisen bodies can be profitable ore (Halter *et al.* 1996).
- *Dolomitization* is the prevalent alteration of limestone adjacent to lead-zinc ore deposits. It is due to import and exchange of magnesium for part of calcium (e.g. Navan, Ireland: Braithwaite & Rizzi 1997).
- Silicate rocks react with CO_2-rich solutions by carbonatization. Calcite, dolomite and ankerite (more rarely siderite and magnesite) are common alteration products adjacent to gold quartz veins in Archaean and Palaeoproterozoic greenstones (Eilu *et al.* 2001). In practice, the distinction of different carbonate minerals is easiest with colouring techniques (Hitzman 1999). Listwaenitization describes carbonated and silicified ultramafic rocks that may be associated with hydrothermal epigenetic gold mineralization. The altered rocks consist of magnesium-calcium-iron carbonates, chromian muscovite and quartz, with various accessory minerals (Halls and Zhao 1995).
- *Tourmalinization* is common in tin (Lehmann *et al.* 2000a), tungsten and gold deposits. If it is very intensive, tough black rocks ("tourmalinites") result that resist both surficial alteration and the geologist's hammer. Tourmalinites mark the proximity of orebodies. In more distal position, pervasive growth of dispersed tiny needles of tourmaline in country rock is only revealed by the microscope.

The study of hydrothermally altered wall rocks is an important subject of economic geology. These rocks reveal the nature of the hydrothermal solutions, they assist in the search for ore because they present a much larger and hence more visible target compared to the actual orebodies, and they allow dating of ore formation because of neogenesis of minerals such as K-feldspar, alunite and mica. Zonation mapping provides a vector pointing to the site of possible ore. In addition, hydrothermal alteration is always accompanied by the dispersion of trace metals around orebodies. The resulting trace metal halos are excellent lithogeochemical prospecting guides. And last not least, several alteration products are valuable industrial minerals (e.g. alunite, kaolin, sericite and vermiculite).

1.1.7 Skarn- and contact-metasomatic ore deposits

Many ore deposits are formed close to intrusive igneous rock bodies. The location of the ore may be at the immediate contact between the intrusion and its host rocks, or at a certain distance. In the first case, the host rocks will be affected by contact metamorphism due to heating (e.g. the formation of andalusite in slates and schists). If carbonate rocks are present, skarn (a Ca-Mg silicate rock) is frequently formed by decarbonation and addition of silica. This process releases large quantities of CO_2 that may pass into the magma inducing profound changes, for example of fO_2. Massive orebodies may occur in proximity to the skarn (proximal contact-metasomatic ore). The ore replaces carbonate rocks (or skarn) by a process called metasomatism. The replacement is the result of the passage of hot aqueous fluids that are given off by the cooling magmatic body or by dehydrating country rocks. If the metasomatic ore formation takes place at a distance from the intrusion, the ore will less likely be associated with skarn rock. Resulting mineralizations are either distal skarn, or distal contact-metasomatic orebodies.

Skarn is an old Swedish mining term for a tough calc-silicate gangue that is associated with certain Palaeoproterozoic iron and sulphide ores. Swedish skarn consists of coarsely crystalline andradite, diopside, various amphiboles, scapolite, quartz and carbonate. Skarn bodies are stratabound and pass laterally into fine-grained banded exhalites and iron formations that are hosted in a suite of felsic and mafic volcanic rocks, carbonates and clastic metasediments. Compaction structures around skarn garnets indicate very early formation of these skarns already during diagenesis of the rocks (Oen & Lustenhouwer 1992). This is overprinted by later metamorphic reactions. Similar diagenetic skarn rocks occur occasionally with submarine sediment-hosted sulphide ore and represent exhalative precipitates of Ca, Fe, Al and SiO_2 in a reducing, carbonate-poor environment. High heat-flow that induced syndiagenetic skarn mineral formation during ongoing sedimentation was probably caused by synsedimentary intrusion of subvolcanic magma (e.g. mafic sills). Calc-silicate skarn rocks are also common in high-grade metasedimentary rocks, for example at the contact between carbonate and silicate strata. This "reaction skarn" expresses local exchange of matter during essentially isochemical metamorphism.

"Skarn" in the context of economic geology

"Skarn" (in North America also called tactite) commonly describes iron-rich rock bodies of Ca-Mg silicates formed from limestone or dolostone by abstraction of CO_2 and hydrothermal addition of SiO_2, Al, Fe and Mg in the contact aureole of intrusions. Most skarn ore deposits are related to intermediate igneous rocks, but association with granites and gabbros is known (Lentz 1998). Often, fertile plutons show evidence of magma mixing that enhances the generation of hydrothermal fluids (Grammatikopoulos & Clark 2006). Emplacement of a hot magma body in cool country rocks causes the build-up of a thermal halo with outward migrating isotherms, driving off water and other volatiles. During this prograde phase, mainly anhydrous minerals are formed that include grossular-andradite, diopside, forsterite and periclase (MgO, if dolomite was present), and part of the ore. Outward from the intrusion, skarn is followed by a narrow zone of wollastonite and a shell of isochemical recrystallization of the precursor carbonate rock to carbonate marble. The export of matter from the cooling magma into the country rocks is due to hot (maximum >700°C) hypersaline melt, saline fluids and gas (Baker *et al.* 2004). The fluid flow in aureole rocks may be quite complex in $T\text{-}XCO_2^{\text{fluid}}\text{-}t$ space. Commonly, initial heating will produce high XCO_2 followed by subsequent passage of magmatic and even meteoric water (Nabelek 2007). Magmatic waters, i.e. hydrothermal fluids continue to exsolve from the intrusion during further cooling and declining pressure. The aqueous fluids represent a retrograde phase, which is characterized by formation of brucite ($Mg(OH)_2$) after periclase and water-rich silicates (amphibole, epidote, clinochlore, talc, chlorite) replacing earlier anhydrous ones, concurrently with the main mass of the ore. Finally, a system of convective cooling by external, non-magmatic water may be established that imprints low-T hydrothermal alterations.

Limestone and dolostone skarn ores are common. Features that resemble skarn in some aspects are also found at intrusive contacts with intermediate, mafic and ultramafic host rocks, because of their relatively high Ca-Mg contents. Iron formations are generally prone to conversion into skarn as in the Swedish prototype. Archaean iron formations of the Southern Cross greenstone belt in Western Australia host 20 mines and numerous smaller gold skarn deposits, with a total production of >260 t gold (1887–2001). The parent intrusion is a peraluminous two-mica granite (Müller *et al.* 2004). Most skarn bodies occur in host rocks adjacent to an intrusion (exoskarn) but occasionally marginal parts of the intrusions are transformed into skarn because of inward mass transport (endoskarn).

Skarn ore deposits can be related to specific magmas and geodynamic positions: Diorites of primitive island arcs produce mainly magnetite orebodies that may have recoverable contents of Cu, Co and Au. In North America, intermediate to felsic, differentiated within-plate intrusions of active continental margins generated some of

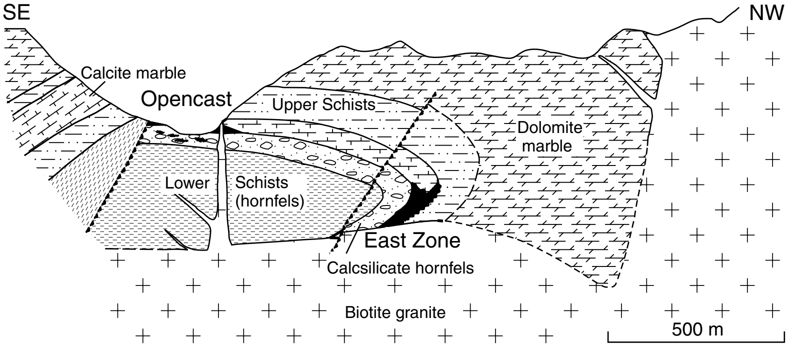

Figure 1.30 Geological section of the scheelite skarn deposit CanTung, North West Territories, Canada (modified from Middelaar & Keith 1990).

the most important tungsten ore deposits Figure 1.30). At CanTung mine, two tungsten orebodies occur in contact metamorphic Cambrian carbonate sediments above a granite stock: In the opencut, the ore consists of scheelite, garnet, diopside and epidote, whereas ore in the underground East Zone is characterized by pyrrhotite and tremolite. In British Columbia, intrusions of Jurassic island arc terranes are related to polymetallic skarn ore of Cu, Fe, Zn-Pb-Ag, Mo, Bi and Au (Ray *et al.* 1995). Mesozoic, post-orogenic and rift-related ilmenite series granites produced skarn deposits of tin with As, Pb-Zn, W, Mo and some Fe-sulphides (China). These consistent relations are a weighty argument for a predominantly magmatic-hydrothermal derivation of the ore elements, which is confirmed by geochemical data on fluid inclusions (Samson *et al.* 2008).

Skarn orebodies display characteristically irregular outlines that can be explained by the two main factors, lithology and structures of the replaced host rocks, which impose chemical and physical controls on permeability and reactivity. Orebodies are often zoned, for example with copper in a proximal and lead-zinc in a more distal position.

Distal contact-metasomatic ore deposits are closely related to skarn ore formation, although skarn rocks may be absent. Ore formation by replacement of carbonate rocks is solely a hydrothermal process. In the Tertiary Pb-Zn-Ag province in Mexico, for example, the connection between proximal skarn to distal stratiform ore ("mantos") is provided by pipe and chimney-shaped orebodies.

Skarn orebodies are a major source of many metals but also of industrial minerals including wollastonite, graphite, asbestos, magnesite, talc, boron and fluorite.

1.1.8 Porphyry copper (Mo-Au-Sn-W) deposits

Porphyry ore deposits are a product of magmatic-hydrothermal activity at shallow crustal levels. Primarily copper, but also molybdenum, tin, tungsten and gold occur closely related to epizonal intrusions of porphyric magmatic rocks (Figure 1.26). Porphyries contain phenocrysts of hornblende, biotite, feldspar or quartz in aplitic groundmass, which solidifies by pressure decay, volatile loss and sudden freezing during rapid ascent. This is the only connotation of the term porphyry ore deposits, not the arrangement or distribution of ore minerals. Because of the large diversity of the group, porphyry deposits of Mo, Sn and W are presented in Chapter 2, whereas the following discussion centres on Cu-Au-Mo porphyry ore deposits, which presently supply ~75% of the world's Cu, 50% of Mo, nearly all of Re and 20% of gold. The most significant characteristics of copper porphyries include:

- plug-like multiple porphyric intrusions below comagmatic volcanoes, formed before mineralization;
- an extraordinary tonnage of magmatic-hydrothermal ore;
- the ore occurs mainly in stockwork vein systems within the intrusion;
- metal contents in ore are low to moderate, and supergene enrichment is often the key to exploitability;

BOX 1.3 Porphyry copper deposits

The average porphyry copper deposit comprises ~1000 million tonnes (Mt) of ore. Common hypogene ore grades are 0.5–1.5% Cu, 0.01–0.04% Mo and <1.5 g/t Au (Sillitoe 2010). Giant deposits enclose >2 Mt, supergiants such as Chuquicamata (Figure 1.31), >24 Mt of copper metal. The largest is El Teniente in central Chile, with >94 Mt of contained copper (Cannell *et al.* 2005). Large copper porphyry open cut mines expose orebodies that extend over several km^2. Alteration halos surrounding ore can be 10 to 20 times this size. Metal contents are generally low but the large mass allows profitable mining. Apart from copper, by-product metals include significant tonnages of Ag, Au, Mo, Re, Pb, Zn, Mn and minor amounts of As, Bi, Sn, W, U and Pt. Clusters of giant deposits that far exceed average copper porphyry size occur in central and northern Chile, and southwestern Arizona to northern Mexico (Cooke *et al.* 2005).

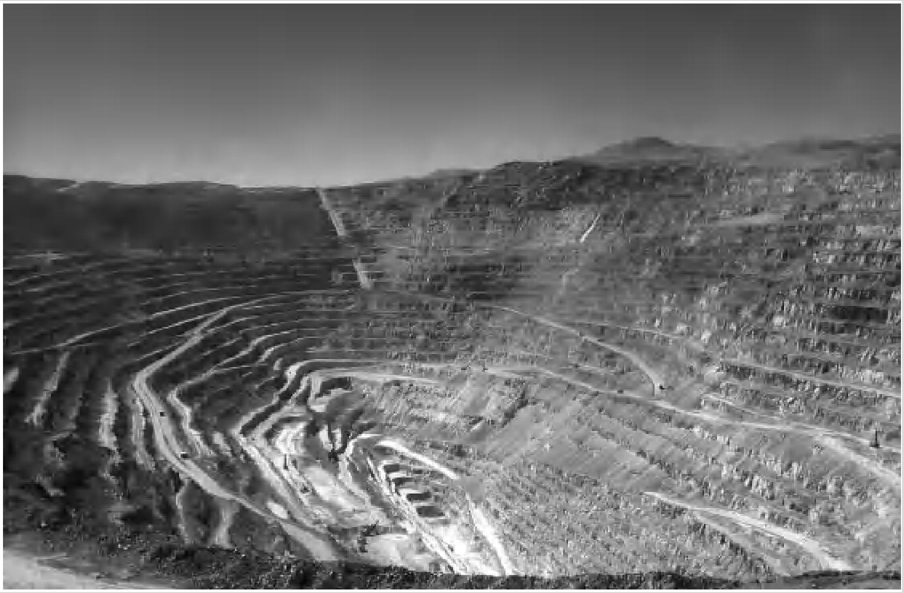

Figure 1.31 (Plate 1.31) Chuquicamata open pit in Chile, one of the world's largest porphyry copper mines. Courtesy Bernd Lehmann, Clausthal.The pit measures 2 × 3 km and approaches a depth of 900 m. Total pre-mining resources were nearly 3000 Mt at 1% Cu and by-product Mo. Annual production is ~1.2 Mt copper and 20,000 t molybdenum plus rhenium.

Porphyry copper systems develop above large parental magma chambers at 5 to 15 km palaeodepth, which establish the heat and flux regime of both the porphyry intrusions and the mineralizing fluids. In a non-telescoped system, the potassic hydraulic fracturing-mineralization-alteration is surrounded by propylitization due to moderate-temperature hydration reactions. Above the porphyry level, advanced argillic (quartz-pyrophyllite-kaolinite-alunite) and vuggy quartz lithocaps may be formed by extreme base leaching. The vuggy quartz level is often the site of epithermal high sulphidation gold mineralization (Sillitoe 2010). Intermediate sulphidation mineralization with higher contents of Pb, Ag, Zn and Mn may be formed at a greater distance from the porphyry centre.

Porphyry copper ore deposits display a hydrothermal alteration zoning that is best characterized by the Lowell-Guilbert (1970) model (Figure 1.32a). Note that this sketch is time-integrated and displayed features originate at different times. Typically, sericitization and the main ore precipitation overprint earlier potassic (mafic minerals replaced by secondary biotite) and propylitic alteration. In practice, there is much variance because of complexities such as repeated intrusive activity and previous alteration of affected rocks (Sillitoe 2010). Hydrothermal systems that produce porphyry ores at depth can extend to the surface where shallow veins and hot springs ore deposits may be formed (Heinrich *et al.* 2004, Heinrich 2005). Skarn ore may be generated at contacts of the porphyric intrusion with carbonate rocks.

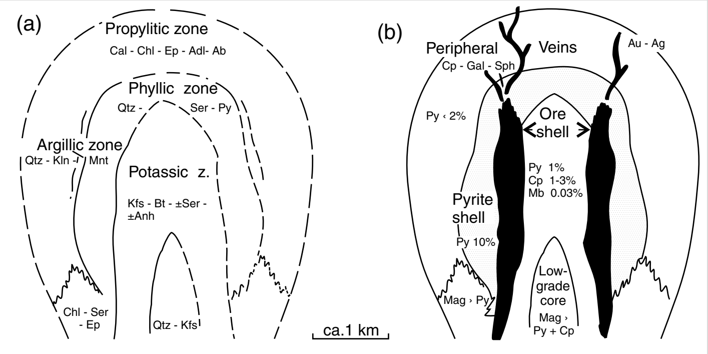
(a)
Propylitic zone
Cal - Chl - Ep - Adl- Ab
Phyllic zone
Qtz - Ser - Py
Argillic zone
Qtz - Kln - Mnt
Potassic z.
Kfs - Bt - ±Ser - ±Anh
Chl - Ser - Ep
Qtz - Kfs
ca.1 km
(b)
Peripheral
Cp - Gal - Sph
Veins
Au - Ag
Py ‹ 2%
Ore shell
Py 1%
Cp 1-3%
Mb 0.03%
Pyrite shell
Py 10%
Mag › Py
Low-grade core
Mag › Py + Cp

Figure 1.32 Schematic arrangement of hydrothermal alteration zones (a) and mineralization (b) in a porphyry copper-molybdenum deposit, according to the venerable Lowell-Guilbert (1970) model. The sequence from potassic to advanced argillic alteration is due to increasing acidity of the fluids. After Lowell, J.D. & Guilbert, J.M. 1970, Society of Economic Geologists, Inc., *Economic Geology* Vol. 65, Figure 3, p. 379.Abbreviations: Ab - albite, Adl – adularia, Anh – anhydrite, Bt – biotite, Cal – calcite, Chl – chlorite, Cp – chalcopyrite, Ep – epidote, Gal – galena, Kfs – K-feldspar, Kln – kaolinite, Mag – magnetite, Mb – molybdenite, Py – pyrite, Qtz – quartz, Ser – sericite, Sph – sphalerite.

Ore formation and the hydrothermal alteration are caused by magmatic fluids and vapours, at temperatures between ~800 and <300°C. More than 90% of the ore is hosted in a vein stockwork in the outer potassic and/or the sericite zone ("ore shell"; Figure 1.32b and Figure 1.33); some ore replaces silicate minerals ("disseminated ore"). Upwards and outwards from the porphyry ore, a halo of small but high-grade gold, silver and base metal vein deposits may be present. At Butte, some of these veins were mined along a distance of 7 km across the district and to 1.5 km depth (Rusk *et al.* 2008). Sulphur isotopes have a magmatic signature, whereas water and strontium isotopes clearly document the passage from early magmatic to late meteoric fluids. During mineralizing events, different fluids pervade the deposit and are trapped in

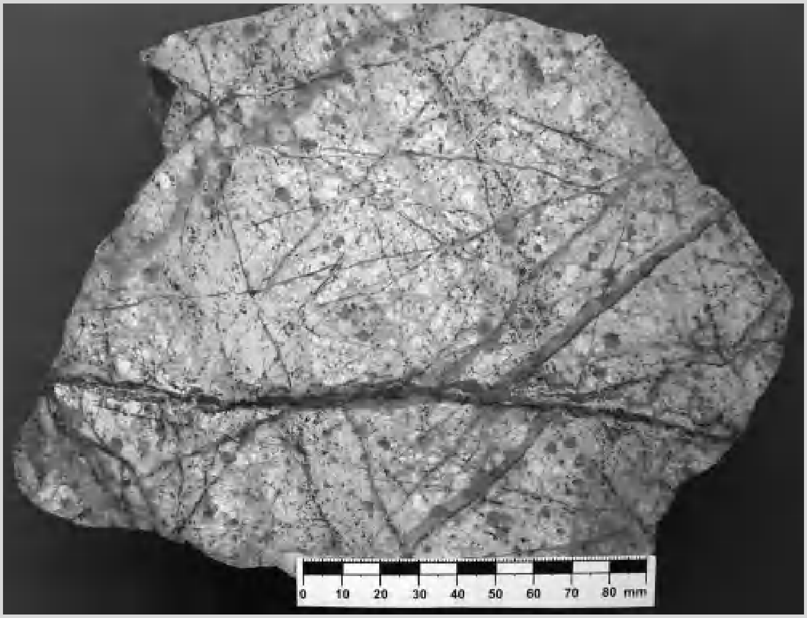
0 10 20 30 40 50 60 70 80 mm

Figure 1.33 (Plate 1.33) Typical copper porphyry ore from Chuquicamata, displaying brecciation and quartz veining, pervasive sericitic (greenish) and argillic alteration. Courtesy Bernd Lehmann, Clausthal.Grey ore in veinlets is largely chalcocite due to supergene enrichment, which reaches 800 m below surface.

fluid inclusions. In most porphyries, main-stage potassic alteration mineralization is connected with co-existing immiscible brine and vapour. Brine is dense (>1.3 g/cm^3) and saline (35 to >70 wt.% NaCl equivalent), with variable contents of K, Na, Ca, Fe, Mo and Cu chlorides (Klemm *et al.*875, 874; Rusk *et al.* 2008). The same elements are found in the multitude of daughter minerals in fluid inclusions (halite, sylvite, anhydrite, chalcopyrite, haematite, Fe-chloride, etc.) of minerals precipitated at this stage. Early fluids have metal ratios that correlate with those calculated for the whole deposit, which is a further argument for a magmatic derivation of the metals (Ulrich *et al.* 1999). Another confirmation is the observation that melt and fluid inclusions co-exist in early hydrothermal quartz (Harris *et al.* 2003). Cogenetic supercritical liquid brine and low-density vapour phase inclusions (D <0.1 g/cm^3) document boiling and unmixing of the fluids. Vapour collects acidic volatile species (SO_2, H_2S, CO_2, HCl, HF) and most Cu and Au, plus much of As, Ag, Sb, Te and B. Vapour flow dominates transport and precipitation. Cooling and contraction of magmatic vapour to a liquid appears to dominate copper mineralization (Klemm *et al.* 2007). Reduction can be induced by magnetite crystallization that triggers sulphate to sulphide conversion. Consequent sulphide precipitation promotes ore formation (Liang *et al.* 2009).

- extensive hydrothermal alteration and metals are vertically and cylindrically zoned in relation to the axis of the intrusion.

Host rocks of copper (Au-Mo) porphyry deposits are shallow (<4000 m), subvolcanic and mostly cylindric intrusions. The parent rocks are frequently calc-alkaline diorites (or the volcanic equivalent andesite-dacite), monzonites (latite) or granites (rhyolite) of I-type that occur in volcano-plutonic arcs above subduction zones, either on active continental margins or in island arcs. Subduction of topographic and thermal anomalies appears to favour copper porphyry genesis (Cooke 2005). Less frequent are Cu-Au porphyry and related epithermal gold deposits in continental collision zones and post-subduction settings (Richards 2009). The parent intrusives are geochemically not peculiar, apart from high oxidation (Mungall 2002). Their hydrous nature, elevated oxidation and SO_2 contents (including anhydrite as a magmatic phase) are the main differentiating characteristics in comparison to the numerous barren intrusions of convergent plate margins. Porphyries on active continental margins are marked by elevated Sn and Mo concentrations apart from copper, those of island arcs more often contain gold as the second metal. Porphyry deposits older than Early Tertiary are rare (Cooke *et al.* 2005) but the oldest date from the Archaean.

Several porphyry copper ore deposits display a strong epithermal signature (cf. "Volcanogenic Ore Deposits") and overprinting of earlier hydrothermal alteration, for example clays replacing potassic zone minerals, as at the gold deposit Ladolam on Lihir Island, Papua New Guinea. Such extreme telescoping is best explained by rapid erosion or a sudden collapse of the original volcano (Sillitoe 1994). Moderate telescoping is common, however, because of contraction of the hydrothermal system with progressive cooling.

Sources of the metals concentrated in porphyry copper ore deposits are probably deeper mafic magmas (Hattori & Keith 2001) but ultimately a fertile mantle. Melts and supercritical fluids that originate in the subducting oceanic crust are oxidizing and dissolve chalcophile metals. Absence of reduced sulphur in the source region is a precondition because otherwise sulphide melts would form, which must lag behind rising silicate liquid (Mungall 2002). In epizonal staging chambers, however, an intermediate step of sulphide melt formation may intervene (Halter *et al.* 2002, 2005). Transfer of the metals from mafic melt into the subvolcanic felsic magma may be enacted by highly metal-charged ore brines (Figure 1.34). The shallow felsic magma is the apparent source of ore fluids that cause brecciation, alteration and mineralization in the solid roof, concomitant with the dynamics of a rising stratovolcano. The activity of individual porphyry systems may last for ~100,000 to several million years; districts are active for 10–20 My (Sillitoe 2010).

1.1.9 Hydrothermal-metasomatic ore deposits

The term "metasomatic ore deposit" implies that the mass of ore was formed by hydrothermal chemical conversion and replacement of a pre-

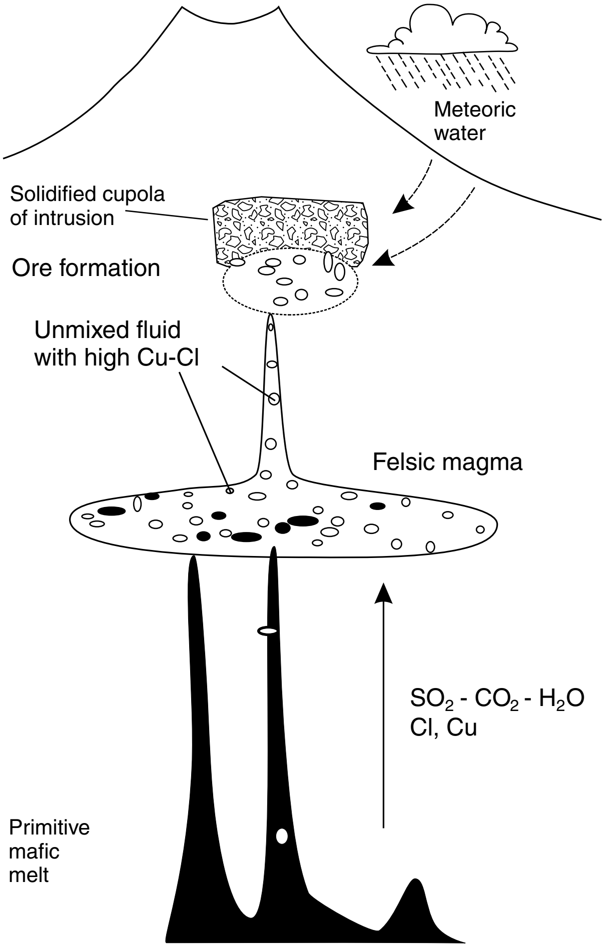

Figure 1.34 Genetic concept of deep magmatic processes preparing the formation of a porphyry copper deposit (modified from Hattori & Keith 2001). With kind permission from Springer Science+Business Media.

existing rock. Local metasomatic processes, for example in ore veins, are ubiquitous co-products of hydrothermal activities, but do not justify attribution to this genetic group. Metasomatic ore formation near igneous intrusions is extremely frequent (cf. Skarn- and Contact-Metasomatic Ore Deposits). In order to avoid repetition, we focus here the discussion on metasomatic ore deposits that have no recognizable genetic relation to magmas. Non-magmatic hydrothermal metasomatic ore formation is usually due to the passage of diagenetic and metamorphic fluids, and especially of evaporative and salt-solution brines (cf. Sections 1.4 and 1.6).

Typically, the metasomatized rocks are marine limestones. This preference can be demonstrated with numerous examples (e.g. many lead-zinc orebodies, gold as at Carlin, USA, magnesite and siderite: Pohl 1988). Main controls of the replacement process include the reactive surface and permeability of the precursor rock, pH and Eh of the mineralizing solutions, and the relative solubility of the participating minerals. A simplified equation 1.7 describes the metasomatic formation of siderite rock (an iron ore) from limestone.

Metasomatic formation of siderite from limestone:

$$CaCO_3 + FeCl_2(aq) \Rightarrow FeCO_3 + CaCl_2(aq) \quad (1.7)$$

In this case, cation exchange is the dominant mechanism, replacing each molecule of calcite

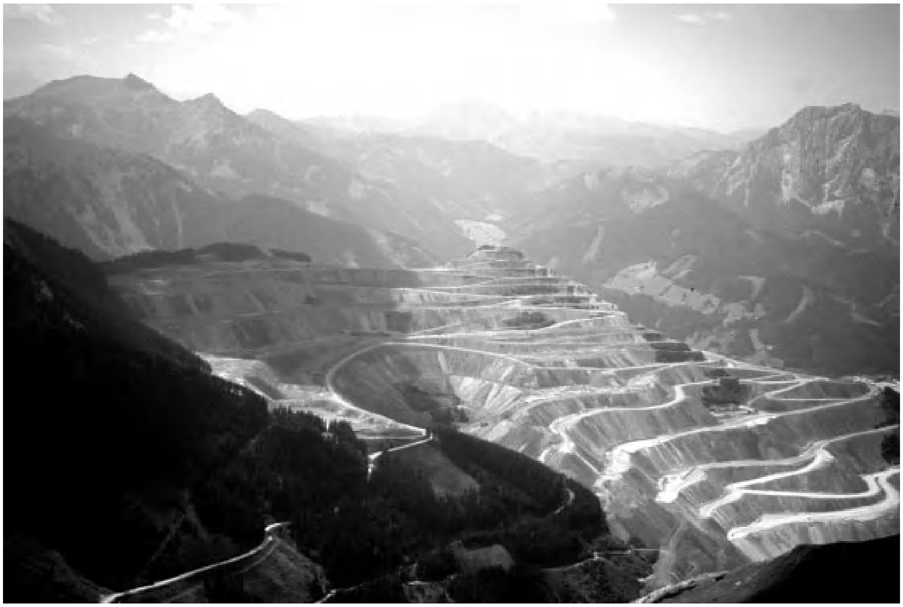

Figure 1.35 The metasomatic siderite deposit Erzberg ("ore mountain" in German) in Austria. The active quarry faces away from the camera. The view shows disposal of barren carbonate host rock.

with one of siderite. Because of the smaller molecular volume of siderite, the resulting ore rock should have a reduced volume. This can be observed in the form of drusy ore at a number of siderite deposits (Erzberg, Austria, Figure 1.35; Ouenza, Algeria), but in many other cases metasomatism exchanges equal volumes. Indicators for this process include the conservation of intricate textures and structures of the replaced rocks (e.g. layering, banding, fossils, stylolites, etc.). Generally, however, metasomatism induces a dramatic change in both chemistry and fabric of the precursor. Some metasomatic ores appear to replace newly deposited soft sediment (e.g. in some magnesite deposits: Pohl & Siegl 1986), but well consolidated precursor rocks are more common.

Hydrothermal-metasomatic ore deposits are often stratabound and occur in the same stratigraphic level across large regions. For example, siderite deposits in North Africa and in northern Spain occur in Early Cretaceous micritic limestone, and lead-zinc ores of the Viburnum MVT district of mid-western USA are confined to stromatolite reefs of the Late Cambrian Bonneterre Formation. Zinc-rich MVT ores in the Tri-State district occur in Mississippian carbonates. In the past, observations like this were believed to prove synsedimentary mineralization. Today, a hydrothermal and epigenetic emplacement is undisputed, but the causes of the preference for certain strata are not always clear. Possibilities include chemical, hydraulic and mechanical parameters.

The emplacement of metasomatic ore is favoured by low-permeability rock horizons (e.g. shales) that form a physical barrier to upward flow (similar to petroleum traps). Focused hydrothermal solutions react more intensively with the carbonate host. Model calculations show that metasomatism is promoted by: i) large temperature differences in flow direction; ii) large focused quantities of fluids; and iii) anomalous phase equilibria (Ferry & Dipple 1991).

The form of many metasomatic deposits is characterized by irregular reaction fronts ("reaction fingering") between ore and host rocks. Higher permeability tongues may be caused by the commonly smaller volume of the product ("induced permeability"). Orebodies are

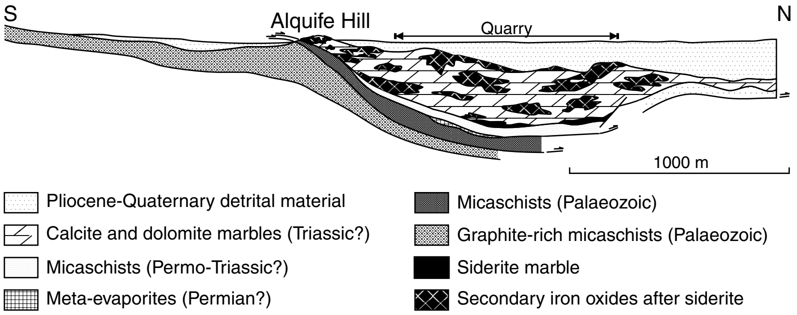
S
Alquife Hill
Quarry
N
1000 m
Pliocene-Quaternary detrital material
Calcite and dolomite marbles (Triassic?)
Micaschists (Permo-Triassic?)
Meta-evaporites (Permian?)
Micaschists (Palaeozoic)
Graphite-rich micaschists (Palaeozoic)
Siderite marble
Secondary iron oxides after siderite

Figure 1.36 Geological cross-section of the Alquife metasomatic iron ore district, Betic Cordillera, southern Spain. Modified from Torres-Ruiz, J. 2006, Society of Economic Geologists, Inc., *Economic Geology* Vol. 101, Figure 3, p. 670. For location refer to Figure/Plate 1.89.

stratabound and cloudy masses with irregular outlines, but some borders mimic structures of the precursor rock (joints, faults, bedding planes). Other ores may take the shape of extensive stratiform bodies (mantos). Both are demonstrated at Alquife in southern Spain (Figure 1.36). In this region, metasomatic siderite was formed during the Triassic by acidic and reducing solutions that leached iron from graphite-rich micaschists in the Palaeozoic basement and ascended along synsedimentary extensional faults into Permo-Triassic cover carbonates. Host rocks and ore were later deformed and metamorphosed by a polyphase Alpine orogeny. In the Tertiary, most of the siderite bodies were affected by supergene alteration and now consist of goethite and haematite.

The flow direction of hydrothermal solutions generates two boundary types of very different nature:

1 In the flow direction, various reactions of mineral neogenesis and isotope exchange migrate with different speed in the form of a chromatographic model (Korzhinskii 1970); assuming kinetically fast reactions, several spatially separate reaction fronts should be the result.

2 Boundaries that laterally limit flow channels (e.g. massive impermeable limestone constricting flow in jointed limestone) can display direct contacts between totally unaltered host rock and high-grade metasomatites (Yardley & Lloyd 1995).

Metasomatism can be accompanied or closely followed in time by mineralization with the character of simple open space filling (veins, fissures, druses, karst cavities). In the North African siderite deposits, this role is played by quartz-barite-fluorite veins, in Bleiberg, Austria by cave-filling ore. Cave ores may include bedded sediments and are a rare, fascinating aspect of hydrothermal systems (cf. "Karst").

1.1.10 Hydrothermal vein deposits

For a long time in the past, ore veins were the most important deposit type. Practice and theory of mining and geosciences grew with the challenges of vein mining, as shown by fundamental books from Agricola (1556) to Lindgren (1933). More recently, the economic relevance of vein mining decreased compared to large-tonnage low-grade operations such as those based on copper porphyries. However, several high-grade base metal vein deposits successfully compete with the mechanized giants.

Veins are tabular bodies of hydrothermal precipitates that typically occupy fissures. Less often, veins originate by metasomatic replacement of rock (replacement veins), propagating from a joint or shear plane. Vein walls range from clean parting planes to "frozen" contacts. Many veins develop upwards into a fan of thinner veins and veinlets (Figure 1.15), which resemble a branching tree. At district scale, veins tend to occur in groups that form vein systems.

Thickness, vertical extent and horizontal length of veins vary widely. Less than 0.5 m thickness may allow profitable mining of high-grade gold and silver ore veins, whereas tin and tungsten require a width of 1 m, barite and fluorite a minimum of 2 m. The world's longest veins may be those of the Mother Lode system of California, with 120 km strike length. Most veins, however,

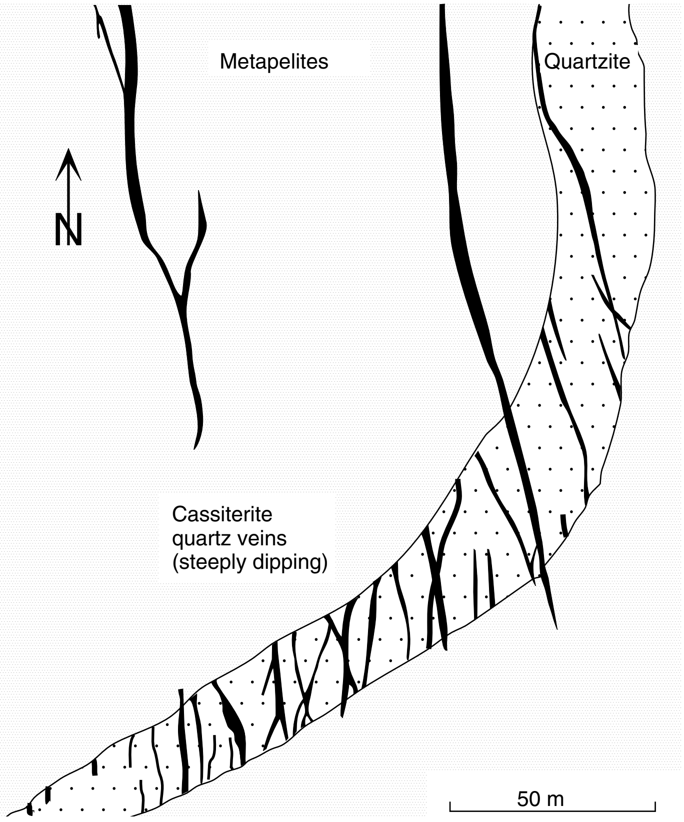

Figure 1.37 Geological map of one level in Rutongo tin mine, Rwanda, showing closely spaced parallel quartz-cassiterite veins (for location, compare Figure 1.16).

have lengths between a few tens to several thousand metres. The disposition of veins in space ranges from horizontal to vertical, but because hydrothermal solutions have a general tendency to flow upwards (more precisely towards lower hydraulic potential) steeply dipping veins are in the majority.

Mechanical properties of host rocks are the most important controls of vein formation, in contrast to metasomatic ore deposits that depend first on chemical properties. Fractures form more readily in competent rocks than in ductile material. Therefore, the cassiterite–quartz (muscovite, arsenopyrite, tourmaline) veins at Rutongo, Rwanda occur preferentially in vitreous quartzites and few cut across low-grade metamorphic schists (Figure 1.37). Very brittle rocks such as dolomite, rhyolite and quartzite are prone to form a network of short fractures instead of spatially separated longer ones (Figure 1.38). In that case, hydrothermal activity may result in stockwork ore. "Stockwork orebodies" consist of numerous short veins of three-dimensional orientation, which are so closely spaced (e.g. 10–30 veins/m in the tin deposit of Tongkeng-Changpo, South China) that the whole rock mass can be mined.

Many vein deposits are spatially and genetically associated with brecciated rock bodies that may host rich ore (Jebrak 1997). As a rule, fissures and breccias have a much higher permeability than most consolidated rocks, which are commonly aquitards. Therefore, these structures focus fluid flow at all scales, from single veins to large structures such as rift faults and crustal shear zones (Weinberg *et al.* 2004). Many fissures, for example the tin ore veins of Cornwall,

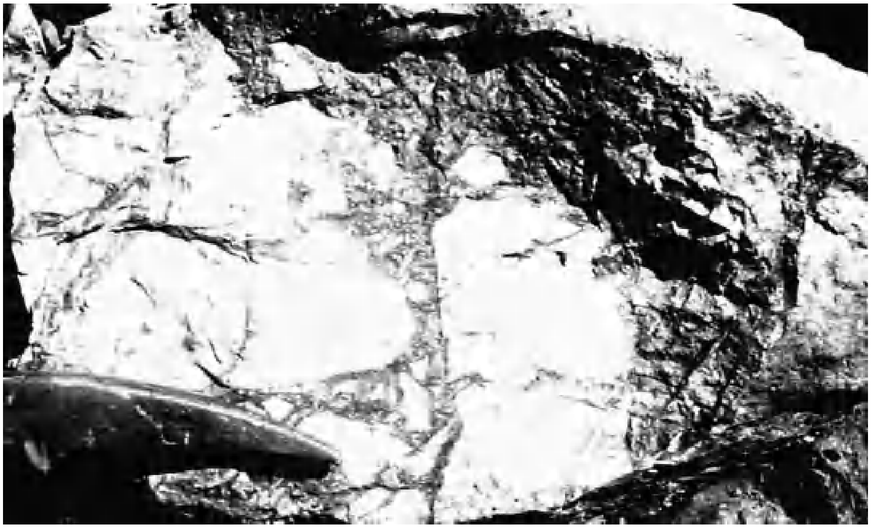

Figure 1.38 Breccia ore at Mammoth copper mine near Mt Isa, Queensland. Supergene secondary chalcocite (grey near hammer) replaces primary chalcopyrite and pyrite in veinlets within quartzite (white).

England, are surrounded by broad zones of intensive micro-fracturing that provide access to fluids from the main flow channel (Dominy *et al.* 1996). It is well-known in the oil industry that in contrast to common permeable faults, clay and shale gouge can transform faults into very effective barriers to fluid flow (Egholm *et al.* 2008). Unconsolidated rocks (clay, sand) are unlikely to fracture but deform ductilely. Typically, this reduces their permeability so that such faults restrict flow.

Veins are channels of former fluid flow. Principally, hydraulic mass flow is a function of hydraulic conductivity and velocity. Flow in a single fissure is controlled by its aperture and secondary properties such as morphology and roughness of the walls. Note that the hydraulic aperture of a vein was hardly ever equal to its present thickness, because most veins were filled while gradually opening. For cases of sheeted vein systems (Figure 1.37), the total cross-sectional permeability can be estimated by incorporating the distance between veins (Lee & Farmer 1993; eq. 1.8). Only in favourable cases, the flow velocity can be measured, for example when upflowing water deposited suspended sediment or hydrothermal precipitates (cf. eq. 1.4 in section "Mineral Succession").

Hydraulic permeability (k) of a single vein and of a sheeted vein system:

$$\begin{aligned} &\text{Single fissure} && \mathrm{k}_{\mathrm{vein}} = (\rho \cdot g/\mu)\cdot(a^2/12) \\ &\text{Sheeted fissures} && \mathrm{k}_{\mathrm{sum}} = (\rho \cdot g/\mu)\cdot(a^3/12d) \end{aligned} \tag{1.8}$$

ρ = density of the fluid (g/cm^3), g = gravitational acceleration (m/s^2), μ = dynamic viscosity (m^2/s), a = aperture (m), and d = distance between veins (m).

Methods of fractal analysis (Mandelbrot 1982) were conceived for studying structures built of many elements. Examples of vein-related topics include the statistical distribution of vein thickness and the spacing of veins, and extrapolation of results into adjacent blocks or to different scales (Roberts *et al.* 1998, Marrett *et al.* 1999). In some cases, the fractal distribution of tectonic features and of mineralization, that is their similarity from microscopic to regional scale, can be used for the definition of new exploration targets (Weinberg *et al.* 2004).

Rock mechanic and tectonic interpretation of vein systems play a central role in vein mining, from creating exploration targets to predicting the shifted position of a vein behind a fault. Mining districts display individual controls that must be identified by careful mapping and structural analysis at all scales. Neogenesis and opening of fissures, shear planes and faults reflect spatial orientation and the ratios of principle tectonic stresses during vein formation (Figure 1.39). The opening of fissures is only possible if normal stress is negative (simple tension) or if fluid pressure (u) is high enough to counteract normal stress (effective stress $\sigma_{eff} = \sigma - u$). This condition is often realized by injection of high-pressured hydrothermal fluids. Many veins display pronounced banding (Figure 1.28) that indicates a correlation between pressure increase of the fluids, movement of the fissure walls and precipitation of hydrothermal fill. This is called "seismic pumping" or "fault valve cycling" (Sibson 1990).

Very large faults and shear zones are rarely the site of hydrothermal mineralization. Orebodies occur rather in clusters of fractured rock near jogs or bends in the large structures. This can be explained by the time-integrated evolution of rock mass permeability after faulting (Sheldon & Mikleswaithe 2007): Main faults that experience a high displacement seismic event enter a healing regime that rapidly reduces permeability. The rock mass at some distance from the fault, however, undergoes a period of weakening that may result in seismic aftershocks. Because this causes elevated permeability for weeks or months after an earthquake, the time-integrated fluid flow will be larger than in the main fault, favouring the formation of ore.

Tectronic control of ore veins

The tectonic control of ore veins may be neogenesis of new fractures or opening of older structures. Both allow an examination of the tectonic processes that were active during vein formation. Not unexpectedly, many veins are associated with large-scale tensional tectonics including rifting (e.g. silver-lead-barite ore veins near the Tertiary Upper Rhine Rift, Figure 1.28; silver veins at Kongsberg near the Permian Oslo Graben; fluorite in the Tertiary East African Rift near Naivasha, Kenya) and late-orogenic relaxation of orogens (e.g. silver veins near Freiberg, Saxony, lead-zinc veins in the Harz Mountains, Germany). However, veins may also originate during convergent tectonics, synchronous with shearing, folding,

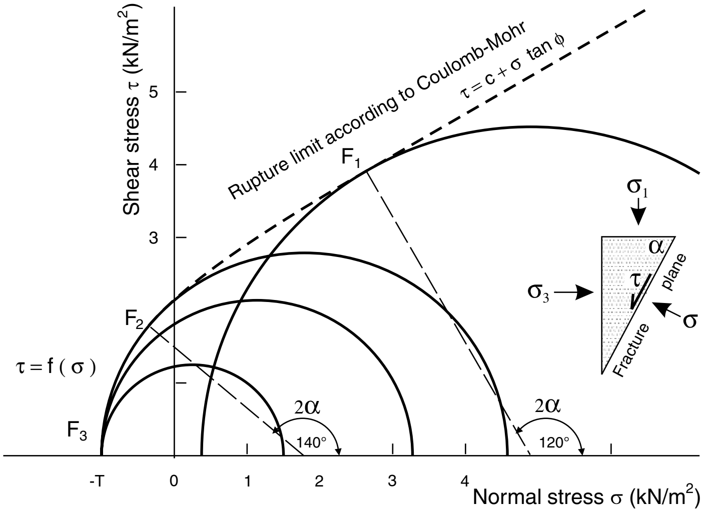

Figure 1.39 The formation of shear fractures (F1), shear fissures (F2) and tensile fissures (F3) with the corresponding angle of fracturing (α), and tectonic stresses $\sigma_1 > \sigma_2 > \sigma_3$ in the Mohr diagram.The inset triangle on the right depicts a section of the upper half of an originally cylindrical sample specimen with the stress geometry of fracture case F1. Fracturing is often assisted by high fluid pressure (u) which reduces strength according to $\sigma_{effective} = \sigma - u$.

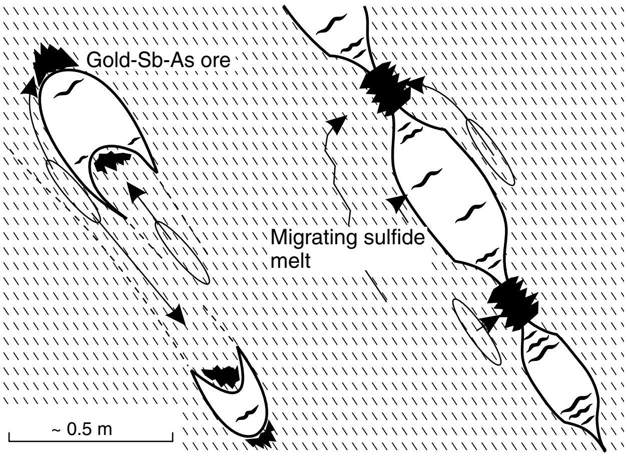

Figure 1.40 Schematic concept of mobilization of disseminated ore melt from high-strain host rock into dilatational sites in folds and boudin necks (Hemlo gold mine, Canada). Modified from Tomkins, A.G., Pattison, D.R.M. & Zaleski, E. 2004, Society of Economic Geologists, Inc., *Economic Geology* Vol. 99, Figure 3 p. 1066.

thrusting and nappe advance (gold quartz veins in Western Australia: Vearncombe 1998; tin and tungsten veins in Central Africa: Figure 1.39; the gold-rich "saddle reefs" in folded shales of Victoria, Australia: Windh 1995). At transitional brittle/ductile conditions, boudinage often controls ore deposition, from the regional to exposure scale (Findlay 1998, Tomkins *et al.* 2004: Figure 1.40). At Hemlo, pre-enriched auriferous sulphides and sulphosalts were partially remelted during deformation and metamorphism. The resulting sulphide liquid migrated to low pressure spaces. Residual ore in the host rocks (baritic metasediments and metavolcanics) includes pyrite and molybdenite (±Au), whereas stibnite, realgar, sulphosalts and gold characterize the solidified and recrystallized sulphide melt.

Vein systems may consist of cross-cutting vein sets that reveal changes in time, including both the stress field and the nature of hydrothermal solutions. At Gifurwe in Rwanda, an early vein generation was injected into anticlinal fold hinges and cut across by later subvertical veins, but both systems have the same paragenesis of wolframite, quartz, muscovite, tourmaline and arsenopyrite (Figure 1.41 and Figure 1.42). Vein formation is late orogenic compressional. Initially, high fluid pressure counteracted vertical rock mass stress, followed by near-vertical fracturing and pressure release.

The distribution of ore in veins is inhomogeneous and only a small part of the total vein fill may be exploitable. Related to either surface or volume, the ratio of economic to uneconomic

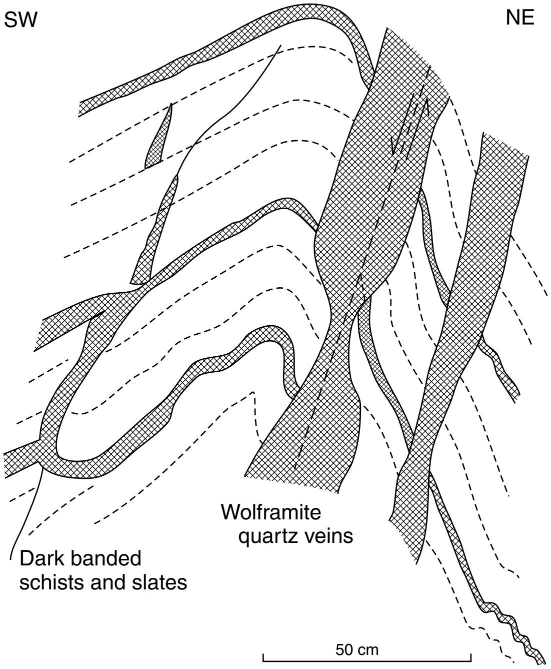

Figure 1.41 Cross-cutting wolframite-quartz veins in folded black shales of the tungsten mine at Gifurwe in Rwanda.

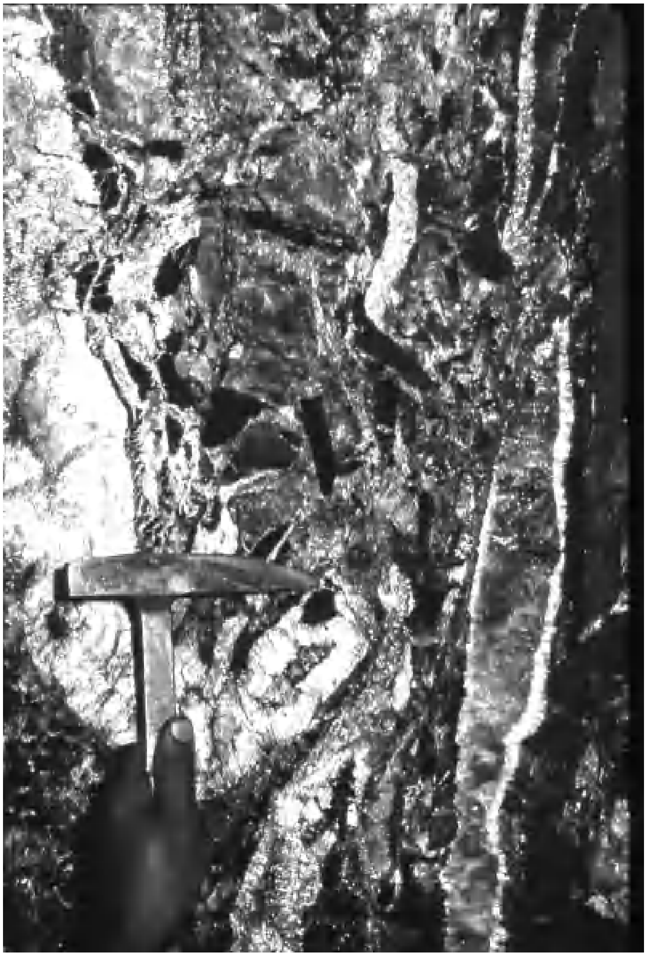

Figure 1.42 Granite-related wolframite veins at Bugarama in Rwanda display a gangue of coarsely crystalline muscovite (white, glittering), dark grey quartz and black shale fragments, which fill steeply dipping bedding-parallel deformation and flow channels between thick competent quartzite beds.

parts of a vein is called the "coefficient of workability" (frequent values are 0.2–0.3). High-grade ore zones ("ore shoots") display distribution patterns that are important guides to exploration (Figure 1.43). During ore deposit formation, ore shoots were preferential channels of fluid flow and ore precipitation. Intersections of veins are often enriched, as are vein contacts with agents of metal precipitation in host rocks mentioned earlier, such as sulphides, organic matter and carbonates. The morphology of a vein surface is never a perfect plane but includes depressions, furrows and highs that are depicted in so-called "Conolly diagrams" (a map of the vein surface similar to Figure 1.43). Replete with data on vein thickness, grade of ore, different host rocks and intersecting structures, these diagrams are extremely instructive.

Metal zonation

Most veins display a change of ore and gangue minerals with increasing depth until a barren zone is reached. The vector of these changes points generally downwards, but may have a strong horizontal component. In the Harz Mountains, Germany, lead and silver predominate at upper levels, whereas zinc appears below. In the same area, barite veins end at depth in a barren

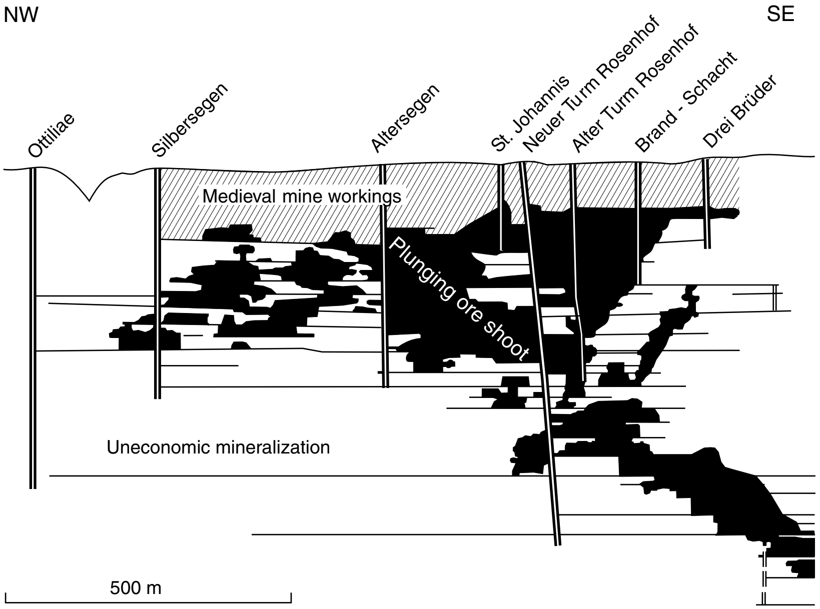

Figure 1.43 Exploited ore shoots (black) of the steeply dipping Rosenhöfer vein, in the lead-silver-zinc mining district west of Clausthal, Harz Mountains, Germany, illustrate the distribution of mineable and subeconomic areas of the vein. With permission from http://www.schweizerbart.de.

quartz zone. Such a *primary zonation* is thought to be due to pressure, temperature and chemical gradients. The term *secondary metal zonation*, in contrast, describes the re-arrangement of elements imprinted by supergene weathering. Spatial zoning models can be used to define hydrothermal centres and exploration targets. In the case of complicated and long-lived hydrothermal systems, metal zone reconstruction should be based on specific activity periods or parageneses of the same age. Thermal and geochemical halos of hydrothermal systems may wax and wane in time, which causes overlapping of zones ("telescoping", Audétat *et al.* 2000).

Vein districts are characterized by recurring parageneses of ore and gangue minerals. In fact, many of these mineral and chemical associations occur worldwide. In the German Erzgebirge, with numerous cross-cutting vein systems, this observation was of high practical relevance to miners and a formal classification of "vein formations" was developed (e.g. "the Pb-Zn-Ag Formation" in the Freiberg District; cf. Stemprok & Seltmann 1994). For descriptive and practical purposes, notations like this are certainly useful. The word "formation", however, is ambiguous.

1.1.11 Volcanogenic ore deposits

The formation of a large number of important ore deposits is closely related to terrestrial and submarine volcanism. We have met two members of this group in earlier chapters; the subvolcanic porphyry ore deposits and the mineralization related to the volcanic section of ophiolites (Cu-Zn-Au ore of Cyprus type). Mid-oceanic deposits, however, are commonly subducted and rarely preserved. Here, other economically significant classes of volcanogenic ore deposits are introduced: i) the submarine volcanogenic massive sulphide (VMS) deposits; and ii) the terrestrial epithermal gold-silver-base metal deposits. Banded iron formations of the Algoma type are also a member of this group (cf. Section 1.3 "Autochthonous Iron and Manganese Deposits").

BOX 1.4 Polymetallic vein fields of Cornwall

Already 3200–2900 BCE (before the Common Era), the tin and copper veins of Cornwall were the destination of adventurous maritime expeditions by the Phoenicians, famous traders in the Mediterranean and beyond. The Cornubian batholith is built of several S-type granite pulses that intruded after the peak of Variscan orogeny (Carboniferous/Permian; from ~300–270 Ma: Chesley *et al.* 1993). The youngest phases of single plutons are fractionated and geochemically specialized, with abundant lithium, boron, caesium and uranium (Chappell & Hine 2006). All granites contain enough uranium and thorium (an average of 11, respectively 19 ppm) to be classified as HHP granites. The relative age of mineralization varies between different plutons. Some veins are synchronous with granites, others apparently up to 40 million years younger. Similar age spreads are displayed by felsic porphyry dykes that cut granites and country rocks, and are controlled by tectonic structures that parallel ore veins.

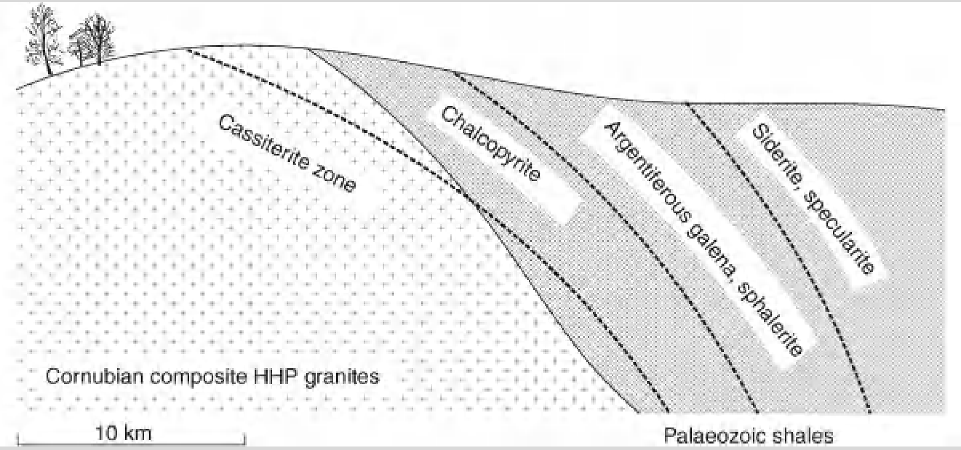

Figure 1.44 Schematic section of primary (hypogene) zonation in polymetallic vein mineralization, Cornwall, England.

Hydrothermal ore veins of Cornwall are zoned about "emanation centres" located in granites, rarely in Palaeozoic country rock schists (Scrivener & Shepherd 1998). Sixty emanation centres are known, with an elliptical shape and a long axis of ~4 km length. The mineralization is not monophase but the product of several activity periods. The oldest episode comprises mineralized pegmatites, sheeted veins with greisen selvages and breccias, all with tin, tungsten and much tourmaline. Highly saline aqueous fluid inclusions with tin, and cogenetic gaseous inclusions with CO_2 and W ± Sn, suggest an origin by unmixing from high-temperature magmatic fluids. The economically prominent main phase of the Cornubian mineralization produced polymetallic (Sn, Cu, Pb, Zn, Ag, Fe, As) veins with a gangue of quartz, tourmaline, chlorite and fluorite, which are very distinctly zoned (Figure 1.44). T_H of inclusions is between 200 and 380°C. The similarity in age of the main polymetallic mineralization indicates formation independent from host granites of varying ages. Relations to younger unexposed pulses of magma are one suggested explanation (Chesley *et al.* 1993). The youngest and last episode of mineralization is represented by low-temperature quartz-fluorite-barite veins with Pb, Zn, Ag and U (the "cross-courses"). Cross-course forming fluids were saline (Na-Ca-Cl), similar to deep formation waters and homogenize at 105–180°C. Until closure of the South Crofty Mine in 1998, the mine production of Cornwall reached a total of 1.75 Mt tin, 1 Mt copper and 0.13 Mt zinc.

Apart from metal ores, Cornubian granites host giant kaolin deposits that occur in the form of pipes, alteration envelopes of veins and horizontal blankets. Many observations suggest kaolin formation by hot, acidic hydrothermal solutions (Dominy & Camm 1998), but water isotopes indicate formation from meteoric water. In fact, many vein mineralizations in Cornwall were precipitated from deeply-circulating meteoric water, with the exception of the early stages of the Permian main phase of Cornubian mineralization, which originated from regional extension, deep heat-flow and crustal melting, followed by fractionation and intrusion of the Cornubian batholith (Chappell & Hine 2006, Shail *et al.* 2003). Later episodes of mineralization were made possible by radiogenic heat production of the granites. Plate tectonic events, such as the opening of the Atlantic, may have favoured deep convection of meteoric and basinal fluids, which leached metals at depth and precipitated ores in the present vein deposits.

Clearly, hydrothermal metal zoning in veins centred on granites is not sufficient evidence for a magmatic source. The example of Cornwall demonstrates coincidence of both the magmatic-hydrothermal and the post-solidus (retrograde-metamorphogenic) mineralization potential of high heat production (HHP) granites.

Important terms

Generally, ores that were formed by hydrothermal solutions venting on the ocean floor are called "submarine exhalative" or "submarine hydrothermal". The second term is preferred by some authors, because the word "exhale" *sensu stricto* implies a gas, not an aqueous liquid. "Submarine volcanic-exhalative deposits" are discerned from "sedimentary-exhalative type" (commonly shortened to "sedex"). Whereas the first are clearly localized in volcanic centres, the second occur in sedimentation-dominated basins. In both cases, the rocks consisting of ore and non-ore minerals (gangue) that result from these processes are called "exhalites" or "hydrothermal sediments". The term "massive ore" designates a body that consists mainly of ore minerals such as base metal sulphides or iron oxides.

Submarine volcanogenic massive sulphide (VMS) deposits

The concept of ore formation caused by submarine volcanic activity, or more precisely, by associated sub-seafloor hydrothermal activity resulting in massive ore mounds on the seafloor, is confirmed by many observations. Their origin by exhalation (outpouring) of metalliferous hydrothermal fluids on the seafloor was recognized by Oftedahl (1958). The concept was further developed by Stanton (1994 and earlier papers), Ohmoto (1996) and Allen *et al.* (2001). Recent exploration of the world's oceans added a wealth of observations from divergent and convergent tectono-magmatic environments, including submarine arc volcanoes (Stoffers *et al.* 2006, Halbach *et al.* 2003). The VMS class encompasses a wide variety of geodynamic and more local genetic settings. Relations to volcanoes range from proximity to quite tenuous connections with volcanism, as in parts of the Southern Iberian Pyrite Belt (cf. Chapter 2.2 "Copper"). VMS-deposits with copper and zinc are hosted by sequences dominated by mafic volcanic rocks, and are particularly abundant in Archaean and Palaeoproterozoic greenstone belts. VMS-deposits with zinc-lead-copper occur in sequences dominated by felsic volcanic rocks sourced from continental crust and are best exemplified by the Kuroko deposits of the Miocene Green Tuff Belt of Japan.

Submarine, volcanic-hosted massive sulphide deposits (VHMS, a non-genetic term) may be characterized in more detail, as follows (Stanton 1994, and cited sources):

> The volcanic rocks are commonly andesites, dacites and rhyolites, basalts are less frequently hosts to significant mineralization (e.g. in Cyprus-type deposits). Throughout ore districts, the deposits occur characteristically in certain volcanostratigraphic horizons and are related to short and singular geological events such as caldera formation (Stix *et al.* 2003), subvolcanic intrusions and generally, enhanced heat flow. Fertile volcanic rocks are petrochemically distinct (Hart *et al.* 2004). The most important metals in these deposits are Fe-Cu-Pb-Zn, with elevated trace contents of Cd-As-Sb-Bi, more rarely including gold and silver. Polymetallic ore deposits are commonly zoned with Fe-Cu at the base, followed upwards by Zn and Pb, and capped by barite, anhydrite or dense SiO_2 exhalites (chert, jasper: Grenne & Slack 2005). This chemical stratification can in some cases be explained by changes in the composition of the hydrothermal solutions. In other cases, a secondary mobilization of more easily soluble components (e.g. zinc) of early precipitates results in this pattern, caused by continuous flow of hydrothermal solutions upward through the earlier metalliferous hydrothermal sediments ("zone refining"). It is thought that in

the precipitates, colloidal textures and framboidal (microcrystalline) pyrite prevailed initially, before zone refining, diagenesis and metamorphism caused coarsening and recrystallization. In the very low-grade metamorphic Archaean ore deposit Sulphur Banks in the Pilbara craton, Australia, pyritic filaments were found in colloidal-textured sulphides, which may represent fossil bacterial colonies. Banding, synsedimentary soft-sediment deformation and graded bedding of sulphides are often observed in VHMS deposits. Ooids and pisoids form where outpouring solutions caused both ore precipitation and agitation of hydrothermal seafloor sediment (Heikoop *et al.* 1996). Breccias are produced by hydrothermal eruptions. Most probably, breccias were first cemented with anhydrite, which is often later removed by low-temperature solutions because of its retrograde solubility. A wide halo of anomalous manganese contents surrounds sites of submarine hydrothermal activity and these horizons survive into high-grade metamorphism, for example as spessartine bands (Stumpfl 1979). Other deposits occur at distinct exhalative centres in regional metalliferous horizons as in the Ordovician Algoma-Type iron formation of northern New Brunswick, Canada (McClenaghan *et al.* 2009). Exhalative systems with low contents of sulphur and dissolved carbonate ions form stratiform skarn, because silica-iron-calcium precipitates develop into metamorphic assemblages of hedenbergite, grossular, Ca-amphibole, wollastonite and diopside.

Iron-rich sulphides occur predominantly with basalts, whereas Fe-Cu-Zn appear in volcanic terranes of andesite-dacites and Fe-Pb-Zn with rhyolites. Water isotope data suggest that the hydrothermal solutions are mainly altered seawater. Therefore, VHMS ore deposits are thought to result from seawater convection and hydrothermal dissolution of metals from pervaded volcanic rocks (Figure 1.10). This hypothesis, however, does not fully explain the ties between specific metals and certain volcanic rocks. Stanton (1994) proposed that a link with the magmatic evolution and degassing of the volcanic rocks may complement the convection hypothesis. The scarcity of Ti, V, Cr, Co and Ni in VHMS deposits, for example, may be due to early precipitation of magnetite from mafic melt which extracts these metals. Also, magnetite crystallization triggers sulphate to sulphide conversion (Sun *et al.* 2004), which tends to abstract chalcophile metals. Stanton's hypothesis is supported by recent research. In the Manus back-arc basin near Papua New Guinea, metal-rich glass inclusions in submarine andesites were found close to a presently active submarine hydrothermal system (Yang & Scott 1996, 2005). Sulphur isotope data from the Lau basin indicate magmatic input (Herzig *et al.* 1998). Mass balance calculations by Beaudoin & Scott (2009) confirmed that a very small fraction (~1%) of metalliferous magmatic fluid mixed with convecting seawater accounts best for Pb-enriched sulphides and volcanic rocks in the Pacmanus vent field.

Boiling P/T of submarine hydrothermal systems depends on the salinity of the fluids, and depth of boiling relative to the seafloor controls both form and location of ore precipitation (Finlow-Bates & Large 1978, Figure 1.45):

1 If boiling takes place below the seafloor, metals preferentially precipitate within the upflow channels, giving rise to stockwork, veins and disseminated ore.

2 Where phase separation and venting coincide at the seafloor, massive orebodies may accumulate.

3 Ore with a sedimentary (e.g. bedded) character results from single-phase fluids that vent below the boiling curve and collect in brine pools.

Accordingly, orebodies of VMS deposits show a great variety of forms, including lenses and blankets (the most common), but also mounds, pipes and stringer deposits (Large 1992).

Volcanogenic massive sulphide deposits occur throughout the geological past from as early as the Archaean. They cluster in periods of supercontinent assembly (Huston *et al.* 2010). Many of the older deposits resemble the Kuroko type (e.g. the Cambro-Ordovician deposits in the Charters Towers District, Queensland, Australia: Monecke *et al.* 2006). Generally, they occur in convergent plate boundary settings. However, the prevailing bimodal nature of the volcanic rocks and geochemical indices imply that most VMS were generated during phases of

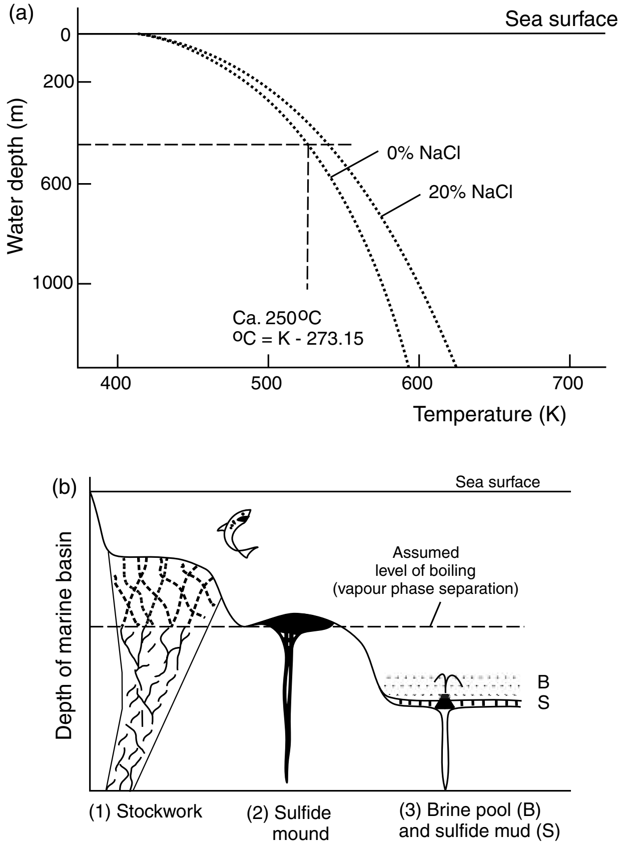
(a)
Sea surface
0
200
600
1000
Water depth (m)
0% NaCl
20% NaCl
Ca. 250°C
°C = K - 273.15
400
500
600
700
Temperature (K)
(b)
Sea surface
Depth of marine basin
Assumed
level of boiling
(vapour phase separation)
B
S
(1) Stockwork
(2) Sulfide mound
(3) Brine pool (B) and sulfide mud (S)

Figure 1.45 Boiling (formation of aqueous vapour) of submarine hydrothermal solutions at subcritical conditions (a) and resulting form and location of submarine ore deposits (b) (adapted from Finlow-Bates & Large 1978). With permission from http://www.schweizerbart.de.

BOX 1.5 Submarine volcanogenic Kuroko type sulphide deposits

Among the submarine exhalative VMS deposits, Kuroko ore deposits are an economically significant subtype (Ohmoto 1996, Morozumi *et al.* 2007). The term "kuroko" is derived from the black lead-zinc ore that was exploited in Japan for centuries. Many mines had also stockwork orebodies of yellow ore ("oko") consisting of pyrite and chalcopyrite (±gold). The deposits occur in a belt ~800 km long, built of Tertiary submarine volcanic rocks. The horizon hosting the deposits is easily recognized because it separates monotonous Miocene "Green Tuffs" (dacitic pumice) in the hanging wall from a bimodal volcanic series below, which is characterized by calderas, rhyolitic and dacitic pyroclastic breccias, and resurgent domes of white rhyolite-dacite. The breccias are the product of submarine neptunian (Allen & McPhie 2009) volcanic eruptions. Explosive pyroclastics occur down to at least 1700 m below sea level at several mid-ocean ridges (Fouquet *et al.* 1999). Geodynamically, the Kuroko province was undergoing strong extension and rifting within a back arc basin of the Tertiary suprasubduction volcanic arcs of Japan.

Early, fine-grained ores of ZnS, PbS, pyrite and barite were formed during extrusion of rhyolite domes by hydrothermal exhalation through submarine vents and mound-building on the seafloor (Figure 1.46). In this figure, white spaces are zones of hydrothermal-sedimentary sulphide ore of copper, lead and zinc, some of which was syngenetically altered (e.g. by zone refining) and recrystallized. The pyrite-rich stockwork of copper (± gold) veinlets is centred below the former. The early ore muds were altered by reaction with upward percolating hot fluids (zone refining) that produced stockwork

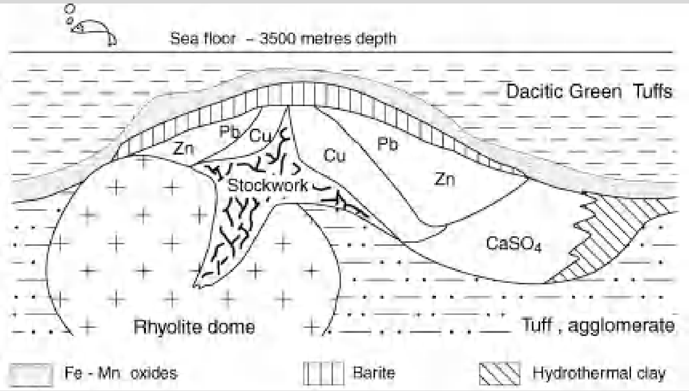

Figure 1.46 Generalized section of a VMS Kuroko type ore deposit (adapted from Finlow-Bates 1980). With permission from http://www.schweizerbart.de.

veinlets with coarse pyrite, chalcopyrite and quartz. Some elements such as Au, Sb, As, Ag and Sn were "distilled" towards the hanging wall of the orebody. Both the stockwork and the ubiquitous ore breccias imply repetitive hydrothermal explosions. Stockworks below exhalative ore beds mark the ascent of the hydrothermal fluids; they are often independent economic orebodies. Distal sedimentary orebodies originate by slumping or mass flow from proximal sulphide mounds. Because of rhyolite dome extrusion, the temperature of the hydrothermal fluids rose during ore formation from 150 to 350°C. Updoming and steepening of ore beds caused complex syngenetic deformation. Due to the considerable hydrostatic pressure, boiling of fluids was rare. Stable water isotopes indicate a seawater origin of the solutions with a low salinity of <5% NaCl (equivalent). Seawater contributed sulphur, but part of sulphide sulphur was leached from the magmatic rocks. Lead isotope characteristics are those of underlying volcanics and sediments. The hydrothermal alteration in the footwall of the massive sulphide ores is concentrically zoned around the stockwork, from innermost K-feldspar and illite to distal montmorillonite and zeolites. Concurrently with alteration, large masses of calcium and barium were leached from the percolated rocks and reprecipitated on the seafloor forming barite, anhydrite and gypsum (Ogawa *et al*. 2005). The hydrothermal fluids were mostly neutral, reduced and had low sulphur contents, probably because in the downward branch of convection SO_4^{2-} is generally removed from solution. Occasionally, clues have been found for the presence of acidic, oxidized and sulphur-rich magmatic fluids of the "high sulphidation type" (Sillitoe *et al*. 1996b; see "Epithermal Ore Deposits" below).

major crustal extension, which may be caused by slab rollback (e.g. in back arcs), resulting in rifting, subsidence and deep marine conditions (Lentz 1998, Allen *et al*. 2001). Present equivalents of VMS-forming processes, such as metalliferous submarine hydrothermal vents in extensional provinces of island arcs, have been discovered in the Okinawa trough and the Manus basin near Papua New Guinea (Yang & Scott 1996). Iizasa *et al*. (1999) describe a submarine gold-base metal deposit off the eastern coast of Japan, with ~9 Mt of ore. The deposit occurs in a large rhyolitic caldera with numerous black smokers that coalesce above faults and form walls. Recently, mining of a gold-rich volcanic massive sulphide deposit at 1600 m water depth is seriously investigated offshore Papua New Guinea. The Solwara orebody contains indicated and inferred resources of ~2 Mt at 6.8% Cu, 4.8 g/t Au and 23 g/t Ag.

Many VMS-deposits have undergone metamorphic overprinting and strong deformation (cf. Section 1.5 "Metamorphosed Ore Deposits"). This may destroy original spatial relations and change rocks to a point where identification of their pre-metamorphic nature is very difficult:

Notable examples are Besshi type sulphide deposits. Besshi is one of numerous comparable mines on the Japanese island of Shikoku. Besshi ore consists mainly of pyrite, chalcopyrite and pyrrhotite, with some sphalerite, gold and magnetite. Deposits occur within the Sangabawa high-P/T metamorphic belt that represents the deepest exposed part of the Mesozoic accretionary complexes in the Japanese island arc. Host rocks include Carboniferous to Jurassic schistose metapelites, metacherts and metabasalts of epi- to mesozonal metamorphic facies that were deformed in the Cretaceous. In the Besshi region, the schists wrap around a large eclogitic ophiolite nappe (Moure & Enami 2008). The orebodies appear to be bound to a regional horizon and are stratiform lenses, either banded or massive, and deformed into spindle-like shapes. Syngenetic formation with host rocks is highly probable. After long disputes, the geodynamic setting was recently affirmed to have been mid-oceanic (Nozaki *et al.* 2008, Watanabe *et al.* 1998). Besshi sulphides are highly deformed and metamorphosed Cyprus Type deposits.

Worldwide, many pyrite-rich beds in metamorphic volcano-sedimentary sequences are known, for example, the "fahlband" (pyritic) gneiss layers in southern Norway. Of course, this does not imply the same genetic setting as that of Besshi sulphides.

Terrestrial epithermal gold, silver and base metal ore deposits

Many important ore deposits are connected with terrestrial volcanism. In previous sections, iron oxide lavas and tuffs, and the subvolcanic porphyry copper ore deposits were mentioned. Here, we focus on a deposit class that is commonly called "epithermal". These deposits formed by near-surface hydrothermal processes (they occur at shallow epizonal depth). Epithermal orebodies take the shape of veins, breccias, metasomatic masses and impregnations within hydrothermally altered host rocks. They are closely related to metalliferous sinter mounds that occur on the land surface ("hot springs deposits"). Epithermal ore formation takes place in the aureole of near-surface subvolcanic magma bodies that induce a high heat flow and a steep geothermal gradient. This is the reason for a commonly restricted vertical downward extension of epithermal orebodies. Primary metal zonation occurs in narrow intervals, or the zones overlap and are "telescoped". Causes for telescoping may be erosion and collapse of volcanoes (Sillitoe 1994) or repeated subvolcanic intrusions that radically change the p/T-field. Epithermal ore deposits are remarkable as a major source of gold, silver, zinc, lead, bismuth and the minerals alunite, barite and fluorite.

Active epithermal systems of today's volcanic regions are mainly investigated in view of their role as an energy source. Energy can be exploited from geothermal systems (Figure 1.47) where heat is transported close to the Earth's surface, usually by a combined action of rising magma, magmatic volatiles and convecting non-magmatic waters.

BOX 1.6 Terrestrial volcanogenic epithermal ore deposits

Epithermal ore deposits are remarkable as a major source of gold, silver, zinc, lead, bismuth and the minerals alunite, barite and fluorite. The descriptor "epithermal" was originally given because ore deposition was thought to have occurred near the surface from low-temperature fluids between 50 and 200°C (Lindgren 1933). Today, the temperatures are better known, but Lindgren's summary of characteristic features is still a valuable guide (freely adapted):

- depth of formation between 0 and 1500 m below the palaeosurface;
- temperature of formation 150–300°C (modern data);
- host rocks may be volcanic or sedimentary rocks, but always close to volcanic centres; ore controls are often faults;
- orebodies occur as veins, breccia pipes and stockworks; stratiform and replacement ore (e.g. in carbonates) is less common;
- main ore metals are Pb, Ag, Zn, Au, Cu, Hg, Sb, Se, Te and Bi; metals occur in native form and as sulphides, sulphosalts, selenides and tellurides;
- gangue includes chert, chalcedony and quartz (often crystalline, e.g. amethyst), chlorite, epidote, carbonates, fluorite, barite, adularia, alunite, dickite, rhodochrosite and zeolite;
- hydrothermal alteration is characterized by moderate to intense silicification, kaolinization, pyritization, dolomitization and chloritization;

- ore textures typically indicate mineral growth in open spaces, in some cases including open space sedimentation; colloform banding is common;
- most deposits have a restricted depth extent; vertical zonation is very pronounced and includes telescoping.

The fluids responsible for epithermal ore formation include magmatic water and vapour, heated meteoric water and in some cases seawater. Magmatic heat and fluids are essential components of the entire hydrothermal system (Figure 1.47). In the centre-right of the figure, oxidized magmatic volatiles and fluids released from subvolcanic porphyry intrusions produce a high-sulphidation Au-Cu deposit ("volcanic-hydrothermal system"). On the left, hydrothermal convection is dominated by meteoric water ("geothermal system"). The heated water dissolves volcanic gas and vapour that are neutralized by reaction with the host rocks. At or after boiling, the solutions precipitate Au-Ag ore of intermediate to low sulphidation type. Solfataras (sulphurous vents) can be associated with the precipitation of native sulphur (S).

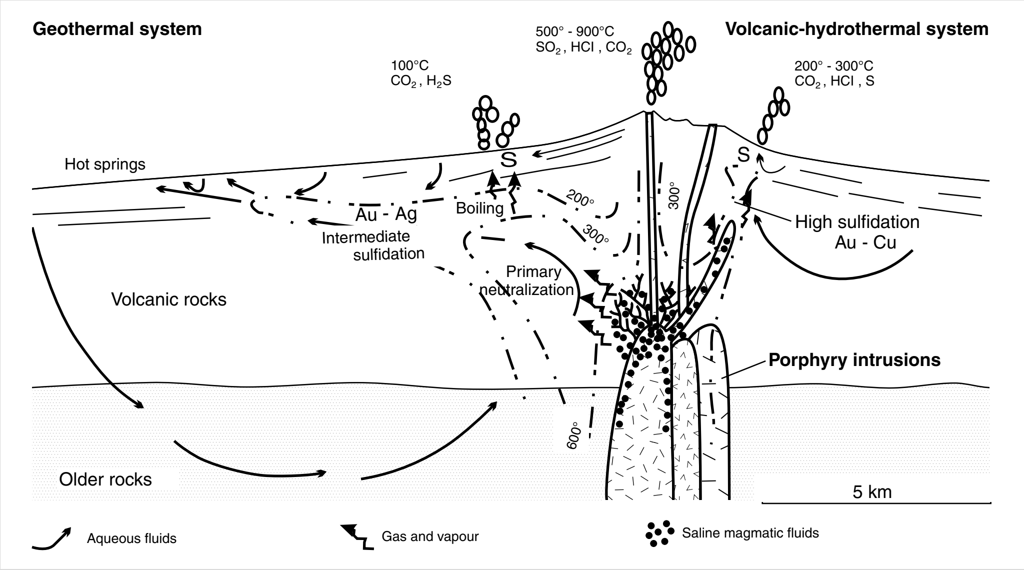
Geothermal system
500° - 900°C
SO₂ , HCl , CO₂
Volcanic-hydrothermal system
100°C
CO₂ , H₂S
200° - 300°C
CO₂ , HCl , S
Hot springs
S
S
200°
300°
300°
Au - Ag
Intermediate
sulfidation
Boiling
High sulfidation
Au - Cu
Primary
neutralization
Volcanic rocks
Porphyry intrusions
600°
Older rocks
5 km
Aqueous fluids
Gas and vapour
Saline magmatic fluids

Figure 1.47 Formation of epithermal ore deposits related to an andesite volcano. Modified from John, D.A. 2001, Society of Economic Geologists, Inc., *Economic Geology* 96, Figure 13, p. 1847.

Salinity of fluids is commonly low (<3%) but may be higher in liquids that lost much vapour. Occasionally, the presence of brines has been noted. Ore precipitation is typically by boiling as the hot solutions move upwards and approach the surface (Robb 2005). Self-sealing of flow channels by precipitates (e.g. silica) is common and causes pressure increase until hydrothermal (phreatic) fracturing or phreatomagmatic eruption releases built-up stresses. Large highly permeable breccia bodies and pipes may result that attract the flow of hydrothermal fluids (Davies *et al.* 2008) and may consequently become bonanza ore. Cyclic repetition of sealing and rupture is reflected in banded ore veins. Mixing of rising hot magmatic gas or boiling fluid with cold groundwater is a possible factor of ore deposition. Where epithermal solutions reach the surface, hot springs establish siliceous sinter deposits. Current formation of hot springs precipitates with high contents of Au, Ag, Hg, Sb and As was described from the Californian Coast Ranges (Peters 1991). Hyperthermophilic microbes (e.g. *Sulpholobus acidocaldarius*) are important actors in these environments. Freshly precipitated siliceous sinters are often filamentous and microbe-rich. They age through a range of silica phases from opal-A, opal-A/CT, opal-CT and opal-C to quartz, with surprisingly rapid transformation rates (Lynne *et al.* 2006).

Several scientific studies illuminate the role of geothermal systems in ore formation (e.g. Taupo Volcanic Zone, New Zealand: Giggenbach 1995, Simmons and Brown 2000, 2007; cf. Ladolam, Lihir Island, Papua New Guinea: Simmons & Brown 2006).

Sulphur is an important component of magmatic volatiles. Near the surface, oxidation of sulphur produces strong acids that react with host rocks. The resulting hydrothermal alteration is very conspicuous because of bleaching and extreme argillization (e.g. alunite, equation 1.5). Alunite can also be formed when oxic magmatic exhalations that are enriched in HCl and SO_2 dissolve in groundwater and react with host rocks (Figure 1.47). This is the environment of the formation of epithermal gold deposits of the **alunite, or high sulphidation type** (Hedenquist *et al.* 1993, Simmons *et al.* 2005). High sulphidation (high fS_2 in oxic conditions) is indicated by ore minerals such as enargite, tennantite and covellite, and by advanced argillic alteration gangue minerals including alunite, pyrophyllite, dickite and kaolinite. In contrast to the former, epithermal deposits of the **adularia-sericite, or low sulphidation type** are produced by reduced and neutral to mildly alkaline fluids that carry H_2S and other reduced sulphur species (Hedenquist *et al.* 1993, Simmons *et al.* 2005). In these deposits, silver and base metals dominate and typical gangue minerals are calcite, adularia and illite (Figure 1.47, White & Hedenquist 1995). Members of the group with exploitable base and precious metals are called "epithermal polymetallic" (Cu-Zn-Pb-Ag-Au-Bi) or "Cordilleran" base metal deposits (Baumgartner *et al.* 2008). High sulphidation epithermal deposits are often in close spatial association with copper-gold porphyries. In active volcanoes, solfatara fields mark this environment. Earlier speculations that there are physical and chemical links between the two deposit classes are confirmed by modelling studies (Heinrich *et al.* 2004, Heinrich 2005) and field observations (Sillitoe 2010). The described sulphidation types of epithermal deposits are end members of a continuum in nature.

Submarine and terrestrial volcanogenic ore deposits are quite different. However, a number of transitional, or hybrid ore forming systems, have been found (Hannington 1997, Naden *et al.* 2005), with a setting at volcanoes emerging from the sea (e.g. Milos, Greece). By definition, all volcanogenic deposits were formed near active volcanoes or subvolcanic centres, and occur in a "proximal" position. A number of submarine base metal deposits display several properties that are similar to bedded volcanogenic ore, but are located at a considerable distance from contemporaneous volcanic activity. Volcanism may be indicated only by thin tuff bands in sediments or known as distant volcanic centres (in parts of the Iberian Pyrite Belt, also at Mt Isa, Australia). This corresponds to a "distal" position. In this case, a genetic connection of mineralization and volcanism is tenuous or even unlikely (cf. Section 1.3 "Sedimentary Ore Formation Systems").

Studies aiming at a full understanding of volcanogenic ore deposits, regardless of scientific or practical objectives, always include investigations of structure, petrogenesis and evolution of the volcanoes, the petrology of synvolcanic intrusions concerning cosanguinity, hydrothermal alteration (Gaboury 2006) and the precise plate tectonic situation (Sawkins 1990a,b). Generally, terrestrial volcanogenic deposits occur in convergent plate boundary and subduction settings, for example in the circum-Pacific "ring of fire". However, they are not necessarily products of subduction and compressional deformation (orogenesis). Many of these systems were triggered by tensional events. Volcanic graben and horst terranes are especially favourable locations (e.g. the Basin and Range Province, USA), as are subvolcanic domes and resurgent calderas of andesitic to rhyolitic composition.

1.2 SUPERGENE ORE FORMATION SYSTEMS

Weathering of rocks and soil formation are the preconditions of most higher life on Earth. They are also at the origin of many important ore deposits. Raw materials that are predominantly produced from supergene mineral deposits include a diverse range of metals and minerals such as

iron, manganese, aluminium, gallium, niobium and kaolin:

The term weathering integrates a number of processes that are caused by the interaction of Earth materials with the atmosphere and the energy flow from the sun. Physical and chemical process groups can be distinguished, frequently with a strong biological component (Banfield & Nealson 1997, Southam & Saunders 2005). Chemical weathering is dominated by reactions between minerals and rocks with meteoric water containing dissolved oxygen and carbon dioxide. The first causes oxidation, for example Fe(II) → Fe(III), the second induces moderate acidity (Figure 1.48, eq. 1.14), especially after passage through a humic soil horizon that multiplies CO_2 concentration in seepage water. Generally, chemical weathering removes mobile cations (e.g. Ca^{2+}, Na^{+}, K^{+}) relative to stable residual components (Al^{3+}, Ti^{4+}). Site-specific conditions of pH and Eh are the main controls on reaction products. Weathering rates are a function of climate. Highest rates occurred during periods of high CO_2 in the atmosphere with consequent warm and humid climate and a profuse growth of land plants as, for example, in the Early Eocene climatic optimum when CO_2 levels reached 1125 ppm (Smith *et al.* 2008).

All forms of life (Figure 1.49) participate in supergene processes. Very direct is the action of land plants, which are the main drivers of rock weathering, not least because they are an important source of oxygen in water and air. Organic acids derived from partial decay of plants intensify rock disintegration. In the Late Archaean and Early Proterozoic, *Cyanobacteria* (blue-green "algae") proliferated to a degree that led to the first oxygenation of oceans and atmosphere ("the Great Oxidation Event"). Archaea were probably always rather specialists for extreme environments, such as very hot, acidic and alkaline settings. In the Mesozoic, diatoms (algae) started to dominate the marine photosynthetic productivity. Remember that for a geologist, the Tree of Life is also a symbol of the time vector of life's evolution on our planet, as first explained by Charles Darwin (1859).

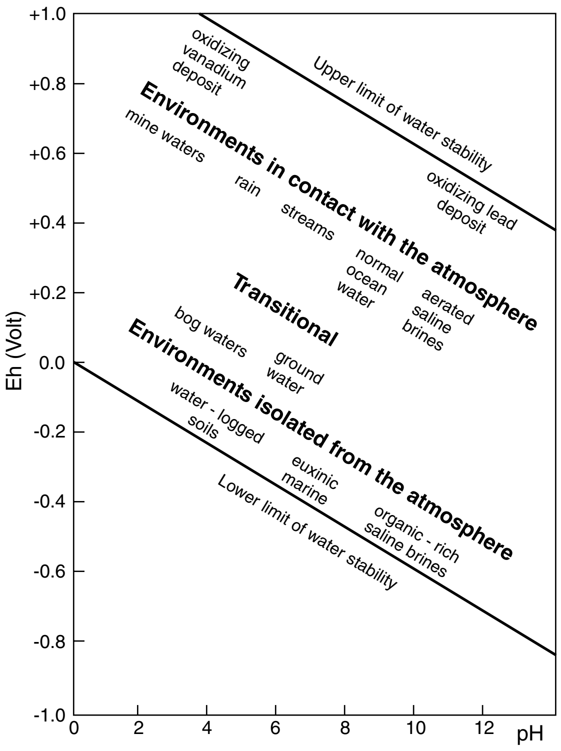

Figure 1.48 Typical Eh/pH range of surface waters (modified from Garrels & Christ 1965). Note that today, the concept of a determinate Eh (pε) is doubted.

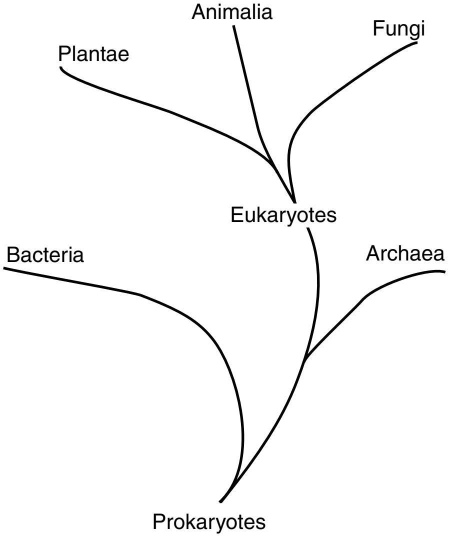

Figure 1.49 The Tree of Life in a very simplified version showing what is poetically called the Kingdoms of Life (consult the complex background in Crandall & Buhay 2004).

The principle of supergene ore deposit formation is the concentration of some dilute but valuable component of the primary rock. Two basically different process types may lead to concentration:

1 The valued component is enriched in a residuum, while much of the rock mass is dissolved and carried away.

2 The valued component is dissolved, transported and concentrated on reprecipitation.

In the latter case, the transport distance is commonly very short (metres to tens of metres). Some ore deposits, however, originate after long-distance transport dissolved in surface and groundwater. Examples include uranium in calcrete and in sandstone, iron in Tertiary river valleys of Western Australia and manganese in limestone karst caves. An important special case of ore formation by weathering with metal transfer by meteoric seepage water is the supergene enrichment of unexploitable low-grade primary mineralizations ("protore"). Many copper, iron, manganese and silver deposits owe an economic ore grade to supergene enrichment processes.

Supergene ore deposits form in regions where weathering is favoured by a humid and hot climate that promotes the profuse growth of vegetation. Vegetation and organic matter affect supergene alteration by two mechanisms. The first is the direct influence of plants on the soil water (e. g. retention). The second is the abundance of organic acids and of microbial activity that promote dissolution of primary minerals. In this environment, iron and aluminium have a very low solubility compared to alkalis and SiO_2. Therefore, they are enriched in the red, clayey-sandy soils of the tropics and subtropics that are generally called laterites (in soil science variously termed "ferralsol", "oxisol", etc.). Ordinary laterites have little value except for making bricks and building roads (the Latin word *later* translates into air-dried brick).

Lateritic ore

Lateritic ore (of Al, Ni, Co, Fe, Mn, Cr, Au, etc.) is formed when exposure of suitable rocks coincides with favourable morphological, hydrogeological and geochemical conditions that enhance dissolution, transport and precipitation (Valeton 1999). Time also has a role – long-lasting weathering under stable conditions may be expected to result in more mature and higher-grade ores, although peaks of lateritization last less than 100,000 years and occur during global greenhouse events (Retallack 2010). This is why supergene ore deposits are preferentially found in tablelands of stable cratons, for example in wide regions of former Gondwana and less likely in young orogenic belts (one exception are bauxites in the European Alps).

Laterite *sensu stricto* designates the upper leached and oxidized part of certain soil profiles with a well-developed vertical zonation (Figure 1.50). Lateritic regolith reaches more than 100 m in thickness. Principally, the lateritic **regolith profile** comprises an uppermost eluvial horizon (A), underlain by an illuvial zone (B) and the altered but still recognizable precursor rock *in situ* (C) that rests on unweathered fresh rock (R). Depending on the groundwater table, zone (B) is often divided into an upper kaolinitic and haematite mottled layer and a greenish-grey smectitic material below. In (A) or in (B), many laterites have hard

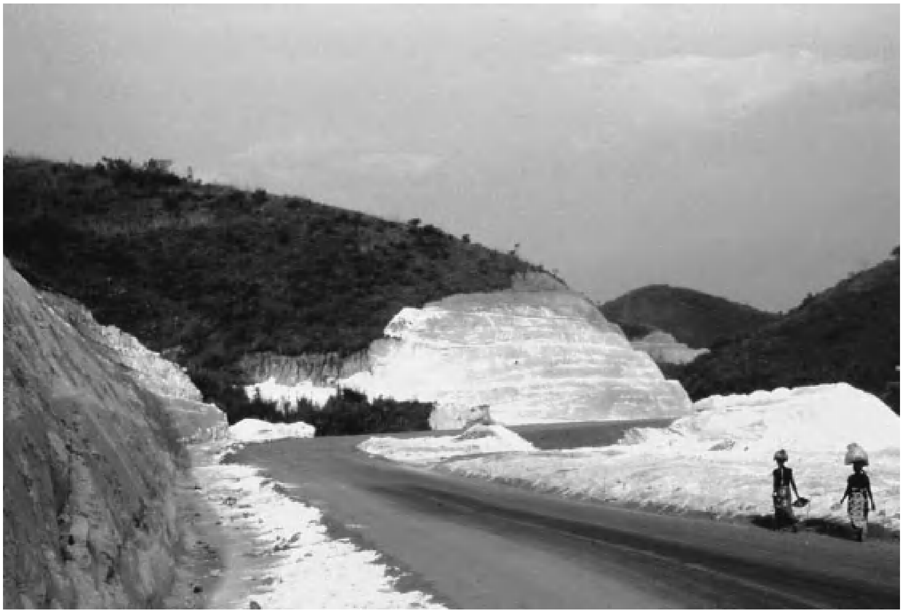

Figure 1.50 (Plate 1.50) Brilliantly white supergene kaolin below red laterite in the rainforest of northern Burundi illustrates lateritic soil profiles which originate by tropical weathering.

crusts (duricrust) that are composed of SiO_2 (silcrete – the geological home of precious opal), iron (ferricrete) or manganese (mangcrete) oxides and oxy-hydroxides. Zone C can be crumbled by hand but often displays an upper clay horizon (feldspars are argillized) and a lower sandy horizon with intact feldspars but vermiculized biotite. The first is called "saprolite", the second "saprock". Colours vary from red and brown to white or grey. Of course, bleaching indicates reduced conditions with dissolution and abstraction of iron, which is caused by organic acids derived from decaying vegetation.

Laterite zonation is due to the effect of seasonal changes between dry and wet periods: During dry seasons, soil water moves towards the surface and evaporates, inducing alkalic conditions that promote silica solubility. In wet seasons, acidic rain water seeps downward, dissolves and reprecipitates matter or takes it out of the system. Textures of lateritic soils include banded crusts, shrinking fissures, concretions, pisolites and oolites, small vertical tubular structures, Liesegang banding and many more. Newly formed solids are often amorphous and colloform, but diagenetic aging into minerals is omnipresent. An example is the transformation of iron hydroxide gel into goethite and haematite (eq. 1.9).

Aging of Fe(III) hydroxide into goethite and haematite:

$$\begin{array}{l} Fe(OH)_3 \rightarrow FeOOH + H_2O \\ 2FeOOH \rightarrow Fe_2O_3 + H_2O \end{array} \qquad (1.9)$$

The crucial factor for effective leaching is water, modulated by hydraulic properties of soil and bedrock that influence the contact time between water and minerals (Gabet *et al*. 2006). Of course, lateritic ore deposits are a variety of soil and consequently their investigation should always include methods and concepts of soil science:

Relative and absolute dating of supergene ore formation remains difficult. Cosmogenic nuclides such as ^{10}Be are usually employed for dating soil formation (Siame *et al*. 2006). If supergene alteration causes the precipitation of new minerals, age determination may be possible. One useful mineral is cryptomelane, a K-bearing manganese ore that can be dated with the $^{40}Ar/^{39}Ar$ method. Based on this approach, ± continuous formation of a supergene manganese deposit in South China from 40 to <2 Ma is revealed (Li *et al.* 2007). Supergene alunite in Chile's giant copper deposits was formed between 45 and 5 Ma, followed by atacamite (dated by ^{36}Cl) during the hyperarid Pleistocene (Reich *et al.* 2009). If haematite is present, palaeomagnetic methods may be useful that also provide a measure of palaeolatitude. Oxygen isotopes of hydrous minerals precipitated from weathering solutions (e.g. goethite, clay, gypsum) are effective archives of the past $\delta^{18}O$ of meteoric water, an important proxy of palaeoclimate (cf. "Isotope Geochemistry").

1.2.1 Residual (eluvial) ore deposits

In residual ore deposits, the economically interesting component is concentrated *in situ*, while weathering removes diluting parts of the rock. Examples are residual and eluvial placers, bauxite, lateritic gold, platinum, iron (Ni, Co) and nickel ores, residual enrichment of subeconomic protore iron and manganese, and industrial minerals such as phosphate, magnesite and kaolin.

The fundamental geochemical principle of the enrichment is the steady activity of a reaction front in soil, while the land surface is lowered by weathering and erosion. At the reaction front, the valuable component is immobilized. Note that this implies that the oldest parts of the profile are near the top of the regolith, and the youngest at the reaction front. The enrichment is due to retention and accumulation of the component of interest contained in the removed rock and soil volume (Figure 1.51). Theoretically, the mass of metal concentrated in stage (3) equals accumulation from the rock volume (R1 + R2). However, the system is not closed, as soil and solutions may move laterally out of it. An illuminating case is eluvial enrichment of phosphate from carbonatites by leaching of carbonate whereas apatite remains in place.

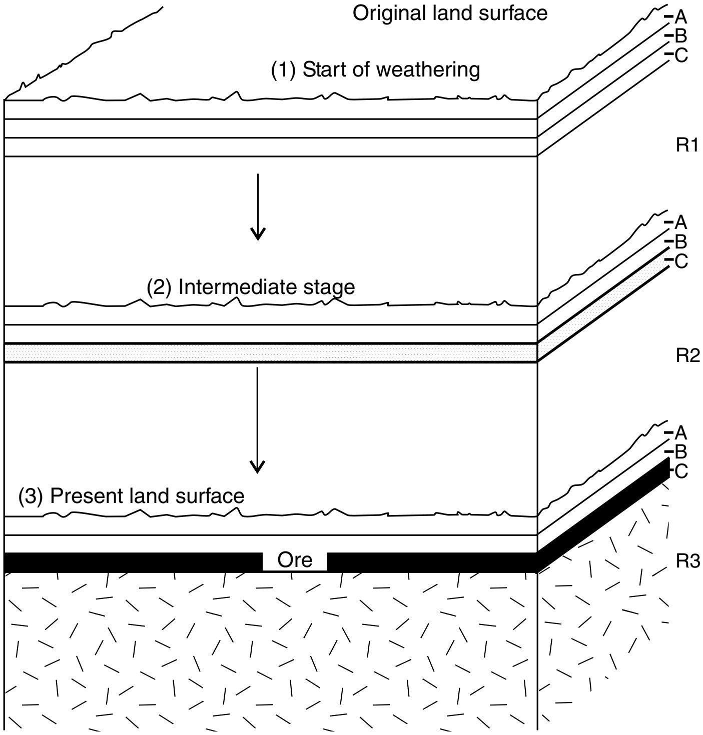

Figure 1.51 Idealized scheme of residual ore deposit formation by enrichment of a valuable component at a reaction front within the regolith (e.g. nickel in C-horizon saprolite).

Residual placers

Residual placers are concentrations of weathering-resistant ore minerals that are due to supergene abstraction of non-ore material. The term *eluvial* (outwash) describes the same result, although with more emphasis on physical removal of barren gangue. Many ore deposits contain heavy minerals that resist dissolution, such as native gold, cassiterite and wolframite. In this case, physical and chemical properties determine enrichment. Residual placers are only stable in flat morphologies, because steeper slopes induce soil creep and with it a down-slope displacement of ore fragments (resulting in colluvial placers). Residual placers often occur at the "stone-line" level of a soil profile, where quartz and durable ore minerals are concentrated.

Bauxite ore deposits

Bauxite ore deposits originate either by *in-situ* weathering of aluminium silicate rocks, or by allochthonous sedimentation after erosion of bauxite soil blankets. Autochthonous upland bauxites (e.g. covering the Dekkan trap basalts in India) are discerned from lowland bauxites that include detrital (sedimentary) deposits. Residual bauxite horizons often extend over large areas and mark regional unconformities that are related to favourable tectonic and climatic conditions (D'Argenio & Mindszenty 1995). Most deposits date from the Mesozoic and the Cenozoic, because the probability of conservation of soil decreases rapidly with increasing geological age. Many aluminium silicate rocks contain an average of 15% Al_2O_3 that must be upgraded by weathering to at least 35% Al_2O_3 to be economically exploitable. Alumina enrichment is caused by leaching of SiO_2 and iron, two substances that are not easily dissolved. The key are the repetitive cycles of favourable pH/Eh conditions in soil water as described above.

Lateritic gold deposits

Lateritic gold deposits as a class are a relatively recent discovery. One of the largest representatives of this group was the Boddington bauxite mine in Western Australia, which until closure in 2001 was the biggest gold mine in Australia with an annual gold production of 2500 kg. Pre-mining resources amounted to 60 Mt of ore at 1.6 ppm Au, apart from bauxite with gold contents of less than 1 ppm. Exploitable gold was located in near-surface, iron-alumina hard crusts that reached a thickness of 5 m and in additional 8 m thick lumpy Fe-Al laterite of the B-horizon. Sources of the gold in soil at Boddington are quartz veins and hydrothermally altered bodies of Archaean greenstone bedrock. Since 2007, resources of 400 Mt of this primary ore with a grade of 0.9 g/t Au and 0.12% Cu are exploited in a new mine. Worldwide, numerous lateritic gold deposits are worked. They are attractive because exploration, extraction and processing of soil is less costly compared with hard rock mining.

Lateritic iron ore deposits

Lateritic iron ore deposits are not an important source of iron, because both deposit size and iron grades are rather low. The ore consists of oolitic, red, yellow or brown haematite and goethite with elevated contents of H_2O, SiO_2 and Al_2O_3. Most deposits take the form of autochthonous or locally transported hard crusts (ferricrete) that reach a thickness of only a few metres. Nevertheless, lateritic iron ore derived from ultramafic source rocks is exploited in several countries (Albania, Greece, Moa Bay, Cuba and in the Philippines) as a high-iron limonite nickel ore (also termed "oxide nickel ore") for pig-iron blast furnaces. In oxide nickel ore, nickel is absorbed in amorphous iron-hydroxides or occurs as inclusions in goethite. The new technology of high-pressure acid-leaching (PAL) appears to alleviate the former economic disadvantage of these ores as a source of nickel.

Residual supergene enrichment of iron preconcentrations is the last upgrading event in the multistage evolution of **high-grade haematite ore deposits** with 60–68 wt.% Fe, which are derived from Precambrian BIF (cf. Section 1.3). Primary BIF are altered, silica-depleted and iron-enriched, in

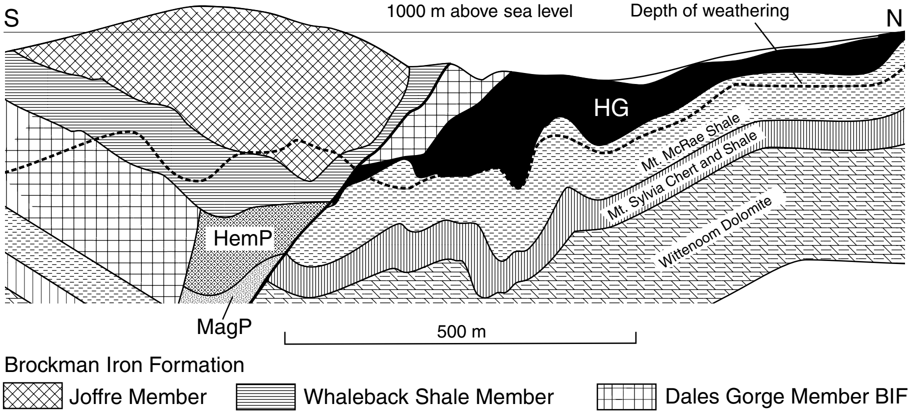

Figure 1.52 Profile of the high-grade haematite orebody at Mt Tom Price, Western Australia. Modified from Taylor, D., Dalstra, H.J., Harding, A.E., Broadbent, G.C. & Barley, M.E. 2001, Society of Economic Geologists, Inc., *Economic Geology* Vol. 96, Figure 5, p. 845.

Western Australia by the passage of diagenetic brines (Thorne *et al.* 2009, Thorne *et al.* 2004). In the vicinity of a normal fault at Mt Tom Price (Figure 1.52), the Brockman Iron Formation of the Palaeoproterozoic Hamersley Group was progressively altered to massive P-rich magnetite bodies (MagP) and microplaty P-rich haematite (HemP). Leaching in the supergene alteration zone is responsible for the final upgrading to economic ore of low-phosphorous high-grade haematite (HG). Note that phosphorous and carbonate abstraction at Mt Tom Price hardly changes iron concentration but makes the ore commercially more favourable.

Residual manganese ore deposits

Residual manganese ore deposits are derived from rocks with above-average manganese contents. Laterites developed from such rocks include hard crusts (mangcrete) or earthy manganese ore that may blanket considerable areas. In contrast to iron that tends to concentrate in the upper soil horizons (ferricrete), the slightly more mobile manganese is typically enriched in lower parts of the laterite profile. Although smaller than sedimentary manganese deposits, lateritic manganese ores are often high-grade and of superior quality. Sources (protore) are manganese quartzites, carbonates and volcano-sedimentary rocks that contain exhalative-sedimentary pre-enriched horizons. In India, metamorphosed Precambrian protore rocks were called gondite. Gondites consist of quartz, spessartine, rhodonite and rhodochrosite with minor amounts of pyrite, alabandite (MnS) and other minerals. Manganese contents in gondites remain below 30%. Weathering removes carbonate and SiO_2, enriching manganese oxides and hydroxides (at Morro da Mina, Brazil to a depth of >200 m). Carbonates and sulphides in gondite promote weathering and ore formation, whereas purely silicate-based gondites only bear thin ore blankets.

1.2.2 Supergene enrichment by descending (vadose) solutions

Lateritic nickel ore deposits are of major economic importance (Gleeson *et al.* 2003). They form by intensive and long-lived tropical weathering of ordinary ultramafic rocks, which enriches nickel (and cobalt). Two types of nickel laterite are distinguished: i) the oxide type in the upper, oxidized iron-rich part of the laterite; and ii) the silicate type in the lower, reduced saprolitic section of the regolith.

Laterite regolith zonation and the redistribution of nickel (Table 1.3) are the result of meteoric water percolating through the soil. Olivine, pyroxene and serpentine are rapidly decomposed by

BOX 1.7 Lateritic nickel deposits

Nickel laterites were discovered by Jules Garnier in 1863 on the island of New Caledonia in the Southwest Pacific Ocean. Exploitation started in 1876. Meanwhile, numerous similar deposits have been discovered worldwide. New Caledonia remains, however, the largest ore province of this type, with a past cumulate nickel production of 3.5 Mt (metal) and considerable remaining resources. Today, 4 large mines are in operation, based on reserves of ~1 Mt nickel in ore at >2.7 wt.% Ni, and 1 Mt of nickel in ore at 2.5–2.7%.

The ultramafic rocks of New Caledonia are part of a giant ophiolite nappe that was obducted during the Eocene and forms most of the island (Paquette & Cluzel 2007; Figure 1.53). Serpentinized and unaltered harzburgite-dunite displays an average 0.25% Ni (mainly in olivine) and 0.02% Co. Lateritization of the exposed ophiolite probably started in the Miocene, resulting in a mature profile (Figure 1.54):

- *Top*: Massive goethitic iron crusts (ferricrete; French *cuirasse*); low residual nickel concentration;
- *Limonite zone*: with residual manganese, chromium and aluminium; mostly bright red-coloured because of haematite traces; earthy or concretionary texture; nickel, cobalt, magnesium, calcium and silica are leached and strongly depleted; in rare cases, residual nickel is exploitable;
- *Nontronite zone*: Ferrallitic, earthy, red and yellow clays are the norm, but in some profiles massive or network silicification is prominent (opal, chalcedony, jasper, etc.); cobalt may occur in exploitable pockets of asbolane ("earthy

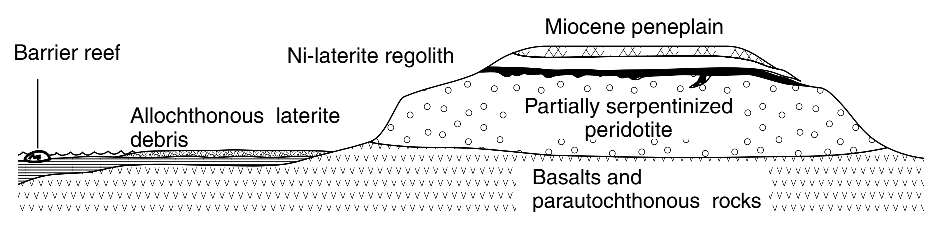
Miocene peneplain
Barrier reef
Ni-laterite regolith
Allochthonous laterite debris
Partially serpentinized peridotite
Basalts and parautochthonous rocks

Figure 1.53 Schematic profile of laterite blanket with nickel ore (black, garnierite-saprolite horizon) above peridotitic rocks such as the New Caledonian ophiolite (not to scale).

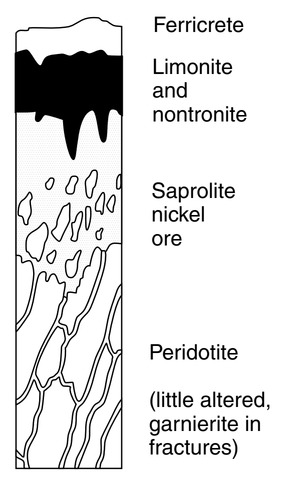
Ferricrete
Limonite and nontronite
Saprolite nickel ore
Peridotite
(little altered, garnierite in fractures)

Figure 1.54 Regolith profile of exploitable nickel laterite in New Caledonia. Note the control of garnierite by joints and fractures of peridotite. Modified from Gleeson, S.A., Butt, C.R.M. & Elias, M. 2003, Society of Economic Geologists, *SEG Newsletter*, Figure 3, p. 13.

cobalt", a variety of wad); occasionally, nickel and manganese are enriched to exploitable grades; the depletion of magnesium is minor, SiO_2 contents are equal to those in unaltered parent rock;

- *Saprolite zone*: This is altered parent rock with clearly recognizable structures and textures of the ultramafics; alteration is controlled by joints; in lower parts of the profile, altered rock includes increasingly fresh cores of parent rock until the base of surficial weathering is reached; the saprolite zone is the main nickel ore horizon, with veinlets, pockets and irregular masses of green garnierite (±chalcedony and magnesite); in the saprolite, olivine and pyroxene are altered to colloform magnesium silicates that age into the minerals antigorite (serpentine), talc and smectitic clays; nickel is taken up by these minerals in their lattice by cation exchange of Mg^{2+} and may reach several percent in the garnieritic ore; along permeable fractures, garnierite can penetrate far into the unaltered rock below the regular base of the regolith;
- *Bottom*: Unaltered hard rock with rare garnierite in joints and fractures.

acidic rain and soil water. From a surface value of ~6, the pH of deeper soil water turns alkaline (pH 8.5). Nickel is dissolved and flushed downward, where it is immobilized by ion exchange with Mg in newly forming magnesium hydrosilicates. A schematic example of this reaction (neogenesis of the Ni-serpentine népouite from serpentine) is given in equation (1.10).

Neogenesis of Ni-silicate in the saprolite zone:

$$Mg_3Si_2O_5(OH)_4 + xNi^{2+}aq \rightarrow (Mg,Ni)_3Si_2O_5(OH)_4 + xMg^{2+}aq \qquad (1.10)$$

Normally, groundwater removes the dissolved magnesium from the system. Some is precipitated as a carbonate (magnesite) in joints. Whether this process is able to form stockwork ore deposits of magnesite remains doubtful (cf. Chapter 3 "Magnesite").

Supergene enrichment of pre-existing mineralization

Supergene, descendent alteration may be exceptionally beneficial where pre-existing uneconomic mineralization or low-grade orebodies are affected. Primary ore (protore) in deeper parts of the weathering profile is upgraded by seepage solutions. For sulphide copper and silver ores, iron oxides and certain uranium ore deposits, this process is of economic significance. Non-sulphide zinc ore produced by supergene enrichment is a less common economically attractive target.

Table 1.3 Typical chemical characteristics (wt.%) of the iron oxide and silicate sections of nickel laterite deposits in New Caledonia (Gleeson *et al.* 2003)

	MgO	Fe_2O_3	SiO_2	NiO
Ferricrete	0.5	84	2	1.2
Limonite and nontronite	1.0	70	2.2	1.8
Saprolite	12.5	11.5	63.2	5.3
Peridotite (little altered)	42.7	9.1	41.3	0.3

The supergene enrichment of sulphide ore is a consequence of near-surface oxidation of sulphides caused by meteoric water seeping downwards through an unsaturated zone. Other agents include dissolved oxygen and microbes that have a role as "self-replicating catalysts" (Sato 1992). These microbes include chemolithotrophic mesophile bacteria such as (Acidi-) *Thiobacillus* or *Leptospirillum ferrooxidans* and extremophile archaea such as *Ferroplasma acidarmanus* (Newman 2010, Edwards *et al.* 2000). In modern metallurgical processing, sulphide-oxidizing microbes are cultivated in leach pads or large vats in order to decompose sulphide ores of, for example, gold, copper, nickel and cobalt.

Because it is kinetically slow, purely inorganic oxidation of sulphides has a minor share in the supergene enrichment process system (e.g. pyrite: Rimstidt & Vaughan 2003, Balci *et al.* 2007). The role of microbes in the oxidation of sulphides is essentially understood but its biochemistry is very complex (Newman 2010, Nordstrom & Southam 1997). *L. ferrooxidans*, for example, attacks the surface of pyrite at $T > 40°C$ and pH 0.7–1.0 by catalytic oxidation of Fe(II) to Fe(III). As an electron acceptor, $Fe^{3+}{}_{aq}$ abiotically oxidizes pyrite. *T. ferrooxidans* has a similar function but prefers cooler and less acidic conditions. Contact of $Fe^{3+}{}_{aq}$ with dissolved oxygen causes

precipitation of ferrihydroxide (Schrenk *et al.* 1998). Yet, the source of the oxygen in sulphate resulting from sulphur oxidation is mainly meteoric water, not atmospheric oxygen, as shown by oxygen-isotope investigations (Balci *et al.* 2007). The oxidation of sulphur and iron in one mole of pyrite (or marcasite) produces four moles of acidity. Consequently, weathering of pyrite-bearing rock (and other sulphides) is a natural or anthropogenic source of extremely acidic solutions (**ARD, acid rock drainage, or AMD, acid mine drainage**).
Oxidation of pyrite-rich copper ore is illustrated by equations 1.11.

Schematic reactions describing supergene oxidation of pyrite and chalcopyrite:

$$\begin{aligned} &2FeS_2+15O+8H_2O+CO_2 \\ &\quad \rightarrow 2Fe(OH)_3+4H_2SO_4+H_2CO_3 \\ &2CuFeS_2+17O+6H_2O+CO_2 \\ &\rightarrow 2Fe(OH)_3+2CuSO_4\ aq+H_2CO_3+2H_2SO_4 \end{aligned} \tag{1.11}$$

The results are acidic solutions, which move dissolved copper, but also silver, zinc and other metals through unsaturated soil down towards the groundwater. Because of their low solubility in oxic environments, iron hydroxides remain near the surface and form the characteristic botryoidal and cellular limonite-haematite masses of the "gossan" (Figure 1.55). Apart from iron, manganese and gold are enriched in gossans. Traces of minor metals in the primary sulphides may be preserved, such as Ag, Pb, Cu, Zn, Cd, Mo, Ni, As and Sb. Gossans are often collapse breccias, because a large mass of the original ore rock was abstracted. Gossans are conspicuous indicators for the possible presence of hidden sulphide ore and therefore, are prime prospecting guides. Gossans can be orebodies in their own right, mainly of gold. Of course, not all supergene limonite-haematite masses are connected with valuable ore ("false gossans"). The distinction is possible by mineralogical (Blanchard 1968) and geochemical investigations.

Below the gossan, a zone of bleaching and silicate weathering (with kaolin, alunite, etc.) is often developed that reflects the former passage of strong acids. Just above the groundwater table, native copper and copper oxides (cuprite, tenorite), carbonates (malachite, azurite), sulphates (gypsum), chlorides (atacamite) and silicates (chrysocolla) display a strikingly varicoloured

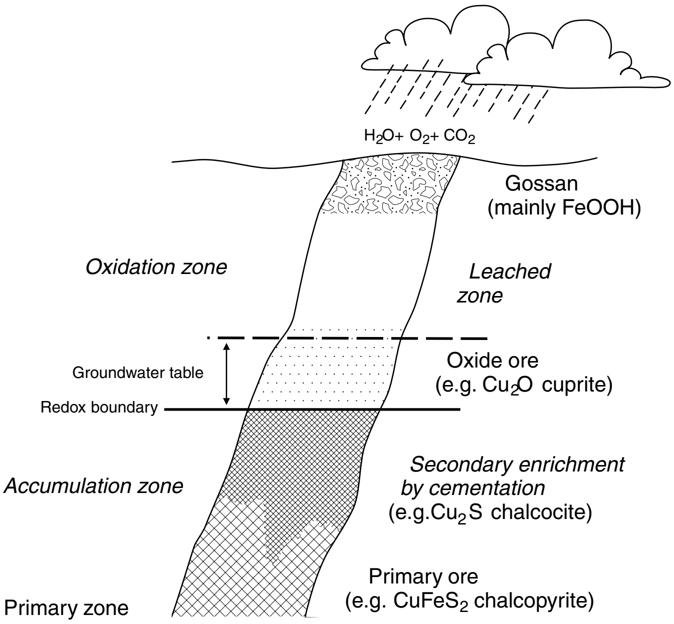

Figure 1.55 Schematic profile of a deeply weathered copper sulphide ore deposit, displaying the supergene "secondary" zonation resulting from redistribution of elements.

paragenesis. In some locations, this zone is enriched to an exploitable volume and grade (Melchiorre & Enders 2003). Prominent examples are several Chilean copper porphyry deposits that have important "exotic oxide" outliers (infiltration deposits, see below). Exotic ores were formed in drainage channels to a distance of about 7 km from the leached portion of the primary deposit (Chuquicamata, El Salvador, El Abra). In the hyperarid Atacama Desert, the copper salt atacamite $Cu_2Cl(OH)_3$ is an economically important ore mineral of oxide orebodies (Reich *et al.* 2008, 2009).

Where percolating water meets the groundwater table, the active reaction front is reached. Here, exothermic oxidation of primary sulphides takes place, as well as the secondary enrichment (Figure 1.55). Microscopy of replacement textures illustrates these processes. This zone is the preferred habitat of the thermophilic microbes mentioned above. Vestiges of the microbes were demonstrated by electron microscopy of contacts between chalcocite and primary sulphides (Sillitoe *et al.* 1996a). Isotope data indicate heating to nearly 100°C (Melchiorre & Williams 2001). The efficiency of secondary enrichment depends mainly on conservation of the acidic environment, but also on favourable hydraulic conditions (e.g. permeability). Carbonates and other basic host rocks that buffer acidity inhibit both organic and inorganic processes, resulting in very little secondary enrichment.

The chemical reactions produce galvanic mineral interactions (Sikka *et al.* 1991) and an electrochemical field near the orebody, which is a very clear target for geophysical exploration methods. Precipitation of enriched ore can be schematized as a cation-exchange reaction that results in formation of chalcocite, covellite or bornite (equation 1.12).

Formation of enriched secondary copper ore:

$$\begin{aligned}&5FeS_2+14CuSO_4\ \text{aq}+12H_2O\\&\quad\rightarrow 7Cu_2S\ \text{(chalcocite)}+5FeSO_4\ \text{aq}+12H_2SO_4\\&CuFeS_2+CuSO_4\ \text{aq}\rightarrow 2CuS\ \text{(covellite)}\\&\quad+FeSO_4\ \text{aq}\end{aligned} \tag{1.12}$$

The primary ore gains more of the valuable metal (here copper), often resulting in spectacularly rich orebodies. Dissolved iron and sulphate are transported away out of the system; part of the sulphate may be reduced by microbes so that additional sulphide is available. It is a frequent observation that many ore deposits are only economically exploitable because of supergene enrichment, based on primary sulphides of poor grade. This is true for a number of porphyry copper deposits, whereas others extract both enriched and primary ore.

Comparative investigation of replacement order showed that more "noble" metals (copper in eq. 1.12) replace more "common" metals (iron in eq. 1.12) that are dispersed. Earlier in this chapter, electrochemical reasons for this behaviour were cited. More noble metals (copper, silver, gold) also exhibit the tendency to occur in the native form, which may be explained by a redox reaction (eq. 1.13):

Formation of native metals by electron exchange:

$$\begin{aligned}&2Ag^{+}+2Fe^{2+}\rightarrow 2Ag^{0}+2Fe^{3+}\\&\text{(in water with dissolved } SO_4^{2-})\end{aligned} \tag{1.13}$$

Overall, weathering of a sulphide orebody comprises a complex system of physical, chemical and biological processes. Often, the observed end products do not match results of thermodynamic calculations. Unexpected parageneses can partly be explained by the argument that at the low temperatures of weathering, the activation energy needed for many reactions cannot be provided. This causes enlargement of thermodynamic stabilities of minerals into what Sato (1992) called "persistence fields" that are in good accordance with geological observations.

Prolonged weathering of a sulphide ore deposit results in a vertical zonation (Figure 1.55 and Figure 1.56) that comprises a leached (oxidation) zone, and a metal-rich cementation zone (supergene blanket), grading into unaltered mineralized rock of the primary zone (protore). In contrast to the primary depth zonation of hydrothermal mineral deposits, the supergene pattern is called "secondary vertical zoning". In stable cratons, oxidation reaches a depth of over 100 m, mainly as a function of the groundwater table that roughly

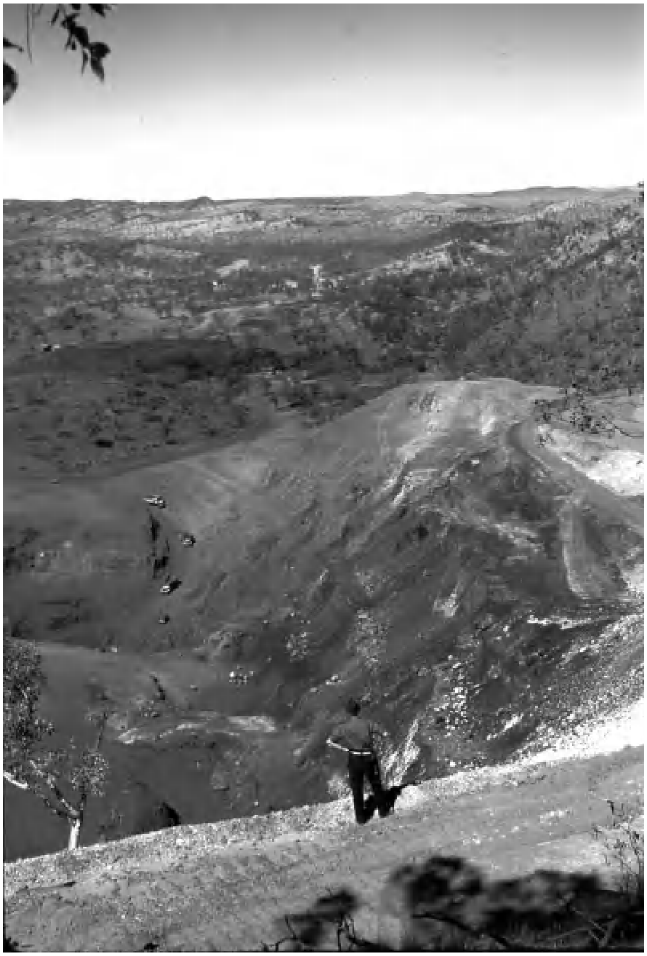

Figure 1.56 (Plate 1.56) For over 100 years, the supergene, high-grade chalcocite ore of the black shale-hosted copper deposit at Mt Oxide in the Mt Isa district, Australia, was the symbolic example of fortune and destitution for investors and miners.Gossan (red) covered an accumulation zone of 55 m thickness which graded into subeconomic primary sulphides. A sizeable ore shoot of 15.9% Cu was extracted by underground methods. Later, the pit was excavated and overall, the deposit yielded 23,000 t of copper (J.H. Brooks in Glasson & Rattigan 1990).

limits the penetration of oxygen dissolved in soil water. In special cases, oxidation occurs to much greater depths (Tsumeb Mine, Namibia to 1160 m: Lombaard *et al.* 1986) or far beneath the groundwater table (e.g. Bougainville, where oxidation "fingers" down along permeable faults). Obviously, the full understanding of a cementation or secondary enrichment deposit requires a thorough reconstruction of the morphological and hydrological evolution.

Iron ore deposits as a product of supergene enrichment

Iron ore deposits as a product of supergene enrichment provide an important part of world iron ore supplies. Protores are usually Palaeoproterozoic BIF (banded iron ore formations), with initial contents of ~25–45 wt.% Fe that are upgraded to 60–63% Fe. Note that there is a sharp divide between: i) medium-grade martite-goethite deposits; and ii) high-grade haematite deposits, which reach a maximum of 68% Fe. Haematite orebodies differ from supergene enrichment systems by reaching a great depth beneath the surface (~1500 m) and huge tonnages (3000 Mt, although most are in the range between 200 and 500 Mt). Based on various observations, current genetic interpretations of high-grade haematite deposits involve mainly epigenetic hydrothermal models (Thorne *et al.* 2009, Clout 2006).

Supergene enrichment is at the origin of common martite-goethite ore (Morris 1985, 1993). However, genetic models are very different from the simple laterite blanket type. It is assumed that near the surface, ferrous iron is leached from BIF by reduced seepage water rich in dissolved carbon and is carried downwards along flow channels such as faults crossing BIF beds. This establishes an electrochemical system that allows flow of electrons. The surface region functions as a cathode, the BIF at depth as an anode. In this system, conversion ("oxidation") of ferrous to ferric iron takes place without the presence of free oxygen. Magnetite is replaced by martite (haematite pseudomorphous after magnetite) or by maghemite. The reaction also multiplies the solubility of silica and other gangue minerals that are leached and replaced volume for volume by goethite (FeOOH). By-product acidity causes transformation of BIF shale bands into kaolinite marker horizons in ore. Orebody growth is upward from depth. If exposed by erosion, lateritic hard crusts may form from this ore, underlain by a friable zone of haematite. Let me add that it is quite possible that martite-goethite protore is hydrothermal just like high-grade haematite preconcentrations; research will soon provide clarification.

1.2.3 Infiltration as an agent of ore formation

Infiltration is a term borrowed from hydrology, where it is used to describe the movement of surface water into soil, porous rock, or karst. Infiltration ore deposits are formed when meteoric waters take up a substance that is dissolved by weathering, and concentrate it after considerable transport by infiltration in a different geological setting. Uranium is an illuminating example, because during surficial alteration it is easily dissolved from ordinary rocks such as granite, gneiss and felsic tuff, and is transported by creeks and rivers for tens to hundreds of kilometres, until infiltrating into an aquifer where reduced conditions cause precipitation and concentration. Certain deposits of copper, iron, vanadium, silver and Pb-Zn-Ba-F are suggested by some scientists to have a similar origin. In the preceding text, we have mentioned Chile's exotic copper deposits as part of the infiltration class. Generally, the metals may be derived from older preconcentrations or from rocks with common trace element contents. Selective weathering of different minerals may produce a pattern of spatial or temporal separation, for example by first leaching traces of uranium, copper and zinc from plagioclase and Fe-Mn oxy-hydroxides, followed by barium, lead and SiO_2 when the more stable K-feldspar is decomposed.

The concentration of solutes in surface and groundwater is generally very low. Enrichment to ore-grade and an exploitable volume is only possible where a large mass flow is focused into a highly efficient filter. For dissolved matter, geochemical barriers are most effective, commonly in the form of a rapid change of pH and Eh. Geological actors include carbonates, H_2S or SO_4 in the pore waters, as well as live, decaying and fossil organic matter (biomats, peat, coal, bitumen), including by-product methane.

Because precipitation takes place in pre-existing rock, infiltration mineralization is clearly epigenetic, not syngenetic. Investigations of infiltration ore genesis always include (palaeo-) hydrogeological methods.

BOX 1.8 Infiltration ore deposits of uranium

Infiltration deposits of uranium are very common and economically important. Oxidative chemical weathering transforms uranium (IV) in rocks to uranium (VI), which forms complex ions with free SO_4^{2-}, CO_3^{2-}, OH^-, alkalis and humates. Under oxic conditions in surface and groundwater, these complexes are stable and allow long-distance transport. Geochemical barriers for uranium are phosphates, arsenates, vanadates and carbonates in percolated rocks, strong reduction (e.g. methane) and sorption by colloids of iron hydroxides, silica and organic matter (Min *et al.* 2005). Correspondingly, uranium infiltration mineralization and ore deposits occur in permeable sandstone and conglomerate (Colorado Plateau, or "sandstone type"), in volcanic ash beds, in faults and breccia bodies, in peat, lignite and coal seams, in asphalt, and in terrestrial calcite crusts of semiarid lands (the "calcrete type"). The genesis of the last includes a pronounced component of evaporation.

The Colorado Plateau is a Precambrian block covered by some 3000–4000 m of little deformed Permian to Eocene sediments. Numerous terrestrial sandstone and conglomerate strata occur in this package. Uranium deposits and occurrences were found in all stratigraphic positions, with the largest endowment in Triassic and Jurassic rocks (Sanford 1990). The time span of mineralization, however, is from 80–50 Ma (Late Cretaceous to Palaeogene), independent of host rock age. The shape of orebodies varies widely, including tabular lenses, sometimes stacked on top of each other, pockets and the characteristic "roll fronts" (Figure 1.57), often in connection with buried river courses. Roll fronts mark the redox boundary in space and time where the infiltrating meteoric water lost its capacity to oxidize the percolated sandstone and to retain uranium in solution. Tabular deposits appear to have been controlled by the interface between two different meteoric water bodies, a stagnant saline brine and freely flowing fresh groundwater that carried uranium and vanadium. In the tabular type, the main ore mineral is coffinite, in contrast to the uraninite of the roll front type. Oxidation/reduction fronts in the aquifers are clearly visible in the field, by red and grey colours of the rocks. Spotty reduction by coal fragments in sandstone caused formation of high-grade ore pockets, but also the complete replacement of large tree trunks by uraninite. It is thought that sources of uranium were the many tuff bands in the sediments, but other possibilities include former basement islands or detrital uraniferous minerals in sandstone. Ore minerals include coffinite, uraninite, vanadium-rich clays and minor sulphides (of Fe, Mo, Cu, Pb, Zn, Se, etc.). Neogene uplift of the plateau caused a late phase of renewed weathering that affected many deposits and produced highly conspicuous varicoloured secondary uranium minerals.

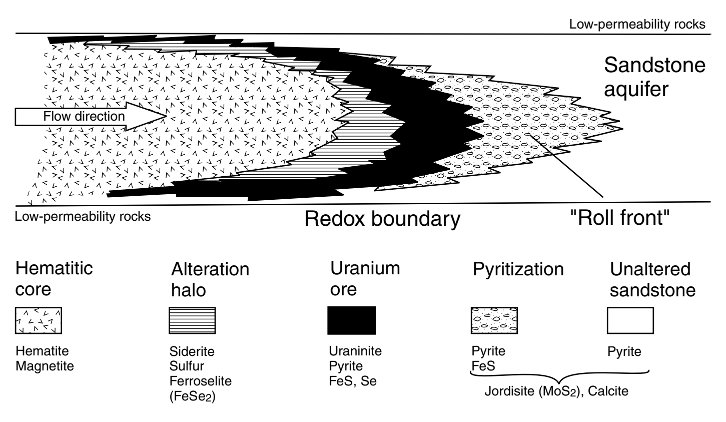

Figure 1.57 Roll front uranium orebodies develop, where infiltrating uraniferous meteoric water passes through a redox boundary.

The example of the Colorado Plateau demonstrates that infiltration ore deposits are formed by meteoric waters that descend into basins – the reverse from diagenetic-hydrothermal ore deposits, which are also found in marginal areas of basins but are formed from ascending basinal solutions (cf. Section 1.4 "Diagenetic Ore Formation Systems"). Copper, lead and silver ores embedded in haematitic sandstone suites ("red bed deposits") may have originated in a way similar to infiltration deposits of uranium (e.g. the Transfiguration deposit in Quebec: Cabral *et al.* 2009). There are, however, viable alternative modes of their formation by basin dewatering, so that each case must be carefully investigated. Resemblance and differences are illustrated by the large sandstone-hosted but diagenetic-hydrothermal Zn-Pb deposit at Jinding, Yunnan, China, with ~220 Mt at 7.4 wt.% combined grade (Chi *et al.* 2007, Kyle & Ning 2002). Sandstone ore of base metals and silver is generally low-grade and therefore at present economically not very attractive.

Formation of karst systems in carbonate rock bodies and the contemporaneous deposition of mineralization in the caves may also be related to **infiltration processes**. However, karst infiltration deposits are more a suspected than a proved deposit class. In the Maghreb Region of northern Africa, numerous small deposits of Pb and Zn (± barite, fluorite) in solution caves were formerly exploited. Following earlier authors who studied lead-zinc karst ores in Europe, many scientists proposed that the North African deposits have formed by concentration of dissolved trace metals originally hosted in the karstified carbonates (Bernard 1973, Zuffardi 1976). Meanwhile, the application of modern research technologies suggests an epigenetic hydrothermal origin, probably related to migrating saline basinal brines. However, the karst infiltration model retains its theoretical validity: Examples may be supergene manganese ores in solution caves of Devonian carbonate rocks in South China (Li *et al.* 2007) and in Cenomanian-Turonian dolostone at Imini, Morocco (Gutzmer *et al.* 2006), or vanadium karst ore in Neoproterozoic dolomites of Namibia (Boni *et al.* 2007).

Karst formation is caused by infiltration of meteoric water, which is enriched in CO_2, for example by percolation through the organic soil horizon. Dissociation of carbonic acid produces acidity (H^+) that is essential in limestone dissolution. Because of a much slower reaction rate, dolomite is less affected by karstification. The reactions of limestone dissolution are described in equation 1.14:

Carbonic acid-induced limestone dissolution:

$$\begin{gathered} H_2O + CO_2(g) \leftrightarrow H_2CO_3 \leftrightarrow HCO_3^- + H^+ \\ CaCO_3(s) + H^+ \rightarrow Ca_2^+ + HCO_3^- \end{gathered} \tag{1.14}$$

There are three possible modes of ore deposit formation in karst:

1 Hydrothermal karst originating from hot ascending fluids (e.g. the famous Carlsbad cave in New Mexico, which was formed by hypogene sulphate solutions: Polyak *et al.* 1998); structural relations such as cementation of host rock karst breccia by sulphides reveal simultaneous calcite dissolution and sulphide precipitation (Figure 1.58); note the possible connection with metasomatic ore formation.

2 Common meteoric karst, formed by downward percolating water with dissolved carbon dioxide, which was later filled by ascending hydrothermal fluids with ore and gangue, independent of karstification.

3 Common meteoric karst, and ± synchronous supergene infiltration of ore elements.

Only the last case answers the definition of a supergene ore deposit. Bernard (1973) discussed the possibility of ore formation in the setting of a common karst system. The hydrogeological zonation is the key (Figure 1.59):

> Underneath the karst infiltration surface is the zone of ± vertical percolation (A). Rain or melt water seeps down rapidly, mechanical erosion and leaching of calcite along flow-tubes are very intensive. Any sediments will be quite coarse-grained. The environment is strongly oxidizing. The following zone of ± horizontal, highly variable water flow (B) is reached where the vertical seepage is collected by underground rivers. Sediments are mainly of the sand and silt grain size. The environment is still oxic and the only mineralization may be barite. In the lower parts of a mature karst system, a zone that is permanently submerged under water (C) can have sections with a "micro-euxinic" environment. Microbes feeding on imported organic matter reduce sulphate to H_2S. Sediments are either very fine-grained or chemical precipitates. Host rocks are silicified and dolomitized; cave walls are encrusted with limonite and clay. Mineralization grows inward and includes sulphides (mainly Pb, Zn, Sb and Cu), fluorite, barite, calcite, dolomite and occasional vanadium ores. Bernard (1973) thought that the metals were derived from the dissolved limestone (carbonates have contents in the ppm-range), but more often infiltration of weathering solutions from surrounding non-carbonatic rocks is assumed.

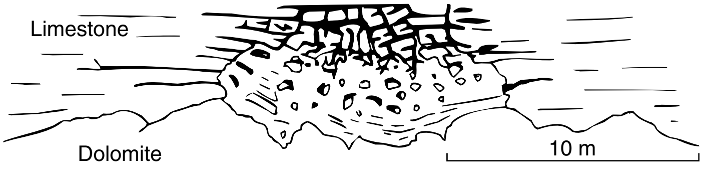

Figure 1.58 Lead-zinc ore (black) in a hydrothermal karst tunnel in Zechstein carbonate, Upper Silesia, Poland. Modified from Sass-Gustkiewicz, M. 1996, Society of Economic Geologists, Inc., *Economic Geology Special Publication* 4, Figure 2, p. 174.

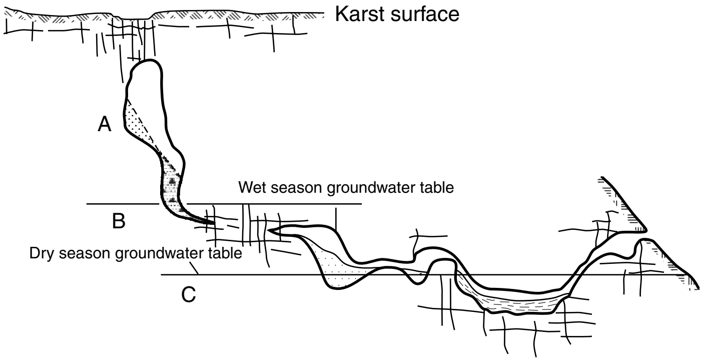

Figure 1.59 Hydrogeological cross-section of a mature karst system (modified from Bernard 1973). With kind permission from Springer Science + Business Media.

Discrimination of supergene karst-infiltration from hypogene mineralization is only possible with modern analytical methods (e.g. a study of fluid inclusions). Observation alone is unable to decide. This is vividly demonstrated by the scientific controversies concerning the origin of the Mississippi Valley type deposits, which lasted more than half a century. Consider the sedimentary geopetal (gravity-induced) structures of ore, gangue and internal sediments in a cave in an Alpine lead and zinc deposit (Figure 1.60). The bedding planes of host and cave fill are nearly parallel. Both were tilted, as shown here by later tectonic movements. Similar to Figure 1.58, repeated caving of the roof is visible. Obviously, the pattern may be due to both ascending or descending solutions. Complicating the situation even more, in a near-surface setting (in this case an emerged reef) both super- and hypogene processes may interact at the same time.

Karst has several properties that may occur alike in hydrothermal and common meteoric water systems (Ford & Williams 2007). These have to be fully understood for rationally exploring and mining karst orebodies. Most important is the observation that thick carbonate strata always have horizons that are more prone to the development of solution caves and tunnels. This is, of course, a first-order guide for finding orebodies. Causes for easier karstification may have been higher initial porosity or brittleness and high purity of the carbonate rock. Clay beds often enhance mineralization by channelling or constricting the flow of water or of hydrothermal fluids. Faults and joints are additional elements that, together with stratigraphic ones, control the three-dimensional structure of a karst system. It is also important to elucidate the fourth dimension, that is the evolution of the system in time. Very practical aspects of mining a karst system concern hazards such as sudden inrushes of water, mud and debris, unstable surroundings of mine openings and damage to water rights owned by third parties.

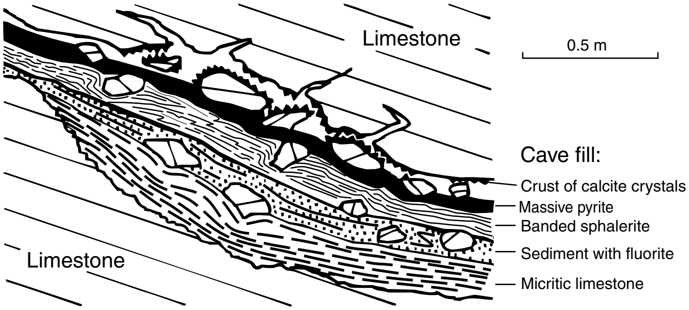

Figure 1.60 Section of a Late Triassic hydrothermal karst cave at Bleiberg, Austria, that shows sedimentary layering involving fluorite, zinc ore and clastic cave sediment.

1.3 SEDIMENTARY ORE FORMATION SYSTEMS

The processes of sedimentation include physical, chemical and biological components. The prevailing regime lends its name to the major subgroups of sediments and sedimentary rocks: mechanical, chemical and biogenic sediments. Sediments are also classified according to the provenance of the material (allochthonous/autochthonous), and the manifold variations of locality and environment of deposition (Nichols 2009). Classifications of ore deposits that originate by sedimentary processes apply analogous criteria.

Allochthonous, terrigenous materials of prime economic importance are gravel, sand and certain clays. The source of the particles composing these rocks is distant from the deposits, the material was transported. Metallic ore deposits of this genetic group are called placers. Placers are mechanical enrichments of heavy and chemically resistant native metals and minerals by flowing or otherwise agitated water.

Autochthonous raw material deposits were formed at the site of the deposit. This group includes chemical precipitates and partially biogenic substances such as carbonates (limestone, dolomite, magnesite), evaporites (rock salt, potassium salt, gypsum), some massive and oolitic ironstones, banded iron formations, marine phosphates, sedimentary sulphide ores and manganese ore beds. Organic formation is the prevailing component for coal, oil shale, diatomite and for part of the limestones (e.g. chalk). All forms of life (Figure 1.49) participate in sedimentary minerogenesis. In sedimentology, soils are also considered as autochthonous sediments. However, ore deposits related to soil formation processes were presented in the preceding section.

Many metalliferous sulphide, oxide, carbonate and sulphate deposits originate by autochthonous sedimentation following hydrothermal exhalation, precipitation of solutes and deposition of ore particles on the seafloor. *Sensu stricto*, all ores with this origin are "sedimentary". However, the different process systems that may cause subaqueous exhalation of ore fluids and the prevailing geological setting must be part of the classification. This is why Cyprus type sulphides are grouped with "Ore Deposits at Mid-Ocean Ridges and in Ophiolites" and Kuroko and Besshi types with "Volcanogenic Ore Deposits". In this section, only those deposits of exhalative-sedimentary character are discussed, which were formed in a sedimentation-dominated environment and distal from contemporaneous volcanism. This is the class of sedimentary-exhalative (sedex) deposits.

Sedimentation is limited to the surface of the Earth, which is also the realm of life and its biogeochemical cycles (Falkowski *et al.* 2008). Therefore, sedimentary ore formation will almost always have a biogenic component (Southam & Saunders 2005). In some cases this is very obvious, for example in phosphate deposits made of bones and coprolites, or a lignite seam composed of fallen trees. In few ore deposits, however, the biogenic component is immediately visible. This is illustrated by sedimentary sulphide deposits that display a very light, biogenic sulphur isotopic composition, although the metals were introduced by hydrothermal-exhalative systems from below the seafloor. The cause for the light sulphur lies in oxygen depletion of seawater around hydrothermal centres and consequently, massive proliferation of anaerobic sulphate-reducing bacteria such as *Desulphobacter* or *Desulphomaculum* (Boschker *et al.* 1998). In the photic zone, green sulphur bacteria (Chlorobiaceae) thrive by anoxigenic photosynthesis. Sulphate-reducing bacteria often form consortia with archaea, whose role is not yet fully understood. These microbe communities reduce seawater SO_4 to H_2S, using organic matter as an electron donor (eq. 1.15). Simultaneously, carbon is "mineralized" to CO_2 or carbonate. As the microbially mediated reduction of sulphur involves a considerable negative isotope effect, metal sulphides formed from this H_2S contain light, "biogenic sulphur". However, a minimal sulphate content in seawater of more than 1 mM is a precondition. Low contents of dissolved sulphate in seawater may have several reasons (e.g. the precipitation of evaporite gypsum: Wortmann & Chernyavsky 2007; cf. Section 4.2.2 "Seawater in the Geological Past"). The maximum isotopic fractionation by bacterial sulphate reduction (BSR) is 46‰, but most natural samples have a much smaller spread. Some rare microbial

BSR-communities produce intermediate-valence sulphur species (like S^0 or $S_2O_3{}^{2-}$) by bacterial sulphur disproportionation (BSD) that results in $\delta^{34}S$ fractionation between sulphate and sulphide approaching 70‰ (Canfield & Thamdrup 1994; Canfield & Teske 1996). Quite often, the involved microbe colonies are fossilized in the form of framboids (microscopic aggregates of pyrite cubes in shale). Earliest evidence for biogenic sulphate reduction dates from ~2.7 Ga. Earlier in the Archaean, bacterial sulphur disproportionation seems to have been the main microbial metabolism (Philippot *et al.* 2007).

Anaerobic microbial (bacterial) sulphate reduction:

$$\underset{\text{(organic matter)}}{106(CH_2O)16(NH_3)(H_3PO_4)} + 53SO_4^{2-}$$

$$\Rightarrow 106CO_2 + 16NH_3 + H_3PO_4 + 106H_2O + 53\,S^{2^-} \tag{1.15}$$

Another frequent form of microbial sulphate reduction occurs at diffuse ("pockmark fields") or vent-like locations ("cold seeps") of methane degassing from sediments or from gas hydrate layers beneath the ocean floor (eq. 1.16). The process is very similar to the one described above.

Anaerobic microbial sulphate reduction and concurrent methane oxidation:

$$SO_4^{2-} + CH_4 \Rightarrow HS^- + HCO_3^- + H_2O \tag{1.16}$$

The precipitation of metals and other elements from exhalations and seawater depends on the presence of suitable partner ions (e.g. HS^-) and pH/Eh conditions. One mode of precipitation is anion exchange, for example mixing of dissolved chloride-metal complexes with H_2S-rich seawater, resulting in sulphide formation. Note that sulphide precipitation results in lowering the pH (equation 1.17). Where redox-sensitive metals are transported across zones of different Eh, for example from the coast into a euxinic marine basin, the precipitates reflect this by lateral zoning. Zones may comprise oxides near the coast followed by carbonates, silicates and finally sulphides in the most reduced environment. Zoning is most noticeable if the same metal is present through all zones as in some iron ore districts. In polymetallic ore deposits, several subzones may be distinguished within the major facies zones.

Production of acidity by sulphide precipitation:

$$\underset{\text{metal ions}}{Cu^+ + Fe^{2+}} + \underset{\text{hydrogen sulphide}}{2H_2S} \Rightarrow \underset{\text{chalcopyrite}}{CuFeS_2}$$

$$+0.5H_2\,(aq) + \underset{\text{acidity}}{3H^+} \tag{1.17}$$

1.3.1 Black shales in metallogenesis

Carbonaceous shales are important host rocks of sedimentary ore deposits. They are fine-grained laminated clastic sediments consisting variably of quartz, carbonate and clay with more than 1% of organic matter. Global black shale units may reflect major perturbations of global carbon and climate cycles, which are controlled by endogenous (tectonics, mantle plume break-out) and exogenous processes (Emeis & Weissert 2009). Their sedimentary environment is characterized by low energy, benthic anoxia and often, by euxinic conditions (associated with stable reduced sulphur species in water above the seafloor). As shown earlier, metal cations dissolved in seawater are precipitated by H_2S and HS^-. The mass of metals dissolved in modern seawater is very large: 13,300 Mt molybdenum, 4400 Mt uranium, 2690 Mt vanadium, 690 Mt zinc and 620,000 t lead. Marine anoxic periods in the geological past may have temporarily reduced the concentrations to less than half of these figures (Algeo 2004).

Organic-rich pelites are generally characterized by elevated contents of redox-sensitive trace elements (including U, V, Mo, Ni, Co, Cr, Cu, Pb, Zn, Cd, Au, Ag, As: Morford & Emerson 1999) and phosphate. Many of the enriched elements are essential for life and their changing concentration in seawater through geological history influenced the evolution of life on our planet (Anbar 2008). Some may have been sourced from continents and entered the sea adsorbed on detrital organic particles. The import of a large mass of plant remains into marine black shale basins is often questioned. Yet, many marine petroleum source rocks produce oil with a considerable fraction of paraffins, whose main precursors are waxes and lipids of plants (Hunt 1996). Apart from continental sources, mid-ocean hydrothermal activity, submarine volcanism and extraterrestrial matter provide parts of the dissolved metal stock. Explanations for preferential metal concentration in marine black shales include:

- Significant metal enrichment may be acquired by the special faculty of marine organic matter to bind trace metals dissolved in seawater (especially Ni, Co, Cu and Zn);
- in contrast to the first group, V, U, Mo and Cr are not fixed by organic species but by reduction;
- elements like Ba, P and Cd are imported from and indicators of a high biological productivity in the upper, oxic layer of the stratified water column.

Manganese (and sometimes even iron) is typically impoverished in black shales relative to ordinary pelites, because it dissolves in the highly reducing bottom sediment pore waters and with increasing consolidation, is flushed out back into the sea. This reduction is in part due to bacterial activity (Kim *et al.* 2004). Low Fe-contents (expressed by low Fe/Ti ratios) inhibit the formation of synsedimentary to early-diagenetic pyrite, favouring the production of significant amounts of H_2S in anoxic pore fluids. This may be an important factor controlling the amount of reduced sulphur available to form ore deposits by capturing metals from migrating fluids.

Accordingly, most black shales have anomalous metal contents, but these are not economically exploitable. The only current profitable use of ordinary black shales is the recovery of the energy inherent in organic matter, either by direct burning or by the production of synthetic oil (cf. Chapter 7.7 "Oil Shale"). The most important economic significance of black shales is their role as the main source of petroleum and natural gas. Similar to the expulsion of hydrocarbons, metals mobilized from black shales during diagenesis or metamorphism can form ore deposits. Some former black shales have been transformed into metamorphic graphite deposits.

Yet, there are many large **sulphide ore deposits hosted in black shales** (with metals such as Cu, Sb, Zn, Pb, Ag and Au), which were typically formed from submarine hydrothermal-exhalative fluids, but precipitation from average seawater without increased hydrothermal input is a plausible alternative. A current example of this scientific controversy is the Chinese Mo-Ni sulphide ore shales (Shao-Yong Jiang *et al.* 2006, Lehmann *et al.* 2007, Wille *et al.* 2008; cf. Chapter 2 "Molybdenum"). Similarly, the European copper shale and the Central African copper-cobalt shale deposits were for a long time considered to be purely sedimentary formations. Meanwhile, the scientific consensus is that both were formed epigenetically by migrating diagenetic, hot fluids (cf. Section 1.4 "Diagenetic Ore Formation Systems").

The distinction between sedimentary and diagenetic ore deposits is sometimes ambiguous, both in theoretical classification and in practical application. The critical difference is the time of concentration of the considered element: Was it effected during sedimentation of the immediate host rocks (by syngenesis) or during later diagenesis (by epigenesis, for example concentration by migrating formation waters)? Isochemical recrystallization during diagenesis or later metamorphism does not justify a different genetic class, except that the sedimentary ore may be called consolidated, lithified or metamorphosed.

Sedimentary ore deposits are increasingly explored and investigated by methods of dynamic basin analysis, sequence stratigraphy and palaeogeographic reconstructions, that were first developed for oil and natural gas exploration (Einsele 2000). These methods encompass concepts such as distinction between sedex-deposits formed during early rifting of a basin and others that originated during later thermal contraction. If the stratigraphic, facies and tectonic evolution of a basin is well understood, it appears possible to predict prospective localities and stratigraphic positions of potential ore (Ruffell *et al.* 1998).

1.3.2 Placer deposits

Sedimentary placer deposits are mechanically formed concentrations of heavy, durable minerals that may occur in transported soil or regolith (colluvial), in fluviatile and in coastal sediments. Aeolian placers (Figure 1.61) and placers in glacial sediments are also known, but rarely of economic

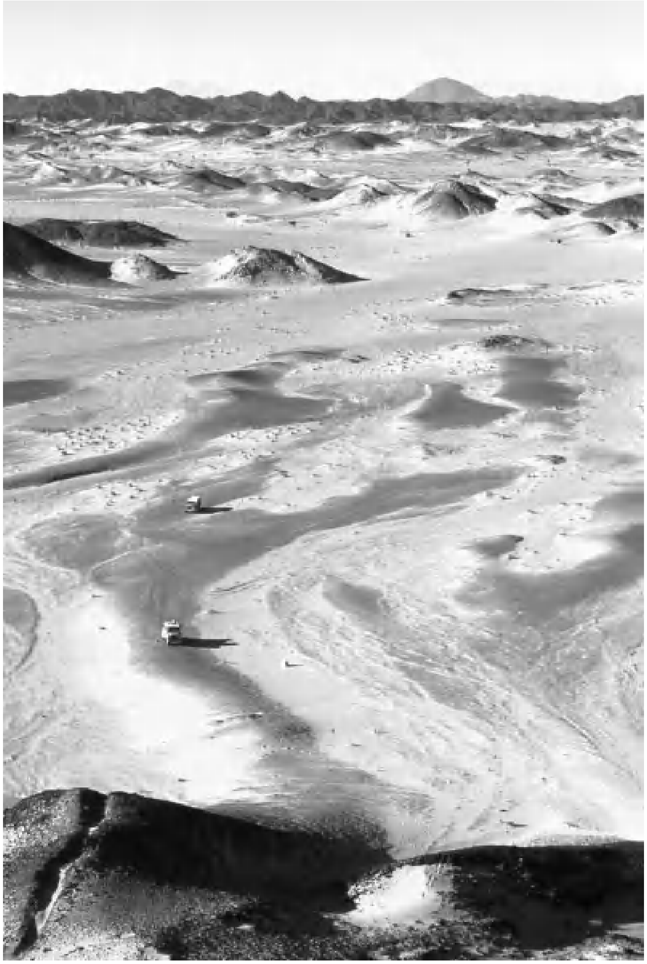

Figure 1.61 (Plate 1.61) Aeolian lag enrichment of magnetite (dark sand patches) at An Kor, Red Sea Hills, Sudan. Note the exploration trench testing the Neoproterozoic primary mineralization in the foreground.

significance. Placer deposits of economic importance are classified as residual, eluvial, colluvial, fluviatile and coastal (for the latter, terms also used include marine and beach placer). Geologically young, usually Quaternary placers (Duk-Rodkin *et al*. 2001) are discerned from fossil placers. Residual and eluvial placers were briefly introduced earlier.

Placers are important sources of gold, platinum metals, tin, titanium (rutile, ilmenite), zircon, rare earth elements (monazite) and gemstones (diamond, garnet, ruby). Precondition of the concentration of placer minerals is their mechanical and chemical durability during weathering and transport, and their elevated density compared with the ordinary rock forming minerals (Table 1.4).

Simple washing in a gold pan (Figure 1.62) easily separates light quartz and feldspar from dark mafic silicates, garnet, ilmenite and magnetite. This dark fraction of "black sand" contains the valuable minerals such as flitters of gold. Note, however, that the same term black sand is often used to describe Canada's giant oil sand resources, which are definitely not placer deposits.

Colluvial placers originate by downslope creep of soil from weathered primary deposits (Figure 1.63). Heavy minerals move to the base of the regolith, whereas lighter and fine-grained

Table 1.4 Density of common placer and gangue minerals (g/cm^3)

Feldspar	2.5–2.8	Monazite	5.2–5.4
Quartz	2.65	Magnetite	5.2
Mafic silicates	ca. 3–4	Columbite	5.2–7.9
Diamond	3.5	Scheelite	5.9–6.1
Topaz	3.5–3.6	Cassiterite	6.8–7.1
Garnet	3.6–4.3	Wolframite	7.0–7.5
Corundum (ruby)	3.9–4.1	Cinnabarite	8.1
Rutile	4.2–4.3	Uraninite	7.5–9.7
Ilmenite	4.5–5.0	Platinum metals	12–21.5
Zircon	4.7	Gold	15–19.3

The density of many minerals varies considerably because of chemical variation. Alloys of native metals vary in composition.

fractions are displaced upwards. Orebodies are sheet- or channel-like bodies consisting of ore (e.g. cassiterite) and gangue (quartz) minerals, and of rock fragments. Colluvial ore minerals at the foot of a slope can be eroded by rivers and reconcentrated by alluvial processes.

Fluviatile, or alluvial placers

Fluviatile, or alluvial placers occur in active stream channels and in older river terraces (Figure 1.63). Heavy mineral concentrations form at morphologically well-defined sites, mainly characterized by changes of flow velocity. Such sites include large boulders, rock bars, gravel beds on the inside bank of river bends, the downstream end of gravel and sand islands (point bars), but also reed patches. Another important trapping mechanism is infiltration of heavy minerals into open pore space of sand-free pebble banks (Hattingh & Rust 1993). This mechanism explains exceptionally high gold grades in the ancient Witwatersrand

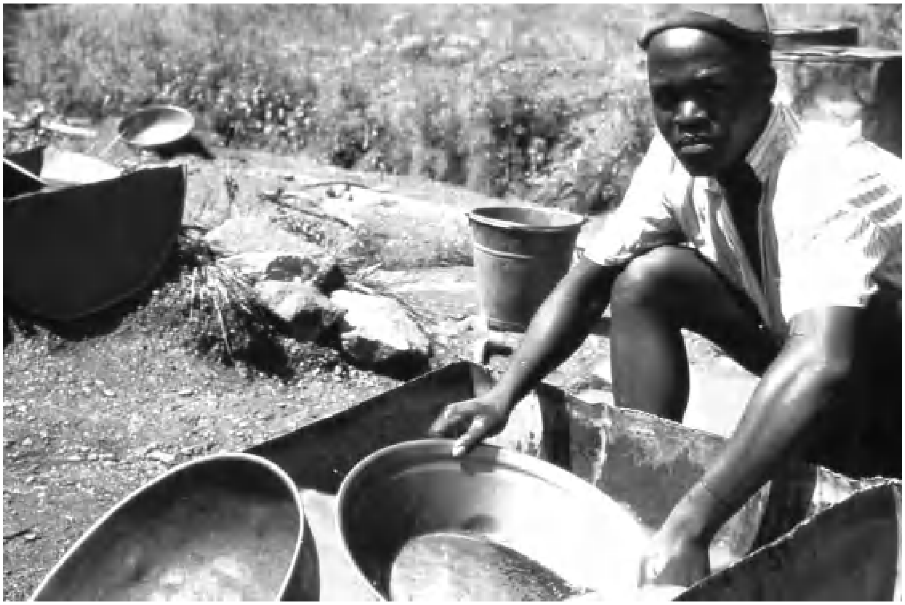

Figure 1.62 (Plate 1.62) Panning cassiterite-columbite ore from Ngara pegmatite, eastern Rwanda. Note the small mass of black ore mineral sand which remains from washing the pan initially filled with ore to the brim.

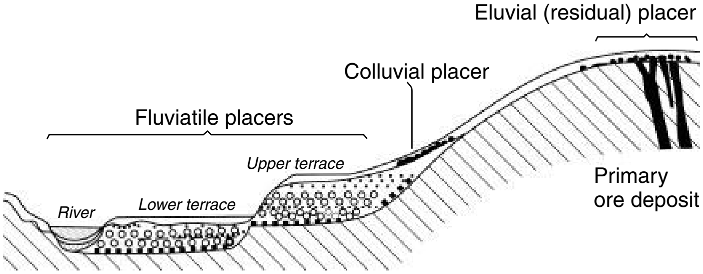

Figure 1.63 Cross-section of a river valley near an outcropping primary ore deposit, which is the source of residual (eluvial), colluvial and fluviatile placers (black dots).

conglomerates (see below). Saxton *et al.* (2008) confirmed experimentally that high-grade longitudinal pebble to cobble bar systems trap gold during their formation from fast-moving suspension flows. Many alluvial placers in mountain stream valleys comprise the whole volume of the valley fill (Figure 1.64). Downstream, trapping sites, such as those mentioned above, control exploitable grades. Alluvial placers rarely extend for more than several kilometres along a valley, because both concentration and grain size of ore minerals diminish with increasing transport distance.

Transport, deposition and density sorting of minerals in flowing water are controlled by factors of "hydraulic equivalence". Originally, this term was used in the sense of "settling equivalence", which refers to the physical principle that the settling velocity of suspended particles in water depends on diameter and density (Stoke's Law, eq. 1.4). Hydraulic equivalence *sensu stricto* results in concurrent deposition of small high density

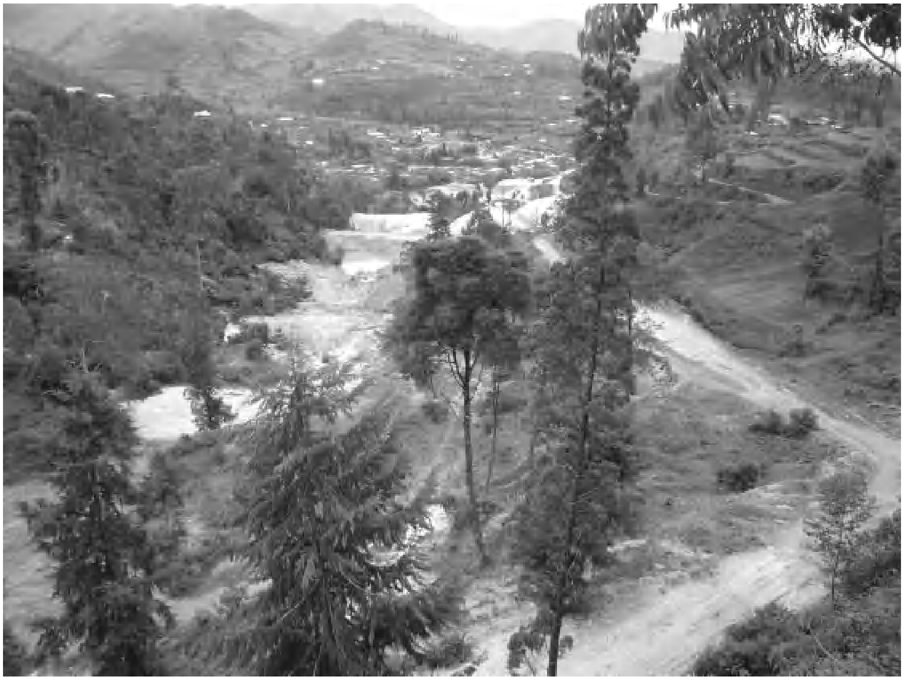

Figure 1.64 (Plate 1.64) Alluvial placer mining near Ruhanga in the tin-tantalum district of Gatumba, Rwanda. After extraction, the devastated valley must be restored. Courtesy B. Lehmann, Clausthal.

grains with larger and lighter ones (e.g. fine-grained gold in coarse alluvial gravel). Meanwhile it has been recognized that concentration of heavy minerals is due to several dynamic processes, which include lag mechanisms: When river sediment is entrained, high density particles tend to remain essentially *in situ*, whereas light particles are removed downstream (this is called "selective entrainment" or, linguistically not quite correct, entrainment equivalence; e.g. James & Minter 1999). Today, the term hydraulic equivalence is usually understood to comprise both settling and entrainment equivalence, and other hydrodynamic factors such as shape, size and surface properties of particles (Carling & Breakspear 2006).

Investigations of fluvial placer formation must include studies of the particular sedimentary system (Fielding *et al.* 2009). Physical models of turbulent mass flow in fast-moving rivers support genetic understanding ("granular physics", Frey & Church 2009). Extensive pebble to cobble longitudinal bar systems of braided rivers at Witwatersrand, South Africa (gold) and Elliot Lake, Canada (uraninite) are believed to have originated in such an environment. Enrichment of the heavy minerals is caused by their tendency to accumulate near the base of a flow where they are easily trapped (Saxton *et al.* 2008).

Often, the highest concentration is located at the base of the valley fill directly on bed rock, but ore is also found above beds of fine-grained or cohesive ground between pebble beds ("false bed rock"). This may be caused by two different mechanisms:

1 The heavy minerals gradually work themselves to the bottom of a pebble bed (this is the hypothesis of an "active bed", Bilibin 1938); or

2 a perpetual and complete reworking of the pebble bed is assumed so that selective entrainment concentrates heavy minerals at the base ("lag deposit").

The second explanation appears to be more likely, because floods provide the main input of energy into erosion and transport processes of river valleys. When exploring for placer deposits, or sampling river sediments for other purposes, it is always advisable to invoke practical aspects of hydraulic models. In addition to hydraulics, chemical and biochemical processes in valley sediments mobilize and reprecipitate elements, including native gold (Reith *et al.* 2010). Chemical mobility of gold in placers is suggested by both the occurrence of very heavy nuggets that could hardly be moved by flowing water and by the occasional observation of idiomorphic, undeformed gold crystals in river sediments:

> Today, geologically young alluvial placers are mainly exploited for gold. Their economic role is feeble, however, compared to the time of the great gold rushes in California, Alaska and Australia in the 19th century. Among fossil alluvial placers, the Archaean Witwatersrand Basin in South Africa hosts by a wide margin the largest gold resources of the world. Because of the costs of increasingly deep mining, however, its share of world gold production is steadily decreasing. It is one of the world's most intensively investigated placer districts (for more details refer to Chapter 2.3 "Gold"). One remarkable result of the research is the reconstruction of the palaeohydrologic situation (Figure 1.65a) showing braided streams, pebble diameters and flow vectors of one of the gold conglomerate beds. Figure 1.65b demonstrates that higher gold contents occur in the middle section of the fan, whereas both marginal (entry front) and basinal areas contain less gold. Geological mapping and precise determination of fluvial facies regimes are essential contributions to a rational exploitation of these superdeep deposits.

The source of ore minerals in placers is an exciting question, both for the practician posing questions such as "Can we locate the primary source?" and for scientists. One way is to estimate the mass balance between erosion and uplift in the source region in comparison to the depositional system. Application of this approach reveals that the mass of gold in the Witwatersrand District can be explained without invoking exceptionally high gold contents in the former source region (Loen 1992).

Coastal placers

Coastal placers are mainly formed in surf zones. In contrast to typical alluvial placers, both light and

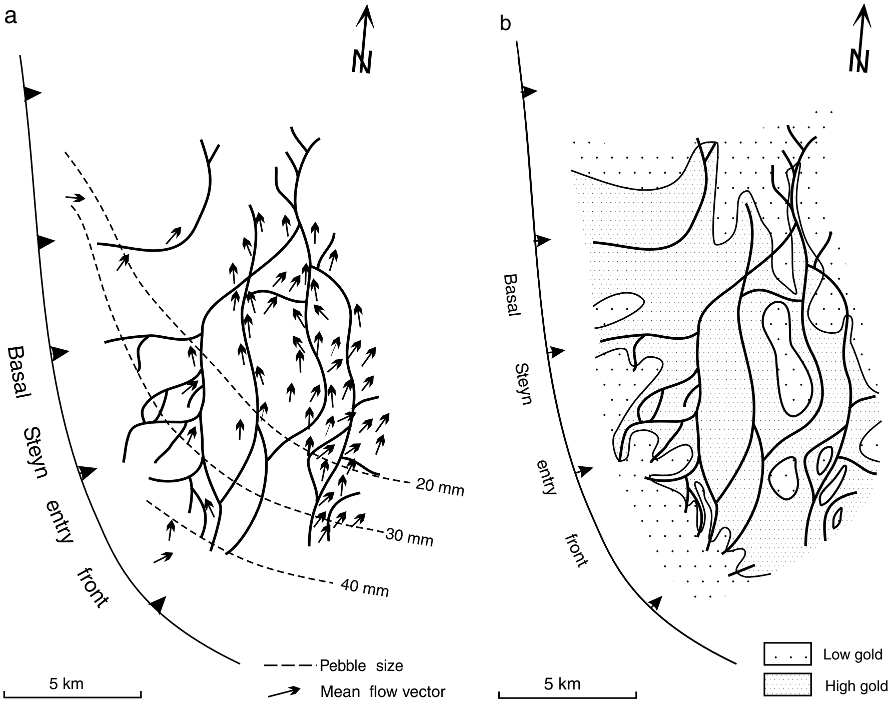

Figure 1.65a,b Facies control of gold deposition in the braided alluvial fan complex of the Basal and Steyn Reefs in the Steyn Mine, West Rand Goldfields, South Africa (after Minter *et al.* 1986). Courtesy Geological Society of South Africa.

heavy minerals occur roughly in the same grain size that is almost exclusively sand. Obviously, the hydraulic equivalence *sensu stricto* has no role in this environment and the critical factor is mainly entrainment equivalence. The incoming surf imposes a turbulent regime that transports suspended sand including heavy minerals towards the beach. When a wave runs out, sand grains settle for a moment. Return flow to the sea is laminar and only light minerals can be entrained. Heavy minerals are enriched in a narrow linear strip along the beach. Other coastal processes may enhance placer formation including tides, lateral currents, wind and especially storms that induce higher waves (Roy *et al.* 2000, Hoefel & Elgar 2003).

Coastal placers are more frequent on stable coasts, because neither strong erosion nor rapid sedimentation is propitious. Single orebodies are elongated narrow lenses or strips of dark sand that may extend over hundreds of kilometres. In some cases, the connection of placers with a river mouth delivering sediment is obvious, but erosion of older coastal strata may also be a source. Sea level changes produced either submerged placers (e.g. during Quaternary glacial conditions, the sea was >100 m below the present level) or deposits above today's sea level associated with the raised beaches of Pleistocene interglacial and older climate epochs warmer than today. Recently, a major new province of marine placers was discovered in the Murray Basin of interior Australia. The placers occur in 400 km long barrier complexes as beds and narrow "shoestrings", which formed in a very shallow transgressive Pliocene inland sea. The barriers developed across more than half of the basin. Many promising coastal placer deposits of coarse-grained (90–300 μm) quartz and the heavy minerals rutile, zircon, ilmenite and altered ilmenite (leucoxene) have been outlined. In lower-energy environments, only low-grade and fine-grained (40–80 μm) heavy mineral sands were deposited. The concentration is attributed to large storms and consequent ground swells, which may have eroded pre-enriched underlying Miocene sands (Roy *et al.* 2000).

Coastal placers can consist of up to 80 wt.% heavy minerals. Their contribution of rutile and zircon to world markets is of high economic importance. They are lesser sources of diamond and cassiterite. Gold and platinum are rare in coastal placers. Iron ore breccias ("detrital iron ore") hosted by Early Cretaceous transgressional sediments in Northern Germany constitute a rarely mentioned type of coastal placers. In this region, oxidized pyrite nodules of emerged Jurassic shales were swept by the surf into depressions that developed due to salt diapirism and subrosion. The ores were low-grade and mining ceased with increasing competition by overseas imports.

1.3.3 Autochthonous iron and manganese deposits

Autochthonous iron and manganese ores are chemical, partly biogenic marine sediments. Today, terrestrial iron ores (including recent bog iron ore, or after diagenesis siderite in black coal) are economically insignificant. In the future, manganese nodules and crusts of the deep oceans may become an essential source of metals. For now, the most important raw materials of this group are enriched parts of marine banded iron and manganese formations (predominantly formed in the Palaeoproterozoic), and ooidal or massive iron and manganese ore beds that are of much younger, Phanerozoic age.

Banded iron formations

Banded iron formations (BIF, including the varieties itabirite, jaspilite, cherty iron formations) are layered, banded (0.5–3 cm) and laminated (<1 mm) rocks containing >15% iron. Essentially, BIF consist of quartz and magnetite layers that form sedimentary units reaching lateral extensions of thousands of kilometres and a thickness of hundreds of metres. Geological setting and associated rocks allow a subdivision of BIF into three types:

1 Algoma type in submarine volcanic settings;
2 Superior type in marine shelf sediments; and
3 Rapitan type, which is closely related to glaciogenic marine sediments (James & Trendall 1992).

Banded iron ores of **Algoma type** are especially common in Archaean greenstone belts, but occasionally, geologically similar deposits formed in younger periods (Figure 1.61). The oldest examples are known in the Isua Belt on Greenland (Whitehouse & Fedo 2007; ∼3800 Ma). Host rocks of Algoma ore are volcanogenic sediments such as greywackes, tuffaceous and magmatic volcanic rocks. Typical ore beds are less than 50 m thick and may display a transition from oxide through carbonate and silicate to sulphide facies. Oxide facies iron occurs as magnetite, haematite is rare (Figure 1.66). Algoma type iron formations extend to several thousand square kilometres, which is quite small compared with Superior type basins. In several districts, numerous exhalative centres with sulphides

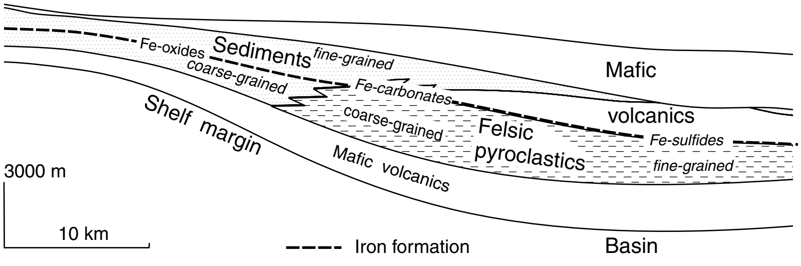

Figure 1.66 Stratigraphical context and facies zones of an Algoma Type volcanogenic iron formation in the Archaean Michipicoten Basin, Canada. Modified from Goodwin, A. M. 1973, Society of Economic Geologists, Inc., *Economic Geology* Vol. 68, Figure 2 p. 919.

and some larger VHMS deposits punctuate Algoma BIF horizons (McClenaghan *et al.* 2009). This observation, and their close association with volcanism, suggest formation on the seafloor by exhalative, hydrothermal-sedimentary processes driven by heat anomalies. Magmatic fluids may also participate in ore formation. Consequently, Algoma type ore is essentially volcanogenic (cf. Section 1.1 "Volcanogenic Ore Deposits").

Banded iron ores of **Superior type** (Figure 1.67) are hosted in sedimentary sequences that include black, organic-rich and silicic shale, quartzite and dolomite, and transgress older basement. Bimodal volcanic rocks (rhyolite and basalt) may occasionally form part of the country rocks. This indicates a sedimentary environment of stable continental shelves covered by relatively shallow seas with some extensional tectonic strain and associated volcanism. Shallow, coastal and deep basinal facies can be recognized (James & Trendall 1992).

Iron formations of the Superior type are marine sediments of global extension. They are preserved in remnants of marine basins that reach tens of thousands of square kilometres. Banding and lamination are remarkably persistent but not all BIF are strictly autochthonous. Chert-free, massive iron sediments locally replacing bedded BIF are interpreted to reflect synsedimentary sifting and deposition by density currents (Lascelles 2006). Truncated beds, flow ripples and synsedimentary deformation structures are recorded. Commonly, BIF contain iron in oxide, carbonate and silicate phases; sulphides are rare. Iron and SiO_2 were deposited as fine-grained ooze (or as a gel), but ooids, concretions and biogenic textures have been observed. Primary precipitates were probably amorphous SiO_2, ferric hydroxide $Fe(OH)_3$ and nontronite (near landmasses, oxic conditions), or precursors of magnetite, siderite and greenalite $[(Fe)_{2\text{-}3}Si_2O_5(OH)_4]$ (far from land; in deeper,

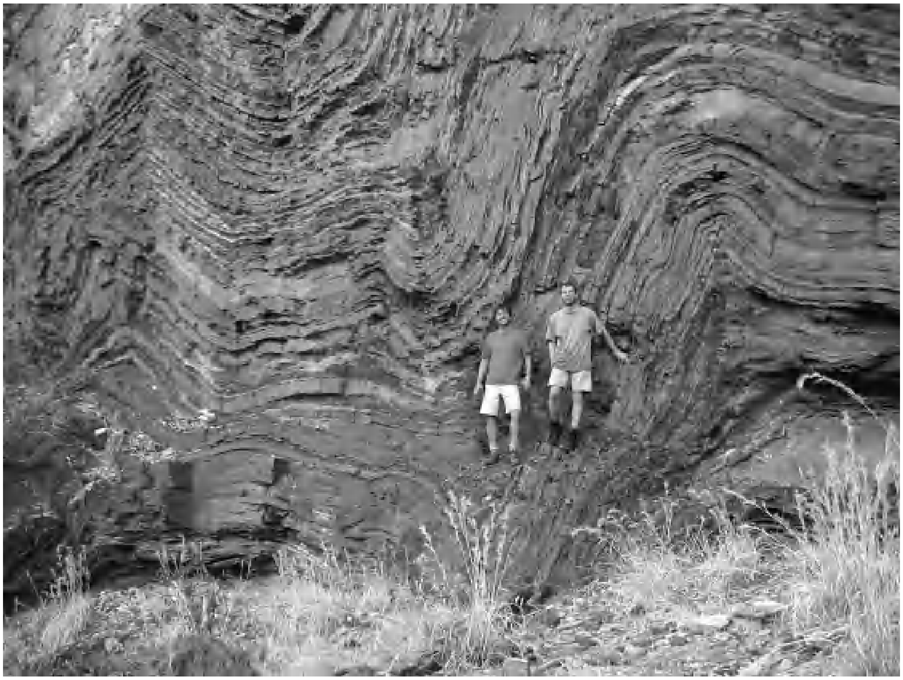

Figure 1.67 (Plate 1.67) Folded and metamorphosed Superior type banded iron formation near Mt Tom Price mine in the Hamersley Gorge (Karijini National Park, Western Australia) with marine scientists Aivo Lepland and Mark van Zuilen kindly posing for scale. Iron-rich beds black, silica (jasper) red. Photograph by Aivo Lepland, courtesy Geological Survey of Western Australia.

dysoxic-anoxic basins). Diagenesis and common low-grade metamorphism produced the ordinary paragenesis of BIF ore, comprising quartz, haematite, magnetite, siderite, minnesotaite [$(Fe,Mg)_3Si_4O_{10}(OH)_2$], stilpnomelane, asbestiform amphiboles and many other Fe-rich silicates. Primary ores have an Fe_2O_3/SiO_2 ratio of 0.98–1.26, typically 25–45 wt.% Fe, <3% each of Al_2O_3, MgO and CaO, and small contents of Mn, Ti, P and S. This discriminates Superior type BIF from other marine sedimentary iron ores. At sufficiently high magnetite grades, the primary ores are exploited as "taconite". Most BIF-based iron ore mines, however, extract parts of iron formations that were enriched either: i) by supergene processes typically resulting in "martite-goethite ore" with 60–63 wt.% Fe; or ii) by hypogene hydrothermal processes forming "high-grade haematite ore", with 60–68 wt.% Fe (cf. Section 1.2 "Supergene Enrichment"). Martite is a term that denotes haematite pseudomorphs replacing magnetite.

BOX 1.9 The origin of Superior type iron formations – still disputed

Superior type BIF occur exclusively in the Late Archaean and Early Palaeoproterozoic (2.6–1.8 Ga). Apart from the formation of giant iron and manganese deposits, the Archaean-Palaeoproterozoic transition includes other remarkable events of Earth history:

- The Lomagundi-Jatuli carbon isotope excursion (Melezhik *et al.* 2004);
- the Earth's earliest (Huronian) glaciation;
- the first global appearance of terrestrial "red beds";
- the earliest abundant calcium sulphate sediments; and
- the Shunga event, a giant accumulation of C_{org}-rich sediments.

The common cause of these changes is probably the rapid expansion of photosynthetic eukaryotes, which was triggered by enhanced nutrient supply and the first formation of an ozone shield in the atmosphere. Most scientists relate the precipitation of the giant mass of iron contained in BIF to the transition of oceans and atmosphere from a reduced to an oxidized state (the "Great Oxidation Event" between 2.45 and 2.2 Ga: Holland 2002, 2005; Anbar *et al.* 2007, Anbar 2008, Kump 2008, Qingjun Guo *et al.* 2009). In the Archaean before oxidation, PO_2 of the atmosphere was <10–5 PAL (present atmospheric level). Other scientists, however, suggest that oxidized seawater existed much earlier (Ohmoto *et al.* 2006, Kesler & Ohmoto 2006).

Sources of iron in BIF may have been:

- submarine-exhalative systems (Kimberley 1994, Morris 1993) similar to today's mid-ocean ridges;
- submarine-exhalative systems associated with intraplate tensional tectonic structures and volcanoes (Bekker *et al.* 2010, Barley *et al.* 1997); and
- continental weathering.

Probably, all these sources contributed iron at different times and locations (Alibert & McCulloch 1993). However, worldwide trace metal contents of Superior type BIF are very low (Morey 1992), arguing against local hydrothermal sources and for homogenized ocean water. Sources of SiO_2 in the chert bands were most probably weathering landmasses (Hamade *et al.* 2003). It is assumed that the ancient oceans were saturated with dissolved silica (as $Si(OH)_4$), resulting in a steady rain of siliceous matter to the ocean floor. The modern oceans are markedly undersaturated in silica and this may be the main reason for the changing character of iron ores, from ancient BIF to more recent ironstones. The banding in BIF can be explained by diurnal to seasonal cycles of biological activity, to temperature fluctuations (Posth *et al.* 2008), or to episodic depletion of ferrous iron in the water column.

Essential parameters of the formation of Superior type BIF are still discussed, apart from the basic agreement that the ores are chemical or biogenic precipitates from seawater (eq. 18).

Oxidative precipitation of dissolved reduced iron forming banded iron formations:

$$2Fe^{2+} + 0.5O_2 + 5H_2O \rightarrow 2Fe(OH)_3 + 4H^+ \qquad (1.18)$$

Many scientists support the following hypothesis: "The atmosphere may have been nearly free of oxygen, while the oxygen in the oceans started to increase. Seasonal blooms of the earliest photosynthetic micro-organisms (cyanobacteria) increased oxygen concentration in seawater that oxidized and precipitated dissolved Fe^{2+}."

Recently, this was both confirmed (Qingjun Guo *et al.* 2009) and vividly contradicted (Ohmoto 2003a, Ohmoto *et al.* 2006). The latter cast doubt on both a low-oxygen atmosphere and the late appearance of cyanobacteria, and propose a euxinic model, with precipitation of iron at the contact between reduced deep water and O_2-rich surface water. Widespread euxinia is confirmed by sulphur isotope and iron speciation data (Reinhard *et al.* 2009). Under anoxic conditions, BIF deposition may have been catalysed by anoxygenic photoautotrophic bacteria (Kappler *et al.* 2005). A third possible precipitation mechanism is abiogenic UV-induced oxidation (Bekker *et al.* 2010). Iron isotope investigations support the concept of a redox-stratified ocean (Rouxel *et al.* 2005) and of an important role of early diagenetic dissimilatory iron reduction (Johnson *et al.* 2008). The worldwide termination of Superior type BIF deposition at ~1.85 Ga may have been caused by the Sudbury impact: Slack & Cannon (2009) suggest that the bolide's oceanic impact destroyed redox layering in the oceans, which impeded dispersion of dissolved Fe(II) from ocean-floor hydrothermal vents. In their thorough review, Bekker *et al.* (2010) conclude that no single parameter explains BIF formation and suggest a control by multiple environmental changes of earth systems.

Manganese formations

In the Transvaal Basin of South Africa, **marine manganese oxide strata (manganese formations, MnF) of the ca. 2.22 Ma Hotazel** Formation occur interlayered with Superior type BIF, which hosts important iron ore deposits. The outstanding feature is, however, that this province (the Kalahari manganese field: Maynard 2010) comprises about half of the world's manganese resources. The concentration of Mn relative to Fe is believed to have been effected by earlier abstraction of iron from seawater and precipitation of BIF. In consequence, the more soluble manganese was relatively enriched and only when PO_2 continued to rise, Mn^{2+} was oxidized to Mn^{3+} and manganese-rich beds were deposited. Note that similar to Superior type BIF, manganese formations are only exploitable if enrichment processes acted on protore (cf. Chapter "Manganese").

Banded iron formations of **Rapitan type** were deposited immediately following the Sturtian (~730 Ma) and the Marinoan (630 Ma) glaciations, during the Cryogenian System of the Neoproterozoic. The name Rapitan is derived from a Sturtian locality in the Mackenzie Mountains, Northwest Canada. Similar occurrences were found in Brazil (Urucum: Walde & Steffen 2007) and in Namibia (Otjosondu). During these glacial events, land and even oceans were widely covered with ice ("Snowball Earth" hypothesis: Hoffman *et al.* 1998), causing a nearly global anoxia and the presence of dissolved ferrous iron in seawater. Inter- and post-glacial melting of the ice caps resulted in formation of glacial sediments, re-oxidation of the oceans, and precipitation of ferric iron and manganese oxides. As marine sediments, Rapitan type iron formations are similar to Superior type BIF, but have little economic significance.

Oolitic iron ore

Oolitic iron ore was exploited from approximately 500 deposits worldwide. Formation of this ore type is restricted to Phanerozoic time. Economically outstanding historic mining districts in the Jurassic of western Europe, and those in the Palaeozoic of the northern USA led to the distinction of "Minette type" (limonitic) and "Clinton type" (haematitic). Always, these ores are sediments of shallow epicontinental seas or of shelf-regions and are interbedded with clastic sediments. Ore beds reach a thickness of about 30 m and lateral extensions up to 150 km. This suggests that eustatic highstands are favourable conditions for their formation, as shown by Young (1992) for the Ordovician deposits of the West-Mediterranean province.

Oolitic iron ore (Figure 1.68) is not banded and contains no primary colloidal silica. Textural varieties include mainly the namesake round accretionary bodies called ooids (earlier termed "ooliths") and pisoids, but also fine-grained iron ore particles forming massive "ironstone" *sensu stricto*. Precipitation of ooids in agitated water is indicated by many observations, including intraclasts of oolitic rock in ooidal matrix, fractured and freshly mantled ooids, cores of ooids formed by quartz, phosphorite and fragments of fossils,

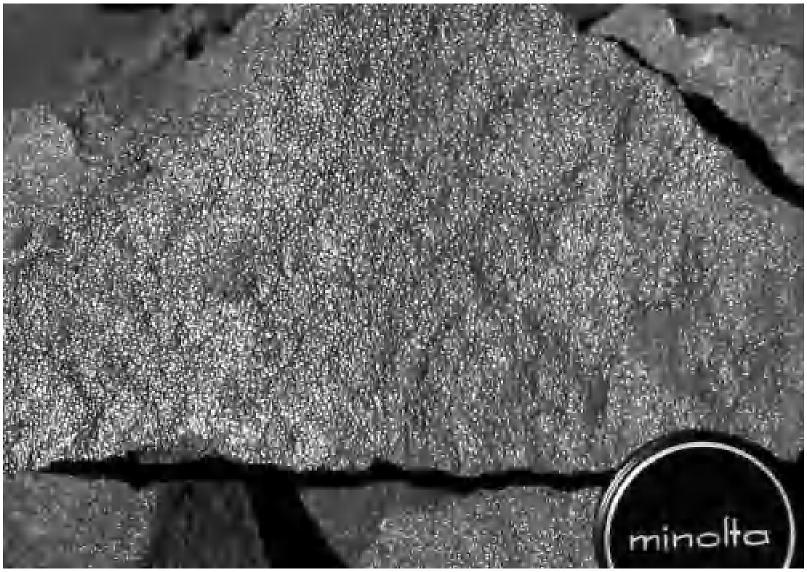

Figure 1.68 (Plate 1.68) Haematitic iron oolite ore formed in a Late Cretaceous marine embayment at Aswan, Upper Egypt.

oblique and cross-bedding. Iron oolite rock of ore grade has closely packed ooids, but host rock bituminous marls of the minette enclose widely disseminated ooids. The ore beds are often connected with rich fossil communities. Fossils are typically replaced and cemented by iron ore minerals. A lateral differentiation of iron facies (e.g. oxic, carbonate, silicate) in oolite beds is rarely clear. Single ooids consist of goethite, haematite, chamosite and siderite (with very little magnetite and pyrite) that alternate in growth zones or in cross-cutting metasomatic zones. Compared to the crustal average, iron and phosphorus are enriched by a factor of 6 (Fe to ~34%, P to 0.6%), similar to Mn, As, V and other elements. An apparent paradoxon is the high percentage of reduced iron in ooids that were formed in oxygen-rich seawater, as proven by the associated fossils.

The coincidence of both sedimentary and diagenetic textures caused very different genetic interpretations. Sorby (1857) thought that originally aragonitic oolitic rock had been replaced by iron ore after lithification. However, many observations favour a synsedimentary supply of iron followed by chemical and biochemical precipitation (Dahanayake & Krumbein 1986). This is supported by many modern submarine studies. Sturesson *et al*. (2000) observed the formation of iron ooids on the submerged flank of an island volcano in the Philippines, where local seawater is enriched with dissolved Fe-Al-Si and oxic ooids are formed. The source of the iron could not be determined; the authors think that submarine hydrothermal springs or ash falling into the sea, or leaching of recent lava flows, are equally probable alternatives. In recent marine sediments of the Niger delta, Porrenga (1967) described the presence of goethite pellets in the uppermost 10 m of sediment, underlain by 50 m of chamositic sediment.

The unlithified sediments at the origin of oolitic iron ore consisted of ooids, pisoids and peloids that originated by rolling on the seafloor. The matrix between these larger grains consists of detrital minerals, fossils, organic material and fine-grained iron-bearing kaolinitic clay (Mücke & Farshad 2005). Subsequent diagenesis, mostly under reducing conditions, caused by bacterial decomposition of organic matter, typically leads to transformation of kaolinite into chamosite (an iron-rich chlorite) and neoformation of pyrite and siderite. Finally, many deposits were upgraded by oxidation caused by meteoric seepage waters.

The source of iron in marine oolitic iron ores were probably lowlands experiencing intensive weathering in tropical climates, where humidity and profuse plant growth produced wetlands discharging river water rich in dissolved organic matter. The Amazon River, for example, annually exports 70 Mt carbon to the sea. Such waters are acidic (pH <5) and dissolve reduced iron (Fe^{2+}). Oxidized iron (Fe^{3+}) may be adsorbed to organic matter and clay (either in colloidal or particle size) suspended in the water. Transport of siliciclastic sediment in these rivers must have been very limited, because this would have diluted the iron. Mixing of river water with seawater (pH >7) provokes immediate precipitation of iron oxy-hydroxides. Other possible iron sources that have been considered are coastal submarine groundwater springs (James 1966) and seawater flowing up from a deep CO_2 zone, where iron is soluble, into coastal waters where it will precipitate (Borchert 1960). Even hydrothermal sources rising from great depth have been invoked (Kimberley 1994).

Because of the availability of higher quality and inexpensive BIF ore, few oolitic iron ore deposits are exploited today. In contrast, genetically equivalent manganese ores occupy a central role in the world economy. Nearly one half of the primary manganese supply is produced from this type of deposit, mainly located in the Paratethys seaway of Eastern Europe and in northern Australia.

Oolitic manganese ore

Oolitic manganese ore occurs in seams within sediments of epicontinental seas, mainly associated with clay, marl and sand (rarely carbonates). The largest province of these ores is the South Ukrainian basin of Eocene-Oligocene age, with many mines around Nikopol. In this region, the sedimentary succession is transgressive, starting with palaeosoil developed on Precambrian crystalline rocks, covered by coal-bearing limnic sediments and finally glauconite-rich sands that announce the sea. The manganese horizon occurs within clastic marine sediments (Varentsov and Muzylev 2001, Figure 1.69):

> The manganese seam of Nikopol reaches a thickness of 4.5 m and an extension along strike of 250 km. A marginal facies of ooids, concretions and earthy masses of manganese oxy-hydroxides (pyrolusite and psilomelane) gives way to a carbonate facies of rhodochrosite and manganocalcite at deeper basinal levels and finally to bluish-green clay with Mn concretions. Sedimentary manganese deposits elsewhere display a similar zonation, for example those of Cretaceous age on Groote Eylant, Australia (Bolton *et al.* 1990). Note that the Australian ores have a complicated history, with sedimentary features overprinted by diagenesis and later supergene, lateritic alteration.

Similar to ironstone and oolitic iron ore, the metal source for oolitic manganese deposits may have been continental weathering (Frakes & Bolton 1992) or ocean-floor hydrothermal venting (Maynard 2010). In principle, manganiferous particles may flocculate and form an enriched bed,

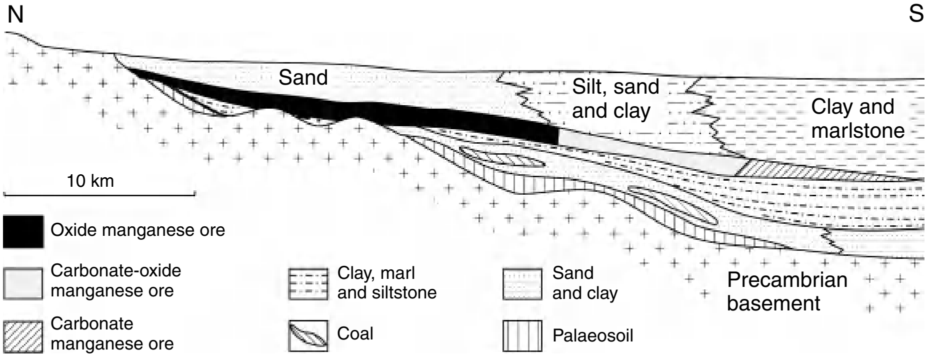

Figure 1.69 Generalized section of facies zones in the Eocene-Oligocene marine-sedimentary manganese horizon in southern Ukraine (adapted from Varentsov & Muzylev 2001).

but a more convoluted path to enrichment is assumed: When the particles settle into the reduced lower section of a restricted sea, they are dissolved, either abiotically or supposedly more often, by microbial anaerobic methane oxidation (Beal *et al.* 2009; eq. 1.18).

Reduction and dissolution of manganese by microbial methane oxidation:

$$CH_4+4MnO_2+7H^+ \rightarrow HCO_3^-+4Mn^{2+}+5H_2O \quad (1.19)$$

This process leads to enrichment of anoxic deep water with dissolved manganese (Mn^{2+}) while iron and other easily reduced metals are precipitated by hydrogen sulphide. Interaction of the Mn-enriched deep water with oxygen-rich marginal zones induces precipitation of Mn oxides, especially during transgressive phases (Roy 1992). This situation is demonstrated by the recent Black Sea with its high Mn^{2+}/Fe^{2+} ratio of deep, highly reduced euxinic water and MnO_2 precipitation in shallow mixing zones with oxic surface water (Force & Maynard 1991). A second viable path to Mn-enrichment is the oxygen minimum zone (OMZ) model; an OMZ develops below high productivity seas but deep ocean water underneath is oxic, not euxinic. Upwelling OMZ water precipitates Mn (and P: Maynard 2010). Plate tectonics, basin configuration and climate cycles control ocean redox conditions favourable for manganese precipitation (Frakes & Bolton 1992).

Manganese nodules

Manganese nodules (Figure 1.70) occur over wide expanses of deep seafloor below the carbonate compensation depth (CCD). In these areas, pelagic sediment (mainly radiolarian ooze) accumulates at a very small rate. In shape and size, the Mn nodules are compared to potatoes but, of course, smaller and larger specimens do occur. Cobaltiferous manganese crusts cover submarine rock outcrops of mid-ocean ridges and of oceanic intraplate volcanoes. Proximity to submarine hydrothermal fields is not essential, although these are surrounded by Mn-rich sediments (e.g. manganese mud mounds of low-temperature exhalations near the Galapagos Islands, the manganese umbers (brown earthy pigments) and Mn-SiO_2 exhalites of many ophiolites).

Economically prospective manganese nodule fields include the Clarion-Clipperton-Zone in the Pacific, the Peru Basin and the central part of the Indian Ocean. Nodules contain ~29 wt.% Mn, 5% iron, 1.2% copper, 1.37% nickel, 1.2% cobalt and 15% SiO_2 (Lenoble 1996). Minor contents of other

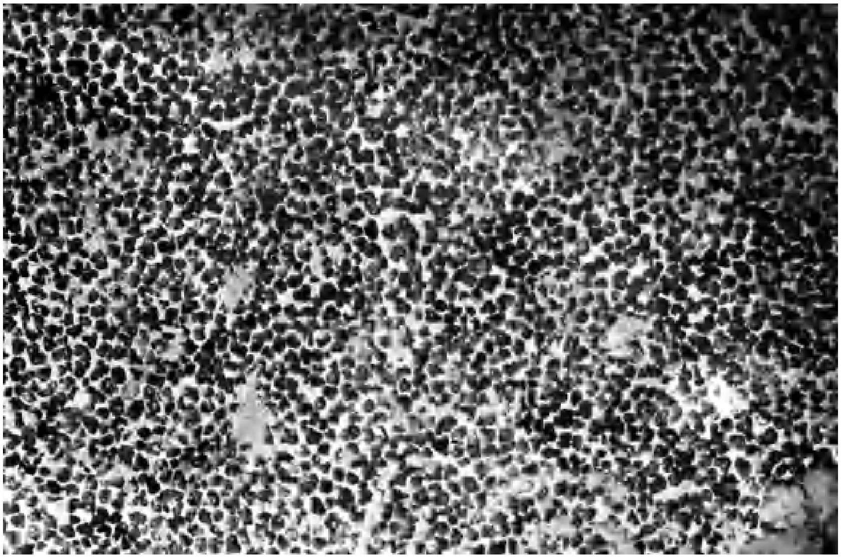

Figure 1.70 Seafloor aspect of polymetallic manganese nodules in the Clarion-Clipperton-Zone (CCZ) of the Central Pacific. The density is here about 20 kg/m^2. Individual nodules have diameters of 3 to 5 cm, the matrix is radiolarian ooze. Courtesy P. Halbach (FU Berlin).

metals including platinum are potentially recoverable. Mn nodules have a botryoidal or smooth surface and consist of concentric shells of amorphous and crystalline manganese and iron oxihydroxides. Formation of the nodules is partly by *in-situ* precipitation from pore fluids ("diagenetic") and partly by attachment of colloidal particles or dissolved matter from seawater ("hydrogenetic"; Hein *et al.* 2005). In both cases, microbial intervention may be essential. Manganese crusts grow mainly by hydrogenetic processes. Nodules and crusts have remarkable contents of valuable metals. The source of these metals are most likely hydrothermal exhalations at mid-ocean ridges, but submarine weathering of Hess Crust serpentinites, extraterrestrial dust and input from land to the oceans may contribute part of the endowment.

1.3.4 Sediment-hosted, submarine-exhalative (sedex) base metal deposits

Sediment-hosted sulphide deposits formed by hydrothermal outpouring on the seafloor compete with porphyry deposits for the role of the largest base metal accumulations on Earth. Clearly, systems forming these ores must be both of large scale and geologically common. Earlier, we have noted that hydrothermal-sedimentary sulphide ores occur in a continuum from: i) a proximal position to submarine volcanoes; to ii) more distal positions where only sparse ash layers in the sedimentary column point to synchronous volcanism; and iii) to purely sedimentary settings. Only the cases ii) and iii) are referred to as sedimentary-exhalative or short, sedex type ore deposits. The first are volcanogenic (cf. Section 1.1).

Distal to volcanism are the locations of Early Proterozoic HYC-McArthur River, Australia and of the Devonian Rammelsberg deposit in Germany (Large & Walcher 1999). Some of the giant Mississippian Zn-Pb-Ag deposits of the Red Dog district, Alaska, are close to igneous rocks but genetically unrelated (see below). Mesoproterozoic Sullivan, BC, Canada, was earlier thought to be purely sedimentary without any magmatic influence ("Sullivan type sulphide deposits"). The choice was not opportune, however, because deep magmatic bodies may have controlled ore formation at Sullivan and the discussion appears to be still open (Slack *et al.* 1998). Hardly any traces of volcanism occur near the Pb-Zn-Ag orebodies within Palaeoproterozoic carbonatic-evaporitic black shales of Mt Isa, Australia, and in the Early Carboniferous carbonate host rocks of Irish deposits.

Sedimentological investigations indicate that the sulphides were deposited in a geologically very short time. The clastic sedimentation rate in the host basins was certainly not exceptionally low,

BOX 1.10 Submarine-exhalative (sedex) base metal deposits

The term sedex implies syngenetic origin of ore and host rocks. Because this cannot always be clearly established, "clastic-dominated lead-zinc ore" was instead proposed by Leach *et al.* (2010). The characteristic setting of these deposits is submarine rifting within epicontinental seas. Orebodies are typically related to faults, synsedimentary tectonic activity and the formation of local subbasins. Pluriphase extensional strain, reefs, sediment-starved restricted basins and distal volcanic centres may be part of the environment (Figure 1.71). Many hydrothermal-sedimentary sulphide ore deposits are close to or enclosed in black shales indicating a state of partial (dysoxia) or severe oxygen depletion (hypoxia to anoxia) of bottom waters. The correlation may be caused by incidental outpouring into a euxinic environment (i.e. anoxic, highly reduced, H_2S stable), or by "poisoning" of a marine sub-basin by profuse amounts of hydrothermal metalliferous fluids. Some sedex ore deposits are hosted by carbonatic silt- and claystones. Cherts are often part of the host sediments.

Sedex orebodies are stratiform and stratabound, and consist of massive, laminated or banded sulphides (Figure 1.72), with varying admixture of clastic matter, barite and other exhalites (SiO_2, haematite, etc.). In appearance they are very similar to volcanic-hydrothermal exhalative (VMS) orebodies; the decisive difference is the sedimentary as opposed to the volcanic genetic setting. Whereas the first are principally controlled by volcanic point heat sources, sedex ore is commonly localized by extensional faults (e.g. basinal growth faults). Single ore beds are either monomineralic or simple

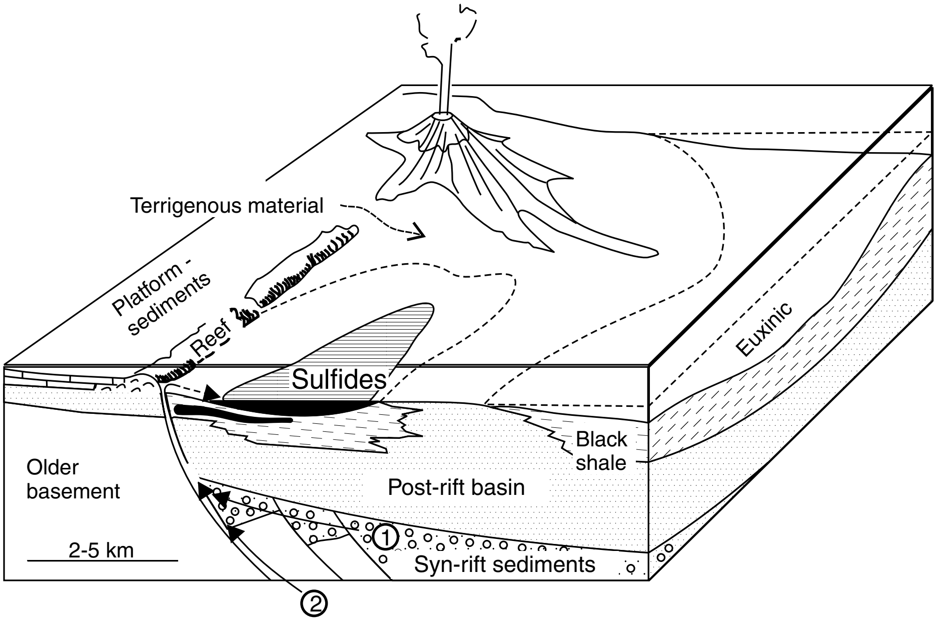
Terrigenous material
Platform - sediments
Reef
Sulfides
Euxinic
Black shale
Older basement
Post-rift basin
2-5 km
①
Syn-rift sediments
②

Figure 1.71 Schematic sketch of the geological setting of an exhalative-sedimentary (sedex) sulphide (-barite) ore deposit in a black shale basin. Note distal rift-related basaltic and felsic volcanic centres.

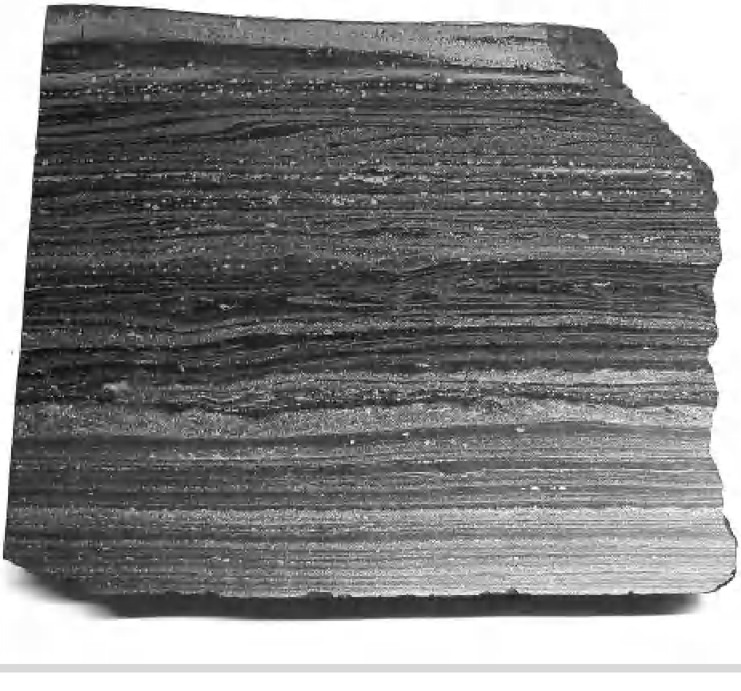

Figure 1.72 (Plate 1.72) Undeformed shale-banded copper-zinc dominated sulphide ore from Rammelsberg sedex deposit (Germany) displays ductile soft-sediment deformation and cross-lamination. Width of image ~20 cm. Courtesy B. Lehmann, Clausthal.

mixtures of galena, sphalerite, pyrite and pyrrhotite, rarely including more than traces of arsenopyrite and copper sulphides. Beds display sharp boundaries with each other, whereas in the same bed, lateral facies changes include decreasing metal grades and often, a metal zonation (e.g. copper in the centre, surrounded by annular zones of Pb, Zn, Ba and Mn). Elevated pyrite contents and geochemical manganese enrichment are found in a wide perimeter of the deposit. Initial ore precipitates were extremely fine-grained ($<5\ \mu m$), often with colloidal organo-metallic phases. Coarser grain size required for economic ore processing is a consequence of diagenesis, orogenic deformation and metamorphism. The unmetamorphosed Palaeoproterozoic HYC deposit, McArthur River district in northern Australia, provides an interesting case history. First reported in 1880, the high-grade but very fine-grained mineralization was technically not exploitable. Serious exploration was only done 80 years later (Logan *et al.* 1990). Total resources of $\sim$125 Mt of ore with 13% Zn and 6% Pb were defined. Again, 30 years later in 1992, a mine was established. New milling and metallurgical methods allow profitable exploitation of reserves comprising 27 Mt at 14% Zn, 6.2% Pb and 63g/t Ag.

Structures and textures of sedex ores confirm the synsedimentary formation by fluids emanating from the seafloor. They include fine lamination, graded bedding, the frequent presence of framboidal pyrite, colloform banding, soft sediment deformation and mass transfer by submarine mudflows (as at HYC: Ireland *et al.* 2004). Fossil hydrothermal vents resembling those of black smokers were found at Silvermines and Tynagh in Ireland providing further proof for exhalative processes. Below the soft sediment surface, early diagenetic replacement and zone refining may take place simultaneously, as at HYC (Ireland *et al.* 2004) and the Red Dog district (Kelley & Jennings 2004). This leaves features of epigenesis that must be weighed against arguments for syngenesis and interpretations may differ as at HYC (Symons 2007). Hydrothermal alteration is only visible where footwall rocks with advection flow paths are exposed (e.g. the "Kniest" at Rammelsberg, Germany, or vein breccias below the Red Dog orebodies, Figure 1.73). If subjacent flow channels cannot be found, heavy hot metalliferous brines may have flowed from elevated outflow points into nearby depressions on the seafloor (Sangster 2002).

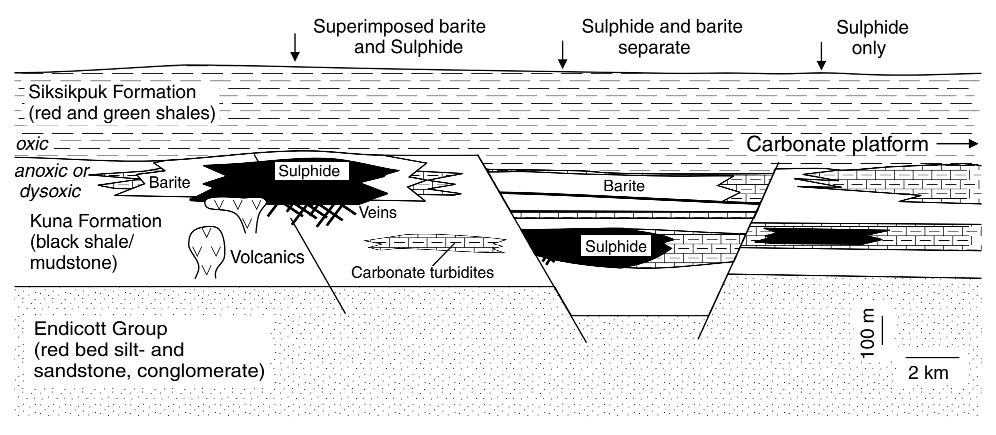
Superimposed barite and Sulphide
Sulphide and barite separate
Sulphide only
Siksikpuk Formation (red and green shales)
oxic
Carbonate platform
anoxic or dysoxic
Barite
Sulphide
Barite
Veins
Kuna Formation (black shale/ mudstone)
Volcanics
Sulphide
Carbonate turbidites
Endicott Group (red bed silt- and sandstone, conglomerate)
100 m
2 km

Figure 1.73 Horst-and-graben architecture of the Late Mississippian Brooks Range Basin, Alaska, hosting the giant Red Dog Zn-Pb-Ge-Ag massive sulphide (and barite) sedex deposits. Modified from Kelley, K.D. & Jennings, S. 2004, Society of Economic Geologists, Inc., *Economic Geology* Vol. 99, Figure 4 p. 1270.

but the sulphide deposition rate was very high. Only this allowed the formation of massive sulphide rocks that are common in this environment.

The source of metals in sedex ore deposits is sought in either the sedimentary basinal rocks (diagenetic) or in the basement underneath (retrograde-metamorphic). Different ratios of Pb-Zn-Cu in mining districts indicate varying lithochemical source material, but also different processes or conditions of metal leaching. Lead isotope data may help to identify the source rocks of metals. Fluids involved in ore formation include:

- deeply convecting seawater and evaporitic brine;
- occluded formation fluids (Slack *et al.* 1998);

- diagenetic water of basinal sediments; and
- fluids mobilized from a deep source (e.g. elevated heatflow from the mantle).

Rising mantle fluids were invoked for giant Broken Hill, Australia by Plimer (1985). Most sedex deposits were generated by migrating formation fluids and seawater or brine fed into convection cells. Convection cells may reach many kilometres downward below the floor of a basin. The metalliferous fluids are either oxidized (SO_4-rich) or reduced (H_2S-rich), depending on the nature of the basin fill. Oxidized, neutral or weakly acidic fluids originate in sediments that are dominated by carbonates, evaporites and haematitic sandstones (e.g. McArthur River, Red Dog), whereas dark shale and sandstone produce reduced and acidic fluids (Rammelsberg, Cooke *et al.* 2000).

The geodynamic environment of submarine, hydrothermal sediment-hosted sulphide deposits is different from Kuroko and Cyprus types, which form near plate boundaries. Sedex deposits occur typically at within-plate locations, such as sedimentary epicontinental shelf regions grading into passive continental margins. This environment combines tensional tectonics and crustal thinning with high heat flow and thermal basin subsidence that all favour fluid convection (Betts *et al.* 2003). The giant Alaskan Red Dog sedex deposits with approximately 40 Mt of contained lead and zinc illustrate these observations (Figure 1.73). The Kuna formation hosting the orebodies is intruded by igneous rocks including mafic sills and rhyolite plugs. Yet, the source of the hydrothermal ore-forming fluids was not magmatic, but brine from evaporating seawater. Sources of the metals were probably fluvial-deltaic red beds of the subjacent Endicott group (Kelley & Jennings 2004).

Because sedex ore deposits are geologically common, both in space and time, numerous members of the group were metamorphosed. Low-grade metamorphism is the most frequent state found (Red Dog, Mt. Isa). Very high-grade metamorphic deposits such as Gamsberg, South Africa (amphibolite facies) and Broken Hill, Australia (granulite facies) are of special scientific interest (cf. Section 1.5 "Metamorphic and Metamorphosed Ore Deposits"). Often, metamorphosed ore displays signs of local mobilization (e.g. cross-cutting coarsely crystalline sulphide veins). In the past, observations of this kind have occasionally caused erroneous epigenetic interpretations of sedex ore formation.

1.4 DIAGENETIC ORE FORMATION SYSTEMS

Diagenesis is "the sum of all chemical, physical and biologic changes undergone by sediment after its initial deposition, and during and after its lithification, exclusive of surficial alteration (weathering) and metamorphism" (Neuendorf *et al.* 2005). The role of diagenesis in the formation of petroleum and natural gas deposits has been known for a long time. Metallogenesis by diagenetic processes was suspected, but decisive evidence could only be assembled in more recent times. Examples of ore deposit types that illustrate the diagenetic realm include the European Copper Shale, many deposits of the Central African Copper-Cobalt Belt, Mississippi Valley type lead-zinc (barite-fluorite-celestite) deposits, and orebodies that originate from brines derived by interaction with salt rocks (e.g. lead-zinc and siderite in Northern Africa). Note that brine *sensu stricto* is defined by a salt content of more than 10% (Table 1.5). Saturation of NaCl in water is reached at a concentration of 26.4% (25°C).

The salinity, or more precisely, the total dissolved solids concentration (TDS) of brines is measured and expressed in two different forms, ppm (g/t) or mg/L (eq. 1.20). In oceanography, "practical salinity units" (psu) are used, which

Table 1.5 What exactly is a brine? Terms for water with different salinities (Davies & DeWiest 1966)

Term	Concentration of total dissolved solids (TDS) in ppm (parts per million) and weight percent	
Fresh water	0–1000	<0.1%
Brackish water	1000–10,000	<1%
Seawater	31,000–38,000	3.1–3.8%
Saline, or salty water	10,000–100,000	<10%
Brine	>100,000	>10%

represent the conductivity ratio of a seawater sample relative to a standard KCl solution.

Contents of total dissolved solids in water and brine:

$$\begin{aligned}&\text{ppm (parts TDS per million TDS+H}_2\text{O)}\\&\text{mg/L (milligrams per litre)}\\&=\text{ppm/density (mg/cm}^3\text{)}\end{aligned}\qquad(1.20)$$

In order to determine the origin of salinity in basinal brines, formation water and hydrothermal fluids, mole ratios of halogens and electrolytes are measured (Botrell *et al.* 1988). Because of its conservative behaviour and small coefficient of partitioning from brine into halite, bromine (Br) is an ideal discriminator between two main solute sources: i) subaerial evaporation of seawater; or ii) dissolution of evaporite salts (mainly halite). Seawater has a characteristic Cl/Br molar ratio of ~655. When seawater evaporates and deposits halite, Br content relative to Cl and Na of the residual brine dramatically increases along the "seawater evaporation path". Consequently, precipitated halite contains little Br (Cl/Br >655, Hermann 1980, Holser 1979). Thus, the congruent dissolution of halite results in high Cl/Br and Na/Br molar ratios and Na/Cl of ~1, very different from the seawater evaporation array. Brines resulting from seawater evaporation have Cl/Br molar ratios distinctly <655. Although halogen ratios appear to be quite conservative (Nahnybida *et al.* 2009), several processes do induce changes, for example leaching of bromine from organic matter (Collins 1975). As a highly organophilic element, iodine (I) is strongly enriched by organisms and an elevated I/Cl ratio is a useful indicator of the passage of solutions through organic-rich sediments (Kendrick *et al.* 2001).

The core of a diagenetic ore formation model is the argument that most sediment includes a large mass of water at the time of deposition ("connate water"). During diagenesis, most of this initial water is expelled by mechanical compaction, with a minor contribution by chemical liberation. When newly deposited, sand may contain 40 vol. % of water, clay 90%, and carbonates ~50%. By diagenesis, the pore space occupied by water is reduced to <1 vol.% at pressures and temperatures approaching the transition to metamorphism. Obviously, all this water must leave the system by flowing upwards and to the margin of sedimentary basins. Drilling for hydrocarbons revealed that water in sediments frequently attains temperatures of more than 100°C and reaches a maximum of about 300°C. By reacting with rocks, the "formation water" acquires a high content of dissolved matter. Where large masses of such fluids pass through geochemical or physical "traps", minerals may be precipitated which concentrate useful elements. Ore deposits that are formed as a result of these processes are hydrothermal and epigenetic.

Stable isotope data prove that part of the water in sediments can have a meteoric origin (precipitation infiltrating basin aquifers), but most is initially occluded seawater. Both the rocks and the pore water chemistry change as diagenesis progresses ("diagenesis of formation water"). Typical formation waters are brines (Table 1.5) dominated by Na-Ca-Cl and with elevated traces of HCO_3, K, I and Br. Compared with seawater, iron, manganese, copper, zinc and many other elements are enriched. Magnesium and sulphate are depleted; the first by neogenesis of dolomite and chlorite, the second by bacterial (eqs 1.15 and 1.16) or thermochemical sulphate reduction to H_2S. In the geological past, however, seawater composition was not constant (cf. Chapter 4.2.2 "Seawater in the Geological Past"). In the Early Palaeozoic, the Jurassic and the Cretaceous, seawater had low concentrations of magnesium and sulphate. Therefore, some basinal brines were dominated by Na-Ca-Cl already at the time of occlusion (Lowenstein *et al.* 2003).

Recently, the presence of **live microbes** was substantiated to a depth of several kilometres below the surface and to temperatures of ~140°C (Schippers *et al.* 2005). Microbes convert organic matter to CH_4 (and CO_2) and produce the methane of biogenic gas deposits. In the near-surface realm of early diagenesis, methanogenesis and sediment dewatering combine to cause methane-rich cold seeps that are sites of submarine barite deposit formation (Torres *et al.* 2003). Many microbes have a role in diagenesis. *Geobacter metallireducens*, for example, catalyses Fe(III) reduction and decomposition of organic substance to CO_2 (Childers *et al.* 2002). In the absence of microbes, for example at higher temperature (>80°C: Thom & Anderson 2008) and greater depth, abiotic sulphate reduction based on destruction of organic matter (here represented by CH_4 and CH_2) is possible (eq. 1.21).

Thermochemical sulphate reduction (TSR):

$$\begin{aligned}&2H^+ + SO_4^{2-} + CH_4 \Rightarrow H_2S + CO_2 + H_2O\\&SO_4^{2-} + 3H_2S \Rightarrow 4S^0 + 2H_2O + 2OH^-\\&4S^0 + 1.33(CH_2) + 2.66H_2O \Rightarrow 4H_2S + 1.33CO_2\end{aligned} \tag{1.21}$$

By disintegrating anhydrite, this process can cause a relative enrichment of $CaCl_2$ in the fluids. NaCl may be retained and concentrated by clay beds acting as a semi-permeable membrane. Probably more often, NaCl brines originate by evaporation at the surface or by dissolution of salt rocks in the basinal sediments. Mature, commonly deep formation waters are mostly concentrated NaCl brines. Maturation and decomposition of organic matter in sediments results in dissolved CH_4, CO_2, H_2, N_2 and higher hydrocarbons (e.g. petroleum). Oxygen induced by infiltrating seawater and meteoric water, and oxygen produced by disproportionation of formation waters is quickly consumed by oxidation of Fe(II) or of organic matter. Therefore, most formation waters display a low redox state, favouring high solubility of many metals. In solution, some metals may occur in the form of organo-metallic complexes (Ni, V, part of Zn and Cu), while others such as Pb, Fe and most Cu and Zn are dissolved as simple ions. The important metallogenetic role of basinal NaCl-brines extends into the realms of metamorphism and even to magmatic ore formation (e.g. iron oxide Cu-Au deposits: Barton & Johnson 1996).

Not all basinal fluids are reduced, and oxidized formation waters are commonly enriched in SO_4. This is possible when the source rocks include predominantly haematitic sandstone and mudrock, limestone, anhydrite and halite, for example in the Rotliegend (Permian) desert and salt lake sediments of Northern Germany. Oxidized fluids are able to dissolve Cu, Pb and Zn, to transport the metals over wide distances and to precipitate ore at suitable traps such as redox fronts established by organic-rich shale (e.g. the European Copper Shale). Barium and iron, in contrast, are insoluble in oxidized fluids and are not part of the resulting ore paragenesis.

Metal uptake in the source region (reaction zone) or along flow paths is a function of kinetic and thermodynamic factors, including rock and water chemistry, T, P, Eh and pH. In contact with formation waters, several common minerals are unstable, including amphibole, pyroxene, olivine and epidote. Their alteration releases trace metals into the aqueous phase. Other mechanisms of liberating metals include ion exchange with clay minerals and simple diagenetic transformation of clays. An example is lead that is often adsorbed on kaolinite, but is released into solution when illite replaces kaolinite.

The flow paths of expelled deep fluids are determined by hydrogeological parameters such as permeable rock units, tectonic disaggregation and the general pressure gradient. Petroleum and gas deposits in crystalline and magmatic rocks clearly demonstrate that diagenetic flow may encompass basement underlying basins. The norm is probably a slowly moving, diffuse compaction flow that loses its dissolved matter by forming pore-cement in sediments or by discharge into seawater. Ore formation will only occur where a large mass of hot brine is focused into preferential flow paths, which may be envisaged as streams within permeable rocks or tectonic structures. In these channels, a rapid drop of temperature or pressure, reaction with host rocks, and mixing with chemically different water may precipitate solutes in a small rock volume. Because of their high permeability, near-surface faults, reefs or karst cavities at the margins of sedimentary basins or basement islands often locate ore deposit formation. Note that traps of diagenetic ore deposits are quite the reverse of petroleum and gas deposits; the first are open flow systems with hydrostatic pressure, whereas the second are closed and often overpressured. The origin of secondary porosity and of caves in carbonate rocks may be caused by metal sulphide precipitation, which produces hydrogen ions (eq. 1.22) that maintain limestone dissolution (eq. 1.23).

Precipitation of metal sulphides by reaction with H_2S:

$$Zn^{2+}+H_2S\,(aq) \Rightarrow ZnS\,(s)+2H^+ \qquad (1.22)$$

Dissolution of calcite:

$$CaCO_3(s)+2H^+ \Rightarrow Ca^{2+}+CO_2\,(aq)+H_2O \quad (1.23)$$

Intracratonic basinal hydrothermal flow systems

There are many variations to the theme of intracratonic basinal hydrothermal flow systems. Some of the more frequent geological driving agents of basin dewatering and fluid migration are the following:

- standard diagenetic dewatering by compaction of pore space (consolidation: Terzaghi *et al.* 1996, Noble 1963), in a slowly progressive process, mainly caused by continuing sedimentation and subsidence in the basin;
- episodic expulsion of brine by increasing overpressure in sand lenses that are enveloped by clay beds of low permeability (Fowler & Anderson 1991); this can be observed as mud-eruptions in the Mississippi delta, although without leading to mineral deposit formation;
- displacement of deep, hot and therefore relatively light brines by cold, heavy groundwater infiltrating from topographically elevated basin margins; this hypothesis assumes that permeable rocks or active extensional faults provide linked-up flow paths (Daubrée 1887);
- tectonic expulsion of formation fluids by a moving nappe pile, causing flow of diagenetic and metamorphic fluids towards the foreland, where transported heat and dissolved matter result in mineral deposit formation (Oliver 1986, Figure 1.74); a present-day analogue are methane-rich hot fluids ejected from the accretion wedge at many subduction fronts;
- fluid overpressures can also be induced by pulses of hydrocarbon generation caused by a rapid thickness increase of cover sediments and consequently of rock temperature; or by a rapid fall of sea levels (Eisenlohr *et al.* 1994);
- Expulsion of formation waters by deep heatflow (e.g. cryptic intrusions, underplating) imposing a wide halo of higher-grade diagenesis; this may trigger submarine venting of fluids resulting in synsedimentary sedex type deposits (Figure 1.71) or of epigenetic ore.

Several of these hypotheses have been tested by Oliver *et al.* (2006), who showed that tectonic extension alone is insufficient for inducing fluid upflow and the main drive is a favourable thermal field. The precise causes, timing and mode of fluid generation and flow in sedimentary basins are a long-standing subject of applied research in the oil and gas industry. Concepts and approaches similar to modelling petroleum systems (Magoon & Dow 1994) considerably advance investigations concerning diagenetic ore formation.

Many diagenetic mineral deposits display strikingly banded textures of newly-formed precipitates that have been called "diagenetic crystallization rhythmites" (DCR) or "zebra textures". The thickness of the bands varies between millimetres and decimetres. They occur in dolomite, evaporite, in sparry magnesite, in siderite and most typically, in stratabound Pb-Zn-Ba-F deposits hosted by platform carbonates. Their formation is attributed to coupling of

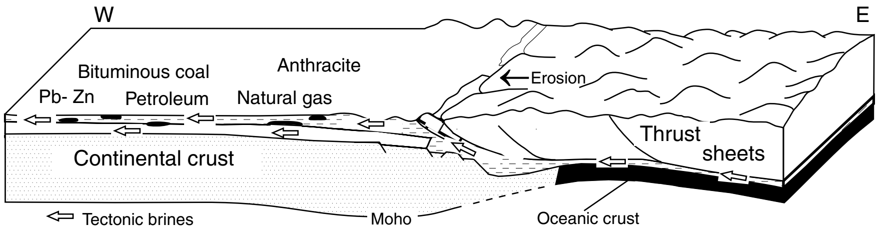

Figure 1.74 Expulsion of fluids ("tectonic brines") towards the foreland from underneath the west-moving nappe pile of the Appalachian Mountain Belt (modified from Oliver 1986).

diffusion with precipitation reactions (Kapral & Showater 1995).

1.4.1 The European Copper Shale

Diagenetic mineral deposits may display properties that resemble synsedimentary features and in a number of cases, only persistent investigations revealed an epigenetic origin from diagenetic solutions. The ambivalence is clearly illuminated by the research history of the European Copper Shale (in German: Kupferschiefer).

In the Central European Permian rift basin, the Copper Shale is a thin stratum that forms the base of the post-Variscan transgressive marine sediments (consult Chapter 4.2.2, "The Zechstein Salt Formation in Northern Europe"). Copper shale is known over an area of more than 600,000 km^2. Basinal Copper Shale intersected in hydrocarbon drillholes displays very low base metal values (Pašava *et al.* 2010). Exploitable metal grades are restricted to southern basin margins (in Germany the Harz District with Mansfeld and Sangerhausen; Silesia in Poland). The Copper Shale of the mining districts is a euxinic sediment deposited in a shallow sea of only a few hundred metres water depth. Ubiquitous fossils of fish and brachiopods indicate that the upper water column was well aerated, whereas deep water was poisoned with H_2S. Continent-derived clastic sediment import was very

BOX 1.11 Copper Shale mineralization

Petrographically, the Copper Shale is a black laminated marly claystone formed from illite, montmorillonite, dolomite, less than 30% organic matter (kerogens include bituminite, vitrinite, fusinite and liptinite: Koch 1997), sulphides, anhydrite or gypsum, phosphates and little quartz. Its footwall is mostly Rotliegend (literally "red footwall" in German) sand or conglomerate, but in some marginal exposures Copper Shale rests directly on folded Variscan basement. The time when Rotliegend sediments experienced reddening (Fe^{2+} oxidized to haematite) is a critical point for a detailed understanding of copper ore introduction (Brown 2009). One obvious possibility is that iron oxide (desert varnish) originally coated the sand grains; palaeomagnetic and illite ages seem to support this assumption (Nawrocki 2000). Hanging wall rocks are lowermost Zechstein carbonates overlain by anhydrite and salt rock. In the North Sea and central Polish basins, the Copper Shale is downwarped to more than 7000 metres below surface. The Copper Shale is not folded but dissected by faults. Fissures and fault intersections are notably mineralized. The bulk of the extracted ore, however, is from stratiform bodies.

As a result of basin palaeomorphology, the Copper Shale horizon occurs in different sedimentary facies: In marginal sub-basins it is quite thin (0.3–0.4 m), rich in Fe, Al_2O_3 and organic substance. Contents of carbonates and quartz as well as thickness increase where shale approaches sills and sand bars. Sills are not mineralized and strikingly red (because of haematite). Miners used to call this barren rock "Rote Fäule" (German for "red rot"). Rich chalcocite orebodies occur at reduction fronts adjacent to Rote Fäule (Figure 1.75; Rentzsch *et al.* 1997).

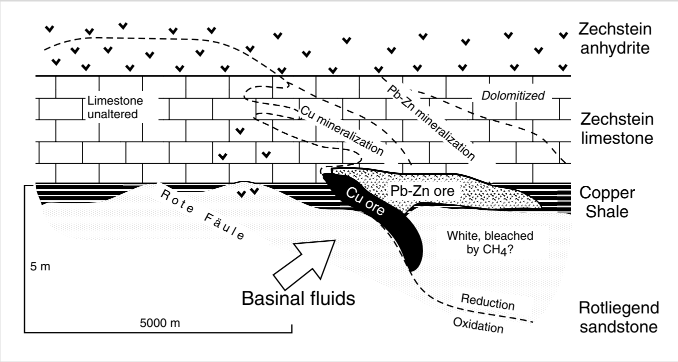

Figure 1.75 Schematic section of a Copper Shale deposit in Northern Germany and Poland (modified from Jowett 1992 with permission from Elsevier).

The sulphides in Copper Shale are of major interest, because they contain the valuable metals. Textural variations from early to late parageneses include (Wodzicki & Piestrzynski 1994):

- Very fine (0.02–0.06 mm), disseminated grains and aggregates, framboids ("mineralized bacteria", Schneiderhöhn 1962) and crusts on organic particles; sulphides consist mainly of pyrite, with occasional traces of chalcopyrite, bornite, chalcocite and marcasite; copper concentrations of a few 100 ppm are considered to have a purely sedimentary origin.
- Spindles, lenses, concretions and thin lenticular bands of sulphides that are parallel to bedding planes; these features reflect diagenetic remobilization within the rock; copper concentrations reach 2000 ppm.
- The main mass of the sulphide ore paragenesis (with base metal contents reaching 3%) replaces rock forming minerals; ore samples may contain 90% chalcocite; microscopic veinlets of different spatial orientation appear in the ore; ore minerals include mainly silver-rich chalcocite, with some digenite, covellite, bornite, chalcopyrite, sphalerite, galena, pyrite and haematite.
- Where no shale is developed on sills, zones of anhydrite pore cementation finger down into bleached footwall sandstone; these zones are mantled by rich chalcocite ore replacing carbonate and clay minerals.
- Thin and cross-cutting veinlets of coarsely crystalline sulphides (bornite, chalcopyrite, tennantite, galena, sphalerite, Fe-Ni-Co sulphides and arsenides) with a gangue of barite, calcite and anhydrite are the latest phase of ore formation; they represent less than 1% of ore produced.

The metals Cu-Pb-Zn display a distinct zonation, both horizontally around oxidized sills and vertically from copper in sandstone and shale to lead and zinc in hanging wall carbonates that are dolomitized (Figure 1.75). However, some copper orebodies extend from bleached footwall sandstone through shale to hanging wall carbonate. Metal contents in exploited Copper Shale deposits in Poland are reported at 1.2–2.8% Cu and 30–80 g/t Ag. Thickness of stratiform orebodies varies from 1.2 to >20 m. Exploitation takes place underground between 600 and 1200 m below the surface. Metals produced include copper, lead, silver, nickel, gold (Piestrzynski *et al.* 2002), palladium, platinum, rhenium, selenium and sulphuric acid. Until 1970, when mining in the Mansfeld District in Germany was terminated, ~1.5 Mt copper had been produced. The nearby Sangerhausen mines were closed in 1990. Economic reserves in Poland are reported as 2.4 Gt of ore; 50% of this occurs in footwall sandstone, 20% in shale and 30% in limestone. The figures underline that a large mass of copper is concentrated within a very small area of the Copper Shale basin.

small and the fine lamination indicates extremely tranquil conditions in the bottom waters.

Genetic interpretations of Copper Shale ore formation have always been dominated by the controversy between syn- and epigenetic models. The difficulty was essentially to determine the time of metal concentration, during sedimentation, or later? Of course, diagenetic ore textures and veinlets were observed, but were they only caused by local remobilization of a metal stock imported earlier? Meanwhile, modern technologies have refined data to a level where epigenetic ore formation during late diagenesis is strongly supported. One of the few mappable characteristics of Copper Shale orebodies supporting epigenesis is their cross-cutting relations with the Copper Shale stratum. In Figure 1.75, this is emphasized by drastically different vertical and horizontal scales revealing the cross-cutting geometry and metal zoning. In underground exposures, Copper Shale orebodies appear to be perfectly stratiform. Epigenesis is also suggested by rings of high-grade ore surrounding red sandstone hills that protrude through the shale. This pattern can hardly be of synsedimentary origin.

Elements of today's diagenetic model of Copper Shale ore formation include hot, oxidized (e.g. sulphate-bearing) Ca-Mg-K-Cl formation waters flowing up from deeply buried Permian molasse red bed sediments and volcanics where they acquired their metal contents (Oszczepalski 2000). Increasing compaction and the low permeability of Zechstein evaporites acting as a seal focused the flow towards basin margins where the metals were precipitated. Possible agents of precipitation include decreasing T and P, mixing with cool, alkaline, meteoric (or sea-) water and most importantly, reduction of fluids by contact with organic matter and sulphides of the shale (Wodzicki & Piestrzynski 1994), and methane in the sandstone (Jowett 1992). The metal zonation of Cu-Pb-Zn is consistent with this model and conforms to the relative solubility of the sulphides (Figure 1.75). To a certain extent, the Copper Shale bed may have acted as a semi-permeable, reactive membrane. The question when exactly the epigenetic Copper Shale mineralization took place is still not satisfactorily answered (Pašava 2010). Evidence has been offered for early diagenetic, Permian (Wedepohl & Rentzsch 2006), to late diagenetic metal introduction during the Triassic (Nawrocki 2000). It appears unlikely that steady-state consolidation of sediments in the Zechstein basin was the driving force. More probable agents are large-scale events, such as the giant mantle plume (Marzoli *et al.* 1999) at ~200 Ma and Triassic-Jurassic rifting phases that punctuated the initial break-up of Pangaea.

Isotope geochemistry supports the diagenetic model of Copper Shale ore formation. Generally, mineralized Copper Shale is isotopically different both from ordinary shale and from red rot. ^{13}C in organic substance is clearly enriched, probably because light carbon was preferentially oxidized and expulsed from the system. Sulphide sulphur with δ^{34}S between −40 and −25‰ implies bacterial reduction of seawater sulphate. Early pyrite contains the lightest, later sulphides heavier sulphur. This suggests: i) a closed system with a restricted mass of available sulphate: ii) later fluids with higher ^{34}S-contents (Jowett *et al.* 1991); or iii) late thermochemical sulphate reduction (Sun & Püttmann 1998). Oxygen and hydrogen investigations of clays resulted in confining the mineralizing fluids to δ^{18}O between 3 and 6‰, and δD from −10 to +3‰, at probable temperatures of 130°C (Bechtel & Hoernes 1993). These characteristics conform to properties of diagenetic formation waters (Figure 1.23).

The copper province of White Pine, Michigan, USA and the African Copper Belt of the Democratic Republic Congo and Zambia are comparable but not identical to the European Copper Shale (cf. Chapter 2.2 "Copper"). All three are included in the non-genetic term of "stratabound and/or stratiform sediment-hosted Cu deposits".

1.4.2 Diagenetic-hydrothermal carbonate-hosted Pb-Zn (F-Ba) deposits

Lead and zinc ore deposits hosted by marine carbonate rocks are a large and heterogeneous group. Single deposits and districts display end member characteristics of syngenetic as opposed to epigenetic hydrothermal ore emplacement. The first are sedimentary-exhalative or volcanogenic (cf. Sections 1.1 and 1.3), whereas the second may have been formed by igneous, metamorphic and diagenetic process systems. In the following discussion, the subject is epigenetic deposits formed by essentially diagenetic fluids. Let us note here that passage of the fluids through igneous intercalations and deeper crystalline basement is not rare. Host rocks are not restricted to carbonates, but world-class deposits in siliciclastic sediments are rare compared to carbonate-hosted deposits (Chapter 2 "Lead and Zinc").

Several provinces or districts with a more homogeneous subset of traits are commonly designated as "types" for discussion. Well-studied types include the "Alpine" (Middle to Late Triassic in Austria-Italy-Slovenia, Figure 1.76), "Silesian" (Mid-Triassic in Poland), "Irish" (Early Carboniferous in Ireland) and "Mississippi Valley" (Pennsylvanian-Permian of the mid-continental USA). Similar deposits occur worldwide, for example in Australia, in several provinces of China and in Mexico. Here, we shall mainly refer to the Mississippi Valley type (MVT) province, because it hosts the most intensively investigated deposits.

The paragenesis of diagenetic-hydrothermal carbonate-hosted deposits is usually very simple, comprising galena and sphalerite, with a gangue of barite, fluorite, pyrite, marcasite, calcite, dolomite, aragonite, ankerite, siderite, quartz, colloform silica (chert) and occasionally, bitumen. Sphalerite appears mostly in colloform-banded texture (sphalerite-wurtzite banding). Low iron and elevated trace contents of cadmium are characteristic. Galena contains little silver. Copper contents are negligible and there are no copper ore deposits of this type. Often, a wide halo of dolomitization due to the passage of brines envelops the ore and many deposits occur at dolomitization fronts (Harper & Borrok 2007). Lead isotopic compositions of districts vary widely and include ordinary (Silesia, Pine Point, Canada) or anomalous lead (southeast Missouri: Goldhaber *et al.* 1995). Sulphur is in part quite heavy and in that case not

BOX 1.12 Mississippi Valley type Pb-Zn deposit characteristics

Large to giant MVT deposits contain 1–20 Mt combined zinc and lead, with an average Zn:Pb ratio of ~3. Even within the type region, a considerable variance of ore-forming processes and modifying factors is observed. This results in variable proportions of metals and minerals in different districts of the Mississippi province. Generally, orebodies are stratiform or at least stratabound, and include tectonic or karst cavity breccias that were cemented by ore and gangue minerals; replacement bodies and cross-cutting veins are not rare (Leach *et al.* 2010). Some ores fill open cavities in carbonate and DCR textures are very common.

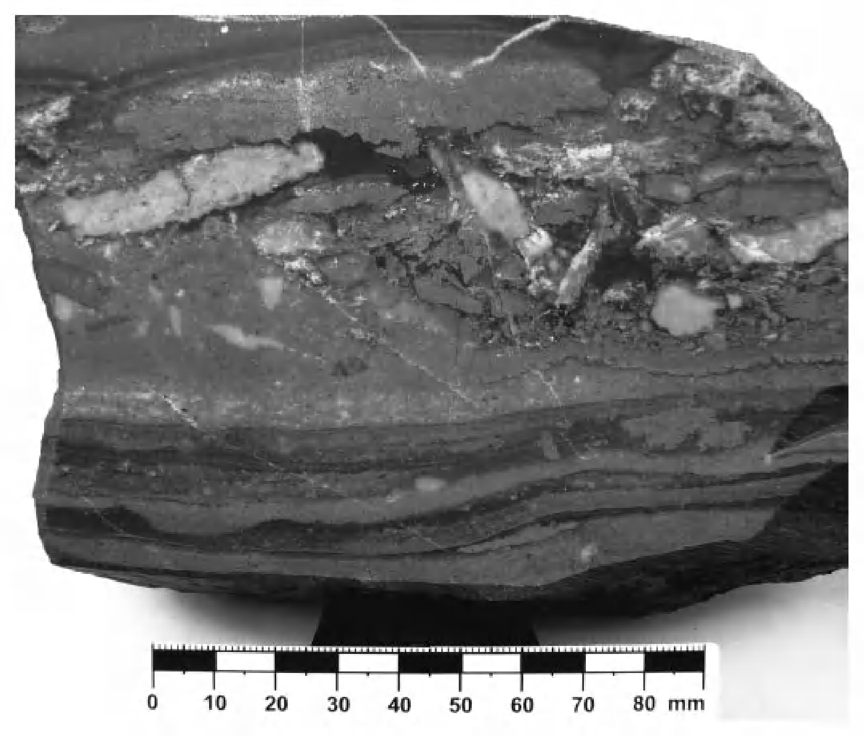

Figure 1.76 (Plate 1.76) Banded and breccia cave ore of brown sphalerite in the historic Lafatsch mine, Karwendel, Tyrol. This is one of the outliers of the Triassic Alpine type carbonate-hosted Pb-Zn deposits. Courtesy B. Lehmann, Clausthal.

World-scale lead deposits were discovered in 1955 in the Viburnum Trend, Missouri, USA. Together with the "Old Lead Belt" nearby, the Viburnum Trend forms a horseshoe-like belt around the Precambrian St Francois Mountains, which are surrounded by Palaeozoic sedimentary basins. During marine transgression in the Cambrian, the mountains were islands with surrounding algal reefs and lagoons, partly of evaporitic facies. The basement is overlain by quartzitic sandstone (Lamotte Sandstone), followed by the carbonatic Bonneterre Formation and dolomites with shale beds.

Most orebodies occur in the Bonneterre Formation within an offshore stromatolitic reef that separates a micritic-clayey basinal facies from coastal oolites. Oolites also fill channels in the reef, form its hanging wall and detrital cones outside of the reef. In the oolitic calcite arenites, long tubular collapse channels are aligned parallel to the coast. Stratabound orebodies occur in these karst-like collapse structures and along faults (Figure 1.77). Both were channels of higher permeability that focused the solutions flowing up from the Lamotte aquifer where it thins out towards the coast.

Apart from galena, the Viburnum ore contains sphalerite, marcasite and rather untypically for MVT deposits, more than traces of chalcopyrite, bravoite and siegenite. Main gangue minerals are quartz and dolomite. Mineralization took place in cyclic pulses that were controlled by mixing of at least two fluids. A weak zoning of Cu-Pb-Zn is compatible with the assumed hydrothermal flow vector.

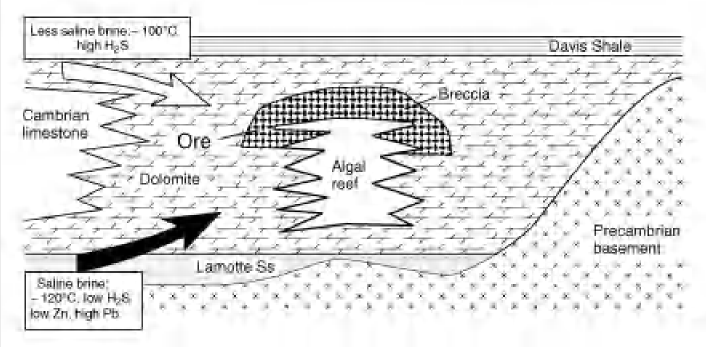

Figure 1.77 Simplified genetic model of the Pb-dominated deposits of Mississippi Valley Type (MVT) in the Viburnum Trend, Missouri. After Plumlee, G.S., Leach, D.L., Hofstra, A.H., Landis, G.P., Rowan, E.L. and Viets, J.G. 1994, Society of Economic Geologists, Inc., *Economic Geology* Vol. 89, Figure 18 (C) p. 1379.

Another important mining area in the MVT province was the Tri-State district, which straddles adjoining parts of the states of Oklahoma, Kansas and Missouri and covers an area exceeding 1200 km^2. This region hosts some MVT deposits, which are characterized by anomalous and highly radiogenic lead (cf Section 1.1 "Isotope Geochemistry"). From 1850 to 1965, Tri-State mines processed an estimated 500 million tonnes (Mt) of ore at a grade of ~3% Zn and 0.5% Pb. Today, the MVT province is past peak production but paradigmatic for environmental remediation of the mining heritage.

In the mid-western USA, different fluids were involved in MVT ore formation. Viburnum District fluids are marked by reactions in the basal sandstone aquifer, whereas Tri-State district fluids display properties of equilibration with marine clay and carbonate (Viets *et al.* 1992). From a southern source, magmatic fluids rich in fluorine were mixed into the diagenetic fluids (Rowan *et al.* 2002). Metal-bearing brines of Mississippi Valley type deposits display the following general characteristics (Roedder 1984, Kendrick *et al.* 2002):

- Salt concentrations above 15 and often >20 % and accordingly, the fluids are brines (Table 1.5); Br/Cl ratios indicate variable fractions of evaporated seawater and salinity derived from halite dissolution.
- General composition is $Cl > Na > Ca \gg K > Mg$; dissolved salts are predominantly NaCl and $CaCl_2$; sulphur concentrations are low, metal contents reach several thousand ppm (Wilkinson *et al.* 2009).
- Brines are usually reduced and moderately acidic.
- Density is always >1 and often >1.1 g/cm^3.
- Temperatures vary from ca. 80–200°C.
- Formation pressures were generally low but above vapour pressure; fluid inclusions evidence of subcritical boiling is hardly ever observed.
- CH_4 in gas bubbles and oil in unmixed droplets are both common, and dissolved hydrocarbons occur in the liquid part of fluid inclusions; often, the fluids are compared to oil field brines.

Precipitation of ore and gangue was probably induced by mixing with near-surface waters that contained reduced sulphur. Some of the latter originated by bacterial sulphate reduction and consumption of organic matter of the carbonate rocks (H_2S-fluids: Plumlee *et al.* 1994, 1995; Figure 1.77). Note the characteristic focusing of ascending fluids into permeable reef carbonates. Reduction may also have been induced by methane and petroleum generated in the heated wallrocks (Anderson 2008).

Rb/Sr ages of Upper Mississippi Valley district sphalerites fall to ~270 Ma (Mid-Permian), the time of Alleghenian/Ouachita orogenesis in the Appalachian Mountain Belt (Brannon *et al.* 1992). Crustal shortening in the east and westward nappe movement are thought to have intensified diagenesis in foreland basins, causing fluid liberation and migration (Figure 1.74).

biogenic but probably due to thermochemical sulphate reduction (TSR, eq. 1.21). As a function of time, strontium isotope ratios of gangue carbonates display higher concentrations of radiogenic ^{87}Sr. This is probably due to an increasing share of strontium derived from clays and other silicates of basinal sediments while diagenesis progresses (Brannon *et al.* 1991).

Diagenetic-hydrothermal carbonate-hosted Pb-Zn (F-Ba) deposits are common in most of the world's marine carbonate platform sequences of Phanerozoic age. This is evidence that the specific metallogenetic process systems leading to this mineralization class are integral to basinal evolution. Although orogenic foreland basins, such as the MVT province, are favourable geodynamic settings, relations to orogeny are not general. Other type regions are related to submarine shelf rifting, to large-scale lithospheric flexure, or to enhanced heat flow and elevated permeability of the crust induced by major plate reorganizations (such as the break-up of Pangaea in Western Europe).

1.4.3 Diagenetic-hydrothermal ore formation related to salt diapirs

In the preceding discussion of diagenetic ore formation, the role of oxidized saline fluids in Copper Shale mineralization and of reduced brines in MVT lead-zinc deposits, were discussed. Also, giant high-grade haematite orebodies derived from BIF were preconcentrated by basinal brines, although the last transformation to economic ore is due to supergene enrichment (Figure 1.52, Thorne *et al.* 2004, 2009). Basinal brines and salt rocks, which are assimilated by magmatic intrusions and consequently leach metals from pervaded rocks, may be the key for understanding the iron oxide-copper-gold class of deposits (Cox & Singer 2007). Of course, the essentially magmatic-hydrothermal IOCG class can hardly be considered as part of the diagenetic process system. In this chapter, brines formed by dissolution and/or dehydration of salt-rich evaporites within basinal sediments shall be singled out for their specific origin.

Most sedimentary basins contain common evaporitic rocks such as anhydrite and rock salt. Dehydration water from evaporites and formation water in contact with these rocks must acquire the character of a saline brine (Table 1.5, eq. 1.20). Other sources of brines in sedimentary basins include evaporated seawater, terrestrial saline lakes and mature formation water. The source of salinity is discerned by determination of halogen and electrolyte ratios (Botrell *et al.* 1988).

Metallogenetic action of brines is especially obvious when salt and epigenetic hydrothermal ore deposits are closely related, in space and time. The best sites for studying this relationship are salt diapir related ore deposits. Salt structures induce peculiar geochemical, hydraulic and thermal conditions in their host sediments (Rouvier *et al.* 1985, Kyle & Price 1986, Pohl *et al.* 1986). Deposits of petroleum and native sulphur in salt diapir cap rocks resulting from the passage of basinal hydrocarbon fluids are known for more than 100 years. However, in addition to oil, some salt diapirs are intimately related to ore deposits (Pb, Ag, Zn and Fe in North Africa), and to non-metallic mineral deposits (barite, fluorite, strontianite; emerald in Colombia).

The southern foreland of the Atlas Orogen in Tunisia and Algeria is underlain by a basin with thick Mesozoic sediments. The package starts with ~1000 m of Triassic evaporites that resemble the Haselgebirge of the Eastern Alps (a melange of salt, anhydrite, clay, dolomite and basalt: cf. Chapter 4.2). Very high subsidence in the Cretaceous reached a total of 8000 m and initiated synsedimentary diapirism that continued into the Eocene, when orogenic folding encompassed the basin. Several large metasomatic siderite and numerous small lead-silver-zinc deposits are found in Triassic cap rocks and in Early Cretaceous limestones where these are in contact with apical parts of the diapirs:

> The largest diapir-related ore deposits in the region are the massive siderite bodies at Ouenza and Jerissa. The siderite replaces Aptian limestone that is in direct contact with salt rock. The limestones are extremely fine-grained (lithographic) and contain numerous rudist (Hippuritoida) fossils, typical for the "Urgonian" facies of Western Europe. Orebodies are stratabound and ore boundaries show marvellous examples of metasomatic fronts. Siderite near the boundaries faithfully preserves bedding, stylolites and fossils of metasomatized limestone and contains large druses of coarse calcite, quartz and tetrahedrite. Figure 1.78 illustrates the margin of a large orebody. Epigenesis of ore is clearly visible as sedimentary textures of host limestones are erased. Antimony fahlore (tetrahedrite), quartz, calcite and aragonite only occur in marginal parts of the ore and are controlled by joints and faults. Within the siderite mass the ore is a nearly monomineralic crystalline rock, with occasional small druses of calcite and dolomite. Ore and host rocks are traversed by rare veins of barite, fluorite and carbonates.

The origin of these deposits is not fully elucidated. It is believed to represent a complex interplay of halokinesis (cf. Chapter 4.3.3) with fluid generation

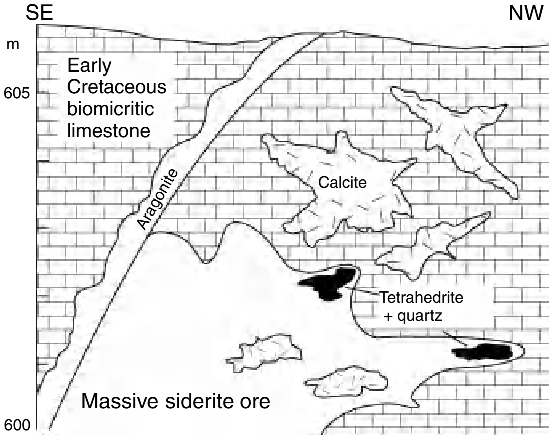
SE
NW
m
605
600
Early Cretaceous biomicritic limestone
Aragonite
Calcite
Tetrahedrite + quartz
Massive siderite ore

Figure 1.78 Metasomatic front of massive siderite ore replacing bedded limestone at Douamis mine, Ouenza, Algeria (For location, refer to Figure/Plate 1.89.)

by diagenesis of evaporites and host rocks. Mass estimates imply that most of the water of the fluids must have been derived from basinal sediments (Bouzenoune & Lecolle 1997). Partial admixture of meteoric or seawater and dehydration brines sourced from the diapir are all possible. At elevated temperature, iron is extremely soluble in reduced, acidic and highly concentrated brines. Precipitation of siderite is induced by drastic pH-change in contact with the carbonates and by sudden lowering of pressure and temperature. In this model, the diapirs and their solution breccia envelope are preferred channels for upflowing deep diagenetic brines (Figure 1.79). In active halokinetic phases diapir salt is permeable.

Many diapirs grow in short spurts of active halokinesis (or halotectonics) that interrupt steady-state passive quietude. During the active phase, major fluid flow may take place. Mineral deposits related to diapirs include petroleum, natural gas, iron, lead,

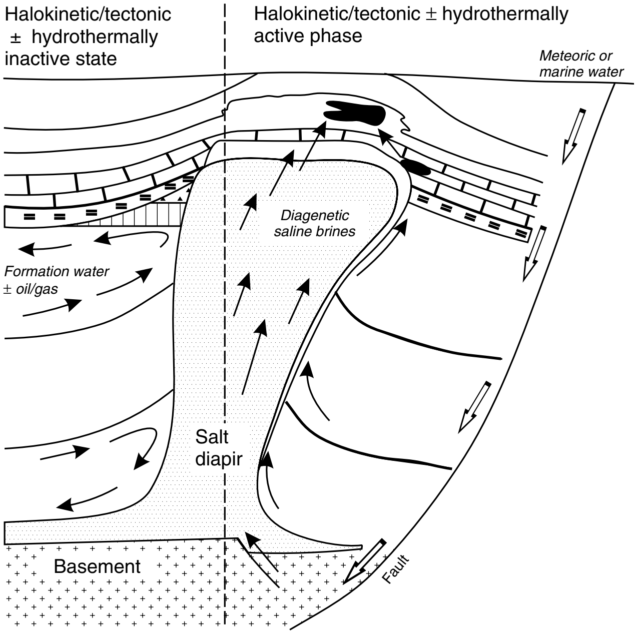
Halokinetic/tectonic ± hydrothermally inactive state
Halokinetic/tectonic ± hydrothermally active phase
Meteoric or marine water
Diagenetic saline brines
Formation water ± oil/gas
Salt diapir
Basement
Fault

Figure 1.79 Diagenetic metallogenesis related to brines released from salt diapirs, based on observations in the Maghreb region in North Africa (adapted from Pohl *et al.* 1986).

zinc, sulphur, barite and fluorite (apart from salts, cf. Chapter 4). Arsenic, antimony, mercury, silver, copper, manganese and strontium mineralization is rarely economically exploitable.

Occasionally, a pre-enrichment of metals in evaporites is invoked. Of course, many terrestrial salt lake brines do contain anomalous and in part exploitable metal concentrations, for example of lithium, tungsten and magnesium. Sabkhas are believed by some to trap metals and elements such as fluorine and barium that are delivered by inflowing groundwater. Later diagenesis may remobilize the pre-enriched elements and produce ore deposits. As yet, the metallogenetic significance of these hypotheses remains untested.

1.5 METAMORPHIC AND METAMORPHOSED ORE DEPOSITS

Ore deposits in metamorphosed terranes may have been formed before, during or after metamorphic processes. This chapter deals mainly with the first category, which are of premetamorphic origin independent from later metamorphic overprinting. This is the class of "metamorphosed" ore deposits.

It is possible to distinguish another class of mineral deposits from metamorphosed ores and minerals, a class that owes its economic interest to largely isochemical metamorphic re-equilibration and recrystallization of pre-existing material which had no use in its original state. Examples provide alumina-rich claystones that were transformed into kyanite or sillimanite deposits, or graphite flakes formed from dispersed bitumen. Among ore deposits, gold may be recrystallized from unrecoverable dilute traces and so turn into recoverable economic ore. In allusion to the term metamorphic rocks, this class may be called "metamorphic" ore deposits (Pohl 1992).

Orogenic (regional) and contact (local) types of metamorphism are most common (Bucher & Frey 2002). In the context of this chapter, ocean floor and dynamometamorphism (due to shearing or cataclasis), extraterrestrial impacts and metasomatic changes to rocks will not be further discussed. Ore deposits that have originated in collisional plate tectonic settings (e.g. island arcs) are most likely affected by later orogenesis and metamorphism. The reverse applies to anorogenic orthomagmatic deposits (e.g. layered mafic intrusions, carbonatites), post-orogenic granitic deposits (tin, tantalum) and superficial alteration deposits (bauxite) which are rarely metamorphosed.

Contact metamorphism of ore in the heated zone around magmatic bodies is usually static (i.e. in the absence of dynamic deformation). Exposure to high temperatures (with a maximum of ~750°C) affects fabric, mineralogy and mineral chemistry (e.g. by driving off water and other volatiles). Fabric changes are confined to a general increase in grain size with rising temperature. Monomineralic ores recrystallize by annealing to "foam" textures (Stanton 1972) that are characterized by triple grain boundary junctions at angles of 120°. Instructive observations can be made at magmatic dyke contacts, where changes affect very narrow zones. The contact zone around the Bushveld Complex reaches hundreds of kilometres. Sulphur release (e.g. from pyrite, eq. 1.24) may induce formation of metamorphic pyrrhotite or even magnetite. Because pyrrhotite (like most sulphide minerals) has a pronounced non-refractory behaviour, retrograde cooling will always bring about equilibration at lower temperatures (Vokes 2000). This is the reason why sulphides have a limited role as geological geothermometers or geobarometers. Iron oxide ore at contacts may recrystallize to a different oxidation state (e.g. haematite to magnetite, eq. 1.24) controlled by the oxygen activity imposed by magma or by heated country rocks.

Oxidation/reduction and sulphidation/desulphidation reactions during metamorphism:

$$6Fe_2O_3 \text{ (haematite)} \leftrightarrow 4Fe_3O_4 \text{ (magnetite)} + O_{2(\mathrm{Fluid})}$$
$$FeS_2 \text{ (pyrite)} + H_2 \leftrightarrow FeS \text{ (pyrrhotite)} + H_2S_{(\mathrm{Fluid})} \quad (1.24)$$

Orogenic metamorphism of ore deposits is common. Temperatures may reach 1100°C and pressures 30 kbar for crustal rocks. Ore metamorphosed in the zeolite, greenschist and amphibolite facies is quite frequent, whereas granulite facies ore is rare (e.g. Broken Hill, Australia). Surprisingly, subducted and high-pressure metamorphic oceanic crust seems to lose mid-oceanic sulphide concentrations: Orebodies hosted in exhumed eclogites and glaucophane schists of subduction zones are very rare (Laznicka 1985). This observation supports assumptions that a part of suprasubduction zone metal concentrations may be mobilized oceanic mineralization.

Orogenic metamorphism is the result of penetrative deformation, while minerals re-equilibrate to new assemblages at geologically elevated temperature and pressure. Volatiles (water, etc.) are partly to wholly (at very high metamorphic grades) removed from the system. Metamorphic rocks exhibit grain coarsening, preferred orientation of minerals and a penetrative fabric (e.g. schistosity, foliation). Ordinary metamorphic rocks display a number of typical deformation styles, including folding, thinning and rupture of fold limbs, thickening of certain rock types in fold hinges and stretching fabrics that produce elongate shapes. Metamorphosed massive sulphide orebodies (and other metallic and mineral deposits) have been shown to react in the same way as common rocks. Generally, sulphides tend to be more ductile than most host rocks, so that fold hinge thickening and thinning of limbs is very characteristic (Figure 1.80 and Figure 1.81). Of course, sulphide layers in ductile rock, such as black shale or migmatite, may exhibit brittle response, for example boudinage. Extreme elongation leads to orebodies shaped like rods, pencils or spindles. Original spatial relations between ore and alteration zones are often severely disturbed and cannot be reconstructed. This is a serious impediment to geological studies and to exploration of these deposits. Also, it explains why a satisfactory understanding of metamorphosed volcanogenic

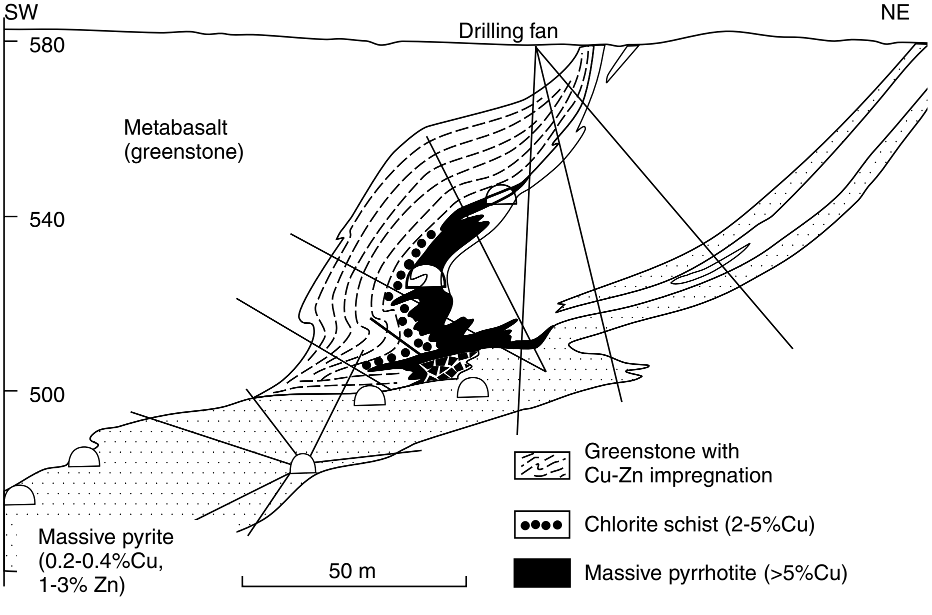
SW
NE
Drilling fan
580
540
500
Metabasalt (greenstone)
Massive pyrite (0.2-0.4%Cu, 1-3% Zn)
50 m
Greenstone with Cu-Zn impregnation
●●●● Chlorite schist (2-5%Cu)
Massive pyrrhotite (>5%Cu)

Figure 1.80 Section of Joma Cu-Zn mine in metabasalt northeast of Trondheim, Norway (Bowie *et al.* 1978). Reproduced with permission of The Institution of Mining and Metallurgy, the Mineralogical Society of Great Britain & Ireland and Maney Publishing www.maney.co.uk. This is an instructive example of orogenic, synmetamorphic deformation of massive sulphide orebodies. Note the drill pattern collared from the surface and from underground mine adits.

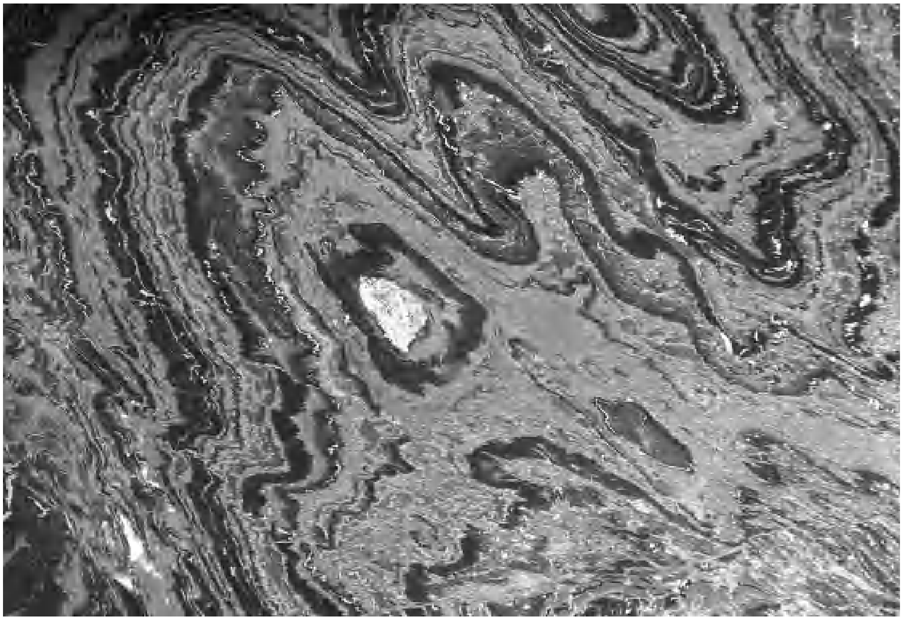

Figure 1.81 (Plate 1.81) Ductilely folded sedimentary bedding in very-low-grade metamorphic shale-banded Fe-Cu-Zn sulphide ore with wispy white dolomite laminae. Note the diffuse axial plane cleavage. Sample from the closure of the orebody synform, Rammelsberg, Germany. Width of image ~20 cm. Courtesy B. Lehmann, Clausthal.

and sedex ore deposits was only recently achieved (Vokes 2000).

An important aspect in studies of metamorphosed ore deposits is the identification of rocks with unusual mineral composition as premetamorphic exhalites or hydrothermally altered rocks (Spry *et al.* 2000b). Quartzites, with or without iron-manganese oxides, are easily identified as former chert, jasper and siliceous sinter. Sillimanite-corundum rock may be metamorphosed alunite alteration; kyanite-andalusite rock might have been advanced argillic alteration and cordierite-anthophyllite schist originally propylitized andesite or basalt (Roberts *et al.* 2003). A premetamorphic potassic alteration and sulphidation halo at the Hemlo gold deposit was transformed by upper amphibolite facies metamorphism into microcline and muscovite-quartz schist, apparently of lower metamorphic grade than the kyanite-bearing host formations (Heiligmann *et al.* 2008).

Oxide ore minerals, especially of iron and manganese, react readily with carbonate and silicate minerals. This caused, for example, formation of the diagenetic-metamorphic skarn rocks in Sweden. Precambrian banded iron formations exhibit many interesting metamorphic features (Stanton 1972). For instance, if alternating magnetite and haematite laminae remain stable, oxygen (and fluid) mobility must have been very restricted. During deformation, haematite typically recrystallizes to micaceous specularite so that the result is a rock similar to biotite schist. Iron silicates and siderite are quite reactive, too. At higher metamorphic grades, siderite loses CO_2 and converts into magnetite or, in the presence of silica, to fayalite (Fe_2SiO_4).

Like iron, manganese is a redox-sensitive and reactive element. During prograde reactions, manganese enters a number of metamorphic minerals, most often spessartine, Mn-rich almandine, rhodonite and rhodochrosite. Rocks of this composition are favourable material for the formation of supergene-residual manganese ore deposits. Elevated Mn-contents of metamorphic silicates (garnet, pyroxene, stilpnomelane, etc.) conserve the geochemical halos of sedex ore deposits and are useful prospecting tools.

Sulphide ore is chemically less reactive, but allows important deductions concerning deformation and heating history. Increase of grain size by metamorphism is important in practice, because processing of coarse ore is less energy-intensive. Controls on recrystallization and deformation of sulphides include pressure, temperature, synchronous penetrative deformation and the presence of fluids. Ductile deformation by creep along certain lattice planes characterizes galena, stibnite (>250°C) and chalcopyrite (>300°C), whereas pyrite (Craig *et al.* 1998), magnetite and arsenopyrite display nearly always brittle deformation. The brittle textures, however, may conceal plastic strain during peak metamorphic conditions (Barrie *et al.* 2010). Banded ores typically display folds and injections formed by galena, while pyrite exhibits boudinage culminating in "augen" (eye) structures. Sulphides may be foliated so that ore textures resemble gneiss. In many cases this is due to pressure solution according to Riecke's principle. If the temperature peak follows well after strain, traces of deformation may be erased by recrystallization to foam textures. The presence of fluids favours recrystallization and local mobilization of sulphides, resulting in the formation of pegmatite-like ore veins in fractures within the orebody or its immediate host rocks.

In contrast to most silicate minerals, sulphides are stable over wide metamorphic P-T conditions. Mineralogical and chemical changes are inconspicuous. Typically, metamorphic recrystallization causes little more than homogenization of pre-existing sulphide minerals and as a consequence, mobilization of trace elements or neogenesis of mineral phases of these elements (Craig & Vokes 1992). Stable isotope systems of the sulphides may be reset by metamorphism. Crowe (1994) reports that sulphur isotopes in chalcopyrite-pyrrhotite assemblages were equilibrated by metamorphism, whereas grains isolated in quartz retained premetamorphic ratios. Orogenic metamorphism may cause a loss of sulphur and formation of pyrrhotite or magnetite from pyrite ("desulphidation"). Sulphur is abstracted by dissolution in prograde dehydration fluids (e.g. water from breakdown of chlorite), mainly in the form of H_2S. These fluids may mobilize metals such as gold and silver that were hosted in the original pyrite/arsenopyrite because they complex with H_2S. Precipitation commonly takes place in the immediate wall rocks, where the fluids encounter minerals with reduced iron. In this way, metamorphic pyrrhotite, gold and silver ores can be formed (Tomkins 2007), for example, in the Bergslagen district, Sweden (Wagner *et al.* 2005, 2007). In the Brunswick No. 12 volcanic-hosted massive Fe-Cu-Zn-Pb sulphide deposit in Canada, however, gold was not upgraded and mobilized, in spite of upper greenschist metamorphism and intensive deformation (McClenaghan *et al.* 2009).

Beginning at low amphibolite facies metamorphism, the formation of sulphide melts from preexisting ore is possible (Frost *et al.* 2002). Metals prone to melting include Au, Ag, As, Sb, Bi, Hg, Te and Tl, some of which are low-melting-point chalcophile elements. Until now, this has only been confirmed at a small number of localities. At Broken Hill, Australia, for example, argentiferous galena fills veins in the sillimanite-facies host rocks near stratiform orebodies (Mavrogenes *et al.* 2001). At the large lode gold deposit of Hemlo, Ontario, Canada, premetamorphic disseminated ore was mobilized as a sulphosalt melt within amphibolite facies host rocks. The melt concentrated into dilatational domains such as boudin necks and fractures (Figure 1.40). Sulphide melts have low viscosities close to those of water and therefore, are highly mobile. During metamorphism and deformation, they migrate like other fluids into structurally favourable traps, although in a limited perimeter.

Note that the observations reported in the last two paragraphs demonstrate the passage from metamorphosed (± *in situ*) to metamorphogenic (metals are dissolved, transported and reprecipitated) ore deposits, which are described in the next chapter.

Generally, most studies of metamorphosed ore deposits confirm that the concept of an essentially isochemical nature of metamorphism is appropriate. Mobilization of matter affects almost exclusively volatile elements and compounds (H_2O, CO_2, O_2, H_2S). As mentioned above, only local remobilization of very small parts of a deposit's total metal stock is observed (Marshall *et al.* 2000, Vokes 2000, Wagner *et al.* 2005, 2007). Therefore, earlier hypotheses are refuted, that metamorphic "regeneration" of pre-existing ore deposits by dissolution-transport-reprecipitation is both ubiquitous and of more than occasional economic significance. It is yet uncertain whether anatectic partial melting induced by metamorphism may be a path to the formation of ore deposits, although selective enrichment of certain metals in the melt fraction is possible (Tomkins *et al.* 2009). In fact, these authors suggest that pre-existing gold mineralization may be recycled through partial melting to form intrusion-related (magmatic-hydrothermal) gold systems. Proven examples for this connection have yet to be found, because the source of fertile igneous rocks is deep crust, whereas the deposits occur rather in the middle and upper crust. The Challenger gold prospect in South Australia seems to represent such a source of felsic auriferous melt. There, exploration drill core displays leucosomes in migmatite, which contain ~8 g/t Au. Round droplets consisting of native gold and sulphides are thought to be frozen ore melt (Tomkins & Mavrogenes 2002).

1.6 METAMORPHOGENIC ORE FORMATION SYSTEMS

Clearly, skarn and contact-metasomatic ore deposits are intimately related to thermal aureoles of magmatic intrusions. They may be said to be products of contact metamorphism, but the causal agent is the interaction with magmatic fluids and not simple change by heating. Therefore, we discussed this group in the magmatic domain (Section 1.1). The formation of ore deposits by regional (most often orogenic) metamorphism, although suspected earlier (Schneiderhöhn 1932), is only now generally accepted. Consequently, "metamorphosed" and "metamorphogenic" ore deposits must be distinguished (Pohl 1992, Spry *et al.* 2000a). Examples of mineral deposits that are members of the metamorphogenic class include orogenic gold (Groves *et al.* 2003), the graphite veins of Sri Lanka, ruby in the Himalayas, several large talc deposits (Rabenwald, Luzenac), certain metasomatic siderite deposits (Erzberg, Austria and Bakal, Russia) and metallic ores (e.g. silver and cobalt in Bou Azzer, Maroc; silver, lead and zinc in western Canada: Beaudoin & Therrien 1999; iron oxide-copper-gold in Australia: Fisher & Kendrick 2008). Generally, deposits of this genetic class were formed from passing hot aqueous fluids and are therefore hydrothermal and epigenetic. Rarely, metamorphic sulphide melting may have been the means of metal migration and concentration, as possibly at Hemlo (Ontario, Canada: Tomkins *et al.* 2004).

In the preceding section, it was argued that apart from devolatilization, regional metamorphism is commonly an isochemical process. Here, this statement must be qualified, in recognition of the mass transfer caused by metamorphic fluids. Orogenic metamorphism induces a large-scale outward flow of heat and fluids (Masters & Ague 2005) that may continue over geological timescales (e.g. 70 million years in the case of the Palaeoproterozoic Ophtalmia orogen, Pilbara, Australia: Rasmussen *et al.* 2005). The metamorphic fluids can be considered as solutions that are in equilibrium with host rocks, and although they are dilute, their sheer mass allows significant transfer of dissolved matter. Even simple field observations of metamorphic rocks provide clues, such as the ubiquitous quartz or carbonate veinlets of epizonal rocks, the unidirectional dissolution of fossils and detrital grains, and the solution schistosity that forms parallel to axial planes. Using these criteria, a loss of ~20% of the original rock mass may not be rare, even at low metamorphic grades. The mass loss of high-grade rocks is probably even higher, but its determination is rarely possible. In cases where identical rocks can be sampled at different metamorphic grades, the mobility of major, minor and trace elements can be quantified. In New Zealand, ore-forming elements (Au, Ag, As, Sb, Hg, Mo and W) are depleted in metamorphic rocks relative to unmetamorphosed protolith samples; the same elements are enriched in the orogenic gold deposits of the region (Pitcairn *et al.* 2006). Some data suggest that even "immobile" elements (e.g. Ti, Zr, Y, Ta) are not reliably conserved, although they are commonly used for petrogenetic and geodynamic investigation of magmatic rocks (Pearce *et al.* 1984, Winchester & Floyd 1977).

Lateral secretion

Lateral secretion is different from the metamorphogenic model. It is best exemplified by the extremely common and ubiquitous generation of quartz and carbonate veinlets from host rocks at low metamorphic grades and of pegmatitic mobilizates at high grades. This interpretation is confirmed by the observation that the paragenesis of these veins depends on the chemistry of the enclosing rocks. Quartz mobilizates, for example, occur in siliceous metasediments, whereas calcite veinlets form in limestone marble and in mafic metavolcanic rocks. In the latter case, veinlets include epidote, chlorite and sulphides. Lateral secretion veins are mostly tensile structures that originate in syn- to late-metamorphic stages. They may contain large crystals of both common and rare minerals, such as the famous Alpine fissure veins (Figure 1.82; Mullis 1996) and many gemstone deposits. Lateral secretion should result in a balanced mass exchange between host rocks and veins. Mobilized elements in the first decrease with proximity to the veins. Because of the chemical equilibrium between fluids and rocks, lateral secretion imprints no hydrothermal alteration on host rocks and stable isotopes reflect equilibrium: The fluids are of a local derivation. A transient pressure gradient induces movement of fluids, which were originally dispersed in the rocks, to the opening fissure. Flow may be along grain boundaries or by diffusion. This system is spatially limited and essentially closed. In its pure form there should be no inflow from beyond its boundary and little outflow. In tectonically quiescent times, temperature and pressure in the fissure and the country rocks are equal, but pressure drops when active extension takes place (Figure 1.83).

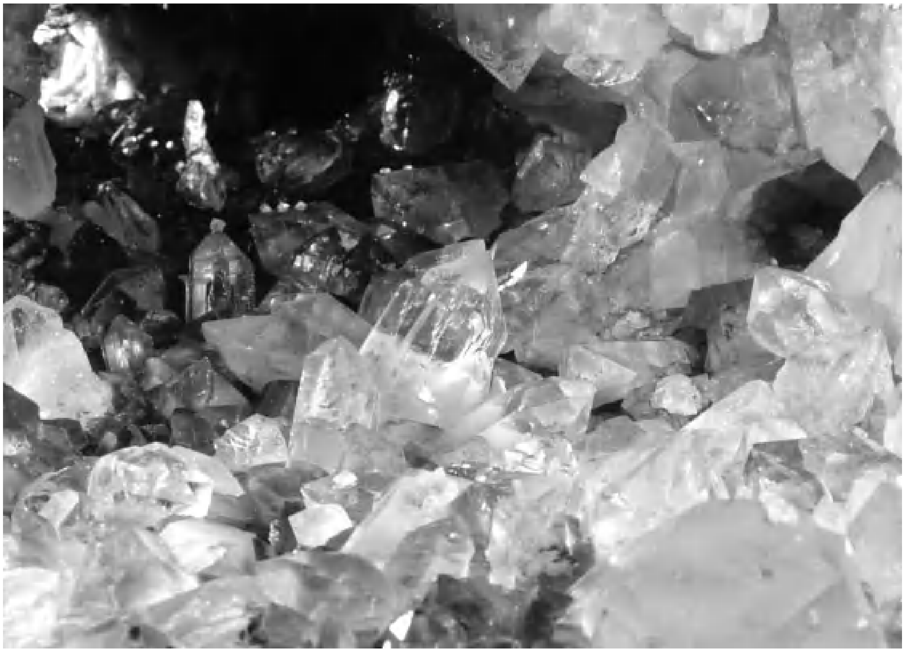

Figure 1.82 Alpine fissure with large quartz crystals encountered in 1974, in Aar granite gneiss (Switzerland) during excavation of an access tunnel to the Grimsel II power station. Courtesy Nagra, Comet, Weisslingen.The crystal cave is now a national geological monument, accessible from Nagra's underground laboratory Grimsel. The fissure formed at ~16 Ma from fluids >400°C. Width of image ~1 m.

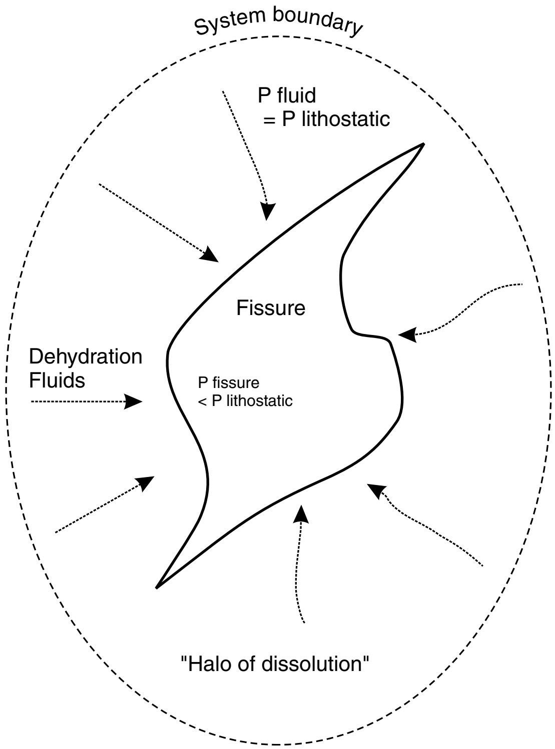

Figure 1.83 Principles of lateral secretion.Changes in the orogenic stress field lead to opening of a fissure. The resulting pressure gradient ($P_{\text{fissure}} < P_{\text{lithostatic}}$) enforces flow of metamorphic fluids into the fissure where minerals precipitate. The system is closed within narrow limits ("halo of dissolution"). The fluids are "dilute solutions" of the surrounding host rocks.

Generally, fluid pressure is lithostatic. Because of the limitations concerning the mass of participating fluids and dissolved matter, a lateral secretion system is not expected to form economic metallic or mineral deposits (apart from pockets of rare mineral specimen). Lateral secretion veinlets demonstrate the retention of metamorphic fluids in a dehydrating rock body. Synchronous shearing is the key to outflow of metamorphic fluids and eventual formation of metamorphogenic ore deposits.

Fluid systems that produce sizeable mineral deposits are open, in contrast to the closed or low flow systems of lateral secretion. In shallower parts of metamorphic complexes, the passage of large masses of deep metamorphic fluids may leave conspicuous clues in the form of regional import of matter (e.g. potassium in the Caledonides: Mark *et al.* 2007). Less visible, oxygen isotope systematics of rocks are changed by the passing fluids (Beaudoin & Therrien 1999). Flow channels of the fluids (e.g. veins) are marked by hydrothermal alteration of the wall rocks. Also, veins are surrounded by trace-metal halos with contents increasing as the vein is approached. Changes of this kind can only be explained by the influence of migrating fluids that have passed through the system. They originated in deeper parts of the orogenic body, where metamorphism was active. Prograde metamorphism liberates large amounts of water by endothermic reactions. This can be substantiated both by simple calculations and by comparative analyses of metamorphic rocks (Hanson 1997).

Metamorphic fluids

Metamorphic fluids originate primarily by chemical release (devolatilization), different from diagenetic fluids. Increasing metamorphism, from sub-greenschist facies to anatexis, produces a steady flow of metamorphic dehydration fluids and a decrease of volatiles in the respective metamorphic rocks. The dehydration reactions (eq. 1.25) are strongly endothermic and consume a heat energy of ~90 kJ per 1 mol H_2O (Bucher & Frey 2002). Shales contain ~4 wt.% water in contrast to mica schist with ~2%. By exothermic reactions, basalt assimilates water during the formation of greenschists to a maximum of ~13%, but only 2% H_2O remain in amphibolite. Siliceous carbonates lose CO_2 due to generation of metamorphic calcsilicate minerals. Decomposition of organic substance in sediments liberates H_2, CO_2, CH_4, N_2 and water. During prograde metamorphism, the "mineralic" NH^{4+} that often partially replaces K^+ in diagenetic silicates (clay, mica, K-feldspar) is expulsed into the fluid phase. Consequently, total nitrogen decreases in metamorphic rocks and the remaining nitrogen becomes isotopically heavier (Bebout & Fogel 1992). Salt and anhydrite are usually dissolved and leave the system. Former evaporite horizons in metasediments may be revealed by newly-formed scapolite and albite, or by remains of anhydrite and of saline fluid inclusions (Fisher & Kendrick 2008).

Example of dehydration reactions at the transition from greenschist to amphibolite:

$$\underset{(\mathrm{Fe,Mg})_5\mathrm{Al_2Si_3O_{10}(OH)_8}}{4\ \text{Chlorite}} + \underset{\mathrm{Ca_2Al_3Si_3O_{12}(OH)}}{18\ \text{Zoisite}} + \underset{\mathrm{SiO_2}}{21\ \text{Quartz}}$$

$$= \underset{\mathrm{Ca_2(Fe,Mg)_3(Al)_2\ Al_2Si_6O_{22}(OH)_2}}{5\ \text{Tschermakite-amphibole}}$$

$$+ \underset{\mathrm{CaAl_2Si_2O_8}}{26\ \text{Anorthite}} + 20\ \mathrm{H_2O} \tag{1.25}$$

Equation 1.25 illustrates the most important mineralogical changes, as chlorite and epidote are consumed and contribute to neoformation of the anorthite (Ca-rich) component of plagioclase and the tschermak (Ca) molecule of amphibole.

Water in metamorphic rocks occurs mainly in OH-groups of hydrous minerals and in fluid inclusions. Grain boundaries also host tiny inclusions. Some fluids fill open fissures and the pore space. Fluid inclusions in low-grade metamorphic rocks are made up of H_2O, Cl, CO_2, CH_4 (e.g. in Alpine fissures) and H_2S and N_2 (Roedder 1984). Abundant cations include Na, Ca and Mg, but salt contents are mostly below 5%. Intermediate-grade metamorphic rocks have fluids with H_2O, HF, F, CO_2, CH_4, CO, H_2 and HS^-. High-grade metamorphic fluids are melt-dominated. Deep drill holes in crystalline rocks sampled small amounts of highly saline fluids of a somewhat enigmatic origin. In the Black Forest, Germany, deep fluids in gneiss are probably derived from Mesozoic seawater (Stober & Bucher 1999). Derivation of deep continental brines at high latitudes by freezing of Pleistocene seawater may be an alternative (Frank *et al.* 2010). Reduction of sulphate in descending brines enriches $CaCl_2$. In granulites, eclogites and sillimanite schists, water content is normally near zero; however, these rocks may contain pure CO_2 inclusions. Frequent daughter minerals in the microscopic inclusions are halite and sylvite that form by desiccation of episodic inflow of small batches of crustal fluids (Markl & Bucher 1998).

Mass balance calculations and isotopic investigations indicate that metamorphic fluids are not solely the product of prograde devolatilization but may mix with basinal and even meteoric fluids. Koons *et al.* (1998) illustrate the variable source of hydrothermal fluids in a cross-section of the New Zealand Alps. Obviously, hot metamorphic terrains build up large hydrothermal systems that are essentially comparable to the smaller convection systems established near magmatic intrusions. Metamorphic ore-forming hydrothermal systems at the deposit-scale can be long-lived (e.g. ~1 million years at Mt Isa: Matthäi *et al.* 2004).

Fluids liberated from rocks undergoing prograde metamorphism acquire economically interesting trace metals (e.g. gold) or other elements (arsenic), either together with the volatiles H_2O, F and Cl from the lattice of transforming minerals, or later along flow channels and in staging reservoirs by reaction of migrating fluids with the wall rocks. Controls of this transfer include the fluid to rock mass ratio, the fluid and rock chemistry, and T, P, pH, Eh and kinetic conditions of the system. Considering that metamorphic complexes will have a comparable average chemical constitution over large distances, expulsed metamorphic fluids should also have an analogue composition over large areas ("compartmentalization": Lefticariu *et al.* 2005). This hypothesis leads to the concept of "fluid provinces". In the Eastern Alps, ore deposits formed in the Cretaceous during the

Eoalpine Orogeny (e.g. siderite, copper, barite, talc) display similar inclusion fluids. This data was interpreted as evidence of a Synorogenic East-Alpine Fluid Province (Pohl & Belocky 1994, 1999). Note that preliminary data on fluid halogen mol ratios and Sm/Nd ages of ore and host rock suggest generation of siderites by deeply circulating evaporative brines in Late Triassic time (W. Prochaska, unpublished).

Many gold ore deposits are interpreted to have a metamorphogenic origin. Common examples are gold quartz veins with sulphides of arsenic, antimony and iron, which occur far from igneous intrusions in black schist, metaturbidites or in greenschist-facies metamorphic rocks. Commonly, they were formed in orogenic belts and at the time of waning orogeny, correlated with late-metamorphic uplift, lateral spreading, deep shear zones and intrusive activity. This is the rationale for the term **"orogenic gold deposits"** (Figure 1.84). Most of the fluids and the solutes are probably of metamorphic origin, but a contribution from other sources including the mantle, magmatic and meteoric domains is possible. Although the gold concentration in metamorphic fluids is very low, focused mass flow through chemical and physical traps formed many large gold deposits.

Time and rate of fluid flow from rock bodies undergoing metamorphism is difficult to determine. Two end-member modes are possible: i) Either fluids formed in the rock mass are conserved and later expulsed all at once ("batch volatilization"); or ii) fluids flow out as they are set free ("Rayleigh distillation"). In geological reality, it may be assumed that both processes act alternately and in various combinations, mainly due to physical boundary conditions (e.g. stress and strain, pore pressures, pressure gradient, permeability, temperature gradient, etc.) imposed by concomitant tectonics and the geological framework. The mineral specimen-rich Alpine fissures, for example, testify to retention of metamorphic fluids until after the

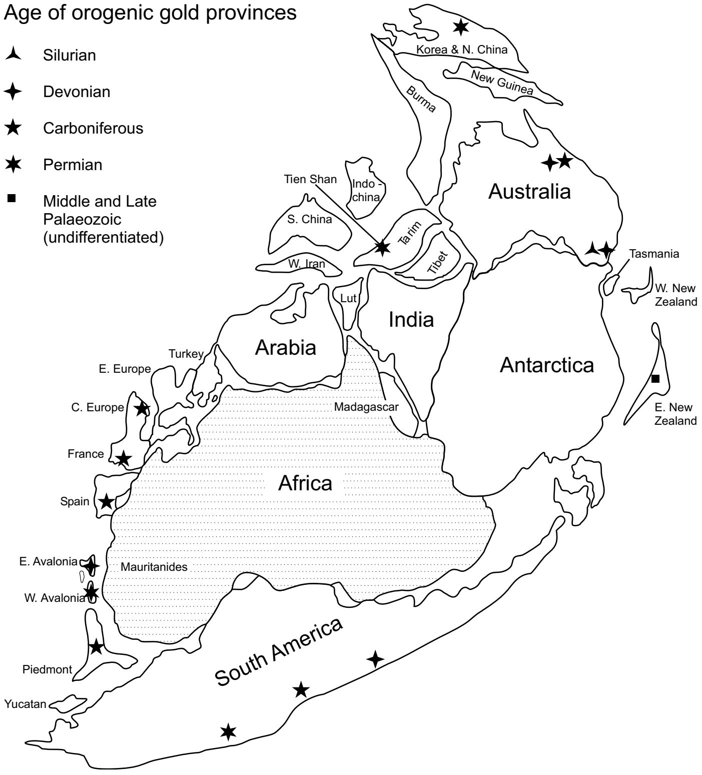
Age of orogenic gold provinces
Silurian
Devonian
Carboniferous
Permian
Middle and Late Palaeozoic (undifferentiated)
Korea & N. China
New Guinea
Burma
Tien Shan
Indo-china
S. China
Tarim
Tibet
W. Iran
Australia
Tasmania
W. New Zealand
Lut
India
Arabia
Turkey
E. Europe
Antarctica
C. Europe
Madagascar
E. New Zealand
France
Africa
Spain
E. Avalonia
Mauritanides
W. Avalonia
South America
Piedmont
Yucatan

Figure 1.84 Large gold ore provinces formed in the Middle to Late Palaeozoic within Gondwana and adjacent plates (adapted from Haeberlin *et al.* 2003 with permission from Elsevier). Active continental plate margins controlled the location of gold ore formation, illustrating the term "orogenic gold deposits".

BOX 1.13 Two end member models of metamorphogenic ore formation

1. Prograde metamorphogenic ore formation. Normally, metamorphic fluids are expulsed in the form of a wide and diffuse flow into regions of lower pressure (Hanson 1997, Jamveit & Yardley 1997). Large regional tectonic structures (shear zones, extensional faults and thrust faults) focus the diffuse flow, because they can be channels of higher permeability (Figure 1.85). The permeability of the lower ductile crust ($\sim$10–15 km beneath the surface, depending on the geothermal gradient) undergoing prograde metamorphism is very low with a flow of only 0.25 m/year (Beaudoin & Therrien 1999) and the pressure regime is lithostatic. Note, however, that even in the middle and lower crust, an interplay between brittle and ductile deformation may occur (Mancktelow 2006). In the brittle upper crust, permeability is much higher and flow in faults reaches 100–1000 m/year. When rising fluids enter this regime, pressure is released and approaches hydrostatic conditions. Descending (e.g. meteoric) water can penetrate as far as the brittle/ductile boundary (Ingebritsen & Manning 1999). Because of these particular conditions, the brittle/ductile transition at ca. 425–375°C is a very frequent location of metamorphogenic ore deposit formation.

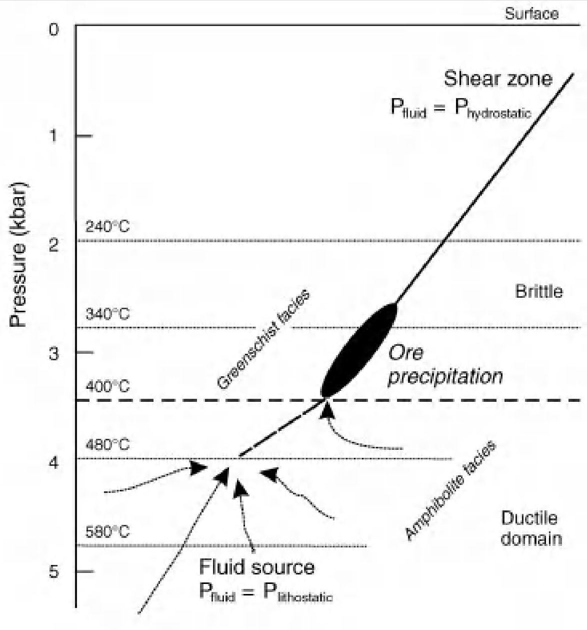

Figure 1.85 Ore deposit formation by prograde metamorphism.A shear zone focuses upflow of metamorphic fluids because of higher permeability. Its crustal-scale vertical extent facilitates transfer of fluids from lithostatic to hydrostatic pressure domains. Ore formation is a consequence of chemical or physical traps. The system is open, the mass flow is unidirectional.

2. Retrograde metamorphogenic ore formation. Many geological observations (e.g. concerning the structural control of orebodies) indicate that ore formation took place long after peak metamorphic conditions (or even totally unconnected to orogenic metamorphism). Petrographic investigations show that cooling and uplift of metamorphic complexes is accompanied by retrograde exothermic reactions of rocks with infiltrating fluids (mainly hydration; Haack & Zimmermann 1996, Yardley *et al.* 2000). Usually, these fluids will be derived from a near-surface reservoir (e.g. meteoric, marine or basinal water). The water descends along structural conduits and in contact with suitable rocks forms hydrous minerals. Oxygen is consumed in oxidation reactions. Tectonic preparation of a large rock surface (e.g. breccias) is favourable. In the reaction zone, rocks and surplus water are heated and country rocks sustain retrograde metamorphism. Heated fluids are charged with dissolved matter. Hydrothermal convection cells are established with hot fluids of low density rising back to the surface. Along the upflow channels, precipitation of dissolved matter from the fluids can form retrograde-metamorphogenic ore deposits (Pohl 1992, Figure 1.86). Convection cells may reach the brittle/ductile boundary, where descending waters mix with deeper prograde-metamorphic fluids, as shown by Templeton *et al.* (1997) in the Alps of

New Zealand. In the European Eastern Alps, many ore deposits are correlated with the second Eocene metamorphic phase. Gold quartz veins in the metamorphic core region of the Penninic unit (Tauern Mountains) were formed by ponded prograde fluids, whereas iron ore in higher tectonic units is the product of mixing of prograde fluids with descending meteoric water (Pohl & Belocky 1999).

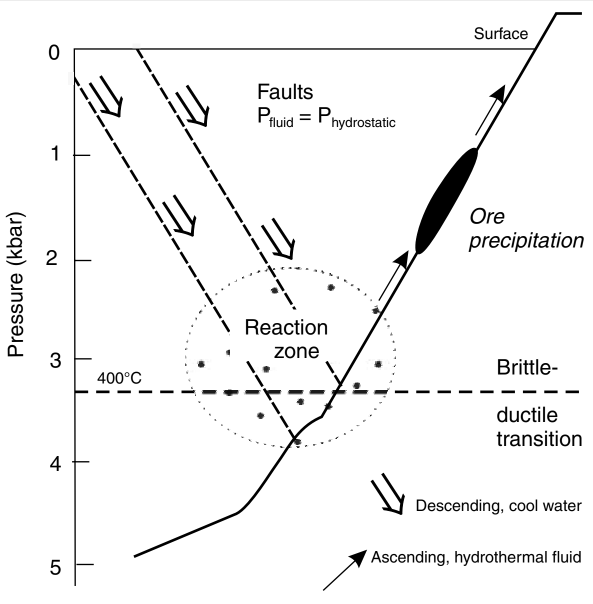

Figure 1.86 Ore deposit formation by retrograde metamorphism. Tectonic extension opens flow paths for descending cool waters that react at depth with hot rocks ("reaction zone"), take up solutes and rise back to the surface as hydrothermal fluids. The pressure regime is usually hydrostatic and the convection system is essentially open.

An instructive concept of ore formation during late-metamorphic cooling processes was described from the Scottish Dalradian belt (Craw & Chamberlain 1996). Infiltrating meteoric water induced an oxidation front that migrated through the orogenic body and facilitated leaching of trace gold. The gold was precipitated in reducing environments of the hydrothermal upflow limb (e.g. in the Tyndrum deposit).

temperature and pressure maximum of metamorphism. Ore deposit formation is more probable when large masses of stored fluid flow off in a geologically short time. This may often be the period of uplift, shearing and distension of metamorphic complexes. Synchronous metamorphogenic ore deposit formation in large areas supports the concept of tectonically activated "fluid pulses".

Many ore deposits, which were formed in stable cratons during geologically short events of major plate reorganizations (Whittaker *et al.* 2007), may be regarded as members of the retrograde-metamorphogenic class. Prominent examples are the unconformity uranium ore deposits in Canada and Australia (cf. Chapter 2.5 "Uranium"). Ore deposits formed during phases of extensional plate deformation, such as Alpine and Irish type Pb-Zn-Ag, often display a retrograde-metamorphogenic component when convection systems reach down into older basement. This is easily revealed by Pb-isotope investigations.

Both models of metamorphogenic-hydrothermal ore deposit formation systems, prograde and retrograde, appear scientifically well founded, but the genetic attribution of specific deposits remains difficult. One reason is that orogenic metamorphism is widespread and operates in settings as different as active continental margins (Andes), in island arcs (New Zealand) and in zones of continental collision (Alps). Regions where mantle magmas heat the crust from below (underplating, deep intrusions, continental extension, rifting) experience mobilization of volatiles and the establishment of deep convection systems. In all these settings, synchronous crustal melting and igneous activity are common, too. This causes difficulties in distinguishing metamorphogenic from magmatic ore deposits (Bucci *et al.* 2004). A severe problem is also that in nature, mixed variants of the theoretical end member models described seem to be prevalent.

1.7 METALLOGENY – ORE DEPOSIT FORMATION IN SPACE AND TIME

> "Deciphering the predisposition of orogen segments for exceptional mineral endowment is one of the most critical as well as intractable metallogenetic research topics"
>
> R.H. Sillitoe 2008

Metallogeny is the science of origin and distribution of ore deposits in geological space and time (de Launay 1913). The term includes both metallic and non-metallic mineral deposits, as does "minerogeny". Note that the adjective form of the word "metallogeny" is metallogenetic, although the abbreviated "metallogenic" is also used. As we have seen in the preceding sections, metallogenesis (ore deposit formation) is a function of the Earth's process systems. Mineral deposits are a by-product of dynamic processes in mantle and crust of the Earth, and of their interaction with hydrosphere and atmosphere. In geological time, these processes occur in geodynamic cycles that produce defined geological entities, such as the Alpine, Variscan and Caledonian orogenic belts, each with characteristic types of mineral deposits.

Important targets of metallogenetic studies are: i) the quest for the source of a valued element, ii) understanding mobilization and transport systems; and iii) the nature of the trap that caused the enrichment resulting in a mineral deposit. Some regions have similar ore deposits dating from more than one geodynamic cycle, for example Palaeozoic to Tertiary carbonate-hosted lead-zinc in the Mediterranean realm and gold in the North American Cordillera (Sillitoe 2008). This is described but not explained by the term "metallogenetic heredity". The word implies that the crust contains a geochemically distinct trace metal reservoir that is the source of repeated mobilization and mineralization. An opposing hypothesis dismisses this notion and claims that ordinary crust or mantle can be the source for most ore deposits. The formation of fertile tin granites, for example, can be traced to average crustal concentrations of tin; the critical factor is highly efficient magmatic differentiation (Lehmann 1990, Figure 1.18). There is no doubt, however, that both crust and mantle are geochemically highly heterogeneous. Anomalous metal contents are possible, and the heredity need not be based on an anomaly of a specific ore metal such as tin, but on other parameters such as redox state or elevated F, Cl, B and Li contents of source rocks that are conducive to mobilization and concentration of tin. This remains unproven, but with a more positive note, Plant *et al.* (1997) demonstrate that regional geochemical maps do allow important deductions about metallogenesis and metal endowment of an area.

The unidirectional evolution of the Earth in time is of superordinate rank compared to geodynamic cycles (Holland 2005, Sleep 2001, Windley 1995). In the 4500 million years (Ma) of geological history, Earth systems experienced severe changes reaching from the atmosphere, the biosphere and the oceans down into the mantle. Of course, metallogenetic evolution reflects these changes (Goldfarb *et al.* 2010). Several deposit-types occur only in certain periods of geological history. Examples include the komatiite-hosted nickel sulphides in Archaean greenstone belts (common from 3.8–2.5, rare until ~2 Ga), banded iron formations of the Superior type (2.6–1.8 Ga), granite-related tin deposits in the Late Palaeozoic and Mesozoic, and uranium in sandstones of Cretaceous and Tertiary age. Another important factor controlling the distribution of ore deposits in geological time is the preservation potential. Just as some rocks are more prone to erosion than others in long-term geological processes (Hawkesworth *et al.* 2009), so are ore concentrations. Preferential exhumation of near-surface deposits and their destruction by erosion must have occurred throughout geological time. This is probably the reason why epithermal and porphyry copper deposits are much more frequent in Phanerozoic compared to Precambrian time (Wilkinson & Kesler 2009, Kesler & Wilkinson 2006).

Impacts of extraterrestrial bodies may have influenced metallogenesis more profoundly than we realize today. The impact origin of the giant structure of Sudbury, Canada and its ore deposits (Dietz 1964) is, of course, generally acknowledged. The bombardment of Earth from space was most intensive during early geological time (ca . 4500–3800 Ma). The imported matter must have been mixed into the mantle. Impact structures on the surface were erased by Archaean crust building and by plate tectonics. Today, about 400 younger impact structures are exposed but apart from Sudbury, there are hardly ever convincing relations with economic ore deposits. Yet, we may ask, for example, if the supergiant ore concentrations in southern Africa (e.g. Bushveld, Great Dyke) could be inherited from extraterrestrial material mixed into the mantle. In contrast, little doubt exists that part of the giant oil and gas resources in the Gulf of Mexico are intimately related to the Cretaceous-Palaeogene boundary Chicxulub impact (Grajales-Nishimura *et al.* 2000).

1.7.1 Metallogenetic epochs and provinces

Useful metallogenetic concepts and terms include (Petrascheck 1965):

- **Metallogenetic Domains** implicate crustal sectors with a comparable geological evolution that include a number of metallogenetic provinces of different ages; examples are the European Alps, the South American Cordillera, or the Archaean Pilbara Nucleus of the West-Australian Shield.
- **Metallogenetic, or Ore Province** combines all deposits that were formed in a major geotectonic unit during one geodynamic cycle, and that are closely related by chemical affinity, form and metal endowment; for example, the tin province in the Late Palaeozoic Erzgebirge of Germany and Czechia; metallogenetic provinces extend over large areas, in contrast to districts.
- **Metallogenetic District, or Zone** describes parts of an ore province; Sillitoe (2008) uses the term "metallogenetic belt" with the same meaning; deposits within such a district are very closely related, single deposit types predominate, and metallogenetic activity was typically restricted to a short geological time Marcoux & Jebrak (1999) distinguish migrating and stationary districts; the latter are thought to be more productive because an energy source (e.g. a mantle plume) remained stationary for a geologically longer time (>10 Ma).
- **Metal Province** describes the distribution of all deposits of one metal (or a group of metals such as Pb, Ag, Zn) irrespective of their age; this illuminates regions of possible metallogenetic heredity.
- **Metallotects** are geological features that have caused formation or localization of mineral deposits; they include major crustal structures (Hough *et al.* 2007), metamorphic, volcanic and plutonic centres, regional geochemical barriers (the European Copper Shale) and discordances (uranium).

Utilization of metallogenetic terms tends to be vague, which is caused by problems of practical application. The main difficulty is often the age attribution of deposits, enforcing a loose definition of metallogenetic provinces and zones in respect of time (Routhier 1980). A statistical method to identify metallogenetic provinces and epochs was presented by Wilkinson & Kesler (2009), built from a large database on porphyry copper deposits. The authors propose to determine regions with a special endowment (metallogenetic provinces) and periods of enhanced deposit formation (metallogenetic epochs), after correcting the age-frequency and deposit-density distributions for loss by uplift and erosion as well as subsidence and burial. Although Wilkinson & Kesler (2009) reveal the Late Eocene and the Middle Miocene as epochs of enhanced porphyry copper mineralization in South America, they state that spatial distribution remains unpredictable. The key to "deciphering the predisposition of orogen segments for exceptional mineral endowment" (Sillitoe 2008) remains improvement of geological understanding.

Metallogenetic maps are produced in order to allow a synopsis of metallogenetic, geological (metallotects) and basic economic data (e.g. the size of deposits). A generalized geological background is used to display information on size and nature of ore deposits. Symbols aim at depicting generalized genetic and morphological information, and the nature of the main metal or mineral (Figure 1.87). Metals are indicated by colour, for example yellow for gold and silver, blue for lead and zinc, red for tin and tungsten, etc. The relative size of deposits is expressed by varying the size of symbols. Usually, boundaries of metallogenetic provinces and districts are shown. Many countries have published national metallogenetic maps. Europe is covered by several sheets of the *Metallogenetic Map of Europe and Neighbouring Countries* (scale 1:1 250 000; Emberger 1984) and by one sheet of the *Mineral Atlas of the World* (scale 1:10 000 000; published by the Commission de la Carte Géologique du Monde, CGMW, Paris, and the Geological Survey of Norway, NGU, Trondhejm 1997 (Juve & Storseth 1977)). Metallogenetic maps and the supporting mineral deposit data banks serve scientific interests, but their main use is practical; they are indispensable for estimates of undiscovered mineral resources and for planning strategic exploration.

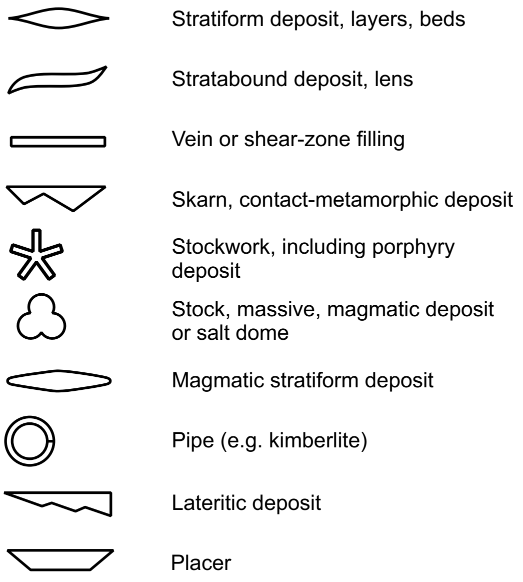
Stratiform deposit, layers, beds
Stratabound deposit, lens
Vein or shear-zone filling
Skarn, contact-metamorphic deposit
Stockwork, including porphyry deposit
Stock, massive, magmatic deposit or salt dome
Magmatic stratiform deposit
Pipe (e.g. kimberlite)
Lateritic deposit
Placer

Figure 1.87 Common morphological and genetic symbols for different deposit types on metallogenetic maps.

1.7.2 Metallogeny and plate tectonics

About 60 years ago, the understanding of global tectonics experienced a revolutionary advance (Kearey *et al.* 2009). Until then, the Earth's crust was considered to move either up or down, but rarely in a horizontal direction. The new concept of plate tectonics recognized that the lithosphere is divided into a number of rigid plates, which display considerable lateral movement. The engine of plate tectonics is convective cooling of the mantle. The resulting lithosphere is in part recycled back into the mantle. Extensional and compressional interactions at plate boundaries are the cause of profusely fertile metallogenetic systems.

The Theory of Plate Tectonics was worked out only recently, but its foundations are much older. The similarity of the coastal geometry of South America, Africa and India, and their sharing Permian sediments with the striking *Glossopteris* flora made already Eduard Suess (1831–1914) speculate that continents were not fixed in time and that in the geological past, the three formed a large supercontinent that he called Gondwana (Suess 1885). Building on this, Alfred Wegener developed the hypothesis of continental drift (Wegener 1924) that is in large parts still valid. Modern understanding of plate tectonics led to great progress in many fields of the earth sciences, including metallogeny (Robb 2005, Sawkins 1990b). Several lines of evidence indicate that plate tectonics may have started to operate as early as 4.4 Ga when a stiff lithosphere had been established (Moyen *et al.* 2006, Furnes *et al.* 2007). Already in the Archaean, ore deposits are known that suggest a suprasubduction zone setting.

Main elements of plate tectonic process systems that are **"metallogenetic factories"** include:

The formation of intracontinental rifts, aulacogens and large sedimentary basins (incipient divergent plate boundaries)

Rifts originate by extensional deformation of lithospheric plates and may or may not evolve into a new plate boundary. Very often, rifting causes thinning of the crust, upflow of hot mantle and updoming of rift shoulders (Tackley 2000). Volcanic activity within the rifts is a frequent consequence, often organized into large volcanic centres ("hot spots": Foulger & Natland 2003). Hot spots can be the origin of three diverging rifts (triple junction). Two of the three rift arms may widen to form a new ocean, whereas the third remains inactive and is called a failed rift arm. Several failed rift arms display thick sediments with bimodal volcanic rock suites, which were later folded by horizontal shortening. Considerable intrusive activity may occur. Settings like this have been called aulacogens (Eriksson & Chuck 1985).

Sediments of continental rifts include early, mainly terrestrial, alluvial clastic infill that can contain uranium, placers and coal deposits. In many cases, a freshwater, saline or marine-influenced lake stage succeeds with beds of salt, gypsum, magnesite, phosphate, valuable clays or oil shale. Full marine ingression into the widening rift and inception of oceanic spreading can induce submarine metalliferous exhalation of the black smoker or brine pool type (Red Sea) and the deposition of thick marine sedimentary sequences. Later, as diagenesis is enforced by rising temperature and pressure, oil and natural gas deposits are generated.

Hot spot-related ore-forming systems include the Bushveld in South Africa, tin-fertile A-granites in Nigeria and worldwide, many alkali-carbonatite igneous complexes. When rifting reaches the stage of a deep graben with vertical displacement at marginal faults approaching kilometres (Scholz & Contreras 1998), hydrothermal convection systems may form, based on the permeable tensional structures, the heat contrast and the hydraulic head imposed by rift shoulder mountains. The ascending branch of these hydrothermal systems typically results in deposits of lead, zinc, silver, manganese, fluorine and barite, which take the form of veins and metasomatic replacement bodies in rift margin rocks, or of ore beds in the graben sediments. Good examples are many Pb-Zn and Mn occurrences in Tertiary sediments on both sides of the Red Sea, and part of the Ag-Pb-Zn-F-Ba veins along the Rhine graben in France and Germany (Figure 1.28). Carbonatites and alkali intrusions with apatite, fluorine, niobium and rare earth element ores characterize the Cretaceous-Tertiary rifts in Eastern and Central Africa. Submarine, epicontinental rifts and half-grabens are related to base metal deposits of the sedex type.

Sullivan in British Columbia, Canada (base metals in the Neoproterozoic Alberta Rift), Mt Isa in Queensland, Australia (Pb-Zn-Cu in the early Mesoproterozoic) and the large deposits of native copper in basalts and of chalcocite in fine sands of the Nonesuch Shale in the Keweenawan Rift (USA, Late Mesoproterozoic) were proposed as remarkable examples of mineralization in aulacogens. The Panafrican Damara Orogen in southern Africa has also been interpreted as an aulacogen, although with exceptionally strong tectonic shortening. Its main mineralizations are late to post-tectonic, including the giant hydrothermal karst pipe Tsumeb with polymetallic ores of Pb, Zn, Cu, Cd and Ge (Chetti & Frimmel 2000), and the uranium-deposit Rössing in alaskitic granite.

Intracontinental basins with prominent ore provinces include the European Copper Shale (Mesozoic), Witwatersrand gold (Late Archaean) and Mississippi Valley type lead-zinc-barite-fluorite deposits (Palaeozoic) in North America.

Major plate reorganizations affect both continental and oceanic systems intensely (Whittaker *et al.* 2007). Within short periods of a few million years, new subduction zones are installed, vectors of plate drift change (wander paths form "loops") and the plates are subjected to new stress fields. Oceanic and continental crust is stretched or sheared, new mantle regions experience partial melting, resulting in magma underplating, the formation of hotspots and the rise of mantle volatiles. Flood basalt volcanism may be a consequence, producing giant Cu-Ni-PGE deposits such as Noril'sk, as well as climate change and global extinction of life due to huge emissions of sulphur and chlorine such as those of the Dekkan traps at the end of the Cretaceous (Self *et al.* 2008). Enhanced heat flow and elevated permeability of the crust are favourable factors for the formation of deep convective hydrothermal systems and of mineral deposits. Mantle volatiles (mainly water and CO_2, with solutes like fluorine, arsenic, etc.) may rise, leach metals, mix with crustal fluids and form ore deposits. Examples of mineralization caused by plate reorganization include the hydrothermal "Saxonian Mineralization" of Europe north of the Alps (Walther 1983), several kimberlite provinces and unconformity uranium ore deposits in Canada and Australia.

The evolution of passive continental margins and the disruption of older ore provinces (divergent plate boundaries)

The opening of new oceans passes from a high heat-flow rift stage into a marine transgression and thermal contraction phase. Relatively shallow, epicontinental seas may form. As the young ocean widens, passive continental margins develop. Sediments include salt, phosphate and hydrocarbon source rocks. Manganese ore beds of the Tertiary Black Sea province, Quaternary metalliferous marine placers and Palaeoproterozoic banded iron ores of the Superior type represent typical marine epicontinental shelf ore deposits.

The separation of continents by rifting and seafloor spreading may cut across older orogenic belts, cratons and other crustal-scale structures. With them, older ore provinces are ruptured and the fragments can be found on remote coasts across an ocean (e.g. the Atlantic borderlands of Africa and South America). In these cases, metallogenetic knowledge acquired on one coast is a valuable tool for work in its twin across the seas.

Seafloor spreading and the production of new lithosphere at mid-ocean ridges (oceanic-divergent, or "constructive" plate boundaries)

This is the domain of ore formation at mid-ocean ridges that was presented earlier in more detail (Section 1.1 "Ore Deposits at Mid-Ocean Ridges and in Ophiolites"). After obduction, the products of these processes are ophiolite-hosted deposits. Many ophiolites, however, were not formed at mid-ocean rifts but in tensional supra-subduction settings including back-arc spreading systems, or rifts of primitive island arcs (e.g. the Cyprus ophiolite). Yet, there is no doubt that all mid-ocean rifts display segments of hydrothermal activity, including black smokers. Related ores are sulphide mounds or mud-pools in a proximate position, iron-manganese oxides (ochres and numbers) and distal manganese crusts and nodules with important contents of Cu, Ni and Co. Oceanic transform faults that offset ridges are apparently not metallotects for mid-ocean metallogenesis.

Subduction of lithospheric plates at convergent ("destructive") plate boundaries

Subduction recycles oceanic lithosphere back into the mantle (Figure 1.88). The trace of subduction on the seafloor is marked by deep oceanic trenches. Volcanic arcs develop on the overriding plate. Between trench and arc, four structural zones are typically developed: Nearest to the

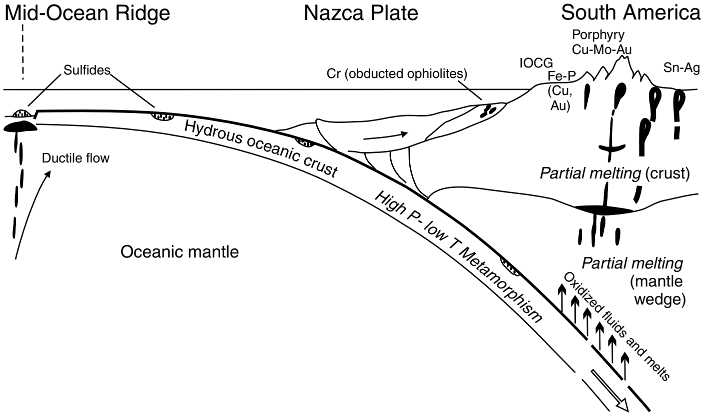

Figure 1.88 Metallogeny of active continental margins with the typical zonation, here illustrated by a schematic profile from the subducting Pacific Nazca Plate through the Central Andes (South America). Adapted from Sillitoe (1972, 2008).

trench (1) an accretionary complex of low-grade metamorphic sediments is followed by (2) a wedge of mainly continental crust with minor oceanic and hydrated mantle material of medium to high-pressure metamorphic grade. This is overlain by (3) a mega-scale melange composed of high-pressure and ultrahigh-pressure oceanic and continental crust fragments that are extruded from the subduction channel. Finally follows (4) the frontal part of the upper plate that carries the volcanic arc. Volcanic arcs in dominantly oceanic settings form island arcs, whereas active continental margins display continental or Cordilleran arcs. Recent primitive island arcs are geologically young (Tonga, Scotia), because maturation sets in quickly and produces arcs with a partially continental character (Japan, Kurile Islands). Other island arcs pass into continental collision belts (Sumatra-Malaysia-Himalaya). Andean volcanic arcs build upon older, strong upper crust that is largely of Precambrian age in both Americas. Behind the magmatic arcs appear back-arc spreading systems that include the back arc basins of island arcs, the continental "molasse" basins and broad distended regions such as the Basin and Range Province of North America.

There is a great diversity of subduction zone configurations, due to many variables including slab density, thickness and length (Schellart *et al*. 2007). Subduction zones show variously high or low trenchward plate velocities, trench retreat (or more rarely trench advance) velocities, slab dip angles and so forth. Trench retreat ("subduction rollback") is caused by the negative buoyancy of the cold, dense descending slab. This places the overriding lithosphere into a state of tension as the subduction zone moves oceanwards and facilitates movement of magmas and fluids (Hamilton 1995). Slab rollback, slab breakoff and delamination of mantle lithosphere allow asthenospheric upwelling that can provide the heat pulses required for ore forming processes, including magmatism and regional hydrothermal fluid systems. Extensive intracontinental compressional deformation migrating cratonwards is explained by flat-slab subduction. This is probably caused by the subduction of oceanic plateaus and plume tracks (Livaccari *et al*. 1981), which typically ends in delamination (foundering) of the slab from the continental lithosphere. This is the environment of Basin-and-Range type tectonic and magmatic provinces (e.g. in Mesozoic South China: Li & Li 2007). Fertile anorogenic magmatism including alkaline basalts, bimodal volcanic rocks and I- and A-type granitoids are characteristic for this setting.

It is important to stress that most of the Earth's richest ore provinces are found above subduction zones. This is conspicuously so along the margins of the Pacific Ocean, which are largely formed by long-lived destructive plate boundaries. Associated are numerous active volcanoes, accounting for the term "ring of fire". Reconstruction of similar settings for stages in the geological past is crucial for strategic exploration planning (Haeberlin *et al*. 2003, Figure 1.84).

Island arc ore deposits may be either allochthonous, which implies tectonic transport, for example of slivers of oceanic lithosphere, or autochthonous, formed within the arc. Allochthonous are first of all the ophiolite-related ores, including chromite (Cuba, Luzon) and platinum placers; Cyprus type sulphide deposits are infrequent. Lateritic nickel ore deposits (New Caledonia) are autochthonous formations. Major autochthonous deposits are associated with the large mass of calc-alkaline to potassic intrusive and volcanic rocks. Of outstanding economic prominence are porphyry and skarn copper-gold deposits, epithermal gold deposits and volcanogenic massive sulphides. Similar to continental margin arcs, sources of the metals may be subducted oceanic crust or the mantle wedge above the subduction zone. The latter was confirmed for Lihir, Papua New Guinea (McInnes *et al*. 1999), which is a giant epithermal gold deposit of very recent geological age (ca. 690 ka). It is significant that some metals such as tin and mercury appear only in older, more complex island arcs with a partially continental character.

Active continental margin ore deposits are often more clearly zoned compared with island arcs, as a function of increasing distance from the subduction zone. In the apparently simple geotectonic setting of Central South America, the results are long and narrow ore provinces (Sillitoe 1972).

Prominent along the western coast within Precambrian basement and Cretaceous plutons are iron-apatite and iron oxide-copper-gold (IOCG) deposits associated with hydrous intermediate magmatism (Sillitoe 2003, Oyarzun *et al.* 2003). A belt of giant porphyry Cu-Mo-Au deposits follows towards the east, roughly along the Neogene-Recent volcanic arc. These mines currently dominate world copper production. Near the eastern margin of the Cordillera, a Sn-Ag belt is developed (Figure 1.88). However, neither this zonation nor all deposits in single belts are synchronous, but are the product of several regional metallogenetic episodes that range from Late Triassic (earliest tin deposits) to Cretaceous (iron and part of copper) and Tertiary ages (most of the copper and tin-silver). Subduction configurations during this time changed considerably (James & Sacks 1999).

The structure of the North American Cordillera is even more complex. One example is the subducting East Pacific Ridge, which is a factor that enhances metallogenetic processes. Partial melting of young, hot subducting oceanic plates favours the formation of oxidized adakitic magmas and of important gold and copper-gold deposits (Cooke *et al.* 2005, Mungall 2002). South Alaskan gold deposits are thought to be related to ridge subduction (Haeussler *et al.* 1995). Another difference is the collage-like nature of the North American Cordillera that consists of many "suspect" or "exotic" terranes, which preserved distinct but interrelated geological records (Colpron & Nelson 2006). This complicates metallogenetic interpretation.

Ore deposit formation above subduction zones is causally tied to the fate of the subducting lithospheric slab of oceanic crust and mantle. At mid-ocean ridges, the crust is largely hydrated and oxidized. When the oceanic slab bends before entering the subduction zone, additional hydration appears to take place (Faccenda *et al.* 2009). Altered basalts, gabbros and depleted mantle peridotites enter the subduction zone as a "cold" slab at geothermal gradients of 15°C/km or less. Along the subduction plane, continental material can be scraped off ("subduction erosion") and taken down to the zone of dehydration and melting. The high-pressure/low-temperature metamorphism of subduction zones converts the rocks to the typical blueschist and eclogite lithologies. Mantle rocks, oceanic crust and its sedimentary cover incur devolatilization and possibly, partial anatexis. Dehydration processes control the structure of slabs from ca. 40 to 150 km depth (Rondenay *et al.* 2008). As a function of T and P, hydrous fluids, anatectic melts or supercritical liquids may be set free (Kessel *et al.* 2005). The latter are characterized by high trace element solubilities and consist of H_2O, Cl, S, CO_2, etc., including large ion lithophile elements (LILE: Ba, K, Rb, Cs, Ca, Sr) and other incompatible elements (U and Pb). This transfer "metasomatizes" the mantle wedge above the subduction zone and triggers widespread melting. Because of relatively high fO_2 (roughly from fayalite-magnetite-quartz [FMQ] to FMQ + 2) sulphide (S_{2-}) and sulphate (S_{6+}) coexist and combine to high total sulphur contents in melts, which favours sulphur saturation and mineralization in the upper crust (Jugo 2009). Extensive formation of sulphide melt during metasomatism and partial melting of the hot mantle wedge would be detrimental, because sulphide melts scavenge chalcophile and siderophile elements such as copper and gold from silicate melt and being heavy, tend to remain trapped in the deep crust (Mungall 2002).

Magma batches rising through the crust continue to change by complex assimilation and contamination processes, until they reach the surface as calc-alkaline melts of andesitic-dioritic nature. These magmas have only ~50% material from the mantle, the other half is derived from the crust. Intrusive and extrusive activity of continental arcs is concentrated in short pulses of 10–15 My ("flare-ups") that occur during and after tectonic shortening (Ducea & Barton 2007). Porphyry copper-molybdenum-gold deposits are direct products of these processes within and above the subduction zone (Richards 2003, 2009). Among many other arguments, this can be substantiated by the observation that localization and metal contents of porphyries are largely independent of their specific setting (e.g. primitive or evolved island arcs, diverse types of active margins). The precise source of the chalcophile metals and gold – oceanic crust or mantle wedge – remains obscure (Dreher *et al.* 2005). A continental source, however, is implied for the metals tin, tungsten and tantalum, because deposits appear only in regions with thick and old crust.

Continental collision

Oceans that were consumed by subduction leave a suture in the newly welded continent, which is marked by ophiolites. One of the most remarkable and metal-endowed sutures worldwide is the Palaeozoic accretionary orogenic collage of the Altaids in Central Asia, with a length of 3000 km (Xiao *et al*. 2009). Usually, continental collision results in the subduction of continental crust (Ampferer or A-subduction), although this is limited by the buoyancy of crustal rocks. The process results in thickened crust below collisional belts and the formation of anatectic S-type granitoid melts. Less frequent are post-subduction Cu-Au porphyries and related epithermal gold deposits, which are formed where former magmatic arcs are involved in the collision (Richards 2009). Continental crust of the lower plate can be subducted to depths of more than 100 km and exhumed after ultrahigh-pressure metamorphism. Also, collision causes giant systems of hydrothermal fluid flow involving metamorphic, basinal and meteoric fluids (Mark *et al*. 2007, Craw *et al*. 2002, Oliver 1986). Similar features are reported from intracontinental mountain belts involving very narrow oceans (Alps, European Variscan Belt) and from purely intracontinental orogens (Kibarides in Central Africa: Pohl 1994). Typically, collisional orogens exhibit: i) granitoid-related deposits of tin, tungsten, gold and rare metals; and ii) deposits formed by migrating metamorphic fluids. Gold is especially common in this setting (orogenic gold deposits: Groves *et al*. 2003). Mineralization in orogenic belts is favoured by phases of extension, because melts and fluids can more easily rise to shallow depths. Extension may be related to orogenic collapse and other post-collisional processes.

Assemblage and break-up of supercontinents

The plate-tectonic evolution of the Earth's crust follows not only the relatively short Wilson cycles (opening and closure of oceans) but also a trend of large-scale cycles of amalgamation of all continental plates into supercontinents and the following break-up. The Phanerozoic supercontinent Pangaea is well-known, existing from the Permian into the Jurassic (~300–175 Ma). Mesoproterozoic Rodinia (~1100–800 Ma) is generally accepted but its assemblage is more contentious because data are insufficient for a unique solution (Torsvik 2003). Older supercontinents are even less well-defined. Supercontinents can be related to specific characteristics of the metallogenetic evolution, including the incidence of anorogenic ore formation (e.g. titaniferous anorthosite-ferrodiorite complexes) and the prevalence of continental, sediment-hosted deposits (Kupferschiefer: Robb 2005). When Gondwana and Laurasia finally fused into the supercontinent Pangaea, the Variscan belt in Europe experienced a short-lived metallogenetic peak of unique fertility. Deep processes inducing initial crustal distension and break-up of Pangaea, at about the Triassic/Jurassic boundary, again produced an ore-forming heat and fluid pulse across much of Europe (Box 1.14).

Apart from the relatively simple plate tectonic model situations described above, many quite complex interaction fields are known today. One recent example is the Gulf of California, where a subducted oceanic ridge passes along strike into a continental rift and ultimately into an intra-continental transform structure (San Andreas Fault). Only rarely, connections such as these can be reconstructed for the geological past so that the precise plate-tectonic setting of some ore deposits may never be fully understood. Yet, the quest for solving a given plate-tectonic puzzle is always scientifically fascinating and results benefit applications of economic geology.

1.8 GENETIC CLASSIFICATION OF ORE AND MINERAL DEPOSITS

> *We can get so wrapped up in debating terms that we forget entirely about the subjects of our original interest: minerals, rocks, geology, and such...*
>
> Stephen A. Langford in *GSA Today*,
> February 2002

BOX 1.14 The metallogenetic evolution of Europe

The following sketch of Europe's metallogenetic evolution is intended to serve as an example that may have implications for other continents. Although the second smallest of all continents (after Australia), Europe is made up of crustal rocks of all ages, starting with an Archaean nucleus in the Arctic North. In the Mediterranean South, subduction and mountain-building are still active. A detailed description of single deposits and districts with their geological frame and with references is available in *Mineral Deposits of Europe* (Volumes 1–5, Bowie *et al.* 1979; Dunning *et al.* 1982, 1989; Dunning & Evans 1986; Ridge 1990). Emberger (1984) provides a succinct report on metallogenetic mapping in Europe. The regional geology of Europe is accessibly presented in the encyclopaedia by Moores & Fairbridge (1997). A geodynamic analysis of metallogeny provide Blundell *et al.* (2005).

Northern Europe (Scandinavia and adjoining Russia) and Northwestern Europe (The British Isles) are largely built of Precambrian and Early Palaeozoic rocks. Mountain belts formed in this time are deeply eroded, so that many preserved ore deposits are metamorphosed or metamorphogenic. The region comprises the Precambrian Baltic Shield and the Lower Palaeozoic Caledonides. In Northern Finland and Sweden, the Baltic Shield contains an Archaean nucleus with attached Proterozoic orogenic belts younging to the southwest, namely the Svecokarelides (ca. 2.0–1.54 Ga) and the Sveconorwegian Province (1200–850 Ma). The Archaean nucleus hosts greenstone belts with little notable mineralization. More prospective seems to be a belt of Ni-Cu-PGE mineralized layered mafic intrusions (Andersen *et al.* 2006), which appear to record a Palaeoproterozoic (2.44 Ga) rifting event. In contrast, the Svecokarelian (also called Svecofennian) belt is well endowed with important mines. Northern Sweden is renowned for "Kiruna-type" magmatic iron oxide-apatite deposits within bimodal metavolcanic rocks and also contains a number of recently discovered iron-oxide-copper-gold deposits (Weihed & Williams 2005). Further south, the Svecokarelides host a broad belt of volcanogenic sulphide ore deposits (Cu, Zn, Pb, Au, Ag, Ni, Co) that extend from Boliden in the Skellefte volcanic arc (Sweden) to Outokumpu-Pyhäsalmi (Finland) and further east to Lake Ladoga (Russia). The geological environment of ore formation included island arcs and oceanic rifting (Nironen 1997; Sundblatt & Parr 1994; Gaal 1990). Recently, exploration for diamonds (in the Archaean), for orogenic gold deposits (both in Archaean and Proterozoic units: Sundblatt 2003) and for platinum in mafic intrusions, resulted in a number of new mines and many promising prospects. Meso- to Neoproterozoic units are moderately mineralized. Only the orthomagmatic titanium ore of the Egersund District in southwest Norway (920 Ma) is of more than local significance. This region was part of the collision zone between Fennoscandia and Laurentia when the Supercontinent Rodinia was assembled.

The Caledonides are the largest metallogenetic domain of the region, with a length of 2700 km and a maximum width of 250 km. The belt resulted from convergence of Baltica and Laurentia, and final closure and suturing of Iapetus Ocean in the Silurian. The Caledonian orogen comprises metasediments and magmatic rocks of Eocambrian to Silurian age, and a large number of significant ore deposits (Grenne *et al.* 1999). During the early rift phase of its evolution (at ~550 Ma), the famous alkali-carbonatite complex at Fen in southern Norway was emplaced. This is the location where terms such as fenite and søvite were coined. Periodically, niobium, iron, thorium and cerium were produced from the Fen carbonatite. Volcanic-hosted massive sulphide deposits resembling the Cyprus type formed in back-arc rifts or in primitive island arcs. In Norway, they were important sources of copper and zinc (Figure 1.80). More recently, exploitable metamorphogenic gold deposits were found in Ireland, Wales and Scotland. Along the thrust front of the Caledonides in Sweden, a number of stratiform lead ore deposits occur in Early Cambrian platform quartzites. These galena impregnation deposits of the "Laisvall type" are thought to be derived from metamorphic fluids, which were mobilized from autochthonous and parautochthonous sediments under the eastward advancing Caledonian nappe sheets. In the Middle and Late Cambrian in Sweden, the platform sediments include oil shales ("alum shales") that represent giant potential resources of synthetic oil, uranium, vanadium, phosphorous, molybdenum and nickel. A "Late Caledonian" phase (~350 Ma) of alkaline intrusions is expressed by the Sokli carbonatite in Finland, exploited for apatite (with by-products niobium and rare earth elements).

The Oslo Graben is an important magmatic, tectonic and metallogenetic rift province in southwest Norway. It is considered here because of its location, although its active phase dates from the Carboniferous and the Permian. The Oslo Graben Province displays remarkable silver and base metals veins (Kongsberg, Figure 1.22), molybdenum impregnations in granite and felsic volcanics, and iron skarn ore. Of about the same age is the alkali ring intrusion of Khibiny on Kola Peninsula (Russia) with its important apatite and nepheline resources.

Central Europe and large parts of Southwestern Europe are underlain by rocks of the Late Palaeozoic Variscan orogen, although large areas are covered by younger platform sediments. Regions near the Mediterranean Sea are shaped by the later (Mesozoic-Cenozoic) Alpine orogeny.

The European Variscides are a complex mosaic of Precambrian microcontinents and of Palaeozoic orogenic belts that were finally welded together and deformed by the Variscan orogeny in the Late Carboniferous (Tait *et al.* 1997).

The Variscan chain in Europe is part of the 10,000 km collisional zone suturing Gondwana and Laurasia when the Rheic Ocean closed to form Supercontinent Pangaea. The development of the Variscan orogen involved major crustal shortening and subduction of substantial amounts of supracrustal rocks, continental and oceanic crust, and mantle lithosphere. Yet, ophiolites derived from Palaeozoic oceanic lithosphere are rare and contain little economic mineralization. Marginal to the region considered in this chapter, however, large ophiolites are present in the Ural Mountains, hosting deposits of chromite, platinum and base metal sulphides (Herrington *et al.* 2003). Silurian submarine hot-spot volcanism is probably the crucial metallotect of the unique and giant mercury deposit Almadén in Spain (Figure 1.89). Large synsedimentary ore deposits were formed during extensional tectonics in Devonian marine strata of the Rhenohercynian shallow sea (volcanogenic iron ore and sedex type zinc-copper-lead sulphides with barite, e.g. Rammelsberg, Germany). Still in a tensional setting during the Early Carboniferous of southern Spain and Portugal, volcanic massive sulphide (VMS) and brine pool sedex deposits in shale constitute the giant massive sulphide ore province of the Iberian Pyrite Belt with pyrite, copper, tin, lead, zinc and gold (Figure 1.89). At about the same time, the syngenetic-diagenetic Irish zinc-lead-silver deposits formed in a shallow sea. Peak synkinematic and synmetamorphic processes during the Variscan orogeny were not fertile. However, giant coal deposits formed from forest mires at tropical latitudes during the Westphalian (Late Carboniferous), located in foreland and intramontane basins of the Variscan orogen. The coal belt in Europe has an east-west extension of ~3000 km and a north-south width of 800 km (Ziegler 1982).

Following the orogenic peak, regional exhumation and post-collisional collapse of the Variscides was strongly affected by transtensional and transpressional wrench-deformation, detachment of subducted lithospheric slabs, asthenospheric upwelling and thermal thinning of the mantle-lithosphere. At ~300 Ma (Stephanian-Early Permian), when Gondwana and Laurasia finally sutured to form Pangaea, the deep-reaching disturbance of the Variscan domain reached its climax with widespread melting of the uppermost asthenosphere and the lithospheric boundary layer. Mantle-derived basic melts underplated the crust, inducing anatexis and the intrusion of granites in the upper crust throughout the Variscides. The most evolved, and youngest phase of these granites was highly fertile: Tin and copper deposits were formed in Cornwall, tin, tungsten, bismuth and uranium ore in the Erzgebirge (Baumann *et al.* 2000, Breiter *et al.* 1999, Stemprok & Seltmann 1994), tungsten, tin, uranium, arsenic, lithium and fluorine in the French Massif Central, tungsten in the Pyrenees, and tungsten (Panasqueira) and tin in Portugal (Figure 1.89). At the same time, C-O-H-N fluids were released from the deep crust that deposited orogenic gold-arsenic-antimony ores in the French Massif Central. It is thought that the reason for this short-lived late-orogenic "metallogenetic peak" was devolatilization of the lower crust by granulite metamorphism (Marignac & Cuney 1999).

In the late Early Permian, magmatism ceased and increasingly larger areas subsided below the erosional base level forming a new system of intracratonic basins. Terrestrial and coastal sediments of the Rotliegend desert sediments contain several deposits and numerous occurrences of uranium. In the Late Permian (Zechstein), the giant salt deposits of Germany, Poland and England formed in a restricted sea, which invaded the desert basins of Pangaea from the north. Potassium salt resources of this basin are second only to those of Canada. The Copper Shale stratum at the base of the transgressive marine Zechstein evaporites is evidence of an early euxinic stage; along the southern basin margins, it trapped epigenetic copper concentrations emplaced in the Triassic. The end of the Permian brought the biggest mass extinction of life in geological history, with the loss of ~95% of all species. Its cause is generally believed to be the eruption of the Siberian and South Chinese Emeishan trap basalts (Kamo *et al.* 2003).

Announcing the break-up of Pangaea, a new Wilson cycle started with crustal distension in the Triassic, which culminated near the Triassic/Jurassic boundary with the formation of a giant magmatic province resembling trap basalts in the later Central Atlantic Ocean (Olsen 1999). This initiated opening of the Tethys and the Atlantic Ocean, and induced a heat and fluid pulse across much of Europe. Copper Shale ore deposits were emplaced as well as numerous karst and vein deposits of Pb-Zn-F-Ba (e.g. Poland: Sass-Gustkiewicz 1996; Germany: Walther 1983). The deposits are located both in Variscan basement (e.g. Schwarzwald, Massif Central) and in the Mesozoic cover from Poland to Spain. Mesozoic, mainly marine sediments of the platform rocks contain oil and natural gas deposits, oil shale and sedimentary oolitic iron ore (Lorraine district in France).

In the Mesozoic and Cenozoic, Alpine and Mediterranean Europe was part of the giant Tethyan-Eurasian metallogenetic domain, which is the product of convergence, subduction and collision of Eurasia with fragments of Gondwana. European Alpine chains include the Pyrenees, the Alps, the Appenines, the Carpathians, the Balkan Mountains, Dinarides, Helennides and Caucasus. Along the convoluted trace of the orogen, the geodynamic character changes from segments with major calc-alkaline magmatism to segments with extensive regional metamorphism. This is attributed to the complex geometry of the collision interface, with numerous microplates and transient oceans (Heinrich & Neubauer 2002). Orogenic compression including formation of the great nappes (thrust sheets of thick rock bodies that moved many kilometres over each other) culminated in the Late Cretaceous and the Early Tertiary. Palaeozoic, and even Precambrian rocks are either part of the nappes or form the basement of microplates. They contain some mineral deposits

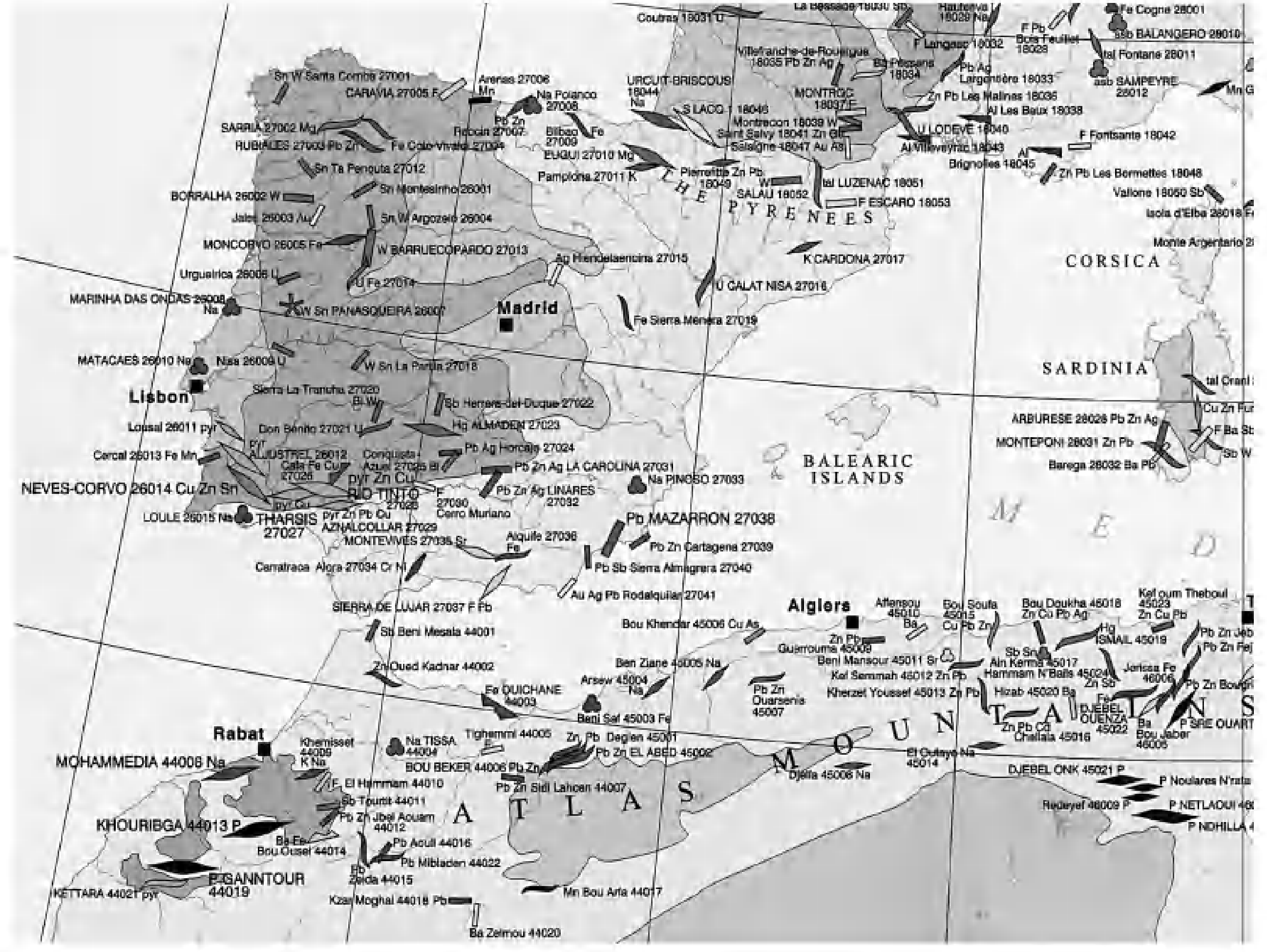
Sn W Santa Comba 27001
CARAVIA 27005 F
Arenas 27006 Mn
Na Polanco 27008
Pb Zn Reocin 27007
Bilbao 27009 Fe
EUGUI 27010 Mg
Pamplona 27011 K
SARRIA 27002 Mg
RUBIALES 27003 Pb Zn
Fe Coto-Vivaldi 27004
Sn Ta Penouta 27012
Sn Montesinho 26001
BORRALHA 26002 W
Jales 26003 Au
Sn W Argozelo 26004
MONCORVO 26005 Fe
W BARRUECOPARDO 27013
Urgueirica 26006 U
U Fe 27014
Ag Hiendelaencina 27015
MARINHA DAS ONDAS 26008 Na
W Sn PANASQUEIRA 26007
Madrid
Fe Sierra Menera 27019
MATACAES 26010 Na
Nisa 26009 U
W Sn La Parrilla 27018
Lisbon
Sierra La Tranche 27020 Bi W
Sb Herrera-del-Duque 27022
Lousal 26011 pyr
Don Benito 27021 U
Hg ALMADEN 27023
Cercal 26013 Fe Mn
pyr ALJUSTREL 26012
Cala Fe Cu 27026
Conquista-Azuel 27025 Bi
Pb Ag Horcajo 27024
Pb Zn Ag LA CAROLINA 27031
Na PINOSO 27033
NEVES-CORVO 26014 Cu Zn Sn
pyr Zn Cu RIO TINTO 27028
F 27030 Cerro Muriano
Pb Zn Ag LINARES 27032
pyr Cu
LOULE 26015 Na
THARSIS 27027
pyr Zn Pb Cu AZNALCOLLAR 27029
MONTEVIVES 27035 Sr
Alquife 27036 Fe
Pb MAZARRON 27038
Pb Zn Cartagena 27039
Pb Sb Sierra Almagrera 27040
Carratraca Alora 27034 Cr Ni
Au Ag Pb Rodalquilar 27041
SIERRA DE LUJAR 27037 F Pb
Sb Beni Mesala 44001
Zn Oued Kadnar 44002
Fe OUICHANE 44003
Rabat
MOHAMMEDIA 44008 Na
Khemisset 44009 K Na
Na TISSA 44004
Tighemmi 44005
BOU BEKER 44006 Pb Zn
F El Hammam 44010
Pb Zn Sidi Lahcen 44007
Sb Tourtit 44011
Pb Zn Jbel Aouam 44012
KHOURIBGA 44013 P
Ba Fe Bou Ousel 44014
Pb Aouli 44016
Pb Mibladen 44022
Pb Zeida 44015
P GANNTOUR 44019
KETTARA 44021 pyr
Kzar Moghal 44018 Pb
Ba Zelmou 44020
Mn Bou Arfa 44017
A T L A S M O U N T A I N S
Coutras 18031 U
La Bessade 18030 Sb
Hauterive 18029 Na
F Pb Bois Feuillet 18028
Fe Cogne 28001
asb BALANGERO 28010
tal Fontane 28011
asb SAMPEYRE 28012
Mn G
Villefranche-de-Rouergue 18035 Pb Zn Ag
Ba Pezens 18034
F Langasc 18032
Pb Ag Largentière 18033
URCUIT-BRISCOUS 18044 Na
MONTROC 18037 F
Zn Pb Les Malines 18036
Al Les Baux 18038
S LACQ 18046
Montredon 18039 W
Saint Salvy 18041 Zn Ge
Salsigne 18047 Au As
U LODEVE 18040
Al Villeveyrac 18043
F Fontsante 18042
Al Brignolles 18045
Zn Pb Les Bormettes 18048
Pierrefitte Zn Pb 18049
W SALAU 18052
tal LUZENAC 18051
F ESCARO 18053
Vallone 18050 Sb
Isola d'Elba 28018 Fe
Monte Argentario 2
THE PYRENEES
K CARDONA 27017
CORSICA
U CALAT NISA 27016
SARDINIA
tal Orani
Cu Zn Fu
ARBURESE 28028 Pb Zn Ag
F Ba Sb
MONTEPONI 28031 Zn Pb
Sb W
Barega 28032 Ba Pb
BALEARIC ISLANDS
M E D
Algiers
Affensou 45010 Ba
Bou Soufa 45015 Cu Pb Zn
Bou Doukha 45018 Zn Cu Pb Ag
Kef oum Theboul 45023 Zn Cu Pb
Bou Khendar 45006 Cu As
Zn Pb Guerrouma 45009
Hg ISMAIL 45019
Pb Zn Jeb
Pb Zn Fej
Ben Ziane 45005 Na
Beni Mansour 45011 Sr
Sb Sn Ain Kerma 45017
Hammam N'Bails 45024 Zn Sb
Jerissa Fe 46006
Arsew 45004 Na
Kef Semmah 45012 Zn Pb
Pb Zn Ouarsenis 45007
Kherzet Youssef 45013 Zn Pb
Hizab 45020 Ba
Pb Zn Bougri
Beni Saf 45003 Fe
Fe DJEBEL OUENZA 45022
Zn Pb Cd Challala 45016
Ba Bou Jaber 46005
P SRE OUART
Zn Pb Deglen 45001
Pb Zn EL ABED 45002
El Outaya Na 45014
Djelfa 45008 Na
DJEBEL ONK 45021 P
P Noulares N'rata
Redeyef 46009 P
P NETLAOUI 46
P NDHILLA 4

Figure 1.89 (Plate 1.89) Metallogenetic overview of Southwestern Europe and adjacent Africa (clipping from Juve & Storseth 1997). With kind permission of NGU, Trondheim. Text and symbols (cf. Figure 1.86) in four classes that indicate relative size of deposits. The geological background is simplified to Hercynian (purple, mainly Palaeozoic); Alpine (yellow, mainly Mesozoic) and cover sediments (light grey, mainly Tertiary). The distance between 5° latitude parallels is ~550 km.

that are clearly older than the Alpine cycle. Other deposits in pre-Alpine rock units originated during the Alpine metallogenetic cycle (e.g. the large metasomatic siderite deposit Erzberg in Austria and orogenic gold-quartz veins in gneisses of the Eastern and Western Alps).

Pre-Alpine basement rocks that are exposed within the Alpine belts allow the reconstruction of a protracted plate tectonic evolution throughout the Palaeozoic, including ocean subduction and the obduction of ophiolites. Some important pre-Alpine mineral deposits in the basement are: i) granite-related tungsten stockwork orebodies at Mittersill (Tauern, Eastern Alps); and ii) sparry metasomatic magnesite lenses in the Eastern Alps and in the Carpathians. The second is clearly different from the Variscan north of the Alps, but the first recalls the rare metal metallogeny of the German Erzgebirge.

In Alpine and Mediterranean Europe, widespread extensional tectonic strain and heating in Mid-Triassic to Early Jurassic time are related to the break-up of Pangaea and caused a major metallogenetic pulse (Jankovic 1997). In the Balkans, associated volcanism is implied in formation of the exhalative iron ore strata at Vareš (Bosnia), the rift-bound mercury deposit of Idria (Slovenia) and a number of lead-zinc deposits. The large lead-zinc deposits in the Southern Alps (e.g. Bleiberg, Mežica) formed in a shallow marine rift zone distal to volcanic activity. Larger oceanic basins existed mainly in the Jurassic and were closed in the Cretaceous. Obducted ophiolites in the Balkans host important chromite mineralization. Cyprus type sulphides are rare and have little economic relevance. Alpine ophiolites are largely barren, from the Eastern Alps to the Pyrenees.

With the inception of the Cretaceous, the tectonic regime in the Alpine realm changed to subduction and convergence. From Romania through Serbia to Bulgaria, arc magmatism is represented by a Late Cretaceous (90–60 Ma) ore-bearing igneous belt, which is referred to as the Banatitic Metallogenetic Belt (or, geographically, the Apuseni-Banat-Timok-Srednogorie belt: Heinrich & Neubauer 2002). Banatites are calc-alkaline intermediate intrusive and extrusive igneous rocks of I-type and magnetite series character. The belt extends for ~750 km with a width of 30–70 km. Copper-gold porphyry and high-sulphidation epithermal gold-copper deposits occur from the Timok district in Serbia (e.g. Bor and Majdanpek) in the west to Bulgaria (Panagyurishte district) in the east. Iron-lead-zinc skarn ore deposits (including Ocna de Fier in Romania: Nicolescu *et al.* 1999) and smaller deposits of iron, molybdenite and bismuth are also considered as legacies of this magmatic metallogenetic belt.

In the western Carpathians (Slovakia) and in the Eastern Alps (Austria), Cretaceous magmatic activity is practically absent. Instead, the onset of continental collision and subduction induced a pervasive flow of metamorphic fluids that produced metamorphogenic deposits of siderite (Erzberg), talc (Rabenwald), and smaller deposits of copper and barite (Pohl & Belocky 1999, Figure 1.90). Coal seams in Late Carboniferous sediments were metamorphosed to exploitable graphite.

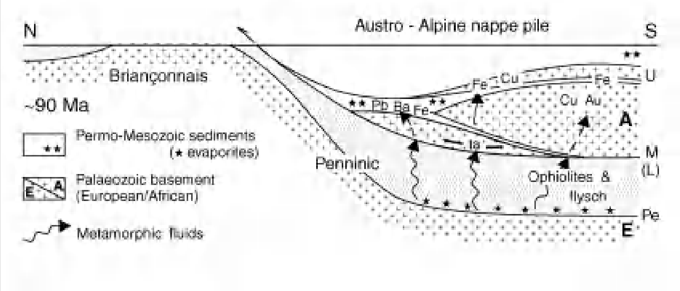
N
Austro - Alpine nappe pile
S
Briançonnais
~90 Ma
Permo-Mesozoic sediments (★ evaporites)
Palaeozoic basement (European/African)
E
A
Metamorphic fluids
Penninic
Fe
Cu
Fe
U
★★ Pb Ba Fe
Cu Au
A
ta
M
(L)
Ophiolites & flysch
Pe
E

Figure 1.90 Metamorphogenic ore formation in the European Eastern Alps.During peak conditions of metamorphism in the Turonian (Late Cretaceous), dehydration affected deeper parts of the nappe pile including Penninic autochthonous cover, oceanic crust and marine sediments with evaporite horizons. ta – Talc at Rabenwald, Pe – Penninic nappes, L-M-U – Lower, Middle and Upper East Alpine thrust sheets.

Intermittent emersion of wide regions of the European and African plates allowed the formation of supergene alteration deposits, most famously bauxite in southern France (Les Baux is the name-giving district), Hungary, Italy and Greece, and nickel laterites in Albania and Greece. Cretaceous convergence between African and European plates caused a wave of compressional deformation in the northern foreland of the Alps ("inversion tectonics"), which can be demonstrated even in North Sea oilfields over 1000 km distant.

In the Early to Mid-Tertiary, major continental blocks collided in the Eastern and Western Alps (Neubauer *et al.* 2000). This led to extensive Barrovian-type regional metamorphism, commonly preceded by an eclogite-facies stage. During the following orogenic collapse and rise of high-grade metamorphic domes, numerous small orogenic gold vein deposits were formed (Monte Rosa, Tauern). Giant lignite basins developed in Germany and Poland, mainly in the Eocene-Oligocene.

Also in the Early to Mid-Tertiary, oceanic sub-basins in the Inner Carpathians and the Apuseni Mountains closed, continental microplates indented into the evolving orogen, and slab break-off and mantle delamination caused asthenospheric incursions (Heinrich & Neubauer 2002). De Boorder *et al.* (1998) suggested that orogenic collapse and slab rupture caused the heat and fluid flow responsible for the subsequent (mainly Miocene) mineralization. In the Apuseni Mountains, gold and base metal ores are related to localized centres and short belts of Tertiary andesitic and rhyolitic volcanism (Neubauer *et al.* 2005). For thousands of years until today, this region was the source of much of the gold produced in Europe. In the Inner Dinarides and the Rhodope Mountains, lead, zinc and antimony deposits occur in similar settings. This magmatic and ore formation style extends into Greece and the Greek islands, where it lasts longer (into the Pliocene and locally, into the Holocene) and where manganese, barite and gold gain a more central role. In Western Europe, Tertiary mineralization includes skarn deposits of magnetite and haematite on the island of Elba, above a granite cupola that intruded Mesozoic sediments some 6 Ma ago. Across the sea in Italy, volcanogenic deposits in the Toscana include epithermal mercury at Monte Amiata. In southern Spain near Almeria, andesitic and rhyolitic volcanoes host epithermal deposits of gold, silver, lead and zinc (Rodalquilar, Figure 1.89). Messinian evaporites along the Mediterranean shores are exploited for gypsum, sulphur, rock salt and potassium salts. The giant strontium deposit at Montevives in the Sub-Betic zone of southern Spain is especially remarkable.

In the Late Tertiary and the Holocene north and west of the Alps, a broad mantle plume caused basaltic volcanism (Goes *et al.* 1999) of little metallogenetic significance. The plume is related to the large crustal break that traverses Europe from the mouth of the River Rhone to the Oslo Graben in Norway. The Upper Rhine Rift is a section of this structure and is endowed with historically important hydrothermal lead-zinc-silver ore veins in the rift shoulders (Figure 1.28), and with oil and gas deposits as well as potassium salt beds in the Tertiary graben fill.

In spite of this reminder that terms and classes are not the first target of science, efforts towards classification are both necessary and useful. Classifications are needed because they clarify terms and provide a common reference frame, and this makes them useful for scientific communication and practical application. Various geological aspects are employed to classify ore deposits, including the presence of certain metals or minerals (e.g. silver, haematite), the form of the orebody (vein, bed, etc.), the local geological environment (submarine or terrestrial volcanism), the plate tectonic setting (island arc, continental margin) and other genetic characteristics such as formation temperatures and fluid chemistry. The thoughts of Lindgren (1933), Niggli (1948) and Schneiderhöhn (1932, 1962) represent important stages of metallogenetic classification. Because ores and useful minerals are basically just rocks, although usually rare ones, a petrogenetic approach is obviously practicable. Main petrogenetic process systems are magmatism, sedimentation, diagenesis, metamorphism and surficial weathering (Figure 1.1). Parallel to other classification systems in science, these five main classes are the root for a branching order of subclasses. Apart from petrogenesis, criteria for ordering often include the local, regional and plate tectonic situation.

However, a stringent genetic classification of mineral deposits is very difficult. One reason for this is that many ore deposits represent a position in a complex multi-dimensional space of well-defined end members. The formation of Kuroko ore deposits, for example, is an interplay of volcanic, intrusive, sedimentary and diagenetic processes. The origin of high-grade BIF-haematite ore seems to comprise sedimentation induced by proliferating marine life, later passage of saline basinal brines and supergene components. May I remind the reader that already Charles Darwin (1859) described lucidly how impossible it is for the naturalist to define species, families and genera of plants and animals only by structural differences. Darwin states "All true classification is genealogical". Ore deposit classification is certainly not easier than establishing biological systems and should also aim for a genetic logic.

Scientific progress continuously modifies and improves genetic models. An ever more detailed understanding of ore-forming processes is the result (Robb 2005). Some practicians of exploration and mining think little of genetic models and prefer a pragmatic and empirical classification. Many scientists employ non-genetic terms of classification, such as "granite-related" or "sediment-hosted stratiform" deposits. Economic geologists use terms such as "deposit styles" (Hough *et al.* 2007) or "deposit types" (Cox & Singer 1986; e.g. copper porphyry type, orogenic gold, lateritic nickel). Attribution to certain styles and types is

Table 1.6 A simple genetic classification of ore deposits

I. Magmatogenic Ore Deposits

1. Orthomagmatic Deposits:
   Sulphide Fe-Ni-(Cu-PGE) ore hosted by Archaean komatiites and subvolcanic ultramafic intrusions; Alpine type Cr-PGM in ophiolites, and seams in layered mafic intrusions; Cu-Ni-PGM "reefs" in layered mafic intrusions; complex mafic-ultramafic intrusions with, for example, conduit-hosted Cu-Ni-PGM; impact magma bodies with Ni-Cu-PGM; Ural-Alaska type ultramafic ring intrusions with Cr-PGM; Ti-Fe in Mesoproterozoic anorthosite-ferrodiorite complexes; orthomagmatic iron ore deposits of iron oxides and apatite in intermediate to felsic igneous rocks (Kiruna type); apatite-Fe-Nb-Zr, or REE-U-F in carbonatite plugs and nephelinite intrusions
2. Pegmatites with ore of Be, Li, Rb, Cs, Ta (Nb), U, Th, REE, Mo, Bi, Sn and W, industrial minerals, gemstones
3. Magmatic-Hydrothermal Deposits:
   Skarn ore, with magnetite-Cu-Co-Au, W, Zn-Pb-Ag, Mo-Bi-Au and Sn-As-Pb-Zn-W-Mo; contact-metasomatic ore (Pb, Ag, Zn); Fe-oxide-Cu-Au (U-REE) deposits (IOCG); porphyry deposits (Cu-Mo-Au, Sn-W); submarine volcanogenic (Kuroko) and volcanic-hosted massive sulphide deposits (VMS); vein deposits (Sn, W, Cu); terrestrial epithermal Ag-base metal deposits; epithermal Au-Ag deposits

II. Supergene Ore Deposits

1. Residual (Eluvial) Deposits:
   Residual placers (e.g. W, Sn); bauxite; lateritic Au, Fe and Mn ore deposits
2. Supergene Enrichment Deposits:
   Enriched sulphide ore (Cu, Ag); lateritic Ni
3. Infiltration Deposits
   U in sandstone; Pb-Zn-F-Ba and Mn in karst cave systems

III. Sedimentary Ore Deposits

1. Allochthonous:
   Colluvial, alluvial (gold, columbite, cassiterite, wolframite, platinum) and coastal (rutile, ilmenite, zircon, monazite) placers
2. Autochthonous:
   Sulphide deposits, mainly in black shales; polymetallic deposits of Cu-Sb-Zn-Pb-Ag (-Au), mostly of sedex type; Palaeoproterozoic banded Fe ore (BIF) of Algoma and Superior type, and banded Mn ore; oolitic Fe and Mn ore; deep sea manganese nodules and crusts (Mn-Cu-Ni-Co-PGM)

IV. Diagenetic-Hydrothermal Ore Deposits

1. Stratabound and/or stratiform sediment-hosted Cu deposits:
   European Copper Shale (Cu); Central African Copper Belt (Cu, Co, Pb, Zn, U)
2. Mississippi Valley type (MVT) Pb-Zn-F-Ba deposits (hosted in marine carbonates)
3. Saline brine-related deposits
   Pb-Zn-F-Ba, metasomatic siderite, preconcentration of high-grade hematite

V. Metamorphosed and Metamorphic Ore Deposits

Metamorphism of pre-existing ore generally improves processing characteristics of ore, but is rarely a factor of metal accumulation and ore formation; metamorphic examples include ± *in situ* redistribution, concentration and recrystallization of gold

VI. Metamorphogenic-Hydrothermal Ore Deposits

Prograde and retrograde metamorphogenic-hydrothermal ore deposits (e.g. orogenic Au deposits in accretion-subduction-collision complexes; part of the Central African Cu-Co ore deposits; Cu in Mt Isa, Australia).

determined by descriptive attributes and relations to certain rock associations (e.g. "turbidite-hosted gold deposits", "alkaline igneous association"– Laznicka 1985, 1993). In this book also, descriptive terms are frequently used. The advantage is that short denominations facilitate communication and that changes of genetic understanding do not enforce new terms. Also, this solves the problem of classifying deposits of intermediate position between genetic end members. Yet, genetic concepts are a strong element in finding new ore deposits (Kreuzer *et al.* 2008), guide rational exploitation and mine closure. Therefore, genesis must be reflected in ore deposit classification.

Guilbert & Park (1986) admirably describe the problems of ore deposit classification but nevertheless argue for the exercise, in spite of shortcomings. In this spirit, I endeavour to provide a simple genetic classification that should help the reader to understand the logic of this chapter's arrangement. As a general rule, the geological setting and the last concentrating process (e.g. sedimentation) determine placement in a certain class, for example formation of metalliferous sediments by hydrothermal fluids venting from the seafloor resulting in sedimentary exhalative (sedex) deposits. In Table 1.6, ore deposit groups and types presented in Section 1.1 are listed with the intention to summarize the genetic panorama. In Chapter 3, a similar overview is provided for selected non-metallic minerals and rocks.

1.9 SUMMARY AND FURTHER READING

Ore formation is an integral component of the Earth's dynamics and of petrogenetic process systems. Ore deposits, however, typically result from the interaction of several processes and modifying factors. Reducing the complexity to simple end member concepts leads to the following shortlist of genetic variety.

Orthomagmatic ore deposits of metal oxides (magnetite, ilmenite, chromite), sulphides (Ni, Cu) and of precious metals (Pt, Pd, Au) are formed by the segregation of solid ore minerals or of ore melt from a large liquid silicate magma body. Gravitational settling of segregates is the basic concentrating factor (Boxes 1.1 and 1.2).

Metalliferous pegmatites originate by fractionation of volatiles (water, boron, fluorine) and rare metals (Be, Li, Rb, Cs, Ta, Sn) into the very last silicate melt batches of crystallizing parental granites.

Magmatic-hydrothermal deposits are formed from metal-enriched magmatic volatile phases which are released by solidifying magma bodies. Copper porphyry systems (Box 1.3) provide economically outstanding examples. Note the great variety within this class, including skarn (e.g. Cu, Zn-Pb-Ag, Mo, Bi, Au) and contact-metasomatic deposits, Fe-oxide-Cu-Au (U-REE) deposits (IOCG), and tin, copper and tungsten veins in the roof of parent intrusions (Box 1.4). Whereas the former are related to intrusive and subvolcanic magma bodies, volcanic-hosted massive sulphides (VMS, Box 1.5) and epithermal gold and silver deposits (Box 1.6) originate near the surface in volcanic centres, either beneath the sea or on land.

Supergene ore deposits result from weathering, which describes the interaction of Earth materials with air, water, life and the energy flow from the sun. During decomposition of rocks, metals are concentrated either *in situ* as an insoluble residuum (e.g. bauxite) or by precipitation after some movement in soil and ground water (e.g. lateritic nickel deposits: Box 1.7). Lateral transport distances of 1 to 100 km characterize infiltration deposits of some metals such as copper and uranium (Box 1.8).

Sedimentary ore deposit formation is foremost the product of exogenous process systems with physical and chemical transport in water. Part of the metals moved is concentrated in rivers (alluvial placers, e.g. Au) and along coasts (coastal placers, e.g. Ti). Most enter the marine realm in aqueous solution from the land or from hydrothermal sources underneath the seafloor. The world's largest metal concentrations formed in the Early Proterozoic when photosynthetic cyanobacteria expanded rapidly, oxidizing the seawater and precipitating iron dissolved in the oceans (banded iron formations; Box 1.9). Many giant base metal deposits (sedimentary-exhalative, "sedex" Cu, Pb, Zn) are the product of hot metalliferous fluids venting on the seafloor. In contrast to mid-ocean black smoker activity, sedex deposits are formed by rifting in shallow epicontinental seas (Box 1.10).

Diagenetic ore deposits are a consequence of physical and chemical changes affecting basinal sediments. With rising temperature and pressure, pore fluids are charged with dissolved matter and eventually are expulsed towards lower pressure regions, commonly basin margins where metals are precipitated. Traps are often low-permeability barriers, which is evident for the most valued products of diagenesis, oil and natural gas. Low permeability and reducing power of the European Copper Shale acted together in concentrating metals transported by oxidized brines (Box 1.11). Worldwide, reduced brines, which resemble reservoir water in oil pools, generated numerous diagenetic carbonate-hosted Pb and Zn deposits (Box 1.12).

Metamorphism affects previously established metal concentrations in two different ways. One group of minerals such as sulphides of Cu, Pb and Zn hardly changes and we call this class metamorphosed ore deposits. Other materials that are only valuable because of transformation into an exploitable ore (e.g. originally dilute traces of gold concentrated by *in-situ* redistribution) may be called metamorphic ore deposits.

Prograde metamorphic recrystallization of large rock volumes liberates a giant mass of dehydration fluids, which transport trace metals into shallow crust where chemical and physical traps precipitate ore (e.g. orogenic gold deposits); this is the prograde metamorphogenic class (Box 1.13). Cooling metamorphic massifs are flooded by surface water, which induces hydration and re-equilibration of high-grade metamorphic rocks. Where tectonic fragmentation provides sufficient permeability, hydrothermal convection systems are established that produce retrograde metamorphogenic deposits (Box 1.13).

Metallogeny is the synthesis of scientific endeavours to understand ore formation. Plate tectonics provide the unifying frame. The world's most prolific metallogenetic domains include supra-subduction island arcs and continental margins (e.g. the Pacific "ring of fire"). The Bushveld in southern Africa, however, with its giant resources of Cr, Pt and V, and many other large ore districts of the world are not related to subduction.

Europe, briefly described as an example of metallogenetic evolution (Box 1.14), is one of the smallest continents and yet provides a fascinating diversity of metallogenetic activity throughout geological history. It can be seen as an assemblage of orogenic belts younging southwards from an Archaean nucleus in the North. Along its Mediterranean margins, subduction, volcanism and ore-forming processes are still active.

For readers who wish to pursue the theme of ore-forming processes to greater detail, Robb (2005) is highly recommended. The present state of the science of economic geology is illustrated and described in the impressive *Economic Geology 100th Anniversary Volume* (Hedenquist *et al.* 2005); be aware, however, that the treatment is selective and at a highly demanding scientific level. An admirable insight into the complexity of ore-forming systems gives Sillitoe (2010) in his paper on "Porphyry copper systems". For details on single deposits and districts, search the extensive and systematic descriptions of thousands of ore deposits worldwide by Laznicka (1985, 1993). Global tectonics is comprehensively presented by Kearey, Klepeis & Vine (2009).

CHAPTER 2

Economic geology of metals

Synopsis

Because of their unique fracture toughness, metals are the most important engineering materials of civilization (Lu 2010) and have many other essential applications. With few exceptions (e.g. only 1–2% of ordinary lead is primordial), metallic elements were part of the solar nebula material that accreted to form the Earth. Within the nascent planet, siderophile metals fractionated into the core and lithophile metals into the crust. In the aeons since then, geological cycling caused concentration of ore deposits. Individual types and the variability of each metal's ore deposits are mainly a function of geochemical properties. In this chapter, the economic geology of more than 40 important metals is systematically presented and illustrated by reference to specific mining districts and deposits. Information for each metal includes its main ore minerals, exploitable ore grade, use of the metal, geochemical behaviour, environmental aspects, a short list of significant deposit types followed by more detailed descriptions, and brief lines on production and resources. Practical notes are added where appropriate.

Many formulae, numbers and various data have been assembled from *Mining Journal, Mining Magazine, Mining Annual Review*, Berkman (2001), Klein & Hurlbut (1999), Neuendorf *et al.* (2005), United States Geological Survey (*USGS Minerals Information Webpages*) and Walker & Cohen (2007). Discrepancies between different sources are not rare. Therefore, in case of the need for highest accuracy, I advise the reader to verify critical data.

2.1 THE IRON AND STEEL METALS

2.1.1 Iron

Common Ore Minerals:

		Max. wt.% Fe	*Density (g/cm^3)*
Magnetite	$FeO.Fe_2O_3$	72.4	5.2
Haematite	α-Fe_2O_3	70	5.2
Maghemite	γ-Fe_2O_3	70	4.8
Goethite	α-FeO(OH)	62	3.8–4.3
Lepidocrocite	γ-FeO(OH)	62	4.0
Siderite	$FeCO_3$	48.2	3.8

Depending on the genetic setting, magnetite displays different concentrations of Ti, Mn, Mg, Al and V. In siderite, Mn and Ca content reaches the percent range. "Martite" is haematitized magnetite, and coarsely micaceous haematite is also known as "specularite". Iron silicates such as chamosite and thuringite, with a maximum of 42% Fe, are rarely of economic interest but are always part of the ore paragenesis in oolitic deposits. "Limonite" is a field term; it may contain variable parts of amorphous and microcrystalline iron oxy-hydroxides.

The cut-off grade for iron ore is ~30 wt.% Fe, although with the exception of the internal

---

Economic Geology Principles and Practice
Metals, Minerals, Coal and Hydrocarbons – Introduction to Formation and Sustainable Exploitation of Mineral Deposits, Walter L. Pohl
© 2011 Walter L. Pohl. Published 2011 by Blackwell Publishing Ltd.

Chinese market, most large producers deliver lumpy ore, concentrate, pelletized and sintered fines with 55–65% Fe. An exception is magnetite ore that can be exploited at relatively low grades, because low-cost magnetic processing is very effective. Iron content of more than 67.5% Fe (after calcining) is required as feed for direct reduction iron (DRI). If carbon dioxide charges are applied to siderite calcining, its role as an iron ore may soon end.

Specifications for marketable iron ore (and concentrate) concern first of all the chemical composition, but also grain size and behaviour in the blast furnace. Ore destined for the blast furnace should resist abrasion and have a good permeability for gas flow. Because large masses of iron ore are transported across the oceans (second only to crude petroleum), mechanical stability during handling and transport is very important. Requirements for metallurgical processes and shipment are attained by sintering or pelletizing fine ore near the mine. Only lumpy ore (6–32 mm diameter) is shipped without upgrading. Sintering may also be applied in order to reduce high water content before transport.

Desirable chemical and mineralogical properties of iron ore are imposed by its main purpose, production of pig iron in the blast furnace. Only ~10% of the world's iron ore is processed to iron sponge by direct reduction technologies. Pig iron or iron sponge, combined with coke, are the main raw materials for the production of crude steel, the toughest of all construction materials (Lu 2010). High iron concentration in ore, low content of SiO_2 and alumina, and coarse grain size are favourable properties. Further desirables are useful content of $CaO + MgO$ ("basic" ore), low phosphorous ($<0.1\%$) and other impurities ($Mn < 2\%$, $Cr < 1\%$, $Ni < 0.5\%$, $S < 0.2\%$, and As, Cu, Zn and $Pb < 0.1\%$). Phosphorus of more than 0.1% is not acceptable, because it adversely affects steel quality. Ti and V interfere with common iron and steel production, but can be valuable by-products of specialized plants. Generally, long-term constant composition of ore is an advantage, because this allows compensation for undesirable properties. Slags from iron and steel production are valuable by-products, not waste. Slags are applied as fertilizers in forestry and agriculture, as part of the cement formula and as aggregates in the construction industry. Some slags, however, may concentrate toxic or environmentally hazardous trace elements.

Non-metallurgical uses of iron ore consume a very small share of total production. They include chemical applications (the sulphate is a fungicide), pigments and abrasives. In the future, iron sulphate compounds might be used for fertilizing the high oceans, because Fe is the main limiting factor of phytoplankton production. Its application is one of the potential geoengineering methods of carbon sequestration from the atmosphere (Boyd 2007). Many specialized mines produce iron oxide pigments (~200,000 t/y worldwide) for colouring construction materials (e.g. bricks), paints (e.g. ochre, specular haematite), animal feed and as a filler in plastics. Typically, these fields demand extremely high quality, both of the ore and its processing.

Geochemistry

The geochemical behaviour of iron is indicated by its namesake position (iron in ancient Greek is *sideros*) in Goldschmidt's siderophile elements (associated with the Earth's iron-nickel core and comprising Fe, Co, Ni, Mo, PGE, C, P, Ge, Sn and Au: Goldschmidt 1958), as a transition metal in the periodic table and its high contents in nearly all rocks and in the continental crust (~5%, range 3–6.5%). Iron's variable oxidation states in nature are of major significance: native iron Fe^0, ferrous (Fe^{2+}) and ferric iron (Fe^{3+}). Reduced iron is commonly mobile and oxidized iron immobile. This causes retention of huge masses of iron in the exogenous cycle of earth processes. Redox states of iron mark certain geological environments, usually controlled by contact with the atmosphere or with organic substances. Of course, surficial alteration induces oxidation, whereas reduced iron occurs in coal seams (siderite), and native iron is found at contacts of basalt with bituminous schists or coal (e.g. Diskø, Greenland).

A large percentage of iron ore was formed or upgraded by weathering and/or sedimentation. Therefore, the geochemical behaviour of iron in the near-surface environment is of the highest interest. Weathering of ferriferous rocks may lead to residual enrichment, as in lateritic iron ore deposits. Some oxidized iron can be mobilized in the form of colloidal or solid oxy-hydroxide particles, adsorbed on suspended clay flakes and chelated with organic matter, but rarely in ionic solution. Stability and formation of ore minerals are well defined in pH/Eh space (Figure 2.1). A lateral disposition of pH/Eh zones in a sedimentary basin induces iron facies zoning (Figure 1.66). Biological activity may contribute to precipitation indirectly by consumption or production of oxygen and CO_2, and rarely in a direct way (iron bacteria: Konhauser 1998; certain fungi). Biological processes (e.g. dissimilatory iron reduction by bacteria) may cause fractionation of the isotopes ^{56}Fe and ^{54}Fe up to $\delta^{56}Fe$ of ±3‰ (related to bulk Earth: Johnson & Beard 2005). Abiotic redox cycling of iron and mineral fluid reactions also produce measurable changes, in spite of the small mass difference of the four natural Fe-isotopes (54, 56, 57 and 58; Staubwasser *et al.* 2006; Whitehouse & Fedo 2007). Black smoker fluids, for example, have isotopically lighter iron compared with sediments and magmatic rocks (Beard *et al.* 2003).

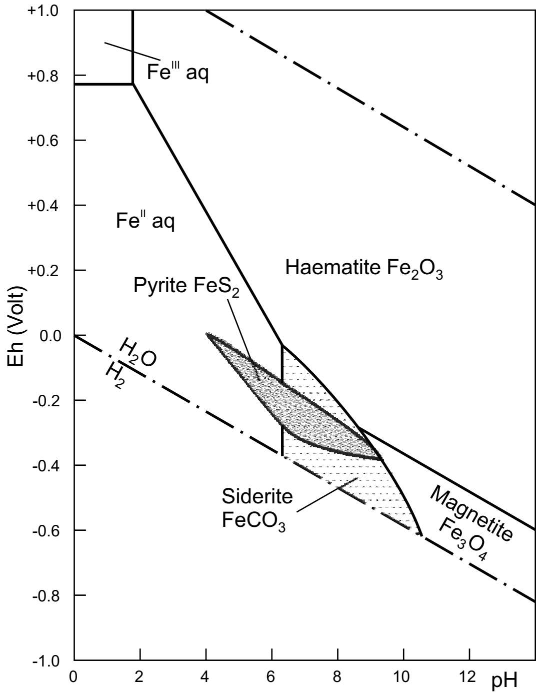

Figure 2.1 Stability fields of oxide, sulphide and carbonate iron phases in water at 25 °C, a total pressure of 1 atm and molarities of Fe, S and CO_3 at 10^{-6}, 10^{-6} and 1, respectively (modified from Garrels & Christ 1965). An increase of the activities of total carbonate or sulphur in solution would expand the fields of siderite or pyrite. The magnetite field would extend into the range of neutral pH if the activities of total carbonate or sulphur in solution were lowered. Compare this diagram with Figure 1.48.

Iron is one of the essential trace elements in supporting biological functions, and only some chemicals are toxic. A risk of fatal iron poisoning by accidental ingestion of iron tablets concerns children below the age of six years. **Essential trace elements** in humans include iron, copper, zinc, manganese, magnesium, chromium, molybdenum, tungsten, cobalt, selenium and iodine (Lindh 2005). Non-metallic elements essential to human health are calcium, chlorine, potassium, phosphorous and sodium (all with recommended daily intake in the gram range) and fluorine. Ocean water was iron-rich in the first half of the Earth's history, but became highly depleted by formation of Palaeoproterozoic banded iron ores (the "Great Oxidation Event"). In the following period, between ~1.8 Ga and 800 Ma, iron was probably abstracted from the oceans into sediments by formation of insoluble sulphides. Since complete ocean oxygenation at ~700 Ma, iron entering the oceans is oxidized to Fe^{+3} and reacts with OH^- to form insoluble oxy-hydroxides (Anbar 2008, eq. 1.18). Because of its biological functions, iron is at present a limiting nutrient in large parts of the world's oceans.

Hydrothermal solubility of iron is positively correlated with fluid salinity and temperature (Fein *et al.* 1992). Elevated chlorine content of hydrothermal solutions is usually caused by dissolution of halite or by convection of evaporated sea water (Barton & Johnson 1996). In acidic, reduced and chlorine-rich fluids, high iron content occurs in the form of $FeCl^+$ and $FeCl_2{}^0$. Rising pressure, fO_2 and pH are negative controls of solubility. Precipitation is induced by falling P or T, by mixing with water of low salinity (e.g. meteoric water), by oxygen access, or by rising pH, the latter commonly being a consequence of contact with carbonate rocks.

Iron ore deposit types

Iron ore deposits occur in a large genetic variety. Two factors of iron concentration are especially prominent – redox changes and the metal's high solubility in reduced saline fluids. The first controls the giant mass of iron in sedimentary deposits, such as Precambrian banded iron formations. Elevated salinity is a common theme in iron concentrations as diverse as iron oxide-copper-gold, skarn, hydrothermal-metasomatic siderite and high-grade haematite ore deposits. Scientific and economic significance suggests the following genetic tabulation:

- orthomagmatic iron ore deposits (intrusive and extrusive; mafic and felsic, alkaline, carbonatitic);
- contact-metasomatic and iron skarn ore deposits;
- magmatic-hydrothermal, epigenetic massive and vein deposits, including an apatite-iron oxide subclass;
- hydrothermal-metasomatic siderite stocks in carbonates (diagenetic or metamorphogenic);
- volcanogenic-exhalative and sedimentary-hydrothermal (sedex) deposits;
- residual, lateritic deposits;
- supergene infiltration "channel" ore deposits;
- terrestrial-sedimentary iron deposits (bog ore, karst iron ore, alluvial magnetite placers);
- marine-sedimentary and associated supergene-enrichment iron ore deposits (magnetite BIF, BIF-derived martite-goethite ore, ironstones, oolitic iron ore, detrital iron ore, coastal placers);
- high-grade haematite ore deposits replacing banded iron formations (pre-enrichment by diagenetic-hydrothermal processes, final supergene enrichment).

Orthomagmatic-intrusive iron ores

Orthomagmatic-intrusive iron ores include the magnetite seams of the Upper Zone of the Bushveld, South Africa (Figure 1.5). Economically most significant is the Main Magnetite Layer with an average thickness of 1.8 m and 1.6% V_2O_5, containing opencast reserves of over 1000 million tonnes (Mt) of ore. Worldwide, numerous small and middle-sized iron ore deposits are associated with gabbro and norite intrusions. Orebodies of this "gabbro type" occur as layers, streaks or veins. Elevated titanium traces in magnetite may interfere with economic use, but some mines thrive on titaniferous magnetite. Orthomagmatic iron ores of the "anorthosite type" often have a paragenesis of haematite and ilmenite, allowing more economic processing. At high ilmenite concentrations, these ores are sources of titanium and iron is the by-product.

For a long period, magnetite-apatite ores at Kiruna and Malmberget in northern Sweden were thought to be orthomagmatic segregations, either subvolcanic or intrusive. More recently, a magmatic-hydrothermal origin similar to Olympic Dam (cf. "Copper") was considered (Hitzman *et al.* 1992). Host rocks are within-plate Palaeoproterozoic felsic volcanic and intrusive rocks (Weihed & Williams 2005). Orebodies are roughly stratabound, tabular and at Kiruna, reach a thickness of 200 m and a strike length of 4 km. This orebody dips at 60° (Figure 1.8) and drilling to a depth of 1500 m confirmed downward continuity. Until 2012, production haulage will be based at the −1045 m level. The large mine voids left after ore extraction are causing significant subsidence of Kiruna town. The ores are massive or banded with apparent cross-stratification. Columnar and dendritic magnetite is suggested to indicate rapid cooling of an ore melt. Vesicular portions may indicate lava flows; and finely banded ore might have originated by ash falls and brecciated ore from pyroclastic breccias (Nyström & Henriquez 1994). Thin apophyses of the ore extend into both hanging wall and footwall rocks. This was earlier thought to prove intrusion of an ore melt. Age determinations demonstrate that ore and volcanic host rocks have the same age (Romer *et al.* 1994). The contrary opinions need not exclude each other and it seems possible that both melts and fluids existed at subvolcanic and extrusive levels. The interaction of ore melt, and later of the solidified massive ore with fluids was substantiated by Harlov *et al.* (2002). The ore paragenesis comprises magnetite, haematite, fluorapatite, actinolite, tremolite and clinopyroxene, with 55–65% Fe and 1–2% phosphorous. Reserves of the district to 800 m below the surface are estimated at 3000 Mt; annual production

> is ~30 Mt. This makes Kiruna the most important iron ore producer of Western Europe.

Orthomagmatic-extrusive iron ores

Orthomagmatic-extrusive iron ores are infrequent, but several deposits are of an impressive size. Some iron oxide melt reached the surface and solidified as lava flows, volcanic agglomerate and tuff; others filled veins and massive bodies within subvolcanic intrusions. Host rocks are felsic and intermediate volcanics that build calderas or shield volcanoes. The FeO_x liquid may result from subvolcanic mingling of mafic and felsic melt (Clark & Kontak 2004). Large deposits of this genetic group, with ore made up of magnetite, haematite, apatite and dendritic pyroxene, are exploited in Chile (El Laco: Nyström & Henriquez 1994; note, however, the objection by Sillitoe & Burrows 2003) and Mexico (Cerro de Mercado: Figure 1.9, Swanson *et al.* 1978, Lyons 1988), both containing ~1000 Mt of ore.

Skarn- and contact-metasomatic iron ore deposits

Skarn- and contact-metasomatic iron ore deposits form in the contact zone of certain gabbros, diorites, syenites and granites that intrude carbonate rocks. Scientific enquiry concerns mainly the derivation of: i) the ore elements; and ii) the fluids that transported these elements. There is no uniform answer, as both ore elements and fluids may originate in the magmatic body, or in nearby host rocks, or in wide regions around these. In the latter case, saline fluids are often prominent,causing regional sodic alteration (e.g. albite, scapolite) and thus forming a link to the IOCG-group of ore deposits.

In the Ural Mountains, economically outstanding skarn iron ore deposits formed in a collisional Late Palaeozoic setting (Herrington *et al.* 2003):

> Orebodies at Gora Magnitnaja occur in Early Carboniferous carbonates and minor volcanogenic sediments, which were intruded by Late Carboniferous porphyric granite. Orebodies are grossly stratiform within an envelope of skarn rock and calcite marble. An early anhydrous paragenesis of mineralization comprises magnetite, garnet and pyroxene, followed by magnetite, haematite, pyrite, chalcopyrite, quartz, epidote and calcite. Total ore in the deposit before mining was ~500 Mt, with an average 56% Fe, 0.8% Mn, 14.85% SiO_2, 1.82% CaO, 0.04% P and 1.94% S. Surficial ore was enriched by martitization. A comparable deposit is Sarbai in Kazakhstan, with a size of 1500 Mt, which was found in 1948 by aeromagnetics. At Sarbai, gangue minerals include Na-Cl-scapolite, clear evidence for the important role of saline fluids in skarn metallogenesis.

Magmatic-hydrothermal, epigenetic, massive and vein iron ore deposits

Magmatic-hydrothermal, epigenetic, massive and vein iron ore deposits occur near many mafic to intermediate calcalkaline plutons of recent or ancient convergent plate margins (Chile, Peru, Central Americas, Sweden and Japan). Some of Phanerozoic age seem to be transitional to iron oxide-copper-gold (IOCG) deposits *sensu stricto* (Groves *et al.* 2010). Preliminary Sm-Nd and Re-Os isotope datas suggest that iron oxide-apatite ore is sourced by the crust, whereas systems with economically predominating copper or gold display a mantle component (Skirrow *et al.* 2007):

> El Romeral in Chile is a magnetite-apatite ore deposit hosted in a Cretaceous andesite porphyry and metasediments near a diorite stock. The largest orebody has dimensions of 850 m by 250 m. The ore consists of sieve-like magnetite with inclusions of actinolite, clinozoisite, titanite, Cl-apatite, andesine, scapolite, chlorite and quartz. This gangue also fills stockwork veinlets surrounding massive ore. The ore clearly replaces hydrothermally altered rock bodies that are limited by faults. The deposit is enveloped by the halo of thermal amphibolite facies metamorphism, at 475–550 °C and 2 kbar. The iron seems to be derived from strongly leached diorite (Menard 1995). Deposits like this can be considered as contact-metasomatic formations in non-carbonate country rocks.

Hydrothermal-metasomatic massive siderite

Hydrothermal-metasomatic massive siderite orebodies are of low grade (~40% Fe) compared with BIF-derived ores (~60%). Districts of some renown include Bakal, Ural Mountains, Russia; Bilbao, Spain; Erzberg, Austria; Jerissa, Tunesia; and Ouenza, Algeria. Typical resources of major deposits comprise several hundred Mt of ore; smaller deposits and occurrences are quite frequent (e.g. the Alquife in southern Spain, Figure 1.36, Figure/Plate 1.89). The heavy-media iron carbonate concentrate can be improved by oxidation in a hot airstream and subsequent magnetic processing, the magnetic fraction attaining nearly 60% Fe:

> Epigenetic siderite occurs in marine epicontinental platform carbonate rocks of Proterozoic to Mesozoic age. The sedimentary association includes clastic sediments and evaporites, and occasionally mafic volcanics. Mineralized carbonates are not part of a specific sedimentary facies, although within single districts certain stratigraphical and lithologic levels are preferred, such as Early Cretaceous lithographic rudist limestones in Northern Africa and Spain. Orebodies are irregular stocks or stratiform lenses, often controlled by pre-existing faults. In detail, ore limits are commonly cross-cutting and cloud-like (Figure 1.78). Apart from the massive siderite ore, cross-cutting veins with siderite, quartz, barite, fluorite and sulphides of lead, zinc and copper (Ouenza, Bilbao) may be present. Contacts between siderite and unaltered carbonate are clearly metasomatic. In Jerissa, within the first several metres inside the siderite body rudists, bedding planes and stylolites are preserved. Further towards the centre of the siderite stock, all remains of the precursor features are effaced and only massive, sugar-grained monomineralic siderite rock is present. Parts of it are drusy and display coarse calcite crystals. At Erzberg (Figure 1.35), the siderite bodies are enveloped by ankerite-dolomite alteration. Footwall and hanging wall of orebodies are frequently formed by low-permeability and incompetent rocks such as shales. None of these deposits exhibit any traces of a redox-zonation (oxide-carbonate-sulphide or silicate facies), which is common in synsedimentary iron ore deposits, both horizontally and vertically. Surrounding carbonates are typically rather pure and have low geochemical iron contents. Nothing indicates that iron was pre-enriched in these rocks.

In conclusion, masses of siderite replacing carbonates are the product of epigenetic hydrothermal processes. The metasomatic replacement may have happened at any time after deposition of the carbonates, from early diagenesis to metamorphism. The giant deposits at Bakal, Russia are hosted by Mesoproterozoic limestones (~1400 Ma), whereas Pb-Pb dates of siderite concur with the Grenvillean orogeny (~1000 Ma: Kuznetsov *et al.* 2005). Possible sources of ore-forming fluids include deeply circulating seawater or evaporitic brines (Strmić Palinkaš *et al.* 2009), formation waters (Torrez-Ruiz 2006), migrating basinal or salt-solution brines (Pohl *et al.* 1986; Bouzenoune & Lecolle 1997) and metamorphic (± saline) fluids (Erzberg: Pohl & Belocky 1994; Bakal, Russia: Kholodov & Butuzova 2004). Only magmatic sources have not been invoked.

Volcanogenic-exhalative and sedimentary-hydrothermal (sedex) deposits

Volcanogenic-exhalative and sedimentary-hydrothermal (sedex) deposits are not significant producers of iron ore but some are co-producers of iron and metals such as Cu, Au, As, Tl, Pb and Zn. Pyrite bodies of the Kuroko, Cyprus and sedex type, which are exploited for the production of sulphuric acid, yield an iron oxide sponge that can be suitable blast furnace feed, provided the chemical composition is acceptable. Volcanogenic and sedex type iron ores may also occur in carbonate or oxide facies. Algoma Type iron ores are part of this group.

Residual, or lateritic iron ore deposits

Residual, or lateritic iron ore deposits, occur above ferriferous mafic or ultramafic bedrocks (mostly ophiolites). From these precursor rocks, they often inherit Cr-Ni-Co that impedes regular metallurgical processing. In addition, these ores contain up to 20% Al_2O_3, have relatively low iron grades and high moisture contents reaching 30%. All this dampens interest in such ores. If concentrations of chromium or nickel reach higher grades, mining may be profitable (Albania, Cuba, Greece, Guinea, Philippines, Western Australia). The material is currently extracted as a high-iron limonite nickel ore ("oxide nickel ore") for Chinese pig-iron blast furnaces. In oxide nickel ore, nickel is absorbed on amorphous iron-hydroxides or occurs as inclusions in goethite. The new technology of high-pressure acid-leaching (PAL) appears to alleviate the former economic disadvantage of processing these ores:

> Conakry, Guinea is a characteristic example of this group. In the deposit, ~6 m of hard ferricrete cover dunite with 10% iron. Run-of-mine ore contains 52% Fe, 12% Al_2O_3, 1.8% SiO_2, 0.25% P, 1.8% Cr, 0.15% Ni, 0.5% TiO_2 and 11% water.

Obviously, residual iron ores are rarely attractive. In contrast, supergene alteration has a prime role in upgrading low-grade protore by supergene enrichment. Of course, this process may in principle act on any genetic variety of iron ore and nearly all near-surface deposits display some enrichment (Figure 1.36). However, Proterozoic banded iron formations of the Superior Type are by far the most important precursor rock, because of their wide distribution and the giant initial mass of iron involved (Figure 1.52).

Supergene infiltration "channel" ore deposits

Around 1990, a new type of giant iron ore deposits began to be developed in the Hamersley Basin of Western Australia, although they had been recognized much earlier in about 1955 (Glasson & Rattigan 1990). Several river courses that drain the Hamersley BIF province towards the east and north are shadowed for many kilometres by table mountains. These are built of iron ore that resisted the erosion that lowered the surrounding land surface. The mountains represent the fill of Early Tertiary broad valleys ("limonite rivers") formed by precursors of recent rivers, giving rise to the term "channel iron ore deposits" (Figure 2.2). In the lower reaches of rivers draining the Hamersley Ranges, part of these ores are buried beneath alluvial valley fill.

> Several of the first mines were sited along Marillana Creek, based on resources of >3500 Mt over a length of 80 km. The ore grades 58% Fe, 0.04% P, 4.9% SiO_2, 1.3% Al_2O_3 and 10% H_2O. It consists of densely packed pisolitic concretions (not ore pebbles) of goethite and haematite. Concretions are partly concentrically banded but also massive. The matrix contains the same iron minerals, and some clay, calcite, chalcedony, and rarely limonitized plant remains. Single orebodies reach a thickness of 100 m. These ores formed by precipitation from ferriferous alluvial groundwater, either directly or by replacement of clastic particles. The source of iron was weathering of upstream outcrops of banded iron formations (Stone *et al.* 2002).

Terrestrial-sedimentary iron ore deposits

Terrestrial-sedimentary iron ore deposits were the first source of the metal for humans, but with the onset of industrialization they were quickly abandoned because the mass of mineralization is commonly very small. Inflow of acidic water produces bog ore in swamps and corresponding siderite ore in coal sequences (Kholodov & Butuzova 2004). Sluggish ferriferous drainage fills karst cavities. Alluvial placers (black sands) are ubiquitous but tiny.

Marine-sedimentary and associated supergene-enrichment iron ore deposits

Marine-sedimentary and associated supergene-enrichment iron ore deposits include BIF, ironstones, oolitic iron ore, detrital iron ore, and coastal placers. Among these, the banded iron formations of the Superior Type dwarf all other sources. However, banded iron formations with their relatively low primary iron grades (25–45 wt.% Fe) are rarely exploited. The bulk of the BIF-iron worldwide is derived from locally enriched

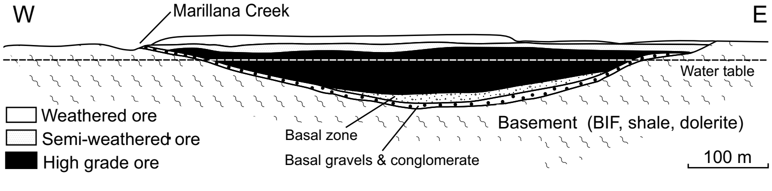

Figure 2.2 Typical cross-section of an Early Tertiary fluviatile ("channel") infiltration iron ore deposit near Marillana Creek in the Hamersley Basin, Western Australia (Stone *et al.* 2002). Note the relief inversion from former valley fill to present table mountain.

sections of banded iron formations (Chapters 1.2 "Supergene Ore Formation Systems", Chapter 1.3 Sedimentary Ore Formation Systems" and Chapter 1.4 "Diagenetic Ore Formation Systems"). These are the "BIF-hosted iron ore deposits" that range from a few million to over 3000 million tonnes at >64 wt.% Fe, although most are between 200 and 500 Mt. Common BIF varieties are described as taconite (a low-grade BIF with $\sim$30% Fe in Minnesota, which can be exploited because magnetic enrichment of magnetite and haematite is feasible), itabirite (a metamorphosed, coarse-grained banded iron formation, Figure 2.3), canga (scree ore deposits) and jaspilite (very low-grade metamorphic, fine-grained iron formation).

Important iron ore mining provinces based on Palaeoproterozoic banded iron formations occur in Australia (Hamersley), South America (Minas Gerais and Carajás in Brazil), North America (Lake Superior, Labrador Trough), Europe (Ukraine with Kryvyi Rih, or in Russian Krivoj Rog, and Kursk Magnetic Anomaly in Russia), Asia (Orissa, Goa, India) and in Africa (Liberia, Angola, Transvaal S.A.).

One of the largest iron ore provinces in the world is the Hamersley Basin in the Pilbara region of Western Australia. The basin covers a surface of $\sim$100,000 km^2 and is built from Neoarchaean to Palaeoproterozoic (2.77–2.41 Ga) sediments and volcanics of the 15-km thick Mt Bruce Supergroup. In the north, these rocks transgress older Archaean rocks discordantly, whereas in the south they are in turn overlain by younger Proterozoic sediments. The Mt Bruce Supergroup starts with basal conglomerates (partly auriferous similar to the Witwatersrand Reefs), basalt, tuff and black shale of the Fortescue Group (1), which are overlain by the Hamersley Group. The Hamersley Group (2) displays five important BIF-horizons (among them the oldest known $\sim$2.6 Ma Superior-type BIF, the Marra Mamba Formation, and the $\sim$2.5 Ma Brockman Iron Formation of Figure 1.52, Figure/Plate 1.67) and intercalated shales, dolomite, and rare bimodal volcanic rocks. The overlying greywackes and basalts of the Wyloo Group (3) are separated from (2) by an unconformity, which is marked by haematite conglomerates. The sediments attest to periods of quiet epicontinental marine conditions, whereas volcanic rocks imply tectonic extension and mantle-derived magmatism. The latter might have contributed to hydrothermal import of iron and silica into the shallow sea (Bekker *et al.* 2010, Barley *et al.* 1997, 1999). In the north, metamorphism and deformation of the rocks is restricted, whereas both increase to the south, reaching greenschist facies and vergent folds approaching the collisional Ophtalmia (Capricorn) Orogen (Rasmussen *et al.* 2005). Several granites are known in the southern part of the basin, with intrusion ages of $\sim$1700 Ma.

Exploitable iron ore resources of the Hamersley Basin are estimated at 22,000 Mt, additional marginal ores at 18,000 Mt. High-grade haematite deposits with 60–68% Fe represent only $\sim$0.1% of the total iron endowment. The bulk of the iron rests in the primary BIF with $\sim$30% Fe and 50% SiO$_2$, which cannot be profitably exploited. Profitable ore types include high-grade haematite, martite-goethite, and pisolitic channel as well as detrital scree ore. Orebodies of the first two types replace BIF *in situ* (Figure 1.52). Mass

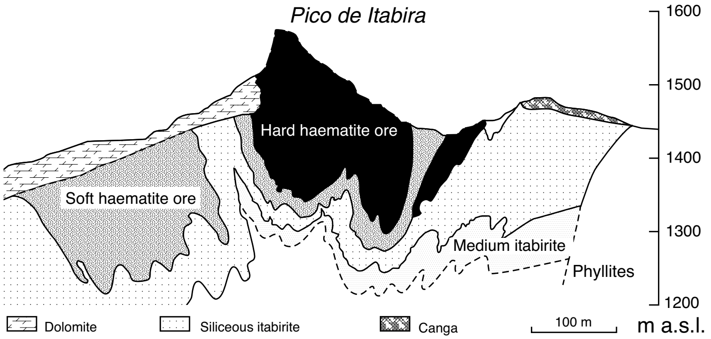

Figure 2.3 Geological profile of the Palaeoproterozoic high-grade haematite deposit of Pico de Itabira, Brazil. After Klein, C. & Ladeira, E.A. 2000, Society of Economic Geologists, Inc., *Economic Geology* Vol. 95, Figure 9, p. 419. Protore-BIF is siliceous itabirite ($\sim$40% Fe). Medium itabirite is moderately enriched to $\sim$58% Fe. Both hard ore and soft ore are high-grade with about 67% Fe. Host rocks are metamorphosed in the greenschist facies.

calculations prove that iron must have been added while silica was removed. Limits to ore are often iron-poor host rocks or faults, and orebodies mirror strike and orogenic structures of BIF packages. Orebodies may reach 70 m thickness and a length of many kilometres so that some of them contain >1000 Mt (Mt Whaleback). All enriched ore occurs near a Tertiary land surface (the "Hamersley surface"). None has been found deeper than 400 m below this level, only primary unaltered BIF.

Banded iron formations of the Hamersley Basin are metamorphosed and consist of quartz and magnetite, with some stilpnomelane (a mineral resembling biotite), carbonate and apatite. Ore derived from this paragenesis by supergene alteration only contains martite and goethite in different proportions, and a gangue of quartz, opal and kaolin. Goethite replaces former quartz bands but may be redissolved. These processes result in various ore classes (as a function of Fe and P content, texture, porosity, strength and mineralogical composition: Clout 2006) that are differentiated for economic reasons. Phosphorous is almost exclusively associated with goethite, so that high-grade haematite is nearly free of it. Goethite-bearing ores contain up to 0.12% P, which is economically problematic. Giant additional reserves of iron ore will be available if technological developments allow cost-effective removal of phosphorous. Average run-of-mine ore in the province is characterized by a mineralogical composition of 70% haematite with 23% goethite, 5% kaolin and 2% quartz, resulting in a chemical composition of 63.5% Fe, 4.3% SiO_2, 2% Al_2O_3 and 3% loss on ignition (mainly water).

High-grade haematite ore deposits associated with Superior type BIF

Generally, martite-goethite ores are thought to result essentially from supergene alteration of BIF (Lascelles 2006), whereas microplaty, porous high-grade haematite ore (Figure 1.52 and Figure 2.3) was explained by metamorphism of BIF that experienced previous supergene enrichment (Morris 1985, 1993, 2003). Recently it was recognized that deep hydrothermal magnetite, haematite and siderite bodies were later affected by supergene leaching and/or oxidation (Thorne *et al.* 2004, Dalstra & Guedes 2004, Taylor *et al.* 2001, Barley *et al.* 1999). Several stages of hydrothermal alteration are indicated, starting with $NaCl\text{-}CaCl_2$ rich brine, followed by leaching of carbonate and apatite in the supergene alteration domain. Oxygen isotopes confirm this model (Thorne *et al.* 2009). The first fluid event is clearly post-metamorphic and dated to ~2000 Ma, which was a period of continental extension (Müller *et al.* 2005). In the hydrothermal models, haematite can be formed from magnetite by hydrothermal leaching of Fe(II) and of silica, without the need of extraneous oxygen (eq. 2.1, Ohmoto 2003b).

Formation of haematite from magnetite by hydrothermal leaching of Fe(II):

$$Fe_3O_{4(Mag)} + 2H^+ \Rightarrow Fe_2O_{3(Hem)} + Fe^{2+}{}_{aq} + H_2O \tag{2.1}$$

Deposits of high-grade haematite reach 3000 Mt of nearly pure iron oxide (Carajás, Brazil) and are by far the largest metal concentrations on Earth. Note, however, that the ore genesis in the Carajás province is also not fully understood (Rosière *et al.* 2006):

The high-grade haematite orebody at Mt Tom Price, Western Australia (Figure 1.52, Figure/Plate 2.4) contained an original resource of 900 Mt at 63.9% Fe and <0.05% P. Situated in the southern greenschist-metamorphic and folded part of the Hamersley Basin, the orebody occurs as a SW-dipping sheet on the flank of an anticline. The deposit extends for 7 km and is up to 1.6 km wide, with a maximum depth of 250 m below the original topographic surface (Taylor *et al.* 2001). Extensional faults channelled basinal brines, which enriched metamorphic BIF in iron and abstracted silica.

Oolitic and detrital iron ore

Large concentrations of oolitic and detrital iron ore occur in the environs of Salzgitter in the Mesozoic foreland of the Palaeozoic Harz Mountains in Northern Germany. Several stratigraphic horizons within the marine platform sediments have been exploited. Mining was terminated in 1976 because of low ore grade and resulting higher costs compared with concentrates from overseas. Overall, ~340 Mt of ore had been produced. Remaining potential resources are estimated at 4000 Mt. The average composition of the ore was 29% Fe, 26% SiO_2, 5% CaO, 0.1% Mn and 0.4% P:

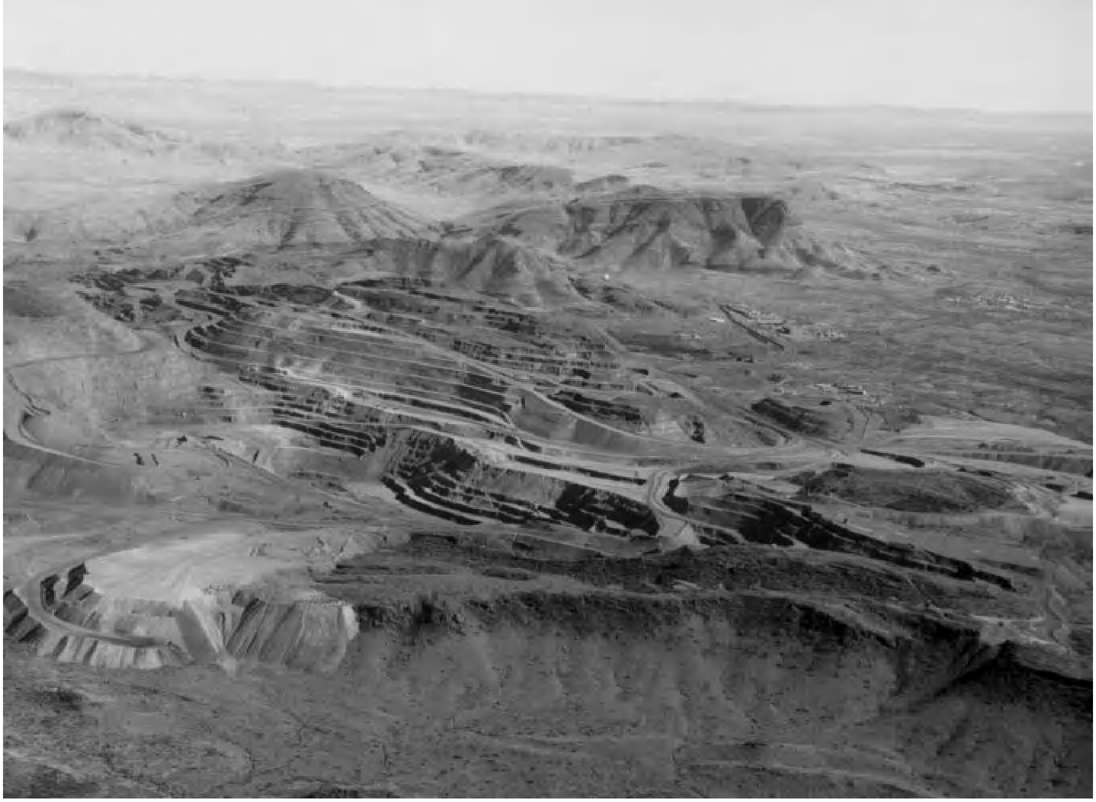

Figure 2.4 (Plate 2.4) Birds-eye view of the high-grade haematite Mt Tom Price mine in the Hamersley Basin, looking to the northwest (cf. Figure 1.52). Southwest dipping Precambrian banded iron formations build the hills that rise above the plains. Courtesy of A.E. Harding, Rio Tinto Iron Ore, Perth, Western Australia.

These iron ores were formed when a shallow epicontinental sea covered parts of Northern and Central Europe, with several large islands and wide landmasses (Figure 2.5). Throughout the Mesozoic, the distribution of land and sea changed continuously. The ore deposits of the Salzgitter district occur near the coast of a southern landmass and smaller islands that originated (and foundered again) by a complicated interaction of the rise of salt diapirs, tectonics and sea level changes. Oolitic iron ores were deposited at different sites in the Liassic, Malm, Early and Late Cretaceous. The last iron ore mine in the district (Schacht Konrad) was not closed, but given a new use as a final storage site for disposal of nuclear waste of low to medium-level activity. A few seams (in the Jurassic) extend across very large areas. Some oolite ore developed above coarse detrital ore that is restricted to the Cretaceous. Detrital iron ore accumulated in localized, very deep troughs that formed by faulting on the flanks of salt diapirs. Sources of the detrital iron ore are siderite nodules and pyritized fossils in Early and Middle Jurassic shales, which were oxidized during phases of emersion. Renewed transgression of the sea imposed a high-energy coastal environment with strong tides, breakers and currents that swept coarse iron oxide detritus into depressions. Some detrital orebodies reached a thickness of 120 m and a length of over 1 km.

Important oolitic ironstone seams were exploited in Lothringia (the limonitic "minette" of Early Dogger age), in the Prague basin (Ordovician), in Algeria (Gara Djebilet, Early Devonian) and in the Clinton District (Alabama, USA, Late Silurian, haematitic). With the exception of China, few mines now exploit oolitic ironstones. This is due to the rather low iron grade and

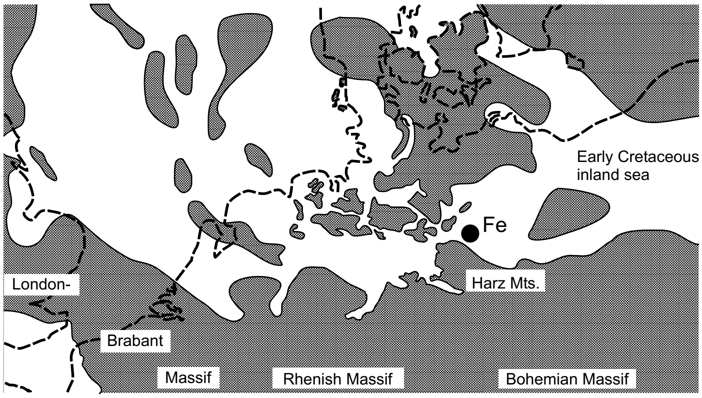

Figure 2.5 Palaeogeographic environment of oolitic and detrital iron ore deposition in the Salzgitter district in Northern Germany. Distribution of land and sea (adapted from Ziegler 1982). Reproduced with permission Shell & Elsevier © (1982). Dashed lines indicate today's coasts. Cretaceous sediments in the island belt of the inland sea include deposits of oolitic and detrital iron ore (black dot, Fe), glass sand, clay and coal.

unwanted high content of phosphorus, aluminium and SiO_2. BIF-ores are both cheaper and of higher quality.

Main producers of iron ore are China, Brazil, Australia, India and Russia. Together, the five countries delivered ~80% of the world total of 2200 Mt (2008; 2300 Mt in 2009: USGS 2010). World crude steel production in 2008 was 1360 Mt (1100 Mt in 2009, after the financial crisis). Iron ore resources are immense, exceeding 800,000 Mt. Exploration for iron ore is directed at large (>100 Mt) or very large (>1000 Mt) deposits of high grade, which are amenable to open pit mining. Geological methods such as mapping are mainly employed. Surprisingly, the usefulness of magnetic methods may be quite limited; in Western Australia, for example, ordinary BIF can be mapped, but not the economically interesting enriched orebodies (Dentith *et al.* 1994). Of course, geochemical exploration methods are hardly useful.

2.1.2 Manganese

Common Ore Minerals:

		Max. wt.% Mn	*Density (g/cm³)*
Pyrolusite	β-MnO_2	63	4.75
Braunite	$3Mn_2O_3 . MnSiO_3$	64	4.8
Hausmannite	Mn_3O_4	72	4.8
Rhodochrosite	$MnCO_3$	49	3.6
Cryptomelane	$K[(Mn^{4+},Mn^{2+})_8O_{16}]$	57	4.3
Manganite	γ-$MnO(OH)$	62	4.3

This list is far from complete, as there are more than 100 manganese-bearing minerals. Predominant are rhodochrosite and braunite. Currently exploited manganese ore is often a mixture of ore minerals, usually of various oxy-hydroxides. Therefore, in mining practice, hard ores are called psilomelane or manganomelane, soft ores are called pyrolusite, and earthy impure masses are called wad. Psilomelane, for example, is commonly a mixture of botryoidal romanèchite $BaMn^{2+}Mn_8{}^{4+}O_{16}(OH)_4$, cryptomelane and todorokite $(Mn,Ca,Mg)Mn_3O_7.H_2O$. Rhodochrosite is chemically variable and may contain Fe, Mg, Ca and Zn. According to their industrial destination, manganese ores are subdivided as metallurgical, chemical and battery grade. Metallurgical grade ore (chiefly for alloying steel and aluminium) must contain a minimum of 46% Mn. Manganiferous iron ore with 10–25% Mn is alternatively used in iron and steel production. Chemical and battery grade ores should have between 70 and 85% MnO_2. Most processors of manganese refuse concentrates with significant contents of non-ferrous metals, such as Ni, Pb, Cu, Co, As, Sb, etc., and phosphorous, earth alkalis, SiO_2 and Al_2O_3. In such cases, the value of the ore depends on possible improvement by processing.

About 90% of the world output of manganese is used in the steel industry, mainly for de-sulphurization and oxygen-control of the melt, but also for alloying. Manganese is added in the form of silico-manganese, high-carbon (HC) ferromanganese and refined ferro-manganese. Silico-manganese is the predominant manganese alloy used in the production of long steel products. Most ordinary steel contains 0.5–1.6% Mn. Special steel for rails, mining machinery and crushers has 11–15% Mn, which raises resistance to wear and fatigue failures. Some stainless steel varieties contain manganese in addition to Cr and Ni. Dry cell batteries are the second important market sector. Zinc-carbon batteries are made directly with good battery ore, whereas synthetic (electrolytic) MnO_2 is prepared for alkali and lithium batteries. Chemicals (e.g. $KMnO_4$, which is used for purification of drinking water) and ferrites (components of many electronic devices) consume only a small part of total production.

For humans and animals, manganese is one of the essential trace elements, because it supports certain biological functions (Lindh 2005). Adverse effects can arise from both deficiency and overexposure, but the latter is very rare except in occupational settings (WHO 2006).

Geochemistry

The geochemical behaviour of manganese is very similar to iron, although it is classified as a lithophile element (Goldschmidt 1958). Manganese, however, displays considerably higher mobility. Its crustal average is ~900 ppm; the Mn/Fe ratio of the crust ~0.02. Mafic magmatic rocks have the highest manganese content (ca. 0.2%), which is negatively correlated with SiO_2, again comparable to iron. Exploitable concentrations of manganese in ore require geochemical separation from iron. Geochemical possibilities of separation are indicated in the Eh/pH diagram, where stable solid Mn-phases occupy a smaller space compared to iron minerals (Figure 2.1). Precipitation of Mn-minerals requires higher oxidation potential and/or alkalinity. This is physically illustrated by the distal manganese halo of submarine hydrothermal sedex ore deposits, where iron concentrates in the proximal facies. Principally, iron and manganese may be separated in the source region, during transport, or by differential precipitation. In the sedimentary realm, redox facies zones similar to iron are less often seen in manganese-rich sediments. In some important mining districts, a carbonate-silicate-oxide succession is observed (Figure 1.69), but never massive sulphide, as with iron because Mn-sulphides are rare.

Like iron, manganese is a redox-sensitive element. Mn(II) is common in minerals of magmatic rocks such as Fe-Mg silicates and carbonates. Its ionic radius is similar to Fe(II), Mg(II) and Ca(II) favouring substitution in rock-forming minerals. In supergene alteration settings and possibly, by sedimentation in the oxic zone, minerals with Mn(IV) are formed. Pyrolusite is the dominant oxide phase at high oxidation potential (Eh) and over a range of pH. The intermediate oxidation state Mn(III) (braunite, hausmannite) originates by partial reduction or oxidation, often related to metamorphism and hydrothermal processes. The Mn(IV) ion is so small that substitution by other elements is restricted, which is one reason why manganese ores of Mn(IV) are practically free of iron. Manganese oxides have a high sorption capacity for cations, and certain trace element associations characterize specific genetic settings (Maynard 2010, Cabral *et al.* 2002, Nicholson 1992).

Manganese ore deposit types

Manganese ore deposit formation and protore concentrations are due to the high solubility of manganese in moderately reduced aqueous fluids, from seawater to hydrothermal systems. Separation of Mn and the geochemically similar and prevalent Fe is due to incidental small shifts in the pH/Eh field. Two genetic modes prevail, hydrothermal-exhalative and marine-sedimentary (Frakes & Bolton 1992, Roy 1992). In many instances, uneconomic primary carbonatic manganese formations were enriched and transformed by supergene processes to valuable oxide ore. In contrast to iron, magmatic Mn-deposits are unknown. Epigenetic hydrothermal manganese ore veins and replacement orebodies are of minor economic significance. Two exotic karst infiltration deposits have recently been described (Li *et al.* 2007, Gutzmer *et al.* 2006).

- geologically young marine-sedimentary manganese deposits (Groote Eylandt, Australia);

- enriched sections of marine-sedimentary Palaeoproterozoic manganese (± iron) formations (MnF), e.g. in the Kalahari Field, South Africa;
- sedimentary-exhalative manganese deposits (Jurassic Molango, Mexico);
- volcanogenic hydrothermal-exhalative manganese deposits similar to Algoma type iron ore (e.g. Nsuta primary ore);
- supergene manganese oxide ore deposits derived from protore (e.g. Nsuta supergene ore).

Hydrothermal vein and replacement origin

An example of hydrothermal vein and replacement origin is Umm Bogma on the Sinai Peninsula, where stratabound orebodies replace Carboniferous dolomite, probably in genetic relation to Tertiary rifting of the Gulf of Suez (note, however, that marine-sedimentary formation was also proposed: Elagami *et al.* 2000). Numerous small epigenetic manganese mineralizations are known along the faulted margins of the Red Sea. Submarine exhalation from hydrothermal systems at rift faults may result in considerable concentrations of manganese (Polgari *et al.* 1991). Ore from hydrothermal deposits can be burdened with undesirable base metal contents.

Hydrothermal-exhalative manganese deposits

Submarine hydrothermal-exhalative manganese deposits are quite common (Polgari *et al.* 1991). Some occur in close proximity to volcanic centres (volcanogenic), others distal to volcanism and within a sedimentary environment (sedex). The first include the manganese-rich metalliferous muds of the Red Sea, the manganese earths (umber) and Mn-cherts of many ophiolites (e.g. Cyprus, Franciscan, California) and manganese beds near submarine volcanoes (Iberian Pyrite Belt). The second group is represented by the giant Molango District in Mexico, by carbonatic manganese ore in black shale basins and Mn-rich metamorphic rocks such as the Proterozoic "gondites" in India, that are an important protore for supergene deposits:

Mineralization in the Molango District occurs as primary to early diagenetic manganese carbonate (rhodochrosite, kutnahorite and Mn-calcite) and supergene battery-grade Mn-oxide (pyrolusite, ramsdellite MnO_2 and manganese oxy-hydroxide). The Late Jurassic Mn-carbonate ore member extends over an area of 50 by 25 km and contains ~1500 Mt manganese. At this time, a complex pattern of marine basins and ridges originated by rifting and deepening of the Gulf of Mexico Basin. This was part of the break-up and distension of Pangaea. The ore bed is underlain by a black, finely laminated, pyritiferous and calcareous shale, which may imply a restricted basin (euxinic) model of formation. The immediate footwall of the ore bed with abundant wood fragments and oyster beds indicates precipitation in shallow oxidizing water. Its hanging wall is formed by alternating limestone and shale. No traces of syngenetic volcanism are known. Exploitable stratiform ore at the Tetzintla mine displayed a thickness of 10 m and up to 30% of manganese in rhodochrosite (Okita 1992). Subeconomic lower grade Mn-carbonates continue upwards in the section for tens of metres. The finely laminated ore consists of rhodochrosite, silty shale and iron oxides (magnetite, maghemite) and is strikingly deficient in sulphur. Mn-carbonate probably formed during diagenesis by Mn oxy-hydroxide reduction coupled with organic matter oxidation. Possible sources for this giant metal accumulation include: 1) seawater, 2) hydrothermal activity and 3) alluvial import from land in the west, with 2 and 3 both equally possible. Overall at present, a sedex origin in combination with submarine rifting is assumed (Okita 1992).

Marine-sedimentary manganese deposits

Marine-sedimentary manganese deposits (Frakes & Bolton 1992) were introduced in Chapter 1.3 "Autochthonous Iron and Manganese Deposits". They occur as oolitic or massive seams in sediments of epicontinental seas. Host sediments comprise mainly clay, marl and sand (rarely carbonates). Similar to ironstones and oolitic iron ores, the metal source for oolitic manganese deposits is usually supposed to be continental weathering and alluvial transport into the sea, but a higher activity of suboceanic hydrothermal sources is also considered. The first hypothesis fits very well with the observation that the interaction of anoxic deep water with manganese dissolved by anaerobic methane oxidation (Beal *et al.* 2009) and oxygen-rich seawater of marginal zones causes manganese oxide precipitation (Roy 1992). However, formation according to the oxygen minimum zone model is equally possible (Maynard 2010). Similar to iron, sedimentary manganese strata reflect climate and redox cycles, affecting oceans worldwide or at local scales:

> The largest metallogenic provinces of this deposit type include the Oligocene Black Sea province (Nikopol, Ukraine: Figure 1.69; Chiatura, Georgia) and the Cretaceous province in Northern Australia, with Groote Eylandt as an important district (Figure 2.6). In the Ukraine, formerly rich oxide ores are depleted and remaining resources are carbonatic with high phosphorous contents. Run-of-mine ore at Groote Eylandt is high-grade with 51% Mn, 3.1% Fe, 3.9% SiO_2, 4% Al_2O_3, 1.9% BaO and 0.16% P_2O_5. Resources are ~160 Mt (USGS 2009).

Precambrian manganese (± iron) formations (MnF)

Similar to BIF, Precambrian manganese (± iron) formations (MnF) are of high economic importance, although comparable to iron, only enriched parts are exploitable. The large Palaeoproterozoic deposits in the Transvaal Sequence of western Griqualand, South Africa are exploited in a number of mines. The sequence comprises sediments and volcanic rocks of a post-Archaean platform basin that experienced very mild later folding and metamorphism. The Transvaal Sequence is remarkably mineralized, with manganese and Superior Type banded iron formations, fluorspar, Pb/Zn, asbestos, andalusite, and dolomite. In the Kalahari Field, manganiferous material >20% Mn amounts to ~13,000 Mt and of this, resources of ~4000 Mt are considered to be economic (constituting 77% of total identified terrestrial Mn-resources). The Mn-rich rocks are believed to have been formed as distal, volcanogenic, hydrothermal-exhalative deposits on the seafloor (Cornell & Schütte 1995). Trace element characteristics are similar to Superior Type BIF, so that a purely sedimentary origin is also feasible, possibly with a very small hydrothermal component (Tsikos & Moore 1997). The concentration of Mn relative to Fe is believed to have been amplified by earlier deposition of thick iron formations, possibly in a restricted sea. A small area (ca. 3%) in the northwestern part of the Kalahari Field displays high-grade ore adjacent to faults. This area contains 20% of high-grade manganese reserves of the world. Agents of enrichment were hydrothermal solutions that leached SiO_2 and $CaCO_3$ from protore and transferred some of the Mn. Opinions differ as to whether this process took place during a synsedimentary hydrothermal phase (Cornell & Schütte 1995, Tsikos *et al.* 2003), or during later deformation and metamorphism (Gutzmer & Beukes 1995).

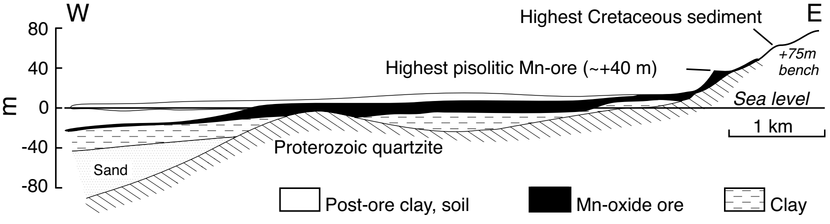

Figure 2.6 Cross-section of the marine-sedimentary manganese deposit at Groote Eylandt, Northern Australia (Bolton *et al.* 1990).The manganese horizon is part of an Early Cretaceous transgressive series. Enrichment by supergene alteration upgraded protore to exploitable grades which occur across an area of >150 km^2.

> The largest mine in the high-grade zone is Mawatwan. Manganese seams occur within an iron formation that overlies basalts. Mining is based on the main manganese seam with an average thickness of 15 m. Far from faults, the seam displays a fine-grained, laminated paragenesis of braunite, kutnahorite Ca(Mn,Mg,Fe)$(CO_3)_2$ and hausmannite, with minor haematite and calcite (Mawatwan type ore). Enriched ore near faults contains 38–50% Mn, is coarsely crystalline, drusy, free of carbonate, and consists of hausmannite and braunite (Wessels type ore). Lenses of coarse sparry Mn-calcite and dolomite are often observed. This deposit is practically free of Mn(IV) minerals.

Supergene manganese ore deposits

Supergene manganese ore deposits are derived from rocks with high but unexploitable manganese concentrations of more than 30%. Above this protore, the laterite blanket often includes hard Mn crusts and earthy Mn ore. In contrast to iron that tends to concentrate in the upper soil horizons (as ferricrete), the more mobile manganese is typically enriched in lower parts of the weathering profile. Although smaller than sedimentary manganese deposits, supergene lateritic Mn ores are often high-grade and, because of effective leaching, of superior quality. Important mining districts exist in Gondwanan continents (South Africa, Minas Gerais, Brazil, Orissa, India, Moanda, Gabon, Nsuta, Ghana) and in China. Source rocks (protore) include spessartine quartzites (Roy 1992: gondite or coticule rock, the second meaning "wetstone"), manganese phyllites, manganese carbonates or any volcano-sedimentary rocks that contain pre-enriched horizons of exhalative or sedimentary origin. Weathering removes or depletes carbonate and SiO_2, enriching manganese oxides and hydroxides. Carbonates and sulphides in protore promote weathering and ore formation, whereas purely silicate-based rocks form thin ore blankets. $^{40}Ar/^{39}Ar$-dating of cryptomelane revealed that the formation of residual Mn-deposits is an extremely slow and long-lasting process (Li *et al.* 2007):

> Oxide ore at Nsuta in Ghana developed from Palaeoproterozoic volcano-sedimentary rocks that were folded and metamorphosed at ~2100 Ma. For a long time, the deposit was a major source of high-grade supergene ores (the total production since 1917 amounts to ~13 Mt). Today, lower grade unweathered primary rhodochrosite ore is exploited from a horizon with a thickness of ~50 m. Resources are estimated at >50 Mt. The ore horizon is banded and is hosted by fine-grained marine metasediments. Its origin is probably similar to Algoma type iron ore ("carbonatic manganese formation": Mücke *et al.* 1999). A new, significant resource of high-grade manganese was found in extensive supergene deposits on the plateaus around Moanda in Gabon.

The leading manganese-producing countries in 2008 were South Africa, Australia, China, Gabon and Brazil. World mine production in 2008 was 13.2 Mt ore, dropping to 9.6 Mt in 2009 (USGS 2010). Manganese production and consumption closely follow the trade cycles of world steel production. Manganese resources are very large, sufficient for hundreds of years. Eighty percent of identified resources occur in South Africa (Kalahari) and 10% in the Black Sea region (USGS 2010). Into the far future, giant potential resources of manganese and other metals exist on the seafloor, in the form of manganese nodules and crusts (cf. Chapter 1.3 "Autochthonous Iron and Manganese Deposits"). At present, economic exploitation of subsea manganese appears hardly conceivable, because land-based reserves are abundant. Geological methods are mainly employed in exploration, eventually assisted by gravity surveys, which rely on the density contrast between ore and host rocks.

2.1.3 Chromium

Ore Mineral:		
Chromite	$(Fe,Mg)O(Cr,Al,Fe)_2O_3$	Density 4.3–4.6 (g/cm^3) Typically 45 to 55, maximal 68% Cr_2O_3

By definition, the mineral chromite contains >25% Cr_2O_3; at lower contents chromiferous spinel is the correct designation. Chromite composition varies within 6–18% FeO, 0–22% MgO, 0–62% Al_2O_3 and 0–30% Fe_2O_3. Some chromites display minor contents of Mn, Ti, V or Zn. The chemistry of chromite is closely controlled by the genetic setting (Pagé & Barnes 2009, Irvine 1965, 1967). In some cases, traces of nickel, copper and platinum metals in chromite ore can be recovered (e.g. from the UG2 chromite seam in the Bushveld; cf. Section 2.3.3 "Platinum and Platinum Group Metals").

Chromium ore may be exploitable at minimum contents of ~20% chromite, provided that a concentrate >44% Cr_2O_3 can be produced at reasonable cost by methods such as gravity separation, magnetic separation and flotation. Very often, however, massive chromitite is exploited. Gangue minerals are typically olivine or serpentine. Producers strive not to market concentrate but the intermediate industrial product ferrochromium.

About 70% of chromium is used for manufacturing stainless steel (Cr 13–25%, 1–10% Ni, 0–5% Mn, 0–5% Mo and 0–1.5% Cu), and of steel alloys with exceptional hardness, durability and tempering properties, for example for aerospace components. Suitable ore for this metallurgical market segment has a high chromium content (>46%) allowing fabrication of high-quality ferrochromium. Zimbabwe, Kazakhstan, Albania, South Africa and Turkey provide metallurgical concentrates. Chromite of intermediate Cr-contents is used in the chemical industry (chemical grade), but also for metallurgical applications. Examples of chemical products include chrome-plated metal and plastics commodities, pigments, salts for wood preservation and tannery, and pure chromium metal ($D = 7.19\,g/cm^3$, melting point 1907 °C), which is a component of special alloys in spacecraft and aircraft. Low-Cr ore with >20% Al_2O_3 and >60% $Al_2O_3 + Cr_2O_3$ (refractory ore) is increasingly sought. It is processed into refractory basic chromite-magnesite (actually periclase = MgO) bricks and mortars, which are used as an internal lining in blast furnaces. Refractory chromite is mainly provided by certain ophiolite-hosted deposits (e.g. Philippines). Chromite of suitable size and durability is also used as a replacement of the more expensive zircon foundry sand.

Both for humans and for animals, chromium is an essential trace element (Lindh 2005). In higher concentrations, however, it is toxic and carcinogenic, especially in the hexavalent ionic state. Because chromic acid and its salts were widely used by small industry such as galvanization and tannery, chromium is a common groundwater pollutant. Another frequent source of pollution is chrome-plated waste in refuse dumps. Cr^{+6} polluted waters can be cleaned by passage through reducing, permeable barriers that are installed in the aquifer. Isotope analysis assists efficiency controls, because light Cr-isotopes are preferentially reduced (Blowes 2002, Ellis *et al.* 2002). Reduction leads to precipitation of insoluble Cr(III) hydroxide $Cr(OH)_3$. It is an environmental curiosity that due to neoformation of carbonates in tailings, mines that process ultramafic-hosted chromium ore sequester enough carbon dioxide from the atmosphere to more than offset greenhouse gas emissions from operations (Wilson *et al.* 2009).

Geochemistry

The geochemical behaviour of chromium is lithophile in Goldschmidt's (1958) classification, because it is most often associated with (mafic) silicates. Nevertheless, the element is enriched to ~0.9 wt.% in the Earth's core, 0.3% in the mantle, and strongly depleted in the crust (~100 ppm). Primary ore deposits are exclusively formed by mantle-derived mafic and ultramafic magmas. The distribution coefficient of chromium between residual mantle and ultramafic melt is near unity. Both reservoirs display equal chromium concentrations (2000–4000 ppm). Peridotite and komatiite contain an average of 2700 ppm Cr, boninite 1000–1500 ppm, gabbro and basalt 200–500 ppm, and granite only 20 ppm.

Chromium traces in rock and soil occur commonly as Cr(III) with an ionic radius of 0.64 Å. Weathering of chromiferous rocks results in oxidation to Cr(VI), which occurs in surface and groundwater as the highly mobile chromate anion $(CrO_4)^{2-}$. Organic matter and other reductants, but also certain microbes, immobilize hexavalent chromium (Nriagou & Nieboer 1988, Richards & Bourg 1991). Cr^{3+} is geochemically similar to Fe^{3+} and Al^{3+}, and therefore Cr is preferentially enriched in organic, ferriferous and aluminous soil, typically in the B-horizon. Black shales and phosphorites concentrate chromium dissolved in seawater by reduction and adsorption. Petroleum inherits chromium from its source rocks. Chromite resists surficial alteration better than most silicates so that eluvial and residual placer deposits are common. Proximal alluvial deposits are also developed, but coastal placers are extremely rare. Although chromite is known in sedimentology as a very resistant heavy mineral tracer, river transport reduces it quickly to very small grain sizes.

Fluids associated with serpentinization and metamorphism provoke mobilization of Cr from disseminated chromite. This is easily recognized in polished sections under the microscope by lighter, iron-rich rims of chromite grains, while cores retain the magmatic composition (Prichard *et al.* 2008). Extreme depletion results in chromiferous iron ore, or relic magnetite in serpentinite. The dissolved chromium is eventually immobilized in newly formed minerals such as chromian chlorite, kämmererite (a chromium clinochlore), fuchsite (a chromium-rich muscovite), uwarovite, emerald and ruby. However, metamorphic-hydrothermal processes only dissipate and never concentrate chromium.

Chromium ore deposit types

Ultramafic and mafic magmas can be oversaturated in respect of chromite by several petrogenetic processes such as: i) magma mixing; ii) assimilation of country rocks; and iii) pressure decrease. Exsolved solid chromite or chromite melt is concentrated by orthomagmatic segregation processes, which reach from quiet gravitational settling to dynamic flow channels. Ore deposits occur either in layered mafic intrusions where tabular seams prevail (stratiform chromite or Bushveld Type), or in the mantle section of ophiolites (podiform chromite or Alpine Type). Chromites of these two main metallogenic settings display a different composition and chemical evolution controlled by the pseudo-stratigraphic position (Figure 2.7). Trace elements provide illuminating constraints on chromite petrogenesis (Pagé & Barnes 2009). A third setting of chromite deposits are concentrically zoned ultramafic ring intrusions of the Ural-Alaska Type (Augé *et al.* 2005). In the Ural Mountains, these intrusions were the source of historically very significant placers of chromite and platinum (cf. "Platinum"). Some Archaean komatiitic intrusions host minor chromite deposits (Rollinson 1997, Prendergast 2008). Note that all chromite is orthomagmatic. Significant genetic settings of chromite deposits include:

- stratiform chromite in layered mafic intrusions (e.g. Bushveld);
- podiform chromite within dunite pods of the mantle section of ophiolites;
- stratiform chromite in ultramafic cumulates of igneous intrusions in ophiolites (e.g. Philippines);
- stratiform chromite in Ural-Alaska Type ring intrusions.

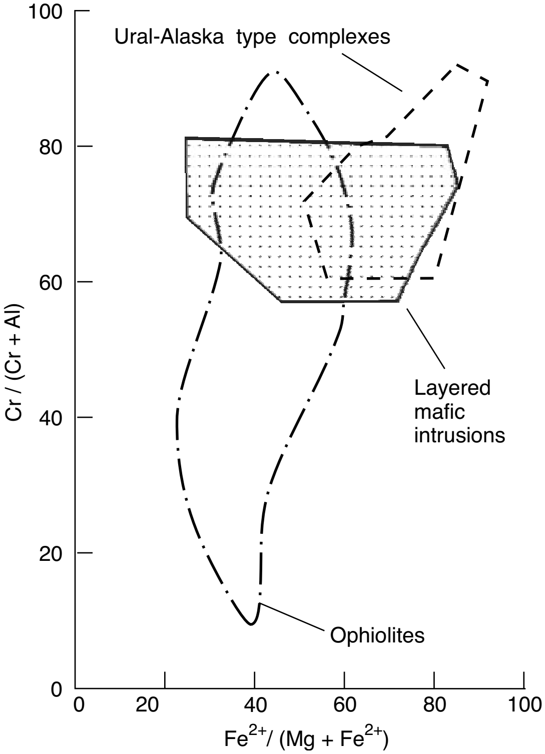

Figure 2.7 Variation of chromium, magnesium, iron and aluminium in chromites of layered mafic intrusions, Ural-Alaska type ultramafic complexes and ophiolites (adapted from Irvine 1967). Reproduced with permission © 2008 NRC Canada or its licensors. Chromium number (Cr #) and magnesium number (Mg #) are the equivalent of the scale shown divided by one hundred.

Stratiform chromite

Stratiform chromite occurs in seams within ultramafic/mafic cumulates of mafic intrusions. In the Bushveld, chromite is concentrated in the Critical Zone (Figure 1.5 and Figure 1.6). Twenty-nine chromite layers in three groups (LG, MG and UG) are distinguished, with a thickness between a few centimetres to 2 m. The seams display a number of "sedimentary" features, including gradual transition to host rocks, lenticular and wedge shapes, synsedimentary folds, erosion channels, splits along strike and eventual convergence. Chromitites consist of fine-grained, rounded and idiomorphic chromite crystals that indicate formation as a solid cumulate phase. Disseminated chromite is found in the matrix between cumulus olivine and pyroxene. Later compaction and sintering may, however, destroy early crystal settling textures, for example, as poikilitic grains overgrow cumulus silicates. These observations confirm the hypothesis that stratiform chromitites are the product of fractional crystallization and gravitational segregation. Chromites at lower levels in the intrusion have elevated Mg and Cr, whereas Fe, Ti and V increase upwards. Two main hypotheses have been proposed to explain the cyclic repetition of chromite formation in the Bushveld: The first invokes mixing of resident and fresh magma injected into the chamber (Naldrett *et al.* 2009), or its assimilation of siliceous roof rocks (Kinnaird *et al.* 2002). The hybrid melt is oversaturated in respect to chromite, leading to extensive chromite (and PGE) crystallization (Spandler *et al.* 2005). The second hypothesis relies on physical, not chemical principles. Pressure changes by injection of new melt batches also induce precipitation of chromite. This explanation better accounts for the giant area covered by the seams, simply because pressure must change instantly everywhere in the melt chamber (Cawthorn 2005b).

> The Bushveld contains giant exploitable resources of ~2300 Mt of mainly metallurgical chromite at >50% Cr_2O_3 (Vermaak 1986). Genetically similar but much smaller deposits occur in the Great Dyke, Zimbabwe and the Stillwater Complex, Montana. In the Great Dyke, massive chromitite dykes (offsets) extend ~100 m downwards into footwall sandstone and conglomerate.

Podiform chromite deposits

Podiform chromite deposits (so-called because they are pouch-shaped like the shell of a fruit) occur in dunite bodies of the mantle section of ophiolites and more rarely, in dunitic and pyroxenitic cumulates of the ophiolitic magma chamber. Orebodies are irregularly dispersed and relatively small (mostly between 0.1 and 1 Mt). Shape, structure and texture depend on the precise origin. Dunites with chromitite occur in tectonized mantle harzburgite, displaying ductile deformation and alignment along flow structures (orebody 4 in Figure 2.8). Both dunite and associated chromite are explained as refractory phases of mantle melts rising beneath mid-oceanic rifts (Thayer 1969). Chromite saturation and formation may be induced by metasomatic reaction of upflowing melt with surrounding harzburgite; assimilation

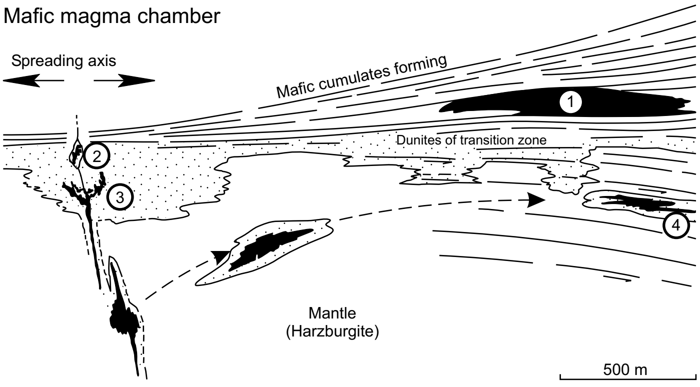

Figure 2.8 Structural locations of podiform chromitite orebodies in ophiolites, deduced from observations at Maqsad, Oman (modified from Ceuleneer & Nicolas 1985). With kind permission from Springer Science+Business Media. (1) Stratiform chromitite in cumulates; (2) Discordant nodule and leopard ore; (3) Disseminated discordant ore segregated from upwelling mantle magma; (4) Concordant orebody in tectonized harzburgite.

of pyroxenes and pressure decrease drive basaltic and boninitic liquids into the field of chromite (± olivine) precipitation (Pagé & Barnes 2009, Zhou & Robinson 1997, Arai & Yurimoto 1994). Chromite and dunite bodies are products of liquid unmixing (or fractional crystallization) and gravitational segregation. In the feeder zone of the mid-oceanic magmatic chamber (Figure 2.8), discordant disseminated (3) and massive ore (2) is formed. Ultramafic cumulates contain concordant lenses and seams of chromitite (1). Podiform chromite ore can be associated with cross-cutting dykes of chromitite that represent oxide melt injected into host rocks. Structural types of podiform chromite ore include the following:

- massive crystalline chromitite, typical for large orebodies; clearly different are:
  - chromitite with foam structures (Stanton 1972) due to crystallization from an oxide melt;
  - chromite cumulate composed of individual idiomorphic crystals, and
  - chromitite displaying ductile deformation features, for example boudinage;
- discontinuous layers of disseminated chromite crystals (cumulate) or flattened aggregates (tectonized) in light-green iron-depleted dunite or serpentinite; some cumulate chromite occurs in net-like structures;
- spotted chromite ore and orbicular (or leopard) chromite ore, elongated in one direction, and typically found in tabular flow structures;
- nodular chromite ore that consists of ovoids sized between beans and plums, also with a constant orientation of the long axis;
- anti-nodular ore with light dunite nodules dispersed in chromitite;
- breccia chromitite ore.

The frequency of rounded structures in podiform chromite (Figure 2.9) is a striking difference

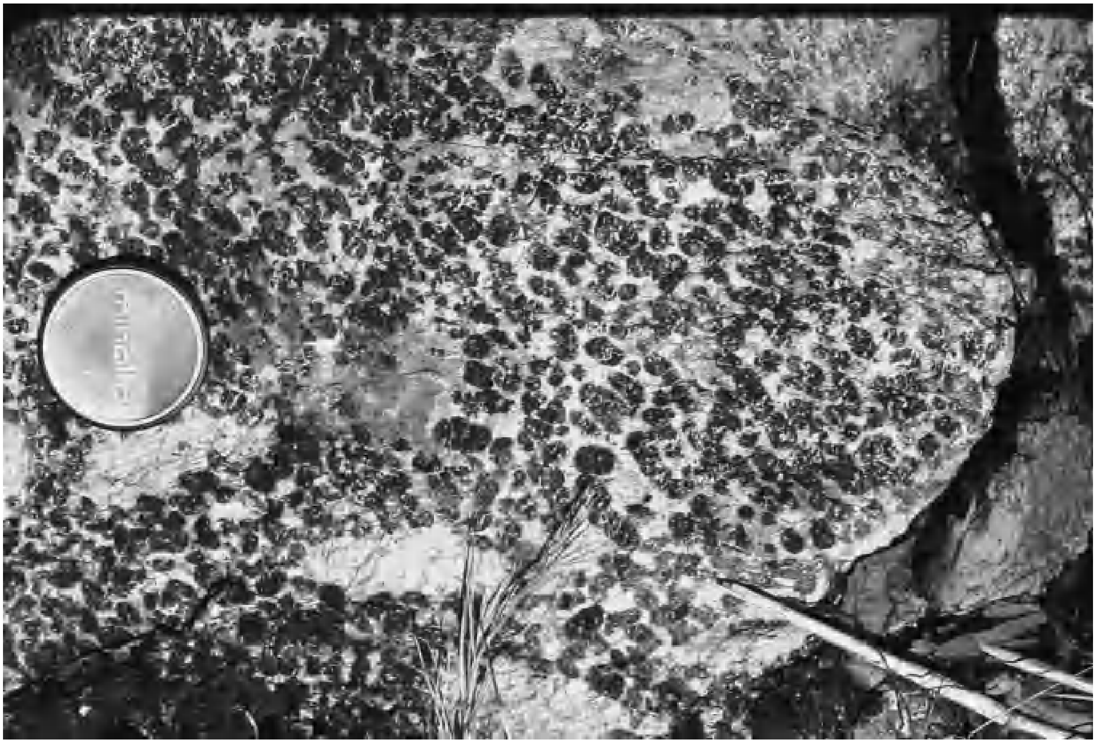

Figure 2.9 (Plate 2.9) Dunite with nodular chromite in the Ingessana Hills, southern Sudan. The hills expose a large Neoproterozoic ophiolite and host several former chromite mines.

to stratiform chromitite, which never displays such features. The cause is probably liquid unmixing of olivine and chromite melt in the former, assisted by aqueous fluids (Matveev & Ballhaus 1998, 2002). The directional structures of chromite ores may be due to viscous liquid flow, or to high-temperature ductile deformation in the mantle. Detailed structural investigations provide fascinating insight into mantle dynamics below oceanic spreading centres (Ceuleneer & Niccolas 1985, Ceuleneer *et al.* 1996). However, the preferred geodynamic setting of podiform chromite ore deposits may be rather suprasubduction fore-arc and back-arc rifts and primitive island arcs than mid-oceanic spreading zones (Zhou & Robinson 1997).

Podiform chromite is chemically different from stratiform ore, with higher Mg/Fe and Cr/Fe ratios, and Al_2O_3 contents up to 62%. Alumina and iron concentrations increase with higher position in the ophiolite stratigraphy (Figure 2.7). This favours formation of refractive ore (e.g. Philippines, Cuba and New Caledonia). The composition of chromites is also linked to the degree of partial melting of the mantle source. High Cr # chromite is believed to originate from higher degrees, whereas low Cr # ore may stem from low degrees of mantle melting (Stowe 1994). Highest chromium and magnesium contents are observed in lowest sections of ophiolites. Compared with stratiform and disseminated ore, podiform chromite orebodies in the mantle section tend to display higher Cr_2O_3 and lower Al_2O_3.

Palaeozoic ophiolites of the southern and middle Ural Mountains display a number of remarkably large chromite and platinum deposits. The largest orebody, Moledeshnoje, occurs in the Kempirsai ophiolite (Kazakhstan). It is 1.4 km long and 140 m thick, and contains ~90 Mt of chromite ore (Melcher *et al.* 1999) with extractable contents of iridium, ruthenium and osmium (Distler *et al.* 2008).

Stowe (1994) pointed out that chromite deposits vary through geological time. Chromite deposits with features similar to the podiform type occur in Palaeo- to Mesoarchaean (3.5–2.9 Ga) greenstone belts. Giant stratiform deposits appear as soon as large cratons were consolidated (2.9–2.0 Ga). Podiform deposits *sensu stricto* emerge with the first modern ophiolites, at ~800 Ma.

In 2008, world production of chromite was ~23.8 Mt, declining to 23 Mt in 2009. Main producers are South Africa (44%), Kazakhstan (17%) and India (15%). Chromite resources are very large and sufficient for centuries of consumption. However, only two countries control 90% of the resources (South Africa and Kazakhstan), implying a certain geopolitical risk.

Exploration for podiform chromite is challenging. Outcropping ore has been found and exploited long ago. Deep orebodies are sought by a combination of detailed geological mapping, structural geology and geophysical methods for locating high-density or magnetic material at depth (gravimetric and magnetic methods). Seismic methods may help to locate massive ore. Stratiform chromite seams are found by geological and petrological investigations. Note that it is always advisable to examine any chromitite for possible by-product platinum element contents.

2.1.4 Nickel

Common Ore Minerals:

		Max. wt.% Ni	*Density (g/cm³)*
Pentlandite	$(Ni, Fe)_9S_8$	35	4.6–5
Nickeline	NiAs	44	7.8
Garnierite	$(Ni, Mg)_6(OH)_8Si_4O_{10}$	30	2.2–2.8

Pentlandite is a component of pyrrhotite formed from mafic and ultramafic melt. Usually, its paragenesis includes minor chalcopyrite and cobalt sulphide, and traces of platinum and gold. Nickeline is a characteristic ore mineral of hydrothermal deposits, and may contain Sb, Co, Fe and S. Garnierite is not a defined mineral, but describes lateritic nickel ore that consists of amorphous to partly crystalline substances similar to talc and serpentine. Other minerals of nickel laterites include Ni-chlorite, Ni-talc, Ni-sepiolite, Ni-montmorillonite and nickeliferous goethite (Gleeson *et al.* 2003).

Economic grades of nickel-only ores are at least 2–3% Ni. Kabanga in Western Tanzania, for example, contains an indicated plus inferred resource of 50 Mt grading 2.7% Ni in sulphide, which makes it one of the most attractive undeveloped deposits in the world. By-production of other metals (e.g. copper, cobalt, gold, platinum) allows extraction of lower-grade ore. Critical controls are properties of the ore related to processing and metallurgy, including separability of deleterious elements (Pb, Zn, Bi, As). High sulphur-content of sulphide ore is favourable because it allows using the energy-saving "flash smelting" process. Lateritic nickel is extracted either by heap-leaching (suitable for ore with little goethite) or by high-pressure acid-leaching (HPAL) at >4 MPa and T >250 °C. Most lateritic nickel ores yield the by-product cobalt. Only recently, nickeliferous limonite ore (that is lateritic iron ore with <1% nickel) has gained the acceptance of international markets.

Use of nickel is favoured by the "seven virtues" of the metal. At 1455 °C, its melting point is high, it is suitable for galvanization and alloying with many other metals, it is ductile, at room temperature ferromagnetic, it forms a stable oxide film in contact with air, is not corroded by alkalis and is a good catalyst. Nickel is one of the heavy metals ($8.9\,g/cm^3$), but neither nickel metal nor its chemical compounds are toxic (the latter with a few exceptions). However, permanent contact with the metal may induce dermatitis and chronic inhalation of nickel sulphide can be cancerogenic. This is contrasted by the metal's role as an essential trace element for humans, animals and plants (Lindh 2005). Nickel's properties allow numerous applications, although >65% of nickel (± Cr, Mn) is used in ductile stainless steel manufacturing. Other major applications are Ni-Cd batteries (in spite of cadmium's toxicity, far from abandoned), the non-toxic rechargeable Ni-hydride (NiMH) batteries, super alloys (e.g. Ni_3AlTi) and catalysts. Ni-based super alloys are heat-resistant and high-strength materials that find applications in aircraft engines, industrial gas turbines, reactors and the chemical industry.

Geochemistry

The siderophile geochemical behaviour of nickel is illuminated by its average contents in magmatic rocks; ultramafics 0.1–0.6%, basalt 0.016%, granite 0.006%. The crustal average of nickel is 99 ppm (Clarke value, Smith & Huyck 1999). Nickel is retained in the mantle when basaltic melts are extracted. One cause of this behaviour is that Mg^{2+} and Ni^{2+} have the same charge and a similar ionic radius, favouring incorporation of the metal in olivine. The fundamental process in the genesis of magmatic sulphide deposits is the extraction of chalcophile metals (e.g. Ni, Cu, Co, and the PGE) from silicate magma into a co-existing Fe-sulphide liquid. As shown in eq. 2.2, the efficiency of the process is a function of the Nernst partition coefficient (D) of a metal between silicate melt (sil) and a sulphide melt (sulph).

Distribution of a metal between co-existing sulphide melt and silicate magma:

$$\mathrm{Sulph_{me}} = \mathrm{D} \cdot \mathrm{Sil_{me}} \qquad (2.2)$$

Extraction efficiency depends on intrinsic (D) as well as kinetic factors (e.g. the R-factor, cf. Chapter 1.1 "Orthomagmatic Ore Formation"). Typical D-values are 40–200 for Co, 100 to >5000 for Ni, 250–2000 for Cu, 1000–100,000 for Pt, ~1500 for Pd and 480–19,000 for gold (Peach *et al.* 1990). Clearly, this will lead to a high concentration of nickel in sulphide melt that interacts with silicate melt. Formation of a sulphide melt depends on sulphur saturation of the magma, which may be caused by:

- assimilation of sedimentary sulphides or evaporitic country rocks, as at Noril'sk ($\delta^{34}S = +10$ to $+12‰$, Li *et al.* 2009);
- derivation of sulphur from undepleted mantle (Sudbury: $\delta^{34}S = +1.7‰$: Naldrett 1999); and
- assimilation of felsic rocks reducing sulphur solubility.

The base metals lead and zinc exhibit partition coefficients near one; sulphide liquid is not enriched.

Polymetallic shales are an interesting low-grade high-tonnage resource of nickel. Examples include the Mo-Ni ore shales of South China (cf. "Molybdenum") and amphibolite-facies Ni-Cu-Co-Zn black schists in Finland. The latter contain ~8% graphite, 9% S, 0.23% Ni, 0.13% Cu, 0.02% Co and 0.5% Zn. The deposits are not far from the Cyprus type massive sulphide deposits at

Outukumpu (cf. Section 2.2.1 "Copper") and are probably derived from ocean-floor hydrothermal fluids pervading organic mud (Loukola-Ruskeeniemi & Heino 1996). In 2008, a mine was launched at Talvivaara, comprising open pit extraction and metal recovery by bacterial heap leaching.

In hydrothermal parageneses, Ni is often present but rarely exploitable. However, the metal's discovery setting and the first industrial nickel source were hydrothermal Bi-Co-Ni veins in the German Erzgebirge (cf. Section 2.5.12 "Uranium"; Stemprok & Seltmann 1994, Baumann *et al.* 2000). In the exogenous cycle, the element is strongly complexed by organic substances, limiting its mobility except under highly oxidizing and acidic conditions (Smith & Huyck 1999). Petroleum, its source rocks, black shales and oil shales all display elevated traces of nickel. Iron hydroxides readily adsorb nickel, and hydrogen sulphide effectively immobilizes nickel.

Nickel ore deposit types

Economically significant nickel deposits are exclusively related to mafic and ultramafic melts originating in the mantle. Nickel concentrations of silicate melts are founded in conditions of mantle melting (e.g. the degree of partial melting, Robb 2005). Extraction of nickel from the silicate melt is initiated by exsolution of a sulphide melt. Efficient partitioning of Ni into the sulphide liquid is favoured by dynamic interaction between the two melts. Segregation of the Ni-enriched liquid, for example by gravity, leads to formation of orthomagmatic sulphidic nickel deposits, which often display co- or by-production of Cu, Co and PGM. Nickel sulphide deposits occur in volcanic and intrusive magmatic systems of different petrotectonic environments (Naldrett 1999):

- noritic intrusives in impact structures (Sudbury, Canada, Figure 1.7);
- intrusive parts of flood basalt systems, related to mantle plumes and extensional deformation of continental crust (Noril'sk, Sibiria);
- troctolitic phases of complex Mesoproterozoic anorthosite plutons (conduit-hosted deposits such as Voisey's Bay, Labrador, Canada: Scoates & Mitchell 2000);
- magmatic rocks of Archaean and Palaeoproterozoic greenstone belts, with the two types:
  1 tholeiitic intrusions (e.g. Pechenga, Kola Peninsula);
  2 ultramafic komatiitic lavas and subvolcanic intrusions (Archaean, cf. Chapter 1.1 "Orthomagmatic Ore Formation" (Figure 1.4).
- synorogenic mafic intrusions in post-Archaean orogenic belts (Jinchuan, Gansu, China).

The instability of mafic minerals hosting nickel under surface conditions and the metal's tendency for adsorption in limonite and for substitution of magnesium are the main factors of supergene lateritic nickel concentration (with Co as a by-product). Two types of lateritic Ni deposits are distinguished:

- oxide nickel ore in the upper, oxidized iron-rich part of the laterite profile;
- silicate nickel ore in the lower, reduced saprolitic section of the regolith.

Orthomagmatic sulphidic nickel deposits

Disputing the title of the world's largest nickel mining district, both Noril'sk (see below) and Sudbury, Canada, are giant accumulations of the metal (Ames *et al.* 2008). Since the first ore was found at Sudbury in 1883 when a railway was constructed, more than 90 deposits have been developed. Total nickel ore exploited plus remaining reserves amounts to 930 Mt, containing over 10 Mt of the metal. Present run-of-mine ore grades are ~1.4% Cu and 1.3% Ni and contain small amounts of ten additional commercialized elements. The search for new orebodies reaches depths of >3000 m. The last newly developed mine Nickel Rim South is based on resources of 13.2 Mt, with 1.7% Ni, 0.04% Co, 3.5% Cu, 2.2 g/t Pd, 0.8 g/t Au and 1.9 g/t Pt.

About 50% of all Sudbury ore occurs in the "sublayer" at the basal contact of the intrusion, other deposits include veins within footwall breccias, or dykes injected far into footwall country rocks ("offsets"). Sublayer orebodies lie in dells of the footwall ("embayments"), which are thought to have originated as settlement terraces of the crater wall during

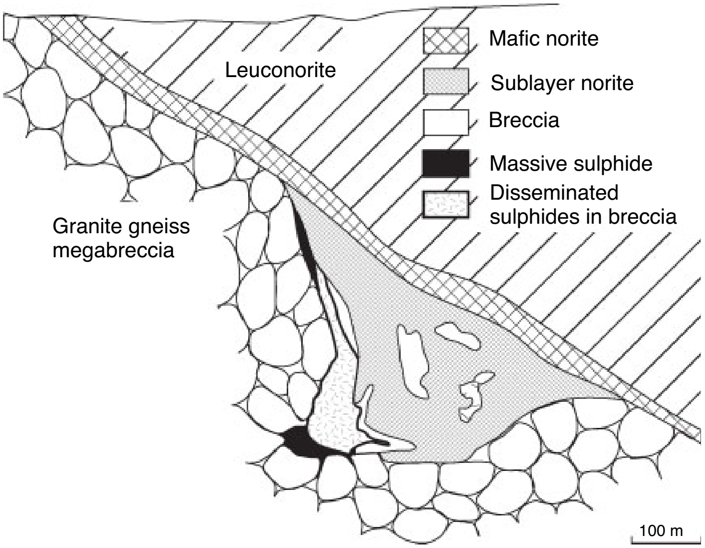

Figure 2.10 The nickel-copper orebody no. 4 at Levack-Mine, Sudbury, Canada, as an example of the characteristic control by sagging terraces of the impact crater (modified from Farrow & Watkinson 1992). With kind permission from Springer Science+Business Media.

impact (Figure 2.10). Massive sulphides collected on the footwall, and with increasing distance, sulphides are more disseminated. Contact ore is rich in Ni, Cu, Pd and Au, whereas contents of Co, Rh, Ru, Ir and Os rise to the interior of the intrusion. This appears to be the result of fractional crystallization of the sulphide melt while it settled downward. The observed paragenesis (pyrrhotite, chalcopyrite, pentlandite, etc.) is the product of secondary unmixing and alteration of a primary Cu-Ni-Fe-S monosulphide phase that solidified at 700–600 °C. In several deposits, magmatic-hydrothermal fluids played a significant role in transport and deposition of metals (Farrow & Watkinson 1992), although initial magmatic sulphide melt emplacement was the dominant process.

The Noril'sk District in western Siberia, Russia, comprises several distinct deposits. Near the northwestern margin of the Siberian Shield, a huge nappe of trap basalts was erupted at the end of the Permian (at ~250 Ma). In the Noril'sk region, its thickness reaches 4000 m. It is underlain by Palaeozoic sediments (Carboniferous coal, Devonian evaporites) and Proterozoic crystalline rocks. Whereas the main mass of the basalts is tholeiitic, the base consists of picritic and alkaline basalts. Mafic and ultramafic sills abound both in the Palaeozoic basement and in the traps.

Noril'sk orebodies are hosted exclusively by differentiated, stratified, gabbroic sills. Outcrops of sulphide ores that initiated exploration are due to an Upper Triassic deformation related to the Taymir Orogen further north. Massive and disseminated ore is exploited. Main ore minerals are chalcopyrite, pyrrhotite and pentlandite, often with important contents of palladium and platinum (10–11 ppm). Average ore grades in the district are 1.7% Ni and 3.1% Cu. With a Ni-production of 330,000 t (2003), the Noril'sk District is probably the world's leading source of this metal. Not all details of the formation of these giant deposits are fully understood. Most authors imply the presence of a mantle plume, deep magma chambers where differentiation took place, assimilation of country-rock anhydrite (Li *et al.* 2009) and, for certain orebodies, further differentiation and unmixing of sulphide melts within the gabbroic sills (Naldrett 1999, Arndt *et al.* 2003). The hypothesis that mineralized intrusions represent a conduit system related to overlying flood basalts was contradicted by Latypov (2007) but re-affirmed by Li *et al.* (2009).

In 1993, the discovery of nickel at Voisey's Bay in Labrador, Canada first pointed to Proterozoic anorthosite complexes as a potential parental setting for magmatic Ni-Cu-Co sulphide ore. The orebodies at Voisey's Bay occur in dyke-like intrusive bodies comprising ferrodiorite, ferrogabbro, troctolite, olivine gabbro and even in country rock gneisses. In contrast to Sudbury, emplacement of the ores was not dominated by simple gravitative separation, but is a product of flow dynamics of the magma. Traps for the heavy sulphide liquids were provided by the complex morphology of the flow channels. The locus of primary segregation was probably much deeper. Orebodies consist of massive and disseminated sulphides and of mineralized intrusive breccias. Main ore minerals are pyrrhotite, pentlandite, chalcopyrite, cubanite and magnetite. Total resources comprise ~137 Mt at 1.59% Ni, 0.85% Cu and 0.09% Co (Li & Naldrett 1999, Naldrett & Li 2000). Production at Voisey's Bay commenced in 2005 at a rate of ~60,000 t/a nickel (plus by-product Co and Cu) contained in concentrate.

The komatiite-hosted nickel sulphide deposits of Western Australia were discovered in 1966 (Hoatson *et al.* 2006). They occur in Archaean greenstone belts of the Eastern Goldfields Province of the Yilgarn Craton. Channels of relatively thin lava flows host high-grade ore (Kambalda Type, Figure 1.4), whereas thick dunite sills contain lower-grade disseminated but much larger orebodies (Mt Keith Type: Fiorentini *et al.* 2007). Past production and remaining resources add up to ~13 Mt of nickel metal contained. The province comprises five world-class nickel deposits (>1 Mt nickel contained). By-product amounts of copper, cobalt, gold and platinum metals are significant.

> Komatiite-hosted nickel-cobalt-copper-PGE sulphide ores are thought to have been formed by a combination of processes: The hot, rapidly flowing lavas eroded and assimilated iron sulphide-rich interflow cherts. Sulphur-saturation of the melt led to unmixing of liquid iron sulphide droplets and stringers. In this liquid, metals with affinity to sulphide melt (expressed by a high distribution coefficient sulphide/silicate melt, see above) were enriched. The efficiency of the enrichment is controlled by a number of parameters including the mass ratio of sulphide/silicate melts, the reactive surface of the sulphide melt, and the dynamics of the flow (e.g. turbulence; Lesher & Campbell 1993). Because of this, sulphide droplets ("blebby ores") often have the highest chalcophile metal contents, whereas massive ores are of lower grade. Overall, upon eruption, komatiites were neither exceptionally rich in metals nor in sulphur. Ore formation is enabled by an external source of sulphur (Bekker *et al.* 2009).

In Finland, a number of orthomagmatic nickel deposits occur within stock- and tube-like synorogenic intrusions of peridotite, pyroxenite and norite. The deposits are aligned over 400 km length in a narrow zone within the Svecokarelian Orogen, which was termed the Kotalahti Nickel Belt. The first ore at the later Kotalahti mine was accidentally found by road builders in 1954. Sulphides are disseminated or brecciated in ultramafic matrix. Kotalahti contained 20 Mt of ore grading 0.7% Ni and 0.27% Cu. Similar to Voisey's Bay, these deposits may have been formed in magma conduits of mafic intrusions.

> Jinchuan, China seems to be a very special case. This is essentially a peridotite body intruded into Proterozoic gneiss and marbles. It was first considered as another magma conduit deposit (Li *et al.* 2004, Ripley *et al.* 2005) intruded at ~830 Ma. The deposit is peculiar because the inducement for sulphide melt formation may have been assimilation of marble material. Most mafic intrusions with Ni-Cu-PGM ore reached sulphur saturation in the magma either by assimilation of sulphur-rich country rocks or of felsic rocks, which reduces sulphur solubility (Naldrett 2004). At Jinchuan, carbonate assimilation may have caused oxidation of Fe^{2+} to Fe^{3+}, thereby reducing sulphur solubility and enforcing formation of an immiscible sulphide melt (Lehmann *et al.* 2007). Jinchuan is the world's third-largest magmatic Ni-Cu-PGM deposit, with 500 Mt of ore grading 1.2% Ni and 0.7% Cu.

Lateritic nickel ore deposits

The origin of this group by supergene alteration of ultramafic magmatic rocks was discussed in Chapter 1.2 "Supergene Enrichment by Descending Solutions" (Figure 1.51, Figure 1.53 and Figure 1.54). This genetic group contributes ~40% of primary world nickel production. Most of the deposits are rather young (Miocene to subrecent) and are still found at tropical or subtropical latitudes (Cuba, New Caledonia, Australia, Southeast

Asia). However, others are older (Mesozoic to Cenozoic: Urals, Albania, Greece: Eliopoulos and Economou-Eliopoulos 2000):

> A number of large new nickel laterite mines are currently (2009) developed on the island of Sulawesi, Indonesia. One of the projects reports installation costs of US$ 1500–2000 million. Total inferred resources of limonitic and saprolitic ore are estimated at 162 Mt and a grade of 1.62% Ni and 0.08% Co. Metal recovery will be based on high-pressure acid leaching.

Land based mineable nickel resources with >1% Ni are estimated to contain at least 130 Mt of metal (USGS 2010). Of this total, ~60% occur in lateritic nickel ore. Considering world production of ~1.6 Mt of refined nickel (2008; 1.4 Mt in 2009), the supply is assured for a long time. Major primary nickel producers are Russia, Canada, Indonesia, Australia and New Caledonia. Giant, but yet uneconomic resources exist on the deep ocean floor. In the central Pacific, ~800 Mt Ni are contained in manganese nodules (Figure 1.70) that grade ~29 wt.% Mn, 5% iron, 1.2% copper, 1.37% nickel, 1.2% cobalt and 15% SiO_2 (Lenoble 1996).

Exploration for nickel ore deposits is very effectively guided by geochemical methods (e.g. nickel concentrations in soil and rocks) and by petrological investigation of magmatic host rocks (keys include sulphur-saturation and PGE contents). In ~1970, the West Australian deposits were found by prospecting gossans with peculiar green coatings (annabergite $Ni_3(AsO_4)_2.8H_2O$ or "nickel bloom"). In 1993, it was again a gossan that led to the discovery of a new important nickel deposit in Labrador (Canada), Voisey's Bay. For detailed investigation of anomalies, magnetic, electromagnetic and induced polarization methods are employed. Drilling and geophysical sections should be closely spaced (~ 30 m). Very deep ore in Sudbury is now sought with new electromagnetic probes that sample a radius of ~300 m around the drill hole. Lateritic deposits are mainly found by geological methods, shallow grid drilling and geochemistry.

2.1.5 Cobalt

Common Ore Minerals:

		Max. mass % Co	*Density (g/cm^3)*
Cobaltite	$CoAsS$	35	6.3
Smaltite	$CoAs_3$	24	6.4
Linneite-Siegenite	$(Co,Ni)_3S_4$	58	4.8–5.8
Carrollite	$Cu(Co,Ni)_2S_4$	28.6	4.5–4.8
Asbolane (cobaltian wad, amorphous)	$Mn(O,OH)_2.(Co,Ni,Ca)_x(OH)_2.nH_2O$	32	3–4
Erythrite	$Co_3(AsO_4)_2.8H_2O$	37	3
Heterogenite	$CoOOH$	61	2–4.5

Cobaltite, smaltite and linneite-siegenite are characteristic for hydrothermal vein parageneses. Carollite is the typical copper belt ore mineral. Pink erythrite guides prospectors to silver ore veins. Asbolane and heterogenite are Co carriers in oxide nickel ore.

In recent years, cobalt is again produced from dedicated mines, not only as a by-product as previously. Nearly 60% of world production is derived from the Central African Copper Belt, with typical ore grades of 2–5% Cu and 0.3–0.5% Co. Cobalt recovery with traditional metallurgy remains low (50–75% of metal content in ore) and bioleaching with much better results is increasingly employed. Cobalt metal ($D = 8.92\,g/cm^3$, melting point 1495 °C) is mainly used for alloying steel, although consumption includes many different cobalt chemicals for catalysts, paint dryers, polymerization promoters and rechargeable batteries, for example in hybrid vehicles. In the near future, cobalt-phosphate catalysts may provide a cheap alternative to platinum for splitting water in order to produce hydrogen as a liquid fuel. Cobalt use in the form of Li-Co dioxides for the production of Li-ion batteries increases rapidly. High-purity metallic cobalt is a component of superalloys destined for the construction of jet engines (~45% of world consumption). For more than 4600 years, cobalt was the basis of blue dye manufacturing.

Geochemically, cobalt is similar to nickel

According to Goldschmidt (1958), both elements are siderophile and cobalt attains highest concentrations in ultramafic (150 ppm) and mafic (40 ppm) magmatic rocks. The average abundance of cobalt in the crust is 29 ppm (Clarke value, Smith & Huyck 1999) and the Co:Ni ratio is ~1:3. Because of the similarity of ionic radii, nickel (0.69 Å) rather associates with magnesium (0.66 Å), whereas cobalt (0.72 Å) substitutes bivalent iron (0.74 Å). Manganese nodules and especially the Fe-Mn crusts of the deep sea floor are enriched to ~1.2% Co, even far from mid-oceanic hydrothermal activity. Seawater contains dissolved Co^{2+} that is fixed in the crusts by oxidation to Co^{3+}. In proximity to hydrothermal vents, precipitation of cobalt does take place, but this is diluted to very low concentrations by the overwhelming mass of iron and manganese. Under surface conditions cationic cobalt mobility is moderate except in strongly oxidizing and acidic environs (Smith & Huyck 1999). Cobalt is not redox-sensitive. Contact with hydrogen sulphide precipitates Co. Cobalt is one of the essential trace elements for humans, animals and plants (Lindh 2005). In the environment it is a harmless element; only some industrial water-soluble compounds are toxic.

Cobalt ore deposit types

Cobalt ore deposits are typically polymetallic. Associated metals include Cu, Ni, Ag, Pb, Zn, Fe, and rarely, uranium. Whereas nickel ore deposits are predominantly orthomagmatic and lateritic, cobalt is a by-product only in these settings. Most cobalt ore deposits are formed by hydrothermal processes. Hydrothermal cobalt occurs in vein and volcanogenic-exhalative deposits (Outokumpu, Idaho, USA: Bending & Scales 2001), but the economically most significant source of the metal is copper ore in the Central African Copper Belt. Significant genetic settings of cobalt include:

- diagenetic-hydrothermal Cu-Co sulphide ore in the Central African Copper Belt;
- orthomagmatic sulphidic nickel ore is nearly always a source of by-product Co (e.g. 0.15–0.22% Co in Sudbury ore; cf. "Nickel");
- lateritic silicate and oxide nickel ores are often a source of by-product Co (cf. "Nickel");
- by-product Co in certain volcanogenic-exhalative pyrite-copper orebodies;
- by-product Co in polymetallic hydrothermal vein deposits of the Bi-Co-Ni type.

The Central African Copper-Cobalt Belt, with numerous ore deposits in Zambia and the D.R. Congo (Shaba, Katanga), is a dominating factor in world cobalt production. Both stratabound and cross-cutting copper orebodies contain ~0.5% Co, mainly in the form of linneite and carrollite (Annels & Simmonds 1984). Cobalt and significant platinum contents indicate leaching of mafic source rocks. Copper-belt deposits are a product of basin-dewatering, probably intensified by deep mafic intrusions with consequent high heat flow inducing diagenetic or metamorphic pulses, and tectonic deformation (for details cf. "Copper").

Minor sources of cobalt include: i) Lateritic Ni-Co ore deposits are an economically significant source of by-product cobalt and contain a high percentage of future resources (Australia, Philippines, New-Caledonia, Moa Bay/Cuba, southeastern Cameroon, etc.). An example is Greenvale near Townsville/Australia where the ore grades 1.6% Ni and 0.12% Co. ii) Several volcanogenic-exhalative pyrite-copper orebodies display recoverable Co-contents, e.g. the Outokumpu district in Finland (0.2% Co) and the Kilembe copper deposit (Kasese, Uganda). At Kilembe, an average 1.35% Co in pyrite concentrate is currently extracted by bacterial leaching. iii) Polymetallic quartz-carbonate veins in the region of Bou Azzer/Morocco are exploited for Co-Ni-As-Au-Ag. Ore grade is reported at ~1% Co, 1% Ni and 3 g/t Au. Cobalt and nickel were mobilized by metamorphic or magmatic fluids from Neoproterozoic (Panafrican) ophiolitic ultramafics (Ahmed *et al.* 2009).

Historically, hydrothermal veins of by-product cobalt associated with Ni-Ag-Fe-(Bi)-S-(U) were the metal's main source, for example in the German Erzgebirge Bi-Co-Ni type, cf. "Uranium"), in Norway and, so prospectors first believed, in Canada:

> In the Cobalt District (Ontario, Canada), the near-horizontal Nipissing diabase sill intruded Archaean greenstones and Early Proterozoic metamorphic clastic sediments (the Huronian "Cobalt Series") at 2219 Ma. All three rock units are cut by joints and faults, which display arsenian Fe-Co-Ni-Ag ore and in places, bonanza ore with native silver. In fact, silver was the target of mining, because at that time, available metallurgical methods were not able to recover cobalt. The district yielded a total of 15,552 t Ag. At present, cobalt recovery may be possible with a new hydrometallurgical technology (Cobatec). Gangue minerals are dolomite, calcite and rhodochrosite, with traces of silicates. The vein orientation is nearly vertical with a northwesterly strike. Vein infill is thin (on average 5 cm), and veins are barren beyond a depth of maximal 100 m below the surface. High-grade mineralization correlates with a thicker facies of the Cobalt Series. Hydrothermal fluids were one-phase liquid and saline; precipitation was induced by mixing with dilute waters at 290–350 °C and 480–1350 bar (Marshall *et al.* 1993). The source of the advected elements remains vague. Lead isotope model ages imply formation of the veins at ~2200 Ma. The emplacement of Nipissing diabase was most likely the driver of regional hydrothermal fluid circulation (Potter & Taylor 2009), but certainly not the direct parent of the mineralizing fluids.

A former cobalt source was the famously rich silver veins of the Permian ore district of Kongsberg, Norway. In the region of nearby Modum, cobalt mines exploited enriched parts of fahlband layers in Mesoproterozoic Svecokarelian gneisses and migmatites. A "fahlband" is a sulphide impregnated (not massive-sulphide) concordant band in metamorphic rocks, which acquires a rusty-brown taint on weathering. In southern Norway, these rocks are hosted in an assemblage including quartzite, mica schist and amphibolites. The disseminates sulphide beds are known to attain a strike length of 11 km and a thickness of 400 m. Metal grades, however, do not allow bulk mining. The dispersed sulphides were probably formed by volcanogenic-exhalative processes. Marginally exploitable cobalt and copper grades (0.1% Co and 0.35% Cu) occur in graphite-rich zones. This enrichment may be an effect of metamorphism. An unusual content of uranium in this ore is striking (Andersen & Grorud 1998).

About 56% of world cobalt mine production (2008 ~76,000 t of metal contained, plunging to 62,000 t in 2009) are contributed by D.R. Congo and Zambia, with an increasing share derived by bioleaching of previous tailings. Congo, Canada, Zambia, Australia and Russia are the biggest producers. About 40% of cobalt supply are a by-product of nickel mining (both sulphide and laterite deposits) and consequently, output depends on the economic cycle of the nickel market. Estimated world reserves of cobalt amount to ~15 Mt. Potential cobalt resources in ocean-floor manganese crusts and nodules are huge, but economic recovery is far from imminent.

2.1.6 Molybdenum

Common Ore Minerals:

		Max. wt.% Mo	*Density (g/cm^3)*
Molybdenite	MoS_2	60	4.7
Wulfenite	$PbMoO_4$	26	6.5–7.5
Powellite	$CaMoO_4$	48	4.2

Molybdenite is the predominant ore mineral of molybdenum mining. Amorphous MoS_2 is called jordisite. As a powellite component, scheelite often carries significant molybdenum. Molybdenite ages can be precisely determined with the Re-Os method. The system is quite resilient after closure and remains stable even at high temperatures (Selby & Creaser 2001). Rhenium concentrations in molybdenite are genetic indicators (Stein 2006): High to very high (>1000 ppm) contents indicate a source in fertile mantle or juvenile crust; intermediate values point to evolved crust, and very low (<10 ppm) levels are characteristic for metamorphogenic molybdenite:

Molybdenite is the main primary source for the rare metal rhenium. ReS_2 contents in MoS_2 reach 1.9%. Much rhenium is recovered from molybdenum-bearing porphyry copper ore in Chile (2008: ~27 t of worldwide 57 t). Together with the platinum group metals (PGM), rhenium is one of the most precious of traded mineral commodities. The metal has high density (21 g/cm^3; melting point 3180 °C), high conductivity and mechanical toughness into high temperature ranges. Rhenium is an important catalyst for gasoline-production from petroleum, but most is used as a component of superalloys (e.g. turbine blades in the aerospace industry). Macroscopic rhenium minerals are extremely rare. A unique occurrence was found in sublimates of a 910 °C hot fumarole-jet situated in a volcanic crater of the Kurile Islands (Korzhinsky *et al.* 1994). The paragenesis of the sublimates comprises rhenium sulphide, molybdenite, halite, sylvite and magnetite.

The exploitable minimum grade of molybdenum ores is ~0.1% MoS_2. Very large deposits can be mined at even lower grades. In the year 2007, for example, the proved reserves at Endako, Canada (Selby & Creaser 2001) were published as 112 Mt at 0.053% Mo. The Ruby Creek project, also in British Columbia, Canada, is based on resources of 213 Mt at an average grade of 0.063% Mo, including a "high-grade" open pit resource of 0.084%. However, ~75% of molybdenum is a by-product of porphyry copper ore mining. Because of the large mass of ore processed at porphyry mines, very low Mo-grades can be economically recovered. The iron and steel industry accounts for about two-thirds of molybdenum consumption, in the form of roasted concentrate ("technical oxide"). Alloying steel with up to 16% Mo results in high strength and resistance to heat and strong acids, which are common in hydrocarbon well pipelines and in desulphurizing plants of coal-fired power stations. Common stainless steel contains ~1% molybdenum. The metal has a high melting point (2623 °C) but relatively low density (10.22 g/cm^3). Further applications are as catalysts in desulphurizing petroleum, for producing chemicals (e.g. orange to yellow pigments), for water treatment, polymers and airbags. Due to its softness and layered structure, molybdenite can be directly used as a lubricant, similar to graphite.

Geochemistry

Molybdenum is a redox-sensitive siderophile element (with a strong chalcophile tendency). Average abundance in basalt is ~0.7 ppm, in granite ~1 ppm. In magmatic rocks, trace molybdenum is hosted by magnetite, titanite and ilmenite (up to 500 ppm), in biotite and amphibole, and even in feldspar. In the presence of reduced sulphur in magmas, most molybdenum is fixed in disseminated MoS_2. The majority of endogenous rocks contain chalcophile Mo^{4+} that is relatively immobile. Economic concentrations are almost exclusively related to high-temperature hydrothermal processes in certain felsic intrusions. Mo is enriched by a factor of 9 ± 4 in a fluid phase that segregates from magma (Audétat & Pettke 2003). In moderately hot hydrothermal fluids, molybdenum is mainly transported as molybdate or molybdic acid species (H_2MoO_4), similar to tungsten. At high temperatures (500–800 °C) molybdenum solubility in KCl solutions reaches 1.5% (Ulrich & Mavrogenes 2008). Characteristically, molybdenite crystallizes from a vapour phase by reaction of hydrated molybdate species ($MoO_3 \cdot nH_2O$) with H_2S as oxygen fugacity falls with declining temperature below the SO_2-H_2S buffer (Hannah *et al.* 2007). Seven naturally occurring stable isotopes of molybdenum with a mass between 92 and 100 are known. When molybdenite crystallizes from vapour, the Mo isotope composition evolves by Rayleigh distillation (Hannah *et al.* 2007).

The estimated Clarke value (crustal abundance) of Mo is 1.2 ppm. Accordingly, molybdenum is less abundant than U, Th, Sc and most rare earth elements. Generally, sediments contain very little molybdenum (<1 ppm). Because the metal is an essential micronutrient, it is enriched in organic matter (coal, petroleum, kerogen, graphite). In oxic river and seawater, Mo is dissolved as a stable molybdate anion ($Mo(VI)O_4^{2-}$). Therefore, with a concentration of 11 µg/kg, molybdenum is the most abundant transition element in ocean water. In euxinic basins with H_2S in deep water, molybdenum and sulphur are precipitated and enriched in organic bottom sediments. Consequently, black shales reach contents of 150 ppm Mo, commonly hosted by pyrite. This process leads to measurable Mo-isotope fractionation (Arnold *et al.* 2004). Modern euxinic sediments, however, reflect the homogeneous seawater isotopic composition (Neubert *et al.* 2008).

By supergene alteration, molybdenite alters to ochreous oxides, including yellow ferrimolybdenite $Fe_2(MoO_4)_3.8H_2O$. These weathering products dissolve easily and the oxidized zone of molybdenum deposits is commonly depleted. Soil and plant samples, however, are useful geochemical exploration media. Molybdenum in sediments is sourced by weathering of ore and rocks, which liberates highly mobile, lithophile, oxidized Mo^{6+}. The dissolved molybdate ion MoO_4^{2-} may be immobilized by Fe-Mn-Al hydroxides (e.g. the deep sea manganese nodules), or by cations including Pb (formation of wulfenite), Cu, Ca, UO_2, Bi and Co, and, of course, by reaction with reduced sulphur (formation of jordisite). Finally, enzymes of most life forms are biochemical traps for traces of molybdenum. Similar to other heavy metals (Fe, Mn, Cr, Co, Cu, Zn), molybdenum is an essential trace element (Lindh 2005), although excessive intake is adverse, especially for cattle. Unlikely sources for a case of molybdenosis (excess of Mo) in cattle were the brickworks of Bedfordshire in England, which worked sulphide and organic-rich Oxford clay.

Molybdenum ore deposit types

Present commercial sources of molybdenum are almost exclusively magmatic-hydrothermal ore deposits associated with I-type subvolcanic monzonitic and granitic intrusions. Monzonite-related sources of molybdenum include the Cu-Mo porphyry deposits of Chile and the USA (cf. Chapter 1.1 "Porphyry Copper Deposits", and "Copper"). Granite-related sources of molybdenum are the molybdenum porphyry deposits (please note the confusing similarity of terms). Large molybdenum porphyries occur in North America and in China (Stein *et al.* 1997). Fertile magmas intruding carbonate rocks produce important polymetallic skarn deposits (cf. "Tungsten"). Significant molybdenum deposits include:

- magmatic-hydrothermal molybdenum (by-product tungsten) porphyry deposits related to granite or rhyolite;
- magmatic-hydrothermal copper (by-product molybdenum) porphyry deposits related to monzonite or latite;
- polymetallic skarn deposits (e.g. Mo, W, Sn, Be, Cu and other metals);
- sandstone type uranium infiltration deposits with by-product Mo;
- ocean-floor hydrothermal (or sedimentary?) Mo-Ni-Cu-Co-Zn ore shales.

Magmatic-hydrothermal molybdenum deposits

Magmatic-hydrothermal molybdenum deposits can be classified according to shape (stockwork, impregnations, replacement, veins), depth of formation (plutonic, subvolcanic), the position of ore related to the intrusion (exo- or endocontact) and, of course, the geodynamic nature of the parental granites (oceanic or continental alkaline rift, or subduction-related calc-alkaline granite).

A unique insight into one possible source of molybdenum-fertile magmas was obtained in Rogaland, Norway (Bingen & Stein 2003). Here, formerly exploited molybdenite and wolframite occur disseminated in felsic mobilizates, which were secreted during the Sveconorwegian granulite-facies metamorphism (1030–970 Ma). Typical molybdenum porphyry deposits (e.g. Questa, USA: Klemm *et al.* 2008) probably take the following path of development: The magma originates in a geochemically enriched lower crust, possibly caused by massive underplating of mafic mantle melts. At shallow crustal levels, rifting and intrusion of high-silica (ca. 75%) leucogranite batholiths and rhyolites characterize ore districts. The parental magma body may be as large as 500 km^3 and is enriched in water, K, Rb, Nb, Sn, W, Mo and F. At mid-crustal levels, fractionation causes formation of water-saturated melt batches and their ascent to subvolcanic levels. Loss of pressure leads to segregation of fluids and frothing of the melt. Bubbles of volatile phases may reach a volume of >50%. This allows vigorous convection of the melt so that fluid contents of large magma volumes are brought upwards, whereas degassed magma sinks downwards (Shinohara *et al.* 1995). Halogen-rich fluids effectively concentrate molybdenum as well as other trace elements (e.g. copper, silver, tin, tungsten, rhenium, bismuth) from the melt. Eventually, single-phase fluids of intermediate density escape upwards, where boiling starts under hydrostatic load at ~420 °C. Molybdenum and other elements concentrate in the resulting brine, which precipitates molybdenite and quartz (note the dissenting view of Hannah *et al.* 2007). The vapour phase may remove copper and sulphur from the system. The high K-content of fluids causes the strong potassium alteration typical for large molybdenum deposits. Isotope data (Pb, O, S and Sr) confirm magmatic derivation of ore fluids. At Endako, Canada, however, early involvement of meteoric water was detected (Selby *et al.* 2000).

Until its closure, the world's largest molybdenum operation was Climax, Colorado, with a pre-mining resources of 500 Mt of ore at 0.25% Mo and minor by-product tin and tungsten. This grade is, of course, much higher than Mo-contents in Cu-Mo porphyry deposits (e.g. 0.028% at Butte). At Climax, Precambrian gneisses and granites are faulted along a NS-structure against Carboniferous sediments. This is one of the deep marginal structures of the Colorado Plateau. In the Tertiary (33–24 Ma), the Precambrian of the upper block was intruded near the fault by at least 11 superimposed rhyolitic stocks, 2 of which are enveloped by caps of mineralization and alteration. The innermost alteration is intensive silicification, surrounded by the ore zone consisting of a stockwork of molybdenite-quartz veinlets with a variable gangue of K-feldspar, biotite, fluorite, topaz, pyrite, magnetite, and distally more huebnerite. Outwards and upwards, zones of sericitization, argillization and propylitization are developed. The apical parts of intrusions display marginal pegmatites ("stockscheider") or rhythmic unidirectional solidification textures (UST) of aplites and pegmatitic quartz with K-feldspar (Figure 2.11).

Climax dominated world molybdenum supply for a long time. Depletion of ore and costs of underground mining eventually enforced closure of the mine. Foresighted exploration had, however, secured several similar deposits (Henderson and Mt Emmons, Redwell, both in Colorado; Mt Hope, Nevada; Questa, New Mexico). Today, the Henderson and Questa mines are leading molybdenum producers.

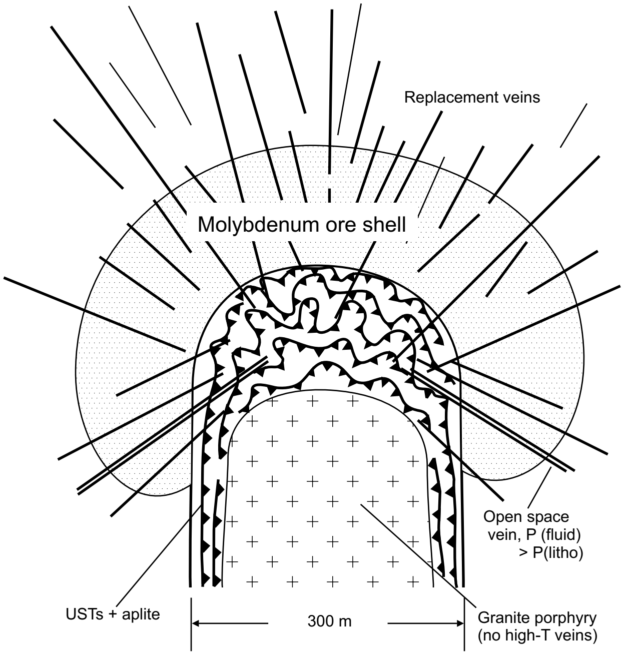
Replacement veins
Molybdenum ore shell
Open space vein, P (fluid) > P(litho)
USTs + aplite
300 m
Granite porphyry (no high-T veins)

Figure 2.11 Schematic section of a molybdenum porphyry ore deposit of the Climax type, Colorado (modified from Shinohara *et al.* 1995). The central granite porphyry is capped by bands of pegmatite and aplite with unidirectional solidification textures (UST) that reflect crystallization from margins to the centre and the former presence of exsolved magmatic-hydrothermal fluids. Replacement veins radiate from this zone into the roof. Concentric veins with open space mineralization prove fluid overpressure but are rare.

An exciting new find is Mesoproterozoic Merlin in Northwest Queensland, Australia, with an interim resource of 13 Mt at 0.8% Mo and 14 ppm Re (Brown *et al.* 2010). High-grade ore occurs in a deformed zone near the contact with granite. In the absence of gangue, molybdenite fills veins and breccias or is disseminated in black metapelite and phyllite. This may indicate precipitation from high-T vapour as proposed by Hannah *et al.* (2007).

Molybdenum porphyries are closely related to Cu-Mo porphyries, although clear differences exist. In the USA, the first are somewhat younger (Mid-Tertiary), and appear in phases of relaxation and extensional deformation of the crust instead of active subduction. The character of parental magmas tends to A-Type compared to mainly I-Type Cu-Mo porphyries. Magmas contain more alkalis and silica. A comparison of metal contents reveal that there are very few transitional deposits between Cu-Mo porphyries and Mo-W porphyries of the Climax Type.

Because molybdenum and uranium are both mobile in oxidized surface water and are commonly precipitated in anoxic environs, many infiltration-derived uranium ores of the sandstone type are a source of by-product molybdenum (e.g. U-deposits near Akouta, Nigeria, with a yearly production of ~400 t Mo).

Mo-Ni ore shales

Of high scientific interest are the Mo-Ni ore shales of the Yangtze platform of South China. The metal-rich horizon is known to extend over ~1600 km at the base of an Early Cambrian shale formation. Economically exploitable ores occur locally and have the form of bedded lenses, with a maximum thickness of 1 to 2 m. The ore consists mainly of organometallic $(Mo,Fe,Ni)[(S,As)_2C_7$ phases with minor sulphides. Grades reach 4% Mo, 4% Ni and 2% Zn, with traces of Au, Ag, PGM, redox-sensitive and base metals. Several important barite deposits occur in the same horizon. Formation by exhalative-hydrothermal fluids venting on the seafloor is supported by several lines of evidence (Coveney & Nansheng 1991, Shao-Yong Jiang *et al.* 2006). A purely sedimentary origin by precipitation from seawater, similar to deepsea manganese crusts was considered by Lehmann *et al.* (2007). Wille *et al.* (2008) suggest that upwelling deep sulphidic seawater caused both molybdenum precipitation and extinction of the Ediacaran fauna. The analogue amphibolite-facies Ni-Cu-Co-Zn black schists of Talvivaara in Finland are suggested to be of ocean-floor hydrothermal origin (cf. Section 2.1.4 "Nickel").

Main producers of molybdenum (2008 ~218,000 t; in 2009 200,000 t Mo) are China, USA and Chile, which also host ample reserves. Exploration for molybdenum employs methods similar to the search for porphyry copper deposits.

2.1.7 Tungsten (Wolfram)

Common Ore Minerals:

		Max. wt.% WO_3	*Density (g/cm^3)*
Wolframite	$(Fe,Mn)WO_4$	76.5	7.0–7.5
Scheelite	$CaWO_4$	80.5	5.9–6.1

Iron-rich members of the wolframite solid solution series are called ferberite (0–20 wt.% Mn) and manganese-rich end members hübnerite (80–100% Mn). Often, wolframite contains traces of Ca, Mg, Nb, Ta and Zn. Endogranitic wolframite (and cassiterite) may have very high, economically recoverable Y and Sc contents (cf. Section 2.5.9 "Niobium and Tantalum", Kempe & Wolf 2005). In scheelite, molybdenum substitutes for tungsten and some scheelites display molybdenum contents of several percent. This drives the short-wave UV fluorescence colour from blue for pure scheelite to yellow. Metasomatic replacement of wolframite by scheelite and the reverse, pseudomorphic wolframite after scheelite may be relevant for ore quality and processing characteristics.

Exploitable grade of primary tungsten ore is typically 0.7 wt.% in vein deposits, 0.3% in high-tonnage orebodies underground, and down to 0.1% in open pits. Because tungsten prices are notoriously volatile, these figures reflect long-term averages. Tungsten is a strategic metal with important military applications. It is heavy, has the highest melting point of all metals

($D = 19.3\,g/cm^3$, $T = 3410\,°C$) and high mechanical strength. Tungsten is used as carbide or alloyed with steel in high-speed metal and wood-working, construction, drilling and mining tools. Light bulbs and many other household applications contain tungsten. Chemical applications include catalysts and pigments. Sodium tungstate is used for fireproofing cloth.

Geochemistry

The geochemical character of tungsten is lithophile. Average contents are 2 ppm in granites and sediments, 0.5–1 ppm in mafic and 0.1–0.8 ppm in ultramafic magmatic rocks. Tungsten displays a siderophile tendency (iron meteorites contain ~1.24 ppm W). Its concentration in crustal rocks ranges from 0.4–70 ppm, with an average of 1 ppm (Smith & Huyck 1999). In several aspects, tungsten is chemically very similar to molybdenum: Both display a range of possible oxidation states (−2 to +6), an ability to form polynuclear complexes, identical atomic and ionic radii, a similar electron affinity and are a mixture of several stable isotopes. However, in contrast to Mo, W(VI) tends to be fixed as scheelite or wolframite, whereas W(IV), which occurs in the rare mineral tungstenite WS_2 is easily solubilized (eq. 2.3):

Solubilization of tungstenite WS_2:

$$WS_2 + 4H_2O \rightarrow WO_4^{2-} + 2H_2S + 4H^+ + 2e^- \qquad (2.3)$$

Trace contents of W in granitoids are due to substitution in Fe-Ti spinel, mica and feldspar. Elevated traces of tungsten are relatively common, for example in Nb-Ta minerals, hydrothermal manganese ores and oceanic manganese nodules (Kunzendorf & Glasby 1992). Anomalous tungsten concentrations are reported from geothermal hot springs and sinters. Brines in sediments of the dry intramontane Searles Lake, California, which are exploited for borax, soda ash and salt, contain 70 ppm of W. The source of tungsten is suspected in scheelite occurrences of the surrounding hills. The concentration of W in seawater is extremely low (1 μg/kg), much less than that of Mo (11 μg/kg). However, like many other heavy metals, tungsten is enriched in marine sediments with high content of organic matter. Bottom sediments of the Okhotsk Sea reportedly display up to 50 ppm W. These observations indicate that tungsten may be enriched in playa lake and marine sediments of volcanic provinces, and that fertile granites may inherit tungsten by melting pre-enriched sediments.

In a fertile crystallizing magma, tungsten is incompatible and concentrates in the exsolving fluid phase (1–1000 ppm). Hydrothermal transport of tungsten at moderately acidic conditions is commonly in the form of tungstic acids (e.g. HWO_4^-, H_2WO_4) or tungstates (WO_4^{2-}) (Wood & Samson 2000). Therefore, at 500–200 °C, neutralization by contact with carbonates, ultramafics and rocks with calcium-rich plagioclase is often the reason for precipitation. Gangue commonly comprises quartz and muscovite (Figure 1.42). Apart from water, ore forming fluids typically contain moderate NaCl-contents (0–15%, rarely up to 55%) and some CO_2 (with N_2, CH_4). However, fluids in wolframite at Panasqueira are free of CO_2, which is present in the quartz gangue (Figure 1.27, Lüders 1996). The solubility of tungsten rises with pressure and temperature, with increasing acidity, with low activities of Ca-Fe-Mn and with fluid salinity. Inverse relations control precipitation (Heinrich 1990). Scheelite formation is favoured by reaction of tungsteniferous solutions with Ca-rich rocks or solutions. In several mining districts (Erzgebirge, Cornwall), the ferberite component in wolframite seems to increase with decreasing temperature. This agrees with theoretical phase relations at constant solution composition but the reverse has been found elsewhere. Clearly, tungsteniferous hydrothermal solutions may have various evolution paths in time, concerning pH, activity of Ca^{2+}, Fe^{2+} and Mn^{2+}, and temperature. Wolframite composition is not a simple geothermometer.

Surficial alteration of wolframite produces yellow ochres that consist of hydrous minerals such as ferritungstite and tungstite ($WO_3.H_2O$). Scheelite may form earthy white anthoinite $WAl(O,OH)_4$. Well-crystallized scheelite and wolframite are quite resistant to chemical weathering and occur in eluvial and colluvial placers. At Fenglin mine (Jiangxi, China), a hematitic gossan above a stratiform ferberite-pyrite-Cu orebody contains

1.5% W. Scheelite and wolframite are both brittle and therefore in water courses quickly reduce to fines. Consequently, alluvial tungsten placers are rare. Chemical tungsten solubility and mobility in surface waters at ambient conditions is very low compared to Mo, due to intensive sorptional precipitation. In the mining environment, the element is no hazard for living organisms or the environment in general. Biologically, tungsten is one of the essential trace elements (Lindh 2005) and a number of microbes employ the element in building enzymes. Hyperthermophilic archaea appear to be obligately tungsten-dependent (Kletzin & Adams 1996).

Tungsten ore deposit types

Tungsten ore deposits are predominantly formed by magmatic-hydrothermal processes related to felsic intrusions (cf. Chapter 1.1 "Granitoids and Ore Formation Processes"). Parental magmas are moderately to highly specialized and display a redox spread from reduced to oxidized (Figure 1.17). The close genetic relations between intrusions and tungsten ores are confirmed by stable isotope data. Ore-stage fluids clearly contain magmatic water (e.g. Zaw and Singoyi 2000). Later flooding by low-T meteoric waters is not rare, however. Deposits include Sn-W greisen and polymetallic tungsten porphyry deposits with Bi, Mo and Sn, which occur in apical parts of intrusions. Wolframite quartz vein fields (Figure 1.15 and Figure 1.16 and Figure 1.41), stockwork orebodies and breccia pipes are preferentially situated in the perimagmatic environment. Scheelite skarn deposits appear in the contact zone with carbonates (Figure 1.32) or with mafic-ultramafic magmatic rocks. Epizonal tungsten ore is rare and of little economic importance. In summary, main deposit types of tungsten include:

- scheelite-only and polymetallic skarn deposits related to felsic intrusions;
- tungsten-only and polymetallic endogranitic greisen and porphyry deposits;
- wolframite quartz vein fields and stockwork deposits within parental granite or in its exocontact country rocks;
- by-product tungsten from magmatic-hydrothermal molybdenum porphyry deposits related to granite or rhyolite.

Close metallogenetic relations between W and Sn are common (China, Erzgebirge, Cornwall: Figure 1.44, Central Africa), but tungsten ore provinces with little tin do exist (western North America). Both W and Sn are enriched in A- and S-Type granites. I-Type granites rarely produce tin deposits, but many important tungsten concentrations. Mo-W porphyry deposits of the Climax Type (cf. Section 2.1.6 "Molybdenum") illustrate the geochemical kinship of the two metals.

The world's largest tungsten (and tin) resources occur in eastern Asia, forming a giant W-Sn-F-U-Nb-Ta-SEE and base metal-Mo province, which is part of the Circum-Pacific metallogenetic realm. Thousands of significant tungsten deposits form a broad belt that reaches from Kamchatka through Korea, Japan, eastern China and Malaysia to Sumatra. The South Chinese provinces of Jiangxi and Hunan are especially endowed with tungsten (± Sn, Mo, Bi, Pb, Zn, Cu and Ag), making China the dominating force in the world tungsten market. Economically most important are skarn deposits, including the world's largest scheelite deposit Shizhuyuan in southern Hunan that contains >1 Mt tungsten, 500,000 t tin, 300,000 t bismuth, 130,000 t molybdenum and 200,000 t beryllium (Huan-Zhang *et al.* 2003). Tungsten porphyry and wolframite quartz vein deposits are also common. Most of these deposits are genetically related to post-orogenic, subvolcanic and intrusive Yanshanian granitoids formed between 190 and 150 Ma (mainly in the Jurassic), which intruded Palaeozoic to Mesozoic sediments and volcanics. Yanshanian granites are of A-, S- and I-Type, the latter producing ores that contain more sulphides. In the Jurassic, South China was a giant Basin-and-Range style magmatic province, which developed after the Indosinian orogeny (Li & Li 2007). Geochemical studies seem to confirm that the granites and their metals are sourced in LIL-enriched mantle and lower crust (Pan & Dong 1999, Minghai *et al.* 2007).

Tungsten deposits in Europe formed during the Late Palaeozoic. Both the northern branch of the Variscan orogenic belt (Erzgebirge, Cornwall, Portugal), and the southern branch (Pyrenees, the French Massif Central, Eastern Alps) host deposits. All are related to Late Carboniferous to

Permian (~300 Ma) granites, which formed as a consequence of the final welding of Pangaea.

Discovered in 1967, the scheelite deposit Felbertal near Mittersill (Salzburg) in the Eastern Alps presents a most interesting case history, as it was initially considered to have been formed by volcanogenic seafloor exhalation. For many years, this hypothesis strongly influenced international metallogenic research and exploration concepts. Host rocks are Cambrian ultramafic (ophiolitic) lenses in mafic to felsic metavolcanics, subvolcanic intrusions and metasediments of a primitive island arc. In the western main part of the deposit, Variscan I-type leucogranites with I- to A-type characteristics ("K1-3 gneisses") intruded these rocks. Locally, the intrusive contact is marked by a pegmatite sheet with large crystals of scheelite, beryl and molybdenite, similar to contact pegmatites ("stockscheider") in the Erzgebirge. Intense orogenic deformation and amphibolite metamorphism both during the Variscan and the Alpidic cycle (at ~280 and 30 Ma) transformed the rocks and their spatial relations profoundly. Orebodies in the western part of the deposit are stockworks of numerous small veinlets of scheelite and quartz (Figure/Plate 2.12a and b), with rare sulphides (Cu, Mo, Bi, Zn, Pb, As), cassiterite and traces of Au and Ag. In an eastern outlier, rich orebodies consisted of fine-grained quartzite lenses laminated by scheelite bands. This "scheelite quartzite" ore type was believed to represent a synsedimentary exhalite but is now interpreted to have originated as large hydrothermal quartz veins, which were later strongly sheared. Various dating methods have failed to provide definitive ages of all rocks and thus to elucidate their role in mineralization (Höll & Eichhorn 2000). Molybdenite Re–Os dating, however, confirmed a Late Palaeozoic age of mineralization (Raith & Stein 2006). Overall, the deposit is of a mixed stockwork, vein and contact-replacement type, produced by magmatic-hydrothermal fluids derived from the leucogranites. The mafic-ultramafic rocks acted as a geochemical trap, by neutralization and provision of reactive calcium. The underground mine exploits ore with ~0.4% WO_3, producing 4500 t/year of scheelite concentrate at 31% WO_3.

Common scheelite skarn deposits – at the contact of granitoids intruding limestone – were exploited at Salau (Ariège) in the French Pyrenees and at King Island in Tasmania, which closed in 1990 but is currently revitalized. Several important skarn ("tactite") deposits occur in the Canadian Cordillera (e.g. CanTung mine, Figure 1.30). Mactung, a large undeveloped tungsten skarn deposit in Yukon, Canada, contains >33 Mt of indicated resources at an average grade of 0.88% WO_3. Planned development is based on 8 Mt with 1.09% WO_3.

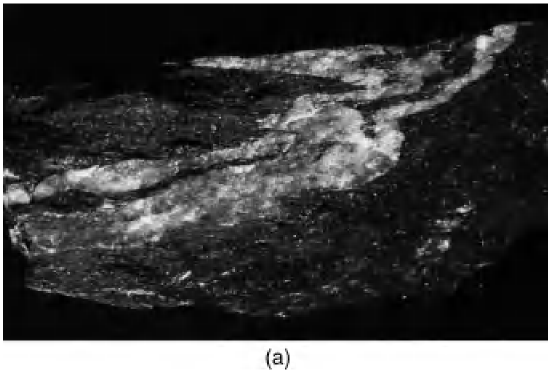

Figure 2.12 a (Plate 2.12a) Folded scheelite-quartz veinlet cutting across foliation of host greenschist at Felbertal mine, Austria. Length of specimen 50 cm.

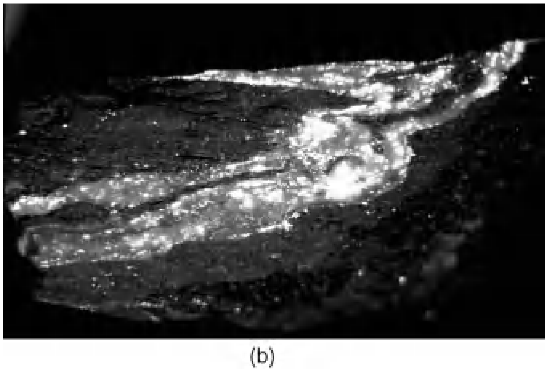

Figure 2.12 b (Plate 2.12b) UV illumination reveals the distribution of scheelite (white).

More than 100 former wolframite mines based on quartz veins near Variscan granite cupolas are known in Portugal. Panasqueira is the largest deposit

(Figure/Plate 1.89), characterized by near-horizontal veins in the apical part of a muscovite-albite leucogranite and in its roof. Intruded rocks include siliceous metapelites and greywackes. The granite forms a small cupola of quartz-muscovite greisen topped by a quartz cap. The vein paragenesis comprises quartz and wolframite, some cassiterite and arsenopyrite, sulphides of Fe, Zn, Cu and Sn, apatite, siderite, Ca-Mg carbonates and fluorite. The paragenetic succession generally follows this enumeration. Near the veins, country rocks are silicified, sericitized and tourmalinized. The horizontal disposition of the veins indicates that fluid pressures were higher than lithostatic stress ($P_{fluid} > P_{lithostatic}$). Vein opening induced phase separation and ore formation (Figure 1.27). Mineralizing fluids were moderately saline and strongly influenced by the organic-rich country rocks (Polya *et al.* 2000). Yearly production at Panasqueira is ~2500 t wolframite concentrate, 100 t cassiterite and 1000 t chalcopyrite.

With a moderate annual production, many quartz vein and tourmaline breccia pipe deposits with ferberite, scheelite, stibnite and other sulphides occur between La Paz and Oruro in the more deeply eroded part of the tin province in the Bolivian Andes. They are genetically related to Tertiary granitoids.

Exploration for tungsten deposits employs geological, petrological and geochemical methods. The conspicuous fluorescence of scheelite in UV-light was the means for many discoveries worldwide, by locating outcropping orebodies and alluvial trails of scheelite.

The world's largest tungsten producers are China (2009, ~80% of the world total of 58,000 t tungsten contained in concentrate), Russia and Canada. China is also the world's biggest consumer of tungsten. Reserves totalling ~2.8 Mt of tungsten metal occur foremost in China, Russia, USA and Canada (USGS 2010). Tungsten concentrates are usually traded in metric tonne units (originally designating one tonne of ore containing 1% of WO_3), today used to measure WO_3 quantities in 10 kg units. One metric ton unit (mtu) of tungsten (VI) trioxide contains 7.93 kilograms of tungsten.

2.1.8 Vanadium

Common Ore Minerals:

		Wt. % V_2O_5	Density (g/cm^3)
Coulsonite (in vanado-magnetite)	FeV_2O_4	variable	5.2
Montroseite	(V,Fe)O(OH)	variable	4.0
Carnotite	$K_2(UO_2)_2(VO_4)_2 \cdot 3H_2O$	20	4.7–5
Tyuyamunite	$Ca(UO_2)_2(VO_4)_2 \cdot 5–8H_2O$	20	3.6–4.3
Vanadinite	$Pb_5Cl(VO_4)_3$	19	6.9

The most important vanadium ore mineral is coulsonite, although in nature this mineral is extremely rare. In common titaniferous magnetite, however, coulsonite occurs as a minor component in solid solution. Montroseite, vanadiferous clays, carnotite and tyuyamunite are minerals of uranium-vanadium ore deposits of sandstone (e.g. Colorado Plateau), karst and calcrete types. Vanadinite is one of a group of vanadium minerals that occur in oxidized lead, zinc and copper deposits (typically with descloizite and mottramite: Boni *et al.* 2007). Patronite (VS_4) is very rare and without economic significance; previously, it was extracted from asphalt at Minasraga, Peru.

Average economically exploitable grades of vanadium-only ores are ~1% V. However, vanadium is predominantly a by-product of iron (and titanium) mining. Several large deposits of this type reach 2.8% vanadium, but content as small as 0.02% V may be utilizable.

Vanadium metal is corrosion-resistant, soft, silver-grey and ductile. It melts at 1910 °C and has a density of 6.11 g/cm^3. Most vanadium (>90%) is used as an additive in the steel industry, for products such as flat-rolled steel, rails, tubes, tools (including medical equipment) and springs. Vanadium stabilizes C and N by the formation of carbides and nitrides that harden and strengthen steel. Ti-Al-V alloys are a component of high-speed airframes. Vanadium oxide (V_2O_5) is used as a catalyst in manufacturing sulphuric acid and for making batteries (e.g. the new generation of $Li_3V_2(PO_4)_3$ batteries for electric cars).

Geochemistry

Vanadium's geochemical character is lithophile (Goldschmidt 1954) with siderophile and biophile tendencies. In nature, vanadium occurs in the three oxidation levels V^{3+}, V^{4+} and V^{5+} and is one of the redox-sensitive elements. Its crustal abundance is ~150 (53–200) ppm (Smith & Huyck 1999). In magmatic rocks, trace vanadium is preferentially included in magnetite, in titanium minerals and in chromite, compared to mafic silicates. Therefore, average vanadium contents decrease steeply from mafic rocks (250 ppm) to granites (20 ppm). As may be expected, pegmatites and granite-derived hydrothermal solutions contain little vanadium. Rare exceptions are mafic or emerald-bearing pegmatites. The green colour of emerald (beryl) is caused by traces of chromium and vanadium. Note that some emerald deposits are not granite-related but products of diagenetic or metamorphic mobilization of black shale-hosted trace elements.

Weathering of primary minerals liberates vanadium. In a humid climate (where soil water is moderately acidic) vanadium is hardly soluble and and is mainly dispersed by mechanical processes. Oxygen-rich, alkaline or strongly acidic seepage and groundwaters of semi-arid and arid climates dissolve V^{5+} or V^{4+} as oxyanion vanadate (VO_3^-) or cation vanadyl (VO_2^+). In such waters vanadium reaches concentrations of several 100 ppm and can be transported over considerable distances (Wanty & Goldhaber 1992). Similar to uranium, precipitation is induced by reduction (especially by organic substances), or by combination with cations such as Pb^{2+}, Zn^{2+}, Cu^{2+}, and UO_2^{2+} (resulting in carnotite formation, e.g. Yeelirrie, Australia) or by inclusion/adsorption in iron and aluminium oxy-hydroxides (e.g. bauxite).

Deep seawater has a uniform dissolved vanadate concentration of 35–37 nmol/kg V (Halbach *et al.* 2003). Most sediments contain little vanadium. Notable exceptions are bituminous rocks (copper shale in Germany and Poland, alum shale in Sweden), sedimentary iron and manganese ores, bauxite, phosphorites and deepsea manganese nodules. Samples of the metalliferous mud pools in the Red Sea contain up to 1.3% V_2O_3 (dry).

Vanadium is one of the micronutrients for humans (Combs 2005) and is essential for many other organisms. In the natural and mining environment, vanadium is harmless but some industrial compounds are toxic. Exceptional vanadium enrichment is known from a number of marine organisms, including the *ascidiacea* (sea squirts) and *holothuroidea* (sea cucumbers) that attain >1% of vanadium (in dry mass). However, the strikingly elevated vanadium trace contents in petroleum, tar and asphalt are not due to biomass concentration but to early diagenetic replacement of magnesium in chlorophyll by the vanadyl ion (Hunt 1996). Vanadium (and nickel) are complexed to porphyrins in the petroleum source rocks and carry the metals on into crude oil. Therefore, petroleum ash may attain 20% vanadium and is an important source of the metal. Large amounts of vanadium are hosted in oil shales. One example is Middle Cretaceous Julia Creek (Australia), with resources of 4000 Mt of shale *in situ*, which contain a recoverable 1700 Mbl of oil and, in oxidized parts of the deposit to ~20 m depth (Lewis *et al.* 2010), measured resources of 200 Mt vanadium ore at 0.4% V_2O_5 and 300 g/t MoO_3. Similar to numerous other oil shale deposits in the world, Julia Creek appears to be marginally not profitable at present market conditions.

Vanadium ore deposit types

At present, significant vanadium ore deposits are almost exclusively orthomagmatic titano-magnetite segregations. Minor or by-product sources of vanadium are certain deposits of uranium, sedimentary iron and manganese ores, combustion residues from coal and oil-burning power stations, steel slags and residues of crude oil processing. Potential sources of vanadium include phosphorite, ocean-floor manganese nodules, iron-rich bauxite, oil shale and tar sand bitumen. The short-list comprises:

- orthomagmatic deposits of V-Ti iron ore in layered and non-layered mafic intrusions;

- infiltration deposits of uranium with by-product vanadium;
- diagenetic heavy oil, oil shale and tar sands are giant potential sources;
- vanadium is one of the potentially recoverable minor and trace elements of sedimentary phosphorites.

Thirty to fifty percent of world vanadium resources (63 Mt according to an estimate by the USGS) occur in the magnetite seams of the Bushveld Complex, South Africa (Figure 1.5):

> The uppermost 1750 m (the Upper Zone) of the Rustenburg Layered Suite contain an average 8% of disseminated magnetite within gabbronorite and magnetite gabbroic rocks. More than 20 seams of massive titanium-magnetite are interbedded with these rocks. Vanadium-contents in magnetite are highest in the lower seams (2.1% V_2O_5) and decrease upward to nearly nil, whereas titanium (TiO_2) increases from 12 to 20%. Apart from magnetite, the seams contain a few percent of silicates and of ilmenite. Open-cut exploitation takes place at Mapochs Mine and in the Brits District, based on the Main Magnetite Layer that has an average thickness of 2 m. The processes contributing to magnetite enrichment in the seams are not fully understood. Possible factors may have been:
>
> - unmixing of silicate and oxide melts;
> - gravitative settling of magnetite liquid or of crystals;
> - multiple magma injection;
> - changes in oxygen fugacity; and
> - changes in pressure (cf. Chapter 1.1 "Orthomagmatic Ore Formation").
>
> The last interpretation is favoured by Cawthorn & Molyneux (1986), because chemical gradients across the seams are very small. It is remarkable that vanadium content in the Upper Zone is concentrated in magnetite, whereas cogenetic silicates contain very little vanadium. This underlines the high partitioning coefficient for vanadium into magnetite from silicate liquid.

Other vanadium deposits of the magnetite-ilmenite type are known in Norway (Rödsand) and Finland (Mustavaara), in the Urals (Gusevogorsk-Katschkanar), in India (Orissa), China (Lanshan, Panzhihua) and in Australia (Barrambie, Windimurra, Coates Siding and Buddadoo, W.A.). Exploration for this deposit type may build on earlier iron ore investigations. In the past, numerous magnetite occurrences in mafic intrusions had been rejected because of elevated titanium contents. At that time, Ti and V were not considered as utilizable by-products.

Most of vanadium mine production (55,500 t of vanadium contained in 2008, 54,000 t in 2009) originates from South Africa (40%), China and Russia. Vanadium extracted from petroleum residues, pig-iron and steel slag, ash from coal-fired power stations and spent industrial catalysts makes up the difference to total world consumption.

2.2 BASE METALS

2.2.1 Copper

Common Ore Minerals:

		Wt. % Cu	*Density (g/cm^3)*
Chalcopyrite	$CuFeS_2$	34	4.1–4.3
Enargite	Cu_3AsS_4	47	4.4
Cu-Tetrahedrite	$Cu_{12}Sb_4S_{13}$	max. 45	4.6–5.1
Cu-Tennantite	$Cu_{12}As_4S_{13}$	max. 53	4.6–5.1
Chalcocite	Cu_2S	80	5.5–5.8
Digenite	Cu_9S_5	79	5.6
Covellite	CuS	66	4.7
Cuprite	Cu_2O	88	6
Malachite	$Cu_2(OH)_2CO_3$	57	4
Atacamite	$Cu_2Cl(OH)_3$	59	3.7

Apart from these important copper ore minerals, many others are known that may locally gain economic importance. Note the distinction between: i) primary ore minerals (commonly the first group listed): ii) secondary enrichment sulphides; and iii) supergene "oxide" minerals (third group). Atacamite associated with gypsum is particularly widespread in oxidized porphyry copper ores of the Atacama Desert (Reich *et al.* 2008). More than 70% of producing copper mines, however, exploit chalcopyrite ore. Copper-tetrahedrite and copper-tennantite are not *sensu stricto* ore minerals but are theoretical end members of complex sulphosalt fahlores that contain Cu, Ag, Fe, Zn, Hg, Cd, Sb, As, Bi, Te, S and Se.

Exploitable grades of smaller copper deposits are 3–5% Cu, whereas very large operations with orebodies suitable for opencut extraction thrive on 0.5% Cu, and even at ~0.3% in the presence of by-product metals such as molybdenum and gold. Sulphide ore is commonly enriched by flotation to saleable concentrates of ~30 to >60% Cu. Concentrates (containing enargite or tennantite) with >5000 ppm As are not accepted by smelters, and deliveries with >2000 ppm As are penalized. This is avoided by removing arsenian minerals during flotation. Other penalty elements include bismuth and antimony. Copper concentrates are processed to cathode sheets by smelting and electrochemical treatment. Noble metals (Au, Ag, PGM) are recovered from anode slimes. Traces of selenium and tellurium can be profitable by-products. High sulphur contents in concentrates allow the energy-saving "flash smelting" technology and production of native sulphur and sulphuric acid. "Oxide" ore deposits, disused mine shafts, tailings and waste rock dumps, and even primary sulphide ores are increasingly treated by microbial, chloride or sulphate leaching in order to extract copper. Copper is stripped from leach solutions by cementation on scrap iron, or with organic chemicals.

Uses of copper are primarily defined by the metal's high conduction of heat and electricity (second only to silver). Over 50% of consumption concerns various products of the electrical and electronics industries. In some of these fields, copper competes with other materials (e.g. glass fibre cables, conducting synthetic materials). Copper metal (melting point 1083 °C, density 8.94 g/cm^3) and its alloys (bronze: Cu + Sn; brass: Cu + Zn) are distinguished by excellent malleability, ductility and resistance against atmospheric attack. Also, copper has strong antibacterial properties. Therefore, water pipes or work surfaces made from copper metal may help to prevent infection. In low concentrations, copper is an essential element for humans, plants and animals (Lindh 2005). However, excess copper is toxic and should be controlled in drinking water (<2 mg/litre: WHO 2006) and in food. In the western United States, soils contain an average of 21 ppm Cu (range 2–300; Smith & Huyck 1999). Among grazing animals, sheep are most sensitive to copper, suffering from deficiency at concentrations (in herbage) <5 μg/g and toxicity at >10 μg/g. Aquatic life displays a similar variance, with fish, for example, being poisoned at levels of dissolved copper acceptable to most other life forms.

Geochemistry

The geochemical properties of copper are dominated by its great affinity to sulphur, which characterizes the "chalcophile or thiophilic elements" Cu, Zn, Ag, Cd, In, Hg, Tl, Pb, Bi, As, S, Se, Sb and Te (Goldschmidt 1958; *chalkos* in ancient Greek denotes copper, *theion* sulphur). Although Cu is redox-sensitive, both Cu^+ and Cu^{2+} are mobile cations under oxidizing conditions (Smith & Huyck 1999). Reduced sulphur and carbonate ions effectively precipitate and immobilize the element in sulphides and malachite, or at higher pCO_2 azurite. Copper forms stable complexes with organic substances. Therefore, black shales, coal and petroleum ashes always have elevated Cu traces. Copper is adsorbed by clay and Mn-Fe oxyhydroxides (e.g. the manganese nodules of the deep sea). Its average abundance in the crust is 68 (14–100) ppm, ~100 in mafic magmatic rocks and ~10 ppm in felsic rocks (Smith & Huyck 1999). Among sediments, pelites have highest trace contents with 70 ppm, carbonates with 6 ppm the lowest. Acidic and sulphur-poor ore-forming hydrothermal solutions transport copper mainly in the form of chloride complexes, such as $(CuCl)^o$ >250 °C and $CuCl_3^{2+}$ or $CuCl_2^-$ at lower temperatures. At high concentrations of reduced sulphur effective transport, for example in the form of CuS $(HS)_2^{2-}$ is only possible if solutions are alkaline (Mountain & Seward 1999). Typical copper concentrations in ore-forming hydrothermal solutions are between 100 and 500 ppm. Sulphur-rich vapours segregating from magma may contain up to 1% Cu (Heinrich *et al.* 1992). HCl-rich volcanic gas can transport 280 ppm copper (Archibald *et al.* 2002).

Many copper ore deposits owe exploitable grades to supergene enrichment processes

(Figure 1.55). Leached sections are characterized by gossans and acidic alteration of silicate rocks. Carbonate host rocks inhibit displacement of copper and its secondary enrichment. Although varicoloured copper carbonates may taint every visible surface of the weathered material, copper contents remain unchanged. However, because of the low cost of leaching operations, even low-grade deposits of oxide copper are attractive exploration targets (Chavez 2000). The common abundance of pyrite in copper ore is the cause why acid rock drainage (ARD) prevention and mitigation is one of the most serious and costly environmental hazards of copper mining (cf. Chapter 5.4 "Mining and the Environment").

Copper ore deposit types

Copper ore deposits are formed in all major metallogenetic process systems. A common feature of the majority is copper transport in oxidized and acidic fluids, and concentration and immobilization upon encountering reduced sulphur. The most important primary genetic groups include:

- orthomagmatic sulphides of Cu-Ni-Co-Fe (± PGM) hosted in mafic magmatic rocks (cf. Section 2.1.4 "Nickel", e.g. Noril'sk and Sudbury, Figure 1.7 and Figure 2.10);
- orthomagmatic to magmatic hydrothermal copper sulphide ore in carbonatite (Palabora);
- skarn and magmatic-hydrothermal replacement deposits, partly in close association with copper porphyry deposits;
- magmatic-hydrothermal porphyry Cu (Mo, Au) deposits that host ~60% of world copper resources (Cooke *et al.* 2005);
- magmatic-hydrothermal, low-sulphur, iron oxide-copper-gold (IOCG) deposits, characterized by large masses of magnetite or haematite (Groves *et al.* 2010, Cox & Singer 2007, Pollard 2006, Hitzman *et al.* 1992; e.g. Olympic Dam);
- copper ore veins, usually intrusion-related (e.g. Cu-Sn in Cornwall, Figure 1.44; San Rafael in Peru, cf. Section 2.2.3 "Tin");
- submarine exhalative massive sulphide deposits, often polymetallic and associated with Au, Zn ± Pb, and even Sn; this group includes Cyprus type deposits (Outukumpu, Finland), volcanic-hosted massive sulphides (Iberian Pyrite Belt, Kuroko type, Figure 1.46), and the sedex group (Figure 1.71), although the latter typically contain more Zn than Cu;
- diagenetic-hydrothermal stratabound/stratiform sediment-hosted deposits (European Copper Shale, Chapter 1.4 and Figure 1.75; White Pine, Michigan; Central African Copper Belt);
- retrograde-metamorphogenic hydrothermal saline brine-related (Copper Belt, Mt Isa);
- secondary copper deposits enriched by supergene processes and oxide ores were briefly described in Chapter 1.2 "Supergene Ore Formation Systems".

Carbonatite-hosted copper at Palabora

The copper-bearing carbonatite at Palabora (Phalaborwa) in northern Transvaal, South Africa is unique, although in some respects resembling the alkali complexes of Kola Peninsula (e.g. Kovdor). Palabora is a Palaeoproterozoic (2030 Ma) complex alkali intrusion hosted in Archaean granite gneisses. The complex displays two intrusive centres: The northern centre consists of olivine-vermiculite-pegmatoid and is the base of the world's largest vermiculite mine. The southern centre consists of carbonatite with peripheral magnetite-apatite ("phoscorite") and copper ore in the middle:

> The Palabora copper orebody is an elliptically shaped, vertical volcanic pipe. Copper grades of ~1% are found in the core and decrease gradually to the periphery with no sharp ore/waste contact. The ore is hosted in banded and transgressive carbonatites, which both contain abundant magnetite. Copper grades located in stringers and veinlets are highest in transgressive carbonatite. Ore minerals include chalcopyrite, bornite and cubanite replacing magnetite. Mineralization is the consequence of the injection of iron and fluid-rich oxidized carbonatite magma. The sequence illustrates an intriguing passage from orthomagmatic (banded carbonatite) to magmatic hydrothermal breccia pipe ore. Outwards, the carbonatite plug is surrounded by rings of pyroxene-vermiculite-pegmatoid, pyroxenite (the main mass) and a marginal fenitic syenite (Verwoerd 1986). Groves & Vielreicher (2001) have considered genetic relations between Palabora, Olympic Dam and the IOCG-family of metal deposits.

The copper orebody has a diameter of ~500 m and extends to a depth of >1300 m. In 2002, the open pit reached a depth of 760 m, having yielded 900 Mt of ore and 4.8 Mt of refined copper. The average copper grade was always low (~0.5%) but recoverable by-products (titaniferous magnetite, sulphuric acid, zirconium oxide, hafnium, uranium, silver, gold and platinum metals) make this a profitable operation. Underneath the open cut, a new underground mine is exploiting ore over a depth interval of 500 m that contains proved and probable reserves of 112 Mt grading 0.56% copper.

Porphyry Cu-(Mo-Au) deposits

Porphyry Cu-(Mo-Au) deposits of great economic prominence are exploited in the western United States (Bingham, Utah, Bisbee, Arizona, Ely, Nevada), in Mexico (La Caridad), in the Chilean Andes (e.g. Chuquicamata, the world's largest copper producer; La Escondida, the latest new mine), in Southeastern Asia (Bougainville, Ok Tedi, Papua-New Guinea), in Iran (Sar Cheshmeh) and in southeastern Europe (Recsk, Hungary, Medet, Bulgaria, Bor, Serbia and Deva, Romania). Porphyry deposits provide 75%, and oxide ore from porphyries nearly 20% of current world copper production (Gerst 2008):

Essential aspects of this deposit type are described in Chapter 1.1 "Porphyry Copper Deposits" (Figure 1.32 and Figure 1.34) and in Chapter 1.7 "Metallogeny and Plate Tectonics" (Figure 1.88). Numbers characterizing Bingham Canyon mine illustrate the singular scale of porphyry deposits. Bingham near Salt Lake City is the largest North American copper and gold deposit. It occurs in the eastern boundary zone of the Basin and Range Province. Selective high-grade mining at Bingham started in 1863 and industrial operations in 1903. Today, the pit is 800 m wide, 1200 metres deep and 4 km long. From this volume 11 Mt of copper were extracted and 5000 Mt of rock had to be moved. Today, Bingham produces annually 250,000 t Cu, 11 t Au, 81 t Ag, 15,000 t Mo and 500,000 t sulphuric acid. Of the total metal endowment of this extraordinary deposit, only ~50% have been removed until now. Three papers in *Economic Geology*, Volume 105, Number 1 (2010) exhaustively describe the metallogeny of the Bingham porphyry deposit. Chuquicamata mine (Figure/Plate 1.31) is nearly twice Bingham's volume. Its past production amounts to 1500 Mt at 1.5% Cu + 0.07% Mo; remaining resources are roughly the same mass.

Magmatic-hydrothermal iron oxide-copper-gold (IOCG) deposits

Magmatic-hydrothermal iron oxide-copper-gold (IOCG) deposits were proposed as a new class of deposits after the discovery of the spectacular copper-uranium deposit at Olympic Dam in South Australia in 1976 (Hitzman *et al.* 1992). The defining difference to other copper sulphide deposits (e.g. porphyries) is the large fraction of iron oxides in the ore, explaining, for example, the controversial (Groves *et al.* 2010) inclusion of Palabora as a magmatic member of this class. Exploration for copper in southern Australia was based on the expectation of ore deposits of Keweenawan (Michigan) or Copper Belt type (Central Africa) in the geologically similar Gawler craton of South Australia. Drilling high-amplitude Bouguer gravity and magnetic aerogeophysical anomalies soon located ore of a wholly unexpected nature.:

The Olympic Dam deposit occurs within an anorogenic oxidized potassic granite (dated to ~1590 Ma), which is set within a Palaeo-/Mesoproterozoic graben (note parallels to Mt Isa and Broken Hill) and is covered by 350 m of younger, unmineralized sedimentary rocks. Host rocks are coarse haematite-rich granite breccias (Figure 2.13) of explosive volcanic and phreatomagmatic origin. The breccia ore contains copper sulphide and by-product grades of rare earth elements, uranium, gold and silver. Total resources are estimated to ~7700 Mt of ore with 0.9% Cu, 0.3 kg/t U_3O_8, 0.3 g/t Au and 1.6 g/t Ag (BHP Billiton 2007). The mineralization appears to be the product of mixing of ascending hot magmatic brines (carrying reduced sulphur species) with shallow highly oxidized haematite-forming groundwater leaching uranium and LREE. The source of copper and gold can hardly have been the host granite (Groves & Vielreicher 2001). Mingling of mafic and silicic melt (Clark & Kontak 2004), deep crust (Heinson *et al.* 2006) and fertile mantle enriched by prior subduction (Groves *et al.* 2010, Skirrow *et al.* 2007) may have contributed to the metal endowment. This setting is very different from the Central African Copper Belt (see below). Additional data about Olympic Dam are provided in Section 2.5.12 "Uranium". Olympic Dam is a textbook case of highly successful exploration that was based on the "wrong" geological model.

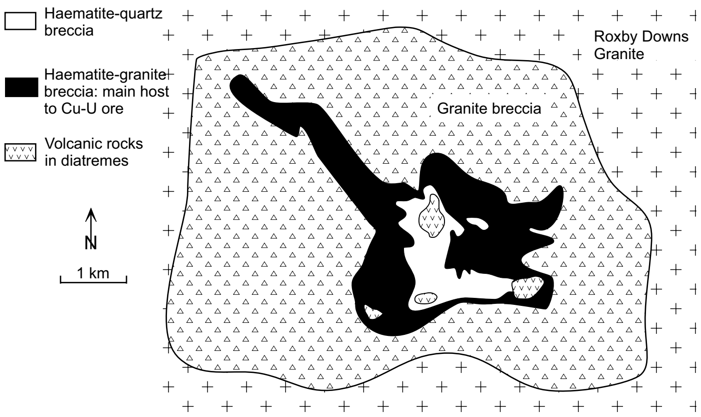
Haematite-quartz breccia
Haematite-granite breccia: main host to Cu-U ore
Volcanic rocks in diatremes
N
1 km
Roxby Downs Granite
Granite breccia

Figure 2.13 Simplified subsurface geological map of the iron oxide copper-gold-uranium deposit Olympic Dam in South Australia, illuminating its origin in a giant complex breccia pipe and diatreme system (modified after Groves & Vielreicher 2001). Note the ore shell surrounding volcanic centres. With kind permission from Springer Science+Business Media.

Cu-Au-deposits of the Cloncurry Type are a subgroup of IOCG-deposits. They derive their name from a district of the Mesoproterozoic Mt Isa copper province in northern Australia (Williams 1998, Pollard 2006, Fisher & Kendrick 2008). The Cloncurry deposits are much smaller than Olympic Dam. Their origin is related to late-tectonic intrusions and saline hydrothermal solutions of mixed origin, including metamorphic fluids (Baker *et al.* 2008). In other IOCG provinces, participation of basinal brines is invoked. Although rather alkaline to subalkaline, the granitoids related to IOCG deposits are petrologically similar to copper porphyry rocks, but hydrothermal alteration is dominantly sodic-calcic. Also characteristic is a strong structural control by major fault systems. Host rocks of ores vary widely. Confirming Clark & Kontak (2004), preliminary Sm-Nd and Re-Os isotope data indicate that fertile (copper-gold rich) IOCG systems display a contribution from mantle-derived source rocks or magmas, whereas "barren" iron oxide apatite ore only carries crustal signatures (Skirrow *et al.* 2007). Iron oxide-copper-gold deposits should be viewed as features of lithospheric scale (Groves *et al.* 2010).

Copper ore deposits of the Cyprus type

Copper ore deposits of the Cyprus type occur in ophiolitic host rocks and have a genetic setting similar to present black smokers (Figure/Plate 1.11) and sulphide mounds. Although common, Cyprus type sulphides have a restricted economic role because deposits are rather small. Copper is named after the island of Cyprus in the Eastern Mediterranean. The Romans called the metal *aes cyprium* and later *cuprum* (metal from Cyprus). Copper extraction on the island was already practised in the 4th millenium BCE and ended with the decline of the Roman Empire at ~500 CE. After rediscovery, industrial operations started in 1921 and eventually, more than 30 cupriferous sulphide orebodies were exploited:

> Pillow lavas of the Troodos ophiolite host all copper orebodies on Cyprus. Most ore is found in the stratigraphic interval between the Lower, hydrothermally altered, and the Upper Pillow Lavas, which are nearly unaltered. Epidote-quartz rocks (epidosites) in the sheeted dykes are thought to mark upflow channels of the hydrothermal fluids (Bettison-Varga *et al.* 1992). From footwall to hanging wall, individual orebodies are zoned as follows: The lowermost expression of hydrothermal processes is the stockwork zone (i) with quartz, pyrite and chalcopyrite in chlorite-quartz rocks. This is overlain by silicified massive sulphide ore (ii) and by the main massive sulphide orebody (iii). There are a number of different ore types, for example "conglomeratic ore" with a matrix of sandy sulphides and "hard compact ore". Both consist of chalcopyrite and traces of sphalerite, but mainly of pyrite, which was formerly used for the production of sulphur. Copper graded 0.3–4.5% and orebodies reached a mass of 50,000 t to 20 Mt. The sulphides are covered by the Ochre Group, goethitic rocks, which have provided pigments since antiquity.

Ochres are clearly different from the darker and browner manganese-iron dominant umber beds of similar use that follow on top of the Upper Pillow Lavas. Both are exhalative precipitates (cf. Chapter 1.3 "Sedex Deposits"). Systematic structural mapping of basaltic dykes and faults suggests genesis of the large sulphide orebodies in fossil rifts near transform faults (Bettison-Varga *et al.* 1992).

Sulphide ore deposits on Cyprus are now depleted, but favourable economic circumstances will certainly result in new finds. The same applies to metamorphic sulphides in the Scandinavian Caledonides, some of which are of the Cyprus type (e.g. Joma, Figure 1.80):

The mining district of Outokumpu in Finland is both economically important and scientifically interesting. From 1910 to 1988, three mines of the district produced a total of ca. 50 Mt of ore averaging 2.8% Cu, 1% Zn and 0.2% Co, with minor amounts of Ni, Ag and Au. In this region, large bodies of serpentinites occur within micaceous gneisses of the Palaeoproterozoic Svekokarelide thrust belt. The serpentinites are thought to be parts of ophiolites, although uncommon ones because basaltic crust is missing. They probably originated as depleted ultramafic mantle rocks exposed on the ocean floor ("Hess Crust"). In this setting, black smoker-related hydrothermal activity produced sulphide ores and non-sulphide exhalites. Typical host rocks of ore (the "Outokumpu Association") include talc-carbonate fels (CO_2-metasomatites), metamorphic skarn, finely laminated quartzite (former exhalite) and black shales (cf. Talvivaara, Nickel). High-grade Cu-Co ore occurred preferentially within the quartzites. The massive sulphide orebody at Outokumpu had a length of 4000 m, a width of 400 m and an average thickness of 10 m. The genetic model of these ores is, of course, not a simple Cyprus type. Its hydrothermal ocean floor setting, however, places it firmly into this family, even if some features remain equivocal (Peltonen *et al.* 2008).

Volcanic-hosted massive sulphide (VMS) deposits

Volcanic-hosted massive sulphide (VMS) deposits are a highly diversified group. Although the attribution is only partially correct (see below), the giant sulphide ore province of the Iberian Pyrite Belt is commonly included in this class. The belt has a length of more than 250 km, from Sevilla in southern Spain to Portugal. Host rocks are part of the southern margin of the Variscan Orogen, comprising a basement of over 2000 m of siliciclastic sediments (phyllites and quartzites), which is overlain by 50–1300 m of bimodal volcanic, sedimentary and rarely plutonic rocks of the Volcano-Sedimentary Complex (Late Devonian to Early Carboniferous) and Viséan to Late Carboniferous flysch (up to 3000 m of greywacke, shale and conglomerates in Culm deepwater facies). During collisional welding of Africa with Iberia in the Westphalian when Pangaea was finally assembled, the belt was deformed by southward thrusting and folding. Metamorphism is of very low to low grade:

More than 80 former and operating mines are known. The deposits form a southern and a northern belt that have contrasting geological settings. In the south, shale-hosted stratiform orebodies are characteristic (e.g. Tharsis, Aznalcollar), whereas in the north, the orebodies are mainly hosted by dacitic or rhyolitic domes, sills and pyroclastic rocks (parts of Rio Tinto, La Zarza, Aljustrel: Tornos 2006, and in the west: Neves Corvo, Relvas *et al.* 2006) and ore formation is clearly synvolcanic.

Until today, ~280 Mt of ore with an average grade of 46% S, 0.7% Cu, 4% Pb + Zn, 30 g/t Ag and 0.8 g/t Au have been extracted in the Iberian Pyrite belt. Total sulphide resources probably reach 2500 Mt. Only one deposit (Rio Tinto) surpasses 500 Mt. This is the world's largest province of massive sulphide ore and a unique concentration of supergiant VMS deposits. The ore paragenesis comprises mainly pyrite, minor chalcopyrite, sphalerite and galena, and traces of arsenopyrite, pyrrhotite, tetrahedrite, Pb-sulphosalts and cassiterite. Gangue minerals are silicates of host rocks and hydrothermal precipitates such as chlorite precursors. Barite and gypsum are rare. Orebodies occur commonly near eruptive centres, either in dark shale/phyllite or in pyroclastic rocks. Shale-hosted orebodies consist mainly of massive and structureless fine-grained pyrite with low base metal and gold content, and of banded and brecciated parts that were formed by debris flows. Several of the massive sulphide bodies contain a significant proportion of siderite. Hydrothermal alteration and stockwork ores are confined to footwall rocks. Manganese-rich jasper in "purple shale" above the sulphide deposits was used for exploration and produced many high-grade supergene Mn ore deposits. Orebodies in volcanic rocks are discordant and replacive, and may be totally enveloped by hydrothermal alteration (silica, chlorite, sericite). The sulphides are medium to coarse-grained and include remnants of altered host rocks. Base metal and gold contents are clearly higher than in the shale-hosted ores. In addition, oxidized facies as well as barite-rich ores are known. Hydrothermal refining, metal zonation (Cu-Zn-Pb), footwall stockworks (with Cu, Zn, Ag and Au, and traces of As, Co, Bi) and breccias are ubiquitous. Sulphur isotope δ^{34}S data ranging from −34 to +21‰ indicate diverse sources of sulphide sulphur, including basement, sedimentary and volcanic host rocks, and reduced seawater sulphur. Microbial reduction of sulphate in a confined system is thought to explain the most negative values (Tornos 2006). The ore forming fluids were saline brines with 3–12 wt.% NaCl equivalent. In spite of intensive research, their origin remains ambiguous. Interpretations range from modified seawater to magmatic derivation (Solomon *et al.* 2002).

The shale-hosted orebodies were formed by exhalation into brine pools, whereas the replacive, volcanic-hosted massive sulphides were precipitated well below the seafloor, in reactive rocks with high permeability. Considering the size of the orebodies, the hydrothermal systems must have reached deep into the basement, possibly driven by deep intrusions. There is a general agreement that extensional tectonics had an essential role (ensialic rifting, pull-apart basins). The basement may have been the source of both fluids and metals (Tornos 2006, Blundell *et al.* 2005).

A number of near-surface orebodies had well-developed gossans with important gold content and rich zones of secondary enrichment which are, however, long exhausted.

The largest Pyrite Belt deposits are Rio Tinto, Tharsis, Aznalcollar and the latest large discovery, Neves Corvo in Portugal. The latter is remarkable because of higher base metal grades including favourable tin contents. The deposit comprises >300 Mt of resources, with 100 Mt of ore at 3.46% Cu, 3.54% Zn, 0.25% Sn, 0.8% Pb and 55 g/t Ag (Relvas *et al.* 2006). Direct host rocks to ore include rhyolitic to rhyodacitic volcanic rocks. An early stage of stringer and massive cassiterite mineralization, some of which formed by direct venting onto the sea floor, was followed by the main stage generation of stratabound massive sulphide ore. Relvas *et al.* (2006) propose that the tin-rich fluids were of magmatic derivation, possibly from a tin granite intruding at depth. The discovery of the five orebodies at Neves Corvo, which are covered by 200–700 m of barren rock, was a highlight of modern exploration methods, in this case a combination of geological mapping and deduction confirmed by regional gravimetric surveys.

Sedimentary-exhalative (sedex) copper ore deposits

Sedimentary-exhalative (sedex) copper ore deposits are here exemplified by reference to the venerable Rammelsberg mine at Goslar, Harz Mountains, Germany. The mine was closed in 1988 after a history of more than 1000 years of exploitation. The orebody occupied a stratigraphic level in the Mid-Devonian Wissenbach Formation, a thick black shale unit with rare felsic tuff bands. Its location is controlled by a synsedimentary fault that separates shale of <150 m thickness from a basinal facies of >1000 m. Several basalt sills occur in the basin a few kilometres distant from the orebody. Variscan orogenic deformation folded the ore lens into an isoclinal, NW-vergent synform (Figure/Plate 1.81). The total ore mass before mining was ~27 Mt with a metal content of 7 Mt (mainly zinc, lead and copper, plus some silver and gold). Gangue included shale, barite, dolomite and ankerite. In the last years before closure, ore graded 19% Zn, 9% Pb, 1% Cu, 160 ppm Ag and 1.2 ppm Au. Shale-banded and laminated ore with synsedimentary deformation structures was prominent (Figure/Plate 1.72). The diagenetic grade of the rocks is within anthracite stability, with some excursions into the graphite field. The ore is strongly recrystallized and locally mobilized. In the footwall, intense silicification of the shale and a stockwork of quartz veinlets with sulphides ("kniest") are thought to mark upflow channels of the submarine hydrothermal system (Muchez & Stassen 2006):

> The stratiform ore bed of the Rammelsberg mine displayed the characteristic vertical ore stratification of sedex deposits: Mineralization sets in with pyrite (i), followed by spotted copper-rich pyrite-chalcopyrite ore (ii), sphalerite and galena (iii), and barite (iv). Transitional ore interbedded or mixed with shale extends laterally and into the hanging wall. Tectonic deformation at Rammelsberg is very intensive; a reconstruction of the orebody's original shape remains conjectural. It may have been elliptical with a long axis of ~1000 m and a thickness of 10–30 m. Observations and data confirm its formation by synsedimentary exhalation of ~300 °C hydrothermal solutions (Large & Walcher 1999). Considering the distal occurrence of synchronous mafic and felsic volcanism, a magma-related heat anomaly at depth can neither be excluded nor confirmed. Figure 1.71 is a tentative illustration of the genetic setting of the Rammelsberg deposit.

Stratabound and/or stratiform sediment-hosted copper deposits

Stratabound and/or stratiform sediment-hosted copper deposits contain large copper resources second only to copper porphyries. Today, most deposits of this class are considered to be of diagenetic origin. Examples include the European Copper Shale (cf. Chapter 1.4 "Diagenetic Ore Formation Systems"), the White Pine District in Michigan and the Central African Copper Belt:

> The White Pine mining district's setting is a Mesoproterozoic rift (1.3–1.0 Ga) with a fill of thick tholeiitic olivine basalt, some andesite and rhyolite, and a transgressive sedimentary cover series. Across a very large area, mineralization is concentrated at the base of the marine Nonesuch Shale and underlying conglomerates flanking an older volcanic massif. The ore bed is siltstone with an average thickness of 5 m and a grade of 1.1% Cu. Stratabound ore contains chalcocite, different from native copper lodes that are hosted in flood basalts of the same region. The stratiform ore is associated with diagenetic dewatering of fluviatile-volcanoclastic rocks of the early graben fill (Swenson & Person 2000). The native copper lodes of the Keweenaw Peninsula on Lake Superior formed ~20–35 Ma later, possibly from hybrid evolved meteoric-metamorphogenic fluids (Brown 2006). Native copper (and silver) accompanied by calcite, chlorite, quartz, epidote and zeolites fill open spaces in basalt flow tops and conglomerates. The district produced more than 6 Mt of copper.

The world's largest province of stratabound copper ore is the Central African Copper Belt of DR Congo and Zambia. Its historic production amounts to >1000 Mt of ore with ~2.7% Cu and by-product Co, but also Ni, Au, Ag, U, Pb, Zn and PGE. It is estimated that more than 190 Mt copper and 8 Mt cobalt remain to be exploited. Both primary sulphides and spectacularly enriched bodies of oxide, carbonate and secondary sulphide ore were extracted:

> Ore deposits occur mainly near the base of Neoproterozoic sediments of the Katanga Supergroup. This succession of dolomitic shales, dolomites, siltstones, sandstones and arkoses reaches a thickness of 11 km. Its basal part is the Roan Group with the Mines Subgroup, which hosts most ore. With an age of <900 Ma, the Roan represents post-tectonic rift and molasse sedimentation of the Kibara orogen grading into sediments of a passive continental margin that developed by extensional break-up of Supercontinent Rodinia. The fragments were rewelded by the main Pan-African orogeny peaking between 570 and 530 Ma, during which the Congo-Tanzania, Kalahari, East Antarctica and India Cratons assembled to form Gondwana. In the Mines suite, anhydrite and dolomitic-magnesitic carbonates are evidence of former extensive evaporite horizons. Similar to the European Rotliegend and the Zechstein salts (cf. Chapter 1.4 "European Copper Shale"), these sediments illustrate the transition from terrestrial settings with playa lakes to coastal sabkhas and shallow-marine conditions. The top of the Roan is capped by the glaciogenic "Grand Conglomérat", a tillite that may be the product of one of the "Snowball Earth" events at ~760 Ma (Hoffmann 1998). The Roan is overlain by marine sandstones, shales and carbonates of the Nguba and Kundelungu Groups. Orogenic deformation (locally called the Lufilian orogeny) terminated sedimentation and created a large orogenic belt (Lufilian Arc) that is characterized by outward vergent folds and nappes. Metamorphic grade increases towards the centre of the orogen, where amphibolite facies with sporadic eclogites is attained and basement windows are ubiquitous.

The Katanga basin formed by rifting and crustal extension that created a wide ocean. This favoured voluminous mafic magmatism; felsic magmatic rocks are less common. Towards the north-northeast, a little deformed failed rift branches off extending to Lake Victoria (the Kundelungu aulacogen). In this region north of the Lufilian arcs, rare mineral deposits are epigenetic and fault-bound (Haest *et al.* 2007).

Copper Belt ore (bornite, chalcopyrite, chalcocite, carollite) is mostly stratabound and hosted in all rocks forming the Mines Subgroup (carbonates, evaporites, sandstones). However, the sandy dark "ore shales" attracted special attention as an easily recognizable lithostratigraphic level. Much of the sulphide ore replaces anhydrite nodules and lenses, together with dolomite and authigenic quartz (Muchez *et al.* 2008). The stratigraphical control of mineralization in single districts is pronounced but varies with greater distance. Some deposits follow a structural control and consequently, have an epigenetic character (e.g. Kipushi). Similar to the European Copper Shale, basin margins adjacent to palaeogeographical highs are preferred sites of ore formation. Deep basinal areas are barren.

The evolution of genetic thinking about Copper Belt metallogeny was last described by Sweeny *et al.* (1991). Syngenetic hypotheses proposed that metals were derived by weathering from emerged areas and concentrated in near-coastal marine sediments. Precipitation would have taken place by reduction in sabkhas or in marginal basins. However, age determinations and structural studies imply more diversity, from pre- to post-orogenic (Torrealday *et al.* 2000). Therefore at present, epigenetic hypotheses are preferred: Metals were transported by oxidized saline formation waters or metamorphic fluids mobilized by diagenesis and metamorphism in the deep basin. Orogeny, or deep mafic intrusions may have provided the necessary driving force (McGowan *et al.* 2003, McGowan *et al.* 2006). The metals were leached from deeply buried sediments and magmatic rocks. This is more plausible than a surficial source considering that Cu, Co and Pt characterize mafic source rocks. The near-surface reducing environment may have been induced by one of the "Snowball Earth" events, by microbial sulphate reduction based on organic matter, or by thermochemical sulphate reduction of methane in suitable traps (Figure 2.14).

Retrograde-metamorphogenic, saline brine-related deposits

The Cu-Pb-Zn-Ag district of Mt Isa in Queensland, Australia is both economically outstanding and scientifically intriguing. Mt Isa is the largest of four supergiant Pb-Zn ± Cu deposits in the region. It occurs within a block of 4.5 km length, 250 m width and 1000 m depth. The estimated total ore content reaches 200 Mt at 3% Cu and 100 Mt at 7% Pb, 6% Zn and 160 ppm Ag (production since 1932 plus remaining reserves). In the year 2000,

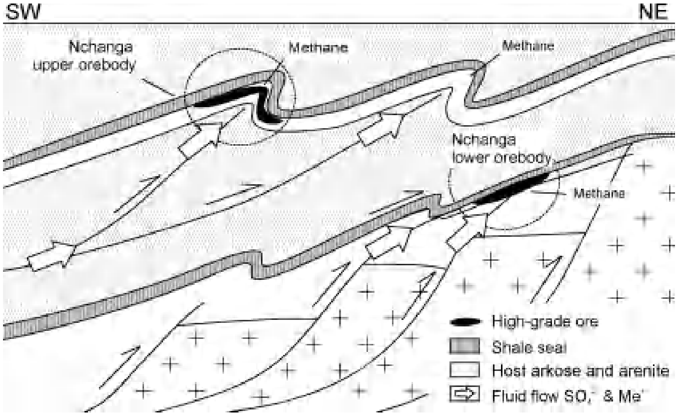

Figure 2.14 Genetic model of the Nchanga copper-cobalt deposits in the Zambian Copperbelt (modified from McGowan *et al.* 2003, 2006). With kind permission from Springer Science+Business Media. Upflowing oxidized, sulphate-rich, basinal fluids (with Cu and Co) are focused by permeable beds and tectonic structures. Low-permeability metapelites above sandstones form traps that probably contained methane. Methane reacting with sulphate of the fluids formed H_2S (thermochemical sulphate reduction), precipitating the metals.

the youngest mine in the district, Enterprise, started operations, based on ore with 4% Cu to a depth of 1800 m:

> Mt Isa district is located in a Palaeo-Mesoproterozoic back arc system that experienced later orogenic deformation (Williams 1998), similar to McArthur River and Broken Hill (cf. section "Lead and Zinc"). At Mt Isa mine, very low-grade metamorphic evaporitic-clastic sediments (deposited at ~1680–1590 Ma) overly a thick mafic volcanic succession. A narrow synform of the sediments was downthrown by a regional fault relative to amphibolite facies basement. Orebodies are stratabound within the Urquhart Shale, a black banded dolomitic marlstone. At depth, the shale abuts tectonically against greenschist facies meta-basalts (Paroo fault, Figure 2.15). Hydrothermal alteration of the basalts is characterized by epidote, Mg-chlorite and rutile. Above the fault, hydrothermal alteration of the Urquhart Shale is pervasive. The resulting coarsely crystalline and brecciated rock consists mainly of Fe-dolomite and quartz ("silica dolomite"). Copper orebodies occur in the form of vein stockworks, massive lenses, and irregular replacement bodies, and cluster near the basal fault (proximal) in extremely silicified rock. The paragenesis includes pyrite, chalcopyrite and pyrrhotite, and minor sulphides and sulphosalts of Ag, As, Zn, Pb and Co. The hydrothermally altered and mineralized body has a length of 2.6 km and a width of 530 m. Before mining, it contained ~20 Mt of copper. All copper ore is enveloped by coarsely crystalline silica dolomite.

The origin of this deposit is undoubtedly due to exceptionally large hydrothermal systems. A plausible syngenetic-synsedimentary model assumed synchronous formation of copper and lead-zinc ores in a sedex-like submarine setting (Finlow-Bates & Stumpfl 1979). This would explain the separation of the metals, because copper typically precipitates within the sub-seafloor feeder zone, whereas lead and zinc remain in solution until

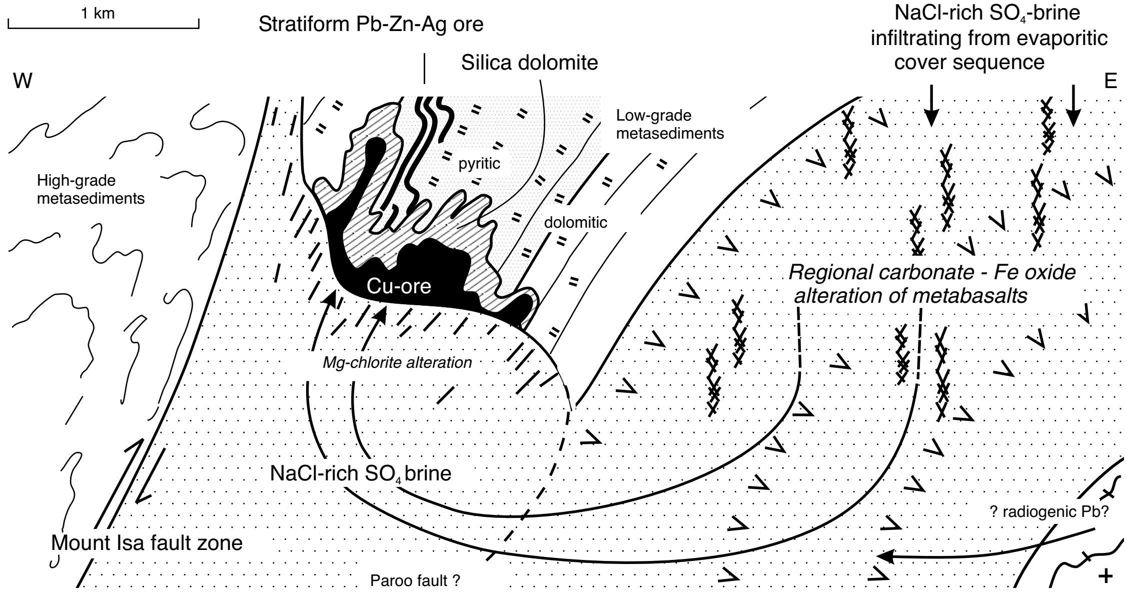
1 km
Stratiform Pb-Zn-Ag ore
Silica dolomite
NaCl-rich SO_4-brine infiltrating from evaporitic cover sequence
W
E
Low-grade metasediments
pyritic
dolomitic
High-grade metasediments
Cu-ore
Regional carbonate - Fe oxide alteration of metabasalts
Mg-chlorite alteration
NaCl-rich SO_4 brine
? radiogenic Pb?
Mount Isa fault zone
Paroo fault ?
+

Figure 2.15 Retrograde-metamorphogenic formation of copper ore at Mt Isa, Queensland, Australia. After Heinrich, C.A., Andrew, A.S. & Knill, M.D. 2000, Society of Economic Geologists, Inc., *Reviews in Economic Geology* Vol. 11, Figure 5 p. 105. Convecting oxidized evaporitic brines leached copper from greenschist-metamorphic continental tholeiites. Precipitation was induced by mixing with reduced, sulphur-rich fluids (not shown).

venting on the seafloor, resulting in stratiform syngenetic ore. Lead isotope model ages of ore at 1653 Ma, alteration of footwall basalts, and high Br/Cl-ratios of fluids indicating an evaporitic origin conform to this model. However, fluids in silica dolomite were trapped at >300 °C and at pressures of 1–2 kbar. This is hardly compatible with a syngenetic sedex setting. Doubts were confirmed by structural analyses of ore control and by $^{40}Ar/^{39}Ar$ ages of hydrothermal phyllosilicates. The new data suggest a late orogenic retrograde-metamorphogenic formation of the copper orebodies independent of the syngenetic lead-zinc-silver ores (Figure 2.15; Heinrich *et al.* 2000; Betts *et al.* 2003, Chapman 2004). Oxidized, sulphur-rich brines extracted copper from the underlying meta-basalts (Gregory *et al.* 2008). Davis (2004) provides structural arguments that imply a late orogenic origin of all ores at Mt Isa, by demonstrating that the overall geometries of both copper orebodies and of high-grade shoots in the Zn-Pb-Ag orebodies are controlled by F4-folds. The implication is that copper and lead-zinc were formed synchronously by the same processes. It can hardly be expected, however, that this is the final word on the formation of the giant metal concentrations at Mt Isa.

Exploration for copper is a multi-technology undertaking based on the whole spectrum of geological, geochemical and geophysical methods (Sillitoe 1995). The search is assisted by indicator minerals in soil, till and stream sediments. Copper porphyries, for example, shed native gold, rutile, tourmaline, garnet, jarosite and alunite (McClenaghan, 2005). Land-based targets are preferably world-class, low-cost potential mines. In the past but also quite recently, successful exploration for copper porphyries was based on the recognition that small high-grade fringe mineralization and alteration point to porphyry ore (Cadia district, N.S.W.; Wilson *et al.* 2003). Exhalative seafloor copper-gold deposits are seriously investigated for submarine mining off Papua New Guinea and New Zealand.

In 2008, world mine production of copper contained in concentrate was 15.4 Mt (in 2009 15.8 Mt), with the major share provided by Chile, USA, Peru, China and Australia. Large resources are available, both on land (3000 Mt) and on the sea floor (manganese nodules: 700 Mt). Land-based resources comprise mainly porphyry (50%) and sediment-hosted deposits (30%). In recent years, the combination of volatile prices, low demand growth, large reserves and surplus mine production capacity combined to make the copper market highly competitive.

2.2.2 Lead and zinc

Common Ore Minerals:

		Max. wt.%	*Density (g/cm^3)*
Galena	PbS	86 Pb	7.5
Cerussite	$PbCO_3$	77	6.5
Anglesite	$PbSO_4$	68	6.3
Sphalerite	ZnS	38–67 Zn	3.9–4.1
Smithsonite	$ZnCO_3$	52	4.4
Hemimorphite	$Zn_4(OH)_2Si_2O_7.H_2O$	54	3.5
Willemite	Zn_2SiO_4	58.5	3.9–4.2

There are few ore deposits that contain only lead or zinc. Most mines are sources of both metals. Therefore it appears rational to discuss their metallogeny combined in one chapter.

Galena is the most important lead ore mineral. Also, it is a common source of silver, with contents from 0.01 to >1% Ag. Silver substitutes for lead in the crystal lattice or forms minute inclusions of silver minerals such as acanthite and tetrahedrite. Microscopic intergrowths are also responsible for traces of As, Sb, Zn, Cd, Bi, Fe and Cu in galena. Sphalerite may contain more than 25% Fe in its lattice, as well as Mn and Cd (up to 5%) in solid solution, and In, Ga, Ge, Tl, As, Se and Hg (Labrenz *et al.* 2000). In fact, sphalerite is the most important source of cadmium, indium, gallium, and germanium (cf. "By-Product Electronic Metals"). Cu, Sn, Ag, Pb and Au in sphalerite are commonly sited in micro-inclusions. The botryoidal finely banded variety of sphalerite that resembles agate consists of both cubic and hexagonal ZnS (wurtzite). Calamine is a miners' name for supergene non-sulphide zinc ore, including

Table 2.1 Properties of lead and zinc metal

	Density	Melting Point	Boiling Point	Remarks
Lead	11.3	327 °C	1740 °C	Corrosion resistant, soft, and ductile
Zinc	7.1	419 °C	907 °C	Corrosion resistant

smithsonite and hemimorphite. Willemite is the typical ore mineral of non-sulphide hydrothermal replacement and vein deposits.

Lowest exploitable grades of lead and zinc ore vary between 6 to 10% of combined metal content. Zinc-rich ores are preferred because the markets value zinc higher than lead.

Whereas lead was already known and used in prehistoric times, production and use of pure zinc metal is a discovery of the industrial age (Table 2.1). Brass, the alloy of copper and zinc, was common in ancient Rome. Today, the key market for Pb is the lead-acid battery for vehicles and for industrial use (85%), followed by paint, glass (e.g. computer screens), various implementations for radiation and noise protection, and ammunition. For humans, lead is extremely neurotoxic and children are especially vulnerable (Plant *et al.* 2005, Troesken 2006). Therefore, its use is tightly regulated. Lead has been phased out as an additive to gasoline, paint and water pipes. Tin-lead alloy solders used in the electronics industry are to be replaced by Sn-Ag-Cu. Todays' urban dust contains a dangerous heritage of earlier use in gasoline (Filipelli *et al.* 2005).

About 50% of total zinc supply is consumed as a protective anticorrosion cover for steel in the construction, automotive and appliances sectors. It is also an ingredient of many alloys including brass (Cu-Zn), of paints and chemicals. A new application is the Ni-Zn battery that is expected to replace Ni-Cd in order to reduce consumption of extremely toxic cadmium (Fergusson 1990, Selinus *et al.* 2005). Cadmium is rapidly becoming a burden for zinc mines because the market cannot absorb the coproduced quantities. For humans, animals and plants, zinc is an essential element (Lindh 2005). More than 300 zinc metallo-enzymes are needed for life functions. One of them is alcohol dehydrogenase that is man's primary defence against intoxication. Zinc is also involved in genetic stability and gene expression, and for proper functioning of the immune system. Zinc deficiency endangers life as much as overdoses of zinc chemicals.

Geochemistry

Among the common metals, lead is a curious exception because most lead is the product of radioactive decay of lithophile uranium and thorium. Radiogenic lead isotopes are fundamental for age dating and for tracing the origin of metal concentrations (cf. Chapter 1.1 "Isotope Geochemistry"; "Uranium"). Following U and Th, chalcophile lead is enriched in felsic magmatic rocks: Mid-ocean ridge basalts have ~2, gabbros 5 and granites 20 ppm (mainly sited in K-feldspar). In rock-forming minerals, Pb^{2+} substitutes for K^+, Na^+, Ca^{2+}, Sr^{2+} and Ba^{2+}. Similar to lead, zinc is chalcophile with a lithophile tendency. Bivalent zinc, however, substitutes strongly for Fe^{2+} and Mn^{2+} resulting in higher zinc contents in basalts (100 ppm) compared to felsic magmatic rocks (40 ppm). Crustal abundance range estimates are 12–20 ppm Pb and 40–200 Zn (Smith & Huyck 1999).

In hydrothermal fluids, lead and zinc rarely occur as simple ions (Pb^{2+}, Zn^{2+}) but are typically complexed with either chloride or bisulphide ligands. Metal-chloride complexes are favoured by elevated salinities and oxidation. At low salinity and <300 °C, $Zn(OH)^+$ und $PbCO_3{}^0$ are possible metal carriers, above this temperature $Zn(HS)_2{}^0$ and $Pb(HS)_2{}^0$. Precipitation mechanisms depend on the nature of the fluids. Common causes are pH-change, cooling, dilution or mixing with other fluids especially those carrying reduced sulphur. Where barite gangue is present, the fluids must have been reduced and acidic because these conditions determine solubility of barium. If barite is absent, oxidized, neutral to alkaline solutions may have formed lead-zinc ore. At low temperatures, precipitation of dissolved zinc by sulphate-reducing microbes seems to be common, often accompanied by dolomitization (Labrenz *et al.* 2000, Vasconselos & McKenzie 2000). High fO_2/fS_2 conditions at temperatures exceeding 150° C (e.g. mixing of hypogene with meteoric waters) favour the precipitation of the non-sulphide zinc ore willemite (Brugger *et al.* 2003).

Under conditions of supergene alteration, galena is more stable than sphalerite, because a thin film of nearly insoluble lead minerals (cerussite and anglesite) quickly develops on all exposed surfaces. Therefore, galena embedded in zinc carbonate is a common observation. In oxidized parts of a sulphide orebody cerussite and anglesite are retained (e.g. Magellan Mine, Western Australia), whereas zinc is more mobile. Downward and lateral displacement by meteoric water flow is characteristic (e.g. Skorpion, Namibia: Borg *et al.* 2003). Some zinc may remain in the cap as "red calamine" but most is dissolved and reprecipitated as "white calamine". This process results in secondary orebodies of the "non-sulphide zinc type" that are economically attractive because the metal can be extracted by low-cost leaching (Large 2001). The formation of secondary zinc-enriched sulphide ores by sulphate-reducing microbes is infrequent (Bawden *et al.* 2003). In geochemical exploration, the higher mobility of zinc in near-surface environment tends to cause wider dispersion halos compared to lead.

Lead and zinc ore deposit types

Lead and zinc ore deposits occur in most genetic groups, although with the notable exception of the orthomagmatic environment. Economically more prominent types include:

- sedimentary-exhalative (sedex), syngenetic-hydrothermal deposits (Rammelsberg: cf. "Copper"; Pb-Zn-Ag ore at Mt Isa);
- diagenetic stratabound, epigenetic, low-temperature hydrothermal ore deposits in carbonates (Mississippi Valley, Irish and Alpine types; salt-diapir-bound and deposits of migrating saline brines; Kipushi in the Central African Copper Belt);
- diagenetic stratabound, epigenetic, low-temperature hydrothermal deposits in siliciclastic sediments (Jinding, Laisvall);
- volcanogenic deposits (Cyprus type Zn only; Kuroko type, Iberian Pyrite Belt: cf. section "Copper");
- contact-metasomatic (high-temperature hydrothermal) and skarn deposits (Bajiazi, China, cf. "Silver");
- vein deposits in various genetic settings (Harz Mountains, Schwarzwald);
- surficial alteration produces *in situ* oxidized lead ore, and transposed secondary zinc orebodies.

Sediment-hosted, submarine-exhalative base metal (sedex) deposits

Sediment-hosted, submarine-exhalative base metal (sedex) deposits, also called clastic-dominated Pb-Zn (Leach *et al.* 2010) were introduced earlier (cf. Chapter 1.3 "Sedimentary Ore Formation Systems", "Copper"). An interesting aspect is the variable metal endowment, such as Zn-Pb-Cu-Ag at Rammelsberg, Germany, but only Zn-Pb-Ag at Mt Isa and Broken Hill/Australia, and Zn-Pb-Ag with a giant mass of barite in the Red Dog district, Alaska (Figure 1.73). Possible explanations of this observation include different availability in source rocks, chemical variables of rocks and fluids, and precipitation mechanisms. For individual deposits, precise understanding of these aspects is rather the exception. Host rocks are commonly carbonaceous shales:

> Lead-zinc-silver orebodies at Mt Isa in Queensland, Australia are stratiform and stratabound within Urquhart shale outside of, but near the huge hydrothermal alteration enveloping copper orebodies. The Pb-Zn-Ag ore is a banded and laminated rock exhibiting synsedimentary soft-sediment deformation. Ore bands consist of galena, sphalerite, pyrite and pyrrhotite, with a thickness from 1 mm to 1 m. Stratigraphical dispersion of ore reaches a thickness >1000 m and a distance of 800 m from the silica dolomite. Lead and silver grades are highest proximal to silica dolomite, whereas highest zinc grades occur more distally. For genetic hypotheses and more details refer to Section 2.2.1 "Copper" (Figure 2.15).

> Before mining, the giant zinc-lead-silver deposit at Broken Hill in New South Wales, Australia held a total of ~200 Mt of ore with the fabulous grade of 25% Pb + Zn. Broken Hill occurs within Palaeoproterozoic crystalline rocks of the Willyama Block, which were

folded and metamorphosed to granulite facies at ~1600 Ma. Peak metamorphic conditions attained 800 °C and 5 kbar (Page *et al.* 2005). At Broken Hill, "Mine Sequence" rocks appear to form an anticline with hanging-wall gneiss on either flank. The mine sequence comprises granite gneiss, amphibolite, Potosi gneiss (probably felsic metavolcanics), banded iron formations with high trace contents of Pb, Zn, Mn and P, siliceous exhalites, sillimanite gneiss (a metapelite, or a hydrothermal alteration rock) and the lode horizon with sulphide orebodies. Characteristic rocks of the lode horizon include Mn-rich garnetite and quartz garnetite, bands of blue quartz with gahnite ($ZnAl_2O_4$) and stratiform pegmatites with green feldspars that contain up to 1% Pb. Granulite facies metamorphism affected all these rocks and the ore. Therefore, Broken Hill is the most famous object for studies of the effects of high-grade metamorphism on sulphide ore. Partial melting of the main base metal sulphide body resulted in a moderately mobile sulphide melt, which was relatively enriched in Cu, Sb, As, Ag, Ni and Au (Mavrogenes *et al.* 2001, Sparks & Mavrogenes 2005). Mobilized sulphides intruded host rocks as far as 100 m from the ore horizon.

Broken Hill ore minerals comprise galena and Fe-rich sphalerite, silver ore minerals, pyrrhotite, chalcopyrite and arsenopyrite. Gangue includes quartz, calcite, Ca-Fe-Mn silicates, garnet, fluorite, gahnite and wollastonite. Individual orebodies have distinct parageneses; "zinc lodes", for example, consist mainly of sphalerite. Age determinations confirm formation of the ore at the same time as immediate host rocks (ca. 1690 Ma: Page *et al.* 2005). Lode horizon rocks and orebodies are metamorphosed sediments that resulted from submarine hydrothermal (sedex) processes. The lithostratigraphic sequence is inverted and the feeder zone to the system has been located (Groves *et al.* 2008). Possibly, part of the ores formed by replacement below the sea floor, while exhalites precipitated above (Parr *et al.* 2004). The nature of the sediments and the bimodal volcanism preceding ore formation suggest an ensialic rift or back arc setting. Syngenetic heat pulses may have mobilized fluids. Playa lake evaporites influenced the evolution of sediments and mineralization (Cook & Ashley 1992).

Low-temperature hydrothermal, carbonate hosted, diagenetic lead-zinc ore deposits

Low-temperature hydrothermal, carbonate hosted, diagenetic lead-zinc ore deposits include a number of different types that have nevertheless many common features. The majority of these deposits are of Palaeozoic-Mesozoic age and occur in little-deformed marine platform carbonates. Ore formation is controlled by palaeogeographic factors, by certain lithological horizons and by faulting. Nature and shape of orebodies are quite variable and include stratiform lenses, veins, breccias, cave fill and metasomatic replacement. The paragenesis is simple, most ores displaying only galena, sphalerite and a carbonate gangue, occasionally with other accessory minerals. Host rocks are dolomitized or silicified ("jasperoid"). Sulphur isotopes indicate derivation of sulphur from seawater sulphate, usually by microbial reduction (refer to Chapter 1.3 "Sedimentary Ore Formation Systems"). A common feature is the absence of igneous activity that might be an agent of mineralization. Positive traits include: i) that weathering may have produced valuable calamine orebodies; and ii) the absence of acid mine drainage (AMD), because both host and gangue carbonates buffer incipient acidity. As a result, the risk of downstream heavy metal contamination is considerably reduced. Economically important provinces or districts gave rise to terms that designate different settings and genetic variations:

Mississippi Valley Type (MVT) deposits were introduced in Chapter 1.4 "Diagenetic Ore Formation Systems" (Figure 1.77). They result from basinal brines that leach metals from sediments and migrate to basin margins where ore is precipitated. Permeable rocks and structures focus fluid flow and exert detailed control on orebody location. Frequent sites of metal precipitation are dissolution cavities that resemble karst pipes. Cave ores in the Triassic limestone of Silesia (Poland) demonstrate synchronous mineralization and cave formation (Heijlen *et al.* 2003, Figure 1.58). This may be due to limestone dissolution caused by sulphide precipitation (eq. 1.21). Mining in some of the US namesake districts has been terminated and today, environmental remediation programmes are carried out.

Alpine Type deposits occur in the Southern Alps, in the border region between Austria, Italy and Slovenia. Orebodies and mineralization are always found in karstifiable Mid- to Late Triassic marine limestone, although the precise stratigraphical level varies. Orebodies occupy veins, hydrothermal karst

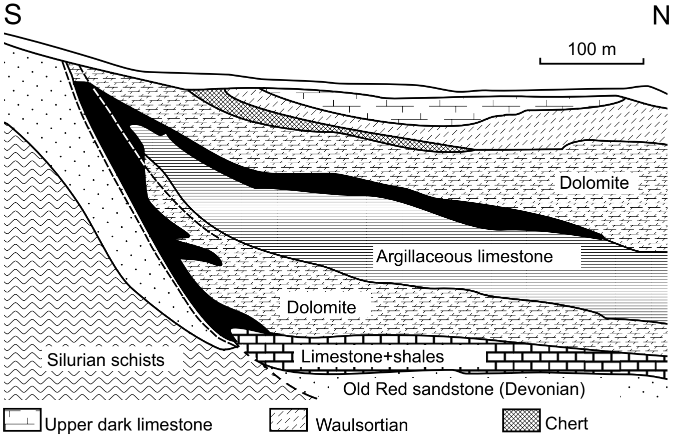

Figure 2.16 Geological profile of the Zn-Pb-Ag deposit Silvermines, Ireland, with cross-cutting fault-controlled and stratabound orebodies in Early Carboniferous lime- and marlstone (modified from Johnston 1999). Orebodies of sulphides and barite in black; "Waulsortian" is a local term for stromatolitic reef limestone.

caves (Figure 1.60, Figure/Plate 1.76) and bedding planes. Sulphide ores display the same age as ordinary host sediments (Schroll *et al.* 2006). An essentially sub-seafloor epigenetic-hydrothermal origin during the Triassic with occasional exhalation of solutions on the seafloor unifies present understanding. There is a connection between tectonic stretching of a marine platform, deep convection of seawater along resulting faults and probably, elevated heat-flow from the mantle. The latter is confirmed by distal mafic volcanism and intrusive processes. The overall geodynamic setting is early distension of the Supercontinent Pangaea initiating its break-up. After a long and profitable mining history, resources of Alpine deposits appear to be exhausted.

Irish Type deposits are so-called because of a cluster of mines and mineralizations in Central Ireland. Deposits are controlled by faults (Figure 2.16) that distended an Early Carboniferous marine carbonate platform together with its basement of Devonian (Old Red) sandstone and Early Palaeozoic metamorphic rocks. The structures facilitated establishment of hydrothermal convection systems, which gradually reached down into Precambrian basement (Figure 2.17). Deepening with time can be deduced from Pb and Sr (Wilkinson *et al.* 2005) isotope data. Sulphur isotopic data indicate microbial seawater sulphate reduction as the source of sulphide sulphur. Fallick *et al.* (2001) summarize the situation briefly by "no bacteria, no giant ore deposit". Ore formed by mixing of shallow waters with deeply circulating seawater-derived evaporative brines with 8–19% salinity and T ~130–240 °C (Wilkinson 2010, Wilkinson *et al.* 2005). Orebodies display variable ratios of Zn-Pb-Ag-Cu sulphides and barite. Some are exhalative-sedimentary, such as the concordant ore in Silvermines (Boyce *et al.* 2003, Figure 2.16), but the majority are epigenetic vein and breccia ores that formed hundreds of metres below the seafloor (Reed & Wallace 2004). Much of the ore lead was leached from Early Palaeozoic basement, confirming genetic models of deep brine convection during synsedimentary basin dilation (Wilkinson *et al.* 2005, Everett *et al.* 2003, Figure 2.17). Lead derived from basement introduces a retrograde-metamorphogenic component into the diagenetic-exhalative setting. Several Irish deposits are giant concentrations of zinc and lead. The largest is the operating Navan mine (>70 Mt Zn + Pb). Historic Silvermines is much smaller, with 18 Mt of ore at 9% Zn+Pb and 23 ppm Ag.

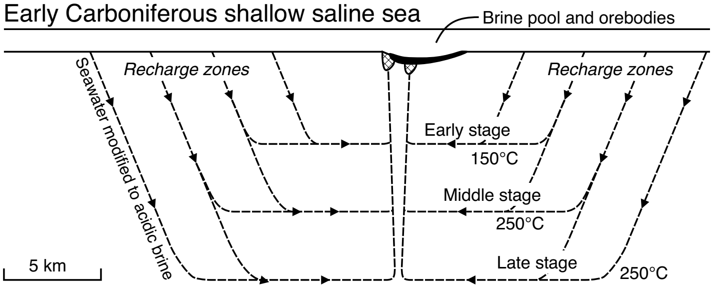

Figure 2.17 Schematic profile of seawater convection favoured by extensional tectonics in the Irish Midlands, synchronous with formation of the large Zn-Pb-Ag deposits in the Early Carboniferous. After Everett, C.E., Rye, D.M. & Ellam, R.M. 2003, Society of Economic Geologists, Inc., *Economic Geology* Vol. 98, Figure 15 B, p. 45.

Pb-Zn deposits related to salt diapirs and migrating saline brines

Pb-Zn deposits related to salt diapirs and migrating saline brines occur in North Africa, the Central African Copper Belt (Kipushi) and the Gulf region of the USA (Chapter 1.4 "Diagenetic Ore Formation Systems"). Numerous epigenetic vein deposits in Western European older basement and the Mesozoic sedimentary cover are related to pervasive mobilization of halite solution and evaporitic formation waters (Jochum 2000). In the Maghreb region of northern Africa (Morocco, Algeria, Tunesia) stratiform Pb-Zn lodes, epigenetic karst-filling ore and veins are related to diapiric Triassic evaporites (Rouvier *et al.* 1985).

> Kipushi (DR Congo) is a large high-grade base metal deposit north of the Central African Copper Belt. Its production from 1923–1993 amounted to ~60 Mt of ore at 12% Zn, 8% Cu, 0.9% Pb and a total of 120 t of germanium (Höll *et al.* 2007). Kipushi ore is hosted in Roan Group dolomites and limestones (cf. "Copper"). Controlling structures include an anticline cored by a dolomite breccia body (vestiges of a former salt diapir) and a fault zone. Orebodies have the form of subvertical chimneys, pipes and stringers. Mineralizing fluids were brines (30–43 wt.% NaCl equiv.), which acquired solutes by salt dissolution (Heijlen *et al.* 2008). Main ore minerals are sphalerite, silver-bearing bornite, chalcocite, chalcopyrite, galena and arsenopyrite. Minor minerals include germanium sulphides such as renierite $(Cu,Zn)_{11}(Ge,As)_2Fe_4S_{16}$ and briartite $Cu_2(Fe,Zn)GeS_4$. Both copper and zinc sulphides were dated to ca. 450 Ma, a Late Ordovician age (Schneider *et al.* 2007). The deposit may have been formed during an extensional tectonic phase. Clearly, Kipushi is not related to the Lufilian orogeny (~550 Ma) as are *sensu stricto* Copper Belt ores.

Diagenetic, stratabound, epigenetic, low-temperature hydrothermal deposits in siliciclastic sediments

Diagenetic, stratabound, epigenetic, low-temperature hydrothermal deposits in siliciclastic sediments ("impregnation" deposits) are rarely of worldwide economic significance, but display interesting metallogenetic traits. Genetic interpretation fluctuated long between supergene infiltration and epigenetic-hydrothermal emplacement. Meanwhile, a number of arguments support the second mode, recalling Oliver's (1986) tectonic brines:

> The lead deposits of Laisvall and Vassbo, and hundreds of smaller mineralizations occur along the Caledonian thrust front in Sweden. The metal province has a width of ~100 km and a length of >2000 km. Host rocks are quartzites and sandstones of the Laisvall Group, an Eocambrian to Cambrian siliciclastic suite that occurs as an autochthon overlying crystalline basement and in allochthonous sheets or slivers between the lower Caledonian nappes, which were overthrust from the west. Mid-Cambrian alum shales served as sliding horizon. The paragenesis consists of galena and small amounts of sphalerite, pyrite, barite, calcite, fluorite and sericite. Ore minerals replace sandstone matrix and form poikiloblastic crystals. Orebodies are stratiform, controls are lithologic (feldspathic sandstone beds between shales of low permeability) and tectonic (nappe thrusts). Ore-forming fluids had a temperature of ~150 °C and 23–26% NaCl equivalent. Lead isotope data identify highly anomalous radiogenic lead (of the J-type). The fluids are interpreted as formation brines expulsed by metamorphism under the advancing Caledonian nappes (Grenne *et al.* 1999). Total resources at Laisvall (before mining) are estimated to 60 Mt at 4% Pb; this makes Laisvall the largest lead concentration in Europe. The Laisvall mine closed in 2002.
>
> The world's largest deposit of this group is Jinding, western Yunnan, China, with reserves of ~220 Mt grading 6% Zn and 1.3% Pb. At Jinding, Triassic to Neogene marine siliciclastic sediments with evaporitic horizons were strongly deformed during the Himalayan orogeny. A structural dome controlled inflow of overpressured basinal fluids and formation of more than 100 orebodies. Overpressures are thought to be due to overthrusting and nappe transport (Chi *et al.* 2007, Kyle & Ning 2002). Sulphides occur disseminated in Cretaceous sandstones and as massive replacement stocks in overthrusted bituminous Triassic limestone (Junlai Liu *et al.* 2010).

Volcanogenic Zn-Pb-(Cu-Au) deposits

Volcanogenic Zn-Pb-(Cu-Au) deposits were described earlier (Kuroko type – Chapter 1.1 "Volcanogenic Ore Deposits", Figure 1.46; Iberian Pyrite Belt: cf. Section 2.2.1 "Copper"). Note that truly oceanic sulphide ore deposits of Cyprus and mid-oceanic type may contain exploitable zinc but very little lead. This is a consequence of the low uranium and thorium concentrations of mid-ocean basalts and generally, of oceanic crust and the Earth's mantle.

Contact-metasomatic and skarn Pb-Zn-Ag deposits

Contact-metasomatic and skarn Pb-Zn-Ag deposits characterize active continental margin metallogeny. Parentage of I-Type granitoid intrusions is frequently observed. Most of these deposits are silver-rich (read more in "Silver" in Section 2.3.2):

> In Europe, the Trepča (or Trepcë) Pb-Zn-Ag mine in Kosovo is a remarkable example of this group. Here, Triassic carbonates and schists are penetrated by the subvertical pipe of a Miocene trachyte volcano (Heinrich & Neubauer 2002). Carbonates proximal to the vent are replaced by anhydrous skarn with pyroxene, garnet, epidote and ore minerals. Hydrothermal ores have been formed outside the skarn rock in large hydrothermal karst caves that contain marvellous crystals of many rare minerals. Massive sulphide ore consists of argentiferous galena, black sphalerite with over 12% Fe, pyrrhotite and pyrite. Important by-product metals are gold, silver, bismuth and cadmium. Traces of indium, gallium, germanium, arsenic, copper, selenium, tellurium and antimony are by-products. Gangue comprises quartz, carbonates and barite; noticeable are large bodies of metasomatic manganese and iron carbonates. Total ore mined plus remaining resources at Trepča are estimated to 60 Mt at 6% Pb and 4% Zn.

Hydrothermal vein deposits

Hydrothermal vein deposits of lead and zinc are economically less favourable because extraction costs are higher than in other deposit types. For ~1000 years, the Harz mining district in northern Germany was a source of silver and lead. Zinc was only extracted since it attained industrial value ~150 years ago. In 1994, the last mine closed (Bad Grund):

> Ore veins of the western Harz Mountains occur in Late Palaeozoic greywacke and shale that were folded during the Variscan orogeny. The veins are part of a late to post-orogenic system of NW-SE striking extensional faults. Down-throw of single faults reaches several hundreds of metres. They can be traced for 20 km and reach a thickness of 70 m. Fault planes display an undulating topography; only certain parts are mineralized (Figure 1.43). Nineteen of these structures host exploitable Pb-Ag-Zn ore. Host rocks are haematitized, silicified, dolomitized and ankeritized, indicating the passage of very different hydrothermal fluids. Vein-fill is banded (similar to Figure 1.28) and displays many druses. The paragenetic sequence is composed of barite, siderite, quartz, dolomite and calcite, apart from ample galena, silver minerals, sphalerite and some chalcopyrite. The Bad Grund mine produced a total of ~1 Mt lead, 2000 t silver and 500,000 t zinc. Remaining resources are large but not economically recoverable.

In spite of intensive research, the genesis of the Harz veins remains enigmatic. The faults formed in response to late-orogenic relaxation of Variscan compressional deformation. Lead and sulphur isotopic composition of ore suggests that both elements are sourced in the Palaeozoic sediments. Mobilization of fluids may be related to a thermal event at ~300 Ma (Carboniferous/Permian boundary), when gabbro and granite intruded near the vein district but derivation from the intrusions is improbable. Fluid inclusions have elevated salt content and this might indicate that the descending branch of convection systems tapped Zechstein brines or dissolved salt from Zechstein evaporites that covered the region during much of the Mesozoic. Some of the vein faults can be traced into nearby Permian cover where displacement is very small, suggesting that faulting (and mineralization) occurred mainly before cover sediments were laid down. Dating of alteration minerals produced ambiguous results; at least one phase of hydrothermal activity falls into the Late Triassic (Schneider *et al.* 2003). This age is shared with many important ore districts in Europe, for example Copper Shale, Pb-Zn in Silesia and in the Alps, and Early Jurassic fluorite veins and sinter barite of the Massif Central in France. Break-up of the Supercontinent Pangaea may be the common cause.

World mine production of zinc (in 2008 11.6 Mt; in 2009 11.1 Mt) and lead (in 2008 3.8 Mt; in 2009 3.9 Mt) is steadily growing. Reserves and resources of lead are large; Australia, China, USA and Peru are best endowed. Main producers are China, Australia, USA and Peru. About 70% of Western

World consumption of refined lead is recycled from secondary sources, whereas for zinc this fraction is small. The primary (mine) production of lead is fluctuating widely because the metal is essentially a co-product of silver and zinc mining. Reserves of zinc are considerable, especially in China, Australia and Peru. Largest producers of zinc are China, Australia and Peru. Exploration for lead and zinc is characterized by geological, geochemical and geophysical methods that are common to most sulphide ores.

2.2.3 Tin

Common Ore Minerals:

		Max. wt.% Sn	*Density (g/cm^3)*
Cassiterite	SnO_2	78	6.8–7.1
Stannite	Cu_2FeSnS_4	27	4.4

Cassiterite is the main ore of tin. Different shapes of cassiterite crystals are characteristic for certain genetic settings. Bipyramidal and short, stocky prismatic crystals are found in pegmatites, greisen and high-temperature veins, whereas long prismas and needle-like crystals appear in lower-temperature hydrothermal deposits. "Colloidal" wood-tin occurs in low-T veinlets associated with rhyolites. Cassiterite usually contains a small amount of iron in substitution for tin and minor to trace concentrations of Ta, Nb, Ge, Sc, Zr, Ga, Be, Hf, In, W, Mn and V, some of which may be valuable by-products. Uraniferous cassiterite is not rare and because of its resistance to alteration is useful for precise U-Pb dating. Stannite is a frequent trace mineral in most tin ores but only attains economic importance in some Bolivian deposits.

Exploitable grades in primary hard-rock tin mines are typically 0.3 to 1.2 wt.% Sn, whereas placers can be mined at <0.01% Sn. At sufficiently large grain size, cassiterite is concentrated by simple gravitative processes (jigs and tables). Very fine-grained cassiterite, stannite and other tin sulphosalts enforce higher investments for treatment (including flotation) and recovery is often poor (<50%).

Uses of tin are manifold because of a combination of positive qualities. Tin metal is not toxic, is soft and melts at low temperatures (melting point 231.9 °C; density 7.29 g/cm^3). Its properties are easily modified by alloying. Examples of common alloys are bronze (Sn with Cu), which was already used in ancient Mesopotamia (~3500 BCE), and tin solder (Sn with Pb) of Roman antiquity but still used in electronic applications. Tin-brass (Sn with Zn) and alloys with Al, Si, Sb and many other metals are more recent developments. Alloys are employed in electrical appliances, vehicles, machinery and buildings. Tin-zirconium alloys are utilized in nuclear reactors. The largest part of production is consumed for tin plating, especially of food and drink containers, and for lead-free solders. Tin chemicals include SnF in toothpaste, amalgam (Ag-Cu-Zn-Sn-Hg) in dental medicine, fillers in plastics and non-toxic chemicals for wood protection. Of all metals, tin has the widest field of uses. Although tin is environmentally benign, arsenopyrite is often part of the ore paragenesis. The fate of the arsenic present in tin mines must be closely monitored.

Geochemistry

The geochemical properties of tin are characterized by its incompatible and lithophile behaviour. Ultramafics contain an average of 0.15 ppm Sn (Jochum *et al.* 1993), mafic rocks 1.2 ppm and felsic magmatic rocks 3.5 ppm. The solubility of Sn in granitic liquids was described by Taylor & Wall (1992) and by Linnen *et al.* (1996, 1998). Trace contents are variously hosted in accessory magnetite, ilmenite, titanite, garnet and in micas. Sn may be extracted from melt or these minerals by reduced, acidic, chloride or fluoride-rich fluids that form during crystallization of specialized felsic magmas. Reduction is favoured by interaction with carbon-bearing country rocks. Highly fractionated granites are characterized by tin contents that may reach 50 times the average for ordinary granite. Rb (Figure 1.17), Li, F, B and many other elements are anomalous, too. Expulsion of fluids, hydrothermal alteration and ore formation cause erratic diminution of Sn in the granite body. Numerous investigations have centred on the geochemical, mineralogical and geological characterization of fertile "tin-bearing" or "tin granites" (Breiter *et al.* 1999, Inverno & Hutchinson

2006). It is, however, probably vain to search for universally valid characteristics of fertility.

Most tin-fertile granites occur near active plate boundaries. This is very obvious for Bolivia and Peru, and the Southeast Asian tin province (Burma to Indonesia), which is the source of nearly 50% of historic world tin production (Schwartz *et al.* 1995). Other significant habitats include collisional orogens such as the European Variscides, the Mesoproterozoic Kibara belt in Africa (Pohl 1994) and the Mesozoic orogen of the South Chinese platform (Figure 1.15). Typically, tin granites intrude at late to post-orogenic time. A third group of tin granites appears as members of A-Type granite suites in anorogenically mobilized cratons (e.g. the Jurassic granites of the Benue aulacogen in Nigeria; Mesoproterozoic granites of Rondonia and the Amazon basin in Brazil). Tin porphyries in the Eastern Andes of Bolivia and Peru may also belong to this group (Figure 1.88). Tectonic control in this province was Tertiary crustal extension. However, most tin granites are S-Type, highly fractionated and strongly reduced (Figure 1.17). High initial Sr-isotope ratios confirm a continental crustal source, which was earlier deduced from geological observations. Good examples are the tin deposits related to the Lebowa granites of the Bushveld Intrusive Complex. The granites are the product of crustal melting induced by the giant mafic magma body. Tin granites tend to have more boron in some provinces and more fluorine ("topaz granites") in others (Lehmann *et al.* 2000). The first typically produce hydrothermal deposits, as in Bolivia, Cornwall and the Kibara belt, whereas fluorine tends to induce greisen and disseminated ores in granite (e.g. in the Erzgebirge and Nigeria).

The volcanic equivalent to tin granites rich in fluorine are topaz rhyolites ("ongonites"), reported in Mexico, USA and Mongolia, with economically insignificant occurrences of wood tin in tuff and other pyroclastic rocks. Topaz rhyolites may be genetically connected with playa lake deposits, such as Li-brines at Searles Lake in California, uranium in playa tuffites, borate and iodine (Warren 1999). Solubility of tin (and Fe) is highest in hot, reduced, saline and acidic solutions. Magmatic high-T fluids carry > 200 ppm reduced Sn^{2+} in chloride complexes (Heinrich 1990). Below 350 °C and at pH 2–7.5 tin is complexed as $Sn(OH)_2$ or $Sn(OH)_4$. Precipitation of cassiterite (Sn^{4+}) is induced by destabilization of the complexes following sudden drops of T or P (boiling), rising oxygen fugacity or pH due to hydrothermal alteration of host rocks, or mixing with fluids of a markedly different composition. Obviously, SnO_2 cannot be formed in the absence of oxygen, but this may be derived from water in the fluids (eq. 2.4).

Precipitation of cassiterite from hydrothermal solutions:

$$\begin{aligned} SnCl^{+}+2H_2O &= SnO_2+Cl^{-}+2H^{+}+H_2 \\ 4Sn(OH)_2+CO_2 &= 4SnO_2+CH_4+2H_2O \end{aligned} \qquad (2.4)$$

The first reaction illustrates why acidic alteration is common in tin deposits, expressed as pervasive sericitization or at lower T, kaolinization. Typical alteration and gangue minerals include quartz, tourmaline, white mica, arsenopyrite and chlorite (e.g. at San Rafael). Grade and mass of tin ore may be controlled by the neutralization capacity of the host rock (Heinrich 1990). Stable isotope data reveal that the water of tin ore-forming fluids is initially of magmatic origin ("juvenile"), whereas later fluids may contain an increasing component of meteoric water. A third possible admixture are water and volatiles distilled from intruded country rocks (e.g. As, S, CO_2, CH_4 and N_2 from black shales at Rutongo, Rwanda; Figure 1.16).

Cassiterite is very resistant against superficial chemical alteration. Eluvial, alluvial and coastal placers of this mineral are common. The distance from the primary source to the point where grades fall below economic limits is controlled by mechanical diminution during transport and by dilution with clastic sediment. Cut-off grades of placers are typically reached after a transport of hundreds of metres to a few kilometres. In contrast to cassiterite, stannite weathers rapidly to souxite (also called varlamoffite, $H_2SnO_3 + aq$), a "mineral" of earthy or colloidal appearance.

Tin ore deposit types

The strongly incompatible and lithophile properties of tin are the foundation of its metallogeny, driving its enrichment in felsic melt with increasing fractionation and its transfer into exsolving magmatic fluids. Primary tin deposits of economic significance range from economically marginal orthomagmatic, through dominant magmatic-hydrothermal (intrusive and volcanic) to volcanogenic-exhalative. Significant tin deposit types are (adapted from Lehmann 1990, Linnen & Samson 2005):

- apical rare element-enriched portions of highly fractionated granites (e.g. Shuiximiao in southeast China);
- rare-element pegmatites with cassiterite as main ore and by-products Ta, Be and Li (Greenbushes W.A.);
- endogranitic magmatic-hydrothermal tin greisen bodies in granite cupolas (e.g. Erzgebirge, Germany);
- magmatic-hydrothermal quartz veins within and above fertile intrusions (San Rafael, Peru);
- magmatic-hydrothermal skarn and contact-metasomatic ore (Dachang, China);
- volcanogenic-hydrothermal, epizonal deposits (Cerro Rico de Potosi, Bolivia);
- by-product tin in volcanogenic-exhalative massive sulphide ore (Neves Corvo, Portugal);
- tin porphyries (Bolivia) as potential future low-grade resources;
- tin placers (Malaysia, Nigeria, Central Africa).

Rare element granites

Granite cupolas, which are enriched in rare metals to the degree that the whole hard rock mass can be considered as ore, are at present not common producers of tin. An example is the endogranitic part of Shuiximiao in southeastern China. A section of the deposit (Figure 1.15, Zhu *et al.* 2001) demonstrates the relations between orthomagmatic Ta-Sn ore within the cupola (albite-topaz-granite), thin Ta-Sn stockscheider pegmatite and Sn-rich pegmatite-aplite bodies intruding the roof. These pegmatites crystallized from highly fractionated hydrous residual melt batches. The igneous section of the profile is at the origin of fan-like magmatic-hydrothermal wolframite-cassiterite-quartz veins. A halo of outcropping F-Li veinlets provides clues for prospectors. Similar are Yichun, South China (Yin *et al.* 1995) and Abu Dabbab, Egypt (Figure/Plate 2.18; cf. Section 2.5.9 "Niobium and Tantalum").

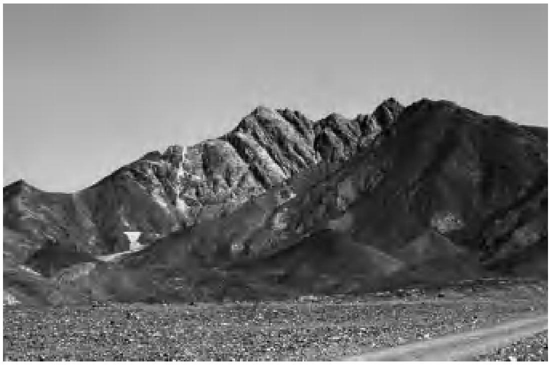

Figure 2.18 (Plate 2.18) Among dark Neoproterozoic volcanic rocks, the white peak of Abu Dabbab leucogranite in the Eastern Desert, Egypt, is striking (although marred by desert varnish). The cupola is investigated for production of tantalum, cassiterite and ceramic-grade feldspar. An exploration adit produced the white waste rock dump on the left slope.

Cassiterite pegmatites

Cassiterite pegmatites are closely associated with fertile granites. In comparison to hydrothermal vein deposits they have been formed at greater depths, usually in a mesozonal setting. However, in some cases both pegmatites and veins occur together (telescoping, e.g. at Musha, Rwanda: Varlamoff 1972, Figure 1.16), and mutual cross-cutting elevations may be developed. In zoned pegmatite fields, tin ore is restricted to certain pegmatite types as in Central Africa (Varlamoff 1972, Figure 1.19) where tin (and in many deposits also tantalum) only appears in pegmatites with albite/microcline, spodumene, muscovite, lepidolite, beryl and quartz. Trace element contents of muscovite in mineralized pegmatite are strongly anomalous in Rb-Cs-Li-Sn. Mining of tin pegmatites is favoured by hydrothermal or supergene kaolinization. Soft rock can be mined by simple hydraulic excavation methods using monitors, in contrast to the high costs that arise from blasting and milling hard rock. A significant example of rare element pegmatites is Greenbushes in Western Australia (cf. Section 2.5.10 "Lithium").

Magmatic-hydrothermal tin deposits

Classical examples of magmatic-hydrothermal tin deposits in Europe include Cornwall (cf. Chapter 1.1 "Hydrothermal Vein Deposits") and the Erzgebirge (Breiter *et al.* 1999, Baumann *et al.* 2000):

> The Erzgebirge is part of the Saxothuringian zone of the mid-European Variscan belt, exposed for a length of ~120 km and a width of 45 km. It is built of Precambrian and Early Palaeozoic rocks that were folded at ~380 Ma (in the Late Devonian). Between 325 and 300 Ma (Late Carboniferous to Early Permian) it was intruded by numerous granite bodies of variable composition (Förster 1999). Investigations of this intrusive suite were the base of the concept of precursor, specialized and mineralized granites (cf. Chapter 1.1 "Granitoids and Ore Formation"). The batholiths comprise large masses of early biotitic granodiorite and monzogranite, followed later by smaller bodies of topaz-biotite-muscovite syenogranites. The youngest members of the latter are highly specialized lithium-mica granites (containing zinnwaldite). Mineralization is genetically related to these lithium granites. Agents of ore formation were fluids exsolved from cooling melt bodies. Ores occur in stratiform greisen bodies within lithium granites (endogranitic), as greisen veins within older granite, in hydrothermal cassiterite-quartz veins located in siliceous metamorphic country rocks and as small metasomatic replacement bodies in carbonates.

Famous greisen tin deposits within granite cupolas of the Erzgebirge are Altenberg, Cinovec (Zinnwald) and Krasno (Schönfeld-Schlaggenwald). At Ehrenfriedersdorf, Sn-W veins were exploited above a cupola containing cassiterite in greisen. The origin of greisen ore within granite cupolas is due to trapping of specialized melts and fluorine-rich fluids. Trapping is controlled by fluid pressure and the stress-state of roof rocks.

Magmatic-hydrothermal quartz vein deposits

Earliest tin mining in Europe took place in western Iberia and in Cornwall (cf. Chapter 1.1 "Hydrothermal Vein Deposits") with its remarkable metal zonation (Figure 1.44). A similar zonation with Sn at depth and superjacent Cu occurs at the giant (>1 Mt of tin) and high-grade (4.7% Sn in ore) San Rafael deposit, that is genetically related to a Late Oligocene S-type granite (Kontak & Clark 2001, Mlynarczyk *et al.* 2003; Figure 2.19). Early hot, reducing and hypersaline fluids were followed by ore-stage fluids, which were more diluted, slightly oxidized and of lower temperature (290–380 °C). This is thought to be due to mixing of magmatic with meteoric water (Wagner *et al.* 2009).

Tin skarn and contact-metasomatic orebodies

Tin skarn and contact-metasomatic orebodies are economically significant because of large resources at high grades. Their formation depends

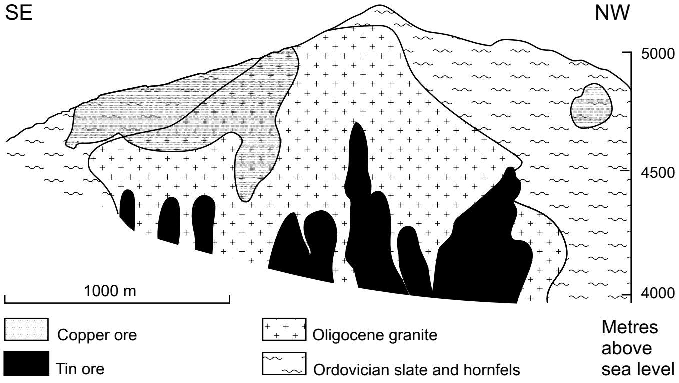

Figure 2.19 Metal zonation, exploitable areas, and granite/schist contact in a longitudinal section of San Rafael vein and breccia deposit, Peru (modified from Mlynarczyk *et al.* 2003). Note the localization of tin within the granite, whereas much copper resides in the Palaeozoic roof schists. The vertical extent (1200 m) of exploitable mineralization is quite remarkable.

on the coincidence of tin-bearing fluids produced from fertile granite and reactive roof rocks. Reactive rocks include limestone, dolomite, dolomitic evaporites, meta-basalts, ultramafics and black shales. Distal tin skarn and metasomatic ores are frequently stratabound. The world's largest tin mining district is probably Dachang, Guangxi, China, where Cretaceous (Yanshanian) S-Type biotite granite intruded Devonian carbonates and calcschists. Within the contact-metamorphic aureole, this resulted in stratiform replacement and stockwork orebodies, and vein fields (Pasava *et al.* 2003, Fan *et al.* 2004a, Minghai *et al.* 2007):

> The ore in the Dachang district contains ~0.8% Sn, 2% Zn and much pyrite; important co-products are In, Sb, Cu, Pb and Ag. Resources are estimated at ~110 Mt of ore. Early anhydrous skarn minerals, such as garnet and pyroxene, have high trace contents of Sn, but the main ore mass is due to the ensuing hydrothermal mineralization. This indicates a multi-phase evolution of fluid expulsion from the granite. Apart from tin ore, stratabound Zn-Cu orebodies (mantos) and W-Sb veins occur at Dachang (Figure 2.20).

Tin porphyries

Tin porphyries are comparable to copper porphyry deposits in respect of large size and low grade. They may reach a tonnage of >100 million, although with grades of only 0.1–0.3% Sn. This is at present not economic, and the lower grade tin porphyries have to be considered as potential future resources:

> Tin porphyries were recognized in the Bolivian tin belt (Lehmann *et al.* 2000). They are closely related to the large (up to 500,000 t Sn) and high-grade volcanogenic tin-silver vein deposits. Tin porphyries are subvolcanic, dacitic to rhyodacitic stocks. The rocks contain phenocrysts of quartz, sanidine, albite and biotite and are brecciated and strongly altered. The hydrothermal alteration zones comprise tourmalinization and silicification in the core, passing into the ore zone with tourmaline, sericite and cassiterite, and a wide halo of propylitization. Locally, richer parts of these breccias are exploited. The Llallagua (also known as Siglo XX) deposit in Bolivia produced ~1 Mt Sn from vein and porphyry mineralization with a bulk grade of ~0.35% Sn. It is centred on a rhyodacite stock emplaced within Early Palaeozoic clastic sediments.

Volcanogenic polymetallic tin-silver vein deposits

Volcanogenic polymetallic tin-silver vein deposits represent the epithermal level of the Bolivian tin porphyries. Somewhat deeper, early, high-temperature (<530 °C) cassiterite-quartz veins pass at shallower levels into sulphides and sulphosalts of Sn, Sb, Ag, Bi, Pb and Zn. The gangue comprises fluorite and siderite, with some scheelite. Later and at low temperature, barren veins with carbonates and hydrophosphate were formed. Shallow epizonal deposits have high silver grades and are known as silver mines (Cerro Rico de Potosi, cf. Section 2.3.2 "Silver").

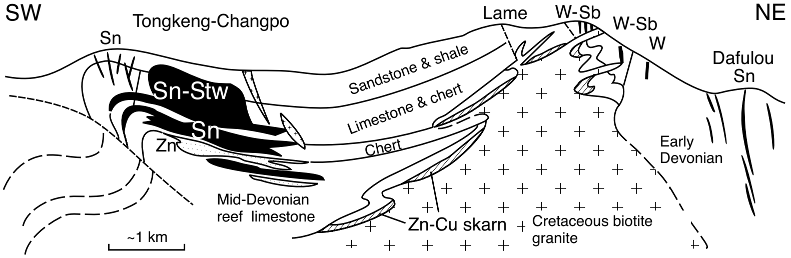

Figure 2.20 The giant contact-metasomatic tin ore deposit Tongkeng-Changpo in the Dachang district, S-China (modified from Fan *et al.* 2004a with permission from Elsevier). Mineralization styles hosted in Late Devonian rocks include a polymetallic stockwork (Sn-Stw), stratiform tin and zinc orebodies, and vein fields with cassiterite, scheelite-fluorite and wolframite-stibnite ore. Zn-Cu skarn ore occurs at the contact between granite and Late Devonian limestone.

Occasionally, tin is an important by-product of volcanogenic-exhalative massive sulphide (VMS) deposits. Over many years, the only tin production in North America was derived from the base metal deposits at Kidd Creek (Ontario), Sullivan (BC) and the Bathurst Mining Camp in New Brunswick, Canada (McClenaghan *et al.* 2009). An example from Europe is Neves Corvo in Portugal (cf. Section 2.2.1 "Copper").

Exploration for tin deposits was traditionally done by systematic panning alluvial sediments for cassiterite along streams and rivers. This was very effective in locating placers, eluvial and outcropping primary deposits. Today, exploration is increasingly directed towards buried hard rock deposits and ancient "deep" placers that are covered by younger sediments or by volcanic rocks (Figure 2.21). Geochemical search for Sn-anomalies in soil and sediments is very efficient. Frequently, rock geochemistry is employed in order to identify fertile and mineralized acidic intrusives (Baker *et al.* 2005). Hidden cupolas of tin granites can by found by geophysical methods (e.g. gravimetric surveys) and investigated by drilling.

China, Indonesia, Peru, Bolivia and Brazil are the world's leading tin producers. World production was 299,000 t in 2008 (307,000 t in 2009; USGS 2010). Large resources occur in China, Brazil and Peru. Because of efforts to reduce the use of lead, demand for tin as a substitute for lead in solder, electrical applications and in shot may increase.

2.3 Precious metals

2.3.1 Gold

Common Ore Minerals:

		Max. wt.% Au	*Density (g/cm^3)*
Native gold	Au (Ag,Cu,Hg,Pd)	70–100	15.0–19.3
Sylvanite	$(Au,Ag)Te_4$	25	8.0–8.3
Calaverite	$AuTe_2$	42	9.3

Native gold may be coarse-grained ("free-milling") or included in sulphide and sulphosalt minerals ("refractory"), where it occurs either in small inclusions or as impurity defects in crystal structures. Native gold contains 2–20% silver (Morrison *et al.* 1991), 0.1–0.5% copper and iron, and trace amounts of bismuth, mercury, lead, tin, zinc and platinum group metals. Gold alloyed with PGE metals is relatively rare (Cabral *et al.* 2002). Electrum is gold with 30–70% silver.

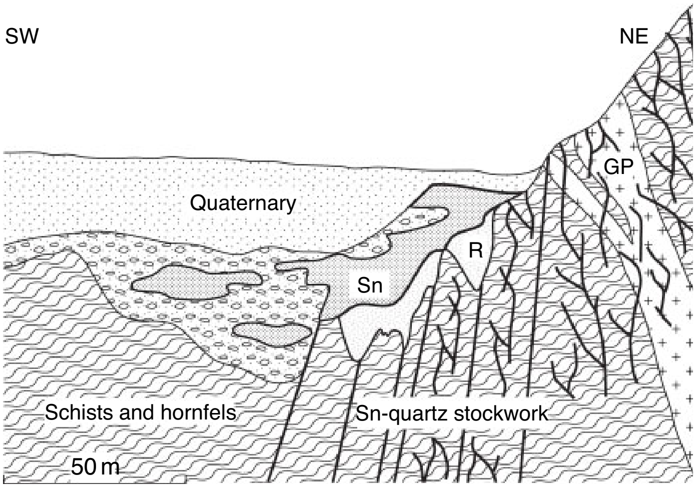

Figure 2.21 Profile of Tertiary escarpment-type tin placers at Tenkeli in northern Jakutia, Russia, due to repeated faulting (modified from Laznicka 1985 with permission from Elsevier). Quaternary alluvial sand and gravel; T = Tertiary gravels; Sn = Tin placer; R = Regolith; GP = Mesozoic granite porphyry.

Apart from copper, gold is one of the earliest metals consciously sought by humans. The oldest known map of a gold mine was drawn in the 19th Dynasty of Ancient Egypt (1320–1200 BCE), whereas the first written reference to gold was recorded in the 12th Dynasty around 1900 BEC. Total gold recovered by humans is estimated at 155,000 t, which would fit into a cube of ~20 m edge length. Gold was always a metal valued for wealth, adornment and strong currency. This is little different today, only ~10% are consumed by industry (e.g. electronics, architectural glass, dental applications). For the future, an increasing role of nano-sized gold particles as catalysts in chemical production, in pollution control and in medical applications is predicted.

Processing costs are an important control on cut-off grades in gold mining. Other variables include extraction expenses, which are very different for underground or open pit mining, dredging of unconsolidated placers and recovery of former mill tailings. The average gold concentration in ore of important mines is currently at ~3 g/t. Alluvial mega-placers can be exploited at grades as low as 0.2 g/m^3. Note that the weight, or more exactly the mass of gold (and platinum) in metal trading is commonly cited in ounces (Troy ounce, abbreviated oz tr). The conversion factor to SI-units is 31.1034 g/oz tr or one metric tonne (1000 kilograms) equal to 32,150.7 troy ounces. Pure gold (24 carat) has a density of 19.3 g/cm^3 and melts at 1063 °C:

> Native gold dissolves in cyanides (e.g. KCN, NaCN) and in mercury, accounting for the chemical part of mine-site processing. Larger grains of free-milling gold are amenable to gravity concentration methods but fine flakes are not. Earlier, fine-grained ore was mixed with liquid mercury (amalgamation); the amalgam paste was separated from gangue and heated to vaporize mercury leaving crude gold bullion. Today, mercury is rarely used in industry and the cyanidation process is preferred. In this process, gold in the ore is dissolved by a very dilute solution of potassium or sodium cyanide producing gold cyanide. This is stripped from the solution by activated charcoal, concentrated and purified by melting (Adams 2005). By cyanidation and low-cost heap leaching, very low-grade ore of ~0.2 ppm Au (=g/t) can be profitably treated. Cyanidation is, however, restricted to ore with a low concentration of cyanicides, which bind cyanide. Common cyanicides include S, Fe, Cu, Ag, As, Cd, Sb, Ni, Co and Zn. Auriferous sulphides, sulphosalts and tellurides ("refractory" ore) are usually pretreated by flotation and oxidation (roasting), causing higher processing costs and consequently, cut-off grades. Humic and bituminous matter in ore is a similar penalty. Refractory "invisible" gold occurs in the form of tiny inclusions (Au^0 <10 μm) or as Au^1 in the crystal lattice of pyrite, arsenopyrite and stibnite. Invisible gold cannot be liberated by milling. The technological solution is oxidation at pressures of 2–3 MPa and temperatures reaching 200 °C (autoclaving) that converts the sulphides to porous and fractured oxides, so that leach solutions can reach the gold. Recent developments include processing such ore with high concentrations of *Thiobacillus ferrooxidans* and *Leptospirillum ferrooxidans*, which oxidize sulphides and make the gold recoverable by heap leaching ("bio-oxidation"). Cyanide solutions are recycled and when spent, are detoxified before release into the environment. Several inorganic and biological processes are available, which decompose cyanide to CO_2 and N_2. Because of hazards posed by cyanides, replacement chemicals are sought, although as yet with little success. Environmental cyanide geochemistry, sampling and analysis are very tricky and require thorough knowledge and experience (Smith & Mudder 1999).

Geochemistry

The geochemical character of gold is strongly siderophile, in contrast to silver, which is chalcophile (Goldschmidt 1958). Accordingly, average gold contents in iron meteorites are 1 ppm, but in the Earth's crust only 0.004 ppm (range 0.001–0.005 ppm: Smith & Huyck 1999). Gold contents in magmatic rocks correlate positively with Fe and S, yet fractionation of felsic melt may lead to economic gold concentrations (Mustard *et al.* 2006). Trace gold of magmatic rocks is variously hosted in sulphides, magnetite, biotite, pyroxene and hornblende. Dissolution behaviour of these minerals controls liberation of gold from source rocks; in passing fluids, sulphides probably dissolve first. Some sediments concentrate gold. Sandstones and conglomerates average

0.03 ppm, coal ashes reach 0.1 and black shale 2 ppm Au. Arsenian iron sulphides of mid-oceanic ridges concentrate gold and silver (28–140 ppm Au, 800–2400 ppm Ag: Halbach *et al.* 2003). Cyprus Type deposits approach grades of 8 ppm Au. The crustal gold/silver ratio is ~1:20 and because of a similar ionic radius and charge, gold and silver are exchangeable in many minerals. Different from silver, gold does not form sulphides but enters a number of rare sulphosalts together with metals such antimony, selenium and bismuth.

In the surface environment, gold is nearly insoluble. More precisely, of all metals gold is least reactive to atoms and molecules when in contact with gases or fluids. This makes it the most noble of all metals (Hammer & Norskov 1995). However, many observations imply that gold in surface systems can be mobile. Examples include the formation of large nuggets that are derived from fine-grained gold in unaltered ore (Youngson & Craw 1993), the common idiomorphic and undamaged octahedral gold crystals of young placers, and the concentration of gold in enrichment zones beneath gossans. Migration may be in the form of dissolved inorganic or organic gold (I) or (III) complexes and with Fe-Mn colloids. The most likely and mobile compound of gold in natural systems at the Earth's surface is probably gold (I) thiosulphate $Au(S_2O)_2^{3-}$. Gold solubility is controlled by the availability of S, Cl, B, I, natural cyanides and Eh/pH. In the tropics, humic acids (especially fulvic acids: Bowell *et al.* 1993) and decomposition products of organic matter (carbonyl CO, NH_3, HCO_3) may support solubility. The precipitation of mobile gold is thought to be assisted by actinomycetes, archaea, fungi and bacteria (e.g. sulphate-reducing bacteria: Lengke & Southam 2007; *Pedomicrobium* films in Alaskan gold placers: Watterson 1992). Certain bacteria (including *Ralstonia metallidurans*) reduce and precipitate gold from soil solution, either within their cells or extracellularly, in order to detoxify their immediate environment. Bacterial biofilms catalyze formation and growth of secondary Au, promoting chemical and nanoparticular mobilization and reprecipitation as bacterioform Au particles that have been described from placers and weathered parts of Au deposits (Reith *et al.* 2010). Due to higher solubility of Ag, Cu and Hg, secondary Au often contains fewer impurities compared to the primary gold. Transported gold particles in placers contain identifiable submicroscopic inclusions of opaque minerals that can be linked to genetic types and even to certain ore districts (Leake *et al.* 1993). Incidentally, this is one of the arguments brought forward against nugget formation by dissolved mobile gold.

In hydrothermal solutions, gold does not form simple ions but combines with anions resulting in Au^+ complexes such as $AuCl_2^-$ and $Au(HS)_2^-$. At the temperatures of supercritical magmatic and metamorphic fluids (550–725°C), high gold concentrations occur based on stable complexes $Au(HS)(H_2O)$ and $Au(HS)_2^-$ (Xiandong Liu *et al.* 2011). In fluids with reduced sulfur, iron and base metals such as Pb, Zn and Cu have a very low solubility. This explains the ubiquitous formation of gold-only ore deposits, in spite of the omnipresence of base metals. Most aqueous gold fluids contain ~0.10–0.25 mole CO_2, which buffers pH (Phillips & Evans 2004), commonly to neutral or slightly acidic state. Nearly pure CO_2 fluids are very rare and their role is not wholly understood (Schmidt-Mumm *et al.* 1997, Chi *et al.* 2006). Typical NaCl content is low, with 1.5–6 wt.%. Oxidation potential E_h is predominantly negative, as demonstrated by Fe^{2+}-rich minerals of alteration halos and veins (e.g. pyrite, ankerite). Precipitation of thiocomplexed gold is induced by falling temperature, pressure and sulphur activity, which may be due to fluid unmixing or boiling, to sulphide precipitation because of reaction with Fe-rich country rocks ("sulphidation"), to dilution or oxidation. In the case of low S-contents in fluids that can be assumed when sulphide and gold in ore are negatively correlated, chlorine complexes may have dominated gold transport. In this case, precipitation of gold is induced by falling temperature, pressure and chlorine activity, or by degassing of CO_2 (e.g. effervescence) because this raises the pH of solutions.

A frequent precipitation mechanism is adsorption of gold on sulphide mineral surfaces (e.g.

pyrite, galena, sphalerite, chalcopyrite, etc.) or colloids. Reduction/oxidation processes also have a role when dissolved Au^{+} or Au^{3+} is fixed as native Au^{0}. This is illuminated by gold enrichment in contact with reducing material (e.g. black shales: Matthäi *et al.* 1995, Copper Shale: Piestrzynski *et al.* 2002). Surface discharge of gold-bearing fluids in volcanic settings (geothermal hot springs) displays co-precipitation of gold with gels of As-Sb sulphides (Broadlands, New Zealand).

Gold ore deposit types

Together with platinum and rhenium, gold is one of the rarest elements. Surprisingly, gold deposits are quite common, in numbers, geographical spread and genetic diversity (Figure 1.3, Table 2.2). Clearly, relatively common crustal fluids are able to mobilize, transport and concentrate gold. Metamorphic and magmatic fluid systems are prolific producers of primary gold deposits. This is illustrated by thousands of gold deposits that formed in orogenic belts from large volumes of crustal rocks with an ordinary geochemical background. The group is called "orogenic gold deposits", which are understood as products of crustal-scale massive flow of aqueous-carbonic metamorphic fluids and of more local magmatic-hydrothermal fluids during orogeny. The majority of primary gold deposits originated in subduction and collision settings. In the American Cordilleras, nearly all major gold deposits are related to magmatic activity and single districts formed in short periods of 5–20 My (Sillitoe 2008). Secondary gold deposits are generated by weathering and soil formation (lateritic gold, cf. Chapter 1.3 "Residual/Eluvial Ore Deposits") or as placers resulting from erosion, transport and sedimentation. The more common genetic types of gold deposits include:

- orthomagmatic by-product gold in sulphide ores formed from segregated sulphide liquid;
- magmatic-hydrothermal (e.g. quartz veins, stockwork orebodies, breccia pipes and breccia bodies, IOCG deposits, copper-gold porphyries, polymetallic skarn, part of shale or turbidite hosted gold deposits; part of orogenic deposits; Carlin type deposits);
- volcanogenic epithermal and hot springs deposits;
- by-product gold in submarine exhalative deposits (VMS and sedex);
- metamorphic local redistribution, concentration and recrystallization of gold;
- metamorphogenic-hydrothermal quartz veins, vein stockworks, replacement and disseminated orebodies; including orogenic deposits (except the magmatic-hydrothermal part of the group) and shale, or turbidite hosted deposits;
- lateritic gold deposits;
- residual placers;
- colluvial, alluvial and coastal placers.

Plutonic (intrusion-related) deposits

Plutonic (intrusion-related) deposits (Lang & Baker 2001) include orthomagmatic and various magmatic-hydrothermal deposit types, for example the iron oxide-copper-gold deposits (IOCG, for more detail, cf. Section 2.2.1 "Copper").

Orthomagmatic origin is illustrated by the discovery of gold in the Triple Group of the Middle Zone of the Eocene Skaergaard Intrusion in eastern Greenland (Andersen *et al.* 1998). Skaergaard is one of the classical examples of layered mafic intrusions, with a long history of scientific studies. Platinum had been the target of exploration, by scanning a large number of Early Tertiary mafic intrusions and tholeiitic flood basalts. Stream sediment samples exposed striking gold contents that were traced back to Skaergaard rocks by lithogeochemical prospecting. The source was located in a sulphidic layer ~2 m thick within banded gabbroic cumulates. Drilling established inferred resources of ~90 Mt with 1.8 ppm gold and comparable palladium plus platinum contents (Andersen *et al.* 1998).

Magmatic-hydrothermal gold deposits include quartz veins, stockwork orebodies, breccia pipes, gold porphyry, skarn and replacement ore. Related intrusions are mostly of felsic or intermediate character. The mineralization occurs within the magmatic bodies (as in Cu-Au porphyries) or in adjacent country rocks (veins, stockwork and skarn ore). Apart from gold, the metal assemblage often includes Bi, W, As, Mo, Te and Sb. Parental granites of gold deposits are not specialized and display both negative and positive redox state (Figure 1.17). Their source may be pre-existing gold mineralization in old continental crust that was recycled by partial melting. It is hypothesized that hydrous and K-alteration surrounding gold concentrations induce preferential dehydration melting. These melt batches add to the metal budget of intrusion-related gold systems (Tomkins *et al.* 2009):

> The enrichment of gold in magmatic fluids is favoured by high oxygen fugacity and high sulphur contents. Early saturation of reduced sulphur causes formation of sulphide droplets in the silicate melt, which abstract gold very effectively. After solidification, accessory sulphides are dispersed in a rock mass with very low, uneconomic overall gold grades (note the difference to orthomagmatic enrichment that is only possible in low-viscosity mafic magmas). Because the solubility of sulphur in silicate melts rises with oxygen fugacity, oxidized magmas of the magnetite series are especially qualified to form profuse amounts of a sulphur-rich volatile phase with a high gold content during fractionation and crystallization. Reduction can be induced by magnetite crystallization that triggers sulphate to sulphide conversion (eq. 2.5; Sun *et al.* 2004). Consequent sulphide precipitation may be the key to gold ore formation (Liang *et al.* 2009). Many gold deposits are related to oxidized potassic granitoids (Pollard 2006: Iron oxide-copper-gold deposits, IOCG) and to hydrous trachyandesitic or shoshonitic magmas that are probably derived from metasomatically enriched portions of lithospheric mantle. Volcanic arc magmas reach high sulphur contents (Jugo 2009). These magmas appear commonly in tensional phases immediately after subduction, accretion and collision (Richards 2009). However, in some cases reduced ilmenite-type granitoids did produce gold deposits, for example in Portugal and in the Kibara belt. This may be due to redissolution of auriferous sulphides by exsolving fluids while the intrusion solidifies.

Magnetite precipitation from magmatic fluids promoting sulphate reduction:

$$\begin{aligned}&12FeCl_2+12H_2O+H_2SO_4\\&\quad=4Fe_3O_4+24HCl+H_2S\end{aligned}\tag{2.5}$$

Copper-gold (molybdenum) porphyries contain gold as a by-product of essential economic importance. Well-known examples are Panguna, Bougainville, Ok Tedi, Papua-New Guinea and Bingham, USA. Recently, Cu-Au porphyries have been discovered in Tibet, in a Middle Jurassic volcanic arc that predates the collision of India and Eurasia (Tafti *et al.* 2009). Gold-only porphyries are less frequent but do occur, for example in the Refugio District in northern Chile (Muntean & Einaudi 2000). The primary ore at the large gold (molybdenum) deposit of Hemlo, Ontario, Canada, which lies in an Archaean greenstone belt near Lake Superior, may have been formed by a premetamorphic porphyry system (Davis & Linn 2003), but is generally classified as an atypical orogenic gold deposit (Heiligmann *et al.* 2008).

Auriferous skarn ore deposits are commonly polymetallic (containing several metals of roughly equal economic share). Gold-only skarn deposits occur in Archaean iron formations of the Southern Cross greenstone belt in Western Australia, supporting 20 mines and numerous smaller exploitations with a total production of >260 t of gold (1887–2001). The parent intrusion is peraluminous two-mica granite (Müller *et al.* 2004).

Stockwork gold deposits are characteristic for metapelitic host rocks. For example, Sukhoi Log in Siberia (Russia) is hosted by Neoproterozoic pyritic black shales and siltstones. Gold was introduced in the Early Palaeozoic (Distler *et al.* 2004; note, however, the different interpretation as a metamorphosed sedex deposit by Large *et al.* 2007 and Chang *et al.* 2008). Cambrian-Ordovician deformed and metamorphosed shales and carbonaceous siltstones host the giant Muruntau stockwork deposit (Uzbekistan), which displays features of intrusion-related orogenic origin (Morelli *et al.* 2007).

An exemplary breccia pipe deposit was exploited by the Kidston Mine, North Queensland, Australia (1985–2001). In this region, felsic Permian ring dyke complexes intruded Proterozoic metasediments and granites. With a surface area of 1300 by 900 m, the nearby Kidston breccia pipe penetrated granite. Felsite and porphyry dykes cut across the pipe. The matrix of the breccia contained free-milling gold (electrum), pyrite, minor arsenopyrite, galena and sphalerite, and quartz with carbonates as a gangue. The breccia fragments were sericitized and carbonatized. Near the border of the orebody breccia, higher-grade sheeted gold quartz veins were developed. Fluids associated with mineralization included saline brines, gas and aqueous inclusions with a low salt content. The latter appear to have controlled gold transport and precipitation, originating by condensation of magmatic vapour (Baker & Andrew 1991). The large open-cut mining potential was only realized when the genetic association of gold mineralization with the breccia pipe was recognized (Lewis 1990). Resources amounted to 90 Mt with ~2.5 ppm Ag and 1.7 ppm Au. Giant copper sulphide breccia orebodies with gold as a by-product are exploited at Olympic Dam in South Australia, which is the largest of the iron oxide-copper-gold deposits (Groves *et al.* 2010, cf. "Copper").

Intrusion-related gold quartz veins may be common, but if there is no visible spatial connection to a potential igneous parent, recognition and differentiation from metamorphogenic deposits is difficult. In the past, all "mesothermal" gold veins (formed at intermediate depth and temperature) were thought to have a magmatic-hydrothermal origin. Mesothermal gold-quartz veins are ubiquitous in plutonic-metamorphic provinces such as the North American Cordilleras, Brazilian, African, Canadian and Australian greenstone belts, and the Pan-African belts of Ethiopia, Sudan and Egypt. Accurate and detailed investigations demonstrate that some of these deposits were in fact formed from magmatic-hydrothermal fluids (Baker *et al.* 2006). A striking common feature is the association of gold with W, Bi, As and Mo, and the localization within tin and tungsten ore provinces. A somewhat exotic observation in this context is that bismuth, or more complex polymetallic low-temperature (200–400 °C) melts such as Bi-Te-S, may scavenge gold from hydrothermal fluids and give rise to economic gold deposits (Tooth *et al.* 2008). Rare minerals such as maldonite (Au_2Bi) and a strong positive Au-Bi correlation in gold ore suggest that this process may have been involved.

Carlin type deposits

The precise origin of "sedimentary rock hosted, disseminated" gold deposits, which are clearly epigenetic is still disputed. The economically most prominent examples occur in Palaeozoic carbonate rocks near Carlin, Nevada, USA, as replacement orebodies that were probably formed in the Eocene (Hofstra & Cline 2000, Hofstra *et al.* 2003). Gold production, reserves and resources of the Carlin trend are thought to exceed 3800 tonnes. Hydrothermal "jasperoid" (silicified decarbonated limestone) and anomalous arsenic characterize alteration. Gold precipitation was induced by sulphidation when H_2S-rich auriferous fluids reacted with reduced iron in the host rocks. One genetic hypothesis implicates an Eocene mantle diapir (Oppliger *et al.* 1997). New dating suggests that the ores formed while a large plutonic complex was emplaced at depth (40–36 Ma: Ressel & Henry 2006). Most of the fluids seem to be meteoric (Henry & Boden 1998) but water and sulphur (Kesler *et al.* 2005) in ore-related minerals have a magmatic (or metamorphic) component. Also, Johnston *et al.* (2008) provide links between Carlin deposits and magmatic activity. Pulsed incursion of magmatic Au-As-Hg-Cu-Te fluids of high-sulphidation epithermal character is suggested by Barker *et al.* (2009). Overall, a distal derivation of the Carlin deposits from calc-alkaline magmatism seems to be the best interpretation (also considered by Sillitoe 2010). Similar deposits have been discovered in Guizhou, southern China, and were suggested to be of late Yanshanian (Cretaceous) metamorphogenic origin (Su *et al.* 2009).

Volcanogenic gold deposits

Volcanogenic gold deposits are located in terrestrial and marine settings. Since Lindgren (1933), the first are called epithermal gold-silver deposits. This class includes many historic, often extremely rich ore districts, such as the Thracian gold of classical Greek and Roman time (essentially in Bulgaria and Romania). In contrast to the old workings, today's epithermal gold mines exploit rather low-grade but high-tonnage orebodies, predominantly sited in the young Circum-Pacific

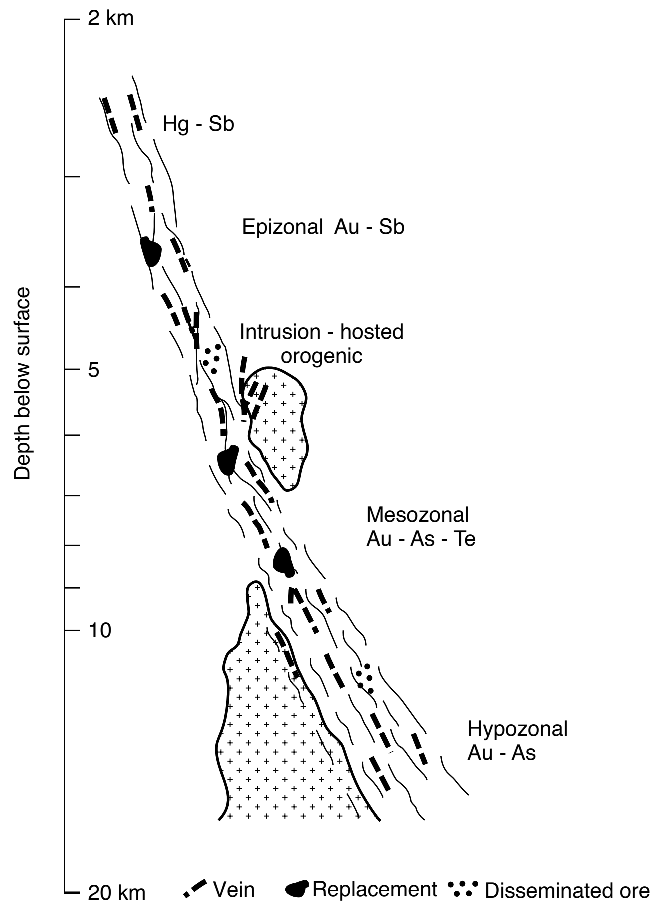

Figure 2.22 Schematic presentation of orogenic gold deposits in the "crustal continuum model". After Groves, D.I., Goldfarb, R.J., Robert, F. & Hart, C.J.R. 2003, Society of Economic Geologists, Inc., *Economic Geology* Vol. 98, Figure 2A, p. 5. The majority of these deposits (>95%) occur in the mesozonal regime (Table 1.2) and within greenschist-metamorphic rocks.

mountain belts (e.g. Ladolam, Lihir). Epithermal gold is infrequently found in Precambrian orogens. One exception is Mahd Ad Dhahab, Saudi Arabia in Neoproterozoic volcanic arcs. Typically, epithermal gold occurs in late- to post-orogenic calc-alkaline andesitic-rhyolitic volcanic fields with a complex magmatic and structural history (Simmons *et al.* 2005). The regional stress field is marked by substantial crustal extension, as in the Tertiary Basin and Range Province, USA. Both stratovolcanoes and calderas with subvolcanic intrusions locate deposits (Milos, Aegaean Sea; Fidji, Pueblo Viejo: Figure 2.22). Note, however, that Pueblo Viejo is an unusual high-sulphidation epithermal deposit insofar as it developed in a largely submarine, island-arc tholeiitic volcanic sequence (Kesler *et al.* 2005).

General characteristics of epithermal deposits are provided in Chapter 1.1 "Volcanogenic Ore Deposits". Epithermal gold deposits are mainly of the "alunite" or "high sulphidation type", but there are important exceptions (e.g. Lihir). Epithermal gold is typically associated with the "volatile" metals and semi-metals Hg, As, Sb, Te and Tl (Figure 2.23). The world's largest epithermal gold deposit is said to be Lihir on Niolam (or Lihir) Island, Papua New Guinea, with resources of ~1300 tonnes of gold in ore >1.5 g/t:

> At Pueblo Viejo, the gold-silver ore is characterized by elevated contents of As and Sb, whereas the more volatile elements Te and Hg migrated in a gas phase closer to the palaeosurface. The ore-forming system consisted of hydrothermal fluids, which interacted

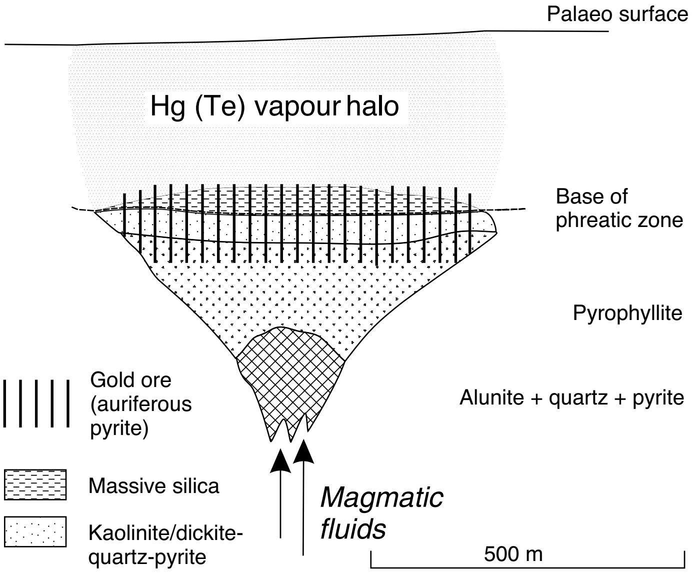

Figure 2.23 Schematic reconstruction of funnel-shaped hydrothermal alteration-mineralization at the epithermal high sulphidation gold-silver deposit at Pueblo Viejo on Hispaniola Island, Dominican Republic, hosted in Early Cretaceous volcanic arc rocks of the Greater Antilles (modified from Kesler *et al.* 2003). Pyrophyllite originated from kaolinite when the deposit and its host rocks were later metamorphosed at 300 °C and 3 kbar (Mueller *et al.* 2008).

with episodic plumes of magmatic vapour. Host rocks are Early Cretaceous sandstones and siltstones with abundant terrestrial plant and algal bituminous matter, which fill a maar-like diatreme together with andesite and quartz porphyry breccias. Oxide ore was exploited earlier (1975–1996: 166 t Au), whereas refractory sulphide resources totalling 195 Mt at 3.25 g/t Au wait for reopening of the mine. The deposit was formed in the Albian (Early Cretaceous) at 109 Ma within a primitive oceanic island arc (Mueller *et al.* 2008).

At Lihir $\sim$400,000 years BP, a sector of a Pleistocene stratovolcano comprising lavas and tuffs of trachybasalt, trachyandesite and latite collapsed into the sea. This caused the conversion of a weak Au-porphyry system into a giant epithermal system hosted by phreatomagmatic breccias (Müller *et al.* 2002). The matrix of these breccias contains disseminated auriferous pyrite, which represents most of the gold ore. Two orebodies cover $\sim$2 km^2 and extend from the surface down to 400 m below sea level. Rocks are hydrothermally altered, including argillic (smectite) and advanced argillic facies (alunite), as well as parageneses of quartz, potassium feldspar and pyrite (±illite, anhydrite, calcite). Epithermal veins with quartz, chalcedony, illite, adularia and pyrite (indicating low sulphidation) contain locally up to 120 g/t of Au. Fluids had low salinity (5–10 wt.% equivalent NaCl), temperatures between 150–250 °C and were mainly of magmatic origin, with some admixture of meteoric and seawater (Gemmell *et al.* 2004). Until today, fluids similar to those that deposited the ore are venting in the crater (Simmons & Brown 2006, Figure 2.24). Wells were drilled to >1 km depth in order to remove hot water before it endangers open pit operations. The inherent geothermal energy is used for producing all electrical power needed at the mine.

The Inner Carpathian Arc of the Alpine orogenic belt, mainly in Transylvania (formerly Siebenbürgen), Romania, supported several thousand years of gold mining. The most famous ancient mining district is the "Golden Quadrilateral" in the southern Apuseni Mountains with several former and current mining centres. The plate tectonic setting was an overall geodynamic regime of northward subduction, modified by slab detachment and brittle tectonics in the crust (Neubauer *et al.* 2005). Orebodies are related to Neogene calc-alkaline volcanoes that developed above thrust sheets of Cretaceous flysch and ophiolites. Epithermal low-sulphidation mineralization is hosted by volcanic vents, sub-volcanic intrusions and rarely by sedimentary country rocks. The volcanic rocks are commonly described as dacites, but may be better classified as biotite and hornblende bearing "quartz andesites" of the IUGS classification. Au, Ag, Zn and Pb have mainly been mined from steeply dipping grey quartz pyrite veins characterized by open space filling

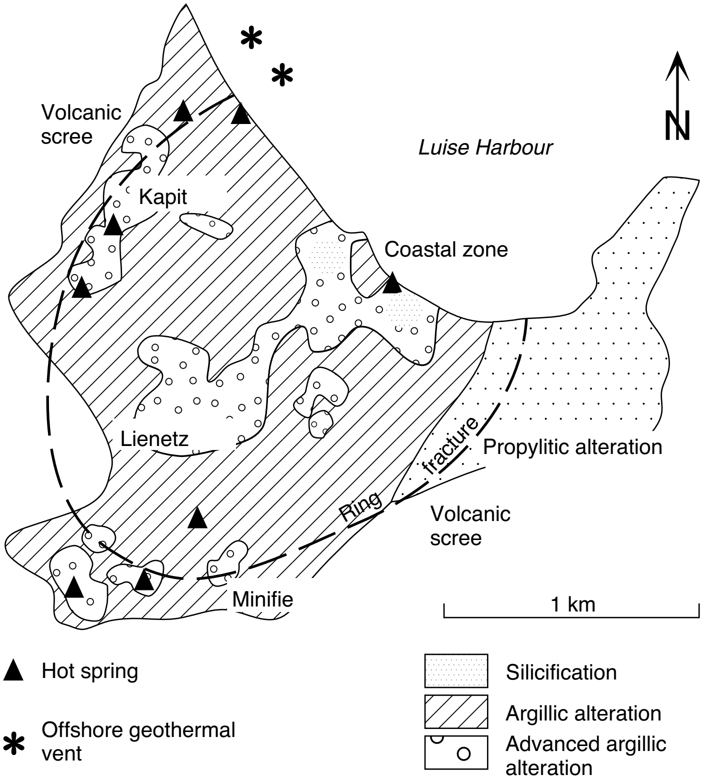

Figure 2.24 Mineralized zones, hydrothermal alteration of volcanic rocks, hot springs in the crater and offshore vents at the giant Ladolam gold deposit, Lihir Island, Papua New Guinea. Lienetz and Minfie are the major orebodies. After Gemmell, J.B., Sharpe, R., Jonasson, I.R. & Herzig, P.M. 2004, Society of Economic Geologists, Inc., *Economic Geology* Vol. 99, Figure 4B, p. 1715.

textures and from hydrothermal breccia zones. Electrum is the main gold carrier, together with pyrite, base-metal sulphides, and a variety of sulphosalts and minor tellurides. Hydrothermal ore zone alteration is characterized by quartz-illite-pyrite, replacement adularia and silicification, and is surrounded by bleached illite-rich dacite. Fluids and metals were sourced from deeper intrusions (Alderton & Fallick 2000):

> Recent exploration revealed Roșia Montană as the largest gold deposit in Europe, set in a maar-diatreme complex (Wallier *et al.* 2006) with identified resources of ~400 Mt at 1.3 g/t Au and 6 g/t Ag. The Sacarimb deposit is noted for its abundant telluride minerals. It is hosted by the vent of an eroded stratovolcano that was built of amphibole-biotite quartz andesite. Two conjugated vein systems with a different paragenesis were developed. Initially and at depth, base metal sulphides were introduced. Tellurides and sulphosalts formed in the succeeding phase, followed by native gold, arsenic and antimony. Main gangue minerals are quartz and carbonates. A wide halo of propylitization surrounds the deposit.

Metamorphic gold deposits

Metamorphic gold deposits owe exploitability to locally confined redistribution and recrystallization caused by metamorphism (cf. Chapter 1.5 "Metamorphic and Metamorphosed Ore Deposits"). In rare cases at high metamorphic temperatures, sulphide melts instead of aqueous fluids may have formed lode gold deposits, as proposed for Hemlo (Ontario, Canada: Tomkins *et al.* 2004) but, of course, based on a premetamorphic concentration (Davis & Linn 2003, Heiligmann *et al.* 2008). The principle may apply to deposits such as Sukhoi Log, Russia, where according to Chang *et al.* (2008) metamorphic recrystallization of early-diagenetic auriferous pyrite liberated and concentrated gold in the hinge zone of an anticline. This giant orebody comprises 1100 t Au averaging 2.45 g/t.

Metamorphogenic gold deposits

The formation of metamorphogenic gold deposits is a consequence of the passage of metamorphic fluids (cf. Chapter 1.6 "Metamorphogenic Ore Formation Systems"). Prograde metamorphic dehydration of volcano-sedimentary rocks takes place during orogenic metamorphism and deep magmatic activity. The generalized model (Kerrich 1999) describes extraction of gold from rocks as an effect of the exudation of crystal water from OH-bearing minerals, at 400–500 °C (3.5–5 kbar) for the greenschist-amphibolite facies transition. In this case, metabasalt yields ~5% H_2O, which follows the pressure gradient to lower P/T domains. The intimate fluid-rock interaction favours dissolution of trace metals. In the case of high H_2S activity in the fluid, iron and base metals are nearly insoluble so that gold is relatively enriched. The model is confirmed by studies in New Zealand, where ore-forming elements (Au, Ag, As, Sb, Hg, Mo, W) are depleted in higher-grade rocks relative to unmetamorphosed protolith samples. The same elements are enriched in the island's orogenic gold deposits (Pitcairn *et al.* 2006). Crustal-scale faults (Willman *et al.* 2010) and shear zones (Weinberg *et al.* 2004) take up the diffuse fluid flow and discharge into fluid escape zones which are often tectonic highs. Even at low gold concentrations, the giant mass of fluids moves a considerable mass of gold. Falling temperature (300–400 °C) and pressure, transition from ductile to brittle mechanical behaviour of rocks and chemical reactions with wall rocks precipitate the gold (Figure 1.85).

Metamorphogenic gold deposits commonly occur in the form of quartz veins and vein stockworks within greenschist facies rocks, but replacement or disseminated orebodies are known (Figure 2.22). The hydrothermal-epigenetic origin is revealed by hydrothermal alteration of host rocks (Campbell-McCuaig & Kerrich 1998) and by isotopic anomalies. Induced nitrogen and certain nitrogen isotope ratios, for example, attest to a distal metamorphic derivation of fluids (Jia & Kerrich 1999, Jia *et al.* 2003).

Many gold deposits in metamorphic terranes postdate the peak of deformation and metamorphism. This implies i) persisting deep metamorphism while the surface cools, ii) ponding of metamorphic fluids at depth, or iii) retrograde-metamorphogenic formation with pervasive flooding of hot rock volumes by outside fluids during uplift, distension and shearing (Figure 1.86; Templeton *et al.* 1997). Apart from retrograde reactions, an oxidation front caused by infiltrating meteoric water may mobilize gold and concentrate the metal in hydraulically favourable tectonic structures (Craw & Chamberlain 1996).

Although most Archaean gold deposits occur in greenschist facies rocks, some provinces display a spread of host rocks from granulite facies to very low metamorphic grade. In Western Australia, hydrothermal alteration changes parallel to metamorphic P/T-conditions of host rocks. Groves (1993) concluded from this observation, that hydrothermal fluid flow systems affected the whole crustal cross-section. This is the essence of the "crustal continuum model". Because metamorphism and melting affect the crust synchronously, both metamorphic and granitoid-derived magmatic fluids may produce gold concentrations, which have been subsumed *as orogenic gold deposits* (Figure 2.22; Goldfarb *et al.* 2005, Groves *et al.* 2003, Groves 1993, Goldfarb 2002). The term avoids purposely a process-related genetic classification in order to stress the coherence of the metallogenetic system.

The majority of gold deposits in Archaean and Palaeoproterozoic greenstone belts are genetically linked to orogenic metamorphism, magmatic activity and major, often crustal-scale shear zones and are prototypes of orogenic gold deposits. Greenstone belts are elongate narrow structures crossing Early Archaean gneiss and granulite terranes, built from felsic to ultramafic igneous rocks, volcaniclastic, siliciclastic and chemical sediments, all intruded by granites. If a generalization of greenstone belt architecture is at all possible, thick suites of primitive ultramafic and mafic volcanic rocks form the base, overlain by intermediate and felsic volcanics, in their turn covered by flysch and molasse-like sediments. Metamorphic grade is usually greenschist to amphibolite facies. Deformation varies from simple sag-basins to folded and overthrusted assemblages. In spite of lingering doubts, there is now a broad consensus that greenstone belts are the product of seafloor spreading followed by subduction-accretion processes in island arcs (Windley 1995). Greenstone belts are distinguished by nickel-sulphide deposits in komatiites, volcanogenic banded iron ores of the Algoma type, massive base metal-sulphide deposits and economically outstanding gold deposits:

> Many greenstone belts host gold quartz vein and stockwork deposits. With a historic production of ~1800 t and reserves plus resources of ~500 t gold, the Golden Mile at Kalgoorlie in Western Australia is among the world's largest. Orebodies extend over 4000 m in length and to a depth of >1500 m. Host rocks are greenschist-metamorphic basalts, which have been deformed by folding and wrench-faulting. Brittle-ductile shear zones control more than 1000 single veins, which together constitute the Golden Mile deposit. A wide halo of hydrothermal chlorite-calcite alteration is developed. Ore is composed of vein quartz and hydrothermally altered metadolerites and pillow lavas. Orebodies consist of breccia and cavity-fill veins, surrounded by a sericite-ankerite-siderite-quartz-haematite-pyrite-telluride alteration zone, which contains most of the gold. One-third of gold is native gold in quartz; nearly one-half forms tiny rounded inclusions in pyrite (with a diameter in the μm-range) and ~25% occurs in tellurides. Geochemically anomalous trace metals include As, Hg, W, B, Sb, Pb and Zn. Fluid inclusions in quartz display CO_2 content and low salinity; formation temperatures were 300–400 °C at pressures of 1–2 kbar. Gold was probably transported in sulphide complexes and co-precipitated with pyrite by reaction with reduced iron in the basalts. The ultimate source of the gold remains uncertain. Some data suggest an origin from deeply buried komatiites and their syngenetic exhalites. The dominantly vertical structures of the Golden Mile imply vertical upflow of the hydrothermal fluids. Based on age dating, McNaughton *et al.* (2005) contemplate a convergent plate tectonic setting of the Golden Mile (and most gold in the Eastern Yilgarn craton) at an active continental margin. The hydrothermal systems would have been generated during the change from subduction to wide-spread crustal melting. Vielreicher *et al.* (2010) demonstrate that gold formation took place at 2.64 Ga, late in orogenesis and overlapped with waning stages of regional metamorphism. After more than a century of selective underground mining, the deposit is now worked as a large open pit (Figure/Plate 2.25).

The important role of ultramafic volcanic rocks as a source of gold in greenstone belts was highlighted by Keays (1995). Until eruption, these magmas remain undersaturated in respect of sulphur, so that a sulphide melt cannot form. This is contrasted by basaltic systems that more easily segregate sulphide melts that concentrate chalcophile and siderophile trace metals such as gold. Because of their high density, sulphide melts, however, are commonly left behind at depth (cf. Chapters 1.1 "Orthomagmatic Ore Formation"; Section 2.1.4 "Nickel"). Komatiites, picrites and boninites exsolve sulphides only when approaching the solidus. The sulphides scavenge traces of Au, Pd, Pt, Ag, Cu, Ni, Zn, Se, Te and some Pb, Mo, Sn, W and Bi. In contrast to silicates and oxides, sulphides are easily dissolved by pervading hot fluids, so that small fluid volumes (e.g. those liberated by metamorphic dehydration) may form relatively concentrated ore fluids.

Ultramafic rocks of greenstone belts and ophiolites are also frequent host rocks of gold ore deposits (Barberton Mountain Land, South Africa, Barramiya, Egypt, Bou Azzer, Morocco). Notable carbon dioxide and potassium addition characterizes hydrothermal alteration in gold deposits where former peridotites are changed into Mg-Fe-Ca carbonate rocks with fuchsite (Cr-muscovite) and quartz. Accessory minerals include talc, serpentine, chlorite, haematite, magnetite, pyrite and residual chromite. These alteration rocks are called *listwaenite* (Halls & Zhao 1995), and may contain gold in quartz veins and pyrite halos. In several locations, they are also sites of Ag, Hg, As, Co and Ni mineralization. Mineralizing fluids are not necessarily metamorphic but this is not infrequent.

Metamorphogenic shale, or turbidite hosted gold deposits

Metamorphogenic shale, or turbidite hosted gold deposits are best illustrated by referring to Bendigo and Ballarat, once fabulously rich gold districts in Victoria, Australia (Phillips & Hughes 1996):

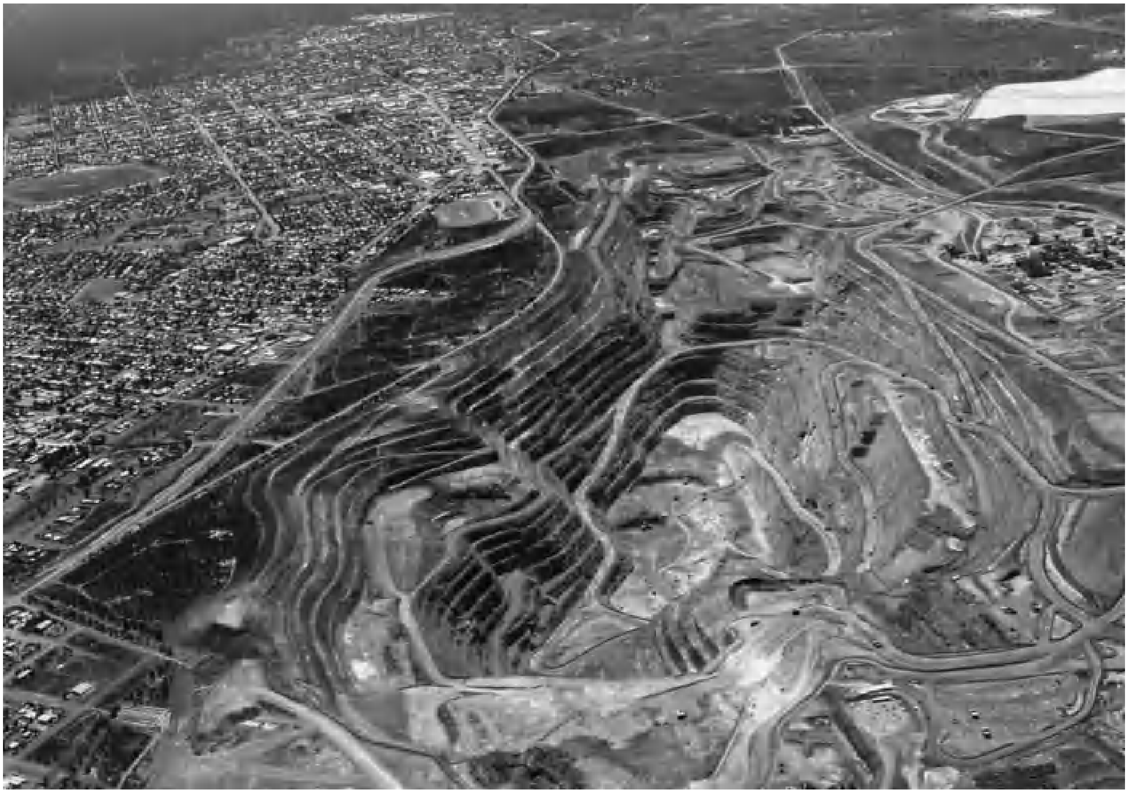

Figure 2.25 (Plate 2.25) The Golden Mile Superpit at Kalgoorlie, Western Australia (2006). Note supergene oxidation in the foreground, the city of Kalgoorlie-Boulder on the left and tailings (white) in the right-hand background. Photo provided courtesy Kalgoorlie Consolidated Gold Mines (KCGM).

Host rocks are Cambrian to Early Devonian turbidites of the Lachlan orogen deposited in deep submarine fans. Shales and greywackes are part of an accretionary wedge above the west-dipping subduction zone along the Pacific Gondwana margin (Fig. 1.84; Hough *et al.* 2007). Deformation progressed from west to east between 455-390 Ma. Concurrent metamorphism liberated fluids from deeply buried Cambrian oceanic and arc-related mafic volcanic crust. Fluid flow was channeled laterally for considerable distances by crustal-scale faults (Willman *et al.* 2010). Deposits consist of quartz veins and concentrate in anticlinoria which served as vertical fluid escape zones.

Early veins form an interconnected fracture mesh controlled by folds, bedding planes, cleavage and reverse faults and are partly deformed. Most gold mineralization was synchronous with peak deformation and metamorphism but extended into later tensional strain (Jia *et al.* 2000). Fluids were CO_2-rich, of low salinity and had temperatures of 135–360° C. The paragenesis comprises free gold, pyrite, arsenopyrite and pyrrhotite in quartz with ankerite and albite. Host rock alteration is macroscopically visible because of proximal bleaching and a wide halo of siderite spots; microscopic features include the introduction of sericite, chlorite, carbonates and pyrite-arsenopyrite (Bierlein *et al.* 2000). High-grade ore shoots occur at the contact with pyritic and graphitic beds ("indicator beds") and lumps of native gold were found that reached 18.8 kg. Since 1851, Victoria State produced a total of 2500 t of gold of which ~40% were derived from quartz veins. The larger part of the total was extracted from placer deposits that included some famously rich bonanzas. The heaviest nugget weighed 71 kg.

Most of the rich metamorphogenic and orogenic gold provinces are restricted to three periods of Earth history: Neoarchaean (2.8–2.5 Ga), Palaeoproterozoic (2.1–1.8 Ga) and Neoproterozoic (~600 Ma) to Early Tertiary (~40 Ma). These timespans include the formation of the first cratons and supercontinents, and of orogenesis, accretion and collision (Kerrich & Cassidy 1994). Among the youngest orogenic gold deposits are Miocene quartz veins in the lowermost (Penninic) tectonic unit of the Alpine orogen in Europe (Pettke *et al.* 1999).

Alluvial gold placers

Recent and fossil alluvial gold placers are, in roughly equal shares, the source of two-thirds of cumulative world gold production. Recent placer districts were the scenes of the epic gold rushes of the 19th century (California; Alaska: Craig & Rimstidt 1998; Yukon, Canada: Lowey 2006; Australia), but today this deposit type has a limited economic significance (Columbia, Mongolia). Among fossil gold placers worldwide, the Neoarchaean Witwatersrand Basin in South Africa is unique: Since its discovery in 1884, 50,000 tonnes of gold were produced. Today, after a long but slow decline the basin delivers each year ~300 t gold, 3000 t uranium and 1000 kg osmiridium. Mining is exclusively underground (except for the reworking of tailings) and at depths approaching 4000 m. Average gold content in ore amounts to 5 g/t. Remaining gold in place is estimated at 800 Moz. The volumes edited by Anhäusser & Maske (1986) are an important source of detailed descriptions of the Witwatersrand gold district and its deposits:

> The Witwatersrand Basin is built of three major volcano-sedimentary successions known as the Witwatersrand Triad that were deposited between 3.1 and 2.6 Ga. The oldest rocks are quartzites, basic and felsic lavas of the Dominion Group, followed by the Witwatersrand Supergroup starting with unmineralized sediments, lavas and banded iron formations (West Rand Group), which are overlain by alluvial fans (the gold-rich Central Rand Group: Figure 1.65). Youngest rocks are the bimodal volcanics of the Ventersdorp Supergroup; in sediments near its base above a tectonic unconformity, several horizons of gold-bearing sediments are exploited. Ventersdorp lavas have an age near 2700 Ma and their feeder dykes cut across the gold reefs (Meier *et al.* 2009). The Witwatersrand Basin is a half-graben with marginal faults in the north that were active during late Witwatersrand and in early Ventersdorp time. Later deformation was caused by the collision between the Transvaal and the Zimbabwe cratons. Several phases of metamorphism did not surpass lower greenschist facies conditions (350 °C and 2–3 kbar), in spite of a total thickness of 20 km. Thermal metamorphism was induced by the emplacement of the anorogenic Bushveld Complex (~2.06 Ga), but not in all gold fields (Rasmussen *et al.* 2007). At ~2.02 Ga, the whole basin was affected by the Vredefort extraterrestrial impact (Hayward *et al.* 2003) that caused widespread brecciation. Parts of the basin are covered by Karroo (Permo-Mesozoic) platform sediments.
>
> Witwatersrand gold is mainly hosted by quartzitic conglomerates of a certain sedimentary facies: Highest contents are found in polymictic bouldery gravels of intermediate grain size building braided channels of former delta fans (Figure 1.65). Both landward coarser gravels and basinward finer sediments contain little gold. The thickness of auriferous beds ("reefs") varies from <0.2 to 4 m. Host rocks are quartzites, schists and little mineralized conglomerates. Many of the auriferous quartz-pebble reefs display visible contents of kerogen and bitumen ("carbon seam reefs", Figure/Plate 2.26a). Geological observations such as truncation by palaeochannels confirm that the organic substance was formed *in situ* by microbial mats (Mossman *et al.* 2008). The organic substance trapped uranium and thorium ("thucholite").
>
> Essentially, gold occurs in the matrix of the conglomerates. Striking are rounded pebbles of pyrite with inclusions of silicates and traces of Au, Ag, Ni, Cu, Pb and Mo. There is also epigenetic hydrothermal pyrite that owes its origin to diagenesis or metamorphism. Native gold predominates in the ore, in the form of detrital grains (50–100 μm diameter) that contain ~10% silver and 2% mercury, and have a rhrenium/osmium age of ~3030 Ma (Kirk *et al.* 2002). Locally, gold is present in thucholite (Figure/Plate 2.26a) and in diagenetic or metamorphic mobilizates (Frimmel & Gartz 1997). Exceptionally, hydrothermal quartz veinlets cutting Witwatersrand rocks are auriferous. Detrital rounded uraninite grains with a diameter of 75–100 μm contain disseminated inclusions of

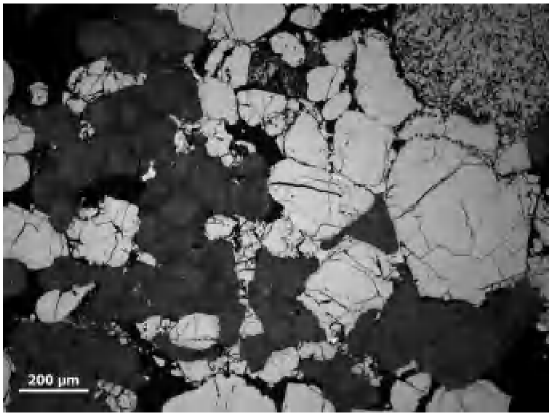

Figure 2.26a (Plate 2.26a) Overview of high-grade gold ore in carbon-rich reef at Elsburg Mine, Witwatersrand, S.A. (plane-polarized reflected light). Courtesy B. Lehmann, Clausthal. The matrix between quartz pebbles (not visible) consists of clastic pyrite (light grey with fissures), pyritized claystone pebbles (top right margin) and clastic uraninite (medium grey with specks of radiogenic lead in galena, white) in thucholite matrix (pyrobitumen, wavy dark grey and black). Gold (yellow) in intragranular pore space is mostly remobilized.

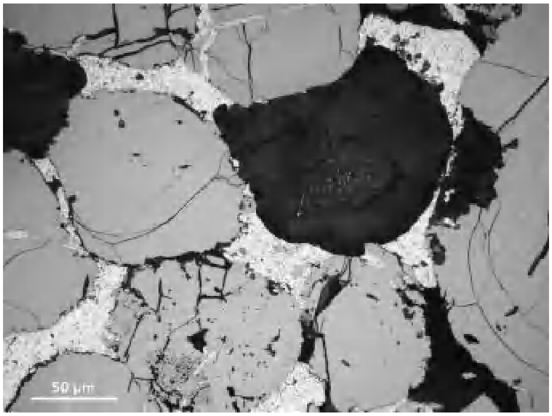

Figure 2.26b (Plate 2.26b) Detailed image of high-grade gold ore in carbon-rich reef at Elsburg Mine, Witwatersrand (polarized reflected light, oblique nicols, oil immersion). Courtesy B. Lehmann, Clausthal. Pyrite (light grey with fissures), gold (yellow, intergranular), uraninite (medium grey speckled with galena) in thucholite (pyrobitumen, wavy dark grey and black).

radiogenic galena (Figure/Plate 2.26b). During metamorphism, some of the uraninite reacted with fluids to form brannerite. Carbon seam reefs may be high-grade sources of gold and uranium. Other heavy minerals in Witwatersrand placers include arsenopyrite, chromite, cobaltite, zircon, chloritized garnet and native osmiridium. The absence of magnetite and ilmenite is not fully understood.

The scientific consensus on the origin of the Witwatersrand gold reefs is the "modified placer model", as described above. Although some scientists favour hydrothermal-epigenetic, possibly metamorphogenic formation processes (the "hydrothermal model", Law & Phillips 2005), geological observations (Meier *et al.* 2009) and rhenium-osmium dating (Kirk *et al.* 2001) refute this hypothesis. The ultimate source of the giant mass of gold is not known. Most probably, the Witwatersrand palaeorivers eroded older greenstone belts. Hydrothermally altered granites and felsic volcanics were present in the catchment area (Robb & Meyer 1995) and may have been a source of gold. Predominant pebbles in the reefs (quartz, quartzite, black schists and chert) provide no clear hint at a specific source. Questions have been raised concerning the popular hypothesis that river transport of pyrite and uraninite would only have been possible under a low-oxygen atmosphere. Falconer *et al.* (2005) described many textures that are similar to the Witwatersrand deposits, including sedimentary and diagenetic pyrite in Tertiary quartz pebble conglomerate placers of New Zealand.

Exploration for gold is exceptional because even today, prospectors and small companies may, with luck, find a new viable deposit. Programmes are based on geological concepts (e.g. structural and lithological controls, metamorphic gradient, etc.) and involve available mineralogical, geochemical and geophysical methods. Specific problems arise during sampling and analysis because of three points:

1 In ore, gold is nearly always irregularly distributed (the "nugget effect") and "clustering" may cause an apparent nugget effect (Dominy & Platten 2007);

2 because of the metal's softness and ductility, homogeneous comminution of gold particles is quite difficult; and

3 gold is much heavier than silicate gangue, resulting in rapid gravity separation, for example within sample bags during shipping.

It is therefore extremely important in every individual project to experiment and work out a procedure that minimizes resulting errors (cf. Chapter 5 "Geological Mapping and Sampling"). Reverse circulation drilling methods provide good recovery of reliable samples, but geological interpretation still needs diamond-drilled core. All sampling and analytical procedures must be checked by well-chosen double and triple samples. For gold, time-tested fire assays and INAA (Instrumental Neutron Activation Analysis) are analytical standard methods. The newly adapted gamma-activation analysis (CSIRO, Australia) provides equal precision and accuracy, but accepts samples weighing several hundred grams, which avoids errors induced by subsampling. Precautions must be taken to avert criminal manipulation of samples, such as "salting" with gold dust or chloride solution.

Geochemical exploration methods for gold are founded in the concept of pathfinder elements. This dates from times when gold analyses were time-consuming and costly, but is still justified by the three problems mentioned above. Compared to gold, pathfinder elements such as Ag, As, Bi and Sb have a considerably less erratic distribution, form larger halos and occur in higher concentrations. They can even be used to evaluate the gold potential of large tectonic-stratigraphic terranes (Plant *et al.* 1997). In specific gold districts, different elements may be identified as useful pathfinders by pilot projects. Knight *et al.* (1999) demonstrated that Au-Ag-Hg-Cu contents of alluvial gold allow correlation with known primary sources of the particles. Particles from unknown sources may suggest a search for undiscovered deposits.

In 2009, the largest gold-producing countries were China, Australia, South Africa, USA, Russia, Peru, Canada and Indonesia. Quite the opposite of other metals, gold mine production rose in the crisis from 2260 t (2008) to 2350 t (2009). The reserves/production ratio of only 20 years characterizes the lively business of gold mining but is no reason to expect "the end of gold".

2.3.2 Silver

Common Ore Minerals:

		Max. wt.% Ag	*Density (g/cm^3)*
Native silver	Ag(Au,Cu,Hg, As,Sb,Bi)	100	10.5
Acanthite	Ag_2S	87	7.2
Proustite	Ag_3AsS_3	65	5.6
Pyrargyrite	Ag_3SbS_3	60	5.8
Stephanite	Ag_5SbS_4	68	6.2
Polybasite	$(Ag,Cu)_{16}Sb_2S_{11}$	74	6.1
Chlorargyrite	AgCl	75	5.5
Freibergite (silver-rich variety of tetrahedrite)	$Cu_6(Ag,Fe)_6Sb_4S_{13}$	18	4.6–5.2

Telluride minerals of silver including hessite (Ag_2Te) and empressite (AgTe) are not a relevant source of the metal, although they are not rare in epithermal and Precambrian gold deposits. Chlorargyrite is important in supergene silver ore; contrary to other salts, silver halides are highly insoluble in aqueous solutions. Carbonates and barite are the typical gangue minerals of silver ore, not quartz as in gold deposits. Silver-only mines commonly exploit ore with a grade >450 g/t. However, ~80 % of the metal's total mine production is silver as a by-product, mainly from copper, lead, zinc and gold ores. Silver contents in galena, sphalerite, pyrite, chalcopyrite and tetrahedrite may be sited in the crystal lattice of the host mineral or form mineral inclusions. Silver as a by-product can be recovered at grades >50 g/t. The economic viability of many base metal and gold deposits relies on by-product silver.

Use of silver is mainly in industrial applications but nearly 40% is consumed in jewellery, coins and silverware. The traditional photographic sector (silver halides in film and photographic paper) continues to decline. Like other native metals in nature, silver was one of the earliest treasures of humans. Pure silver metal has a density of 10.49 g/cm^3 and melts at 960.8 °C. Its properties include strength, malleability, ductility, electrical and thermal conductivity, sensitivity to, and high reflectance of light and the ability to endure extreme temperature ranges. Silver is part of fabricated goods such as electronics, plasma display panels, rechargeable and disposable batteries (the "button" style, which have up to 35% silver by weight), rechargeable Ag-Zn batteries, electroplating metal for steel bearings, solders for water pipes, catalysts for production of ethylene oxide (the starting-substance for plastics), electrical appliances, computers and solar energy mirrors for electricity production. Medical applications are based on the high toxicity of silver ions to microorganisms.

Geochemistry

Silver is a chalcophile element (Goldschmidt 1958). The crustal abundance of silver is estimated to range from 0.02 to 0.1 ppm (Smith & Huyck 1999). Among sediments, black shales, phosphorites and oil shales have the highest contents. Magmatic differentiation has no discernable influence on concentrations, although basalts display higher contents than granites (0.1 compared to 0.04 ppm). This is explained by differing sulphide contents. Similar to gold, silver in hydrothermal solutions rarely occurs as a simple monovalent Ag^+ ion. Sulphide and chloride complexes are more common (Stefansson & Seward 2003). In magmatic and epithermal systems, aqueous vapour may transport AgCl in concentrations relevant for ore deposit formation (Migdisov *et al.* 1999). Geothermal waters in the Salton Sea field in Southern California contain 0.8–2 ppm silver, and sulphide scales in the steam production boreholes concentrate silver to a maximum of 7%. Ore mud in the Atlantis-II-Deep of the Red Sea has an average of 18 ppm Ag and 0.3 ppm Au. It is believed that the subduction of ocean-floor metalliferous sediments has a major role in the metallogeny of convergent plate boundaries (Figure 1.88).

Silver is not redox-sensitive and displays oxidation states Ag^+ and Ag^0. In the near-surface environment, silver is scarcely mobile except under very acidic conditions ($pH < 3$: Smith & Huyck 1999). Sulphide oxidation mobilizes silver in the presence of ferric sulphate solutions. Silver is also mobile in dilute nitrate solutions. Upon encountering chloride ions, chlorargyrite is formed. At the base of the oxidized zone of silver deposits, downward seepage typically precipitates native silver (eq. 1.13), whereas silver sulphide enrichment (neoformation of acanthite similar to chalcocite in copper ore deposits) is rare. Chlorargyrite is more common in arid lands where evaporation tends to concentrate halogens near the surface (e.g. in the giant Pb-Zn-Ag deposit at Broken Hill, South Australia). Organic substances effectively immobilize silver by chelation, resulting in enrichment of humic soil or coal near outcropping ore.

Silver ore deposit types

Most primary silver ore deposits are hydrothermal and epigenetic (Graybeal *et al.* 1986). All of the hydrothermal realms (magmatic, metamorphic, sea-floor exhalations, diagenetic) are potential sources of silver, commonly at the by-product level. However, most large silver deposits are magmatic and occur in the Cordilleras of North and South America. This is believed to be the result of the singular longevity of the convergent plate boundary of the eastern Pacific rim. Supergene, secondary silver ore deposits are the result of local enrichment by descending solutions, or by groundwater in arid regions that may have migrated over considerable distances before forming "red bed" or similar infiltration deposits of silver.

By-product sources of silver include many of the vein mining districts in Europe, where silver was the original target of operations in the Middle Ages. Examples are the northern Alps (Tyrol), Kongsberg (Norway), Erzgebirge and Harz (Germany) with argentiferous veins of lead-zinc and of the Bi-Co-Ni "formation" (cf. Section 2.1.5 "Cobalt", Section 2.5.12 "Uranium"). In the 17th century, many of these vein-based mines were abandoned when large amounts of silver from newly discovered America flooded Europe. A common genetic signature of the vein districts north of the Alps is their formation from hydrothermal convection systems related to extensional tectonic deformation. Today, by-product silver is recovered from porphyry copper ore, polymetallic base metal deposits, the Copper Shale in Poland and, of course, from nearly all gold mining operations. Many volcanogenic and sedex massive sulphide deposits yield by-product silver (e.g. Cannington in Australia that may at present be the largest single source of silver in the world; Walters & Bailey 1998). Silver as an economically significant ore constituent occurs in the following genetic classes:

- skarn, contact-metasomatic and replacement ore deposits;
- volcanogenic polymetallic massive sulphides;
- volcanogenic epithermal veins, stockworks, disseminated ore and breccias;
- sedex polymetallic massive sulphides;
- metamorphogenic veins;
- infiltration deposits ("red bed type");
- supergene enrichment deposits.

Skarn and contact-metasomatic ore deposits

High-temperature skarn and contact-metasomatic ore deposits of silver (typically with lead and zinc) in carbonate rocks are economically prominent. In contrast to this group, low-temperature diagenetic-hydrothermal lead-zinc deposits (e.g. Mississippi Valley and Alpine Type) rarely have noteworthy silver. Silver-rich deposits occur in the contact zone of intermediate to felsic intrusions. Large silver skarn ore provinces occur in the American Cordilleras and in China. In southern North America, Palaeozoic and Mesozoic carbonate rocks are intruded by fertile Tertiary plutons. Ores contain silver, lead, zinc and pyrite, with minor amounts of Mn, Cu, As, Sb and Au. Gangue is dominated by calcite, quartz and dolomite. Barite, siderite, fluorite, rhodonite, rhodochrosite and the characteristic "jasperoid" are less ubiquitous. Jasperoid is hydrothermally silicified limestone (see also Section 2.3.1 "Gold") that occurs distal to parent intrusion contacts, associated with dolomitization. Proximal carbonate alteration is characterized by skarn paragenesis and recrystallization. Silver is often concentrated in tetrahedrite and tennantite [$(Cu,Ag,Zn,Fe)_{12}(As,Sb)_4(S,Se)_{13}$] and associated with galena. Orebodies are variously veins, stratabound replacement flats (mantos) and cross-cutting pipes (chimneys). Main control of ore is elevated palaeopermeability of the carbonate rock bodies, due to lithology, tectonics or hydrothermal karst. Impermeable roof rocks may have focused the aqueous magmatic-hydrothermal fluids. Fluid inclusions imply formation temperatures reaching 500 °C in the anhydrous phase of skarn formation (Baker *et al.* 2004). Water is of magmatic origin.

In China, silver-rich vein, skarn and replacement deposits occur in contact zones of Yanshanian Mesozoic granites that intruded Neoproterozoic and Early Palaeozoic sediments. Silver content of ore reaches 200 g/t in addition to by-product amounts of tin, tungsten, copper, lead, zinc, antimony and bismuth (Wu *et al.* 1993):

> One of the largest skarn deposits in China is Bajiazi. Total reserves are estimated to comprise 220,000 t Zn, 150,000 t Pb and 1647 t Ag, in ore grading 186 g/t Ag (Zhao *et al.* 2003). Orebodies occur near the contact of a Jurassic quartz-monzodiorite with Proterozoic dolomites, following a NW-striking fault zone that channelled fluids (Figure 2.27). Metasomatic veins and irregular replacement masses occur along a distance of 3.4 km (Figure 2.28). Skarn zones from the intrusive contact outwards include a proximal Mg-facies with magnetite and molybdenite, followed by Mn-Mg-skarn with sulphides of Fe, Cu, Pb, Zn and Ag, and by distal Mn-skarn with Ag, Pb and Zn. This succession reflects reaction of magmatic fluids with the dolomite and temperatures falling from >500 to ~340 °C. Lead isotope data imply that base metals and probably silver, too, are derived from deep lower crust.

Epithermal vein silver ore deposits

Volcanogenic veins, stockworks and hydrothermal breccias include mainly epithermal vein silver ore deposits with some of the largest silver producers known. Like epithermal gold deposits they are associated with Tertiary volcanic belts, including subvolcanic intrusions. Prominent examples are Guanajuato in Mexico, and the upper part of Cerro Rico de Potosí in Bolivia:

> Since 1548 when Spaniards arrived, Guanajuato yielded ~35,000 t silver and 175 t gold. Most of this was extracted from one giant vein (Veta Madre) that has a mineralized strike length of 16 km and reaches a thickness of tens of metres and a depth of 2000 m below surface. The structure occupies the marginal fault of an Eocene-Oligocene rift that is filled with coarse clastic sediments and a thick volcanic pile of

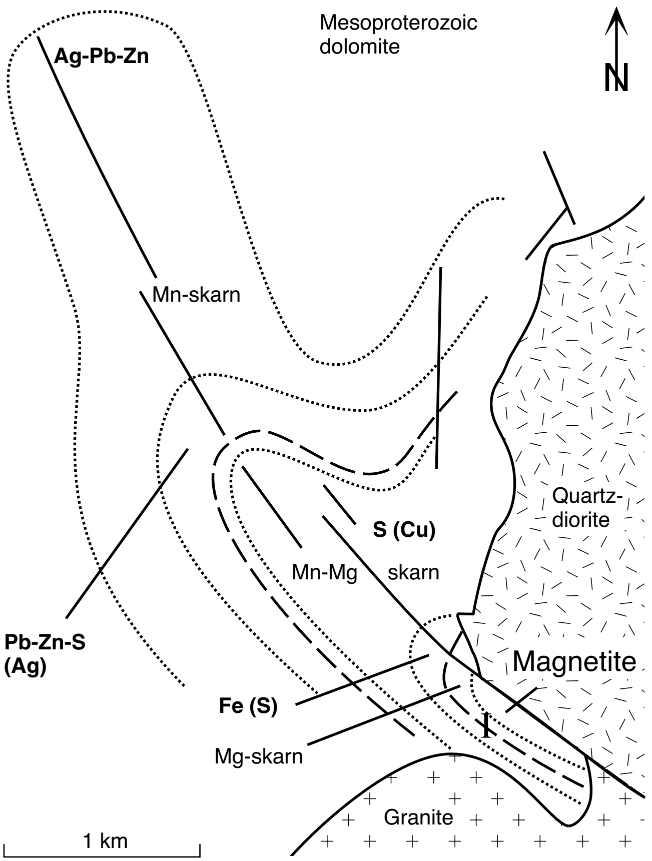

Figure 2.27 Geological zonation map of Ag-Pb-Zn skarn in the contact zone of the Jurassic quartz monzodiorite intrusion at Bajiazi, China; note alignment controlled by a fault zone (modified from Zhao *et al.* with permission from Elsevier). Dotted lines delimit different skarn zones: Proximal magnetite is followed by Fe(S) = magnetite-pyrite-pyrrhotite, S(Cu) = sulphides of Cu-Fe-Zn-Pb-Ag, and distal Pb-Zn with silver contents increasing to the Northwest.

intermediate and felsic rocks. Subvolcanic intrusions are assumed at depth. The fill of Veta Madre consists of quartz, calcite, galena, sphalerite and chalcopyrite, with native silver, silver sulphosalts and selenides. The hydrothermal alteration of host rocks comprises K-metasomatism (adularia), sericitization, kaolinization and propylitization, hinting at an affinity to porphyry copper ore systems. Already the first geological visitors of the Guanajuato mining district classified it as an epithermal deposit. Today, it is one of the prominent members of the "low sulphidation" subclass with formation temperatures of 250–300 °C (Mango *et al.* 1991).

Famous Cerro Rico de Potosí is an extinct Neogene volcano built of tuff and explosion breccias that mantle a dacite porphyry core (Cunningham *et al.* 1996; Figure 2.29, Figure/Plate 2.30). It is built on Ordovician shales. Hydrothermally altered volcanic and basement rocks host numerous ore veins. The past production from the mountain is estimated at between 30,000 and 60,000 t of silver, and the same metal mass is thought to exist in remaining resources grading ~100 g/t Ag and 0.10–0.17% Sn. Potosí is probably the largest silver deposit on Earth. Apart from silver, considerable tonnages of by-product metals tin and zinc have been extracted, with minor copper and lead. A primary hydrothermal zonation is clearly developed, arranged around a high-temperature centre with cassiterite, wolframite, bismuthinite and arsenopyrite. This passes into a lower temperature paragenesis of sphalerite, galena and silver sulphosalts. Primary silver minerals are mainly freibergite and acanthite. However, oxidation has affected the uppermost 300 m of the mountain, where a secondary supergene paragenesis developed. Hydrothermal alteration in the centre is characterized by quartz and tourmaline, followed upwards by strong argillization and a vuggy quartz cap. This is characteristic for extremely acidic hydrothermal alteration

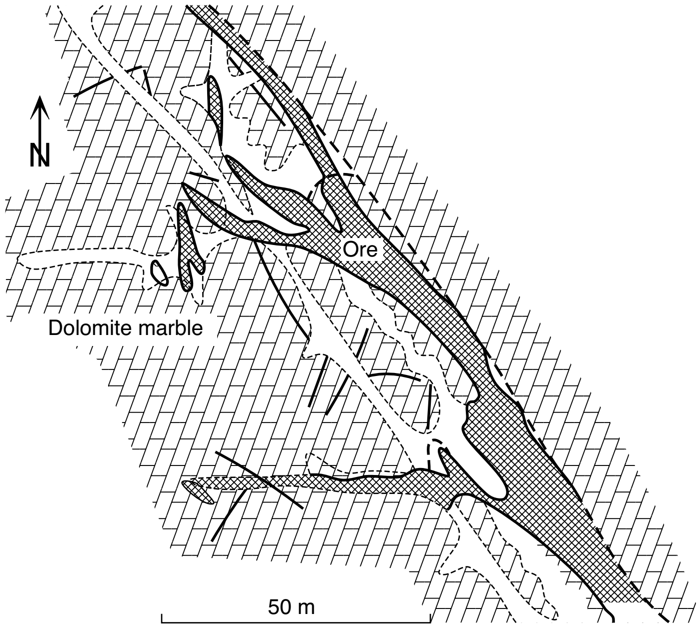
N
Ore
Dolomite marble
50 m

Figure 2.28 Geological mine map (155 m level) of Ag-Pb-Zn orebody at Bajiazi, China (modified from Zhao *et al.* 2003). Copyright (2003) with permission from Elsevier. Orebody is hatched. Ore minerals include sulphides, sulphosalts and native silver; gangue is made up of pyroxmangite $(Mn,Fe)_7[Si_7O_{21}]$, rhodonite, spessartite and phlogopite. Dashed lines designate underground mine tunnels.

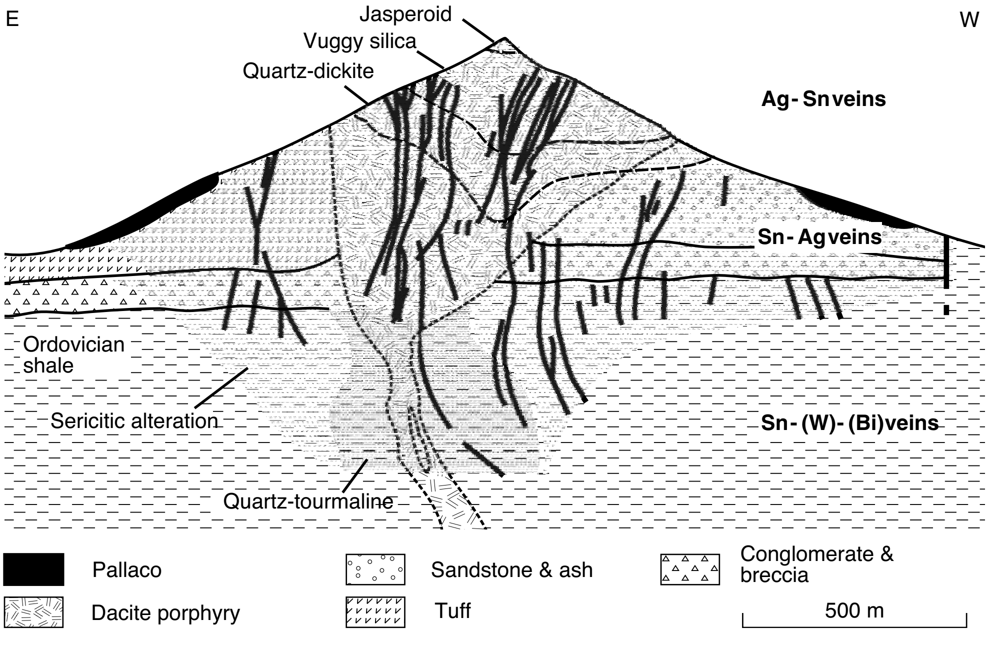
E
W
Jasperoid
Vuggy silica
Quartz-dickite
Ag- Snveins
Sn- Agveins
Ordovician shale
Sericitic alteration
Sn- (W)- (Bi)veins
Quartz-tourmaline
Pallaco
Sandstone & ash
Conglomerate & breccia
Dacite porphyry
Tuff
500 m

Figure 2.29 Vertical zonation of the polymetallic silver-tin ore veins at Cerro Rico de Potosí, Bolivia. After Bartos, P.J. 2000, Society of Economic Geologists, Inc., *Economic Geology* Vol. 98, Figure 2, p. 647. Note the typically epithermal hydrothermal alteration in the upper part of the mountain. In contrast, the subjacent porphyry system displays a central pipe of silicification and tourmalinization that is surrounded by a wide halo of sericitization. "Pallacos" are silver-mineralized mass flow deposits that slumped from higher parts of the volcano.

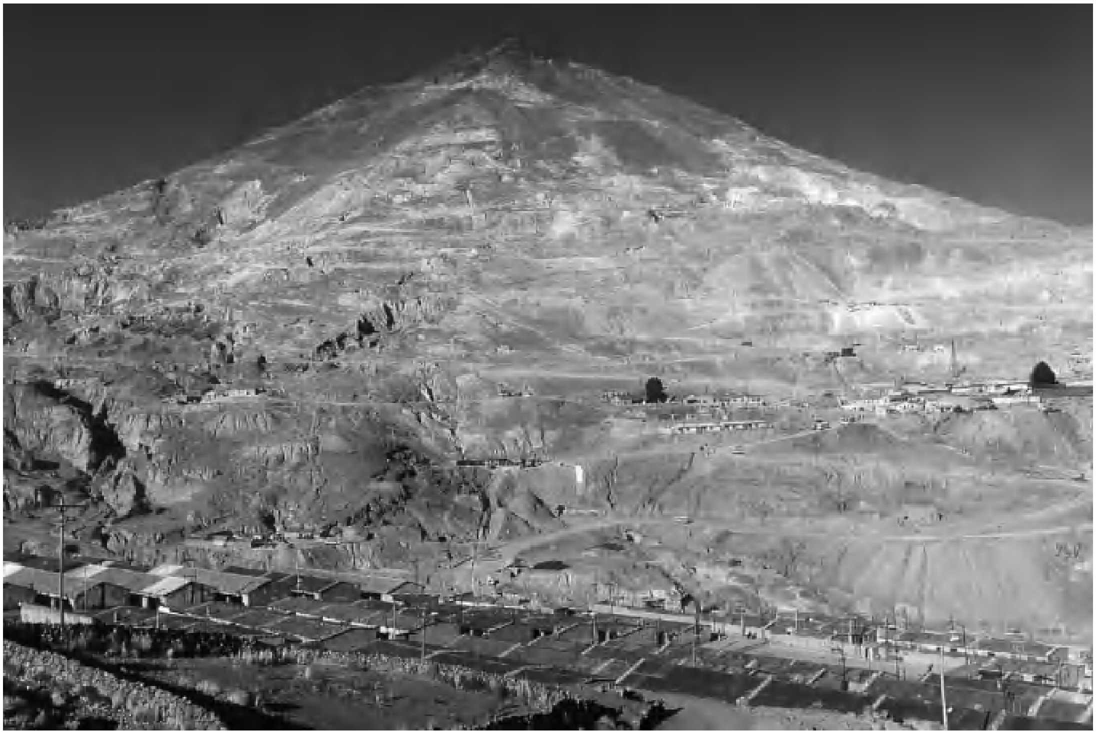

Figure 2.30 (Plate 2.30) Cerro Rico de Potosí, Central Cordillera, Bolivia, contained the world's largest pre-mining silver concentration. Courtesy B. Lehmann, Clausthal. Visible are ubiquitous traces of vein mining on the slopes and the oxidized cap of the Miocene volcano. During the 17th century, Potosí was the principle source of fabulous wealth for Spain and of silver inflation in Europe.

> of the high-sulphidation type of epithermal ore formation (Sillitoe *et al.* 1998). The vertical extent of mining reaches 1150 m. Conglomerates, breccias, and slide masses (pallacos) at the foot of the mountain are large potential silver orebodies (Bartos 2000). In 2008, the first pallaco mine went into operation.

Cerro Rico de Potosí is a revealing example of the evolution of a giant epithermal deposit from a subjacent porphyry. Stable isotope characteristics of water in the mineralizing fluids are predominantly magmatic (Cunningham *et al.* 1996). The deposit illustrates the vertical metal zonation that is characteristic for the Bolivian silver-tin province. The deepest mineralization carries tin, tungsten and bismuth, and at intermediate levels appear copper, zinc and tin (e.g. San Rafael, Figure 2.19). The uppermost levels are rich in silver and antimony, but little tin (Sillitoe *et al.* 1998).

Epithermal silver of a different setting occurs disseminated in felsic volcanic rocks in strata-bound and stratiform orebodies within permeable volcanic tuffs and interbedded clastic sediments. Deposits are controlled by calderas or subvolcanic intrusions. Ore grade is low but large-scale open pit mining allows profitable extraction. Silver is associated with sulphides of Fe, Zn, Pb and variable Cu, Au, As, Sb and Mn. Hydrothermal gangue in pore space or replacing host rock minerals includes pyrite, quartz, opal and minor amounts of sericite, carbonates and adularia. Decreasing base metal contents correlate with increasing gold relative to silver and with higher formation temperatures. Because of their apparent insignificance, disseminated silver (and gold) ores are a more recent discovery in the vicinity of former high-grade mines.

It is both a scientifically and practically interesting problem to understand why epithermal silver and gold deposits tend to either gold or silver-dominant end members, with few cases of more balanced contents. Tentative explanations include the characteristic vertical zonation with gold ore near the surface, passing into silver and base metal ore beneath. However, most large epithermal gold deposits do not have a deeper silver and base metal zone. There must be more fundamental metallogenic reasons, such as varying gold and silver content in the source rocks, or different chemical evolution paths. Redox control may be one critical factor. Bolivia's silver-tin deposits are related to felsic rocks of the ilmenite type formed from reduced melt implying H_2S-rich magmatic fluids. By contrast, gold porphyries and associated epithermal deposits are oxidized, magnetite type and segregate a volatile phase that is dominated by SO_4.

Metamorphogenic vein deposits

Metamorphogenic vein deposits of silver are surprisingly rare compared to gold deposits of this class (although, of course, metamorphogenic gold always contains some silver). However, there is one significant example that may encourage search for this type. In the Coeur d'Alene district (Idaho), several large silver veins are known in an area of 50 by 20 km:

> In addition to silver, Pb, Au, Zn and Cu were also produced at Coeur d'Alene. Host rocks of exploitable veins are low-grade metamorphic, clastic sediments of the Mesoproterozoic Belt Supergroup that were intruded by Cretaceous monzonites. Furthermore, major strike-slip faults cut through the region, which have been related to the origin of the vein structures. Ore formation is controlled by late orogenic reverse faults formed in greenschist facies conditions (Wavra *et al.* 1994). Vein ores appear mainly in competent quartzites and siltstones (Mauk & White 2004). Although veins are thin, the high-grade ore allows exploitation to >2400 m below the surface. The veins are unusually persistent; one, the Morning Star, was followed for 1300 m along strike and down-dip for 2300 m. Main ore minerals are galena, sphalerite, silver-rich tetrahedrite, chalcopyrite, pyrrhotite and arsenopyrite, in a gangue of siderite and quartz. Vertical and horizontal zonation is obscure. Formation conditions were ~350 °C and 1–3 kbar. Even modern methods have not given a clear understanding of age relations. Apparently, part of the vein fill (Zn, Pb) is of Proterozoic age (ca. 1 Ga), whereas silver, antimony and gold were introduced between the Late Cretaceous and Early Tertiary (Eaton *et al.* 1995, Leach *et al.* 1998, Mauk & White 2004). Both phases of mineralization are believed to have been metamorphogenic, with the latter possibly influenced by a thermal gradient induced by Late Cretaceous (Laramic) intrusions.

Infiltration, or red-bed silver ore deposits

In spite of silver's low solubility in the surface environment, infiltration deposits of silver are not insignificant. Because metalliferous meteoric water is more typical for arid regions, the bulk of clastic host rocks display the name-giving pronounced red colour. Apart from silver, uranium and copper are often enriched in this setting. A famous example for exploitable red-bed silver is the historical district of Silver Reef, Utah, where Triassic sandstone carried strata-bound ore. Above the groundwater table silver occurred as chlorargyrite and below in the saturated zone as acanthite and native silver. Fossil plant remains were the focus of rich ore pockets, which is characteristic of this deposit class. At the Silurian Transfiguration Cu-Pb-Zn-Ag deposit in Quebec, Canada, red-bed seepage reduction and metal sulphide precipitation was achieved by a hydrocarbon-bearing fluid rising from basement slate (Cabral *et al.* 2009). In the western USA, several red-bed copper and uranium deposits had profitable silver content.

Important silver-producing countries include Peru, China, Mexico, Chile, Bolivia, Australia, Russia, USA, Poland and Canada. Mine production in 2008 was 21,300 t of Ag-metal (21,400 t in 2009). One-third of annual silver consumption is satisfied by recycling of scrap. Poland, China and USA host large silver resources in polymetallic and gold deposits. Geochemical methods combined with geological models are most effective in exploration for silver ore deposits.

2.3.3 Platinum and Platinum Group Metals

Common Ore Minerals:

		Max. wt.%	*Density (g/cm^3)*
Native platinum (alloyed with other PGM and/or Fe)			14–19
Cooperite	(Pt,Pd)S	~82 Pt	~9
Braggite	(Pt,Pd,Ni)S	~59 Pt and 20 Pd	~10
Sperrylite	$PtAs_2$	54 Pt	10.5
Moncheite	$(Pt,Pd)(Te,Bi)_2$		10.24

The six platinum group metals (PGM) or elements (PGE) comprise relatively light ruthenium (Ru), rhodium (Rh) and palladium (Pd) with a density of ~12 g/cm^3, and the heavy metals osmium (Os), iridium (Ir) and platinum (Pt, density 21.45). Natural alloys of these elements with iron are common (ferroplatinum). Concentrates of PGM ore may be composed of many more minerals (Cabri 2002). Sulphides and chromite are important carriers of PGM ("invisible" PGM, e.g. in the Merensky Reef). Palladium is preferentially hosted in sulphide minerals, primarily in pyrrhotite.

Cut-off grades of primary platinum deposits fluctuate widely with processing characteristics. Coarse-grained ore can be extracted at 3 g/t Pt equivalent, less favourable ore requires 5 to even 10 g/t. A new mine in the Bushveld (Maandakshoek mine) exploits ore from the 63 cm thick UG2 chromitite reef with an average of 8.16 g/t Pt equivalent. After dilution with host rock, run-of-mine ore grades 7.5 g/t PGE + Au. Sulphides at Sudbury contain up to 1 g/t Pt + Pd in sperrylite. In spite of the low content, the metals are profitably recovered as a by-product during copper and nickel electrolysis. Placer platinum is mined at grades as low as 0.5 g/t, for example in the Russian Far East. Averaging 2.5 g/t PGM, tailings of past chromite processing in the Bushveld constitute an attractive ore.

Platinum metal has a high melting point (1769 °C) and like gold, dissolves only in aqua regia (nitro-hydrochloric acid). It is a good electrical conductor, a useful catalysing agent and is highly resistant to corrosion and oxidation. Although other platinum group metals do have differing properties in detail, the general trend is the same. Platinum's main use (~60%) is as a catalyst in the petrochemical and automotive industries, closely followed by production of "white" precious metal jewellery. Platinum is also employed in the electronics industry (e.g. LCD-screen glass), fuel cells in vehicles and in many medical applications. Palladium and rhodium are foremost used as autocatalysts for benzine engines, rhodium being especially effective in reducing NO_x to nitrogen. PGM autocatalysts, however, are increasingly replaced by less expensive silver.

With these applications, platinum metals are obviously beneficial for the environment. Because of their low solubility in surface water and body fluids, they are not a health hazard. PGM ore processing, however, may involve more problematic elements (e.g. sulphur, arsenic), the fate of which in the mine environment has to be carefully investigated and controlled.

Geochemistry

Platinum group metals are distinctly siderophile elements, like Au and Re. This is emphasized by the frequent occurrence of natural alloys of PGM with iron (4–21%) and the platiniferous fayalite ("hortonolite") dunite pipes of the Bushveld (Figure 1.5) A chalcophile tendency is expressed by the common occurrence of PGE minerals that include elements such as Sb, As, Bi, S, Se and Te. Fe-Ni meteorites containing 1–10 ppm PGM attest to the siderophile character of PGE. During formation of the Earth, PGE were fractionated into the core. They are depleted in Palaeoarchaean komatiites, but relatively enriched in Neoarchaean komatiites. This change is explained by transfer into the mantle of platiniferous cosmic matter bombarding the Earth during the period from 4.5 to 3.8 Ga (Maier *et al.* 2009).

Crustal abundance of platinum and palladium is roughly equal to gold (Pt 0.005 ppm, Pd 0.01 ppm, Au 0.004 ppm: Smith & Huyck 1999). Generally, ultramafic and mafic igneous rocks have relatively high and granites low PGE trace content. Geochemically anomalous traces occur predominantly in chromian spinels and sulphides. Au-rich copper porphyry ores reach 0.05 g/t Pd + Pt (Tarkian & Stribrny 1999). Mid-oceanic sulphide mud at the East Pacific Rise displays up to 1% PGE in pyrite and marcasite, similar to oceanic manganese nodules and crusts. Black shales trap platinum (e.g. gold and platinum in certain parts of the Copper Shale in Poland). Fractionation of platinum elements is often investigated using the ratio Pt + Pd/Ru + Os + Ir or Pt/Pd, and by relating data to C1-chondrites. PGE in ophiolitic chromites, for example, have roughly chondritic concentrations (0.1–1) of Ru + Os + Ir ("IPGE") but only 0.01 Pt + Pd. The reverse is found in chromites and the Merensky Reef of the Bushveld Complex, where Pt + Pd reach 4 times chondritic concentrations. Generally, Ru + Os + Ir are enriched in early crystalline phases formed from a mafic melt, whereas Pd, Pt and Au rather segregate into residual liquids.

Mafic and ultramafic igneous rocks host practically all primary PGM ore of the world. Felsic and intermediate magmatic systems are virtually free of platinum metals. Mafic layered intrusions, and among them the Bushveld Complex, outweigh by far all other geological settings of platinum deposits. Three genetic models of PGE mineralization in layered mafic intrusions are prominent: i) involvement of a sulphide melt; ii) coprecipitation with chromite; and iii) chromatographic extraction of PGE by fluids (Boudreau & McCallum 1992):

> Ad i) Reduced sulphur in the magma is the key to formation of PGE ore. Sulphur solubility of melts is controlled by iron content, temperature and the SiO_2 concentration (Cawthorn 2005a). Sulphur saturation by change of one of these parameters leads to formation of dispersed droplets of a sulphide melt that contains ~35–40% S and 50% Fe, with some copper and nickel. This melt is a very effective collector of PGM, due to the high distribution coefficient from silicate to sulphide melt ($>10^5$ for platinum; cf. Section 2.1.4 "Nickel", eq. 2.2). Silicate/sulphide melt mass ratios (R) of ore-forming systems are commonly moderate to low (Naldrett 2010). Dynamic factors influence the transfer from silicate to sulphide melt. Transfer will be more efficient if sulphide droplets remain suspended for a longer period and react with more silicate magma. Vigorous convection is probably of greatest importance (convective scavenging). Enrichment may be further enhanced if sulphide droplets sink through several convection cells (cascade enrichment: Rice & von Gruenewaldt 1994). One common element of models implies mixing of two or more magma pulses, with freshly injected sulphur, inducing sulphide melt formation (Naldrett 2010, 1999). In this case, redissolution of earlier sulphide melt may increase the concentration of PGE (Kerr & Leitch 2005, Hinchey & Hattori 2007). With increasing fS_2, Pt + Pd are enriched relative to Os-Rh (Fleet & Wu 1993). This may be a clue to exotic PGM fractionations in platinum deposits.

> Ad ii) and iii) Platinum ores in igneous rocks that contain very little sulphur (e.g. Stillwater and Bushveld, excepting the Merensky Reef, see below) and possibly never developed a sulphide melt obviously demand a different explanation. In that case, the concentration of PGM may have been caused by chromite precipitation (see below), or by residual volatile-rich liquids. Complex fluids, hydrous or hydrosaline melts may form in fertile magma bodies during crystallization (Stumpfl 1986, Boudreau & McCallum 1992, Mathez & Mey 2005) or are injected into the chamber from the footwall. Experiments indicate that at temperatures ~1000 °C, such liquids contain little water but much salt and chlorine and are capable of concentrating PGM.

Similar to gold and silver, hydrothermal transport of platinum metals occurs commonly in the form of chloride or sulphide complexes. At reduced conditions below ~300 °C, bisulphide complexes prevail; oxidized, saline fluids carry Pt and Pd in chlorine complexes (Xiong & Wood 2000). Precipitation from oxidized fluids is enforced by reduction, as for example at the footwall of the European Copper Shale, where upwelling Rotliegend (Early Permian) basinal brines encountered organic matter, methane and diagenetic sulphides. In the 300 °C hot brines at the geothermal energy field of the Salton Sea, Southern California, Au, Pt, Pd and Rh occur at a concentration of ~1 ppb each. Platinum is dissolved as $(PtCl_4)^{2-}$ or $Pt(HS)_2$. When the brines are pumped to the surface, boiling sets in at a certain depth and gold is precipitated. In contrast to gold, PGM remain in solution. Gold scales reach concentrations of 0.1% (McKibben *et al.* 1990).

Metamorphic hydrothermal fluids formed PGM-Au-quartz-sulphide veins in schists of the Pounamu region (Southern Alps, New Zealand),

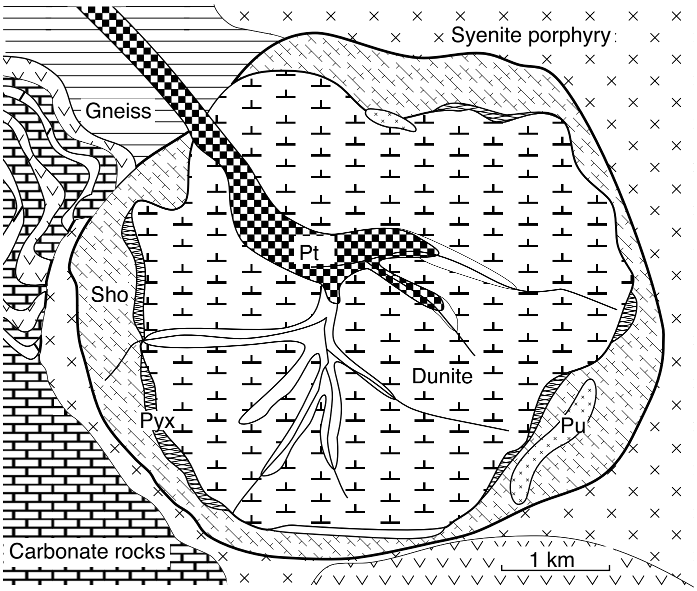

Figure 2.31 Geological map of the Inagli ring intrusion of the Alaska, Urals type, Aldan Shield, Russian Far East, with alluvial platinum placers (modified from Tolstykh *et al.* 2002). Copyright (2002) with permission from Elsevier.
Sho – Shoshonite (trachyandesite),
Pyx - Pyroxenite, Pu – Pulaskite (syenite),
Pt - Platinum placer.

which are related to serpentinite and talc serpentinite bodies. Still enigmatic are the platiniferous quartz veins of the Waterberg deposit near the southern boundary of the northern limb of the Bushveld Complex. The veins occupy a fault between Rooiberg felsites and Triassic sandstones (McDonald & Tredoux 2005, Armitage *et al.* 2007).

During supergene alteration, platinum elements resist dissolution like gold and are enriched in placers that range from residual to coastal settings. Also like gold, they are not completely insoluble, especially in complex ore, and limited chemical transport does take place. In near-surface meteoric waters, platinum elements form hydroxi- (e.g. $PtOH^+$), thiosulphate, organic and PtCl complexes (due to trace chlorine from sea spray). Residual PGM reside in gossans (frequently together with gold) and in lower horizons of laterites. Actually, lateritic platinum concentrations ("oxide ores") are not rare but rarely economic. As the solubility of the different platinum elements is not identical, weathering of primary PGE ore leads to relative enrichment of Pt over Pd (Oberthür *et al.* 2003) and of the notably immobile metals Os + Ir. The ratio Pt/Os + Ir is a measure of the maturity of weathered platinum occurrences. In this connection it is remarkable that Witwatersrand gold mining produces annually ~1000 kg Os and Ir, but no platinum. Precipitation of dissolved platinum elements is provoked by reduction (e.g. in contact with Fe^{2+}) or by changing pH. Large platinum crystals form in alluvial placers, as for example in the Aldan Shield of the Russian Far East. Primary sources are zoned intrusions of the Alaska, Urals Type (Figure 2.31). Platinum placers contribute ~50% of Russia's impressive annual PGM production, whereas those of Colombia and New Zealand have little international significance.

Platinum group element ore deposit types

The key to economically significant primary PGE deposits is the extraordinary efficiency of orthomagmatic processes in concentrating traces of the elements to exploitable grade. This is restricted to only three petrogenetic settings:

1 layered mafic intrusions (Bushveld, South Africa, Great Dyke, Zimbabwe);
2 mafic intrusions related to flood basalts (Noril'sk, Sibiria; cf. Section 2.1.4 "Nickel"); and
3 ultramafic complexes of the Alaska, Urals type (Urals and Russian Far East, e.g. the ring complex Inagli, Jakutia, Russia).

Naldrett (2010) shows how the petrological association and magma types control PGE metallogeny. The wider genetic variety including significant by-product sources comprises:

- orthomagmatic PGE ore with by-product base metals or chromium in layered mafic intrusions;
- orthomagmatic co-product PGE in base metal ore of intrusions related to flood basalts;
- orthomagmatic by-product and PGE-only ore in ultramafic intrusive complexes of the Alaska-Urals type;
- orthomagmatic by-product PGE in gabbro/norite hosted base metal sulphides;
- orthomagmatic by-product PGE in chromitite of the ultramafic section of ophiolites;
- orthomagmatic by-product PGE in platiniferous nickel sulphides of Archaean komatiites;
- by-product PGE in diagenetic-hydrothermal stratabound/stratiform sediment-hosted copper deposits (European Copper Shale);
- supergene lateritic PGE deposits;
- residual and colluvial PGE placers;
- alluvial and coastal PGE placers.

The Bushveld Complex in South Africa provides nearly 80% of world platinum mine production (Vermaak & Van der Merwe 2000, USGS 2009):

> Two major platiniferous horizons occur in the lithostratigraphic succession of the Rustenburg Layered Suite (Figure 1.5), The Merensky Reef and the UG2 chromitite. Both are part of the upper, cyclic section of the Critical Zone. Platinum in the Bushveld was discovered in 1924 by the geologist Hans Merensky (1871–1952), whose achievement was acknowledged by the name Merensky Reef. This is one of several stratiform "pegmatoids" (coarse-grained, thin layers) in the Critical Zone. It is a thin (0.4–2 m) pyroxenitic band (Figure/Plate 2.32), with orthopyroxene as a cumulus-phase and plagioclase both as cumulus and intercumulus phase, and displays considerable lateral variation (Naldrett *et al.* 2009). The Merensky Reef is a curious geochemical hiatus with petrochemical features, such as initial Sr-isotopes and the Cr/MgO-ratio pointing to either Critical (U-type, komatiitic, PGE-rich) or Main Zone (T-type, normal tholeiitic) magma (Naldrett 2010), but apparently excluding magma mixing (Seabrook *et al.* 2005). In addition, the reef is a physical hiatus by its close relation with an unconformity surface (marked by "potholes") in the ultramafic cumulate at the base of the Merensky Cyclic Unit (Viljoen 1999). The reef displays thin chromitite bands, locally olivine, and pockets of magnetite, amphibole, biotite-phlogopite, white mica, quartz and talc, which attest to the former presence of an aqueous fluid phase (Wilson *et al.* 1999). The reef is relatively sulphur-rich and chalcophile element concentrations can be modelled by sulphide segregation from a silicate melt (Barnes *et al.* 2009). The magma-mixing hypothesis was updated by Naldrett *et al.* (2009) in the "lateral mixing model": Along the cumulate-magma interface, a newly injected more primitive melt pre-enriched in PGE to ~200 ppb spread out laterally. Magma mixing resulted in segregation of a sulphide melt scavenging PGE, nickel and copper. The PGE enrichment of the inflowing Merensky melt is assumed to have originated by redissolution of previously enriched sulphides in a staging chamber. Exploitable volumes of the reef contain 0.5–2% of chalcopyrite and pyrrhotite/pentlandite, which host invisible platinum. Average grades are ~4–8 ppm PGM (ca. 60% Pt and 30% Pd) with by-product gold credits. Platinum elements occur in the form of native ferroplatinum and minerals of PGE with S, Te, As and Sb.

> The UG2 chromitite seam occurs ~150 m below the Merensky Reef. It comprises a main layer (<1 m thick) of massive chromitite of 75–90% chromite with plagioclase as the dominant interstitial mineral, the "Leader Triplets" in the hanging wall and a footwall plagioclase pyroxenite pegmatoid (Leeb-Du Toit 1986). Large-scale mining of UG2 only started in ~1980, when the problems of metallurgical processing were mastered. However, the low sulphur content continues to impede metallurgy by the traditional matte process and a new roasting-smelting technology is now embraced. Today, UG2 is a more important Pt-source than the Merensky Reef. In the chromitite ore, Fe-Cu-Ni sulphides have a minor role and compared to the Merensky Reef, ferroplatinum is much less abundant. Laurite (RuS_2), platinum-palladium sulphides and discrete rhodium-bearing phases occur as tiny inclusions between tightly packed chromite grains. Geochemically, all chromite layers in the Bushveld have elevated PGM-contents. Kinnaird *et al.* (2002) suggested that platiniferous chromitites (and the Merensky Reef) originated by jets of fresh mafic magma that hit the roof of the intrusion and assimilated felsic material (Figure 2.33). Because silica contamination reduces its solubility, chromite would have been precipitated, scavenging PGEs and

settling down to the floor of the magma. In this model, aqueous fluids in the Merensky Reef caused a limited redistribution of platinum elements during cooling of the system. The genetic discussion continues, however, and other processes such as ejection of hydrous melts from lower, consolidating cumulates, or pressure fluctuations in the magma body are proposed to explain the formation of PGM-enriched chromitites (Mathez & Mey 2005, Cawthorn 2005a,b).

Lately, a new zone of giant Pt deposits has been discovered in the northern limb of the Bushveld Complex. In this area, Main Zone gabbronorites are underlain by a 10–400 m thick package of pyroxenitic rocks with PGE and base metal sulphide mineralization, designated earlier by Hans Merensky as the Platreef, that overly sediments of the Transvaal Group and Archaean basement. Rocks of the Lower and Critical Zones are absent (Holwell & Jordaan 2006). Mining started in 1992 at Sandsloot north of the town of Mokopane.

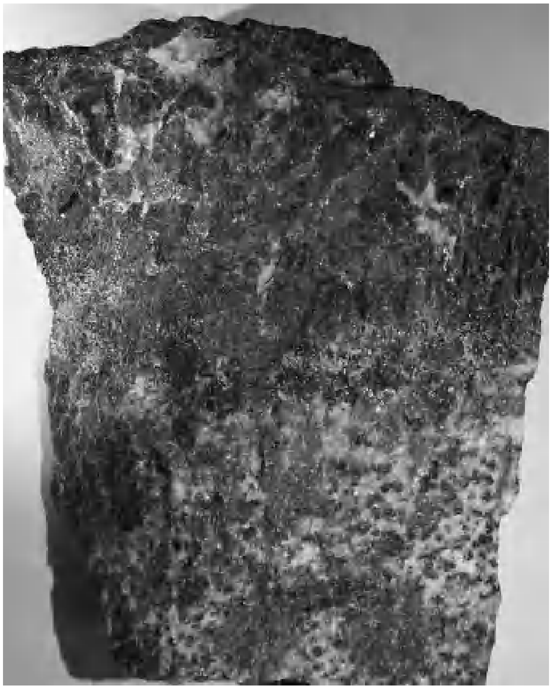

Figure 2.32 (Plate 2.32) Merensky Reef at Impala mine, S.A., with footwall anorthosite (lower part), a thin chromitite band in the middle and the pegmatoid reef on top (orthopyroxene, plagioclase and the sulphides pentlandite-pyrrhotite- chalcopyrite). Height of sample is ~15 cm. Courtesy B. Lehmann, Clausthal.

With its dunite core sourcing Pt placers and marginal olivine-bearing trachyandesite the Inagli ultramafic ring complex is a textbook example of Alaska-Urals type intrusions (Figure 2.31). Placer mining ceased in 2008. Alluvial placers in the Western Cordillera of Columbia are related to zoned ultramafic intrusions (Tistl 1994). Economically more spectacular is Nizhny Tagil in the Ural Mountains, because of both rich eluvial and alluvial platinum placers, and historic underground mines (Augé *et al.* 2005). The dunite unit at Nizhny Tagil consists of olivine and minor chromite that accumulated from mafic magma in an open flow-system. Chromite ore occurs in schlieren and massive lenses, which reach 100 by 5 m, and were formed by dynamic concentration of chromite crystals in magma conduits. Chromitites are enriched in PGE. Augé *et al.* (2005) suggest that the reason for coprecipitation is a physical affinity between chromite and PGE-phases.

By-product platinum is widespread, especially in norite and gabbro intrusions of different genetic lineage (e.g. Sudbury, Lac des Iles and Voisey's Bay in Canada; Montchegorsk and Pechenga on Kola Peninsula). In these deposits, PGM and gold are associated with Cu-Ni sulphides and pyrrhotite. Typically, palladium is concentrated over platinum (Noril'sk Pt:Pd ~1:4; Lac des Iles 1:10; Hinchey & Hattori 2007). Nickel sulphide concentrates of komatiite deposits are also a source of by-product platinum. Platiniferous chromitites of ultramafic sections of ophiolites are relatively rare but may support smaller mining operations (Albania, Ural Mountains, Ethiopia, Shetland: Lord & Prichard 1997). High PGE concentrations in podiform chromitite are probably controlled by a favourable degree of mantle melting (Prichard *et al.* 2008). Several platinum placer districts, for example alluvial and coastal placers in New Zealand, are sourced from nearby ophiolite hills.

PGM mineralizations in the European Copper Shale at Lubin and Polkowice mines in Silesia, Poland are economically of little weight but of scientific interest. At the redox border between Rote Fäule (oxidized) and the Cu-Ag sulphide zone (reduced), noble metals are enriched to 1460 ppb Pt, 824 ppb Pd, 13.5 ppm Au and 160 ppm Ag, although in a very thin boundary layer. Remember that this redox front experienced a giant mass flow

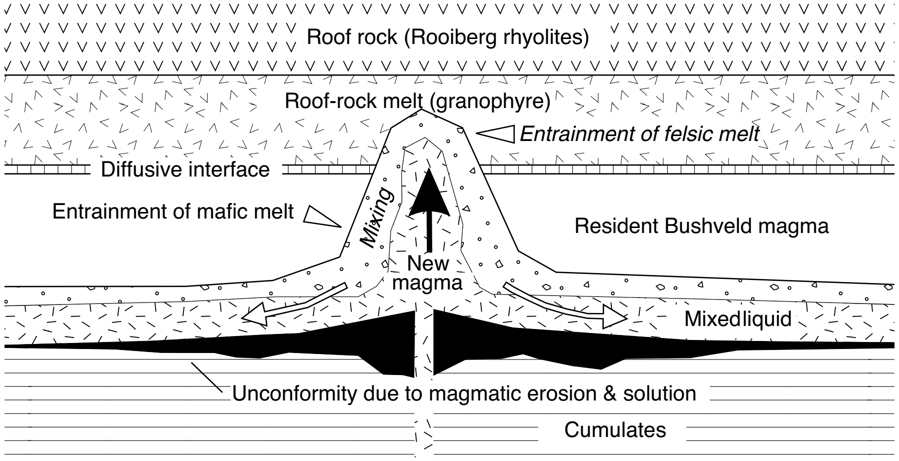
Roof rock (Rooiberg rhyolites)
Roof-rock melt (granophyre)
Entrainment of felsic melt
Diffusive interface
Entrainment of mafic melt
Mixing
Resident Bushveld magma
New magma
Mixedliquid
Unconformity due to magmatic erosion & solution
Cumulates

Figure 2.33 Model of chromium and platinum ore formation in the Bushveld Complex, caused by injection of fresh melt into the magma chamber, silicic contamination and mixing with resident liquids. Precipitated platiniferous chromite (black) accumulated on the floor of the magma chamber (modified from Kinnaird *et al.* 2002). By permission of IMM London & Maney Publishing (www.maney.co.uk/journals/aes).

of hot, oxidized basinal brines (cf. Chapter 1.4 "European Copper Shale").

Exploration for platinum deposits requires geological and petrological models, followed up with geochemical and geophysical surveys (e.g. induced polarization for sulphides). Prime targets are sulphide-enriched sections, chromitite (Ohnenstetter *et al.* 1999) and magnetite seams (Maier *et al.* 2003) of layered mafic-ultramafic intrusions. Sections of ophiolites displaying chromite mineralization are second-order targets. Lithostratigraphic mapping assisted by geochemical data on silicate minerals is essential. Large areas are scanned by heavy mineral and sediment sampling of streams, and by grid-sampling of soil (Prendergast *et al.* 1998). Pathfinder elements for sulphide-associated PGM mineralization include Cu, Ni, Ag, As and Te. More than 100 years ago, Merensky used the frequent association of Pt with Ni and Cu (resulting in green staining of outcrops) in his discovery of the Bushveld platinum ore deposits. Of course, the method fails to discover native alloys of PGM in the absence of base metal sulphides (Potter 2002).

Leaders of primary platinum production are South Africa and Russia, followed by Canada, Zimbabwe and USA. World production in 2008 was 189 tonnes Pt (falling to 178 t in 2009) and 204 t Pd (195 t in 2009). Russia and South Africa equally share world supply of palladium. Although South Africa's reserves and resources of PGM in the Bushveld are very large indeed (>90% of the world's), exploration elsewhere is quite active. Demand, but also recycling, continue to increase.

2.4 Light metals

2.4.1 Aluminium

Common Ore Minerals:

		Wt. % *Al_2O_3*	*Density* *(g/cm^3)*
Gibbsite (Hydrargillite)	$Al(OH)_3$	65	2.4
Boehmite	γ-AlO(OH)	85	3
Diaspore	α-AlO(OH)	85	3.4
Alunite	$KAl_3[(OH)_6(SO_4)_2]$	37	2.7
Nepheline	(Na,K)[$AlSiO_4$]	36	2.6

Aluminium metal ($D = 2.7\ g/cm^3$, melting point 660 °C) is commonly produced from bauxite, which is loose soil or a hard rock with 30–65% Al_2O_3. Bauxite consists of Al-minerals such as gibbsite, diaspore and boehmite, and amorphous alumogel in varying proportions. Gangue minerals include kaolinite, quartz, haematite, goethite, ilmenite/rutile/anatase and zircon. Alunite and nepheline (a co-product of certain apatite mines) with marginal Al_2O_3 content were at times used for the production of alumina or Al-metal. Among the oxy-hydroxides, gibbsite is preferred because it is easily soluble in the standard Bayer digestion method, whereas diaspore is least soluble. For a timely planning of plant technology, the distribution of various Al-minerals (and reactive silica) in the deposit must be carefully mapped. Reactive silica (commonly in kaolinite) is undesirable. Fe_2O_3 and quartz are not soluble but should not exceed low contents. Exploitable bauxite ores contain >35% Al_2O_3. Enrichment of alumina by processing bauxite is rarely feasible and selective mining is the common means to guarantee targeted run-of-mine grade. One exception is deposits in the Darling Range (Western Australia), where quartz can be separated by simple processing. Metamorphosed bauxite with the paragenesis corundum and magnetite is called emery, a raw material for the production of abrasives.

Aluminium is the most important of the non-iron metals. About 95% of bauxite produced is processed into aluminium metal. The remaining 5%, typically ore of very high quality ("chemical grade") with >52% Al_2O_3, serves as an industrial raw material for numerous special products (e.g. abrasives, portland cement, calcium-aluminate cement, technical ceramics, glass, chemicals, paints, enamels and refractories). Favourable attributes of aluminium metal such as light weight, strength (Lu 2010) and excellent corrosion resistance allow its use in numerous applications from building air frames to food packaging (the metal is not toxic). Alloys of aluminium with other metals including lithium, scandium and magnesium are produced for specific uses.

In the Bayer digestion technology, bauxite is leached with NaOH. Alumina $Al_2O_3{\cdot}xH_2O$ is precipitated from the aluminate solution. After drying, the precipitate is mixed with natural or synthetic cryolite Na_3AlF_6, fluorite, $LiCO_3$ and NaCl, and is reduced by electrolysis to metallic aluminium in an electric arc furnace. Insoluble residue of leaching is alkaline (pH 8–13.5) "red mud", which contains mainly quartz, calcite, haematite and goethite. Because bauxite is extremely leached, elevated trace contents of elements such as Sc, Ga, V, U, Th, REE, P and Ti are rarely observed. In some cases, Sc (Kempe & Wolf 2005, Wiesheu *et al.* 1997), V and Ga are extracted from red mud. Red mud is not radioactive nor toxic, apart from its caustic nature. Commonly, it is disposed of in settling ponds. Revegetation of pond sediments after closure is an interesting problem (Courtney & Timpson 2005). Recently, red mud was investigated for environmental applications such as lining waste disposal sites, for neutralizing acid mine waters, and for immobilization of toxic heavy metals (Snars & Gilkes 2009). At the Kwinana aluminium plant, Western Australia, red mud is reacted with CO_2 from the power station in order to neutralize negative environmental effects of both waste products.

Geochemistry

With an abundance of 8% (range 7.4–9) lithophile aluminium is the third most abundant element in the Earth's crust after oxygen (47%) and silicon (27%). In spite of its abundance, enrichment to exploitable grades and tonnages is relatively rare. The key to economic concentrations of aluminium is humid-tropical weathering leading to the formation of laterites (oxisols, ferralsols) and exploitable bauxite (cf. Chapter 1.2 "Supergene Ore Deposits"). The solubility of aluminium in natural waters is very low, except as Al^{+3} ion below about pH 4. The element is not redox-sensitive. During supergene alteration, primary alumosilicate minerals of rocks (e.g. feldspar) are first hydrolysed to kaolinite, followed by formation of colloidal aluminium hydroxide and silica. Above pH 4.5, silica is more soluble than alumina, resulting in residual enrichment of Al. At pH >5.6 (Figure 1.48), gibbsite forms from alumina colloids. Seasonally changing tropical climate favours these processes, because dry season soil water rises and evaporates towards the surface. The resulting alkalic soil moisture dissolves SiO_2, which is flushed out with Na, K, Ca and other soluble elements when rainy season water infiltrates. Low pH/Eh induced by organic acids favour iron mobility and depletion (Figure 2.1), producing bauxite with low iron contents. Ageing (soil diagenesis) transforms gibbsite into boehmite and diaspore, and consolidates the original aluminous soil into solid bauxite rock.

Bauxitization is essentially the enrichment of alumina by abstraction of rock-forming elements including silica, alkali and alkali earth elements. Likewise, minor and trace elements are either depleted or enriched. The resulting distribution pattern of elements in bauxite deposits are powerful tools that allow investigation of genetic parameters, including identification of source rocks, physico-chemical conditions of alteration and the degree of element mobility (Nesbitt 1979, Mameli *et al.* 2007). Indicators of specific source rocks are the more immobile elements such as Ti, Zr, Nb, Ga and Th.

Aluminium ore deposit types

Only supergene geological processes enrich aluminium to exploitable grade based on dissolution of other rock constituents and the extremely low solubility of its oxy-hydroxides. Drivers are greenhouse maxima of global climate cycles (Retallack 2010). The resulting ore, bauxite, is residual aluminous soil. The nature of footwall rocks of bauxites is used to differentiate between: i) laterite, or silicate bauxite (developed on silicate rocks); and ii) karst, or limestone bauxite that occurs above limestone karst surfaces or in karst depressions. In short, significant genetic variants of aluminium deposits include:

- supergene residual bauxite in autochthonous soil blankets;
- resedimented detrital allochthonous bauxite.

Laterite bauxites

Laterite bauxites are most often products of autochthonous weathering, but as in most soils, local erosion and resedimentation are not rare (Bardossy & Aleva 1990). The bauxite-bearing laterites form soil profiles of several metres to tens of metres thickness that blanket old, usually Mesozoic-Tertiary land surfaces. Later erosion causes interruption of "highland" bauxites by incised valleys. Bauxite scree develops on the slopes, and sedimentation of fines in depressions results in deposits of allochthonous detrital bauxite (Figure 2.34). Textural varieties of bauxite soils comprise massive, concretionary, pisolitic, spongy and cellular types. The quality of bauxite can be directly related to the source rock chemistry: Both the Dekkan and West Australian bauxites above dolerite have high iron and titanium content. Generally, the lower part of a laterite profile is often clayey, and several bauxite mines co-produce high-grade kaolin or smectite clay from the same pits (e.g. Weipa, Australia with a production of 100,000 t/y of paper-grade kaolinite).

Australia hosts several of the largest laterite bauxite districts of the world. Important mining districts are Weipa (Cape York Peninsula), Gove (Northern Territory), Darling Ranges (Figure/Plate 1.1, 1.2) and Kimberley (Western Australia):

> The Weipa bauxites form bright red cliffs on the shore of the Gulf of Carpentaria that had already been observed by the earliest Dutch explorers. Their potential was only recognized in 1955 during an oil (!) exploration campaign (Schaap 1990). Extraction started in 1963. The bauxite laterite occurs over Palaeogene arkosic sand, silt and clay, and in some areas on Cretaceous marine sediments. The laterite

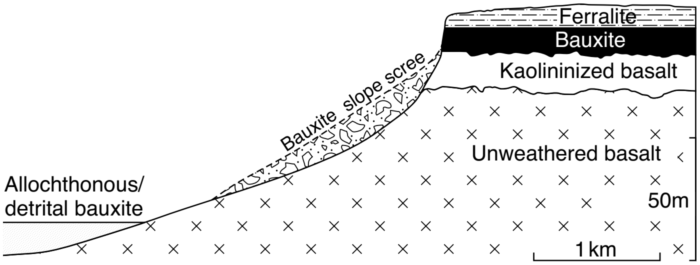

Figure 2.34 Sketch of morphological position of bauxite deposits in the Dekkan Plateau (India).

profile is covered by several metres of younger soil. Bauxite extends over an area of ~11,000 km^2 with an average thickness of 2 m, thickening in places to 12 m. It consists of loose and little cemented pisoliths formed from concentric layers of gibbsite and boehmite, with accessory kaolinite, quartz, anatase and haematite (Taylor & Eggleton 2004). Average grade of the bauxite bed in the mine is 52–55% Al_2O_3, 5–9% SiO_2 and 7–16% Fe_2O_3 (Abzalov & Bower 2009). The horizon is underlain by 1–2 m of ferricrete and a kaolinitic saprolite. Normally, soil pisoliths form in a substrate. At Weipa, winnowing processes seem to have eroded the fine matrix, while the pisoliths were hardly transported as evidenced by geochemical relations to the bedrock (Taylor & Eggleton 2004). Reserves and resources of the district are very large.

Large bauxite blankets derived from phyllites, greenschists and gneisses occur in tropical western Africa (Guinea, Ghana and Sierra Leone). Across the Atlantic Ocean, important bauxite provinces include the Guiana Shield (e.g. Surinam) and the Amazon Basin in Brazil. Worldwide, laterite bauxite is found in humid and warm climate zones that have hardly changed their latitudinal position since the Mesozoic. Pre-Mesozoic bauxites are rare and have little economic significance. This appears to be mainly due to the high geological probability of soil erosion compared with its preservation. Undoubtedly, the absence of land plants in earlier geological times is another factor. Bauxites of the Tikhvin Type and karst bauxites are examples of unusually effective geological preservation of soil.

Allochthonous laterite bauxites of the Tikhvin Type are found in former morphological depressions, similar to young detrital bauxites. Deposits in the Tikhvin mining district occur in Palaeozoic rocks of the Moscow basin (Russia) along a strike length of 260 km. Bedrocks underneath the bauxite are spotted bluish-grey sandy and micaceous shales of Devonian age and locally Early Carboniferous (Tournaisian) marlstones, dolomites and limestones. Bauxites were deposited during the Viséan and are covered by later Viséan and Quaternary sediments. During the period of bauxitization, the area was above sea level and was drained by a number of large valleys descending towards an ocean in the east (which was soon afterwards consumed in the collisional Variscan Ural Mountains). Bauxite deposits fill the upstream sectors of these valleys where they form long, narrow (<100 m) and thick (40 m) bodies. The ore is reddish-brown without bedding structures or size-grading. Gibbsite, boehmite and kaolinite are main minerals, with some secondary calcite. The ore contains 35–49% Al_2O_3 and up to 18% SiO_2. Devonian shales are thought to be the original source rocks.

Karst bauxites, or limestone-hosted bauxite deposits

Karst bauxites, or bauxite deposits formed on carbonate rocks (Bardossy 1982), are quite different from laterite bauxites. They rarely occur as blankets but fill karst depressions of variable form and origin. Karst bauxites in Mediterranean Europe are commonly associated with carbonate rocks of Mesozoic and Cenozoic age (Combes 1984). Main ore minerals are boehmite and diaspore. Other important karst bauxite provinces occur in the Caribbean Islands, the Ural Mountains, Vietnam and southeastern China.

Both karst and bauxite formation occur in phases of emersion that may be expressed by unconformities or periods of non-deposition. In Mediterranean Europe, this includes several short time spans between the Middle Triassic (e.g. Montenegro) and the Eocene (Dalmatia, Istria, northwest Hungary). Karstified footwall limestones are always marine deposits, whereas hanging-wall sediments developed above bauxite may either be transgressive marine (Figure 2.35) or terrestrial lacustrine sediments that can host coal deposits (Gant in Hungary, Laussa in Austria). Like laterite bauxites, karst bauxites record warm and humid climates ("greenhouse conditions"), and favourable tectonic and morphologic configurations (D'Argenio & Mindszenty 1995):

> Form and thickness of karst bauxite deposits are determined by the relief of the depositional site, which is a function of the duration of the karstification process, the nature of the limestones, and of the difference between the altitude of the karst plateau and the drainage system. Deeper karstification

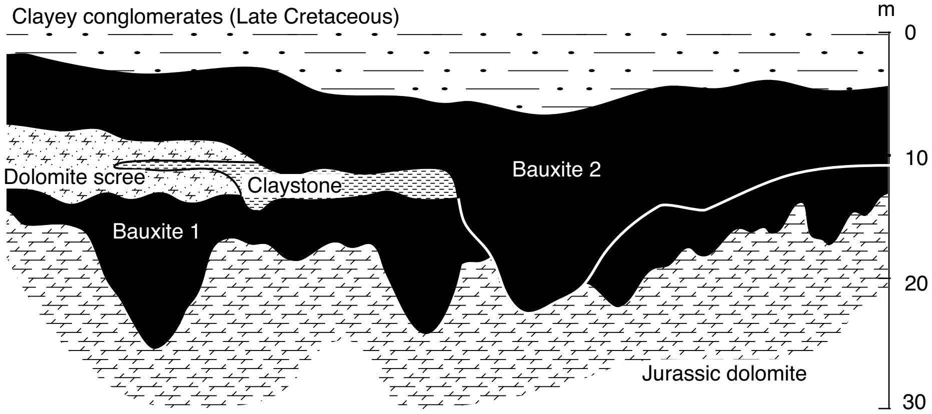

Figure 2.35 Synthetic section of the sedimentary succession in the karst bauxite deposit Uston (Languedoc, France, modified from Combes 1984). Reproduced by kind permission of Total. Clearly, there were two periods of bauxite sediment formation that are separated by erosional unconformities and deposition of clay and dolomite scree. For location of Les Baux district refer to Figure/Plate 1.89.

results from a large height difference resulting in orebodies of 80 m thickness at Niksicka Zupa (Montenegro) and 50 m in the Haute Var (Provence). Bauxite orebodies are often longitudinally arranged along certain structural features of the bedrock (e.g. faults) or along former karst valleys. The ore of Iharkut (Hungary) filled a deeply incised canyon.

Autochthonous or allochthonous formation of karst bauxites was long disputed. One of the early theories proposed derivation of bauxite from silicate minerals that were enclosed in the karstified limestone. However, karstifiable carbonate rocks have typically very low silicate contents, so that this "terra rossa hypothesis" can only explain a few exceptional situations, as in Sardinia (MacLean *et al.* 1997). Mineralogical and geochemical research showed universally that the precursor rocks of karst bauxites were silicate rocks and not the footwall carbonates. Actually, most karst bauxites have an ordinary laterite bauxite origin and are detrital bauxite sediments, after erosion and transport. Discussions also thrived on the observation that karst plateaus rarely display surface river flow. So, how can the import of detrital material into isolated depressions be explained? The solution to this question lies in a nearly-submerged state of the karst, which enabled rivers to inundate its surface. In some cases, aeolic transport of volcanic ash may have been the source of silicates (Jamaica).

Note, however, that the nature of the sediment that is now karst bauxite may have been quite different at deposition. Erosion may have moved either bauxite or saprolite clays of the laterite profile and even rock particles. Bauxitization may have taken place after sedimentation in the karst depressions. The bauxite must have been imported when it is interbedded with clay (Figure 2.35). Karstification may continue after deposition resulting in apparent metasomatic replacement of carbonate by bauxite. Tectonically reversed bauxite bodies experienced renewed carstification in Provence (France), resulting in bauxite-filled sinkholes in the stratigraphic roof.

Apart from bauxite, alunite (a product of acidic hydrothermal alteration, cf. Chapter 1.1) and nepheline are potential ores of aluminium. At present, only one mine reports production of alumina from nepheline rock, Kiya-Shaltyr in southern Siberia, Russia. Ore is a nepheline syenite body that forms part of an ultramafic alkaline complex. Resources comprise 94 Mt of rock with 26–27% Al_2O_3 (average nepheline syenite contains 21% Al_2O_3). Desired run-of-mine grades are reached by selective mining. There is no further concentration. Processing only comprises pulverizing and sintering with limestone, which is followed by alkaline leaching. Yearly production attains ~1 Mt of high-grade alumina.

In the reconnaissance stage, exploration for bauxite deposits builds mainly on geological methods, because geochemical and geophysical tools are hardly applicable. During detailed follow-up work, electrical, soil radar and magnetometric methods may be useful. Field determination of bauxite is often hampered by the wide variability of colour, consistency and texture of the ore. Therefore, mineralogical (e.g. portable field spectrometers PIMA, etc.) and chemical analyses are indispensable. For large sample numbers in the field, simple determination of loss on ignition and colorimetric tests may help to assess ore grade.

In 2008, world mine output was ~200 Mt bauxite or 39 Mt aluminium, dropping to 36.9 Mt in 2009. Australia, China, Brazil, Jamaica, Guinea and India are significant producers. Reserves and resources are very large (Hostermann *et al.* 1990), mainly of laterite bauxite.

2.4.2 Magnesium

Ore Minerals:

		Wt. % Mg	*Density (D, g/cm³)*
Forsterite	Mg_2SiO_4	34	3.2
Dolomite	$CaMg(CO_3)_2$	12	2.8
Brucite	$Mg(OH)_2$	41	2.4
Magnesite	$MgCO_3$	28	3.0
Carnallite	$KCl.MgCl_2.6H_2O$	8	1.6
Bischofite	$MgCl_2.6H_2O$	11	1.6

Very diverse mineral raw materials, natural and industrial brines, and seawater are used for the production of magnesium and of magnesium compounds. The first four minerals listed above occur in nearly mono-mineralic rocks with potentially recoverable magnesium content. These ore rocks include forsteritic dunite, dolomite (cf. Chapter 3 "Carbonate Rocks"), brucitite and magnesite (cf. Chapter 3 "Magnesite"). A project in Quebec, Canada, which was to produce magnesium from serpentine tailings (~24% Mg) of the former asbestos mines, failed for economic reasons.

In spite of low Mg-contents, the salt minerals carnallite and bischofite are used for magnesium and magnesium compound production (Russia, Ukraine; cf. Chapter 4.1 "Salt Minerals and Salt Rocks"). Solution mining (Veendam, Netherlands) and processing of potassium salts yields co-product $MgCl_2$ brines, which are convenient for further chemical and metallurgical manufacturing.

Processing of hard rock magnesium "ore" often involves leaching with HCl, resulting in intermediate product $MgCl_2$. The salt is reduced by electrolytic melting, yielding magnesium melt and chlorine gas. In China, the world's largest Mg-producer, the Pidgeon process route is preferred, in which calcined dolomite or magnesite are reduced with ferrosilicon or aluminium. Magnesium metal production requires a high energy input so that availability of cheap energy is a precondition for economic success. Environmentally acceptable disposal of discarded processing water and sludge constitutes another significant cost. It can be reduced by using raw materials that are free from contaminants.

Applications of the extremely light magnesium metal (density 1.74 g/cm^3, melting point 650 °C) employ the pure metal or aluminium alloys. Magnesium-aluminium alloys are mainly consumed for beverage container making. About 40% of magnesium is used for die casting in the car industry in order to reduce weight and fuel consumption. Other sectors include the space, aircraft and chemical industry. Lesser qualities serve as agents of desulphurization of iron and steel.

The largest sector of magnesium compound consumption is the use of magnesium oxide (magnesia) as a refractory material in furnace linings for the production of iron and steel, nonferrous metals, glass and cement. Also, MgO and other compounds, such as brucite, are used in agriculture, chemical, environmental and construction products (cf. Chapter 3 "Magnesite").

With 2.1% in the Earth's crust, magnesium is the fourth-abundant metallic element after silicon (27%), aluminium (8%) and iron (5%). Magnesium is one of the lithophile earth alkali elements.

Average MgO content in common rocks amounts to ~6.7% in basalt, 3.3% in andesite and 0.4% in rhyolite; average dunite contains 38% MgO. The element is not redox-sensitive and is mobile in all surface environments (Smith & Huyck 1999). In low concentrations Mg is essential for humans, animals and plants, and for this reason is commonly added to animal feed and fertilizer (Lindh 2005).

Sources of magnesium for metal and Mg-compounds production

- seawater, natural brines and residual brines from potassium salt processing;
- dunite, serpentine, dolomite, brucite and magnesite rock.

Seawater with 0.3% $MgCl_2$ or 0.86 g/L Mg is an unlimited source of magnesium. Some playa lake brines (Dead Sea, Great Salt Lake) contain recoverable magnesium as one of several products:

> The Dead Sea, shared by Israel and Jordan, occupies a transtensional basin along the Dead Sea transform fault that links the divergent plate boundary of the Red Sea to the convergent Alpine Taurus Mountains in southern Turkey (Garfunkel & Ben-Avraham 1996). The brine surface of the Dead Sea at ~415 m below sea level represents the lowest continental surface on Earth. The depression is 80 km long and 20 km wide, and receives drainage from ~40,000 km^2. Very little rainfall, high temperatures and very high evaporation characterize the climate. With a water depth of ~300 m, the Dead Sea is an interesting example of present deep-water halite sedimentation (Warren 2006). The lake brine displays a salinity of around 280‰ compared to 35‰ of seawater, although it contains relatively more Ca, Mg, K and Br, and less sodium, sulphate and carbonate. This brine is pumped into fields of fractionation ponds in the Southern Basin of the Dead Sea, which cover an area of roughly 130 km^2. A little gypsum and much halite are first precipitated followed by carnallitite. The salts are harvested and processed into potash, sodium chloride, magnesium chloride, magnesium oxide, hydrochloric acid, chlorine, caustic soda and magnesium metal. From residual brines of carnallite precipitation ponds, bromine and $MgCl_2$ are extracted before the waste brine is returned to the northern Dead Sea.

Reserves and resources of raw materials for magnesium metal production are practically inexhaustible and widely available. Leading producers include China (>80% of the total), Russia, Israel and Kazakhstan. In 2008, world production of magnesium metal amounted to 810,000 t, but fell to ~700,000 t in 2009.

2.5 MINOR AND SPECIALITY METALS

2.5.1 Mercury

Common Ore Minerals:

		Wt. % Hg	*Density (g/cm^3)*
Cinnabar	HgS	86	8.1
Native mercury	Hg	100	13.5

Metacinnabar (Hg,Fe,Zn)(S,Se), the tetrahedrite schwazite $(Cu,Hg)_3SbS_{3-4}$ and calomel $HgCl_2$ are common Hg-minerals, although not in ore-forming quantities. Sulphides and sulphosalts of other metals (e.g. Sb, As, Cu, Fe) may make up part of the paragenesis; antimony and gold are occasional by-products of mercury. Typical gangue minerals are quartz, carbonates and barite. Cinnabar is a heavy mineral and durable in surficial alteration settings. Proximal eluvial and alluvial placers are not rare. Hypogene native mercury is characterized by elevated concentrations of Cu, Ag, Sb, Fe, As and Zn, whereas secondary supergene mercury contains only trace amounts. The same elements are concentrated in cinnabar, which condensed from a gas phase, in contrast to hydrothermal cinnabar (Barnes & Seward 1998).

Worldwide, mercury mining has nearly ceased. Formerly, typical grades of mercury ore were between 0.6 and 2% Hg. Mercury metal (density 13.55 g/cm^3; melting point –38.87 °C, boiling point 356.9 °C) and chemical compounds were used for the production of chlorine and caustic soda (in the form of native Hg as a cathode in salt electrolysis), of paints, batteries and numerous chemicals and pharmaceuticals (e.g. dental amalgam). Supporting mercury use, USA and EU are currently phasing out general service incandescent light bulbs in favour of mercury-containing compact fluorescent bulbs in a drive to save energy. Also, mercury is widely used in the fluorescent tubes that form the backlight to liquid crystal displays (LCDs) of television sets and numerous other electronic devices. In many parts of the world, application of gold amalgamation in small-scale and artisanal mining is still widespread.

Mercury is a powerful neurotoxin that is especially enriched in aquatic food-webs (Selinus *et al.* 2005, Plant *et al.* 2005, Alloway 1990, Fergusson 1990). Ionic mercury contamination, for example from coal burning, is rapidly converted by microbes to methyl mercury, which is highly toxic when accumulating in living tissues. Bioremediation of soil by genetically modified plants seems to be the best choice (Omichinski 2007). Today, mercury's use is strictly controlled, and recycling is employed where it cannot be replaced by other metals. Sources of mercury, as well as natural and anthropogenic cycles including environmental aspects, are presented in detail by Parsons & Percival (2005).

Geochemistry

The geochemical behaviour of mercury is chalcophile. Its average content in the continental crust, in granite and basalt is ~0.08 ppm (range 0.03–0.5, Smith & Huyck 1999). Mercury occurs in the three oxidation states Hg^0, Hg^{+1} and Hg^{+2}. It has a strong affinity to organic matter, live or dead, so that shales, especially black shales are enriched compared with magmatic rocks. The European Copper Shale, for example, contains an average of 0.13 ppm Hg. Petroleum, natural gas, formation waters and coal all have elevated Hg-contents. From certain reservoirs, the oilfield Cymric, California produced petroleum with 21 ppm Hg and water with 0.2 ppm Hg, and the methane outgassing from it was saturated with mercury, which condensed in the gas pipelines. Worldwide, many geothermal power stations have problems with mercury in the extracted vapour. The world's largest geothermal power field, The Geysers, California, "produces" ~50 kg Hg^0 per year. These observations suggest how mercury is transported in geological systems: Mercury is more mobile in a gas phase or a hydrocarbon fluid than in aqueous solution. Its characteristic geochemical association comprises other "volatile" and semi-metals, including As, Sb, Te and Tl (Figure 2.23).

Traces of mercury occur in many sulphide ores, because Hg substitutes for Cu, Ag, Zn, Cd, Bi, Pb and other metals. It is also a frequent companion of gold, antimony, barite and strontium ore, resulting in considerable by-production of mercury. During orebody formation, mercury vapour forms wide primary dispersion halos (cf. Chapter 5.2 "Geochemical Exploration"), which makes it useful as a pathfinder element.

In reduced, low-sulphur hydrothermal fluids of >200 °C, Hg^{2+} occurs in complex ions such as $HgS(H_2S)^0{}_2$ in the aqueous phase; yet, Hg^0_{aq} is probably more abundant than Hg^{2+} and behaves like a dissolved gas (Varekamp & Buseck 1984). The solubility of Hg^0 in hot fluids is very high (400 ppm at 300 °C), but drops rapidly with decreasing temperature (only 0.5 ppm at 100 °C). As the fluid ascends along open fractures, it cools and begins to boil, and Hg^0_{aq} is partitioned into the vapour phase. Diffusion of Hg between the liquid and vapour bubbles enriches the light isotopes (Smith *et al.* 2005). Loss of H_2S to the vapour phase during boiling causes reduction of Hg^{2+} in dissolved complex ions (eq. 2.6).

Mercury vapour formation by dissociation of complex Hg-bearing ions:

$$HgS(H_2S)^0_2 + H_2 \Rightarrow Hg^0_g + 3H_2S_g \qquad (2.6)$$

Petroleum is a common component of hydrothermal solutions transporting mercury. This suggests an important role of Hg-complexing organic molecules (Fein & William-Jones 1997). Salt concentration seems to have little impact on Hg solubility. Most mercury deposits were formed at 60–150 °C. In this case, condensation of Hg^0 from the gas phase and formation of HgS from the aqueous phase may cause precipitation. Sources of mercury are probably quite often siliciclastic sediments with elevated organic matter contents. From this pool, both mercury and hydrocarbons can be distilled by heat pulses during diagenesis or low-grade metamorphism. The only reason for the connection of mercury mineralization with volcanism may be localized strong heat flow, not magmatic degassing. Magmatic extraction of mercury from the Earth's mantle and crust, however, remains a viable model.

Mercury ore deposit types

Likely examples of mercury deposit formation (or considering the ban on Hg-mining, "mineralization") can be studied at several active geothermal emanation centres. Discharge rates that may produce deposits have been described from Ngawha, New Zealand and Sulphur Bank, California. Submarine hydrothermal vents with high mercury delivery have been discovered off New Zealand (Stoffers *et al.* 1999). Based on these observations and on the study of older mercury deposits, common characteristic include:

- mercury deposits are formed near or at the surface (rarely >200 m below the surface; with 800 m, the deepest mining took place at New Almaden, California);
- formation temperatures are mostly <200 °C;
- ore is typically mono-metallic (mercury only) and mono-mineralic (cinnabar);
- hydrothermal alteration is dominated by silicification and carbonatization;
- very few mines delivered most of total historic world production.

Overall, volatile mercury is concentrated in shallow epizonal and hydrothermal settings, which are commonly related to circumscribed heat anomalies, rifting and volcanism. At a number of sites, a metamorphogenic origin is indicated and mercury deposits may mark the tops of orogenic gold systems, as supposed in the Californian Coast Ranges (Figure 2.22; Groves *et al.* 2003). Significant genetic mercury deposit types include:

- volcanogenic-hydrothermal;
- metamorphogenic-hydrothermal.

Sulphur Bank Mine in the northern Coast Ranges, California, was one of the major historic mercury producers of North America and one of the first locations where volcanic geothermal systems were recognized as modern analogues to epithermal deposits. The deposits lay in a broad hill of Pleistocene andesitic lavas on the shore of Clear Lake. Andesites above the groundwater level are strongly altered. Only boxwork quartz and elemental sulphur indicated mineralization, the latter giving the site its name. After discovery in 1856, borax and sulphur were extracted. Prospecting shafts below the groundwater level soon exposed mercury ore with highest grades in fault gouges impregnated with fine-grained cinnabar. Nearby fissures in argillized andesites also contained HgS, with some pyrite, markasite, stibnite, quartz and calcite. The vertical extent of mineralization was only ~100 m, hosted by andesites, lake sediments and Mesozoic greywacke. The mine yielded a total production of ~5000 t Hg:

> ^{14}C-dating of wood in the oldest Hg-bearing lake sediments allowed determination of the onset of mineralization at ~34,000 years BP. Even today in the former open pit, thermal springs deposit HgS, markasite, pyrite and native sulphur. Cl in these waters is remarkably low, whereas CO_2, B, NH_3 and iodine are strongly enriched. Contents of liquid hydrocarbons and methane indicate derivation of the fluids from marine sediments by thermal maturation and diagenesis. Compared to local meteoric waters, both deuterium and the heavy O-isotopes are enriched, giving rise to earlier speculations that the geothermal water has a deep source (metamorphic?). A regional comparative investigation, however, showed that the composition of the waters is best explained by meteoric-dominated systems with repeated vapour loss at depth (Sherlock 2005).

Sulphur Bank is part of a large mercury district in California. Single deposits typically lie about subvolcanic intrusions marked by geothermal activity. Yet, the fluid source is thought to be rather metamorphic than magmatic, possibly related to overthrusting of Mesozoic sediments by the Coastal Ranges or to subvolcanic heat flow. Most of the deposits are hosted by serpentinites of the Franciscan Complex, sited within a halo of hydrothermal silica-carbonate alteration. This suggests that the fluids were rich in CO_2. Mercury probably was transported as vapour-phase Hg^0 at 200–240 °C (Peabody & Einaudi 1992). Until 1973, the Californian mercury province played a major role in world production. Today, its interest lies in close genetic and spatial relations to some hot springs gold deposits (Sherlock 2005).

Almadén in Spain is the largest mercury concentration in the world ($\sim$300 km southwest of Madrid; Figure/Plate 1.89). It is the source of $\sim$30% of total historic world production and encloses 30% of remaining world resources of mercury, although the mines are indefinitely closed since 2002. From prehistoric times, mining took place in the district, with prosperous peaks during Roman (200 BCE to $\sim$400 CE) and Arab (711–1492 CE) occupation, and again in the Renaissance (16th century). This bequeathed a heavily contaminated landscape (Molina *et al.* 2006):

> At Almadén, steeply dipping Ordovician and Early Silurian sediments contain quartzite bands with lenses of cinnabar impregnations and veins. Enclosing black shales display native mercury ore. The stratabound orebodies extend for hundreds of metres along strike and dip. Most orebodies occur near Ordovician-Devonian volcano-sedimentary rocks that include black shales, sills, lava flows, tuffs and diatreme breccias ("frailesca") of heavily altered alkali-basaltic and tholeiitic volcanics (Figure 2.36).
>
> In this setting, cross-cutting bonanza orebodies were exploited (Jebrak *et al.* 2002). Typical ore grades in quartzite were 1%, but in places reached 20%. Radiogenic and stable isotope studies of the hydrothermal alteration zones suggest a magmatic derivation of the fluids. Lead isotopic compositions point to a mainly sedimentary source of Pb and probably Hg, although a magmatic contribution cannot be excluded (Higueras *et al.* 2005). ^{40}Ar/^{39}Ar illite dating shows that hydrothermal alteration is contemporaneous with magmatism (Hall *et al.* 1997). Sulphur isotopes imply Ordovician shales as source for both cinnabar and pyrite sulphur. Overall, the origin of this giant deposit with a total mercury endowment of $\sim$320,000 t is insufficiently understood. Mantle metasomatism, rifting, magmatism, diatreme formation, hydrocarbons formed by maturation of organic matter and hydrothermal convection in sediments and magmatic rocks may all have had a role (Hernandez *et al.* 1999, Higueras *et al.* 2005).

Presently, China and Kyrgyzstan operate mercury mines. World production in 2008 was an estimated 1320 t refined mercury (1280 t in 2009). Consumption is estimated to $\sim$2000 t per

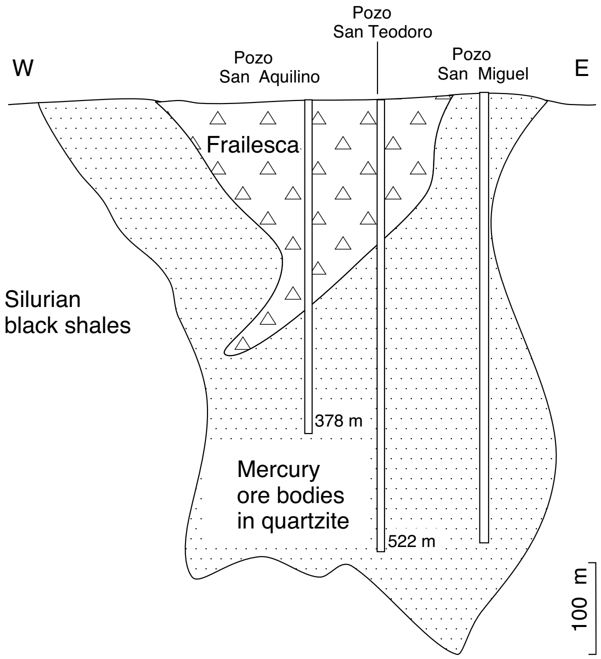

Figure 2.36 Schematic profile of the giant mercury deposit of Almadén, Spain (modified after Hernandez *et al.* 1999). With permission from Springer Science + Business Media. The main orebodies occur in the Criadero quartzite (Earliest Silurian) near mafic volcanics and diatreme rocks (frailesca), rarely in black shales. Highest-grade ore occurred near the surface. Concentrations decreased with increasing depth. For location refer to Figure/Plate 1.89.

year, not least because many gold producers use amalgamation (e.g. China, Indonesia and South America). However, many mines and smelters processing ore with traces of mercury have to pay for permanent disposal. Small amounts of mercury continue to be sold from the stockpile at Almadén, from decommissioning of chlor-alkali plants worldwide and by geothermal power stations. Recycling is an important market factor. Mercury is traded in traditional units that are called flasks (one flask containing 34.5 kg of refined mercury).

2.5.2 Antimony

Common Ore Minerals:

		Wt. % Sb	*Density (g/cm^3)*
Stibnite (antimonite)	Sb_2S_3	71	4.6
Tetrahedrite (Antimony fahlore)	$Cu(Ag,Fe,Zn)_3 Sb(As,Bi)_{3,25}$	variable	4.6–5.1

The most common antimony ore mineral is stibnite, which may host traces of Au, Ag, Fe, Pb and Cu. Other antimony-bearing minerals are of minor economic significance. These include native antimony and a number of sulphides, sulphosalts, oxides, antimonates and antimonites. Weathering of primary antimony minerals produces grey-coloured ochres and greyish-white senarmontite. Antimony ore is often a carrier of important by-product Au and Ag, but also of undesirable As and Hg. Prevailing gangue minerals are pyrite, quartz and carbonates.

Mining grades in antimony-only deposits are usually >3% Sb. Many lead, silver and copper ore concentrates yield by-product antimony during metallurgical processing. Antimony is traded as a metal (density 6.62 g/cm^3; melting point 630.5 °C, boiling point 1750 °C) or oxide. The most important antimony compound is the trioxide Sb_2O_3, which is used as a flame retarder applied to plastics, textiles and building materials (~65% of mine production). Other applications of antimony compounds include fireworks, ceramics and glass. Antimony metal is part of various alloys, mainly with lead in storage batteries, sheet and pipe metal, and ammunition.

Geochemistry

Similar to mercury and arsenic, geochemical concentration of antimony in near-surface epizonal hydrothermal systems is striking. It is a chalcophile element such as As, Hg and Pb, and its geochemical behaviour is intermediate between mercury and lead. Igneous rocks contain an average of 0.2 ppm Sb (granite and basalt alike), whereas pelitic sediments reach 2 ppm Sb. Antimony's crustal abundance is 0.15–1 ppm (Smith & Huyck 1999). Antimony occurs in valence states Sb(V) and Sb(III).

Oxidation of stibnite results in formation of antimony oxides with colourless senarmontite ($Sb_2^{III}O_3$) as the most common phase. In oxidized and near-neutral pH surface or groundwater, senarmontite may yield dissolved Sb at concentrations to ~50 mg/L (Craw *et al.* 2004). Dissolved antimony is toxic and contents in drinking water should not exceed 0.003 mg/L (Australian Drinking Water Guidelines). At low intake, antimony poisoning is very similar to clinical effects of arsenic. High doses of antimony are lethal but exposure is very rare. Epizonal hydrothermal metal deposits (e.g. gold) are most likely sources (Milham & Craw 2009). Mobile antimony tends to be immobilized and geochemically enriched in iron oxy-hydroxides.

Antimony in hydrothermal fluids may be derived from degassing magma or from pelites, especially those rich in organic matter. Mobilization of trace antimony from pelites is observed in heated aureoles of igneous bodies or of orogenic metamorphism. This behaviour relates antimony to other "volatile" metals and semi-metals such as Hg, As, Te and Tl (Figure 2.23). Antimony complexes, for example $Sb_2S_2(OH)_2$ or $H_2Sb_2S_4$ are vehicles of hydrothermal transport. Comparable to mercury, Sb solubility is mainly controlled by temperature (~10,000 ppm Sb at 300 °C and only 1 ppm Sb at 100 °C). Neither pH nor H_2S-activity or fO_2 exert a noteworthy influence. Precipitation is caused by falling temperature, either because of adiabatic cooling with dropping pressure, or by mixing with cool near-surface waters. Fluid inclusions in quartz of antimony deposits confirm entrapment at low temperature. Late Variscan (Carboniferous/Permian) antimonite mineralization in the Armorican Massif (France), for example, was formed at 140–160 °C (Bailly *et al.* 2000).

Antimony ore deposit types

Deposits of volatile antimony are formed in epizonal low-temperature hydrothermal settings. Mobilization may be due to diagenetic heat and fluid pulses, or to volcanogenic, magmatic and metamorphogenic process systems. Important antimony ore deposit types include:

- hydrothermal-exhalative sedex deposits (e.g. Xikuanshan in China), of considerable economic importance;
- epizonal hydrothermal replacement ore in limestone and dolomite, controlled by low-permeability traps and fracture zones, and characterized by pronounced silicification; antimonite is commonly the prevailing ore mineral, but deposits that are transitional to epithermal gold deposits of the Carlin type are known (e.g. Alshar in Macedonia with arsenic, gold and important reserves of thallium: Volkov *et al.* 2006);
- antimony ore veins associated with orogenic gold systems, base metals, and granite-related tin and tungsten (Hillgrove, Australia; Bolivia: Dill 1998);
- terrestrial hot springs deposits as parts of metamorphogenic systems caused by extensional (graben) tectonics in volcanic regions (e.g. part of the ores at Murat Dagi, Turkey: Gokce & Spiro 1994).

Antimony deposits are more numerous in young orogenic belts than in geologically old terranes, due to deeper erosion of older mountain belts and consequent loss of near-surface metal concentrations. Numerous antimony vein and replacement mineralizations occur in Tertiary provinces of andesite and rhyolite volcanism. Other antimony provinces may have formed during late-tectonic flooding of the crust with granites. In Variscan Europe, a preponderance of metamorphogenic mobilization is assumed (Wagner & Cook 2000), but antimony deposit formation coincided with a period of granite intrusion and distension after folding (Munoz *et al.* 1992). Gold-antimony ore in shear zones of the Archaean Murchison Greenstone Belt in South Africa is interpreted as the epizonal expression of an orogenic gold system (Figure 2.22).

In South China, important sedex deposits are exploited, of which Xikuanshan is the largest (Fan *et al.* 2004b). Two ore beds attaining a thickness of 5 m and an extension of several thousand square metres occur between grey chert bands within a Late Devonian suite of black shale, dark marl and limestone (Figure 2.37). Ore strata consist of antimonite, quartz and calcite and traces of other sulphides. Stockwork antimony ore with additional barite and fluorite occurs below the strata to a distance of ~200 m. The deposit is surrounded by a large halo of anomalous Sb traces. With $\delta^{34}S$ of 6.6‰, sulphur isotopes in antimonite are thought to reflect biogenic sulphate reduction. During the Devonian, the area was a shallow marine platform undergoing extensional strain.

Many of China's large and smaller antimony deposits are probably magmatic-hydrothermal products of the Mesozoic Yanshanian granites, which display remarkable metallogenic fertility (e.g. Dachang, Figure 2.20; cf. Section 2.1.7 "Tungsten", Section 2.3.2 "Silver", Section 2.2.3 "Tin" and Section 2.5.9 "Tantalum"):

> The Au-Sb-W deposits near Woxi have combined reserves of ~1.8 Mt with an average grade of 13 g/t Au, 4.5 % Sb and 0.5 % WO_3. Host rocks are purple-red slates of Mesoproterozoic age. Bedding-parallel quartz veins (<1.5 m thick) account for most of the production, although cross-cutting veins are also exploited. The ore contains scheelite, wolframite, stibnite, native gold, pyrite and other sulphides. Hydrothermal wallrock alteration is pronounced. Nd-Sr-Pb isotopic characteristics imply a granitic source of the hydrothermal fluids, although granites are not known in the district (Peng & Frei 2004). Together with textures reminiscent of bedding, this absence of granites has led to genetic interpretations that invoke a sedex-like origin comparable to Maucher's (1965) once popular "volcano-sedimentary Sb-W-Hg formation".

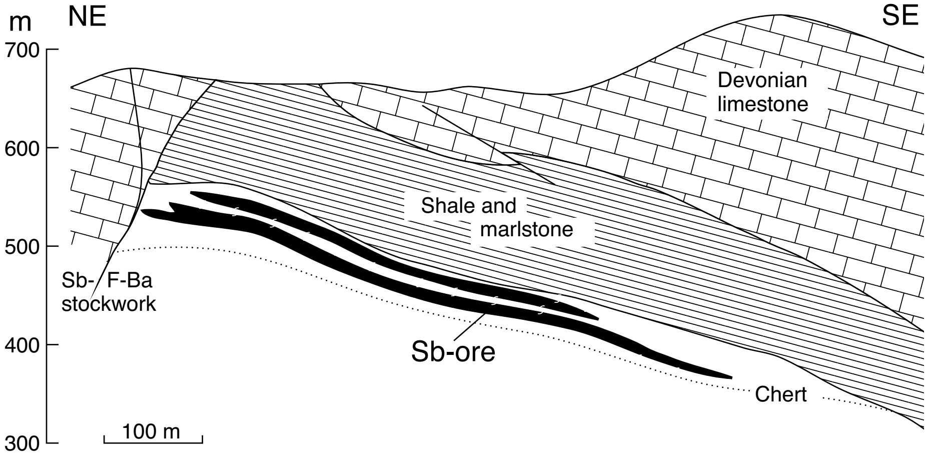

Figure 2.37 Stratiform sedex antimony orebodies in Late Devonian sediments at Xikuanshan, Hunan, China (after Fan *et al.* 2004b). Copyright (2004) with permission from Elsevier.

Significant metamorphogenic deposits occur in the Archaean Murchison Greenstone Belt, South Africa, along a shear zone that extends over 55 km (termed the "Antimony Line") and is marked by strong hydrothermal alteration. Komatiites, for example, were transformed into conspicuous massive talc-carbonate rocks. Host rocks of orebodies include quartz-chlorite and quartz-muscovite schist, quartzite, metabasalt and banded iron formations. All these rocks display alteration in greenschist facies and addition of CO_2:

> Orebodies consist of quartz veins and impregnation zones with traces of scheelite, magnesite and talc, which were originally worked for gold, but present mining aims for antimony with by-product gold. Ore minerals include antimonite, tetrahedrite and complex sulphosalts. $\delta^{34}S$ data imply a magmatic source of sulphur, probably leached from komatiites. Carbonate $\delta^{13}C$ ($-4.7‰$) is too heavy for biogenic carbon and suggests a deep origin of CO_2. The crustal-scale shear zone (Figure 2.22) may have allowed upflow of mantle fluids. The proposed genetic model emphasizes deep metamorphic fluids that distilled antimony and gold from metapelites (Pearton & Viljoen 1986). Orebody characteristics and metamorphogenic hypotheses applied to the orogenic antimony-gold deposit Wiluna in Western Australia are very similar (Hagemann & Lüders 2003).

The World's leading producer of primary antimony is China (2008 >90% of a total of 197,000 t; in 2009 falling to 187,000 t), followed by Bolivia, Russia, South Africa and Tajikistan. Recycling of used car batteries satisfies an important part of demand.

2.5.3 Arsenic

Common Minerals:

		Wt. % As	*Density (g/cm^3)*
Arsenopyrite (mispickel)	FeAsS	46	5.9–6.2
Loellingite	$FeAs_2$	73	7.4

The semi-metal arsenic occurs in many more minerals composed of elements such as S, Se, Te, Tl, Cu, Fe, Ni, Co and the platinum group elements (PGE). Arsenopyrite is especially common in gold ore and often contains the gold. "Invisible" gold in arsenopyrite may occur in the form of tiny inclusions or in its crystal lattice (possibly with Au-As bonds). Gold-rich parts are variably certain growth zones, or fissures, or the rims of grains. Elevated trace contents of nickel and cobalt in arsenopyrite are not rare. Formerly, the less common sulphides realgar (red, AsS) and orpiment (yellow, As_2S_3) used to be precious pigments for artists, in spite of their toxicity.

Arsenic is a by-product of processing ore of metals such as Ag, Cu, Zn, Sn and Au. The amount of arsenic produced by mines and metallurgical plants worldwide is much higher than consumption. Sulphide ore roasting results in sublimation of "white arsenic" As_2O_3 that is known as an infamous poison and a medical restorative. Today, use of arsenic is strictly limited, for example to pest control chemicals in agriculture (banned in the EU) and wood conservation products such as Cu-Cr arsenate in aqueous solution, that is non-toxic after drying. Arsenic compounds are used as pesticides, herbicides, insecticides and in various alloys. Traces of arsenic are added as a micronutrient to plant fertilizers. High-purity arsenic metal (density 5.72 g/cm^3; melting point 817 °C, boiling point 613 °C) is increasingly required for the production of high-capacity semiconductors (e.g. gallium arsenide). Yet, the unfavourable market for arsenic forces many mines and metallurgical plants to dispose of all As-bearing material as hazardous waste. One example is the Giant Mine, Yellowknife, Canada, where between 1948 and 1999, a total of 215 tonnes of gold and 237,000 t of arsenic trioxide dust were produced. The dust was stored underground in mine voids where it is immobilized by freezing, because the mine lies in a permafrost zone (Royle 2007). Former metallurgical plants were often a source of arsenic contamination in their neighbourhood, by roasting and smelting of base and precious metals concentrates. Arsenic-contaminated soil can be bioremediated by planting and harvesting the fern *Pteris vittata* (Gonzaga *et al.* 2007).

Trivalent arsenic is more toxic than other forms. Doses of more than 100 mg of arsenic will cause acute poisoning, whereas chronic exposure impairs health and increases the risk of cancer. The main path of arsenic intake of humans is drinking water. Plants cultivated on contaminated soil are less frequently a source of critical exposure. Therefore, acceptable maximum levels in drinking water are generally set to 10 μg per litre, the intervention level for soil in residential areas to 55 mg/kg dry mass (The Netherlands) and the inspection value for agricultural land to 200 mg/kg (Germany). In small concentrations, however, arsenic is an essential element (Oremland & Stolz 2003). Healthy humans contain ~18 mg As, that must be continually replaced because of the short biological half-life (10–30 h) of the element in the body (Lindh 2005).

Geochemistry

Arsenic is one of the more "volatile" metals and metalloids such as Hg, Sb, Te and Tl (Figure 2.23). Arsenic exhibits redox-sensitive behaviour with oxidation levels −3, 0, +3 and +5. It is geochemically similar to phosphorous and peculiar because it forms both anions and cations. Its crustal abundance is estimated at ~2 ppm (range 1.7–5) similar to contents in average granite (1.5) and basalt (2 ppm; Smith & Huyck 1999). Sediments contain more arsenic than magmatic rocks, with highest contents in pelites (~13 ppm). Coals have particularly high arsenic trace concentrations. In the USA arsenic (like Hg and Sb) is specified as a hazardous air pollutant (Chapter 6.5 "Applications of Coal Geology").

With gold and silver, arsenic shares an elevated solubility in the presence of H_2S, which immobilizes other metals (Fe, Pb, Zn, Cu). The prevailing species of arsenic in hydrothermal solutions is $H_3AsO_3{}^0$ (aq), with As^{+3} at pH 1–8 and T up to 275 °C. Geothermal fluids often have very high arsenic content (~50 ppm), with varying ratios of As^{+3} and As^{+5}. In magmatic and hydrothermal vapour above ~400 °C, arsenic is enriched in the form of $As(OH)_3$ compared to the liquid phase (Pokrovski *et al.* 2002, 2005).

Weathering of arsenian iron sulphides produces intermediate realgar and orpiment, and arsenates such as the greenish scorodite $FeAsO_4.2H_2O$. Similar to antimony, As^{+5} is mobile as oxyanion ($AsO_4{}^{3-}$) in oxygen-rich water and As^{+3} in strongly reduced groundwater. Mobile arsenic is efficiently immobilized and geochemically enriched in iron oxides, sulphides, in siderite concretions hosted by claystone, in phosphorites and black shales. Mine-derived acid seepage is often contaminated, even where only traces of arsenic occur in the ore (Zhu *et al.* 2003). Under oxidizing conditions and at pH 5–7, arsenic is hardly mobile and virtually immobile if iron-rich particles are abundant (e.g. hydrous ferric oxide precipitated from mine water); transport is limited to suspended solids (Smith & Huyck 1999). Because arsenic was not measured in earlier national geochemical surveys, the distribution in the Earth's surficial materials is poorly known (Plant *et al.* 2005).

Unrelated to mining, natural arsenic concentrations in aquifers and/or groundwater of Holocene lowland valleys throughout the world are a hidden hazard. In the Ganges delta, this caused humanity's biggest mass poisoning (Nordstrom 2002, Smedley & Kinniburgh 2005). Earlier, millions of people in the region had relied on surface water. From 1980 to 1990 thousands of drinking water wells were drilled to provide "safe", microbially clean water. Of these wells, nearly 50% had As of >10 micrograms/litre. Sadly, this was only recognized after numerous people had developed skin and internal disorders, including cancer. With 2–20 ppm, the As-contents in Ganges river sediments are quite ordinary. Spots of elevated dissolved arsenic occur in low-sulphate groundwater in the presence of reactive organic matter, which supports strong microbial reduction of iron oxides and oxy-hydroxides releasing adsorbed arsenic (Fendorf *et al.* 2010). Well-drillers should be wary of extracting water from reduced, grey sediments.

Arsenic mineralization types

Arsenic is mobilized from crustal material, transported and precipitated wherever hot aqueous fluids and vapours are cooled, including magmatic, diagenetic and metamorphic systems. As a chalcophile element it is concentrated in many sulphidic ore deposits. Processing these ores, for example roasting, liberates arsenic (III) oxide, which can be recovered.

Arsenopyrite and arsenian pyrite $Fe(S,As)_2$ are common in pyrite-rich copper ores (e.g. volcanogenic Boliden, Sweden; sedex Rammelsberg/Germany), in metamorphogenic silver (Kongsberg, Norway) and cobalt-nickel ore veins (Bou Azzer, Morocco: Ahmed *et al.* 2009), in numerous gold deposits (distally magmatic-hydrothermal Carlin, USA) and in many tin deposits (magmatic-hydrothermal Renison Bell in Tasmania and Altenberg; Erzgebirge in Germany). Arsenopyrite, realgar and orpiment are often part of the paragenesis in metamorphogenic, volcanogenic epithermal and hot springs deposits of gold, antimony and mercury.

Main producers of arsenic are China, Chile, Morocco, Peru, Russia, Kazakhstan and Belgium. Annual world production is ~53,000 t (trioxide). Many mines find arsenic a liability, which requires permanent disposal. Arsenic is hardly ever the target of exploration but retains its important role as a useful pathfinder element for geochemical gold exploration.

2.5.4 By-Product Electronic Metals (Selenium, Tellurium, Gallium, Germanium, Indium, Cadmium) and Silicon

"Electronic metals" is not a strictly defined term. Several non-ferrous and semi-metals used for manufacturing electronic equipment are treated in separate parts of this chapter (e.g. copper, antimony, arsenic, gold). Here, concise information is provided about elements that occur in minor or trace amounts in ores of more common metals. With the exception of silicon, the electronic elements are typically by-products of the processing of sulphide ore of base and precious metals. Consumption of single electronic metals is of the order of tens or hundreds to a few thousand tonnes per year. With a market of ~20,000 t/year for cadmium and 40,000 t/year for silicon, the two are clearly set apart. In metal trading, the electronic metals are part of the "minor metals", but this sector expands rapidly. For applications as functional electronic materials, an extremely high purity is required and refining creates most added value. Because this is often limited to specialist companies, raw and intermediate materials may be shipped across the oceans so that their true origin remains uncertain. Also, recycling (e.g. of electronic scrap) is an important and often undisclosed source.

Selenium

Selenium (melting point 217 °C, density 4.79 g/cm^3; crustal abundance 90 ppb: Smith & Huyck 1999) is primarily recovered from copper sulphide ore. Selenium also occurs in uranium ore of the sandstone and unconformity types (Figure 1.57; cf. Section 2.5.12 "Uranium"). Because of similar chalcophile geochemical characteristics, Se (and Te) partially substitute for sulphur in many sulphides. Selenium is also enriched in epithermal Au-Ag ore, in skarn and various base metal deposit types. Large selenium-only deposits are known in China (La'erma and Qiongmo in the western Qingling mountains, and Yutangba in Hubei province: Xiong 2003). Under oxidizing conditions in surface water, the element occurs in anionic form but is immobilized by reduction. This effect concentrates selenium in organic matter-rich sediments such as black shales, phosphorite and coal. Enrichment of selenium relative to sulphur is favoured by oxidizing conditions in the haematite stability field (Simon *et al.* 1997, Xiong 2003). Selenium minerals (e.g. $FeSe_2$, PbSe) are rare and economically insignificant. Selenium is unusual in that it is both photovoltaic and photoconductive. Yet, ~65% of selenium is used in glass and pigments manufacturing (yellow, orange, red). Examples of electronic applications (10%) are certain photovoltaic cells (e.g. solar panels). In recent years, it is also used as an additive in the production of electrolytic manganese metal. Selenium, tellurium and sulphur can perform as vulcanizing agents in rubber compounding. For humans, animals and plants, selenium in low quantities is an essential element (Lindh 2005). For this reason it is a common additive to animal feed and to fertilizer. Humans suffer from dietary deficiency at intakes <40 µg/day and from toxic effects at >400 µg/day (Fordyce 2005). Because most rocks contain very low concentrations, selenium-deficient environments are far more widespread than seleniferous ones. Selenium is nearly exclusively a by-product of electrolytic copper refining. Output, therefore, is tied to countries that process copper concentrates (e.g. Japan, USA, Belgium), and to the vagaries of the copper market. World production is ~1500 t/year (USGS 2010).

Tellurium

Tellerium (melting point 449.5 °C, density 6.24 g/cm^3; crustal average 4 ppb) is a very rare chalcophile metalloid. Trace amounts are found in many gold ores (e.g. sylvanite $AgAuTe_4$ in Transylvania (Romania) and in gold deposits of the Western Australian greenstone belts; cf. Section 2.3.1 "Gold"), in silver ore (Bolivia), in coal, lead ore and in many large copper ore deposits. The latter are the chief source of tellurium recovered as a by-product of electrolytic copper refining. The world total refinery production may be assumed at ~500 t/year (metal). In the USA, ~50% of tellurium is used as an alloying agent for iron and steel, 25% for catalysts and chemical purposes, and only 8% for electronic applications such as CdTe solar cells. The latter application is thought to expand rapidly, because the CdTe technology produces the lowest-cost solar electricity (Zweibel 2010). The use of cadmium in photovoltaics is contentious. Tellurium is mildly toxic, similar to selenium.

Gallium

Gallium (melting point 29.78 °C, density 5.907 g/cm^3), with an estimated crustal average of 17 ppm (Smith & Huyck 1999) is as abundant as Pb (16 ppm). In contrast to galena, Ga-minerals are very rare (e.g. gallite $CuGaS_2$). Chalcophile gallium is relatively enriched in meteorites, in sedimentary iron ore deposits and in gossans, in sphalerite and sulphosalts, in coal (with some production from flue dust), pegmatites and greisen. However, most commercial gallium is derived from bauxite, because Ga^{3+} substitutes for Al^{3+} and Fe^{3+} in common rock-forming minerals. Due to the low solubility of α-GaOOH in the weathering environment between pH 3–8 (Wood & Samson 2005), Ga is enriched to 30–60 ppm in bauxites. During

Bayer-Process leaching, Ga is precipitated from the sodium-aluminate solution, providing >95% of primary world production (2008: 111 t; 78 t in 2009). Minor sources of economic gallium (plus Cd and Ge) are sphalerite concentrates (e.g. in the Mississippi Valley Province, USA). Ga, Ge and In in sphalerite usually reflect substitutional coupled solid solution. In some coals and in petroleum ash, gallium and germanium occur in recoverable concentrations. Gallium is mainly used in electronic applications (e.g. GaAs-base integrated circuits, LED-light emitting diodes, solar cells). Consumption of gallium is expected to increase with the production of gallium arsenide wafers for integrated electronic circuits, competing with silicon.

Germanium

Germanium (melting point 937.4 °C, density 5.32 g/cm^3; crustal average 1.4 ppm) is mainly a by-product of the smelting of certain sulphidic copper and zinc ore concentrates, with grades of several 100 ppm Ge (Höll *et al.* 2007). Examples of primary (mining) sources of this type are Kipushi (cf. Section 2.2.2 "Lead and Zinc"; St Salvy, France), the Tristate District (USA), Petsamo (Russia), Tsumeb (Namibia; where large masses of germanite $Cu_{13}Ge_2Fe_2S_{16}$ have been extracted), Bor, Serbia and Red Dog (Alaska: Figure 1.73). Germanium can also be enriched in the weathering environment, for example in the Apex deposit (Utah), where the element occurs adsorbed in jarosite and goethite/haematite (Wood & Samson 2005). Ash from coal-combustion can be an economic source of germanium (Chapter 6.1 "The Chemical Composition of Coal"). Germanium minerals are rare. Chemical properties and the geochemical behaviour of siderophile (Goldschmidt 1958) germanium are largely similar to silicon. Germanium is applied in the production of polymerization catalysts for PET-plastics (35%), of infrared lenses and optical fibres for wiring the internet (ca. 25%), and electronic and solar cell applications (12%). The world refinery production (~140 t/a) is dominated by China and USA. Secondary sources and recycling are important features of the market. Germanium displays the best performance of all semiconductor elements and accordingly, demand is expected to grow.

Indium

Indium (melting point 156.17 °C, density 7.31 g/cm^3) has nearly the same relative abundance in the Earth's crust as silver (50 ppb In against 70 ppb Ag), but never occurs in sufficient concentrations to be mined in its own right. It is chalcophile and concentrates in sulphides (Schwarz-Schampera & Herzig 2002). Most indium is a by-product of tin, high-temperature zinc and copper ores at grades of up to 1000 g/t concentrate. In the form of copper indium diselenide, indium is used as a transparent absorbing semiconductor in solar cells. The metal is applied as a surface coating in bearings and in low-temperature fusible alloys (e.g. solders). Its most prominent application (~80%) is in the form of indium-tin oxide as a transparent conductor in liquid crystal display (LCD) screens. A large part of the world's refinery production (2009: 600 t) comes from China, the Republic of Korea, Japan and Canada (one important source is granitic-hydrothermal orebodies at Mt Pleasant, New Brunswick: Sinclair *et al.* 2006).

Cadmium

Cadmium (melting point 320.9 °C, density 8.65 g/cm^3) also is a by-product of zinc ore processing. Because of NiCd battery recycling, the refinery production of Cd (2009 ~19,000 t) provides only ~80% of world consumption. Uses of cadmium include NiCd batteries (~ 80% of total consumption, with Cd as an oxide), pigments, stabilizers, coatings and in small quantities, specialized alloys and electronic products. In the future, solar panels with Cd-S/Cd-Te are expected to win wide acceptance, because cadmium compounds provide a perfect match to the spectrum of the sun. In spite of the successful introduction of non-toxic Li-ion batteries, NiCd batteries experience a rennaissance in the favoured electric vehicles. Cadmium is extremely toxic and its use and recycling are strictly controlled (Selinus *et al.* 2005). Cadmium's geochemical character is chalcophile and its average crustal content ~0.1 ppm. Pelites, phosphorites and manganese nodules concentrate cadmium to ~25 ppm. Sphalerite carries cadmium either in solid solution or as tiny inclusions of CdS (greenockite), to a maximum of 5% (average contents are 0.3%). Refined cadmium metal production originates predominantly from Asia (Korea, China, Japan) and North America (Canada and Mexico).

Silicon

Silicon (melting point 1410 °C, density 2.329 g/cm^3) is currently the most important electronic material. Nearly all micro-electronic equipment in electronic and photovoltaic applications is based on ultra-pure (and doped) silicon. Annual consumption of semiconductor-grade silicon is estimated to ~40,000 t/year. Read more about silicon in Chapter 3 "Quartz".

2.5.5 Bismuth

Common Ore Minerals:

		Wt. % Bi	*D (g/cm^3)*
Native bismuth	Bi	100	9.8
Bismuthinite	Bi_2S_3	81	6.8

Common impurities in native bismuth include Fe, Te, As, S and Sb. Oxidation of primary bismuth minerals produces the yellow or greyish-green bismuth ochre minerals bismutite $(BiO)_2CO_3$ and bismite α-Bi_2O_3.

Bismuth is a non-toxic heavy metal (9.79 g/cm^3). Because of its low melting point (271.3 °C) it is used in lead-free solders and a variety of other alloys. It is also a metallurgical additive (steel), a replacement for lead in plumbing and a raw material for chemicals (yellow pigments, pharmaceuticals, cosmetics). Increasingly, lead shot is replaced by an alloy of 97% bismuth with 3% tin.

Geochemistry

Bismuth is an extraordinary element because its only natural isotope ^{209}Bi is unstable, although with a half-life of 2×10^{19} years. Its daughter by radioactive α-decay is stable ^{205}Tl (Marcillac *et al.* 2003). Bismuth's average crustal abundance is ~0.2 ppm. Its geochemical behaviour is chalcophile and like Sb and As it is one of the "volatile" metals. Trivalent bismuth is among the elements that are highly enriched in the continental crust, compared to primitive mantle. Bismuth is concentrated by magmatic and hydrothermal processes. The element is an essential component in low melting-point assemblages such as the Au-Bi-Te-S system, which is common in magmatic-hydrothermal gold deposits (Tooth *et al.* 2008). Under oxidizing conditions, bismuth is moderately mobile, but immobile in all reduced environments.

Bismuth deposit types

Bismuth occurs as a by-product in tin pegmatites, in tungsten, copper, gold and lead skarn deposits, and generally in magmatic-hydrothermal mineralization related to granites. It is an essential component of hydrothermal Bi-Co-Ni (U-Ag) veins, for example at Jachymov, CSR (cf. Section 2.5.12 "Uranium"). Workable deposits with bismuth as main metal are extremely rare; one is Tasna in Bolivia.

Cerro Tasna mine (or Tazna, presently on standby) is one of the southern Bolivian tin-silver belt deposits. Orebodies occur in the roof of a Tertiary felsic intrusion. Host rocks of the deposit are metapelites that were transformed into proximal quartz-tourmaline fels, overlain by an argillized zone. Numerous veins occur in the altered rocks, with a paragenesis of native bismuth, bismuthinite, chalcopyrite and ferberite. Gold occurs locally. Elsewhere in Bolivia, bismuth is a by-product of silver and tin ore (e.g. Potosí).

The world's largest single concentration of bismuth is the scheelite skarn deposit in Shizhuyuan, China (Huan-Zhang *et al.* 2003; cf. Section 2.1.7 "Tungsten"). By-product bismuth is derived from the processing of copper and lead ore, rarely also from ores of tin, zinc, molybdenum, cobalt, gold and silver. In some cases, bismuth is a detrimental part of ore concentrates and lowers its value. Most of the world bismuth production (2008 ~7700 t;

in 2009 7300 t) originates in China, Mexico, Peru, Bolivia and Kazakhstan.

2.5.6 Zirconium and Hafnium

Common Ore Minerals:

		Max. wt.% ZrO_2	*Density (g/cm^3)*
Baddeleyite	ZrO_2	94	5.5–6
Zircon	$ZrSiO_4$	67.2	max. 4.68

Baddeleyite is exploited as a by-product of hard-rock mining (its only present source is Kovdor in Russia; cf. Chapter 3 "Phosphates"). Zircon is an accessory in many common rocks and very stable in the surface environment. Therefore, it is enriched in the heavy mineral fraction of clastic sediments and is a by-product of ilmenite and rutile placer mining. Zircon and baddeleyite typically contain ~1.5 to 4% hafnium and a maximum of 4000 ppm uranium and 2000 ppm thorium (Hanchar and Hoskin 2003). This makes the extremely robust zircon highly suitable for petrological studies and age dating with the U-Pb method. However, the radioactive decay of alpha-emitters U and Th causes chemical and physical changes in zircon ("damage domains") that may finally reach an amorphous state with low density. In that case, age determination is highly problematic. Many placer zircons contain micro-inclusions of other minerals (e.g. of P, Fe, Ti, etc.) that decrease their market value. Zircon concentrates should have grades of >65% ZrO_2. Exploitable placers commonly contain 0.2–3% zircon. Zirconium is not toxic, but zircon's radioactivity enforces careful management from the mine to the end user. Therefore, zircon with U + Th <500 ppm is preferred.

A high percentage of traded zircon is used as a mineral, for example in abrasives, foundries and refractories (glass, cement). Milled to very fine particle size, zircon is applied in ceramic frits and opacifiers (tiles, tableware and sanitary ware). Zircon is also added to TV glass and computer screens to block X-rays. Some zircon is processed to synthetic zirconia (ZrO_2, an important ceramic material) and zirconium metal. Zirconium metal is an outstanding refractory material due to its resistance to high temperatures (melting point at 1852 °C, boiling point 3580 °C, density 6.5 g/cm^3) and chemical attack. This accounts for its use in the chemical and space industriers, and in the form of zirconium alloy tubes as containers of fuel pellets (rods) in nuclear reactors. Zircon is considered as a material in which to immobilize the plutonium isotope ^{239}Pu over geological time scales. ^{239}Pu and other actinides are waste products from uranium-fuelled nuclear reactors:

Hafnium (density 13.09 g/cm^3, melting point 2222 °C) is geochemically very similar to zirconium but with a crustal average of 4.9 ppm being less abundant. Hafnium is recovered as a by-product of zirconium metallurgy. Its separation from zirconium is expensive, however. Hafnium uses are in superalloys for gas turbines, control rods for nuclear reactors and, although in small quantities, manufacturing microprocessors for the latest generation of computer chips.

Geochemistry

As a lithophile element (similar to Ti und Hf) zirconium has a relatively high crustal abundance of 160 (130–400) ppm. Zircon is a common mineral in igneous rocks, clastic sediments and their metamorphic equivalents. Primary enrichment of zircon has been noted in alkaline magmatic rocks. Subeconomic concentrations are known in pegmatites. Hydrothermal zircon concentrations are rare. One example is epithermal zircon and uranium impregnation of felsic volcanic rocks at McDermitt caldera, Nevada (Castor & Henry 2000; cf. Section 2.5.12 "Uranium"). In surface waters, zirconium displays a very low solubility. Zirconium salts are of low toxicity; the element has no known biological function.

Zirconium deposit types

Zircon deposits are almost exclusively coastal placers that typically display a combined valuable heavy mineral content of 4–10 weight %. Co-product minerals are mainly rutile and ilmenite. Exploitable hard-rock concentrations of baddeleyite are only known in alkali complexes (Kovdor, Russia, which in 2007 produced ~5 Mt iron concentrate, 2.5 Mt apatite and 8200 t baddeleyite). At Palabora, South Africa, Zr-production was terminated in 2002. In the near future, zircon is expected to become a by-product of large sand-moving industries, such as the Canadian tar sand operations (cf. Chapter 7.6).

One important region of zircon-rich coastal placers occurs in Geographer Bay, south of Perth in Western Australia. In this area, Precambrian granulite and gneiss are overlain by Mesozoic clastic sediments. Pleistocene to Recent coastal cliffs and surf platforms are cut into the Mesozoic, at elevations of 0–76 m above sea level. Heavy minerals are enriched at the base of each strandline. The oldest and highest group of deposits occurs near Yoganup, in a cross-section consisting of lenticular orebodies (Figure 2.38) that reach a length of 30 km and a width of 1500 m. The heavy mineral content of the Yoganup level surpasses 10 Mt:

> The highest-grade black sands of Yoganup occur just above Mesozoic or Pleistocene sediments. Their base is marked by a coarse coastal conglomerate that grades into black clayey sands with monazite and 15–20% zircon in the heavy mineral fraction. This is overlain by sandy clay (10% zircon in HM) and yellowish-brown aeolian sand (6% zircon in HM). Overall, the HM fraction contains an average of 65–80% ilmenite, 10% magnetic leucoxene, 10% non-magnetic leucoxene, 5–12% zircon, <1% rutile, and 0.2–1.1% monazite. The majority of heavy minerals occur in the 100–150 μm grain size range (fine sand). Towards the sea and upwards, both overall HM content and fractions of monazite and zircon decrease.

A new province of mineral sand deposits was lately discovered in the Pliocene inland sea sediments of the Murray Basin, Victoria, Australia. The Douglas deposit, for example, is based on several strips of HM sands occurring over an area of 4 × 8 km. The subhorizontal HM sand beds occur between fine-grained sand and clayey silt horizons 10–15 m below the surface (Figure/Plate 2.39). Measured and indicated resources comprise ~45 Mt at 11.3% HM. Fractions of valuable HM in the total mass of heavy minerals are 8% rutile, 10% zircon, 41% ilmenite and 4% non-magnetic leucoxene (Whitworth 2009). In the Tertiary Eucla Basin of western South Australia, the Jacinth-Ambrosia mine is based on resources containing 9.5 Mt HM composed of an extraordinary 48% zircon, 28% ilmenite and 4% rutile. Average grade is 6.5% HM.

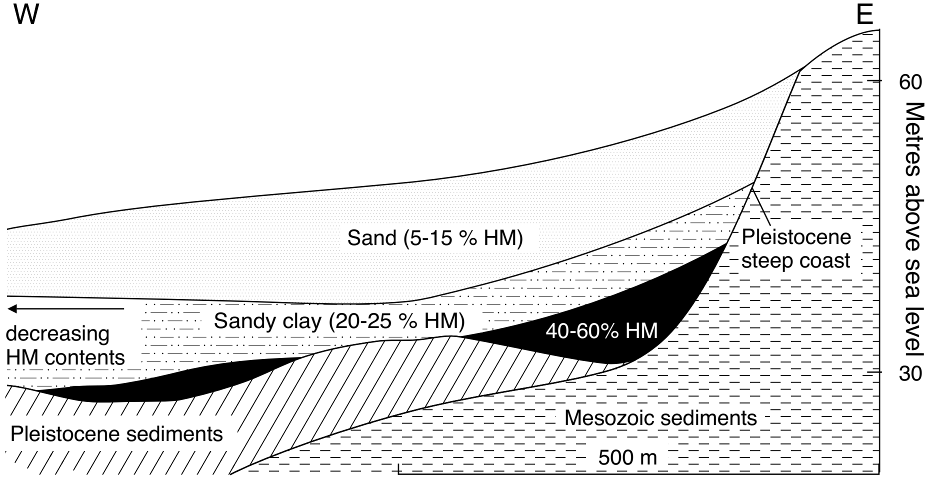

Figure 2.38 Geological section of Pleistocene coastal placer deposits near Yoganup, Western Australia (modified after Welch *et al.* 1975). The heavy mineral (HM) fraction consists of max. 80% ilmenite and leucoxene, 12% zircon, and minor parts of rutile, monazite and xenotime. Near the surface, ilmenite is altered to leucoxene but this decreases with increasing depth. Black = High-grade black sand.

Coastal placers are explored by grid drilling, which is carried out in prospective areas defined by geological modelling. Reverse circulation or sonic drilling is used for precise sampling. With increasing refinement of the grid, the geology of coastal sediments and the distribution of heavy minerals are better understood. Important factors of feasibility, apart from HM content, include the thickness of the overburden, a minimal induration of the ore bed, low content of deleterious "slime" and clay, the grain size distribution, surface characteristics of HM minerals, the mineral composition and the degree of ilmenite oxidation (Jones 2009). Content of uranium and thorium traces in zircon may result in the need to control risks of radioactivity. Many coastal landscapes constitute a precious environment and are valued by society. In spite of efforts to preserve biota and to re-establish nature after mining, the social licence for extraction of heavy minerals may be unattainable in some areas. One way of avoiding this conflict of interests is exploring older inland seas (e.g. the Murray and Eucla basins, Australia). Rehabilitation of heavy mineral placer mines is much less complicated compared to metal sulphide or coal pits (Jones 2009).

Annual world production of zircon amounted to ~1.3 Mt (2008) and 1.2 Mt in 2009. Australia, South Africa and China are major sources, producing from placers. Identified zirconium resources are very large (~56 Mt: USGS 2010). Nevertheless, the availability of zirconium is decreasing and prices are rising. One reason for this situation is the dependence of by-product zirconium production on titanium placer mining.

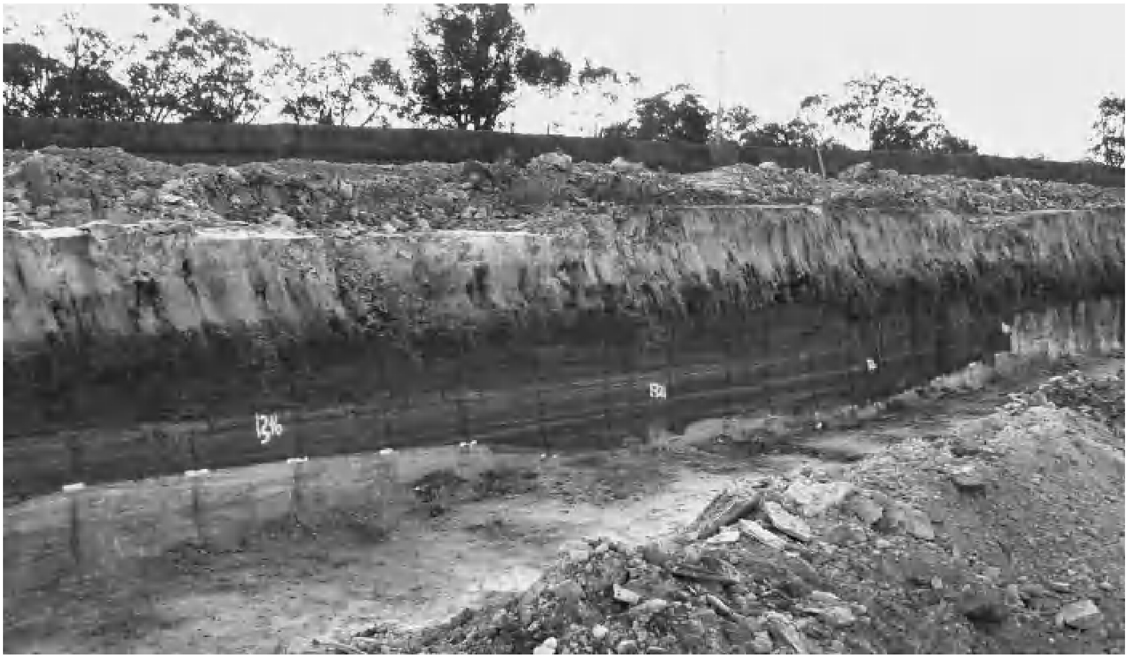

Figure 2.39 (Plate 2.39) Bondi East heavy mineral deposit near the southeastern margin of the Murray Basin in Victoria, Australia, looking north at an active mine face, which has been cleaned up for channel sampling and detailed mapping. Courtesy David Whitworth (Iluka Resources). Barren overburden is removed; upper low-grade ore (ca. 10% HM) is white sand with 30% clay. Note the near-vertical incision of the high grade ilmenite-zircon-rutile sand (dark, 50–70% HM) at the right of the image. The footwall consists of barren massive silty sand (white). Patchy oxidation is ubiquitous.

2.5.7 Titanium

Common Ore Minerals:

		Wt. % TiO_2	*Density (g/cm^3)*
Rutile	TiO_2	>95	4.2
Anatase	TiO_2	>95	3.8–3.9
Ilmenite	$FeTiO_3$	52 (35–70)	4.5–5.0

With an average crustal abundance of 0.5% Ti (range 0.24–0.96%), or 0.8% TiO_2, titanium takes the ninth place of the most common elements in the Earth's crust. It occurs in ~50 different minerals, but only the above listed are of technical importance. Possibly, perovskite $CaTiO_3$ found in carbonatites and nepheline syenites may one day be considered as an ore.

Ilmenite is characterized by limited substitution of Cr, V, Mg and Mn, rarely Nb and Ta. Elevated contents of colouring metals such as iron reduce its quality, as do traces of uranium and thorium. The wide range of TiO_2 content is due to intergrowth of primary ilmenite with haematite, because at >950 °C a complete solid solution exists between Fe_2O_3 and $FeTiO_3$. Consequently, ilmenite concentrates of orthomagmatic ore contain only 35–40% TiO_2. Titaniferous magnetite with even lower TiO_2 content is of little use except in some cases as an ore of vanadium (cf. Section 2.1.8 "Vanadium"). Ilmenites of secondary deposits with a history of weathering, erosion and sedimentation reach a maximum of 70% TiO_2 by leaching of iron. *In-situ* weathering of magnetic placer ilmenite transforms it into non-magnetic leucoxene, a fine-grained, amorphous substance or a "mineral" with a structure like rutile or anatase with 70–90% TiO_2 (Mücke & Chaudhuri 1991). Primary rutile is only known as an accessory mineral in rocks; enriched hard-rock occurrences are still subeconomic. Its high resistance to weathering and transport, however, leads to concentration in placers.

Lowest exploitable grades in placers are ~1% for ilmenite and 0.1% for rutile. Extraction from hard rock ore dictates grades ten times as high (the Titania mine at Tellnes in Norway, for example, works with ilmenite ore of 18% TiO_2). Ilmenite and leucoxene satisfy >90% of the world's demand for titanium minerals. Traded concentrates should be free of radioactive trace minerals, such as monazite (Th) and xenotime (U).

Roughly 95% of titanium production is used as white and highly opaque TiO_2 pigment that substitutes for lead oxides because it is not toxic. The pigment is mainly used for manufacturing enamels, paint, paper and plastics. Other applications are in the chemical industry and as a UV-blocker for skin protection. As there is not enough natural rutile available to satisfy demand, ilmenite is used for the production of "synthetic rutile". Rutile's main use is as a fluxing agent in welding rods. Titanium dioxide is produced by dissolving rutile, ilmenite and leucoxene in sulphuric acid (the sulphate process). Iron compounds are removed and the remaining solution is hydrolized, precipitating hydrous titanium dioxide, which is washed and calcined. The sulphate process accommodates lower grade ilmenite, but the resulting high Fe and low pH waste water is problematic. Therefore, low TiO_2 ilmenite is less attractive and the alternative chloride process is preferred, although it requires higher grade ilmenite (>60%) and rutile.

Titanium metal is produced from titanium tetrachloride ($TiCl_4$), which is prepared by chlorinating natural or synthetic rutile in the presence of carbon. $TiCl_4$ is reacted with molten magnesium (or with sodium) at ~850 °C, resulting in formation of titanium sponge that is further processed to market-grade metal. Titanium is a non-toxic, soft, ductile, lightweight metal (density 4.5 g/cm^3, melting point 1668 °C, boiling point 3260 °C), with excellent corrosion resistance and a higher strength and flexibility than steel. However, its production is expensive, resulting in high prices (~200 times the price of aluminium). Therefore, use of pure titanium and different alloys concentrates on the aerospace industry, in desalination and petrochemical plants, cars, cameras, laptops, medical devices and sporting equipment. In 2008, world production of titanium sponge amounted to ~170,000 tonnes (USGS 2009).

Geochemistry

In many rocks, titanium is one of the major elements. Highest content occurs in mafic (0.9–2.7%

TiO_2) and alkalic magmatic rocks (0.1–3.3%), and in eclogites (1.0–6.0%). Titanium is a tetravalent lithophile high field strength (HFS) element. Because only oxide minerals of titanium can be economically processed, geological systems that favour the formation of oxides are required, which is realized in certain magmas and by high-grade metamorphism. Metamorphism does not affect Ti-concentrations but releases titanium from titanite $CaTiO(SiO_4)$, titaniferous biotite and hornblende at amphibolite-granulite and blueschist-eclogite transitions. Titanium recrystallizes as an oxide, mostly rutile (Bucher & Frey 1994). This is the reason why granulites and eclogites are optimal source rocks for titanium oxide placer deposits. Ferrogabbroic eclogites may reach TiO_2 content of >6%, almost exclusively in the form of rutile. Such rock bodies (e.g. Piampaludo, Ligurian Alps; Sunnfjord, Norway; Shubino, Urals) are important potential resources of titanium (Force 1991).

> Titanium is geochemically rather immobile and a reference element for many petrogenetic investigations (Pearce *et al.* 1984). An illuminating example is the alteration halos of copper porphyry ore deposits. In unaltered porphyry, titanium occurs in titanite, biotite and hornblende. All three minerals are destroyed during hydrothermal alteration and fine-grained rutile is present in the new paragenesis. The original TiO_2- contents of the rock remain unchanged.

Similar to zirconium and hafnium, titanium displays a very moderate to low mobility in surface environments. It constitutes no environmental or health hazard. Currently, titanium metal is the most common material used for medical implants in the human body.

Titanium ore deposit types

Titanium deposits include primary, orthomagmatic concentrations in intrusive rocks of anorthosite-ferrodiorite, tholeiitic and alkaline basalt association, but foremost secondary alluvial and coastal placers. Orthomagmatic and titanium placer concentrations may be upgraded by supergene residual enrichment. High-grade metamorphic rocks constitute potential hard-rock rutile sources.

Orthomagmatic titanium deposits

Igneous hosts of orthomagmatic titanium deposits are Proterozoic massif anorthosite complexes and tholeiitic layered intrusions; nelsonitic melts occur in association with alkali basalts (Clark & Kontak 2004). During cooling, titanium and iron are concentrated in an immiscible oxide melt that accumulates by gravitation at the base of the magma chamber where massive layers of ilmenite with magnetite or haematite accumulate. In some cases, the melt filled interstitial spaces of cumulates or intruded footwall rocks forming dykes. Massive nelsonitic ore consists of ilmenite, rutile, magnetite and apatite. Phosphorous reduces the solidus temperature of the liquid. Examples of primary titanium ore deposits include the giant Lac Tio (Allard Lake) and other mines in Canada, Tahawus (Sanford Lake) in the Adirondack Mountaions, USA, Otanmäki in Finland and Tellnes in Norway (Duchesne 1999; cf. "Iron"):

> Tellnes in southwestern Norway produces ~1 Mt/a ilmenite concentrate with a grade of 44% TiO_2 from banded ilmenite norite intruded into the centre of an anorthosite province (ca. 920 Ma). Reserves amount to ~57 Mt TiO_2. The sill crystallized *in situ* to a cumulate facies with an average of 40% ilmenite concentration. The ilmenite displays haematite exsolutions and a Cr-content, which decreases upwards as magnetite increases (Blundell *et al.* 2005, Duchesne 1999).

Similar to Tellnes, not all deposits were formed by liquid unmixing of an ore melt. At the Koivusaarenneva mine in Finland, solid-phase ilmenite was gravitatively enriched from silicate liquid (Kärkkäinen & Bornhorst 2003). In this deposit, a gabbro sill contains several strata with 15% ilmenite and 6% vanadium-magnetite, which segregated during lateral magma flow in the sill.

Primary titanium concentrations in akaline complexes occur preferentially with pyroxenite (e.g. jacupirangite consisting of titanian augite, magnetite and nepheline). Other common rocks in these complexes are nepheline monzo-syenites and a carbonatite core in the centre. The type locality for the name "ilmenite" is an alkaline complex in the Ilmen Mountains near Miask, Urals, Russia. The ore consists of ilmenite, magnetite and perovskite, with changeable amounts of rutile, brookite (a rutile polymorph), titanite $CaTiO(SiO_4)$, apatite, carbonates and silicates. High trace contents of Nb, Th and REE in several of these minerals are frequent but rather detrimental for use as a titanium ore. Lateritic leaching removes gangue and enriches titanium in the form of anatase. In Minas Gerais, Brazil hosts a province of Cretaceous ring complexes, some of which display supergene residual titanium mineralizations (e.g. Tapira carbonatite), while others have bauxite, uranium, REE and phosphate deposits.

Coastal placer deposits

Coastal placer deposits are the main economic source of titanium. Placers provide ~55% of world production and contain 45% of known resources. The quality of placer concentrates is superior to primary hard rock ore, because they consist essentially of ilmenite-leucoxene and rutile. Extraction and processing of unconsolidated beach sands is inexpensive and consequently, economically recoverable grades may be lower than the average crustal abundance of titanium. The formation of these placers is the product of a complex interaction of source area, weathering (climate), erosion, alluvial transport, marine dynamics, wind and the morphological evolution of the coast. Most large deposits date from the Quaternary and occur above and inland of today's coastlines, attesting to formation during former sea level high-stands of interglacial periods. Older deposits are more affected by supergene alteration. Youngest deposits are sections of Holocene beaches. Mining of titanium minerals below present sea level, concentrated at low-stands during glacial periods is uncommon (in contrast to cassiterite and diamond). Typically, coastal placer orebodies are sand beds with a thickness of 10 m, a width of 100–1000 m and a length of over 10 km. HM sands are well-rounded, equigranular and medium- to fine-grained. Both beach and dune sand may be mineralized.

Nearly all titanium placers comprise valueless heavy minerals such as magnetite, tourmaline, sphene and apatite, and others that may be profitable co- or by-products. The most important of these is zircon, occasionally monazite and silicates such as kyanite and garnet (Port Gregory, Western Australia). Combined valuable heavy mineral (VHM) contents are commonly in the range of 4–10 wt.%.

Australia is endowed with large titanium placers both on its eastern (Queensland, New South Wales, Victoria) and its western coast, especially south and north of Perth (Figure 2.38). The high chromium content of ilmenite in the eastern deposits reduces the value of concentrates considerably and rutile is the main product. In the west, chromium is at acceptable levels (<0.03%). Extraction of heavy minerals in Australia is now moving into interior Australia. In the Murray Basin, Pliocene (palaeo-) coastal barrier placers are estimated to contain over 50 Mt of rutile, ilmenite and zircon (Roy *et al*. 2000). The Douglas mine, for example, commenced operations in 2004, based on a resource of 45 Mt at 11.3% heavy minerals (Whitworth 2009). The Richards Bay deposit near Durban in South Africa is a broad belt of aeolian sand with ilmenite, monazite and some leucoxene. Ilmenite is mainly produced at Quilon in Kerala, India. Large coastal placer districts are mined or under investigation in China, Florida, USA, Sri Lanka, Thailand and Madagascar. In Canada, work is in progress to produce titanium minerals and zircon from oil sands in Northern Alberta. Note that in this case, the heavy minerals are not enriched, as these sands are not placers. The envisioned profit is constituted by the economy of scale, because of the giant mass of sand turned over by the oil industry (cf. Chapter 7.6 "Tar Sand").

Alluvial placers

Economically exploitable alluvial placers of titanium oxides are rare. One reason for this is the small volume of most alluvial placers, considering that favourable deposits should contain >1 Mt of recoverable titanium minerals. A second point is that alluvial placers more often contain unaltered ilmenite, resulting in low titanium content of concentrates. Exceptions include Gbangbama in Sierra Leone, where rutile is derived from a granulite source area and cassiterite placers in Malaysia, where by-product rutile is sourced from highly specialized felsic intrusions ("tin granites").

The world's titanium resources are very large. World production in 2009 was 5.2 Mt ilmenite and 530,000 t rutile (TiO_2 contained). Leading producers are Australia, South Africa, China and Canada (the latter sourced from hard rock mining). Worldwide search for new deposits is intensive, mainly targeting coastal placers (for notes on exploration refer to Section 2.5.6 "Zirconium and Hafnium"). Exploration, reserve estimation, extraction and rehabilitation of coastal placer deposits differ in several aspects from hard rock deposits (Jones 2009, Lee 2001). Increasingly, communities prefer non-mining uses of their coasts, which restricts accessability. It is assumed that because of this, primary titanium ore deposits will soon gain economic importance (e.g. the rutile-eclogites in the Norwegian Sunnfjord).

2.5.8 Rare Earth Elements (REE, Lanthanides)

Common Ore Minerals:

		Max. wt.% REE-oxide	*Density (g/cm³)*
Monazite	$(Ce,La,Y,Nd,Sm,Th)PO_4$	65	4.6–5.4
Bastnaesite	$(Ce,La,Y)CO_3(F,OH)$	75	4.9
Xenotime	$Y(HREE)PO_4$	61	4.8
Loparite	$(Ce,Th,Na,Ca)_2(Ti,Nb)_2O_6$	36	4.6–4.9

The lanthanide series of the rare earths group comprises 14 elements from lanthanum to ytterbium. Of the actinide series of the rare earths group, only uranium and thorium are economically significant (cf. "Uranium"). Valued REE include cerium (Ce), praseodymium (Pr), neodymium (Nd), samarium (Sm), europium (Eu), gadolinium (Gd), terbium (Tb) and dysprosium (Dy). Yttrium (Y), scandium (Sc) and thorium (Th) are not rare earths *sensu stricto*, but have physical and chemical properties, and uses that are similar to REE ("pseudolanthanides"). Based on relative atomic mass, the elements La to Sm are called light (cerium, or LREE) and Eu to Lu heavy (yttrium, or HREE).

There are ~250 minerals containing rare earths but only the four listed above are economically important. Although natural processes never separate individual REE, monazite and bastnaesite contain mainly LREE (La, Ce, Pr, Nd), whereas xenotime and loparite host significant HREE content (Möller *et al.* 1989).

Monazite is a common accessory mineral in intrusive, and amphibolite to granulite facies metamorphic rocks. Based on U-Th-Pb isotope systems, it serves as a useful geochronometer. Sourced from eroding land, the mineral is enriched in placers where it can be a co- or by-product of ilmenite, rutile, zircon, cassiterite and gold extraction. Monazite is singled out by its γ-radiation due to daughter nuclides of thorium, which makes radiation a convenient proxy for estimating REE content. The sources of xenotime are mainly granites and pegmatites, which host the mineral as a disseminated accessory. It is a minor component in alluvial tin placers and coastal mineral sands.

Bastnaesite is the major ore mineral of hard rock REE deposits. Mining grades are ~2–6% rare earth oxide (REO), the range being due to content of the more valuable REE. Orthomagmatic and magmatic-hydrothermal apatites of carbonatite and alkali complexes (cf. Chapter 3 "Phosphates") contain anomalous REE yet the concentrations are commonly sub-economic. Until 1998, 0.85% REO was recovered from apatite and loparite concentrate produced from nepheline syenite pegmatites of the Khibiny and Lovozero massifs, Kola Peninsula, northern Russia (cf. Section 2.5.9 "Niobium and Tantalum").

Uses of REE started more than 100 years ago with Welsbach mantles for coal gas lanterns made of 99% thorium dioxide and 1% cerium dioxide. Today, ~98% of consumption concerns what is called *mischmetall* (German for "mixed metal"), which is an alloy of unseparated REE in the proportion inherited from ore (usually cerium, lanthanum, neodymium and several minor REEs). It is used in steel-making, for producing petroleum-refining catalysts, for lighter flints and in magnesium metallurgy. The separation of individual REE is elaborate and costly. Enrichment of single elements to 60–90% allows more specialized uses such as colouring glass and ceramics, and the production of high-strength magnets (e.g. Nd-Fe-B, $SmCo_5$). Extremely pure (>99.99%) REE are required in small amounts only. Eu and Y, for example, are employed as phosphors in television and computer screens, neon tubes and X-ray equipment, and for some Laser machines. Other applications include superconductor technology, hydrogen storage and catalytic converters for automobiles. Toyota's Prius hybrid car reportedly contains >22 kg of REE in nickel-hydride batteries, braking systems, exhaust converters and electric motors. Chinese scientists report that traces of REE in fertilizer considerably improve agricultural harvests.

Geochemistry

All lanthanides have a similar geochemical behaviour, commonly occur in trivalent state and form stable compounds. Exceptions are europium that displays both trivalent and bivalent states, and cerium with an additional oxidation state of Ce^{4+}. Consequently, the distribution of europium and cerium in natural systems is a function of redox conditions, which control enrichment or depletion ("anomalies") relative to other lanthanides. Furthermore, geological processes can lead to fractionation between light and heavy REE caused by the difference in atomic mass and ionic radius. This allows improved understanding of earth processes. Anomalous REE-distribution is compared with C1 chondrites and shale composites (Gromet *et al.* 1984).

The combined average crustal abundance of lanthanides (including yttrium) is estimated at nearly 200 ppm (Clarke value), with cerium (66.4 ppm), lanthanum (34.6 ppm) and yttrium (31 ppm) being most abundant (Smith & Huyck 1999). In spite of their name, REE are several orders more abundant than gold, for example. Lanthanides are lithophile elements. In rocks, REE are mainly concentrated in accessory minerals (monazite, titanite, zircon, apatite) and occur as trace elements in amphibole, pyroxene, feldspar, garnet and mica. Differing ionic radii cause a tendency for enrichment of heavy REE in certain minerals (xenotime, garnet, zircon) and of light REE in monazite and bastnaesite. In hydrothermal systems light REE are more mobile than heavy REE. The mobility of the small, highly charged REE, Y and Zr ions, depends on the availability of intermediate and hard ligands such as chloride, fluoride, sulphate and carbonate. As these are common, considerable hydrothermal mobility is the result (Lottermoser 1992). Magmatic bodies that have segregated much fluid or interacted with passing fluids (e.g. tin granites) display a strong loss of LREE. High salinity and CO_2 content of fluids are crucial factors of REE mobilization, transport and REE ore formation.

Under oxidizing and acidic conditions on the Earth's surface, REE are mobile, similar to uranium (but note the near-immobility of thorium). At circum-neutral pH mobility is reduced and the presence of iron-rich particles effectively immobilizes REE. In reduced environments, REE are virtually immobile, as are uranium and thorium.

Rare earth ore deposit types

REE deposits occur in a number of genetic classes and types, but most deliver by-product REE only. Hard rock economic concentrations and pre-enriched REE as protore for supergene enrichment are primarily related to magmatic systems:

- orthomagmatic to pegmatitic magnetite-apatite with REE (associated with alkali complexes, e.g. Kola Peninsula; cf. Chapter 3 "Phosphates");
- pegmatites (REE accessory minerals recoverable with ore of tantalum and tin);
- skarn deposits, e.g. allanite $(Ce,Ca,Y)(Al,Fe)_3(SiO_4)_3(OH)$ of the former uranium mine Mary Kathleen in Queensland, Australia;
- orthomagmatic to magmatic-hydrothermal ore in carbonatite dykes and intrusions (Mountain Pass), and in associated veins;
- magmatic-hydrothermal, low-sulphur, iron oxide-copper-gold (IOCG) deposits, characterized by large masses of magnetite or haematite (e.g. Olympic Dam, cf. Section 2.2.1 "Copper");

- hydrothermal-metasomatic ore in dolomite-carbonatite (giant and singular Bayan Obo, North China, with the largest LREE reserves in the world);
- volcanogenic-hydrothermal fluorite-bastnaesite breccia and vein mineralization (Gallinas Mountains, New Mexico);
- residual lateritic REE concentrations developed in regolith on carbonatites (Mrima Hill Kenya; Araxá, Brazil; Mt Weld, Australia);
- residual enrichment in autochthonous saprolite above granite, referred to as "lateritic ion-adsorption clays", with valuable heavy REE in Jiangxi, South China;
- placers (mostly monazite as a by-product of titanium and zirconium extraction from coastal placers).

Magmatic-hydrothermal Bayan Obo (Baiyenabo) in Inner Mongolia, China, is both economically outstanding and genetically extremely complex. Total reserves comprise 1500 Mt of haematite and magnetite, 100 Mt with 6% $LREE_2O_3$ (monazite and bastnaesite), and 1 Mt with 0.13% Nb_2O_5. Country rocks are Mesoproterozoic slates, sandstones and quartzites. The origin of dolomite hosting the ores remains undecided as either sediment or carbonatite. Unquestioned carbonatite dykes intruded the suite at around 440 Ma. Fluid inclusions in ore and gangue minerals have elevated salinity and CO_2 contents. At formation pressures of 1 kbar, episodes of phase separation (boiling) are indicated. The fluids have characteristics that can be related to carbonatites and alkali complexes (Smith & Henderson 2000). However, the origin of this giant deposit remains disputed (Fan *et al.* 2004, Yang *et al.* 2008). It displays features of both (magmatic) carbonatite and (magmatic-hydrothermal) oxide-copper-gold (IOCG) deposits (Wu 2008).

An orthomagmatic monazite-apatite dyke crystallized from residual liquids of anorthositic magma at Steenkampskraal in Namaqualand, South Africa. From 1952 to 1963, the mine was an important producer of thorium and REE:

> Mining was based on a steeply dipping dyke with monazite ore in a volume of 350 × 200 × <4 m. Ore consisted of monazite, apatite, chalcopyrite and zircon, in places with magnetite, quartz, plagioclase and biotite. Host rocks are Mesoproterozoic intrusions of anorthosite, charnockite, hypersthenite and other rare igneous rocks (the Roodewal Suite) in a large granite gneiss batholith. Roodewal rocks and the monazite ore were intruded during a regional granulite facies metamorphic event. The tabular orebody may have been formed by unmixing of a residual anhydrous phosphorous melt from anorthositic liquid (Andreoli *et al.* 1994).

From 1965 to 1995, Mountain Pass in San Bernardino County, California was the world's largest source of LREE (Castor & Nason 2004). The mine is presently in a care-and-maintenance state and is planned to be back in production by 2012:

> Within an area of 10 × 2.5 km metamorphic rocks are intruded by a swarm of Mesoproterozoic (1.4 Ga) ultrapotassic granites, syenites and shonkinites. Several bodies and dykes of carbonatite are syngenetic with this intrusive suite. One of the carbonatites encloses stockwork-like vein fields with a paragenesis of bastnaesite, parisite $(Ce,La)_2Ca(CO_3)_3F_2$, calcite, dolomite, siderite, barite and quartz. Exploited ore grades were 5–15% REO (99.5% LREE, mainly lanthanum, neodymium and praseodymium). Reserves are estimated at >20 Mt with 8.9% REO based on a 5% cut-off grade (Castor 2008).

Breccia pipes and veins in the Gallinas Mountains (New Mexico) developed in Permian sediments in connection with Tertiary alkalic rhyolite and trachyte laccoliths. Although formerly several iron ore and fluorite mines were worked and REE-mineralized ore is present, resources are too limited for extraction under present market conditions:

> Vein fill and matrix of breccias are dominated by fluorite, with smaller amounts of bastnaesite, quartz, barite, pyrite, magnetite and haematite. Host rocks near mineralization are fenitized. REE and fluorine are probably derived from degassing subvolcanic magma bodies. In the magmatic-hydrothermal fluids, REE were complexed with fluorine. Mixing with Ca-bearing formation waters caused precipitation of fluorite and consequently of REE, and formation of bastnaesite (Williams-Jones *et al.* 2000).

Residual enrichment blankets

Residual enrichment blankets above granites of mixed REE (mainly yttrium, samarium, europium and gadolinium) in autochthonous saprolite are exploited in Jiangxi, South China. Source rocks are Mesozoic granites with bulk REE contents between 300 and 400 ppm. Primary carriers of REE in the granites are zircon, apatite and allanite. However, REE fluorocarbonates were found on grain boundaries and in microscopic fissures of silicate minerals, and replacing altered biotite. These observations are thought to present evidence of deuteric (post-solidus) magmatic-hydrothermal alteration, which produced the easily soluble REE fluorocarbonates accessible for supergene leaching and enrichment (Ishihara *et al.* 2008).

Residual lateritic regoliths

Residual lateritic regoliths above carbonatite are at present rather niobium (e.g. Araxá, Brazil) and/or apatite deposits. Most display enrichment of REE, but recovery preoccupied metallurgists and scientists for many decades. Although some production from lateritic ore is reported, a general breakthrough has not happened:

> A new effort is under way at Mt Weld in Western Australia. Mt Weld reserves are reported as 7.7 Mt at 12% REO + Y, including a high grade part of 1.2 Mt with 16% rare earth oxides. The estimate is calculated using a minimum content (cut-off grade) of 4% REO *in situ*. The high grades are due to supergene enrichment (Figure 2.40, Lottermoser 1995). The main carrier of REE content is secondary Th-depleted monazite. The main product of the mine will be phosphate with by-products Nb, Ta, Y (3.1%) and HREE (3.9% of total REE). A first batch of ~800,000 t of ore grading 15.4% REO was mined in 2008.

Coastal placer characteristics are presented in Chapter 1.3 "Sedimentary Ore Formation Systems" and in Section 2.5.6 "Zirconium and Hafnium" and Section 2.5.7 "Titanium". Note that for >15 years, the thorium content of monazite from most operations precluded its use as a rare earth feedstock.

Main producer countries of REE are China, India and Brazil. Annual world production amounts to ~124,000 t REE-oxides (USGS 2010). Largest reserves and resources occur in China, which dominates world markets of REE with nearly 97% of world production. Many potential deposits of mainly LREE are known elsewhere, however. Demand for, and consumption of different rare earths vary considerably. Generally, light REE are in oversupply, whereas demand for Eu and several scarce REE (Nd, Dy and Tb) increases. Recoverable contents, price and geopolitics of these latter explain the curious situation that exploration and new developments are undertaken in spite of giant REE resources. Carbonatites are an easy target for magnetic, gravity and radiometric methods. Testing for ore is mainly based on shallow drilling.

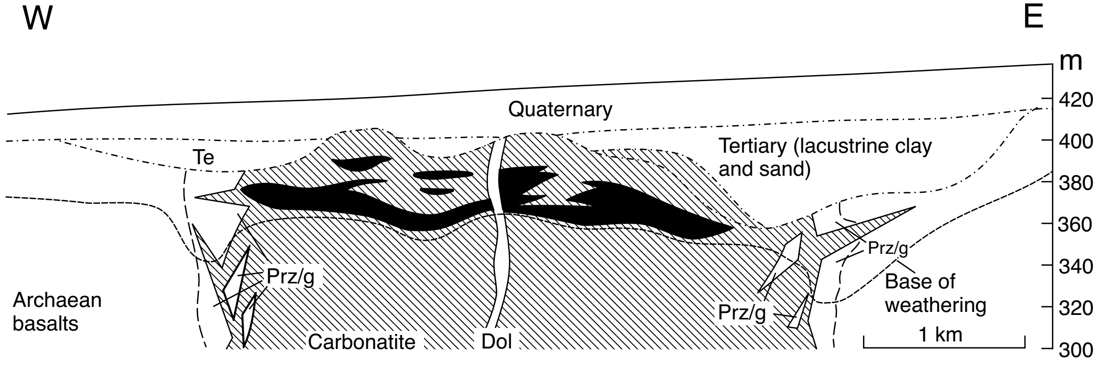

Figure 2.40 Section of the residual phosphate-niobium-tantalum-yttrium-rare earth deposit at Mt Weld in Western Australia (modified after Duncan & Willet 1990). Metal-rich phosphates (black) occur within a deep lateritic weathering profile of Proterozoic carbonatite. Near the intrusive contact, basaltic country rocks are altered to phlogopite (Prz/g). Dol – a dolerite dyke.

2.5.9 Niobium and Tantalum

Common Ore Minerals:			*Density (g/cm^3)*
Niobite	$(Fe,Mn)(Nb>Ta)_2O_6$	31–79% Nb_2O_5	min. 5.2
Tantalite	$(Fe,Mn)(Ta>Nb)_2O_6$	52 to 86% Ta_2O_5	max. 7.9
Pyrochlore	$(Na,Ca)_2(Nb,Ti,Ta)_2O_6(O,OH,F)$	56–73% $(Nb,Ta)_2O_5$ +3–6% LREE-oxides	4.2–4.5
Microlite (tantalum-rich end member of the pyrochlore series)	$(Na,Ca)_2Ta_2O_6(O,OH,F)$	max. 80% Ta_2O_5	6.3
Wodginite	$MnSnTa_2O_6$	max. 70% Ta_2O_5	7.3

Note that pure niobite and tantalite are unknown in nature; they are theoretical end members of a solid solution series called columbite. Tantalite is defined by an Nb/Ta atomic ratio of <1. "Columbite" is occasionally used to designate Nb-rich minerals of the columbite group, because in America until 1949, the element niobium was called "columbium". Before discovery of pyrochlore in carbonatites of Brazil and Canada, columbite was the main source for both tantalum and niobium. The chemical composition of columbites is commonly presented in the "columbite quadrilateral" that depicts changes in the Fe/Mn and Nb/Ta ratios (Beurlen *et al.* 2008). With increasing fractionation of pegmatites, columbites are enriched in tantalum and manganese. Columbites contain traces of Mg, Bi, Sn, W, Ti, Sc, REE, Th and U. In concentrates, the latter may enforce radiation protection measures. Inclusions of columbite and other Ta-minerals in cassiterite of pegmatite deposits are frequent. As columbite is initially free of lead and because of its resistance to later alterations, the mineral is useful for U-Pb dating of granites and pegmatites (Romer *et al.* 2007). Scandium in columbite and related minerals may reach >6 wt.% (Kempe & Wolf 2005):

Scandium (density 3.0 g/cm³, melting point 1539 °C) is a typical dispersed element. Its Clarke value (25 ppm) is higher than that of tungsten and lead (1.2 and 13 ppm, respectively) but concentrations and minerals of this element are extremely rare. Together with Y it is one of the "pseudolanthanides" (cf. Section 2.5.8 "Rare Earth Elements"). In igneous rocks, Sc^{3+} is positively correlated with Fe^{2+}. Because scandium is preferentially enriched in clinopyroxene, amphibole and ilmenite, high-silica magmatic rocks have low contents (3–5 ppm). Scandium may be enriched to economically significant by-product grades in bauxite, nickel laterite, carbonatites, phosphorites, Ti-placers, Ta-Nb ore, wolframite, cassiterite, uranium ore and in zircon (Wood & Samson 2005, Kempe & Wolf 2005, Wiesheu *et al.* 1997). Among other applications, scandium is useful as a grain refiner in aluminium alloys, and in solid oxide fuel cells.

Pyrochlore is chemically variable; for example, calcium can by substituted by Ba, LREE and U. Therefore, pyrochlore tends to be radioactive and metamict, i.e. its crystal structure is damaged by radiation. Often, its paragenesis includes minerals of Ti, U, Th and REE. Bariopyrochlore is the main ore mineral at Araxá. Formerly in Russia, niobium was produced from loparite concentrates derived from nepheline syenites of the Kola Peninsula. Loparite is a perowskite ($CaTiO_3$) containing Nb and Ce. Compared with pyrochlore, however, loparite is economically not competitive. Exploitable niobium ores have minimal grades of ~0.3%, although at Araxá the ore contains 2.5% Nb_2O_5. Tantalum ore is extracted at cut-off grades of ~0.03% Ta_2O_5, generally as a co-product of cassiterite and other minerals. Because of easy overgrinding, recovery of columbite by crushing and milling hard-rock ore is often as low as 50%.

Table 2.2 Properties of tantalum and niobium metal

	Density (g/cm^3)	Melting Point	Boiling Point
Tantalum	16.7	2996 °C	5429 °C
Niobium	8.57	2477 °C	4927 °C

Tantalum metal is grey, heavy and very hard, but malleable and ductile. It has a high melting point exceeded only by tungsten and rhenium (Table 2.2). Tantalum alloys with other elements display great strength, good ductility and high melting points. Niobium is mainly noted for its enhancement of strength in alloys.

Most niobium is consumed for production of micro-alloyed steel (with ~0.03% Nb) used for high-pressure pipeline tubes, offshore petroleum drilling and exploitation platforms, and automobiles. Nickel-free stainless steels contain 0.5 and superalloys ca. 5% niobium (e.g. heat-resistant equipment, jet engines). Niobium-titanium (-zirconium) alloys are materials suitable for supraconducting magnets. Some niobium, but 65% of tantalum supply is destined for the electronic sector. The remainder of tantalum production serves in manufacturing cutting tools (tantalum carbide), high-temperature alloys (e.g. turbines of gas-fired power stations) and extremely corrosion-resistant equipment of the chemical industry. There are also medical applications (e.g. implants) based on tantalum's total inertness to body fluids. Most electronic-grade tantalum metal is used as a capacitor core, together with some Ta-pentoxide as dielectric barrier. Tantalum is essential for portable electronic devices such as mobile phones, laptop computers, digital cameras and navigation systems in cars and aeroplanes.

Geochemistry

The geochemical behaviour of niobium and tantalum in crustal processes is nearly identical. Both are incompatible and lithophile high-field-strength elements (HFSE). With a crustal abundance of 20 ppm, niobium is more common than tantalum (~2 ppm). Both elements are enriched in highly differentiated granites, in alkali granites and syenites, in carbonatites and in rare-metal pegmatites. Niobium outweighs tantalum in carbonatites and syenites, whereas the latter prevails in granites and pegmatites (Figure 1.18). Columbite saturation in F- and Li-rich granitic melt at 600 °C is reached at 2000–4000 ppm Ta+Nb. In hydrothermal systems, niobium and tantalum are extremely immobile (Linnen 1998). Therefore, columbites crystallize from melts and not from hydrothermal fluids (Lichtervelde *et al.* 2007). Columbite is very resistant to surficial chemical alteration but is rapidly reduced to fines by alluvial transport. Accordingly, only residual and proximal eluvial/alluvial placers are preserved.

Niobium and tantalum ore deposit types

- Nb > Ta: Lateritic regolith (residual supergene enrichment blankets) above carbonatite intrusions (Araxá, Brazil, potentially Mt Weld, Australia);
- Nb > Ta: Hydrous schlieren of hard rock carbonatite or nepheline syenite with magmatic pyrochlore (Araxá, Brazil; Niobec, Canada);
- Ta > Nb: Rare-element granites ("tantalum granite") with tantalum-rich columbite and cassiterite (Yichun, South China: Yin *et al.* 1995; Figure 1.15; potential future mines include Ghurayyah in Saudi Arabia and Abu Dabbab in Egypt)
- Ta > Nb: Rare-element pegmatites of the Li-Cs-Ta type with tantalum-rich columbite and cassiterite (e.g. Wodgina and Greenbushes in Australia: cf. Section 2.5.10 "Lithium", Figure 2.41)
- Ta > Nb: Tin placers (Malaysia, Nigeria, Central Africa).

Alkali complexes

Alkali complexes with carbonatites and nepheline syenites occur along continental rifts or in zones of extensional crustal thinning. However, the primary hard and low-grade rocks are rarely mined. More than 90% of the mines extract residual supergene enrichment blankets. At Araxá in Minas Gerais, Brazil, unweathered carbonatite contains only ~1.5% Nb_2O_5 compared to regolith ore with 2.5% Nb_2O_5. The complex has a diameter

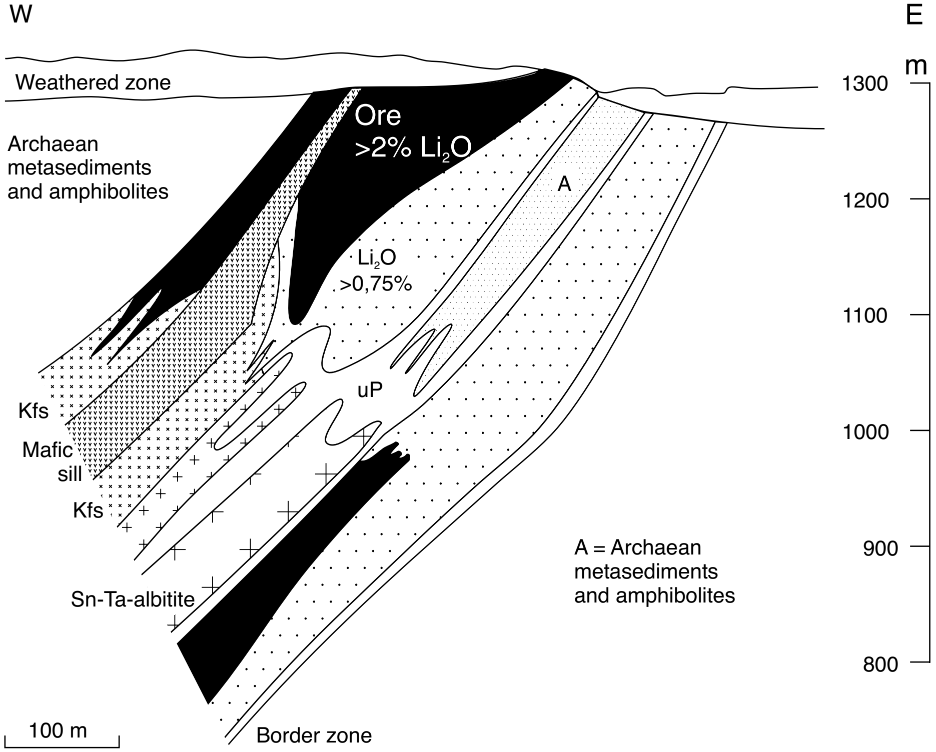
W
E
m
Weathered zone
Ore
>2% Li_2O
Archaean
metasediments
and amphibolites
A
Li_2O
>0,75%
Kfs
Mafic
sill
Kfs
uP
Sn-Ta-albitite
A = Archaean
metasediments
and amphibolites
1300
1200
1100
1000
900
800
100 m
Border zone

Figure 2.41 Cross-section of the Archaean Greenbushes Sn-Ta-Li pegmatite in Western Australia (after Hatcher & Clynick 1990). Note the complex and irregular internal zonation. uP is undifferentiated pegmatite. Part of the weathered zone (regolith) contains high-grade kaolinite. The underground mine was closed in 2006.

of ~5 km. Weathering reaches to a depth of 240 m. Reserves and resources amount to ~450 Mt.

Tantalum contents improve the viability of such deposits, whereas elevated concentrations of radioactive elements are detrimental. Because of commonly high phophorous (±magnetite and phlogopite) content in the protore (the unaltered carbonatites), the supergene ores are phosphate-rich and rather constitute phosphate ± REE deposits like Mt Weld, with estimated resources of 273 Mt at 0.9% Nb_2O_5 containing 145 Mt of Ta_2O_5 ore at 0.034% (cf. Section 2.5.8 "Rare Earth Elements", Figure 2.40). Recovery of Nb and Ta from the supergene ore at Mt Weld is expected to comprise gravity and magnetic separation, flotation, caustic and acid leaching (Aral & Bruckard 2008). The origin of the giant REE-Nb-Fe deposit Bayan Obo in Northern China remains disputed (Fan *et al.* 2004).

Tantalum granites and pegmatites

Tantalum granites and pegmatites are typically derived from highly fractionated, hydrous, residual melt batches of felsic magma bodies. Similar to lithium, tantalum is enriched in extremely fractionated felsic magmas at <0.05% of the original volume (Evensen & London 2002). The resulting rocks are marked by magmatic albite, often grading into monomineralic albitite (Figure 2.41). Post-solidification metasomatic-hydrothermal albitization is also possible (Schwartz 1992). In a scientific deep continental drilling programme, the Late Palaeozoic lithium-tantalum-tin granite of Beauvoir in the French Massif Central was intensively investigated. Results showed that only magmatic processes including fractionation contributed to metal enrichment (Figure 1.18), and hydrothermal metasomatism could be excluded (Raimbault *et al.* 1995). However, Beauvoir is a kaolin mine with minor by-production of cassiterite (800 g/t Sn) and columbite (190 g/t Ta plus 120 g/t Nb).

The Abu Dabbab area in Egypt is part of the Neoproterozoic basement east of the River Nile. In this province, the youngest (and smallest) intrusive members of a suite of post-tectonic granites are either mineralized or associated with tin and tungsten pegmatites, and quartz vein deposits:

> Abu Dabbab is a small conical mountain (Figure/Plate 2.18) built of the apical part of a granite cupola. The exposed rock is fine-grained leucogranite consisting mainly of albite and some microcline, quartz and muscovite. Ore minerals are disseminated in the uppermost 130 m of the granite beneath the roof. The paragenesis comprises Ta-rich columbite, cassiterite, pyrochlore, monazite, rutile, zircon, magnetite, galena and sphalerite. Total resources are estimated at 40 Mt at 252 ppm Ta_2O_5, 116 ppm Nb_2O_5 and 0.01% Sn. A bankable feasibility study proposed to produce mainly Ta_2O_5, cassiterite and ceramic-grade feldspar. Nearby prospects at Nuweibi in Egypt are comparable (Helba *et al.* 1997). Ghurayyah in Saudi Arabia is thought to be the world's largest potential Ta-(Zr) deposit (385 Mt of ore containing 94,000 t Ta_2O_5).

Tantalum pegmatites are not rare, with deposits known in many countries (Canada, Brazil, Ethiopia, Australia: Figure 1.20 and Figure 2.41). The Kenticha deposit in Ethiopia is a highly fractionated subhorizontal Li-Cs-Ta pegmatite sheet with a thickness approaching 100 m, which is related to Late Neoproterozoic I-type granites. Exploitable tantalum grades occur in its upper zone characterized by spodumene and high concentrations of Rb, Cs and Ga (Küster *et al.* 2009). Numerous, relatively small deposits of this type are common in Rwanda, Burundi and Eastern Congo. Swarms of pegmatites form districts (e.g. Gatumba in Rwanda: Figure 2.42). The giant subhorizontal pegmatite sheet at Manono (D.R. Congo) resembles the Kenticha and Bernic Lake (Canada) pegmatites. Central African tin-tantalum pegmatites are associated with late-tectonic, Early Neoproterozoic tin granites of the Kibara orogen, which are related to the final assembly of Supercontinent Rodinia. Varlamoff (1972) discerned lithium-rich internally zoned pegmatites with by-product beryl

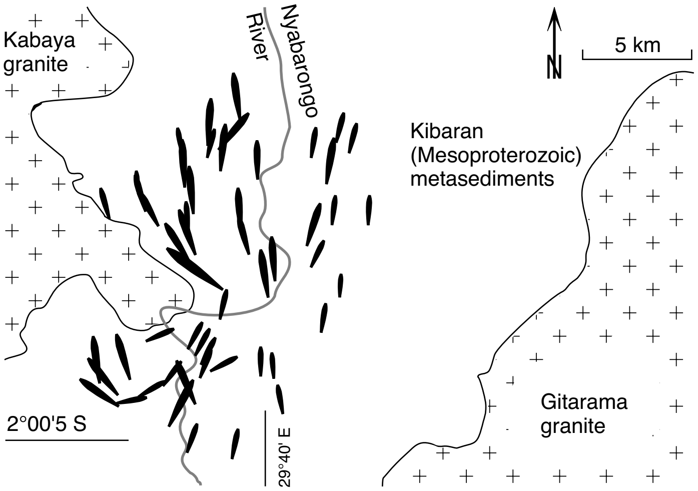

Figure 2.42 Sketch map of the Kibaran (ca. 950 Ma) pegmatite dyke swarm in the Gatumba tin-tantalum mining district, Rwanda. Near Nyabarongo River, Kabaya granite attains the character of a tin granite. From 1928 to 1985, the district produced about 18,000 t of cassiterite and 2000 t of columbite concentrate, from regolith ore of an average combined grade at 0.5 kg/m^3.

and tantalum plus tin and unzoned albite-rich tin-tantalum pegmatites. The latter contain the ore minerals columbo-tantalite ("coltan"), cassiterite, spodumen, some lepidolite, beryl and muscovite (e.g. at Gatumba). In the recent past in Central Africa, mining was artisanal and geared to high-price periods. Earlier semi-industrial hydraulic mining was limited to near-surface zones of supergene alteration with soft-rock ore. Unaltered hard-rock ore was hardly ever exploited.

Tantalum-niobium placers are commonly derived from pegmatites and occur in their immediate neighbourhood. The main resource is cassiterite with columbite as a by-product. Tantalum of tin placers in Malaysia and Thailand takes the form of strüverite inclusions in cassiterite. Strüverite is a tantalum-bearing rutile (Fe,Mn, Ti)(Ta,Nb)$_2$O$_6$). Tantalum occurring in this context is stripped from slags of tin smelters.

The world's niobium reserves are large, with >98% located in Brazil. The world's primary niobium production of 63,000 t niobium contained in concentrate (2008; 62,000 in 2009) is dominated by Brazil (92%, mainly from Araxá mine), followed by Canada. The world's annual primary tantalum production is near 800 t tantalum contained in concentrate (USGS 2010); Australia (50%) and Brazil (15%) were the largest producers. Tantalum reserves in the ground are largest in Brazil, closely followed by Australia. Supply and consumption of tantalum are occasionally out of balance, as demonstrated by Boeing delaying production of its new 787 Dreamliner aircraft in 2007 because of a tantalum shortage. Very high tantalum metal prices in the period 1999–2000 incited a wave of tantalum exploration that resulted in the discovery of many significant prospects. At the same time, previously known tantalum granites were explored in detail. In the future, a number of new hard-rock mines may produce from these sources. Exploration for niobium and tantalum is based on alluvial heavy mineral and geochemical surveys of rocks, soil and sediments (Sweetapple 2000). Because of large variations within single pegmatites, columbite chemistry appears to be of little use for tantalum prospecting (Beurlen *et al.* 2008).

2.5.10 Lithium

Common Ore Minerals:

		Wt. % Li_2O	*Density (g/cm^3)*
Amblygonite	$(Li,Na)Al[(F,OH)\|PO_4]$	10	3–3.1
Lepidolite	$K_2Li_4Al_2[(F,OH)_2\|Si_4O_{10}]_2$	5	2.9
Petalite	$LiAlSi_4O_{10}$	5	2.4
Spodumene	$LiAl[Si_2O_6]$	8	3.2
Zinnwaldite	$K(Li,Fe,Al)_3(F,OH)_2$ $(AlSi_3O_{10})$	5	2.9–3.1

Lithium contents of ore minerals are commonly smaller than listed because of substitution of Li^+ by other elements. Spodumene is formed at higher pressures than petalite. Lepidolite and zinnwaldite are potential sources for the rare metal rubidium (crustal abundance 120 ppm, density 1.532 g/cm^3, melting point 38.9 °C). The Rb-Sr dating method is based on the radioactive isotope ^{87}Rb (half-life $4.75 \cdot 10^{10}$ years). Rubidium is used for manufacturing catalysers, atomic clocks for GPS, solid-state lasers and luminescent materials. Yearly traded mass is in the kg range:

> Lithium minerals may be associated with pollucite $CsAlSi_2O_6.H_2O$, which is the main carrier of **caesium** (crustal abundance 3 ppm, density 1.892 g/cm^3, melting point 28.64 °C), as in the Bernic Lake rare metal pegmatite (Tanco mine, Manitoba), which contains 300,000 t pollucite with an average Cs_2O content of 24% (USGS 2010). Other sources include caesium beryl exploited from Li-rich pegmatites (Figure 1.20) and lithium brines. Caesium is part of X-ray tubes, atomic clocks, scintillometers, magnetometers and special glasses. Most of it is processed into caesium formate (CsOOH) brine, which is non-toxic and displays a high density (2.3 g/cm^3) making it a useful ingredient of high-pressure and high-temperature drilling fluids (e.g. ultra-deep holes in hydrocarbon exploration).

Exploitable hard rock lithium ore contains >1% Li_2O (3.5–4.5% at Greenbushes). However, most mines co-produce metallic ores (tantalum, tin) and minerals (lithium minerals, feldspar, quartz).

Accordingly, economic comparison of different deposits can hardly ever be reduced to lithium grades (Garrett 2004). Because of high processing costs, lithium minerals (mainly spodumene and petalite) are rarely used for the production of Li-metal and chemicals, but are preferred as fluxing agents for manufacturing heat-resistant glass, pyroceramics and enamels. In these applications, very low impurities of Fe, Mn, Ti and Cr are crucial.

Lithium carbonate and chloride extracted from natural brines are converted to lithium fluoride for aluminium reduction plants. A smaller share is consumed for production of lithium metal and chemicals. With a density of 0.53 g/cm^3, lithium is the lightest metal of all (melting point at 180.5 °C, boiling point 1336 °C) but is too reactive for transport and use. Alloys with aluminium are employed in the aerospace industry. Chemical applications include lubricants (grease), pharmaceuticals, rechargeable and non-rechargeable lithium batteries, which have higher energy density and lighter weight compared to NiCd and NiMH. Forthcoming electric vehicles mainly depend on Li-ion batteries. In the nuclear industry, lithium is employed for the production of tritium, which is required for thermonuclear fusion reactors and for nuclear weapons. In nuclear power plants, lithium serves as a neutron absorber and heat exchanger.

Geochemistry

Lithium is an extremly lithophile element with a small atomic and ionic radius. Its crustal abundance is 30 ppm (range 18–65; Smith & Huyck 1999), basalts contain an average of 5 and granites 20 ppm. Lithium is enriched in highly differentiated granites and pegmatites, and forms ore deposits together with tin, tantalum and beryllium. All three rare alkali metals lithium, rubidium and caesium are geochemically closely related to the abundant potassium (2.6% in the crust). Like nearly all alkali elements, lithium is soluble in surface waters as a mobile cation. This results in elevated trace concentrations of lithium in pelites, formation and oil-field waters (e.g. 100–700 ppm in Arkansas and Texas), and significantly, in terrestrial saline (playa) lakes. In the western USA, some volcanic tuffs altered to montmorillonite are enriched in lithium substituting for magnesium (hectorite). The stable lithium isotopes ^{6}Li and ^{7}Li are efficient tracers of hydrothermal processes in the crust (Chan *et al.* 2002).

Lithium is employed as a pharmaceutical for the treatment of psychic disorders. In nature, the element (as Cs and Rb) is harmless in all forms. WHO (2006) does not set a limit for lithium in drinking water.

Lithium ore deposit types

Lithium ore deposits of economic significance are restricted to only two genetic classes:

- Rare element pegmatites with lithium minerals and commonly, with exploitable by-product contents of Sn, Ta (>Nb) and Be (e.g. Greenbushes, W.A.); the mines produce concentrates of lithium minerals;
- Lithium brines of playa lakes or pumped from subsurface aquifers (e.g. Salar de Atacama, Northern Chile; Salar de Uyuni, Bolivia); operations market lithium carbonate or chloride.

Large rare element pegmatites are exploited in Western Australia (Greenbushes), Canada (Tanco mine, Bernic Lake) and in Zimbabwe (Bikita). The giant Kibaran (ca. 900 Ma) Manono tin-tantalum pegmatite in Maniema Province, Congo, has an untested potential of lithium minerals (Figure/Plate 2.43):

> The Greenbushes pegmatite in Western Australia (Figure 2.41) was worked for tin (and tantalum) since 1888, mainly from weathered and alluvial sources. More recently, spodumene and kaolin were extracted. In the 1990s, a deep hard-rock open cut and a large underground operation were established which made Greenbushes one of the world's leading tantalum and spodumene mines. The pegmatite dykes are sourced from highly fractionated "tin granites", which intruded greenstone belt rocks at ~2800–3000 Ma, and are controlled by crustal-scale shear zones and more local structures (Sweetapple & Collins 2002, Sweetapple 2000, Partington *et al.* 1995). In 2010, Greenbushes' capacity comprised 600,000 t/y of ore feed up to 260,000 t/y of spodumene concentrate at 7.5% Li_2O.

Lithium brines can be exploited at much lower cost compared with hard rock minerals. Brine deposits occur in the western USA, Argentina, China (Quaidam salt basin and Tibet) and Chile. Vast potential deposits are known in Afghanistan, Bolivia and Peru. Bolivia's Salar de Uyuni (Figure/Plate 2.44) is thought to contain 50% of world lithium resources (USGS 2009). Generally, it is assumed that lithium in continental salt basins and salt lakes originates by meteoric leaching of young volcanic rocks (in Nevada from rhyolites), or by volcanic degassing and hydrothermal fluids. The second opinion appears to be supported where lithium associates with borates. Enrichment by evaporation is evident:

> The Salar de Atacama in the Chilean Altiplano contains a significant part of the world's known lithium resources. This is a dry depression in 2300 m altitude with an area of 3200 km^2. A halite facies occurs in the centre of the basin. The sediments in this area contain brines with 1510 to 6400 ppm Li, important contents of potassium (as well as traces of Rb and Cs) and boron. The brines are pumped from subsurface lake beds into shallow constructed ponds, where solutes are concentrated by natural evaporation. Traces of sulphate and Mg:Li ratios of $\sim$6:1 significantly increase processing costs. Products are $LiCO_3$, KCl, K_2SO_4 and H_3BO_3.

Lithium resources of the world are very large. In 2009, an estimated 150,000 t of lithium minerals were produced worldwide. First was Australia with nearly 76% of the total, followed by Portugal, Canada and Zimbabwe. In the same year, a total of $\sim$10,000 t of lithium carbonate equivalent (LCE) was extracted from natural brines in Chile ($\sim$70% of world production), China, Argentina and USA.

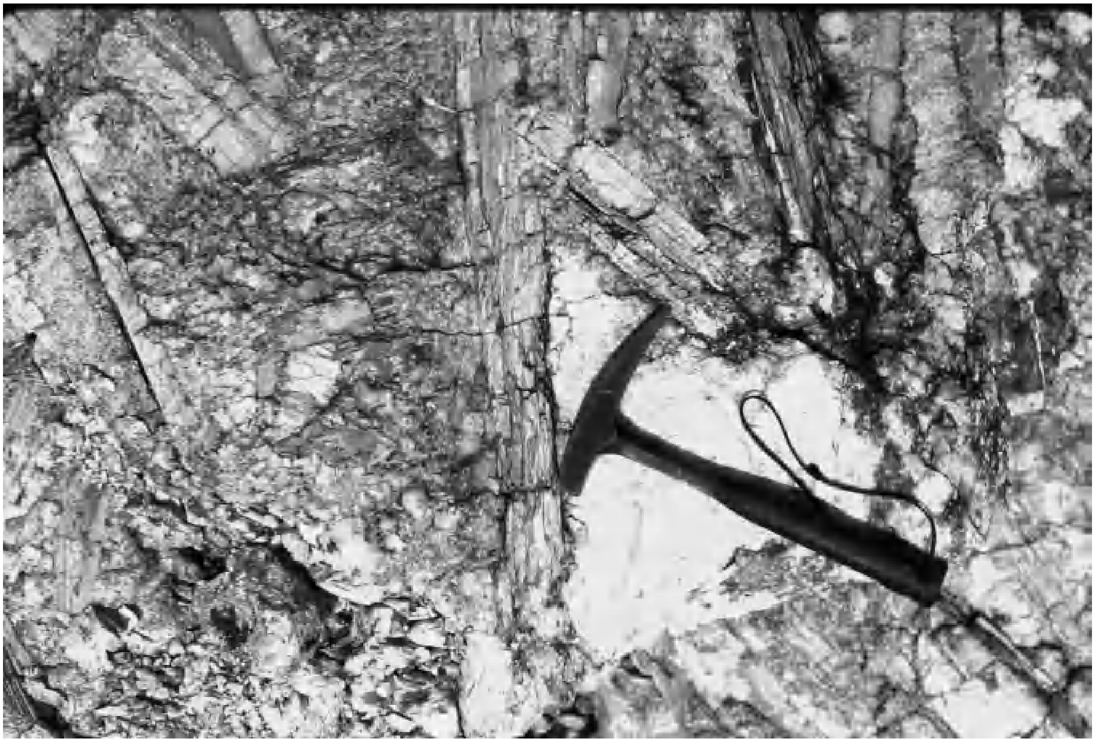

Figure 2.43 (Plate 2.43) Giant Manono pegmatite in D.R. Congo is a sub-horizontal sheet and asymmetrically zoned. An upper marginal zone is made up of near-vertical palisades of spodumene (with microcline) and patches of stanniferous albitite (centre).

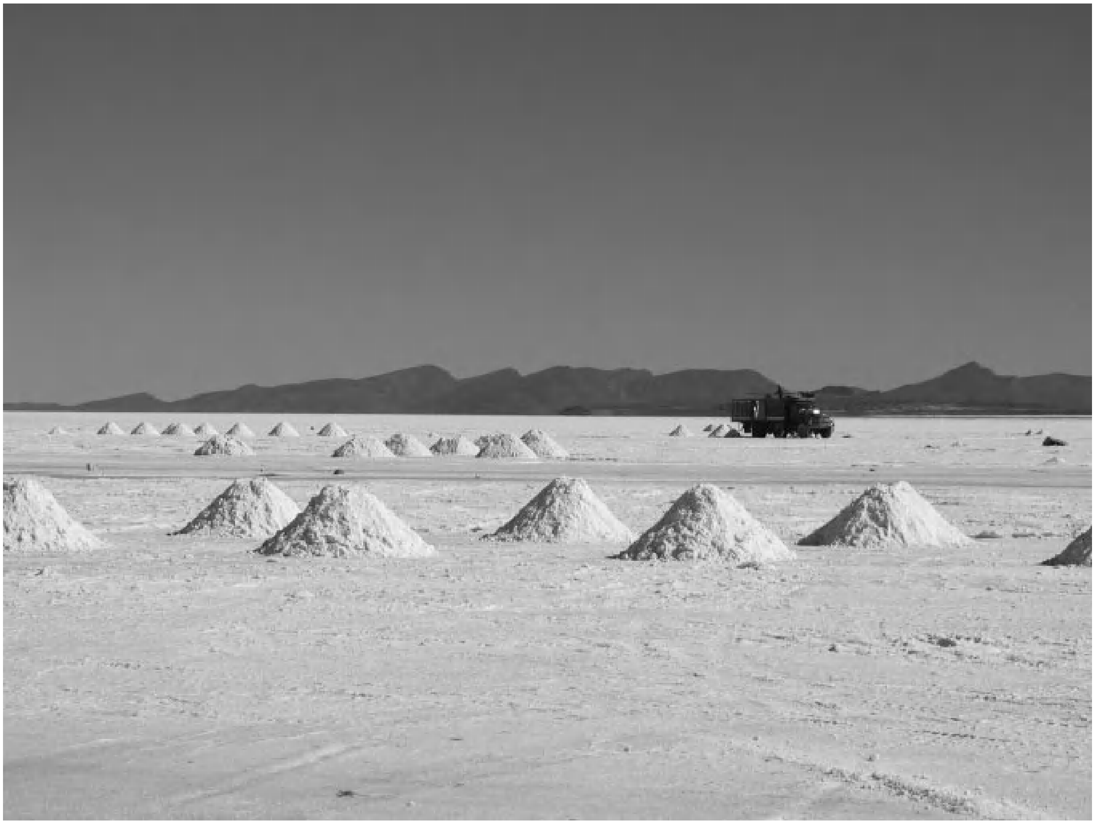

Figure 2.44 (Plate 2.44) Artisanal salt production at Salar de Uyuni, at 3500 m altitude in the Altiplano of Bolivia: One of the largest salt lakes on Earth, the salar contains giant resources of lithium, potassium, boron and magnesium in brines below the surface. The background mountains are part of the Central Cordillera, which hosts Cerro Rico de Potosi. Courtesy B. Lehmann, Clausthal.

2.5.11 Beryllium

Common Ore Minerals:

		wt. % BeO	*Density (g/cm^3)*
Beryl	$Al_2Be_3Si_6O_{18}$	14	2.65–2.8
Bertrandite	$Be_4(OH)_2Si_2O_7$	15.1	2.6

Although 28 minerals are known, in which beryllium is an essential constituent, only two are found in sufficient quantity and concentration to allow commercial extraction. The beryllium content in beryl is commonly lowered by the presence of Na, Rb, Li and Cs. H_2O, CO_2 and fluorine are lodged in large structural channels of the mineral. Deep green, transparent beryl is an extremely valuable gemstone (emerald). In emerald, up to 2% Cr + V replace Al in the crystal lattice. The pale, greenish-blue colour of aquamarine is due to content of 0.1–0.3% Fe^{2+}. Bertrandite occurs like beryl in miarolitic granites, greisen and pegmatites, where it is commonly formed by alteration of beryl. Frequent impurities in bertrandite include Al, Fe and Ca. Its main commercial source is tuffites in the USA.

Exploitable beryllium ores have minimum concentrations from 0.1 to 2% Be, depending on grain size, purity, texture and co-products.

Beryllium is a very light ($D = 1.85\,g/cm^3$) strong metal with a high melting point (1280 °C, boiling point 2970 °C). It displays good mechanical properties, oxidation resistance, and high thermal and electrical conductivity. Beryllium is useful in a number of applications, for example by hardening alloys (~75% of consumption) and in ceramics. Alloys with Cu are most common, mainly in the telecommunications, computer, aerospace and vehicle markets. Beryllium is an eminently important material for nuclear and military equipment.

Geochemistry

Beryllium is one of the lithophile, incompatible earth-alkali elements with a very low crustal abundance (2.5 ppm; Grew 2003). Basalts contain an average 0.5, granites 5 ppm Be. In chemical properties, beryllium resembles magnesium and aluminium. Its atomic and ionic radius is smaller than that of lithium. Beryllium dissolves readily in acidic and alkalic hydrothermal solutions. Natural beryllium only consists of the stable isotope ^{9}Be. In the atmosphere, "cosmogenic" ^{10}Be is produced by cosmic ray spallation of oxygen and nitrogen. It is radioactive and decays with a half-life of 1.51 million years to ^{10}B. Cosmogenic ^{10}Be accumulates at the Earth's surface, where its long residence time makes it useful for measuring processes such as soil erosion, soil formation from regolith, the development of lateritic ore deposits and variations in solar activity (Siame *et al.* 2006).

In natural oxidized water, beryllium occurs in trace quantities ($<1\,\mu g/L$), because its oxides are nearly insoluble. Be^{2+} is somewhat mobile in acidic waters at $pH < 3$. Nearly all beryllium emitted into the atmosphere by humans results from oil and coal combustion for electric power generation. The element seems to have no biological function and is specified as a hazardous air pollutant by the US Clean Air Act (1990). In the past, toxicity of very fine-grained beryllium metal dust and several compounds affected industrial workers who developed occupational diseases. Today, workplaces appear to be adequately controlled. For the general public, beryllium exposure is toxicologically not relevant.

Beryllium ore deposit types

Similar to lithium, beryllium is enriched in extremely fractionated late liquids and fluids of felsic magmas (<0.05% of the original volume: Evensen & London 2002). These liquids form pegmatitic beryllium deposits. Much less common are similar melts in the volcanic environment, which are related to epithermal beryllium impregnations in tuffite. Several of the world's emerald deposits hosted in black shale are possibly of diagenetic or metamorphogenic-hydrothermal origin, but doubts remain. Economic sources of beryllium are only:

- epithermal stratiform volcanogenic beryllium impregnations in rhyolite tuffite;
- rare element pegmatites of the lithium-caesium-tantalum (LCT) type.

Several epithermal stratiform volcanogenic beryllium deposits occur in the area of Spor Mountain in Utah, USA. The region is part of the Basin and Range Province. Between 42 and 6 Ma, several phases of volcanism took place. Early eruptions produced intermediate lava flows and tuffs but after ~21 Ma, alkali-rhyolite tuffs and ignimbrites were deposited. Topaz rhyolite tuffite beds (the "beryllium tuff") with abundant clasts of subjacent Palaeozoic basement dolomites host the ore. In the basement, upflow channels exhibit uraniferous fluorite that was exploited in the past. Fluids invaded permeable tuffites between less porous rocks and replaced dolomite with bertrandite, uraniferous fluorite, chalcedonic quartz and manganese oxide (Lindsey 1977). Hydrothermal alteration enclosing beryllium ore (>1000 ppm Be) comprises adularia and argillization zones, including lithium-bearing trioctahedral smectite. Mining started in 1968. Production rates at Spor Mountain amount to ~45,000 t/y of bertrandite ore at ~0.35% Be. Similar mineralizations are known elsewhere. A rarity is the occurrence of beryllium skarn at the contact of a Tertiary rhyolite laccolith intruding Cretaceous limestone at Round Top in western Texas.

Beryl is a characteristic minor mineral in rare element pegmatites of the lithium-caesium-tantalum (LCT) type that are mainly exploited for cassiterite, columbite and lithium minerals; beryl

(± elevated Cs-contents) is a by-product. Beryl is more often enriched in zoned pegmatites, preferentially in the wall zone or adjacent to the quartz core where coarse and even giant crystals can be found (Figure 1.19 and Figure 1.20; Sweetapple 2000). Beryl in unzoned pegmatite tends to be very fine-grained and recovery is more expensive. Worldwide, beryl extraction from pegmatites used to be quite common when artisanal or semi-industrial mining allowed selective recovery. Today, only large pegmatite bodies warrant the investment for industrial processing plants.

Emeralds are extracted from beryllium pegmatites that intruded chromium-rich rocks (e.g. ultramafics in Pakistan: Arif *et al.* 1996; talc schists in Zambia). However, some emerald deposits are hosted by black shale and are a product of diagenetic or metamorphic hydrothermal processes:

> Emerald deposits in Colombia occupy the first place in the world, both concerning quality of the gemstones and quantity of annual production (estimated at 2 t/y). Near Muzo, 100 km northwest of Bogotá, emerald occurs in fault-bound veinlets in thinly banded black shale and limestone. This is part of the strongly folded Cretaceous marine suite of carbonates, sandstone, shales and evaporites, which builds the Eastern Cordillera. Mineralization is structurally controlled by a thrust plane (Pogue 1917). The paragenesis of the emerald-veinlets includes calcite, dolomite, quartz, fluorite, pyrite and muscovite, which were precipitated from saline brines (up to 40% NaCl equiv.) at 290–360 °C and P~1 kbar. Hydrothermal alteration of black shales includes bleaching, carbonation and albitization. For the miners, the resulting light "cenicero" (Spanish for "ash rock") indicates the presence of emeralds. Cr and V of the emeralds are probably derived from the organic matter-rich host rocks. Hydrothermal fluids have the character of deep formation or low-grade metamorphic water. Dissolution of gypsum and halitite provided salinity. Migration of fluids was induced by Eocene-Oligocene orogenic compression and salt tectonics. The source of beryllium remains disputed. Hypotheses include dissolution from black shale near the deposits (Giuliani *et al.* 1999) or abstraction from deep basinal sediments and transport in mobile Be-F complexes (Banks *et al.* 2000). Pogue (1917), however, mentioned the occurrence of a pegmatite in the area, and suggests genetic relations with a buried intrusion.

Annual world mine production of beryllium in concentrate is ~200 tonnes (but only 140 in 2009; USGS 2010). More than 80% of the total is from Spor Mountain (USA), the remainder from China and Mozambique. The search for beryllium ore depends on a combination of well-planned sampling, and the availability of chemical and X-ray determination equipment. In the field, portable "beryllometers" (gamma-ray neutron generators) are used to measure *in-situ* Be-contents.

2.5.12 Uranium (and Thorium)

Common and Characteristic Ore Minerals:

		Max. Density (g/cm^3)
Uranium		
Uraninite (Pitchblende)	UO_2	9.7
Brannerite	$(U,Ca,Ce)(Ti,Fe)_2O_6$	6.3
Coffinite	$U(SiO_4)_{1-x}(OH)_{4x}$	7.2
Autunite	$Ca(UO_2)_2(PO_4)_2.8\text{–}12H_2O$	3.2
Carnotite	$K_2(UO_2)_2\ (VO_4)_2.\ 3H_2O$	5.0
Thorium		
Uranothorite	$(U,Th)SiO_4$	variable
Thorite	$ThSiO_4$	5.3
Thorianite	$(Th,U)O_2$	9.7
Monazite	$(Ce,Th)PO_4$	5.3

There are more than 200 different minerals containing uranium; those listed above are common in workable deposits. The first three minerals host uranium in its reduced state (U^{4+}), whereas the following are samples of a large number of minerals containing the uranyl ion $UO_2{}^{2+}$ and uranium in its oxidized state (U^{6+}). Most uraninite is partially oxidized and the composition lies between UO_2 and U_3O_8. Well crystallized uraninite was probably formed at higher temperatures and has elevated trace contents of Th, Ce, Y, and Ca. At lower temperature, the botryoidal, massive or friable soot-like pitchblende is more common, which contains less of these impurities. Radioactive decay of uranium results in trace contents of radioactive daughter nuclides such as radium and stable elements lead and helium (Table 2.3).

Table 2.3 End products of radioactive decay of uranium and thorium

$^{238}U \rightarrow {}^{206}Pb + 8\,{}^{4}He$
$^{235}U \rightarrow {}^{207}Pb + 7\,{}^{4}He$
$^{232}Th \rightarrow {}^{208}Pb + 6\,{}^{4}He$

Pb and ^{4}He are used for age determination of ore, minerals and rocks (cf. Chapter 1.1 "Isotope Geochemistry"). Radiogenic lead in uraninite may form galena inclusions (Figure/Plate 2.26). During geological times, however, passing fluids can selectively remove lead or uranium, concealing the true age of mineralization. Depending on age and geological fate, uraninite contains 45–85 wt.% U.

Thucholite is not a mineral but a complex bituminous material with high uranium and thorium content, and visible pyrite or galena. It has been noted in pegmatites, but was only extracted as uranium ore from Witwatersrand conglomerates where earlier it was thought to represent algal mats. An origin from migrating hydrocarbons was suggested by Parnell (1996).

Economic ore grades of large hard-rock uranium mines can be as low as 0.2% U_3O_8. Most mines produce ore of ~1%. Cut-off grades depend on commercial and technological constraints, because prices of the metal fluctuate widely and the ore paragenesis determines processing costs and recovery. Therefore, uranium reserve tonnages are commonly related to certain market price levels. Of course, mines with exceptional grades such as Cigar Lake and McArthur River in Canada with 14% and even >30% U_3O_8 are beyond such considerations. An example of extremely low grade and yet feasible uranium mining is the calcrete deposit Langer Heinrich in Namibia, which since 2006 produced ore of 0.06% U_3O_8 from a reserve of 50 Mt.

Uranium mining by *in-situ* leaching (ISL) is suitable for low grade (e.g. 0.12% U_3O_8 in the Honeymoon project, Southern Australia) near-surface ore in aquifers. Nearly all uranium produced by Kazakhstan is from relatively small ISL mines. Characteristic examples are permeable mineralized sandstone beds interbedded between aquitards. The aquifer is grid-drilled and leach fluid is injected. This may be an aqueous solution of sodium hydrogen carbonate or simply CO_2, alternatively H_2SO_4 and O_2. The resulting pregnant solution is pumped from production wells and processed for recovering uranium in marketable form. *In-situ* leaching is a very small-impact extraction method. The environment is hardly affected and after the end of operations, the aquifer is remediated.

In-situ leaching (ISL) provided 36% of world mine production (2009) and ~60% was derived from open pit and underground mines (www.world-nuclear.org; June 2010). "Acidic" (quartz-rich) ore is leached with hot sulphuric acid, whereas "basic" (e.g. carbonate-bearing) ore is treated with a solution of soda and sodium bicarbonate. From the liquor, uranium is precipitated as ammonium diuranate ("yellow cake") or oxide.

During leaching, 226-radium of the ore is not dissolved. Radium, with geochemical properties similar to barium, remains in the tailings, which are commonly neutralized and disposed of in tailings dams. Care must be taken if the waste material contains sulphides: In contact with oxygen most sulphides produce acid, which mobilizes radium that may then contaminate groundwater or the environment. Radium is an emitter of α-radiation with a half-life of 1620 years and poses a considerable risk. Its dispersion can be blocked if the acid-generation potential of the tailings is reliably neutralized (e.g. by mixing with red mud waste from alumina production; cf. Section 2.4.1 "Aluminium"). Another serious hazard is radium's daughter element radon, a noble gas and α-emitter with a half-life of only 3.8 days. In the UK, indoor inhalation of natural radon and short-lived decay products of natural radon cause thousands of cancer deaths per annum (Appleton 2005). In outdoor air, radon is quickly diluted.

The principle health hazards posed by uranium are its chemical toxicity (notably in drinking water) and the radiological properties of some of its decay products, especially ^{226}Ra and ^{222}Rn (Appleton 2005). Radionuclide contamination by man includes nuclear weapons (mainly testing), nuclear accidents and, to a lesser extent, nuclear power generation and re-processing of spent fuel. Uranium is also emitted into the atmosphere by oil and coal combustion for electric power generation. It is specified as one of the hazardous air pollutants by the US Clean Air Act (1990) and is closely controlled. The average dose from these sources over most of the Earth's surface, however, is small compared to natural radioactivity (Plant *et al.* 2005). WHO (2006) proposed a provisional guideline value of uranium in drinking water at 0.015 mg/litre but notes that 0.03 mg/l may be sufficiently protective of kidney toxicity. Let us not forget that uranium is omnipresent in the environment and that all living matter contains traces of uranium and other radioactive nuclides.

In civil applications, uranium is almost exclusively used as a fuel for base load electrical power production in nuclear power stations (Wilson 1996). For this purpose, no carbon-free alternatives exist. Yet, nuclear reactors can be quickly controlled to make room in the grid for unpredictable fluctuations of wind and photovoltaic electricity production. Worldwide in 2009, 439 power reactors were operating in 30 countries. Fifty-seven were under construction, mainly in China (23), Russia, South Korea, India, Japan and Canada. Natural uranium is composed of three isotopes (Table 2.4).

Table 2.4 Naturally occurring uranium isotopes

^{238}U	99.27 wt.%	half-life (a) = 4.468×10^9
^{235}U	0.72 wt.%	0.703×10^9
^{234}U	0.0057 wt.%	2.47×10^5

Uranium 234 is a member of the ^{238}U decay series; its concentration is a function of the radioactive equilibrium between both isotopes. The precise $^{238}U/^{235}U$ ratio of natural uranium depends on genetic conditions (Bopp *et al.* 2009).

> In water-cooled nuclear fission reactors, only ^{235}U is consumed that was previously enriched to ~3–5% of $^{238}U+^{235}U$. Future breeder reactors are supposed to make additional use of the energy contained in the more common ^{238}U. Major differences between nuclear and fossil power production are in the amount of fuel required and in resulting emissions. For a typical power station of 1000 megawatt (MW), annual fuel requirement is ~3 Mt of coal, or if nuclear, 170 tonnes of natural uranium. Seven million tonnes of CO_2 and 300,000 tonnes of ash are generated annually by a coal-fired plant, compared with ~27 t of spent fuel (or 1 t of processed waste) from a nuclear station. Also, considering the uncertain future of oil availability, supply and price, the nuclear industry is well positioned to produce hydrogen as a transport fuel.
>
> Of all energy sources, the nuclear energy cycle has the lowest impact on the environment, as it produces no harmful emissions (CO_2, toxic elements, etc.) and requires very little land. Risks associated with nuclear power generation, reprocessing of spent fuel, and with disposal of spent fuel and other toxic and radioactive nuclear waste are major points discussed in science and society. Safe waste disposal is one of the most important demands of society from the geosciences (cf. Chapter 5.5 "Deep Geological Disposal of Dangerous Waste").

Highly enriched uranium (to >90% ^{235}U) is only produced for nuclear weapons. Depleted, almost pure non-fissile ^{238}U is mainly used for its high density (19.1 g/cm^3, melting point 1132 °C). Applications are limited and include bullets and shells, chemical catalysts, but also sailing boat keels and parts of Formula 1 racing cars. Because of increasingly tighter control of radioactive material, civil application of non-fissile uranium will probably cease.

Thorium is composed of only one isotope (apart from a short-lived daughter nuclide), ^{232}Th with a half-life of 1.405×10^{10} years. It is not fissile and is rarely used for nuclear power production. However, thorium can be converted to fissile ^{233}U by neutron irradiation and the Molten Salt Reactor Process is considered to potentially satisfy future energy needs. India built a first small reactor of this type in 1996 and since then launched a major programme to use its large thorium reserves. The Subcontinent has little uranium, but is endowed with coastal placers containing ~400,000 t of Th in monazite, promising energy for hundreds of years. Non-nuclear uses of thorium (11.7 g/cm^3, melting point 1842 °C) include the production of incandescent mantles for gas lamps (~50% of consumption; but Th is increasingly replaced by yttrium compounds), Mg-Th alloys for high-temperature applications, and various electronic, chemical and metallurgical applications. However, most non-energy uses of radioactive thorium are being phased out.

Geochemistry

The geochemical character of uranium and thorium is lithophile (Goldschmidt 1958). In common magmatic rocks, uranium reaches its highest average abundance in granite (4.8 ppm; Th 17 ppm). Large granite bodies with high U and Th-contents are heated by radioactive decay (High Heat Production, or HHP granites). This has geological consequences (e.g. hydrothermal mineralization in Cornwall) and may be a source of environmentally benign geothermal energy. For several decades in the past and in current projects, the European Union supports the development of technologies for harvesting geothermal heat and electricity at sites in Cornwall and Alsace. As large ions with a high charge, U(IV) and Th(IV) are geochemically similar to the rare earth elements. They are incompatible in relation to common igneous silicate minerals and are preferentially concentrated in accessories such as allanite, monazite and xenotime. Traces occur in zircon, orthite, apatite, titanite and magnetite. In many granites, however, a large part of uranium and thorium is held in intergranular films (compare recent findings concerning REE in S-Chinese granites: Ishihara *et al.* 2008). These films and radiation-damaged accessory minerals are easily soluble. As much as 90% of total uranium and thorium in granites may occur in this form. Felsic volcanic rocks are also a source of readily soluble uranium, mainly from glass phases.

Uranium and thorium are enriched in late melts and fluids segregated from cooling felsic magma bodies. The distribution of U and Th between melt and fluids is a function of the fluid composition. A purely aqueous fluid dissolves little U and Th, but both elements are enriched in fluids when fluorine concentrations rise. Uranium and thorium are separated if the fluid is dominated by CO_2 and Cl, because in this case uranium is soluble but thorium is retained in the melt or in refractory solids. This explains, for example, the low concentration of uranium in granulite and its enrichment in carbonatite. In magmatic-hydrothermal fluids, uranium occurs mainly in the form of chlorine and carbonate complexes of U^{+4}, whereas both Th and U form fluorine complexes (Keppler & Wyllie 1990). Uranyl-carbonate complexes (in circum-neutral conditions) or uranyl-chlorine complexes (in acidic conditions) prevail in hydrothermal solutions of low temperature ($<200\,^{\circ}C$; Kojima *et al.* 1994). Changing pH, degassing of CO_2 and reduction precipitate UO_2 from these solutions.

The geochemical behaviour of uranium and thorium in the exogenic cycle (Burns & Finch 1999) is peculiar because of the low solubility of thorium and REE in near-surface environments, in sharp contrast to uranium, which is easily dissolved by oxidation. Primary uranium minerals are first transformed into brown, yellow and green intermediate oxides, and dissolve finally to form the mobile uranyl ion $UO_2{}^{2+}$, which can be transported over large distances by surface and groundwater. The uranyl ion is complexed by carbonate, fluoride, sulphate and phosphate anions. Most common is transport as an anionic uranyl-carbonate complex. Aqueous colloids with sorbed uranium (VI), such as amorphous iron hydroxides, may carry much higher concentrations than simple solutions. Precipitation of uranium is induced by adsorption (e.g. clay minerals, organic matter, Fe-Mn-Al oxy-hydroxides) or by reduction. Common reducing factors in geological settings include H_2S, Fe^{2+}, CH_4, petroleum and organic substances. In the laboratory at room temperature and in limited time, dissolved uranyl is efficiently immobilized by humic substances without being reduced (Wood 1996, Nakashima *et al.* 1999). Rapid reduction in natural systems is probably encymatically catalysed by microbes, for example by sulphur-reducing bacteria (Lovley *et al.* 1991, Min *et al.* 2005). It is assumed that the organically-bound uranyl is reduced during diagenesis. Peat and coal (Figure 2.43), phosphate rocks (40–250 ppm U), black shales and oil shales always display elevated but rarely exploitable uranium concentrations. Examples include the Cambrian alum shales of southern Sweden (~300 ppm U; Leventhal 1990) and the European Copper Shale (180 ppm: Piestrzynski 1990). The ash from large power stations burning coal or petroleum may be a feasible source of uranium. Some petroleum and associated formation waters carry significant

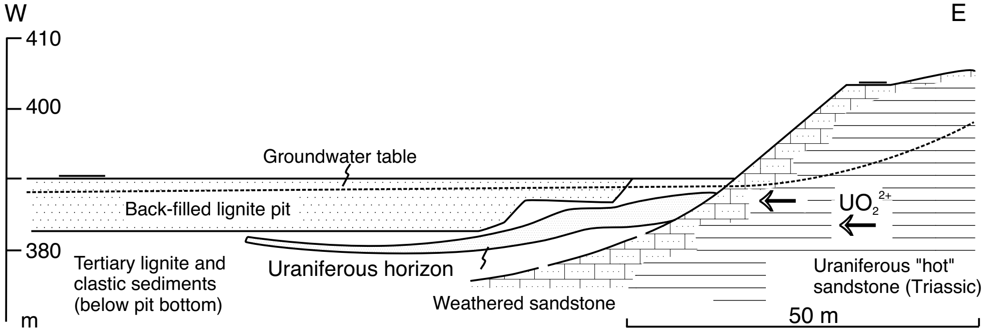

Figure 2.43 Uranium infiltration at the margin of the Tertiary lignite basin Wackersdorf, Germany. Groundwater passing through uraniferous ("hot") Late Triassic sandstone flowed into marginal basin sediments (impure coal, carbonaceous clay and sand) that immobilized uranium by adsorption and reduction. Peak contents reach several thousand ppm of uranium.

uranium contents, for example in the Ukhta field in the South Russian Pechora Basin.

Ordinary surface and groundwater contains less than 1 ppb (1 µg/L) uranium (Merkel *et al.* 2002). Several tens of ppm may occur in water that was in contact with uranium-anomalous rocks or with ore. Average ocean water concentration of uranium is ~3 ppb. Seawater is the source of uranium in phosphorite and black shale. Because of the large water volume, the oceans contain ~5000 Mt of uranium (Algeo 2004). Evaporation of seawater causes enrichment of uranium in brines. Thorium is commonly insoluble and immobile in contact with oxic surface water, apart from physical transport in flowing streams. Rarely, complexing elements such as Cl, Br, F or I in brines may lead to exogenetic chemical mobility of thorium.

Natural nuclear reactors

Natural nuclear reactors have been found in uranium deposits of the Oklo District, Gabon (Jensen & Ewing 2001, Figure 2.44). At Oklo, uranium ore is extracted from faulted Palaeoproterozoic siliciclastic sediments transgressing Archaean granites. During the mineralization process, the critical mass of massive pitchblende was reached at 14 sites exposed by mining, where the chain reaction of nuclear fission started to operate. Criticality of the reactors was dated to 1950 Ma and proved by the presence of long-lived fission products. The first of these reactors was discovered in 1972 when the reason for a strong depletion of ^{235}U in certain ore shipments from Oklo was investigated. Today, the natural assembly of a nuclear reactor is not possible because the concentration of fissile ^{235}U in modern uranium is too low. The preservation of the Oklo reactors is remarkable, considering the shallow burial and the high mobility of uranium and its daughter and fission nuclides. This makes Oklo one of the demonstration sites for the long-term safety of engineered underground disposal facilities. Note that the rocks of Oklo are fractured and permeable, so they would certainly not be chosen for the construction of a nuclear waste repository. Coogan & Cullen (2009) suggested a causal connection between the "Great Oxidation Event" and an assumed abundance of widespread near-surface uranium deposits that developed into natural fission reactors. Under a reduced atmosphere, detrital uranium must have been common. First islands of oxygenation by early photosynthesis might have established aqueous cycling and concentration of uranium at redox boundaries.

Thorium mineralizations originate almost exclusively by magmatic, magmatic-hydrothermal

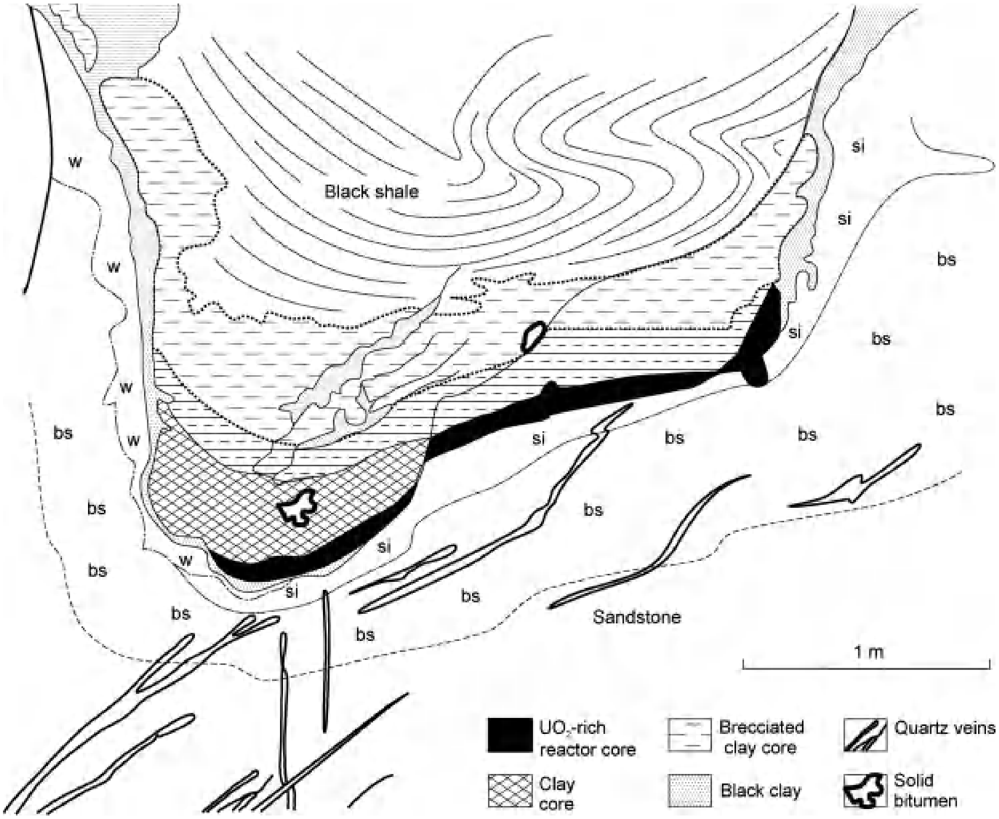

Figure 2.44 Underground mine exposure of the Palaeoproterozoic Rzoke nuclear reactor in the uranium mine Okelobondo in Gabon (after Jensen & Ewing 2001). Ascending uraniferous hydrothermal fluids precipitated uraninite at the contact between black shales and sandstone. Locally, critical mass and concentration of ~15% UO_2 were reached and nuclear fission started to operate. Water and petroleum (now pyrobitumen) functioned as neutron moderators. Note the pouch-like sagging form. Abreviations: w – white, leached shale; bs – bitumen-rich, si – silicified sandstone.

and sedimentary processes. Thorium is commonly a by-product of mines exploiting rare earth elements and copper. Thorium concentrations are found in pegmatites with uranothorite, thorite, orthite and zircon, in carbonatites (e.g. 0.01% in ore at Palabora, South Africa) and in hydrothermal veins with thorite, bastnaesite, monazite and apatite in the vicinity of alkali complexes and carbonatites. In practice, only coastal placers with monazite as a by-product of ilmenite and zircon mining are a relevant source of thorium.

Uranium ore deposit types

Exploitable concentrations of uranium are formed in a broad spectrum of geological systems, but foremost in magmatic, magmatic-hydrothermal, retrograde-metamorphogenic, supergene alteration and infiltration, and sedimentary settings (compare Cuney & Kyser 2009, Cuney 2009). The mobility of uranium in oxic surface waters and seepage solutions explains a large number of different uranium ore deposits that were formed by fluids convecting in the shallow crust. This group includes the richest deposits of uranium (the "unconformity type"). Due to the generally reduced state of common diagenetic and prograde metamorphic fluids, uranium is rarely mobile or enriched in these process systems. Exceptions occur where oxidized solutions were involved. A stringent genetic classification of uranium deposits remains elusive (cf. Cuney 2009, Dahlkamp 1993). Therefore, generally used descriptive terms are included in the following brief overview of significant uranium deposit types, supplemented by genetic information. The order of the list reflects economic importance, from highest to lowest:

- unconformity deposits (saline brines, retrograde metamorphogenic; e.g. Athabasca District, Canada);
- magmatic-hydrothermal uranium in iron-oxide-Cu-Au (U-REE) deposits (IOCG) (Olympic Dam, South Australia);
- infiltration deposits in sandstone (Kazakhstan);
- ancient alluvial placers (Witwatersrand);
- orthomagmatic deposits in felsic intrusions (Rössing, Namibia);
- post-magmatic hydrothermal uranium in HHP granites, characterized by protracted cooling and flooding with meteoric water;
- basinal brine-related, granite-hosted disseminations and veins (Limousin, French Massif Central);
- infiltration/evaporation deposits in dry river channels and palaeovalleys: calcrete, and palaeochannel deposits (Yeelirrie, Western Australia, Lake Frome region in southern Australia).

Unconformity uranium deposits

Unconformity uranium deposits occur in ancient cratons close to the unconformity between an Archaean to Palaeoproterozoic igneous and metamorphic basement, and a cover of younger clastic sediments. Orebodies may be basement and sandstone-hosted. This class contains over 40% of world reserves, mainly in two provinces: i) the Alligator River District of the Northern Territory in Australia (Jabiluka, Ranger, Narbarlek); and ii) the Athabasca District in Saskatchewan, Canada (Rabbit Lake, Cigar Lake, Key Lake and the new McArthur River mine). The Athabasca basin produces ~30% of annual world primary uranium, with average mining grades from 0.5 to >20% U_3O_8:

> Cover rocks in the Athabasca District are fluvial to marine red sandstones with conglomerates at the base and several intercalations of evaporites and felsic volcanic rocks. The suite is called Athabasca Group and reaches a thickness of 1500 m. Its age is <1750 Ma. The basement includes Palaeoproterozoic metasediments in amphibolite and granulite facies, and Archaean gneiss domes. The unconformity is marked by lateritic palaeosoil and is hardly tilted. The metasediments display bands of graphite-bearing rocks, which control uranium orebodies where they coincide with reactivated permeable basement structures. Several periods of more intensive fluid circulation and perturbation of uraninite in the Athabasca Basin have been dated by U-Pb ages and neoformation of alteration silicate minerals (Fayek *et al.* 1998). The main uraninite ore formation event, however, took place at ~1590 Ma (Alexandre *et al.* 2009).
>
> Until discovery of McArthur River, the Key Lake deposit (exploited 1982–1997) was the largest high-grade uranium mine in the world, with 2.15% U_3O_8 in run-of-mine ore and considerable reserves (90,000 t U_3O_8; compare Chapter 5.3.2 "Ore Reserve Estimation"). The ore zone had a width and height of 15 by 100 m, and a strike length of 3.6 km (Figure 2.45). The ore was dominated by uraninite with some coffinite; gangue included a considerable mass of nickel and arsenic sulphides, and traces of Co, Fe, Cu, Pb, Zn, Mo and Se. Occasionally, thucholite occurred in pockets. The alteration halo displayed outer illitic and inner illite-chlorite zones surrounding the orebody. Above the mineralized core, rocks are silicified and tourmalinized. This extends from basement into overlying sandstones, providing a vector to ore, which is mainly explored by core logging with infrared reflectance field spectrometry. Alteration was reducing, made conspicuous by the change from red to green or grey. Microthermometric investigations imply mineralization at 150–250 °C and 0.75 kbar, and salt contents in the fluids of ~30% NaCl-equivalent.
>
> Exploited since 1999, the McArthur River deposit considerably exceeds Key Lake. Grades are ~21% U_3O_8 and geological resources are estimated to 188,000 t of uranium oxide (Jamieson & Spross 2000). The nearby Cigar Lake mine suffered a crown pillar failure and underground flooding in October 2006, from which it had not recovered by early 2010.

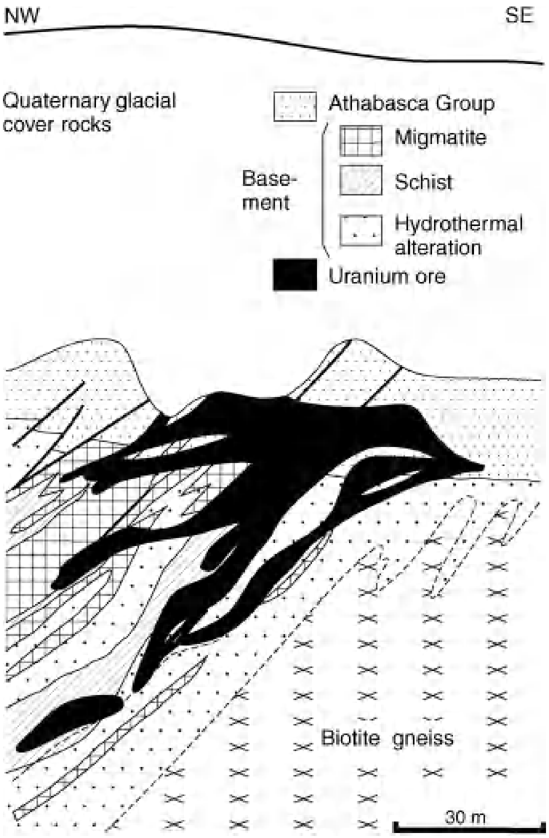

Figure 2.45 Schematic section of the unconformity uranium deposit Key Lake in the Athabasca District, Canada. After Dahlkamp, F.J. 1978, Society of Economic Geologists, Inc., *Economic Geology* Vol. 73, Figure 6, p. 1435.

The genesis of unconformity deposits is undoubtedly hydrothermal and epigenetic (Alexandre *et al*. 2005, 2009). The uranium may be derived from uranium-rich phases (e.g. apatite, zircon, monazite) in both cover and basement rocks. In the Athabasca district, orthogneisses appear to be the most likely source. The gneisses are strongly altered and uranium-depleted to a depth of 200 m below the unconformity (Hecht & Cuney 2000). Hydrothermal convection systems were controlled by permeable fault structures in the basement. Oxygen-rich basinal brines derived from Athabascan evaporites descended into the basement leaching uranium. Heated at depth to >250 °C, they were reduced by contact with graphite schist on the upflow-branch or by electron gain from Fe^{2+} of basic rocks, resulting in formation of haematite (Komninou & Sverjensky 1996). Precipitation of uranium is a consequence of reduction. Once initiated by tectonic movements, hydrothermal convection must have continued until mineral precipitation terminated all permeability, because uranium decay produces heat (cf. "HHP-granites"), making such systems independent from external energy. In conclusion, the formation of unconformity deposits combines elements of ore formation by migrating oxidized saline brines and of retrograde metamorphogenic hydrothermal processes.

Uraniferous iron oxide-copper-gold (IOCG) deposits

IOCG deposits (Groves *et al.* 2010) are represented by one single, albeit giant deposit: Olympic Dam near Roxby Downs in South Australia (Figure 2.13, cf. Section 2.2.1 "Copper"). Although most IOCG systems have anomalous uranium and LREE traces, typical grades <0.1 wt.% U_3O_8 are at present too low for profitable exploitation, except in deposits with economic grades of copper and gold (Hitzman & Valenta 2005):

> At Olympic Dam, host rock is the Roxby Downs granite (1590 Ma), which is comagmatic with volcanic rocks (Skirrow *et al.* 2007). The magmas are magnetite series and include both A- and I-Type compositions. Immediately after solidification the granite was brecciated and the breccias were the site of pervasive magmatic-hydrothermal mineralization and alteration, probably interacting with surface-derived fluids. Main minerals introduced were haematite, sulphides, uraninite, quartz, sericite and fluorite (Hitzman *et al.* 1992; Groves & Vielreicher 2001). Breccia bodies have a wide cross-section and are steeply plunging. A first batch of mineable reserves of 450 Mt with 2.5% Cu, 0.08% U_3O_8, 0.6 g/t Au and 6 g/t Ag was outlined for initial operations. Total metal endowment is estimated at >1 Mt uranium, apart from 30 Mt Cu, 1200 t Au and 7000 t Ag. Hosting ~40% of the world resource base of uranium, Olympic Dam is the largest deposit of this metal yet known.

Sandstone, or infiltration deposits of uranium

Sandstone, or infiltration deposits of uranium are very common and occur in all continents, mainly in sediments younger than 400 Ma. Individual deposits are usually rather small and have low grades (0.1–0.2% U_3O_8). Fluvial arkose sandstones of epicontinental, semi-arid basins are most frequent host rocks. Sources of uranium are felsic volcanics or granites that were weathered and eroded in up-lifted basin margins. Uranium dissolved in surface waters infiltrated aquifers in the basin fill. Conditions of mobilization, migration and precipitation can be explored by determination of U-Th nuclides and daughter elements (Reynolds *et al.* 2003, Bopp *et al.* 2009). Uranium is immobilized by reduction (typically at elongate, sinuous fronts and at roll-front deposits, cf. Chapter 1.2 "Infiltration as an Agent of Ore Formation"; Figure 1.57), but also by fluid mixing and pH change in the form of tabular orebodies (Spirakis 1996). The world's greatest provinces of uranium sandstone deposits include the Colorado Plateau, USA (Tertiary), Chu-Sarysu and Syrdarya basins in Kazakhstan (Late Cretaceous to Palaeogene: Petrov 1998) and the Agadez Basin in Niger (Carboniferous). Lodève near Montpellier, France is a peculiar trap of uranium because the means of precipitation was bitumen in faults, joints and pores of tuff and silt bands in Autunian black shale (Carboniferous-Permian boundary; Schlepp *et al.* 2001).

> Figure 2.46 shows a typical sandstone deposit: After initial underground ore extraction, an infiltration deposit in Cretaceous sandstone of southern Saxony was exploited by *in-situ* leaching with dilute sulphuric acid from 1967–1990, yielding 18,000 t uranium. The ore horizon sandstone is draped over Palaeozoic granite and granodiorite. It includes disseminated pitchblende and much pyrite. Sandstone beds are aquifers separated by aquitards. During uranium leaching, the water table was controlled by pumping in the shafts. Since 1999, remediation of aquifer 4 is carried out by flushing with fresh water (Biehler & Falck 1999). Some uranium continues to be recovered from this operation and a small production will extend well after 2010.

Ancient fluviatile placers

Uranium is a by-product of gold exploited from ancient fluviatile placers ("quartz pebble conglomerates") of the Neoarchaean Witwatersrand gold province in South Africa (cf. Section 2.3.1 "Gold"). In certain gold reefs, the matrix between pebbles contains silt-sized rounded grains of uraninite, coffinite and brannerite (UTi_2O_6). The last two were probably produced by diagenetic or metamorphic alteration of primary uraninite. Pyrobitumen bands (thucholite ore, Figure/Plate 2.26) with a thickness between 0.2 and 50 mm were either algal mats or migrated petroleum (Parnell 1996). Similar ancient uranium placer deposits occur at Elliot Lake in Canada and Jacobina in Brazil. Because of the rapid oxidation of uraninite in oxic conditions, its alluvial transport in the geological past is one of the arguments put forward for extremely low oxygen contents of the Archaean atmosphere (cf. Chapter 1.3 "Banded Iron Formations").

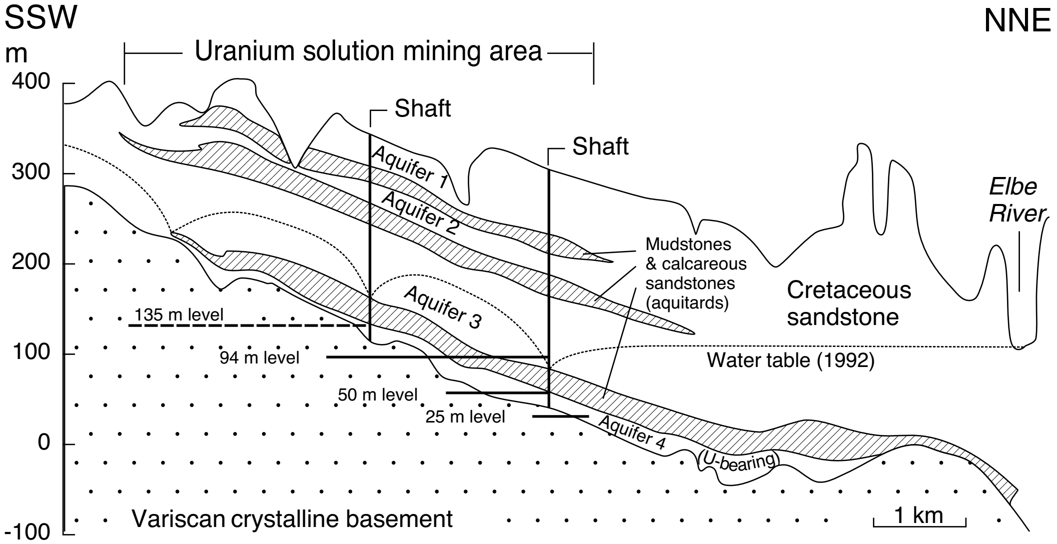
SSW
NNE
m
400
300
200
100
0
-100
Uranium solution mining area
Shaft
Shaft
Aquifer 1
Aquifer 2
Aquifer 3
Aquifer 4
(U-bearing)
Mudstones & calcareous sandstones (aquitards)
Cretaceous sandstone
Elbe River
Water table (1992)
135 m level
94 m level
50 m level
25 m level
Variscan crystalline basement
1 km

Figure 2.46 Underground *in situ* leaching of the sandstone-hosted uranium infiltration deposit Königstein in Saxony. Leaching took place in blasted chambers. With kind permission by Wismut GmbH, Chemnitz.

Uranium deposits related to igneous rocks

Uranium deposits related to igneous rocks occur in association with granites, rhyolites, alkali massifs and carbonatites. Orthomagmatic uranium deposits are rare because accessory uranium minerals are hardly ever concentrated to economic grades. However, elevated traces may be a source of uranium in hydrothermal ore deposits if post-magmatic fluid convection systems are established as, for example, in HHP-granites. Higher uranium concentrations occur only in fractionated late liquids and fluids of felsic magmas. Examples are pegmatites (e.g. Madagascar), which cannot compete with today's large and high-grade deposits:

Rössing in Namibia is one of few large orthomagmatic uranium deposits (Berning 1986). At ~500 Ma, post-tectonic leucogranites (alaskites) intruded intensively folded metasediments and mafic metavolcanic rocks of the Panafrican Damara orogen. The intrusives are mainly alkali-feldspar granites with <5% mafic minerals and variable texture, including aplitic, granitic and pegmatitic variants. The intrusion caused contact metamorphism expressed by cordierite in metapelites and skarn at contacts with metabasalt. Alaskites form sheeted dykes, parallel or oblique to hostrock schistosity, and diffuse larger bodies that attain a thickness of 100 m. U/Th and $^{87}Sr/^{86}Sr$ ratios in some members of this suite are high, possibly indicating a derivation of the melts from metasediments. Uranium is almost exclusively present as uraninite; small (30–50 μm) rounded grains are disseminated in alaskite, together with biotite, zircon, monazite, apatite and titanite. Minor phases include fluorite, sulphides (Fe, Cu, Mo, As) and oxides of Fe, Mn and Ti. Not all alaskites are mineralized; proximity to methane-bearing semipelitic and carbonate-banded metasediments seems to be a first-order control (Kinnaird & Nex 2007). Resources are estimated to ~166,000 t contained U_3O_8 at the very low grade of 0.035%.

Granite-related uranium deposits in South China are an important source of uranium. At Dalongshan in Anhui province, high-grade uranium ore was found at the contact between a Cretaceous alkali-feldspar granite and Jurassic sandstone hornfels in the hanging wall. The pluton is a HHP-intrusion; careful age investigations showed that cooling was very protracted. Hydrothermal mineralization took place while the pluton cooled from 300–150 °C, ~25–30 million years after emplacement (Zhao *et al.* 2004).

Uranium ore veins and disseminations in Variscan basement regions of France (Armorican Massif and Massif Central) defy a simple genetic classification:

> Post-orogenic (ca. 310 Ma) Variscan S-Type leucogranites with 12.5 ppm U host the uranium deposits. The ore occurs in pipes and veins of "episyenites", which are the alteration product of granite after hydrothermal removal of quartz. The leached rock displays a connective porosity of 20–30% and striking druses of adularia, quartz, fluorite and dolomite. The uranium mineralization is independent of this post-magmatic Permian hydrothermal activity and much younger (Middle Jurassic). Apparently, the episyenites offered preferential flow channels when low temperature (ca. 100 °C) oxic diagenetic brines from adjacent sedimentary basins invaded the crystalline basement. Uranium ore was precipitated with illite-smectite clay in episyenite (Patrier *et al.* 1997). The brines probably took up uranium by dissolution of uraninite disseminated in fertile leucogranite. The largest uranium mining district in the Massif Central is Limousin, based on cross-cutting uranium veins and mineralized episyenites in leucogranite. Single orebodies are rather small but cumulate production reaches 35,000 t U_3O_8, at grades of 0.1–0.6% U_3O_8.

Rhyolite tuffs, tuffites and volcanogenic limnic sediments in calderas are frequently mineralized with uranium. Tertiary U-Th-rich topaz rhyolites in the western USA display numerous epithermal (cf. Section 2.5.11 "Beryllium") and infiltration deposits as in the McDermitt caldera (Nevada-Oregon). At McDermitt, breccias near the main ring fault are epithermally impregnated with uranium and zirconium ore (Castor & Henry 2000). Playa lake sediments in such settings may be economically exploitable. The largest rhyolite-related uranium deposit is probably the Streltsovka caldera in Transbaikalia, Russia (Chabiron *et al.* 2003).

Palaeochannel and calcrete deposits

Palaeochannel and calcrete deposits of uranium form in palaeovalleys with little present groundwater flow. Examples of the calcrete type occur in Western Australia (yet undeveloped Yeelirrie: Cameron 1990) and Namibia (Langer Heinrich, producing since 2007). Langer Heinrich operates with reserves of 30 Mt at 0.06% U_3O_8. Several significant palaeochannel deposits were recently discovered in the Lake Frome region of southern Australia.

> Due to the dry and hot climate in central Western Australia, former river valleys hardly ever carry surface water. Drainage is mostly confined to buried channels in the alluvial sediments. Yeelirrie lies in the lower reaches of one of the valleys before it enters a saline lake basin. In this area, the groundwater table is several metres below surface. High evaporation in the unsaturated zone leads to precipitation of metasomatic and concretionary Ca-Mg carbonates (channel calcrete or caliche). Uranium is concentrated in the lowest calcrete and underlying alluvial clays, mainly just below the groundwater table. The uraniferous calcrete orebody is some 6 km long, 0.5 km wide and up to 8 m thick. Pockets and crusts of carnotite characterize the ore. Total resources of the deposit are estimated at 52,000 t U_3O_8 with an average grade of 0.15% (Cameron 1990). Its discovery in 1972 was due to a total-count aeroradiometric survey financed by the Australian state. Uranium and potassium at Yeelirrie are derived from weathering of granites at basin margins, but mafic rocks in the basement of the basin are probably the source of vanadium. Calcrete formation and mineralization are geologically young, although radioactive equilibrium is usually present. The ore at Yeelirrie was precipitated in an oxic environment, not by reduction. Infiltrating uranium was immobilized solely by formation of the insoluble vanadate. The palaeochannel deposits in South Australia seem to have precipitated uraninite by microbial reduction and show displacement of radium from uranium (Dickson & Giblin 2007).

Hydrothermal vein deposits or uranium

Hydrothermal vein deposits of uranium lost their former prominent role when the potential of uranium in weapons and energy production was recognized during World War II. Intensive prospecting for the new strategic metal soon brought discoveries of new deposit types (e.g. sandstone ore) that could be exploited with lower-cost mining techniques compared to underground stoping of narrow veins. When mining of silver and lead in the Erzgebirge (*ore mountains* in German, *Krušné hory* in Czech language) reached a peak during the 16th century, by-breaking pitchblende was discarded as useless. Even after the discovery of uranium by Klaproth in 1789, nearly 100 years passed before an application for the element had been found. Beginning in 1863, pitchblende was mined at Joachimsthal (Jachymov) for the production of dyes. Until 1912, this mine was the most important source of uranium (and radium) in the world. It acquired scientific fame when Marie Curie discovered the new elements radium and polonium in pitchblende from Joachimsthal (1898). The mine was operated well into the recent past, until 1968. Over the last 50 years, it developed into a spa based on radon dissolved in thermal water, which is recommended for alleviating numerous serious ailments such as rheumatic diseases and asthma. A brief introduction to the wider geological setting is provided in Section 2.2.3 on "Tin":

> The Joachimsthal uranium deposit is not only of historic importance but also of great scientific interest. It is peculiar because apart from uranium, five different metals were present in commercial quantities. In classical economic geology this assemblage was called the Bi-Co-Ni-Ag-As (±U) vein formation (Baumann *et al.* 2000, Stemprok & Seltmann 1994). Some 200 veins occur at Joachimsthal within an area of 35 km^2 but only 8 were major silver producers. Two vein sets are developed: The older prominent "morning veins" striking roughly east-west and the smaller "midnight veins" north-south. The latter contained most of the ore, although their thickness rarely surpassed 10–30 cm. A Proterozoic metasedimentary sequence of phyllites and mica schists hosts the veins. Carbonate, pyrite and graphite-rich bands in the metasediments exerted a strong lithological and chemical control on ore shoots (Ondruš *et al.* 2003). The metasediments are underlain by the Variscan Karlovy Vary (Karlsbad) batholith, at depths from 500–800 m below the surface. The batholith is composed of several phases intruded between 310 and 290 Ma, with a uranium-rich younger generation and ending with highly fractionated, very small rare element-fertile granite intrusions (Breiter *et al.* 1999). A gross depth zonation is developed in the veins, with silver (±As) nearest the surface, followed by Bi-Co-Ni-As and uranium below just above the roof of the batholith. Veins within the granite are barren. The paragenesis associated with pitchblende is composed of dolomitic carbonates, pyrite and blackish-violet fluorite (Figure/Plate 2.47). Uraninite ages from Joachimsthal vary between 5 and 285 Ma (Ondruš *et al.* 2003). Only the oldest age, 285 Ma, can be considered primary. Younger ages indicate disturbance of the system or dissolution and reprecipitation of pitchblende. The absolute age of the polymetallic Bi-Co-Ni-Ag-As ore is not yet constrained but structural relations suggest that it was formed after the uranium (Ondruš *et al.* 2003). In conclusion, uranium mineralization at Joachimsthal is related to Variscan felsic magmatism. Protracted cooling similar to the Chinese deposits mentioned above (Zhao *et al.* 2004) may best explain the post-magmatic formation age.

Supergene enrichment uranium deposits

Ronneburg in Thüringen (Germany) is an interesting example of a supergene enrichment uranium deposit. During the period 1950–1991, the district provided the former Soviet Union with a total of 113,000 t uranium, in spite of low grade (Lange 1995). Host rocks are strongly folded and very low-grade metamorphic shales occurred in a region where an antiform is traversed by a broad fault zone. Most ore was extracted from shales, banded cherts and argillaceous limestones of Late Ordovician to Early Devonian age. Unaltered shales are characterized by high contents of organic C (5–9%), pyrite (S 2–3.5%) and 30–50 ppm uranium. Orebodies are blanket-shaped but independent of bedding. Mineralization is clearly controlled by the density of rock fracturing and the resulting palaeo-permeability. Pitchblende, chlorite, carbonates, sulphides and arsenides are most important minerals of the ore. Pitchblende ages fall into two groups of Early Permian (Rotliegend, ~300–270 Ma) and Mid-Cretaceous (120–90 Ma). Ore at Ronneburg had an average grade of 850 ppm U. The enrichment was induced by supergene alteration and dissolution of uranium by infiltrating meteoric water. The oxidation zone extends to a depth of 100 to a maximum of 1000 m. Below the redox boundary, uranium was immobilized by reduction

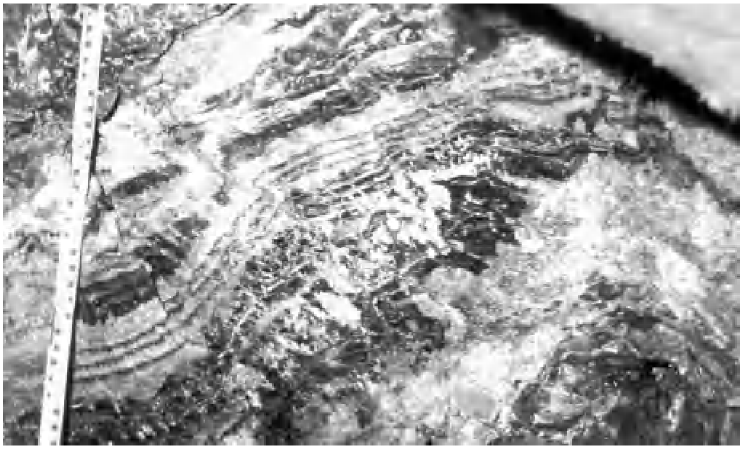

Figure 2.47 Uraninite vein at Hartenstein mine (1530 m level) in the Erzgebirge, Germany. Courtesy Volker Lüders, GFZ Potsdam. Uraninite in dark bands, the light gangue comprises pink dolomitic carbonates, pyrite and Bi-Co-Ni sulphides. This is one of nearly 2000 uraniferous veins in the district. Between 1946 and 1991, total production was ~80,000 t uranium contained in concentrate. From outcrops around Schneeberg in the southwest the vein field plunges to great depths in the northeast, about parallel to the roof of an underlying granite batholith. Height of image ~50 cm.

and concentrated in a secondary enrichment zone with a thickness between 200 and 400 m.

Exploration for uranium is singular because of the application of radiometric methods. ^{238}U, ^{235}U and ^{232}Th are long-lived alpha and low-energy gamma emitters. Together with ^{40}K and the respective daughter nuclides they generate most of the natural radioactivity. Daughter nuclide chains of uranium and thorium comprise one or more radioactive gas species. In the case of ^{238}U this is ^{222}Rn (radon), itself an alpha emitter with a half-life of 3.8 days (André-Jehan and Feraud 2001, Appleton 2005). The thorium decay chain includes ^{220}Rn (half-life 51.5 seconds) that is also called thoron. Radon is quite mobile, for example by diffusion, and is used for locating buried uranium anomalies, which cannot be detected by measuring surface gamma radiation. In practice, a prospect is covered with a grid of shallow (<10 m) open drillholes (>80 mm) and after equilibration with soil gas, the radon concentration in holes is determined with commercial probes. Radon dissolved in groundwater can also be a useful guide. Because of its short half-life, thoron mobility is very limited.

The decay series of uranium and thorium reach a secular equilibrium after ~300,000 to 400,000 years. For the more abundant ^{238}U, the daughter nuclides ^{234}Th and ^{214}Bi have a prominent role, because both emit high-energy gamma radiation. ^{214}Bi is the base for the determination of "equivalent" U contents (eU) using gamma ray spectrometry. This is of great practical interest because gamma radiation penetrates further (up to ~1 metre of low-density material) facilitating detection. Most common techniques of radiometric uranium and thorium exploration are based on γ-radiation. Provided that uranium and its daughters are in equilibrium, the intensity of γ-radiation is positively correlated with uranium concentrations, which can easily be calculated.

However, discrepancies between radiometric and chemical determination of uranium contents are not rare (Brooks 2008). These "errors" result from the different mobility of uranium and its daughter nuclides ^{234}Th, radium, radon and ^{214}Bi. In the case of geologically young uranium (e.g. in post-glacial peat, sandstone and calcrete) equilibrium is not fully established and the daughter nuclide spectrum is incomplete. Consequently, eU will not point to the uranium. The reverse is not rare in "moving" roll-front deposits, where uranium is leached on the upstream side, but not its daughters. In this case, eU will be high but little uranium may be present. The differential movement of nuclides of the uranium decay series is extremely useful for timing transport processes. Reserve estimations of uranium deposits must be based on a good understanding of the local disequilibrium situation (Bowden & Shaw 2007).

Equipment employed in uranium exploration includes thallium-activated sodium-iodide scintillation detectors (scintillometers measuring total gamma counts), which are also available as spectrometers that allow separate determination of eK, eU and eTh. Instruments are employed in cars and aeroplanes to prepare radiation maps of larger areas. Hand-held versions are used for reconnaissance in difficult terrain and for detailed mapping of prospects. Borehole probes are available, but note that in many cases it may be better to work with prompt fission neutron (PFN) logging systems that allow determination of *in-situ* uranium contents (Givens & Stromswold 1989), both in operating mines and in exploration. Mapping uranium distribution in cut and polished ore specimen is most efficiently carried out with the scanning electron microscope (SEM). Of course, uranium exploration employs other mineralogical, geochemical and geophysical methods, apart from radiometric surveys.

Identified and inferred uranium resources at mining costs <130 US $/kg are estimated at >5.5 Mt (U metal content). Largest resources occur in Australia, Kazakhstan, Russia, South Africa, Canada, USA, Brazil and Namibia. Since 1945, ~2.5 Mt uranium has been produced worldwide, of which nearly 50% were destined for military purposes. Annual world mine production is ~50,600 t U (2009). Main producing countries are Kazakhstan, Canada, Australia, Namibia, Russia and Niger. The balance to annual consumption of ~70,000 t U required by the world's nuclear reactors is made up from secondary sources, including former nuclear weapons, re-enrichment of depleted uranium and stockpiles. Large potential resources assure future supplies, but new mines and technologies will be needed, especially for eventual recovery from seawater.

Specific problems of uranium production and use start at the mine with strict control of radiation exposure of miners and people living nearby, both during operations and after closure (Merkel *et al.* 2002). In this respect, uranium mines are highly regulated. Safe keeping of closed mines and mine waste facilities is complex. Remediation of uranium mines in Canada, France and Germany provides exemplary case histories (Daroussin *et al.* 1998). The public has accepted the results of these efforts, but disposal of nuclear waste is still hotly discussed, although the geoscience community is largely supportive of deep permanent geological storage. Results of comprehensive research programmes are available and field experiments confirm the feasibility of underground storage (Chapman & McCombie 2003, Gibb & Attrill 2003, Miller *et al.* 2000, Hollister & Nadis 1998). Hazard from high-level nuclear reactor waste is initially due to the short-lived radionuclides ^{137}Cs (half-life 30.17 years) and ^{90}Sr (28.64 years), followed by ^{241}Am, ^{243}Am, ^{239}Pu, ^{240}Pu and ^{237}Np from 10^3 to 10^5 years. Afterwards, ^{99}Tc, ^{210}Pb, and ^{226}Ra dominate the remaining radioactivity that is equivalent to ore containing 0.2% U (Plant *et al.* 2005). Generally, the hazard of nuclear energy production is little different from other large-scale energy sources and the sum of benefits and risks may be best balanced by using all available technologies (Lovelock 2006).

2.6 SUMMARY AND FURTHER READING

A cursory inspection of this chapter reveals that the short lists of significant deposit types for specific metals are never identical. Even closely related metals such as iron and manganese, or lead and zinc exhibit substantial differences. Yet, if one would be asked to devise an ore-forming system for a certain metal, its geochemical properties should provide valuable clues. Many metals, for example, are redox-sensitive and their solubility and transport by aqueous fluids is limited either to a reduced (Fe, Mn) or an oxidized state (U, Mo). A drastic redox change immobilizes such metals. Other controls on ore formation include the tendency to form sulphides (Cu, Zn, Ag, Cd, In, Hg, Tl, Pb, Bi, As, Se, Sb, Te), their "volatility" (Hg, As, Sb, Te, Tl) and tendency for enrichment in extremely fractionated batches of felsic melts (Sn, W, Ta, Mo, U, Th, Rb, Cs, Li, Be). Geochemistry also helps to conjecture potential source materials for certain metals. If extraction by aqueous hot fluids is envisaged, basalt would be a favourable source of zinc and copper, whereas uranium and lead should be sought in granite. Clearly, geochemical study of ore formation is vital.

Yet, understanding the variety of physical constraints that are implicated in ore formation is not less important. Pressure and temperature gradients from the Earth's interior to the surface drive a flow of liquids and fluids, which is involved in ore formation. Mantle and crustal dynamics combine in the global process system of plate tectonics. Specific ore deposit types (e.g. copper porphyry) occur in well-defined settings. Yet, the apparently simple system of metal source, transport and trap displays an unlimited variety, modulated by very many factors. This is not to discourage the pursuit of ever better understanding but is a word of caution not to take my simplified presentation of the fascinating world of geochemical cycling and metal concentration for the full account.

More detailed geochemical information is provided in the *Encyclopedia of Geochemistry* by Marshall & Fairbridge (1999) and amplified in the voluminous *Treatise on Geochemistry* edited by Holland & Turekian (2003). To readers seeking more details concerning deposits mentioned in this book or additional examples, I recommend the extensive and systematic description of thousands of ore deposits worldwide by Laznicka (1985, 1993). Geodynamic controls of metallogeny can be studied in Blundell *et al*. (2005), based on the example of Europe. For a thorough presentation of geology and ore formation, the book by Guilbert & Park (1986) is unsurpassed. Berkman (2001) provides a blend of valuable scientific and very practical information (watch out for the next edition, which should appear in 2011). To my knowledge, there is no recent comprehensive book on environmental management of metal mines, but the two SEG volumes *The Environmental Geochemistry of Mineral Deposits* edited by Plumlee & Logsdon (1999a) and Filipek & Plumlee (1999) are very useful. The *Essentials of Medical Geology* edited by Selinus *et al*. (2005) offer a treasure-trove of relevant information. Production and resources figures, and concise information about use and market trends of single metals are available in the United States Geological Survey's *Minerals Information Webpages* (USGS 2010).

PART II

Non-Metallic Minerals and Rocks

Economic Geology Principles and Practice
Metals, Minerals, Coal and Hydrocarbons – Introduction to Formation and Sustainable Exploitation of Mineral Deposits, Walter L. Pohl
© 2011 Walter L. Pohl. Published 2011 by Blackwell Publishing Ltd.

CHAPTER 3

Industrial minerals, earths and rocks

Synopsis

Industrial minerals are valuable economic raw materials, which are not used in the production of metals or energy. Compared with metals and other non-metallic resources, they are mainly processed by physical methods. Both definitions, however, are not without exceptions and some attributions to the group are rather by tradition. Typical examples of industrial minerals are talc, mica and andalusite. Several ore minerals such as chromite, bauxite and rutile also have industrial applications, but the bulk of production feeds metallurgy. Industrial rocks and earths typically comprise multi-mineralic hard and unconsolidated rocks, which are mainly used in the construction industry (granite, sand, gravel, clay). Together with salts (Chapter 4), industrial raw materials form the class of non-metallic and non-energy rocks and minerals. Because of multiple and ever changing uses, and a wide genetic variety (cf. Table 3.1), neither supports a particularly illuminating subdivision of industrial minerals, rocks and earths. Therefore, the order in this chapter is simply alphabetical. The selection of about 30 materials is based on geological and economic interest.

Uses of minerals and rocks encompass all human activities, from the mundane (e.g. road building aggregate) to industry (refractories for steel-making), food production (apatite and sulphur) and high technology applications (quartz for electronics). In many cases, high-technology conversion of fairly common raw materials into refined products (e.g. micronized fillers in plastics) is the key to economic success. Therefore, market considerations are a major component from the exploration stage to evaluation and development of a deposit (Border & Butt 2001). Feasibility characteristically depends on successful industrial-scale production trials in cooperation with potential customers.

Economic data and facts were assembled from *Mining Journal, Mining Magazine, Mining Annual Review*, Berkman (2001), Neuendorf *et al.* (2005), *United States Geological Survey (USGS minerals information webpages)* and Walker & Cohen (2007). Discrepancies concerning details are not rare between different sources. Therefore, where highest accuracy is sought, I advise the reader to verify critical data.

Economic Geology Principles and Practice
Metals, Minerals, Coal and Hydrocarbons – Introduction to Formation and Sustainable Exploitation of Mineral Deposits, Walter L. Pohl
© 2011 Walter L. Pohl. Published 2011 by Blackwell Publishing Ltd.

Table 3.1 Exemplary genetic classification of non-metallic mineral deposits

I. Magmatogenic Mineral Deposits
  1. Orthomagmatic Deposits:
    Apatite as a coproduct of titanium ore (nelsonite) of Mesoproterozoic anorthosite-ferrodiorite complexes and in apatite-magnetite ore; olivine (dunite) associated with ophiolites and ultramafic intrusions; apatite and limestone in carbonatite; apatite nephelinites in alkali complexes; alkali feldspar in granite
  2. Pegmatites:
    Mica, K-feldspar, amblygonite, spodumene and petalite; chemical, electronic and optical quartz; various gemstones and valuable crystals of many rare minerals; apatite schlieren in carbonatite
  3. Skarn and Contact-Metasomatic Mineral Deposits:
    Andalusite, asbestos, boron, fluorite, graphite, magnesite, talc, wollastonite
  4. Magmatic-Hydrothermal Deposits:
    Vein deposits of amethyst, barite, fluorite, talc; rock bodies resulting from hydrothermal alteration. i.e. alunite, kaolin, pyrophyllite, trass; protoliths of kyanite quartzites; phlogopite, sericite, vermiculite
  5. Volcanogenic Mineral Deposits:
    Barite of VMS deposits; diamond in kimberlite and lamproite; native sulphur
II. Supergene Mineral Deposits
  1. Residual and Eluvial Deposits:
    Residual placers of diamond, kyanite, sillimanite; phosphate-rich soil ("phoscrete") above carbonatite; bauxite and kaolin blankets on aluminous silicate rocks; bentonite on mafic igneous rocks; asphalt forming at oil seeps
  2. Infiltration Deposits:
    Barite and fluorite of karst infiltration origin; magnesite in alluvial sediments; evaporative brines of playa lake basins (e.g. boron, iodine, lithium, soda)
III. Sedimentary Deposits
  1. Allochthonous:
    Gravel, sand and certain clays (kaolin); alluvial and coastal placers (diamond, andalusite, kyanite, sillimanite); volcaniclastic rocks
  2. Autochthonous:
    Coal, oil shale, diatomite, phosphorite and most limestones; evaporites (rock salt, potassium salt, gypsum/anhydrite, borate minerals, trona and other salts in playa lakes); sedex barite; bentonite, zeolites
IV. Diagenetic Mineral Deposits
  1. Petroleum, natural gas, liquid native sulphur
  2. Sulphur in sulphate cap rocks of salt diapirs
  3. Mississippi-Valley type barite-fluorite in marine carbonates
  4. Saline brine-related deposits:
    Emerald in black shales; dolomite and magnesite in marine carbonates
V. Metamorphic Deposits:
  Graphite, sericite, muscovite, emery, andalusite, kyanite, sillimanite, quartzite
VI. Metamorphogenic-Hydrothermal Deposits: Asbestos, magnesite and talc in ophiolites; vein graphite (Sri Lanka).

3.1 Andalusite, kyanite and sillimanite

Andalusite, kyanite and sillimanite are chemically identical (Al_2SiO_5) but structurally different minerals. Their use is very similar, based on refractory properties, an intermediate content of alumina (50–63%) and intermediate basicity (between quartz and magnesia). Untreated and calcined concentrates of these minerals are mainly used in the iron and steel industry and in manufacturing special ceramics. Today, sillimanite is the least traded of the three minerals. Historical predominance, however, bequeathed us the commercial term "sillimanite minerals". The calculated Al_2O_3-content of the three minerals is 62.9%. In practice, market products have less Al_2O_3 because of inclusions of other minerals that cannot be removed by physical processing. Traded concentrates should have 56–60 wt. %Al_2O_3, Fe_2O_3 <1% and very little alkalis. Coarse-grained products command higher prices.

The thermal expansion of andalusite and sillimanite (6 and 4 vol. %, respectively) is so small that the uncalcined minerals can be used directly for blocks and mortars applied as an inner cladding of furnaces. Kyanite, however, expands by 16–18 vol. % and has to be calcined before application. In some instances, raw kyanite can be useful, for example when shrinkage of clay upon burning is to be compensated. Calcining at temperatures between 1100 and 1650°C converts the natural $Al_2O_3 \cdot SiO_2$ to a mixture of 88 wt. % needle-shaped crystals of mullite ($3Al_2O_3 \cdot 2SiO_2$, density 3.17 g/cm^3) and 12 wt. % SiO_2 (cristobalite, or glass). Up to a temperature of ~1810°C, mullite is very stable under thermal, chemical and mechanical stresses. Due to these properties, mullite is used to line furnaces for the production of iron, steel, other metals, glass, ceramic products and cement. Mullite is also synthesized in large quantities by mixing and calcining kaolin + bauxite or quartz + alumina. Natural occurrences of mullite are known (Mull, Scotland) but are too small to warrant economic interest.

The aluminosilicates andalusite, kyanite and sillimanite are **metamorphic minerals**, which formed in aluminium-rich rocks by orogenic or contact metamorphism (Holdaway 1971). Average pelites have Al_2O_3-contents of 14–17%, similar to most igneous rocks, except ultramafics (e.g. 1.82% in dunite). Higher contents are found in anorthosite (average 25.86%) and nepheline syenite (21%). The Al_2O_3-enrichment required for economic exploitability in many deposits (>20% to 40%) is an interesting scientific question that is not always easy to answer. The metamorphic veil often hides evidence about the origin of the precursor rock (Ihlen 2000). One known agent of aluminium concentration is surficial weathering (cf. Chapters 1.2 "Supergene Ore Deposits" and 2.4 "Aluminium"). Former kaolin-rich soil horizons or sands may be one genetic explanation. Kaolin also is formed by hydrothermal alteration in granitic and felsic volcanic environments and these altered rocks are possible precursors, too. Investigations of Norwegian kyanite quartzites favour the latter hypothesis, substantiated by very low content of alkalis that are always present in sedimentary quartzite (Müller *et al.* 2007). In deep shear zones of high metamorphic grade, fluids may transform common granitoids into strongly peraluminous ($Al_2O_3 > NaO + K_2O$) kyanite mica schists (Sassier *et al.* 2006). Metamorphic fluids concentrate aluminium by preferential leaching of SiO_2 and alkalis. This is favoured by elevated fluorine contents (Nabelek 1997). Hydrothermal kyanite in quartz veins is rather rare, because of the low solubility of Al in aqueous fluids (Bucholz & Ague 2010).

Mutual pseudomorphic replacement of the three closely related minerals is very common and is a function of the metamorphic P/T/time path. With rising pressure, andalusite is replaced by kyanite and both by sillimanite, when the temperature increases. Retrograde metamorphism results in muscovite replacing the aluminium silicates. The extent of pseudomorphism or replacement may be one of the controls of product quality.

All three alumosilicate minerals occur in alluvial placers, which were formerly important sources. At present, kyanite and sillimanite are locally significant by-products of coastal placer mining.

3.1.1 Andalusite

Andalusite (density 3.16–3.20 g/cm^3) occurs in contact-metamorphic metapelites of the heated aureole of magmatic intrusions and in low-pressure amphibolite facies metasediments (Bucher & Frey 2002). Undesirable inclusions in andalusite include staurolite, chloritoid, biotite, sericite, graphite, Fe-oxides and TiO_2. The main producer of andalusite is South Africa, from the vast contact zone of the Bushveld Complex. Initially, the mineral was exploited from alluvial placers. Today, hard rock mining of primary deposits prevails (Siegers & Lange 1991). The second major producer is France with the Glomel mine in the Bretagne. Ordovician slates in the contact zone of a granite intrusion contain ~15 wt. % andalusite in large porphyroblasts (1–4 by 10–40 mm). The run-of-mine ore is crushed and pulverized. From this, andalusite

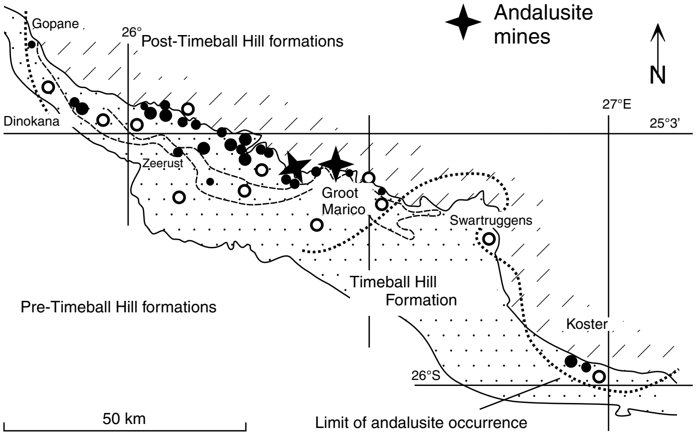

Figure 3.1 Andalusite in the northwestern thermal contact zone of the Bushveld Intrusive Complex (modified from Hammerbeck 1986). Courtesy Geological Society of South Africa. Black circles denote andalusite contents in weight percent: <5%, 5–10% and >10%.

is concentrated by flotation, high-intensity magnetic and heavy media separation:

> Near Groot Marico in the Northwest Province of South Africa, the Timeball Hill Formation of the Palaeoproterozoic Transvaal Series hosts andalusite deposits. However, only pelitic metasediments within certain metamorphic subzones characterized by index minerals are prospective (Figure 3.1), including zone A (chiastolite, biotite, cordierite, epidote, minor andalusite) and zone B (chiastolite and biotite). Zone C (biotite plus minor andalusite) and zone D (spotted slate) are not favourable. Chiastolite is a variety of andalusite with dark carbonaceous inclusions forming a cruciform design.

Andalusite is generally preferred to kyanite, because it can be used without calcination, thus saving energy. Most of the world production of andalusite in 2009 originated from South Africa (260,000 t) and France (65,000 t). The development of new mines depends mainly on markets, because andalusite-bearing contact aureoles are not rare.

3.1.2 Kyanite

Kyanite (density 3.55–3.66 g/cm^3) is common in aluminous metasedimentary and meta-igneous rocks that experienced medium-pressure and medium-temperature orogenic metamorphism (Bucher & Frey 2002). Metamorphic host rocks of kyanite are quartzite, schist and gneiss containing kyanite as porphyroblasts or in crystalline masses. Secretion quartz veins developed by dehydration reactions in these rocks and certain pegmatites can also be enriched with coarse-grained kyanite. Minimum exploitable grades of hard-rock kyanite deposits are ~20 wt. %. Muscovite and garnet are often associated with kyanite and can be economically important co-products. Kyanite contains abundant solid inclusions (e.g. muscovite) that influence its value. In the surficial weathering environment, kyanite is very stable and as a heavy mineral, it is enriched in alluvial and coastal placers:

> Large primary kyanite deposits occur in the eastern USA. At Henry Knob in South Carolina, a thick bed of quartzite interbedded with Precambrian gneiss had contents of ~20% kyanite (and pyrite) over a strike length of several kilometres. Most of today's world production of kyanite is derived from the Willis Mountain mine in Virginia, USA (2009 ~80,000 t after 115,000 t in 2008). Indicated reserves at Willis Mountain amount to 65 Mt at 25% kyanite. Together with many smaller occurrences, Willis Mountain forms a "kyanite belt" within the central Virginia volcanic-plutonic province. Country rocks include Palaeozoic mafic to felsic volcanic rocks, volcaniclastic metasediments, granites and tonalites. Kyanite quartzites

are thought to have originated by severe leaching in high-sulphidation (advanced argillic) alteration systems, resulting in quartz-kaolin protoliths (Owens & Pasek 2007).

Small quantities of kyanite are produced in India, Simbabwe, Brazil, Sweden, Spain, Russia, Ukraine and China. Indian kyanite was renowned for its large grain size, but export ceased because of dwindling reserves. In Russia, deposits are hosted by Archaean metasediments of the Kola Peninsula. Apart from kyanite, the ore schists contain quartz, sillimanite, staurolite, muscovite and graphite. Exploitable high-grade lenses with >20% kyanite occur over a strike length of 200 km of the schist zone. Several potential deposits are known in the East African Mozambique belt, a complex Neoproterozoic orogen. In Kenya, eluvial placers of kyanite were exploited at Murka Hill near Voi Township until 1960. On the ridge, the source kyanite quartzites contain dispersed high-grade pockets. Today, the former mine lies within Tsavo National Park.

3.1.3 Sillimanite

Sillimanite (density 3.23 g/cm^3) occurs in many metasedimentary rocks that experienced low- to medium-pressure and high-temperature orogenic or contact metamorphism (Bucher & Frey 2002). Typical rocks that may have exploitable sillimanite grades are biotite-sillimanite hornfels, cordierite-sillimanite gneiss and quartz-mica-sillimanite schists. Lateral secretion quartz veins in these rocks and, rarely, in pegmatites, can be enriched with coarse-grained sillimanite. However, exploitable grades of hard rock sillimanite are infrequent. Consequently, sillimanite has the least significance of the aluminosilicates. The mineral is probably exploited in China in order to supply refractories to its steel industry but statistics are not published. In India it is a by-product of coastal placer mining (~24,000 tonnes in 2009). Very small quantities of the formerly famous sillimanite-corundum "balls" from Assam are still traded. In South Africa, minor sillimanite production is derived from the contact halo of the Bushveld Igneous Complex.

3.2 ASBESTOS

		Density (g/cm^3)
Chrysotile asbestos ("white asbestos")	$Mg_3Si_2O_5(OH)_4$	2.5
Crocidolite asbestos ("blue asbestos" or "Cape blue", a variety of the amphibole riebeckite)	$Na_2(Fe^{2+}, Mg)_3 Fe_2{}^{3+}Si_8O_{22}(OH)_2$	3.2
Amosite asbestos ("brown asbestos"; the formula describes grunerite)	$(Fe{>}Mg)_7 Si_8O_{22}(OH)_2$	3.1–3.25

Generally, the commercial and industrial term asbestos refers to minerals of the serpentine and amphibole groups that occur as bundles of thin, flexible and separable fibres. All asbestos minerals are characterized by a length to width ratio (the "aspect ratio") of >100:1. "Amosite" is a trade name; mineralogically it may consist of anthophyllite, grunerite, gedrite or cummingtonite. Tremolite and actinolite are other common amphibole minerals that may occur in asbestiform varieties. Exploitable asbestos ore typically contains 5–6 wt. % fibres with a length of 20 mm.

For over 4000 years, asbestos was considered as a magic safeguard against fire. Only a few decades ago, its hazards for human health were discovered. When handled, for example in asbestos board manufacturing, asbestos fibres disintegrate readily and release microscopic needle-like particles. Inhalation of these particles causes a number of serious respiratory diseases and other health problems, especially benign and malignant lung diseases (Kane 1993, Gibbons 2000, Selinus *et al.* 2005). Therefore, mining and the use of asbestos in industrial countries have been virtually terminated. Naturally occurring asbestos exposed by weathering and erosion always caused a background of asbestos fibres in the air. Human intervention (e.g. road building, quarrying and agriculture) may locally aggravate the risk. Authorities should identify rock bodies that contain asbestos and if needed, establish control measures such as suppression of dust during excavation and farming (Van Gosen 2007). Exposures of naturally asbestos-bearing rocks can be detected by airborne spectral mapping (Swayze *et al.* 2009). There is no evidence that ingestion of asbestos with drinking water is hazardous to health (WHO 2006). Note, that blue asbestos poses a much greater health hazard than chrysotile.

Useful properties of asbestos include resistance against heat (permanent temperatures of 400°C and peaks to 1000°C) and many chemicals, as well as low conductivity of heat and electricity. Chrysotile asbestos made up >90% of past asbestos production and represents >99.5% of remaining world production, due to termination of amphibole asbestos exploitation. For some applications, fibre length and tensile strength are important. Asbestos' exceptional insulation and fire-resistance properties have been used in numerous products and industrial applications (e.g. tiles for Space Shuttle Columbia). An important sector of asbestos use is the building industry, because many countries with a rapidly growing population continue to use low-cost asbestos cement for roofing and water pipelines.

3.2.1 Asbestos mineralization types

Asbestos deposits include (1) hydrothermal veinlet stockworks in ultramafic rock bodies, (2) hydrothermal stockworks in mafic intrusive or extrusive rocks, and (3) hydrothermal-metasomatic alteration of iron formations. Asbestos occurrences of minor economic role are (4) hydrothermal veinlets in contact-metamorphic dolostone and (5) metasomatized alkalic intrusions (Libby, Montana) and carbonatites (Mountain Pass, California). In most cases, either contact or orogenic metamorphism established the hydrothermal systems, but magmatic fluids are equally capable of producing asbestos. Essentially, a suitable combination of chemical rock composition, pervasive rock fracturing, silica-bearing fluids and favourable (commonly lower greenschist facies) T/P-conditions cause formation of asbestos minerals.

Ultramafic-hosted asbestos deposits

These are complex stockwork mineralizations in partially or totally serpentinized dunite, peridotite or pyroxenite. With exceptions (e.g. Zimbabwe: Great Dyke; South Africa: Barberton Greenstone Belt), these rocks are parts of ophiolite sheets. Extensional fracturing of the rock bodies, possibly during ophiolite obduction, allowed access of mineralizing fluids. High fluid pressures and pure extension favour formation of valuable "cross fibre" veinlets, where fibre growth is vertical to the walls of the fracture. Shear-hosted "slip fibre" or unoriented "mass fibre" have low value. Chrysotile, like most of the asbestos minerals, forms under P/T-conditions of the lower greenschist facies. Because low-T hydrothermal chrysotile excludes iron very efficiently, magnetite is a frequent by-product of the rock-fluid reaction producing chrysotile. Average olivine with a composition of $Fo_{90}Fa_{10}$ transforms into serpentine with 5–10 vol. % magnetite (eq. 3.1).

Chrysotile asbestos formation (serpentinization) from olivine:

$$\underset{\text{Forsterite}}{2Mg_2SiO_4} + 3H_2O \rightarrow \underset{\text{Chrysotile}}{Mg_3Si_2O_5(OH)_4} + \underset{\text{Brucite}}{Mg(OH)_2}$$

$$\underset{\text{Fayalite}}{3Fe_2SiO_4} + O_2 \rightarrow \underset{\text{Magnetite}}{2Fe_3O_4} + 3SiO_{2aq}$$

$$3Mg_2SiO_4 + SiO_{2aq} + 2H_2O \rightarrow 2Mg_3Si_2O_5(OH)_4 \tag{3.1}$$

Mines processing ultramafic-hosted ore (e.g. Ni, Cr, asbestos) sequester enough carbon dioxide from the atmosphere to more than offset greenhouse gas emissions from operations. This is due to the formation of carbonates in tailings (Wilson *et al.* 2009).

The largest (or after the Ural Mountains in Russia and Khazachstan, the second largest?) chrysotile asbestos deposits in the world were exploited near Thetford in Quebec, Canada. They occur in harzburgitic mantle of Ordovician fore-arc ophiolites near the western margin of the Appalachian orogen (Pagé & Barnes 2009, Hébert & Bédard 2000; Figure 3.2). Mining was terminated in 2003.

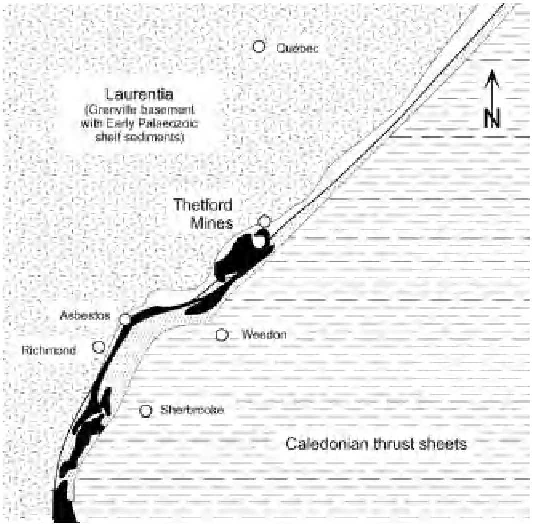

Figure 3.2 The asbestos-rich ophiolite (black) near Thetford south of Québec, Canada highlights the suture of Iapetus Ocean closed by the collision between Caledonian nappes and the Laurentian continent (after Hébert & Bédard 2000, La Chronique de la recherche minière). © by permission of BRGM, www.brgm.fr.

Asbestos deposits related to Precambrian banded iron formations (BIF)

Asbestos deposits related to BIF were mined extensively in South Africa until closure a few years ago. Large deposits occur in the Palaeoproterozoic Transvaal Supergroup:

> Amosite asbestos (grunerite) was exploited in the Penge area in northeastern Transvaal province. Certain horizons of the Penge Iron Formation are mineralized at tectonic highs (domes) that were formed by the interference of two fold systems. The later phase of folding and a regional thermal metamorphism are thought to be related to the Bushveld intrusion (Beukes & Dreyer 1986a). In this area, rosettes and ubiquitous thick prismatic masses of grunerite are regional products of metamorphism. Asbestos was only formed where syn-metamorphic folding and doming provided low-pressure domains that attracted fluids. Asbestos orebodies had a thickness of a few metres only, but a horizontal extension of 3 by 1.5 km. Fibre length reached 76 cm.
>
> The South African crocidolite asbestos deposits occur along a distance of 400 km in a belt between Prieska and Botswana. Here also, the deposits are controlled stratigraphically by iron formations of the Transvaal Supergroup. The largest mine was Pomfret near the Kalahari Desert. Thin beds with an extension of 1.5 by 2 km were exploited. The sodium of the riebeckite-like asbestos was probably derived from mafic tuffs that are intercalated with the iron formation (Beukes & Dreyer 1986b). Fibres were short (1–18 mm) and structurally controlled by competent bands of the iron formation, similar to saddle veins. The asbestos ore rock contained ~12 wt. % of fibres. Processing included crushing, airlifting the fibres and classifying different grades. Nearly the whole production was used for manufacturing asbestos cement.

Main producers of asbestos are Russia (50%), China, Brazil, Khazachstan, Canada and Zimbabwe. Because of regulations, production in most western industrial countries was terminated. World production in 2009 amounted to ~2 Mt (USGS 2010). Asbestos is substituted by wollastonite (cf. "Wollastonite"), ceramic, glass and steel fibres, and with fibres made from carbon, cellulose and synthetic organics. Most of these materials are too expensive for roofing and similar applications in buildings, explaining why asbestos continues to be used in less affluent countries.

3.3 Barite and celestite

		Density (g/cm^3)
Barite	$BaSO_4$	3.9–4.5 (calculated 4.468)
Witherite	$BaCO_3$	4.3

Nearly 300 minerals are known to include barium, but barite and witherite are the only natural resources used by industry. In its crystal structure, barite readily incorporates strontium (0.1–5%), lead (0–0.2%, usually ~0.17%) and calcium ($CaCO_3$ 0–5%, usually 2.8%). Often, barite is associated with Pb-Zn sulphides, fahlore, manganese oxides, stibnite, fluorite, carbonate and quartz. Some of these may be co-products of barite mining. Elevated trace contents of mercury are common in barite and have to be controlled during processing and marketing.

Barite is a low-cost mineral and is mainly extracted in open pits. Underground exploitation may be economically feasible if the material is of high quality (e.g. for white filler or medicinal blanc-fixe production). Veins should have a minimum thickness of 2 m and the deposit must include at least 0.4–1 Mt $BaSO_4$. Generally, a high content of $BaSO_4$, high density and whiteness facilitate marketing processed barite.

Barite is heavy, non-abrasive, inert, non-corrosive, insoluble and non-toxic. This qualifies the mineral particularly for use in the petroleum and natural gas industry. More than 85% of world barite production is employed for regulating the density of drilling fluids by adding finely ground (micronized) barite to a maximum of 40% by weight of the fluid. For similar reasons, heavy concrete is made with barite. It also serves as a non-abrasive, dense and chemically inert filler in plastics, paper, rubber and paints and, due to its high adsorption capacity for hard radiation, as a shield in nuclear reactors, X-ray laboratories and in faceplate glass for television cathode ray tubes, but not in flat-panel monitors. Barium chemicals are made by reduction of barite with coal or coke to produce barium sulphide ("black ash"), which is reacted to form chloride, hydroxide or carbonate. Chemically precipitated $BaSO_4$ (blanc-fixe) is employed in medicinal X-ray diagnostics and increasingly in paints and other specialized fields. Witherite and technical barium carbonate are useful additions in glass and ceramics (as a flux), and in chemicals, ferrites and photographic papers.

Strontium is chemically similar to calcium and barium, and is part of group 2 (alkaline earths) of the periodic table of the elements. Strontium consists of four stable isotopes, but only the ratio $^{87}Sr/^{86}Sr$ is commonly employed in geological investigations. ^{87}Sr is composed of a primordial and a radiogenic component from the decay of ^{87}Rb (Schreiber & Tabakh 2000, cf. Chapter 1.1 "Isotope Geochemistry"). In the environment, strontium is harmless. The nuclear fall-out isotope ^{90}Sr (half-life 28.9 years) is dangerous, however, but is also used in cancer therapy. Natural celestite (also called celestine, $SrSO_4$, <43.88% Sr, density 3.9 g/cm^3) and rarely, strontianite ($SrCO_3$, density 3.8 g/cm^3) are processed into a range of strontium chemicals, which are essential in many products. Previously, strontium was merely regarded as a provider of red colour in fireworks and signals. At present, consumption is growing fast because many applications of strontium carbonate are similar to those of barium carbonate (see above) but strontium is often preferred. Strontium metal (density 2.64 g/cm^3, melting point 777°C) is alloyed with aluminium and silicon for improved casting, for example of car engines. The only source of strontium occurring in large exploitable deposits is celestite. Celestite deposits are mainly associated with evaporites (Figure/Plate 3.3), more rarely with carbonates and other rocks.

Celestite deposits are typically stratiform, but various features suggest a replacement origin during diagenesis, as in Coahuila State, northeastern Mexico. These stratabound celestite deposits occur in Mesozoic sediments close to horst structures. Homogenization temperatures of fluids vary from 50 to 160°C, salinities from 0 to 19 wt. % NaCl equivalent pointing to basinal brines, which leached Sr from basement-derived clastic rocks and precipitated celestite upon mixing with meteoric waters. Together with deposits and numerous occurrences of Zn, Pb, Ba and F, the Coahuila strontium deposits are considered as one of the nearly two dozen Mississippi Valley Type provinces of North America (Gonzáles-Sánchez *et al.* 2009). Low-temperature hydrothermal epigenetic veins and veinlets occur in limestone (e.g. Cyprus). The largest producing celestite district is Granada in southern Spain with the Escúzar and Montevives mines in Tertiary basins of the Betic cordillera. In this district, diagenetic celestite occurs in beds of gypsum and stromatolitic limestone of a flat-lying Late Miocene (Messinian) sequence. Strontium was probably mobilized during early diagenesis by the conversion of gypsum to anhydrite (cf. "Gypsum and Anhydrite"). The world production of strontium amounts to 500,000 t (2008). Main producing countries are Spain, China and Mexico (USGS 2009).

3.3.1 Geochemistry

Barium is lithophile and closely related to calcium, strontium and radium. Like lead, Ba^{2+} (ionic radius 1.35 Å) replaces K^+ (1.38 Å) as an incompatible LIL-element in many rock-forming minerals to contents of several percent. Basalts contain ~250 ppm, whereas felsic magmatic and clastic sedimentary rocks attain 600 ppm Ba. Its crustal average is 430 ppm Ba (Sr 350 ppm) with a range of 179–1070 (Sr 150–480 ppm; Smith &

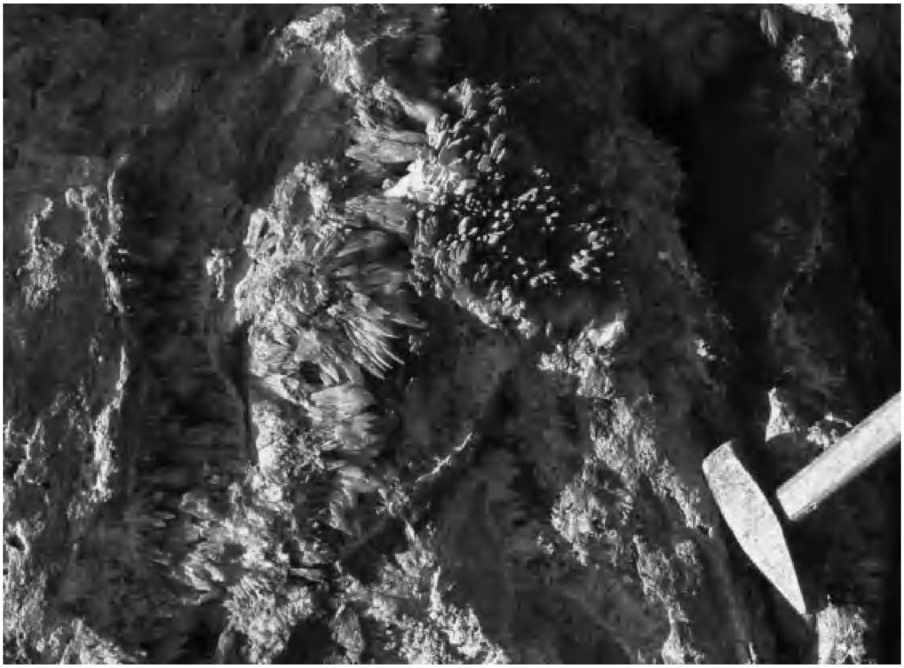

Figure 3.3 (Plate 3.3) Celestite crystals in roughly bedding-parallel solution cavities of Neogene gypsum at Wadi Essel, Red Sea Coast, Egypt.

Huyck 1999). Barite forms in the seawater column and its accumulation in bottom sediment corresponds with biological productivity. Relative to aluminium, barium (or barite) is enriched in pelagic sediments of highly productive seas. During weathering, diagenesis, metamorphism and hydrothermal processes such sediments are a ready source of barium. Reduced and acidic conditions facilitate barium mobilization from rocks (Cooke *et al*. 2000). Therefore, barite deposits are common and barite is a frequent gangue mineral in hydrothermal mineralization. In hydrothermal solutions, the element is transported in the form of chloride complexes such as $BaCl_{2(aq)}$. Upon encountering SO_4^{2-} ions (e.g. oxidized brines or seawater) barite is precipitated. Witherite forms at lower oxygen fugacity and alkaline conditions ($pH > 8$). Witherite and barite are resistant against weathering and nearly insoluble in water and dilute acids, so that outcropping deposits are marked by strikingly white exposures and boulders. Some dissolution may take place, however, caused by sulphate-reducing microbes (Bolze *et al*. 1974). Because of their low solubility, barite and witherite are not hazardous, but all soluble compounds of barium are toxic, especially the chloride. For application as a rat poison, the chloride used to be prepared from witherite.

$SrSO_4$-concentrations in barite may assist genetic interpretation. Because celestite and barite are isostructural, a complete solid solution series exists between both minerals, although most samples plot near one end or the other of the series. Higher $SrSO_4$-contents in barite appear to characterize hydrothermal veins formed at elevated temperatures, whereas synsedimentary and early diagenetic barite contains little strontium. Because barite is practically free of rubidium, the isotopic ratio $^{87}Sr/^{86}Sr$ of barite generally represents the composition of the host fluid at the time of mineral formation. This allows the distinction of two groups of stratiform barite (Maynard *et al*. 1995). The first is associated with Pb-Zn ore and displays clearly radiogenic Sr (implying derivation from continental crust),

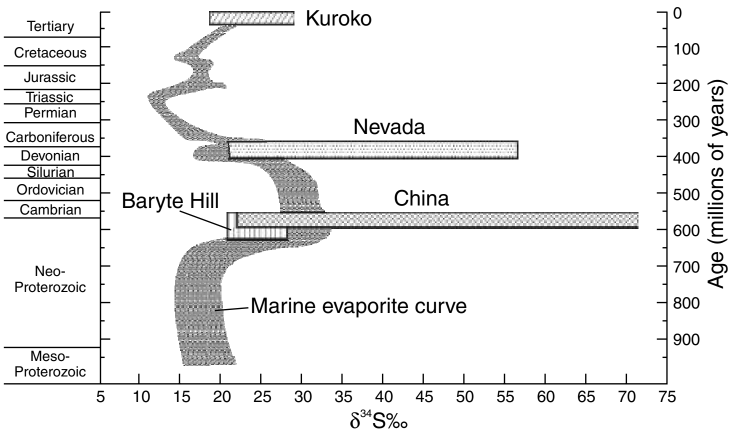

Figure 3.4 Sulphur isotope characteristics of marine stratiform barite deposits compared with standard seawater sulphate $\delta^{34}S$ (after Clark *et al.* 2004 with permission from Elsevier).

whereas the second is unrelated to base metals and has a low $^{87}Sr/^{86}Sr$ ratio inherited from a rubidium-poor source (e.g. oceanic crust). Of course, sulphur and oxygen isotope data on barite also support genetic investigations (Paradis & Lavoie 1996, Paytan *et al.* 2002, Johnson *et al.* 2004). As a general rule, both modern biogenic trace barite in marine sediments and volcanic-hydrothermal deposits (Kuroko, Baryte Hill, South Carolina) display sulphur isotope characteristics near contemporaneous seawater, whereas sedex barite often contains very heavy sulphur (Figure 3.4). This is due to microbial sulphate reduction (cf. "Sulphur"), which results in enrichment of isotopically heavy SO_4-ions in closed basin waters and in pore fluids of sediments during early diagenesis. The resulting light H_2S may escape as a gas or form pyrite (Clark *et al.* 2004). Metamorphism can affect both Sr-contents and the isotopic composition (Sr, S, O) of barite (McClung *et al.* 2007).

3.3.2 Barite deposit types

Barite deposits are almost exclusively the result of hydrothermal fluids convecting in the shallow crust. However, the basic chemical model of barite precipitation involving a geochemical redox barrier (reduced fluids with dissolved barium mix with oxidized waters containing SO_4^{2-}) also allows formation of barite by infiltration (cf. Chapter 1.2 "Supergene Ore Formation Systems"). Reduced migrating meteoric water may take up barium during weathering and eventually deposit barite. Examples of this genetic model include karst barite (Sardinia), stratabound barite in evaporites and in red sandstone. At submarine "cold methane seeps" of continental slopes, sulphide-poor barite sinters are formed, which resemble certain Palaeozoic barite deposits (Torres *et al.* 2003). Ranked according to economic importance (Clark *et al.* 1990), the following genetic types of barite deposits are discerned:

- diagenetic-hydrothermal submarine sedex barite deposits (e.g. the barite and witherite province of southern China);
- volcanogenic-hydrothermal exhalative submarine barite (associated with VMS orebodies, e.g. Kuroko Type);
- epigenetic-hydrothermal barite veins, hydrothermal karst cave fill and metasomatic barite masses in carbonates (commonly diagenetic-hydrothermal; e.g. Silvermines, Ireland, and the Appalachian district in southwest Quebec: Paradis & Lavoie 1996);
- epigenetic-hydrothermal barite veins in non-carbonate host rocks (e.g. schist and greywacke at Bad Lauterberg, Germany);
- terrestrial, hydrothermal-exhalative barite deposits (comparable to travertine sinter, e.g. Les Redoutières, France);
- infiltration barite in karst (Sardinia, Fleurus, Belgium);
- evaporite-hosted barite deposits (e.g. Pessens, France);
- residual barite placers formed by supergene alteration of outcropping deposits.

Submarine, hydrothermal-exhalative barite deposits

These deposits can be very large. Commonly, barite is a co-product of base metal mining. Barite is either part of the ore paragenesis or occurs as a separate nearly monomineralic seam. Kuroko (Figure 1.46) and sedex deposits (China, Nevada, Alaska, Figs. 1.71, 1.73) are prominent types. In chemical sedex stratification, barite occurs with galena or follows immediately after galena. This may be due to zone refining by redissolution of barite in the sulphide zone and precipitation on encountering sulphate. The volcanic environment of the Greek island of Milos seems to recall Kuroko features. However, barite at Milos occurs in the form of beds, tubular and irregular masses that replace Pliocene volcanic tuff. Nearby kaolin deposits clearly point to the transitional position of mineralization from marine to terrestrial and epithermal. Sulphide-poor barite deposits in marine black shales and chert, such as those of South China and Nevada, were probably formed in a setting comparable to recent submarine barite sinters, which form at seeps of cold methane-rich pore waters on passive continental slopes (Figure 3.5, Torres *et al.* 2003):

> Barite and witherite deposits of southern China occur in sequences of Neoproterozoic-Cambrian marine black shales and chert, those of Nevada in comparable sediments of Ordovician-Devonian age. In both regions, the host sediments formed on submarine continental slopes. The conspicuous linear arrangement of deposits implies a control by synsedimentary faults (Clark *et al.* 2004). One of the largest sedex barite deposits on Earth is Mangampeta in southern India, with ~37 Mt of reserves. Giant accumulations of Mississippian-age sedex barite associated with the largest known massive sulphide deposits (Red Dog district, Figure 1.73) have been found in the western Brooks Range, Alaska. They contain as much as 2000 Mt barite. At present, however, these geological resources are clearly second to the metal potential of the region.

Hydrothermal barite veins

An example for hydrothermal barite veins, in this case formed from basinal fluids, is the Wolkenhügel mine near Bad Lauterberg in the German Harz Mountains:

> The mine exploited a thick steeply dipping vein over a length of 1100 m and a depth of 350 m. The economic section is but a small part of the total exposed length of the vein structure (8.5 km). The mine was worked from 1838 to 2007, with a total production of ~4 Mt of barite. Host rocks include Devonian and Early Carboniferous greywacke, shale and siliceous limestone. Near the vein, these rocks are variously bleached, silicified, carbonatized and chloritized. The vein displays two different parageneses. The hanging-wall part consists of crumbly quartz and carbonate, which remained after leaching of

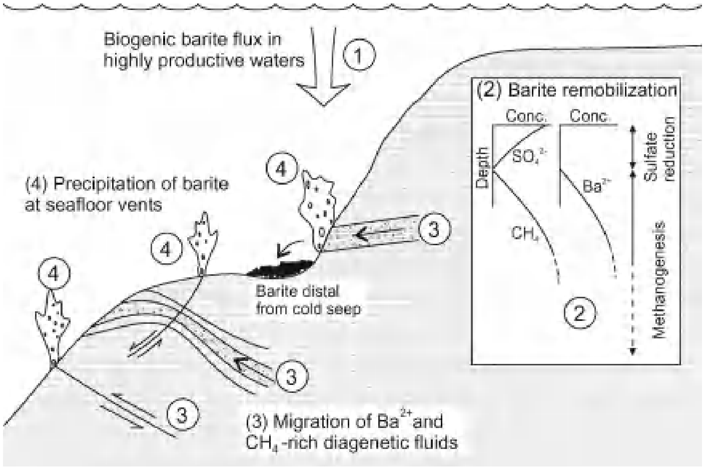
Biogenic barite flux in highly productive waters
①
(2) Barite remobilization
Conc.
Conc.
Depth
SO_4^{2-}
Ba^{2+}
CH_4
Sulfate reduction
Methanogenesis
②
(4) Precipitation of barite at seafloor vents
④
④
④
③
③
③
Barite distal from cold seep
(3) Migration of Ba^{2+} and CH_4-rich diagenetic fluids

Figure 3.5 Submarine formation of barite deposits by venting of early-diagenetic barium and methane-rich fluids on the sea floor ("cold seeps", Torres *et al.* 2003). 1 – Biogenic barite production in the water column of coastal upwelling zones; 2 – Mobilization of sediment-hosted trace barium by reduction and methanogenesis; 3 – Migration of fluids with dissolved barium and methane in permeable sediments or faults; 4 – Precipitation of barite by mixing of diagenetic fluids with seawater at seepage vents on the sea floor, formation of "milky-white smokers", sedimentation, possible mechanical erosion and redeposition of barite.

> anhydrite cement. The footwall part of the vein consists essentially of massive and banded coarsely crystalline barite with some quartz, carbonate and traces of sulphides (chalcopyrite, pyrite, tetrahedrite). Barite thickness reaches 30 m. Run-of-mine ore assayed 89% $BaSO_4$, 3.4% $SrSO_4$, 6% SiO_2 and 1% $CaCO_3$. The deposit formed during a Late Cretaceous tectonic phase that activated faults and induced convection of meteoric water. On the downflow path, the water dissolved overlying Permian salt. Barium was leached at depth and concentrated in the upflow limb, where the hot brine mixed with cool sulphate solutions.

Terrestrial barite sinter (hot springs) deposits

Genetically interesting as well as economically significant was the terrestrial barite sinter (hot springs) deposit of Les Redoutières near Chaillac on the northwest margin of the French Massif Central (Sizaret *et al.* 2004):

> Here, migmatites of the Variscan basement are transgressively overlain by coastal red sands of earliest Liassic age (203 Ma). In a shallow basin, these sands contained a stratiform barite deposit, which reached 20 m thickness and comprised ~4 Mt of $BaSO_4$. The mine closed in 2006. The ore bed displayed both horizontal and vertical zonation (Figure 3.6). Thin banding of red to yellow barite and brown goethite was characteristic, the latter becoming more abundant upwards. The banding was affected by synsedimentary brecciation and by deformation due to dehydration and gravitational consolidation of the hydrothermal precipitates. On the eastern side of the barite deposit, a near-vertical fluorite (-barite-) vein (Rossignol) had been mined until recently. In this vicinity, the barite sinter displayed an elevated content of fluorite. Obviously, both vein and surficial sinter deposits were derived from one hydrothermal convection system. The sinter formed by mixing of Ba-F-fluids (110°C, 21% NaCl equiv.) of deep origin with surficial SO_4-solutions (Ziserman 1980). A genetic relation to intensified heat flow, early rifting and extensional strain associated with the opening of the Atlantic Ocean is assumed.

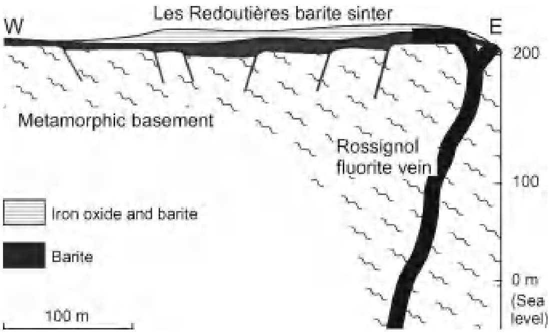

Figure 3.6 Section of Early Jurassic barite sinter deposit Les Redoutières near Chaillac, France, formed from hydrothermal solutions ascending through Rossignol fluorite vein (cf. Figure 3.17). After Sizaret, S., Marcoux, E., Jébrak, M. & Touray, J.C. 2004, Society of Economic Geologists, Inc., *Economic Geology* Vol. 99, Figure 2C, p. 1109.

Barite deposits in karst

Barite deposits in karst may be epigenetic (ascending hydrothermal) or a product of supergene weathering and infiltration into existing karst caves (descending meteoric water):

> The former Fleurus mine in southern Belgium was sited in a karst depression of Viséan limestones on the northern flank of the Namur synclinorium. The doline was filled with Early Cretaceous terrestrial, lignitous sediments that enclosed a barite bed reaching a thickness of 25 m. Barite textures resembled travertine and the bed enclosed sediments, implying syngenesis. Dejonghe (1989) proposed derivation of the barium by weathering of surrounding Late Carboniferous rocks and precipitation by sulphate-bearing groundwater in the karst lake. The mine yielded a total of ~1.1 Mt until closure in 1987.

Epigenetic-hydrothermal karst barite and barite veins occur in Morocco and elsewhere in western North Africa (the Maghreb region). They are considered to be products of deep basinal fluid convection systems that were established in Triassic and Jurassic times, when the Atlantic Ocean started to open (Valenza *et al.* 2000; Figure 1.79).

Evaporite-hosted barite deposits

The Pessens deposit is located on the southern margin of the French Massif Central and, like Chaillac in the North, in transgressive Early Jurassic sediments:

At Pessens mine, the base of the Liassic rocks comprises stromatolitic dolomites, anhydrite and variegated claystone. To the north, its facies changes to terrestrial coal-bearing sediments, whereas in the south, black marine claystone prevails. In the deposit, barite replaced dolomite, resulting in a stratiform shape of the orebody. There is little doubt that the evaporitic bar served as a geochemical trap for barium transported by reduced fluids. Its derivation, however, remains ambiguous. The source may have been either weathering rocks on land or diagenetic pore water of the marine claystone. The mine closed in 1983 after production of ~1.2 Mt of barite.

Production and consumption of barite closely follow the economic fate of the petroleum and natural gas industry. Because of high prices of hydrocarbons and the consequent intensified drilling, world production peaked at 8 Mt (2008). Largest barite producers were China (57%), India, USA, Morocco and Iran. Because of a sharp reduction of drilling in the economic crisis of 2009, production fell to 5.5 Mt (USGS 2010).

3.4 BENTONITE (SMECTITE ROCKS)

$$\text{Montmorillonite } (Na,Ca)_{0.3}(Al,Mg)_2Si_4O_{10}(OH)_2.nH_2O \quad D = 2\text{–}3\,g/cm^3$$

Bentonite is a soft clay or brittle claystone composed of 60–95% smectite and other clay minerals, and minor components such as quartz, feldspar, biotite, amphibole, zircon, apatite, volcanic glass and colloidal silica (e.g. opal-CT) (Figure 3.7). Smectites comprise the dioctahedral montmorillonite group (montmorillonite, beidellite and nontronite), the trioctahedral saponite group (saponite, hectorite) and swelling mixed-layer illite-smectite with a prevailing smectite component. All these minerals display a high ion exchange capacity, but only a few have the remarkable ability to absorb large quantities of water resulting in volume increase. Ideally this "swelling" reaches the state of a thixotropic gel. Isomorphic substitution of octahedral Al^{3+} by Mg^{2+} and Fe^{3+}, or of tetrahedral Si^{4+} by Al^{3+} in smectites causes a surplus negative charge, which is neutralized by cations in the interlayers (often Ca, but also Na, Li, etc.: Alther 2004). Diagenesis converts smectite to mixed-layer illite-smectite. The resulting rock has been termed K-bentonite, which is common but of limited use. Low-grade metamorphism leads to the growth of sericite and chlorite ("metabentonites") and final loss of swellability.

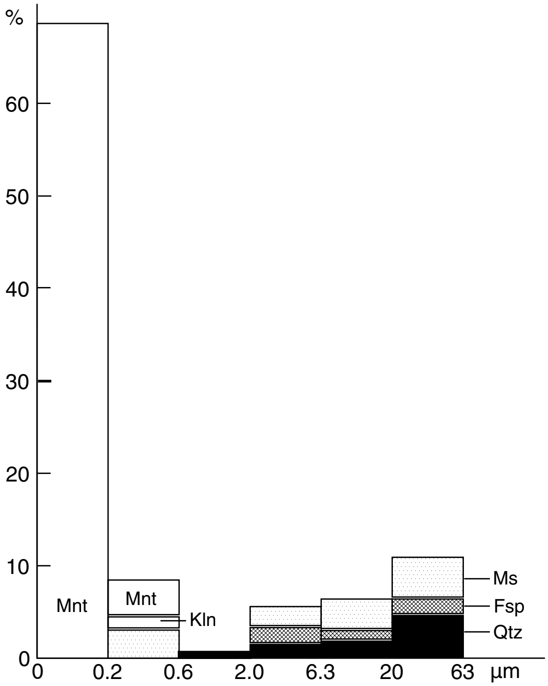

Figure 3.7 Grain-size distribution and mass percent of minerals in bentonite from Moosburg in eastern Bavaria, Germany (after Unger *et al.* 1990). With permission from www.schweizerbart.de. Mnt – Montmorillonite, Kln – Kaolinite, Ms – Muscovite, Qtz – Quartz, Fsp – Feldspar.

Similar to some types of bentonite, **attapulgite** (palygorskite) $(Mg,Al,Fe^{3+})_2Si_4O_{10}(OH)\cdot 4H_2O$ and **sepiolite** $Mg_4Si_6O_{15}(OH)_2\cdot 6H_2O$ are mainly used as lightweight industrial spillage absorbents (Galan 1996). In contrast to bentonite, the minerals do not swell in the presence of water or other liquids. One of the largest sepiolite deposits of the world is exploited at Vallecas near Madrid, in Miocene gypsiferous green marls that are interpreted to be playa lake sediments. Yearly production is ~0.5 Mt from two layers of

> earthy sepiolite. The dense, massive and white sepiolite ("meerschaum") extracted near Eskishehir, Turkey is a different modification that is used for carving ornamental objects. The largest deposits of attapulgite are worked in the Quincy-Attapulgus region of Georgia and Florida, USA, but the mineral is also produced in Spain (Kendall 1996). Very large resources of attapulgite are known in Senegal, although at 50,000 t/yr present production is moderate. Authochtonous deposits of supergene montmorillonite-palygorskite above basalt rock and resedimented lacustrine sediments are exploited in Jiangsu and Anhui provinces, China. The formation of palygorskite from montmorillonite is explained by evaporitic pedogenesis, with dissolution of sodium and calcium and import of magnesium and silica (Long *et al.* 1997).

Industrial classification of bentonite stresses technical properties including thixotropy, base exchange, swelling and adsorption capacity (Christidis & Scott 1996). Two types of bentonite are distinguished: i) The sodium, high-swelling type, derived from volcanic ash deposited in shallow marine or playa lake environments; and ii) the calcium (±Mg), low-swelling type that evolved from volcanic ash settled in freshwater environments (Alther 2004). The second is more common and less valuable than the first. Note, however, that Cretaceous calcium-montmorillonite in southeast England has been used for centuries under the trade name "Fuller's earth". For the standard swelling test, 1 g of bentonite is added to 100 mL of demineralized water. One gram of dry Ca-bentonite swells from 1–2 mL, and 1 g of Na-bentonite swells up to 16 mL in volume. Na-bentonite adsorbs six times its weight in water (Alther 2004). Swelled water-saturated bentonite forms a gel with a certain mechanical resistance, because the platelets are negatively charged at edges and positively charged on planes. Electrostatic forces cause gelification, but the gel is easily liquefied by stirring (taking the state of a sol). This transformation gel-sol-gel (thixotropy) is essential for use in drilling mud. Poorly swelling betonites can be improved ("activated") by homogenizing moist bentonite (~30 wt.% H_2O) with 2.5–6% hygroscopic soda ($NaCO_3$), resulting in replacement of Ca^{+2} and Mg^{+2} by Na^{+}.

Natural bentonite (as opposed to processed products) below the ground surface is grey or bluish-green (reduced). Near the surface, oxidation of iron causes yellow and brown colours (Figure/Plate 3.8), and the stiff clay-rock decomposes into small fragments and soft clay. Bentonite is extracted in open pits and stockpiled for maturing, the principle of which is to spread and rework the material periodically in order to advance oxidation and disaggregation:

> In the field, bentonite is not easily recognized because the rock resembles ordinary marlstone. Identification may be assisted by unusual colours (red, green, gray and blue; typically yellow when weathered) and by a slippery feel or waxy appearance. Polyhedral fragmentation in the dry state and a soapy surface after wetting and, of course, swelling are characteristic. Samples from bentonite outcrops are deceiving; drilling and trenching is recommended for recovery of representative material. Wet sieving and XRD analysis of the clay fraction are standard laboratory procedure. Specific tests depend on the intended market. Bentonite seams of 0.5 m thickness can be exploited if conditions are favourable. However, working smectite-rich clays is awkward because of their peculiar hydraulic and mechanical properties (Terzaghi *et al.* 1996).

Bentonite is used: (i) raw, after little processing such as removal of coarser grain fractions and drying; or (ii) activated by chemical treatment with acids or alkalis. Heat activation (iii) is a more recent way to improve desired properties. Sodium bentonite is used raw as a drilling mud component, a binder for pelletizing ore fines (e.g. 0.5–1.5% in iron ore pellets), for the treatment of water contaminated with heavy metals or hydrocarbons, for soil improvement, as a filler in paint and putty, for supporting deep open trenches in civil engineering and as a binder in foundry moulds made from sand. Acid-activated bentonite (bleaching earth) is employed as an adsorbent in refining and decolourizing oil, fat, wine and beer, as an inert carrier of insecticides, a fire drencher, cat litter (the largest market segment) and for absorption of spilled fuels. Alkali-activated bentonite is mainly used in thixotropic drilling muds and as a binder in pellets and foundry sand.

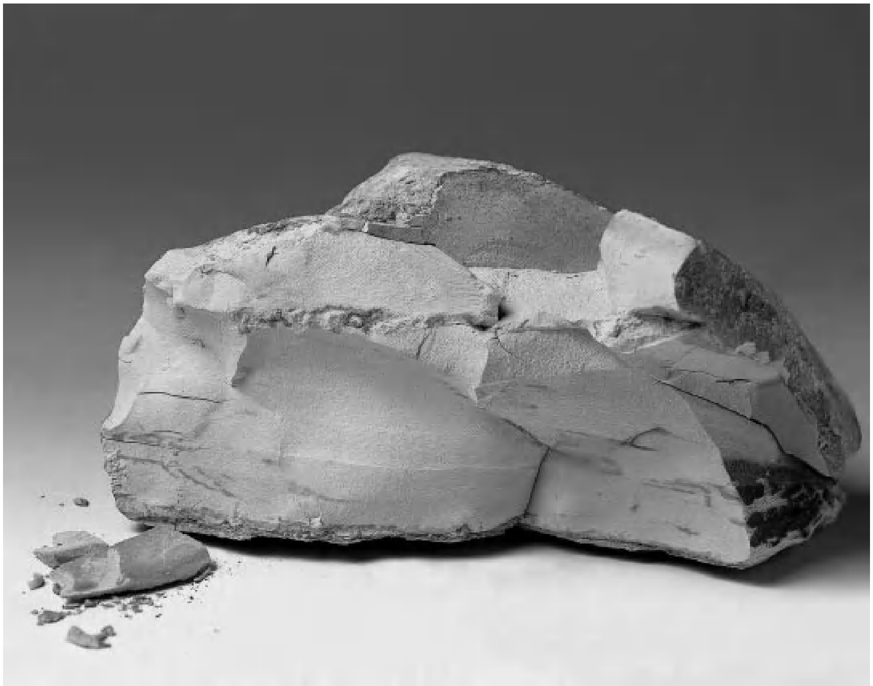

Figure 3.8 (Plate 3.8) Bentonite sample from Moosburg mining district, Germany. Copyright © Süd-Chemie AG 2009.

Synthetic smectites are commercially produced for special purposes (e.g. laponite®) as a colourless gel in medicine, cosmetics and numerous other small-volume applications.

For humans and the environment, bentonite is harmless. Actually, it is one of the edible earths used as a medicine and for other reasons ("geophagy", Selinus *et al.* 2005). Bentonite is an important material in environmental engineering. Its high plasticity and swelling capacity, united with low permeability make it a most effective sealing material. Its high adsorption capacity minimizes the mobility of harmful substances. Typical applications are landfill liners and the sealing of underground repositories containing toxic or radioactive waste.

3.4.1 Bentonite deposit types

Bentonite deposits originate by alkaline alteration of volcanic rocks and especially of glass-rich felsic ash. Some deposits are detrital clays with a high proportion of smectite or of swelling mixed-layer minerals. Consequently, the following settings of bentonite formation are distinguished:

- alteration of volcanic ash under alkaline conditions, by reaction with seawater (Wyoming, England: "Fuller's earth"; Milos, Greece) or with terrestrial evaporative alkaline brines (Bavaria);
- hydrothermal, alkaline alteration by seawater convection at half-submerged felsic volcanoes (Milos, Greece);
- autochthonous weathering of basic tuff, basalt and ultramafic rocks resulting in smectite-rich soil;
- smectitic clay as a marine or playa lake sediment.

Bentonites of high quality are geologically young. The name is derived from the Cretaceous Benton Group volcano-sedimentary rocks in eastern Wyoming, USA, where swellable sodium bentonite was found more than 100 years ago. The Hardin and Black Hills districts still are the world's largest source of high-grade sodium bentonite.

Tertiary and Quaternary tuffs host the large bentonite and kaolin deposits of the Aegean islands, with the island of Milos the most remarkable of all. Several exposures on Milos show that pyroclastic rocks were transformed into either kaolin or smectite, indicating passage of acidic (hot) and alkalic (cool, seawater?) fluids at different times. Kaolin formation supersedes the smectite phase and although pH-boundaries are very sharp, kaolin pervades bentonite in the form of irregular tubes, veins and stockwork veinlets. Such complex distribution patterns complicate selective exploitation. Acidic hydrothermal alteration of bentonite is in principle similar to acid activation but the product lacks the desired properties, possibly because of ageing (Kaufhold & Decher 2003). Rheological and swelling properties are positively influenced by smectite concentration but decrease with opal-CT content. Sodium bentonite is mostly derived from rhyolitic tuff and calcium bentonite from andesite (Christidis & Scott 1996). Also in a marine island volcanic setting, low-temperature hydrothermal alteration of Tertiary andesitic-dacitic tuff near Serrata in the Sierra del Cabo de Gata, Almeria, Spain produced large bentonite deposits. Pits form a wide circle around the gold-mineralized caldera at Rodalquilar (cf. Chapter 2 "Gold").

Economically important bentonite deposits occur in the East Bavarian Tertiary molasse zone (the foreland basin north of the Alps). In the Neogene of the region Mainburg-Landshut-Malgersdorf, shallow, hydrographically closed basins accumulated a suite of volcanic ash-derived bentonite beds, silt, sand and impure freshwater carbonates. Hot and dry climate conditions caused periodic alkalinity. The sediments are undeformed. Laterally, smectite contents of the yellow, bluish-green to olive-green bentonite beds change little (Figure 3.7, Figure/Plate 3.8), whereas vertical differences are considerable. The bentonized rhyolitic tuff beds can be related to the distant Transylvanian-Pannonian volcanic province (Unger *et al.* 1990).

World production of bentonite is ~10 Mt (2009), with USA first (40%) followed by Greece and Turkey. Reserves and resources are very large. Fuller's earth (calcium bentonite) adds another 3.5 Mt (2009) to world smectite production.

3.5 BORON

		% B_2O_3	*D* (*g/cm*^{3})
Borax (tincal)	$Na_2B_4O_5(OH)_4 \cdot 8H_2O$	36	1.7
Kernite (rasorite)	$Na_2B_4O_6(OH)_2 \cdot 3H_2O$	51	1.9
Ulexite	$NaCaB_5O_6(OH)_6 \cdot 5H_2O$	43	1.9
Probertite	$NaCaB_5O_7(OH)_4 \cdot 3H_2O$	50	2.1
Colemanite	$CaB_3O_4(OH)_3 \cdot H_2O$	51	2.4
Szaibelyite (ascharite)	$MgBO_2(OH)$	41	2.7

The list names the most commonly extracted boron ore minerals, out of more than 230 that contain boron (Garret 1998). Minor sources of boron include some silicate minerals, playa lake brines and boric acid from volcanic fumaroles. Elemental boron does not occur in nature. In many cases, water-rich minerals such as borax are aqueous precipitates that age by dehydration to higher-grade minerals such as kernite. Near the surface, kernite readily rehydrates to borax. Colemanite is often seen to replace ulexite and borax, but can also be a primary epigenetic phase (Miranda-Gasca *et al.* 1998).

Boron is mainly traded as anhydrous boron oxide (B_2O_3), as mineral concentrates and boric acid (H_3BO_3). Worldwide, most boron is consumed in the borosilicate glass industry. Certain enamels, ceramics, agricultural chemicals, pharmaceuticals, detergents, wood preservatives and fluxing agents also require boron. Grinding media (boron carbide is harder than corundum) and buildings for radiation protection (because boron absorbs neutrons) are further sectors of boron use. A future perspective may be $NaBH_4$ as a hydrogen storage material for vehicles that run on fuel cells. The metalloid boron (density 2.34 g/cm^3, melting point 2075°C) is very hard and useful in a number of specialized applications.

Boron is an essential nutrient for humans, animals and plants, but is moderately toxic in higher concentrations. Human intake is mainly with food, but increasingly through drinking water prepared from treated sewage effluent. In 2006, WHO set a provisional drinking water guideline value to 0.5 mg/litre. The threshold for normal plant growth is 15 mg/kg boron in soil.

3.5.1 Geochemistry

Boron is a lithophile element with a crustal abundance of 10 ppm (range 3–50: Smith & Huyck 1999). Granites (15 ppm) contain more boron than basalt (5 ppm). Boron has one of the smallest ionic radii of the common elements and displays incompatible behaviour in magmatic systems, leading to strong enrichment in hydrous liquids, magmatic fluids and vapours. Elevated boron concentrations mark marine pelites (100 ppm), the magmatic gas phase (BF_3, BCl_3, etc; e.g. Larderello in Toscana, Italy) and many terrestrial hot springs (boric acid H_3BO_3). Mud volcanoes associated with gas and oil fields emit much boron. Based on seawater with 4.6 ppm B, boron is enriched in potassium-magnesium salts of marine evaporites. An example is boracite ($Mg_3ClB_7O_{13}$), which was formerly by-produced from potash seams of the Stassfurt mining district in Germany. In the surficial environment, oxy-anions of boron (II) and (III) are very mobile.

Isotope investigations imply that boron in magmatic rocks, geothermal systems and fumaroles is mainly derived from pelites. The considerable mass difference between ^{10}B and ^{11}B causes strong fractionation in many geological processes, including the formation of boron minerals (Swihart *et al.* 1996). Boron in terrestrial settings is characterized by negative $\delta^{11}B$, whereas marine borates (e.g. in evaporites) exhibit positive values, similar to modern ocean water with delta ^{11}B ~40‰.

3.5.2 Boron deposit types

Current commercial boron extraction is mainly based on boron mobilized ("distilled") from crustal rocks by volcanism or deep heat anomalies (e.g. intrusions). Boron concentration takes place by evaporation in confined evaporative lake basins, either: i) syngenetically from lake brines; ii) during early diagenesis from pore water; or ii) in some instances as at Sonora, Mexico (Miranda-Gasca *et al.* 1998) epigenetically from hydrothermal solutions. Metamorphic borate deposits are exploited on Liaoning Peninsula, China. A large boron skarn deposit occurs in the Russian Far East (Dalnegorsk).

Most boron is extracted in one of four borate provinces: i) Southwestern USA; ii) western Anatolia; iii) the High Andes (Argentina: Alonso *et al.* 1991, Bolivia, Chile, Peru); and iv) Kazakhstan and Tibet.

California hosts the major North American boron deposits, in Miocene playa lake sediments, as at Boron (Kramer) and the nearby Death Valley area in the Mojave Desert. A Pleistocene equivalent with brine-filled crystal mush is exploited at Searles Lake in the Mojave Desert:

> Kramer is the largest of these deposits, with resources >100 Mt of ore. It lies within a borate zone 8 by 1.6 km that represents a small sub-basin within a large Tertiary playa valley. The orebody is a lenticular mass of borax and kernite ~1600 m long, 800 m wide and 100 m thick, with several intercalations of smectite clay. Locally, the borate bed rests directly on basalt. Concentrated (saline) geothermal spring waters are supposed to have flowed into the lake, where they sank to the bottom and on cooling precipitated borax (Siefke 1991). Exploitation takes place in a large open pit. Elsewhere in California, deep borate orebodies are extracted by borehole leaching (e.g. the new mine Fort Cady, with reserves of 138 Mt B_2O_3 at 410 m below the surface).

> Searles Lake is a Pleistocene equivalent to the Tertiary borate playa lakes. The deposit consists of muddy evaporitic sediments, which contain halite, trona, borax and other salts. These minerals prevail in two "salt layers" that are exploited by solution mining. The brine contains 1–1.2% B_2O_3, as well as recoverable sodium bicarbonate and sodium sulphate. Here, the

boron supply is assumed in thermal springs along the Sierra Nevada frontal faults (Smith 1979).

The Salar de Atacama in the Chilean Altiplano is a large dry saline flat. Lake sediments contain brines with lithium, potassium (as well as traces of Rb and Cs) and boron. Solutes are concentrated in constructed ponds by natural evaporation. Products include H_3BO_3 (cf. Chapter 2 "Lithium").

Turkey probably hosts the world's largest boron resources. Early Miocene lakes occupied a series of elongate extensional rift basins that formed in a continent-continent collisional setting. Lake sediments comprising limestone, tuff, marls and gypsum are intercalated with felsic calc-alkaline volcaniclastic beds. Sediments reflect an evaporative setting and changing shallow to deep-water phases. Borates were deposited in subaqueous settings as seams of laminated borax, as at Kirka (Figure/Plate 3.9). Towards lake margins, a zone of ulexite is followed by a broad colemanite rim (Helvaci & Orti 2004). Five main borate mining districts are worked. With resources of nearly 1000 Mt Bigadiç is the largest deposit of colemanite-ulexite on the Earth. Here, two 30 m thick borate horizons occur in a sequence dominated by volcanic tuff that is covered by basalt. Borates are hydrothermal-sedimentary precipitates in yellow and white banded sediments. Gypsum and dolomite occur with borates and confirm evaporative conditions. Borate textures show that initial growth took place in the soft amorphous precipitates (early diagenetic), although later diagenetic changes are evident (Helvaci 1995). Here, colemanite remains the marginal facies, but the basin centre is occupied by ulexite (Helvaci & Orti 1998).

Liaoning Peninsula in China is an important province of magnesite, talc and boron mining. The marginal facies of a Palaeoproterozoic rift basin is characterized by clastic sediments and carbonates including magnesite. The central part of the basin is built of footwall meta-arkose, alkali rhyolite, Mg-rich metasediments and hanging-wall meta-turbitites. Borates occur in the Mg-carbonates and

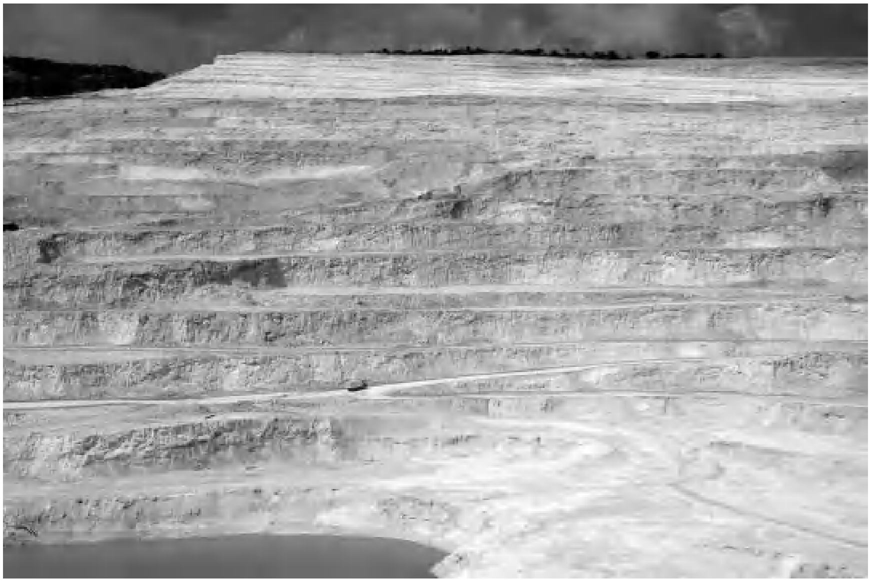

Figure 3.9 (Plate 3.9) Borax mine Kirka in western Turkey is one of the world's largest boron producers. Courtesy Walter Prochaska, MU Leoben. Formed in a Miocene evaporitic lake (Helvaci & Orti 2004), the borax ore (lower part) is enveloped in limestone and overlain by claystone and banded limestone, tuff, marl and chert. Gangue of borates comprises realgar, orpiment, gypsum, celestite, calcite, dolomite and smectite clay. Ore thickness reaches 145 m, resources comprise >110 Mt of 45% B_2O_3.

silicates that are now magnesite marbles, partly with phlogopite, forsterite-diopside fels or serpentinite, all with much magnetite. Borate ore consists of lenses and masses of suanite ($Mg_2B_2O_5$) and ascharite [also called szaibelyite, $MgBO_2(OH)$]. Orebodies have the form of breccias, stockworks, masses or dispersed stratabound nodules in metasediments. Because of amphibolite facies metamorphism and strong deformation, genetic keys are ambiguous. One of the possible interpretations includes a former playa lake setting similar to the Californian and Anatolian deposits (Peng & Palmer 1995).

Russia procures ~80% of its boron requirements from the skarn ore deposit at Dalnegorsk near Vladivostok. Triassic carbonates were intruded by a Cretaceous granodiorite. The resulting skarn consists of danburite ($CaB_2Si_2O_8$), datolite ($CaB(OH)SiO_4$), wollastonite, hedenbergite and garnet (Crowe *et al.* 2001).

Exploration for boron is based on the observation that borate in salt lake sediments occurs in massive beds or displacive crystals embedded in mud and gypsum. Along strike, the seams reach extensions of several hundred metres and appear to be centred on former hydrothermal springs. After barren intervals, the same horizon may again host exploitable borate. Margins of arid basins with volcanic activity are principally prospective. Deposits that can be worked by open pit mining are preferred. Basinal deeps are explored by drilling. The present limit of underground mining of borates is probably 400–500 m below the surface. Below this depth, brine and solution mining may still be an economic proposition.

The world production of primary boron in 2009 amounted to ~6 Mt B_2O_3, mainly from Turkey (~35%), USA, Argentina, Chile and Russia (USGS 2010).

3.6 CARBONATE ROCKS: LIMESTONE, CALCITE MARBLE, MARLSTONE, DOLOMITE

		Density (g/cm³)
Calcite	$CaCO_3$	2.6–2.8 (calculated 2.7)
Dolomite	$CaMg(CO_3)_2$	2.85–2.95 (2.876)

The density of carbonate rocks (specimen) varies within a wide range from 1.8–2.85 g/cm^3. Large samples of many cubic metres are preferred for the determination of *in-situ* rock mass weight per volume (e.g. for reserve estimation). In the mineral dolomite, part of the magnesium may be replaced by ferrous iron and manganese.

In this chapter, carbonate and carbonate-clay rocks are presented that are exploited as industrial raw materials. Specific requirements of rocks quarried for building stone, ornamental use and road ballast are not discussed, nor is magnesite (cf. "Magnesite"). The majority of industrial carbonate production is based on autochthonous, abiotic/biogenic marine sediments. Viable deposits of terrestrial (calcrete), lacustrine, hydrothermal (travertine: Guo *et al.* 1996) and magmatic origin (carbonatite: Notholt *et al.* 1990) are less frequent. With few exceptions such as recent oolite sands and earthy chalk, sedimentary carbonate rocks are consolidated by diagenesis and occur as hard rocks. Metamorphic equivalents including calcite and dolomite marble are often chemically less pure but many make excellent white fillers. All investigations of carbonate rock deposits must include methods of sedimentology and carbonate petrology. In practice, carbonate rocks are classified according to calcite and dolomite content (0–10% dolomite = limestone, 10–50% dolomitic limestone, 50–90% = calcitic dolomite, and 90–100% = dolomite), and the percentage of clay and quartz impurities (limestone with 0–5% clay, marly limestone 5–35%, marl or calcareous clay 35–65%, marly clay 65–95%, and clay 95–100%). If the mudrocks are indurated, add "-stone" as in marlstone when referring to these rocks.

Carbonate rocks are extremely important raw materials for industry, the building sector, agriculture, forestry and environmental engineering. Potentially exploitable resources should be mapped, recorded and protected by land use regulations.

Generally, carbonate rocks are processed by washing, crushing and calcining at temperatures of 800–1050°C in kilns of varying construction (Oates 1998). Resulting products are lime CaO (± MgO) and CO_2. Pure calcite loses 43.8 wt. %, but practice shows that the production of 1 t CaO consumes 1.8–2.2 t limestone. For shipping, lime is pulverized and often hydrated to calcium hydroxide $Ca(OH)_2$. In contrast to calcining limestone, natural marl that is destined for cement production, or a mixture of ground limestone and clay, is "sintered". Sintering designates heating to incipient melting (>1280°C). Only a small part of carbonate rocks is used in uncalcined form, for example in forestry as a mild and slowly acting basic soil conditioner.

3.6.1 Limestone

Limestone consists of calcite (rarely of aragonite) and minor amounts of iron, magnesium, quartz, clay, pyrite, phosphate and organic matter. Reef limestones are often quite pure because clastic silicates are nearly absent, but may have spurious (diagenetic) dolomite contents. Bedded limestones tend to have higher clay and quartz fractions. An efficient field method for determination and visualization of undesirable non-calcitic components in limestone is short-time immersion in diluted hydrochloric acid, which dissolves calcite and exposes a relief of dolomite and silicates. Comparison with samples of known mineralogical and chemical composition allows on-site provisional estimation of quality.

Desirable properties of limestone include a specified chemical and mineralogical composition, calcining performance, grindability, etc. as a function of the intended use. Low MgO thresholds, for example, are applied in steel and calcium carbide production and for de-acidification of water. Generally, low contents of SiO_2, Al_2O_3 and Fe_2O_3 are stipulated and their level determines possible uses. Sulphides and phosphates interfere with pig iron and steel manufacturing where carbonate rocks are used as a slag-forming flux. In all metallurgical and combustion processes, alkali element contents, which are often derived from contact with saline waters should be <0.05%. Resistance to size reduction during loading, transportation, unloading and calcination in industrial kilns is advantageous. Note that all limestone deposits comprise parts with differing qualities, which must be identified. Surficial alteration, and especially karstification, are frequent causes of impaired quality. If at all possible, higher-grade parts should be separately extracted in order to maximize economic benefits. Viable carbonate rock deposits should have a minimum tonnage of 500,000 t (for white filler or lime production) and ten to several hundred million tonnes for cement manufacturing.

Limestone is one of the most versatile and essential commodities. More than 70% of limestone products are used in chemical and metallurgical processes (e.g. iron, steel, glass, paper, sugar), including large amounts for flue gas desulphurization, water treatment, cement and fertilizer production. There are numerous smaller and specialized uses of limestone and lime.

High-grade carbonate fillers are micronized carbonate rocks with a high whiteness. This is compromised by dark minerals or joint coatings such as iron and manganese oxides, organic matter and pyrite. Silicates that give a white powder upon grinding (e.g. muscovite) are not harmful. In Europe, numerous suitable deposits are exploited, based on Cretaceous chalk, other marine limestones and calcite marbles. The last reach the highest degrees of whiteness.

3.6.2 Metamorphic calcite (and occasionally dolomite) marbles

Calcite marbles are in high demand for the production of high-whiteness fillers and coatings (1–10 μm) for the paint, paper and plastics industries. Country rocks are typically amphibolite, mica schists and paragneiss. A recent example is the new Kristallina mine near Vitipeno (Sterzing) in northern Italy. The deposit has a strike length of ~4 km and a width of 300 m (Pine *et al.* 2006). As is increasingly common in Europe and in North America, extraction will be by underground mining because of environmental and societal considerations. For more than 2000 years, ornamental marbles have been exploited from Mesozoic metamorphic carbonates at Carrara in Italy (Meccheri *et al.* 2007).

3.6.3 Marlstone

Marlstone with 35–65% clay and **argillaceous limestone** (>50% $CaCO_3$) are the most important components of cement production (Hewlett 1997).

Cements are hydraulic binders reacting with water to solid "hydrates". Cement production begins with sintering ground limestone and clay in a kiln. The resulting "clinker" is ground to a fine powder. Cement clinker consists of tricalcium silicate, tricalcium aluminate and tetracalcium aluminoferrite (Saint John *et al.* 1998). Because rocks with a suitable chemical composition ("natural cement marls") are relatively rare, the feed for cement factories is mixed from limestone, marlstone, claystone, quartz sand and iron ore. Almost all cements used for manufacturing concrete are based on Portland cement (the name originates from the similarity of concrete to Portland stone, a Jurassic oolite used as a traditional building material in England). The raw mix for Portland cement consists of 75% $CaCO_3$, 3% Fe_2O_3, a maximum of 4% dolomite and silicates with a ratio of SiO_2 to Al_2O_3 of 3–6. Only small amounts of sulphur, alkalis (Na, K) and phosphorus are admissible. Elements such as As, Sb and Hg, which volatilize at the high sintering temperatures in the kiln, must be carefully monitored in order to avoid emissions into the environment. The described mass ratio requires that cement factories are located near limestone or natural cement marl deposits. Other components may be hauled from greater distances. Supplementary cementitious materials (SCM), such as pozzolans, pulverized fly ash from coal-fired power plants or blast furnace slag, may substitute for part of the cement formula. Main environmental issues related to cement production are high energy consumption and carbon dioxide emissions.

Among speciality cements, calcium-aluminate cements are important for applications in underground mining and tunnelling. Also called "fondu" (French for melted) cements, they are made from a mixture of limestone and low-silica bauxite resulting in Al_2O_3 contents of 40–50% (exceptionally up to 80%). The raw mix is melted and after cooling, finely ground. In concrete prepared with aggregate and water, the fondu cement hydrates to calcium-aluminium hydrate and Al-hydrate without secreting free Ca-hydroxide like Portland cement. Upon curing, water is given off and strength-developing phases crystallize, mainly monocalcium aluminate ($CaAl_2O_4$). Concrete made from fondu cement displays a high chemical resistance against sulphate and acids, a rapid strength development and no release of alkalinity to mine and tunnel water.

3.6.4 Dolomite

Dolomite rocks are formed from the mineral dolomite, some calcite and the same minor and trace minerals as listed for limestone. Dolomite rocks are rarely primary sediments but are usually formed by diagenetic Mg-metasomatism (dolomitization) of limestone. This involves the passage of Mg-bearing solutions, although non-diagenetic sources of Mg-fluids are possible (cf. "Magnesite"). Metasomatic dolomites form rocks of a friable crystalline (saccharoidal) nature near unconformities, faults and fractures. Incomplete conversion or later recalcitization are quite common. Therefore, dolomite rock bodies, which are sufficiently large, pure and homogeneous for utilization, are less widely available compared to low-Mg limestones.

Dolomites are used raw, calcined and sintered. The first includes applications as a filler and extender, as a fluxing agent in the iron and steel industry, and as a magnesium-fertilizer in agriculture and forestry. Calcined dolomite is a rapidly acting fertilizer, neutralizes acid waters and is the solid reagent in manufacturing seawater magnesite and magnesium metal. Sintered dolomite (at 1600–1950°C) in the form of mortar or blocks is a useful refractory in the iron, steel, cement and lime industry. The sintering aptitude of dolomite is a function of crystal size and decrepitation upon heating. Mineralogical methods can give first indications but full-scale industrial trials are indispensable. High-purity dolomites are required for Mg-metal, seawater magnesite and brucite $Mg(OH)_2$ production. Detailed specifications for different uses vary widely. Strict requirements exist for glass-making and refractory dolomite (high MgO; Al_2O_3 and Fe_2O_3 below 1.5%, SiO_2 <0.5%). Similar to limestone, an improvement of the extracted dolomite by mine-site processing is hardly possible (except the removal of chert from chalk, or of fine impurities by washing). Accordingly, the exploration of dolomite deposits requires closely spaced sampling, preferably by coring. Extraction will be selective so that different qualities can be separately marketed.

World production of lime and calcium hydrate in 2009 was 280 Mt (USGS 2010), ~10% less than in 2008. Of the total, a share of 68% was recorded from China, followed by USA, Japan, Russia, Brazil and Mexico. Cement production reached 2800 Mt. Of all mineral raw materials, cement consumption's growth is highest.

3.7 Clay and clay rocks

Clay rocks are cohesive unconsolidated or indurated clastic sedimentary rocks with an important size fraction <0.002 mm (2 μm), which mainly consists of clay minerals such as kaolinite, illite, montmorillonite, chlorite and mixed-layer clay minerals (Figure 3.7 and Figure 3.10). Apart from clay minerals, clay and claystone contain fine-grained clastic silicates (quartz, mica, feldspar), biogenic matter (carbonatic microfossils, kerogen, coaly particles) and diagenetic minerals (marcasite, pyrite, carbonate, phosphate). Nearly monomineralic, high-grade clays such as bentonite and kaolin are separately discussed. Here, emphasis is on lower-grade plurimineralic clays, which are products of *in-situ* weathering, erosion and resedimentation in lake basins or in the sea. These clays are mainly used for the production of bricks, stoneware and numerous other essential baked, fired and sintered products.

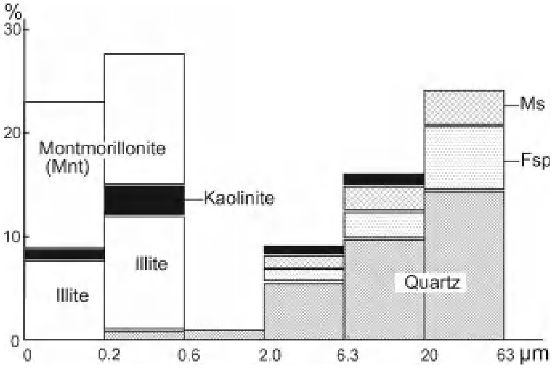

Figure 3.10 Grain-size distribution and mass percent of minerals in Cretaceous marine sealing clay from Dolgen near Hannover, northern Germany (company data). With permission from www.schweizerbart.de.

Basically, clay rocks consist of three groups of minerals, which determine possible uses: (1) 35–55% clay minerals that provide plasticity, (2) inert minerals giving strength (e.g. quartz, or flint) between 25 and 45%, and (3) 25 to 55% reactive fillers ("fluxes") such as illite and feldspar. Two main groups are distinguished: refractory and non-refractory, or ceramic clays. Of course, properties of naturally occurring clay rocks are modified at will (within economic boundaries) by an admixture of various components: Kaolin and bauxite, for example, raise the melting temperature; quartz and feldspar flour dilutes group (1) minerals, and barium carbonate prevents bloom defects. Oxides of Fe, Cu, Ni, Co, Mn, Cr, Ti, Zn and Sn are more common members of the palette that may be used to colour fired ceramics. Glazing is applied in order to seal porous surfaces of stoneware and for decoration. Different glazes are mixed from ingredients such as illitic or bentonitic clay, talc, ash prepared from various plants, barium carbonate, halite, borax, calcite, alkali feldspar and nepheline syenite.

3.7.1 Clay deposit types

Clay deposits are products of supergene alteration, erosion and sedimentation. Those still found above silicate rock from which they formed are part of autochthonous or moderately relocated soils (kaolin, loam). Most clay deposits originated by erosion and short transport in limnic or fluvial settings. Clay beds in the footwall of peat (or lignite, coal) typically display reduced iron and alkali element content, because of the passage of acidic and humic waters. This favours formation of kaolin and results in refractory grade. Numerous examples can be cited, including the "fire clay" in Carboniferous coal basins of England or in Tertiary basins of Czechia. Marine clays are rarely of high grade but may be usable after prolonged weathering.

Refractory clay

Refractory clay (fire clay) displays incipient melting at >1580°C. This is mainly a function of elevated Al_2O_3 content provided by kaolinite, diaspore or boehmite. Substances that cause melting at low temperatures ("fluxes", i.e. Ca, K, Na, Fe) should amount to <3 wt. %. Some refractory clays contain more SiO_2 ("acidic" clay), whereas others are Al_2O_3-rich and particularly suitable for the production of chamottes (calcined clay). Synthetic calcined mixtures of clay and bauxite, for example, are manufactured to replace natural refractories such as andalusite. In most cases, fire clay deposits are chiefly composed of kaolinite that does not burn white and therefore, is of lesser value (cf. "Kaolin").

Flint clay is a hard compact microcrystalline to crystalline claystone with a conchoidal fracture mainly composed of well-ordered kaolinite. Flint clay is highly refractory, with a quality between kaolin-illite plastic clays (ball clay) and high alumina nodular clays characterized by diaspore or boehmite.

Geological, mineralogical and technological investigations are required for exploring a fire clay deposit. Critical properties, which are tested with standardized methods, include plasticity, the behaviour during heating and sintering, melting point and chamotte quality. Chamotte is used as a refractory lining in kilns and furnaces, whereas acidic clays are applied as a binder in foundry moulds, and for bricks, tiles and whiteware of extra quality.

Ceramic, non-refractory clays and loams

Ceramic, non-refractory clays and loams soften by incipient melting below1520°C. Compared to refractory clays they display lower contents of Al_2O_3 and relatively more iron and alkalis. With decreasing value, the following subgroups are distinguished:

- Fine ceramics, or potter's clay, must have good plasticity and fluidity for casting ceramic pieces, low air drying and firing shrinkages, high green strength before firing (no cracking) and favourable firing properties. The colour after firing should be white, or as light as possible ($Fe_2O_3<1\%$), or a pleasant red ($Fe_2O_3>7\%$). Clays with these characteristics consist mainly of kaolinite and illite, possibly with some mica and montmorillonite. Coarse-grained minerals (of iron, or carbonates) and rock fragments are unwanted. In contrast to kaolin (china clay) that gives a vitreous body, potter's clay is porous after firing and must be glazed. In Devon and Dorset in England, extensive deposits of poorly to fairly ordered kaolinite-illite ("ball") clays are found at deeper levels of Eocene and Oligocene lacustrine to brackish basins (Bristow & Robson 1994). The source of the clay was most probably a former kaolin blanket on the Culm shales and granites of Cornwall. The material is nearly free of iron and gives a white or cream-coloured body. Because of its favourable small grain size it is very plastic. This makes it an excellent complement to kaolin of low plasticity. Blending different clays in order to attain desired properties is an important skill of both artist potters and producers of industrial ceramics and stoneware.
- Coarse ceramic clay contains more silt, sand and other impurities than potter's clay (pyrite, iron hydroxides, carbonate, organic matter). Roofing tiles and frost-resistant clinker bricks are made with the best material, whereas lesser qualities are used for bricks, drain pipes and other construction stoneware (also called "earthenware"). Geological aspects of brick clay deposits and brick making are described in detail by Bell (1993).
- Loam is the common material for brick-making. It is a mixture of sand, silt and clay of brown or yellow colour, often with humic matter and abundant weathered and fresh rock fragments. Loam is a product of supergene alteration affecting alumosilicate rocks, loess or clay. In northern latitudes, unweathered aeolian loess deposited by glacial dust storms contains no clay minerals and is of little use. Loam is either found *in situ* as a soil horizon, or eroded and resedimented. Most bricks are fired, but the advantages of using unfired clay bricks and binder ("earth masonry"), such as a healthy indoor environment and low environmental impact over the whole life-cycle of the material lead to increasing use. In some regions people prefer red-fired bricks requiring elevated iron contents. The red colour will be subdued if the loam contains calcite; fired bricks turn out yellow. Of course, the firing colour can be manipulated by additives: Coal and sawdust cause black, and manganese oxides dark purple colour.

Expanding clay

Expanding clay is distinguished by a considerable volume increase when rapidly heated to 1100–1200°C. After curing for several months in exposed dumps, the raw clay is usually shredded and pelletized. Upon heating, the round pellets expand and form little balls with a diameter of up to ~5 cm. These balls ("light expanded clay aggregates") display a vitreous dense skin and a cellular inside. Different qualities and processing allow adjustment of bulk density from ~250–950 kg/m^3. Low-density expanded clay makes an ideal aggregate for lightweight concrete. In loose form it is also used for sound and heat insulation.

Expanding clays are normally free of quartz sand, therefore plastic, and contain little iron. Prevailing components are illite and smectite. The molten skin should form before the main body expands. Therefore, melting at relatively low temperature is desired and this requires high contents of fluxes (up to 30%). The expansion may be caused by reduction of iron compounds in reaction with organic matter, liberating CO_2. Degassing of calcite and pyrite may also be involved. Many deposits exploit expanding claystone and even Palaeozoic shales are known as adequate raw materials. Therefore, the suitability of likely rocks should be tested at a semi-industrial scale, in addition to laboratory methods. One expanding clay deposit at Fehring in southern Austria occurs as a sediment in a Pliocene freshwater maar lake. The material consists of illite, montmorillonite, kaolinite, vermiculite, muscovite and mixed-layer clay minerals.

Sealing clays

Sealing clays are a traditional material for control of permeability in hydraulic and civil engineering, such as building the core of earth dams. Recently, they are widely employed in the construction of landfills and the remediation of abandoned hazardous sites, both as hydraulic and geochemical barriers. The suitability depends on properties, such as cation exchange and adsorption capacity, swelling (if smectites are present), high plasticity and low permeability. Best practice demands that sealing clay barriers, which are supposed to protect ground or surface water, should be composed of several layers of different mineral composition. Because of economic reasons, sealing clays are normally not processed apart from homogenization and curing. In northern Germany, a Cretaceous marine montmorillonite-illite clay deposit at Dolgen near Hannover is the main supplier (Figure 3.10).

Large (>1 Mt) clay occurrences with a reasonably homogeneous composition and a favourable location are always potential deposits. Even in an unexplored state, they should be mapped and protected by land-use planning agencies. Indeed, even common brick loam resources are limited, at least in many industrial countries. Detailed investigations of clay deposits must consider the typically high inhomogeneity and include possibly hazardous trace element contents (cf. Chapter 2 "Molybdenum"). Intensive geological, mineralogical and technological investigations are required before reserves, possible products and marketing of different clay qualities can be reliably estimated. Many technological tests are time-consuming and expensive, whereas investors always expect rapid answers. Note that internationally leading clay mining districts and companies making clay products typically have a long history of learning and development.

Worldwide clay production amounts to ~500 Mt/year.

3.8 DIAMOND

Diamond (C, Density 3.5 g/cm^3) is foremost a valuable gemstone but large quantities of diamond are used in industry. Diamond is remarkable because of its hardness (10 on the Mohs scale), a high refractive index that causes its singular brilliance, the highest thermal conductivity of any mineral, mechanical toughness and high electrical resistivity.

Natural diamond occurs in the following varieties:

- Diamond *sensu stricto* includes transparent crystals, of which the highest valued are colourless ("white") and flawless (without visible inclusions). Different colours are caused by impurities.

- Bort and ballas describes globular aggregates of small diamonds with a confused radial or granular structure. The term bort is also used to designate natural diamonds of lowest quality or similar synthetic stones and waste from gem cutting that can only be used in industry.
- Coated diamonds are characterized by an opaque outer shell of diamond containing impurities such as graphite and other inclusions, and a gem-quality core
- Carbonados are black, sintered, porous diamonds that contain reduced metals or metal alloys, carbides and nitrides, but no terrestrial mineral inclusions. They are possibly of extraterrestrial origin.

> The size (mass) of gem diamonds is measured in carat (1 ct = 200 mg); the minimum for industrial recovery is ~5 mg. Most rough stones produced from diamond mines are under 0.5 carat in weight. Diamonds with ~1 ct are relatively common and stones to ~300 ct are rare. Larger diamonds, however, are so extraordinary that they are usually given a name (e.g. *Cullinan,* the largest rough gem-quality diamond ever found with a weight of 3106 ct or 621 g). The value of gem diamonds depends on size, transparency, colour, flaws, cut and other factors.

> Industrial diamond is foremost an abrasive that is used for drilling, grinding, sawing and polishing. Useful properties apart from its hardness include toughness, resilience against aggressive chemicals and high-temperature stability. Applications are numerous, ranging from microsurgery to deep drilling for petroleum and cutting large monolithic dimension stones. Most of this market is served by synthetic diamonds.

Exploitability of diamond deposits depends on the combination of grade and value of the diamonds produced. Most mines exploit grades between 0.05 and 2.0 ct/t, corresponding to 0.01–0.4 ppm C. One of the recent new mines, Diavik, Northwest Territories, Canada, extracts kimberlite ore grading 3.9 ct/t in an open pit; the recovered diamonds have an average value of 96 $/ct. Letseng in Lesotho, the world's highest diamond mine (3200 m above sea level) operates with ore of 1 ct/100 t but an average value of nearly US$ 1000/ct. Diamond placers of Gbenko, Guinea have a grade of only 20 ppb; probably, this operation works the lowest- concentrated "ore" in the world, which is only possible because the recovered diamonds are valuable gems >1 ct. Diamond ore processing utilizes dense media separation, cyclones and X-ray fluorescence sorting.

3.8.1 Source and formation of diamonds

Most diamonds formed in the Earth's lithospheric mantle, at high pressures and relatively moderate temperatures. Diamonds are brought to the surface by volcanic eruptions that originate from these source regions defined by the "cool" 40 mW/m^2 mantle geotherm of Pollack & Chapman (1977). Such conditions are realized beneath continental cratons with deep keels ("lithospheric roots"). A small part of diamonds found in kimberlites and alluvial deposits, however, has its source below the lithosphere in the asthenosphere at depths of ~250–410 km, the transition zone (~410–670 km) and even in deep mantle (>670 km; Tappert *et al.* 2009). Sublithospheric diamonds identified in South Australia, southern Africa and South America are thought to be derived from deeply subducted Permian crust related to a formerly active margin of Gondwana (Tappert *et al.* 2009).

Carbon isotope data of diamonds display a wide spread of $\delta^{13}C$ from +4 to −41‰. This points either to very different sources of the carbon, including biogenic matter or to strong fractionation during diamond formation (Moore 2009). Subducted oceanic and sedimentary source material is indicated by sulphur and Pb-isotopes of sulphide inclusions in eclogitic diamonds (Eldridge *et al.* 1991, Tappert *et al.* 2005). In one case, even staurolite inclusions have been found (Daniels *et al.* 1996), confirming a contribution of crustal material, most probably by subduction. Comparative analyses of carbon and N-isotopes, however, led to contrary views (Catigny *et al.* 1998, Haggerty 1999).

Lithospheric diamond forms in the upper mantle below continents, at pressures between 43–65 kbar (4–6 GPa, ~135–200 km depth) and at mean temperatures of 1100–1200°C (Gurney *et al.*

2010, Mitchell 1986, 1991, Kennedy & Kennedy 1976). The stability of diamond is favoured by extremely reducing conditions and the presence of CH_4-H_2O-H_2 fluids or of carbonate melts (Frost & Wood 1997). In Yakutian kimberlites, the paragenesis of diamond, chromite and Cr-rich garnet is explained by the passage of CH_4 fluids through harzburgite that originally contained neither diamond nor garnet (Malkovets *et al.* 2007). Oxidation of methane, as exemplified by eq. 3.2, may induce diamond formation.

Diamond formation by oxidation of methane reacting with Fe_2O_3 in chromite:

$$Fe_2O_3 + CH_4 \rightarrow C_{diamond} + 2H_2O + 2FeO(\text{in chromite}) \quad (3.2)$$

Microdiamonds with a grain size of <0.4 mm or a mass <0.001 ct have been found in many rocks, including ultramafics, basalts, chromitite of ophiolites, ultrametamorphic gneiss (Davies *et al.* 1993), meteorites and impact rocks. Some originated in the lower mantle (>660 km: McCammon 2001) and in ultrahigh-pressure parts of subduction zones (Griffin *et al.* 2002, Barron *et al.* 2005). Of course, microdiamonds are economically insignificant.

3.8.2 Diamond deposit types

Most valuable diamonds formed in lithospheric mantle roots (Gurney *et al.* 2010). Once formed, diamonds may be entrained as xenocrysts by mantle magmas that rise rapidly to the surface, where they form volcanic edifices. If the ascent of the magma is too slow, diamond will be graphitized or resorbed. Primary diamond deposits occur commonly in subvolcanic pipes, sills and dykes of alkalic ultramafic rocks (kimberlites and lamproites). Weathering of diamondiferous rocks liberates diamond, because the mineral is highly resistant to supergene alteration. Enrichment and formation of secondary diamond deposits takes place either in autochthonous weathered material (eluvial placers) or after erosion and transport (alluvial and marine placers). Transported placer diamonds are often more valuable gemstones than those of primary deposits.

The first primary diamond deposits were found in South Africa in ~1870 (Wilson *et al.* 2007). Until then, only secondary sources (placers) were known. The newly discovered deposits were soon recognized as "pipes", vents and diatremes of explosive volcanism. The diamondiferous rocks filling pipes in the Kimberley district of South Africa were called kimberlite.

Kimberlites

Kimberlites are petrographically very complex and always strongly altered K-rich ultramafic volcanic rocks. Like many volcanic rocks, kimberlites display phenocrysts dispersed in a groundmass. The groundmass is dominated by carbonate, serpentine/olivine, phlogopite and diopside; phenocrysts include olivine, phlogopite, picroilmenite, chromium-rich pyrope, perovskite ($CaTiO_3$) and accessory diamond (Mitchell 1986, 1991). Several unaltered Devonian-Carboniferous kimberlites in Siberia contain magmatic Na-K chlorides and Na-K-Ca sulphates, which may be assimilated from Cambrian evaporite host rocks, or derived from the mantle (Maas *et al.* 2005). The rapid rise of kimberlites is attributed to high CO_2-contents in the source region of the mantle and high pressures during ascent (Wilson & Head 2007). Spera (1984) calculated that kimberlites rise with ~10–30 m/s through lithospheric mantle, accelerating to trans-sonic speed in the crust. When the magma reaches the surface, volcanic explosions lead to a sharp pressure decrease in the vent and an implosion of the walls. Sudden freezing of the melt initiates the fluidization stage, which produces the final form of the pipe and its brecciated diatreme facies infill. Commonly, kimberlites occur in volcanic fields that comprise hundreds of pipes and dykes, with very few, typically the earliest of successive generations, having economic diamond contents.

Before erosion, the surface expression of kimberlite volcanoes must have included craters, often maar-like, with a low rim of volcaniclastic ejecta (Figure 3.11). For the first time, this facies of volcaniclastic kimberlite was observed in the Fort à la Corne kimberlite field, Saskatchewan, Canada (Leckie *et al.* 1997). At this locality, Early

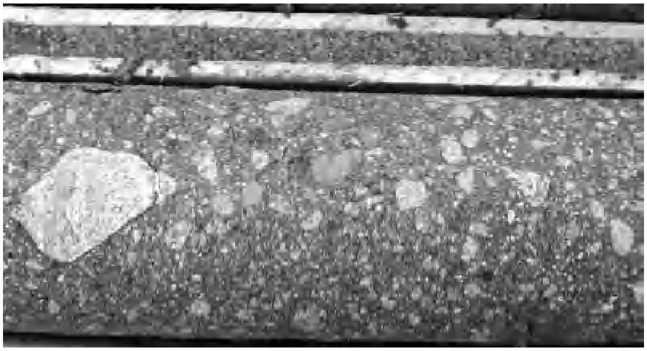

Figure 3.11 At Ekati Mine, Northwest Territories, Canada, diamonds are recovered from volcaniclastic lithic kimberlite tuff (here seen in drill core laid out in the core box). Courtesy W. Prochaska, MU Leoben.

Cretaceous sediments contain terrestrial diamondiferous lapilli tuff, which is overlain by olivine crystal tuff. Subsequent transgression caused enrichment of diamonds in the surf zone. Since 2002, the Ellendale mine in northern Australia exploits diamonds from Miocene lamproitic pyroclastites. Remains of the crater facies are known at Mwadui, Tanzania and in the Jwaneng and Orapa pipes, Botswana. However, most kimberlite pipes have been eroded to the level of the deeper diatreme zone, which is characterized by steep and smooth walls that converge inwards with depth and by a circular cross-section. The deepest zone attained by mining is the root zone, which contains a high fraction of country rock breccias and has a very irregular form. The root zone gives way to narrow non-brecciated hypabyssal kimberlite dykes, which are commonly too low-grade for mining. Some mines in South Africa, however, do exploit dykes. The whole profile may have had an original vertical extent of ~2000 m. The deepest kimberlite mines in South Africa reach a depth of 1000 m:

A paragon of diamondiferous kimberlites was the De Beers Pipe near Bultfontein in the Kimberley district (South Africa, Figure 3.12). Discovered in 1871, the mine was closed in 2005 when reserves were exhausted. Total production was ~5 tonnes (25 Mct) diamonds. During later years, mining was underground with average ore grades of 20 ct/100 t. Individual kimberlite generations had different diamond concentrations: DB1 and DB2 contained only 6.6 and 3.5 ct/100 t, respectively, whereas DB3 had 60.8 ct/100 t.

Diamondiferous kimberlite (and lamproite) and the diamonds always contain inclusions of mantle rocks. Peridotitic mantle inclusions include olivine, pyroxene and Cr-pyrope, e.g. in the Kimberley district with additional magnesite, graphite and anatase at the Finch pipe. Eclogitic inclusions are characterized by pyrope-almandine and omphacitic pyroxene, and also by kyanite, coesite and sulphides (e.g. Argyle, Australia). Peridotitic inclusions may have harzburgitic or lherzolitic character. Extraordinary is the coincidence of all three types of inclusions in diamonds of

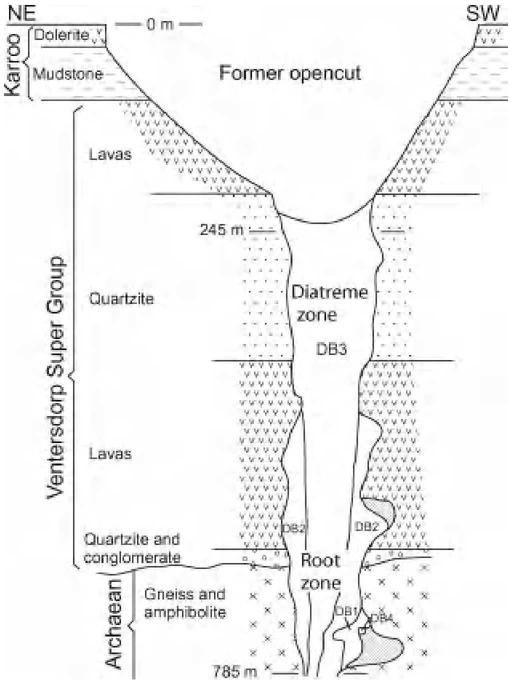

Figure 3.12 De Beers Kimberley diamond pipe, South Africa (modified from Clement *et al.* 1986). By kind permission from Geological Society of South Africa. Hatched: Root zone breccias; DB1-4 are different kimberlite generations.

the Premier Mine, S.A., where the oldest (Archaean) diamonds contain harzburgitic, those of Palaeoproterozoic age lherzolitic and the youngest diamonds that crystallized shortly before eruption of the kimberlites (1180 ± 30 Ma) display eclogitic inclusions. It is hypothesized that the harzburgites are residues of komatiite melting; the lherzolites may be related to formation of basaltic Bushveld melts (Richardson *et al.* 1993) and eclogitic inclusions are probably derived from Kibaran subducted oceanic crust. Part of the eclogitic diamonds stand out by light δ^{13}C, very low nitrogen contents, irregular form and absence of colour (Type II diamonds). Moore (2009) presented evidence that these diamonds crystallized in pegmatitic melts injected into the thermal aureole of kimberlite melt bodies. Type II diamonds associated with pegmatitic megacrysts cause the outstanding value of gemstones from Letseng (Botswana), Jagersfontein and Premier mines (South Africa).

Kimberlites are closely related to carbonatites and other alkali magmas. Kimberlites are thought to originate by a very small degree of melting of metasomatized subcontinental lithospheric mantle (Mitchell 1986, 1991). Some kimberlites that originate in the lower mantle are petrologically related to mantle plume magmas (Tachibana *et al.* 2006) or to deeply subducted oceanic slabs (Tappert *et al.* 2009). The Mainpur kimberlite field in India is synchronous with and genetically related to the Deccan flood basalt event (Lehmann *et al.* 2010), one of the largest igneous outpourings on Earth, which was emplaced ~65 Ma ago. Others may be sourced in an unusually enriched asthenospheric mantle (Paton *et al.* 2007). Typically, however, diamondiferous kimberlites occur within old cratonic nuclei that experienced tensional tectonic deformation ("Clifford's rule", Clifford 1966), for example in the early stages of the break-up of supercontinents. This hypothesis originated in Africa where Cretaceous kimberlites seem to be controlled by a system of faults and lineaments that are related to the opening of the Atlantic and Indian oceans.

Lamproites

The role of K-Mg-rich lamproites as sources of diamonds was only discovered in 1980, when the important deposit at Argyle, Australia was found. Phenocrysts and groundmass of these extrusive or hypabyssal rocks consist of olivine, K-richterite (a tremolite) and diopside, often with minor titanium-phlogopite and leucite or sanidine (Peccerillo 1992). Diamondiferous lamproites appear to be saturated in SiO_2, in contrast to kimberlites. Lamproite melting may be controlled by higher partial pressure of H_2O and fluorine, whereas kimberlite melting is favoured by elevated pCO_2.

In both kimberlite and lamproite, diamonds are xenocrysts or exotic fragments, which were entrained from the mantle source and lifted to the surface. Ages of diamonds and their igneous host rocks are typically very different; diamond formation in the lithospheric keels is episodic and can be related to the geodynamic evolution of the host craton (Gurney *et al.* 2010). In the Cretaceous (ca. 100 Ma) Orapa and Finch pipes, S.A., diamonds display a formation age of 990 and 1580 Ma. Yet, there is ample theoretical and experimental evidence that diamonds do crystallize from fluid-rich, alkaline carbonate melts similar to kimberlites.

Argyle in Northwest Australia is the largest primary diamond deposit in the world. Mining started in 1985. The AK1 pipe is a volcanic crater filled by olivine lamproite lapilli tuff covering an area of 1.6 by 0.6 km. At 1200 Ma, lamproite intruded Mesoproterozoic sedimentary siliciclastic rocks. Lamproite dykes cut across the pyroclastic rocks, which contain the diamonds. The crater fill is the product of multiple phreatomagmatic eruptions caused by contact of the lamproite magma with groundwater (Boxer *et al.* 1989). The diamonds formed at ~1.6 Ga, contain eclogitic inclusions and have a δ^{13}C of −9 to −12‰ PDB (Boxer & Jaques 1990). In 2001, reserves at Argyle were 54 Mt at a grade of 3.0 ct/t and resources 166 Mt at 2.5–3.0 ct/t. The open pit operation was terminated in 2007 and extraction moved underground. Gem quality diamonds >2 ct are only ~1% of production, but famous for their rare colours (champagne, cognac and pink stones: Figure/Plate 3.13). Apart from Argyle, more than 100 other lamproites and kimberlites have been found in Western Australia, including Ellendale mentioned above. With an age of only 20 Ma (Early Miocene), this swarm is the youngest of this rare igneous family in the world.

Recently, in the Bunder district of Madhya Pradesh, India, eight lamproite pipes were discovered. Two

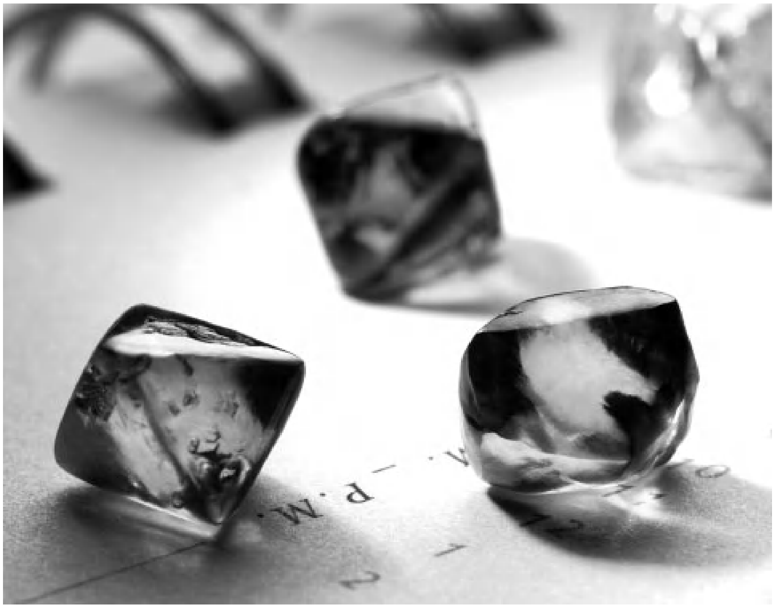

Figure 3.13 (Plate 3.13) Champagne-coloured octahedral diamond crystals from Argyle, Australia. Note the macroscopic (eclogitic) inclusions. Courtesy Rio Tinto © Argyle Diamonds.

coalesced pipes at Atri display a surface extension of 17 ha and host inferred resources of 37 Mt at a grade of 0.7 ct/t, which are amenable to open-pit mining and conventional diamond recovery.

Diamond placers

Diamond placers owe their origin to the high density and remarkable mechanical and chemical resilience of the mineral. This allows for multiple erosion/sedimentation cycles explaining placer deposits without known primary sources and especially, the discovery of spectacular single stones. Geologically very early fossil placers include the Palaeoproterozoic conglomerates near Vila Nova in Brazil. Geologically young and recent placers occur in higher river terraces and present river beds. An excellent example for the connection between primary and secondary deposits are the diamond placers along Bow River in Western Australia, which occur downstream of the Argyle AK1 pipe. Based on large reserves with an average grade of 0.3 ct/t, the annual production was (in 1991) 960,000 ct. Highest diamond grades occurred in the oldest, highest level terraces. Gem quality stones contributed ~20% of production, confirming the experience that transport results in higher-quality diamonds. Most alluvial diamonds have values of the order of US$ 450–500/ct, in contrast to diamonds from kimberlites pipes and dykes that commonly fall into the range of US$ 30–150/ct. A famous example of rich alluvial placers occurs along Orange River in Southwest Africa. The diamonds were eroded in post-Cretaceous time from kimberlites in central South Africa. From the Tertiary to the Holocene, the diamondiferous gravels were reworked due to a complex evolution of the river system (De Wit 1999). Note that in 1866, South Africa's first diamond (Eureka with 21.5 ct) was found on the banks of Orange River.

Marine (coastal) and submarine placers of diamond, noted as a source of gems averaging over US$ 350/ct, are exploited in southwestern Africa (mainly Namibia). Near Gibeon in the upper reaches of the area draining to the coast, many kimberlite pipes are known, but none is diamondiferous. Due to the wide Quaternary sea level variations, both submarine (low-stand, formed during glacial times) and onshore deposits (high-stand, formed during interglacial periods) are present, sourced from the Orange and Olifants rivers. From the Orange River delta, diamonds were transported northwards along the coast to a distance >150 km. Diamond contents and stone size in the beach complex are closely correlated to specific sedimentary settings (Spaggiari *et al.* 2006). Buried bedrock gullies of the Sperrgebiet host famously rich gem diamond concentrations (Jacob *et al.* 2006).

Diamond exploration

Diamond exploration uses a combination of geological, geochemical and geophysical methods (Michel 1996). Clifford's rule, that most likely old cratons have diamondiferous lithospheric roots, still applies with few exceptions (e.g. Argyle), and crustal tectonics control kimberlite fields (Gurney *et al.* 2010). Regional-scale exploration always includes the systematic collection of heavy mineral samples from regolith or drainage systems. "Indicator minerals" for kimberlites and lamproites include high-Mg ilmenite (picroilmenite with >8 wt. % MgO and >0.5 wt. % Cr_2O_3), chromian diopside, chromian spinel or chromite, Cr-rich pyrope, low-U zircon, phlogopite and, of course, microdiamonds (Figure 3.14; Muggeridge 1995). Infrared reflectance spectrometers are routinely used to scan samples, such as drill core, in order to detect favourable indicator minerals. Argyle was found by the recovery of diamonds 20 km downstream from the primary deposit during routine drainage sampling. Major and trace element compositions of indicator minerals can be valuable guides to diamondiferous kimberlites and lamproites (Griffin & Ryan 1995). In humid climates, soft weathered kimberlites of subcropping pipes form maar-like depressions that can be detected in satellite images. Other methods include geochemical soil sampling in order to spot anomalies of Ni, Cr and Co, supplemented by airborne and ground geophysical surveys searching for magnetic, electromagnetic and gravimetric anomalies. At Argyle, however, a range of airborne and ground geophysical methods failed to produce a definitive response over the pipe (Dentith *et al.* 1994). Once kimberlites or lamproites have been found, their diamond potential must be evaluated (Rombouts 2003). Routinely, very large samples (several hundred tonnes) are processed in order to recover sufficient diamonds for a preliminary evaluation. One tested sampling method is deep, large-diameter (584 mm) drilling. Similarly, the evaluation of diamond placers requires processing of large

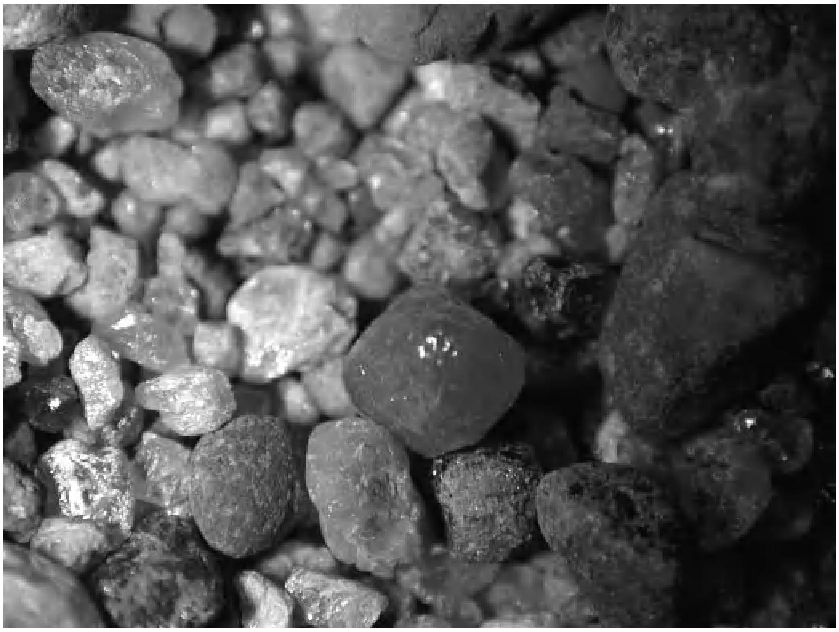

Figure 3.14 (Plate 3.14) Heavy minerals concentrate from glacial till in the region around Ekati, N. T., Canada, where more than 150 kimberlite pipes have been found. Courtesy W. Prochaska, MU Leoben. Indicator minerals on display include dark green Cr-diopside, pale or transparent yellow eclogitic garnet (?), light grey picroilmenite, dark grey chromite, dark red Cr-pyrope, bright green olivine and one octahedral diamond (centre, diameter ~1.8 mm).

samples. Meticulous investigation of all aspects of the deposit is required for rational exploration and extraction. Understanding distribution and value of the diamonds is crucial. For valuation of diamonds found, a minimum sample should comprise at least 2000 ct of macrodiamonds. Microdiamonds cannot be evaluated.

After the unexpected discovery of the giant diamond deposit Argyle in Northwestern Australia (1983) in a geological unit that was thought to be unprospective, a worldwide exploration rush revealed many new diamond fields. Examples are Northwestern Canada (Ekati and Diavik mines, Northwest Territories), Finland and USA (Kelsey Lake, Colorado). Yet, among more than 10,000 kimberlites known in the world, less than 100 mines have been established and only 15 are really significant.

Mine production of natural diamonds in 2008 was 72 Mct (14.5 tonnes) and little less in 2009 (USGS 2010). Ranked according to weight, the largest producers were Congo (DRC), Australia, Russia, South Africa and Botswana. About two-thirds of the total is from primary deposits, one-third from placers. Only ~20% of the production is of genuine gem quality. Because of this divergence, ranking according to value puts Botswana first, followed by Russia, Angola and Canada. The rapidly growing demand for industrial diamonds cannot be satisfied by mining natural diamonds. China alone produces ~4000 Mct/yr (or 800 tonnes) of synthetic diamonds that can be designed to specifications of the customer (e.g. grain size from crystals and grit to powder, homogeneity, structure). Most synthetic diamonds are made from graphite by the High Pressure/High Temperature (HPHT) technology at T >1400°C and P >59 kbar in a metallic melt. Heat-resistant doped semiconductors are produced by the Chemical Vapour Deposition (CVD) technology. Even the production of synthetic gem diamonds is possible, at a fraction of the price of natural diamonds. The consequences for diamond mining are not clear. One strategy against the competition by man-made diamond gems is certification ("branding") of natural stones. Unregulated artisanal mining of diamonds is a bane for certain regions, as it leads to extreme exploitation of people and brutal civil wars, especially in tropical Africa. Solutions are being sought by industry, governments and NGOs (e.g. the Kimberley Process Certification Scheme 2003).

3.9 DIATOMITE AND TRIPOLI

Diatomite (alternative names include diatomaceous earth and kieselguhr) consists of microscopic skeletons (frustules, 50–100 μm) of unicellular algae of the phylum *Bacillariophyta*. Structurally in two halves (valves) – hence their name – their cell walls are made up of amorphous opaline silica ($SiO_2 \cdot nH_2O$, density 2.0–2.25 g/cm^3), which diatoms polymerize from dissolved silica (Figure 3.15). In ocean water, the common form of silica is orthosilicic acid H_4SiO_4. The estimated 100,000 extant species of diatoms take many forms, as do ancient ones, and this may influence specific uses. In lakes and oceans, diatoms are part of the plankton that feeds fish and other animals. Because of their huge total mass they are one of the main sources of atmospheric oxygen. It is estimated that 40% of all organic carbon fixation on our planet (photosynthetic transformation of carbon dioxide and water into sugars, using light energy: eq. 6.1) is carried out by diatoms, about equal to all of the world's tropical rainforests. A steady rain of diatoms sinks

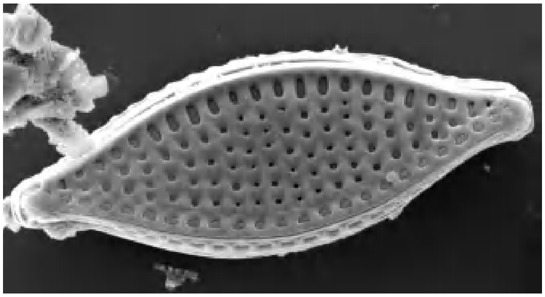

Figure 3.15 Electron microscope image of the skeleton of diatom *Nitzschia lancettula* f. *minor* which is characteristic for Pleistocene diatomite at Adami Tulu Sida (Ethiopia), illustrating the delicate sieve-like structure that is the base for many applications of diatomite. Length of image 15 μm. Courtesy Juliane Fenner, © BGR Hannover.

to the floor of water bodies. Under favourable conditions, diatoms "bloom" and this results in useful concentrations if other sedimentary input remains low. Diatoms only became widespread in the Cretaceous and exploitable deposits are mainly of Tertiary and Quaternary age.

As a sedimentary rock, exploitable diatomite often includes a minor component of organic substances, quartz, pyrite/marcasite, clay, calcite and volcanic ash. SiO_2 contents are most often $>80\%$, the best grades have $>90\%$ (Lompoc, California). Of course, gradation into diatomaceous clay or silt is common. In outcrops, the material resembles friable chalk with a white to greenish colour. High organic matter and sulphide contents give it a dark grey or brown colour. Raw diatomite can hold $\sim60\%$ water. Dry, loose diatomite has a very low density of 0.12–0.25 g/cm^3.

Diatomite is usually extracted in open pits and crushed in spiked rolls and hammer mills. The material is then dried and ground at $\sim100°C$. Because diatoms are very delicate, enrichment is preferably carried out in cyclones and air separators, not in aqueous slurry. For some applications (e.g. polishing), the concentrate is calcined at ~800–1000°C or flux-calcined at 1000–1200°C, resulting in stronger silica particles. In addition, this procedure burns organic matter and gives the product a white or pink colour. Commercial products are divided into grain size classes.

Useful properties of diatomite include the high silica content, low density and high porosity (Kogel *et al.* 2006). The advantage of silica is its chemical inertness. Typical uses include heat and sound insulation, filtering of liquids (e.g. clarification of swimming pool water and beer), filtering of microbial contaminants such as bacteria, protozoa and viruses in public drinking water systems, as a filler in rubber, plastics, paper, paints and bitumen, as an ingredient in cement and as a carrier powder in nitrogen fertilizer and insecticides. Small amounts find applications in cosmetics and polishing wares. Similar to sepiolite, much diatomite is used as cat litter and industrial spillage absorbent.

Amorphous opaline diatomite does not cause silicosis. However, the World Health Organization cautions that diatomaceous earth with a crystalline silica content over 3% should not be ingested by humans or animals. Crystalline silica content may be elevated in heat-treated products.

3.9.1 Diatomite deposit types

Diatomite deposits result from localized profuse growth of diatoms in a geologically short time. This is favoured by a high and continuous availability of dissolved silica, in addition to essential nutrients (e.g. P, K, N). Geothermal springs in volcanic settings (Iceland) and settling of glass tuff into lakes and coastal lagoons provide soluble silica (Denmark; California). As a consequence, most diatomite deposits occur in volcanic districts.

Freshwater diatomite

Present diatomite formation can be studied in Iceland. Diatomite is recovered from the shallow bottom of Myvatn Lake near subaqueous discharge sites of geothermal springs. The French Massif Central hosts Europe's largest diatomite deposits, related to a chain of basaltic-trachytic volcanoes whose activity lasted from the Late Miocene to Early Holocene; the Murat deposit actually is a former maar lake filled with diatomite. In Africa, economically important diatomites occur near volcanic centres along the East African Rift. In the Neogene and Quaternary, diatomite formed during times of wet climate in huge lakes in and near the Rift Valley and the Afar depression of Ethiopia. High-grade diatomite occurs in Pleistocene Lake Galla sediments at the foot of Aluto volcano.

Glacial/interglacial diatomite

In the Lüneburg area of northern Germany, diatomite formed during Quaternary interglacial warm periods, in elongate, narrow lake basins excavated by the inland ice during glacial phases. Deposits reach a thickness of tens of metres and several kilometres length. The material is finely banded and in deeper parts olive-green to black-coloured by organic substance and pyrite. Near the surface, white and grey colours prevail, because of oxidation and leaching above the groundwater table. Remaining resources comprise >12 Mt exploitable diatomite, but because of environmental considerations, extraction was stopped in 1994. Considering the absence of proximal volcanism, elevated silica availability is explained by rapid interglacial weathering of rock flour exposed after retreat of the glacial ice shield.

Marine diatomite

The Eocene moler earth of northern Jutland, Denmark, is formed by interbedded marine strata of light diatomite and argillized bentonitic ash tuff. The deposit reaches a thickness of 60 m. Shear deformation underneath the southward-moving Quaternary ice sheets left strata folded and disrupted. High clay and iron contents impede use as a filtering material, but dried, calcined and sintered products find a ready market, which includes insulation bricks, absorbents (cat litter) and coating material (e.g. for fertilizer). California has large diatomite deposits of marine and freshwater origin. South of Lompoc, diatomite deposits occur in Neogene marine sediments. The higher part of the Middle and Upper Miocene Monterey Formation comprises hard opaline cherty shale and chalcedonic chert, with intercalated pure diatomite. Diatomite is also hosted by the overlying Sisquoc Formation in 25 beds between clay layers.

World production of diatomite in 2009 was ~2.2 Mt. Major producers are USA, China, Denmark and Japan (USGS 2010).

3.9.2 Tripoli

Tripoli is similar to diatomite but of different origin. Like diatomite, it is used as a fine, mild abrasive and as a filler and extender in elastomeres, paints and plastics. Originally, the term was coined for diatomaceous material traded at the port of Tripolis (Libya). Today, "tripoli" designates residual earthy, very fine-grained, non-diatomaceous silica accumulations, which result from weathering of chert, flint and siliceous limestone (Neuendorf *et al.* 2005). Constituent silica phases depend on the source material and may vary from amorphous opal to low-temperature quartz (often chalcedonic). Typical grain sizes range from 1–10 μm, but include particles as small as 0.1 μm. Commercial tripoli grades 98–99% silica, with traces of alumina and iron oxide. White colour is characteristic but yellow, brown and red material is also extracted. Tripoli is classified as carcinogenic and may cause silicosis. This must be taken into account when the material is handled. The volume of world mine production is not recorded; its magnitude is probably several 100,000 tonnes per year.

3.10 FELDSPAR

Orthoclase, microcline	$KAlSi_3O_8$	$D = 2.5–2.6\ g/cm^3$
Albite	$NaAlSi_3O_8$	2.6
Anorthite	$CaAl_2Si_2O_8$	2.8

Feldspar is a main component of most igneous rocks and of many metamorphic and sedimentary rocks. It is one of the most common minerals. However, only the two first listed alkali feldspars or members of their solid solution series (K-Na feldspar, perthite) are of major industrial significance. These desired feldspars occur mainly in felsic and alkaline magmatic rocks. Feldspar of most intermediate and mafic rocks is rich in calcium (plagioclase, a solid solution series of albite and anorthite). Plagioclase lacks important properties and is, therefore, rarely of economic interest.

Potassium, or K-feldspar has a theoretical composition of 64.8% SiO_2, 18.3% Al_2O_3 and 16.9% K_2O, but always contains some sodium, traces of calcium and tiny flitters of haematite that give the mineral its pink to red colour. Pure albite is composed of 68.8% SiO_2, 19.4% Al_2O_3 and 11.8% Na_2O. Minor kaolinization of feldspar is acceptable.

Use of feldspar is mainly (ca. 85%) in the production of porcelain and technical or glazed ceramics (whiteware), and glass. In ceramics and porcelain, the role of feldspar is that of a fluxing agent for lowering the melting temperature of a ceramic body during firing and formation of a glassy phase. As a component of glass melts, feldspar provides alumina for improved hardness, thermal endurance, durability and resistance to chemical corrosion. Increasingly, feldspar is employed as a filler in plastics, paints and rubber. The intended use controls the precise specification for processed sales products: Main variables are the contents of alkalis, alumina, free silica and of iron. Iron is generally unfavourable because it induces undesired colours. Alumina content of glass is also lifted by adding kaolin, bauxite or kyanite, but either higher costs or iron contents may be a handicap. As a standard flux, the glass industry uses soda ash so that alkali contents of feldspar are less critical.

Earlier, feldspar was extracted from coarsely crystalline pegmatites and manual sorting delivered a pure product. Today, processing of run-of-mine ore to concentrate includes methods such as comminution, flotation, and electrostatic and high-intensity magnetic separation. Pegmatites continue to be significant primary sources, but other magmatic rocks gain significance. This is, of course, due to the economy of scale resulting from exploitation of large homogeneous rock bodies. Examples include nepheline syenite (Brazil, Canada, Norway, Russia and Turkey), aplite (Japan, Elba), alaskite (USA), albitite (Sardinia, Vysoki Kamen, CZ), phonolite (Eifel, Germany), rhyolite (Saar-Nahe, Germany) and Cornish stone (partly altered sandy granite in Cornwall). In Norway, white anorthosite is quarried for the production of mineral wool, fillers and extenders; its use in glass and ceramics production is limited. The world's largest feldspar pegmatite is reportedly Pippingarra near Port Hedland, Western Australia, with a length of 1.5 km and a width reaching 200 m.

Prospective deposits must have a suitable size, and reasonably constant processing characteristics and product composition (compare Greiling *et al.* 2005). Low iron contents are always stipulated. Remember in this context that many pegmatites are paragons of inhomogeneity, so that compliance with these conditions may be very difficult. Product specifications are best reconciled with potential users. Co-production of quartz and mica should always be considered. World mine production of feldspar in 2009 was ~19 Mt (after 22 Mt in 2008). Largest producers are Turkey, Italy and China. Reserves and resources are extensive.

3.11 FLUORITE

		Max. wt. % F	*Density (g/cm^3)*
Fluorite (Fluorspar)	CaF_2	48.9	3.18

Numerous minerals contain fluorine but only fluorite and fluorapatite are industrial sources of the element. Fluorite regularly contains traces of rare earth elements substituting for Ca (particularly Y and Ce), which activate the namesake fluorescence (and thermoluminescence) of the mineral. They also cause many colour variations of fluorite, but other elements and hydrocarbon inclusions are also involved. Different colour bands always differ in trace element geochemistry. Frequent cations in fluorite include Sr and Y, whereas Al, Ba, Cd, Mg, Mn, Na, K and U + Th are less common. Minor and trace element variations mark certain fluorite generations in any one deposit, and even different deposit types in a fluorine province. This may assists exploration. The deeply purple colour of some fluorites is attributed to uranium content, or more precisely, to radiation damage affecting the crystal lattice. Fluorite ages can be determined by the Sm-Nd isotope isochron method (Munoz *et al.* 2005). Frequent U + Th content of several tens of micrograms per gram allows application of the $(U\text{-}Th)/^4He$ dating method (Pi *et al.* 2005). Common gangue minerals of fluorite ore include quartz, carbonate, barite, galena and sphalerite. Beware that sellaite MgF_2 is easily mistaken for fluorite but less valued. Fluorite resists supergene alteration and tends to form visible outcrops. It may even be enriched by dissolution of carbonate gangue and host rocks.

Industrial fluorine requirements are mainly satisfied by fluorite. Until closure in 1987, natural cryolite Na_3AlF_6 was extracted from a singular pegmatite deposit near Ivigtut in western

Greenland. Meanwhile, synthetic cryolite is made from fluorite for a flux in electrolytic melting of aluminium. An increasing source of fluorine is fluorapatite $Ca_5[F(PO_4)_3]$ processing in the phosphorus fertilizer industry (cf. "Phosphates"), which results in considerable quantities of hexafluoride silicic acid H_2SiF_6.

Large fluorite deposits with resources of several million tonnes are exploited at grades of 15 to 20% CaF_2, smaller ones require 30 to >40%.

Fluorite's main use is as a flux in numerous metallurgical processes and this is the reason for its name (*fluere* in Latin means "to flow"). Large quantities are consumed in the iron, steel and cement industries. Fluorite concentrate is accepted as "metallurgical grade" if it contains >60% CaF_2 at good granularity and low contents of SiO_2, S and Pb. The chemical industry requires >97% CaF_2 and very low sulphide and phosphorus concentrations. This "acid grade" fluorspar is used for the production of fluoric acid by dissolution in H_2SO_4 yielding anhydrite as a by-product. Fluoric acid HF is the base for many industrial processes, for example cryolite synthesis, the production of propellant gas and of perfluorocarboxylates that are used in large quantities for consumer products such as Teflon. Gaseous UF_6 is the preferred means for enrichment of ^{235}U for energy and weapons. Metallurgy and chemical industry consume most fluorite in about equal shares. Extremely pure and transparent fluorite (and sellaite) is used for lenses and prisms, but most optical material is made synthetically.

For humans, fluoride is an essential element, but within narrow limits. Both too low and too high intake cause visible damage to teeth and other health problems (Edmunds & Smedley 2005). Drinking water should contain from 0.7 to 1.2 mg/l F (Dissanayake 2005), but not more than 2 mg/l. In order to protect the population, the dissemination of fluoride into the environment must be strictly controlled. In industry, recycling or safe disposal is the rule. A contraction of demand for acid-grade fluorite was caused by recycling combined with the ban on halone and CFCs (chlorofluorocarbons) by the Montreal Protocol 1987, because these substances deplete the stratospheric ozone layer. Production of HCFCs (hydrochlorofluorocarbons) in developing nations will stop in 2013. Newly developed HFCs (hydrofluorocarbons) that are benign to stratospheric ozone support fluorite mining. Although HFCs are strong greenhouse gases they may be acceptable, because at low concentrations they cause very little radiative forcing in the atmosphere (Shine & Sturges 2007).

3.11.1 Geochemistry

Lithophile fluorine (Goldschmidt 1958) is remarkably enriched in mantle volatiles, as evidenced by fluorine contents in phlogopite of kimberlites reaching 8500 ppm. Mantle-derived carbonatites and igneous alkali rocks also contain much fluorine, commonly in the form of fluorapatite segregations, which may be large enough to support important mines (e.g. Khibiny, cf. "Phosphate"). With an estimated crustal abundance of 500 ppm (range 270–800: Smith & Huyck 1999) fluorine is the most common trace element. Fluorine is a component of all magmas. Its concentration rises from mafic (400 ppm) to granitic rocks (735 ppm), although actual contents depend on the individual degassing history of a magmatic body. Metapelites contain an average of 500 ppm F, carbonates 330 ppm and seawater only 1.3 ppm. In common rock-forming minerals, fluorine (F^-) substitutes for OH^-. Therefore, mica, amphibole, apatite, clay and other hydrous minerals are carriers of fluorine traces. Accordingly in most rocks, fluorine is freely available. This explains why fluorite is a common gangue mineral in hydrothermal ore deposits and why fluorite deposits are so widespread.

Volcanic vapours contain fluorine as an HF^o phase, causing strong alteration of rocks. Cooling magma bodies may liberate giant amounts of fluorine. Fumaroles in the Valley of the Ten Thousand Smokes, Alaska are estimated to eject some 200,000 t/y fluorine into the atmosphere. Carriers of fluorine in hydrothermal solutions include F^-, HF^o, HF_2^-, SiF_6^{2-}, CaF^+ and BF_4^-. Solutions are mainly acidic and precipitation of fluorite is induced by contact with limestone or dissolved calcium, raising pH. In the surficial environment, fluorine is equally soluble and mobile, and is precipitated by earth alkalis.

Many fluorite occurrences and deposits occur in certain stratigraphical and lithofacies units that are marked by regional geochemical fluorine anomalies. Examples include Carboniferous sandstone in the central Russian Platform, Zechstein (Late Permian) saline dolomite in Germany (Ca2 und Ca3: cf. Chapter 4 "Salt Formation in the Geological Past"), Triassic sediments of the Morvan near the French Massif Central and in the Eastern Alps, and Cretaceous limestone in Mexico. This observation can be explained by either synsedimentary exhalation and dispersion of fluorine or by pervasive epigenetic hydrothermal processes.

3.11.2 Fluorite deposit types

The formation of fluorite deposits is mainly a consequence of magmatic and hydrothermal-diagenetic systems. Magmatic-hydrothermal deposits are connected with carbonatites, alkaline magmatic rocks, granites and rhyolites. Economic fluorite concentrations are commonly located in the roof of intrusions, where magmatic volatiles reacted with host rocks. However, the majority of fluorite deposits have no connection with magmatic process systems. They include fluorite-rich members of the Mississippi Valley Type class, epigenetic hydrothermal veins, stockworks, pipes and metasomatic masses, and stratiform fluorite hosted in sediments. Diagenetic processes and basinal fluids are often implicated, but there is no single genetic explanation for non-magmatic epigenetic fluorite deposits. In some cases, degassing of the mantle may have transferred fluorine into crustal hydrothermal systems (e.g. in Europe during the Triassic break-up of Pangaea).

Magmatic-hydrothermal fluorspar deposits

These deposits are exploited in Mexico, South Africa, Canada and China:

The volcanogenic deposit Las Cuevas near Zaragoza in Mexico is the world's largest fluorite mine, with reserves of 28–30 Mt at 84.5% CaF_2. Fluorite with some calcite and silica fills hydrothermal karst cavities in Early Cretaceous limestone in contact with a Tertiary rhyolite breccia. In South Africa, magmatic degassing of the Bushveld granites (cf. Chapter 1.1 "Orthomagmatic Ore Formation") produced the fluorspar deposits of Vergenoeg and Buffalo mines. Host rocks are contact metamorphic sediments of the Transvaal Group and rhyolitic Rooiberg felsites ("leptites") in the roof of the granitic intrusions. Orebodies consist of vein systems, which are injected either into bedding planes of quartzites (Buffalo), or into cross-cutting structures within a pipe (Vergenoeg). Some veins carry only fluorite, others display a gangue of apatite, siderite, quartz, chlorite and sphalerite. High trace contents of uranium and rare earth elements are characteristic. Resources of the Buffalo deposit are estimated at >50 Mt, those of Vergenoeg at 100 Mt.

With ~12 Mt of ore at 30% CaF_2, Amba Dongar, Gujarat, India is one of the largest carbonatite-associated fluorite deposits. The intrusion is located within the giant late Cretaceous Indian flood basalt province (Deccan traps), with which it is genetically related. Numerous veins of fluorite with barite, chalcopyrite, dickite, galena and pyrite occur at the contact of carbonatite with fenitized sandstone. The mineralization originated by mixing of magmatic fluorine-rich fluids with calcium-rich formation water in the sedimentary country rocks (Palmer & Williams-Jones 1996).

Diagenetic-hydrothermal fluorite deposits

These deposits are very common. In the English Peak District, the famous ornamental fluorite ("Blue John", Figure/Plate 3.16) was introduced by diagenetic fluids during a late stage of the main Variscan deformation. The Illinois-Kentucky district within the type area of Mississippi Valley type (MVT) deposits was the source of most fluorite produced in the USA. The spatial coincidence does not, however, support *a priori* an origin comparable to MVT lead-zinc deposits. Geological position and geochemical modelling (Plumlee *et al.* 1995) make it very likely that these deposits originated in connection with HF-CO_2 degassing of Permian alkali complexes, although these are poorly exposed. The authors imply that rising magmatic gas dissolved in basinal brines, which migrated along faults and formed the large fluorite veins, mantos (in limestone) and breccia orebodies of the cryptovolcanic Hicks Dome.

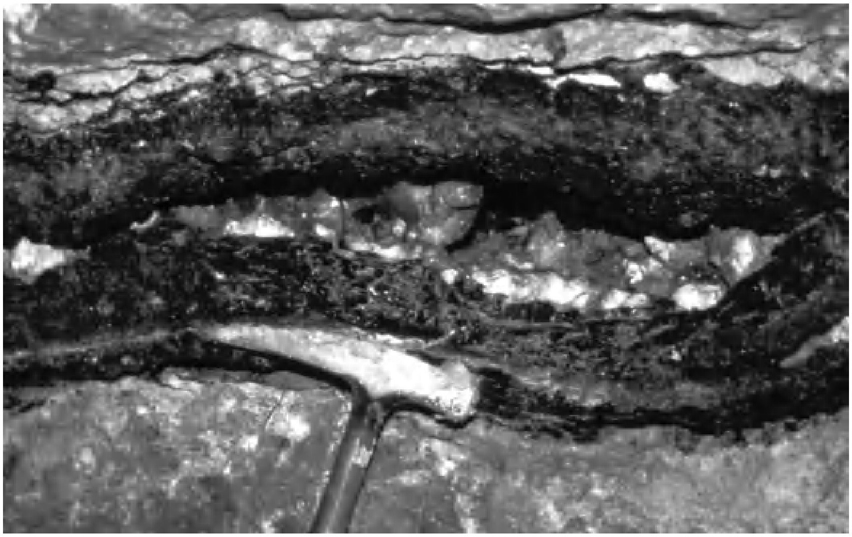

Figure 3.16 (Plate 3.16) Banded dark blue, purple and yellow hydrothermal fluorite ("Blue John") filling karst pipes and replacement bodies in Carboniferous limestone, Derbyshire, England. Light crystals in the central cavity are calcite. Courtesy Volker Lüders, GFZ Potsdam.

A remarkable fluorite province occurs around Witkop mine near the town of Marico in western Transvaal, South Africa. Orebodies are located below an unconformity of the Palaeoproterozoic Malmani Dolomite (of the Transvaal Supergroup), where it is covered by shales, chert with banded iron formations, breccias and conglomerates of the Pretoria Group. Below the unconformity plane, the dolomites are severely karstified, which proves emersion to subaerial levels. Stratiform fluorite impregnates stromatolitic dolomite of the karst zone ("algal ore"), and cements collapse breccias of black dolomite ("block spar"). Gangue includes quartz, calcite, dolomite, pyrite, talc, tremolite and sphalerite. The ore contains only 16% fluorite but open pit mining allows economic extraction. Potential resources of the district are very large; at a cut-off grade of 10% CaF_2 they amount to 1000 Mt. Ore formation is bracketed between deposition of the Pretoria Group (because unmineralized Malmani dolomite forms transgressive breccias) and intrusion of the Bushveld Complex (because the ore paragenesis is clearly contact-metamorphosed as demonstrated by the presence of talc, tremolite and graphite formed from petroleum droplets). Many of these observations suggest a genetic affinity to MVT deposits. Basinal brines are thought to have mobilized trace fluorine from the sediments. Precipitation occurred below the impermeable barrier at the unconformity. A connection with a phase of large-scale fluid mobilization at ~2.0 Ga is assumed, triggered by the Kheis orogeny along the western margin of the Kapvaal craton (Duane *et al.* 1991).

Hydrothermal veins and hydrothermal-metasomatic deposits

These deposits may be produced by several geological process systems. Magmatic and diagenetic origins were mentioned above. Tensional tectonics, including continental rifting (e.g. Kenya) and distension of cratons by a network of smaller faults and shears (e.g. Late Variscan Europe), are further activators of fluorine metallogeny. It is possible that in some of these cases rising mantle volatiles, degassing of deep magma bodies and leaching of crustal rocks play a similar role, as recently proposed for the Rio Grande Rift (Partey *et al.* 2009).

The fluorite orebodies of the Kerio Valley in Kenya occur on the western border fault of the East African Rift. Proterozoic calcite marbles, gneiss and quartzite are exposed at the foot of the escarpment, which rises ~1300 m to the highlands above. Near the fault, the marbles host metasomatic fluorite masses that are controlled by cross-cutting structures. The gangue includes chalcedony, adularia, pyrite and chlorite, indicating epithermal conditions. Kaolinization of feldspar in country rocks is a prominent hydrothermal alteration. This sector of the rift displays Miocene and Recent basaltic to Na-rhyolitic volcanoes, fumaroles and hot springs that discharge much fluorine. The precise provenance of the fluorine remains open, however, because degassing magmas and older volcano-sedimentary rocks in the rift are equally possible sources. Note that the alkaline playa lakes Magadi, Nakuru und Elmenteita in the Rift Valley of southwest Kenya all have fluorine concentrations between 1100 and 1700 μg/L. Nevertheless, these lakes provide a favourable habitat for millions of pink flamingos *(Phoenicopterus minor)*.

Europe north of the Alps experienced several phases of "reactivation" following its consolidation by the Variscan orogeny, caused by large-scale tectonic processes such as the rifting and opening of the Tethys, Atlantic and Penninic oceans in the Jurassic, and a Tertiary phase of renewed rifting. During these periods, hydrothermal fluids were repeatedly generated and invaded both the metamorphic basement and the sedimentary cover. A number of formerly important epigenetic fluorite deposits resulted from these events, including the early Jurassic (Hettangian) fluorite (-barite) veins in the French Massif Central (Morvan) near Chaillac (Sizaret *et al.* 2004; cf. "Barite", Figure 3.6 and Figure 3.17). The Rossignol vein was filled in two stages: The first is remarkable by its open space sedimentation at low velocities of the ascending fluid. The second stage produced a fluorite-barite breccia and the barite sinter deposit on the surface. Fluids had low temperature (110°C) and high salinity (19–22% NaCl equiv.). Total production by underground mining amounted to 800,000 t at 50–60 wt. % CaF_2.

Exploration for fluorite is mainly based on geological and geochemical methods. Rock, soil and water analyses with the ion-selective fluorine probe are useful guides to prospective anomalies. In contrast to the brightly purple or green fluorite samples commonly seen, much ore-grade fluorite is not easily recognized. Because of its mobility, fluorine is also a useful pathfinder element whenever it forms part of the paragenesis, for example in many Pb-Zn-Ba deposits in carbonate rocks, in REE-carbonatites and in certain tin granites.

In 2009, 5 Mt fluorspar were produced worldwide after 6 Mt in 2008. With 60% of the total, China is the largest producer, followed by Mexico, Mongolia, South Africa and Russia. Identified resources amount to ~500 Mt of CaF_2 contained, and global resources of fluorine in phosphate rock are estimated at 1300 Mt fluorite equivalent (USGS 2010).

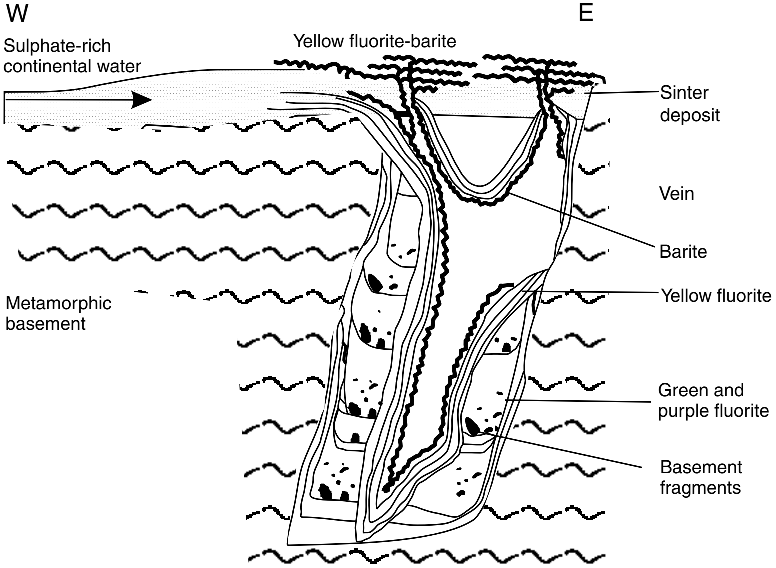

Figure 3.17 Schematic profile showing the evolution of Rossignol fluorite (barite) vein and its surficial barite sinter deposit Les Redoutières near Chaillac, France (not to scale). After Sizaret, S., Marcoux, E., Jébrak, M. & Touray, J.C. 2004, Society of Economic Geologists, Inc., *Economic Geology* Vol. 99, Figure 13B, p. 1120.

3.12 GRAPHITE

Natural graphite (C, Density 2.1 to 2.3 g/cm^3, calculated 2.27) often contains traces of hydrocarbons and of nitrogen. Its melting point is nominally at 3652–3697°C, but graphite sublimes instead of liquefying. The degree of graphitization is commonly characterized by X-ray diffraction and Raman spectroscopy (Lespade *et al.* 1982). Related to the grade of structural ordering, several varieties of graphite are distinguished. Optically, graphite is defined by reflectance $R_{max} > 9\%$, semi-graphite by R_{max} from 6.5–9% (Kwiencinska & Petersen 2004; cf. Chapter 6 "Coal"). Graphite is considered to be a "one-mineral" geothermometer (Luque *et al.* 1998), because its differential thermal analysis (DTA) maximum is thought to correlate with formation temperature. Natural graphite is intergrown with minerals such as sulphides and silicates. In practice, determination of carbon content is routinely done by combustion and the mass of residuum is termed "ash".

Graphite is one of the softest solids known (and diamond, the other natural crystalline modification of carbon, one of the hardest). The most important properties of graphite are softness and low friction, because of weak bonds between lattice layers; it displays high conductiviy of heat and electricity, resistance to acids and to temperatures reaching 3000°C in the absence of oxygen (in air, graphite oxidizes at 400–500°C). Grain size and carbon contents of graphite concentrate are main controls of its possible use. Highly valued flake graphite, with platelet diameters from >1 to 0.018 mm, is distinguished from the fine-grained and less valuable microcrystalline, or "amorphous" graphite. Massive crystalline lumpy graphite ("Ceylon lumps") is preferred to graphite dust (<100 µm). Although for some uses low carbon contents (say >40%) are acceptable, most traded concentrates grade >85 and even >90% carbon. Sulphides and abrasive or reactive minerals in concentrate are generally undesirable.

Flake graphite can be extracted at a minimum of 3–5% graphite in rock, whereas amorphous graphite ore requires grades >45%. Concentrates are prepared by flotation, wet-mechanical methods, cyclones and air separators. Very pure grades that reach C >99.9% are made by chemical refining of concentrates. Graphite resists supergene alteration, so that perfectly preserved flakes are found in decomposed rock and even in autochthonous soil. Extraction of weathered deposits is economically very attractive, compared with the high cost of separating the delicate flakes from fresh and hard rock. Accordingly, unweathered deposits stipulate higher ore grade (e.g. 16–18% C in Lac Knife, Quebec).

Large quantities of graphite are used for manufacturing foundry crucibles and moulds, and for recarburizing steel. Modern crucibles are highly complex composite materials, with 20–50 wt. % of flake graphite, depending on the properties required. Other possible ingredients include tar and pitch, silicon carbide, silicon metal or alloys, aluminoborosilicate glass and aluminosilicates (mullite). Quartz-rich graphite is used as an acidic and reducing slagging agent in iron blast furnaces. Graphite is also used as a lubricant, as a filler in paints, for manufacturing electrodes and as a substitute for asbestos in brake lining. Durable refractory bricks and mortars result from mixing flake graphite with magnesite or alumina. Small amounts of high-purity graphite play an important role in electrotechnology (e.g. lithium ion batteries), as a neutron moderator in fission reactors and in uranium-carbide nuclear fuel elements. Synthetic graphite and substances resembling graphite (e.g. carbon black) are made from petroleum coke in electric furnaces at 2600–3000°C. Several synthetic products have a different market from natural graphite (e.g. electrodes in electric arc furnaces, carbon fibres). Others compete with amorphous graphite (paints and anticorrosive protection). In the future, widespread use of fuel cells may require much graphite.

The source of graphite carbon is investigated by stable isotope analysis (Hoefs 2009, Faure & Mensing 2004). $\delta^{13}C$ of graphite ranges from −2 to −23‰, indicating a predominantly biogenic source of carbon with admixture of carbon derived from marine carbonate rocks, for example by calc-silicate formation (decarbonation) during metamorphism. With an average of 0.1–0.2 wt. %, graphite is a common accessory or trace mineral of igneous rocks. Isotope data indicate that even this magmatic carbon is mostly of organic derivation, possibly by assimilation of sedimentary country rocks (Luque *et al.* 1992).

3.12.1 Graphite deposit types

Graphite deposits commonly occur in rocks that experienced orogenic or contact metamorphism. Most large deposits are (1) metamorphic mineral deposits *sensu stricto,* with graphite derived by nearly isochemical transformation of sedimentary or diagenetic organic substances, including coal, kerogen and hydrocarbons. Whereas synthesis of graphite at ambient pressure requires very high temperatures, well-ordered graphite of metamorphic rocks typically originates at only 300–500°C, but at 2–6 kbar (greenschist facies metamorphism). Very large flakes seem to be restricted to amphibolite facies rocks. Coeval shear strain boosts graphite formation in experiments (Ross & Bustin 1997, Bustin *et al.* 1995) and natural graphite formation is enhanced by penetrative shearing during orogenic metamorphism. Apart from pressure, shear strain and temperature, controls on graphite formation include the type of organic precursors, the composition of the fluid phase, the available reaction time and the presence of minerals that may catalyse the reaction. Graphite-mineralized pegmatites, hydrothermal veins and shear zone-hosted deposits are clearly (2) epigenetic and mostly metamorphogenic deposits formed by migrating supercritical carbon-bearing fluids or fluid-rich magma.

The principle of epigenetic graphite formation is illustrated by the reactions of eq. 3.3 (Frost 1979).

Formation of graphite from hydrothermal C-O-H fluids at high T/P:

$$\begin{aligned}&2\mathrm{C}_{\text{solid}} + 2\mathrm{H_2O} \rightarrow \mathrm{CH_4} + \mathrm{CO_2}\\&\text{Mobilization}\qquad\text{Transport}\\&\mathrm{CH_4} + \mathrm{CO_2} \rightarrow 2\mathrm{C}_{\text{graphite}} + 2\mathrm{H_2O}\\&\qquad\qquad\text{Precipitation}\end{aligned} \tag{3.3}$$

Extremely reducing conditions are not required for stabilizing and precipitating graphite. Precipitation may be induced by fluid/rock interaction (e.g. chlorite formation by hydration, thus reducing $x\mathrm{H_2O}$), by fluid mixing and by redox-change. Isochemical precipitation is a consequence of falling temperature or rising pressure. Fluid-precipitated graphite is always well-ordered, even fine-grained "amorphous" varieties. The formation of high T/P carbon-bearing fluids is most often a consequence of metamorphism, but magmatic degassing can also produce graphite (Luque *et al.* 1998).

Orogenic metamorphic graphite

Orogenic metamorphic graphite is a common constituent of metasediments such as schists, quartzite, marble and paragneiss (Figure 3.18):

> In the Eastern Alps, deposits (e.g. Kaisersberg) are located in Late Carboniferous epimetamorphic sediments of the Upper East Alpine tectonic unit (Figure 1.89). Host rocks of graphite seams (former coal) include phyllites, slates, quartzite and conglomerates. Intensive folding, faults and shearing complicate underground extraction. Graphitization of the coal occurred during a Late Cretaceous-Palaeogene phase of orogenic deformation. Graphitization of the original coal is variable and some of the material is meta-anthracite. Structural ordering and crystallization are incomplete, because of weak synmetamorphic strain. The result is typical "amorphous" graphite with its main market in foundry applications.
>
> In the Variscan Bohemian Massif, graphite is associated with amphibolite-facies metamorphic rocks. Country rocks of graphite include amphibolite, calcite marbles, paragneiss and schists that are probably

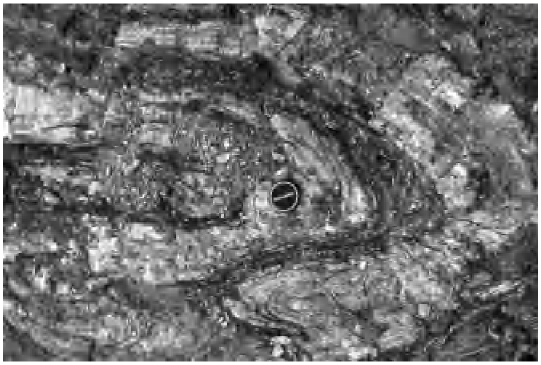

Figure 3.18 Graphite (dark bands) in folded amphibolite facies Palaeoproterozoic paragneiss at the abandoned Kanziku mine near Tsavo National Park, Kenya.

marine sediments of Early Palaeozoic age. Graphite occurs throughout the extension of this large crystalline basement block with mining districts in Austria, Czechia and southeastern Germany. Most of the deposits produced fine-grained flakes, but included "amorphous" portions. The Moldanubian graphites are "metamorphic oil shales" (former kerogen and/or bitumen-rich mudrocks). Accessory minerals in this ore include alkali feldspar, plagioclase, quartz, phengitic muscovite, Mg-rich dravitic tourmaline, kyanite, Mg-calcite and traces of dolomite, rutile, corundum, apatite, pyrite, pyrrhotite and chalcopyrite. Anomalous geochemical concentrations of Ni, Co, Cr, Mo, V and Se confirm deposition of the precursor sediments in a sea characterized by massive proliferation of life and euxinic conditions (cf. Chapter 1.3 "Black Shales").

Comparable graphite deposits in metamorphic sediments are exploited in the Canadian Grenville Orogen (e.g. Graphite Lake, Ontario with famously large and pure flakes), in Norway and in Madagascar that is also a source of highly valued flakes, although with a low output.

Contact metamorphic graphite deposits

These deposits can have very large reserves, but most exploit material of low crystallinity and flake diameter. In addition, irregular distribution of grades, relic coal and anthracite complicate extraction. La Colorada in Sonora, Mexico is reportedly the world's largest contact metamorphic graphite district. Dykes, sills and stringers of white granite intrude coal seams in Triassic limestone producing soft, amorphous graphite, natural coke and anthracite. Graphite seams reach a thickness of 8 m. Compared to world output, the district's production of ~10,000 t (2009) is insignificant.

Epigenetic graphite deposits

Epigenetic graphite deposits may take the form of cross-cutting veins or impregnations of shear zone material. Although not unique, the most famous deposits of the first occur in the late Archaean charnockitic terrain of Sri Lanka (Ceylon). Since 1834, they are a source of highly valued crystalline lump graphite (apart from chips and microcrystalline fractions):

Sri Lanka's deposits consist of vein fields with tens to over 100 single veins that reach a length of 500 m and a width of 3 m. Vein fill is variably either pure graphite, or graphite associated with a gangue of quartz, biotite, feldspar, pyroxene, calcite, apatite and pyrite. Some of the veins seem to be syngenetic with pegmatite. Coarsely crystalline flakes and needles of graphite are oriented perpendicular to the vein walls and banding reflects progressive vein growth. Phyllic graphite parallel to vein walls is a product of shearing. Sri Lanka graphite reaches a reflectance R_{max} of nearly 15%. Formation temperatures are estimated at 700–800°C. Genetic interpretation of these deposits is not sufficiently supported by data. With $\delta^{13}C$ between −2 and −9‰, graphite carbon of Sri Lanka is possibly derived from the mantle, but a mixture between organic and carbonate carbon cannot be excluded. Granulite metamorphism at depth or the intrusion of charnockitic magmas are likely means of mobilizing a carbon-rich volatile phase (Farquhar & Chacko 1991).

Exploration for graphite combines geological and geoelectric methods. Often, chance encounters during geological mapping (and notes in mapping reports) give initial clues. In weathered deposits, pitting and trenching is more revealing than drilling. When embarking on detailed investigations of a prospect, quality criteria (flake size and purity) and processing properties must be a parallel part of the work towards establishing reserves. The achievable array of products decides the commercial feasibility.

World production in 2009 amounted to ~1.1 Mt natural graphite, little different from 2008. China leads with ~70% of the total (both flakes and amorphous graphite), followed by India, Brazil, North Korea and Canada. Sri Lanka is still a source of valuable lumps, although with a low output (7000 tonnes). Reserves and resources of graphite are large. Any development of new mines depends on China's market control.

3.13 GYPSUM AND ANHYDRITE

		Density (g/cm^3)
Gypsum	$CaSO_4 \cdot 2H_2O$	2.3
Anhydrite	$CaSO_4$	2.96

Nearly monomineralic rocks of the two common calcium sulphates are exploited but in most applications, gypsum is preferred. Impurities in gypsum rock may be anhydrite, clay and carbonate, with accessory kerogen, bitumen, authigenic quartz and soluble salt. The same gangue occurs in anhydrite rock with soluble salts more common. Anhydrite rock is usually strong, massive and finely crystalline. Alabaster is a very fine-grained, massive and pure (>99%) gypsum rock that is used for ornamental purposes, preferably when it is snow-white and translucent. Alabaster originates by near-surface supergene solution and reprecipitation of gypsum. In arid and semiarid climate zones, ascending soil solutions may form gypcrete, similar to calcrete. Gypsite is an earthy variety of gypsum mixed with sand and soil. Selenite designates crystals of translucent and colourless gypsum.

Gypsum and anhydrite cannot be enriched by mine-site processing; therefore, run-of-mine material must meet buyers' stipulations. These include specification of purity (usually a minimum of 70–80% gypsum or anhydrite), carbonate contents (commonly <5%), MgO <2% and soluble salt contents ($NaCl + MgCl_2 + MgSO_4$) <0.02%. For many applications, white colour (low Fe-Mn concentration) is desired.

Gypsum is composed of 32.6% CaO, 46.5% SO_3 and 20.9% H_2O. When heated to ~65°C, $1^1/_2$ moles of water are lost and the remaining solid is very reactive "plaster of Paris". The relic $^1/_2$ mole of water is retained strongly until 95°C, when dehydration is quickly completed and the structure of the solid transforms into a polymorph of anhydrite (Klein & Hurlbut 1999). This "dead-burned" gypsum sets (hardens) very slowly. Most gypsum is consumed in the building industry, in the form of the fast-setting semihydrate $CaSO_4 \cdot {}^1/_2H_2O$, for example for wallboards and mortar. An average house in the United States is said to contain 7 tonnes of gypsum. Uncalcined gypsum is used as a retarder in Portland cement and as a calcium soil conditioner and sulphur fertilizer in agriculture. Small amounts of high-purity gypsum are used for industrial processes, such as smelting and glass-making.

Anhydrite may be added to the cement powder instead of raw gypsum, in order to retard setting of concrete. In deep coal mines, anhydrite is used for fire prevention as a backfill and plugging material in galleries. Note that anhydrite hydrates strongly and fast under ambient conditions (eq. 3.4), resulting in a volume increase of ~60%. This "heave" is quite a nuisance in mining, tunnelling and road building (Bell 1993).

Dehydration of gypsum and hydration of anhydrite:

$$CaSO_4 \cdot 2H_2O \leftrightarrow CaSO_4 + 2H_2O \qquad (3.4)$$

3.13.1 Deposits of gypsum and anhydrite

Deposits of gypsum and anhydrite are formed as chemical sediments of evaporating marine or terrestrial water bodies. Therefore, common country rocks of the calcium sulphates include dolomite, saline claystone and salt rocks such as halitite (cf. Chapter 4 "Salt Deposits – Evaporites"). With increasing concentration of seawater, calcium sulphates are precipitated after carbonate rocks and before rock salt. Gypsum is slightly soluble in fresh water (13.78×10^{-3} mole/L at 25°C and atmospheric pressure). Its solubility displays a positive correlation with temperature and salinity, but the maximum solubility at ~58°C does not change significantly with fluid salinity. Contrasting the behaviour of gypsum, the solubility of anhydrite is retrograde; it increases with falling temperature. The primary precipitate of calcium sulphate is gypsum; only at temperatures higher than 56–58°C, anhydrite is the thermodynamically stable phase. In sabkhas, conditions of gypsum and anhydrite stability switch easily so that multiple transformations are observed (eq. 3.4). With increasing overburden, however, already in early diagenesis anhydrite is the stable phase, at 50–70°C (Jowett *et al.* 1993). Dehydration of gypsum mobilizes a considerable mass of water and most of the strontium is abstracted with the dehydration water. Somewhere along the flow paths, celestite ($SrSO_4$, the principle ore of strontium) may precipitate and fill joints and rock cavities, replace beds or form irregular masses that can be economically attractive (cf. "Barite"). Overall, textures, structures and geochemistry of gypsum and anhydrite include the heritage from sedimentary formation and diagenetic alterations, and therefore reflect conditions from basin palaeogeography to the history of burial and uplift (Kasprzyk & Orti 1998).

Isotope data (D, O and S) provide a deeper understanding of gypsum and anhydrite formation. We have seen earlier that sulphur isotopes in seawater ($\delta^{34}S$ of sulphate) display strong variations with geological time (Figure 3.4). Also, stable isotopes allow deductions about conditions of sedimentation and diagenesis of calcium sulphate rocks. Gypsum and alabaster of the Paris Basin, for example, were not extracted from Tertiary seawater but leached from older Permian and Triassic evaporites. Messinian gypsum deposits in the Mediterranean region, by contrast, are direct precipitates from Neogene seawater. Sulphate ions in the Canadian McKenzie River system are derived from pyrite oxidation in the eroding mountains and not from sedimentary sulphate (Calmels *et al.* 2007). D and O isotope data usually allow a unique genetic attribution of associated water. Note that hydration water in gypsum is enriched in ^{18}O by ~4‰ compared to the water from which it is derived. The precise age of geologically young gypsum (and many other evaporite rocks) can be determined with the U-series disequilibrium method (Reich *et al.* 2009).

Many gypsum deposits originated by hydration of anhydrite rock, which was uplifted to the near surface by geological processes. Access of meteoric water initiates supergene gypsification that may reach a depth of several tens of metres. The anhydrite underneath often displays large karst cave systems. In the overlying gypsum, sinkholes and caves are ubiquitous and the surface resembles karst morphology of carbonate rocks ("gypsum karst", Figure 3.19). The processes of gypsification and karst formation are a function of the groundwater system, morphology and the nature and spatial arrangement of rock bodies. Sinkholes and caves may be filled with collapse breccias comprising gypsum and dolomite, and often with earthy impurities. Breccias can be cemented by calcite. In that case, leaching of gypsum fragments is the path to formation of cellular rocks termed "rauhwacke" (Schaad 1995).

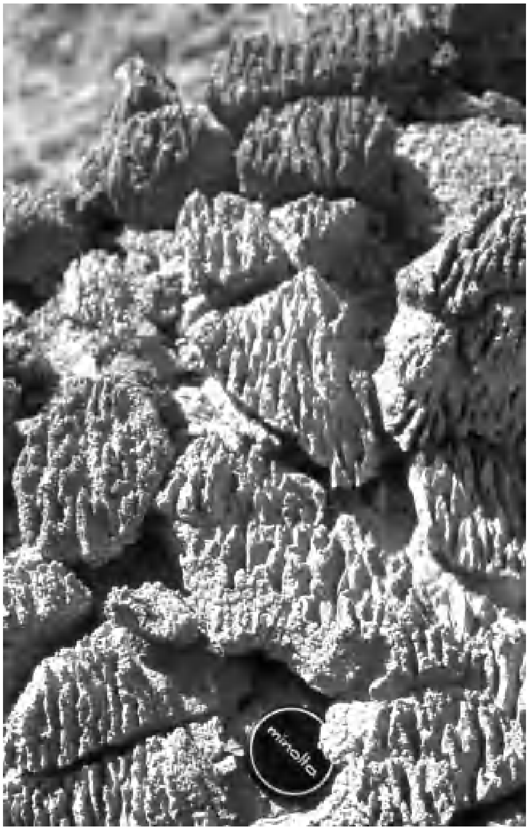

Figure 3.19 Gypsum outcrop at Wadi Essel, Red Sea Coast, Egypt, provides a model of full-scale gypsum karst morphology. Flutes and joint-controlled furrows also characterize the karst surface at the scale of tens to hundreds of metres.

Australia hosts a variety of young gypsum deposits. Its arid coasts are lined by numerous salinas (coastal salt lagoons), which originated due to the worldwide post-glacial rise of seawater levels. With rising oceans, valleys of Pleistocene dune belts were filled with seawater that evaporated (Figure 3.20). Sediments formed in these salinas consist mainly of gypsum, including solid masses of selenite near the base and banded gypsum sands. Near the margins, aragonite may occur. Holocene dry climate periods caused formation of gypsite dunes. All these varieties of gypsum are extracted

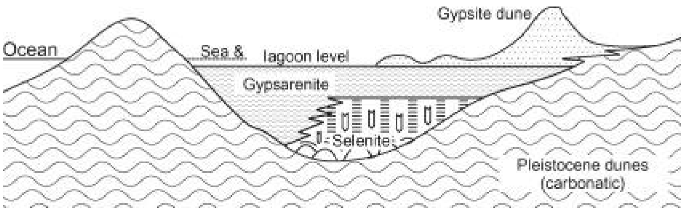

Figure 3.20 Schematic section of a Holocene coastal gypsum lagoon in South Australia (after Barnes 1990). Water level in the lagoon is lowered by evaporation.

and stockpiled for several years in order to reduce salt content by exposure to rain. Coastal Lake Macleod in Western Australia is essentially a dry lagoon of 100 by 30 km in size. Here, gypsum is extracted with a floating dredge, while salt brine is pumped from a deeper aquifer and harvested from evaporation ponds. In South Australia, gypsum was deposited in Pleistocene tidal Lake Alexandrina that developed at a highstand mouth of the Murray River, today some 50 km from the coast. This gypsum is well drained and free of salt.

Gypsum is mainly exploited in quarries and exploration is limited to near-surface deposits. Geological maps provide first guides. In the field, karst morphology and sulphate in spring water (determined by reaction with $BaCl_2$ solution) may provide clues. Georadar and drilling are employed to define shape and nature of the karst surface underneath soil cover, of the base of gypsification and of waste material filling karst caves. Often, this can only be done with a very close spacing of drillholes. Gypsum karst landscapes are ecologically peculiar and mining intentions may therefore be resisted. It is advisable to obtain a valid mining licence as early as possible in the course of investigations.

Gypsum and anhydrite are low-cost raw materials and deposits are common. Most countries are self-sufficient. Nevertheless, considerable quantities are internationally traded. World mine production in 2009 was ~152 Mt. Largest producers were China, Iran, Spain, Thailand and USA (USGS 2010). Synthetic gypsum is a by-product of coal-fired electric power plants and other smoke-stack industries, of phosphate processing and of de-acidification of industrial waste water (e.g. TiO_2-production). In the USA, synthetic gypsum accounts for ~22% of the total domestic gypsum supply. It is used like natural gypsum, except for special cases where elevated trace contents of heavy metals, acids, chlorine, soot and its small grain size may be problematic. Still unsolved is the problem of phosphogypsum. The production of 1 tonne of phosphoric acid from phosphorite results in ~4.5 tonnes of calcium sulphate. Unfortunately, the processing of raw phosphate ore specifically concentrates radionuclide (226) radium in the sulphate phase. ^{226}Ra emits (222) radon by radioactive decay and this inhibits nearly all uses of phosphogypsum, except for those plants that process phosphate ore with very low contents of radionuclides.

3.14 KAOLIN

		Density (g/cm^3)
Kaolinite	$Al_2Si_2O_5(OH)_4$	2.1 (aggregates) 2.6 (crystals)
Dickite	same as K.	2.6
Nacrite	same as K.	2.6
Halloysite	$Al_2Si_2O_5(OH)_4 \cdot 2H_2O$	2.09
Allophane	$xAl_2O_3 \cdot ySiO_2 \cdot zH_2O$	~1.9

The four first listed kaolin minerals ("kandites") are dioctahedral phyllosilicates made of 39.5% Al_2O_3, 46.5% SiO_2 and 14% H_2O, corresponding to a formula $Al_2O_3 \cdot 2SiO_2 \cdot 2H_2O$. On heating, the structurally bound water escapes at different temperatures: 390–450°C for kaolinite and 510–575°C for dickite. Kaolinite forms generally by weathering and low-temperature weakly acidic hydrothermal alteration (50–150°C). Compared to kaolinite, dickite and nacrite are rare and originate at higher hydrothermal temperatures (~150–300°C). Macroscopically crystalline nacrite is a characteristic gangue of high-temperature gold and tin ore. Kaolinite may have a well-developed crystal structure or, not surprising for a low-temperature mineral forming in soil, a disordered structure. Because this affects some uses, the degree of disorder is routinely measured by X-ray diffraction and expressed in figures between 0 (disordered) and 2 for nearly perfectly ordered kaolinite (Hinckley 1963). Allophane is poorly ordered or X-ray amorphous gel and is mainly found in soil. Allophane and halloysite are generally precursors of kaolinite and are not acceptable in high-grade kaolin products. However, halloysite and allophane-rich clay can be marketable.

Whereas mineralogical terms concerning kaolinite are well defined, the application of the geological and commercial term "kaolin" is much less precise. Kaolin clay in nature displays wide compositional variations and some commercial kaolin hardly contains kaolinite. It is important to remember the origin of the word kaolin from the Chinese *kau-ling*, which simply designates a location where clay for porcelain manufacturing was excavated and which was the source of the earliest samples sent to Europe. Meanwhile "kaolin" has captured many other industrial applications so that its suitability for porcelain-making is of lesser relevance.

Kaolin, or China clay rocks consist mainly of kaolinite and residual minerals of the precursor rock, for example quartz, potassium feldspar, very often muscovite and sericite, or biotite and tourmaline. Frequent accessories include anatase, goethite, haematite and crandallite-goyazite (Ca-Sr hydrophosphates). Kaolin rocks are commonly soft and clayey materials in the sand to clay-size fraction. Highest quality kaolin is brilliantly white. Commercial kaolin deposits contain between 10 and 60% kaolinite. By- or co-production of other minerals (mostly quartz sand, but also feldspar and mica) may materially improve the earnings of a mine. Kaolinite is concentrated from run-of-mine material by wet or dry processing, and upgraded by a number of chemical, physical and magnetic methods. Iron oxy-hydroxides, which are often carriers of toxic heavy metals (As, Pb, Cd, Hg), are removed by leaching and magnetic separation. However, few applications require preparation of a mineralogically pure kaolinite concentrate. Some admixture of minerals such as illite and sericite may be acceptable. Higher contents of illite, other clay minerals and iron diminish kaolin quality and cause transition to kaolinitic clays that include fire clay, ball clay (with 30–80% kaolinite) and flint clay (cf. Section 3.7 "Clay and Clay Rocks").

Useful properties of kaolinite include its chemical inertness, white colour, opaqueness, softness, small grain size (0.5–50 µm in nature), plasticity, high melting point (1850°C), white colour after burning, low electrical and thermal conductivity, low absorption and cation exchange capacity, and good dispersivity. Kaolin's chemical composition is suitable for manufacturing synthetic zeolites. By curing with the appropriate fraction of NaOH, zeolite A, for example, with an atomic ratio of $Na:Si:Al = 1:1:1$, can easily be prepared (Dyer 1988).

More than 60% of all traded kaolin is used as filler in paper pulp and for coating paper surfaces. Coating grade kaolin is the purest and most valuable kaolinite product. In the paper sector, kaolin is competing with similar white fillers such as barite, calcite, gypsum and talc, but several properties of these substitutes are not identical with kaolinite. High-grade kaolin is also applied as functional filler in paint, rubber, plastics, pharmaceuticals and after calcining (700–1200°C), as the main ingredient of porcelain (china clay). Lesser grades, commonly dry-processed, are added to ceramics of minor quality (for whiteness), to refractory mortar, cement and fertilizer. Because of the wide field of applications, the suitability of kaolin for specific uses can only be investigated by both mineralogical and appropriate technological methods.

3.14.1 Kaolin deposit types

Kaolin deposits are typically formed by surficial alteration of leucocratic feldspar-rich rocks (leucogranite, granulite, rhyolite, andesite, arkose) or of illite-rich claystone. Iron-rich rocks are unsuitable precursors. Feldspar and other Al-silicates are kaolinized by acidic meteoric water percolating near-surface rocks. This induces hydrolysis that liberates alkalis (Na, K, Ca) and SiO_2 into solution, which leaves the system (eq. 3.5). The reduction of the original rock's silica content connects kaolinization with the formation of bauxite. There are two main process systems where acidic waters may react with suitable rocks, that is (1) supergene autochthonous weathering and (2) hydrothermal alteration. Autochthonous kaolin soils may be eroded and resedimented, resulting in (3) sedimentary kaolin deposits. Rarely, kaolin forms in sand as a pore cement from infiltrating supergene solutions ("kaolin sand"). Discrimination between the various lines of kaolin genesis is based on geological arguments, and data such as the variation of O- and H-isotopes of water in the kaolinite crystal structure (Harris *et al.* 1999, Gilg & Sheppard 1996).

Formation of kaolinite from potassium feldspar:

$$\begin{aligned} &\underset{\text{Feldspar}}{2\mathrm{KAlSi_3O_8}} + 9\mathrm{H_2O} + 2\mathrm{H^+} \\ &\rightarrow \underset{\text{Kaolinite}}{\mathrm{Al_2Si_2O_5(OH)_4}} + 2\mathrm{K^+_{aq}} + \underset{\text{Silicic acid}}{4\mathrm{H_4SiO_4}} \qquad (3.5) \end{aligned}$$

Autochthonous, supergene kaolin deposits

These deposits form extensive, often remarkably white blankets above unaltered rocks (Figure/Plate 1.50). Similar to other mature soils, kaolin is prevalent in pluvial, and wet and dry (savannah) tropical climate. Related soils include laterite, bauxite and peat. The last case is prone to form kaolin with very little iron, because this is efficiently leached by organic acids. Unleached kaolin may contain goethite, siderite or pyrite. The quality of supergene kaolin is often impaired by elevated contents of halloysite. Generally, the lower part of a laterite profile is clayey and several bauxite mines co-produce high-grade kaolin or smectite clay from the same pits (e.g. Weipa, Australia with a production of 100,000 t/y of paper-grade kaolinite). Examples of large provinces of supergene kaolin include giant deposits in Russia (South Urals: Gorbachev *et al.* 2004, 2007), Brazil and USA (Austin 1998):

> High grade kaolin of the Amazon Basin was developed in the last decades. In this province, kaolin is part of an ancient lateritic regolith that formed a peneplain above Cretaceous sediments, magmatic rocks and a Precambrian crystalline basement. The regolith's former kaolinitic B-horizon was exposed by erosion and iron was removed where tropical forests and peat covered the land (da Costa & Moraes 1998). Resources amount to >500 Mt.

Sedimentary kaolin deposits

Sedimentary kaolin deposits are a valuable part of the world's largest kaolin provinces in the south-eastern USA (Georgia and South Carolina) and in Brazil (Amazonia). The American deposits are hosted by transgressive sediments of Late Cretaceous to Early Tertiary age, marginal to the Piedmont province. Cretaceous kaolin (and bauxite) is a product of *in-situ* supergene alteration, whereas the younger, Tertiary deposits have been formed by resedimentation of eroded older kaolin and by kaolinization of bauxite.

Hydrothermal alteration deposits of kaolin

These deposits occur in both volcanic and plutonic igneous rocks, provided feldspar content was high. Epithermal kaolinization is a characteristic by-product of high-sulphidation gold deposits but is, of course, independent of exploitable gold contents. Associated minerals are commonly halloysite, alunite and silica, but also dickite and nacrite, as in Mexico. Hydrothermal kaolinization of plutonic rocks characterizes geochemically specialized granites. This may be caused by strong acids (H_3BO_3, HCl and HF) in the fluids segregating from such melts. The result of fluid-rock interaction within the granite cupolas and their roof is greisen formation and kaolinization:

> The largest hydrothermal kaolin province in the world is Cornwall, with estimated resources of 5000 Mt kaolinized rock containing ~10 wt. % kaolin. Cumulative production amounts to 100 Mt of wet-processed kaolin. Deposits are zones of kaolinized granite that are several 100 metres long, 150 m wide and >250 m deep. Host rocks are Variscan granites including specialized lithium granites as the youngest phase. In the large pits around St. Austell zones of kaolinization are controlled by sheeted tin-tungsten quartz veins.

Very thin greisen bands line the vein contacts with the granite whereas kaolinization extends for tens of metres. Plagioclase is preferentially kaolinized, in contrast to K-feldspar that is sericitized. Quartz grains display lobate solution surfaces. Assuming that Al_2O_3 was immobile during alteration, a removal of SiO_2 (−27%), Fe_2O_3 (−59%), MgO (−27%), CaO (−88%), Na_2O (−98%), K_2O (−33%) and F (−56%) can be calculated. The total rock volume has been reduced by 28%. In the Goonbarrow pit the kaolinization affected not only granite but also felsic dykes ("elvans") that cut across the quartz veins. This sets 280 ± 2 Ma as the maximum age of kaolinization and confirms a hydrothermal formation process. Other observations, however, point to supergene processes (e.g. the oxygen and hydrogen isotope composition of kaolinite that suggests a meteoric origin of the water). The apparent contradiction is resolved by assuming two major steps in the formation of these deposits: An initial hydrothermal kaolinization was later (in the Tertiary?) overprinted by weathering and leaching of iron (Dominy & Camm 1998).

World mine production of ~30 Mt kaolin (2009) was provided by USA, Uzbekistan, Czechia, Germany, Ukraine, Brazil, United Kingdom and many other countries (USGS 2010). Consumption decreased by 15% compared to 2008, because of lower demand in world paper markets. World reserves and resources are enormous (~20,000 Mt).

3.15 MAGNESITE

Measured densities of the mineral magnesite $MgCO_3$ vary between 2.9 and 3.2 g/cm^3 (theoretically 3.0). Magnesite rock, however, has an average mass of only 2.7 t/m^3, due to porosity, dolomite contents and tectonic fracturing. Industrial use of brucite $Mg(OH)_2$ (density 2.37 g/cm^3) is similar to magnesite, especially for environmental applications, because its acid neutralizing capacity is very high. Exploitable deposits of natural brucite are rare (China, USA); usually it is made by reacting seawater with calcined dolomite. "Seawater magnesite" is produced in the same way. The synthetic products are in some aspects superior to natural magnesite because they can be "designed" to stringent specifications. In several plants, seawater as a source of magnesium is replaced by natural brines (Dead Sea, Great Salt Lake, Utah) and by residual brines of salt solution mining or of carnallite processing.

For most applications, the suitability of magnesite depends on low contents of Fe, Ca, Al and SiO_2. Because of the similarity of the ionic radii of Fe^{2+} and Mg^{2+} (0.83/0.75Å), solid solution of several percent $FeCO_3$ is not rare. Magnesites with higher Fe-contents (called breunnerite at 5–30% and mesitite at 30–50% $FeCO_3$) and Mg-rich siderites are not common. Some magnesites display traces of haematite as a reddish pigment, which indicates early exposure to an oxidizing (and saline) environment. Ca-contents may be caused by substitution in the crystal lattice but are more often due to the presence of dolomite. Dolomite occurs in host rock inclusions or in the form of the conspicuously white, coarse dolomite crystals ("horse teeth"), which appear in druses and veinlets traversing sparry magnesite rock. SiO_2 in magnesite occurs as quartz or chalcedony and in a number of silicate minerals such as talc, phlogopite, sepiolite, enstatite or clay. Several of these minerals bequeath Al-contents to products.

Untreated magnesite can be employed as a filler and slowly acting alkaline soil conditioner. Most applications, however, rest on its calcination (decarbonation) to the oxide (magnesia, MgO, melting point 2827 ± 30°C, density 3.58 g/cm^3). High-temperature calcination at 1500–2000°C results in unreactive, "dead-burned" refractory sinter magnesia, which is used as a basic lining in containers of molten steel. This consumes ~75% of total magnesia produced. Magnesia sinter of good quality is expected to contain >95% MgO, <1.5% CaO, <1% $Fe_2O_3 + Al_2O_3$ and <1.5% SiO_2 with a lime-silica ratio of 2:1. Bone magnesite reaches these requirements more easily. Sparry magnesite often needs to be upgraded by removing contaminants before sintering. Lately, magnesia sinter for special applications in the steel industry is melted in electric arc furnaces, resulting in very dense, granular "fused magnesia". "Electric-grade fused magnesia" is valued as an isolating powder in domestic heating appliances. "Hard-burned" magnesite is calcined at temperatures between

1000 and 1500°C. Its moderate reactivity is useful in animal feed and fertilizer. Calcining magnesite between 700 and 1000°C results in chemically reactive "caustic" or "light-burned" magnesia, which is used for floor cements and isolating boards, and in various applications including paints, paper, plastics, sealants, surface coatings, rigid PVC and polyolefin films. In industrialized countries, environmental applications consume much of the caustic magnesia produced. These include de-acidification of forest soil, desulphurization of combustion gas and chemical treatment of water.

"Seawater magnesite" is competing with natural magnesite. In 2009, seawater and natural brines accounted for ~55% of US magnesium compounds production. Synthetic magnesite, magnesia and magnesium metal are produced by reacting calcined dolomite with seawater (0.13% Mg), or with brine resulting from carnallite dissolution and KCl-recovery, or with natural evaporitic brines (e.g. Great Salt Lake, Dead Sea: cf. "Magnesium"). The intermediate product magnesium hydroxide can be further processed into magnesia (by dehydration) and calcined to the desired degree of reactivity. Compared to natural magnesite, the synthetic product may have higher MgO-contents, but its production (eq. 3.6) requires more energy.

Production of magnesium hydroxide from seawater or brine:

$$\underbrace{(CaCl_2 + MgCl_2 + H_2O)}_{\text{Brine}} + \underbrace{(CaO \cdot MgO)_{\text{solid}}}_{\text{Calcined dolomite}} + 2H_2O \rightarrow \underbrace{2Mg(OH)_{2\,\text{solid}}}_{\text{Mg-hydroxide}} + 2CaCl_{2\text{aq}} + H_2O \qquad (3.6)$$

3.15.1 Magnesite deposit types

Magnesite deposits (Pohl & Siegl 1986, Pohl 1990) of economic significance are formed by very different process systems. Virtually all are epigenetic:

- The first is desilication and carbonatization of Mg-rich ultramafic igneous rocks by CO_2-rich fluids that may have a magmatic, diagenetic, metamorphic or mantle degassing origin; the product is cryptocrystalline, or bone magnesite.
- The second is essentially the percolation of meteoric or low-temperature hydrothermal water through ultramafic rock massifs, dissolving Mg; the solutions discharge in freshwater or saline lakes, or infiltrate terrestrial basinal sediments; this setting is supergene mobilization followed by infiltration; magnesite precipitates occur in continental limnic sediments as cryptocrystalline, banded, nodular, or sinter-like magnesite.
- The third is characterized by metasomatic replacement of marine dolomite and limestone by cation exchange of Mg for calcium; this rests on the provision of Mg-chloride bearing solutions whose prevalent origin is probably evaporation in emerged parts of marine carbonate platforms; periodically magnesium-enriched seawater (Lowenstein et al. 2003; Lowenstein 2001) may have played a role; the genetic model is a combination of evaporation, infiltration and synsedimentary (early) diagenesis; this magnesite is commonly coarsely crystalline (sparry) and stratabound.

Ultramafic-hosted, or Kraubath type deposits

The name Kraubath is derived from a former mine in Styria, Austria. This magnesite occurs in strikingly white veins, stockworks, massive bodies within, or as caps above ultramafic rocks (Figure 3.21). Common host rocks are dunites, peridotites and serpentinites. Typically, these are parts of ophiolites, but mafic intrusions may also host magnesite occurrences (e.g. Bushveld). Most deposits of this type are related to a former land surface, with caps and stockworks near the surface, whereas some veins extend downwards for hundreds of metres. Magnesite veins can be very thick (up to 45 m at Mantudi, Euboea, Greece) and reach a length of 4 km (Susehiri, Turkey). Vein fill is nearly monomineralic magnesite but occasional quartz, chalcedony and calcite are observed. Near veins and stockworks, the host rocks are hydrothermally altered to "brown serpentinite", which consists of fine-grained serpentine, chlorite, deweylite, montmorillonite, nontronite, inherited chromite and goethite:

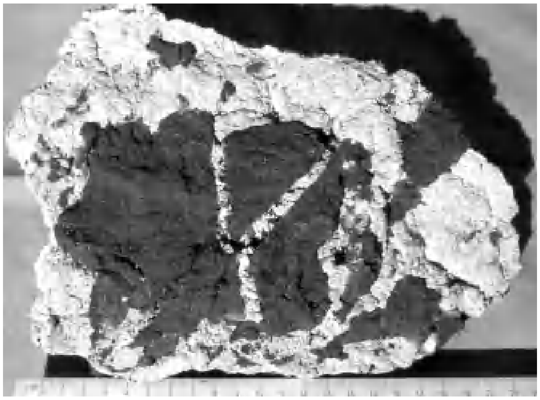

Figure 3.21 Dense white "bone" magnesite with a little quartz (grey, translucent) filling fractures in dunite is a product of near-surface hydrothermal carbon dioxide reacting with olivine (Kinyiki Hill, Tsavo, Kenya).

> Ultramafic-hosted magnesite is brilliantly white and cryptocrystalline. Grain sizes are mostly in the micrometer range; granular and fibrous textures are reported. Impurities include traces of Ca-Fe-Mn carbonates. The term "bone magnesite" describes its porcellaneous lustre and conchoidal fracture. Small veinlets often display ptygmatic folding. The surface of magnesite pockets may exhibit a characteristic colloform "cauliflower" texture and desiccation cracks. These magnesites are probably derived from a gel that consisted of Mg-hydrocarbonates such as nesquehonite $Mg(HCO_3)(OH){\cdot}2H_2O$.

Magnesite deposits of the Kraubath type are principally the product of the reaction between ultramafics and CO_2-rich aqueous fluids (eq. 3.7).

Magnesite formation from dunite:

$$\underset{\text{Forsterite}}{Mg_2SiO_4} + 2CO_{2aq} \rightarrow \underset{\text{Magnesite}}{2MgCO_3} + SiO_{2aq} \qquad (3.7)$$

If this chemical process is interpreted as an *in-situ* metasomatic replacement of dunite by magnesite, an increased volume should result. This is hardly ever observed, with the exception of the ptygmatic veinlets mentioned above. Also, chromite grains of the host rock are extremely rare in the magnesite. The obvious interpretation is that magnesite precursor colloids have moved within opening vein fissures. At the same time, silica was removed in solution (otherwise siliceous magnesite would have been formed, which is not rare but useless). There are two principal possibilities for the origin of the CO_2-rich fluids: i) infiltrating meteoric water; and ii) hydrothermal fluids from a deeper source (Pohl 1990, Fallick *et al.* 1991). The CO_2 of ascending fluids could be of magmatic, diagenetic, metamorphic and mantle derivation (Abu-Jaber & Kimberley 1992a, b). Stable C and O isotopes in ultramafic-hosted magnesite vary from 3 to $-20‰$ for $\delta^{13}C_{PDB}$ and 19 to $36‰$ $\delta^{18}O_{SMOW}$ indicating a variable mixture of different sources (Fallick *et al.* 1991, Zedef *et al.* 2000). An instructive parallel may be drawn to the Californian mercury deposits that are genetically connected to magnesite-SiO_2 stockworks in serpentinitic host rocks (Peabody & Einaudi 1992).

Lacustrine, or Bela Stena type magnesite deposits

These deposits occur in lake basins, which are underlain or surrounded by hills of ultramafic rocks. The ultramafics may contain Kraubath type magnesite and not infrequently, both deposit types grade into each other. The magnesite rock is similar in both types. At Bela Stena in the Miocene Jarandol Basin, Serbia, massive to laminated micritic magnesite forms a thick concordant lens in pelitic clastic sediments and zeolitized andesitic tuff. Nearby, several borate beds have been found (Obradovic *et al.* 1992). Tertiary lake sediments near Bozkurt, Denizli in Turkey contain pure magnesite beds. At Eskishehir (Turkey) magnesite veins in ultramafic rocks extend into lake sediments forming elongate zones of the famous meerschaum (sepiolite) deposits. In the Tertiary basin at Aiani-Kozani (Greece), hydrothermal springs exiting in the lake have produced large sinter masses of hydromagnesite $Mg_4(OH)_2(CO_3)_3{\cdot}3H_2O$, huntite $CaMg_3(CO_3)_4$ and some magnesite, occurring along concealed faults. Laterally, the sinters pass into thick beds interstratified with the lake sediments. The sinter carbonates have high degrees of whiteness and are exploited as fillers (Stamatakis 1995). Hydromagnesite stromatolites occur near seeps on the shores of the alkalic Salda Gölü Lake in southwestern Turkey. Erosion products are transferred to deeper

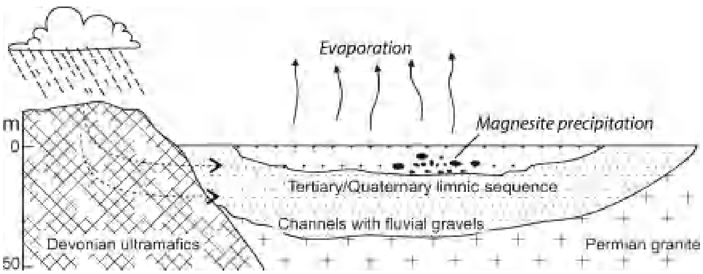

Figure 3.22 Principles of the assumed supergene leaching, infiltration and evaporation origin of the limnic magnesite deposit at Kunwarara in Queensland, Australia (modified from Wilcock 2000).

water and form hydromagnesite mud (Braithwaite & Zedef 1996).

At Kunwarara in eastern Queensland (Australia), a very large deposit of nodular cryptocrystalline magnesite was discovered in Tertiary-Quaternary alluvial and lacustrine sediments adjacent to hills formed by ultramafics (Wilcock 2000). The basin is over 60 km long. Magnesite nodules and lumps displace red fine-grained sand and grey magnesitic mudstone which form the upper section of an infill of ~40 m thickness. Black clay covers the exploitable horizon which may be controlled by fluviatile meanders. The magnesite-enriched blanket is proven in an area of 30 km^2, with an average thickness of 8 m. Total resources approach 800 Mt. These magnesites probably orginate from infiltrating meteoric groundwater derived from the hills (Figure 3.22). Precipitation of the magnesite may have been induced by evaporation in dry, either seasonal or longer, climate-controlled periods. Organic matter and bacterial activity in the deeper basin sediments could also have had a role.

All these observations confirm that Bela Stena type deposits are formed from low-temperature or ambient aqueous solutions that discharge in lakes or infiltrate terrestrial basinal sediments. Magnesium is leached from nearby ultramafic rocks and transported along variably deep flow paths. Hydraulic head is probably provided by topographical elevations surrounding the basins. Deeper convectice systems may be driven by geothermal heat, as indicated by elevated trace contents of boron and arsenic in Neogene lacustrine magnesite-huntite of Southwest Turkey. The precipitation of magnesite and related minerals is controlled by physical and chemical conditions at the sites where spring waters enter the lakes or react with pore water in sediments.

Marine carbonate-hosted, or Veitsch type

Veitsch type magnesite (the name is derived from a formerly important mine in Styria, Austria) forms large replacement masses and stratiform lenses in marine platform sediments. Deposits are mainly found in Proterozoic and Palaeozoic rocks and are rare in both Archaean and post-Palaeozoic times. Country rocks comprise dolomite, limestone, black and grey pelites, sandstone, conglomerate and mafic volcanic rocks. Metamorphism may vary from very low grade (Eugui-Asturetta in Spain) through greenschist facies (the majority of deposits) to upper amphibolite facies (Namdechon, Korea, Liaoning, China) and possibly to granulite facies (Snarum, Norway, although this is a somewhat enigmatic occurrence):

Typically, the magnesite rock of these deposits is massive and sugary to coarse-grained. Its colour may be white, grey, black, yellowish, reddish or brown. Many deposits have parts with a "pinolitic" texture (Figure 3.23). The term designates the presence of white, elongated magnesite crystals ("pinolites" resemble the edible seeds of *Pinus pinea*) in a fine-grained dark matrix, that consists of clay or chlorite, organic material, pyrite, talc and dolomite. Clearly, pinolite growth displaced the dark matrix. The long axis of the pinolites may form an irregular fabric or three-dimensional rosettes, or they may grow perpendicular from bedding planes, joints and stylolites resulting in mono- or bipolar fabrics. In the magnesite rock, traces of bedding may be preserved; less frequent are various sedimentary fabrics such as cross and oblique bedding, ripple marks, erosion channels, syn-sedimentary breccias and desiccation fissures. Beds of limestone, dolomite and chert may occur between magnesite rock bodies. In the magnesite, traces of pyrite (and other sulphides) and bitumen are common, whereas haematite and plant remains are

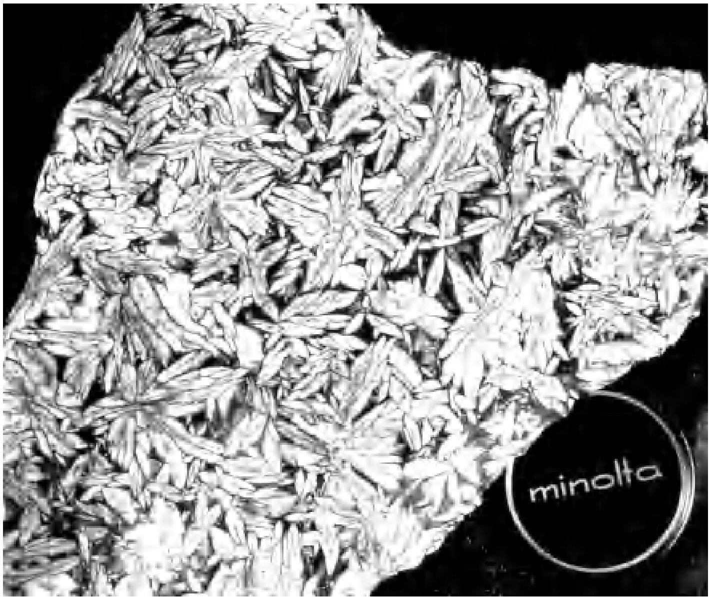

Figure 3.23 Pinolite-textured magnesite from Hohentauern Mine, Austria. Note the crystal rosettes and general displacement of formerly dispersed impurities by crystals growing during diagenesis.

very rare. Most of these features are sedimentary or early diagenetic, others imply late diagenetic (e.g. stylolites) or even metamorphic conditions. Contacts to host rock clearly display metasomatic replacement. Normally, this affects carbonates, but replacement of meta-pelite, quartzite and chert was reported. Generally, magnesite rock bodies are enveloped by a dolomitic alteration halo.

The genesis of sparry magnesite deposits is the result of different geological process systems that lead to magnesium metasomatism of precursor limestone or dolomite (eq. 3.8). Epigenetic and hydrothermal, or sedimentary to early diagenetic, low-temperature processes in the marine environment are possible actors.

Magnesite formation by Mg-metasomatism of limestone:

$$CaCO_3 + Mg^{2+}{}_{aq} \rightarrow MgCO_3 + Ca^{2+}{}_{aq} \qquad (3.8)$$

Abundant data supporting metasomatic replacement of precursor carbonates by magnesite have been published in the past. Replacement of already lithified carbonates by magnesite was described for Eugui, Spain (Lugli *et al.* 2000) and Rubian, Spain (Kilias *et al.* 2006). In the replacement model, the most probable transport medium of Mg is chloride solutions. Dissolution of Mg, transport and precipitation of magnesite are a function of temperature, pressure, salinity, relative activities of Mg and Ca and possibly biogenic factors. Microbial mediation by sulphate-reducing bacteria (equations 1.15 and 1.16) probably plays a role for magnesite formation as it does for dolomite precipitation at low temperatures (Vasconcelos *et al.* 1995).

The hydrothermal epigenetic model is supported by thermodynamic modelling and experiments showing that higher temperature favours the formation of (dolomite and) magnesite. Different sources of hydrothermal Mg-fluids have been proposed in the past, including deep magmatic intrusions, metamorphism of carbonates or of ultramafic rocks, contact metamorphism of dolomite and late diagenetic formation waters (basinal brines) that have reacted with dolomite. Also, some sparry magnesites may have formed like dolomites, by downward infiltration of seawater into carbonate platforms, which were heated from below, for example by synsedimentary magmatic activity (Wilson *et al.* 2000) or rifting (Powell *et al.* 2006). Another potential Mg-source is the incongruent dissolution of carnallite caused by the passage of Mg-undersaturated fluids (eq. 3.9). In the Permian salt deposits in Germany, carnallite is often the primary potassium salt mineral. Near fault zones in many deposits, the carnallite beds have been changed into sylvite (KCl) by brines, which were saturated in NaCl but not in $MgCl_2$. KCl is much less soluble than $MgCl_2$. Obviously, partial dissolution of carnallite is one way of producing Mg-rich brines, which may react with carbonate rocks along their further flow paths, forming "late diagenetic" or "hydrothermal" dolomite and magnesite.

Incongruent dissolution of carnallite as a source of dissolved magnesium:

$$KCl \cdot MgCl_2 \cdot 6H_2O \rightarrow KCl_{solid} + MgCl_{2aq} + 6H_2O \quad (3.9)$$

Sedimentary and early-diagenetic models of sparry magnesite metasomatism are closely related to concepts of dolomite formation. Because of kinetic limits, magnesite is rarely a primary sediment, comparable to dolomite (McKenzie & Vasconcelos 2008). An exception is anoxic environments that support sulphate reducing microbes (Vasconcelos *et al.* 1995). Ammonium resulting from biogenic breakdown of organic matter (eq 1.15) favours magnesite formation (eq. 3.10).

Ammonium-induced magnesite formation:

$$MgCl_2 + 2NH_3 + CO_2 + H_2O \rightarrow MgCO_3 + 2NH_4Cl \quad (3.10)$$

This reaction was first observed in soda production plants working with the Solvay process (Waeser 1926). Deelman (2001) demonstrated that small oscillations of the concentration in the solution favour the precipitation of magnesite. Deeper horizons of arid land typically contain high concentrations of nitrogen (Walvoord *et al.* 2003) that may induce oscillating NH_3-contents in brines infiltrating from emerged carbonate platforms.

Direct primary sedimentation of magnesite has been proposed by evaporation of $CaSO_4$-poor Proterozoic seawater (Frank & Fielding 2003). Recent early diagenetic replacement formation of magnesite is common, for example in the sabkhas of the Arabian Gulf. This confirms that evaporitic conditions favour magnesite precipitation. Traces of a former evaporitic environment in magnesite deposits are known. They include occurrences of anhydrite, gypsum and possible dissolution breccias at Sunk, Styria; Asturretta, Spain; Liaoning, China (cf. "Borates") and sabkha-playa sediments at Palaeoproterozoic magnesite occurrences near the White Sea in Russia (Melezhik *et al.* 2001). More often, however, the facies of the precursor sediments indicates a subtidal marine environment. In that case, magnesite may have been formed by infiltrating evaporative brines from nearby emerged regions (Pohl 1990), similar to the reflux model proposed for dolomitization (Jones *et al.* 2002). Investigations at the Satka deposit (Urals) confirm this model (Ellmies *et al.* 1999). Similarly, sparry magnesites in the Neoproterozoic and Cambrian of British Columbia, Canada, occur near emerged evaporitic parts of platform carbonates (Simandl & Hancock 1996). Powell *et al.* (2006) describe Middle Cambrian submarine brine seeps in Burgess Shale, spatially associated with magnesite and talc deposits.

Probably all these processes may contribute to form sparry magnesite deposits by low to moderate-temperature metasomatism. However, although Veitsch type magnesite rocks are relatively rare, they are not exotic and rather common geological processes should dominate their genesis. This is most probably the diagenetic realm and brines derived from evaporated seawater are the most likely source of magnesium. It is possible that the common abstraction of Mg from diagenetic pore waters in sedimentary basins by chlorite is the limiting factor for magnesite deposit formation.

Magnesite rock is quite resistant against supergene alteration. Commonly, outcrops show conspicuous massive rocks that may be white (if poor in Fe) or yellowish-brown (in case of elevated Fe). Magnesite pebbles can be traced for considerable distances in rivers. For exploration, geological methods are very effective.

With ~12,000 Mt, the world's resources and reserves of magnesite are very large and many regions have not yet been investigated for this mineral. More than 90% of the total is sparry magnesite, whereas resources of cryptocrystalline magnesite are much smaller. Brines and seawater, however, are practically inexhaustible. Leading magnesite producers are China (~56% of world mine production), Turkey, Russia, Slovakia and Austria. World production of magnesite is ~18 Mt per year.

3.16 MICA (MUSCOVITE, PHLOGOPITE, VERMICULITE)

		Density (g/cm^3)
Muscovite	$KAl_2(OH)_2(AlSi_3O_{10})$	2.8–2.9
Phlogopite	$KMg_3(F,OH)_2(AlSi_3O_{10})$	2.8–2.9
Vermiculite	$Mg_{0.3}(Mg,Fe,Al)_{3.0}(OH)_4(Si,Al)_4O_{10}\cdot 8H_2O$	2.4

These three minerals of the mica group are economically significant (Madhukar & Srivastava 1995). Vermiculite is structurally similar to talc and is essentially derived by alteration of biotite and phlogopite. Due to elevated iron-contents, unaltered biotite is of little practical use. Phlogopite (Mg-mica) resembles biotite in composition but is nearly free of iron. By substitution of iron (II) for magnesium, a continuous solid solution series is established, which makes a clear distinction between biotite and phlogopite impossible. Muscovite is chemically rather simple, with only minor substitution of K (by Na, Rb, Cs), Al (by Mg, Fe^{2+}, Fe^{3+}, Li, Mn, Ti, Cr) and (OH) by F. Its sodium equivalent paragonite, although isostructural with muscovite, is not miscible at low to moderate temperatures.

3.16.1 Muscovite and phlogopite

Muscovite (white mica) and phlogopite (amber mica) have similar uses. However, there are differences because muscovite is less heat-resistant compared with phlogopite. Upon heating, water loss of muscovite commences at 400–500°C, whereas phlogopite remains stable to 850–1000°C. Obviously, phlogopite is preferable for high-temperature applications. Both minerals display a perfect basal cleavage and can be split into thin sheets. The sheets are flexible, elastic, resistant against heat shock and exhibit excellent electrical insulating properties. Mica sheets are mainly used in the electronic and electrical industry. Smaller flakes and scrap are produced for many applications, including drilling additives, paint, plastics, roofing and rubber.

Sheet mica is extracted from muscovite pegmatites (cf. Chapter 1.1 "Ore Deposits in Pegmatites"). Associated minerals include quartz and feldspar, minor tourmaline, beryl, tantalite and spodumene. Large crystals, called "books", or crystalline aggregates of mica are usually concentrated in the wall zone of pegmatite bodies, but also in pockets and lenses within the main mass. Zoned pegmatites are more favourable for mining than unzoned chaotic bodies, because this facilitates exploration and extraction. Mining and dressing the sales products to blocks, plates and sheets requires highly skilled manual labour. This explains why sheet mica production is virtually non-existent in high-wage countries. Sheet muscovite deposits are known to occur in China, India, Russia, Madagascar, Zimbabwe and Brazil. Sheet phlogopite is very rare compared with muscovite; it occurs in pegmatitic pyroxenite dykes that intrude gneiss and granite (Madagascar, Canada).

Flake and scrap ("ground") mica: Muscovite and phlogopite are mass-produced by mechanized extraction of pegmatites and other micaceous rocks (e.g. weathered and kaolinized granites and alaskites, mostly of S-type, sericite phyllites, micaschists, phlogopitized peridotites). They are also a by-product of kaolin, feldspar and Li-Ta mining. Hard rocks are comminuted (therefore the term "ground mica") and mica is enriched by wet or dry processing methods. Dry grinding results in a greasy product, which is useful for roofing, paper and drilling fluids. Wet grinding produces thinner, glossy platelets, which embellish paint (e.g. metallisé paints of vehicles), facing plaster, plastics and gypsum wallboard.

The Neoarchaean (2.61 Ga) Siilinjärvi carbonatite complex in Eastern Finland hosts an important deposit of glimmerite consisting of phlogopite (Figure/Plate 3.24), apatite and carbonate.

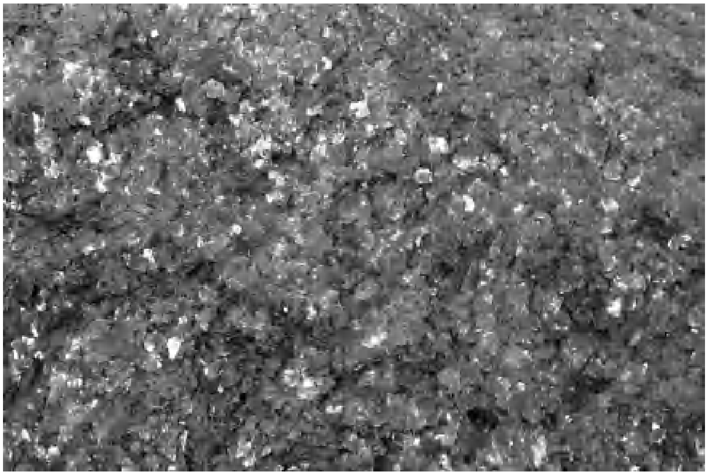

Figure 3.24 (Plate 3.24) Concentrate of phlogopite flakes produced at Siilinjärvi, Finland, is processed for use in decorative paint, special plastics and fire protection coatings. Courtesy LKAB 2010.

Sericite phyllites are essentially composed of fine-grained (<200 µm) white mica. They form at low metamorphic grades below temperatures of ca. 400–450°C. Above this temperature, grain size increases so that the mineral is "muscovite" and at 580–600°C white mica finally breaks down to K-feldspar and aluminium silicate. White micas in metamorphic rocks include muscovite, paragonite (sodium mica), celadonite (iron) and phengite (magnesium). Some uses may exclude specific white mica minerals. Many sericite-rich deposits are products of hydrothermal ("phyllic") alteration of feldpathic rocks (cf. Chapter 1.1 "Hydrothermal Alteration", eq. 1.6), including orthogneiss, aplite and felsic volcanics. The fluids responsible for alteration may be magmatic (La Crocetta, Elba, Italy: Maineri *et al.* 2003) or metamorphic. An example for the latter is "leucophyllite" in the Eastern Alps (Austria). Leucophyllites are rocks that consist of sericite, Mg-chlorite and quartz. Precursor rocks were Palaeozoic granite gneiss and Permian quartz porphyry. During the Cretaceous orogeny, metamorphic fluids were channeled along shears and nappe boundaries, and in some locations caused pervasive sericitization (Prochaska *et al.* 1997).

3.16.2 Vermiculite

Vermiculite of economic quality is visibly micaceous (>3 mm). Microscopic aggregates occur in soil and sediments but have no commercial value. Vermiculite develops from biotite or phlogopite through replacement of interlayer K by hydrated Mg (Na, Ca) cations resulting in expansion of the structure. Concurrent oxidation of Fe(II) to Fe(III) is characteristic. This alteration of the micas may be caused by low-temperature hydrothermal systems or by intensive tropical weathering. The name of the mineral derives from the observation of worm-like growth and buckling when it is heated. Heating vaporizes interlayer water and the vapour drives expansion. The extent of expansion is the main measure of quality; a minimum of 6-fold exfoliation is expected, but 50-fold volume increase is possible. An extremely important second criterion for marketable vermiculite is the total absence of asbestos. Raw vermiculite is processed at the mine site by crushing, screening and winnowing into a concentrate of large flakes (16–0.25 mm) and a bulk density of 640–1000 kg/m^3. Near consumer markets, the concentrate is expanded by flash heating to ~870°C in a furnace, yielding a sales product density of 52–192 kg/m^3. A new microwave exfoliation process promises to reduce energy consumption to about one fifth.

Expanded vermiculite is extremely light and porous, and has a high internal surface. This results in properties such as efficient thermal and acoustic insulation and high adsorption capacity. The heated mineral has a good thermal stability and no known health risks. Therefore, it replaces asbestos in many applications. Most vermiculite is used in the building industry (for fireproofing, heat and sound insulation) and in agriculture (for soil improvement, replacing peat). This is similar to applications of perlite and pumice (cf. Section 3.27 "Volcaniclastic Rocks") or of expanded clay aggregates. Smaller amounts of vermiculite are consumed as industrial fillers or in environmental engineering (e.g. absorbents for oil spills).

Vermiculite deposit formation requires the presence of rocks that are chemically predisposed to formation of massice biotite and phlogopite. Therefore, common host rocks are ultramafic magmatic rocks. Pervasive flooding by hydrothermal fluids causes transformation of the primary olivine and pyroxene of these rocks into nearly monomineralic mica bodies. Vermiculite may be generated during waning hydrothermal conditions or by later surficial alteration. One giant deposit in South Africa (Palabora) and deposits in the USA and in China produce the bulk of world supply:

> Large vermiculite deposits occur in Virginia, South Carolina and Montana. One of the largest deposits in the world was the mine near Libby in Montana (Figure 3.25). An alkalic Cretaceous ring complex with pyroxenites and nepheline syenites intruded Precambrian metasediments (Boettcher 1967). In the centre, a pyroxenite plug is altered to biotite and vermiculite. Vermiculite has been drilled to over 300 m depth below the surface indicating that hydrothermal systems, probably related to later syenite phases, were the cause of mica formation. A high incidence of asbestos-related deaths and respiratory diseases affecting miners and townspeople led to closure of the mine in 1990 when the vermiculite ore was found to contain tremolite asbestos (Van Gosen 2007).
>
> At Palabora (South Africa) >200,000 tonnes of vermiculite are produced annually from a pyroxenitic-syenitic and carbonatitic alkali complex. The carbonatites are a source of copper, zircon, magnetite and apatite (cf. Chapter 2 "Copper"). Vermiculite is extracted from pegmatitic phlogopite-diopside-apatite-olivine rocks with contents of >15% vermiculite and a grain size of >0.45 mm. Generally, alteration of phlogopite to vermiculite reaches from the surface to a depth of 50 m, which is thought to indicate a supergene origin. In some drillholes, however, vermiculite was found at depths exceeding 400 m. Accordingly, a hypogene hydrothermal formation cannot be excluded.

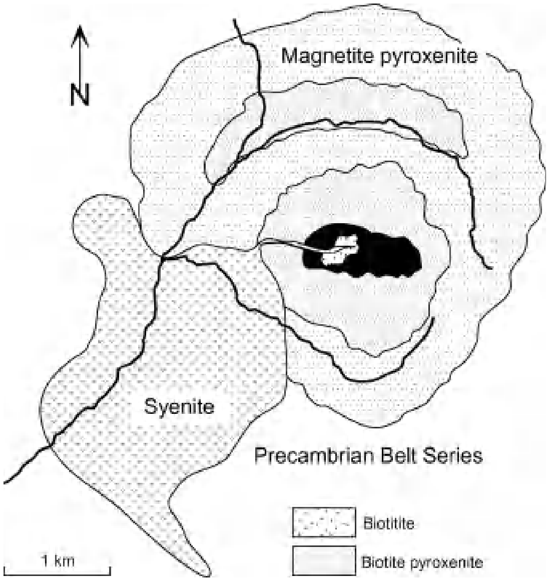

Figure 3.25 Geological setting of vermiculite in the Mid-Cretaceous alkaline-ultramafic Rainy Creek Complex, near Libby, Montana (adapted from Boettcher 1967). By permission of The University of Chicago Press. Vermiculite ore formed from biotite-pyroxenite (black) surrounds a central pipe of biotite that was intruded by alkalic syenite dykes. The ore had about 30–50 wt. % vermiculite content.

Occurrences of vermiculite often line the contacts between ultramafic rocks and intruding pegmatites. Reaction of felsic hydrous melt with ultramafics produces corundum and kyanite-bearing pegmatites ("plumasite"; in Kenya with ruby and sapphire: Pohl *et al.* 1980). Marginal alteration displays a characteristic zoning of distal anthophyllite and proximal phlogopite, chlorite and vermiculite.

The world's annual sheet mica production amounts to ~5200 tonnes per year, almost only from India and Russia. Largest producers of ground mica are Russia, USA and Finland; world production in 2009 was 380,000 tonnes. Vermiculite is provided to world markets by only three countries: South Africa, China and USA. In 2009, world production amounted to 550,000 tonnes (USGS 2010).

3.17 OLIVINE

Olivine	$(Mg,Fe)_2SiO_4$	Density 3.2 (forsterite) – 4.4 g/cm^3 (fayalite)

Forsterite (Mg) and fayalite (FeII) are end members of a continuous solid solution series. Manganese and calcium may substitute part of Mg and Fe. Valuable olivine is generally forsteritic. Already in antiquity, it was mined as a semiprecious, clear and translucent mineral (peridote) on tiny Zebirget Island (St Johns) in the Red Sea, Egypt. About 100 years ago, nearly monomineralic olivine rocks (dunite) were first used as a refractory material. With a melting point of 1890°C, Mg-rich forsterite is understandably preferred to Fe-rich fayalite (1205°C).

Olivine is in demand for manufacturing special refractories, but mainly (75% of total consumption) as a slag conditioner similar to dolomite in pig iron production. In this sector, iron content of olivine is accepted. The use of olivine is advantageous because it replaces dolomite and reduces coke consumption, thereby diminishing CO_2 emissions. Olivine is also used for sintered heat-storage elements in electrical heating appliances where it competes with magnesia made from magnesite. Olivine makes good foundry sand because compared with quartz, the mineral displays a lower expansion when heated. It requires less binder (e.g. bentonite) so that steam development during casting is reduced. However, other alternatives such as zircon and chromite sand are less easily damaged by sudden heat shock. Olivine sand is also a useful abrasive (hardness $6^1/_2$–7) and poses no hazard concerning silicosis.

Olivine is very prone to hydration and weathering (cf. Chapter 1.2 "Lateritic Nickel Ore Deposits"). Hydration is easily measured by the loss on ignition (weight %). It should be minimal where refractory application is the target. Unaltered dunites and olivine-rich peridotites are quite rare. However, the propensity to alteration is very useful if the aim is sequestering CO_2 into stable minerals. Ground dunite rock may be one means of immobilizing carbon dioxide. The reaction (eq. 3.6, Section 3.16.1 "Magnesite") is exothermic and the heat might be recovered.

Common accessory minerals in dunite including chromite and pyroxene can be removed by processing. The same applies to joints coated with serpentine and magnesite, but net-textured serpentinization of olivine grains at the microscopic scale impedes some applications. When heated, hydrated minerals give off steam that fractures the grains.

3.17.1 Olivine deposits

Pure and unaltered (hydrated) forsterite fels (dunite) is the preferred olivine raw material. Deposits occur in ophiolites and in complex intrusions of the Alaska-Urals type.

The world's largest olivine mine is Åheim in western Norway (Figure/Plate 3.26). Polymetamorphic Palaeoproterozoic gneisses enclose a large (5 × 1 km) ultramafic body with dunite and several eclogite inclusions (Sturt *et al.* 2002). The dunite is enveloped by a narrow (100 to a maximum of 300 m) serpentinization mantle, which is due to interaction with metamorphic fluids. Exploitable dunite comprises ~50 vol. % of the ultramafic body. The extracted rock displays a loss on ignition of <2 % and consists of 91% forsterite and 7% enstatite, as well as some serpentine, chlorite, chromite and spinel (Figure/Plate 3.27). With a capacity of 2.4 Mt per year, Åheim is reported to provide >50% of olivine sand produced worldwide.

International statistics on olivine (dunite) production are incomplete and most is probably comprised in the giant class of "crushed stone and aggregates". A large seaside quarry at Atammik between the capital Nuuk and Maniitsoq in Greenland, with an annual production of 1 Mt, was put on hold in 2009.

3.18 PHOSPHATES

Apatite	$Ca_5(F,OH,Cl)(PO_4)_3$	~40 wt. % P_2O_5	D = 3.2 g/cm^3

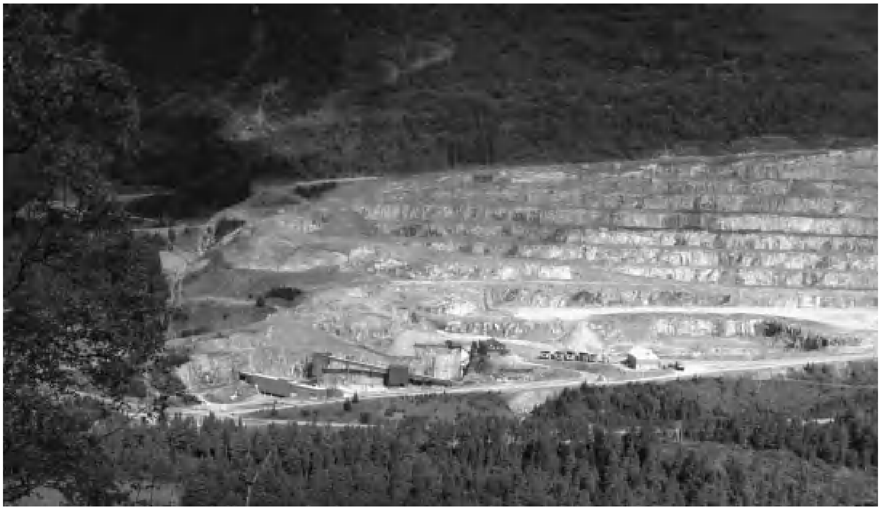

Figure 3.26 (Plate 3.26) Part of the Åheim (Almklovdalen) olivine quarry in southern Norway. Courtesy of Håvard Gautneb, Geological Survey of Norway, Trondheim.

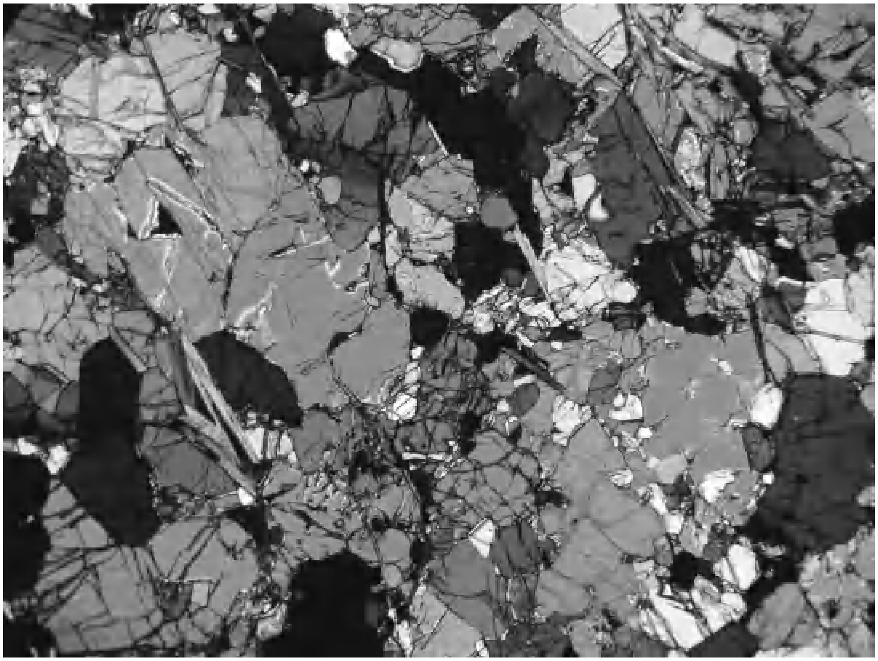

Figure 3.27 (Plate 3.27) Åheim dunite in thin section (crossed nicols). Olivine grain diameter is 1–2 mm. Note the fractures with weak net-textured serpentinization. Courtesy of Håvard Gautneb, Geological Survey of Norway, Trondheim.

Apatite is chemically highly variable. Calcium may be substituted by Mn, Sr, Na, Mg, U or REE. Fluorine and (OH) can be replaced by Cl and (CO_3). Silica (SiO_4) or (SO_4) may take the place of (PO_4). Therefore, many different names have been proposed for varieties of apatite (Kohn *et al.* 2002). Apatite is very useful for radiometric age determination by the fission-track method (Wagner & van den Haute 1992). Because of its low closure temperature of ~100°C, the mineral supports thermochronological studies of the cooling history of geological rock bodies. Phosphorites, or phosphate rocks are apatite-rich weathering crusts and sedimentary rocks that consist of fine-grained apatite with a gangue of carbonate, clay, quartz, pyrite, glauconite and organic matter. The crypto-crystalline apatite is called collophane or francolite. Francolites are a very heterogeneous group of carbonate-fluor apatites.

The phosphate content of a rock is usually expressed in weight percent P_2O_5, or % tricalciumphosphate ($= 2.185 \times P_2O_5$) and % elemental phosphorus ($= 0.436 \times P_2O_5$). Cut-off grades of phosphorite vary from 15 to 30% P_2O_5. Carbonatite-hosted apatite ore can be profitably mined at ~8% P_2O_5.

Wherever feasible, apatite and phosphorite ores are selectively extracted ("direct shipping ore"). Elevated contents of carbonate, iron oxides, kerogen and clay are undesirable in fertilizer production, as they cause higher sulphuric acid consumption. Comminution, washing, sieving and flotation are employed to remove impurities in order to reach a marketable concentrate grade of >30% P_2O_5. Apatite concentrate always contains minor and trace elements, some of which may be recovered as by-products (U, Th, F, V, REE: Dill & Kantor 1997). If left in the product stream, some of these elements may cause an undesired geochemical heritage in phosphate fertilizer, or contaminate the environment of phosphate mines (Abed *et al.* 2008). Problem elements include Cd, Cu, Ni, Cr, Pb, Zn, Hg, As and Se. For example, waste rocks left after mining the phosphatic shales of the Permian Phosphoria Formation in SE-Idaho release selenium, causing adverse effects to aquatic resources in the region (Hamilton & Buhl 2004, Hein 2004). Sludge from processing phosphate in Togo endangers the coastal environment (Gnandi *et al.* 2005). Several of the trace elements are not associated with apatite but with organic substance and pyrite in the ore. Elevated cadmium concentrations of some phosphorite deposits in western Africa are a serious problem, but many sources in the same region have acceptable low concentrations. Of course, the industry strives to mitigate environmental consequences, but operations with very low contents of hazardous elements find this to their advantage.

Phosphorus is one of the six major elements — H, C, N, O, S and P — that are required to build all biological macromolecules (Falkowski *et al.* 2008). P is an essential constituent of desoxyribonucleic acid (DNA), ribonucleic acid (RNA) and many other parts of organisms (bones, teeth, shells). It is one of the three main nutrional elements (P, N, K), which are indispensable for plant growth. Consequently, over 90% of world phosphorus production is consumed as fertilizers in agriculture. In fertilizer production, the concentrate is first reacted with sulphuric acid in a wet process, in order to make phophoric acid. Calcium sulphate is a by-product ("phosphogypsum"). The most common fertilizers ammonium phosphate and superphosphate are made by reacting phosphoric acid with ammonium or with apatite concentrate. Untreated phosphate is of little use to agriculture, because apatite dissolves too slowly. A minor part of phosphate is used for manufacturing elemental phosphorus, animal feed and chemicals.

The possibility of marketing the by-product phosphogypsum as a building material is determined by its contents of radionuclides of the uranium decay series. Radium (226) and its daughter radon (222) exhaling from plaster are the main hazard. Elevated contents impede use of the gypsum in the building industry and much of it is stored as waste. In Florida, phosphogypsum tailings reach a mass of ~1000 Mt. Efforts to exploit this potential resource of nuclear fuel have recently intensified. Phospho-gypsum from Siilinjärvi in Finland, in contrast, is sold as a filler for paper.

Phosphorus is foremost an essential element for all life forms and in natural occurrence is not hazardous. Yet, high concentrations of phosphorus disturb the ecology of rivers and lakes. In the industrial countries, eutrophication by phosphorus in detergents was common in the years 1960–1970. Mitigation by building water treatment plants and replacing P-detergents with zeolites was one of the great environmental achievements of the period.

3.18.1 Geochemistry

Phosphorus is a minor component of all magmas, with highest concentrations in mafic (1400 ppm) and intermediate melts (1660 ppm). Its crustal abundance is between 480 and 1300 ppm, shales contain 700 ppm. In magmas, the element displays incompatible behaviour but is precipitated in early apatite if calcium is available. Enrichment in late melts (pegmatites) and fluids is only possible at low calcium activity. Phosphorus is siderophile and associates with many magmatic and sedimentary iron ores. Hydrosaline melts and saline fluids may be responsible for the enrichment of phosphorus in spectacular magnetite-apatite ore, as at Kiruna (Sweden) and in some apatite orebodies of carbonatites and nephelinites. Apatite crystallizing from hydrous residual melt batches is marked by elevated fluorine and chlorine concentrations. The element occurs in eight different oxidation states, but valency (V) is most common.

Weathering releases phosphate into rivers and oceans. At surface conditions, pentavalent phosphorus in oxyanions is extremely mobile, except in the presence of adsorbing iron oxide particles. Seawater is largely oversaturated (50–100 ppb P) but in wide parts of the oceans, phosphorus occurs in biologically limiting concentrations. Nevertheless, a steady rain of biomass sequesters phosphorus into oceanic sediments. Main agents appear to be diatoms and common marine cyanobacteria that accumulate polyphosphates in their cells. In the bottom sediment, polyphosphate particles nucleate and authigenic growth of (carbonate-fluor) hydroxi-apatite takes place (Diaz *et al.* 2008). Overall, phosphorus is strongly enriched in the deep ocean as a result of continental runoff, marine phytoplankton production and the remineralization of biomass raining down to the ocean floor. Marine phosphorites are formed where cold, more acid and P-enriched deep water flows up into shallow regions off continental margins promoting high biological productivity ("oceanic upwelling"; Robb 2005). Subrecent phosphate rich sediments have been found on many continental shelves (e.g. southwestern Africa and Peru). As a result of biological processing, modern marine phosphates have $\delta^{18}O_P$ of ~19–26‰ (SMOW), compared to ~6–8‰ that are characteristic of apatite in igneous rocks.

Phosphorite of wide shallow epicontinental seas (e.g. northern Africa, Arabia) cannot be explained by upwelling, but is due to fluvial import of phosphorus (Glenn *et al.* 1994). In both cases, phosphorus availability causes a synergetic increase in the density of life, supporting the food chain from phytoplankton to fish and birds. Under anoxic conditions in C_{org}-rich bottom sediments, large sulphur bacteria such as *Thiomargarita namibiensis* gain energy by oxidizing sulphide with nitrate as an electron acceptor. At the same time, they release phosphate into the pore waters, which results in the high degree of supersaturation that is required to overcome the kinetic nucleation barrier to apatite precipitation (Schulz & Schulz 2005).

3.18.2 Phosphate deposit types

Phosphate deposits include marine (rarely lacustrine) sediments, guano (Nauru and Christmas Island) and fluid-enriched parts of magmatic bodies (mainly carbonatite and alkali complexes: Notholt *et al.* 1990).

Sedimentary phosphorites

Sedimentary phosphorites represent the largest part of world P-resources (>90%) and yield most of annual phosphorus production (northern Africa, China, Middle East and USA). They are marine sediments of shallow seas (<200 m depth) and form lenses or beds of considerable extension. Lateral passage to non-phosphatic rocks is gradual. Host rocks may be pelitic (often oil shale), calcareous or psammitic; associated chert bands are characteristic. As a rule, deposits occur in little deformed platform sequences (e.g. northern Africa) but also in strongly folded (Kara Tau, Kazakhstan, midwestern USA) and metamorphic phosphate strata (Siberia: Guliy 1995). Many deposits owe their exploitable grade to enrichment by supergene alteration, both by dissolution of carbonate matrix and by (limited) transfer of phosphate in solution ("phoscrete"). Mechanical erosion and concentration of phosphate nodules similar to coarse detrital iron ore at Salzgitter in Germany is caused by high-energy submarine currents. A rapid oscillation between high and low energy states characterizes many submarine areas of phosphorite enrichment (the "Baturin cycle"):

> Phosphorites are highly variable ranging from soft and earthy to hard rocks, with a grain size from silt to coarse pebbles and nodules, or fine-grained pelletoid and dense. Colours vary from white to green and brown. Apart from cryptocrystalline francolite, bone fragments, fish teeth, dolomite, calcite, chalcedony, kerogen, pyrite and detrital components (quartz, etc.) are common. Some phosphorites consist mainly of phosphatized bone breccias and coprolites. The macroscopic and microscopic variability of phosphorite makes it an eldorado of sedimentologic research (Glenn *et al.* 1994).

The earliest marine phosphate deposits occur in the Palaeoproterozoic of Siberia. Geological periods of enhanced phophate deposition include the Cambrian (Asia, Australia), Permian (Phosphoria Formation of North America: Piper & Link 2002, Hein 2004), Late Cretaceous to Eocene (Saudi Arabia, northern Africa, northern South America) and Miocene (Florida, North Carolina). The increase of phosphorite with decreasing age is an effect of the evolution of life:

> One of the oldest of the large deposits occurs in Early Palaeozoic platform sediments of the Mt Isa region in Queensland, Australia, with resources of >2000 Mt at 17% P_2O_5 that include 40 Mt at 31% of direct shipping ore. Al Jalamid in Saudi Arabia is a new mine exploiting a Cretaceous deposit with reserves of ~213 Mt. The phosphate horizon contains ~21% P_2O_5 and extends over 18 km^2 with an average thickness of 6.5 m. Planned production is 5.3 Mt/y of phosphate concentrate containing 32.5% of dry P_2O_5.

Magmatic phosphate deposits

Magmatic phosphate deposits occur in alkaline and carbonatite complexes (Figure 1.14, Figure 2.40 and Figure 3.28) and in layered mafic intrusions. Brazil, Canada, Russia and South Africa host notable resources. Most carbonatite-hosted deposits are only exploitable because of supergene enrichment (e.g. Araxa, cf. Chapter 2 "Niobium and Tantalum").

For many years, the ultramafic-carbonatitic Palabora Complex in South Africa was an important source of apatite, apart from metals such as Cu, Zr, Hf and and Fe in magnetite (cf. Chapter 2 "Copper"), and other minerals (vermiculite). Before the change to underground mining of copper, annual production used to be ~3.5 Mt fluorapatite concentrate. Ore rocks included apatite-rich pyroxenite and the so-called phoscorite, which surrounds the copper ore of the central carbonatite pipe. Typical phoscorite consists of 25% apatite, 35% magnetite, 18% calcite and 22% phlogopite, some serpentine and chalcopyrite. Average *in-situ* grades were 10% P_2O_5. High apatite concentrations were correlated with more phlogopite, implying that fluid-enriched melts concentrated phosphorus:

> Geologically less complex is the alkali ring intrusion of Khibiny near the town Apatity on Kola Peninsula (Russia). It was formed after the Variscan orogenic peak (300–280 Ma), intruding Archaean and Proterozoic basement. Today's erosion level exposes a cross section at subvolcanic depth with a diameter of ~35 km (Figure 3.28). Rings formed successively from the margin to the centre comprise nepheline syenite, ijolite, apatite nephelinite and foyaite. P-enriched sections of apatite nephelinites are exploitable apatite ore. The ore horizon rocks occur as concordant intrusive bodies that reach a length of 20 km and a thickness of 250 m, and were probably injected into late ring fissures. The ore consists of apatite, nepheline, aegirine and hornblende, and traces of sphene and titanomagnetite. Ore grades exploited in two open pits are 12.3 and 16% P_2O_5. Today, apatite ore is the only commercial product (~900,000 t/a), but earlier, nepheline was exploited as an aluminium ore and baddeleyite as a source of zirconium and hafnium. The comparable Kovdor Complex in Russia, near the border to Finland, produces annually ~2.5 Mt of apatite besides iron ore and zirconium oxide.

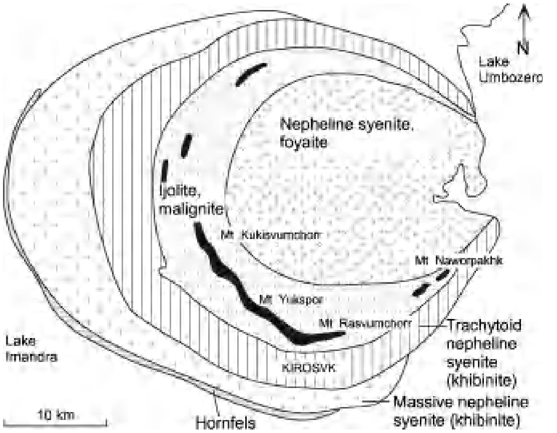

Figure 3.28 Generalized geological map of the alkali ring intrusion at Khibiny, Kola Peninsula, Russia. Exploited horizons of apatite-nephelinite in black. Modified from Notholt *et al.* (1990). By permission of IMM London & Maney Publishing (www.maney.co.uk/journals/aes).

The ultramafic alkaline Fanshan Complex in northern China is an important source of phosphorus fertilizer, based on a reserve of 76 Mt of apatite ore at 11% P_2O_5, with by-product magnetite (Neng Jiang *et al.* 2004).

With a diameter of 80 km, the Cambrian Sept-Îles Complex in Quebec, Canada is one of the largest layered mafic intrusions of the world. However, the greater part of the outcrop is underneath the sea. Of three magmatic cycles that produced the intrusion, the oldest terminates with the 250 m thick "critical zone" of which nearly 100 m consist of magnetite-ilmenite-apatite rock (nelsonite). Its formation is thought to be due to orthomagmatic liquid immiscibility (Cimon & McCann 2000). Mining reserves amount to 110 Mt with 15 wt. % apatite and 16% ilmenite.

Phosphate reserves are very large (16,000 Mt) and shared by many regions of the world, although ~40% occur in northwestern Africa (USGS 2010). Additional very large potential phosphate resources are known in offshore regions of Namibia and Mexico. World phosphate production in 2009 was 158 Mt. Largest producers were China, USA, Morocco, Western Sahara and Russia.

Exploration for phosphorus is based on geological models. Both sedimentary and magmatic apatite is marked by traces of uranium and radiometric methods can help in recognizing P-anomalous outcrops. Apatite was so named after the Greek word *apatein* that is translated as "to deceive", because it is not easily identified. Phosphorite may attract attention because of bone fragments and fish teeth, but radiometric methods help at all scales of investigation. Carbonatites, alkali complexes and layered mafic intrusions are located by a combination of remote sensing, photogeology and aerial magnetic surveys.

3.19 QUARTZ AND SILICON

Quartz	SiO_2	Si = 46.7 wt. %	Density 2.65 g/cm^3

Quartz is economically the most important among all silica minerals. Other silica polymorphs include tridymite, cristobalite, coesite, stishovite and amorphous silica (opal *sensu lato*). With the exception of opal (diatomite), quartz is the only one of these minerals that is widely used. It is also the most common of the group, especially in magmatic, metamorphic and sedimentary rocks. Hydrothermal quartz usually originates at T>120°C. Many quartz deposits are possibly precipitates from silicothermal fluids (Wilkinson *et al.* 1996), which are liquids with ~90% SiO_2 that coexist with an aqueous supercritical fluid in a wide temperature field (~300 to >750°C). Quartz (silica) solubility at surface conditions is extremely low; it rises with increasing T, P and pH. Quartz occurs in low- and high-temperature forms. At 573°C and atmospheric pressure, the first transforms instantaneously to high quartz. This causes a small volume increase ($D_{HQ} = 2.53$) that may be a problem in certain high-T applications. Most natural quartz is twinned. Critical properties are chemical purity and crystallinity. Quartz consists of 46.7% silicon and 53.3% oxygen. Although natural quartz is commonly quite pure, it does contain structurally bound trace elements (B, Li, Al, Ge, Ti, Fe, Mn, Ca, K, Na, P) in its lattice. Common point inclusions are H_2O, AlOH and LiOH. Fluid inclusions (with dissolved salts) are frequent. Variable quantities of inclusions define sectors of quartz crystals (Ihinger & Zink 2000). The melting point of natural quartz varies about 1650 ($\pm$ 75)°C. Note that whenever quartz is drilled (in the mine) or pulverized during processing, the hazard of inhaling fine dust must be excluded, because prolonged exposure leads to lung complaints such as silicosis (Ross 1999).

Silicon is a lithophile element, with an approximate crustal average of 27% (Smith & Huyck 1999). It is the second most abundant element after oxygen. Silicon occurring in sand and glass is made up of stable isotopes ^{28}Si (92.23%), ^{29}Si (4.67%) and ^{30}Si (3.1%). Native silicon is extremely rare in nature:

> The metalloid **silicon** (melting point 1410°C, density 2.329 g/cm^3) is currently one of the most important electronic materials, apart from its mass market in the metallurgical and chemical industries. For electronic applications, silicon is produced from high-purity quartz (HPQ) raw materials. Melting, followed by reduction with carbon and reaction with chlorine is employed in order to produce liquid silicon tetrachloride, that is purified by repeated distillation. It is then reacted with magnesium in order to precipitate native silicon, which is further purified by metallurgical zone, or chemical refining to a final impurity content of $<10^{-9}$. Ultrapure silicon is not conductive. For electronic use as a semiconductor, silicon is doped with other elements (P, Sb, B, In, etc.) constructing negative and positive transistors in minimal space. Nearly all microelectronic equipment is based on silicon. Yearly world consumption of electronic and photovoltaic grade silicon is estimated at 100,000 t/year.

Quartz of metallurgical quality is used for the production of quartz glass, silicon alloys (with Cu, Al), silicon metal, silicon carbides and ferrosilicon, which is important in the cast iron and steel industry. Most silicon metal is used in the form of aluminium-silicon alloys for manufacturing cast parts in the automotive industry. Fumed silica is produced at high temperatures, mainly as a filler for silicon rubber and for paints. Worldwide in 2009, production of metallurgical silicon (>98% Si) was ~5.4 Mt. Ferrosilicon accounts for about four-fifths of this amount. Largest producers of ferrosilicon were China, Russia, USA, South Africa and Norway, and of silicon metal, China, Brazil, Norway and France (USGS 2009).

Very pure (>99% SiO_2), lumpy (>20 mm) quartz concentrate or processed quartz sands constitute the base for chemical grade silicon. One path of processing leads to glass fibre cables, semiconductor silicon chips for micro-electronic applications, and photovoltaic (solar) cell panels (solar grade silica). Compared with metallurgical use, the electronic applications account for only a small percentage of total silicon demand. The alternative path provides silicon for the chemical industry (e.g. silica gel, silanes, silicones), which is the second largest sector of chemical grade silicon use. Silica gel, for example, is an important industrial adsorbent for drying process air and extracting heavier hydrocarbons from natural gas.

Quartz crystals are required in the electronics and optical industry. The largest part is consumed in electronics as frequency-control oscillators, timers and frequency filters in a wide range of products, for example communications equipment, watches, computers and television receivers. Properties that make quartz singularly useful for these applications include its piezoelectricity, dielectric capacity and a high acoustic hardness. Electronic quartz must be very pure, untwinned and faultless. As natural quartz of this quality is rare, crystals are hydrothermally cultured in autoclaves. Natural quartz crystal material is only required as seeds (lascas) for synthetic crystal growth. Optical quartz must be transparent and untwinned. It is used for manufacturing UV-transparent prisms and cells, and for certain lenses, for example in high-temperature equipment (<1100°C).

3.19.1 Quartz deposit types

Economic quartz deposits include quartz in granite pegmatites, hydrothermal vein quartz, sedimentary and metamorphic quartzites, and mature clastic sediments such as quartz sand and gravel.

Deposits of quartz include material of very different quality and value. Sandy gravels for road construction are at the lower end and quartz of sufficient purity for electronics is the most valued of all industrial silica materials. High-purity quartz is defined by a content of trace elements $<50\,\mu g/g$. High-purity quartz deposits include quite varied genetic types, such as silica caps ("quartzolite") of specialized granites (Figure 3.29), granitic pegmatites, hydrothermal quartz veins, quartzites (cf. Section 3.21 "Quartzite") and mature clastic sediments such as quartz sand and quartz pebble deposits (Désindes *et al.* 2006). Müller *et al.* (2007) identified kyanite quartzites as a new source of high purity quartz (cf. "Andalusite, Kyanite and Sillimanite"). Detrital deposits are more profitable than hard rocks because of cheaper extraction, less energy-intensive processing and higher quality due to natural preselection by weathering and transport. However, the preselection hypothesis is contradicted by Cox *et al.* (2002), who propose that non-siliceous, less durable pebbles are removed by diagenetic factors (e.g. *in-situ* dissolution). Major sources of lascas are Brazil, Canada, Germany and Madagascar. Cultured quartz crystals are exported by China, Japan and Russia. Considering that high-quality quartz raw materials are quite rare, prospects of favourable size and processing characteristics should always be explored and developed. Close cooperation with industrial customers is essential.

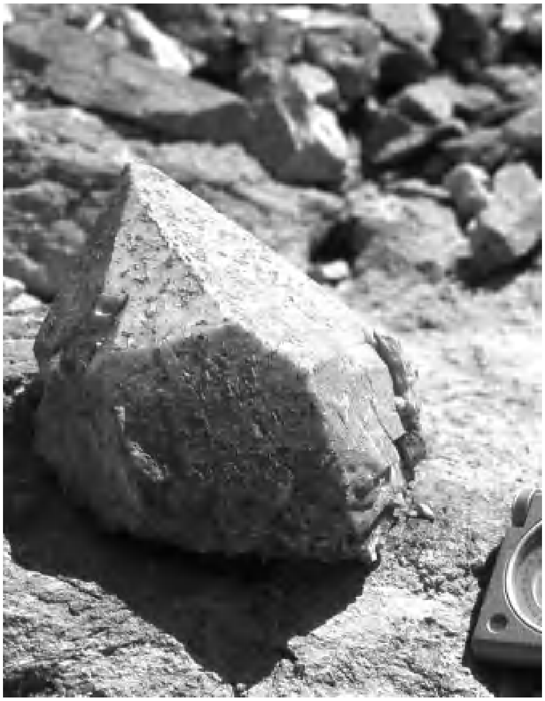

Figure 3.29 The massive silica cap of the Panafrican Nuweibi rare metal granite, Eastern Desert, Egypt, is made up of large upright unidirectional quartz crystals.

3.20 QUARTZITE

Quartzites are hard and brittle sediments or metamorphic rocks that consist chiefly (>80%) of quartz. Rock density is ~2.6–2.7 t/m^3 and bulk density of crushed quartzite ~1250–1350 kg/m^3. Fragments of crushed quartzite are angular with a rough surface, low porosity, high strength, and resist wear and weathering. This makes quartzite a valuable road-building aggregate.

However, high-quality quartzite is also an industrial raw material. Based on its high melting point (>1700°C) refractory-grade quartzite with >96% SiO_2 is used for the production of "acidic" refractory bricks and mortars. Note that the transformation of low silica polymorphs (e.g. low quartz) into tridymite (~900°C) and cristobalite (>1470°C) by heating in the furnace may result in irregular expansion and consequent damages to the refractory lining. Therefore, transformation behaviour must be investigated if the refractory market is sought.

Metallurgical-grade quartzite is used for the production of silicon metal and ferrosilicon (cf. Section 3.20 "Quartz"). Quartz consists of 46.7% silicon and 53.3% oxygen. Quartzite (or quartz) are reduced by graphite electrodes at >1780°C in electric arc furnaces. For this process, a high chemical and pyrometallurgical reactivity is desirable. These properties can be predicted by microscopic confirmation of a high percentage of strained, strongly undulatory and highly cataclastic quartz grains, which provide a large reactive surface when thermally shocked. Also, favourable reactivity is correlated with higher solubility of quartzite in NaOH. Deleterious impurities include Al, Fe, P, Ti and Ca. Of these, only alumina and calcium can be removed with slag. Some quartzite deposits may yield highest quality material that can be used for chemical and electronic products (cf. Section 3.20 "Quartz").

3.20.1 Metamorphic quartzite deposits

Metamorphic quartzite deposits are usually derived from sedimentary quartz sandstone precursors, by orogenic or contact metamorphism. Müller *et al.* (2007) suggest that kyanite quartzites are a product of hydrothermal alteration and propose these rocks as a new source of high purity quartz with co- or by-product kyanite (cf. Section 3.1 "Andalusite, Kyanite and Sillimanite"). In contact metamorphic zones, silica-rich, cryptocrystalline hornfels can occur near more granular quartzite.

Metamorphic quartzite is commonly massive or slightly foliated. Quartz grains are typically equidimensional or somewhat elongated and have clear boundaries, resulting in a simple mosaic texture. A higher percentage of grains with a diameter above 2–3 mm impedes a number of upper-value uses. Cataclastic structures and lattice defects are often observed, without necessarily lowering the value. Quartzites with accessory mineral content of >4% are not suitable for higher-value uses; common impurities include mica, feldspar, garnet, pyrite and goethite. Because of brittleness, many quartzites are densely jointed and brecciated. Although this facilitates extraction, joints and faults may be pathways for seepage and groundwater flow and with it, introduction of impurities. Careful mapping of grade classes and selective mining is the key to quality control. Remember that whenever quartz is drilled (in the mine) or pulverized during processing, the hazard of inhaling fine dust must be excluded, because repeated exposure provokes silicosis (Ross 1999).

3.20.2 Sedimentary quartzite

Sedimentary quartzite is an unmetamorphosed sandstone that consists mainly of quartz grains, which are cemented by silica. The cement may be opal (some quartzites have >30% X-ray amorphous silica), chalcedony or microcrystalline quartz. The rocks are smooth, extremely hard and tough, and break into sharp-edged fragments with a conchoidal fracture surface. The silica-cement is evidence of solution and reprecipitation of SiO_2. Two geological process systems provide models for explaining these observations:

- migrating alkalic formation or shallow groundwater, which is common in tropical wet and dry (savannah) climate (related to silcrete);
- dissolution, for example by kaolinization, and transport of silica by complexing with dissolved organic matter.

In Tertiary lignite basins of central and northern continental Europe, sedimentary quartzite boulder horizons in sand are very common and illustrate the second model. Organic acids combined with reduction cause very low iron concentrations (cf. Section 3.22 "Quartz Sand and Gravel"). Bennet *et al.* (1991) provided analytical and mineralogical proof of the high SiO_2-solubility in lower parts of peat profiles.

Exploration for quartzite is best guided by published geological maps and reports, and narrowed down by geographical factors such as the availability of land for quarrying. High-grade quartzite is located by wide-spaced regional sampling. Most of the quartzite produced worldwide makes up part of the giant mass of "crushed stone and aggregates" (cf. Section 3.22 "Quartz Sand and Gravel"). Its share in world silicon production (~5.4 Mt in 2009) is not recorded.

3.21 QUARTZ SAND AND GRAVEL

Sand is one of the most common natural materials in our life, but has many little-known fascinating aspects (Welland 2009). Sand (0.06 to 2 mm grain diameter, dry loose density $\sim$1.3 t/m^3) and gravel (2–63 mm, dry density $\sim$2 t/m^3) are defined by grain size. They are sedimentary, non-cohesive (loose) and unconsolidated clastic rocks. Sand consists mainly of minerals such as quartz, calcite and silicates, with traces of heavy minerals (cf. Chapter 1.3 "Placer Deposits"). Gravel is more often a mixture of quartz and rock fragments. Both sand and gravel grains display shapes that are described as angular to rounded. Of course, gravel and sand in the ground have higher densities because of partly or wholly water-saturated pore space (saturated densities of gravel ~2.3 t/m^3 and sand ~2.15 t/m^3). Concerning possible uses, two subgroups are differentiated:

- industrial sand (glass and foundry sand; quartz flour, well-packing and cementing sand, abrasive sand);
- building sand and gravel (concrete aggregates, construction fill, mortar sand, various concrete products).

Properties of natural sands and gravels control eventual use. Favourable are minimal contents of iron, calcite, clay, salt, humic and bituminous matter, heavy minerals, and suitable grain form and grain size distribution. Some negative properties can be alleviated by processing, which includes washing, classifying, attrition and flotation.

3.21.1 Industrial sand and gravel

Industrial sand and gravel is defined by higher quartz contents and lower impurities compared with building sand. Industrial specifications are very narrow. Main consumers are glass and metal casting factories. SiO_2 should be at least 96% and for flat glass >99%. Glass sand implies very low (<0.008%) to moderate Fe_2O_3, $TiO_2<0.03\%$, $Al_2O_3<0.2\%$ and $CaO+MgO<0.05\%$. Accessory heavy minerals (zircon, chromite, kyanite) may be deleterious. Grain size should be 0.1–0.6 mm (medium sand) and angular grain shape is preferred. Note that there are glasses with very different requirements. Sand for green bottle production may contain as much as 4% Fe_2O_3.

Quartz sand of the high chemical purity described is the basic raw material for glass production, with ~70 wt. % in the formula. Because most commercial glasses belong to the soda-lime-silica variety, main components of the glass mixture include quartz, soda (Na_2CO_3 to ~15% Na_2O) and calcined limestone or dolomite (10%). Minor additions are made to improve properties of melting, forming and use: Alumina (Al_2O_3) for chemical durability and reduced devitrification, sodium sulphate for purifying and salpetre for decolourizing. Heat-resistance is improved by adding boron (B_2O_3). K_2O and BaO enhance the hardness of optical glass. PbO is added to produce decorative glass as it increases the refractive index. Traces of metal oxides such as CoO (blue) and Cr_2O_3 (orange) colour glass. Pure silica glass (vitreous silica) is produced for its excellent high-temperature stability, optical properties and thermal-shock resistance. It is more expensive because of the high temperature required for melting quartz (~1700°C) and the great viscosity of the melt.

Industrial sand deposits

Pure quartz sand deposits occur predominantly in repeatedly eroded and recycled mature sediments, because only quartz and the most durable heavy minerals (e.g. zircon) survive multiple chemical and mechanical attacks. Sand deposits form in coastal marine (Figure 2.5, Figure/Plate 3.30), fluvial and aeolian process systems. High-quality sands seem to be marked by proximity to peat and emersion surfaces and this is probably a genetic factor: Water infiltrating the soil beneath bogs and tropical forests is loaded with dissolved organic carbon (DOC) and organic acids that leach alkalis and cause reduction and microbial methanogenesis in the sand. Iron is reduced to Fe^{2+} and dissolved. DOC production and export rise during geological periods of elevated CO_2 content in the atmosphere (Freeman *et al.* 2004). Favourable hydraulic conditions in the sand aquifer, especially persistant percolation, allow removal of dissolved impurities. Many glass sand operations extract fossil sand of raised beaches (deposited and purified in interglacial warm climate). Recent coastal sand must be desalinated by washing with freshwater.

Quartz flour is prepared from high-purity quartz sand by metal-free grinding. Micronized to <3 µm, the flour is used as a functional filler, for example in ceramics, paint and plastics.

Abrasive quartz sand (hardness 7) competes with garnet, olivine and slag-derived abrasive products. Garnet and olivine are preferred, because quartz and slags may endanger the health of workers (by silicosis, or hazardous metals such as As and Pb).

Foundry sand is slightly cohesive sand that allows manufacturing of moulds and cores for

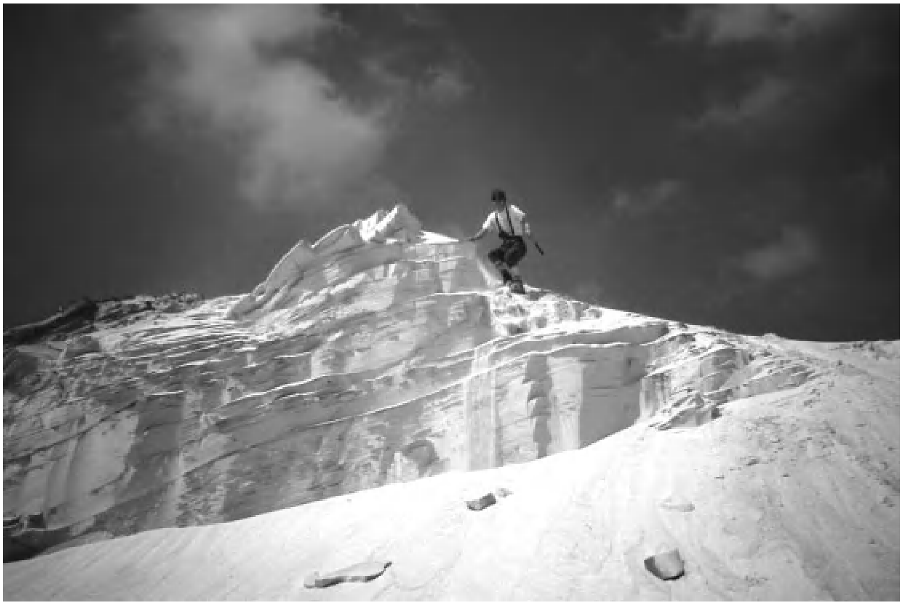

Figure 3.30 (Plate 3.30) High-grade industrial sands at Uhry in northern Germany were deposited in a shallow bay of the Late Cretaceous sea north of the Harz Mountains and chemically upgraded when the sea retreated westwards and tropical forests covered the area.

metal casting. For this use, sand should contain cohesive grain fractions (clay and silt) and must tolerate heat. Specified grain size distribution, rounded grains and high gas permeability are expected. Although lower silica content is acceptable (85–95%), carbonate and mica contents are rejected. Because many of these properties display considerable variations in natural deposits, foundry sands are increasingly "synthesized" by mixing pure components such as glass sand and bentonite or fire clay as a binder. Foundry sands are also prepared from chromite, zircon, staurolite and olivine.

World production of industrial sand and gravel in 2009 amounted to ~112 Mt. The largest producers (>5 Mt) were USA, Italy, Germany, United Kingdom, Australia, Poland, France and Spain.

3.21.2 Building sand and gravel

The most important use of building sand and gravels is the provision of aggregates for concrete. Aggregates are materials composed of natural or crushed, hard, sound and durable particles of non-reactive minerals. This covers sand, gravel and crushed rock. In comparison with industrial sand, quality may be lower and the grain spectrum wider. Alluvial and glacio-fluvial pebble sands are common near moraines and in terraces and valleys of rivers. The high competition for land in river plains, for example by housing and industry, agriculture, nature preserves, roads and railways, groundwater extraction, etc., continuously reduces the accessability (Cook & Harris 1998) of areas for sand and gravel extraction (Figure 3.31). In spite of substitution by construction and demolition debris, such as used asphalt, bricks and concrete, by metallurgical slag and combustion residues of coal power stations, high-quality natural sand and gravel are still needed for critical concrete structures, such as bridges and high-rise buildings. Shrinking resources of this material must be protected, preferably by a strict land-use planning programme. An alternative is to develop aggregate sources far from densely populated areas, such as the megaquarries on the coasts of Northern Europe and Greenland. This is feasible for delivery from coast to coast, because maritime

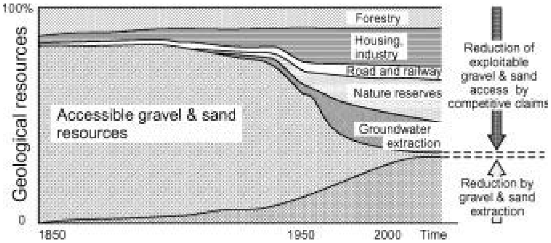

Figure 3.31 Various demands of society on fluvial landscapes diminish accessible gravel and sand resources to a point were protection by planning authorities and maritime import from far-away coasts are inevitable.

bulk transport is very economic, but doubts remain concerning the costs of supplying inland destinations.

> Specifications for concrete aggregates are closely regulated and subject to industrial standards (Primel & Tourenq 2000). Some important points concern:

- the petrographical composition (quartz and quartz-rich pebbles or fragments are favourable, whereas weathered, schistose, friable fragments are deleterious as are pebbles of coal, clay, marl and alkali-reactive chert, opal and flint: Scott 1993, Michel *et al.* 2003).
- Grading, investigated by sieving and illustrated by cumulative particle size curves. Unfavourable compositions can be adjusted by adding or substracting a size class, although within limits. A high fraction of cobbles (>63 mm) or of silt and fine sand is not favourable.
- The grain shape; rounded fragments are preferred to angular or platy ones. Pebbles should display a high uniaxial compressive strength and frost resistance.

The investigation of potential sand and gravel deposits is mainly carried out by trenching and drilling. The aim of investigations is a full understanding of the three-dimensional architecture of the deposit (Kostic *et al.* 2007, Miall 1996), of the quality distribution and of the quantities involved. In a phased approach, widely spaced drilling (~500 m) and geophysical line surveys (electrical resistivity sounding) can establish whether sand and gravel are at all present in the required quantity (Annels 1991). For detailed exploration, grid sampling distance should be less than 200 m. Spacing can be adjusted (e.g. by calculating variograms) as soon as sufficient data are available. Although cheap and quick auger drilling is sometimes used for sampling gravel and sand prospects, only wide-diameter, airlift reverse circulation holes provide reliable samples, both above and below the groundwater table. Use of water-based drilling fluids is discouraged because fines will be lost. Vertical sample profiles should be prepared from a minimum of 5–10 kg material per metre, and this must be weighed and documented. If larger grains are present, the minimum size of a truly representative sample expands exponentially – a maximal grain diameter of 50 mm requires a sample mass of 250 kg (Berkman 2001). It is important to remember that small samples are always a compromise that widens error margins (Pitard 1993). Washed particle size analysis is preferred to dry sieving. The presence and percentage of boulders and cobbles (>63 mm) is best determined by excavating test pits using a hydraulic excavator. Soil mechanical properties determine pit slope angles (Terzaghi *et al.* 1996) and as a consequence, the exploitable volume of the deposit.

Sufficient volume and homogeneity, acceptable overburden thickness, depth and a water table position allowing extraction either in pits or by dredging, and a favourable distance to potential buyers are further criteria. Environmental considerations concern foremost the position of the groundwater table in relation to the deposit and consequent problems of groundwater protection. It is most important to obtain a valid planning consent to extract the minerals as early as possible in the course of investigations. Later restoration of the land (including pit lakes) must guide all actions from early stages of development. In the past, sand pits and rock quarries were too often abandoned without environmental clean-up. Financial assurance requirements during licensing are one possible enforcing measure.

In 2009, 800 Mt of building gravel and sand were produced in the United States (USGS 2010). This was one-fifth less than a year before, illuminating the severity of the financial and economic crisis. Crushed stone, the alternative major construction aggregate, is increasingly replacing natural sand

and gravel, especially in more densely populated areas of the world. In the USA, a total of 1100 Mt of crushed stone was produced in 2009, comprising ~70% limestone and dolomite, 14% granite, 7% basalt and lesser quantities of sandstone, quartzite, marble, volcanic cinder and scoria, calcareous marl and slate. Most of the total was used as aggregate for highway and road construction, and only a small part for chemical and metallurgical uses, including cement and lime manufacturing. Although reserves and resources are very large, zoning regulations and alternative claims on land are expected to cause future hard rock, sand and gravel operations to be located at increasingly greater distance from high-population centres. This will, of course, affect prices.

3.22 SODIUM CARBONATE, SULPHATE AND ALUM

		Density g/cm³
Trona	$Na_3H(CO_3)_2 \cdot 2H_2O$	2.14
Natron	$Na_2CO_3 \cdot 10H_2O$	1.45

In addition to natural sources, the demand for sodium carbonate ("soda ash" Na_2CO_3) is satisfied by synthetic soda made via the Solvay or ammonia-soda process using halite and limestone (eq. 3.11). "Soda" designates any of the common sodium compounds such as the oxide, hydroxide, carbonate and bicarbonate. End use of soda ash is mainly in glass manufacturing, followed by chemicals, soap and detergents, pulp and paper production, water treatment, bentonite activation, animal feed and flue gas desulphurization, dechlorination and defluorination.

Synthetic soda production by the Solvay process:

$$2NaCl + CaCO_3 \rightarrow Na_2CO_3 + CaCl_2 \qquad (3.11)$$

Sodium carbonate deposits are either beds of soda carbonate salts (commonly trona) or brines that are harvested from shallow aquifers and from playa lake water (cf. Chapter 4.2 "Salt Lakes"). Trona-forming brine is strongly alkaline with a pH >9, alike to existent soda lakes (Eugster & Surdam 1973; e.g. East African Rift).

The largest deposits of trona occur in the Green River Basin, Wyoming, USA, with >47,000 million metric tonnes of exploitable resources. Sediments in the centre of Eocene Lake Gosiute reflect repetitive lacustrine expansion-desiccation cycles. They comprise 42 beds of trona and horizons of displacive intrasediment nodules, formed in shallow playa lakes. Within an area of >2000 km², 25 exploitable trona beds are known (Dyni 1996) with a thickness attaining 14 m at depths from 120 to over 1000 m below today's surface. Interbedded thin dolomitic oil shales represent deeper water phases. The frequency of oil shale beds (cycles/metre) and by implication, the trona beds, is a function of orbital signals including precession, obliquity and eccentricity (Meyers 2008). Other members of the sedimentary suite are dolomitic limestone, mudstone and numerous beds of halite (Fischer & Roberts 1991). The Green River Basin is the world's largest producer of soda ash, with an annual output of ~15 Mt of trona ore.

Brines are exploited at Searles and Owens lakes in California (with co-products salt, sodium sulphate and borax), and from the subsurface in the Roma area, Queensland, Australia, containing an average of 14 g of Na_2CO_3 per litre. In Lake Magadi in the East African Rift Valley, Kenya, on the foot of carbonatite volcano Oldoinyo Lengai, Holocene trona beds are 7 to 40 m thick, sourced from geothermal springs and precipitated by evaporation (Eugster 1970). Fluorine contents in this trona ore are significant, occurring in the form of 22 wt. % villiaumite (NaF) and ~6% fluorite. Extraction is by dredging. The rate of replenishement of the deposit is reported to exceed production, which makes Magadi one of the rare examples of literally sustainable mining. In neighbouring Tanzania, a project to exploit soda from Lake Natron is disputed, because of possible negative consequences for the lake's famous flamingo population.

The annual production of soda ash (natural and synthetic) is ~40 Mt/a, but only 12 Mt are primary mining products, almost wholly from the Green River Basin. In Turkey, two newly discovered and very large trona deposits are presently prepared for production: Kazan with resources of 600 Mt at 31% trona and nearby Beypazari with 230 Mt at

70% trona. China leads in the production of synthetic soda.

3.22.1 Sodium sulphate

In several aspects, sodium sulphate is comparable to sodium carbonate; both the environment of formation (as at Searles Lake, USA) and their uses, such as powder detergents overlap. Two minerals provide most of industrial supply (apart from industrial sources, such as lead-acid battery reclamation): Thenardite Na_2SO_4 with a density of 2.67 g/cm^3, and mirabilite or Glauber's salt $Na_2SO_4 \cdot 10H_2O$, $D = 1.49$ g/cm^3. The solubility of sodium sulphate is a function of temperature. Below 32°C, solubility decreases until mirabilite precipitates; above the transition point, thenardite is the stable phase and precipitation is favoured by rising temperature. This curious behaviour caused an accumulation of ~80 Mt Na_2SO_4 in Holocene saline lakes of southern Saskatchewan and south-eastern Alberta in Canada. More than 5.5 million saline lakes are counted in the post-glacial moraine plains of Canada. Only 100 of them have permanent salt beds at depth (thenardite, dolomite and gypsum) or a recoverable harvest of autumnal coldwater precipitates (mirabilite; Warren 2006). Other sources of solid sodium sulphate ore are exploited in Spain and Turkey, and giant deposits similar to the cold playas of Canada exist in saline lakes of Siberia and China. In Kara Bogaz Gol (Turkmenistan), a bed of 3–8 m thick cryogenic sodium sulphate was exploited that may date from the ice ages (cf. Chapter 4.2 "Salt Formation Today"). Primary annual production of sodium sulphate is estimated at 4 Mt (USGS 2010). Largest producing countries are USA, Spain, Canada and Mexico.

3.22.2 Alum salts

Alum salts are a large group of hydrated double salts, i.e. sulphates of triple-valence (+3) and single-valence (+1) ions. The alum of greatest commercial importance is potash alum $KAl(SO_4)_2 \cdot 12H_2O$. Alum occurrences are not infrequent and for over 2000 years, native alum was extracted from sulphuric acid-altered felsic volcanic rocks or weathered pyritic schists. The Swedish alum shales (kerogen and V, U, Mo, Ni-rich black shales of Middle and Late Cambrian age) were so called for constituting a source of this important chemical. Since medieval times, alunite rock (alumstone) $KAl_3(SO_4)_2 \cdot (OH)_6$ $D = 2.6–2.8$ g/cm^3 was employed for manufacturing potash alum. Alunite deposits are formed by the interaction of sulphuric acid with alumosilicates such as feldspar (eq. 1.5); they are usually volcanogenic (cf. Chapter 1.1 "Volcanogenic Ore Deposits") or supergene, as a product of acid-generating sulphide oxidation (cf. Chapter 1.2 "Supergene Enrichment by Descending Solutions"). With today's easy availability of low-cost sulphuric acid, alum is commonly made from shales, leucite, bauxite or clay. Alum has important uses in the pharmaceutical, textile, sugar, paper, paints and other industries. It is also used as a flocculant in water purification.

3.23 SULPHUR

Sulphur	S	Density 2.05–2.09 g/cm^3

Native sulphur is a pale yellow, brittle solid. It occurs in two polymorphs: orthorhombic sulphur is stable at low temperatures, which is the reason why it is sometimes called "sedimentary" sulphur. The monoclinic polymorph of sulphur is quite rare in nature. It is stable above 95.5°C and typically crystallizes from melt ("volcanic sulphur"). Sulphur melts at 115°C and boils at 445°C. Sulphur liquid density varies from 1.8 g/mL just above the melting point to 1.6 g/mL at the boiling point. All native sulphur ages in time to the orthorhombic modification. Often, native sulphur contains trace amounts of arsenic, selenium and tellurium.

Native sulphur is not the only feasible source of the element. Ferrous and base metal sulphides have contents between 53.3% S (pyrite) and 13.4% S (galena), and metallurgical fabrication of the metals results necessarily in co-production of sulphur or sulphuric acid. The metallogeny of these deposits is presented in Part I of this book. Coking plants and desulphurization of coal-burning power plant fumes also recover by-product sulphur. Sulphur might be extracted from anhydrite (23.5% S) and gypsum (18.6% S) (cf. Section 3.13 "Gypsum and Anhydrite"), but this is economically not feasible.

The main source of industrial sulphur, however, is petroleum refining and sour natural gas processing, which make up >70% of annual production. In sour gas, hydrogen sulphide (H_2S) is a natural component, whereas petroleum yields H_2S during refining. Hydrogen sulphide is converted to elemental sulphur by the Claus process (eq. 3.12). Almost all of the remaining 30% is produced as SO_2-gas from non-ferrous metal smelters and the roasting of pyrite, which is the most economic path of sulphuric acid production. Mining of elemental sulphur is now rare.

Conversion of H_2S to elemental sulphur by the Claus process:

$$2H_2S + O_2 \rightarrow 2S + 2H_2O \qquad (3.12)$$

Demand for sulphur depends primarily on the activity of the phosphate fertilizer industry (cf. Section 3.19 "Phosphate"). Sulphuric acid is needed to produce superphosphate from phosphorite, apatite and ammonium sulphate. Over 90% of all recovered sulphur is converted to sulphuric acid ("the work horse of the chemical industry"), which is one of the most widely used of all chemicals. For example, sulphur and sulphuric acid are essential for making insecticides, dyes, pharmaceuticals, explosives, rubber and for preserving food. In the future, climate engineering (Wigley 2006) may be a new use of sulphur, because injecting aerosols or aerosol precursors (i.e. SO_2) into the stratosphere can provide a negative forcing of the climate system and offset part of the positive forcing that is attributed to increasing greenhouse gas concentrations in the atmosphere.

3.23.1 Geochemistry

Sulphur is a nonmetallic element of lithophile character. Its crustal abundance is estimated at 500 ppm (range 260–1200 ppm: Smith & Huyck 1999), which is about equal to chlorine and fluorine. Large crustal reservoirs of sulphur include evaporites and seawater (oxidized, S^{6+}), as opposed to sulphides and organic substances, including hydrocarbon fluids (reduced, S^{2-}). Both oxyanions and hydrogen sulphide are rather mobile, but sulphates and metal sulphides tend to immobilize sulphur. Intermediate-valence sulphur species prevail in the shallow marine diagenetic setting. Sulphur is essential to life. It is one of the six major elements – H, C, N, O, S and P – that are required to build all biological macromolecules (Falkowski *et al.* 2008). The biological fluxes of the first five of these elements, including sulphur, are driven largely by microbially catalysed, thermodynamically constrained redox reactions. Geological cycling of sulphur can be illuminated by studying isotopic fractionation (cf. Chapter 1.1 "Isotope Geochemistry").

3.23.2 Deposit types of elementary sulphur

Deposits of elementary sulphur occur (1) by magmatic degassing in volcanic settings and (2) as a product of microbial sulphate reduction of gypsum/anhydrite in the presence of organic matter, petroleum and natural gas (cf. Chapter 1.3, eq. 1.15). Occasional encounters of liquid sulphur in deep drillholes traversing anhydrite-carbonate sediments are of scientific interest (Hunt 1996). This sulphur is the result of abiotic thermochemical sulphate reduction (eq. 1.21; for details refer to Chapter 1.4 "Diagenetic Ore Formation Systems").

Volcanogenic sulphur deposits form by sublimation and precipitation of elemental sulphur on crater walls, near solfataras, at H_2S-fumaroles and hydrothermal sulphurous springs (e.g. Vulcano, Italy). This is an oxidation/reduction process (eq. 3.13). Some sulphur may collect in gas flow channels and in brecciated and porous wall rocks (Figure 1.47). Later heating to temperatures above the melting point causes formation of liquid sulphur flows, which are known to occur from time to time on several volcanoes in Chile and Japan. Mining of volcanic sulphur is, however, mainly based on disseminated sulphur in volcaniclastic rocks.

Abiotic formation of elemental sulphur:

$$\begin{aligned} 2H_2S + 3O_2 &\rightarrow 2SO_2 + 2H_2O \\ 2SO_2 + 4H_2S &\rightarrow 6S^0 + 4H_2O \end{aligned} \tag{3.13}$$

Sedimentary or more precisely, diagenetic and biogenic sulphur deposits are formed by reduction of SO_4-sulphur in sulphate rocks (gypsum, anhydrite). This is catalysed by anaerobe microbes in oxygen-depleted settings. The process is mediated by consortia of sulphate-reducing bacteria and archaea. Common sulphate-reducing bacteria include *Desulphovibrio desulphuricans* and *Clostridium nigrificans*. In this context, organic matter is the source of energy, frequently provided by diagenetic migration of oil or gas. Bacteria assimilate dissolved $(SO_4)^{2-}$ and hydrocarbons into their system and secrete H_2S and CO_2. Equation 3.14 describes this process for the case of anaerobic methane oxidation. The role of archaea is not yet fully understood.

Anaerobic methane oxidation and microbial formation of elemental sulphur:

$$\begin{aligned} SO_4{}^{2-} + CH_4 &\rightarrow HS^- + HCO_3{}^- + H_2O \\ 2HS^- + 0.5O_2 &\rightarrow 2S^0 + H_2O \end{aligned} \tag{3.14}$$

HS^- is oxidized to elemental sulphur, whereas $HCO_3{}^-$ reacts with calcium released from the sulphate rock by precipitating secondary aragonite or calcite. Oxidation of HS^- is possible by reaction with SO_4, by mixing with oxygen-bearing meteoric water, or by autotrophic bacteria that use part of the resulting CO_2. The participation of biota in these processes is illuminated by the enrichment of the light isotopes ^{32}S and ^{12}C in the products (sulphur, limestone) compared with the source material (gypsum, hydrocarbons). One mole of gypsum/anhydrite yields $\sim ^1/_4$ sulphur and $^3/_4$ white, massive or cellular limestone. The calcite cap rocks above salt diapirs are often major hydrocarbon traps. This coincidence led to the discovery of sulphur.

Sulphur in shallow marine sediments, such as the deposits of Sicily formed by similar diagenetic-biogenic processes. For many centuries in the past, Sicily was the leading source of sulphur. Since ~1900, pyrite roasting and sulphur extraction from salt domes in the Gulf region of the southern USA began to dominate markets. Sulphur mining in Sicily declined and the last mine working to a depth of over 300 m closed in 1988:

> Sicilian sulphur was exploited from Miocene (Messinian) evaporitic sediments of the Caltanisetta and other basins. The sedimentary sequence comprises basal clay, bituminous diatomite (called "tripoli"), overlain by limestone, gypsum/anhydrite, halitite (rock salt) and potassium salt, which are covered by more sulphates, gypsarenite, calcarenite, mudstone and calcareous marl (Zuffardi 1989). The whole package is strongly folded and faulted. Sulphur orebodies occurred in sulphate rocks as stratiform lenses of 1–2 m thickness (max. 30 m). Ore formed thin veinlets of sulphur parallel to bedding planes and joint-controlled pockets. Run-of-mine ore comprised native sulphur, sulphate, carbonate, bitumen, rare sulphides and celestite. Sulphur contents used to be 20–25 wt.% S at a cut-off grade of 15% S.

> In the Gulf regions of southern North America, native sulphur occurs in the caprock of salt diapirs that are mantled by Miocene and Pliocene mudrocks, sandstone and limestone. Because some of the earliest bonanza oil fields in America had been found in caprock and in updomed host sediments of diapirs, the occurrence of sulphur was known. Extraction, however, became only feasible when Herman Frasch introduced a novel hot-water melting process at Sulphur Mine, Louisiana, in 1894. Extraction by the Frasch process involves pumping overheated water (with 150–165°C far above the melting temperature of sulphur) at high pressure downhole into the orebody; molten sulphur is brought to the surface via an inner pipe. Meanwhile, more than 100 similar onshore and offshore deposits were found. Typically, the sulphur-bearing caprock displays a thickness of 40–120 m and is traversed by numerous lenses, beds, pockets and veins of elementary sulphur (Figure 2.32). Economic grades were ~20–40%. Remaining resources are gigantic, in spite of 100 years of intense exploitation. Frasch-mining of sulphur ceased, however, because of its high energy costs compared to by-product sulphur from the hydrocarbon industry.

> Large, at present uncompetitive occurrences of native sulphur resembling those of the Gulf occur in the Carpathian foredeep of southern Poland, Romania and Ukraine. The province forms a narrow corridor that extends over ~1500 km length and contains a sizeable part of world resources of native

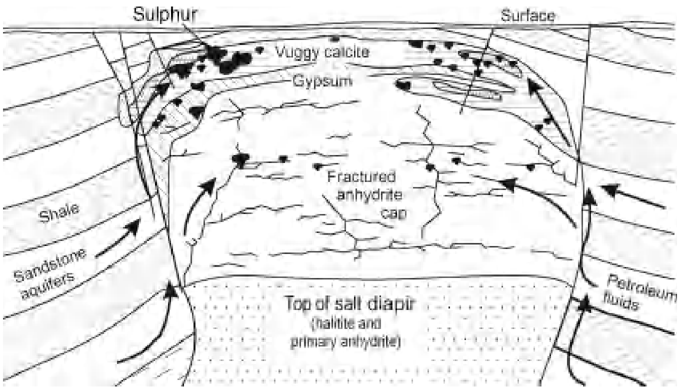

Figure 3.32 Schematic section showing formation of native sulphur deposits in caprock of salt diapirs in the Gulf of Mexico region. Black arrows indicate flow of hydrocarbon fluids. Not to scale. After Ruckmick, J.C., Wimberly, B.H. & Edwards, A.F. 1979, Society of Economic Geologists, Inc., *Economic Geology* Vol. 74, Figure 1, p. 471.

> sulphur. Concentrations are associated with Miocene evaporites that are interbedded with clay, marl and sand of the Neogene molasse basin. Here also, formation of sulphur is related to migrating hydrocarbons and appropriate flow paths (Parafiniuk *et al.* 1994). This connects diagenetic-biogenic sulphur mineralization with petroleum traps, although closure by beds of low permeability is rarely observed. On the contrary, an open system appears more favourable because it provides access of meteoric water, oxygen and seed microbes.

In 2009, world production of sulphur amounted to 70 Mt. Of this total, about two-thirds were "recovered sulphur", which designates by-product sulphur of sour natural gas processing, sour crude refining, tar sands processing and stack gas clean-up. "Mined sulphur" includes elemental sulphur recovered by conventional mining and the Frasch method. Mined sulphur production continues to decline. Pyrite mining yields annually ~6 Mt and non-ferrous metal smelters ~18 Mt. In the future, the share of sulphur derived from oil and gas processing is expected to grow, because of an overall increase of the quantity treated and of higher sulphur concentration in crude petroleum and gas. Sulphur resources are very large.

3.24 TALC AND PYROPHYLLITE

Talc	$Mg_3(OH)_2Si_4O_{10}$	$D = 2.7$–$2.8\,g/cm^3$	Mohs hardness 1

In talc, small amounts of Al and Ti may substitute for Si, and Fe (II) may replace some of the Mg. Traces of iron and nickel in talc lend it a greenish colour; grey-green talc rock is rich in chlorite. It is rare to find monomineralic talc in exploitable volumes. More common are talc rocks with a gangue of colourless chlorite (leuchtenbergite, a magnesium-rich clinochlore containing little or no iron), magnesite, dolomite, amphibole, quartz and pyrite. Steatite is a dense unfoliated talc rock, which can be worked by carving. Soapstone is another term for steatite but is also applied to metamorphic talc-mica-chlorite-amphibole-pyroxene rocks, or in Norway, to talc-carbonate rocks, which are used for cutting dimension stone, fire places and ovens (Sturt *et al.* 2002). Talc schists are foliated schistose talc rocks.

Talc has a number of unique properties including softness, chemical stability, refractory nature and low thermal and electrical conductivity. Applications of talc are numerous. Much is consumed in production of fine and electrical ceramics, paints (as extender), paper (for stabilizing resin, as a filler and coater), refractories, plastics (filler), insecticides, cosmestics, pharmaceuticals, rubber and roofing fabric. Specifications vary with use. Talc destined for paper or as filler must have a high whiteness. Ceramics demand high SiO_2 and MgO contents as well as a favourable firing behaviour. Cosmetics require high talc grade and absolute absence of acicular (asbestiform) minerals. In most applications of talc, asbestiform fibres are acceptable but enforce costly precautions during extraction and processing. The content of talc in some commercial products is of little importance, whereas colour, whiteness, adherence to narrow grain size specifications and an extremely high specific surface may be crucial.

Like most sheet silicates, talc and talc rocks have a very low shearing resistance. Consequently, open cut mining slopes are prone to collapse, as are underground stopes. The economic fate of a mine may depend on delivering a constant quality of run-of-mine ore to the processing plant. Even large deposits still use handpicking for highest quality material, apart from grinding, flotation and optical laser-based sorting for the majority of run-of-mine material. Talc is an environmentally benign mineral and talc mining has a very minor impact on the environment.

3.24.1 Talc deposit types

Most talc deposits originate by hydrothermal addition of silica and water (OH^-) to Mg-rich ultramafic rocks or carbonates (dolomite, magnesite) resulting in replacement talc ore. The majority of deposits are generated during orogenic metamorphism (they are metamorphogenic). A smaller number is due to magmatic-hydrothermal contact-metasomatic processes.

Talc is part of the metamorphic paragenesis in siliceous metadolomite, where it forms in a relatively closed system at high lithostatic pressures. Talc deposits with high concentrations of the mineral and large volumes are chacteristically controlled by shear zones and faults (similar to the San Andreas Fault in California: Moore & Rymer 2007). Seismic pumping (Sibson 1990) is probably involved and phases of free hydrothermal flow and low, hydrostatic pressures may be essential, because import (SiO_2, Mg) and export (Ca, CO_2) of matter must be achieved. Hydrothermal synthesis of talc was demonstrated at temperatures above 300°C. Kinetic limitations occur below that temperature. In nature, talc is definitely formed at lower temperature, including the diagenesis of evaporites and the saprolite zone of soil formed on ultramafic rocks (cf. Chapter 1.2 "Nickel Laterites").

For the hydrothermal formation of talc from ultramafics, magnesium-rich rocks such as magnesian dunite are more suitable than iron and aluminium-rich varieties. The talc-forming reaction is summarized in equation 3.15.

Hydrothermal formation of talc from dunite:

$$\underset{\text{Forsterite}}{3Mg_2SiO_4} + 5SiO_{2(aq)} + 2H_2O \rightarrow \underset{\text{Talc}}{2Mg_3(OH)_2Si_4O_{10}} \qquad (3.15)$$

Clearly, the addition of dissolved silica is needed for the formation of talc from dunite/olivine. Because most ultramafic rocks contain pyroxene besides olivine, talc formed from these rocks will be associated with retrograde amphibole that may be acicular. Chlorite and serpentine are common gangue minerals. If the hydrothermal fluids contained CO_2, carbonate minerals are part of the paragenesis (eq. 3.16). Talc derived from ultramafic rocks often displays iron contents in the percent range, and traces of nickel and chromium. Some ophiolites comprise huge masses of metasomatic talc-carbonate rocks (e.g. those of the Pan-African Orogen in Saudi Arabia and Northeast Africa). The bulk of these rocks cannot be utilized, having low talc and high iron concentrations.

Talc-carbonate rock formation by carbonation of serpentine:

$$\underset{\text{Serpentine}}{2Mg_3Si_2O_5(OH)_4} + 3CO_2 \rightarrow \underset{\text{Talc}}{Mg_3(OH)_2Si_4O_{10}} +$$
$$\underset{\text{Magnesite}}{3MgCO_3} + 3H_2O + 1.5\,O_2 \qquad (3.16)$$

Exploitable talc concentrations in ultramafics typically follow structures that controlled hydrothermal flow, such as stockwork bodies, but many are relatively small and irregular veins. Worldwide, ~30% of talc is derived from ultramafic rocks:

In eastern Finland along an Early Proterozoic rift and ophiolite belt marked by copper and nickel deposits (Outukumpu and Talvivaara) large ultramafic-hosted talc deposits are exploited. Locally, metamorphic fluids converted Svecokarelian ophiolites into talc-breunnerite soapstone and talc schist with >50% talc. Near Lahnaslampi, a vertically elongated lens of this material with a cross-section of 200 × 500 m contains >30 Mt of talc. Flotation yields ~200,000 t/year of talc products and ~1000 t/y nickel concentrate as a by-product from accessory sulphides.

Carbonate-hosted talc deposits

Carbonate-hosted talc deposits provide ~70% of world production. Talc is formed from dolomite or magnesite by reaction with hydrothermal SiO_2 solutions. With magnesite, this is easy to understand. However, even replacement of dolomite by talc is possible without the need to add magnesium (eq. 3.17).

Hydrothermal formation of talc from dolomite:

$$3CaMg(CO_3)_2 + 4SiO_{2(aq)} + 4H_2O + 6H^+ \rightarrow Mg_3(OH)_2Si_4O_{10} + 3Ca^{2+}_{(aq)} + 6H_2CO_3 \qquad (3.17)$$

Large metasomatic talc bodies can only form in an open system that allows evacuation of Ca and CO_2, because otherwise the reaction would soon cease. Theoretically, talc formation according to this reaction should cause a volume decrease of ~14% and drusy textures should develop. This was never observed, however. As an explanation, some scientists propose hydrothermal supply of magnesium in addition to SiO_2 derived from outside of the system. Observations of talc replacing non-magnesian rocks such as limestone, and even non-carbonate rocks (e.g. quartzite and radiolarite in deposits of northern Spain: Tornos & Spiro 2000) are also cited as evidence of extraneous Mg-supply called "magnesium metasomatism" (cf. Section 3.16.1 "Magnesite"). Most probably, both alternatives occur in nature – derivation from the rock *in situ*, and hydrothermal supply from outside. Hydrothermal fluids of carbonate-hosted talc deposits often are saline brines. One plausible explanation is that dolomite and magnesite rocks hosting talc deposits may be residual members of evaporites. It is also possible that migrating fluids dissolved salt elsewhere (Powell *et al.* 2006).

Talc in carbonate rocks is generally of better quality compared to ultramafic-hosted talc. Common gangue minerals are chlorite (if metapelites are involved) and carbonate. Trace element concentrations are very low. Dolomites host larger talc deposits than magnesite, because of the commonly denser fracturing, which made the original rockmass more permeable for hydrothermal solutions. Of course, dolomite is also more common compared to magnesite. Talc in magnesite tends to occur in shells around cores of magnesite rock.

Trimouns, Luzenac in the French Pyrenees is the largest dolomite-hosted talc deposit in Europe (Moine *et al.* 1989). At ~1700 m above sea level, the talc-bearing zone extends for more than 5 km along the eastern slope of the Massif of St Barthelemy. Its footwall is formed by mica schists and migmatite (Figure 3.33, Figure/Plate 3.34). Crystalline basement rocks are overlain by an epizonal metamorphic suite of dolomite (Ordovician), sericite schist (Silurian) and calcite marbles with bands of quartzite (Devonian). The sediments were overthrusted as a nappe during the Variscan Orogeny (Late Palaeozoic). In the Cretaceous, an Alpidic (Pyrenean) transtensional deformation affected the region and the thrust plane experienced renewed intense shearing. The Ordovician dolomites are partially replaced by talc and in the shear zone, blocks of dolomite, quartzite, mica schist, gneiss and pegmatite float in a mass of talc. The talc zone reaches a thickness of 80 m and dips with 40–80°

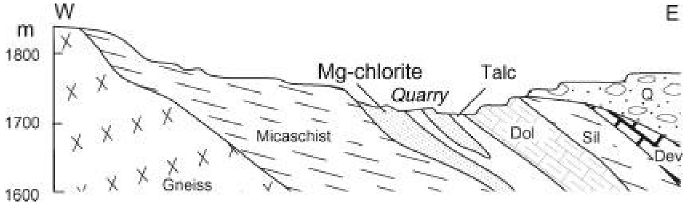

Figure 3.33 Simplified geological profile of the talc deposit at Trimouns, Luzenac in the French Pyrenees (adapted from Schärer *et al.* 1999). Mg-chlorite fels derived from micaschist and pegmatites; Talc (white) derived from dolomite; Dol – Ordovician dolomite; Sil – Silurian black schists; Dev – Devonian calcite marbles; Q – Quaternary. For location refer to Figure/Plate 1.89.

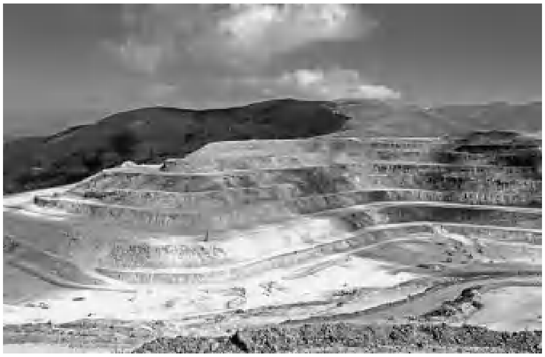

Figure 3.34 (Plate 3.34) Eastward bird's eye view of the talc quarry at Luzenac in the French Pyrenees. White talc marks the working face. © Philippe Psaila/SPL/PictureDesk.com.

to the East. The footwall part of the deposit consists of 70–90% grey chlorite and 10–30% talc. Pure talc (>80%) occurs only in the hanging wall part. Chlorite is derived from silicate rocks by magnesium metasomatism (Moine *et al.* 1989), whereas talc clearly replaces dolomite which is best illustrated by banded talc that passes into equally banded dolomite. Fluid inclusions reveal formation by saline brines (~30 wt. % NaCl) at ~300–350°C and 2–3 kbar. The hydrothermal system was unusually long-lasting, active for at least 16 million years (112–97 Ma). This was supported by simultaneous Pyrenean tectonics, fluid migration and metamorphism (Schärer *et al.* 1999). Talc resources of the Trimouns deposit are estimated at 20 Mt.

The Rabenwald deposit in Eastern Austria also occurs in a shear zone, in this case, however, within Lower East Alpine basement gneisses (Figure 1.89). The shear zone dips with 6° southeast, almost parallel to the slope on which talc is exploited in an open pit. The shear zone reaches a thickness of tens of metres and consists of large blocks of magnesite that float in schistose talc-chlorite rock. The magnesites are thought to be remnants of Palaeozoic sediments (cf. "Magnesite") which were overthrust and thinned out by nappe movement. Magnesite was consumed by talc formation and only single blocks remain (Prochaska 1989). Host gneiss was hydrothermally altered and transformed to fine-grained quartz-phengite-chlorite (-kyanite) rock. Paragenesis and fluid inclusions data support formation of the deposit at 500–550°C and 8–9 kbar (Moine *et al.* 1989). However, the extreme conditions probably have prevailed only during an early tectonic phase of deep burial (as shown in Figure 1.89), whereas talc was formed later at 350–400°C and 3 kbar (Pohl & Belocky 1999). A connection with deep fluid systems and metamorphism provoked by the Cretaceous nappe formation in the Eastern Alps appears likely.

In several talc districts, granite intrusions caused formation of talc deposits although, of course, granites do not release Mg-rich fluids. Consulting the reactions above (eq. 3.15 and 3.17), the explanation is straightforward: The intrusions establish hydrothermal systems with dissolved silica. On interaction with ultramafic or dolomite rock, talc can be the result (e.g. Göpfersgrün in Southern Germany:Hecht *et al.* 1999):

Skarn-related hydrothermal deposits of talc in the metamorphic aureole of granite occur in Korea (Shin & Lee 2002). Near Hwanggangri a Cretaceous granite intruded Cambro-Ordovician metasediments and produced a wide skarn zone. During the anhydrous phase of skarn formation, dolomite was transformed into magnesian calcsilicates. Subsequent flow of magmatic fluids at T<400°C through permeable structures in Mg-skarn provoked talc formation. The authors suggest that the magnesium of the talc is inherited from dolomites.

3.24.2 Pyrophyllite

Pyrophyllite $Al_2(OH)_2Si_4O_{10}$ (density 2.65–2.85 g/cm^3, hardness 1–1.5) resembles talc closely. In a number of applications it is exchangable with talc. When calcined, its refractory stability extends to higher temperatures, including those common in the iron and steel industry. It occurs in foliated (phyllitic) form and as compact wax-like masses. When heated, pyrophyllite exfoliates strongly but positive identification requires X-ray diffraction techniques. With few exceptions, pyrophyllite is the result of advanced argillic hydrothermal alteration affecting intermediate to felsic volcanic, mainly volcaniclastic rocks (Herrmann *et al.* 2009). At Pueblo Viejo, for example, pyrophyllite was induced by magmatic volatiles condensing into meteoric water. Similar to kaolinization, the process is characterized by depletion of silica, alkali elements, calcium, magnesium and iron.

Pyrophyllite is also a common metamorphic mineral formed at low to moderate pressure and T <400°C. Pyrophyllite replaces kaolinite at ~200–300°C by reactions such as 1 kaolinite + 2 quartz → 1 pyrophyllite + H_2O. At higher temperature (~400°C) pyrophyllite decomposes to alumosilicate (kyanite or andalusite), quartz and H_2O (Bucher & Frey 2002). Numerous deposits of pyrophyllite occur in Japan and Korea. In USA and Canada, Precambrian volcanics host important pyrophyllite deposits.

World production of talc and pyrophyllite in 2009 was 7.2 Mt, mainly from China, the Republic of Korea, India, USA, Finland and Brazil (USGS 2010). Available statistics rarely differentiate between talc and pyrophyllite.

3.25 VOLCANICLASTIC ROCKS

Volcanic processes create a wide diversity of mineral deposits, including numerous metallic and non-metallic resources. Bentonite, borates and zeolites are valuable industrial minerals with close genetic relations to volcanism. The heat of shallow magmatic bodies is a prolific source of geothermal energy. Under suitable climate conditions, volcanic soils are among the worlds' richest for farming. Here, we shall briefly describe the role of quite common volcanic rocks that meet essential needs of human societies.

Volcaniclastic rocks comprise all fragmented volcanic material, whatever its origin, dispersion and depositional sites. One example is naturally cemented ash (tuffite) which is often used as a building stone, apart from many other applications (Heiken 2006). Note that tuffites are the host rock for the proposed high-level radioactive waste repository at Yucca Mountain in the southwestern USA. Scientific and more practical data resulting from 20 years of investigations at this site are singularly comprehensive (Stuckless & Levich 2007).

Volcaniclastic rocks provide much of the "crushed stone and aggregate class" of raw materials for the building industry (cf. Section 3.22 "Quartz Sand and Gravel"). Of course, the chemical and mineralogical composition of volcanic rocks varies widely. Generally, loose and cemented volcanic ash contains crystals, glass shards, pumice and lithic fragments in variable proportions. As concrete aggregates, uncemented ash (<2 mm grain diameter) and lapilli (2–64 mm) are preferred substitutes for alluvial sand and gravel. In this application, favourable grain size and mechanical properties are positive criteria, whereas the presence of concrete-damaging substances (salt, sulphate, alkali-reactive silica) is negative. Preliminary petrological examinations of aggregate resources are indispensible. Any material that contains >0.25 wt. % opal, >5% chalcedony, >3% glass and cryptocrystalline acidic to intermediate material produces a severe alkali-silica reaction in concrete (expansion and cracking by formation of a hydrous gel), unless low-alkali cement is used. The alkali-aggregate reaction can be avoided by including pozzolanic supplements in the aggregate mix, which immobilize Na_2O and K_2O.

3.25.1 Pumice

Pumice consists of loose and unaltered volcanic rocks that originate by frothing of intermediate to felsic melts. Pumice particles consist essentially of highly vesicular volcanic glass. Fine ash and blocks (>64 mm) are of little use and the main economic interest lies in lapilli (2–64 mm). In felsic systems porosity of pumice reaches 90% and the material floats on water. In the building industry, grain diameters of 2–16 mm are preferred. Of course, grain classes are separated and mixed to consumers' specifications. Weathered or hydrothermally altered material is rejected (except for pozzolanic rocks, see below). Bulk weight should be below 1000 kg/m^3, because the most common application of pumice is the production of lightweight concrete by mixing it with lime or cement. Building blocks made from this mixture have a high heat and acoustic insulation capacity. Minor uses include horticulture, filtering and artificial aging (stonewashing) of cloths such as jeans. Industrial pumice mining is centred in Turkey, Italy, Greece and Chile. Resources are very large. World production in 2009 was estimated at 20 Mt (USGS 2010).

After fallout, volcaniclastic rocks may experience various alterations, such as the influence of acid (hydrothermal) or alkalic waters (seawater, playa lake brines), elevated temperature and humidity (aging, supergene alteration). This leads to formation of mineral deposits such as bentonite and zeolite, which are described in special sections of this chapter. Other useful products of alteration include perlite and trass.

3.25.2 Perlite

Perlilte is a hydrated glass-rich volcanic rock of rhyolitic composition, with a perlitic texture. It is generally derived from lava flows or resurgent domes, rarely from pyroclastics (Shackley & Allen 1992). The perlitic texture is often a visible onion peel-like concentric cracking, caused by expansion of the glass upon hydration. Water molecules diffuse into the glass in exchange for Na^+ followed by K^+, which move out of the system. Perlitization commences at ~3 wt.% H_2O. Obsidian (with less water) and pitchstone (with much more water to ~10%) are different from perlite, but transitions are reported, for example in Iceland: Perlites formed by hydrothermal alteration of rhyolite extruded beneath glaciers in Iceland display 2–8 wt.% water content, with perlitization increasing at higher water concentrations. The water is of meteoric derivation (Denton *et al.* 2009).

Rapid heating to 900–1150°C at atmospheric pressure expels the water, while the glass softens and expands. Expanded perlite is a white, lightweight and durable material that resists decay. Similar to pumice, it is used as an aggregate for making lightweight concrete for heat and sound insulation. There are many other applications, such as producing paint, ceramics, foundry sand, drilling muds, filters, abrasives, matrices for hydroponic plant culturing and loose filling material in insulation and packaging. Usability is mainly controlled by the swelling capacity, which is measured by comparing the bulk density of raw and swelled material. In the field, the swelling aptitude of prospective rocks can be estimated by heating grains of 1–2 mm diameter with a blowtorch. Volume increase should be a minimum of 6–10 times; even 20 times is quite common. Typical traded perlite weighs ~80 kg/m^3.

Perlite deposits and resources exist in many regions with widespread felsic volcanism. Similar to pumice, transport costs tend to limit international trade. Available statistics reveal Greece, USA, Turkey and Japan as leading producers (world production 1.7 Mt in 2009). No data are available for China and other likely producing countries. Greece hosts very large (the worlds' largest) and high-quality resources in the Aegaean Sea, especially on Kos and Milos islands.

3.25.3 Trass

Trass is not a petrological term, but designates non-welded massive ash and pumice deposits (rarely lavas), which have acquired pozzolanic properties by hydrous alteration. Trass is one of the *pozzolanic raw materials*. This term is derived from a deposit of natural cement (leucite tuff) near the village of Pozzuoli, Naples (Italy). The namesake deposits seem to have been exploited in ancient Rome as early as 2300 years ago. The words cement and concrete are derived from Latin *caementum* and *concretus*. Pozzolanic materials are either natural or man-made siliceous, often amorphous substances that react readily with calcium hydroxide, which is a by-product of the hydration of Portland cement. Calcium hydroxide or calcite produced by ageing are relatively soluble if concrete is submerged in water. In contrast, calcium silicates resulting from the reaction with pozzolans are insoluble in water and the concrete is durable. The essential property of pozzolans is an elevated content of reactive SiO_2 (and Al_2O_3) phases. Apart from trass, natural pozzolans include chert, calcined diatomite and even oil shale ash. Man-made are fly ash, dehydrated kaolin ("metakaolin") and silica fume (a by-product of silicon metal or ferrosilicon alloy manufacturing). For application, trass is finely ground and mixed with Portland cement or lime making the concrete harden, even under water. The pozzolanic properties of hydrated tuffs are best determined by serial tests in the laboratory. Sampling must make certain that the natural heterogeneity of altered volcanic rocks is sufficiently constrained. Trass is always extracted in open pits. Upgrading by processing is not possible.

The genetic variability of trass deposits can be shown by reference to Western Europe: The deposit Andernach at Laacher See, Eifel, Germany originated in the late Pleistocene during the giant eruption of a maar volcano (Schmincke *et al.* 1999). Hot phonolitic pumiceous ash was deposed in a shallow lake. The material consists of analcite, phillipsite and SiO_2 glass phases (Liebig & Althaus 1998). The bed has a thickness of ~9 m and covers an area of 8 by 2.5 km. Trass is also exploited in the Miocene impact structure Nördlinger Ries in southern Germany. This material is derived from suevite, a polymict impact breccia containing sedimentary and crystalline lithic fragments, and glassy impact-melt shards in montmorillonite matrix (Liebig & Althaus 1998). Suevite was pervasively altered by alkaline hydrothermal fluids that produced montmorillonite, saponite, illite, analcite, erionite and clinoptilolite (Osinski 2005). In Austria, trass is extracted from the flank of a Miocene trachyandesite volcano near Gossendorf. Pyroclastic rocks were strongly altered by acidic hydrothermal fluids (Klammer 1997). This material consists essentially of alunite, kaolinite and opal-C/CT phases.

As reported above, only pumice and perlite are considered in international statistics. Volcanic rocks used in the building industry or in manufacturing cement are part of the giant mass of crushed rock that is briefly quantified in the description of "Quartz Sand and Gravel" in Section 3.22.

3.26 WOLLASTONITE

Wollastonite	$CaSiO_3$	Density 2.8–3.0 g/cm^3

Calcium in wollastonite may be substituted by several percent of Fe and Mn, and lesser Mg or Al. This can reduce the value of the product, either by lowering whiteness, or by causing less desirable electric, physical and chemical properties. Frequent gangue minerals of wollastonite are diopside-hedenbergite, tremolite (beware of asbestiform varieties), vesuvianite, grossular-andradite, graphite, quartz, plagioclase and calcite.

Exploitable wollastonite ore has a minimum content of ~30% $CaSiO_3$. Saleable by-products (e.g. garnet sand, calcite) allow mining lower grades.

Usually, wollastonite occurs in coarse, bladed masses, but after crushing and grinding the mineral is acicular to fibrous. The needles have a high strength that is the key to many uses of wollastonite. It is applied as a component or filler in the production of ceramics (especially tiles), plastics and rubber, paints, adhesives, isolating material, in ceramic abrasives and building elements. Fibrous wollastonite substitutes for asbestos, as in paint, refractory materials and in welding rods. The most important properties of processed wollastonite are: i) percentage and shape of fibres (length/thickness); and ii) reflectivity and whiteness. Depending on the intended use, very low chemical reactivity and weight/volume loss due to heating, and the mineral's alkaline reaction in emulsified state (pH 9.9 in 10% water slurry) may play a role.

3.26.1 Wollastonite deposit formation

Wollastonite is a product of contact-metasomatism (skarn-formation) of limestone and calcite marble. Isochemical regional metamorphism of siliceous limestone does not form sufficiently high grades of wollastonite. Although it is theoretically possible that the silica in skarn is derived from impurities in the original calcite rock, investigations show that it is commonly introduced by magmatic-hydrothermal fluids (Grammatikopoulos & Clark 2006). Exotic elements in the skarn; such as W, Cu and Au; serve as monitors for the passage of magmatic fluids. Wollastonite forms according to reaction 3.18, at T ~500 to >700°C and P at 100–500 MPa (1–5 kbar); corresponding to highest-temperature hornblende hornfels and pyroxene hornfels facies.

Contact-metasomatic formation of wollastonite:

$$\text{Calcite} + SiO_2(aq) \rightarrow \text{Wollastonite} + CO_2(aq) \qquad (3.18)$$

CO_2 must leave the system. as otherwise the reaction would stall. In a closed system, quartz and calcite can coexist stably side by side, even under conditions of the granulite facies. Therefore, mass transformation requires an open system. For wollastonite formation, the fluid phase must be mainly aqueous with a low CO_2-content (X_{CO2} <0.3). High fluid/rock ratios are needed in order to dilute and export the CO_2 generated by the reaction. This prerequisite for the formation of a wollastonite orebody is achieved by a considerable mass flow of magmatic water outwards through the nascent wollastonite zone. Because during the prograde stage of contact metamorphism, decarbonation reactions and high X_{CO2} prevail, conditions of wollastonite formation are mainly realized during the retrograde path (Nabelek 2007).

Exploitable wollastonite concentrations are not common. The first mines were established in 1943, in the Willsboro district of the Adirondack Mountains in New York State. Until today, this district is a globally significant producer. The deposits occur in the Mesoproterozoic Grenville Orogen (Tollo *et al.* 2004):

> Many of the wollastonite deposits in the Adirondacks occur near the contact of anorthosite with calcite marble. The Valentine deposit and many smaller occurrences are the product of a quartz-syenitic intrusion into granulite-facies metasediments (Gerdes & Valley 1994). At the contact, calcite marbles were transformed into a skarn shell 60 m wide, that contains coarsely crystalline wollastonite and minor amounts of calcite, diopside and secondary prehnite. Reserves are >7 Mt ore. Megascopic boundaries between the wollastonite skarn and calcite marble are irregular in shape but sharp. Oxygen isotope ratios in calcite marble remain unchanged right up to the skarn boundary. As there is hardly any silica in the marbles the SiO_2 must have been delivered by hydrothermal fluids.

> An important wollastonite deposit is exploited near Lapeenranta in southern Finland, not far from calcite marble deposits at Ihalainen. At Lapeenranta, a large body of calcite marble with bands of fine-grained quartzofeldspathic metavolcanic rock ("leptite") floats in a giant intrusion of Mesoproterozoic Rapakivi granite. The marbles are traversed by swarms of granitic, pegmatitic and mafic dykes. The whole assemblage experienced strong thermal metamorphism that provoked the formation of wollastonite orebodies (with a gangue of quartz, grossular, diopside and serpentinite). The average wollastonite grade is 25–30%; grinding and flotation are employed to produce a concentrate of >90% wollastonite with very little iron. Resources are estimated to >30 Mt.

Wollastonite production continues to increase. In 2008, processed wollastonite world output was ~600,000 t. China was the leading producer (70%), followed by India, USA, Mexico, Spain and Finland. Spain has several potential deposits (Galan & Caliani 1997; Figure 3.35). Prospecting is based on geological models. It is advisable to carry out processing tests early in investigations, because many occurrences do not yield a product of sufficient quality (Gracia *et al.* 1999). Considerable tonnages of wollastonite are produced synthetically from quicklime and quartz sand ("cyclo-, pseudo-, or β-wollastonite", a high-temperature phase).

3.27 ZEOLITES

		Density g/cm³
Analcime (analcite)	$NaAlSi_2O_6 \cdot H_2O$	2.3
Chabazite	$Ca\ (K,Na,Sr)Al_2Si_4O_{12} \cdot 6H_2O$	2.1
Clinoptilolite	$(Na,\ K,Ca)_{2\text{-}3}(Al,Si)_{18}O_{36} \cdot 11H_2O$	2.1
Erionite	$(Ca,K_2Na_2)_2(Al_4Si_{14}O_{36}) \cdot 15H_2O$	2.0
Ferrierite	$(K,Na,Mg)_{4.4}(Si,Al)_{36}O_{72} \cdot 20H_2O$	2.2
Mordenite	$(Na_2Ca,K_2)Al_2Si_{10}O_{24} \cdot 7H_2O$	2.1
Phillipsite	$(K,Ca,Na)_2(Si,Al)O_{16} \cdot 6H_2O$	2.2

This list includes the few economically prominent zeolites from more than 70 zeolite minerals in nature (Bish & Ming 2001). Note that cation ratios may vary so that formulas and specific densities provided are only indicative. Zeolites are crystalline hydrated alumosilicates of alkali and alkaline earth elements with a zeolite structure and with the capability of cation exchange and reversible dehydration. The zeolite structure is a three-dimensional framework of anionic tetrahedra (AlO_4 and SiO_4) similar to feldspar, with interconnected micropores, which contain water and exchangable cations. When heated, many zeolites fuse readily and display marked swelling, giving

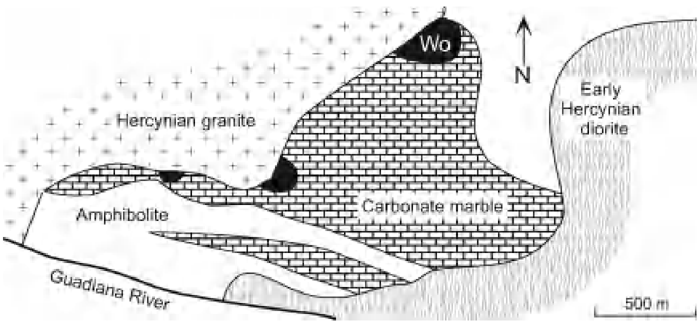

Figure 3.35 Schematic geological map of wollastonite prospects (black) near Merida, southwest Spain, at the contact between Early Palaeozoic carbonate rocks and Late Palaeozoic granite (modified after Galan & Caliani 1997).

rise to the name zeolite, from the Greek word for *boiling stone*. Contrary to dehydration of minerals with (OH) groups, zeolite water is lost continuously with increasing temperature. At ambient temperature, water is readily re-absorbed. This behaviour singles out thermogravimetric analysis as a suitable method for identification of zeolites.

Zeolite use is based on the mobility of water and cations in the pores and channels of the framework. The ease of cation exchange is the precondition for numerous applications, such as water softening (removal of dissolved earth alkalis). Because the overall size of zeolite channels accepts only molecules below a certain diameter, the separation of large and small molecules ("molecular sieving") is another application of zeolites. Designed zeolites are synthesized for industrial purposes, exemplified by reacting a saturated kaolinite solution with NaOH or sodium silicate at elevated temperatures. Upon cooling, gel agglomerates form first, within which nucleation and crystallization of zeolite take place (Mintova *et al.* 1999). Other applications of zeolites include nitrogen fixation in drinking water treatment, desiccation, deodorization (cat litter), adsorption of spilled fuel and of radioactive contamination (e.g. for purifying water and milk, as at Chernobyl after the 1986 accident, and as a filler between waste containers in storage facilities). Zeolites are also used for filtering oil, desulphurization of stack gas and as filler in paper, fertilizer, cement and toothpaste. K-rich clinoptilolite is useful as a slowly acting fertilizer. For environmental reasons, synthetic zeolites are preferred as cleaning agents instead of sodium phosphate in powder detergents. Synthetic zeolites are essential as catalysers in cracking heavy hydrocarbons such as petroleum and methanol in order to produce light fuels. In many countries, zeolitized tuff is extracted as a dimension stone, because such rocks are easily worked in the natural moist state but harden by drying. Furthermore, zeolite-rich rocks are much employed for the production of lightweight building materials and as pozzolans in manufacturing seawater-resistant concrete.

Zeolite-rich rocks are extracted in open pits. Zeolites forming part of natural rocks cannot be enriched. No processing is done apart from drying, milling, sieving and in some cases, acid treatment in order to remove exchangable cations.

Zeolite minerals are ubiquitous in nature, although commonly only in very small concentrations, for example in joints and vesicles of volcanic rocks and disseminated in sediments. Subgreenschist metamorphic rocks may contain appreciable amounts of zeolites, in the case of mafic rocks typically represented by low-T stilbite ($CaAl_2Si_7O_{18}\cdot 7H_2O$) and heulandite {$CaAl_2Si_7O_{18}\cdot 6H_2O$} and high-T laumontite {$CaAl_2Si_4O_{12}\cdot 4H_2O$} plus wairakite ($CaAl_2Si_4O_{12}\cdot 2H_2O$). Associated minerals include analcime, mixed-layer clays, albite and quartz (Bucher & Frey 2002). Overall, metamorphic zeolite formation is the result of hydrous alteration at low temperatures. As temperatures increase beyond 250–300°C, zeolites disappear and prehnite-pumpellyite take over.

3.27.1 Zeolite deposit types

Generally, only rocks with over 50 wt. % zeolite content (zeolitites) are considered as economically exploitable. High grades like this are favoured by high reactability of the hydrating rock, provided by small grain size (e.g. volcanic ash) and an amorphous state of particles (e.g. silicic volcanic glass). An alkaline aqueous environment (pH 8–10) with desirable cations is best provided by terrestrial salt lakes (Hall 1996, 1998). In addition, moderately elevated temperatures (50–300°C) favour zeolitization (Hall 1998). Geothermal waters and groundwater in terrestrial volcanic settings are commonly acidic to extremely acidic. This inhibits zeolite formation and geological factors must act in favour of alkaline conditions. Common causes of alkalinity are evaporation in closed inland lake basins and ocean water with a pH of ~8.4. Further possibilities include mobilization of alkalis from volcanic glass, or advection of alkalis from elsewhere (e.g. groundwater that dissolved limestone).

Most zeolitites are geologically young (Tertiary-Quaternary), because zeolites age with time to form denser minerals. However, exploitable heulandite and mordenite deposits were reportedly found in Carboniferous rocks of New South Wales, Australia (Flood 1991).

Erionite deposits are exploited from alkaline lake deposits in the western USA. Layers of rhyolitic tuffs in the lacustrine deposits were zeolitized by lake brines or pore fluids. In some cases, low-temperature hydrothermal alteration is evoked. The famous landscapes of Cappadocia in Turkey are formed of erionitic rhyolite ignimbrites. However, the residents of the towns of Karain and Tuzköy in the area suffer from an elevated incidence of pleural mesothelioma, lung cancer and asbestosis. This is attributed to the asbestiform shape of erionite dust, with very thin (<0.5 mm) and long (>10 mm) needles (Ross 1999). Other fibrous zeolites include natrolite and scolecite.

Mordenite is present in playa lake deposits (e.g. Green River Basin, Wyoming) but is particularly characteristic for alteration related to near-surface hydrothermal systems with temperatures of ~100°C. In Bulgaria, mordenite deposits are exploited that originated by deposition of volcanic ash into an Oligocene sea.

Clinoptilolite is extracted from alkaline lake sediments. Its precursor rocks are typically rhyolitic glass tuffs. Several deposits are worked in the western USA, which display a zoned alteration: A central zone with highest pH and authigenic alkali feldspar is surrounded by an analcime zone. This is followed by the broad zeolite zone with erionite, clinoptilolite and mordenite. The outer margin is characterized by chabazite and phillipsite. Outside of the lake, where groundwater chemistry is nearly normal, volcanic glass is fresh or partly altered to montmorillonite. The same succession is observed vertically because pore water in playa lake sediments acquires higher alkalinity with increasing depth. Most probably, the zonation is also a product of changing environmental conditions in geological time. Several of the large Neogene borate basins in Turkey contain important clinoptilolite resources in the footwall of borate seams (e.g. Bigadiç, cf. "Boron"; Sirkecioglu & Erdem-Senatalar 1996). Clinoptilolite deposits are quite common so that numerous applications have been developed for this material and research is continuing.

In 2007, world production of natural zeolites was an estimated 2.5–3 Mt. Main producers were China, the Republic of Korea, Japan, USA, Indonesia, Turkey and Hungary (USGS 2008). Most of the production was probably used in low-value applications, including lightweight aggregate, pozzolanic cement and soil conditioners. Areas of geologically young volcanism and adjacent playa lakes with tuff beds are most prospective. The potential to locate additional large and high-quality zeolite resources is high. However, zeolite minerals can only be ascertained and precisely characterized by advanced mineralogical methods.

3.28 SUMMARY AND FURTHER READING

In my view, industrial minerals and rocks are deeply interesting. Like metal deposit, they occur in all genetic process systems (Table 3.1). Let us summarize the genetic setting of significant resources presented in this chapter:

1 Orthomagmatic: Alkali feldspar (in granite), apatite, limestone (carbonatite) and olivine (in dunite);

2 Pegmatites: Alkali feldspar, Li-minerals and quartz;

3 Magmatic-hydrothermal: Alunite, kaolin and phlogopite;
4 Skarn and contact-metasomatic: Boron, fluorite and wollastonite;
5 Volcanogenic: Exhalative barite (VMS), diamond in kimberlites and lamproites;
6 Supergene: Kaolin, phosphate and vermiculite; infiltration/evaporation brines of playa lake basins with boron, iodine, lithium and soda;
7 Sedimentary: Gravel, sand and clay; volcaniclastic rocks, diatomite, phosphorite; most limestones; diamond placers, borate minerals, trona, zeolites and sedex barite;
8 Diagenetic: Dolomite and magnesite; sulphur in evaporites;
9 Metamorphic: Andalusite, some asbestos, graphite, kyanite and sillimanite;
10 Metamorphogenic: Part of asbestos, graphite, magnesite and talc.

The evironmental record of exploiting and utilizing this group of resources is inconsistent. Consider the carbonates dolomite, limestone and magnesite. These bases are essential for food production, environmental engineering and numerous other utilizations. Magnesite and dolomite are the means for producing the light metal magnesium. which is central to minimizing the CO_2 footprint of all liquid fuel-based traffic. Yet, the three minerals must be calcined for further processing and are, therefore, an important source of carbon dioxide. The only seriously hazardous substances are probably amphibole asbestos, fluorine and certain zeolites. Unwanted traces of problematic elements occur in phosphorite and even in quite ordinary clay. Investigations and precautionary measures are compulsory.

More information on this group of raw materials is found in the exhaustive volume by Kogel *et al.* (2006), in Ciullo (1996) and Harben & Bates (1990). Genetic processes are at length explained in Robb (2005). Metamorphism, which is important for a number of the described minerals and rocks, can be explored in Bucher & Frey (2002). Continental saline lakes, which are the main habitat of several of the discussed materials, are revisited in Chapter 4 of this book and thoroughly described by Warren (2006).

CHAPTER 4

Salt deposits (evaporites)

Synopsis

In economic geology, the term "salt" generally refers to rocks consisting of halite (sodium chloride) and other water-soluble minerals. Salt is a common member of evaporitic sequences. Evaporites are precipitations from a saturated brine in sedimentary systems driven by solar evaporation (Warren 2006) and are chemical sediments. They form along coasts or on continents, resulting in the terms marine as opposed to terrestrial, or continental salt deposits. Most hard rock halite and potassium salt deposits are derived from seawater. About 50% of the total mass of evaporites in the Earth's crust are salt rocks *sensu stricto* (mainly consisting of halite), which are the subject of this chapter. The other half is composed of gypsum and anhydrite (cf. Chapter 3 "Industrial Minerals").

In several respects, salts are very peculiar. They are water soluble, for example, but have the lowest permeability of all common rocks. Consequently, they confine crustal water flow and form effective traps for petroleum and natural gas deposits. Cycling of saline waters in the crust is an important agent of ore formation (cf. Chapter 1 "Diagenetic Ore Formation Systems"). Also, salt is one of the few *sensu stricto* sustainable natural resources, because its mass contained in ocean water is very large indeed.

Currently, the role of salt rocks for building inexpensive underground spaces is rapidly growing. Large leached caverns dedicated to the storage of petroleum products and natural gas are an important example. Wind energy may be temporarily stored in salt caverns in the form of compressed air from which it is easily reconverted to electricity. Toxic industrial waste is safely disposed in deep salt bodies (cf. Chapter 5.5 "Deep Geological Disposal"). Critical public reactions to underground storage of radioactive waste were particularly fruitful by spurring research on salt, which generated a wealth of new knowledge.

The aim of this chapter is to introduce important salt minerals and salt rocks, their formation as observed today and in the geological past, their diagenesis, metamorphism and deformation characteristics, and specific aspects of applied salt geology.

Rock salt (NaCl, common salt, halite, sodium chloride) is not only an essential part of the diet of humans and most animals (~20% of salt consumption), but primarily an important raw material for the chemical industry (~60% of consumption). Most halite is used for the production of chlorine, soda ash (Na_2CO_3) and sodium hydroxide (NaOH, caustic soda), which are basic chemicals for glass, paper, PVC and aluminium metal manufacturing. Sodium chloride is an

---

Economic Geology Principles and Practice
Metals, Minerals, Coal and Hydrocarbons – Introduction to Formation and Sustainable Exploitation of Mineral Deposits, Walter L. Pohl
© 2011 Walter L. Pohl. Published 2011 by Blackwell Publishing Ltd.

essential nutrient for humans and grazing animals, because a plant-derived diet must be supplemented by salt. Plant growth, however, is impeded by elevated salt concentrations in soil. In humans, high salt intake (~1 g per kg of body weight) in a short time is fatal, whereas ~4 g per day is the recommended intake (Paracelsus, 1493–1541: "The dose makes the poison"). Some of salt's applications pose potential risks for the environment, such as the production of organo-chlorides (Thornton 2000). Salt is needed for de-icing roads (in the United States ~40% of total consumption: USGS 2010). De-icing may locally increase Cl-concentration in surface and groundwater, which might impact on sensitive biota and resources of drinking water. Note, however, that WHO 2006 does not set guide values for chloride and sodium in drinking water because the elements are *"Not of health concern at levels found in drinking-water"*. Salt deposits are very common and few countries rely on imports. Harvesting salt from seawater in coastal salt pans by solar evaporation is feasible and inexpensive along all low-latitude coasts. This technology must have been discovered when Neolithic humans changed from nomadic to agricultural life and first felt the need for salt. Rock salt is mainly extracted by solution methods. Therefore, salt is cheap and rarely traded over long distances. Yearly world production of sodium chloride is ~260 Mt (2009) from 110 different countries. Largest producers are China, USA, Germany, India, Canada and Australia. Resources are practically unlimited, because rock salt beds are huge and widely distributed, and this is backed up by salt dissolved in ocean water, salt lakes and subsurface brines. Present production is based on all four sources.

In contrast to sodium chloride, potassium salt rocks are relatively rare and primary production is restricted to only 12 countries, although about 40 different potassium-bearing salt basins are known worldwide (Goncharenko 2006). Major producers are Canada (Saskatchewan), Belarus, Russia, China, Germany, Israel and Jordan. The latter extract potassium by solar evaporation from Dead Sea brines, precipitating carnallite (K-Mg chloride) with by-product bromine (cf. Chapter 2.4 "Magnesium"). Potassium is the fifth most important element in terrestrial biomass, after C, O, H and N. It is one of the three essential plant nutrients (N-P-K) and consequently, agriculture consumes over 95% of production. K^+ is the most abundant cation in the human body and an essential nutritional element for humans and animals. Potassium is also needed for the production of various industrial products (soap, glass, building materials, drilling fluids). The minimum grade for hard rock and deep solution mining of potassium salts is ~10% K_2O. Most potassium deposits are formed by chloride minerals (~90%, mainly sylvite) and KCl with ~60% K_2O is the most common form of K-fertilizers. Potassium sulphates contribute only 4% of world production; they are recommended for Cl-sensitive crops such as tomatoes, tobacco and potatoes. In 2008, primary world production of potassium salts amounted to 36 Mt (K_2O), but dropped to 25 Mt in the crisis year 2009 (USGS 2010). Resources are very large.

Agriculture and forestry have increasing demand for magnesium. This is partly satisfied by co-production of kieserite ($MgSO_4 \cdot H_2O$) that is common in certain potassium salt beds (e.g. Sigmundshall, near Hanover, Germany). Other possible by-products of processing potassium salts are occasionally rubidium and caesium (with 50–1700 ppm in K-salts), boron (e.g. boracite) and bromine (partly replacing Cl in chloride minerals, concentrations reach 5000 ppm). Processing of carnallite for potassium fertilizer production results in waste brines with elevated sodium chloride and Mg-chloride content. These brines can be used for the production of magnesium metal or of synthetic magnesite. Separation and concentration of specific salts is carried out by flotation, electrostatic separation, thermal dissolution-crystallization and heavy media separation. Waste brines of salt processing are regarded as an environmental hazard. In central Europe, geological disposal in deep saline aquifers is the preferred option.

Terrestrial salt deposits and brines also contain exploitable halite and potassium salts, but their striking feature is the chemical variability of precipitated compounds. Of course, this reflects the geochemically and environmentally diversified setting of salt lakes on land as opposed to the

Table 4.1 Important potassium salt minerals

		g/cm^3	% K_2O
Sylvite	KCl	1.99	63.1
Carnallite	$KCl \cdot MgCl_2 \cdot 6H_2O$	1.6	17.0
Kainite	$KCl \cdot MgSO_4 \cdot 3H_2O$	2.15	18.9
Langbeinite	$K_2SO_4 \cdot 2MgSO_4$	2.82	22.6
Polyhalite	$K_2SO_4 \cdot MgSO_4 \cdot 2CaSO_4 \cdot 2H_2O$	2.77	15.5

homogeneous chemistry of ocean water. Resulting economic resources include lithium, borate, iodine, bromine, sodium carbonate and sodium sulphate. Several of these substances are commonly classified as industrial minerals (cf. Chapter 3).

4.1 SALT MINERALS AND SALT ROCKS

4.1.1 Salt minerals

Tables 4.1 and 4.2 provide a selection of economically significant and characteristic minerals from the large number of salt minerals in nature. Halite and the potassium salts (sylvite more than carnallite) are eminently economic raw materials. Minerals of Table 4.2 include other salts of economic (kieserite, natron, mirabilite, trona) and genetic interest.

Table 4.2 Important salt minerals of magnesium, sodium, calcium and boron

		g/cm^3
Bischofite	$MgCl_2 \cdot 6H_2O$	1.59
Blödite	$Na_2SO_4 \cdot MgSO_4 \cdot 4H_2O$	2.23
Boracite	$MgCl_2 \cdot 5MgO \cdot 7B_2O_3$	2.90
Epsomite	$MgSO_4 \cdot 7H_2O$	1.67
Glauberite	$Na_2SO_4 \cdot CaSO_4$	2.8
Gaylussite	$CaNa_2(CO_3)_2 \cdot 5H_2O$	1.99
Halite (rock salt)	$NaCl$	2.16
Kieserite	$MgSO_4 \cdot H_2O$	2.57
Mirabilite	$Na_2SO_4 \cdot 10H_2O$	1.49
Natron	$Na_2CO_3 \cdot 10H_2O$	1.45
Tachhydrite	$2MgCl_2 \cdot CaCl_2 \cdot 12H_2O$	1.66
Thenardite	Na_2SO_4	2.66
Trona	$Na_3H(CO_3)_2 \cdot 2H_2O$	2.14

Table 4.3 The composition of potassium salt rocks (potassites)

Sylvinite	sylvite + halite
Hartsalz	sylvite + kieserite (± anhydrite, langbeinite) + halite
Carnallitite	carnallite + kieserite + halite
Kainitite	kainite + halite
Langbeinitite	langbeinite + halite

4.1.2 Salt rocks

Salt rocks consist of water-soluble salt minerals as defining major phases, minor (e.g. anhydrite) and accessory minerals (e.g. talc, magnesite, clay). The most common salt rock is almost monomineralic halitite, consisting of halite. Potassium salt rocks ("potassites") always contain more than one salt mineral, usually in thin separate layers and beds, resulting in the following common varieties (Table 4.3):

Often, carnallitite resembles a breccia or conglomerate composed of fragments of halite and sulphates, which float in a matrix of carnallite. This results from the mechanical contrast between the ductile carnallite and the brittle sulphates. Initially, strain induces boudinage and intensive folding (Figure 4.1). Kainitite is typically the product of supergene alteration affecting carnallitite seams. Kainite at Caltanisetta, Sicily, however, is considered to be a primary sediment. Potassites without a sulphate component (mainly sylvinite, the "chloride type") provide the majority of world potash production, whereas those with sulphates (e.g. langbeinitite: the "sulphate type") are more restricted.

Rock salt (halitite) frequently forms nearly monomineralic rock masses. Common banded halitite displays dark and lighter layers; in dark bands, anhydrite, polyhalite, organic matter and clay are enriched (Figure 4.2). Very pure (often recrystallized) salt rock is preferably extracted for nutritional use. In the Eastern Alps and in Poland, a chaotic breccia of halite, shale, dolomite and anhydrite (Figure 4.3) is called *Haselgebirge* (ancient German for "salt rock"). Many halitites are brightly colour-banded, which helps to

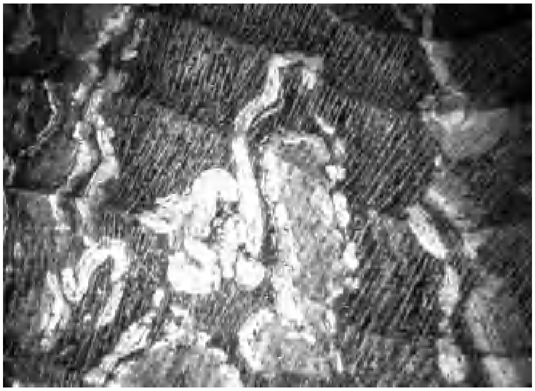

Figure 4.1 Potassium seam Stassfurt in the Asse mine, Northern Germany, made up of intensively folded beds of carnallite (dark reddish-brown, highly ductile), grey halitite and white kieserite (thin bands). The long and narrow Asse salt wall is the product of compressional intraplate deformation (inversion) during the Late Cretaceous. Near-parallel scratches and ridges are typical traces of excavation by a continuous mining machine.

investigate deformation within deposits. Some rocks such as carnallitite and minerals such as polyhalite are usually brilliantly red, but salt rock colours are not generally diagnostic. Colouring is due to tiny inclusions or to lattice defects (Sonnenfeld 1995). As in other rocks, a reduced state is expressed in grey and greenish colours, which are caused by clay, bitumen and iron sulphide phases. The much more common reddish colours of salt rocks are due to an oxidized state expressed by the presence of tiny haematite needles and platelets. Conspicuous blue halite is produced in the laboratory by irradiation that causes lattice defects and liberates minute particles of native sodium. In nature, the passage of diagenetic solutions may have leached bromine from halite, inducing the same effect.

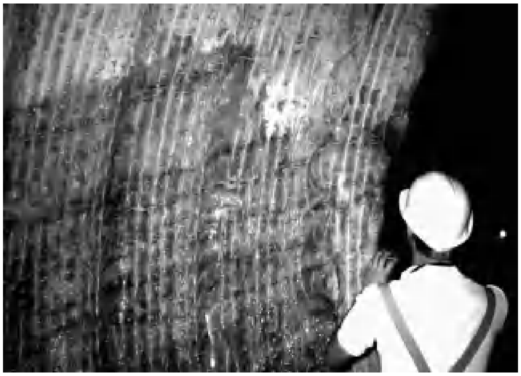

Figure 4.2 Anhydrite-banded Stassfurt halitite below carnallite seam in Asse mine, Northern Germany. Each couplet consists of ~1 cm thick light-grey anhydrite and ~10 cm halitite; bedding dips moderately to the left. Near-vertical structures are grooves left by a continuous miner.

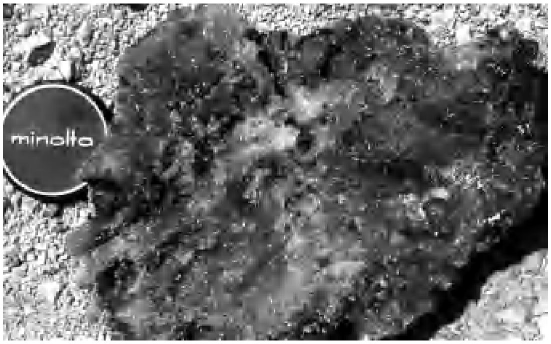

Figure 4.3 (Plate 4.3) Haselgebirge sample from Bad Aussee mine near Salzburg, Austria. This variety displays a red halite matrix with dispersed angular fragments of black claystone.

Most salt rocks contain a small proportion (<0.5%) of organic matter derived from algae, microbes and airborne remains of terrestrial higher plants (e.g. pollen, black carbon). Higher contents of kerogens and bitumen are restricted to clayey and anhydritic rocks associated with salt.

Salt rocks are investigated by petrographical (in thin and polished sections) and by chemical methods. Dubious potassium minerals in drill core and mine exposures can be made visible by spraying with a solution of Mg-dipicrylamine inducing a red colour. A portable scintillometer helps to identify the higher γ-ray activity of potassites.

Fluid inclusions

Salt rocks in little deformed platform sediments contain >1 wt.% H_2O, but deformed salt (e.g. in diapirs) has normally <0.1% water. In both cases, the water occurs in microscopic and submicroscopic fluid inclusions. Inclusions in diapiric salt are mainly located at grain boundaries. Little deformed salt is more likely to show intracrystalline inclusions along growth zones (Horita *et al.* 1996). Vreeland *et al.* (2000) found viable "spores" of bacteria in inclusions of this type within Permian salt crystals from Carlsbad, New Mexico. However, recrystallization of salt rock is so common that original brine inclusions are rare. Prevalent inclusions have been sealed in at various times during diagenesis and deformation of the salt rocks. Investigations of brine inclusions by measuring the temperature of homogenization (T_H, heating) and salinity (freezing) allow only limited interpretation. Informative data are rather expected from diagenetic minerals that are more stable than salt, for example sulphate and authigenic quartz (Attia *et al.* 1995). Formation temperature can be estimated from T_H after strong cooling (Roberts & Spencer 1995). The chemical composition of inclusions is measured by EDS Electron Microscopy (Energy Dispersive X-ray Spectroscopy) and ICPMS (Inductively Coupled Plasma Mass Spectrometry) at temperatures below −190°C (Garcia-Veigas *et al.* 1995, Zimmermann 2001).

Gas in salt

In some salt mines, explosive gas-driven salt outbursts are not rare. This happens when mining exposes salt that contains gas under high pressure, comparable to coal outbursts (Guan *et al.* 2009). In the Permian salt strata of the Werra district in central Germany, "crackly" salt (giving off a crackling noise when submerged in water) indicates hazardous areas. In this region, CO_2 and N_2 were introduced by sills, veins and pipes of Tertiary basalt volcanism. Salt in Wielicka, Poland, contains nearly pure CH_4. Nitrogen is common in salt of the Caspian basin and in Carlsbad, New Mexico. Deep German Zechstein salt occasionally includes thermochemical H_2S (Chapter 1.4, eq. 1.21). Trace amounts of gas occur in all salt rocks (Potter *et al.* 2004). Similar to salt rock colour, there is a clear disparity of salt with a prevalence of oxidized (O_2, CO_2) in contrast to reduced gas (alkanes, i.e. CH_4, H_2, H_2S).

Geochemical investigations enhance insights into many processes related to salt formation and assist practical applications.

Bromine

This halogen element is a very useful measure of the degree of evaporation (the concentration) of a seawater-derived brine and an important tracer of the origin of diagenetic fluids (Botrell *et al.* 1988; cf. Chapter 1.4). During halite precipitation, bromine is enriched in the liquid phase relative to chlorine, with increasing concentration of a brine (Herrmann 1980). The distribution coefficient for bromine between precipitated halite and the brine varies from ~0.12 to 0.3. Early halite contains little bromine (~50 ppm in contrast to ~500 in co-existing brine; seawater 67, continental crust 3–7 ppm Br), whereas halite of potassites contains over 10 times as much (up to 600 ppm; Figure 4.4). Epsomite-precipitating brine concentrates Br to ~2500 ppm. Consequently, bromine analysis of

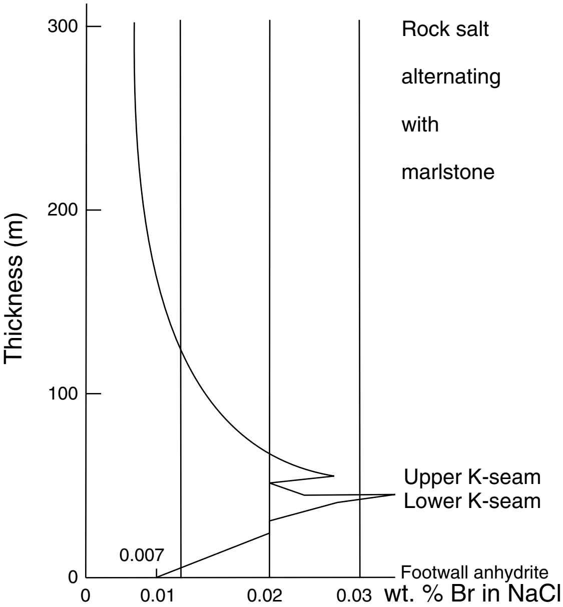

Figure 4.4 Bromine concentrations in halite of the Oligocene salt formation in the Upper Rhine Valley (Reproduced from Herrmann 1980 with permission from Elsevier)

halites is the best tool for potassium salt exploration. In thick packages of halite sediments, bromine profiles assist stratigraphical correlation and support derivation of mass balance models for salt basins concerning inflow, outflow and evaporation. However, disturbance of original bromine characteristics is possible by post-sedimentary processes, such as recrystallization, diagenetic brine migration and the influence of meteoric water (Siemann & Schramm 2002). Yet, a comparative study of little deformed bedded Zechstein 2 halitite and the same stratigraphical interval in diapiric salt of Northern Germany displayed the same trend of bromine concentrations rising towards potassium seams; in diapirs, only the variance of data is reduced (Küster *et al.* 2009). Most non-marine salts display low bromine contents.

Bromine (Br_2, liquid density 3.1028 g/cm^3, toxic) is an important by-product of brine exploitation and to a minor extent of seawater and rock salt processing. Annual world production is estimated at ~440,000 tonnes, mainly in USA, Israel, China and Jordan. Reserves and resources are very large, and considering the total mass of seawater, practically unlimited. Bromine and bromine compounds are foremost used as flame retardants in plastics of electronic and electrical equipment. Numerous other applications include drilling fluids, brominated pesticides, mercury capture at coal-fired power stations and water treatment.

Isotopic geochemistry of evaporites

Several isotope systems contribute to a deeper understanding of formation, diagenesis and metamorphism of evaporites. Similar to bromine, boron is enriched by evaporation and salt precipitation. Fractionation of $^{10}B/^{11}B$ allows the discrimination of marine and terrestrial evaporites, even after salts have been dissolved and only tourmaline remains (Perez Xavier *et al.* 2008). Sulphur isotope analyses of recent and fossil marine sulphates (mostly anhydrite) allow a reconstruction of seawater sulphur isotope characteristics in the geological past (Figure 3.4). The variations can be explained by two major factors driving the global sulphur cycle:

1 ^{34}S of the oceans reaches a minimum at times of profuse precipitation of marine sulphate rocks, because heavy sulphur is preferentially incorporated in sulphate (e.g. in the Late Permian); and

2 heavy sulphur is enriched in ocean water when light sulphur is extracted by formation of sulphides in marine bottom sediments (as in the Late Neoproterozoic and Early Palaeozoic).

Earlier than ~2100 Ma, the sulphur cycle's control was atmospheric and fundamentally different. Higher precision of past seawater $\delta^{34}S$ can be reached by analysing deep-water barite (Paytan *et al.* 2004). Chlorine isotopes are useful for analysis of geologically young salt, because of the occurrence of cosmogenic radioactive ^{36}Cl with a half-life of 301,000 years. Different stable Cl-isotope ratios $^{37}Cl/^{35}Cl$ characterize earth reservoirs (crust and seawater $\delta^{37}Cl \sim 0‰$; mantle slightly negative; standard is mean ocean chlorine SMOC), mark certain genetic processes and preserve this evidence through strong deformation (Eastoe & Peryt 1999), subduction and magmatism (Nahnybida *et al.* 2009, Banks *et al.* 2000). The method was employed to prove that deep brines in country rocks of the Palo Duro halite in Texas did not originate by meteoric dissolution but are original Permian residual brines (Eastoe *et al.* 1999). Strontium isotopes are used for investigating complex sedimentary and diagenetic processes (Schreiber & Tabakh 2000). Carbon isotopes of methane in potassium salt provide arguments for a perfect preservation of sedimentary and early diagenetic features (Potter *et al.* 2004).

Stable oxygen and hydrogen isotopes of water in fluid inclusions of salt rock provide clues to the sedimentary environment (e.g. terrestrial or marine) and eventual post-sedimentary fluid passage through salt rocks. This is a point that is especially important in connection with radioactive waste disposal in salt rocks. Compared to seawater, evaporation shifts water isotopes to higher concentrations of ^{18}O and ^{2}H (Figure 4.5). Red Sea water, for example, displays $\delta^{18}O + 2$ and $\delta D + 11‰$. Strong evaporation of brine in the halite precipitation phase causes a decline in heavy isotope content, because heavy water volatilizes more easily from concentrated salt solutions. This "salt effect" is caused by stronger

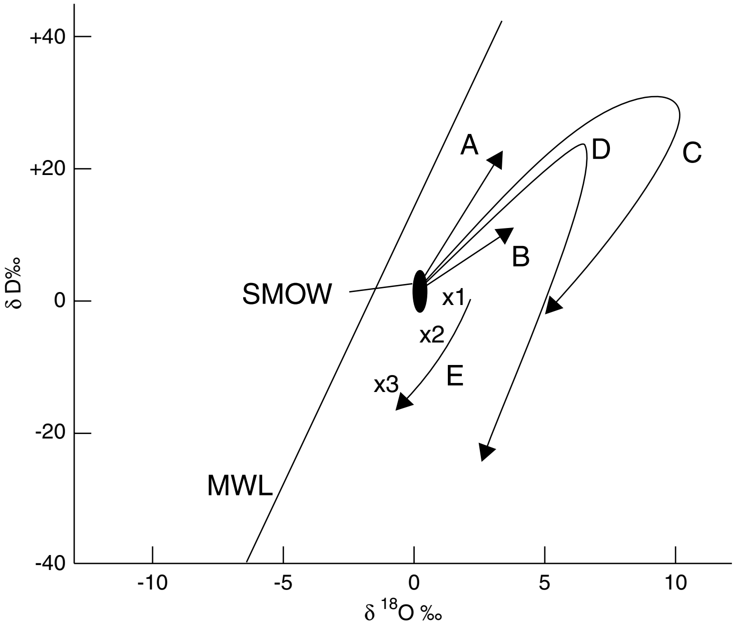

Figure 4.5 Stable hydrogen and oxygen isotope ratios in evaporating seawater and brine (modified from Kyser & Hiatt 2003 with permission from Elsevier). A demonstrates initial changes by evaporation in humid, B in arid climate. C and D illustrate experiments and natural systems evaporating until halite precipitation. Trajectory E is derived from salt pans on the Caribbean Bonaire Island; sample x_1 shows situation just before gypsum is precipitated, x_2 at the onset of halite formation and x_3 after the main halite stage with first K-Mg salt deposition. SMOW = Standard Mean Ocean Water, MWL = Meteoric Water Line.

attachment of light water molecules in hydration spheres of ions and in changes of the structure of water that are caused by dissolved salts. The strength of the salt effect depends on concentration and the prevailing salt ($CaCl_2 > MgCl_2 > MgSO_4 > KCl = NaCl > Na_2SO_4$; Horita *et al.* 1993). The result is the characteristic evaporation loop in the water isotope system (Figure 4.5). Note that primary isotope characteristics can be disturbed by the ingress of meteoric and formation waters, or by passage of dehydration water of gypsum interbedded with salt.

Isotope dating

The precise age of geologically young gypsum and many salts can be determined with the U-series disequilibrium method (Ku *et al.* 1998). The method is based on the inclusion of ^{238}U in authigenic minerals under exclusion of its decay chain (uranium series) nuclides. The earliest products of radioactive decay include ^{234}U and ^{230}Th. Their increase towards secular equilibrium with the parent nuclide is a function of time and is used for dating. However, the common recrystallization of evaporite minerals severely limits general application of the method.

The age determination of geologically ancient salt is normally based on palaeontological examination and radiometric age-dating of host rocks. Considering the mobility of salt, this may be questionable and wind-blown pollen or spores of surrounding vegetation enclosed in salt are used as controls. Radiometric age dating is done with systems such as K/Ar, K/Ca, Rb/Sr and U/He, but the resulting model ages may be sedimentary or diagenetic. Salt rocks rarely contain minerals that are reliable vessels for the intact preservation of mother and daughter nuclides.

Impermeability

The impermeability of salt rocks in respect to water, petroleum and natural gas is extremely important, because salt-related traps confine many giant hydrocarbon deposits (Warren 2006, cf. Chapter 7.3 "Petroleum and Natural Gas Deposits"). Radioactive waste disposal projects prompted much research on salt rock permeability. Data on halitite in the Asse mine

(Northern Germany) confirm extremely low intrinsic permeability [k]. *In situ* and distant from mine openings, k is below $1.10^{-21}\,m^2$, whereas destressed and dilated salt on side walls of tunnels displays a mean k of $1.10^{-16}\,m^2$ that equals 1.10^{-4} Darcy (Peach 1991). Note that during rapid upflow of a diapir, or under the influence of a volcanic field (e.g. Hesse, Germany), salt may be temporarily quite permeable, comparable to rocks undergoing penetrative shearing during metamorphism. In this environment, fluid migration is part of a dynamic chemical, energy and mechanical flow. Permeability is provided by processes such as dissolution, precipitation, grain boundary sliding and creep cavitation.

4.2 THE FORMATION OF SALT DEPOSITS

4.2.1 Salt formation today

Examples of present salt formation are salt lakes in California, Chile, Tibet and Utah, the Dead Sea, sabkhas on the coast of the Arabian-Persian Gulf and numerous salt lagoons on arid coasts throughout the world. However, there exist no large marine basins of salt formation as in the geological past. This is one reason why early research on salt formation started with coastal salt works (Figure/Plate 4.6; Usiglio 1849). Salt production, however, aims at monomineralic solids, and processes in salt works are not full replicas of natural salt formation, because back reaction between precipitates and brine is prevented. Yet, the back reactions are prime controls on the mineralogical composition of natural salt rocks.

The solubility of salt in water is expressed either as mass fraction (g/kg) or concentration (g/L). Note that resulting figures are different and should not be confused (Table 4.4).

The term "salinity" is used to describe the salt content of water. Here also, the units of Table 4.4 are used, and others such as per cent (%), per mil (‰, equal to grams per thousand) and ppm (parts per million, or grams per tonne). The density of seawater measures between 1020 and 1050 kg/m^3.

Water of the high seas has a mean salt content of 3.5 wt.% (35 g of salt in 1000 g of ocean water) with a range of 3.1–3.8%. Lower salinity is observed in polar seas (2.9%) and values of more than 3.5% are reached in confined seas at low latitudes (e.g. Red Sea). Independent of concentration, composition and proportion of dissolved salts display little variation: Important cations are Na^+, K^+, Mg^{2+}

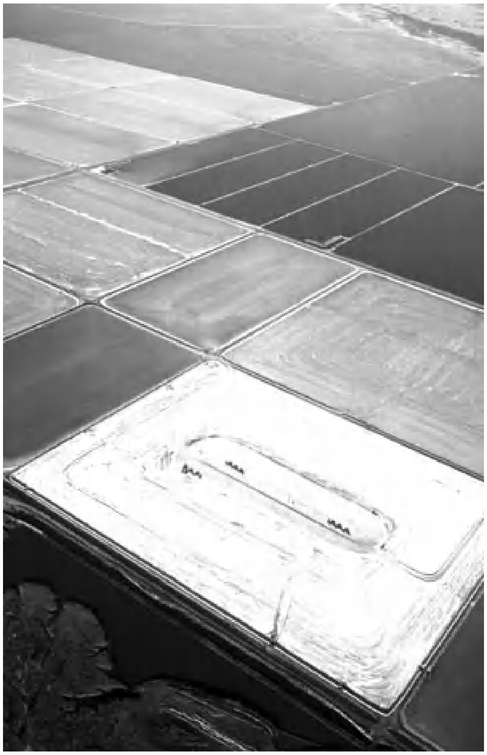

Figure 4.6 (Plate 4.6) Solar seawater evaporation pans for industrial salt production on the West Australian coast. Courtesy Dampier Salt Ltd and Rio Tinto Minerals. Seawater is first concentrated to specific gravity 1.21 in order to precipitate carbonate and gypsum. Different grades of salt are crystallized between brine gravity 1.21 and 1.275. Harvesting is visible in the foreground. The remaining K-Mg brine ("bittern") may be processed or pumped back into the sea.

Table 4.4 Solubility of NaCl in water at different temperature (cf. eq. 1.20)

T °C	0	10	20	100
g/L	356.85	358.70	360.54	388.89
g/kg	263	264	265	280

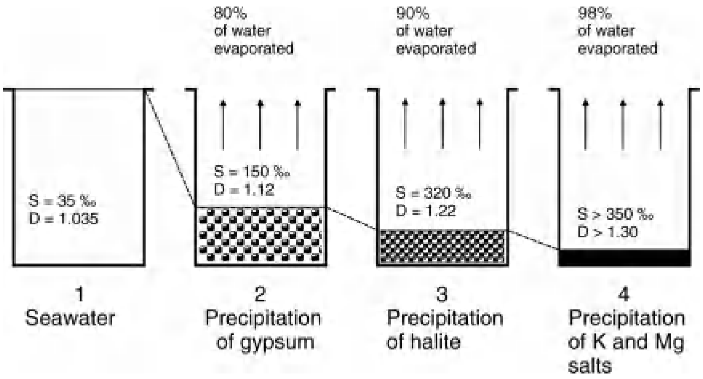

Figure 4.7 Simple demonstration of the major stages of evaporite formation by evaporation of seawater in a beaker (inspired by Rouchy & Blanc-Valleron 2006). S is the brine's salinity, D its density in g/cm^3. The brine in beaker no. 4 has a very bitter, unpleasant taste which is at the origin of the term "bittern salts".

and Ca^{2+}, anions include Cl^-, SO_4^{2-} and HCO_3^-. $CaSO_4$ and $MgSO_4$ may be present in non-ionized compounds. One litre of seawater with the density of 1035 kg/m^3 contains the following salts: 27.2 g NaCl, 3.35 g $MgCl_2$, 2.25 g $MgSO_4$, 0.74 g KCl, 0.12 g $CaCO_3$ and 1.27 g $CaSO_4$. Ten-fold concentration is needed for halite precipitation to start. Saturation of NaCl in water at 25°C is reached at a concentration of ~26.6% (Table 4.4). The total mass of salt dissolved in the oceans is gigantic. The volume of ocean water amounts to 1370.10^6 km^3 (Walker & Cohen 2007). Palaeozoic salt basins contain ~13% of NaCl in present seawater.

Undisturbed evaporation precipitates salts as a function of solubility. First to reach saturation are calcite or aragonite (often later dolomitized), followed by gypsum or anhydrite, halite and ending with highly soluble potassium-magnesium chlorides and sulphates (Figure 4.7). The high solubility of the latter, called "bittern salts", is the reason why they are rarely formed and once precipitated, are easily redissolved.

More than 150 years ago, the precipitation of salt minerals caused by increasing concentration of brines was experimentally investigated by the pioneers Usiglio, Van't Hoff and D'Ans. Braitsch (1971) summarized their results. Thermodynamic modelling by Eugster *et al.* (1980) and Harvie *et al.* (1984) confirmed most of the earlier deductions.

Details on bittern salt precipitation changed from earlier simple models. The precipitation sequence had been thought to be bloedite, epsomite, epsomite and kainite, and finally carnallite and kieserite. However, several variables were not considered in the laboratory, which cause variations in the precipitation path from seawater. One example is the formation of polyhalite (e.g. by replacing earlier anhydrite) that changes brine composition so that epsomite is followed by carnallite and kieserite (Figure 4.8; Eugster *et al.* 1980). Generally, back reactions between brine and solids are decisive (Figure 4.9), but may remain incomplete. The terminal paragenesis is principally bischofite, carnallite, kieserite, halite and anhydrite. Observations show that bloedite and kainite are rare as primary minerals in salt deposits. However, kainite can be formed when polyhalite cannot crystallize, because SO_4 is depleted, for example due to an excess of calcium as supposed for the Caltanisetta district, Sicily (Garcia-Veigas *et al.* 1995). SO_4 depletion may be forced by bacterial reduction.

Deviations from the normal precipitation sequence are also possible by depletion of magnesium caused by earlier dolomitization or by formation of Mg-rich clays. Carnallite precipitation is inhibited by algal blooms that enrich nitrogen hydrides (e.g. urea), which complex $MgCl_2$. This might explain primary sedimentation of sylvinite and of langbeinitic hartsalz that are the most frequently exploited "potassium ore", for example in Western Canada. Secondary, early to late diagenetic sylvite is typically the product of carnallite exposure to brines undersaturated with $MgCl_2$. Tachhydrite cannot be precipitated from modern seawater but only from brines rich in $CaCl_2$. It is striking that worldwide, Cretaceous potassium salts are associated with tachhydrite. The most probable solution for this conundrum is to admit

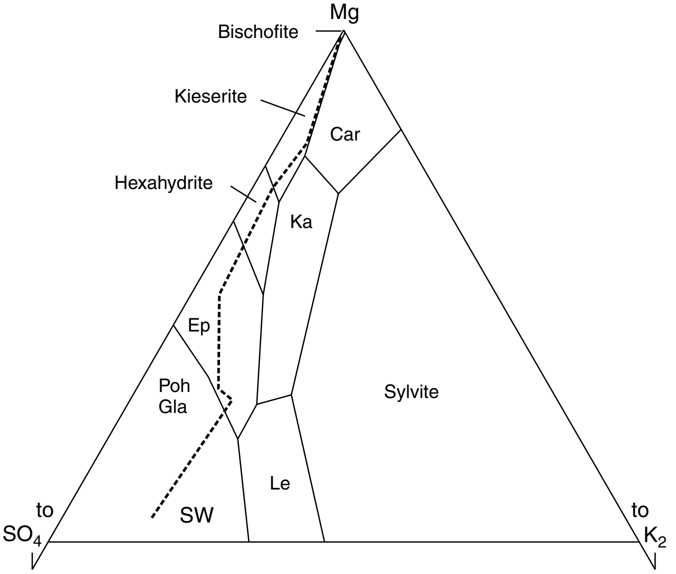
Mg
Bischofite
Kieserite
Car
Hexahydrite
Ka
Ep
Poh
Gla
Sylvite
Le
SW
to
SO4
to
K2

Figure 4.8 Jänecke diagram ($SO_4 + K_2 + Mg = 100$) of the standard precipitation sequence from evaporating present seawater, starting at the halite stage and ending with bischofite $MgCl_2$ (thick black line). Adapted from Eugster *et al.* (1980 with permission from Elsevier. Note that this path applies only to geological periods with $MgSO_4$-rich seawater. SW = Seawater, Poh = Polyhalite, Gla = Glauberite, Le = Leonite, Ka = Kainite, Car = Carnallite.

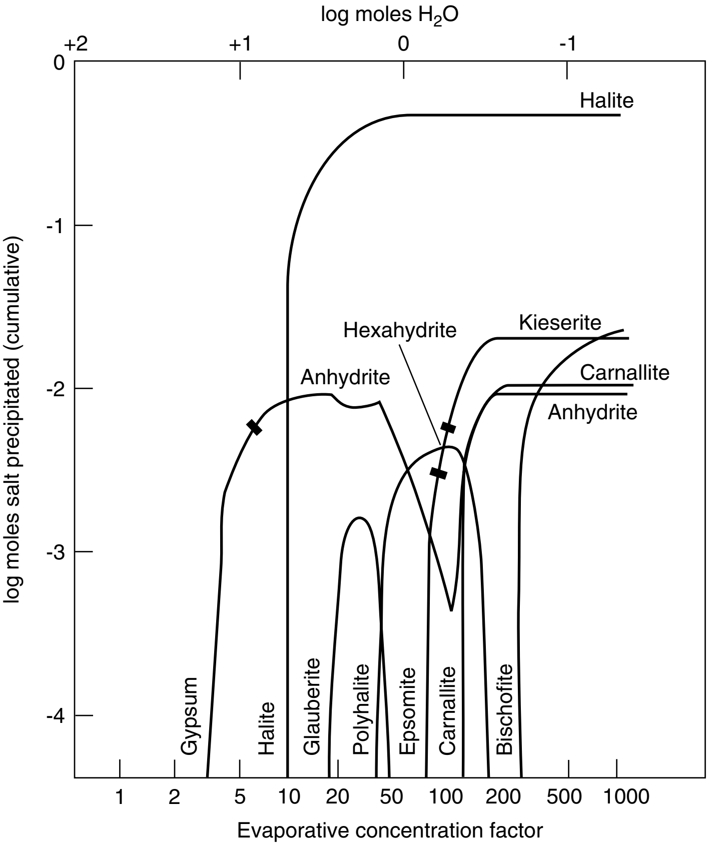

Figure 4.9 Cumulative formation and resorptive back reaction of important minerals during evaporation of present seawater (after Hardie 1991). Reproduced with permission of Annual Reviews, Inc.

that past seawater composition was not constant (see below).

Whatever the details, increasing seawater evaporation produces a suite of salt minerals and rocks that is termed the progressive salt precipitation sequence. In nature, however, the last members of the sequence will rarely be formed and very often, a more advanced paragenesis is overlain by salts produced by less concentrated brine. The regression is called a recessive sequence. Both combine to form an evaporative cycle. Most salt basins comprise a number of cycles. A complete progressive sequence can be subdivided into distinct stages or zones, which follow the facies rule by either forming a vertical (in time), or a lateral (two-dimensional) succession (Table 4.5).

Complete evaporation of a seawater column of 1000 m produces a salt layer of only 18 m thickness (Figure 4.10), with thickness ratios of Table 4.6. Clearly, it is impossible to explain the formation of hundreds of metres of monotonous halitite by simple static evaporation in closed basins. Likewise, the thickness relations between various salt rocks (e.g. halitite vs. potassites) in salt deposits deviate considerably from the theoretical ratios. Natural evaporites obviously formed in dynamic and partially open systems, with both inflow of fresh seawater and outflow of concentrated brines.

Terrestrial evaporites are even more variable than marine salt formations, because local conditions in the catchment region control available ions. Exploitable deposits of salt minerals such as soda, trona, mirabilite and thenardite are only known in terrestrial salt formations.

Table 4.5 Mineral associations forming six stages or zones of a progressive salt precipitation sequence

Top	6. Bischofite (bischofite, boracite, carnallite, halite, kieserite, anhydrite) or tachhydrite zone (sylvite, tachhydrite, halite)
	5. Carnallite zone (carnallite, halite, kieserite, anhydrite)
	4. Mg-sulphate zone (halite, polyhalite, kieserite, anhydrite, magnesite)
	3. Halite zone (halite, anhydrite, dolomite, magnesite)
	2. Gypsum zone (primary gypsum or anhydrite)
Footwall	1. Carbonates (limestone, dolomite)

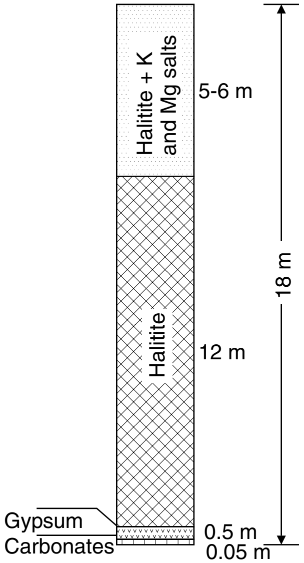

Figure 4.10 Evaporation of a seawater column of 1000 m in a closed system precipitates a salt layer of 18 m thickness, including 6 m of potassium-magnesium salts. Because halitite sequences often reach a thickness of hundreds of metres with very little K-Mg salts it is obvious that salt formations formed in open systems.

Climatic parameters

Salt formation is only possible when evaporation exceeds precipitation and inflow. Today, this is

Table 4.6 Thickness of salts deposited by complete evaporation of seawater in a closed system (normalized to 100 m halitite; Braitsch 1971)

Thickness (m)	Evaporite facies
38	Bischofite (halite, kieserite, carnallite)
3.6	Carnallitite (carnallite, halite, kieserite)
13.7	Mg-sulphates (kieserite, halite)
10.8	Polyhalite (halite, polyhalite)
100	Halitite (halite, anhydrite)
4.8	Gypsum (3 m if dehydrated to anhydrite)
0.37	Calcite

most common in the Earth's arid latitude belt between 15–35° with a mean at 23 ± 4° (Evans 2006). Air involved in tropospheric Hadley-Ferell circulation descends on these regions of both hemispheres and induces desert climate conditions. Near the equator, evaporites are rarely formed because high precipitation surpasses evaporation. Distance from the oceans ("continentality") and rain shadow effects may cause deserts at higher latitudes and independent of tropical atmospheric dynamics. Examples are deserts and recent salt deposits in China and Tibet. Cool, upwelling seawater contributes to desertification in coastal areas, for example in Namibia and Chile. Halite can be formed at relative air humidity $>65\%$ but K-Mg salt precipitation is restricted to humidity $<35\%$ (Schreiber & Tabakh 2000).

Exceptional loci of salt formation are lakes and mud flats in polar deserts of Antarctica, for example hypersaline lakes such as Don Juan Pond of the McMurdo Dry Valleys, which is probably the most saline lake on Earth, with 413 g of $CaCl_2$ and 29 g of NaCl per kg of water. Neoproterozoic equivalents were discovered in Svalbard, where glacial diamictites of the 635 Ma Marinoan Snowball Earth glaciation display carbonate and sulphate contents (Bao *et al.* 2009). Thousands of Holocene salt lakes are known in the moraine plains of Canada, and about 100 contain exploitable sodium sulphate beds (Warren 2006). In this climate, salt precipitation is "cryogenic", not solar evaporative, because sodium sulphate solubility decreases with falling temperature. Calcium sulphate solubility reaches a maximum at ~40°C and drops with both rising and falling temperature. Purely as a function of temperature (disregarding salinity), the stable mineral below the maximum is gypsum, above it anhydrite.

However, profuse marine salt formation is restricted to subtropical high-pressure zones. Cooler parts of the globe are rather sites of much smaller terrestrial salt pans or salt lakes. In this context, ancient salt deposits can generally be considered as indicators of specific palaeoclimatic and palaeogeographical settings (Evans 2006). Only in the Late Permian, evaporites formed throughout Pangaea, spanning equatorial regions and high latitudes (Torsvik & Cocks 2004).

The physical environment

Salt can be formed from terrestrial or sea water and from mixtures of both. Terrestrial salt formation is prominent in endorheic (that is hydrographically closed or nearly closed) continental basins and depressions with high evaporation. In deserts, efflorescence from soil is ubiquitous due to evaporative pore water rise to the surface. Crusts of salt, gypsum and calcrete form in this way or deeper in the soil profile. Dry or marshy salt mudflats develop in shallow depressions and on the shore of salt lakes. Examples of the first include the salt marshes of Kazakhstan between Wolga River and the Urals, the shotts (also spelled "chotts") of Northern Africa and the Great Kavir in Iran. The Great Kavir is the lowest swampy part of the giant salt desert of Central Iran, Dasht-e Kavir, which is ~800 km long and over 300 km wide.

Salt lakes (playa lakes, salinas)

These are typically ephemeral lakes in lowest parts of undrained desert basins. In the geological past, many present-day salt lakes were large freshwater lakes (e.g. Lake Bonneville, the pluvial predecessor of Great Salt Lake, Utah). This fact highlights the surprising conclusion that present global climate is of exceptional aridity. Worldwide, tectonic rifts and transform faults preferentially host salt lakes (e.g. Dead Sea). These lake basins are surrounded by mountains where most precipitation takes place. On entering the basin, downflowing streams build alluvial cones and fans of sediment fining away from the escarpment (Figure 4.11). Wide sandy and clayey plains (these are the namesake "playas" *sensu stricto*) slope down to the lake. Springs occur where groundwater is forced to the surface by encountering less permeable sediment. Along faults, geothermal springs are aligned with typical precipitates of travertine, SiO_2 and Si-Al oozes. Mudcracks, efflorescent crusts and early diagenetic (authigenic) salt crystals characterize dry supralittoral mudflats. Salt content increases towards the lake with the concentration of the pore-fluid brine until the sedimentary banding of

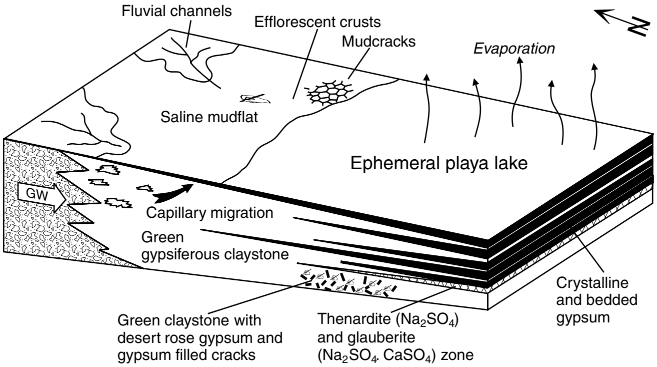
Fluvial channels
Efflorescent crusts
Mudcracks
Evaporation
N
Saline mudflat
Ephemeral playa lake
GW
Capillary migration
Green gypsiferous claystone
Crystalline and bedded gypsum
Green claystone with desert rose gypsum and gypsum filled cracks
Thenardite (Na_2SO_4) and glauberite (Na_2SO_4. $CaSO_4$) zone

Figure 4.11 Schematic block diagram showing environmental elements of sedimentation in Late Miocene playa lakes of the Beypazari Basin, Central Anatolia (Yagmurlu & Helvaci 1994). This basin contains important deposits of trona, gypsum, oil shale and lignite. GW – groundwater inflow from alluvial fans.

the clays is totally disturbed by displacive crystalline salt.

Apart from siliciclastic and volcanogenic sediments, subaqueous sediments of salt lakes include banded carbonates, black clay, gypsum, halitite, trona and other salts, depending on climate and the chemical composition of inflow. In the Dead Sea, for example, 15–20 varves are present in carbonate mud, which was deposited on the lake floor between 1900 and 1975. Humid years and extreme floods are thought to have caused the few prominent bands. In 1979, the meromictic (permanently stratified) Dead Sea overturned and entered a mode of alternating holomictic/meromictic states (Enzel *et al.* 2006). Since 1982, coarsely crystalline halite accumulates on the floor of the lake, for the first time since more than 300 years. Most playa lakes are very shallow with just a few metres of water, but the Dead Sea reaches a depth of ~400 m. In the fresh sediments, bacterial sulphate reduction produces H_2S or FeS_2-phases. Methanogenic microbes turn out CH_4 and the gas forms bubbles in the sediment that can be fossilized. Although the salinity of perennial saline lake waters varies considerably (in the Dead Sea up to ~300,000 mg TDS/L = total dissolved solids per litre), a lower boundary of 5000 mg/L is often used to define saline lakes. At this salinity most ordinary freshwater organisms cannot survive. However, many specialized (halophile and/or alkaliphile) organisms thrive at high salinity and alkalinity, including species of algae, bacteria and archaea. *Halobacterium*, for example, is an archaeon known to be extremely resistant to UV and gamma radiation. Microbes and halophilic algae floating in the sun-lit, aerobic, nutrient-rich brines are characterized by carotenoid and rodopsin pigments, which cause the deep red colour of salt lakes and salt pans (Figure/Plate 4.12a; Boetius & Joye 2009). These organisms contribute to the frequent occurrence of oil shale and petroleum source rocks in fossil playa lakes (Figure 4.12b), e.g. in the Eocene Green River Basin, USA. Alkalinity can reach extreme $\mathrm{pH} \sim 12$ as in the soda lakes of East Africa and South America.

Although most terrestrial salt lakes are alkaline, acidic saline lake waters do exist (e.g. Lake Tyrell in Victoria, Australia, where water is a dilute solution of H_2SO_4 with a pH of 2–4). This can be caused by sulphide oxidation and production of acidity in the watershed and a lack of acid-consuming rocks. Acidic lake waters are common in volcanic regions. An ancient example are fluid inclusion brines in Permian halite of the mid-western USA with a $\mathrm{pH} < 0$ (Counter Benison *et al.* 1998).

The provenance of ions concentrated in salt lakes is varied, but the larger part is provided by weathering of rocks making up the watershed. Surface and groundwater carry the dilute inflow into the basin (Figure 4.11). Provenance from surrounding rocks was verified for Neogene evaporites in the Atacama desert of Northern Chile (Pueyo *et al.* 2001). Another source may be dissolution of older evaporite beds, which can be recognized by inherited isotope characteristics of the younger sulphates. Import of matter by volcanic and geothermal processes is quite common (e.g. tungsten, fluorine, boron, lithium, or volcanic ash transformed into bentonite or zeolite).

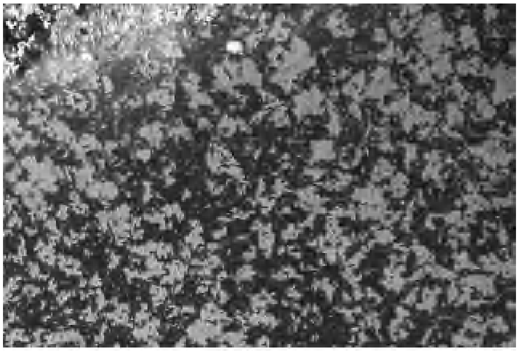

(a)

Figure 4.12 a (Plate 4.12a) Salt rafts floating on brine at the shore of Lake Katwe, western Uganda. Katwe is a large maar lake due to Pleistocene volcanism. It draws seepage water from close-by fresh Lake Edward. The dark red colour of the brine is caused by teeming micro-organisms. Upper left corner is organic-rich mud.

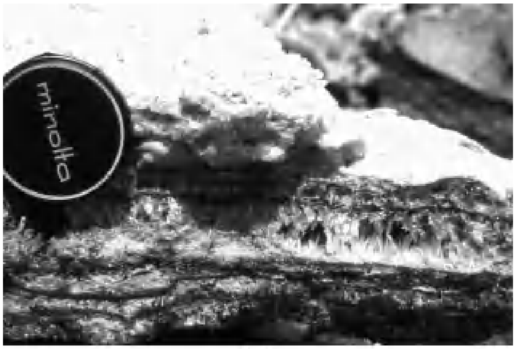

(b)

Figure 4.12b Salt harvested from the shallows of Lake Katwe. Note alternating layers of black organic mud and salt, and the bipolar growth of elongated clear halite crystals. Voids are, of course, brine-filled when *in situ*.

The evolution of brine chemistry and precipitates with increasing evaporative concentration is primarily a function of the $HCO_3/Ca + Mg$ ratio (Eugster & Hardie 1978), modified by other parameters and processes. Three major geochemical paths have been recognized:

1 Inflow with a high $HCO_3/Ca + Mg$ ratio produces alkaline Na-CO_3-Cl-(SO_4) brine (the soda lake type);

2 a low ratio causes gypsum precipitation and residual brines characterized by Ca-Na-Cl-(SO_4), final precipitates are halite, glauberite and mirabilite;

3 an intermediate ratio leads first to precipitation of alkaline earth carbonates (calcite, aragonite, Mg-calcite), followed by a rich diversity of brine evolution and evaporite deposition.

Precipitation of K-Mg chlorides and sulphates takes place in salt pans at the stage of near-dryness. On the shores of Dabusun salt lake in the Qaidam basin, China, potassium salt is forming today (Casas *et al.* 1992). Poikilitic carnallite crystals occur in halitite layers of a rhythmic halitite-clay succession. In clay bands, carnallite forms displacive crystals. Obviously, this carnallite precipitated from pore solutions within the sediments. Saturation is explained by evaporation on the surface causing high Mg-K concentration. The heavy brine seeps downwards, where lighter and less concentrated pore water is displaced. As the brine cools, carnallite is precipitated 0–13 m below the surface. Potassite seams in ancient salt sequences may have formed in a similar way.

Marine salt formation can be observed on the world's coasts, in two differing morphological settings – salt lagoons and sabkhas. The first are bays disconnected from the open sea, which receive fresh seawater only through a narrow channel or by seepage through a barrier (e.g. a sand spit; Figure 3.20). Sabkhas are saline flats hostile to most life forms, which occur along desert coasts throughout the world (e.g. the Arabian coast of the Persian Gulf).

Sabkha

A sabkha (Arabic for salt flat; also written sebkha) is a coastal saline surface dropping down to the highwater level beach. An essential part of the definition is the specific hydrological regime of salt formation within the sediment by capillary evaporation (Warren 2006). The sabkhas of Abu Dhabi were first intensely investigated. It was found that high evaporation causes an upward flow of increasingly concentrated water from a saline water table to the surface. Within the capillary fringe, gypsum or anhydrite, dolomite, magnesite and halite are precipitated. The derivation of water and dissolved ions was sought in the nearby sea, either by occasional flooding ("sea-water flooding model") or by lateral suction of seawater and groundwater ("evaporative pumping"). More recent quantitative hydrogeological investigations indicate that most dissolved matter is supplied by inland groundwater ("ascending brine model", Wood *et al*. 2002). Seawater seems to have only a minor role. Anyway, because of several reasons, foremost the minor salt accumulation, sabkhas cannot explain the formation of salt deposits.

Marine salt lagoons

Marine salt lagoons (saltern, salinas) are omnipresent features on arid and semi-arid coasts. They illustrate many phenomena that have been observed in the ancient salt giants, but are orders of magnitude smaller. Already Ochsenius (1877) used this approach in an attempt to explain the origin of the Late Permian salt formations in northern Europe, when he drew parallels with the Garabogazköl (Kara Bogaz Gol) on the eastern shore of the Caspian Sea in Turkmenistan:

> The Garabogazköl bay covers a surface of $\sim$18,000 km^2 and has a maximum depth of 15 m. Originally, a 100–500 m wide channel connected the bay with the Caspian Sea and evaporation lowered the water level in the bay, probably by $\sim$0.5 m. Annual water flow through the channel was 18–26 km^3. In 1878, total salt content of the Caspian Sea was 13‰ (about one-third of ocean water), but with a notably different composition. Salinity in Kara Bogaz Gol was 285‰ and precipitates included gypsum, mirabilite and some halite. At times, a 3–8 m thick bed of cryogenic sodium sulphate (cf. Chapter 3 "Sodium Carbonate") was exploited that may date from the ice ages. Ochsenius (1877) especially studied the role of the barrier between sea and bay. In later years, the Caspian Sea suffered from a drawdown caused by drought and human intervention and the bay fell dry, but recently the former lake level was restored by a climatic return to wet years. Considering the chemical difference between the parent water body and ocean water, and the preponderance of mirabilite in the precipitates, it is obvious that Garabogazköl is a poor example for marine salt deposition.
>
> Lake Assal in Djibouti may much better represent a salt basin fed by seawater and comparable ancient equivalents are known along passive continental margins (Jackson *et al*. 2000). Assal is a crater lake in the Afar Depression of northeastern Africa, close to the Gulf of Aden. In this region, the giant African rift system passes into an oceanic spreading ridge. The setting is similar to Salton Sea in Southern California. Lake Assal region is very arid and hot, with resulting high evaporation. Lake Assal is 155 m below sea level. Through a barrier of Pleistocene volcanic rocks, sea water seeps into the lake and convects through hot rock and rises in hot springs. Lake Assal water is a saturated brine with a salinity of 34.8%. A broad salt flat supporting several commercial salt diggings occurs along its northwestern shore. Starting up in 2010, a large-scale solar salt project is planned to produce 4 Mt/year of salt from sea water.

Geologically young marine salt lagoons have a history of oscillating water levels that deposit a succession of shallow-water and subaerial sediments. Evaporites with these characteristics represent a marine shallow water facies. This is in contrast to evaporitic sediments laid down in deeper water and in central parts of large salt basins that have no modern equivalent.

Shallow water evaporites

Characteristic sediments of shallow water evaporites are laminated sulphates interbedded with algal mats, clastic gypsum sands with graded bedding, broken crusts (tempestites) and gypsum dune sands (Figure 3.20). *In-situ* grown poikilitic and replacive crystals, and nodular sulphates form in the soft sediment from pore brine. In places, profuse growth of white sulphate nodules leaves only stringers of dark matrix. Resulting textures are called "mosaic", or "chicken wire texture". Similar soft-sediment processes lead to enterolithic textures of thin sulphate or more rarely magnesite bands, presenting the appearance of intestinal convolutions. Selenitic, that is clear colourless gypsum crystals with typical swallow-tail twins grow to a length of several metres. They form palisades and rosettes near the surface, pushing up small hillocks. Repetitive cycling between subaqueous and subaerial conditions is caused by changes of water level (e.g. storm-driven flooding) and climatically controlled rhythmic salinity variations (Peryt 1996). In the characteristic shallow water evaporite successions, structure and texture of gypsum and anhydrite deposits are the key to understanding the sedimentary environment.

In a salt lagoon, halite can crystallize at the brine surface or on the bottom. At the surface, halite first nucleates in the form of tiny hopper crystals. These are very distinct inverted pyramidal skeletal crystals that grow mainly along the water surface (in two dimensions). Hopper crystals assemble to plates (Figure/Plate 4.12a) and when their weight is too large for floating, founder and end up as detrital halitite on the lagoon bottom. Halite precipitating in shallow water (<2 m) on the bottom grows in the shape of elongate vertical crystals that appear like palisades in a cross-section ("chevron texture"). Under the microscope, both halite types display growth zones by linear and planar arrangement of brine inclusions. Displacive halite crystals in clay grow both in subaqueous and subaerial conditions. Clastic halite sand may be formed by brine flow. Halite pisoids originate on beaches by wave action. Halite ooids indicate involvement of bacteria (Castanier *et al.* 1999). The porous mushy halite sediment is rapidly lithified by clear halite cement. Only centimetres to decimetres below the surface, halitite is commonly a hard rock.

In ~1970, salt reefs started to grow in large solar evaporation ponds that had been built in the southern Dead Sea. The aim of these basins was to precipitate halite and to use the residual brine for production of potassium, magnesium and trace elements such as bromine. These salt reefs are mushroom shaped, round or elongate build-ups with a height measured in metres. They coalesce and tend to partition the ponds into thousands of small compartments that enclose stagnant brine. Instead of being extracted according to planning, carnallite precipitates uselessly in the small basins enclosed by reefs. The epidemic afflicted several hundred km^2 of salt works both in Israel and Jordan (Talbot *et al.* 1996). Salt reefs have not been reported from ancient salt deposits. Most probably, cross-sections of such structures have been observed in salt mines but their significance may have been missed.

4.2.2 Salt formation in the geological past

Similar to the deposition of large masses of coal, large salt deposits cluster in distinct geological periods and regions. Traces of halite are very common in the geological record. Large salt formations, however, with a thickness of hundreds of metres and an areal extent of thousands of km^2, and with valuable potassium salt seams are quite restricted. Major controls for their formation are climate and a favourable tectonic configuration of sedimentary basins. Before discussing this in more detail, let us briefly look at the chemistry of seawater through geological time.

Seawater in the geological past

Ample evidence demonstrates that salinity, chemical characteristics and the composition of dissolved matter in seawater varied considerably during geological history (Coggon *et al.* 2010, Anbar 2008, Horita *et al.* 2002, Knauth 1998). Therefore, many observations deduced from modern seawater may not be applicable to the geological past. The average water temperature probably declined from ~70°C in the Archaean to ~20°C 800 million years ago (Robert & Chaussidon 2006). Sulphate was rare in Precambrian seawater until the Mesoproterozoic, when it started to rise and reached ~75% of today's concentration with the onset of the Cambrian (Kah *et al.* 2004). Since the Cretaceous, seawater is highly undersaturated with respect to silica, because of the emergence of silica-consuming diatoms (Grenne and Slack 2005). The isotopic composition of the oceans is a function of the size of polar ice sheets. Changing CO_2 content in the atmosphere shifts seawater pH. The pre-industrial state is estimated at pH~ 8.17 and since, rising CO_2 lowered pH by ~0.1 units ("acidification"). Considering that CO_2 contents in the geological past were nearly always much higher than today (Normile 2009), significantly less alkaline seawater was certainly the norm. $\delta^{11}B$ in marine carbonates is a proxy of ancient ocean pH which varied between ~7 and 8.5 (Kasemann *et al.* 2010). Ocean water probably was virtually free of oxygen and iron-rich

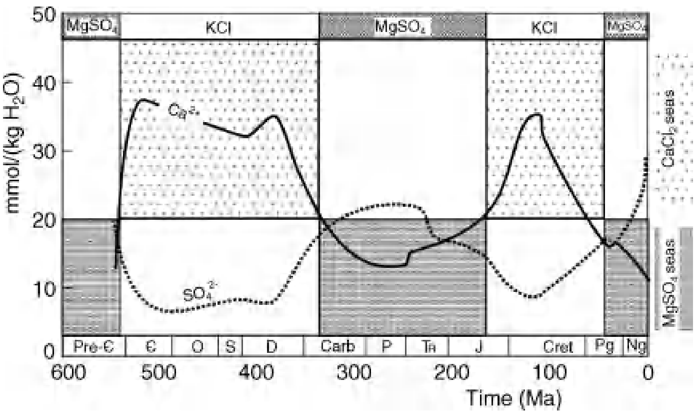

Figure 4.13 Secular variation of Ca^{2+} and SO_4^{2-} concentration in seawater during the Phanerozoic (after Lowenstein *et al.* 2001, 2003). These changes controlled deposition of marine sulphate, and chloride or sulphate type potassium salts.

in the first half of Earth history. The oxidation state of atmosphere and ocean in the Precambrian controlled the seawater SO_4^{2-} concentration (Fike *et al.* 2006) and the bioavailability of essential trace elements (Anbar 2008). Between 1.8 and 0.8 Ga, H_2S sulphur probably prevailed in ocean water and only after complete ocean oxygenation at ~700 Ma, dissolved SO_4^{2-} sulphur became the norm (Anbar 2008). In the Permian, oxygen concentration in the atmosphere reached 35% compared with today's 21%. This induced unusually high oxygen concentration in the oceans. At other times, anoxia was prevalent (e.g. Mid-Devonian, Early Jurassic) and biota abstracted sulphur, which was fixed in reduced sediments. Low sulphate concentration in seawater can also be caused by mass precipitation of gypsum (Wortmann & Chernyavsky 2007). Apart from abstraction in evaporites, changes of major cation concentrations in seawater can be induced by:

- varying input of river water and sediment (continental weathering);
- fluctuating rates of spreading and hydrothermal convection at mid-ocean ridges (stripping Mg from seawater, Coggon *et al.* 2010, Conrad & Lithgow-Bertelloni 2007); and
- changing rates of seawater alteration by reactions on ridge flanks and across the ocean floor in general (Demicco *et al.* 2005).

Conspicuous are the secular variations of the Mg/Ca ratio and of the Na^+ and SO_4^{2-} concentrations, which have caused systematic variation of potassium salt rock composition (e.g. the chloride/sulphate facies: Hardie 1996, Horita *et al.* 2002). During the Late Precambrian, in the Permo-Triassic and from the Tertiary until today, considerable $MgSO_4$ (kieserite) contents in potassium salts are evidence for high Mg/Ca ratios (>2.5) and for elevated Na concentrations. The reverse is observed from the Cambrian to the Devonian and in the Cretaceous, with deposition of chloridic, sylvite-rich K-Mg-Ca salt rocks (Figure 4.13).

Periods of evaporite formation

In the Archaean, only traces of evaporites are known; some of the Isua rocks of Greenland display evaporitic features. Cherts with an age of 3.3–3.5 Ga in the Pilbara Nucleus of Western Australia contain pseudomorphs after halite crystals. In the Proterozoic, the former presence of salt rocks is suggested by relatively frequent proxies, such as anhydrite, albite and scapolite (Evans 2006). The oldest known halitites occur in Neoproterozoic sediments of Australia, Pakistan (Salt Ranges), Iran and Oman (Hormuz Salt). Together with earliest Phanerozoic evaporites, these giant salt accumulations mark the termination of the 1.5 to 2 times higher salinity of Precambrian compared to later ocean water (Knauth 1998).

Beginning with the Cambrian, salt formation and its preservation was much more common than before (Evans 2006, Warren 1999, 2006). During the Cambrian, the first and one of the largest of the Earth's salt giants (exceptionally large evaporite basins) was formed in Siberia. Other important Cambrian salt formations occur in Pakistan and in the Persian Arabian Gulf region. Silurian salt is known in the Baltic States, USA and Australia. Devonian salt formations in western Canada (the Prairie Evaporite) are the base for the country's role as the world's largest potassium producer. Thick Devonian salt is present in the Dniepr-Donets Basin of Belarus and Ukraine. On the supercontinent Gondwana, Permian salt was formed in several areas, including the mid-western USA (Carlsbad, New Mexico), the forelands of the Ural Mountains, in the north European Zechstein basin (England, Northern Germany, Poland) and in the Eastern Alps (Ziegler *et al.* 1997). Triassic salt is exploited in southwestern Germany, in the North African Maghreb province, Britain and Spain. Jurassic salt of the Smackover and Louann salt formations seals many of the extremely rich oilfields of the Gulf of Mexico province. With 2.4 million km^3, this is the largest of all saline giants on Earth (Evans 2006). Cretaceous salt formations in the Khorat Plateau, Thailand, host potassium salt seams of significant economic potential (El Tabakh *et al.* 1999). Cretaceous salt also occurs in the Amazon province and in Egypt. Of Palaeogene age are potassium deposits in the Spanish Ebro basin and in the Upper Rhine Graben. Neogene salt is exploited in the northern foreland of the Carpathian Mountains and has an important role by sealing hydrocarbon reservoirs in the Red Sea, the northern Arabian Gulf (the Fars evaporites above the Asmari limestone reservoir) and southern Iran (Gachsaran evaporites). With an age of ~5.9–5.3 Ma, the Messinian evaporites in the Mediterranean region are the youngest of the marine saline giants (Ryan 2009).

Environments of evaporite formation in the geological past

In geodynamic terms, large masses of evaporites are likely to occur in four main settings:

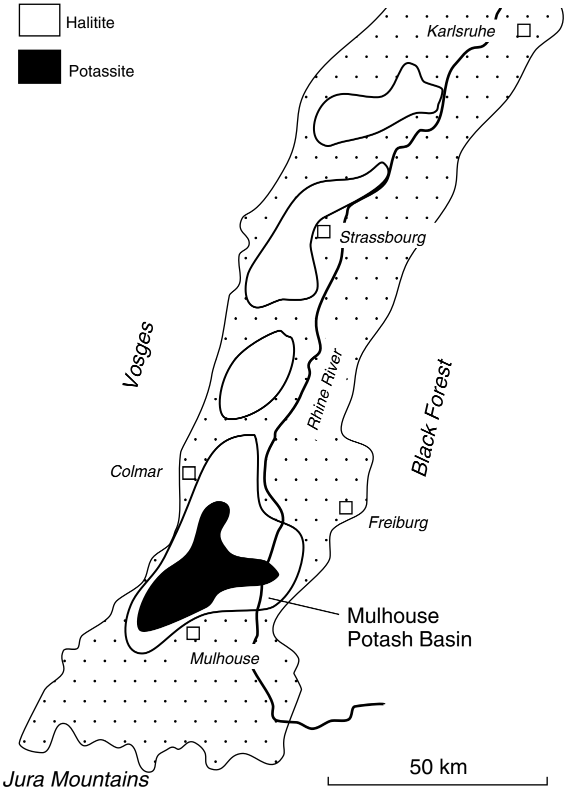

Figure 4.14 Early Tertiary (Middle Eocene-Early Oligocene) syn-rift evaporites in the southern Upper Rhine Graben contain potassium salts of the chloride type. Dotted areas include a gypsum-zone surrounding the salt, and marginal non-evaporitic rift sediments of alluvial fans and plains, and lacustrine limestone (modified from Warren 1999).

1 in continental rifts (e.g. Upper Rhine Graben: Blanc-Valleron 1997; Figure 4.14);
2 in rifts that precede the opening of a new ocean and in transitional early stages of the newly born sea (Red Sea, passive continental margins);
3 in late-orogenic foreland basins of mountain belts (e.g. the Carpathian foredeep);
4 in wide epicontinental basins (e.g. Zechstein within Pangaea).

A somewhat unique case is the intracollisional setting of Mediterranean oceanic basins hosting the Neogene Messinian evaporites:

> When the Straits of Gibraltar closed in the Late Miocene (5.96–5.33 Ma: Krijgsman *et al.* 1999) by collisional movement of Africa and Eurasia, the Mediterranean Sea was isolated from world oceans and quickly dried out (the "Messinian salinity crisis": Hsü 1972). Marginal shallow salt basins such as in Sicily and Spain formed first, followed by halitite on the sea floor at >3 km below the Atlantic Ocean surface (Clauzon *et al.* 1996). Salt precipitation started under deep basin/deep water conditions (see below) and ended with a deep basin/shallow water stage and the desiccation of the Mediterranean to residual salt pans on the former sea bottom (Ryan 2009). Messinian basinal evaporites reach a thickness of ~2000 m and extend over wide areas beneath the Mediterranean Sea. With a volume of 1 million km^3 (Evans 2006), the Messinian is the fourth-largest of the presently known "saline giants" (Figure 4.15b).

Deep water evaporites

Many fossil evaporites display a sedimentological character that points to deposition in deep water, in contrast to the shallow setting of virtually all present evaporite formation. Striking evidence for a deep-water facies includes turbidites (Rimoldi *et al.* 1996), mass flows (East Alpine "Haselgebirge", see below), and the bedding and lamination of salt rocks that is constant for hundreds of kilometres (German Zechstein, see below). Laminites of the shallow-water facies are laterally confined; wedging out of single bands occurs after a few metres and usually can be ascertained within one exposure.

Laminites of deep-water halitite are typically banded by thin dark bands in a lighter mass of salt. Usually, the dark laminae consist of sulphates with accessory clay, carbonate and organic substance. Certain stratigraphical levels may be characterized by cm-scale, often folded or boudinaged anhydrite bands (Figure 4.2). In certain periods during formation of the Zechstein salt, the system oscillated 100 to 1000 times between halitite and anhydrite deposition. Certain layers of this anhydrite can be nodular or acicular, indicating replacement of primary gypsum. With 1–10 mm, dark bands in halitite are commonly thinner than light pure salt bands with a typical thickness of 10 cm. These rhythmic sulphate bands are laterally very persistent and obviously represent planar bedding planes.

Halite of the deep-water facies crystallized either on the brine surface, where evaporation is strongest, or in the case of stratified salt concentrations at depth where supersaturated brine flowing down from basin margins precipitated halite during cooling. Mass-flow of salt mush from basin margins is a further

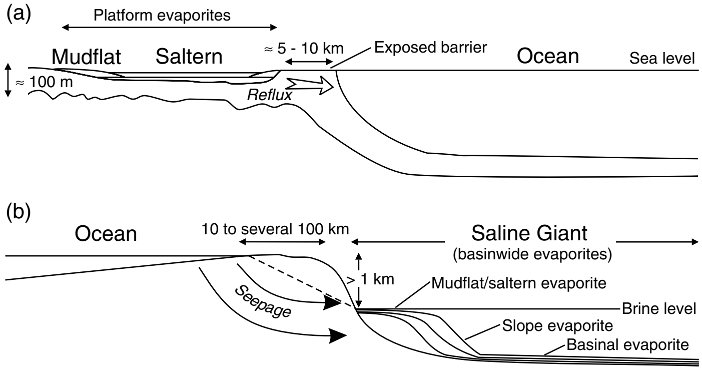

Figure 4.15 Coastal salt lagoons, or saltern (a) are common in hot and dry regions of the world, but no present-day example exists for the immensely large salt-filled basins (b, saline giants) of the geological past (after Warren 1999).

possibility. Regularly laminated halite, however, is rather due to a steady rate of salt formation, not to singular events. Either chevron crusts forming on the floor or a rain of hopper crystals and halite plates are the most probable salt depositing processes. The lamination of deep-water salt rocks resembles glacial lake varves. In melt water lakes, one varve (a couplet) consists of a light and coarse summer layer and a thin, dark winter layer. Consequently, one glacial couplet represents one year. The "halovarves" of salt rocks were equally assumed to reflect an annual rhythm, hence the German salt miners' term "Jahresringe" (annual growth rings) that is also used in English papers. Confirming this hypothesis, Messinian gypsum-dominated couplets were most likely deposited annually and even reveal a strong influence of El Niño Southern Oscillation (Galeotti *et al.* 2010). The causal relation would be dry and wet seasons, with dark bands forming during more humid periods. Generally, the 11-year solar cycle (sunspot cycle) and even longer climate cycles caused by orbital oscillations are equally possible causes.

Palaeogeography

The spatial distribution of evaporite zones, or facies (Table 4.5) is a function of morphology and hydrology of a salt basin. Often, a vector of increasing concentration can be observed, for example from a leaky barrier to more distal parts of the basin. In other cases, the bottom reflux of hot brine from margins causes salt precipitation of high evaporative facies in deeper, central parts of the basin. In the case of desiccating basins without an influx from the sea, evaporite zones are arranged in rings with increasing concentration from margin to centre. Apart from the scientific quest for understanding, mapping and analysing the spatial and temporal distribution of evaporite facies is of great practical value. Exploration and extraction of evaporite resources, such as potassium salt, are substantially facilitated.

Basin models and isolation models

Two hypotheses can explain the great thickness of fossil salt formations: i) synsedimentary tectonic subsidence similar to orogenic siliciclastic flysch and foreland basins; and ii) previously formed, deep depressions, which are gradually filled with sediments. It has been argued against the first that the high sedimentation rate of halite reaching 14 cm/year in present salt lagoons surpasses measured tectonic subsidence rates by several orders of magnitude. Furthermore, the predominant deep-water facies of ancient evaporites can only be explained by formation in deep basins. But, of course, even deep basins may be sites of tectonic subsidence. We now know that the specific combination of tectonic and non-tectonic contributions to evaporite sedimentation varies between individual basins. Shallow basins display salt formations of lesser thickness. Three principle basin models cover most natural variations of evaporite deposition (Sonnenfeld 1991; Figure 4.16), but complex and mixed systems are the common case:

- deep basins with deep-water facies evaporites (e.g. part of Zechstein, see below);
- deep basins with shallow-water facies evaporites (basinal Messinian salt in the Mediterranean);
- shallow basins with shallow-water facies evaporites (Danakil Rift: Hardie 1990; marginal Messinian salt in the Mediterranean).

At first sight, the predominance of certain salt rocks such as halitite or sulphates over hundreds of metres of evaporite sedimentation is a paradox. Table 4.6 and Figure 4.10 provide thickness relations that theoretically result from closed-system evaporation of seawater. This is, however, hardly ever observed in nature. The rule is the formation of one facies (e.g. halitite in the Zechstein) as a background, which is punctuated by intercalations of higher and lower concentration. This implies preservation of a narrow concentration range for a long period, which may require backflow (reflux) of brines with salts of higher solubility to balance inflow as already realized by Ochsenius (1877). Reflux may occur below the inflowing seawater (near-surface reflux) or through permeable rocks of the barrier (seepage reflux, Figure 4.15a). If reflux is not possible, for example in desiccating deep basins (Figure 4.15b), a constant concentration grade can only be preserved by a delicate equilibrium between seawater inflow, evaporation and the mass of water and

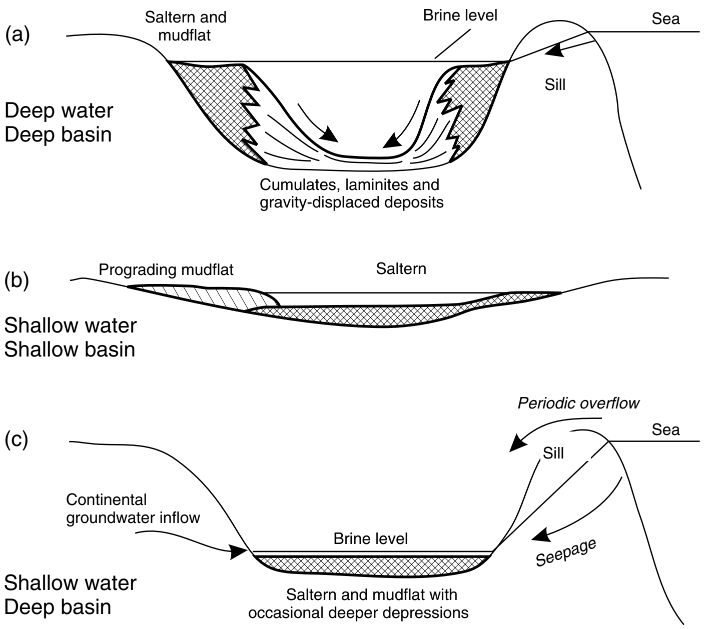
(a)
Saltern and mudflat
Brine level
Sea
Sill
Deep water
Deep basin
Cumulates, laminites and gravity-displaced deposits
(b)
Prograding mudflat
Saltern
Shallow water
Shallow basin
(c)
Periodic overflow
Sea
Sill
Continental groundwater inflow
Brine level
Seepage
Shallow water
Deep basin
Saltern and mudflat with occasional deeper depressions

Figure 4.16 Schematic basin models of deep and shallow evaporite basins, including possible combinations with deep-water and shallow-water sedimentation (modified from Warren 1999).

salts in the basin. Mathematical modelling of the mass balance in natural settings is most instructive (Eugster 1984).

The Zechstein (Late Permian) salt formation in Northern Europe

The major salt formation of Europe is the Zechstein (originally a German miners' term, translating as *pit rock*). In Germany, England, The Netherlands and in Poland, former and presently active mines provide access to ancient deepwater evaporites, although potassium salt seams represent desiccation phases.

In wide parts of Europe, the Variscan orogeny ended with deposition and folding of giant coal measures in the Late Carboniferous. Extension and gravitational collapse of the orogen in the Permian and thermal contraction of the lithosphere induced formation of the wide north-central European Permian rift basin. This was an arid land below sea level, which accumulated continental red sandstones, shales and conglomerates, felsic volcanic rocks, minor coal and playa-lake evaporites of the Rotliegend sequence. The arid setting is a stark contrast to the organic-rich sediments of the tropical Late Carboniferous coal measures. Burial of peat depressed atmospheric CO_2 to very low concentrations, amplifying continental glaciation within Gondwana, which lasted from 326 (late Early Carboniferous) to 267 Ma (Mid-Permian, Horton & Poulsen 2009). Waxing and waning of the extensive ice sheets controlled climate and sea levels. The end of Gondwanan glaciation caused a rapid climate change from humid-equatorial to desert conditions in wide parts of Pangaea. The global Late Permian climate was hot and dry. Boreal forests and coal swamps only formed at highest latitudes and reptiles lived within 15° of the South Pole (Torsvik & Cocks 2004, Ziegler *et al.* 1997). Final ice melting led to sustained sea level rise and the Zechstein basin was flooded. The first sediment deposited was a black shale bed (the European Copper Shale). Because the connection to world oceans was restricted and arid conditions unbroken, the basin developed into a large evaporite pan receiving the Zechstein sequence.

Exploitable Permian salt is restricted to the Zechstein. At this time, ocean water flowed through a restricted channel between Norway and

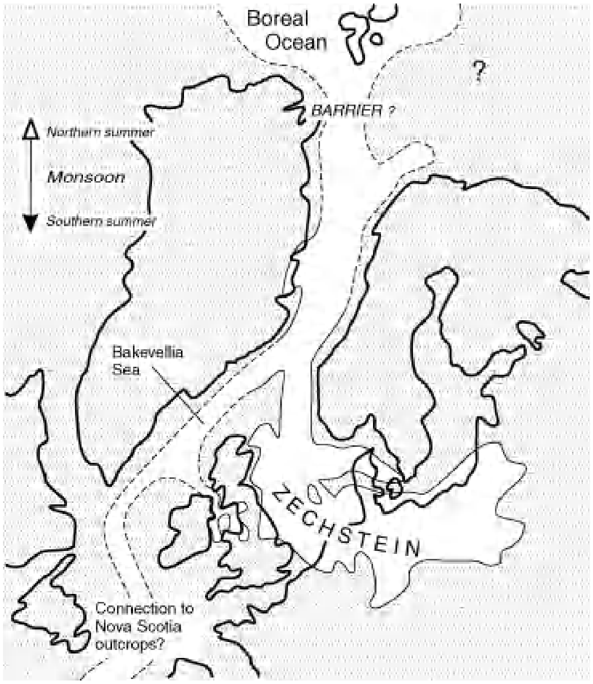

Figure 4.17 Palaeogeographic sketch of the Zechstein Basin in Pangaea before the Atlantic Ocean began to open (adapted from Ziegler 1982 and Warren 1999). The basin was at about 20° northern latitude (Torsvik & Cocks 2004). Inside this giant landmass, the climate was extremely dry and displayed a seasonal change of monsoonal wind direction.

Greenland (a graben?) from today's Arctic into the centre of northern Pangaea (Figure 4.17). Nearly everywhere in the basin, four cycles of evaporite sedimentation (Z1–4) can easily be distinguished. Two rather stunted ones (Z5–6) have been added in recent years by deep drilling for oil and gas. Each of the cycles starts with clastic sediment (commonly clay indicating high water levels), which is followed by carbonate, sulphate, halitite and Mg-K salts (reflecting progressive desiccation). Above the potassium seams, a thin recessive package of halitite and anhydrite forms the hanging wall, before a new cycle starts with a clay bed. Most of the formation names date from pioneer times of potassium salt mining in Germany during the second half of the 19th century, after Liebig (1842) had discovered the principle of inorganic plant fertilizers, and K-salts became a lucrative commodity. In terms of sequence stratigraphy (Miall 1997), a new stratigraphical classification of the Zechstein suites comprises ZS 1–8 (Strohmenger *et al.* 1996), somewhat different from the traditional cycles as represented in Table 4.7. With a total volume of only 200,000 km^3 (Evans 2006) the Zechstein evaporites are not among the saline giants.

Near the margins of the basin and around islands emerging from the saline inland sea (e.g. Harz Mountains), shallow-water carbonate and sulphate "reefs" or "walls" were building up. Bryozoa formed the Werra Carbonate (Ca1), whereas Ca2 and Ca3 were built by algae. In deeper parts of the basin, the carbonates pass gradually into dark, banded and thinner limestones or dolomites (Figure 4.18). In certain deeps, thin bituminous "smelly shales" represent the time horizon of marginal carbonates. These rocks are a source of exploitable hydrocarbons. Marginal sulphates display shallow-water facies characteristics. From the coastal sulphate walls, mass flows and turbidites descended into the deeper basin. Water depth, however, was not constantly deep but oscillated between deep and shallow. A moderate drawdown can be assumed for the halite-sulphate laminates. Nearly dry conditions are indicated for the formation of potassium salts, mainly by sedimentary features of the seams. Potassium seams consist of carnallite or sylvite layers, with bands and

Table 4.7 Simplified lithostratigraphic scheme of Zechstein evaporites (thickness mentioned relates to type area of rock units)

Lower Triassic	
Late Permian	
Zechstein 6 (Friesland Series, 3–4.5 m)	Friesland Clay, Halitite, Anhydrite
time mark 252 Ma	
Zechstein 5 (Ohre Series, 7.5–11 m)	Upper Border Anhydrite Upper Siltstone Border Anhydrite Ohre Halitite Banded Anhydrite Salt-fragment Clay
Zechstein 4 (Aller Series, 34–130 m)	Upper Aller Clay Border Anhydrite Aller Halitite Aller Anhydrite (or “Pegmatite Anhydrite”) Lower Aller Clay (“Red Salt Clay”)
time mark 253 Ma	
Zechstein 3 (Leine Series, 150–345 m)	Upper Leine Clay Leine Halitite (enclosing *Potassium Seams Riedel and Ronnenberg)* Main Anhydrite Leine Carbonate (Ca3: “Flaggy Dolomite”) Lower Leine Clay (“Grey Salt Clay”)
time mark 254.5 Ma	
Zechstein 2 (Stassfurt Series, 210–750 m)	Upper Stassfurt Clay Upper Stassfurt Anhydrite (“Hanging wall Anhydrite”) Cover Halitite *Stassfurt Potassium Seam* Stassfurt Halitite Lower Stassfurt Anhydrite (“Footwall Anhydrite”) Stassfurt Carbonate (Ca2: “Main Dolomite”, or basinal “Smelly Shale” facies)
Zechstein 1 (Werra Series, 200–420 m)	Uppermost Werra Anhydrite Uppermost Werra Halitite Upper Werra Anhydrite Upper Werra Clay Upper Werra Halitite *Hessen Potassium Seam* Middle Werra Halitite *Thüringen Potassium Seam* Lower Werra Halitite Lower Werra Anhydrite Nodular Anhydrite Shale Werra Carbonate (Ca1: “Zechstein Limestone”) Lower Werra Clay (“Copper Shale”)
time mark 258 Ma	Werra Conglomerate (“Zechstein Conglomerate”)
Rotliegend (Middle and Early Permian)	

intercalations of halite, anhydrite and kieserite. Kieserite bands in carnallitite or sylvinite are nodular, brecciated or enterolithic. Upright carnallite crystals grew in Mg-sulphate mud, comparable to shallow-water selenite. Bright red colours mark some of these rocks, foremost the massive carnallite bands, and attest to the horizon of a K-seam in areas of non-deposition or of later dissolution. This striking oxidation supports the assumption of very shallow water to dry conditions.

The end of the Permian period saw the largest mass extinction of life in geological history, with the loss of ~95% of all species. Its cause is generally believed to be the eruption of the Siberian trap basalts (Kamo *et al.* 2003). In Early Triassic time, a 1000 m thick blanket of terrestrial red sediments of the Buntsandstein group covered the Zechstein evaporites.

The sulphate walls of basin margins (Figure 4.18) tended to form mechanically unstable steep slopes. When the basin desiccated during formation of potassium-magnesium salts, dry rock falls and avalanches may have affected the oversteepened cliffs. During high-water periods, debris slides descended into deeper parts of the basin. Resulting sediments resemble turbidites. Impressive examples of evaporites with a strong imprint by gravity mass flows occur in the Miocene of the Carpathian foredeep of southern Poland, Romania and Ukraine, and in the Permian salt of the Eastern Alps (Austria).

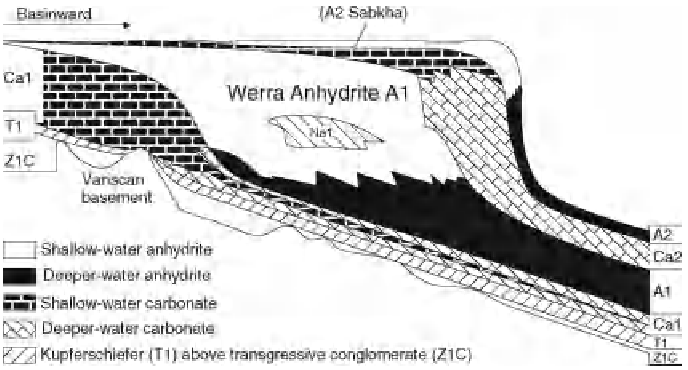

Figure 4.18 Characteristic cross-section of a sulphate "wall" on the southern margin of the Zechstein Basin (after Braitsch 1971). With permission from Springer Science + Business Media. In this setting little salt was formed, and non-saline rocks of Zechstein Cycles 1 (Werra) and 2 (Stassfurt) are in direct contact. Not to scale.

Permian salt in the Eastern Alps (Austria)

Late Permian (to earliest Triassic?) salt deposits occur in the Northern Calcareous Alps, a tectonic subunit of the Upper East Alpine thrust sheets (Figure 1.89). Anhydrite and gypsum deposits are exploited over the whole outcrop length of this unit (some 600 km) but salt is restricted to a central part from Salzburg to Tyrol. The sediments imply a rift setting within Pangaea that later developed into the Meliata Ocean, which is one of the ephemeral Tethys-related oceans that opened and closed during formation of the Alpine orogen in Central Europe (Neubauer *et al.* 2000). Terrestrial sediments and bimodal volcanics of Permian age resemble the Rotliegend and display remnants of arid alluvial fans, flood plains, siliciclastic sabkhas and playa lakes. First orogenic deformation of the Calcareous Alps took place in the Middle Jurassic, when nappes formed and during advance, shed and buried thick turbiditic wildflysch (a tectonic-sedimentary melange) along their fronts. Kilometre-sized blocks of Permian evaporites and marine shelf sediments were embedded in the wildflysch (Frisch & Gawlick 2003). In the following prolonged period of Alpine orogenic deformation, the salt was very mobile and is now found along nappe thrust-soles, in anticlinal traps, or in stocks that faintly resemble salt diapirs.

Salt mining in the region started in Neolithic times. An ancient term for the peculiar salt formation of the region is *Haselgebirge* (in German), which translates as "salt rock" or "salt mountains". The characteristic Haselgebirge rocks are debris-sheets and mega-breccias within bedded and massive halitite. Rock debris includes fragments of anhydrite, dolomite, claystone, basalt and halitite. Opinions on the origin of the breccias are still not settled. Interpretations vary from synsedimentary mass flows entering salt lagoons (with a tectonic overprint) to a purely tectonic origin during overthrusting and nappe propagation. The intensive deformation, or more probably the chaotic incidence of mass flows severely limits stratigraphical subdivision. The following lithological units are discerned (Schauberger 1986):

- *Grüntongebirge* (white halitite, anhydrite, greenish clay and sandstone), and
- *Rotsalzgebirge* (red banded halitite with anhydrite, polyhalite, glauberite and Mg-Na sulphates; black and red clay; Figure/Plate 4.3) make up most the total thickness (possibly 1000 m) of the salt formation. The second displays the highest K-Mg contents of all units. It is assumed that these two units are synchronous but deposited in different facies, the first in coastal lagoons with considerable terrigenous siliciclastic import, the second in areas of repeated desiccation;
- *Buntes Salztongebirge* (red and white halitite with black, green and red clay, and numerous horizons of rounded to subangular fragments of vesicular basalt and mafic tuffite) may be an intermediate facies between the first and the second (Schauberger 1986);
- *Grausalzgebirge* (grey halitite with red and grey clay fragments, black dolomite) indicates reduced conditions, probably in deeper parts of the basin.

Relative age relations of the lithological units remain unresolved.

The preponderance of red colours indicates prevailing shallow water and oxic conditions. Thick anhydrite and dolomitic anhydrite bodies are marginal equivalents of the salt formation. S and Sr isotope data confirm that the Alpine evaporites were formed from Permian seawater (Spötl & Pak 1996).

Bromine concentration in halite varies between 50 and 350 ppm (Spötl 1989). The higher figures imply concentrations typical for the Mg-sulphate zone and approaching the potassium facies. Potassite rocks, however, are unknown. In blocks of anhydrite and clay, which slumped into salt basins, polyhalite and accessory kieserite are not rare. This makes it probable that high salinity was locally reached in marginal positions, but not sufficient for precipitation of carnallite or sylvite. An alternative possibility is loss of former potassium salt minerals by later dissolution, considering that Alpine salt formations must have experienced several events of pervasive fluid passage. Yet, viable halobacteria and haloarchaea have been isolated from Haselgebirge halite and were successfully cultured (Stan-Lotter *et al.* 2003).

The Alpine salt bodies also display features of a tectonic melange that originated when, during the Late Jurassic, the evaporites acted as the ductile sole of the (higher) Hallstatt nappes moving over deeper tectonic units of the Northern Calcareous Alps (Spötl 1989). Many observations support this statement, such as inclusions of giant fragments of much younger country rocks (Triassic to Cretaceous). Tectonic deformation was intense when the frontal wildflysch was overridden by the nappes. However, already Schauberger (1986) presented arguments for a sedimentary origin of the peculiar claystone debris-sheets in salt. Most workers now agree that the haselgebirge is a modified mass flow sediment. Supporting arguments include the continuity of certain lithofacies over a considerable distance. In the Hallstatt mine, for example, basalt and basalt tuffite occur in an indentifiable lithostratigraphical horizon of the salt body. Some of the debris flows display rounded, others only angular fragments; this can be explained by different water-solid ratios of distinct mass flows. Round pebbles of clear halite are part of the debris. Halite, clay and sulphates in the debris are derived from basin marginal shallow-water settings, or from a siliciclastic sabkha. Affirmative observations include cross-bedded sulphates, mosaic-textured nodular anhydrite, sulphate pillows that may have been selenite hillocks, polyhalite replacing anhydrite, rare calcrete and red carnelian fragments, and the common occurrence of displacive clear halite crystals in claystone. Most of the debris fragments are densely jointed but not deformed; joint fissures are filled by fibrous or scaly halite. The combined evidence points to haselgebirge formation in a halite-stage restricted sea within a rift basin that was bordered by arid alluvial flood plains, desert mountains and distant volcanoes. Accumulating shore sediments had the character of a siliciclastic sabkha. Earthquakes related to rifting released debris flows from clastic basin slopes and sulphate walls (Figure 4.19).

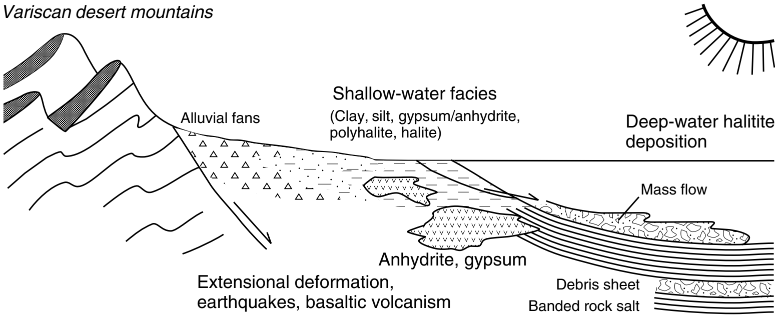
Variscan desert mountains
Shallow-water facies
(Clay, silt, gypsum/anhydrite, polyhalite, halite)
Alluvial fans
Deep-water halitite deposition
Mass flow
Anhydrite, gypsum
Extensional deformation, earthquakes, basaltic volcanism
Debris sheet
Banded rock salt

Figure 4.19 Schematic sketch of Permian Haselgebirge formation by salt-anhydrite-clay debris mass flows in rifts of the nascent Eastern Alps.

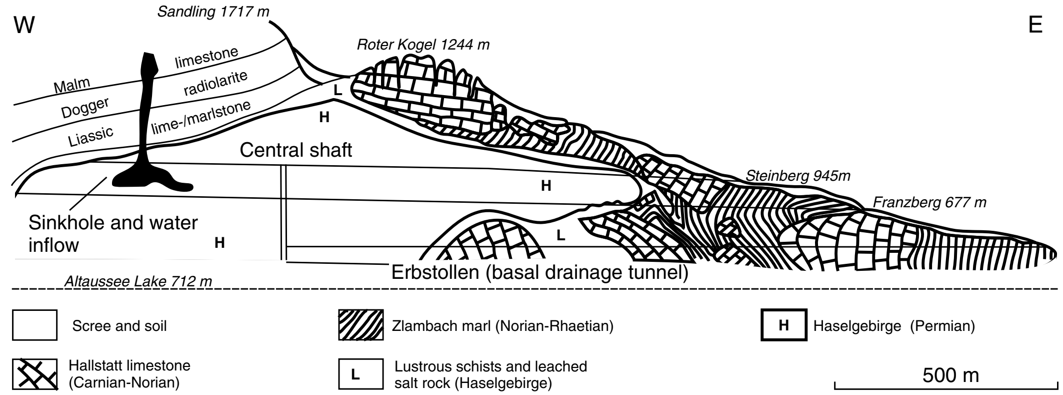
W
E
Sandling 1717 m
Roter Kogel 1244 m
Steinberg 945m
Franzberg 677 m
Malm
Dogger
Liassic
limestone
radiolarite
lime-/marlstone
L
H
Central shaft
H
L
Sinkhole and water inflow
H
Erbstollen (basal drainage tunnel)
Altaussee Lake 712 m
Scree and soil
Zlambach marl (Norian-Rhaetian)
H Haselgebirge (Permian)
Hallstatt limestone (Carnian-Norian)
L Lustrous schists and leached salt rock (Haselgebirge)
500 m

Figure 4.20 Geological section of Altaussee salt mine, Austria. With kind permission from Salinen Austria AG.

Facies and thickness variations of post-salt sediments near Alpine salt deposits suggest that already in the Triassic, salt pillows and possibly diapirs were formed. The position of the salt at the base of nappes is supposed to have facilitated movement of thrust sheets, which imprinted strong deformation on earlier salt structures. Illite crystallinity, vitrinite reflectance and fluid/rock reactions record a complex deformation and thermal history differing between, and even within individual outcrops (Spötl *et al.* 1998). The resulting "salt mountains" (Figure 4.20) faintly resemble common salt diapirs.

In the Eastern Alps, the extraction of salt from the salt-clay rocks was traditionally carried out by underground construction of solution chambers ("Laugwerk"). Low grade salt-clay rock (Haselgebirge) contains 30–40% NaCl, medium-grade 40–60% and rich portions have 60–70% salt. Masses of pure salt were exploited by hard rock mining methods. Today, the Alpine salt mines have been converted to borehole leaching operations, as in the Altaussee salt mine (Figure 4.20). The mine lies above the Altaussee Lake level and is drained by a basal tunnel. The Haselgebirge salt body is enveloped by a thin mantle of impermeable claystone ("lustrous schists"). Several decades ago, ancient near-surface leaching caverns in the west had caused local roof collapse (a sinkhole) and inflow of water, that was successfully plugged.

4.3 POST-DEPOSITIONAL FATE OF SALT ROCKS

4.3.1 Diagenesis and metamorphism of evaporites

Like other sediments, salt rocks are altered by recrystallization, neogenesis of minerals and the passage of various fluids, beginning at precipitation. In the past, scientists studying the highly soluble potassium and magnesium salts considered even their early diagenesis as a kind of metamorphism. However, this term should be restricted to truly metamorphic evaporites (see below):

Calcium sulphate is commonly precipitated as gypsum, except at elevated temperature in highly saline pore waters when anhydrite is stable. Diagenesis always alters gypsum to anhydrite, so that anhydrite may be either sedimentary or diagenetic (Jowett *et al.* 1993). In some cases, replacement of gypsum by anhydrite can be seen under the microscope. Chemical clues for a replacement origin of anhydrite include lower strontium contents, because some strontium is always abstracted when dehydration takes place. Mechanically and chemically, anhydrite is very stable, but $CaSO_4$ undersaturated brines may leach anhydrite and deposit halite. The conversion of gypsum to anhydrite induces a 40% volume reduction. However, the liberated water plus solid anhydrite occupies ~11% more volume than the original gypsum. If the system is closed, overpressures may result that can cause intraformational brecciation.

Table 4.8 Dehydration reactions of common salt minerals

Mirabilite ($Na_2SO_4 \cdot 10H_2O$)	⇒ Thenardite (Na_2SO_4) + $10H_2O$ (at 32.4°C)
Epsomite ($MgSO_4 \cdot 7H_2O$)	⇒ Hexahydrite ($MgSO_4 \cdot 6H_2O$) + H_2O (at 26°C)
Hexahydrite ($MgSO_4 \cdot 6H_2O$)	⇒ Kieserite ($MgSO_4 \cdot H_2O$) + $5H_2O$ (at 31°C)
Carnallite ($KCl \cdot MgCl_2 \cdot 6H_2O$)	⇒ Sylvite (KCl) + $6H_2O$ + $MgCl_{2aq}$ (max. 167.5°C at 32 MPa, function of pressure)

Ordinarily, the $CaSO_4$ brines resulting from dehydration leave the system.

Halitite*:* Newly formed salt sediment is a loose mush of salt crystals with a high pore fraction, which is filled with brine. More solid salt crusts also contain large brine inclusions (Figure 4.12b). Investigations in present salt-forming lagoons revealed that the pore volume is rapidly diminished by continuing salt precipitation. In geologically very short time and at a depth to a few metres, lithified salt rocks are formed. Increase of temperature and pressure during main stage diagenesis provokes recrystallization, often to equilibrium grain boundaries (foam structures).

For over one hundred years, the precise origin and diagenesis of potassium-magnesium salt rocks challenged numerous scientists and our present understanding is far from complete. D'Ans (1969) and Braitsch (1971) summarized details about results acquired during the pioneering times of salt research. In the earlier papers, diagenetic reactions with passing fluids at stable temperature ("solution metamorphism") are distinguished from alterations caused by rising temperature ("thermal metamorphism"):

- Fluid-related diagenesis of potassites is best explained by an example: If a sodium chloride-saturated but Mg-poor solution passes through carnallite, incongruent dissolution of the carnallite extracts $MgCl_{2aq}$ and leaves a solid residue of sylvite. Carnallitite will be transformed into sylvinite or hartsalz. If the brine-flow continues, KCl is leached also and the potassium seam is impoverished. Thin bands of red halitite may be the only witness to the former presence of a K-seam.
- Thermal diagenesis describes neogenesis of minerals by heating. The most common case is dehydration, which is a strong proof for temporary permeability and an outflow from the observed system. Many reactions of this type are known (D'Ans 1969, and earlier papers). The reactions can be used directly as geological thermometers, except for those that are also a function of pressure (Table 4.8).

Water originating by dehydration (e.g. of gypsum) within a salt formation, or entering a salt body from outside is quickly saturated with NaCl. In principle, this inhibits further flow within halitite, except under strong temperature or pressure gradients. Experiments in the Asse mine demonstrated that saturated brine in tiny fluid inclusions moves towards a heating element, obviously because salt solubility rises with temperature. Another possibility is flow within induced porosity, when NaCl-brines pass through soluble K-Mg salts. Flow takes place until the brine is in equilibrium with the surrounding salt rocks. The accumulated evidence shows that the passage of diagenetic brines through salt bodies is common. Numerous exposures in potassium mines display low-temperature fluid-induced sylvite formation from carnallite (Figure 4.21). This is an obvious contradiction to the earlier statement of the extremely low intrinsic permeability of salt, proved by high-technology measurements as well as geological observations (e.g. salt trapping high-pressured methane). The solution to the conundrum can only be found in geologically short events that mobilize or deform salt strongly, including faulting, volcanism and diapiric upflow (Peach 1991) within a field of steep pressure and/or temperature potentials.

The alteration of K-Mg salts and sulphates starts at the moment of precipitation (cf. back reactions of Figure 4.9) and continues through early and main stage diagenesis. The accumulated petrologic history of potassites is complex. For example, the distribution of carnallitite, sylvinite, hartsalz and residual halitite in the undulating K-seam Thüringen in the Werra District (Figure 4.21) is controlled by relative elevation (the primary

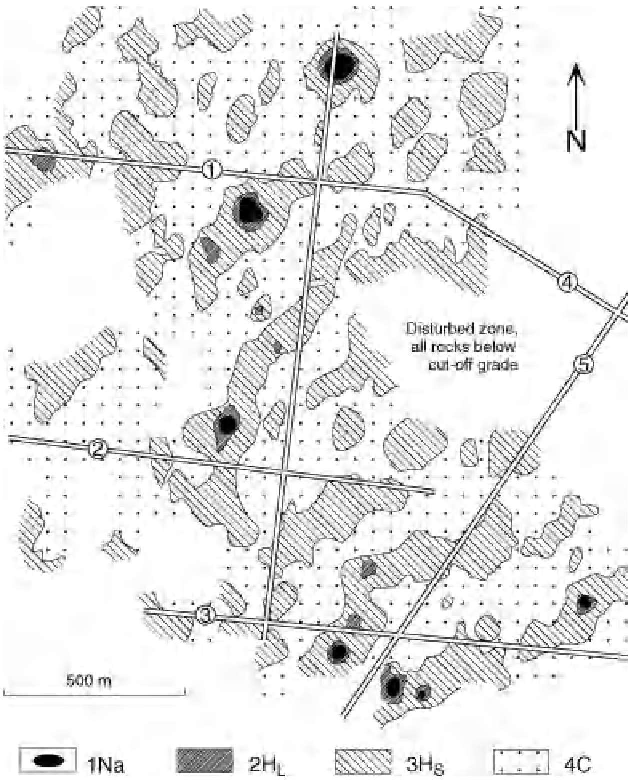

Figure 4.21 Facies map of near-horizontal potassium seam Thüringen (Zechstein 1) in the Herfa mine, Hesse, Germany (Braitsch 1971). In elevated positions of the seam, residual halitite (1Na), langbeinitic hartsalz ($2H_L$) and sylvinitic hartsalz ($3H_S$) replace the "basinal" carnallitite 4C). The alteration is attributed to early diagenetic supergene leaching or to migrating fluids mobilized by Tertiary volcanism.

carnallite only occurs in depressions) and, to some degree, by proximity to faults. Tectonics and fluid migration associated with volcanism are the accepted interpretation of observations, but early diagenetic processes such as meteoric leaching cannot be excluded.

Less changeable minerals in salt, mainly carbonates and silicates, provide further restrictions concerning conditions of diagenetic change. Chlorite is formed from kaolinite and montmorillonite, phengite from illite and albite from NaCl and clay. Mg-rich tourmaline, talc and sepiolite attest to higher Mg-concentration in pore fluids, as does magnesite replacing dolomite. Authigenic quartz crystals are useful for microthermometry. Finely fibrous SiO_2 aggregates (e.g. in chert bands) consisting of lutecite with >20% moganite indicate the former presence of salt (Heaney 1995).

Contact metamorphism

Contact metamorphism of salt rocks in the vicinity of subvolcanic dykes is not rare because salt, rifting and volcanism are often closely related. Numerous basalt/salt contacts have been exposed by mines in the Werra District, Germany. At the surface, the region is dotted with Tertiary volcanic cones and lava flows. In the salt mines below, the dykes widen in salt and cause a halo of alteration. At ~80 m from the dyke, distal carnallite is first altered to kainite. With decreasing distance, K-Mg chlorides are impoverished until only residual halitite is observed. At the actual contact, many rare minerals are formed. Note that this alteration is hydrous, melting of salt is not observed (the melting temperature of halite is 801°C). The basalt in the dyke is profoundly altered and soaked with salt. A similar situation was described from eastern Siberia by Grishina *et al.* (1992).

Orogenic metamorphism

Orogenic metamorphism of evaporites usually results in the removal of soluble salts with the metamorphic fluid flow. Anhydrite, however, is more stable and is reported from amphibolite facies metamorphic rocks. When salts are leached during metamorphism, relatively subtle clues remain that point to the former evaporitic nature of rocks. Indicators are higher concentrations of minerals with unusual contents of Na, Mg, Cl, B and SO_4, including scapolite (Frietsch *et al.* 1997), lapis lazuli (lazurite), Mg-tourmaline, phlogopite and albite (Cook & Ashley 1992). Talc-kyanite rocks called "white schists" are believed to represent Mg-rich pelites metamorphosed at conditions of high pressure and low temperature during lithospheric subduction (>8 or 9 kbar and 700 ± 50°C: Bucher & Frey 2002). Meta-pelites of evaporitic lineage may be chemically distinct by elevated contents of Mg, Li and F, and higher Li/Mg and B/Al ratios compared to averages. While evaporites are changed by metamorphism, so are the metamorphic fluids that have passed through them. They acquire the character of brines and consequently cause alteration of large rock volumes in the periphery, such as albitization and scapolitization. Also, they may induce mineralization (cf. Chapter 1.4 "Ore Formation by Migrating Saline Brines").

4.3.2 Deformation of salt rocks

Salt is highly deformable. Nearly all salt rock bodies display folding and flow structures, even those that are interbedded with little deformed sediments. Potassium seams in flat, tabular evaporites display internal recumbent folds. In salt diapirs, their high ductility is emphasized by flow fold patterns that resemble banded calcite marbles in high-grade metamorphic settings.

Underground mine openings in salt slowly close by ductile convergence of walls. After tens or hundreds of years, only traces of former human presence are seen in solid salt, such as timber or iron rails. This illustrates that salt rocks can be considered as highly viscous Newtonian fluids. Enduring, weak differential stresses cause ductile flow, whereas sudden loading at high stress ratios provokes brittle fracture (Hunsche & Hampel 1999). The flow of salt is termed "creep", because it cannot be seen. Depending on the relative values of shear and normal principal stress, creep may lead to volume increase (dilatation) or decrease (contraction). Dilatation (expansion) is regularly observed near mine openings. It causes elevated permeability and mechanical damage, and often ends in brittle failure (e.g. spalling). Dilatant strain may explain some cases of the above-mentioned episodically higher permeability of salt for passing diagenetic fluids.

Creep of salt is macroscopically free of fractures or fissures. Microscopic examination of etched sections reveals, however, that single salt grains are disjointed by microstructures into numerous subgrains. Integrated movement of subgrains produces the overall creep. Microfractures "jump" across grain boundaries. This results in the characteristic polygonal textures of mechanically strained salt. A second mode of creep is achieved by solution transfer, grain boundary migration and diffusion. Migration of dislocations (one-dimensional crystal lattice defects) constitutes a third component of creep (Miguel *et al.* 2001). High rock and fluid pressure, but also higher humidity and temperature of mine air promote the rate of viscoplastic deformation of salt. Seasonal variations of these parameters in a mine at 650 m below the surface still influence the rate of creep (Kwon & Kim 2005). There is no lower boundary of loading for inducement of creep. In geological time spans, salt deforms at very low stress ratios. This is illustrated by the Hormuz salt glaciers of Iran (Kent 1979), which flow under their own weight. In this desert region, glacier movement accelerates after a little rainfall.

Any change of humidity, temperature and the stress field such as the opening of a new mine tunnel cause a variation of the deformation rate ("transient creep"), which returns to steady state creep only after adjustment to the changed parameters. Mathematical modelling of salt and associated rocks is possible with non-linear physically-based material laws exemplified by eq. 4.1 (Hunsche & Hampel 1999).

Creep of salt rock:

$$\varepsilon^\star = A.\ \exp[-Q/(R.T)].\sigma^n \qquad (4.1)$$

ε^* = rate of creep; A = structural parameter (type of salt); Q = activation energy; R = universal gas constant; T = temperature in K; σ = stress deviation (MPa); n = stress exponent (usually 5–7). A, Q and n are determined by experiments. All modes of salt deformation, from elastic-brittle behaviour to creep and failure, are described by composite material laws (Swift *et al.* 2001).

Experiments as well as practical experience in salt mines show that at comparable conditions, different halitite rocks display characteristically unequal creep rates. In the Zechstein mines, Z2 Stassfurt Halitite (Table 4.7) displays a distinctly higher creep rate compared with Z3 Leine Halitite. This is not always a function of visible petrographical parameters, although in this case, grain size and admixture of clay and anhydrite are different. Strength and deformation characteristics of haselgebirge are clearly a function of salt content. Carnallitite creeps like halitite but with a ten-fold rate and fails after much less strain. This explains the sudden collapse of whole extraction panels in potassium mines, which may cause earthquakes. An earthquake of this type originating in the former potassium salt mine Teutschenthal near Halle (Germany) had a local magnitude of 4.8 (1996).

During deformation, salt rocks may acquire directional grain textures but recrystallize ("heal") readily. Traces of deformation, such as foliation in Leine Halitite of the Asse mine (Germany) and in the Khorat Plateau (El Tabakh *et al.* 1999), macroscopic fissures, or microscopic translation planes and pressure twinning are rarely preserved. Normally, separation planes in salt including faults, fissures, joints and schistosity are only recognizable if marked by some fill material. Common fills include secondary fibrous halite, bischofite, carnallite, sylvite and anhydrite, as well as gas, petroleum and brine.

Although the deformation of salt rocks is generally ductile, some are strikingly brecciated. Reports describe breccias of halite and even of highly ductile carnallitite. It is speculated that very low fluid pressures during deformation might explain these observations.

Different deformation characteristics distinguish the various salt rocks and the intercalated clays, sulphates and carbonates. Salt rocks are less competent and tend to flow, i.e. deform ductilely. Competence (resistance to flow) increases from sylvite to carnallite to halite. Whereas salt rocks flow even at near-surface conditions, associated sulphates, claystone and carbonates tend to react by brittle deformation and display jointing, fissures and boudinage. Typical disharmonic folding results from the widely different mechanical properties of evaporites and their country rocks.

4.3.3 Forms and structures of salt deposits

In epicontinental platform settings of little-deformed sedimentary suites, and with less than ~1000 m overburden, basin-wide salt-bearing evaporites occur in the form of essentially flat tabular strata. As mentioned above, even in little deformed salt beds, internal folding is observed. Associated more competent and brittle country rocks display fractures and limited tilting, but no ductile deformation. Examples include the Devonian Prairie Evaporite in Saskatchewan (Canada), Devonian salt in the Moscow basin (Russia, Ukraine) and Permian (Zechstein) salt in the Werra district of Hesse (Figure 4.21 and Figure 4.22), which occupies a marginal platform position relative to the main Zechstein basin. Note that in this region, only the first Zechstein cycle is fully developed. Mining is based on potassium seam Thüringen with a thickness of ~2 m. A mechanized room and pillar mining method is used in order to minimize the hazard of roof failure and water inrush. Waste brines of potassium salt processing are injected into the Flaggy Dolomite aquifer (Figure 4.22).

Extensional tectonic deformation often causes considerable movement of salt masses. Agents include modification of the load and stress field and the opening of flow paths along faults. In the Mesozoic Basin of Northern Germany, pronounced mobility of Permian salt first occurred during tectonic east-west extension in the Late Triassic (Mazur & Scheck-Wenderoth 2005), which was an initial phase of the break-up of the supercontinent Pangaea. During this time, salt glaciers formed on rift flanks (Mohr *et al.* 2007) and allochthonous salt intruded into higher stratigraphical levels.

Compressional tectonic deformation shifts salt into locations of lower pressure, generally

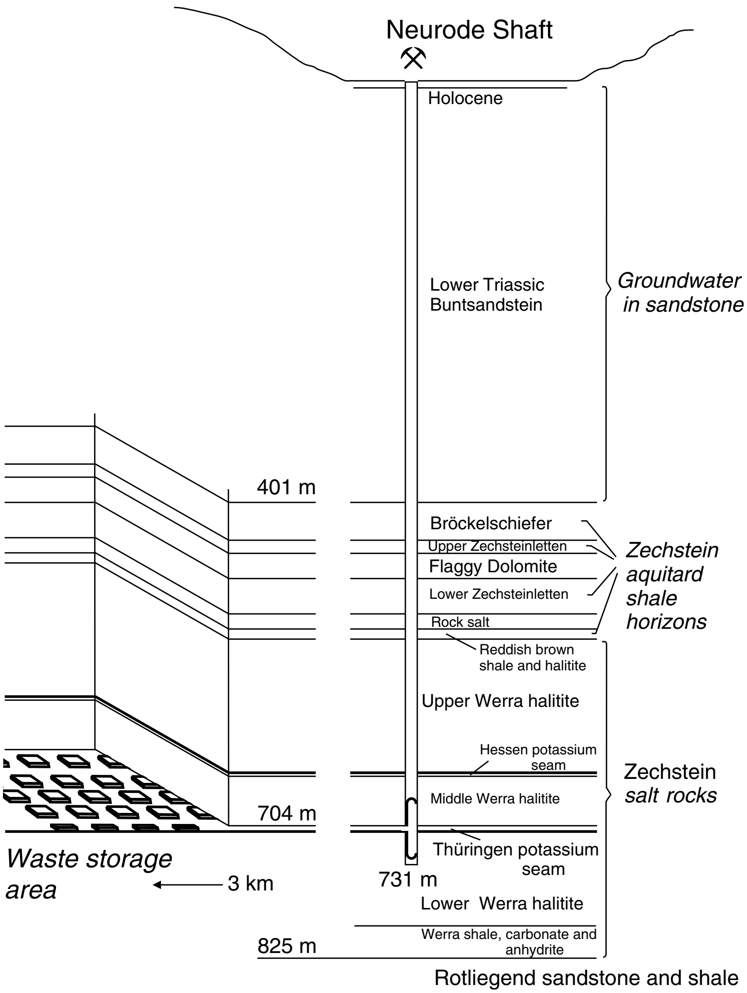
Neurode Shaft
Holocene
Lower Triassic Buntsandstein
Groundwater in sandstone
401 m
Bröckelschiefer
Upper Zechsteinletten
Flaggy Dolomite
Lower Zechsteinletten
Rock salt
Zechstein aquitard shale horizons
Reddish brown shale and halitite
Upper Werra halitite
Hessen potassium seam
Middle Werra halitite
Zechstein salt rocks
704 m
Thüringen potassium seam
Waste storage area
3 km
731 m
Lower Werra halitite
Werra shale, carbonate and anhydrite
825 m
Rotliegend sandstone and shale

Figure 4.22 Geological profile of the potassium salt mine Herfa-Neurode in the Werra region, Hesse, Germany, indicating the position of the storage area for toxic and chemically aggressive industrial waste. Note the characteristic pattern of room-and-pillar mining. With kind permission from Kali & Salz AG, Kassel.

anticlinal fold cores and salt ridges (Ings & Beaumont 2010). Often, the salt-bearing evaporites constitute a detachment horizon between folded cover rocks and brittle, faulted basement underneath. An excellent example of the resulting thin-skinned fold and thrust belts provide the Jura Mountains (Switzerland-France: Philippe 1994). Similar effects show seismic images produced for gas exploration in northeastern Germany; this region experienced north-south compressive tectonic deformation ("inversion") in the Late Cretaceous-Early Palaeogene (Kley & Voigt 2008, Mazur & Scheck-Wenderoth 2005, Kossow *et al.* 2000). Flow of salt into anticlines forming elongate salt pillows is balanced by abstraction of salt below adjoining synforms.

Salt in Alpine-type fold and thrust belts induces detachment and facilitates movement of nappes (c.f. haselgebirge in the Eastern Alps). The form of salt deposits in this setting is the combined result of early diapirism, salt flow, tectonic shortening and possibly, late diapirism. The melange of Alpine thrusting, nappe movement, folding and repeated salt flow is not easily resolved (Figure 4.20).

The characteristic form of salt deposits in thick epicontinental sedimentary basins and in passive continental margin settings are salt domes, or

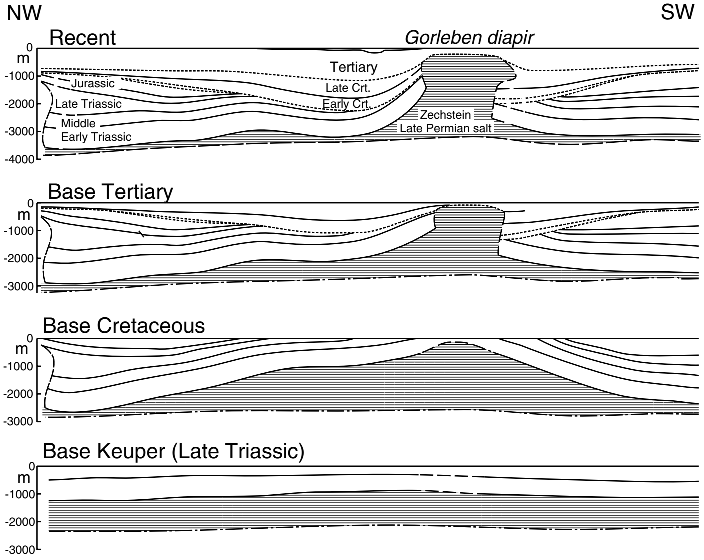

Figure 4.23 Characteristic development stages of a salt dome, here illustrated by the Gorleben diapir, Northern Germany (modified from Zirngast 1991). With permission from www.schweizerbart.de. This salt body is under investigation as a future repository for high-level radioactive waste. The salt-pillow stage was reached in the Late Jurassic. Active diapirism took place in the Early Cretaceous and was followed by passive diapirism, which continued into the Tertiary. The salt diapir in the West was formed much earlier.

diapirs. In diapirs, the salt pierced its former roof and intruded younger sediments, quite similar to small granite stocks (Figure 4.23). Host rocks in contact with the up-flowing salt are dragged upwards and ductilely bent, and slabs of the roof are pushed to the side and occasionally overturned. Plug-like parts of the roof may be uplifted for several kilometres (Perthuisot & Rouvier 1992). Phenomena like this are thought to originate during a stage of early, *active diapirism,* which is the process of forceful intrusion of salt into roof rocks. During this stage, the permeability of salt is relatively high, similar to rocks undergoing metamorphic shearing. The crest of an active diapir may break through the sediments to the surface, on land or under water cover.

Active diapirism is usually followed by a downbuilding phase, when the diapir rises passively (passive diapirism), while sediments accumulate in the rim synclines. At shallow depths where horizontal stresses are small, or at the surface, diapirs expand horizontally. This results in carrot or mushroom-like cross-sections of diapirs, the formation of salt tongues and coalescing salt canopies (e.g. Great Kavir Basin of northern Iran: Jackson *et al.* 1991). Salt glaciers that flow laterally off outcropping diapirs, either below the sea or subaerially, may result in allochthonous salt sheets. On the top, the sheets may carry a sedimentary package (Figure 4.24). The feeder stems beneath a diapir may close so that supply of salt from below is cut off ("pinched-off salt domes": Jackson *et al.* 1998). Manifold are the variations of diapiric salt structures; even in one district, tower-like diapirs occur near elongated walls (Figure 4.25).

The internal structure of salt diapirs is characterized by ductile flow deformation. In spite of the drastic change of the outer form from tabular shape to a plug or wall, the lithostratigraphical order is commonly well preserved. Bromine profiles are little different from undeformed stratigraphical equivalents (Küster *et al* 2009). The oldest, originally deepest salts occur in the centre, mantled by younger and higher beds (Figure 4.26). Many salt diapirs display internal folding with nearly vertically plunging fold axes ("curtain folds"). Certain diapirs, such as some in the American Gulf Coast region, are composed of several individual intrusions separated by "anomalous zones", which contain inclusions of host rocks, brines, gas and petroleum.

The thermal conductivity of salt rocks (6 W m^{-1} °C^{-1}) is about three times higher compared with common country rock sediments (1.5–2.5 W m^{-1} °C^{-1}). As

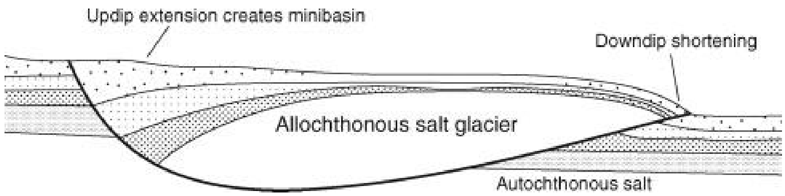

Figure 4.24 Schematic profile of a composite salt-sediment glacier, showing one possibility (a gravity slide or flow) of the origin of allochthonous salt sheets (Fletcher *et al.* 1995). AAPG [2010] reprinted by permission of the AAPG whose permission is required for further use. Salt glaciers that formed on the sea floor in the geological past are not easily recognized. Here, tensional and compressional features are pointed out that may assist in discrimination from laterally intruded salt sheets.

a result, heat flow in salt is higher and temperatures exhibit characteristic anomalies. Relative to adjacent host rocks, salt is warmer in the upper part of the diapir and cooler at its base (Figure 4.27, Manhenke & Beer 2004). Because temperature is a primary control on kerogen maturity and hydrocarbon formation, the thermal properties of salt exert important constraints on petroleum and gas deposits (Thomson & Lerche 1991). Also, the fluid flow regime around diapirs is determined by temperature gradients. The difference of temperature and salinity that is induced by the contact of salt with permeable sediments causes convection in adjoining aquifers. This may induce clogging of pores by precipitation of minerals such as anhydrite (Kühn & Günther 2007).

Salt intrusions are initiated in either compressive or distensive tectonic settings. The first are mostly pierced salt-cored anticlines, the second are rooted in normal faults and rifts. Salt intrusions connected to anticlines are very prominent in Romania, in Tunis and Algeria, and in the Zagros fold belt of Iran. Often, the linear tectonic control is expressed by a long strike length of salt structures ("salt walls") that appear on maps as swarms of "salt lines". In Northern Germany, the pattern can be simplified to (1) Late Triassic N-S directed transtensional structures that parented more isolated diapirs, and (2) Late Cretaceous cross-cutting transpressional salt walls striking NE-SW.

Another large group (3) is constituted by salt diapirs that have no recognizable tectonic trigger and whose upflow and intrusion appears to be totally autonomous. These stocks are round or elliptic in map view, appear to be randomly distributed through a region and cut through little disturbed cover rocks. Part of the Gulf Coast and German diapirs conform to this description. For a long time, the origin of non-tectonic salt diapirs was hotly disputed.

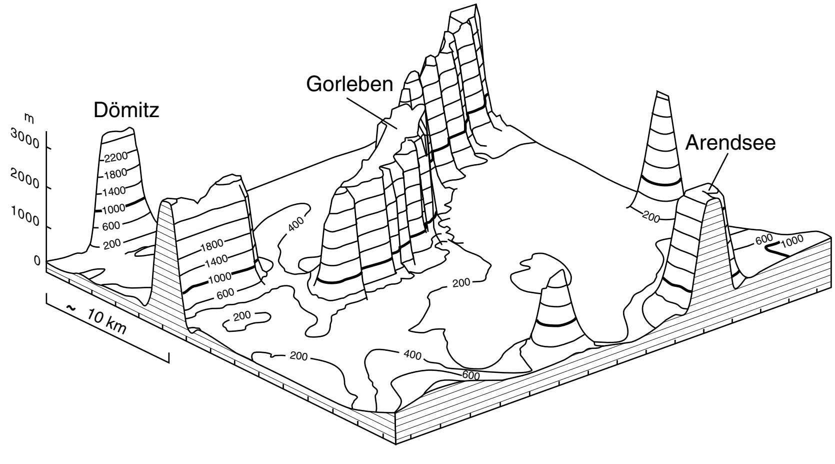

Figure 4.25 Salt structures in the Gorleben region, Northern Germany (modified from Zirngast 1991). With permission from www.schweizerbart.de. Overhangs of diapirs are not shown. Prior to salt flow, the total thickness of the Zechstein salt was about 1400 m.

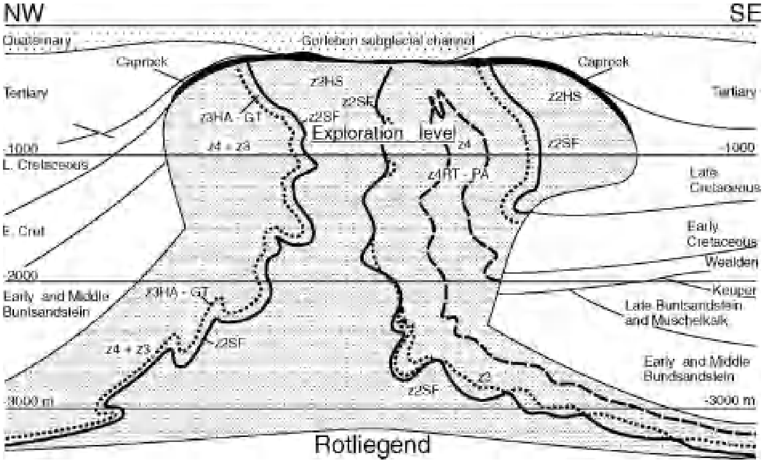
NW
SE
Quaternary
Gorleben subglacial channel
Caprock
Caprock
Tertiary
Tertiary
z3HS
z2SF
z2HS
z3HA - GT
z2SF
Exploration level
z4 + z3
z4
z2SF
-1000
-1000
L. Cretaceous
z4RT - PA
Late Cretaceous
E. Cret
Early Cretaceous
Wealden
-2000
Keuper
Early and Middle Buntsandstein
z3HA - GT
Late Buntsandstein and Muschelkalk
z4 + z3
z2SF
Early and Middle Bundsandstein
z3
z2SF
-3000 m
-3000 m
Rotliegend

Figure 4.26 Geological profile of the Gorleben salt diapir, Northern Germany, which is explored as an underground repository for highly radioactive waste (modified from Köthe *et al*. 2007). With permission from www.schweizerbart.de. The envisaged storage depth ("exploration level") is 800 m below ground surface, within a massive body of Z2/Z3 halitite. PA = Pegmatite Anhydrite, RT = Red Salt Clay, HA = Main Anhydrite, GT = Grey Salt Clay, SF = Stassfurt Seam potassite (carnallitite), HS = Main Salt, caprock black. Note the easterly overflowing body of Z2 salt; is this a former submarine salt glacier?

The physical base for an explanation of the upflow of salt was provided by Arrhenius & Lachmann (1912), who recognized that salt rocks are lighter (less dense) than clastic sediments and carbonates forming their hanging wall. This is a system of inverted density like the classical Rayleigh-Taylor (RT) instability. After early diagenetic pore filling, the density of halitite deviates

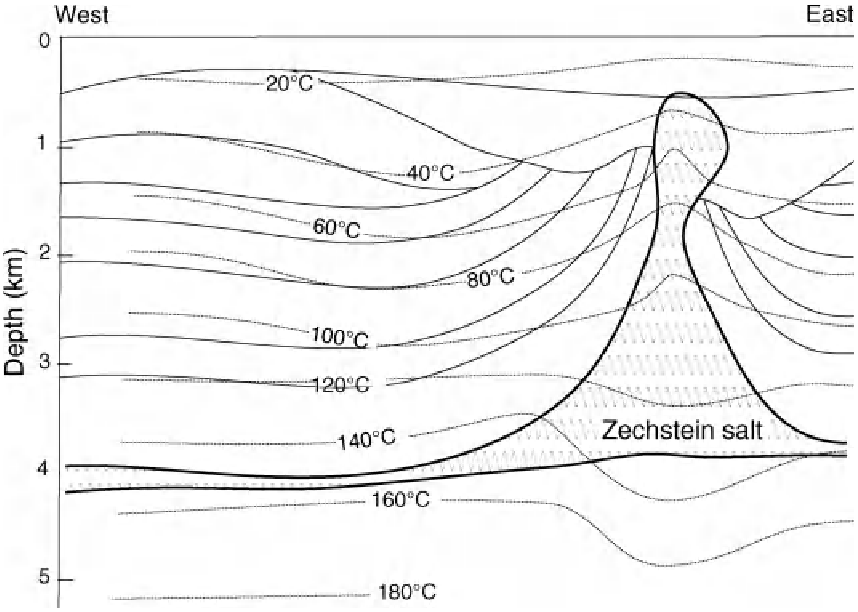
West
East
0
1
2
3
4
5
Depth (km)
20°C
40°C
60°C
80°C
100°C
120°C
140°C
160°C
180°C
Zechstein salt

Figure 4.27 Cross-section of geology and temperature field imposed by the Kotzen salt diapir, Brandenburg, Germany (Manhenke & Beer 2004).

little from the average of 2.2 g/cm^3. Unconsolidated sediments display a density of 1.6 to 1.9 and in fully compacted state 2.6 to 2.8 g/cm^3. The difference illuminates the potential energy of such a system. Very subtle factors may trigger lateral and upward flow, including small elevation differences of the footwall, either of tectonic (faults) or morphological nature (buried hills: Figure 4.26). In a similar manner, weight differentials in the hanging wall of the salt (e.g. lateral facies change) induce flow. At the stage of thin cover before RT instability is established, a system of viscous pressure ridges and minibasins may form, e.g. in the Gulf of Mexico (Ings & Beaumont 2010).

When Trusheim (1957) analysed characteristics of salt structures in Northern Germany, he divided the process of diapirism into several stages (Figure 4.23):

1 Once the "critical overburden thickness" (density inversion) is exceeded, salt starts to flow towards lower pressure domains, first forming "salt pillows". Updoming above the pillow crest and lateral abstraction of salt from the source salt layer result in formation of "primary rim basins" (sag, or minibasins), which allow precise timing of salt movement. Using this method, updoming of Zechstein (Late Permian) salt pillows (i.e. Gorleben during the Jurassic) was measured at an average of a few millimetres per year.

2 "Active diapirism" designates the breakthrough of salt into cover rocks. At the same time, "secondary rim basins" are initiated and filled. The piercement may be associated with high upflow velocities of the salt, possibly reaching metres per year.

3 Once the high potential energy of active diapirism is spent, the diapir continues to grow in the mode of "passive diapirism". Sediment accumulating in "tertiary rim basins" displays unconformities, off-diapir debris flows, salt extrusions (Jackson *et al.* 1991) and salt glaciers. In Northern Africa, salt tongues extend laterally to >1000 m from the Triassic diapirs along unconformity planes, probably formed as submarine extrusions (Perthuisot & Rouvier 1992).

In this connection, Trusheim (1957) introduced the term *halokinesis* and defined it as salt flow that is only due to gravity potential. He contrasted halokinesis with *salt tectonics*, which is salt flow related to regional tectonic processes. Of course, the terms designate opposites that in nature may not be clearly separated. More intensive salt flow occurs nearly always in times of tectonic strain (Kossow *et al.* 2000). In conclusion, diapirism is basically the product of compensation processes following density inversion, but is very often triggered by tectonic events (Daudre & Cloetingh 1994, Nalpas & Brun 1993).

4.3.4 Supergene alteration of salt deposits

Salt solubility in water is very high. Accordingly, salt on the surface is only preserved in an arid climate. In humid climate zones, salt is leached by infiltrating precipitation and moving groundwater. Because of its extremely low permeability massive salt rock is an aquiclude. Therefore, salt will be removed by dissolution until a deep saturated brine pool (in the pores of an aquifer) becomes stable and very little flow or additional solution take place. In such settings the salt forms the lower boundary of a brine aquifer. The boundary plane is commonly a level, mirror-like surface below the brine aquifer, which often is a cap-rock dissolution breccia (Figure 4.28), but may include clastic rocks as at Gorleben. In some cases, the salt surface displays channels or is inclined. Dissolution of salt reaches considerable depths. At Gorleben, for example, the salt surface occurs 250–300 m below sea level, with the local land surface and River Elbe at 20–30 m a.s.l. (Figure 4.26).

Subsurface solution of salt has been termed "subrosion". The removal of mass by subrosion enforces adjustment of overburden, often leading to collapse and formation of sinkholes. Depressions fill with groundwater (forming lakes: Figure 4.28) or with younger sediments.

The rate of subrosion is of high interest, because it is one of the critical parameters of a security case for salt domes destined to take up nuclear waste. Its determination is not simple; methods used include groundwater flow models and mass balance calculations, geomorphological analyses, geological data (e.g. the subsidence of precisely

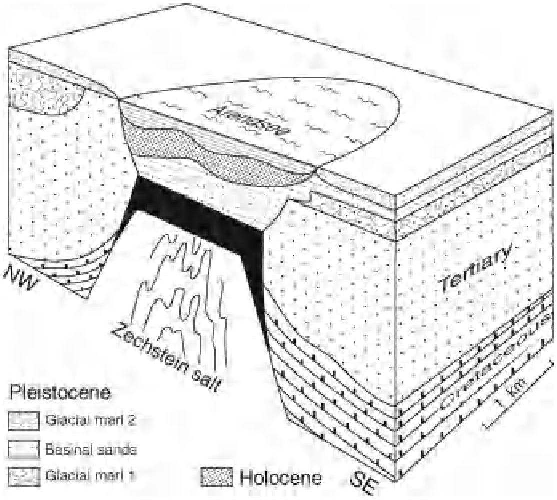

Figure 4.28 Formation of a large collapse lake by Pleistocene and Holocene subrosion of salt at depth. Arendsee Zechstein salt diapir, Northern Germany. With permission from www.schweizerbart.de. A catastrophic collapse event last happened in 1685. Black = caprock.

dated rocks) and the rate of caprock formation. In most investigated locations of Northern Germany, the rate is clearly <1mm per year. At Gorleben, the Holocene rate of subrosion is minimal (0.01–0.05 mm/a), after relatively high rates during glacial periods of the Pleistocene (0.1–0.4 mm/a: Köthe *et al.* 2007), when rivers surged beneath the ice shield. At present, stable and upward-moving diapirs are known in the area. If the rate of diapir rise is higher than the rate of subrosion, morphological elevation is the result.

Dissolution of salt at depth produces nearly stationary saline groundwater and brines (Table 1.4, Chapter 1.4 "Diagenetic Ore Formation Systems"), which display a density stratification. Hydraulic anomalies, however, may cause upflow of saline tongues and the formation of salt springs and licks. In earlier times, salt springs were an important source of salt for humans and wildlife. Today, they are often used for therapeutic baths. Note that little disturbed saline springs and wetlands are biological treasures, which host rare forms of life.

As a by-product of subrosion, the less soluble components anhydrite and clay of the salt rocks form residual enrichment bodies of "cap rock". In this supergene setting, most anhydrite is rehydrated to gypsum. Exceptions occur in highly saline and warm brine pools in lowermost cap rock, which stabilize anhydrite. At higher levels above the salt surface and at lower salt concentration in the groundwater, a breccia of grey, crystalline gypsum is the prevailing rock (gypsum cap rock). Salt rocks with higher contents of argillite, such as the Alpine haselgebirge, develop a residual clay envelope, which is advantageous in mining practice because of low permeability, whereas gypsum cap rock is commonly highly permeable.

Cap rock

Cap rock bodies above salt domes should be carefully studied when a deposit is to be developed, whatever the aim of the operation (Figure 4.20 and Figure 4.26 and 4.28). The thickness of cap rock fluctuates from a few to hundreds of metres. Cap rocks are commonly bedded and preserve a record of the subrosion history. Remember that the youngest beds in the cap rock are the lowest, directly above the salt, and the oldest lie uppermost. Stable isotope investigations of crystal water in neogenetic gypsum provide information about: i) the origin of the water (ocean, or meteoric); and ii) the climatic background of past subrosion. In some cases, brine channels occur between cap rock and the salt, which transport gypsum or anhydrite sand and pebbles. This is one origin of the typical banding of gypsum cap rock. The supergene alteration may affect flanks of diapirs too, forming an anhydrite, clay or gypsum mantle. When hydrocarbons gain access to gypsum cap rock, biogenic sulphate reduction takes place with consequent formation of secondary calcite/dolomite, sulphides and native sulphur (Figure 3.32).

The thickness of the cap rock is a measure for the volume of leached salt rock, if the percentage of anhydrite and clay in the dissolved volume can be estimated. Modifying factors have to be considered, such as glacial erosion or dissolution of gypsum. In the higher parts of gypsum cap rock bodies, percolating seepage and groundwater may produce fissures, pipes and caves, which are filled with water, rubble, sediment or soil, originating by earth falls. Deeper down, cavities are filled with brines. The surface, if exposed, displays all the characteristics of a karst landscape. Because of these properties, gypsum cap rock causes considerable mechanical and physical difficulties for surface installations, drilling and shaft building, which are aggravated by the saline brines that lower the required temperature for the freeze shaft-sinking technology.

Supergene alteration

Supergene alteration of salt rocks beneath the salt surface affects the more easily soluble potassium-magnesium salts. Generally, potassium seams that crop out on the salt surface may display alteration to more than 100 m below the halitite surface. Below the glacial channel filled with sand and gravel at Gorleben, Germany (Figure 4.26), carnallitite was locally found to be altered at 170 m below the top of the salt. This alteration is zoned: K and Mg salts are totally dissolved immediately below the salt surface and only coarsely crystalline residual halite is observed. Red colouring by haematite marks this halite as an equivalent of the K-seam. Kieserite is rehydrated to hexahydrite. This surficial zone is underlain by an interval with sylvite derived from carnallite. If the original carnallite contained kieserite, sylvite is associated with nodules and crusts of schönite (picromerite $K_2Mg[SO_4]_2{\cdot}6H_2O$). This is underlain by a kainite zone, or cap above the unaltered carnallite. Kainite forms either from sylvite + kieserite according to eq. 4.2, or from carnallite + sulphate by abstraction of easily soluble $MgCl_2$.

Supergene formation of kainite from hartsalz:

$$\underset{\text{kieserite}}{MgSO_4.H_2O} + \underset{\text{sylvite}}{KCl} + 2H_2O \rightarrow \underset{\text{kainite}}{MgSO_4.KCl.3H_2O} \quad (4.2)$$

Because kainite is easily processed to KCl fertilizer, it was preferentially exploited in the early days of potassite mining. However, its proximity to water-bearing anhydrite caprock caused a number of crown pillar failures and consequent water inrushes that usually enforced the closure of afflicted mines.

4.4 From exploration to salt mining

4.4.1 Exploration and development of salt deposits

Indications for the presence of evaporitic rocks in the search area are outcrops of gypsum, gypsum karst surface features (e.g. sinkholes), wetland depressions or lakes above rock salt beds, salt licks, ponds and saline springs, and saline biotopes. Salt in groundwater can be a guide to shallow salt rock bodies:

> Because of its higher density, saline water resulting from leaching of buried salt principally collects in deepest parts of basins or of aquifers. Nevertheless, even in lowland plains like Northern Germany, with saltwater usually >200 m below the surface, saline springs are not rare. This is due to forced hydraulic convection, for example by an elevated hydraulic head induced by infiltration from basin-marginal hills. Possibly even more common are barriers that constrict the cross-sectional area of flow, as at Gorleben. Some brines may rise because they were heated at depths resulting in lower fluid density.

Geophysical surveys serve to outline prospective areas of near-surface salt. Gravimetric methods are most efficient because of the density difference between salt and most country rocks (Figure 4.29). Seismic reflection and refraction surveys define depth and borders of the salt rock

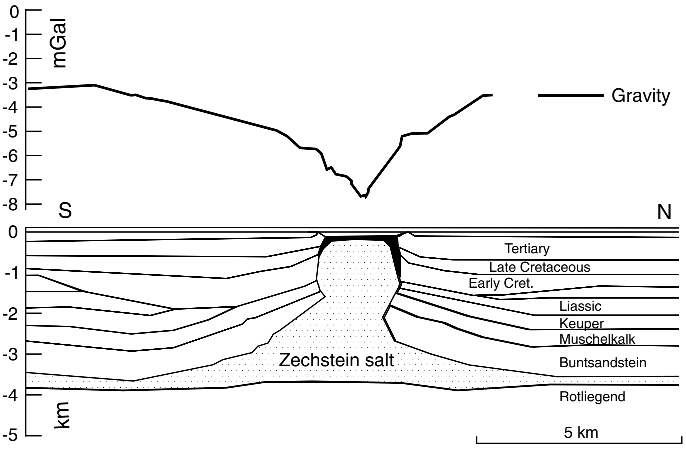

Figure 4.29 Geological profile of the Arendsee Zechstein salt diapir in Northern Germany, and the Bouguer anomaly caused by the low density of the salt body (modified after Gabriel & Rappsilber 1999). Note that gravity is generally expressed in gravity units (g.u.), with 1 mGal equal to 10 g.u.

body. Geophysical data collected for hydrocarbon exploration are valuable tools for assessing salt features. However, the methods described reveal little of the internal structures of a salt body, so that drilling is indispensable. Note that the world's largest potassium salt province in the Devonian Prairie Evaporite Formation of Saskatchewan, Canada, had been found accidentally in the 1940s by petroleum exploration drilling. The same happened later in northern Thailand, but development of the large (10,000 Mt), high-grade, "world-class" carnallite resource is yet to be realized. Resistance by affected communities and the less favourable processing costs of carnallite compared to sylvite are cited as causes.

> Salt's high solubility is a specific problem for drilling. In order to avoid caving, the flush fluid must be saturated with NaCl and if potassites are encountered, in addition with KCl, $MgCl_2$ and $MgSO_4$. Because many salt minerals are transparent, geological drill core logging is facilitated by illumination across the core. For precise lithostratigraphical attribution, down-hole geophysical surveys are standard procedure. Natural gamma radiation, acoustic velocity, density and neutron porosity logging are especially useful. Sampling for bromine analyses should always be included.

Even near-horizontal and little deformed tabular potassite seams may exhibit laterally changing facies of significant economic impact (Figure 4.21), as well as slight undulations or small faults affecting mining. Therefore, preliminary exploration drilling needs a minimum of 2–3 holes per km^2. This is later improved by variography (cf. Chapter 5.3). In order to reach a similar understanding of the internal structure of a salt diapir, many more holes are necessary. Early drillholes are planned to penetrate only 10–20 m into the salt, as the induced hydraulic paths may later cause grave problems in spite of careful plugging. Oriented coring and geophysical logging provide sufficient data for drawing preliminary geological maps and sections. Based on these and as a function of the project's aims (e.g. salt mining, hydrocarbon or waste storage), a minimal number of deep-penetration boreholes are drilled.

Exploration and reserve calculation are supported by basin models. These models integrate data and observations (e.g. lithostratigraphy, structures, geochemistry, isopach maps and diagenetic facies) into a holistic image (Sonnenfeld 1991).

4.4.2 Geological practice of salt mining

For any underground salt mine, detailed geological maps are indispensable. This aims at establishing the local lithostratigraphical standard profile (and deviations from it) and is supported by geochemical (e.g. bromine) and physical parameters. Rational mine planning depends on geological maps, sections and block diagrams. Nature and spatial structure of cover rocks, and their hydrogeology

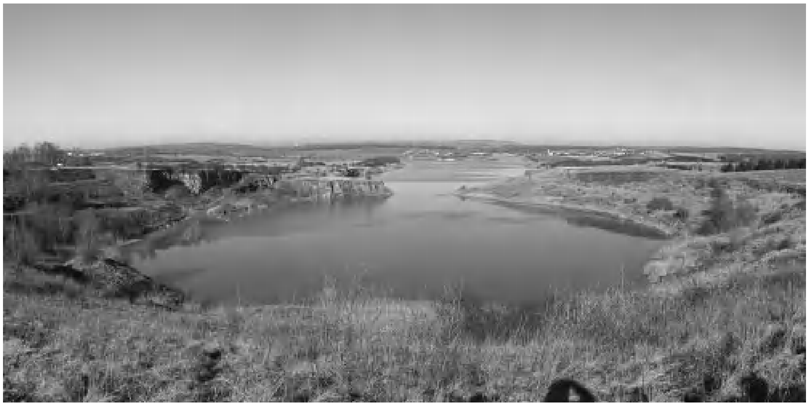

Figure 4.30 (Plate 4.30) Historic salt exploitation by borehole solution at Haraucourt (Meurthe-et-Moselle, France) caused these flooded collapse craters. The deposits are subhorizontal Late Triassic (Keuper) salt beds at shallow depth. Courtesy Christian Wolkersdorfer, CBU, Sydney, Canada.

have to be explored in sufficient detail to understand potential hazards. Inclusions of non-salt rock bodies (e.g. dolomite, anhydrite, clay, basalt) and tectonic disturbance zones deserve special attention, because they may allow inflow of, or hold water, brine and gas. Quality and quantity of potassite seams is illustrated by isopach maps, maps of K_2O grade and of potassite rock facies. Mining blocks, reserves and grades are calculated both by conventional and by geostatistical modelling methods.

Important raw materials exploited from recent or ancient salt lakes include trona, halite, mirabilite/thenardite, borates, gaylussite, celestite, nitrate, zeolites, clay, sepiolite, oil shale and brines. Extraction often relies on pumping brines from lakes or from subsurface aquifers of dry salt lakes (I, Li, Mg, KCl, NaCl). Underground mining of solids is rare (exceptions include trona in the USA and rock salt in the Atacama Desert), and open pits are the standard. Exploration and exploitation of salt lake resources are always based on extensive sedimentological and chemical investigations. Salt lake systems are rather fragile and human interference can cause dramatic changes. In most cases, however, diverting freshwater inflow for other uses such as agriculture is the major impact and mining activities are of little consequence.

Solution mining

Today, rock salt is usually extracted by solution mining. The most common variant is drilling a vertical hole into the salt body, either from underground or from the surface. Fresh water is injected through an outer tube into the drillhole section where salt is exposed, whereas brine is pumped from near the bottom of the growing solution cavern. Critical geological parameters include nearby non-salt rock bodies (affecting safe enclosure and the mechanical stability of the cavern), the presence of potassites (causing irregular and unstable parasitic cavities) and the risk of surface subsidence and collapse (Figure/Plate 4.30). Solution caverns are developed and widened to design size and shape by skilful management of freshwater inflow and brine level. Progress is mainly controlled by sonar echometric surveys. Specific problems occur in the presence of carnallite, because the system easily converts to incongruent solution resulting in solid-phase sylvite. Using heated fluid may alleviate this problem. In contrast to carnallite, sylvite-rich potassites are more easily dissolved. In Canada and USA, borehole solution mining of sylvite salt reaches depths of more than 1400 m.

The establishment of storage caverns for oil, gas, compressed air and industrial waste follows the same principles.

Hard rock mining

Hard rock mining of rock salt is characterized by the excavation of large underground chambers that are separated by pillars. Cavern dimensions of 70 by 50 m (horizontal) and 25 m (vertical) are not rare. As mentioned earlier, potassium salt rocks display a lower mechanical stability and the supporting pillar surface may have to be larger than the excavated rooms (Figure 4.22). Engineering geological and rock mechanical methods are essential tools to control the stability (Jeremics 1994). In most cases, long-term stability is aimed for, including the time after mine closure. Collapse is a hazard because it may lead to ingress of unsaturated formation or meteoric waters from outside and to damaging earthquakes. Therefore, the calculation of pillar dimensions of salt must include stress state and properties of country rocks, not only salt rock mechanics. In order to minimize hazards for the local population and for groundwater protection, near-surface underground openings of a salt mine may have to be backfilled with salt tailings and fines.

Among the greatest hazards in underground mining of salt are **water and brine inflows**. It is important to distinguish between waters sourced: (i) from host rocks of the salt deposit; (ii) brine pockets within the salt rocks; and (iii) mining-induced moisture (e.g. condensation).

Only inflows from the country rocks, such as carbonates, sandstone, shale and cap rock are dangerous. As a function of their hydraulic parameters and structural position, these rocks may be conduits for formation water, shallow groundwater or surface water. In all three cases, salt along flow paths will be dissolved, so that plugging is extremely difficult or simply impossible. Typically, the flow rate increases steadily from an initial trickle and if the country rocks are profuse aquifers (as in the case of most gypsum caps), the mine will have to be abandoned. The only efficient precaution is to design the mine in a way that a thick salt pillar is left intact adjacent to the country rocks. A rare example of successful plugging was reported from a salt mine in Austria (Figure 4.20). The most efficient counter measures are screens of sealing injections.

Brines that are occluded by salt rocks may suddenly drain into mine openings or drillholes. This can be damaging but is mostly a nuisance. If larger brine-filled cavities are expected, geophysical detection and forward drilling should be employed as a precaution. It is important to regularly measure brine flow rate, temperature, closure pressure and its chemical composition. Main questions concern: i) the brine's origin; and ii) its ability to dissolve salts occurring in the deposit. Halite-saturated brine, for example, is perfectly able to dissolve potassium salts, potentially causing grave damage. Isotopic tracers of inflowing water of unknown origin should always be examined (including $^{87/86}$Sr, ^{18}O, ^{2}H and ^{3}H; Botrell *et al.* 1996). This will be the only reliable base for judging hazard and risk. Mining-induced moisture (e.g. condensation from ventilation air, drilling fluid, backfill humidity) is usually harmless but may accelerate deformation.

Gas in salt mining

All salt rocks contain a mixture of gas including N_2, O_2, hydrocarbon gas, CO_2 and H_2S. Usually, this gas occurs in trace concentrations and presents no risks. Higher contents that are easily diluted by the ventilation air flow may locally occur in all mines. Some mines, however, experience sudden inflow of hazardous gas volumes. H_2S is toxic at concentrations above 0.007 vol.% in air, highly concentrated CO_2 and N_2 are asphyxiating and CH_4 is flammable and explosive. Both slow degassing and sudden gas-driven blow-outs or "outbursts" can be dangerous. High-pressured gas trapped in salt rock "explodes" from the working face into mine openings, filling them with salt grit and gas. This is very similar to coal outbursts (Guan *et al.* 2009). One of the largest salt outbursts on record took place in 1953 in the potassium mine at Menzengraben in Germany, where a volume of $\sim$700,000 m^3 CO_2 and $\sim$65,000 t of salt were suddenly fluidized. Advance recognition of gas-rich salt bodies is not simple but is possible with a combination of geophysical methods and forward drilling. Proximity to clay, anhydrite and basalt rocks is a general indicator. Destressing gas-charged salt rock by drillholes and safety management measures for personnel are recommended precautionary procedures.

Disturbance of the groundwater system

Disturbance of the groundwater system around salt mines is hazardous because any change of the hydraulic potential (e.g. by pumping) may draw unsaturated water to the salt and intensify dissolution (subrosion). Resulting earth falls and general subsidence may induce costly damages. Drillhole disposal of waste brines from salt processing plants (e.g. $MgCl_2$) must target deep saline, not freshwater aquifers. Salt mining waste retention facilities include surface dumps of anhydrite/gypsum, halite, clay and slimes that result from potash ore beneficiation. This may cause release of solutes into surface or groundwater. Permissible salt concentrations of emissions must not be exceeded. Note, however, that in regions with profuse precipitation, local brine seeps are quickly diluted. Natural and man-made saline springs may be ecologically singular and valuable sites, because they support rare and specialized life forms.

Closure of mines

Closure of underground salt mines is foremost a decision between "dry" and "wet" variants. Overall, sealing a dry mine (Fuenkajorn & Daemen 1996) against water inflow is probably preferable to controlled flooding. A dry mine that is mechanically stable and absolutely water-tight is safe. In Northern Germany, hundreds of salt mines that operated over a century ago were flooded, either intentionally or by accident. The first modern monitoring programme of a flooding process was applied at the Hope mine near Hannover in 1984. It confirmed that water in the shaft (and presumably in the mine) very soon reached a stable density layering with: i) slightly saline fresh water at the top; ii) a saturated NaCl brine; iii) NaCl-KCl brine; and iv) a lowermost body of $MgCl_2$-NaCl-KCl brine (Wolkersdorfer 2008). The safety of flooded mines may be compromised by slow strength loss of salt pillars, changing water levels, inflow of fresh water that causes renewed solution and convective brine overturn because of temperature differences. Sudden earth falls are the main hazard, with highest incidence in the immediate perimeter of old shafts.

4.5 SUMMARY AND FURTHER READING

Solutes derived from continental weathering are concentrated in terrestrial salt lakes and in the oceans, mixed with matter vented by hydrothermal activity. In hot and dry climate zones, intensive evaporation induces precipitation of salt minerals and rocks. The available ions and the degree of evaporation determine the precise paragenesis of salts to form. Economically significant salts derived from ocean water include chlorides of Na, K and Mg, sulphates of K and Mg, and minor components such as bromine. Continental salt lake resources overlap with the first but are particular by producing boron, I, Li, Mg, K and Na chloride, Na and Li carbonate, and Na, Mg and Sr sulphate. Salt lakes and brines are an important source of environmentally useful metals such as lithium and magnesium.

Only in the last 600 million years of earth history, salt rocks are common, due to profound changes in ocean water state and composition. Chemical changes of ocean water continue into recent geological time. By definition, salt rocks are easily soluble in water. Yet, salt rocks in the upper crust tend to be well preserved for geological time periods. One explanation for unexpected survival in basinal sediments is the prevalence of saline pore fluids derived from seawater evaporation instead of undersaturated water. Salt rocks function as seals for moving subsurface water, petroleum fluids and natural gas. Salt rocks conserve geologically ancient life; viable bacteria and archaea have been isolated from Permian salt, more than 250 million years old.

Formation and preservation of large salt formations require a favourable physical setting. Arid climate, a wide sea cut off from the main ocean and a narrow channel providing continuous inflow is the basic model. Deep and shallow basins are distinguished. Evaporation lowers the water level in the saline sea, resulting in steady-state ocean water inflow. In time, concentration levels for halitite and finally potassite precipitation requiring near-dryness are reached. Intermittent or final isolation may lead to total desiccation.

Coastal solar salt operations are a tangible model of marine salt formation, although with one important difference. Salt production aims at pure products. Therefore, K-Mg bitterns are pumped from the halite pans before bittern salts precipitate. In nature, however, back-reaction with previously formed solids is the rule and is part of earliest salt diagenesis. Like sediments, salt rocks change with increasing temperature and overburden pressure, and survive into metamorphic sequences, although rather in chemically anomalous rock compositions than as actual salt beds.

Salt rocks are very ductile compared with carbonates, sulphates, shales and sandstones. Small pressure differences cause salt to flow from higher to lower potential. This results in many exotic salt intrusions distant from the source bed. The most flamboyant products of salt flow are the diapiric salt domes – salt pillars vertically rising to the surface from the source bed through pierced hanging wall rocks. Unstable inverted density layering is the physical driver for diapir formation. Salt diapirs are a rich source of benefits for humans, because they provide near-surface exploitable halite and potassite, sulphur and oil, deep natural gas and safe storage for liquid fuels, methane, wind energy and hazardous waste (cf. Chapter 5.5 "Deep Geological Disposal of Dangerous Waste").

To francophone readers I suggest Rouchy & Blanc-Valleron (2006) for a discerning introduction to evaporites. A profound and detailed description of evaporites is offered in the two books by Warren 2006, 1999). Warren is also the best source to study the relations between hydrocarbon deposits and evaporites. The volume about salt diapirs in Iran, by Jackson *et al.* (1991), is full of wonderful images and offers a framework for the mechanics of diapirism. *Applied salt rock mechanics* by Jeremics (1994) still is the only complete treatment of the subject, but should be supplemented by reading papers such as Kwon & Kim (2005). *Salt, a world history* (Kurlansky 2002) is illuminating, comprehensive and entertaining.

PART III

The Practice of Economic Geology

Economic Geology Principles and Practice
Metals, Minerals, Coal and Hydrocarbons – Introduction to Formation and Sustainable Exploitation of Mineral Deposits, Walter L. Pohl
© 2011 Walter L. Pohl. Published 2011 by Blackwell Publishing Ltd.

CHAPTER 5

Geological concepts and methods in the mining cycle: exploration, exploitation and closure of mines

Mente et malleo ("With intelligence and hammer" – the venerable motto of geology)

Synopsis

Civilization depends on freely available raw materials. To assure supply, ores and minerals extracted by mining must continuously be replaced by new reserves. Beyond satisfying the present demand, an additional requirement results from the growth of the world's population and its increasing standard of living. This implies that exploitable reserves are identified and prepared for mining, out of previously assumed but not sufficiently known, or undiscovered mineral resources. Commonly, this activity proceeds in several stages, from reconnaissance exploration for potential mineral deposits (target generation), through detailed follow-up exploration (investigation of targets), to evaluation (development of a new mine, or final rejection). Stages may be omitted, for example in cases of companies buying prospective mineral occurrences, or when new orebodies in active mining districts ("brown fields") are discovered and developed.

The secure provision of metals and minerals depends not only on geological and technical availability but also on economic, institutional, societal and legal conditions. In an ideally free and well regulated market economy, raw materials supply would never be a problem. Indeed, it is wonderful how well market forces work in our real world, although many regions are far from free. Conflicts and crises surrounding the petroleum and gas markets, however, are a warning that national and international political efforts to ensure essential supplies should never cease. Of course, the same is true for scientific and technological work to provide needed metals and minerals.

Economic Geology Principles and Practice
Metals, Minerals, Coal and Hydrocarbons – Introduction to Formation and Sustainable Exploitation of Mineral Deposits, Walter L. Pohl
© 2011 Walter L. Pohl. Published 2011 by Blackwell Publishing Ltd.

All activities that serve mineral raw materials supply, from exploration to extraction, including mine closure and reclamation, must be optimized according to the three criteria:

1 environmentally sound;
2 sustainable; and
3 socially compatible.

The same criteria rule the provision of underground waste repositories, mines that are specifically designed for deep disposal. Waste storage mines are constructed in analogy to natural toxic and radioactive rock bodies that have been conserved for many million years.

This chapter presents essential geological concepts and practices concerning the life-cycle of a mine, from reconnaissance exploration to closure.

5.1 ECONOMIC CONSIDERATIONS

Economic extraction of minerals requires that all costs (for exploration, detailed investigation, development, mining, processing, credit financing, taxes, environmental mitigation and closure) are covered by returns (gross revenue from selling mine products) and that reasonable profits remain for investors (Wellmer *et al*. 2007). This basic rule may be disregarded, but always at a cost to somebody. Overriding reasons may concern the national economy (e.g. the need of foreign currency income), socio-economic conditions (employment), or the wish to retain a national supply and knowledge base for certain strategic metals and minerals.

Possible returns are conditional on the price of metals and minerals. Normally, prices are found by free interplay of supply and demand, for example on the London Metal Exchange. This applies to a number of metals including gold, lead and tin. Strong price fluctuations are a problem that severely complicates the financial planning of mines. The risk is particularly difficult for new mining projects and is aggravated by the long lead time (often 5–10 years) from the decision to open a new mine until the first products can be sold. Other mining sectors typically conclude long-lasting contracts with reliable price agreements (e.g. many industrial minerals). Because the competition is lively, mining companies hardly ever have the market power to dictate prices. Some states, however, have a near-monopoly on specific raw materials, which may disquieten purchasers (e.g. European Commission 2010).

Apart from prices, the size of reserves, the geological situation, beneficiation costs, geographical situation, infrastructure, social conditions and political risk are important parameters of the feasibility of a mining operation.

Resources and reserves are the primary factor of the viability of a mine. The terms describe estimated mass and quality of ore, and imply a lower (resources) or a higher degree of confidence (reserves). Hardly any obstacle will prevent exploitation of large and rich deposits, whereas low-grade or small occurrences cannot be mined, even if all other parameters are optimal. Average or minimal (so-called "cut-off") grades for various ores are provided in Chapter 2 of this book. In Table 5.1, order-of-magnitude estimates illustrate the smallest total metal content of a viable deposit and an appropriate ore grade.

The mass of metal contained is essential information, because the investment for establishing a mine must relate favourably to returns from selling the metal (as contained in concentrate). Even small mines commonly require an initial

Table 5.1 Minimal total metal mass and corresponding metal concentrations in ore ("grade") for economic ore deposits

Iron	1 000,000 t Fe	60% Fe
Manganese	30,000 t Mn	45% Mn
Copper	50,000 t Cu	3% Cu
Tin	5000 t Sn	1% Sn
Gold	1 t Au	0.001% Au

investment of ~50 million US $. Very large operations, such as giant copper or iron mines, cost well over 1000 million US $. Therefore, already at the stage of exploration, figures like those of Table 5.1 are important guidelines.

In addition, reserves are an essential control on the optimal output capacity of a mine expressed in tonnes/day or per year. Most mines operate for a period of 3 to 30 years. Based on the same reserve figure, high annual production shortens the life of a mine compared to low extraction rates. The search for an optimal rate is carried out by calculating costs and returns for different production rates. The rate offering the highest overall profit is the best choice, but may be moderated by other considerations.

Exceptionally large deposits ("giants", Laznicka 2006), such as several porphyry copper deposits in Chile, are economically most attractive. Overall, large-scale mining costs less per unit of metal produced, even if ore grades (e.g. kg copper per tonne) are relatively low. Very large reserves allow investment in technologies that reduce costs of all mining and processing activities. Open pit operations are more economic than underground mines. The result is that small underground mines need higher grade ore (e.g. 3% Cu) compared to giant open cut mines, which are profitable at low grades (e.g. copper porphyries with 0.4% Cu but reserves of several hundred million tonnes). Yet there are many small mines that are quite profitable. An interesting development is the trend of co-producing several minerals from the same deposit. In this case, unit costs of extraction are balanced by returns from more than one product. Examples are co-production of clay, sand and lignite in large open pits, or tantalum, kaolin, feldspar and quartz sand from pegmatite.

The **geological situation** controls expenditure from early field investigations to mining and final mine closure. Form, spatial arrangement and variability of orebodies, as well as mechanical and hydrogeological properties of ore and host rocks, influence profitability. Simple unfaulted bodies of a mineral resource (e.g. a coal seam), the quality of which hardly changes with distance, is economically very favourable. This allows for wide-spaced drilling (saving costs) as a base for reserve estimation and mine planning. After an initial phase of adjustments, operating conditions during the period of exploitation remain stable for a long time. The contrary applies to strongly deformed (e.g. metamorphic sulphides) or to highly discontinuous orebodies, including many metasomatic ores such as lead-zinc sulphide in carbonate rocks. Ore deposits of this kind always cause higher costs, from exploration to production. Highly fractured or hydrothermally altered host rocks may have unfavourable and therefore costly mechanical and hydraulic properties. High inflow of water leads to rising costs for pumping that have caused the economic collapse of innumerable mines. However, a good grade of the ore allows mining even under extremely difficult conditions as at Lihir, with ore temperatures of ~100°C and the ever-present danger of geothermal outbursts.

The **feasibility of beneficiation** is an important precondition for the economic success of a mineral resource project (Table 5.2). Factors that control processing, concentration and the resulting recovery include grain size, type of intergrowths, and the physical characteristics of ore and gangue minerals. Contents of minor and trace elements in the concentrate may be advantageous (e.g. gold in copper ore) or very costly and a useless liability

Table 5.2 Mine to metal – five important terms

Run-of-mine ore is commonly a mixture of ore and gangue minerals, often diluted with by-breaking host rocks (e.g. copper ore with 1.2 wt. % Cu)

Ore dressing (or processing) describes mine-site operations that reduce waste (gangue) and enrich ore minerals to "concentrates" of metals (e.g. a copper concentrate with 62 wt. % Cu), which can be sold to smelters

Metal recovery is the ratio between the mass of metal contained in a specific *in-situ* volume of ore and in concentrate produced from this volume

Tailings describes the useless part of ore removed by processing (say ~95% of the above-mentioned copper ore) consisting of gangue minerals such as silicates, carbonates and quartz; safe tailings storage is an economic and environmental liability; because of ever-improving processing methods, older tailings may be today's ore

Metallurgical processing isolates metals from concentrates (by smelting, electrolysis, leaching, etc.) and refines them to marketable grade or purity. Mines are rarely large enough to warrant the establishment of mine-site metallurgical operations, but exceptions do exist (e.g. Mt Isa, many gold mines).

such as arsenic. Gold ore with large gold grains (free-milling gold) can be processed with cheap gravity methods. The extraction of fine-grained gold usually involves cyanide leaching, which imposes considerably higher costs for plant and operating expenses. Also, the use of cyanides enforces environmental monitoring and risk reduction measures that imply further costs. Sub-microscopic gold in sulphides induces an additional processing step, that is roasting (oxidizing) the ore before leaching (Milham & Craw 2009). The flue gas from roasting kilns may have contents of SO_2, As, Sb, Hg and other volatile elements, which cannot be emitted into the environment. Clearly, when all these costs have to be covered, gold content per mass unit of ore must be much higher in the last case compared with free-milling gold.

The geographical situation comprises parameters such as remoteness, morphology, altitude and climate, which are complemented by infrastructural factors including accessibility by road and railway, free availability of, or competing claims on land, water and energy. Social conditions are increasingly the crucial factor for the decision to launch an exploration project or a new mine. Social aspects include the density of population, its acceptance of, or aversion to industry, the availability of a suitable work force and environmental regulations. All the above combined dictates the minimum size and grade of an ore deposit. The long-term political stability will be the final test for a project – a high risk of doubtful security, financial, fiscal and legal conditions imposes a very different business model compared with expectations of long-term stability and peace.

5.2 THE SEARCH FOR MINERAL DEPOSITS (EXPLORATION)

In my view the greatest value is added by the geologist who starts with nothing other than some ideas and goes out into the desert and finds an orebody
J.K. Ellis (Chairman of BHP Australia, 1998)

5.2.1 The pre-exploration stage

Every search for mineral deposits starts with collection and interpretation of existing data concerning the geological, metallogenetic and mining background. Geological maps are indispensable sources because to the expert, they reveal potentially occurring deposits. Terrestrial volcanic centres with advanced hydrothermal alteration, for example, may host gold mineralization. Small, late-phase granite cupolas can have extractable contents of tin and tantalum. Volcanic playa lakes are favourable settings of zeolite, borate and lithium deposits. Many exploration successes, even most recent ones, were based on a knowledgeable re-interpretation of public geological maps and a careful reading of the explanatory notes. For example, an incidental reference to an alunite occurrence on Lihir Island, Papua New Guinea, in a mapping report induced a search for epithermal gold mineralization. The results were overwhelming, as Lihir is now one of the largest gold concentrations in the world, with a total gold content exceeding 1300 tonnes:

> Allow me here a plea for geological mapping: It is regrettable that the relevance of systematic geological mapping for a reliable supply with minerals and metals, but also for the rational management of land, water and the environment is not more widely recognized. In industrial nations the mining industry may be expected to finance such services, although within limits. In developing parts of the world, however, geological map coverage is often poor and dated. Although they are very useful, relatively low-cost satellite images and geophysical coverage cannot replace the experienced geologist's groundwork. Good geological maps are a significant factor for the transition from agricultural to industrial societies. This is demonstrated by the first geological map ever made, by William Smith in England, and published in 1815, for entirely practical reasons (in this case canal building).

The choice of target regions for exploration is often based on large-scale geological models that use information published in the scientific domain. Regions with favourable conditions are selected, such as large sedimentary basins with synsedimentary tensional tectonics and well-developed reduced and oxidized compartments (prospective for base metals), or belts of late-orogenic highly differentiated felsic intrusions (rare metals such as tin), or metamorphic massifs affected by large shear zones (gold). Large deposits are typically formed where the geological structure is generously proportioned.

Seafloor exploration for metals and minerals is still rare, except for aggregate and submerged coastal placers of diamonds and cassiterite. With rising prices of minerals, deep-sea resources including phosphorite, sulphides, gold and manganese nodules gain economic attraction. Several seafloor mining projects are currently developed, for example gold-rich volcanic massive sulphide deposits at ~2000 m water depth offshore of Papua New Guinea and New Zealand.

Geological concepts may be supplemented by formal quantitative mineral resource assessments (Singer & Menzie 2010). The pre-exploration desk study presents a concept of the proposed future work, including geoscientific, logistic, legal and financial components, as well as previews of the physical and social environment. Remember, however, that exploration is not only a scientific and technical enterprise but foremost an investment. As with any investment, potential rewards and risks must be clearly defined and continuously updated (Kreuzer *et al.* 2008).

In 2008, a total of 14,400 million US$ was spent on exploration for non-ferrous metals and industrial minerals (excluding coal), but expenditure dropped to 8400 millions in the global financial crisis year of 2009. Most is dispensed in work near existing mines and very little in unspecified "grass roots" exploration. About one-fifth of the annual budget is destined for gold exploration. Significant funds are spent in the search for base metals, iron ore, coal, uranium, diamonds and platinum group metals. A small part of the total exploration budget targets other metals and minerals.

5.2.2 Geological exploration

> *About thirty years ago there was much talk that geologists ought only to observe and not theorize. How odd it is that anyone should not see that all observation must be for or against some view if it is to be of any service!*
>
> Charles Darwin (Letter from the Beagle,
> September 18, 1861)

Geological concepts and methods are the indispensable base for any exploration project (Kreuzer *et al.* 2008, Kelley *et al.* 2006, Bevier 2005, Sillitoe 1995, Glasson & Rattigan 1990). Geology is both the starting point and the unifying frame for merging and analysing data resulting from a wide variety of methods. Today, standard practice in mineral exploration is to analyse data in two dimensions using GIS (maps and cross-sections in Geographic Information Systems) and to identify targets by empirical means. Increasingly, three-dimensional and four-dimensional (three-dimensional plus time) modelling is employed by explorers for integrating multiple datasets, such as geology, geophysics, geochemistry and drillhole data, including concepts such as past fluid flow. This approach emulates the "petroleum systems" method (cf. Chapter 7) in the oil and gas industry. Three-dimensional numerical models of coupled fluid flow and deformation, for example, assist in orogenic-gold exploration (Potma *et al.* 2008). Resulting models can be visualized and tested. Based on these tools, predictive capabilities are considerably advanced.

Due to increasing mineral raw materials demand and prices, exploration frontiers are shifting to deeper and lower grade mineralization in more remote locations. Worldwide, new discoveries will increasingly be of this nature.

Fundamental strategies of mineral exploration include:

- exploring large areas systematically, either searching for all possibly occurring metals and minerals ("grass roots exploration") or, more commonly, for only a few attractive resources;
- selecting specific regions for their geological resemblance to known metallogenetic provinces or districts;
- investigating districts hosting known mineralization and mines, motivated by improved geological understanding that suggests the presence of undiscovered ore;
- exploration for specific raw materials (e.g. marble of high whiteness) is guided by the search for locations with geological properties that resemble commercially viable deposits.

Several spectacular exploration successes of the last decades illustrate different strategies:

Olympic Dam, Australia: A large Neoproterozoic volcano-sedimentary basin in South Australia was selected for its resemblance to base metal-rich basins in Africa and North America. The presence of satellite-image lineaments and copper-depleted basaltic rocks similar to the Keweenawan rift in Michigan was felt to be especially encouraging. The reward was the discovery of the giant Cu-Au-U deposit near Olympic Dam (c.f. Chapter 2 "Copper", "Uranium").

Mt Isa, Australia: This is one of the largest base metal deposits of the world (c.f. Chapter 2 "Lead and Zinc", "Copper"). Geological research motivated exploration along strike of the major structure that controls ore at Mt Isa. This resulted in the discovery of several deposits and the development of new mines such as Hilton, George Fisher and Valhalla, recalling the motto "if you wish to hunt elephants, go to elephant country".

Skaergaard, Greenland: The benefit of applying new concepts to well-known geological sites was demonstrated by geologists who investigated the platinum potential of large layered mafic intrusions based on genetic models of the Bushveld deposits. Many new discoveries were made, but one especially remarkable (though still undeveloped) Au-Pt deposit was found at Skaergaard (c.f. Chapter 2 "Gold"). Previously, this intrusion had been described in all petrology textbooks and was the site of much scientific work, including the discovery of sulphide immiscibility (Wager *et al.* 1957).

Voisey's Bay, Canada: Even today, some mineral deposits are found by accident. In 1994, diamond prospectors in eastern Labrador, Canada happened upon a small gossan. Trace metal contents and its location within olivine-gabbros suggested an exploratory electromagnetic survey. The results revealed the presence of sulphides, which are now known to be part of the Ni-sulphide deposit Voisey's Bay. Total published resources are 137 Mt at 1.59% Ni, 0.85% Cu and 0.09% Co (Naldrett & Li 2000, Naldrett 2004).

Lisheen, Ireland: The location of Irish base metal deposits is known to be controlled by stratigraphy (usually the base of Early Carboniferous stromatolitic Waulsortian limestones) and tensional synsedimentary growth faults (c.f. Chapter 4 "Lead and Zinc"). A combination of geochemical and geophysical methods was used to scan areas underneath overburden reaching a thickness of 300 m above the prospective horizon. This depth had been hidden from earlier explorers. Suggestive anomalies were soon found and examined by diamond drilling. Only the seventh drillhole revealed ore. In 1994, 22 Mt of ore at 11.5% Zn, 1.9% Pb and 26 g/t Ag were proven and a new mine was born.

Earlier, the discovery of new deposits was pursued by geologists, miners and enterprising non-professionals who scanned the land systematically for traces of ore or other indications of mineralization such as gossans ("prospecting", Figure 5.1; Locke 1921). Promising indications were examined by trenches, shafts and adits, usually with the aim of immediate exploitation. Meanwhile, however, the chance to discover hitherto unknown ore outcrops on the land surface is very small, because early prospectors worked quite thoroughly. Today, large buried deposits are targeted and the search is guided by geological concepts. Modern exploration is characterized by multi-professional teams and systematic methodology (Kreuzer *et al.* 2008, Sillitoe 1995, Magoon & Dow 1994). Of course, experienced individuals with exceptional metallogenetic knowledge may still be the key to success.

The essence of geological concepts is descriptive and genetic models of mineral deposits (Cox & Singer 1986). Appropriate geological, geochemical and geophysical parameters that characterize targeted deposit types are combined to build "exploration models". In practice, locations are sought that display anomalous indicator parameters within the ordinary geological background. These locations are called "anomalies", or "prospects". Exploration projects commonly expose many anomalies that have to be ranked for prospectivity and investigated in more detail. Experience shows that most anomalies are found to be of no economic interest. Exploration teams strive for early rejection of barren prospects (negatives) in order to avoid useless expenses. Reliable identification of good prospects is essential, whereas both false negatives and false positives must be avoided:

The distribution of formerly exploited copper deposits and mineralizations in the Cloncurry-Mt Isa district provides an instructive example. Apart from the world class Mt Isa deposit, 262 sites produced >10 t, 70 >100 t, 14 >1000 t and only 6 including Mt

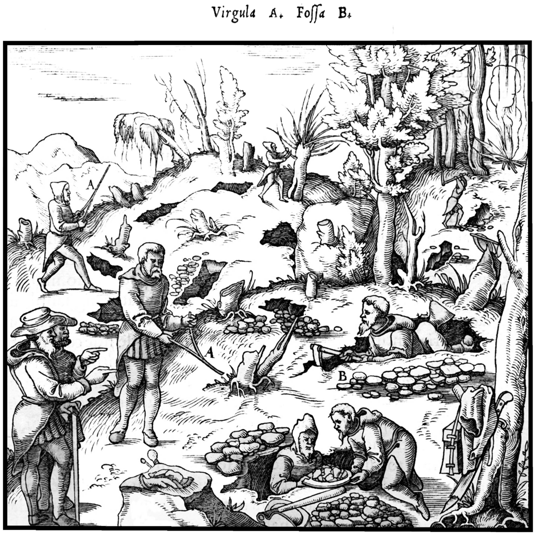

Figure 5.1 Prospecting in Europe during the 16th century (Agricola 1556). Courtesy Thomas Hofmann, © Geological Survey, Vienna, Austria. Agricola explains that the divining rod (*Virgula* A) is useless and that only physical indications of hidden ore should be regarded, such as ore fragments in trenches (*Fossa* B) and streams, stressed vegetation, indicator plants and tiny temperature differences of the soil, which are made visible by frost and dew.

Oxide (Figure/Plate 1.56) yielded >10,000 tonnes of copper (J.H. Brooks in Glasson & Rattigan 1990). Some of the tiny mines may have enriched a lucky artisanal miner, but would never support an industrial mining operation. The essence of exploration is to identify potential mines among the large number of anomalous locations.

The strategy of exploration programmes directs work from the initial regional scale to smaller areas, with costs increasing as reconnaissance methods are succeeded by detailed investigations, and the pursuit of resemblance to models changes to collecting hard data. Different metal and mineral deposits require distinct approaches, but a general pattern can be sketched as follows:

1 Reconnaissance exploration. Reconnaissance aims at rapid and low-cost sorting out of prospective and unprospective parts of an area. Typical methods used include interpretation of published geological maps, satellite images and aerial photographs, aerogeophysics, heavy (indicator) minerals and geochemical sampling of stream sediments (e.g. for diamond exploration), and other regional geochemical surveys. On-the-ground geological reconnaissance and verification mapping, and on-site inspection of prospects are indispensable.

2 Detailed follow-up exploration. In this phase, prospective locations and anomalies (prospects) are examined to a degree that allows a preliminary appraisal of their potential. Essential data include the geological setting, contours and nature of the suspected orebody. Useful methods include detailed geological mapping, geochemical and ground-based geophysical investigations, shallow trenching and some drilling. This work will rapidly expose the low potential of most locations. Note, however, that in some famous cases perseverance, in spite of disappointing first drillholes, was well rewarded (e.g. Olympic Dam). Retained prospective locations are submitted to a prefeasibility study, which presents the case of potentially profitable exploitation by comparison with mines working similar deposits.

3 Evaluation. Evaluation aims to provide comprehensive data that allow the final decision to develop a mine or to defer development. In this phase, drilling is intensified and first mine exposures are made in order to provide large samples for semi-industrial scale processing trials. Results are indispensable for the assessment of metal or mineral recovery and of product quality. Access to ore and host rocks facilitates determination of rock mechanical and geohydrological behaviour. Together with drilling and assaying results, these data serve to estimate reserves (and resources) of the deposit. The next step is realistic planning of the future mine and its processing plant and infrastructure. At this stage, investment, operating costs and the probable future income can be calculated. Assessment of environmental and social costs is possible. Of course, evaluation is done by a team of professionals. Evaluation of a mining project concludes with the compilation of a *feasibility study*. A feasibility study is the required base for a decision to develop a mine and for an investor (e.g. a bank) to finance the project.

Note that wherever exploration is likely to lead to new mining activities, environmental studies must be taken up as early as possible (Plumlee & Logsdon 1999b). It would be a costly error to defer this work to the last stages of developing a new operation.

5.2.3 Geological remote sensing

The term "remote sensing" refers to techniques that are used to measure and interpret the interaction between distant matter and electromagnetic energy. Some of these techniques (e.g. electromagnetic methods) are commonly assigned to geophysics. Geological remote sensing is mainly based on natural electromagnetic waves radiating from the Earth's surface. Main observation platforms are aeroplanes and satellites. Interpretation focuses on geospatial features (Sabins 1999, Drury 2001). Photogeology was the first remote sensing method widely employed and remains a useful tool. A new dimension of remote sensing opened up in 1972, however, when the first satellite images (Landsat ERTS-1) became available. Today, Landsat TM and more recent satellites producing high-resolution images are standard exploration and mapping tools.

Only part of the electromagnetic spectrum between ∼0.3 μm (micrometre) and 50 cm wavelength is useful for remote sensing. This span comprises visible light (0.38–0.78 μm), near and middle ("thermal") infrared, and microwaves (Figure 5.2). Radiation emitted from the surface of interest is recorded. "Passive" remote sensing uses reflected sunlight, whereas "active" methods are based on reflected induced radiation (e.g. by radar equipment mounted on aircraft and satellites).

Different minerals, rocks, soils and plants reflect radiation in specific wavelengths, which is obvious considering our subjective colour perception of visible light (from short-wave violet to long-wave red). By dividing the spectrum between ∼0.3 and 20 μm into more than 200 distinct spectral bands ("hyperspectral mapping", e.g. NASA's Earth-observing satellite Hyperion), specific reflection characteristics are recorded. Based on comparative spectral data at different scales, from space to ground truth in the field and laboratory measurements, the method allows identification of minerals and rocks, different

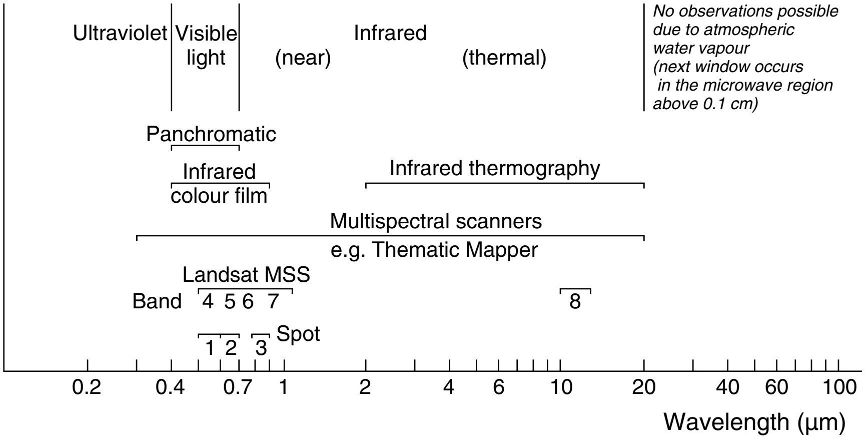
Ultraviolet
Visible light
Infrared
(near)
(thermal)
No observations possible due to atmospheric water vapour (next window occurs in the microwave region above 0.1 cm)
Panchromatic
Infrared colour film
Infrared thermography
Multispectral scanners
e.g. Thematic Mapper
Landsat MSS
Band 4 5 6 7
8
1 2
3
Spot
0.2
0.4
0.7
1
2
4
6
10
20
40
60
100
Wavelength (μm)

Figure 5.2 Wavelength regions in the lower electromagnetic spectrum frequently used in geological remote sensing. Note that the infrared region extends to a wave length of 0.1 cm, but this long-wave IR heat radiation cannot be observed from space because of absorption in the atmosphere (resulting in the greenhouse effect).

soils, types of hydrothermal alteration (Mauger *et al.* 2007), gossans and the discrimination of healthy and stressed plants. From 20–1000 μm, atmospheric interference is too strong for reliable interpretation. Radar bands used in Earth observation include 3 (X), 5.6 (C) and 25 cm (L). These waves penetrate clouds and vegetation and provide morphological images. Synthetic aperture radar (SAR) sensors excel by high resolution. Radar is most valuable for mapping topography that reveals geological and man-made structures (e.g. the paired system of TerraSAR-X and TanDEM-X launched in 2010).

The foundation of modern remote sensing was the development of optomechanical radiometers in the years after 1960. Before, only analogue photographic films with high resolution were used. The new technology allowed building *multispectral scanners(MSS),* which excel in spectral resolution but have relatively poor spatial resolution. These systems record several sections ("bands") of the electromagnetic spectrum synchronously for the same target area ("pixel"). Landsat pixels cover a surface area of 30 × 30 m, but modern satellites have a much better resolution. Reflection intensities for each band are digitally registered. For better evaluation, ground surveys with the new generation of portable spectrometers are invaluable. The instruments produce data across the full spectral range (350–2500 nm, visible light to infrared) at very high resolution and allow mineralogical characterization of soil, rocks and alteration zones which occur in the survey area.

MSS technology and hyperspectral mapping are also possible from aircraft, but only satellites provide nearly total coverage of the Earth that is available to the general public. Much used are the workhorses of the LANDSAT series (1–7). The French SPOT series offers better resolution (10 × 10 m pixels) and stereographic capabilities. The US-Japanese ASTER (*1999) satellite carries 5 bands in the short-wave infrared (SWIR) range, enabling detection of different clays, carbonates, sulphates and other minerals. Typical products offered are:

- paper images (e.g. black-and-white of single bands, or colour-coded composites);
- electronic copies of the digital dataset of one scene; and
- variously processed data.

One Landsat scene covers an area of 185 × 185 km. In dry and arid lands, geological evaluation with simple visual methods provides excellent insight into large-scale features, which are best visible in near infrared images. However, the full potential of satellite data can only be achieved by combining all available spectral bands in digital processing. This allows enhancing contrasts, linear structures, gossans and hydrothermal alteration, correcting topography and the production of artificial stereo pairs (similar to aerial photographs). Digital image processing combined with GIS makes it possible to combine results of remote sensing with topographic (e.g. digital elevation models, DEMs), geophysical and geochemical information.

In geologically well explored areas, satellite images have mainly assisted in the recognition of large-scale structures (lineaments) that defied earthbound mapping. After the first elation, it was soon realized that large structures rarely control the location of ore deposits. Yet, tectonic control is frequent and aids rational exploration. Geologically less explored regions of the Earth, possibly making up 75% of the land surface, can be economically and quickly surveyed with satellite data. Resulting maps at 1:50,000 to 1:1000,000 support an efficient and effective exploration programme. TM data allow easy recognition of gossans and of hydrothermal clay, alunite and mica zones (Ruitenbeek *et al.* 2005). Famous successes include the discovery of large copper porphyries in northern Chile (Collahuasi and Ujina; Sabins 1999). More recently, remote mapping at a scale of 1:10,000 became feasible, because digital panchromatic and colour images of IKONOS (1999) and QUICKBIRD (2001) have a resolution as small as 0.6–4 m. Space photographs in cartographic quality taken from manned platforms are available for certain regions of the Earth.

The geological interpretation of aerial photographs is employed for smaller areas that are to be mapped in great detail. Most countries offer a full coverage of black-and-white photographs at scales between 1:20,000 and 1:50,000. Repeated runs many years apart may be available and are very useful for retracing the landscape evolution, which is essential for environmental work. In addition, different vegetation, moisture and illumination may reveal subtle features. In most cases, panchromatic film and high-resolution cameras provide excellent pictures. Lateral (30%) and longitudinal overlap (60%) allow stereoscopic viewing and mapping. Very precise (orthorectified) topographic and geological maps are prepared from aerial photographs. Amended by groundwork, these maps are an excellent means for detailed exploration. In special cases, colour or infrared colour films are employed for better recognition of certain features (e.g. hydrothermal alteration zoning).

Optimal results of remote sensing are obtained in arid and semi-arid regions that have little soil and vegetation cover. Humid landscapes yield little geological information, apart from structures. Vegetated hydrothermal alteration cannot be mapped, although anomalous heavy metal contents may be discernible by stressed plants because their reflection deviates from that of healthy ones.

5.2.4 Geochemical exploration

A first modern overview of distribution and mobility of elements in the Earth was written by V.M. Goldschmidt and posthumously published (Goldschmidt 1958). More recently, Holland & Turekian (2003) edited a voluminous and comprehensive presentation of geochemistry. Although not directed at practicians, both are valuable sources for applied geochemistry, such as exploration and environmental investigations.

Geochemical methods of exploration are based on the observation that most ore deposits are surrounded by zones (halos), which deviate chemically from ordinary host rocks. Chemical deviations may be expressed by enrichment or depletion of certain minerals, elements, isotopes and by other systematic differences. Various ore deposit types display characteristic halos, which can be found by analysing samples of rocks, soil, plants, water, soil gas (Figure 5.3) and of sediments in streams and lakes. Graphical and statistical processing of geochemical data helps to define locations that may indicate ore ("geochemical anomalies"). The scale of investigations, for example the density of sampling, varies from geochemical mapping at the continent scale (1 sample/ 5000 km^2) through an intermediate mesh (1 sample/300 km^2, Reimann *et al.* 2007) to very detailed local sampling of, for example, soil above a prospective geophysical anomaly.

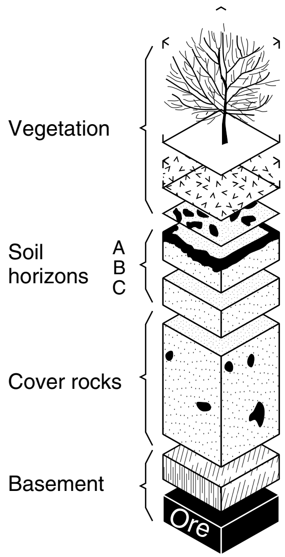

Figure 5.3 The variety of geochemical samples that can be collected and analysed to assist in the search for buried ore deposits.

Geochemical exploration results in a large number of analytical data. Statistics are used to discern anomalous and therefore potentially prospective results, such as simple frequency plots (Figure 5.4) and more advanced methods (Carranza 2008). Concentrations of elements in unmineralized rock bodies always fluctuate around a mean value (background). Samples with higher concentrations (above a certain threshold) may indicate subtle or very clear geochemical anomalies. Of course, anomalies must be considered within their petrological context. Ultramafic bodies, for example, within metasediments must cause Ni and Cr anomalies that have no prospective value. In such cases, data have to be sorted by source rocks into

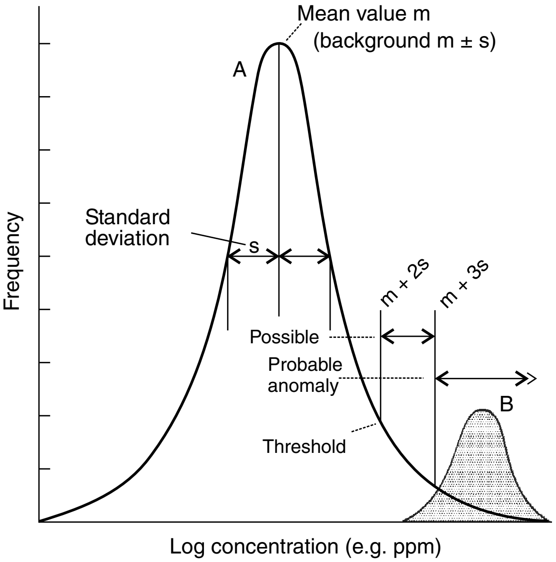

Figure 5.4 Schematic diagram of the frequency distribution of two different populations of geochemical data. The distribution of geochemical data is typically lognormal. Population A may be considered as an ordinary geological background (e.g. the serpentinized mantle section of an ophiolite), population B as expression of a mineralized zone such as chromite in serpentinite. Note that the concentrations which mark background and threshold are not necessarily defined as shown in the plot.

different populations, which are then evaluated for anomalies indicating possible mineralization. In the same project, a lower threshold can be used for regional exploration (e.g. finding mineralized zones) and a higher one for locating the best targets for drilling.

Primary geochemical anomalies

Primary geochemical anomalies are formed as a by-product of the processes that concentrate ore. Geochemical halos enveloping the actual ore are caused by the "primary dispersion" of elements. When, for example, hydrothermal solutions deposit ore in a vein, some of the fluid permeates into wall rocks causing different alterations (cf. Chapter 1.1 "Hydrothermal Host Rock Alteration"), which include chemical changes. About the central Cu-Mo ore zone, porphyry copper ore deposits display shells and caps of elevated Pb-Zn, Au and an extensive outer halo of more mobile elements such as As, Ag, Sb, Hg, Tl, Te and Mn. These halos are three-dimensional, whereas others are essentially two-dimensional, such as those associated with sedex deposits, which are restricted to the same stratigraphical horizon. Primary trace element halos considerably enlarge the targets of geochemical exploration. Consequently, a higher sampling distance can be set, reducing costs. Also, as demonstrated by the halos surrounding copper porphyries, associated and more mobile elements ("pathfinder elements") may be more suitable for finding prospective locations than the elements concentrated in ore.

Secondary geochemical anomalies

Secondary geochemical anomalies are formed by processes that acted on the deposit after its formation. Most frequent are chemical consequences of near-surface mobilization, weathering and erosion, which transfer elements from the orebody or its primary halo to till, soil, plants, groundwater and soil gas. Erosion moves particles and dissolved matter into streams, where traces may be detectable at great distances from the source. This is why stream sediment sampling is a most effective method of reconnaissance and regional exploration. The post-formation redistribution of elements from an ore deposit is called "secondary dispersion". In the processes that cause secondary dispersion, the variable mobility of elements is of great significance. Elements with a higher mobility under surficial conditions enlarge the anomalous zone. A project targeting polymetallic deposits of Pb, Zn and Cu, for example, would use mobile Zn for regional sampling with a low density, whereas dense sampling of Zn-anomalies for Cu and Pb should reveal the drilling targets (Figure 5.5).

The mobility of elements in secondary dispersion is strongly influenced by factors including the nature of rocks, climate, vegetation, relief and groundwater flow. The complex interaction of these natural factors has been called "landscape geochemistry" (Fortescue 1992). Nearly ubiquitous influence of human activities, such as industry, agriculture and building, overprints the natural state. Geochemical exploration projects must consider the possible presence of perturbance by "anthropogenic dispersion".

Effective distinction between prospective and non-significant geochemical anomalies is desirable. To this purpose, non-geochemical data such as the geological setting are consulted. Based solely on the geochemical data, the contrast between background and the anomalous data is employed. High contrast is considered to affirm the significance of an anomaly. Controls of the contrast include the primary metal contents in ore compared to host rocks, the mobility of the elements investigated and dilution with barren material. Because contrast is so important, most geochemical work in exploration starts with an orientation phase, which is expected to identify the most suitable sample material and other constraints for the main phase work. For unconsolidated soil, stream and lake sediments, contrast is a function of the chosen grain size, the soil horizon (depth) and the extraction method. If sufficient contrast of target element concentrations cannot be reached, possible pathfinder elements should be tested.

Geochemical exploration programmes

Geochemical exploration programmes may be designed for the reconnaissance of large areas or for detailed investigation of prospective locations. Regional sampling is done along roads and water courses, whereas sampling grids are typically designed for local investigations. In the first case, sampling distances are measured in kilometres, in the second rather in metres. The orientation of the sampling grid is best chosen to support geological mapping, geophysical surveys and later drilling. Orientation sampling serves to select suitable field methods and the most appropriate analytical methods. This allows final planning of the main phase of the sampling programme, including logistics.

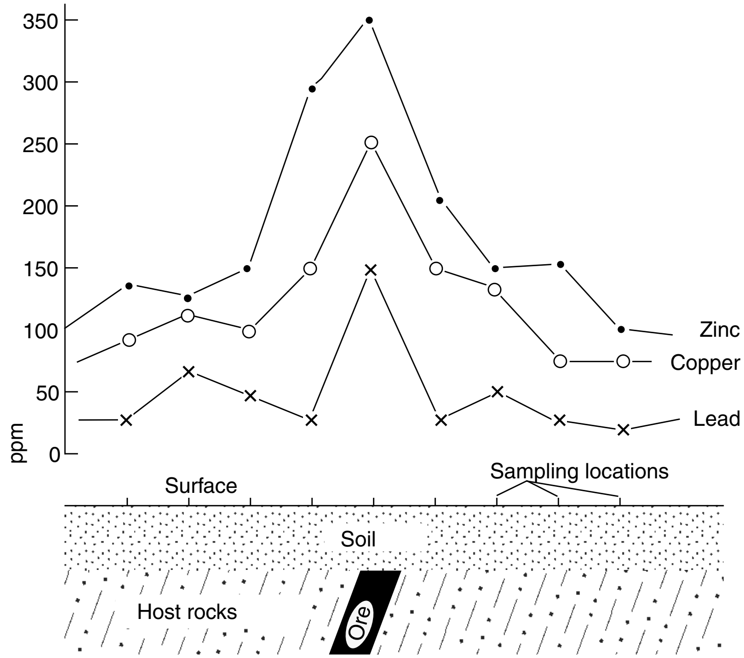

Figure 5.5 Differential secondary dispersion of zinc, copper and lead in soil above a tabular base metal orebody in siliciclastic host rocks. The profile is drawn along a geochemical sampling, or grid line.

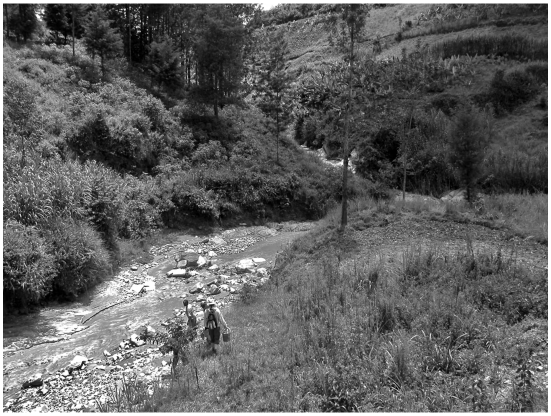

Figure 5.6 (Plate 5.6) Environmental stream sediment and water sampling (including *in-situ* determination of pH, T and Eh) in the Gatumba tin-tantalum mining district, Rwanda.

Stream sediments

Stream sediments (Figure/Plate 5.6) are extremely efficient means to discover geochemically anomalous zones in large regions and with low sampling density, but only if a well-developed drainage system is present. Where suitable water courses are absent, remarkable results are achievable with wide-spaced soil samples (e.g. Australia), till and lake sediments (Canada, Finland). The sediment sample from an active river bed is considered to represent an average of its upstream watershed. If mineralization or its dispersion halo is exposed in the drainage area, chemical traces must occur in the sample. Because coarse material dilutes trace element concentrations (and thus lowers the contrast), fine-grained stream sediments (clayey and silty mud) are preferred. Samples are sieved in order to submit a homogeneous fraction for analysis (often −80 mesh corresponding to −180 μm). Samples for indicator mineral investigations (McClenaghan 2005) are collected parallel with the stream sediments. In specific cases, such as expected loss of fine-grained gold, or environmental work aiming at volatile pollutants, freeze-sampling is employed (Petts *et al.* 1991). Organic substances and Fe-Mn ooze in surface waters adsorb dissolved metals more than clay minerals. Geochemical results from such samples have to be treated apart from common siliciclastic sediment. Water pH, T and Eh should be measured at each sample site, because large variations strongly influence the mobility of elements. Interpretation of data should always consider the geochemical characteristics of rock types occurring in the watershed as a geogenic background. If a reference to common average contents of elements is intended, one of the worldwide clay rock standards is more appropriate than the crustal average (Reimann & de Caritat 1998, Gromet *et al.* 1984). Fine-grained sediments should only be compared with material of similar grain size.

Soil sample geochemistry

Soil sample geochemistry calls for detailed orientation work, because success depends on sufficient understanding of soil layering and genesis (Butt *et al.* 2000), which control element mobility (cf. Chapter 1.2 "Supergene Ore Formation Systems"). Often, present distribution patterns are a legacy of several superposed soil formation phases. Autochthonous soils must be discerned from transported ones. Allochthonous soil is of little use in exploration, although exceptions do occur: In Western Australia, nickel concentrations are anomalous in the B-horizon of transported soil above buried Ni-mineralization. This totally unexpected feature is explained by nickel transfer from deep roots into leaves and from rotting litter back into the soil. Many elements are enriched in the B-horizon of a regolith profile, but there are important exceptions. Ferriferous nodules or pisoids, which are common in areas of lateritic cover, can be useful geochemical guides to ore in bedrock (Smith *et al.* 2000, Smith & Singh 2007). In South Australia, even pedogenic calcrete is sampled for locating subcropping gold-quartz veins (Mauger *et al.* 2007).

Geochemical exploration with rock samples

Geochemical exploration with rock samples, or selected minerals is based on specific geological-petrological models. Examples include the regional sampling of granites in order to locate fertile intrusions, the discrimination of prospective and barren porphyries by analysing copper in biotite, and the identification of rare metal pegmatites by muscovite analyses. Also, rock geochemistry is useful for tracing orebodies in complex structural settings. Certain hydrothermal alteration zones (cf. Chapter 1.1 "Hydrothermal host rock alteration") are easily recognized and help to point development adits or drillholes towards ore. Isotope investigations complement data on elemental distribution, mainly at a more local scale. Whole rock stable isotope mapping around centres of epigenetic mineralization, for example, often reveals very clear anomalies that are useful for finding orebodies (Hoefs 2009, Holk *et al.* 2008). Remember that with all solid materials, the mass of a representative sample is a direct function of the grain diameter. The rules of sufficient sample mass and careful diminution, homogenization and sub-sampling must be strictly followed (cf. *Geological Mapping and Sampling*; Gy 1992, Pitard 1993).

Soil air and atmospheric air sampling

Soil air and atmospheric air sampled near the surface may contain traces of Hg, H_2S, SO_2 and metals, which are possible keys to buried sulphide and gold deposits, and radon may indicate uranium ore (Klusman 1993, Hale 2000). Although technological innovation in this field is intense, persuasive case histories are not widely known and more common geochemical methods seem to suffice. It appears possible, however, that future search for deep orebodies buried below today's commonly shallow targets between the surface and ~400 m depth will profit from these methods.

Biogeochemical exploration methods

Biogeochemical exploration methods ("phyto-exploration") have a demonstrated success rate but are not equally often used as stream sediments and soil samples. Plant roots "sample" soil and soil water, and thus transfer geochemical information to their organs above the ground. Samples are usually taken from live plants. Orientation surveys assist to find suitable plant species and because of organ-specific accumulation, favourable parts of individual plants. Possible choices include leaves, twigs (that must have the same age), or bark. Sampling is relatively cheap because drilling and digging is not needed. Regional and local anomalies of metals and pathfinder elements can be ascertained.

Water samples

Water samples collected from springs, wells, boreholes and streams are rarely useful for exploration. Dissolved metal contents in water are usually very low (in the ppb range) and vary strongly with pH and Eh. This makes interpretation difficult. Yet, regional datasets on ground and surface water chemistry may provide important clues to several deposit types. Of course, water geochemistry is always an essential part of environmental monitoring of mine sites (Ficklin & Mosier 1999).

Analytical methods of exploration geochemistry

Samples are dried, sieved, sub-sampled and ground until 100% pass an 80 mesh (180 μm) screen. For analysis, a small aliquot (0.2–2 g) is usually prepared in aqueous solution. Partial solution by weak acids, which only dissolve weakly adsorbed elements, is one common procedure. The other is complete dissolution by aqua regia, or a multi-acid mixture combining hydrofluoric, hydrochloric, nitric and perchloric acids at low temperatures and pressures. The choice is guided by the speciation of the elements of interest in the sample. If the main interest concerns metals weakly adsorbed on clay and organic matter, partial solution is recommended. For determination of elements sited in the crystal lattice of minerals, such as barium in muscovite of metamorphosed distal sedex exhalites, total dissolution is indicated. Methods of *sequential elution (sequential extraction)* provide an understanding of metal speciation in soil, lake and stream sediment samples: Total metal content of a sample is the sum of several species occurring:

- as exchangeable ions;
- carbonates;
- adsorbed to Fe-Mn oxy-hydroxides;
- in sulphides; and
- silicate minerals (Rao *et al.* 2008).

Defining the most suitable dissolution variant for a specific project is one of the aims of an orientation survey.

Geochemical laboratory equipment for exploration and environmental studies is nearly identical (Crock *et al.* 1999). The workhorses of instrumental analysis are inductively coupled plasma-atomic emission spectroscopy (ICP-AES) and inductively coupled plasma-mass spectrometry (ICP-MS). Other useful methods include X-ray fluorescence (XRF), instrumental neutron activation analysis (INAA), gamma-activation analysis, atomic absorption spectroscopy (AAS) and electrochemical means such as specific ion electrodes.

In the field and in mines, portable X-ray fluorescence (XRF) analysers are increasingly used for on-site data acquisition. Colorimetric and other simple field methods remain useful, but deliver semi-quantitative data for elements (e.g. As, Cu, Zn, Mo, W, Ni) and ions (e.g. SO_4^{-2}). They are chosen when quick results are more important than accuracy, for example in remote regions. A decision to use such methods should only be made after trials with preliminary samples and consultation with an experienced analyst.

Analytical data in exploration geochemistry need not in all cases equal the absolute element content in a sample, or in other words, *accuracy* may not be essential. Deviations of ±30% from the absolute figure (e.g. an international laboratory standard) are tolerated, if the relative error remains within narrow limits. In contrast, excellent reproducibility of results, that is high *precision,* is absolutely required. This is the base for any data evaluation, especially if the contrast between background and anomalies is small. In all geochemical programmes, *error control* is a fundamental aspect. Errors may be introduced during sampling, sample processing and transport, and in the laboratory. It is good practice to repeat at least 10% of sampling. Analytical errors are revealed by inserting the same sample or a standard of known composition repeatedly into the series (Arbogast 1990). Control by another laboratory is advisable. Based on a collection of control data, it is possible to calculate total error margins and the confidence interval (Taylor 1997).

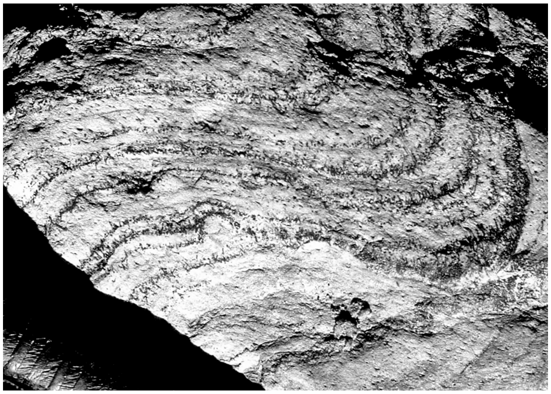

Figure 5.7 Tourmalinization is common around pegmatite and granite-related ore. Near cassiterite vein deposits at Rutongo, Rwanda, the growth of black tourmaline needles in quartzite was controlled by folded bedding planes and a weak schistosity.

Indicator minerals

Indicator minerals are increasingly used as a complementary tool to geochemistry. Indicator minerals are characterized by elevated density (>2.8 g/cm^3) and a good preservation potential in the weathering environment (McClenaghan 2005). Of course, their application in diamond prospecting has a long tradition. Other deposit types, however, also display specific indicator minerals. Porphyry copper systems, for example, shed gold, rutile, tourmaline, garnet, jarosite and alunite. Many rare metal deposits are enveloped by tourmalinization halos (Figure 5.7).

Presentation and interpretation

Data resulting from geochemical exploration should always be presented in maps, because the search is first of all for spatial variation. Statistical calculations are a useful complement, if geology and structure are not too diverse. Point-symbol maps (Howarth 1983) represent the basic tool (similar to Figure 3.1), which can be amplified by wavelength filtering to produce a map of residual anomalies (Ludington *et al.* 2006). Principle component analyses of multi-element data and plotting the factor distribution may provide valuable guides for regional exploration. The correlation of geochemical results with geology, geophysics and topography is investigated using GIS (Carranza 2008). Examples for complex presentation and interpretation can be found in geochemical atlases which provide data at different scales.

Environmental geochemistry

Geochemical work is not finished with the discovery and preliminary quantification of a potential ore deposit, but reaches a second climax during detailed investigations and preparation of the feasibility and environmental impact studies. The pre-mining environmental state of the future mining area must be documented, including natural and anthropogenic characteristics of bedrock, regolith, surface and groundwater. Establishing the geochemical landscape (Fortescue 1992) is a central task. Considering this requirement, costs of re-sampling may be saved by imposing high accuracy standards on all exploration geochemistry. High resolution, multi-media and multi-element mapping is an important part of environmental impact studies, which are the foundation of operational and administrative decisions throughout the life of a mine, including closure.

The methods of environmental geochemistry differ little from its application in exploration. In fact, investigations and interpretations of non-mining anthropogenic dispersion might profit from the study of the highly developed methods and accumulated experience of geochemical exploration. One example concerns the unreflected reporting of heavy metal concentrations without reference to natural (geogenic) boundary conditions- such as background and variance.

5.2.5 Geophysical exploration

The foundation of geophysical exploration methods are the varied physical properties of ore and gangue minerals, fluids and rocks (Ellis & Singer 2007, Keary *et al.* 2002). Passive geophysical survey methods use natural potential fields (e.g. magnetism, gravity). Active methods rely on interaction of induced artificial fields with the subsurface (e.g. electrical conductivity, seismics). "Inversion" designates the computation of geophysical models purely from measurements. These models are inherently ambiguous. Useful interpretations are only obtained when independent constraints are available, for example geological models, drillhole and petrophysical data. Petrophysical properties of rocks and ore are the critical link between geophysics and geology.

Geophysical methods with a depth penetration to several hundred metres below the surface are commonly employed in the search for solid mineral deposits. Geophysics extend the validity of geological and geochemical data to this depth, which currently limits the economic exploitability of most minerals and ores. However, the reason for using geophysics is not always depth penetration. Geophysical investigations of near-surface ores such as coastal placers, for example, contribute valuable continuity to deposit modelling, for example between drillholes. Also, identification and mitigation of mining-induced environmental problems may profit from geophysical surveys (Ackman 2003, Rucker *et al.* 2009).

In cases of strong incentives to extend the search to greater depth, which common surface-based geophysical methods cannot reach, magnetotelluric methods (MT) are used. Another approach was developed in Canada, where base metal deposits such as those of the Sudbury District are explored to more than 3000 m depth: Deep drillholes are sited on geological evidence to penetrate a prospective rock body, which is scanned by downhole geophysics for signs of ore.

Geophysical surveys complement other exploration methods at all scales. Regional geological and geochemical work is supported by geophysical data measured from aircraft and helicopters. Frequently used aerogeophysical methods include magnetics, electromagnetics, radiometry and gravimetry. For detailed and more local exploration on the ground, many more methods are available that allow a high density of observations at higher accuracy and improved validity. Borehole geophysical surveys result in the highest resolution of data (Ellis & Singer 2007), especially in conjunction with geological, physical and chemical core logging results.

As with geochemical surveys, geophysical methods reveal a *background* that is characteristic for ordinary rocks of an area and distinctive *anomalies*, which illuminate physical contrasts. The magnitude of an anomaly is a function of: i) the contrast between host rocks and the anomalous material; ii) the size, spatial orientation and shape of the anomalous body; and iii) the depth from the surface. The last is essentially due to the general law of inverse-square attenuation of a geophysical signal as a function of distance. Identification and interpretation of geophysical anomalies are often quite challenging, not unlike weak geochemical indices.

'A considerable number of geophysical exploration methods are available for mineral exploration and each method exists in several variants. The specific choice is a function of the geological and exploration model of the targeted deposits (Shen *et al*. 2008), of general conditions such as remoteness, climate and human land use, and of the costs. Methods that require the placement of electrodes in the soil, for example, cannot be deployed in permafrost regions. Electrolyte-rich highly conductive soil and groundwater in semi-arid lands limits the depth penetration of most electrical methods. Some well established geophysical methods in exploration include the following (Milsom 1996).

Magnetometry

Measuring the magnetic field is relatively straightforward, with portable instruments on the ground, borehole probes and instruments for aerial surveys (Airo *et al*. 2004). Various types of magnetometers are available, including "scalar" sensors that measure total magnetic field and "vector" sensors providing directional data. The latter include the traditional fluxgate and the new supersensitive SQUID (Superconducting Quantum Interference Device) magnetometers. The intensity of the magnetic field is measured in nanoTesla (previously gamma; 1 nT equals 1 gamma). The Earth's total field varies from ~30,000 (equator) to 65,000 nT (poles). Regular diurnal variations of the field are enforced by currents in the ionosphere and reach 10–30 nT. Solar activity, such as spots and flares, cause short-term irregular disturbances ("magnetic storms"), with amplitudes that may surpass 1000 nT. Field work must be suspended during magnetic storms. The magnetic properties of rocks differ by several orders of magnitude. Exploration tends to look for strong deviations from the background field, which are commonly caused by minerals of high susceptibility, such as magnetite, pyrrhotite and maghemite. Haematite has a very small susceptibility and many iron ore deposits do not produce magnetic anomalies. Magnetite and sulphide ore deposits can be located with magnetic surveys, but also kimberlites and other rocks that host magnetic minerals. Airborne magnetic surveys benefit geological mapping, especially in regions with thick cover of soil, moraine sheets or water (on land and offshore). One of the most relevant tools for detailed mapping are measurements of the anisotropy of magnetic susceptibility (ASM; Mezeme *et al*. 2007). Results of magnetometry are presented in maps and in sections with distance as horizontal and the magnetic signal as vertical axis.

Electric current methods

Conductivity (Siemens per metre, S/m) or its reciprocal, resistivity (Ohm), are determined by measuring voltages associated with electric currents flowing in the ground, either induced or natural. Rocks and minerals have widely varying resistivity, with lowest values displayed by clay, saline pore water, acid rock drainage, sulphide ore, native metals and graphite, whereas common rocks and minerals have low conductivity. This contrast is used for exploration. Electric current methods rely on placing electrodes in the ground, commonly two metal stakes (e.g. steel rods) for passing current into the subsurface and two non-polarizing electrodes for measuring the induced potential in volts. Several time-tested arrays of electrode layout are possible. Moving cables, electrodes and equipment from one point (traverse station) to the next makes these methods laborious and slow. They are typically used for local and detailed investigations.

- *Spontaneous potential methods (SP)* rely on electrochemical processes caused by weathering orebodies that straddle the groundwater table. The conductive material concentrates the flow of oxidation-reduction return currents, producing a negative anomaly at the surface. Typical targets for SP-surveys are sulphides, graphite and magnetite. The method is very cheap and simple; only two non-polarizing electrodes, cables and a voltmeter of very high impedance are needed. Today, SP surveys are little used in exploration, because methods such as EM (see below) more reliably detect orebodies. However, SP is useful for locating flowing groundwater (e.g. in a leaky tailings dam) by an effect that is termed "streaming potential". Large-scale natural potentials in the earth are investigated with *telluric* and *magnetotelluric methods (MT).* Practical application finds MT mainly in the hydrocarbon industry. Hybrid-source magnetotelluric systems are capable of measuring electrical resistivity and the magnetic field in great detail, over depth ranges of a few metres to greater than one kilometre. This method is successfully employed for exploration of coal, petroleum, uranium and other metals (Shen *et al.* 2008).

- *Electric resistivity surveys* require the four electrodes described above. Two different aims are pursued:
  1 "Resistivity profiling" is in principle a tool for mapping the shallow subsurface. In this variant, the distance between electrodes is not changed and the whole array is moved across the country, allowing recognition of gravel, sand and clay, massive orebodies, faults and steep rock contacts.
  2 "Resistivity sounding" utilizes the larger depth penetration of currents as electrodes are set farther apart. The method reveals the vertical sequence of different rocks but only works well if interfaces between beds are largely horizontal. Resistivity surveys have been "mechanized" for hydrogeological mapping in Denmark by placing the electrodes on a long trailer pulled by a tractor (Thomsen 2004). Improvement is also possible by placing electrodes in boreholes. Resistivity methods help to locate massive sulphide bodies, acid rock drainage (Rucker *et al.* 2009), graphite, salt water intrusions on the coast, water-filled sand and gravel aquifers and indirectly, alluvial tin and gold placers.
- *Induced polarization methods* (IP) are much utilized in exploration because they are able to detect sulphide ore minerals (e.g. of Cu and Mo in porphyries) and other conducting minerals (graphite flakes in gneiss), which are disseminated in a matrix with high resistivity. Induced polarization is activated by passing a pulse of current via two electrodes into the ground. This charges electronically conducting particles, not unlike capacitors. When the activating current is terminated, discharge from the particles produces currents, voltages and magnetic fields. The transient voltage spike (polarization effect) is measured at the surface via two non-polarizing electrodes. It is a measure of the number, or more precisely the total surface, of conducting particles in the ground. A higher signal indicates more intense mineralization. IP systems work either in the frequency domain or the time domain; frequency domain equipment is generally lighter and more portable. Different electrode configurations are possible. Note that clay minerals display "membrane polarization", which is the cause for most IP effects encountered in the field. IP is successfully employed to a maximum depth of ~600 m.

Electromagnetic methods (EM)

EM are very often utilized in geophysical exploration. EM works without a physical contact to the ground (no electrodes), which is an advantage for use above ice, water, swamps, frozen or arid ground. Many different surveying systems are available, for aerial and surface deployment. Today, even highly conductive surface zones such as salt lakes can be penetrated with equipment like MagTEM (magnetic field sensor transient electromagnetic technology). The principle of TEM is that an alternating current is passed through a square loop of cable, which induces an electromagnetic field in the ground. Decaying currents in the subsoil are measured with a receiver coil or a magnetometer. If the primary field encounters a good conductor, "eddy" currents flow and this produces a secondary electromagnetic field. Its strength and relative phase compared with the primary field indicate possible ore. Typical targets are kimberlites, sulphides (e.g.

Ni-Cu in Voisey's Bay, Canada), graphite (as a guide to unconformity deposits of uranium) and water-bearing faults. Increasingly, natural electromagnetic fields are measured concurrently with induced fields. The magnetotelluric method (MT) is a passive electromagnetic technique used for exploring the conductivity structure of the Earth from tens of metres to a depth of several hundred kilometres. Main applications are in hydrocarbon exploration.

Gravity methods

Gravity methods in exploration are based on detecting variations of the Earth's natural gravity field. The measure of gravity is acceleration expressed in gravity units (1 g.u. = 1 μm/s^2; earlier, named after Galileo, 1 Gal = 1 cm/s^2 or 1 mGal = 10 g.u.). Modern instruments (gravimeters) reach an accuracy of 0.1 g.u., which is approximately a 100 millionth of the Earth's field. Gravity gradiometers are designed to measure gradients of geological gravity changes. Surface gravity at a specific location is a function of the rocks underneath, of the distance from the Earth's centre of gravity, of latitude and relief. Because one metre difference in height of the gravity station causes a change of 3.086 g.u., elevation relative to the theoretical sea level reference surface must be determined to an accuracy of ±3 cm. Surveying is usually the most costly part of gravity operations. Geological factors cause relatively small changes of gravity. Therefore, the above-mentioned effects on readings must be removed by calculations, including the tidal drift of gravity (±1 g.u.). The corrected, "residual" or "extended" Bouguer anomalies, and in some cases gravity gradients, are presented in maps and in profiles. Interpretation of shape, density and depth of bodies, which cause the measured gravity pattern. are derived by calculations based on geological models.

Gravity can be determined by airborne systems, on the ground, in the sea and in underground mines. Regional gravity maps serve mainly science and hydrocarbon exploration, but are increasingly utilized in exploration for minerals and metal ores (Hildenbrand *et al.* 2000). Orebodies of solid minerals are distinguished from ordinary rocks by greater (chromite, sulphides) or smaller density (kimberlites, salt diapirs: Figure 4.29). One of the notable achievements of gravity exploration in the recent past was the discovery of the base metal deposit Neves Corvo in the Iberian Pyrite Belt (cf. Chapter 2.2 "Copper"; Leca 1990).

Radiometric methods

Radioactive decay of uranium, thorium and potassium, and of certain daughter nuclides of the first two releases gamma radiation, which is measured with portable instruments on the ground, with equivalent systems on board of aeroplanes and helicopters (Airo *et al.* 2004) and with borehole probes. Scintillometers or spectrometers are usually employed. The second use energy sills of γ-radiation to distinguish between the three elements and to estimate their concentrations. Measurements of γ-radiation in the field are snapshots of a random process and readings vary, even with the same instrument. Geologically-sourced radiation forms peaks superimposed on a background of scattered cosmic (mainly solar) and terrestrial radiation. The high geochemical mobility of K and U in surficial environments, compared to the nearly immobile Th, is the motive for the common use of ratios (U/Th, K/Th) in maps. Application is primarily in the search for uranium, but numerous other utilizations have been found. Determination of gamma-radiation is a very convenient and low-cost tool to distinguish rocks, from regional mapping to borehole logging. It facilitates recognition of potassium salts in halitite, beach placer horizons in sand and phosphorite in marine sediments. Potassium-rich rocks, such as certain granites or zones of hydrothermal K-alteration, can be detected. Aerial and ground use, however, are restricted to areas with little soil cover, because most radiation on the surface comes from the uppermost 10–50 cm; deeper sources below soil remain undetected. Read more about radiation surveys in Chapter 2.5 "Uranium".

Tomographic methods

Remarkable new developments in exploration geophysics include tomographic methods, which produce spatial images of geological bodies, for example ore between the surface, drillholes and mine tunnels. Various means of excitation are used, including acoustic, sonar (ultrasonic), radar, radio and seismic waves. Tomography allows larger distances between exploration adits and drillholes, and considerably lowers costs. In addition, the risk of overlooking orebodies is reduced. A convenient method of near-surface reconnaissance is *ground penetrating radar* (GPR), which maps interfaces of materials having different electrical properties, elucidating bedding planes, moisture and clay content, voids and man-made objects. Applications include imaging the internal structure of dunes, beaches, fluvial deposits, karst, buried channels and lake deposits (Baker & Jol 2007). *Multifunctional geophysical systems* are designed to measure several physical parameters at the same time or in rapid sequence. Seismic methods are rarely used in hard-rock mineral exploration but are the workhorse of hydrocarbon search. Yet, successful location of uranium orebodies with three-dimensional seismics is reported from the Athabasca Basin, Canada. Coal and lignite seams are routinely scanned by seimics in great detail, in order to guide mechanized mining. The future of exploration geophysics will be ever greater resolution and increasing depth penetration in order to locate the next generation's mineral deposits.

Geophysical borehole surveys

Most geophysical methods have been adapted for drillholes in mineral resources exploration with the typically small diameters (~1/10th compared to petroleum and gas drilling, for which they were originally developed; Ellis & Singer 2007(Figure, 5.8); cf. Chapter 7.4 "Exploring for Petroleum and Natural Gas"). Wireline logging methods (so-called because probes suspended from a wire cable are lowered into the hole) include total gamma, gamma spectroscopy, density by gamma/gamma, laterologs (resistivity and SP), electromagnetic induction (conductivity), borehole deviation, hydrochemistry and magnetic susceptibility. Acoustic (sonic) scanners are employed for the determination of mechanical rock properties, seismic wave velocity, the direction of joints and borehole breakouts, which reveal horizontal stress directions (Bartlett & Edwards 2009). Optical scanners ("borehole videos") provide information on orientation, frequency and aperture of fractures, bedding and lithology. A recent development is logging while drilling, for example the application of prompt gamma neutron activation analysis (PGNAA) that allows determination of main and minor elements of rocks and fluids in the borehole walls. Uranium is measured with prompt fission neutron (PFN) logging systems that allow determination of *in-situ* uranium concentrations (Givens & Stromswold 1989), both in operating mines and in exploration.

Dentith *et al.* (1994) provide a useful collection of some 50 case histories of geophysical exploration in Western Australia, illuminating both advantages and limitations of most methods mentioned above. In any one project, the variety of geophysical methods and their wide availability rapidly lead to copious data, which can only be processed by computing with appropriate software. The required expertise, both in the field and office, is best obtained from specialized companies. The highest efficiency in identifying good prospects, however, can only be expected if cooperation between geophysicists and the field geologists is ensured.

5.2.6 Trenching and drilling

> *The difference between successful and unsuccessful exploration companies is a dramatic difference in the amount of diamond drilling they do.*
>
> S. Muessig 1998

Potential orebodies that are indicated by geological, geochemical and geophysical exploration methods must be examined by physical exposures. In most cases, this is done by drilling, but trenching (costeaning) through the overburden may reveal valuable information. Exploration pits, deep trenches and adits are not regularly made in this phase of investigations. Similar to the preceding reconnaissance exploration work, the objective of detailed follow-up exploration is identification of the most promising prospects,

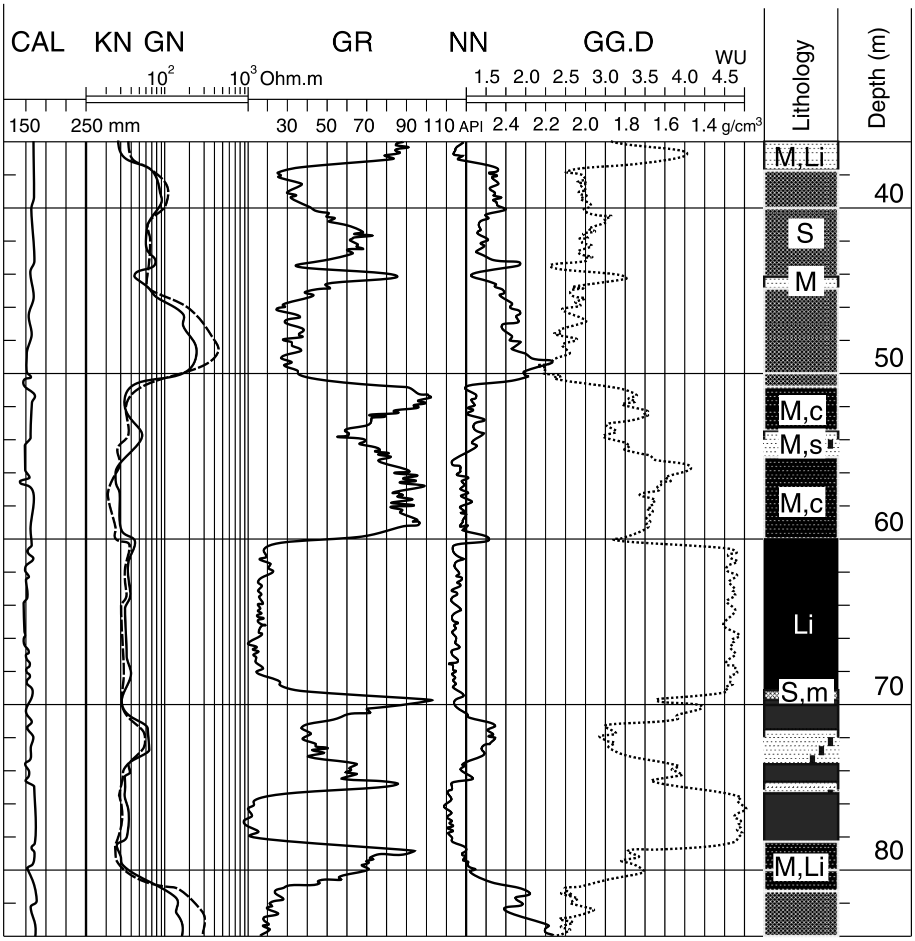

Figure 5.8 Geophysical characteristics of lignite and host rocks in a borehole log. With kind permission by Geophysical Services GGD Leipzig. *CAL* (caliper) records the borehole diameter; *GN* (natural gamma) displays γ-radiation (usually of ^{40}K in clay; API units); *KN and GN* are resistivity logs (Ohm) with electrode distances at 0.5 and 1.0 m, respectively; *NN* (neutron/neutron) provides porosity and water content (in water units, WU), *GG.D* (gamma/gamma) reports density. Clearly, sand (S), silt (M, Ms sandy, Mc clayey, MLi lignitous) and lignite (Li) can easily be distinguished.

whereas locations with insufficient potential are discarded. For prospects that display essential characteristics, such as resources (tonnage) and ore grade which resemble profitable working mines, the detailed follow-up phase ends with the preparation of a prefeasibility study.

Planning for the trenching and drilling programme is based on the presumed geological model. The programme includes maps and sections showing the required drillholes and exposures, and their description. Technical details and the sequence of execution are proposed. Intermediate targets (milestones) that can be assessed are described. Fund-controlling recipients of the programme proposal often stipulate a comparison of costs and potential rewards of the planned work.

This is founded in the principle that for a company, drilling is an investment that must be justified.

Pits, trenches and shallow drillholes

Pits, trenches and shallow drillholes are made in soil and soft rock in order to expose near-surface ore, alteration zones and host rocks for detailed geological mapping and sampling. Trenches, tens to hundreds of metres long, may be excavated by manual labour, trench excavators and bulldozers. Pits and shallow shafts provide large samples (e.g. of gold or diamond ore). Shallow drillholes can be sunk with various tools. In unconsolidated loose rocks, such as tin placers, scoops with a valve, light-cable and tool-boring rigs, or augering equipment may be used. Hole depths of ~60 m are possible. Experiments with radiotracer gold particles showed that in non-cohesive material, dry augering is the best method to recover representative gold contents (Clarkson 1998).

Rotary percusson air blast drill rigs

Rotary percussion air blast drill rigs (RAB), also called top, or down-the-hole hammers (DTH), are commonly used in quarries and open cut mines for drilling blast holes at diameters from 25–400 mm to depths of 100–200 m. In exploration, low costs may be an argument for using this method, aiming at quick data acquisition. Compressed air is used in order to lift rock cuttings and dust from the bit to the surface, between the drill pipe and the wall of the hole. The hole is typically open and casing (lining), which keeps the wall rocks from falling in, is not installed. Rock flour and cuttings from DTH-holes are useful samples, but higher accuracy is obtained with reverse circulation (RC) hammers (Figure 5.9). The drill-string of RC-hammers consists of two pipes: The compressed air flows down between the inner and the outer pipe, whereas the rock chips are lifted in the inner pipe. This avoids erosion of wall rocks, which may mix with the cuttings, resulting in diluted samples. The large sample size and the high speed of penetration are important advantages of DTH compared to diamond drilling. RC-drilling has become a standard where high accuracy is essential and coincides with closely spaced (and therefore expensive) drilling, as in gold exploration and mining. Most RC drill rigs are constructed for holes to ~500 m depth, but the largest machines are capable to drill to 1500 m.

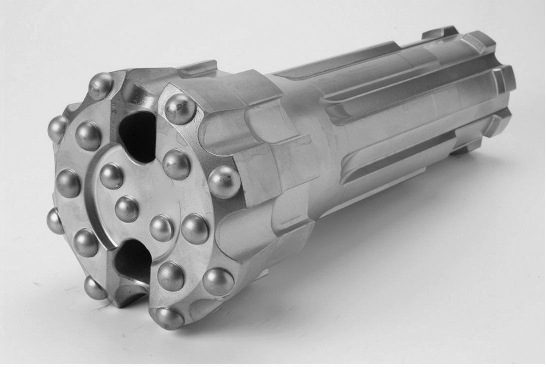

Figure 5.9 Reverse circulation hammer bit. Photograph by Leon Bird, copyright Sandvik 2010. Note the wide openings, which guide air flow and cuttings into the inner tube.

Sonic drilling

Sonic drilling is a new technology that produces excellent cores from mixed hard and soft rocks (e.g. nickel laterite, alluvial overburden, mineral sands, coal spoils) and friable ore such as the manganese oxide ore at Moanda, Gabon, down to ~60 metres depth. It is based on using high frequency vibration and some rotation.

Diamond core drilling

Diamond core drilling is the most common method employed in exploration for mineral deposits in hard rocks. This technology is two to three times more expensive than RC, but has several advantages compared with hammer drilling, not least the smaller disturbance of the environment. Small diamond drills can be carried

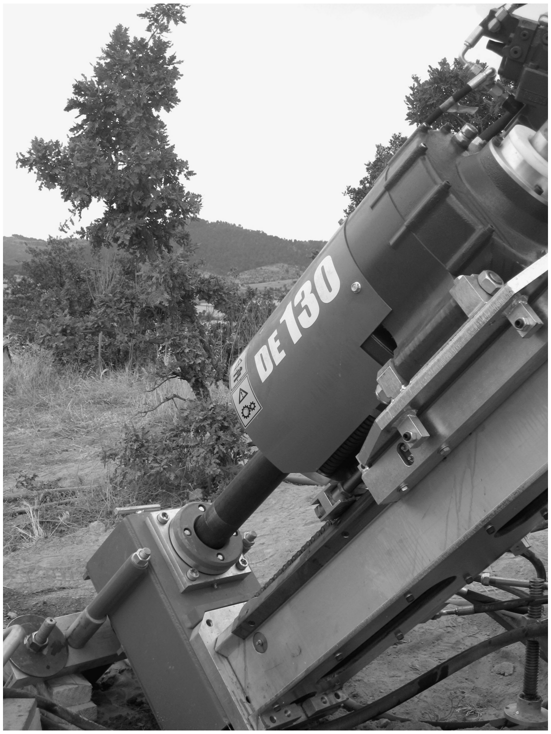

Figure 5.10 Sandvik DE 130 portable exploration diamond drill rig in Turkey. Photograph by Muzaffer Bayazitoglu, copyright Sandvik 2008.

on foot by geologists (Figure 5.10) and average-sized rigs can be pulled by common four-wheel drive vehicles. RC rigs, in contrast, are much heavier. Some machines are produced that can alternatively be equipped for diamond or RC operation. Diamond coring is relatively easy in solid rock, but asks for considerable skill in the more common cases of rapidly changing hard material (quartz), solid rock and soft material (clay, fault gauge, etc.). Ideally, the core taken from a hole is a complete and coherent sample of the ground. Cores provide a wealth of information, such as lithology, rock boundaries and structural data. Core samples are used to determine (assay) ore grade as well as geochemical, mineralogical and petrophysical parameters. The essential determinant of the significance of core-derived data is *core recovery* (Annels & Dominy 2003), defined as the ratio of the length of recovered core to the length drilled. Low core recovery impedes quantitative interpretation of important properties, such as ore grade and ore boundaries. Therefore, core recovery of more than 90% is stipulated with drilling contractors. Other strict rules must be agreed, such as careful extraction of the core and its packing in properly labelled core boxes, and marking individual core runs. Drilling should be supervised on site by experienced geologists. Proper storage of core is needed for the duration of the project (if the prospect is rejected) and for the whole life of the resulting mine if the deposit is feasible. Note that although onerous, storage is much cheaper than repeat drilling.

Exploration drillholes for ore and minerals are rarely sunk to depths greater than a few hundred metres. In cases of well-known geology and a reasonable expectation of high rewards (e.g. Witwatersrand, Sudbury), diamond drillholes are driven to more than 5000 m depth. Not only for deep holes, *directional core drilling and borehole deviation surveying* are standard procedures. Inclined and deep drillholes (deeper than ~200 m) must be surveyed for deviation, which is too frequent to be ignored. Reliable estimation of resources and reserves, and precise mine planning is impossible if the location of orebodies, faults and risky zones, such as water-rich or weak rocks, is not accurately known. Normally, low-cost electronic multishot (EMS) downhole instruments based on magnetometers are used, but in steel-cased holes, or in the presence of magnetite and pyrrhotite, nonmagnetic survey instruments (e.g. gyroscope-based) must employed. The first are prone to considerable errors, which may cause wrong resource estimates. Nordin (2009) advises to control all EMS data by occasional gyroscope runs.

Neglect of deviation surveying can have drastic consequences: In 1989, resources of the newly discovered base metal deposit Louvicourt, Quebec, Canada were estimated, based on diamond drilling to 830 m depth, to >30 Mt of ore at 3.1% Cu and 1.34% Zn. After underground development and additional drilling of 80,000 metres (similar to Figure 1.80), the reserves were recalculated in 1994 to 15.7 Mt. The company had to admit that the grave error was due to drillhole deviation.

Geological logging

Considering the high costs of drilling, a maximum of information must be extracted. Geological logging of core and drill cuttings is common practice. State-of-the-art standard procedures are best learnt from large companies and reputed geological state surveys. Digital processing is the norm, but intricate geological features may be most faithfully recorded by hand-drawings at scales larger than 1:100 (1 cm = 1 m). Whenever samples are removed from the core box, markers with a sample number must be put in the empty places. Sample numbers are composed of the drillhole name and an individual number that must be singular in the company's database. Colour photographs of the core complement other documented data, but cannot replace the above-mentioned sketches. The differentiation of macroscopically similar minerals, such as carbonates, may be facilitated by colouring techniques (Hitzman 1999). Semi-automated methods of mineralogical analysis are increasingly employed in field geology, core logging and metallurgy. Host rock and hydrothermal alteration minerals of core and drilling chips can be determined by portable infrared field spectrometers, such as TerraSpec™. Automated instruments (HyLogger™) developed by the Australian Commonwealth Scientific and Industrial Research Organization (CSIRO) measure simultaneously 190 bands in the 400–2500 nm (visible light to infrared) or 7000–14,000 nm (thermal infrared) range of the electromagnetic spectrum, which allow a very precise assessment of minerals, their crystallinity and chemistry. Portable XRF (X-ray fluorescence) analysers can be employed to provide an initial overview of metal contents of the core.

Geophysical borehole logs are ideally complementing the geological description. They are indispensable for percussion drillholes and for cases of high core loss (Ellis & Singer 2007). The choice of methods depends primarily on physical properties of ore and host rock, with other modifying factors.

A basic rule in **planning drillholes** is that whenever possible, orebodies should be penetrated at right-angles. Accordingly, steeply dipping orebodies are drilled by nearly horizontal holes, and those with low-angle dips by vertical or inclined holes. Local constraints, such as steep terrain that limits the choice of collar sites, may enforce disregard of this rule. Often, drillholes are arranged in fans (cf. Figure 1.80) parallel to gridlines, preferably along profiles that were established for geochemical and geophysical surveys. The distance between drillholes is essentially a function of the assumed continuity and variability of the orebody. As soon as sufficient data are available, geostatistical methods help to adjust distances (cf. "Ore Reserve Estimation and Determination of Grade") but geological experience remains indispensable. The first drillholes are aimed at the centre of the assumed orebody, in order to confirm the presence of significant mineralization. Large pipe-like deposits (kimberlites, copper porphyries) are explored and sampled by vertical holes in quadratic or rectangular grids. However, such unidirectional drilling may induce serious errors, if ore distribution is non-isotropic. In the Cu-Au porphyry deposit Bougainville (Papua New Guinea), ore grades calculated from vertical drilling were later found to be lower than excavated ore. Vertical pipes of rich ore had not been sufficiently sampled. Note that this was a lucky case, with more metal present than originally estimated. Too often, the reverse ruined a mine.

The decision to abandon a prospect, or to continue with detailed exploration in spite of a series of negative results, may be very difficult. A wrong decision may cause financial loss, either because of costs for an unjustified prolongation of investigations, or because the income from a good orebody is not realized. Of course, every drillhole will be judged on meeting expected targets. Yet, negative results should not lead to precipitous abandonment of a prospect. One example of the rewards of persistence is Olympic Dam, where only the tenth drillhole hit exploitable copper ore. Naturally, every new drillhole is carefully evaluated in a drilling campaign and results suggesting variations of the programme are incorporated.

Hydrogeological and geotechnical data

In mine-development projects, groundwater and surface water investigations are hitherto carried out very late, i.e. usually during feasibility studies. In many cases, this is a costly mistake. It is much better to routinely collect water data already during detailed follow-up exploration drilling. Key data needed by the hydrogeologist and the geotechnical engineer can easily be assembled by the team carrying out the drilling. The geologist should always record observations concerning the overburden (lithology) and the depth of weathering. Mines have been lost by mud or water inrushes caused by insufficient information on the thickness and nature of the crown pillar. For the fresh rock, minimum data include core recovery, rock quality designation (RQD: Deere 1964) and basic observations on fractures and joint systems. Drillers should record data on penetration rates, rest water levels, water inflow and fluid loss in the drillhole. This will form the basis of a conceptual groundwater model and allows preparation of hydrogeological contour maps with little additional costs, compared with the need to drill new holes for the same purpose later. At the same time, risks concerning water supply for the mine, its management and security will be exposed, as well as hydrogeological and geotechnical hazards affecting the project.

With completion of the detailed follow-up drilling and trenching phase, and availability of laboratory reports, a formal report must be prepared that comprises: 1) a concise technical description of work done; 2) a detailed presentation of geological, geophysical and geochemical results; and 3) three-dimensional graphic presentations of all essential parameters of the supposed deposit. On this base, 4) a first valuation of the mineralization is possible, mainly by comparing the deposit to key data of currently working mines. The whole report (1–4) is called a *prefeasibility study*. A positive outcome of this study may lead to the decision to start a full *feasibility study*, with the aim to establish sufficient reserves and all information needed to develop the new mining operation. The feasibility study will not be complete without an environmental impact assessment (EIA), the consideration of native title and cultural heritage sites, and an extensive consultation of all stake holders.

Never forget that every drillhole must be safely sealed (Fuenkajorn & Daemen 1996) when it is to be abandoned. If several aquifers are present at depth, they must be separated by barriers (seals). Holes that are to be accessed again at a later time must be plugged in such a way as to preclude hazards for humans and animals.

5.3 DEVELOPMENT AND VALUATION OF MINERAL DEPOSITS

Getting the geology right is fundamental
Roy Woodall 2007 (Director of exploration,
Western Mining Corporation WMC)

The science of economic geology is preoccupied with rather theoretical problems, foremost the details of ore forming processes. The practice of economic geology is dedicated to make mining operations economically profitable. In open-cast or underground mines (Figure 5.11), this includes many diverse obligations (Marjoribanks 1997, Berkman 2001). Some more important examples of geological tasks in mines are:

- planning, management and interpretation of drilling programmes, of geochemical and geophysical surveys, and of exploratory drifts, in order to locate new resources and to outline reserves;
- geological mapping of all rock exposures, underground and in the open pit, at a detailed scale (commonly used are 1:100–1:500); establishing a geological surface map of the mining area (1:1000–1:10,000); logging all drill core from the mine and its surroundings at a suitable scale (e.g. 1:100), with due consideration for rock mechanics and hydrogeology (mining), grade (economics) and ore mineralogy (processing); drafting geological serial sections;
- sampling of exploration drill core, adits and trenches, and of day-to-day ore extraction sites (grade control);
- data management of returns from the laboratory, including data validation;
- geological and mineralogical investigations of ore, in order to improve processing and maximize recovery ("geometallurgy"; Petruk 2000);
- calculation, valuation and reconciliation of reserves;

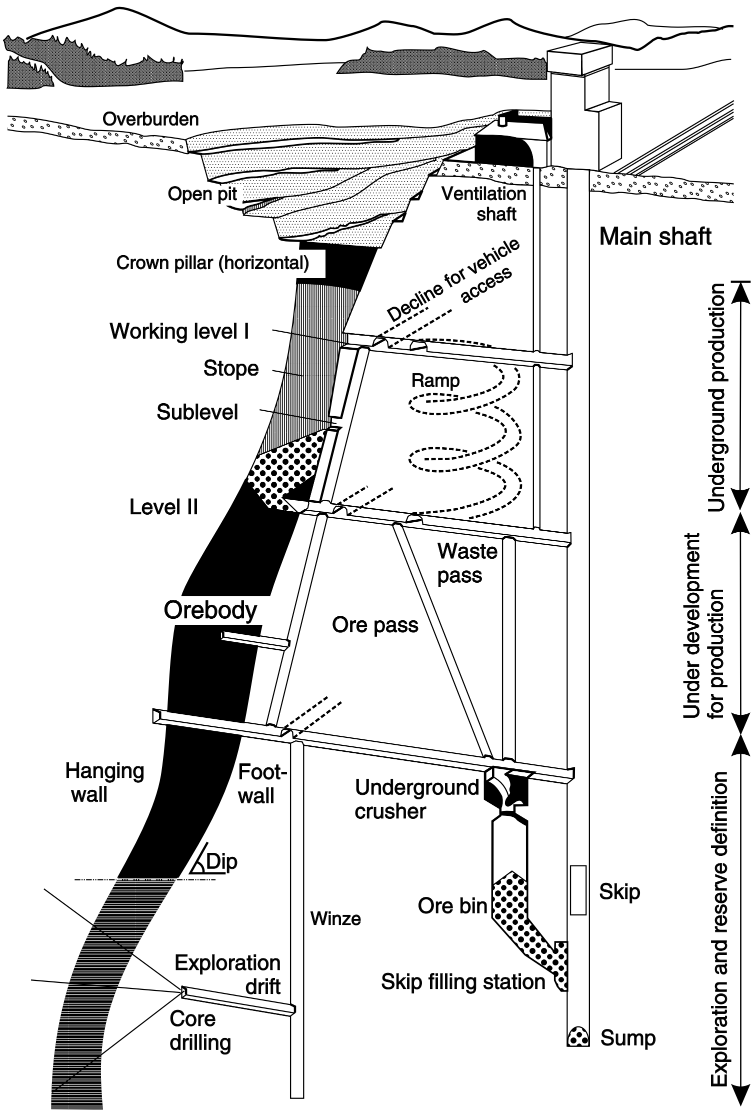
Overburden
Open pit
Ventilation shaft
Main shaft
Crown pillar (horizontal)
Decline for vehicle access
Working level I
Stope
Ramp
Sublevel
Level II
Waste pass
Orebody
Ore pass
Hanging wall
Foot-wall
Underground crusher
Dip
Winze
Ore bin
Skip
Exploration drift
Skip filling station
Core drilling
Sump
Underground production
Under development for production
Exploration and reserve definition

Figure 5.11 Simplified section of a mine that first exploited a steeply dipping planar orebody in a pit (open cut) and is now extracting ore underground. Note the vertical segmentation between (1) ongoing production, (2) development for future extraction, and (3) exploration aiming at the definition of new mining reserves as a replacement for extracted ore.

- design and continuous improvement of the genetic model of the deposit;
- engineering geological examinations of soft and hard rocks, ore, waste rock dips, tailings dams, open cut slopes, etc. (cf. Jaeger *et al.* 2007, Hoek & Bray 1981 for opencut work; Hoek & Brown 2003 and Brady & Brown 2004 for underground mining);
- geological input into subsidence damage cases;
- resolution of geological water problems, either concerning the draw-down cone caused by mining, or unexpected hazardous inflow;
- acquisition of environmental data, including appraisal, based on the environmental impact statement (EIS) that had to be submitted with the

application for the mining licence; day-to-day tasks in mining operations include environmental monitoring of the mine and its surroundings.

Of course, a number of these tasks are executed in teamwork with other company professionals and with external consultants. In this chapter, only those duties are briefly sketched that relate to economic geology.

5.3.1 Geological mapping and sampling

Geological mapping of natural outcrops and of man-made exposures is the most important task of the mine geologist. A complete and up-to-date documentation of all geological data is the precondition for both day-to-day management and for serious decisions concerning, for example, a large drilling programme. Field mapping should be carried out at suitable detail (e.g. at 1:100), whereas display scales of geological mine maps and sections should be equal to the geodetic mine plans. Never neglect preparing geological overview sections through the mine. One mine I knew suffered a catastrophic mud inrush because a stope was driven upwards into water-logged hanging wall sediments. Nobody had ever asked where exactly the hard rock/overburden boundary was. This mine had to be abandoned. Modern mine management software includes components for geological work. Integrated digital processing of geological data and of mine planning is standard in most mines. The practical arts of geological mine mapping have been admirably described by McKinstry (1948), but consult also Marjoribanks (1997).

Sampling

The mining industry devotes considerable efforts to acquire accurate analytical data for resource estimation, grade control, metallurgical accounting and commercial transactions. However, sampling and sample preparation are not always given the attention they deserve. If the samples submitted to the laboratory are not representative, there is little point in using expensive analytical equipment. The most important rule for correct sampling is that all parts of the ore, concentrate, slurry or other material being sampled must have an equal probability of being collected and becoming part of the final sample for analysis. The logic of sampling is to collect a minimal mass (of grams, kilograms, tonnes) that equals a certain parameter (e.g. gold content) of a much larger mass (hundreds or thousands of tonnes). In the laboratory, sample preparation for analysis again includes carefully controlled diminution of the mass (subsampling), until fractions of a gram will be used for actual analysis. This final aliquot must still replicate targeted properties of the original large mass. Note that the term sampling may include specialized measurements with tools appropriate to the minerals under investigation, such as downhole gamma probes and prompt fission neutron borehole probes for *in- situ* determination of uranium in ore.

Most of the sampling problems occur in the field, where conditions cannot be as strictly controlled as in the laboratory. The problems are often of a very practical type, such as cutting a slit of a given geometry through a succession of hard quartz veinlets alternating with soft mineralized host rock. Random chip samples may favour soft over tough rock. Of fundamental interest is the need to estimate the *smallest sample mass* that will guarantee that the sample is representative of the whole. One controlling variable that has been recognized very early is the grain size. When comparing a very coarse-grained granite (e.g. displaying feldspar laths 10 cm long) with aplite from the same melt, but consisting of small equigranular grains of less than 1 mm diameter, it is obvious that the aplite can be represented by a much smaller sample compared to the granite. Another variable is the frequently irregular distribution of the ore mineral in the ore rock. In many gold orebodies, most of the gold resides in rich pockets, whereas the overwhelming mass of the ore rock is of low grade. This type of occurrence is commonly compared to gold nuggets in alluvial mining. When statistical processing of sample data indicates such an unpredictable behaviour, a *nugget-like* distribution is implied. There are many theoretical papers on how to find solutions to both grain size and nugget problems. In mining practice, the use of nomograms or specific software is common (Gy 1992, Pitard 1993, Berkman 2001).

Grade control

The practical execution of sampling depends on the conditions at the site and the precision to be attained (Gilfillan & Levy 2001). The lowest quality have samples that are picked at random from an outcrop or from an ore heap. Slits of a defined geometry (e.g. 10 cm square) are recommended if they can be cut to plan. Drillhole or reverse circulation blast hole dust and cuttings may suffer from differential settling of the (usually heavy) ore minerals and the (light) gangue minerals, or of problems with moisture. Diamond drillhole cores may have a diameter too small for representativity, core-splitting may introduce serious errors (Brooks 2008) and core loss is an ever-present risk. In spite of this, continuous sampling methods are generally preferable to discontinuous procedures. But no method is without problems and this has to be considered before starting a sampling campaign. If possible, different sampling techniques should be tested and compared before settling on a specific method. And a final advice – never underestimate the importance of accurately measuring the density of samples (Lipton 2001).

Subsampling

Subsampling designates procedures that reduce the total mass sampled (e.g. from a slit in an orebody exposure) to the few grams of powder in a small bottle that is all a modern laboratory requires for analysis. The key are stepped cycles of grain size diminution (by crushing and pulverizing), splitting (halving or quartering) and rejection of one half or three quarters of the sample. The choice of the correct splitting device is crucial, especially in cases where the ore is much heavier than the gangue (gold, uranium, etc.). Traditional riffle splitters work badly in these cases, because they are prone to cause gravity separation. Rotary splitters avoid this trap. Whatever the technique, error control is the central task in a sampling campaign. Always try to check on errors by submitting well-chosen and unrecognizable doubles of samples to the laboratory.

Geometallurgy

Geometallurgy describes procedures to model the distribution of different ore types in a mine (Petruk 2000). We have seen earlier, that mine-site processing of run-of-mine ore is an important determinant of economic success or failure of an operation. During a feasibility study, not only the variability of metal contents in ore, but also of metallurgical recovery over the life-time of the future mine, must be studied and modelled. Automated methods of mineralogical analysis, such as QEMSCAN (an electron beam technique that combines a scanning electron microscope, four X-ray detectors and a software package developed by CSIRO, Australia), provide the required data. *Geometallurgical (ore) domains* comprise parts of the orebody with similar geochemical, mineralogical, textural and processing properties. Predicting grindability and metallurgical performance is critical. The development of small-scale tests based on diamond drill cores allows multiple sampling of an orebody opposed to the traditional pilot-plant scale sample of several 100 tonnes taken from one accessible location of yet undeveloped reserves.

5.3.2 Ore reserve estimation and determination of grade

From the scale of a single mine or a mining company to national and supranational stock markets and resource planning, knowledge about the physical and economic availability of raw materials is needed for rational decisions. Therefore, international efforts to standardize measuring and reporting of mineral reserves and resources have reached a wide acceptance.

The total geological quantity of a specific raw material is termed the "mineral resource base". This includes both known and unknown quantities. However, only ore that has reasonable prospects for eventual economic extraction may be included in any estimate. Based on increasingly reliable data on quantity, quality and exploitability of minerals, McKelvey (1973) proposed a matrix ("McKelvey Box"), which differentiates between prognostic (undiscovered) resources, identified resources and reserves. Reserves are only that part of resources that is thoroughly investigated and proved to be exploitable with a high degree of confidence.

Prognostic resources

Strategic planning for the future availability of metals and minerals relies on estimates of prognostic resources. Often, dire predictions are made about the world running out of specific metals (Club of Rome: Meadows *et al.* 1974), coal or crude oil. In 1974, the reason for the prediction of depletion in the 1990s was the erroneous use of reserve instead of prognostic resource figures. Even today, this mistake is commonplace. Because of obvious reasons, quantification of undiscovered resources is notoriously difficult. Most methods proposed are based on extrapolation of identified resources (including reserves and past production) in well investigated tracts to geologically similar, less well-known parts of the globe (Singer & Menzie 2010, Gautier *et al.* 2009, Singer *et al.* 2005) or to greater depth beneath the surface (Kesler & Wilkinson 2008). Such exercises demand geological and metallogenetic maps, and mining databases.

In estimating undiscovered resources, statistics have an elementary role. Studying the negative correlation between tonnage and grade of metal ores, Lasky (1950) proposed a log-normal distribution (Lasky's Law). In a log-log diagram, the same data pairs form a line with a slope determined by an exponent D between 0 and 3 reflecting a fractal nature (equation 5.1).

Fractal distribution of ore tonnages and related grades (Turcotte 1997):

$$C_{ore}/C_{min} = (M_{min}/M_{ore})^{D/3} \qquad (5.1)$$

C_{ore} is the average grade of the tonnage M_{ore}, C_{min} the minimal grade included of the mass M_{min}, D is the fractal dimension. M_{min} may be the mass of ore exploited at the lowest-grade mine, or even source rock from which ore in a district is thought to be derived (consider the metamorphogenic model of gold deposits leached from crust with trace contents).

Based on this correlation, undiscovered resources can be estimated. A different mathematical approach (density functions) was applied by Gerst (2008), aiming at an estimate of cumulative grade-tonnage curves for continental copper resources.

Discovered mineral resources

Discovered mineral resources result from exploration and detailed follow-up work. According to increasing geological certainty, they are subdivided into *inferred, indicated and measured resources* (Figure 5.12). The last category infers that mass and grade are known with a high level of confidence. Methods for measuring confidence are typically based on drillhole or sample spacing and geostatistical criteria (Abzalov & Bower 2009). Resources are normally not acceptable as a base for commercial mining. There are, however, some projects, such as *in-situ* leaching (ISL) of uranium, which must rely on drilling only, so that mere resources and no reserves at all can be estimated until production starts.

Mineral, or ore reserves

Mineral, or ore reserves are only that part of an indicated or measured resource that can be economically mined. Only reserves justify commercial mining. Investigations supporting this attribution must include mining, metallurgical, economic, marketing, legal, environmental, social and political factors (the "modifying factors"). The modifying factors are time-bound variables. Mineral reserves are subdivided into *probable* and *proved,* the first with a lower degree of confidence.

Statistical and geostatistical methods are indispensable in the determination of different levels of confidence. The principle can be illustrated by varying density of geological observations (Figure 5.13). In a mine exploiting a simple planar orebody (e.g. a fluorspar vein, or a steeply dipping sedex ore deposit), proved reserves must be physically outlined on three or four sides. Probable reserves are those parts that are only exposed along two mine openings (or closely spaced drillholes).

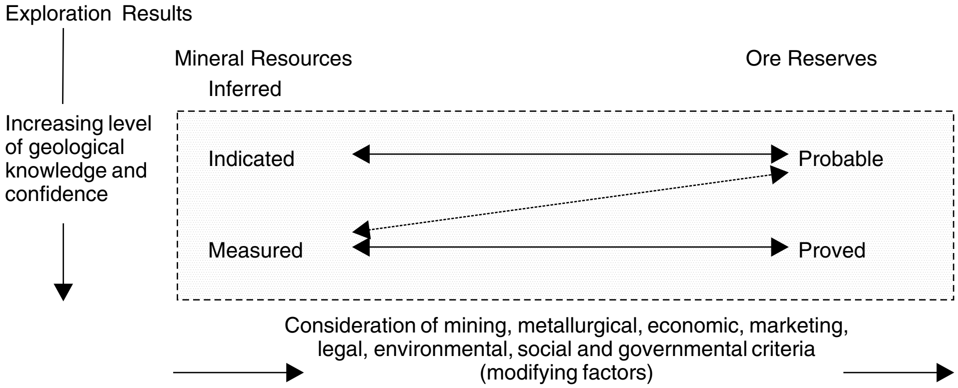
Exploration Results
Mineral Resources
Ore Reserves
Inferred
Increasing level of geological knowledge and confidence
Indicated
Probable
Measured
Proved
Consideration of mining, metallurgical, economic, marketing, legal, environmental, social and governmental criteria (modifying factors)

Figure 5.12 General relations between exploration results, mineral resources and mineral reserves as defined in the JORC Code (AusIMM 2004). It is noteworthy that proved reserves can fall back to the measured resources category.

Measured resources are usually the result of detailed drilling but of insufficient quality or incomplete data for classification as reserves. Indicated mineral resources are derived from the geological orebody model and supporting physical observations.

Investigations for resource estimation include work in six stages:
1 provide a sufficient quantity of data of appropriate quality (precise and accurate);
2 develop a well-founded geological deposit model (including data that link mineralogy and metal recovery);
3 use statistical methods in order to understand the distribution of analytical data in the deposit;
4 choose a suitable interpolation model for grades, considering both the geological model and the statistics;
5 calculate tonnage and grade, either globally or for parts of the deposit;
6 prepare the report, clearly outlining resource categories and respective confidence of figures presented.

Each of these points represents a complex system of scientific and technical approaches, which influence the results. Not all uncertainties can

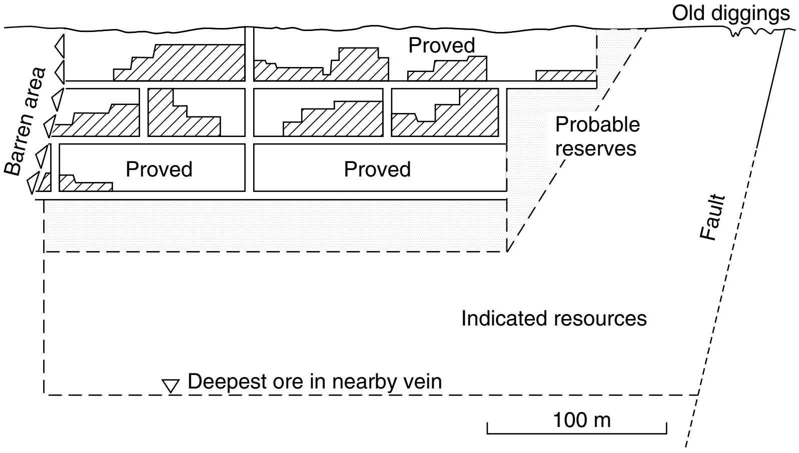
Old diggings
Proved
Barren area
Probable reserves
Proved
Proved
Fault
Indicated resources
Deepest ore in nearby vein
100 m

Figure 5.13 Proved and probable reserves of a vein deposit in relation to geometry of actual underground exposures, and indicated resources supported by the geological model and some drill hole intersections (not shown). Shaded areas are extracted parts of the orebody.

be resolved and some assumptions must be made. This is why the product is termed a "resource estimate" (not a calculation), even if advanced mathematical methods are used. It must always be remembered that users (e.g. banks) of the resulting figures will take them at face value and derive potentially serious financial and organizational decisions. Note also, that resource estimates are essentially numerical models of orebodies. Similar to other such models in the earth sciences, they can hardly ever be true replicas of nature (Oreskes *et al.* 1994).

Because of the economic impact, for example on financial markets and industry, all major industrial countries developed norms for estimating and classifying reserves. In Europe, a common standard is prepared by the Pan-European Reserves and Resources Committee (PERC 2008). A widely lauded and internationally adopted example is the Australian system (Joint Ore Reserves Committee or JORC Code: Edwards 2001, AusIMM 2004). The United Nations Economic and Social Council (1997) presented a proposal that was hoped to meet the requirements of private and state-controlled mining industries, as well as governmental needs for mineral inventory classification. In this system (UN International Framework, Figure 5.14), three axes are presented, including: i) the degree of geological assessment (geological axis); ii) the degree of economic viability (economic axis); and iii) the stage of feasibility assessment (feasibility axis). The latter is a new aspect specifically aimed at potential investors. Another proposal for a third axis was put forward by BGS (British Geological Survey), concerning information on the accessibility of deposits considering environmental, legal, social and political factors (Cook & Harris 1998). The intention is to visualize which part of reserves is really available for mining, in contrast to those that are blocked by other claims. In the future, mining will increasingly depend on modifying factors. Purely geological reserves unavailable for exploitation are meaningless (Weatherstone 2005).

Practical procedures of **calculating quantity and grade** of a mineral deposit are modified according to type, form, raw material contained and mode of data collection (Annels 1991). In simple cases,

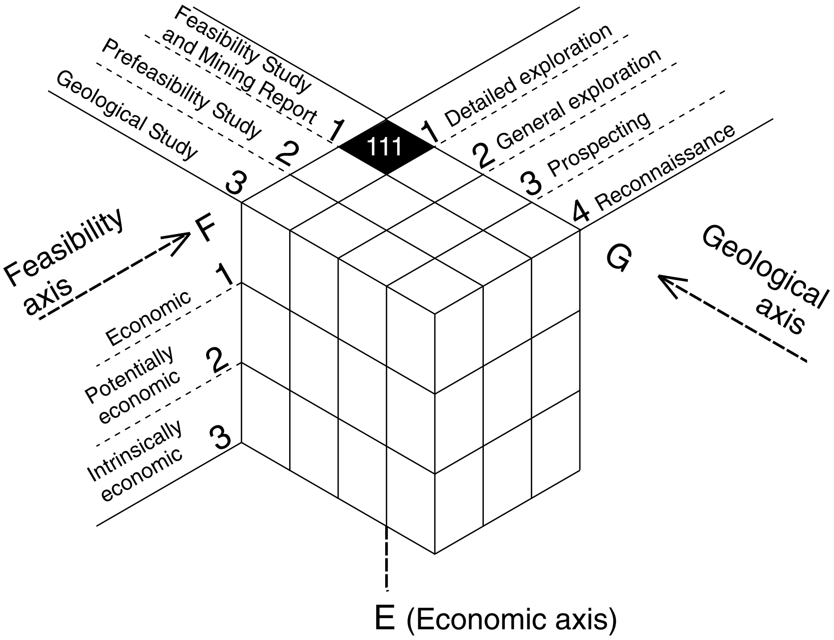

Figure 5.14 The tri-axial UN Framework Classification of mineral reserves and resources. Courtesy UN Economic and Social Council (1997). Numbered codes apply to each block. Block 111 represents proved reserves, 121 and 122 probable reserves (coordinates E-F-G). All other blocks are various resource classes.

such as homogeneous planar bodies (e.g. a seam of chromite or of coal), a simple volume-by-density formula can be applied (eq. 5.2).

Simple calculation of in situ *tonnage*:

$$Q = F \cdot D \cdot M \tag{5.2}$$

If the recoverable metal mass in a specified volume of ore is required, the formula is enlarged by the introduction of factors that take account of ore left in place (mining loss, for example in safety pillars) and the loss during metallurgical processing (eq. 5.3).

Simple calculation of recoverable metal content:

$$P = Q \cdot G \cdot A \cdot V \tag{5.3}$$

Q = ore *in situ* (t), F = surface to be mined (m^2), M = average thickness of ore (m), D = specific weight or bulk density of ore (t/m^3), P = recoverable metal content (t), G = average metal content in ore (% or kg/t), A = correction factor for mining loss, V = correction factor for processing loss.

Note that the specific weight of ore (D) must be determined using large samples, because in this case the aim is to quantify a physical property of the rock mass including joints and fissures (Bieniawski 1989, Lipton 2001), in contrast to ore rock (a specimen, for example). If appropriate, dilution of the ore by unavoidable extraction of host rock must be included. Dilution is, of course, a factor that increases costs. Polymetallic ore grade is often reported in terms of a single equivalent grade of one major metal such as gold or copper. It is usually obtained by taking the *in-situ* value (grade multiplied by price) of each of the individual metals, adding these values and calculating the grade of the same value of the primary reported metal. The result can be very misleading if the recovery of individual metals is not considered. Therefore, the preferred measure of equivalent grade is the net smelter return (NSR).

Usually due to practical considerations, parts of a deposit (single orebodies or blocks of ore) are separately submitted to ore reserve estimation. Some orebodies with a longitudinal continuity but varying contours are depicted by serial sections (wire frames) that may be based on drilling fans, such as those shown in Figure 5.11. In such cases, exploitable ore surface in cross-sections and distance between sections are measured (Figure 5.15). The ore volume can be estimated by applying eq. 5.4.

Simple estimation of ore volume from serial sections:

$$\begin{aligned}\text{Volume}\,(m^3) = {} & 0.5 \cdot (F_1 + F_2) \cdot b_{1-2} \\ & + 0.5 \cdot (F_2 + F_3) \cdot b_{2-3} + \ldots \text{etc.}\end{aligned} \tag{5.4}$$

The role of weighting

Variability of some factors of special importance, such as varying thickness of a gold vein, sample length along core, or density of ore impose the need for weighting (Wellmer *et al.* 2007). Average grade of an ore vein with varying contents of lead and, therefore, variable density can only be correctly calculated by weighting (eq. 5.5).

Weighted average content (G_w) as a function of thickness (M) and density (D):

$$G_w = \frac{M_1 \cdot D_1 \cdot G_1 + M_2 \cdot D_2 \cdot G_2 + \ldots \text{etc.}}{M_1 \cdot D_1 + M_2 \cdot D_2 + \ldots \text{etc.}} \tag{5.5}$$

The determination of the lowest grade in an orebody that can be economically mined (the "cut-off grade") is of paramount importance (Rendu 2008, Lane 1997). By definition, this is the grade where mining and processing costs are equal to proceeds from the sale of the product. The cut-off grade is the limit between ore and waste rock. Its determination is not simple, as the parameters that determine the optimal cut-off grade are not only the given geological properties of the deposit but include time-dependent factors such as varying metal prices, shallow or deep location of stopes and the cash-flow strategy of the operation. Therefore, different cut-off grades will apply during the life-cycle of a mine and at one point of time, in different parts of the mine. When setting cut-off grades, the aim will always be to maximize the profit of a mine. In recent years, maximization of the net present value (NPV) of the mining operation is the main measure of optimizing the cut-off grade (Nieto & Bascetin 2006).

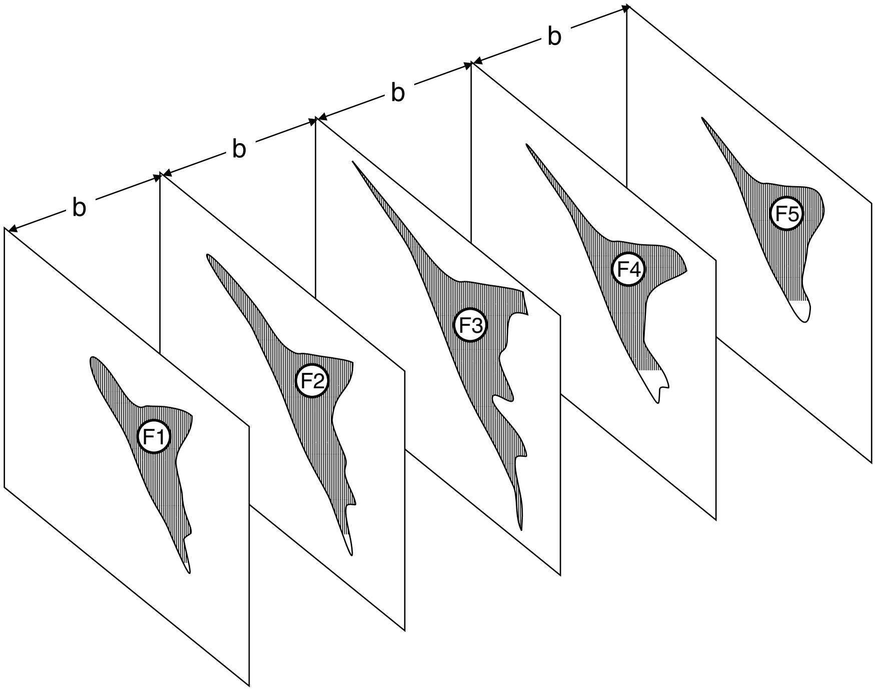

Figure 5.15 Serial profiles of an orebody (wire frames) are one of several methods to estimate the volume of ore. This drawing is inspired by the Deilmann orebody at Key Lake uranium mine, Canada.

Geostatistic modelling

Geostatistical modelling is an important part of ore reserve estimation. Geostatistics were first developed by Matheron (1971) and Krige (1981), originally aiming at a higher accuracy of gold reserve estimates. The difference between geostatistics and ordinary statistics is that geological parameters depend on the site of a measurement (e.g. the laterally changing thickness of a coal seam), whereas each throw of a dice is independent from the previous one. Commonly in geology, smaller distances between sample locations cause a higher correlation of measured values. This can be used for various predictive purposes, especially in reserve estimation. The most important step in geostatistical modelling is therefore the quantification of the spatial correlation of sample properties ("regionalized variables"):

> Semivariograms are computed in order to quantify the spatial correlation and directional properties of various parameters, such as ore grade, mineral paragenesis, thickness, etc. (Figure 5.16). Variography (or "structural modelling") is an important tool that reinforces geological understanding of a deposit (Guibal 2001). Typical uses of variograms are: i) optimizing the sampling density (e.g. the drilling grid distances); and ii) helping to define the geological model ("domaining") for resource evaluation. Domains are then subdivided into blocks for calculation of tonnage and grade of ore contained. Common computational methods employed include *kriging* (i.e. minimizing the error of estimation; Matheron 1971, Isaaks & Srivastava 1990) and *conditional simulation*, allowing extremely complex models and providing a measure of precision and probability (Abzalov & Bower 2009, Khosrowshahi & Shaw 2001).

It is very important to remember that geostatistical methods cannot replace meticulous geological data acquisition and interpretation. They are computational tools that rely on good geology and extend its reach. Erroneous applications include calculating a variogram with data that comprise

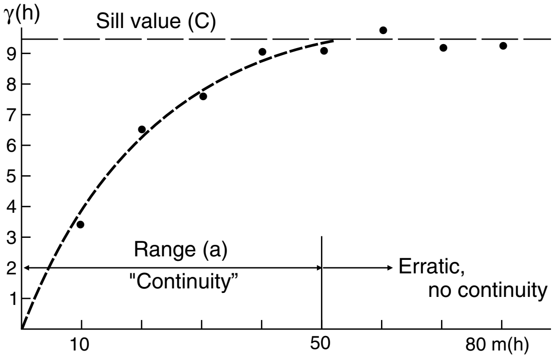

Figure 5.16 Example of a simple experimental semivariogram with a fitted model (black line), that may be used to determine the optimal sampling distance in an orebody. γ (h) is the variance of values at different sample distances (lag-distance [h] here in 10 m steps). When reaching the sill at range (a), γ (h) equals the variance of the total population (C) and the predictive value of γ (h) – the covariance – is lost. Optimal sample distance would be a/2.

distinct domains. Practical experience with geostatistical resource evaluation has shown that results (e.g. of kriging) should always be checked with different methods, including conventional "manual" ones (Sinclair & Blackwell 2002). In Australia, comparative runs with commercial software resulted in severe differences, provoking the demand that all resource announcements should be accompanied by a manual calculation (Swain 1997). Much can be learned from a comparison of reserve estimates and quantity produced. For the uranium mine Key Lake (1982–1997, cf Chapter 2.5 "Uranium"), the original reserve estimate systematically deviated from later production figures. The estimated tonnage had been too low and the predicted grades were hardly ever reached. The explanation for this disparity was an unplanned dilution of the ore by ~25% of host rock (Mistry *et al.* 1999).

Reserve management and reconciliation

The lesson of Key Lake and many similar cases is that reserve management and reconciliation is an important task. Predicted grade of reserves, *in-situ* grade of ore produced, grade delivered to the processing plant and mass of metal in concentrate must be carefully supervised (Fouet *et al.* 2009, Gilfillan & Levy 2001). The results are a measure of the overall metal recovery of the operation, but also of problems at different points in the mining process. For some time now, reconciliation results ("factors") are required information by international reserves and resources reporting codes such as JORC.

Many placer deposits of gold and diamond, but also some lode gold deposits, show a high nugget effect. A *nugget* is a large lump of gold lying about that will certainly please the finder. Of course, one lucky find would hardly be a rational cause for opening a mine. If gold in a mine is said to have a nugget-like distribution, an important part of the total content in the ore is present in erratic pockets of high concentration. This causes severe problems in ore reserve estimation. In such cases, channel sampling of the four walls of a pit may yield four different results, which in turn show little relation to the bulk sample from the pit. Common geostatistical methods cannot solve this problem, because in this case the area of influence of single samples is negligible. At the Bendigo gold mine (New South Wales, Australia), most of the gold content in each tonne of ore is present in just 5–15 very coarse gold particles (Johansen 2005). Investigations of large bulk samples of placers at Bendigo have shown that the grain size distribution is relatively stable at different total grades and can be presented in a type curve (Figure 5.17). Estimation of the grade of any sample from the mine appears to be possible by determination of gold in the lower part of the grain size curve. The method is reported to allow reliable grade estimates based on small samples like drill cores.

Reserves of a mineral deposit are a first-order control on economic evaluation, whether decisions concern the opening of a new mine, the value of company shares, the sale of a deposit, or securing a credit. Therefore, the execution of reserve estimation carries considerable responsibility. This translates into the condition that experts involved must have a demonstrated high professional standard ("competent person"), independence and ethical integrity. Australian rules are an excellent example (AusIMM 2004, 2005; Edwards 2001).

5.3.3 Valuation of mineral deposits

The term "mineral resource wealth" tempts the non-professional to consider undiscovered or undeveloped minerals in the ground as an economic value. This is not strictly correct because an income from buried minerals can only accrue when they are extracted. Only mining creates wealth for investors, miners, contractors and the whole economic space. It is true, however, that minerals in the ground are an *economic potential* and therefore can be the object of trading and speculation.

Investing in a mine is basically providing funds in the expectation of being repaid in the future and, of course, with interest. This translates in economic terms to "the *present value or worth* (P) of a sum (A) to be received or paid at some future date is such an amount as will, with compound interest at a prescribed rate (i), equal the sum to be received or paid in the future (n years)". Accordingly, the present value is less than the future income, because that must be discounted (eq. 5.6).

Present value of future income calculated by discounting:

$$P = A/(1+i)^n \tag{5.6}$$

In periods of high interest rates, the present value of future income falls rapidly to near zero. With an interest rate of 15% per year, an income (A) in 15 years from now has a present value of only 0.123 A and 0.001 A for 50 years. At common interest rates of 7.5% and a period of 15 years, the result is a present value of 0.338 A. This illustrates why the development of ore reserves (a future income) beyond a period of 15–20 years is

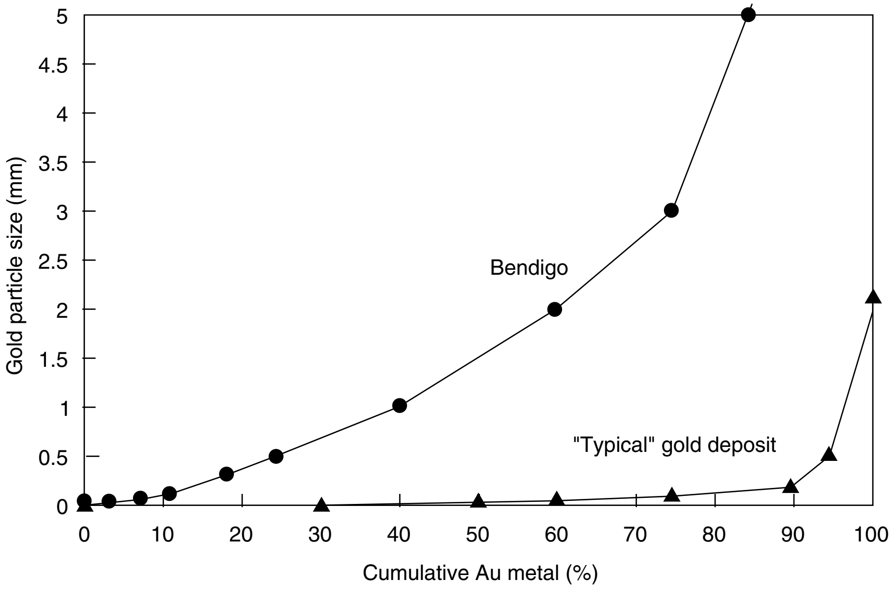

Figure 5.17 Gold particle size distribution at Bendigo, Australia compared to a "typical" gold deposit (Johansen 2005). At Bendigo, coarser (and fewer) grains control the total grade. Determinations of the characteristic grain size/metal content relations in a deposit allow improved grade estimations in spite of high nugget effects.

economically wrong, except in special cases (e.g. a coal mine producing for an attached thermal power plant with an amortization time of 25–30 years). In the recent past in Australia, exploring and developing a new mine caused average costs of 50 million US$. It is obvious from the above given figures that ore reserves drilling for a time 30–50 years beyond the start of operations of this mine just adds to the costs, but does not contribute to earnings. Capital markets would not support such wilful waste, because investments in exploration and mining compete with other uses of capital.

Of course, future income and interest rates are uncertain and estimates should be given with error margins. Often, average figures of the recent past are used, but cannot be projected with 100% confidence into the future. The volatility of markets for many raw materials (e.g. tungsten, tin, cobalt, lead, zinc, gold, petroleum) is proverbial, whereas industrial minerals have relatively smaller price fluctuations. The consequence is that the present value of an ore deposit can be large or small, simply as a function of the assumed future metal price. Because the time of high prices cannot be predicted, the estimate and an investment related to the deposit (e.g. buying shares of the mine) are subject to a *risk*. Apart from the risk due to the product market, further risk factors are political, social and fiscal. All risks must be identified for a specific project and included in a formal *risk analysis.* High risks always reduce the present value of a project (e.g. the share price). In economic calculations, risk can be allowed for by using higher discounting rates.

Methods of cost-benefit analysis

Founded on these basic principles, **various methods of cost-benefit analysis** were developed that can be used for the valuation of mining projects (Rudenno 1999). Taking into account that in the first years most mines cause high costs, whereas income accumulates in later years, the practical evaluation method termed *cash flow analysis* contrasts yearly costs (C) with expected returns (R). Resulting figures are discounted and their sum represents the *net present value(NPV)* in the year zero (eq. 5.7).

Valuation of a mining project with discounted cash flow analysis:

$$\mathrm{NPV} = (R_0 - C_0) + \frac{R_1 - C_1}{(1+i)} + \frac{R_2 - C_2}{(1+i)^2} + \ldots \frac{R_n - C_n}{(1+i)^n} \tag{5.7}$$

A positive *NPV* indicates that expected income is higher than projected expenses and the difference illuminates the presumed profit which determines the feasibility of an investment. A negative *NPV* indicates a non-profit or loss situation so that the project should be abandoned, although the option of higher product prices in the future might be considered. Apart from *NPV*, other guide values include the *internal rate of return(IRR)* and the *payback period*. The *IRR* is determined by calculating the interest rate (i) for a net present value of zero. The payback period is the number of years that is needed to recover the sum initially invested by net returns. This exposes clearly when the first true profits may be expected. Typical payback periods for metal mines are from 3–8 years.

Feasibility study

The phase of development and valuation of a mining project concludes with the compilation of a feasibility study. This is a full documentation of geology and reserves, mine planning, processing methods, infrastructure, work and construction plans, costs, markets, cash flow analysis, social, legislative and fiscal frame, financing, environmental management during the extraction period and closure plans including landscaping, recultivation and renaturalization.

5.4 MINING AND THE ENVIRONMENT

> *The mine of the future will be a waste management project*
>
> N. Weatherstone 2005 (Rio Tinto)

Large mining operations (Figure/Plate 5.18) affect surrounding communities, flora and fauna, land and water, similar to other major industrial operations. Yet there are differences that are clear to any casual observer. Typically,

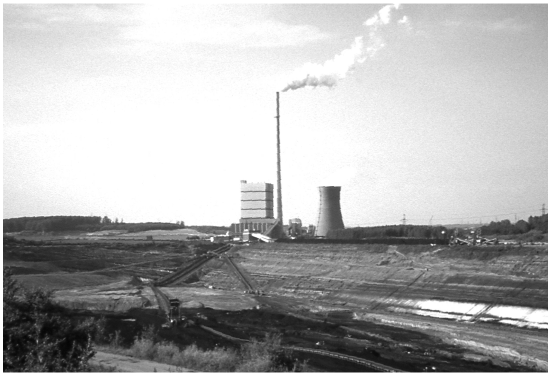

Figure 5.18 (Plate 5.18) Lignite pit Schöningen in northern Germany with its captive power station. Coal extraction takes place at the pit bottom. Overburden and combustion residues are used to refill nearby exhausted pits. Flue gas cleaning yields by-product elementary sulphur. Note white sands on bench to the right. Strata are limnic and marine due to marine transgression during the Palaeocene-Eocene thermal maximum.

mines change the landscape profoundly and they bequeath much visible waste. This is one of the main reasons for public misgivings about mining. Concern for future societal acceptance of mining inspires visions, such as the Zero Waste Mine (Wolkersdorfer 2009).

Large quantities of waste are a consequence of most mining and quarrying operations. Although the major part of this is inert and non-hazardous, disposal, at least in densely populated areas, is often a space problem. Possible solutions include storage of waste in underground mining voids and converting it into useful products such as aggregate for the building industry. Today, the relatively small mass of potentially hazardous waste produced by mines is properly regulated by the authorities and managed by the operators. In the past, this was quite the reverse. The wealth created by mines was of first importance, whereas their impact on people and the environment was hardly noticed.

The earliest anthropogenic heavy metal spike known occurs in sediments of the estuary of Rio Tinto in southern Spain; it is due to Copper Age mining (~2500 BCE; Leblanc *et al.* 2000). In our time, the mining industry invests heavily in procedures that promise sustainability and minimal environmental risk. It is not rare to encounter post-mining landscapes that are truly improved compared to their virgin state. Examples are the refuges for rare species of animals and plants in re-naturalized quarries, clay pits and pit lakes, in contrast to surrounding agricultural land. Citizens and media have hardly taken notice of this new face of the industry, but are shocked by images of careless mining that is often a by-product of weak and corrupt governance. To call for an end of all mining is hardly helpful. Environmental improvement of working mines and reclamation of abandoned exploitations is only possible if sufficient funds are available. It makes no difference if private or public funds (Figure/Plate 5.19) are used; in both cases, quantitative and qualitative growth is the precondition. Economic growth, however, cannot take place without mineral raw materials. The rational conclusion is that exploitation of mineral resources is not the problem, but in its "green" and modern execution, represents the key to sustainable development.

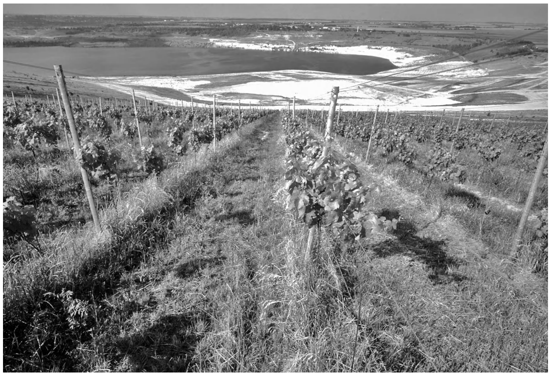

Figure 5.19 (Plate 5.19) Recultivation of the lignite pit Geiseltal in northern Germany during the flooding operation in 2005. Photograph by Christian Bedeschinski 2005. © LMBV (Lausitzer und Mitteldeutsche Bergbau-Verwaltungsgesellschaft mbH). The sunny slope on footwall limestone in the foreground was planted with grapevines. The Eocene lignite seam attained a thickness of 100 m in a large salt subrosion depression within Triassic limestone measuring 5 × 15 km. Because of the induced alkalinity, the coal was famous for exceptional preservation of vertebrate fossils and of chlorophyll in green leaves. Exploited through nearly 300 years, original lignite resources were 1600 Mt.

Environmental impact assessments

Environmental Impact Assessments (EIA) are complex studies that must be carried out and approved by the authorities when operations are licenced. The potential environmental problems specific to mining, which have to be considered are listed below. The same list will serve for preparing a mine-closure project or the reclamation of abandoned mines. Mining may disturb local society, natural flora and fauna (the biosphere), soil and regolith (pedosphere), the geological environment below the regolith (the geosphere) and surface or groundwater (the hydrosphere). Possible impact on the spheres must be studied by a multidisciplinary group. Their role includes the responsibility of asserting the precautionary principle (Foster *et al.* 2000) by predicting hazard and risk, and by cooperating with the management to prevent damaging incidents. Note that in technical context, the term "hazard" designates a damaging event that threatens people, environment or property with a specific probability (e.g. once in ten years). "Risk" is the financial or other consequence of the damaging incidence multiplied by the probability.

5.4.1 Potential environmental problems related to mining and mine-site processing plants

- Visible alterations of the landscape:
    - o *Temporary.* Disturbance of the ecosystem (e.g. by clearing the site), relocation of water courses, drainage of wetlands, removing soil, laying new roads;
    - o *Lasting.* "Scars" in the landscape; new water courses, ponds and lakes; lowering, tilting or raising the land surface; landfills, waste rock tips; pit lakes, settling ponds, tailings dams.
- Effects concerning the aquatic and/or hydrologic environment
    - o *Temporary.* Because of dewatering, all mines (except dredging operations) act as a well (Figure 5.20). The consequence is often a wide draw-down cone, influencing nearby groundwater, drinking water well-fields, wetlands, or medicinal and recreational springs. Water pumped from a mine into rivers and lakes or issuing from ore processing may be loaded with dissolved matter, suspended particles (e.g. iron hydroxide ochre, clay, mica) and acidity from oxidizing sulphides (AMD or ARD – acid mine or rock drainage: Verburg *et al.* 2009, Younger & Robins 2002, van Geen *et al.* 1997; concerning the formation conditions of AMD refer to Chapter 1.2 "Supergene Enrichment of Pre-Existing Mineralization").
    - o *Lasting.* Partly as above; long-wall underground coal mining induces subsidence and lowering of the land surface, so that undrained depressions may fill with water; a concurrent reversal of the hydraulic gradient may enforce expensive surface and groundwater management. Lakes filling former open pits can have problems with acid rock drainage from the pit walls or from waste rock and with unstable underwater slopes. Even pit lakes in rocks that contain no toxic or acid-producing compounds, such as sand pits in river valleys, cause chemical changes in passing groundwater (e.g. loss of CO_2, oxidation); the quality of drinking water pumped from wells downstream of the pit can be affected.

      Note that "*empirical studies of mineral deposits in the context of their surrounding watersheds are thus an important and needed next step in the development of improved predictive methods to help anticipate, mitigate, and remediate the potential environmental effects of mineral-resource development*" (Plumlee *et al.* 1999a).
- Surface damages affecting private or public property:
    - o Legally, mines are responsible for compensating damages and losses that are caused by their activities. Subsidence above coal and salt mines, gas and oil fields may damage roads, canals, railways and buildings (Brady & Brown 2003, Bell 1998). The large underground iron ore mine at Kiruna, for example, induces considerable subsidence that is predicted to last 100 years, eventually enforcing a relocation of Kiruna town. Mine dewatering can lead to drinking water wells falling dry. The attribution of damages to mining is often

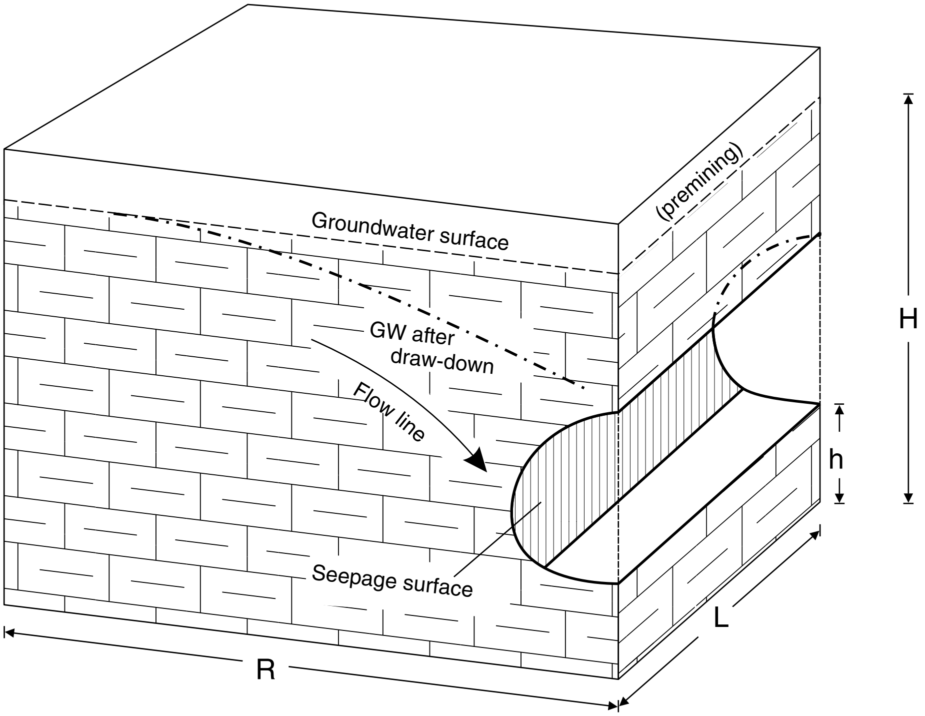

Figure 5.20 Cross-section of a mining tunnel drawing groundwater (Wittke 1990). With permission from Springer Science + Business Media. Once the hanging-wall rocks are fully drained after establishment of the tunnel, steady-state seepage into the tunnel will take place. The rate of water inflow Q (in m^3/s per length-metre of the tunnel, without vertical unsaturated seepage from above) can be estimated by equation (5.8) $Q = 2k.(H\text{-}h/R).F$ (k = rock mass permeability in m/s, R, H and h in m; cf. sketch; F = potential seepage surface in m^2). For total quantity of water entering, multiply Q with L = length of tunnel drawing seepage in metres.

dubious and such cases have to be settled in court, involving legal and technical experts.

- Collapse of underground mining voids or of pit walls, affecting the surface:
  - o Disastrous accidents of this kind have occurred in working operations, but sudden cratering is more frequent above old, abandoned mines. A general rule is that only open mine workings situated between the surface and ~100 m depth are likely to break through to the surface. In rare cases, large voids at much deeper levels have triggered chimney caving, which reached the surface (Brady & Brown 2004). The resulting earth falls, collapse craters and crown holes endanger people, buildings, infrastructure and groundwater (Goetz *et al.* 1994).
- Hazards associated with rock tips, tailings dams and settling ponds:
  - o Many waste facilities contain problematic material, which may be a source of contamination of soil and water by hazardous compounds and elements (Figure 5.21). This subject is enlarged on below.
  - o Physical hazards include dam breaks, landslides and mudflows, in most cases caused by exceptionally heavy rains. Flotation tailings consist of gangue and by-breaking host rock of the ore (Figure/Plate 5.22). They are typically very fine-grained; the silt-like material tends to liquefaction and in that state can form destructive mud-flows (Ritcey 1990). Accidents of failing tailings dams occurred in the base metal mine Los Frailes in the

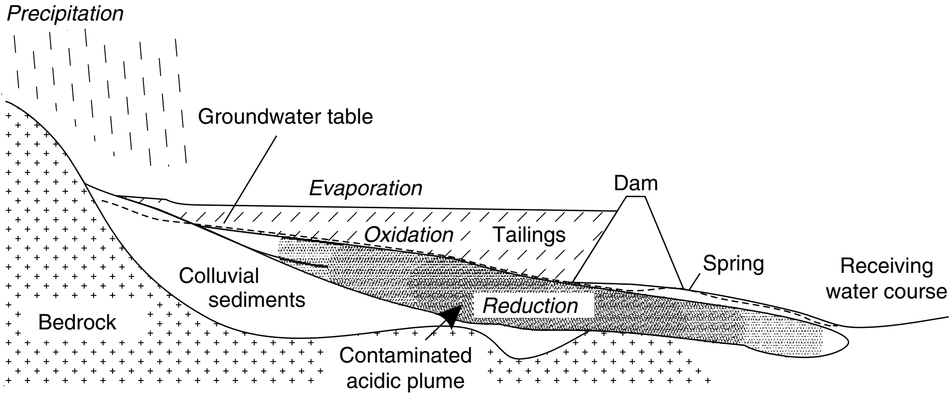

Figure 5.21 A tailings dam receiving fine-grained flotation tailings. After Alpers, C.N. & Nordstrom, D.K.,1999, Society of Economic Geologists, Inc., *Reviews in Economic Geology* 6, Figure 14.8 b, p. 314. Material containing pyrite and heavy metals with a small acid-neutralizing capacity (low Ca and Mg) is a potential hazard for the environment. Seepage water (shades of grey) can spread contamination.

South Iberian Pyrite Belt (April 1998: Ollas *et al.* 2005) and near Baia Mare in Romania during reworking of an old settling pond in order to recover gold (February 2000). Dam failure by overflow or by piping is the most frequent cause for these accidents (Richards & Reddy 2007, Terzaghi *et al.* 1996). The impact of tailings on the environment can be minimized if they are stored underground as hydraulic or paste fill in disused mine openings.

  - Pyrite-rich black shale ("reactive shale"), oil and coal-bearing shale are prone to spontaneous auto-ignition, usually after a lengthy period of slow temperature increase. Old coal washing tips may contain so much unrecovered coal that they self-ignite and burn.
- Contamination of the environment by toxic elements and/or heavy metals:
  - Apart from the main metals and minerals targeted by extraction, many orebodies and immediate host rocks display minor

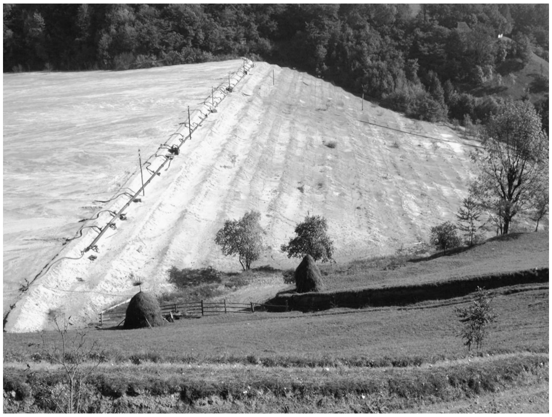

Figure 5.22 (Plate 5.22) The dam retaining the tailings pond of Baia de Aries gold mine in Valea Sartas, Romania. Courtesy Wolfhart Pohl, Washington. The image demonstrates the usual technology of "upstream building" with the main tailings discharge pipe placed along the crest of the dam, and a series of outlet risers which dispense the slurry into the reservoir. Coarser material settles near the dam, preserves stabilizing permeability, and serves to build it up, whereas slimes are washed to the centre of the pond. Permeable dams are not advisable for toxic material (e.g. cyanide).

concentrations of hazardous elements (Alloway 1990, Fergusson 1990, Plumlee & Logsdon 1999a). Examples include the semimetals Hg, Se and Te in the hanging wall above epithermal gold ore (Figure 2.23, and As, Co, Cr, Cu and Ni of gold mine tailings in South Africa (Aucamp & Schalkwyk 2003). The hazard posed by toxic elements can be better evaluated if sequential extraction methods are used, because total contents may be readily soluble, or safely hosted in resilient minerals (Rao *et al.* 2008). Remember also that mining-derived contaminants have to be evaluated in the context of the local natural background geochemical landscape (Fortescue 1992), which is nearly always anomalous in mineralized areas (Selinus *et al.* 2005). Geochemical fact sheets useful for environmental practice were provided by Reimann & Caritat (1998).

- Gas seepage:
  - o Abandoned coal mines may be a source of CO_2 that collects in nearby depressions or in the basement of buildings. The lighter methane is no less dangerous, although it will be retained in different traps such as unaired rooms. Enhanced gas flow is typically related to changes of meteorological air pressure. Methane can also be emitted from old petroleum and natural gas wells that were not properly sealed. Former uranium mines, their waste rocks and settling ponds may be

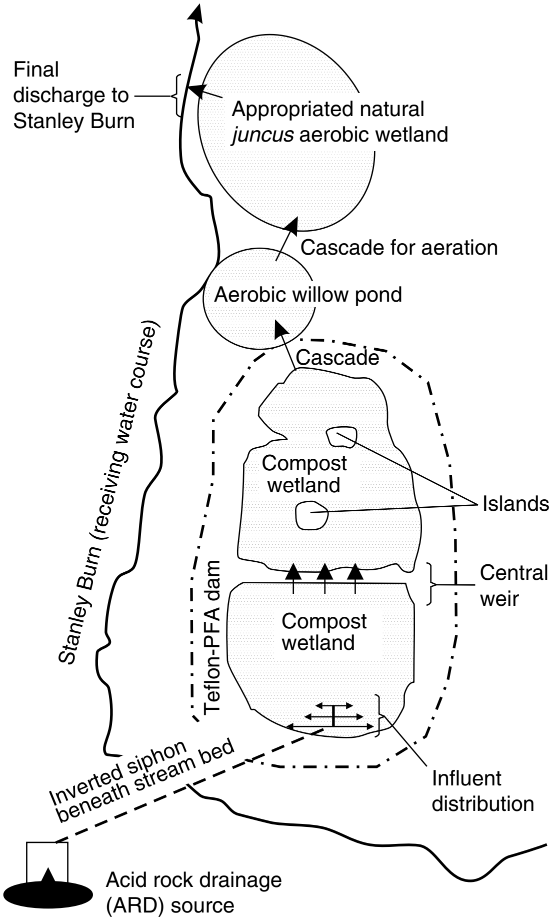
Final discharge to Stanley Burn
Appropriated natural *juncus* aerobic wetland
Cascade for aeration
Aerobic willow pond
Cascade
Stanley Burn (receiving water course)
Compost wetland
Islands
Central weir
Teflon-PFA dam
Compost wetland
Inverted siphon beneath stream bed
Influent distribution
Acid rock drainage (ARD) source

Figure 5.23 Constructed wetlands at Quaking Houses near Newcastle, UK, which serve for passive treatment of acidic water seeping from spoil heaps of former hard coal mining (after Younger 2002). By permission of IMM London & Maney Publishing (www.maney.co.uk/journals/aes). The acid rock drainage waters have pH ~ 4.5 and contain dissolved SO_4, Fe, Al, Mn and Zn. Main agents of remediation are aeration and anaerobe microbes, which thrive in a compost and horse manure substrate. Discharge water is purified and has a pH of 6.7. *Juncus* are rushes.

sources of radon. Radon's hazard lies in its α-radiation that acts on the lungs when the gas is inhaled, increasing the risk of cancer.

- Dust emissions:
  - Dust is a frequent complaint of people who live near operating pits, quarries, transport routes and bulk handling sites such as ports. For mapping dust distribution, hyperspectral methods using aerospatial data are most efficient. Spraying roads and tracks with water (possibly mixed with a coagulant) and other dust-suppressing technologies bring relief.
- Shaking, vibration, ground motion, earthquakes:
  - At close distances from a mine, blasting of rock and ore can be felt and buildings may suffer minor damages. The effect is minimized by special blasting techniques. Large rock falls and the collapse of underground voids spread uneasiness. Vibrations and noise of heavy duty traffic can incense the population.
  - As a secondary effect of mining, faults may be reactivated, resulting in earthquakes (up to magnitude 6 in parts of the Witwatersrand mining district). Similar magnitudes are reached when large sections of underground mine voids collapse (e.g. potassium salt mines in Germany). In exceptional cases, damages to buildings and loss of human lives may occur (Gibowicz & Kijko 1994, Klose 2007).
- Hazards associated with mine-site processing plant:
  - Some ore processing routes imply the use of chemicals that have to be very carefully handled. Examples include cyanides (Smith & Mudder 1999), strong acids, alkalis, organic compounds and mercury. Several accidental cyanide releases have been widely reported (e.g. in 2000 at Baia Mare in Romania, affecting rivers Tisza and Danube). Less known is the worldwide contamination of rivers with mercury, caused by artisanal gold miners employing the amalgam method of extraction. In some rivers, alluvial gold particles are rimmed by mercury derived from this source (McCready *et al.* 2003).
- Environmental hazards by emission of gases or of trace metals from metallurgical plants (Coppin *et al.* 1996):
  - Regulated gaseous emissions include CO_2, CO, SO_2, SO_3, H_2S, NO, NO_2, F and dioxin (halogenated organic compounds). In historic mining and smelting districts, downwind contamination of land with hazardous trace elements such as As, Cu, Pb and Zn (in the Iberian Pyrite Belt: Chopin & Alloway 2007), or Se, Cd and Hg (Harz Mountains, Germany) is an unwelcome heritage. Today, large efforts are expended to minimize emissions.
- Greenhouse gas (GHG) emissions:
  - such as CO_2 and CH_4 arise throughout the life of a mine. Well-planned management of energy use can reduce emissions and energy costs. GHG compensation is possible by acquiring carbon credits through increasing carbon storage in waste land, for example, by temporary biofuels production or reforestation. Due to the formation of carbonates in tailings, mines that process reactive rock, such as ultramafics, sequester more carbon dioxide from the atmosphere than needed to offset greenhouse gas emissions from operations (Wilson *et al.* 2009).
- Societal problems:
  - In an abstract way, new mines pitch the interest of the consumers of minerals who wish for low prices and assured availability, against the affected population who fear the loss of their familiar quality of life. The consumer of mineral products, however, is anonymous and will deny any joint guilt, but the mining company is an easy target for opponents of change. It is, of course, true that for the local population, very large mines fundamentally change all aspects of life. From the landscape to the infrastructure, bewildering alterations take place. The daily way of life and relations between locals are under pressure. Part of the workforce will be professional migrants. Management and staff of the mine have to understand the stress this causes and act in such a manner that the

population is not antagonized. Ethical action and the quest to mitigate negative outcomes must always be the rule. It may not be sufficient to act according to laws and regulations, because minor problems can be understood as major injustice and finally threaten the project.

- Similar to the installation of a new mine, mine closures can have grave social consequences and minimizing these must be part of the planning. Social reconciliation must always be ranged at top priority.

Meanwhile, a rich experience in solving the listed problems has been acquired. Most mines blend unobtrusively into their environment and the local society. Many communities are proud of "their" mine. In some cases, aspired solutions could not be found:

Such an example is the tailings management of the Ok Tedi Cu-Au mine in Papua New Guinea. Mining is based on a copper-gold porphyry and skarn deposit related to a monzonite intrusion (Rush & Seegers 1990). The deposit had been found by a weak (<500 ppm) copper anomaly and chalcopyrite-bearing magnetite pebbles in stream sediments (Sillitoe 1995). Ore grade is low (0.7% Cu and 0.8 ppm Au) but resources total several hundred Mt. The operation's viability depends on throughput of large masses. Because of the mine's location in steep mountains, extremely high precipitation (8–10 m/year) and frequent earthquakes, safe tailings and waste rock disposal near the mine is impossible. In order to prevent future acid rock drainage, waste is mixed with limestone. The only feasible disposal method is tipping the waste material, amounting to $\sim$30,000 m^3/day, into the headwaters of the Ok Tedi River. Near the mine, this causes build-up of mine-derived sediment in the river valley. Further downstream, a high load of suspended matter and copper contamination have negative consequences for the river and the people (Hettler *et al.* 1997). The mine expends many efforts to mitigate the damage. In view of the economic advantage for local people and the whole country and in spite of the negative effects, the mine enjoys majority support.

Waste rock and tailings

Waste rock and tailings of many mines, even if mechanically safe, are a potential source of environmental impact (Lottermoser 2007). This is because weathering of such materials may liberate: i) toxic or harmful elements; ii) salinity; iii) acid water; and iv) radioactive nuclides (Jambour *et al.* 2003). Geological, morphological, climatic and mining parameters are different for every individual site and must be considered (Hartwig *et al.* 2005). The *acid formation potential* is an important characteristic of waste; it is controlled by gangue and ore minerals. During oxidation, arsenopyrite, pyrite, chalcopyrite, pyrrhotite, marcasite and sphalerite produce much acidity, whereas galena, chalcocite and sulphates do not (Jennings *et al.* 2000). However, many sulphates are only stable in dry conditions and dissolve during wet seasons, liberating heavy metals and acidity (Alpers *et al.* 2000). Wastes may contain acid-neutralizing agents such as calcite. If net acidity results from experiments (e.g. humidity cell tests) and geochemical modelling, preventative counter-measures may be considered. These include

- liming (application of $Ca(OH)_2$ or of pulverized limestone, dolomite, brucite and magnesite) in order to raise pH, which also immobilizes many metals;
- minimizing access of water and oxygen, for example by covering the waste with clay, gravel and soil, or by flooding it with a few metres of water; and
- installing active or passive treatment if the seepage water can be captured.

"Active treatment" implies dosing the seepage with chemicals in a water treatment plant, whereas "passive treatment" is typically done by means of *constructed wetlands* (Younger 2000, Figure 5.23, Figure/Plate 5.24 and 5.25). In many of these systems, ferric iron is first precipitated (e.g. in cascades, Cravotta 2007, and stepped settling ponds) before acidity is neutralized by passing the contaminated water over open beds or through buried drains of crushed limestone. The next stage is precipitation of chalcophile metals in a reducing environment, provided by shallow ponds packed with compost, peat and animal manure that support a teeming phytoplankton and microbial community (Ledin & Pedersen 1996). Their main function is to reduce the sulphate of

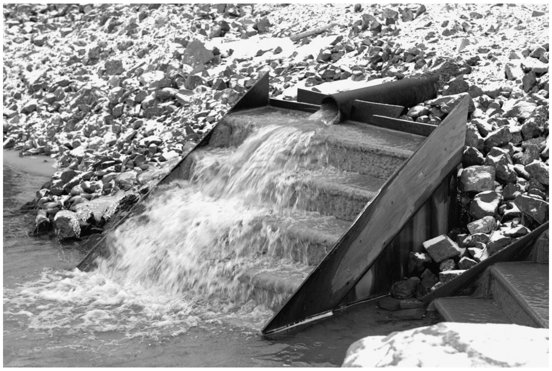

Figure 5.24 (Plate 5.24) Cascades for aerating mine water from the abandoned Dominion number 25 coal mine on Cape Breton Island, Canada. Oxidation initiates precipitation of colloidal red oxyferrohydrate, which gradually matures into minerals such as goethite, ferrihydrite and jarosite. Courtesy Christian Wolkersdorfer, CBU, Sydney, Canada.

the acid drainage. In compost beds, phosphate is often the limiting nutrient. Treatment in constructed wetlands needs little human intervention, except to renew the reactive materials. Contaminated groundwater flowing off a site can be treated by *permeable, reactive barriers* (Lapointe *et al.* 2006). Best practices and mitigation technologies related to sulphide mineral oxidation, acid mine drainage and metal leaching are described in the online GARD Guide (Verburg *et al.* 2009).

Generally, a well-planned water management is indispensable throughout the whole life-cycle of every mine, from the stage of feasibility and environmental impact studies to post-closure care (Younger & Wolkersdorfer 2004, Younger 2006, Kumar *et al.* 2010). A worldwide investigation of past mine water studies presented as part of environmental impact statements revealed significant errors and usually underestimated environmental impacts (Brown 2010). This can be illustrated by the example of hydrological studies, which are often based on only one annual cycle. It is impossible, however, to predict extreme precipitation and flooding from one year's data. Yet, extreme events are the common cause of dam breaks, landslides and mudflows. Clearly, error analysis of data is required (Taylor 1997) and upper and lower bounds of hydrological conditions affecting a mine must be determined.

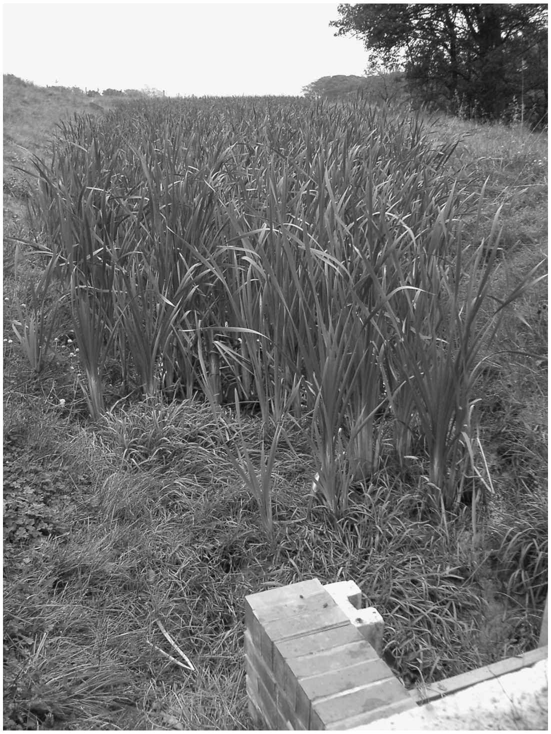

Figure 5.25 (Plate 5.25) Polishing reed bed as the last element in a passive treatment system consisting of a combined reducing and alkalinity-producing (RAPS), and wetland system for acid mine drainage from an abandoned coal mine (Bowden Close near Durham, County Durham, UK). Courtesy Christian Wolkersdorfer, CBU, Sydney, Canada.

Remediation of soil

Remediation of soil contaminated by mining or metallurgy is possible by cultivating and harvesting metal-accumulating plants ("phyto-remediation", Whiting *et al.* 2002). Of course, suitable species must be identified for every contaminant and location. Based on successful decontamination examples, the method is now applied to natural metalliferous soil, in order to extract metals ("phyto-mining", e.g. Ni in soil surrounding nickel laterite deposits, with certain *Alyssum* species). A lower-cost alternative for numerous orphaned mines may be "phyto-stabilization", which only aims at covering the hazardous material with plants so that erosion and surface run-off are reduced.

Closure of mines, reclamation of post-mining landscapes and ecosystems restoration

For more than 100 years, the closure of mines is regulated by the authorities. In the past, legal provisions aimed at protecting the public against physical or property damage (e.g. by open shafts and tunnels) and the land was to be restored to benefit the post-mining economy. Enforced measures were mainly technical, such as filling shafts and erecting fences, allowing partial recultivation (Aston 2001). In more recent times, mine-closure has to be carried out in a way that protects people and the environment durably against damages. Reclamation is enforced by the law. The target of reclamation is a landscape that is useful for industry, residential or recreational purposes, agriculture or forestry (recultivation). Wherever possible, parts of the land should be dedicated as oases of nature and wildlife habitats with minimal human intervention (renaturalization). Although every mine is a specific case, reclamation often includes the following actions:

- Take appropriate measures against physical danger to people (e.g. by permanently sealing shafts and tunnels: Fuenkajorn & Daemen 1997).
- Check and substantiate the stability of all near-surface and of large deep underground voids (Brady & Brown 2004).
- Investigate possible alternative uses of mine openings, such as disposal of moderately hazardous waste, geothermal energy production (in the case of flooded mines: Watzlaf & Ackman 2006), as a collector of drinking water, a tourist attraction, etc.
- Carry out landscaping while the mine is still active and heavy equipment is available (creating a new surface in consideration of destined use, average and extreme rainfall, erosion control, geotechnical and hydrogeological properties of rocks and soils present, including revegetation possibilities); if feasible, plan for topographic diversity, springs, step-pools, wetlands and lakes, that will commonly raise the land's value.
- Design suitable cover systems and final landforms for mine waste storage facilities
- Replace and amend topsoil for seeding and planting.
- Restore ecosystems in such a way as to provide humans with ecosystems services (e.g. food, flood and erosion control, areas for recreation and aesthetics, and clean water: Palmer & Filoso 2009).
- Model hydraulics and if needed, the water chemistry of the post-mining surface, flooded mine voids and ground water systems (Wolkersdorfer 2008).
- Construct a new surface drainage system.
- Plan for treatment (active or passive) of mine water and of seepage from mine waste, if needed.
- Envisage and model the geochemical landscape that will be the result of reclamation; note that the baseline to be attained (e.g. the concentration of hazardous substances) can hardly be lower, or better, than the pre-mining natural state of the land.
- Analyse hazard and risk of earthquakes that may be caused by flooding after mine closure (Klose 2007).
- Devise a monitoring programme.

Geoscientific aspects of reclamation

Chemically unstable waste rock and tailings (e.g. containing sulphides) should be either stabilized with pH-buffering materials, or covered so that oxygen access is minimized (Tordoff *et al.* 2000, Patterson *et al.* 2006). Cover material may be water, clay or residual organic waste from industry and agriculture (including energy crops). Surface run-off should conform to standards of ordinary surface water, suitable for fishing, bathing and water birds. The time needed for filling mine pits and country rock aquifers to a new post-mining groundwater level ("groundwater rebound": Adams & Younger 2001) has to be calculated based on hydrogeological models (Gandy & Younger 2007, Fontaine *et al.* 2003). Flooding of opencut and underground mines may degrade groundwater, mainly by oxidation and dissolution of minerals in mine openings and adjacent permeable host rocks. Appropriate planning will often be based on forward modelling of the geochemical evolution of the water (Marcuello *et al.* 2006,

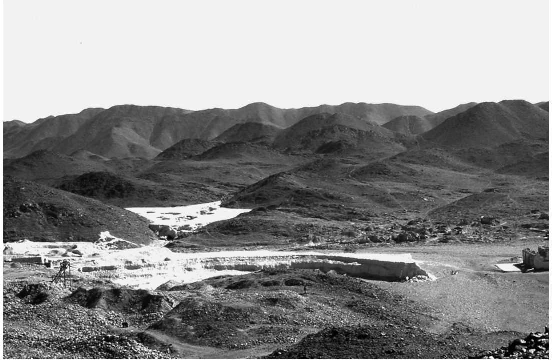

Figure 5.26 Stamp mill tailings (white) left by the former Gebeit gold mine, Red Sea Hills, Sudan. Tailings such as these are not only a possible source of contamination, but also a profitable resource if reprocessing is feasible.

Bowell 2003, Davis 2003). Based on this, preventive measures or remediation methods may be designed. Acidification of pit lakes can be prevented or remediated either by chemical treatment (addition of lime, sodium hydroxide) or by supporting microbial alkalinity production (Totsche *et al.* 2006).

Note that mine waste and abandoned mines may not only be an environmental problem, but develop quite often into important assets (Figure 5.26). A first point is their role as a habitat for many rare and threatened species, from metal-tolerant and extremophile archaea and bacteria to plants and animals, thus helping to preserve biodiversity (Batty 2005). The second concerns the frequent case that presently uneconomic mines may enter a new productive phase. Because of this, it is paramount to include the investigation of a possible mining future in all "final" mine closure projects. As commodity prices rise and more efficient technologies are employed, cut-off grades fall steadily, leading to reclassification of former *in-situ* low-grade mineralization, current and historical waste to "ore deposits" in their own right. Novel technologies are available, including low-cost microbial techniques (e.g. heap leaching of waste rock in Western Australia with 0.4% nickel). Even simple aggregates of low quality are so expensive that waste rock recycling may be profitable. Therefore, reprocessing of tailings and waste rock is increasingly seen both as an attractive investment and as a means to finance environmental remediation of abandoned mines. A striking example is the Kolwezi tailings project in the D.R. Congo, with 113 Mt measured resources at an average grade of 1.29% copper and 0.32% cobalt. A third positive aspect is that certain mine wastes sequester so much carbon dioxide from the atmosphere as to more than offset greenhouse gas emissions from operations (Wilson *et al.* 2009). This is due to supergene neoformation of carbonates from silicates, for example tailings and waste rock from ultramafic-hosted asbestos, chromium, diamond and nickel operations.

Clearly, principles and tools for socially and environmentally sustainable mining and mine site restitution are highly developed. Already, they have been embraced by most large mining companies. Yet, the transition to "green" mining has only started. For the near future, we may expect an avalanche of innovation and penetration of best practice execution throughout the world. Wise national and international governance should aim to support this change

5.5 DEEP GEOLOGICAL DISPOSAL OF DANGEROUS WASTE

With the preservation of numerous deposits and occurrences of toxic or radioactive substances over geological time-scales (e.g. the natural fission reactors in Gabon, Figure 2.44), nature demonstrates the feasibility of secure disposal of waste in deep repositories (Rempe 2008, Miller *et al.* 2000). Among professionals, the consensus is that surface disposal of dangerous industrial waste that is only confined by technical systems is not sufficient to guarantee long-term safety. In contrast, waste that rapidly loses its hazardous properties (e.g. processed urban or low-level radioactive waste) may safely be disposed of in shallow pits and subsurface vaults. Of course, even this requires geological guidance for appropriate sites. The advantage of deep disposal is the large envelope of rock that protects the repository against exogenic geological processes (e.g. erosion, weathering) and against intentional or accidental human intervention. In addition, deep rocks contain very little water that hardly moves because of low permeability and flow potentials. This inhibits mobilization and dispersion of dangerous substances, and restricts movement out of the repository to geological time-scales.

Essentially, deep geological disposal simulates, with technical means, conditions that allowed preservation of mineral deposits in the geosphere. Deep repositories may be considered to be "constructed mineral deposits".

Most important conditions for safe repositories include:

- a mildly reducing environment (*natural analogues* for this demand are deposits of sulphide ore, coal, petroleum and gas, uranium and natural fission reactors);
- absence of, or extremely small hydraulic flow;
- any water present should be in chemical equilibrium with the host rocks (formation waters); both ascending hydrothermal and descending oxygen-rich surface waters should be absent;
- tectonically disturbed rocks must be avoided because hydraulically conductive faults may cause oxidation to depths more than 10 times of the average surficial alteration.

Various technical solutions of deep disposal have been devised (Figure 5.27). Frequently, underground voids of producing or exhausted mines are used (including caverns that result from solution mining of salt). For disposal of high-heat producing ("hot") radioactive waste, new, specially engineered mines are constructed. In mountainous areas, tunnels or caverns may be prepared (e.g. Yucca Mountain: Stuckless & Levich 2007). The oil and gas industry disposes of brines and CO_2 in deep drillholes (Klusmann 2003). Similarly, many factories pump waste water into deep saline aquifers. In the future, deep sequestration of CO_2 will probably increase as this is one solution that allows continued use of coal for energy production without the hazard of aggravating climate change. At much greater depths, reaching 6 km below the surface, borehole disposal of plutonium in granite is considered.

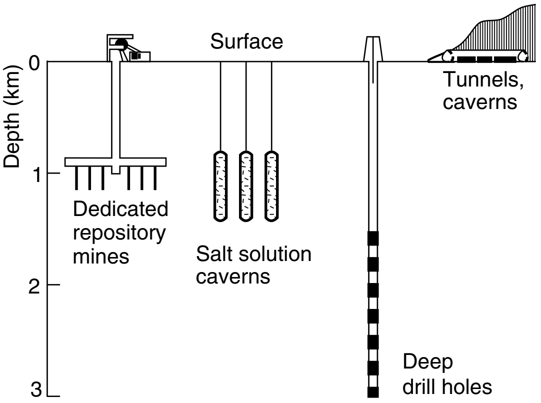

Figure 5.27 Technical variants of geological disposal of hazardous waste (modified from Herrmann & Knipping 1993). With permission from Springer Science + Business Media.

As a rule, deep disposal in mines utilizes the concept of *multiple barriers* (Figure 5.28). At depth, mine openings suitable for receiving waste are newly made, or voids remaining after extraction of minerals (e.g. salt) are refurbished. The first

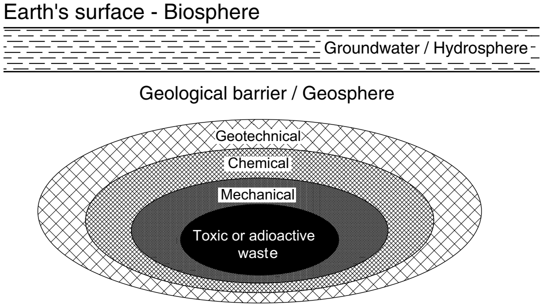
Earth's surface - Biosphere
Groundwater / Hydrosphere
Geological barrier / Geosphere
Geotechnical
Chemical
Mechanical
Toxic or adioactive waste

Figure 5.28 The concept of multiple barriers is employed to protect biosphere and groundwater from dangerous contaminants. Deep geological disposal relies mainly on a geological barrier that is supported by additional measures (constructed barriers). Chemical barriers, for example, may be concrete that maintains an alkaline environment inhibiting solubility of many elements. Physical barriers include absolutely tight containers.

(innermost) barrier concerns conditioning the waste in order to minimize its reactivity and mobility (e.g. by controlled oxidation of organic matter; vitrification; solidification of all liquids). The second barrier inhibits dispersion of dangerous substances by mechanical means (e.g. stainless steel containers, or a capillary barrier as proposed for Yucca Mountain: Carter & Pigford 2005). The third barrier employs chemical reactions (e.g. bentonite as an alkaline absorbent). The forth barrier provides geotechnical stability of storage voids and reliable sealing of access shafts and tunnels (Fuenkajorn & Daemen 1996, 1997). This is to assure long-term functionality of the fifth and most important, the geological barrier.

The *geological barrier* is required to provide sustained protection of the biosphere, similar to natural systems, for example high-grade uranium deposits. Nuclear waste requires highest standards but constitutes only about 1% of the total mass of dangerous industrial waste. For nuclear waste repositories, the geological barrier should be thick and homogeneous and exclude water. Appropriate rock bodies can be thick halitites (Gorleben, Germany, Figure/Plate 5.29: Bornemann *et al.* 2008; Carlsbad, New Mexico), mudstones (Mol, Belgium; Bure, France; Mont Terri, Switzerland: Arnould 2006; Konrad, Germany), gneiss and granite (Olkiluoto, Finland; Äspö, Schweden; Grimsel, Switzerland), or volcanic rocks (Yucca Mountain, Nevada: Stuckless & Levich 2007). The choice among these possibilities is often limited by the geological availability. Finland, for example, has no thick salt or mud rocks, but ample granite.

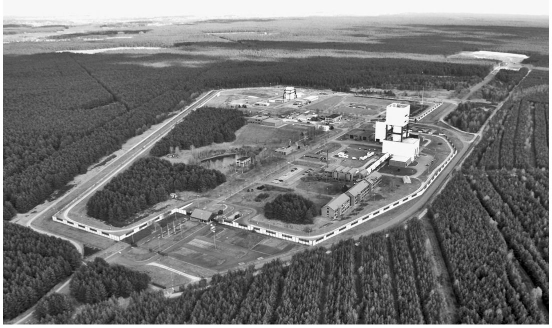

Figure 5.29 (Plate 5.29) Gorleben mine in northern Germany is destined (although not yet licensed) to function as a repository for heat-producing radioactive waste in salt rock. The aerial view shows surface installations, the two shaft buildings, waste disposal and Elbe River in the far distance to the left. © Bundesamt für Strahlenschutz, Germany.

The former oolitic ironstone Konrad mine near Salzgitter, Germany is destined to receive intermediate and low-level radioactive waste. Geology makes it an ideal deep repository. Late Jurassic sediments are here buried to >1000 m depth in a broad trough adjacent to a salt diapir. A bed of oolitic ironstone is interbedded with impure limestone of the Coral Oolite Formation. In Konrad mine, the iron ore bed had a thickness of 6–18 m with 33% Fe. From 1965–1976, ~7 Mt of ore were produced. Chambers in the ore horizon are to be filled with waste. The geological barrier consists of overlying Cretaceous mudrocks with a thickness of 750–1000 m (Figure 5.30). Because of overconsolidation, the mudrocks are very dry.

For many years, moderately dangerous waste has been buried in underground mine voids or in open cuts created by the extraction of minerals, accumulating a large body of theoretical and practical experience. In Germany, most of the slag, ash and filter dust of coal power stations and communal waste incinerators are disposed of in potassium salt or in coal mines. Toxic industrial waste is preferentially buried in salt mines, including Herfa-Neurode, Hesse (Figure 4.22). In some mines, waste serves as a fill, supporting the mechanical stability of underground voids. Until recently, intermediate and low-level radioactive waste was stored in the former salt mines at Morsleben and Asse in northern Germany.

Thick salt formations are well suited for the disposal of toxic and radioactive waste (Herrmann & Knipping 1993). Salt rocks have an extremely low permeability for water and gas, which ensures enclosure and inhibits contaminants entering the hydro- and biosphere. In a relatively short time, mine voids in salt rocks close by plastic flow (creep), thus strengthening the rock barrier. Furthermore, rock salt is resistant against moderate heating (~200°C) and radiation.

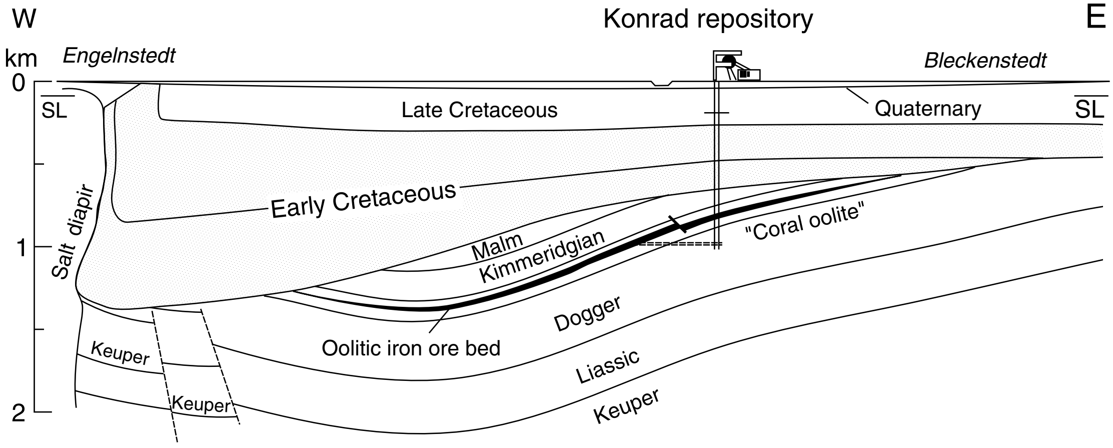

Figure 5.30 Geological profile of the Bleckenstedt Trough north of the Harz Mountains, Germany, with the Konrad repository for intermediate and low-level radioactive waste, in a former oolitic iron ore mine (iron ore black). SL = Sea level. With permission from www.schweizerbart.de.

Repositories for radioactive waste

Repositories in salt rocks for heat-producing high-level radioactive waste require extremely detailed and meticulous investigations. An exemplar case is the enormous scientific and technical exploration work at the Gorleben salt diapir in Northern Germany (Figure/Plate 5.29, Figure 4.26; Klinge *et al.* 2007, Köthe *et al.* 2007, Bornemann *et al.* 2008). Important geoscientific aspects of this kind of work comprise:

- The selection of adequate salt rock bodies is primarily controlled by geological parameters. In many regions of the world, existing geophysical data acquired during hydrocarbon exploration are very valuable data sources (Jenyon 2008). Ideal targets are large halitite masses with a minimum of tectonic disturbance, which are covered by low-permeability mudrocks. However, as with establishing a new mine, infrastructure, economic and social parameters will be crucial for a successful project.
- The tectonic stability of a salt rock body refers to the inherent buoyancy of light salt compared to surrounding sediments. Within a short geological time, resulting upflow might lift the repository to the surface. Many ("active") salt diapirs in Northern Germany rise at rates of between 0.01 and 0.5 mm/year. Stable, that is tectonically "inactive", diapirs have no measurable upflow. This can be controlled by long-term geodetic surveys, but the geological upflow history of a salt body should be established in order to strengthen the case for a durably inactive state.
- The hydrologeological stability of a salt body depends on the rate of salt dissolution (present and past) where it is in contact with aquifers. Salt diapirs with a history of strong subrosion such as Arendsee (Figure 4.28) are unsuitable. In many cases, however, the surface morphology will be less striking and may be of no help. A thorough investigation of the caprock and the hydrogeological situation is absolutely required (Gorleben: Klinge *et al.* 2007).
- A favourable internal structure of the salt formation, including a large dry salt body (halitite) with a minimum of hydrous mineral components at the required depth. Large anhydrite masses are better avoided because they may contain brine. Also, because of anhydrite's high density, large blocks tend to gradually sink downwards (Koyi 2001).

Results of geoscientific investigations are building blocks for assessing the longevity of the geological barrier between waste and biosphere. For some nuclides that are contained in radioactive waste, a "proof" of safety (the technical term is "safety case") is required for periods approaching one million years. Clearly, the nature of possible changes in that time and the associated risks cannot be known with certainty (Macfarlane & Ewing 2006). Yet, earth scientists commonly agree that deep disposal is the safest option, but disagree often on the safety of a specific site. Considering the relatively high level of natural background radiation, however, even a nuclear repository need not be absolutely tight. Small masses of nuclides seeping out may be lost in the ubiquitous natural background (Selinus *et al.* 2005).

5.6 SUMMARY AND FURTHER READING

Metals and minerals serve human needs such as housing and in use, are consumed. The mining industry provides the required raw materials. For continuity of supply, a steady rate of replacement is required involving new mines. The search for new deposits is an important part of the industry's activities and of economic geologists' professional duties and responsibilities.

Let us here acknowledge the drivers in this field. Worldwide, about 2000 stock exchange-listed companies are active in non-ferrous metal exploration. International and state organizations (e.g. China), unlisted companies and specialists for iron ore and minerals may add another 1000 to this figure. It is a great achievement, that this relatively small industry sector supplies the world with an adequate number of new prospects, mines and raw materials.

Strategies and methods of the search for minerals and metals ("exploration") build on the large body of metallogenetic science and utilize all available technologies, from electron microscopy to interpretation of satellite images. Nearly all deposits display subtle halos of anomalous geochemical and mineralogical composition, and many have physical properties such as high density or conductivity, which allow detection through thick sterile overburden. Different deposit types are characterized by specific sets of geological environment and properties which are combined in "exploration models" that guide the search.

Potential deposits indicated by preliminary work ("prospects") are investigated in more detail, usually by drilling. Drilling is first aimed at the centre of the assumed orebody, in order to confirm the presence of significant mineralization. Core samples obtained are thoroughly analysed and as data density and coverage increases, a detailed image of the mineralized body evolves. Ore resource quality and quantity are estimated. In a prefeasibility report, the results are compared with working mines of a similar type. Very often, this leads to final rejection of the prospect.

In the case of accumulating evidence that the prospect resembles orebodies supporting flourishing operations, work turns to assembling all data that are needed to prove the viability of a new mine. This includes more drilling and bulk sampling, in order to affirm sufficient reserves which justify the investment – remember that establishing new mines costs from 50 to 2000 million US$. Mine planning, processing and geometallurgy, environmental state and management of the future mine, financing and economic viability, social reconciliation and many more aspects have to be investigated to such a degree that the decision to open the new mine is fully supported. The resulting feasibility document equally serves licensing authorities and investors.

It is very important to understand the precise meaning of the terms "reserves" and "resources". Reserves are only that part of resources that is thoroughly investigated and proved to be exploitable with a high degree of confidence. Reserves are essentially determined by economic recoverability and are the foundation of mining operations. Reserves provide collateral security to investors and stock markets. This role provoked the elaboration of reserve reporting codes, e.g. by JORC in Australia. Outlining reserves in the ground is a costly undertaking, which must be financed before any profit is made from future income by extracting and selling the ore. The present value of future income is a function of time, because it results from discounting. Income due in 40 years from now is practically worthless. Therefore, reserves are hardly ever substantiated for a period beyond this mark.

Resources are principally less well-known or even unknown. Measured resources may be disclosed for a deposit in order to show that the mineralized body is much larger than reserves, but are not bankable. Unknown resources, however, are the subject of scientific enquiry and the hopes of explorers. This is that part of the total geological endowment of the Earth with a certain metal or mineral that may one day satisfy human needs. It is the stock from which new discoveries are wrested.

Few mines have no visible impact on people and environment. During the working period of a mine, unaesthetic changes to the land, artificial water bodies, increased traffic and dust, noise and vibration, and perturbation of the local community all may cause rejection of the operation. Yet, the "social licence" is essential. Why are some communities proud of their mines and others wish them away? Mine closure, however, is not without its own social problems.

Technical problems of mine closure first comprise measures to ensure safety for people and animals, such as sealing tunnels and shafts. Land and ecosystems are restored to some use, ranging from brown field industrial plots to nature preserves. Reprocessing old mine waste, such as shale tips with 10% coal fines, may pay for remediation. Tailings should be landscaped and covered in order to avoid leaching of hazardous elements. Parts of mines may be destined to allow nature its course, in order to create islands of biodiversity.

Principles and tools for socially and environmentally sustainable mining and mine site restitution are pioneered by the large mining companies. The transition to "green" mining is on its way. The face of the future extractive industry will be very different from that in the past.

Readers searching for a more profound introduction to mineral exploration are directed to Moon *et al.* (2006). If you have access to a good library you might enjoy Evans (1993). In order to learn more about geological concepts, models and methods that are the indispensable base for any exploration project, read Kreuzer *et al.* (2008) and Kelley *et al.* (2006). My favourite sources, however, for better understanding geological exploration, are Glasson & Rattigan (1990) and Sillitoe (1995). The first assembled 50 valuable case studies from Australia, tracing geological exploration from the time when in ~1850 the first geologists arrived in the colony. Sillitoe provides a wealth of useful detailed information and concludes that the key to finding ore deposits is "experienced geologists in the field and a generous drilling budget". In my view, these two books should be compulsory reading in all exploration training programmes. *Quantitative Mineral Resource Assessments* by Singer & Menzie (2010) shows how to estimate number, tonnage and grade of undiscovered deposits. Modern insight into geochemical exploration is provided by Carranza (2008) and geophysical methods are explained in more detail in the book by Keary *et al.* (2002). Various facts and figures that may be needed in practical work are assembled in Bell 1993, 1998), Berkman (2001) and Walker & Cohen (2007). Environmental problems of mining and possible solutions are broadly covered in Bell & Donelly (2006) and Warhurst & Noronha (2000). I recommend the two *Environmental Geochemistry of Mineral Deposits* volumes by Filipek & Plumlee (1999) and Plumlee & Logsdon (1999), for a scientific yet accessible level. Readers who wish to explore the economic aspects of environmental issues should consider reading Gilpin (2000) and Lomborg's (2001) provocative *Skeptical Environmentalist*.

PART IV

Fossil Energy Raw Materials – Coal, Oil and Gas

Carbon is the element of Life on Earth – six major elements, carbon, hydrogen, nitrogen, oxygen, sulphur and phosphorous are required to build all biological macromolecules. Carbon dioxide in the air, and water are used by plants in photosynthesis of carbohydrates, such as cellulose. By photosynthesis, terrestrial global gross primary production (GPP) removes ~123,000 million tonnes carbon (MtC) of CO_2 per year from the atmosphere (Beer *et al.* 2010), compared to human emissions by burning fossil fuels of ~7,000 MtC/yr. Most bacteria and archaea, and all higher animal life forms including humans, use the reduced carbon of carbohydrates as food and breathe out carbon dioxide. Life is an important part of the Earth's carbon cycle. However, the planet contains other reservoirs of carbon and carbon dioxide, including the mantle, the crust, ocean floors and permafrost lands with methane gas hydrates. The Earth constantly degasses carbon dioxide and peaks occur with large outpourings of volcanic eruptions at the surface. Yet, during the last 450 million years, carbon dioxide concentration in the atmosphere has decreased steadily (Normile 2009), mainly because of the proliferation of plants on land, carbonate-fixing biota in the oceans and carbon burial in the subsurface. By burning fossil fuels, humanity reversed this trend from a pre-industrial ~280 to a present 388 ppm CO_2 in the atmosphere. Beginning in Pleistocene glacial times, the role of reduced carbon for humans has increasingly changed from food to fuel.

Fossil fuels include coal, petroleum, natural gas, tar (heavy crude oil) and oil schists. Coal's peak role as an energy raw material was reached early in the 20th century. Since then, oil has displaced coal to second rank. In 2009, the world's primary energy supply (ca. 11,164 Mt oil equivalent) was provided by 34.8% from petroleum, 23.8% natural gas, 29.4% coal, 6.6% hydroelectricity and 5.5% nuclear power (*BP Statistical Review of World Energy* 2010). BP sources are limited concerning renewable energy, but do report that geothermal, wind and solar electricity generation combined account for approximately 1.7% of global electricity generation. The International Energy Agency (IEA) provides more detailed data and projections about renewables

---

Economic Geology Principles and Practice
Metals, Minerals, Coal and Hydrocarbons – Introduction to Formation and Sustainable Exploitation of Mineral Deposits, Walter L. Pohl
© 2011 Walter L. Pohl. Published 2011 by Blackwell Publishing Ltd.

CHAPTER 6

Coal

> *... plants are a significant geological force of nature – a critical missing feedback linking biology, chemistry, and physics that has shaped our planet's history ...*
>
> David Beerling 2007

Synopsis

For industrial nations, abundant energy in the form of coal was the fundamental precondition for development (Freese 2003). Considering examples such as China and India, this is not different today. Development requires bounteous and low-cost energy, which involves sacrificing the pre-industrial farming society with its perceived peaceful and sustainable life. For liberating the inherent energy, coal must be combusted, resulting in various hazardous emissions that have to be controlled. Coal's most widely discussed emission is carbon dioxide because of its influence on global climate. This feeds a lively debate about the future of coal.

This chapter starts with a concise introduction to coal utilization, production and resources, including information on possible carbon dioxide mitigation strategies. To lay the base, the ensuing sections discuss the substance of coal, its formation from peat deposited in ancient wetlands and the processes that make coal from peat. We then look at weathering of coal, which often involves self-ignition and natural coal seam fires. Practical aspects of coal science, such as its application in exploration, reserve estimation, mining and environmental mitigation, conclude the chapter.

At present, the major utilization of coal is electricity production. China, for example, derives ~80% of its electricity from coal and the United States 50%. Cokes produced from certain hard coals, and anthracite, are ideal reductants for processing oxide metal ores and are also used in many other industrial processes (e.g. soda ash and carbide manufacture, cement-making, hydrogen production by steam reforming). Domestic heating is a minor sector of coal use. In the near future, the production of liquid fuels from coal and lignite, based on the Fischer-Tropsch synthesis and similar processes ("coal-to-liquids technology"), is expected to expand considerably. This is due to increasing economic viability, as prices of petroleum and natural gas rise. South Africa has a long tradition of providing its liquid fuel needs by this technology. Today, many more countries, which have limited natural hydrocarbon but large coal reserves, plan to take this route (e.g. Australia,

Economic Geology Principles and Practice
Metals, Minerals, Coal and Hydrocarbons – Introduction to Formation and Sustainable Exploitation of Mineral Deposits, Walter L. Pohl
© 2011 Walter L. Pohl. Published 2011 by Blackwell Publishing Ltd.

China, India, New Zealand, USA). Gasification is emerging as an improved technology for electricity production from coal, resulting in lower sulphur dioxide, nitrogen oxide, mercury and particulate emissions, compared to a conventional pulverized coal power plant. The IGCC (integrated gasification combined cycle) process also uses less water and can be more economically retrofitted for carbon capture.

This scenario implies that in the future, production and use of coal will continue to grow. Is this supported by sufficient coal resources? Today's deposits that can be exploited under existing economic and operating conditions ("proven reserves") contain ~ 826,000 Mt. Of this total, one half comprises black coal and anthracite, the remainder brown coal and lignite (*BP Statistical Review of World Energy* 2010). World production of coal and lignite in 2009 was ~7023 Mt (equal to 3409 Mt of oil equivalent). The largest producers of hard coal are China (45.6%), USA, India, Australia, Russia and South Africa. Germany is the leading lignite producer, followed by USA, Greece and Australia.

Dividing reserves by annual production (R/P) gives the so-called "static period of availability" of coal reserves at ~120 years (Figure 6.1). Of course, the ratio does not define the end of coal, because additional giant resources are available. It illustrates only the difference between coal and other raw materials, concerning the rules for defining coal reserves and the long-term nature of planning. At face value, coal reserves are assured for a much longer time than petroleum (at the end of 2009 ~46.7 years, the Canadian oil sands not included) and natural gas reserves (~63 years). As explained in Chapter 7, oil and gas production will continue far beyond this period. Additional giant energy resources are available if today's uneconomic coal occurrences can be made useful, for example by new extraction technology or *in-situ* gasification.

More than 60% of world coal reserves occur in the USA, Russia and China. With nearly 30%, the USA hosts the largest reserves of all countries. Black coal (anthracite and bituminous coal) reserves occur in USA, China, India, Russia, Australia and South Africa. Significant brown coal (sub-bituminous coal and lignite) reserves occur in USA, Russia, China, Australia, Ukraine, Colombia and Canada.

Carbon capture and storage must result in a higher price of electricity and requires giant investments. Economists are divided on the best mitigation path to take. Should the huge sums needed for a reduction of anthropogenic CO_2

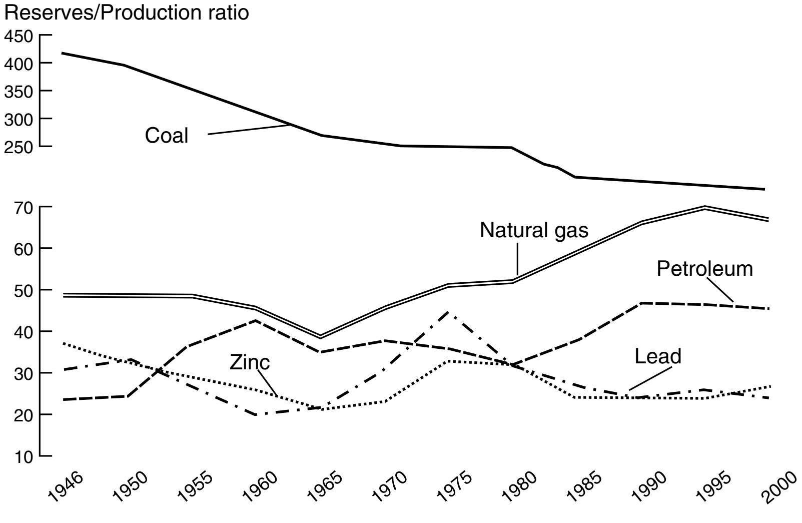

Figure 6.1 Evolution of the reserves to production ratio R/P (also called "life-index" or "R/C ratio") of energy raw materials coal, petroleum and natural gas, compared to lead and zinc, from 1945 to 2000 (adapted from Wellmer 2008). With permission from www.schweizerbart.de. The rapid fall of the R/P ratio of coal is not due to depletion, but to gradual world-wide acceptance of stricter rules for declaring reserves (cf. Chapter 5.3.2 "Ore Reserve Estimation and Determination of Grade"). In 2010, R/P ratios were 47 years for oil, 63 for gas and 120 for coal (BP 2010).

BOX 6.1 Coal and carbon dioxide

Worldwide, there are ~2100 coal-fired power plants. Burning coal implies the generation of waste gases, including CO_2, SO_2 and NO_X. The two latter can be reduced to low levels by better combustion and flue gas cleaning technologies. Reduction of greenhouse gas (GHG) carbon dioxide emissions progresses only gradually, however, mainly by more efficient combustion and by saving energy. The energy yield was improved from ~33% in the past to 55% in modern coal-fired power plants. Even so, coal-burning accounts for roughly one-third of the CO_2 generated by human activity (a total of 7 Gt per year, Normile 2009). One tonne of black coal containing 80% C generates nearly 3 t CO_2. Today, the public, governments and industry are prepared to take more radical counter measures against CO_2 (and other) emissions into the atmosphere. This is certainly desirable, even if a leading role of CO_2 as a control on climate is not undisputed and the climate's sensitivity to a doubling of CO_2 may be commonly overestimated (Plimer 2009, Kirkby 2008, Royer *et al.* 2007). About 75% of the greenhouse effect is due to clouds and water vapour and 20% to CO_2 but without CO_2 and minor GHGs, Earth would rapidly fall into icehouse state (Lacis *et al.* 2010). Present data are insufficient to decide if climate change increases or decreases evaporation (Dolman & de Jeu 2010) which is a significant factor of the Earth's surface energy balance. Stratospheric water vapour is unexpectedly revealed as an important climate driver (Solomon *et al.* 2010). For the last five years, the energy balance of the Earth defies climate modellers (Trenberth & Fasullo 2010).

Apart from reducing fossil fuel use, two mitigation strategies against the increase of atmospheric CO_2 concentration are mainly pursued (Lackner 2003): i) Net carbon storage in forestry and agriculture, including soil improvement by adding biomass or char; and ii) carbon-capture and storage systems (CCS) that include underground sequestration in mature oil and gas fields, in deep coal beds and in deep saline aquifers. The last has been practised for many years in the Norwegian offshore gas field Sleipner (Bickle *et al.* 2007, Figure/Plate 6.2). Worldwide available pore space is thought to be very large (Figure 6.3). Less credible, CO_2 might be disposed of as a liquid in deep oceans, in zeolites, and in magnesite made from serpentinite and dunite. CO_2 capture technologies, more than sequestration, are costly. Two technologies of capturing CO_2 are currently favoured: The first binds CO_2 on monoethanolamine (MEA) or ammonium carbonate in order to separate it from nitrogen in the flue gas, whereas the second burns the coal with pure oxygen.

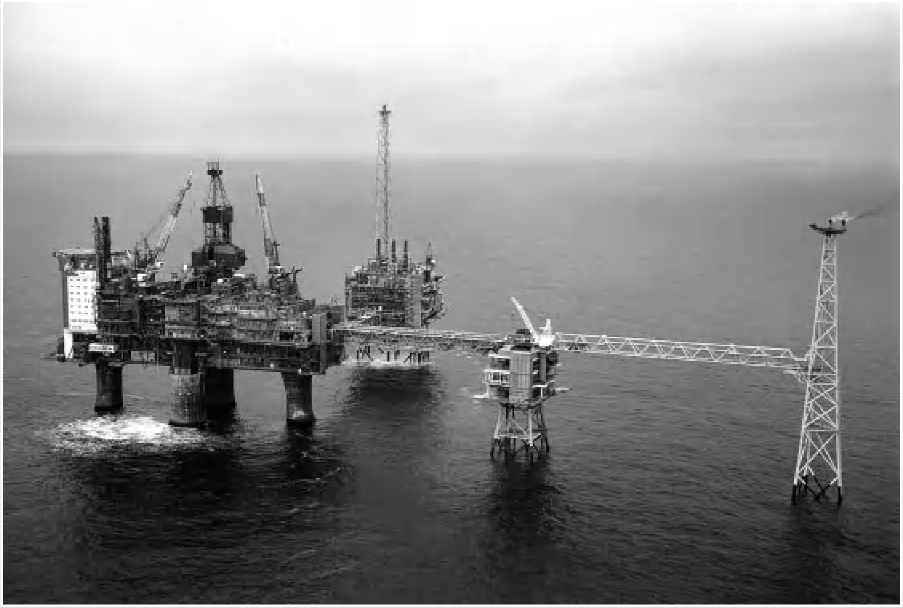

Figure 6.2 (Plate 6.2) Sleipner platform in the North Sea off Norway is the world's first large-scale geological CO_2 sequestration operation. On the platform, carbon dioxide is separated from natural gas and pumped into a sub-seafloor aquifer. © Øyvind Hagen, Statoil.

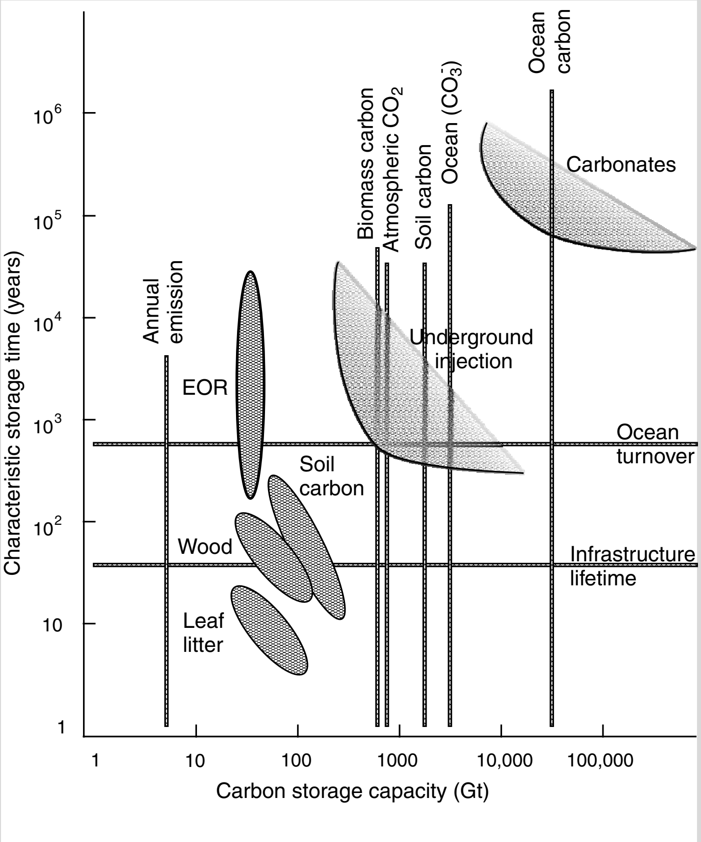

Figure 6.3 Comparison of several significant variants of CO_2 sequestration, their estimated storage capacity and time of immobilization (modified from Lackner 2003). Reprinted with permission from AAAS. Carbonates guarantee the maximum of isolation time, whereas biomass is short-lived. Advisable seem to be EOR (enhanced oil recovery) and deep injection with its large capacity.

At ambient pressure and temperature, carbon dioxide is a gas (density 1.98 g/cm^3) that is 1.53 times heavier than air. At moderately low temperatures (31.1 to −56 °C) and a pressure from 5–73 bar, CO_2 is a liquid heavier than water. Above its critical point at 31.1 °C and ca. 73 bar, carbon dioxide transforms into a low-viscosity supercritical fluid. This is the state of concentrated CO_2 in geological reservoirs at depths below ∼500–1000 m. With a density of 0.5–0.7 g/cm^3, supercritical CO_2 is less dense than brine or petroleum but more dense than methane. Within the reservoir, injected CO_2 is gradually dissolved in formation water and commonly occurs as ionic HCO_3^- (eq. 1.14). In time, it may be immobilized by precipitation of carbonates such as calcite. Leakage from CO_2 repositories to the surface must be minimized, not only because escape defies the purpose of storage, but also in order to prevent hazards to human and animal life. Carbon dioxide gas is an inert asphyxiant and because of its density, collects in calm depressions and basements. Humans react to CO_2 concentrations of 4–5% in air by accelerated breathing and discomfort, at 7–10% persisting for several minutes by fainting (Weinstein & Cook 2004). Maximum work exposure is set to 0.5%. Because of the perceived hazard, offshore sites such as Sleipner are probably more acceptable than onshore storage in densely populated regions (Schrag 2009). Haszeldine (2009) presented a map of CO_2 emission sites in Northwest Europe and a draft of possible pipelines and storage fields in the North Sea.

Once captured, CO_2 is liquefied, dried and pumped down into geological reservoirs. This technology is well-known in the oil and gas industry because for many years, supercritical carbon dioxide has been used to displace hydrocarbons from reservoir pore space in order to enhance oil recovery. One example is the almost pure magmatic CO_2 from Bravo Dome gas field in New Mexico, which is used for carbon dioxide injection to maximize oil recovery in western Texas. The comparable but less practised CO_2-enhanced methane recovery (ECBM) from deep unexploitable coal seams may offer another path of CO_2 geosequestration (Ozdemir 2009). In the Rangely Oil Field, Colorado, loss of injected carbon dioxide by micro-seepage to the atmosphere is a fraction of natural methane seepage (Klusmann 2003). The safety case for geological CO_2 storage is gaining strength (Houston *et al.* 2007) and in a North Sea oil field CO_2 pool, seal performance for >70 million years has been demonstrated (Lu *et al.* 2009). For prospective storage sites, the main questions that must be answered concern: i) the pressure management; and ii) the fate of the displaced pore fluid (Schrag 2009). Although large-scale capture and geological sequestration of CO_2 still present technological challenges, CCS may soon be widely employed, provided that clear regulations assure companies of a long-term business perspective (Haszeldine 2009). Overall it is expected that in a few decades, CO_2 emissions from coal, oil and gas power stations will be reduced to unproblematic levels similar to the successful mitigation of SO_2 and NO_x. On that base, fossil fuels can yet provide long-term sustainable energy for the world's industry and humans (Haszeldine 2009, Jaccard 2006).

emissions be provided now because of ethical considerations (Stern & Taylor 2007), or "ramp up" slowly as conventional economic analysis (Nordhaus 2007) indicates? For the second more realistic case, a strategy might be prepared to arrest a possible "run-away" warming of the Earth's climate, when the upper limit of the IPCC (UN Intergovernmental Panel on Climate Change) temperature rise is near. This includes various techniques of *climate engineering* (Wigley 2006). Injecting aerosols or aerosol precursors (i.e. SO_2) into the stratosphere can provide a negative forcing of the temperature and offset part of the positive forcing due to increased greenhouse gas concentrations. Volcanic eruptions provide natural examples of this effect. In June 1991, Mt Pinatubo blew ~10 Mt sulphur into the stratosphere and caused detectable cooling without disruption of the climate system. Another method might be fertilizing the upper oceans with iron in order to amplify biomass production, enhancing carbon storage by burial of organic matter in ocean floor sediments (Boyd 2007). Such actions could slow warming and provide time for the huge investments needed to reduce human CO_2 emissions.

6.1 THE SUBSTANCE OF COAL

6.1.1 Coal types

Coals are solid, combustible, fossil sedimentary rocks that formed from land plants (*Embryophyta*) profusely growing in ancient wetlands. After deposition, the peat was covered by sediments, usually clay and sand. Diagenetic processes acting on the material caused an overall enrichment of carbon (coalification). The difference between coal, peat and coal shale is important because in many countries the state controls coal mining, whereas peat and coal shale belong to the land owner.

Peat, the soft sediment in mires and fens, is the precursor of coal, which is a hard rock. Low-grade lignites (bog coal) are intermediate between mature peat and mature lignite. The limit between peat and lignite is rather a matter of convention. In some countries peat may be an important source of energy.

Coal shale and bituminous shale can be valuable raw materials, for example in cement production (cf. Chapter 3 "Carbonate Rocks"). These rocks are remarkable because they self-ignite and burn slowly when dumped on waste rock tips without special precautions. Generally, the limit between coal and coal shale may be set at 50 wt. % combustible substance (dry basis). However, coal with more than 30 wt. % of non-combustible matter is rarely used as a fuel. Coals with higher content of mineral matter (e.g. clay, silt, sand, carbonates, sulphides), but not exceeding 50%, are called "impure coals". If feasible, mine-site processing is often employed to upgrade the coal content of low-grade impure material.

The distinction between brown coal and black coal originated in Europe, because there is such an obvious difference between Tertiary low-rank brown and Carboniferous high-rank black coal, with rare intermediate quality deposits. The first has a low calorific power and its use is restricted to energy and heat production, whereas the second is a prime fuel and a valuable industrial reductant (e.g. for iron melting). The terms brown coal and lignite are widely considered as synonymous. The terms "black" or "hard coal" are little used

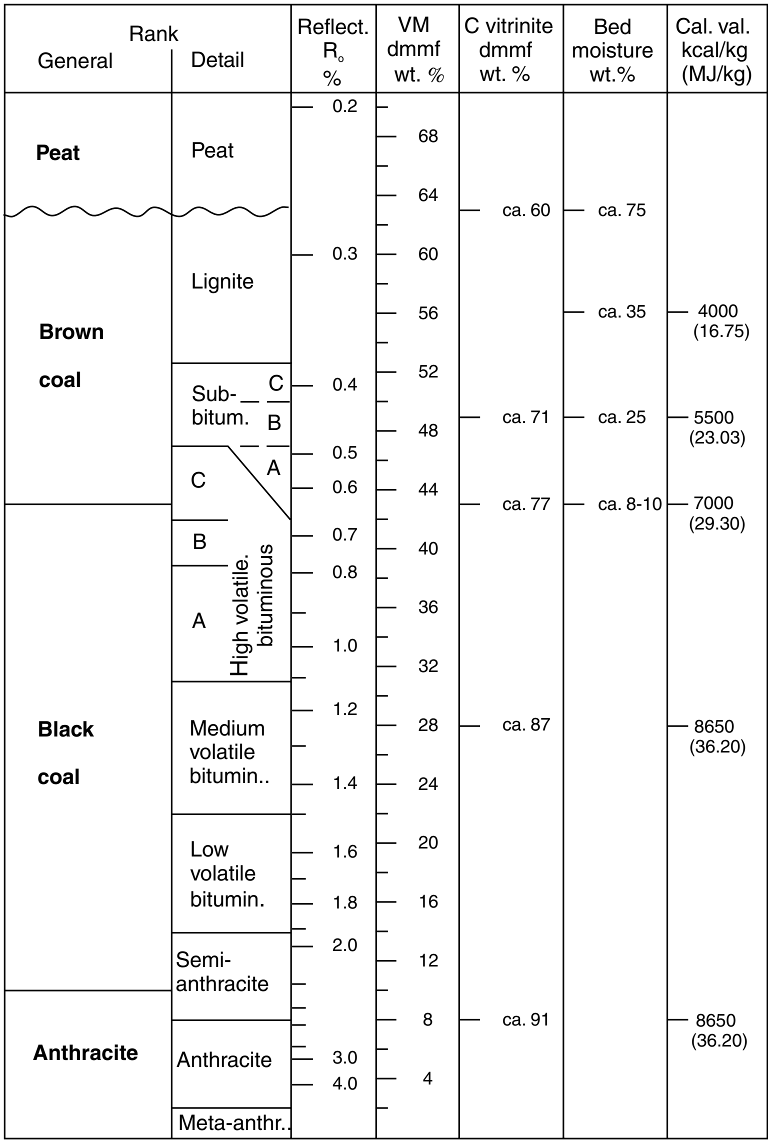
Rank
General
Detail
Reflect. R_o %
VM dmmf wt. %
C vitrinite dmmf wt. %
Bed moisture wt.%
Cal. val. kcal/kg (MJ/kg)
Peat
Peat
Brown coal
Lignite
Sub-bitum.
C
B
A
C
B
A
High volatile. bituminous
Black coal
Medium volatile bitumin..
Low volatile bitumin.
Semi-anthracite
Anthracite
Anthracite
Meta-anthr.
0.2
0.3
0.4
0.5
0.6
0.7
0.8
1.0
1.2
1.4
1.6
1.8
2.0
3.0
4.0
68
64
60
56
52
48
44
40
36
32
28
24
20
16
12
8
4
ca. 60
ca. 71
ca. 77
ca. 87
ca. 91
ca. 75
ca. 35
ca. 25
ca. 8-10
4000 (16.75)
5500 (23.03)
7000 (29.30)
8650 (36.20)
8650 (36.20)

Figure 6.4 Classification of coal according to rank with reference to important properties (modified from Taylor *et al.* 1998). With permission from www.schweizerbart.de. The international unit for calorific value in the SI-System is *Joules*. Conversion: 1 kcal = 4.1868 kJ [d.m.m.f. = calculated to dry and mineral matter free, i.e. pure coal substance].

in English; the common terms are "bituminous coal" and "anthracite" (Ward 1984, Thomas 2002).

Low rank coals (lignite and sub-bituminous coal, Figure 6.4) are subdivided according to water content. Bituminous coals are mainly classified by % volatiles liberated at high temperature in the absence of oxygen. This underlines that at differing rank, suitable parameters for coal classification vary. Some observations on macroscopic characterization of coal types include the following:

Lignites

Lignites are yellow or brown coals that can be cut with a knife. Lowest rank soft, earthy or crumbly lignite is called "bog coal"; it occurs in thick banded seams that are not jointed. In certain horizons, upright tree stumps or fallen logs are numerous. Exposed bog coal crumbles quickly because of drying and shrinkage. Seams occur at little depth below the surface and country rocks are unconsolidated sediments. "Lumpy" lignites are harder and more consolidated and on extraction break into large fragments. This type is made up of brown tree stumps, logs and branches. The seams are banded, either by thin layers of clastic sediment, detrital coal, or by charcoal and charred woody debris (fire horizons). Lumpy lignite occurs at a depth to a few hundred metres below moderately consolidated sediments. Today, lignites are exclusively used for large electricity production units.

Sub-bituminous coal

Sub-bituminous coal ("black lignite") is markedly brittle. With increasing rank (from C to A, Figure 6.4) its colour varies from dull brown to lustrous bright black. Fossilized wood can still be recognized. The seams are closely jointed and banded. On drying, dull coal disintegrates into small cubic lumps, whereas lustrous sub-bituminous coal with lower water content changes little. Sub-bituminous coal occurs at a depth of several hundred metres below medium-consolidated sediments.

Bituminous coal

Bituminous coal occurs in well-consolidated sediments (e.g. sandstone, shale) and both coal and host rocks are jointed. From low to high rank, the main varieties are:

- high volatile bituminous (gas coal);
- medium volatile bituminous (coking coal); and
- low volatile bituminous coal (steam coal).

There is little macroscopic difference between the three; all bituminous coals are brittle and composed of thin dull and bright bands. As volatile substance content decreases, banding and layering of coal wanes and disappears when the anthracite rank is attained. Natural coking coals and commercial blends that provide good coke are most valuable. Non-coking bituminous coals are burned in power plants and general industry; gas coal is especially suitable for the production of liquid fuels.

Anthracite

Anthracites are black, and display a metallic lustre and a conchoidal fracture. Due to the very low content of volatile matter, anthracites burn with little smoke and with short flames. They are preferred for steam and heat generation. Meta-anthracite is transitional to graphite. In fact, a sizeable part of traded "graphite" is meta-anthracite.

The coal varieties described so far are *humic coals*. They originate from land plants and peat, and represent the majority of all coal extracted. Many deposits of humic coal contain a minor part of less common coal varieties. These include *sapropelic* (boghead and cannel coal, schungite) and *liptobiolite* coals. Sapropelic coal is formed as a bottom sediment in stagnant anoxic water from small particles of plant residues, spores and foundered mats of floating algae. The sediment is putrefied rather than peatified. Liptobiolites consist of plant material that resists oxidation on the peat surface (e.g. spores, pollen, wax, resin, amber) and accumulates in situ or after transport by wind and flowing water.

Boghead coal

Boghead coal (torbanite) is composed of characteristic algal colonies (e.g. *Pila, Reinschia*). Boghead is of blackish-brown or greenish-black colour and gives a brown streak. Similar to cannel coal, it is very fine-grained and homogeneous, and presents a conchoidal fracture. Boghead occurs with humic coals or forms independent seams that may grade into oil shale and petroleum source rock as mineral matter content increases. Volatile matter content of boghead is very high, so that the material is preferably used for "synthetic oil" production. On heating in a retort, up to 800 litres of oil per tonne may be recovered (cf. 7.7 "Oil Shale").

Cannel coal

Cannel coal burns like a candle when ignited, explaining its name given by miners. It is black with a greasy dull lustre and has a black streak. Often found in the upper part of humic coal seams, it forms thick slab-like beds. Constituents are mainly derived from vascular plants and comprise uniformly fine-grained particles such as spores, resins, plant debris, black carbon and algae (Hutton & Hower 1999). Siderite lenses and bands are frequent in cannel coal and beds may pass into massive siderite. Cannel coal occurs in all major coal fields of the world. *Jet (gagatite)* is similar to cannel coal and both can be worked into black jewellry and ornamental articles. However, jet originates from tree logs that were embedded in bituminous shale (e.g. in the Jurassic beds of Yorkshire). *Schungites* are Palaeoproterozoic equivalents of sapropelic coal, formed from mats of Cyanobacteria and of exuded bitumen (Medwedev *et al*. 2001, Melezhik *et al*. 2004).

Liptobiolites

Liptobiolites are concentrations of plant constituents that resist aerobic weathering. In Eocene lignite seams in Germany, bands of yellow, light brown or pink *pyropissite* are common. Pyropissite is essentially composed of pollen, wax, resin and leaf cuticles in variable ratios. Often, the strata are more prevalent near margins of coal basins, yet formed as aquatic sediments. Pyropissite can be ignited similar to cannel coal. *Amber* is re-sedimented fossil resin, occurring in large lumps that the plants produced to seal and protect wounds and to discourage herbivores. Earliest amber dates from the Carboniferous (Grimaldi 2009). In the Palaeocene-Eocene, major amber deposits were formed in deltas and shallow water along the southeastern shore of the Baltic Sea (Kharin *et al*. 2004). Baltic amber was already highly valued by Neolithic people ~13,000 years ago and traded throughout Europe. Amber is used for the production of ornaments, special lacquers and chemicals.

Saline coals

Saline coals contain elevated gypsum, NaCl and KCl, because of contact with brines (Yudovich & Ketris 2006a). In Northern Germany, chloride-sulphate brines are common in the vicinity of subcropping Permian salt formations (Figure/Plate 5.18). Where brines infiltrate lignite and sub-bituminous coal, severe problems arise for boiler operations, because alkalis, silica and iron tend to combine in fouling surfaces of steam generators in power plants. Leaching of salt deposits is also the reason for the salinity of underground water pumped from black coal mines near Cracow, Poland; coal quality, however, is hardly affected because the small porosity of bituminous coal inhibits absorption of salt. Saline mine waters can also be a result of aridity, as in Australia (Côte *et al*. 2007).

This overview shows that coals are described according to the three parameters:

1 rank (grade of diagenesis);
2 type of organic precursor; and
3 content of inorganic substance.

Traded coal is often a mixture from different seams and deposits. Its characterization is based on technological and commercial parameters (calorific power, water content, volatile content, coking properties, etc.) that are translated into numeric codes (Gayer & Pesek 1997, Thomas 2002). These codes are shorthand descriptions of quality and possible use.

6.1.2 Petrography of coal

Most coals are very heterogeneous, both macroscopically and under the microscope. This is aggravated by the fact that organic constituents exhibit a continuously changing chemical composition as rank increases, very different from the stable properties of minerals. Because of these impediments, it took more than 100 years to develop an internationally recognized system of coal petrography. Its base is the Stopes-Heerlen System, which was first presented by Marie C. Stopes at Heerlen, Netherlands in 1935.

A full description of the composition of a "coal rock" can only be carried out with a microscope (Taylor *et al*. 1998). Yet, macroscopic features are useful for a preliminary approach, similar to the field description of ordinary rocks. In this way, mine exposures or drill cores of coal are examined and the occurring coal varieties ("lithotypes") and interbedded non-coal rocks are recorded in a ply-by-ply manner. Under the microscope with a 25- to 50-fold magnification, the organic constituents of coal ("macerals") are determined. The microscopic quantification of different macerals making up coal layers ("microlithotypes") provides a precise characterization of coal.

Lithotypes

Lithotypes are layers in coal that can be macroscopically distinguished. Bituminous coal always consists of thin bright and dull layers that trace sedimentary bedding. Bright layers are *vitrain*, dull ones *durain*. Vitrain is more brittle than durain and narrowly jointed by cleats. Thick vitrain displays conchoidal fractures. Parting planes of coal are often covered with numerous soft and friable fragments of coal with a silky lustre, resembling charcoal. This is *fusain*. *Clarain* consists of alternating thin laminae of vitrain and durain.

These four coal lithotypes form pure coal; many seams, however, contain mineral matter as thin strata of clastic sediment, in mixed coal/mineral material, and as concretions or joint-fillings. Clay and silt are the most common diluting materials; with increasing content, impure coal (<20 vol. % clay, $D < 1.5$), carbonaceous shale (20–60 vol. % clay, $D = 1.5$–2.0) and coaly shale (>60 vol. % clay, $D > 2.0$) are distinguished.

Lignite lithotypes cannot be described in the same terms as bands of bituminous coal. Visible wood remains ("xylite") are often present and these sections of a seam are called *xylite-rich coal*. Stratified or unstratified detrital humic groundmass is *matrix coal*. Charcoal horizons consist of *charcoal-rich coal*, and coal containing clastic minerals, carbonates and sulphides is *mineral-rich coal*. Colour and degree of gelification can be used for a subdivision into lithotype varieties (e.g. black gelified matrix coal). Charcoal (fusain) is very common in Tertiary coals, possibly because oxygen content in the atmosphere was higher (23% in the Eocene) favouring the incidence of peat fires. Remember that by photosynthesis (eq. 6.1), vigorous plant growth causes increasing oxygen concentration in the air parallel to depletion of CO_2. When reduced carbon is buried, as in coal, surplus oxygen remains in the atmosphere (Garrels *et al.* 1976, Falkowski & Isozaki 2008).

Documentation of macropetrographical analysis is commonly presented in the form of seam sections that are valuable tools for investigating lateral facies variations. Brightness logs (ply-by-ply % of vitrain) are used in exploration to characterize the coking potential of individual seams.

Macerals

Microscopic investigations of coal started with thin sections. The introduction of polished sections and microscopy under incident light (Stach 1935), later completed by the techniques of oil immersion, luminescence and fluorescence microscopy, was the foundation of modern coal petrology (Taylor *et al.* 1998, Sykorova *et al.* 2005). Macerals are organic coal constituents visible at magnifications between 25 and 50 times and have differing optical properties, hardness and shape (Stopes 1935). The term was deliberately chosen for its similarity to the word "minerals". Macerals may be recognizable parts of plants or products of their degradation. Organic macerals are not crystalline substances. In bituminous coal, three groups of macerals are distinguished: i) vitrinite group; ii) liptinite group; and iii) inertinite group:

Vitrinite group macerals are mainly derived from wood. Vitrinite is very bright and is either cellular (Figure 6.5, *telinite*) or homogeneous (Figure 6.6, *collinite*). Vitrinite is the purest and most constant constituent of coal. This is the reason for its use as a sensitive and precise means of coal rank determination. *Huminites* (Figure/Plate 6.7, Figure 6.8) are those macerals of lignites and sub-bituminous coals that would form vitrinite at higher rank.

Liptinites (earlier called exinite) comprise macerals that originate from plant matter, which resists humification, including spores, pollen, resins, waxes and fats. Liptinite is common in dull coal bands. It is rich in hydrogen and, together with hydrogen-rich ("perhydrous") vitrinite, is the main source of volatile matter (and of natural gas and petroleum: Wilkins & George 2002). Illuminated with UV or blue light, liptinite demonstrates fluorescence. Cannel and boghead coal are predominantly liptinitic. During

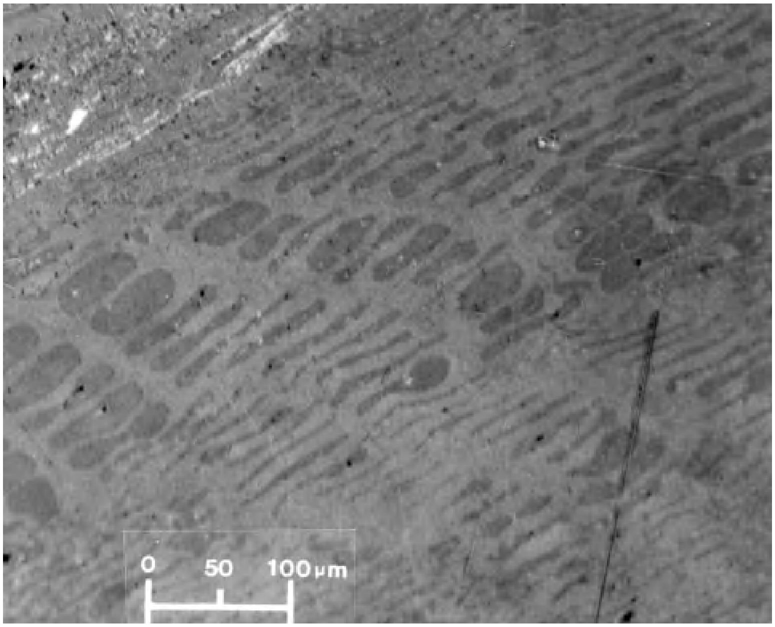

Figure 6.5 Microphotograph of the coal maceral telinite (a vitrinite; clearly recognizable cell walls of more or less intact but humified plant tissue) in Pennsylvanian bituminous coal, USA. Reflected light, oil immersion. Courtesy of Maria Mastalerz and Indiana Geological Survey.

coalification, beyond coking coal, liptinites produce much methane. The concurrent loss of hydrogen leads to an appearance that approaches vitrinite. Liptinite group macerals derived from plants include *sporinite* (Figure 6.9), *cutinite* (epidermis of leaves), *resinite* and *alginite*. Fluorescence distinguishes the macerals *fluorinite* (derived from fats and oils), *bituminite* (decomposed algae, bacteria, proteins) and *exudatinite* (diagenetically mobilized bitumen). Liptinites are indicators of wet conditions or even open water in mires, so that elevated clay content of liptinite-rich coal is not unusual.

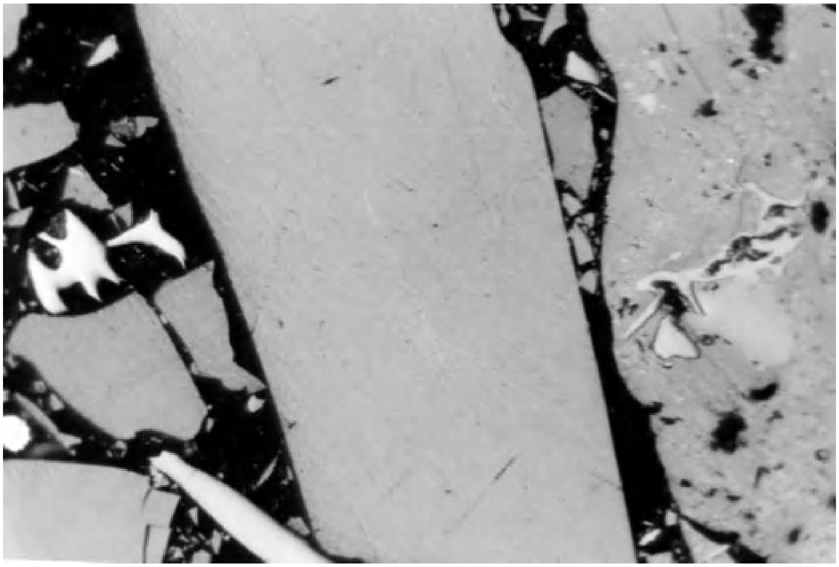

Figure 6.6 Microphotograph of the coal maceral collotelinite (vitrinite, more or less homogenized) in Pennsylvanian bituminous coal, USA. Reflected light, oil immersion; long side of image 0.5 mm. Courtesy of Maria Mastalerz and Indiana Geological Survey.

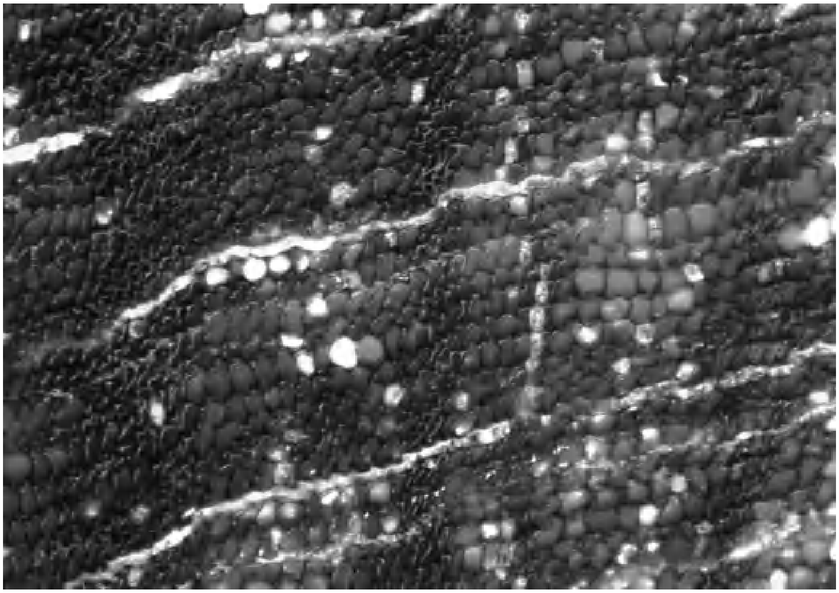

Figure 6.7 (Plate 6.7) Microphotograph of the coal maceral textinite (a huminite; ungelified woody tissue with intact botanical cell structures) in Tertiary lignite, Poland. Reflected light, oil immersion; long side of image 0.5 mm. Courtesy of Maria Mastalerz and Indiana Geological Survey.

Inertinites are coal constituents whose chemical composition changes little as rank increases and that do not melt during coking. All inertinites have high carbon and low hydrogen content and reflect strongly under incident light. Many inertinites originate from precursors of vitrinite group macerals. Their notable properties are due to partial oxidation during early stages of coal formation (Moore *et al.* 1996). The most

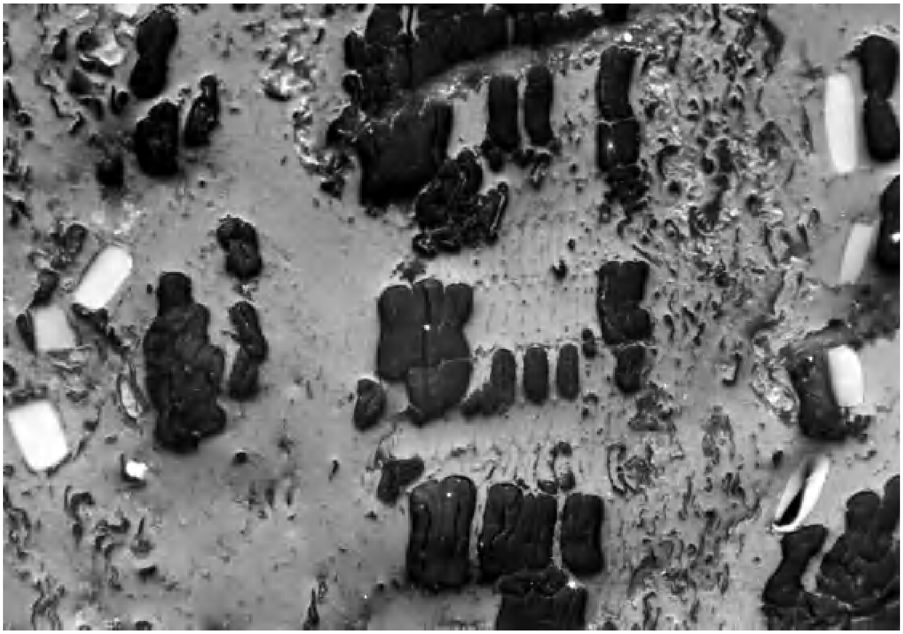

Figure 6.8 (**Plate 6.8)** Microphotograph of the coal maceral ulminite (a huminite; more or less gelified woody tissue) in Tertiary lignite, Poland. Reflected light, oil immersion; long side of image 0.5 mm. Courtesy of Maria Mastalerz and Indiana Geological Survey.

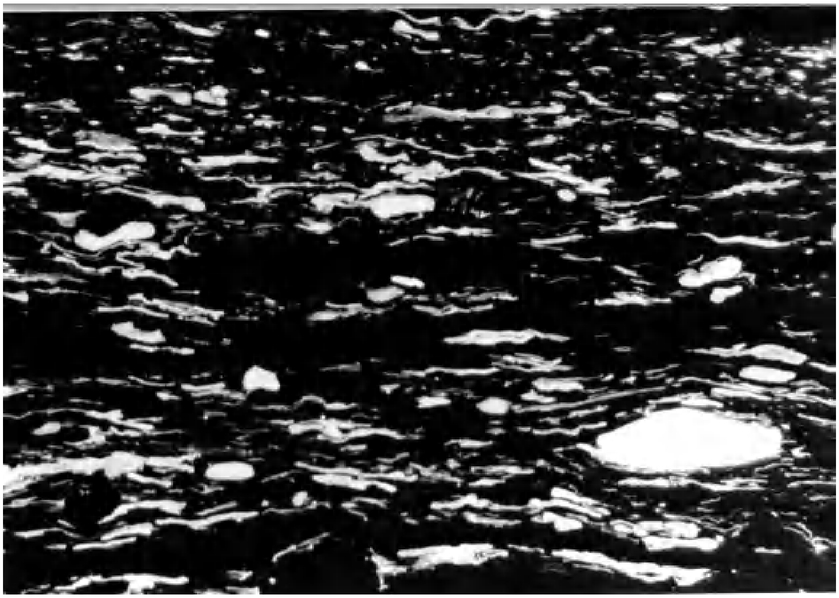

Figure 6.9 (Plate 6.9) Microphotograph of the coal maceral sporinite (liptinite; wax-coated fossil spores and pollen) in Pennsylvanian bituminous coal, USA. Fluorescent light; long side of image 1.0 mm. Courtesy of Maria Mastalerz and Indiana Geological Survey.

frequent inertinitic component of coal is *fusinite* (Figure 6.10). Under the microscope fusinite exhibits the cellular structure of wood and its anatomic details. Former cell lumina may be filled with humic gel or mineral substance (clay, carbonate, pyrite, etc.). *Semifusinite* is intermediate between fusinite and vitrinite. Most fusinite is fossil charcoal produced by forest fires that were ignited by lightning (Guo & Bustin 1998). The degree of carbonization correlates with temperature, as illustrated by tree logs that were externally carbonized but preserve a core of ordinary vitrinite. Small rounded particles of inertinite are called *macrinite*. *Micrinite* particles are very tiny and originated probably as airborne soot or carbon black. In Tertiary brown coals, a very common inertinite, besides fusinite, is *sclerotinite* that consists of round

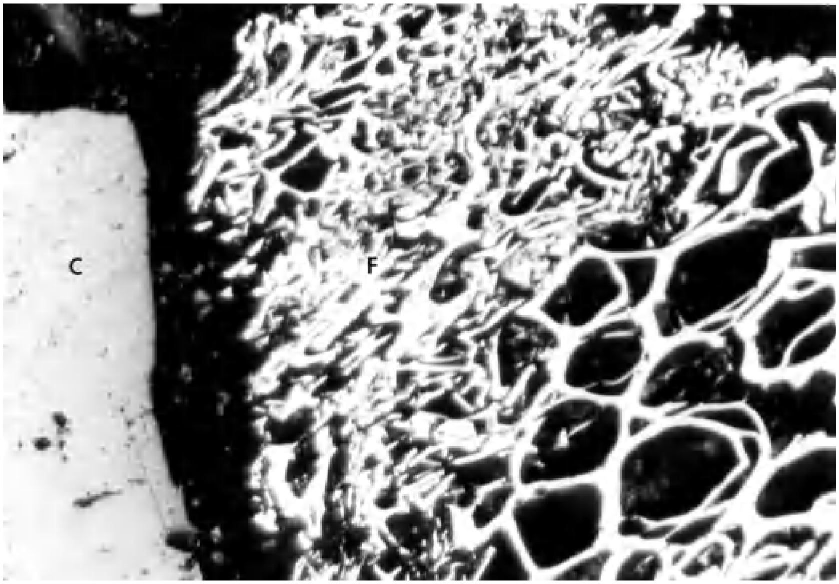

Figure 6.10 Microphotograph of the coal maceral fusinite (an inertinite; highly reflecting, well-preserved cellular structure inherited from ligno-cellulosic cell walls) in Pennsylvanian bituminous coal, USA. F-fusinite, C-collinite. Reflected light, oil immersion; long side of image 0.5 mm. Courtesy of Maria Mastalerz and Indiana Geological Survey.

or oval, brightly reflecting particles with one or several cavities. Sclerotia are remains of mycelia, spores and other fungal tissues.

Microlithotypes

Microlithotypes are defined by common associations of macerals. They can be mono-, bi- and trimaceralic, for example *vitrite, vitrinertite* and *vitrinertoliptite* (Taylor *et al.* 1998). Microlithotypes are determined with the microscope and recorded in seam sections. They are useful for an interpretation of conditions in the former swamp. Diessel (1986) proposed that the degree of decomposition of plant tissue (TPI = tissue preservation index measured by the ratio humotelinite/humodetrinite) and the relative water level vs. peat oxidation (GI = groundwater index, the huminite/inertinite ratio) can be used for the determination of facies and plant communities. Controls using peat of known depositional facies showed that pH and the microbial decomposition of peat are additional obligatory parameters of facies interpretations (Dehmer 1995). Coal petrography alone is probably not sufficient for identification of swamp type and facies (Moore & Shearer 2003).

6.1.3 The chemical composition of coal

Coals are extremely heterogeneous mixtures of various organic substances and of inorganic material, including water, inorganic colloids and minerals. The chemistry of the organic matter depends on the fraction of different macerals (the coal type) and the degree of diagenetic changes (rank, or maturity of coal). Full chemical analysis of coal is little used in practice but its complex organic compounds are determined for scientific elucidation (Bustin *et al.* 1997; Hatcher & Clifford 1997). In chemical terms, coal consists of aromatic nuclei, cross-linking bridges and adhering functional groups containing oxygen, sulphur and nitrogen.

In practice, large numbers of coal samples are analysed by standard procedures that include proximate and ultimate analysis. This is sufficient to control the quality from underground grade control to the final shipping product. Fewer samples will be analysed for data, such as potential atmospheric pollutants in the coal, the chemical composition of ash, the grain size distribution and coking properties. Proximate analysis includes the determination of moisture, volatile matter (fixed carbon), ash content and calorific value (heat energy per unit mass). Ultimate analysis serves to reveal the content of the major elements C, O, H, N and S in coal. Online X-ray fluorescence analysis of lignite and coal destined for power plants targets mainly elements that contribute to slagging and fouling of boilers (Si, Ca, Fe, K, Al, S, Na). The data are used for overall coal quality management, blending and automatic alarms, if critical parameters are exceeded.

Organic precursors and chemical compounds of coal

Cellulose $(C_6H_{10}O_5)_n$ is the major component of higher plants. By means of the chlorophyll, plants synthesize carbohydrates such as cellulose from carbon dioxide in the air plus water (eq. 6.1). In wood and bark, cellulose is reinforced by *lignin.* Lignins are a group of complex organic polymers containing aromatic nuclei with side chains. Molecular weight of lignin macromolecules surpasses 10,000 units. They are more resistant against microbial attack compared to cellulose. Different plants and even parts of plants have diverse lignin types and concentrations (5–45% in dry substance). Plants use wax, cutine (leaf surfaces) and suberine (bark) as a protection of the surface of vegetative organs. Sugars (glucose $C_6H_{12}O_6$), starch (polysaccharide carbohydrates) and proteins are rapidly decomposed by microbes in the peat. Much of the nitrogen in coal is inherited from protein in plants and microbes.

Simplified formula of cellulose production by photosynthesis – The fundamental reaction of life:

$$6CO_2 + 5H_2O \rightarrow C_6H_{10}O_5 + 6O_2 \qquad (6.1)$$

Lignin and cellulose are precursors of huminite and vitrinite. Cellulose and lignin are detectable in xylite and humotelinite of lignites but not in subbituminous coal. They are transformed by humification into humic substances (Kögel-Knabner 1993) that form the bulk of coal. Humic substances are heterogeneous mixtures of organic compounds that are divided into fulvic acid, humic acid and humins. They are colloidal dark-coloured complex substances, with a high molecular weight built from the elements carbon, oxygen, hydrogen and nitrogen. All contain an aromatic nucleus and various functional groups. When fulvic acid transforms into humic acid, both oxygen content and solubility in KOH decrease; humins are insoluble:

> Yellow to red-brown hydrophilic *fulvic acids* occur in soil, peat and wetland water. They have a molecular weight of 400–1500 and dissolve in both acidic and alkaline water. *Humic acids* are brown to black, hydrophobic and have a higher molecular weight. Soluble in alkaline water, they flocculate under acidic conditions. Both organic acids form salts (fulvates, humates) with cations including Na, Ca, Mg, Fe and Al. Black humins are the product of ageing of humic acids and their salts. Among the humates, *dopplerite* (the calcium salt of humic acid) is relatively common. It is a gel-like substance filling cavities in lignite seams. It shrinks and cracks on drying, and turns into a brilliant black material with conchoidal fracture. Generally, the early transformation of peat by *humification* is followed by a stage of more or less pervasive *biochemical gelification*.

Spores, pollen, resins, waxes and fats are *lipids* formed by higher plants. Lipids change little during humification and biochemical gelification. Severe alteration begins only with the onset of maturation to bituminous coal. In brown coal, part of the lipids can be determined under the microscope, but much remains undetected and is only revealed by organic solvent extraction (e.g. wax by benzene). *Chlorophyll* is normally destroyed before peatification. Macroscopically visible chlorophyll in lignites is very rare; one famous locality was Geiselthal in Germany (Figure/Plate 5.19).

Humins evolve during coalification by increasing *aromatization*. As functional groups, bridges and side-chains of nuclei are broken down, and islands of well-ordered structural elements ("crystallites") grow larger. During coal maturation, aromatic clusters are increasingly arranged into flat sheets that resemble the graphite lattice.

Volatile matter, fixed carbon and chemical composition

Run-of-mine coal contains water and minerals (ash). Data on moisture and ash content allow the calculation of the fraction of pure coal (dry, ash-free = d.a.f., or more precisely, dry, mineral matter-free = d.m.m.f.) in a sample. Data on coal's chemical composition and yield of volatile matter are of both practical and scientific use.

Heating a water-free coal sample under exclusion of air induces processes of pyrolysis and carbonization. This results in release of flammable gas ("town gas" as opposed to natural gas), liquids and vapours that condense to tar. Because high temperatures are attained, liberation of volatiles from minerals (e.g. water from clay, CO_2 from carbonate) must be accounted for. The term "volatile matter" (VM) describes the mass loss of the sample due to abstraction of organic and other volatiles. Volatile matter content of coal decrease with increasing rank (Figure 6.4), whereas the share of non-volatile (or "fixed") carbon increases. Fixed carbon is therefore as useful as volatile matter for measuring coal rank.

The elements making up coal are predominantly inherited from the peat-forming plants. Main elements are carbon, hydrogen and oxygen, with nitrogen and sulphur as minor components. Pure coal of high-volatile bituminous A-rank with 84% C has an average chemical composition that can be expressed by the "formula" $C_{10}H_7O$.

The continuous enrichment of carbon and the decrease of hydrogen (and oxygen) with increasing rank have been known for a long time (Figure 6.11). During lower rank coalification, oxygen diminishes rapidly, because of the loss of CO_2 and H_2O. A strong decrease of hydrogen occurs between high-volatile bituminous A-rank coal and anthracite. During this stage of coalification, a large volume of methane (CH_4) is released. The resulting bend in the coal band is sometimes termed a "jump of coalification". In parallel with chemical changes, several physical alterations are also observed, such as an increase of reflection and a decrease of liptinite fluorescence.

Sulphur occurs in many forms in coal, including massive, coarse, or very finely disseminated

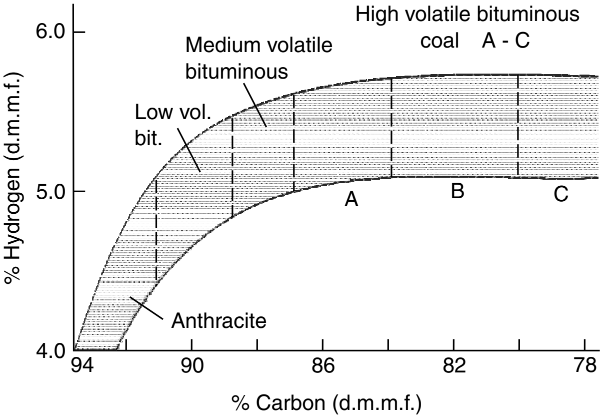

Figure 6.11 An updated rendering of Seyler's (1933) illustration of coal chemistry in carbon-hydrogen space. The diagram displays the typical composition of humic coals (the coal band), the increase of carbon with higher rank, and the rapid drop of hydrogen content at about the rank of coking (medium volatile) coal (d.m.m.f. = dry mineral matter free).

pyrite, soluble sulphate, acid-volatile sulphides (AVS) and organic sulphur. Only a small part of organically-bound sulphur is inherited from plants, which host the element in the form of aminoacids (C-S-form) or as ester-sulphate (C-OSO_3; e.g. in polysaccharides, phenol, etc.). In coals that are S-rich, most sulphur is derived from bacterially reduced sulphate. Pyritized bacterial colonies in coal have been demonstrated (Southam *et al.* 2001). Sulphate is commonly imported: i) by flooding of the peat mire with seawater; and ii) by sulphate-carrying groundwater that seeps into the peat from the surroundings, either during or after formation of the peat. In the first case, sulphur is concentrated in the upper part of the seam, whereas in the second, sulphate infiltrates from the footwall.

Sulphur content can be exceptionally high in coal seams with carbonate-rich host rocks. This setting induces alkaline conditions in the mire (e.g. in the Everglades, Florida, USA, up to pH 8.6). Seawater flooding has a similar effect. Higher pH favours sulphate-reducing microbial activity and the resulting H_2S will combine with iron or with organic substances in the peat. Alkaline swamps may even conserve calcareous fossils and skeletons of vertebrates (Geiseltal is famous for its Eocene fauna; Figure/Plate 5.19). In the Schöningen lignite pit (Figure/Plate 5.18), numerous boulder-like calcite concretions occurred in the seam where its footwall was formed by karstified Triassic limestone. Extraction of the lignite was severely impeded. This problem had not been recognized when mining reserves were defined by drilling.

Seams that were inundated with seawater are characterized by elevated sulphur, ash and nitrogen content. Coals that are derived from unusually acidic peat (with a pH as low as 3.3 compared with average peat of pH 4.8–6.5) contain little sulphur. Acidic swamps may be indicated by kaolinized footwall rocks of coal seams. Exceptionally low sulphur content of 0.06% (air-dried) has been reported for the high-volatile bituminous B-coal from the Tanjung mine in Borneo. The product is sold under the trade name of "Envirocoal"; resources are estimated at >1000 Mt:

> Sulphur in coal is undesirable because in boilers it is oxidized to SO_2 and enters the flue gas. Likewise, sulphur in coking coal diminishes product quality. Mitigation of inorganic sulphur is possible by mine-site coal processing (e.g. removal of pyrite) but is not feasible for organically-bound sulphur. Several technical solutions for withholding sulphur from the atmosphere are applied in power stations, although not without repercussions on the price of electricity.

Nitrogen is foremost inherited from proteins in the peat. During coalification, it enters the coal macromolecules. Coking or gasification of coal generates ammonia that can be a valuable by-product. For burning, however, low-nitrogen coal is preferred, because elimination technologies such as reduction of NO_x to N^0 or NH_4 are costly.

Nitrogen is a biogenic element of coal. Plants contain a number of trace elements, including Ca, N, K, P, S, Mg and Fe, but also Na, Si, Al, Mn, B, Ba, Sr, Zn and Cu. Several of these elements are selectively enriched in biomass and the resulting coal. The enrichment may be quantified by the biological accumulation coefficient (eq. 6.2).

Biological accumulation coefficient B_s as a measure of preferential enrichment of elements in organic substance:

$$B_s = \frac{\%\ \text{in ash of organic substance}}{\%\ \text{Clarke crustal average}} \qquad (6.2)$$

B_s-values >10 are commonly determined for P, S, Se, Cl, Br and I, values between 1 and 10 for Ca, Na, K, Mg, Sr, Zn and B, whereas most other elements are comparatively depleted ($B_s < 1$). World average chlorine content of coal amounts to 340 ± 40 (hard coal) and 120 ± 20 ppm (brown coal: Yudovich & Ketris 2006a). The world average for ash is 1435 ppm Cl compared to a Clarke of 126 ppm. The selenium average is 1.6 ± 0.1 ppm and 1.0 ± 0.15 ppm, respectively for hard and brown coal, compared with a Clarke value of 0.05 ppm (Yudovich & Ketris 2006b). Note that the enrichment is not literally "biological" but represents accumulation from the live plants ("inherent elements") to late diagenesis (Swaine 1990). Furthermore, comparison with average shale should be more relevant than with Clarke values, which include basalts (Reimann & de Caritat 1998). Of course, the geogenic background of the watershed must be considered in the interpretations.

Accessory metal content in coal has little economic significance, mainly because of low and fluctuating in-seam content. In power stations, however, some metals may be enriched in the ash to extractable grades (both bottom and fly ash). Metals that were occasionally produced from coal ash include vanadium, germanium and uranium. Coals with anomalous germanium content occur in America, Australia, China and Russia (Seredin *et al.* 2006). Metalliferous (Seredin & Finkelman 2008) and especially uraniferous coals are ubiquitous. In coal, uranium is adsorbed on organic matter. This may be due to: i) syngenetic enrichment from waters draining the former hinterland of the peat swamps; or ii) later, epigenetic input. The first has an equivalent in today's uraniferous mires in Sweden, whereas the second is typically due to the later passage of uranium-bearing groundwater (e.g. Wackersdorf, Figure 2.43). REE are enriched to 300–1000 ppm in giant coal deposits of the Russian Far East, possibly sourced from nearby volcanic rocks (Seredin 1996).

Trace elements in coal are determined by sedimentary and diagenetic conditions. Their distribution is usually irregular, so they are rarely useful for identifying specific seams in multi-seam deposits. An exception may be the ratio Al/La-Sc (Chyi & Medlin 1996). Several trace elements are harmful, either for power station operation (Na, Cl, etc.) or for the environment (e.g. arsenic, mercury, radioactive elements). Therefore, a thorough geochemical investigation of all coal deposits is mandatory. This must include the determination of the preferred carrier (mineral or maceral) of significant elements and of speciation. In many cases, ecologically sensitive elements are concentrated in pyrite, kaolinite and illite, in which case removal by coal processing may be feasible (Palmer & Lyons 1997). The fate of hazardous trace elements in power stations and especially the level of stack emissions must be monitored (Huggins & Goodarzi 2009). Anticipatory mitigation is required.

Clearly, peat and coals are extremely efficient *geochemical barriers*, due to processes that include biochemical accumulation, reduction, sorption and ion exchange. Import of elements into swamps may occur by surface water, seawater and groundwater. Seawater influence is indicated by higher content of B, Sr, Mg and, of course, Cl, Na, SO_4, Ca, K and Br. Groundwater may contribute U, V, Mo and in case of contact with saline brines or evaporite rocks, Na, K, Ca, Mg, Cl, B, Sr, Br and SO_4. Hydrothermal epigenetic metal enrichment in lignites is rare (Seredin *et al.* 2006), whereas most hard coals exhibit traces of mineralization by the passage of diagenetic (basinal) fluids.

Isotopic investigations of coal are mainly based on the elements C, O, H and N. Isotopic composition is a function of coal age, geographical latitude, mean annual temperature (reflected in the D/H ratio), dominant plants (carbon isotopes), isotopic character of precipitation including seasonal variations (Jahren & Sternberg 2008) and coal maturity and degassing history (Whiticar 1997). Carbon in coal is clearly enriched in ^{12}C relative to the source (atmospheric and mantle) carbon, because photosynthesis strongly discriminates against $^{13}CO_2$. The Middle Miocene Yallourn seam lignites (Latrobe Valley, Australia), for example, have $\delta^{13}C$ (PDB) values from −25.3 to −27.3‰ (Holdgate *et al.* 2007). Cyclicity correlates well with the deep-sea $\delta^{13}C$ marine organic record. Contrary to earlier assumptions, the oxygen isotope ratio ($\delta^{18}O$) of cellulose is not a reliable proxy of ambient temperature and relative humidity (Helliker & Richter 2008). The source of nitrogen may be discerned, because little fractionation takes place when plants or microbes assimilate nitrogen from air ($\delta\ ^{15}N_{Plants}$ from −3.1 to −0.4‰), whereas uptake of nitrates enriches heavy nitrogen. The release of methane during coalification initially mobilizes light carbon and hydrogen. Theoretically, this should translate into an enrichment of heavy isotopes in coal. However, depletion of ^{12}C during coalification cannot be measured, because the seams are a giant reservoir of carbon. Deuterium, however, is slightly enriched (Schoell 1983). Rhenium-osmium ages of pyrite may be used to investigate the diagenetic evolution of coal deposits.

Water in coal

Water is an essential component of brown coal. Lignites contain between 30 and 75 wt. % water (Figure 6.4). This figure reveals why power stations burning these low-grade "wet" coals are built near the mines. The water content of bituminous coal and anthracite is low (from 9–2.5%) and this explains why they are shipped across the world's oceans.

Coal contains water in four possible forms:

1 surface, or adventitious moisture;
2 hygroscopic moisture in capillaries;
3 adsorbed water; and
4 mineral moisture.

Drying higher rank coal in air removes surface water. Hygroscopic and adsorbed water are termed "inherent moisture" and are determined by heating to 105°C. Mineral moisture is mainly a component of clay in coal. Surface water content reflects conditions of sampling, for example rain or drought. Yet coal samples are always hermetically sealed on site, because adventitious moisture influences mass calculations and processing of coal. Compared with inherent moisture, lignites have little surface moisture. However, on drying in air, lignite looses even hygroscopic and adsorbed water and may crumble into low-value coal dust.

Gas in coal

Methane is the most common gas occluded or adsorbed in coal seams. It may be accompanied by minor fractions of ethane and propane, and by traces of hydrogen and helium. Some coal seams contain large amounts of carbon dioxide. Whereas the source of CO_2 is usually external to the coal measures, for example volcanogenic, methane is produced during coalification within the seam. Abiotic methane production from liptinites begins with the coalification jump from sub-bituminous coal B to A rank. Medium volatile bituminous (coking) coals have the highest content (10–30 m^3 gas per tonne of coal). Methane mixed with 5–14% air is highly explosive ("fire damp"). The largest mass of gas is formed from humic substances during continuing maturation to anthracite. It is estimated that 1 kg of coal produces ~200 litres methane during maturation from high volatile bituminous coal B to anthracite. Because country rocks of higher-grade bituminous coals are increasingly permeable as jointing intensifies, 90–95% of methane produced migrates away from the seams. This is one reason why the actual gas content of coal *in situ* cannot be predicted (Bustin & Clarkson 1999). Only the ash-content correlates (negatively) with gas in coal, because gas is almost exclusively hosted by organic material. If the migrating gas encounters a trap capped by impermeable rocks (in northern Germany, usually Zechstein salt rock, cf. Chapter 4), important and even giant gas deposits can form (e.g. Groningen, Netherlands). Most lignites and sub-bituminous (C and B) coals are methane-free. Yet, underground extraction of brown coals is not without its own dangerous gases – poisonous CO and asphyxiant CO_2 can form by slow oxidation in parts of the mine with stagnant air. CO_2 collects in hollows, as it is

1.53 times heavier than air. Increasingly, methane gas released from coal mines is used for heating, power generation, as a vehicle fuel, or for chemical manufacturing. Mine methane that cannot be used should be flared off, as conversion to CO_2 lowers the greenhouse effect (Gayer & Harris 1996).

Only a fraction of the carbon dioxide adsorbed in coal seams is derived from coalification. If high content is encountered, the source is usually igneous or otherwise endogenous. Faults and permeable sandstones have been identified as conductors. In the past, several mines suffered catastrophic carbon dioxide blow-outs, filling the mine openings not only with the asphyxiating gas but also with coal dust. The precondition for gas-driven coal outbursts are high *in-situ* gas pressures in the coal. *Coal outbursts* are violent and spontaneous ejections of powdered coal and gas from the working coal face (Guan *et al.* 2009). Coal dust in air is by itself explosive and very destructive but methane is often involved. Seams with a clayey hanging wall are prone to trap gas and to impede natural degassing. In that case, a slow advance of extraction, deliberate fracturing and loosening of the rock mass, and drainage boreholes may decrease gas pressures. Ordinary degassing of CH_4 and CO_2 is not dramatic. Gas blowers occur along joints, or gas bubbles rise in water channels along mine tunnels. Coal mines and oil or gas fields tend to be well separated, but in a few cases, a near neighbourhood did cause accidents (Nottinghamshire, UK, Stevenson 1999).

Ash and minerals in coal

It is important to understand the difference between ash and minerals in coal (Ward 2002). Ash represents incombustible matter in coal measured by controlled oxidation (burning) of a sample at 700–850 °C ("high-T ash"). This causes loss of CO_2 from carbonate, SO_2 from sulphides and H_2O from clay. The mass of ash is less than the original mass of minerals in coal. Because coal ash consists essentially of oxides, its chemical composition is investigated with analytical methods used for silicate rock analysis. Calculation of norm percentages of minerals in coal from high-T ash data is very imprecise. It is recommended to determine minerals directly by appropriate methods after careful drying and oxidation at low temperature (150 °C: "low-T ash").

Ash of run-of-mine coal has various sources:

- wall rocks extracted with coal;
- minerals that were transported into the swamp, diluting the organic material (e.g. clastic or volcanic sediments);
- diagenetic minerals introduced after sedimentation;
- salts dissolved in pore water; and
- the inherent biogenic mineral matter content of plants (e.g. silica of *equisetum*). Matrix coal (of lignite) or dull, bituminous coal contains more ash than bright coal:

> Ash content and calorific value of coals are negatively correlated. Generally, high ash coal is economically less desirable and is a bigger environmental burden. If possible, ash content of run-of-mine coal is reduced by one of three technologies: i) Processing in a dense liquid medium washing plant; ii) in heavy media cyclones; or iii) in jigs (separating particles of different density by pulsations immersed in water). All methods rely on the increase of coal density as a function of ash content. Because of the increasing need to manage scarce water resources (e.g. in Australia), novel dry processing methods for upgrading coal are employed wherever possible.

Minerals in bituminous coal include silicates, carbonates, sulphides, sulphates, phosphates and others. Apart from minerals, immature lignites may contain amorphous and semi-ordered substances, such as allophane instead of kaolinite.

Quartz is very common in coal, mostly of detrital origin, but also as a chemical precipitate such as silicified tree logs, which occur in many lignites. Kaolinite is the most frequent clay mineral in coal, both as clastic sediment and as an authigenic and diagenetic mineral. Other clay minerals that are not rare in coal include montmorillonite, illite and mixed-layer clays. Illites in anthracite are remarkable because of high content (45–80 mole %) of NH_4 instead of K, due to pronounced liberation of nitrogen in this coalification stage (Daniels *et al.* 1994). Coal seams formed in volcanic surroundings may have high zeolite content (e.g. Beypasari, Anatolia: Querol *et al.* 1997). Pyrite (and other sulphides including sphalerite, marcasite, and galena) can be found filling cell lumina, or as framboids, idiomorphic crystals, small bedding-parallel lenses, thin coating of joints and in cross-cutting veins. All this indicates that sulphide formation starts with early diagenetic microbial sulphate reduction (Southam *et al.* 2001) and continues into late diagenetic stages with inflow of basinal hydrothermal fluids. Carbonates in coal comprise siderite, ankerite, calcite and dolomite. Siderite and dolomite form syngenetic layers or concretionary horizons in coal seams. The preservation of uncompressed cells in concretions is due to very early lithification. Carbonates in cleats (joints) of coal must have been introduced during late diagenesis. Sulphates in coal are products of natural pyrite oxidation by meteoric waters. Some may form by exposure to humid mine air. Exceptions are sulphates in saline coal that are derived from invading brines. Authigenic apatite and Sr, Ba and Ca aluminophosphates are trace minerals in all coals (Ward *et al.* 1996).

Minerals in coal influence the feasibility of exploiting the coal (Ward 2002). Some minerals may cause geotechnical problems, for example montmorillonite clay in opencut mining in a high-precipitation landscape. Processing, transport, storage, combustion, coking and coal liquefaction can all be affected. Pyrite is critical, because its oxidation induces acidity from the mine through processing to coal and waste rock tips. Also, pyrite is a common carrier of undesirable trace elements such as As, Hg and Sb. In the boiler, the fusion temperature of the ash is very important. Most combustion chambers cannot deal with low-melting ash due to higher content of montmorillonite, chlorite, carbonates, sulphates and pyrite. As a radical solution of the problems caused by unfavourable minerals in coal, acid-alkaline leaching has been proposed. Its product is nearly pure organic matter (UCC = ultra clean coal). Note that fly ash and slag from large-scale burning of coal can be useful by-products that find application in producing cement, concrete and ceramics, as a source of alkalinity in environmental technology, as a road construction material and as a self-hardening fill in underground mines.

Physical properties

The density of coal increases with both rank and ash content. Lignites have a density of ~1.2 (range 1.1–1.25), bituminous coals 1.35 (1.2–1.5) and anthracites 1.5 (1.34–1.8) g/cm^3. As a rule, coals are less dense than clastic country rocks at the same level of diagenesis (lignite-associated sand 1.8 and silty clay 2.0; sandstone hosting bituminous coal 2.0–2.4, shale 2.0–2.5 g/cm^3). The density of coal of a specific rank correlates positively with ash content. The density difference between low-ash and impure coal is the base for coal processing methods that strive to reduce the percentage of pyrite, country rock material and impure coal.

The hardness of brown coals increases with lower water content. Bituminous coals are hard but brittle and this may cause excessive comminution by handling. Generally, markets prefer lumpy coal to fines. Grindability of vitrain is higher than that of durain, so that vitrinitic coals are more susceptible to fining.

Optical translucence of coal decreases with higher rank, whereas reflectance and anisotropy increase. This is caused by more pervasive ordering of aromatic rings and clusters. Reflectance is determined quantitatively under the microscope using polished mounts of coal (Taylor *et al.* 1998). The degree of reflectance [R] is determined as a percentage of the incident light. Because reflectance correlates closely with coal rank and chemistry, its determination provides a very precise measure of coalification (Figure 6.4). The same technology is used to determine the maturation level of dispersed organic particles in sediments and due to its predictive capabilities, this method has a central role in petroleum and natural gas exploration.

Under the microscope, coals are birefringent. With crossed Nicols, extinction positions are normally parallel and at right-angles to bedding planes. The same anisotropy is exhibited by reflectance. The maximal reflectance [R_{max}] is found parallel to bedding, and R_{min} at 90° to sedimentary stratification. This is caused by the anisotropic molecular structure of coal, which is imprinted by vertical lithostatic stress σ_V and associated strain. Coal seams that were deformed in an orogenic stress field with horizontal stress σ_H larger than σ_V, display oblique extinction angles (Petrascheck 1954).

The inherent heat energy is one of the first parameters for assessing coal. It is expressed as specific energy, or calorific value of coal, which is the amount of heat available per unit mass [kJ/kg]. The calorific value increases during coalification to the stage of medium volatile (coking) coal; further maturation causes no little change (Figure 6.4). Water and ash reduce the available energy. The first because of the energy needed to heat and evaporate the moisture, the second because of several endothermic reactions, but foremost the reduced amount of pure coal mass. Because of these relations, coal for power production is not traded per mass unit but for its inherent energy yield.

Cokeability

Coke is the vesicular and fused solid residue that forms when coking coal is heated in the absence of air to a temperature of several hundred to 1000 °C. If non-coking coals are treated in the same way, the residue is not coke but char (less porous or unfused solid). Coke is a highly valued energy carrier and reducing agent of the iron and steel industry. Important properties of coke include lumpiness, mechanical strength and durability. Apart from coke, saleable by-products of the process of carbonization are coal, or town gas (hydrogen, methane, other hydrocarbon gases, carbon monoxide), crude benzole, coal tar and ammoniacal liquor (Ward 1984).

Cokeability depends on the coincidence of coal becoming plastic ("fluid") when heated coinciding with volatile release forming gas bubbles. The result is swelled and porous coke. The coking process can be adapted to different coals by technological parameters, but rank and the ratio of macerals control the feasibility. Coke is often compared to concrete; inert components (the pebbles) are bound by a reactive matrix (cement). Liptinite is an excellent swelling agent, vitrinite a moderate one. Inertinite and most minerals remain unchanged. Vitrinite determines plasticity and gas release, because liptinite content is rarely above 5% of the total coal mass. In the case of high inertinite content, it is preferred to have it mixed with vitrinite, because this will stiffen the pore walls of the coke. Generally, vitrinite content (brightness) and its maturity are the main controls on cokeability.

Lignites and anthracites are not cokeable. However, many ingenious ways of making coke from non-coking coal have been developed. One example is the blending of reactive material such as coking coal or bitumen with inert additives (anthracite, carbon black). The mass is then formed into high-pressure briquettes. After coking, the briquettes are a valuable smokeless fuel.

Synfuels (coal-to-liquids technology)

With rising petroleum prices, worldwide production of liquid fuels from coal is rapidly expanding. One of the largest plants is still the facility at Secunda, South Africa, that was built to cope with an apartheid era fuel embargo. Unfortunately, underground storage of the waste product CO_2 was not planned and today the plant is the Earth's single largest point source of carbon dioxide emissions (20 Mt/y).

> Synfuels production is carried out by several industrial processes, basically variations of the Fischer-Tropsch synthesis. The principle is gasification of coal in the presence of steam and some oxygen at high temperature and pressure. Two separate gas streams are produced, "synthetic gas" with the composition $CO + H_2$, and waste CO_2. The synthetic gas (or syngas) is then converted by hydrogenation in the presence of catalysts into products such as gasoline, diesel fuel, jet fuel or chemical feedstocks. Combined with underground CO_2 sequestration, synfuels have a smaller carbon footprint than petroleum-based fuels.

New developments in underground and *in-situ* gasification of coal support hopes that this technology may finally reach profitability. Underground production of syngas eliminates all costs of mining and transport. Syngas can be directly burned to produce electricity, or converted to synfuels and to pure hydrogen by removal of CO_2. Since nearly 50 years, the world's only commercial plant of underground gasification of coal (UGC) combined with electricity generation operates in Uzbekistan. In the Surat Basin, Australia, a demonstration plant produces diesel fuel from UGC syngas. In Britain, *in-situ* gasification of deep coal below the Firth of Forth, combined with carbon dioxide capture and sequestration, was licensed in 2009. It is claimed that the UGC process can be applied to deep, high ash, conventionally unexploitable coal, which would immensely widen the resource base of coal.

6.2 PEAT FORMATION AND COAL DEPOSITS

Even though coal is chemically and petrographically very different from other sediments, it is an integral constituent of many sedimentary sequences. Peat deposition occurs in diverse terrestrial, limnic and coastal settings. Sufficient understanding of a coal deposit, including very practical aspects, can only be acquired by a comprehensive study covering all aspects of the evolution of a coal basin.

6.2.1 Types and dimensions of coal seams

Coal occurs in beds (strata) that are called seams. Many coal seams have a tabular shape characterized by a large areal extension but low thickness. Very thin strata that cannot be economically extracted are referred to as coal bands, or stringers. Two main types of coal seams can be discerned, which impose quite different approaches, from exploration to extraction:

- Concordant seams occur over large areas intercalated among strata of host sediments of the same age; lateral changes in seam thickness and facies are very gradual.
- Discordant seams typically occur above a stratigraphical unconformity and constitute the base of transgressive sediments; discordant seams display considerable and rapid lateral changes.

Discordant seams originate by:

- regional subsidence of previously formed landscapes with depressions, which are semi-closed and support a high groundwater table such as karst and broad valleys;
- local subsidence of the surface on the downthrow side of normal (tensional) faults; or
- above salt rock bodies undergoing subrosion.

The thickness of coal seams typically amounts to a few metres (black coal) or a few tens of metres (lignite). Exceptions include the Tertiary (Eocene-Miocene) brown coal seams in the Latrobe Valley, Victoria, Australia, which are supposedly the thickest on Earth, with a maximum of 320 m of coal (Holdgate *et al.* 2007, Barton *et al.* 1993; Figure 6.12). The district's youngest (Middle Miocene Yallourn) seam alone is 100 m thick and covers a stratigraphical record of 1.3 My. A black coal seam at Fushun in China reaches 200 m (Figure 6.13). However, extremely thick coal strata are very rare (Volkov 2003).

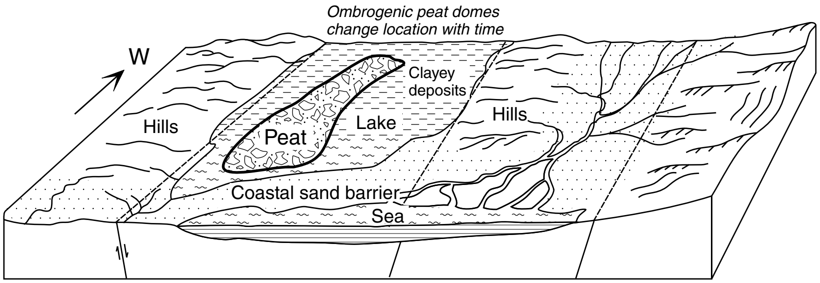

Figure 6.12 Schematic reconstruction of the palaeogeographic setting of Miocene peat formation in the Latrobe Valley, Victoria, Australia, in a wide tectonic graben (Holmes 1993). Ponding of water favourable for peat growth was caused by a coastal sand barrier and high global sea levels. Recoverable resources of the District are estimated at 37,000 Mt of earthy lignite with low ash contents and calorific value, and 60–70% moisture.

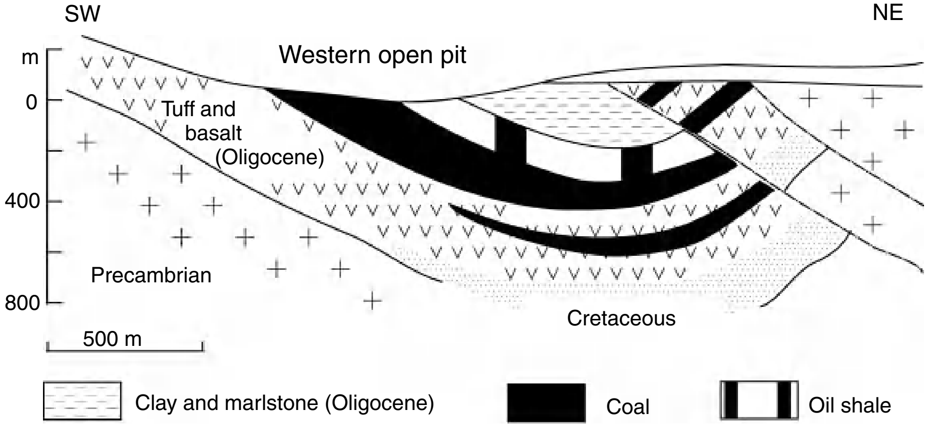

Figure 6.13 Geological section of the Palaeogene bituminous coal and oil shale deposit Fushun in Liaoning, China, illustrating the extraordinary thickness of the seam (Volkov 2003). With permission from Springer Science + Business Media.

Compaction of peat

Like all sedimentary rocks, peat, lignite and coal are compacted when covered by overburden rocks. In engineering geology, the *consolidation theory* explains and describes mathematically the increasing density and decreasing porosity, permeability, water content and thickness during compaction (Terzaghi *et al.* 1996). The same phenomena affect peat but at shorter time-scales. In addition, a part of peat consolidation is a function of synsedimentary biological activity. Therefore, most geological methods that aim to determine the original thickness of peat transformed into a coal seam target the (total) peat thickness at the time of deposition of the first overburden rocks (Widera *et al.* 2007). Consolidation during peat formation ("self-consolidation") is generally disregarded. Nadon (1998) vividly argued that self-consolidation of peat explains most of the total compaction and that this takes place in the few uppermost metres of the peat profile. Deep, mature peat is assumed to have compacted to 0.2–0.3 m, compared to near-surface material 1 m thick. The main means of measuring consolidation in buried peat or coal are lenses of clastic sediments of the same age, either on top of the down-warped coal surface or interbedded with it (Widera *et al.* 2007, Nadon 1998). Of course, for a precise determination of the coefficient of coal consolidation, the compaction of the clastic sediments should also be determined. Because it is much smaller than that of organic substance, it is often disregarded. If measurements are impossible, the traditional rule of thumb may be helpful: Six metres of peat consolidate to 3 m of lignite and to 1 m of black coal.

The areal extension of coal seams is typically quite small for local discordant seams (a few km^2), whereas concordant seams reach very large dimensions. The Pennsylvanian (Late Carboniferous) Pitsburgh seam in the Appalachian foreland basin (Virginia) occurs discontinuously over an area of ~30,000 km^2. It is historically one of the most important sources of coal in the United States, with an exploitable area of 5600 km^2 (Cross 1993). The spread of the Katharina seam in northern Germany (210 × 50 km) is comparable. In the Tertiary lignite district of Saxony and Thuringia (Germany), the main seam is developed over 750 km^2.

6.2.2 Concordant and discordant clastic sediments in coal seams

Thin strata of clastic or volcanogenic sediments in coal seams (dirt bands, partings, tonstein) are quite frequent. They divide the seam into several coal sub-layers that are called plies. Non-coal bands display a thickness from 1 to more than 50 cm.

Dirt bands are an economic disadvantage, because the material dilutes run-of-mine coal. Fine-grained clay and silt predominate, whereas bands of sand, carbonates and volcanic tuff are less frequent. In black coal, sideritic ironstones and even siderite oolites have been reported. In many cases, certain bands form recognizable key horizons that assist coal seam correlation. In that respect, tonstein bands (kaolinized pyroclastic tuffs) can be useful marker beds, because they often possess specific properties (e.g. crystals, glass shards, pumice), which designate particular beds. In addition, they contain trace minerals such as zircon and sanidine that allow precise radiometric dating. Thick kaolinitic partings may be a source of valuable fire clay. Bentonitic bands are rare in coal seams, because of the generally acidic environment of peat-forming wetlands.

The lateral evolution of coal thickness, number of plies and partings is depicted by seam sections, which are positioned on mine maps (Figure 16.6). The resulting seam facies maps reveal genetic and practical information, such as estimates of the likely dilution of coal in reserve blocks. Partings may be very useful when thick seams are to be exploited in benches (slices), if they can be utilized to delimit roof and floor of the slice. Dirt bands may laterally thicken to the extent that a seam is split in two or more unexploitable coal stringers.

Clastic strata in coal implicate shallow lakes and inflow of sediment-laden water into the swamp. Thick coal seams form when subsidence is such that profuse plant growth is maintained. For optimum conditions, groundwater levels should oscillate little about a mean, just covering the peat surface. In the case of higher subsidence, the swamp surface and with it the plants drown in open water. Clastic sediment deposition is the consequence, especially towards basin centres where seams tend to split by increasing thickness of dirt bands (Figure 6.14 and Figure 6.15). Mineral matter content of the coal (ash) rises in parallel

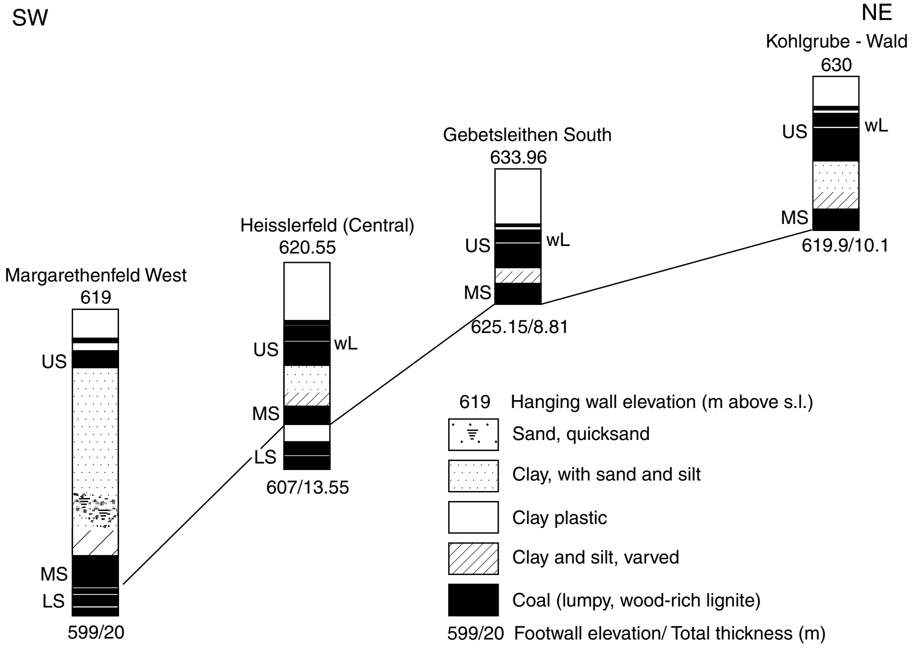
SW
NE
Kohlgrube - Wald
630
US
wL
MS
619.9/10.1
Gebetsleithen South
633.96
US
wL
MS
625.15/8.81
Heisslerfeld (Central)
620.55
US
wL
MS
LS
607/13.55
Margarethenfeld West
619
US
MS
LS
599/20
619 Hanging wall elevation (m above s.l.)
Sand, quicksand
Clay, with sand and silt
Clay plastic
Clay and silt, varved
Coal (lumpy, wood-rich lignite)
599/20 Footwall elevation/ Total thickness (m)

Figure 6.14 Part of the seam facies map of a lignite basin. The sections indicate a more limnic centre in the southwest and dryer conditions in the northeast (Hausruck, Austria; Pohl 1968). Thickness of seams (LS = Lower, MS = Middle and US = Upper Seam) and facies of clastic sediments are clearly a function of the relative altitude. wL is a thin kaolinitic marker bed in the Upper Seam (volcanic tuff).

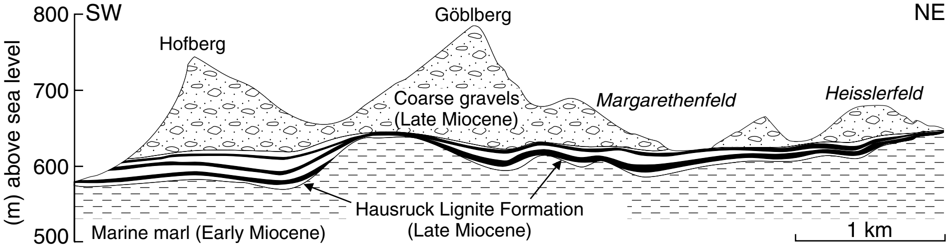

Figure 6.15 Geological section of the southwestern part of the Hausruck lignite district, Austria (Pohl 1968). The drawing uses different vertical and horizontal scales in order to single out the thin Hausruck Lignite Formation (seams in black). Observe that its thickness is greater in basin centres than at higher elevations.

until content surpasses acceptable levels. Dry swamp areas (deep groundwater levels) and basin-marginal positions of the swamp display increasing oxidation and microbial destruction of plant matter, which thins the coal seam to a band resembling forest floor litter. Swamp margins may be associated with clastic fans built up by creeks, which reach out into the seam in the form of sand and gravel beds.

The different facies zones of a coal swamp are more profoundly distinguished by the inclusion of petrographical, chemical and palaeobotanical methods. Two papers by Teichmüller 1958, 1991) about the Lower Rhine Valley lignites in Germany stimulated research and discussion of swamp facies. In this broad graben basin, Oligocene and Early Miocene sediments pass from a southern freshwater swamp to a northwestern marine bay of the North Sea (similar to the setting of the Latrobe Valley, Figure 6.12, Schäfer *et al.* 2005). Swamps occupied a broad tectonically subsiding embayment, which was surrounded on three sides by land. Teichmüller postulated three main wetland facies zones: (1) a marginal broad zone of forest swamp which graded into (2) wide reed expanses and (3) shallow water with deposition of humic sapropels. Alternating dark and light bands of woody lignite and assumed reed coal make up most of the seam. Like other sedimentary facies changes, this was considered as the vertical expression of a horizontal oscillation of facies zones (1) and (2). Moosbrugger *et al.* (1994) described in great detail one of the forest bands, which is mainly composed of conifers of the *Taxodiaceae* and *Cupressaceae* families with a few interspersed palm trees. Teichmüller based her interpretation on a comparison with the cypress swamps of the southeastern coastal USA. Meanwhile, supposedly better equivalents were discovered in the swamp forests of Southeast Asia. Tropical swamps in Indonesia consist of woody dark layers, which are the base for ombrogenic peat domes made of pale, earthy and oxidized material (Esterle & Ferm 1994). The same interpretation is used to explain colour-banding in the giant Morwell lignite deposit (part of the Latrobe district, Figure 6.12), which is interpreted to reflect orbitally forced climate oscillations (Large *et al.* 2004).

In the Hausruck lignites, nearly all coal is characterized by a preponderance of *Sequoia* wood, including giant tree trunks and numerous forest fire horizons (Pohl 1968). Near the basin margin in the northeast, the lignite seam is quite thin and displays high ash content. Towards the south, coal thickness increases until it reaches a maximum of 7 m. The Hausruck Lignite Formation attains a total thickness of 30 m in the southwestern depocentre and the seams contain increasing mineral matter, both as ash and in dirt bands, until the impure coal is not marketable. A peculiar varved limnic clay above the Middle Seam is a useful marker (Figure 6.14). Taken together, these observations imply a high and relatively dry setting in the northeast that grades into a lower and mostly limnic basin in the southwest. Geochemical methods confirm this model (Bechtel *et al.* 2003).

Some bodies of clastic sediments are drastically different from the thin clastic strata in coal seams, by exhibiting a short lenticular shape (in cross-section) but a great length in map view. The sediments include clay, sand and coal fragments. Cross-sections of these clastic bodies in coal can be very complex, because their compaction is small compared to peat. Contacts are often slickensided and fractured. These structures are infilled channels of meandering creeks and rivers in the swamp. Actually, vegetation is the clue for stabilization of river banks and of meandering single-thread channels (Tal & Paola 2007). In the Pennsylvanian coal fields of Illinois, USA, a giant swamp river is known with a width of 3–8 km and a length of 275 km.

It is important to distinguish clastic inclusions formed during peat formation from clastic infill deposited by streams, which cut into the seam from a base in the hanging wall (incised channels, or washouts). In Illinois, Middle Pennsylvanian channels in coal measures were incised when a glacial climate period induced low sea-levels and seasonally dry climate (Falcon-Lang *et al.* 2009). Very deep incisions were made by rivers flowing beneath inland ice shields, which covered northern Europe in the Pleistocene. The subglacial erosion was well exposed in open pits exploiting Miocene lignites in the Lausitz District (Germany). Fluviatile washouts are identified by sharp erosive contacts instead of the transitional character between peat (coal) and synsedimentary channels. In the Hausruck District, washouts take the form of round potholes (scours) of 30 m diameter and 10 m depth, which are filled with alluvial gravel and sand resembling the overlying coarse sediments of the large Late Miocene alluvial fan of a large river originating in the Alps (Figure 6.15).

Some seams are cross-cut by clastic dykes, which usually originate in a bed of sand or mud that is present in the hanging wall. Arguably this is an effect of synsedimentary earthquakes. Dykes, swamp channel fill bodies and washouts are always serious and costly challenges to mechanical coal extraction.

6.2.3 Peat formation environments

Coals originated in former wetlands of coastal and inland settings (Greb & DiMichele 2006). The formation of peat deposits requires that:

- a profuse growth of higher plants is possible;
- dead plant material is covered by water so that oxidation and microbial decomposition is restricted; and
- that only a minimum of clastic sediment enters the peatland.

Most important is a suitable water level; if the water is too deep, higher plants cannot survive. If the swamp falls dry, peat and plant matter will be rapidly decomposed. Also, a water level that is favourable for the growth of higher plants will indirectly limit introduction of clastic sediment.

Both transgression and regression of the sea may promote the formation of peatlands. In the first case, the rising sea dams up coastal freshwater so that swamps form. As the waterline slowly migrates landwards, the swamps drown and peat beds are covered by marine sediment (e.g. coastal sand or shallow water carbonate mud). Many Palaeozoic coal seams in Northern Europe and in Eastern Australia (Herbert 1997), but also Tertiary lignite deposits in the Mediterranean realm attest to this course of events. Regression causes peat formation when the retreating sea exposes wide coastal flats where swamp forests thrive (e.g. the giant Miocene lignite deposits of Lausitz, Eastern Germany: Standke *et al.* 1993). In this case, marine sediments are found below the seam that is covered by terrestrial deposits.

Low-lying swamps (fens) develop in depressions or vales of the land, such as alluvial interchannel areas, moraine hills, constricted river bends, volcanic craters and in drowning karst dolines. Even in such terrestrial surroundings, the water table rise may be caused by eustatic increase of the sea level. Shallow lakes first develop a stage of floating peat that accretes on the lake margin. Next, a luxuriant and diverse flora expands across the former lake. Such low-lying swamps promote minerotrophic and eutrophic conditions with a high rate of organic production, but result in coal with high ash and elevated sulphur content. In contrast to ombrogenic bogs, fens are important sources of CH_4 and contribute to CH_4 and CO_2 fluctuations in the atmosphere. As greenhouse gases, both are factors of climate variations.

Ombrogenic, oligotrophic **raised swamps (bogs)** occur in regions of high precipitation. Raised bogs

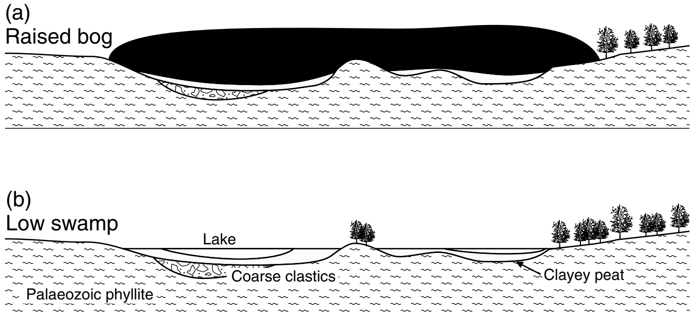

Figure 6.16 Simplified evolution of peat formation in the Miocene coal basin at Leoben, Austria, from an early, rather unproductive stage of a low-lying swamp (a) depositing high-ash peat to (b) a highly productive raised bog (modified after Gruber & Sachsenhofer 2001). Copyright (2001) with permission from Elsevier.

are independent of morphology and may even grow on mountains, although with a small chance of preservation. The transition from an original low-lying swamp into a raised bog is often observed ("domed peat deposit", Figure 6.16). The domes reach impressive dimensions. On the coastal plains of Sarawak Island, Pleistocene-Holocene peat domes attain 20 m thickness and a surface of 1000 km^2 (Staub & Esterle 1994). Raised bog peat differs from low-lying swamp peat by low ash and sulphur concentrations, acidic pH and less decomposition. However, low concentration of limiting nutrients (Ca, P, K, N) may severely curb productivity. Remember that six major elements – H, C, N, O, S and P – are required to build all biological macromolecules (Falkowski *et al.* 2008). Coastal raised swamps of the Indonesian islands are most probably the modern equivalents of ancient low-sulphur and low-ash coal (Cobb & Cecil 1993). In the Northern Hemisphere, lignin-free *sphagnum* (a moss) is at present the most important peat-producer of raised bogs.

The majority of coals are autochtonous, derived from plants that grew at, or near their present location in the seam. The opposite, allochthonous formation of coal from transported plants or peat is quite rare. Upright trees, tree stumps and seat rocks (root horizons in footwall sand or clay) are indicators for autochthonous coal. Stump horizons in German lignites are ubiquitous (Moosbrugger *et al.* 1994), and some stumps display over 1500 annual growth rings (Kurths *et al.* 1993). This implies coal formation periods with very stable conditions and little incremental peat deposition. Allochthonous seams are characterized by a high siliciclastic fraction, high ash, rounded coal fragments, non-oriented driftwood masses, rapidly varying seam thickness, discordant boundaries and cross-bedding within the coal. Allochthonous origin is relatively more common in Gondwana coal (Begossi & Della Favera 2002, Glasspool 2003). Of course, much plant matter in all swamps is transported for short distances and may be called "parautochthonous". This is especially obvious for the char fragments of fire horizons, which form continuous laminae of the lithotype fusain (Lamberson 1996).

The formation of swamps and extensive peat deposits, and the preservation of peat and its transformation into coal, require a set of favourable factors including climate, tectonics and palaeogeography.

Climate is an essential control on peat-forming plant communities. Sufficient precipitation is the basic precondition. It should not fall below 40 mm/month, even in dry seasons. Monthly average temperatures should remain above 10 °C, because this is the minimum that supports lush plant growth. Tropical, warm and humid forest swamps are optimal for a high production rate of plant substance, where trees grow within 7 to 9 years to heights of 30 m. Growth in cooler climates is much slower, with an estimated peat increment of 0.5–1 mm/a compared to 1–4 mm/a in the tropics (Falcon-Lang *et al.* 2009). Although many major coal deposits originated in tropical climate zones, significant coal resources formed in temperate and even cool climates. The Late Carboniferous (Pennsylvanian) coals of Europe, North America and China were deposited in swamp forests of *Sigillaria* and *Lepidodendron* at tropical latitudes (Ziegler *et al.* 1997). These rain forests were ecologically quite heterogeneous (DiMichele *et al.* 2007). Glacial climate cycles, however, induced long phases of dry tropical vegetation, which are poorly represented in the fossil record (Falcon-Lang *et al.* 2009). The giant Permian coal deposits of the Southern Hemisphere, with their boreal *Gangamopteris-Glossopteris* flora, formed during the same Permo-Carboniferous glaciation in a cool and humid climate, although possibly with tropical summer temperatures (Rayner 1996). Burial of peat depressed atmospheric CO_2 to very low concentrations. Waxing and waning of the ice sheets controlled climate and eustatic sea levels.

> The typical Permian flora of southern continents was one of the main arguments when Suess (1885) recognized the former land connection between Africa, Madagascar and India, and called this landmass "Gondwana". Today we know that Australia, Antarctica and much of South America were also part of Gondwana. Gondwana and Laurasia finally collided at ~300 Ma, resulting in the formation of Supercontinent Pangaea (Torsvik & Cocks 2004), which was the stage for Permo-Carboniferous glaciation and peat formation.

Coal seams are terrestrial climate archives, just like recent peat deposits (Large *et al.* 2003). The density of stomata on fossil cuticles allows an estimate of atmospheric CO_2 concentrations back into the Palaeozoic (Retallack 2001). A coal formation in northeastern Greenland just straddles the end-Triassic extinction and displays a ^{12}C spike that is attributed to sudden release of methane from gas hydrates on the ocean floor (Beerling 2007). At the same time, foundering and rifting of Pangaea started with the outpouring of basalts in the Central Atlantic Magmatic Province (Marzoli *et al.* 1999). Exceptionally fusinite-rich (40–60%) Mid-Cretaceous seams in British Columbia, Canada, testify to unusually frequent swamp fires, which were probably caused by dry climate periods (Lamberson *et al.* 1996). The iridium anomaly and botanical extinction caused by the Chixculub impact at the Cretaceous/Tertiary boundary were confirmed in a coal seam of New Zealand (Vajda & McLoughlin 2004).

Wetlands are significant factors of climate regulation, by preserving large masses of carbon in the form of peat and coal (Beerling 2007). Today's wetlands cover a surface of 250–500 Mha and contain 110–450 Gt C_{org}. In comparison, the mass of $C(CO_2)$ in the atmosphere is ~780 Gt. Clearly, an important function of peat and coal sedimentation is abstraction of CO_2 from the atmosphere and concurrent cooling of climate. At the same time, burial of organic matter is the cause of a net oxidation of the atmosphere via photosynthesis (Falkowski & Isozaki 2008). When CO_2 concentration in the atmosphere decreased to very low levels in the Late Palaeozoic (Figure 6.17), the Earth's climate fell into glacial mode. The

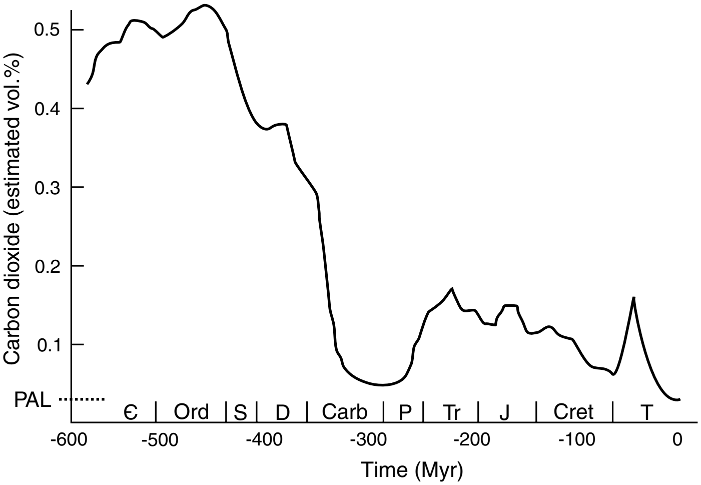

Figure 6.17 Reconstruction of CO_2-levels in the Earth's atmosphere from the Cambrian until today (cf. Normile 2009) based on geochemical models (Berner & Kothavala 2001) and various proxy data (Retallack 2001). Adapted by permission from Macmillan Publishers Ltd: *Nature* copyright (2001). Error margins are not shown. PAL is the present atmospheric level at ~0.039 volume % CO_2 in air. At about 635 Ma in the Neoproterozoic Marinoan Snowball Earth glaciation, pCO_2 had been as high as 1.25–8% (Bao *et al.* 2009).

resulting Gondwanan continental glaciation lasted from 326 to 267 Ma (Horton & Poulsen 2009). At the end of the Permian period, the eruption of the giant Siberian trap basalt province (Kamo *et al.* 2003) terminated the period of low CO_2 concentration in the atmosphere, although the long-term draw-down was only interrupted. The reverse – warming of the climate – is a consequence of swamps falling dry and oxidation of peat and coal, including burning it in power stations (releasing CO_2). Warming is also caused by methane released into the atmosphere through the activity of microbial methanogens in wetlands. However, the Earth's carbon cycling remains incompletely understood (Normile 2009). Our planet encloses other reservoirs of carbon and carbon dioxide, which share in the control of atmospheric carbon dioxide, and climate is influenced by a plethora of processes apart from the CO_2 cycle (Plimer 2009, Solomon *et al.* 2010). During the last ice age and its numerous glacial/interglacial periods, carbon dioxide varied from ~180–300 ppm, but the variations were not the cause but the consequence of temperature amplitudes between -9 and $+3\,^{\circ}C$ (Shackleton 2000).

Tectonic processes provide the slow subsidence that enhances peat thickness by balancing swamp growth. This includes all scales of tectonics, from wide epeirogenic flexure of intracratonic basins and platforms to the formation of orogenic foredeeps and local rift valleys (Figure 6.12). Post-orogenic intramontane basins are formed by tensional or shear strain of thickened orogenic crust. Embryonic folding of a basin during peat sedimentation may cause thinned seams over future anticlines and thickened coal in the depressions (e.g. Sydney District, Australia; Wise *et al.* 1991). Rim synclines of salt diapirs and walls (Figure/Plate 5.18) may collect large volumes of peat.

Palaeogeographical reconstructions of important coal basins of the Earth lead to an enhanced understanding of the conditions that support the formation of large coal deposits (Rowley *et al.* 1985). Palaeogeographical reconstructions at the scale of coal-forming wetland landscapes are useful for exploration and exploiting coal. A problem of such reconstructions for the geological past is the absence of recent examples of giant wetlands, because in the Holocene, continents are in a state of emergence and general dryness. Today, there is no wetland resembling the Westphalian coal belt in Europe with an East-West extension of ~3000 km, and a North-South width of 800 km (Ziegler 1982). Coal "giants" were typically deposited in periods of marine ingression into continents, at relatively higher sea levels than today. Therefore, instead of relying on the rules of actualism, facies analysis of the sediments associated with coal seams is the basis for modelling the sedimentary environment. Work in the foreland of the Appalachian Mountains resulted in the establishment of the Allegheny model that gained worldwide acceptance.

The Allegheny model is based on the observation that thick coal formations consist of disconformity-bounded stratigraphical repetitive sequences of sediments that have been termed "cyclothems" (Figure 6.18). Cyclothems were originally defined as "designating a series of beds deposited during a single sedimentary cycle of the type that prevailed during the Pennsylvanian period" (Wanless & Weller 1932). The concept and its significance are still discussed today (Horton & Poulsen 2009, Weibel 2004, Wilkinson *et al.* 2003). Sediments making up cyclothems can be related to several depositional environments, which are the key to the recognition of favourable peat-forming areas (Thomas 2002, Ward 1984):

- *Marine shelf* Fossiliferous shale, sandstone and carbonates, rarely dark phosphatic shale, all deposited in relatively deep water and far from the shoreline; no coal;
- *Delta front, coastal barriers and brackish lagoons* Mainly quartzites that are interbedded either with shale and carbonates (seawards) or with dark shale and thin coal beds (landwards); the shoreline may be marked by the occurrence of flint;
- *Lower delta plain* Lagoonal or deltaic shales that are overlain by silt and sandstone, incised by sandy alluvial channels; thin coal beds are ubiquitous, either in abandoned channels or in wide coastal swamps between active flow channels;
- *Upper delta plain and broad alluvial plains* Terrestrial clastic rocks and thick coal seams; peat formed in wide swamps covering inundation

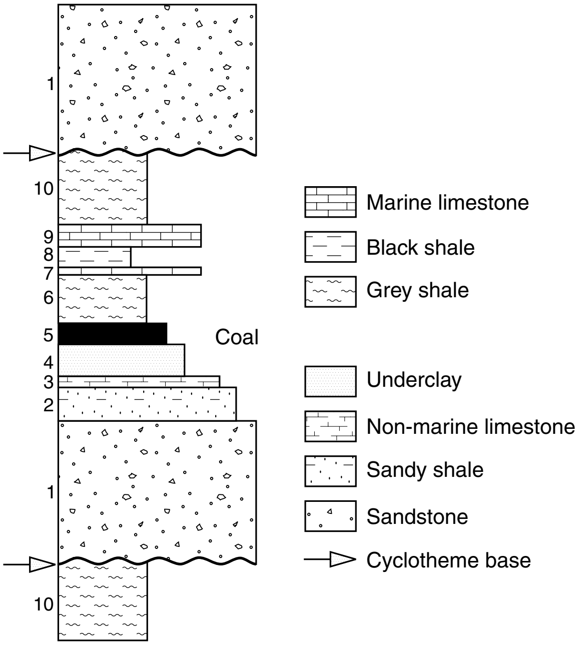

Figure 6.18 The "ideal" cyclothem (modified from Wanless & Weller 1932 and Wilkinson *et al.* 2003). Wilkinson *et al.* argue, however, that the apparently regular succession of sediments in cyclothems is accidental. The variable width of the column emphasizes different lithologies and grain size.

plains, lakes and abandoned channels; coal seams contain clastic interbeds; generally, fining-upward sediments are characteristic.

The formation of Pennsylvanian cyclothems may have been controlled by: i) eustatic glacial forcing of sea levels; or ii) tectonic impulses. The first can be caused by orbital control of sea levels and climate oscillations related to the Milankovitch theory (Heckel 1986), or by greenhouse gas control. There is little doubt that most cyclothems reflect global change of sea levels due to waxing and waning of continental ice sheets. Estimates of the glacial-eustactic amplitudes during the Pennsylvanian vary around ~100 m, similar to the Pleistocene. Glacial-eustatic cyclothems are separated by lowstand terrestrial units or by exposure surfaces. Orbital insolation changes are controlled by the Earth's precession, obliquity and eccentricity, with recurrence sinusoidal periods of ~20, 40 and 100 kyr, 400 kyr and 2.5 Myr. The short cycles provide a possible time-scale to single cyclothems. In the Pleistocene, a combination of orbital control and consequent greenhouse gas decrease to less than 280 ppm CO_2 equivalent, is thought to have caused growth of ice sheets and fall of sea levels by 120 m. Simulations of Late Palaeozoic orbital cycles, glaciation and sea levels at different $p\mathrm{CO}_2$ (Horton & Poulsen 2009) suggest that orbital cycles alone only account for ~10 m sea level change; greenhouse gas forcing must be induced to replicate observations.

Global extent of glacial eustasy caused by Late Palaeozoic glaciation of Gondwana translates into the probability that single cyclothems should be datable events worldwide (Miall 1997). The origin of specific cyclothems is still discussed. The Carboniferous coal measures of northern Germany, for example, were deposited in coastal swamps of the Variscan foredeep (Figure 6.19) and display many cycles of marine transgression and regression. Resulting cyclothems are considered eustatic-tectonic by Süss *et al.* (2000) and glacial-eustatic by Hampson *et al.* (1999).

6.2.4 Host rocks of coal

A siliciclastic nature of rocks hosting coal is the norm (Figure/Plate 6.20). Exceptional cases include Late Permian coal seams in southern China, which rest on marine platform carbonates.

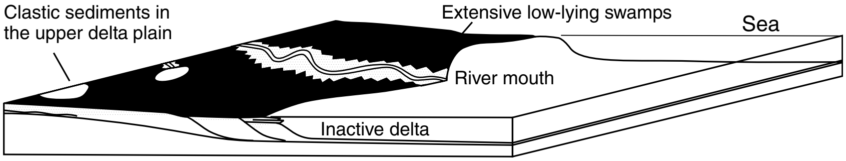
Clastic sediments in the upper delta plain
Extensive low-lying swamps
Sea
River mouth
Inactive delta

Figure 6.19 The largest expansion of Late Carboniferous paralic swamps in northern Germany occurred at times of beginning transgression of the sea. In sequence stratigraphic terms, this is an "early transgressive systems tract" (Hampson *et al.* 1999). Black – peat areas.

This coal contains marine fossils and is enriched in organic S, Na, Mg and Ca. A setting similar to recent coastal mangrove swamps is assumed (Shao *et al.* 1998).

An appropriate study of host rocks is a vital part of scientific and practical investigations of coal deposits. Sedimentological data are needed for palaeogeographical models and for resource estimation, physical properties determine mining methods and costs. Note that rocks associated with coal always display grey colouring; red (haematitic) sediments are free of coal. The grey colour of host rocks is, of course, simply a result of the reducing sedimentary-diagenetic environment and is caused by fine-grained organic substances and pyrite. In rare cases, the connection between former swamps and nearby hills is exposed and lateritic (red) soil is observed. An example is the paralic (coastal) Late Carboniferous seams of the Sydney basin on Canada's Atlantic seaboard,

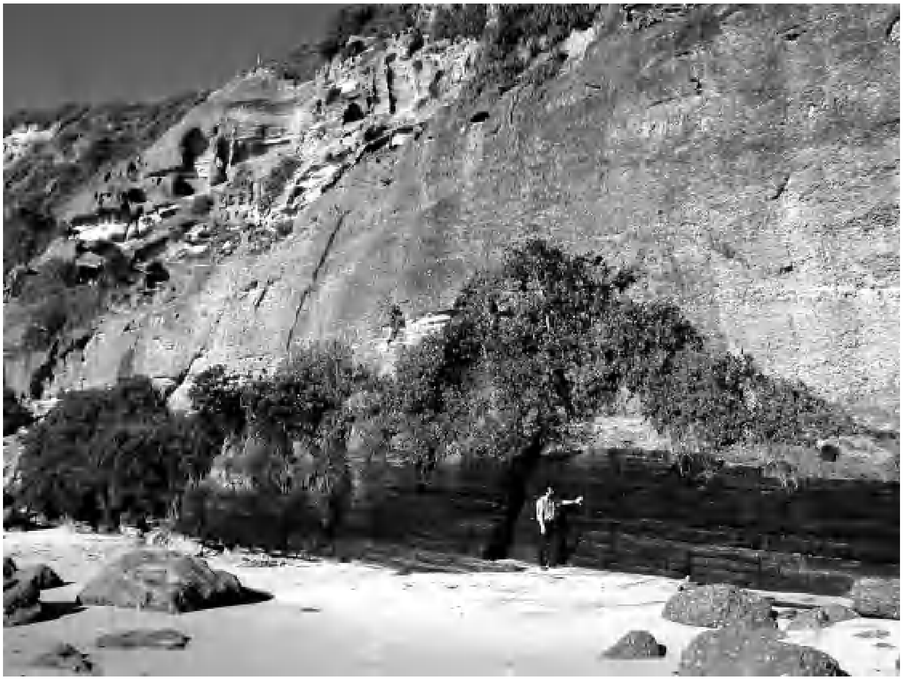

Figure 6.20 (Plate 6.20) Outcrop of Permian Great Northern coal seam below fluvial conglomerate on the Pacific shore, Sydney basin, New South Wales, Australia. Note vertical joints and subdivision of seam into plies. Courtesy of Keith Bartlett, Minarco-Mineconsult, Tuggerah, NSW.

which are interbedded with transported red soil and calcrete nodules (Tandon & Gibling 1997). Autochthonous calcic vertisols are attributed to glacial dry climate spells in the Mid-Carboniferous of Illinois (Falcon-Lang *et al.* 2009).

Floor (footwall) of coal seams

Coal seams may be in direct contact with older basement (Figure 6.16), but are more commonly underlain by clastic sediments of the same age. Plant roots and their symbiotic fungal associates secrete organic acids that dissolve mineral particles in the soil to liberate nutrients needed for growth. This enhances the rates at which continental silicate rocks undergo abiotic chemical weathering (Berner *et al.* 2003, Berner 1997). Organic acids dissolved in seepage water from the mires act as reductants and break down soil minerals. In the case of good drainage, iron and alkalis are removed, resulting in bleaching, kaolinization and the upgrading of quartz sands. In consequence, valuable kaolin, illitic fireclay and high-grade sand or quartzite deposits in coal districts are not rare. Also, the downward seepage of water removes large quantities of CO_2 from the atmosphere, for example by calcite formation in deeper parts of the aquifers. At the same time, dissolved matter entering the sea favoured proliferation of marine carbonate-forming life. The combined effect is the steady drop of atmospheric CO_2 during the Palaeozoic (Figure 6.17), while land plants emerged and colonized the Earth's terrestrial surface and as a side-effect, lowered ambient temperatures.

A characteristic footwall rock of seams is *seat earth,* or *underclay,* which is the soil that supported the peat-forming vegetation. The material is typically fine-grained (clay and silt) but may be sandy. Coalified remains of roots are abundant and reach a depth of 10 m below coal seams. Siderite concretions mark many of these horizons as former gley and semi-gley soil.

Roof (hanging wall) of coal seams

Thinly stratified carbonaceous shale with numerous leaf fossils, cannel coal and bituminous shale are characteristic roof rocks of Late Palaeozoic coal seams in the Northern Hemisphere. These rocks indicate deglaciation, rising oceanic and local water levels, and drowning of the swamp. In contact with air, as for example on waste dumps, these rocks are prone to self-ignition. Sand as a roof rock of seams in orogenic foreland basins may have originated by subduction earthquakes and consequent tsunamis. Also possible is a genetic equivalence with the mud deposited by Hurricane Katrina over wide wetland areas of Louisiana, USA (Turner *et al.* 2006). Coals with marine hanging wall rocks contain relatively more ash, sulphur and nitrogen, and more volatile matter than is expected from the rank of nearby freshwater coal. The elevated bitumen concentrations shift coking behaviour. These negative consequences of seawater inundation require a considerable time; peat in Panama, which was submerged by an earthquake below sea level in 1991, displayed little alteration three years later (Phillips *et al.* 1994). A relatively thin roof of freshwater clay and silt provides sufficient sealing to prevent negative consequences of marine transgression on coal quality (Eble & Greb 1997).

6.2.5 Marker beds in coal formations

At scales of less than 10,000 years and 10 km distance, coal seams must be considered as diachronous beds, except if the opposite can be proved, for example by a tuff marker bed. At larger time spans and distances, seams may be used as time markers. They are, however, a rather poor basis for chronostratigraphy but serve very well in lithostratigraphical work. In mining applications such as seam correlation, the latter has proved its high worth.

Lithostratigraphical orientation is most important in coal districts with numerous seams, which are deformed by folds, faults and overthrusting. Lithological marker horizons, fossil-rich bands, characteristic host rocks, palaeosoils and recognizable dirt bands in single seams, such as tuff and fire horizons, all serve to build a lithostratigraphical division, and to match an unknown seam into the system, for example after driving a tunnel through a fault with uncertain throw.

Marine marker horizons are the product of transgression of the sea over coastal peat swamps or freshwater mud flats. In the Ruhr District, Germany, 40 exploitable seams and 18 marine marker horizons are distinguished. These marine flooding events are traceable throughout Europe and already long ago served to establish international stratigraphical boundaries. Typical rocks are dark banded shales with a rich fauna, in part open marine pelagic, whereas others display a fauna of a few species in brackish settings.

Volcanic tuff horizons are very useful correlation markers, because ash falls mark actual time horizons. When a tuff band cuts through a seam at an oblique angle, the seam is diachronous. In European and North American, Carboniferous coal seams, tonstein (German for "claystone") horizons are relatively frequent. They represent kaolinized rhyolitic tuff with recognizable characteristic rhyolite quartz, former glass shards, sanidine, zircon and ilmenite. With a thickness of <10 cm, many tonstein bands are known over thousands of square kilometres. Kaolin originated in the acidic swamp; later diagenesis transformed much kaolin into illite (e.g. Sabero, Spain: Knight *et al.* 2000).

6.2.6 Coal formation in geological space and time

A large number of coal basins were formed in coastal swamps and are called *paralic* (Greek for "by the sea"). Marine marker horizons clearly indicate the proximity of the sea and its occasional invasion. Limnic coal basins formed in intracontinental and often intramontane swamps and display freshwater-dominated rocks. The term "limnic" is not fully satisfactory because little coal originated in lakes. The majority was deposited in a "telmatic" (wetland) or terrestrial (raised bog) environment. Of course, host rocks of "limnic" coal are mainly of limnic and fluviatile facies, with occasional volcanic and marine influence.

The geodynamic nature of coal basin settings suggests a classification along the following lines:

1 *Foreland and molasse basins* are caused by downflexure of the lithosphere, due to subduction and the advancement of an orogenic front. Sediment fill is very thick (up to 8000 m in the North European Carboniferous) and of continental derivation, but mainly deposited in the sea. Paralic seams are numerous, although thin (1–2 m) and cover a large surface. The sedimentary package is folded and faulted, with a decrease of strain from the orogenic front towards the foreland. Examples are giant coal deposits in the Appalachian foreland (Cross 1993), the North-Variscan foredeep of Europe (Drozdzewski 1993), the Bowen Basin west of the Tasman orogenic belt in Australia and the Karoo Basin north of the Cape belt in South Africa (Cadle *et al.* 1993).

2 *Intramontane and intermontane basins* are the result of late-orogenic distension and collapse of mountain belts, and of large transform or shear structures, which create transtensional, transpressional and simple pull-apart basins. Sediments are predominantly limnic and alluvial with marine intercalations. The base of the infill may be a discordant seam. The number of seams is rarely more than 10, but the thickness of individual seams may surpass 100 m. The total thickness of coal formations is rather limited. Tectonic strain varies widely. This type is well illustrated by the Early Tertiary Raton and Powder River basins in North America, although the two originated during the Laramide orogenesis as isolated fragments of a former Cretaceous foreland basin.

3 *Intracontinental and platform basins* Coal-bearing sediment sequences display a thickness of a few hundred metres only. Few seams are developed but some may reach great thicknesses. The seams are constant and attain large areal extensions to several 10,000 km^2. Bedding is nearly horizontal to moderately inclined. This type of coal basins is the result of slow, wide-ranging epeirogenic subsidence of stable cratonic regions. Examples include Gondwana coal basins north of the *sensu stricto* Karoo Basin in South Africa and India, the Tunguska Basin in Central Siberia and the lignites of Eastern Germany.

Times of peat (coal) formation

Earliest rocks resembling coal are known from the Archaean Witwatersrand gold placers (cf. Chapter 2 "Gold"); the so-called carbon leaders are graphitic pyrobitumen seams, which may be derived from algae. Plants first invaded the land

~470 million years ago (in the Silurian). In the geologically short time since, they have diversified and profoundly moulded the Earth's climate and the evolutionary trajectory of life (Beerling 2007). Humic coal became only a possibility with this conquest. The earliest known vascular plant is fragile and leafless *Cooksonia* (425 Ma). In the early Devonian, the first tiny leaves are found (*Eophytophyllon bellum*). Later during the Devonian, terrestrial vascular plants became so widespread that atmospheric CO_2 concentration fell rapidly, caused by intensified weathering (Figure 6.17, Berner 1997). At the same time, the oxygen concentration in air started to rise, reaching a peak of ~35% in the Permian (compared with the present atmospheric level of 21%).

The oldest coal deposits date from the Late Devonian of Arctic regions (Asia, northern Europe, Canada), with fossils of genus *Archaeopteris* as the earliest tall trees. Well-developed seat rocks are known in Quebec (Elick *et al.* 1998). Since then, coal was formed in all geological stages. Two main periods of coal formation, however, stand out because of the sheer mass of coal contained: The Late Carboniferous-Permian and the Late Cretaceous-Tertiary, which contain ~55 and 26%, respectively, of world resources. Both are related to late orogenic dynamics of continental collision (the Variscan and Alpidic cycles, respectively). Late Palaeozoic coals of the northern hemisphere (China, Europe, North America) formed in a relatively short time span of ~30 Ma in the Late Carboniferous. During this time, the region passed the tropical rain forest zone while Pangaea drifted northwards. Most of the coals of the Gondwanan part of Pangaea (Australia, Africa, Antarctica, India, South America) were deposited later, in the Early and Mid-Permian. Coal formation in both hemispheres is intimately controlled by continental glaciation lasting from 326 to 267 Ma (Horton & Poulsen 2009).

6.3 THE COALIFICATION PROCESS

The natural process system, which transforms plant material into coal, is called coalification, as proposed by Gümbel (1883). Gümbel coined the term in order to stress the contrast with carbonization that is provoked by anoxic heating of wood in a charcoal pile. Coalification can be considered to consist of a first stage that takes place in the swamp during peat formation, and a second stage that begins with deposition of cover rocks above the peat. The first is also called "peatification" and is primarily a biochemical process. The second, geochemical coalification is essentially abiotic, driven mainly by increasing temperature and pressure. The domain of coalification is largely equivalent to that of diagenesis, the term applied to inorganic sediments (cf. Chapter 1.4 "Diagenetic Ore Formation Systems"), and to "maturation", which is used in the hydrocarbon industry to describe changes of dispersed organic matter in sediments related to oil and gas generation.

6.3.1 Biochemical peatification

Most peat-forming wetlands have an oxidized near-surface layer but at little depth, reducing conditions prevail. A fully developed vertical redox-stratification may include oxic, suboxic, sulphidic and methane zones with increasing depth. The aerobic oxic zone is defined by the presence of dissolved oxygen in pore waters and is generally very shallow. The suboxic zone is identified by accumulation of dissolved Fe(II) and Mn(II) in the pore waters and is anaerobic. Due to sulphate reduction, dissolved H_2S builds up in the sulphidic zone. Organic matter degradation by anaerobic methanogenesis sets in when sulphate is depleted to levels that do not support microbial respiration. Lateral variation of the zonation is considerable (Koretsky *et al.* 2007).

Dead plant matter in the swamp is decomposed by bacteria, archaea, actinomycetes and fungi. Synthesis of humic macromolecules occurs by microorganisms proliferating on organic residues (Kögel-Knabner 1993). Different products are due to the respective redox environment and the fate of various building materials of the plant. Sugars, starch, pectine and protein are rapidly metabolized, as is cellulose, which is not protected by lignin. Lignin is preferentially attacked by fungi; the effect is transformation into solid humic substances under preservation of shape (Hatcher & Clifford 1997).

Cork (suberine) and tannine-impregnated tissues are only in part microbially decomposed. Wax and resins remain unaffected. Lipids such as pollen, spores and cuticles preserve both shape and material composition. Some peats display enrichment of carbon to 60% (d.m.m.f.) already near the surface; the increase of carbon towards depth is slow and in rare cases attains a maximum of ~64% C. Clearly, carbon is not a useful parameter for the determination of peat maturity.

Only abiotic changes such as condensation, polymerization and reduction take place below ~10 m under the surface. Most conspicuous are decreasing porosity and water content of the peat as a function of increasing consolidation. Some observations suggest that water content is reduced by 1% for every 10 m; such experimental data collected from a specific deposit may serve well for studying the maturity distribution. The transition from peat to bog coal and lignite is a matter of convention, with no natural limiting mark. Water, free cellulose and carbon content, or the ease of cutting may be parameters taken into account (Figure 6.4, Taylor *et al*. 1998).

The most significant process of peatification as a precursor of coal formation is humification, which is a limited oxidation of lignin, cellulose and proteins. Humification may be followed by biogenic gelification. Microbiota are the key to more intense decomposition. Preconditions for high microbial activity include: i) a rather basic pH of the swamp: ii) the availability of sufficient nutrients (Ca, P, K, N): iii) elevated temperature; and iv) free oxygen in surface water. Therefore, high biogenic gelification is one of the indicators of swamp facies. In some cases, clearly variable gelification of different plies in one coal seam has been observed.

Burial of the peat by alluvial, limnic or marine sediments terminates the biochemical peatification process, and geochemical coalification takes over.

6.3.2 Geochemical coalification

Petrographical, chemical and physical properties of coal change with increasing rank. Peat and bog coal are little different, but already in sub-bituminous coal organic constituents are markedly changed. This observation provoked remarks that coalification may be better considered as a kind of metamorphism and not of diagenesis (Hower & Gayer 2002). Taking into account, however, that host rocks of coal experience diagenesis while coal rank increases, using the term metamorphism appears highly impractical.

Humins evolve during coalification by increasing aromatization, condensation and clustering (Hatcher & Clifford 1997). As functional groups, bridges and side-chains of nuclei are broken down, islands of well-ordered structural elements ("crystallites") grow larger. During coal maturation, aromatic clusters are increasingly arranged into flat sheets that resemble the graphite lattice.

During coalification, elemental ratios of H/C and O/C change, and decomposition reactions liberate water, CH_4 and CO_2 or CO (Kopp *et al.* 2000). Note that in certain districts, $C_{2\text{-}4}$ hydrocarbon gas may occur apart from methane. In the Ruhr District, Germany, this "wet gas fraction" attains 70%. In addition, all humic coals exude a little bitumen similar to crude oil. Coal as a source rock for oil deposits, however, is uncommon (Wilkins & George 2002).

6.3.3 Measuring the degree of coalification

Quantitative determination of coal rank relies on chemical and physical changes during coalification. Because these changes are not equally distinct over the whole rank scale, certain methods are preferred in specific rank regions.

In lignites and sub-bituminous coals, moisture decreases rapidly with increasing rank (Figure 6.4), which makes its determination a useful parameter of maturity. In Australian (Holdgate 2005; Figure 6.12) and Lower Rhine bog coal, water content decreases 3–5% per 100 m depth increment, and in the sub-bituminous coal of Borneo at 1% per 100 m. This loss of water is caused by a reduction of the pore volume, but also chemical loss of hydroxyl (-OH) and other organic groups. Factors that influence gradual loss of water include burial depth, time, seawater contact, lithotype and tectonic strain (e.g. folding). Moisture of bituminous coal changes little and is of no use for rank determination.

In mining practice, the rank of black coal is measured by volatile matter yields. Because macerals display different content of volatiles, bright lithotype layers (vitrain) are preferably used for precise rank measurements. The reverse, i.e. fixed carbon ($\% \mathrm{C} = 100 - \% \mathrm{V.M.}$) may also serve to express rank. Increasing coal rank reduces volatile matter and increases fixed carbon content. Already in 1873, Hilt had reported that the rank of black coal in a shaft increases with depth (Hilt's law). The gradient is locally different but the average decrease of V.M. is ~1.4% per 100 m. Sivek *et al.* (2008) show that in the Upper Silesian coal basin, deviations from the average are due to elevated pressure in tectonically deformed areas, to thermal influence from igneous intrusions and even to palaeoweathering.

The standard method of rank measurement, however, is the determination of vitrinite reflectance (Taylor *et al.* 1998). This is carried out with a photometer mounted on a microscope, by illuminating a polished surface of coal with non-polarized light under oil immersion and measuring the reflected fraction of the incident light. In routine work, particle mounts are prepared and reflectance is measured. Statistical evaluation reveals the mean of random reflectance (R_r or in oil immersion $R_{r,o}$, often written R_o), which correlates closely with coal rank. Reflectance determined with polarized light on oriented coal samples reveals an anisotropy of high (R_{max}), intermediate and low (R_{min}) values. In little deformed coal seams, R_{max} is oriented parallel to bedding and R_{min} across it at a right-angle. This is due to the gravity-induced natural stress field, which causes growth or adjustment of structural lamellae into near-horizontal bedding planes. Deviations from this ordinary spatial arrangement may occur in folded seams and are important keys for resolving the relative timing of coalification and deformation, and for reconstruction of the palaeo-stress field. Average reflectance increases from ~0.3% (of incident light) for lignite to ~4% for anthracite. The increase is much steeper in high-rank compared to lower rank coals (Figure 6.4).

Changes of macerals of the liptinite group can also be employed for studies of coal rank (Taylor *et al.* 1998). Illuminated with blue or long-wave UV light under the microscope, liptinites exhibit fluorescence (Figure/Plate 6.9). The intensity of fluorescence is highest in peat and lignite and decreases with higher rank. Quantitative measurement of rank is possible up to the so-called coalification break at ~29% V.M. (high volatile bituminous coal). At higher rank, in medium volatile bituminous coal, liptinites approach vitrinite in chemical and optical properties and the two cannot be distinguished. Precursors of liptinites are mainly paraffinic (aliphatic) waxes and lipids of plants, which are very stable during peatification. In the sub-bituminous stage, liptinites exude bitumen, just like petroleum source rocks. Subsequently, methane is released until liptinites loose their petrographical identity.

Physico-chemical investigations of structural change during coalification, such as aromatization, condensation and clustering, also reveal much about the coalification process (Hatcher & Clifford 1997). This is, however, hardly ever applied in practice, in contrast to the methods presented above. Visualization of coalification data in relation to geological features is provided by maps and sections, which display rank by contours of equal water and V.M. content, or reflectance.

6.3.4 Causes of coalification

Many observations in coal mines provide arguments concerning the agents of coalification, including:

- time, because older coal is commonly of higher rank;
- temperature, because coal in proximity of igneous rocks is upgraded and deeper coal is subject to higher heat flow;
- pressure, which also rises with depth;
- tectonic strain, as in the same basin undeformed coal tends to display lower rank compared to folded seams; and
- swamp facies, which partly controls volatile matter content.

Currently, a dominating role of temperature is generally accepted, but the influence of other factors is not negated (Sivek *et al.* 2008, Hower & Gayer 2002).

Thermal metamorphism of coal

Thermal metamorphism of coal in contact with magmas continues to provide a deeper understanding of coalification (Mastalerz *et al.* 2009). Of course, quantification of the temperatures that acted on coal excites much interest. Estimates are made by comparison with results from laboratory experiments, or are derived from the assumed liquid and solidus temperature of the magma and the heat conductivity of host rocks and coal. Actually, with a high heat capacity and one of the lowest heat conductivity coefficients of geological materials (0.016–0.148 W/[m.K], Bychev *et al.* 2004), coal is an excellent insulator. To give one example, coal intruded and covered by Permo-Triassic trap basalt in the Tungus Coal Basin, Siberia, was heated to a maximum of 650–700 °C (Pavlov *et al.* 2005).

Generally, coal affected by the heat aureole of magmas displays reduced moisture and volatile matter content (higher rank), whereas ash yield increases. Black coal is visibly altered above ~300 °C and, above 500 °C, obtains an appearance that resembles industrial coke. Natural coke and graphite often occur as a thin fringe with hexagonal jointing along the contact. Natural coke can be formed from coal that is not cokeable, because of too high V.M.; this observation indicates that confining pressure had an influence. The coke fringe is followed by thermally altered coal, which is dense, hard and dull, and may be hexagonally jointed. Vitrinites in the intermediate zone exhibit incipient melting, loss of volatile matter and exudation of tar. Softening induces viscous plastic flow of coal that destroys sedimentary bedding. Fluid coal may be injected into host rocks resembling a dyke. Haematite may replace pyrite and abundant CO_2 causes deposition of much carbonate, both in coal and in the igneous rock body, which is itself heavily altered. This raises the ash content of coal. Water vapour or supercritical fluid may form at the igneous contact, impeding vitrinite alteration (Barker *et al.* 1998).

Lignites are strongly dehydrated near the contact, which induces cracks and joints. Coke formation is less frequent but confirmed. Anthracites hardly melt and, without exhibiting visible alteration, are upgraded to meta-anthracites, which are commercially extracted and marketed as graphite (cf. Chapter 3, "Graphite"):

> The West Siberian Tungus Coal Basin extends over ~1.2 M km^2 and hosts a thick Permo-Carboniferous coal-bearing series with many important coal seams. Total coal resources are estimated to reach 40,000 Mt (Pavlov *et al.* 2005). Trap basalts covered and intruded the coal sequence at the Permo-Triassic boundary. This induced a short pulse of thermal metamorphism that upgraded previous lignites and sub-bituminous brown coal to coking coal rank, anthracite, and even graphite. At the same time, the process must have released enormous volumes of CO_2, methane, water vapour and hydrogen sulphide that contributed to the near-extinction of life on Earth. In the northern part of the Tungus Basin, the coal series is covered by low-permeability rocks and Pavlov *et al.* (2005) speculate that giant resources of coal-bed methane may be trapped in this area.

Deep igneous intrusions may impose a wide halo of regional thermal coalification, with a peak in the anthracite stage (e.g. in the western Lower Saxony Basin of northern Germany: Kus *et al.* 2005). Rapid rise and denudation of metamorphic massifs may also impose a regional coalification gradient (Sachsenhofer 2000). In the Eastern Alps, Tertiary coal occurs in many intramontane basins (Figure 6.16). Over a distance of ~100 km from east to west, rank increases from lignitic to high volatile bituminous B. The highest rank occurs proximal to the Tauern Window, a tectonic unit that was metamorphosed in the Eocene and unroofed in the Miocene (Neubauer *et al.* 2000).

Geothermal coalification by subsidence

In contrast to spatially circumscribed heat sources, the geothermal field of the Earth provides ubiquitous heat energy. Heat flow from depth provokes a temperature rise with increasing depth, which is called the *geothermal gradient*, with an average of ~25–30 °C/km. However, the geothermal gradient varies with lithology; it may be as low as 14 °C/km for highly conductive salt and 47 °C/km for insulating coaly shale. Other variations are due to the tectonic setting. Subsidence of a coal basin shifts coal into higher temperature conditions, which intensify coalification. The depth arrangement of rank reflects the wide or narrow spacing and the shape of isotherms (contours of equal T). Coalification isolines may be used to reconstruct the geothermal gradient responsible for coalification.

The coalification gradient is a function of geothermal gradient and lithologies at a specific location. Based on quantitative estimates of overburden and heat flow at the time of coalification, calculation of coalification temperatures is possible. If time is not a limiting kinetic factor (see below), typical coalification temperatures are ~50–200 °C (sub-bituminous and bituminous coal). Anthracite is formed at 200–300 °C, which is the reason why this rank is relatively rare. Often, anthracitization is clearly related to magmatic heat sources, but there are other genetic possibilities. In the Appalachians, hot tectonic brines, which are expulsed from the westward moving nappe pile, are considered to have been the agents of heating (Figure 1.74, Daniels *et al.* 1994). Anthracite occurring on the northern margin of the South Wales Basin (UK) was formed by the passage of hot basinal fluids, which were displaced by cool water due to a topographic gradient (Gayer *et al.* 1998). Another hypothesis suggests that the commonly moderate extension of anthracite fields might be explained by an early synclinal downwarp, which is now concealed by later strong deformation such as folding and inversion (Lyons 1991).

The coalification temperature can be calculated from vitrinite reflectance data (e.g. from a drillhole profile) and an estimate of palaeoheat flow derived from specific geological constraints. One of several models was proposed by Sweeny & Burnham (1990). The model is based on chemical kinetics (eq. 6.3). Calculations based on this model demonstrate that coalification represented by reflectance (% R_o) is mainly controlled by temperature, whereas the reaction time exerts a much smaller influence (Figure 6.21).

ARRHENIUS-equation describing the kinetics of an endothermic chemical reaction (here coalification):

$$k = A \cdot e^{-E/RT} \qquad (6.3)$$

k = reaction rate (1/m.y.), A = specific reaction constant (frequency factor, 1/m.y.), E = activation energy (kJ/mol), R = universal gas constant ($J.K^{-1} \cdot mol^{-1}$) and T = temperature in Kelvin (°C + 273).

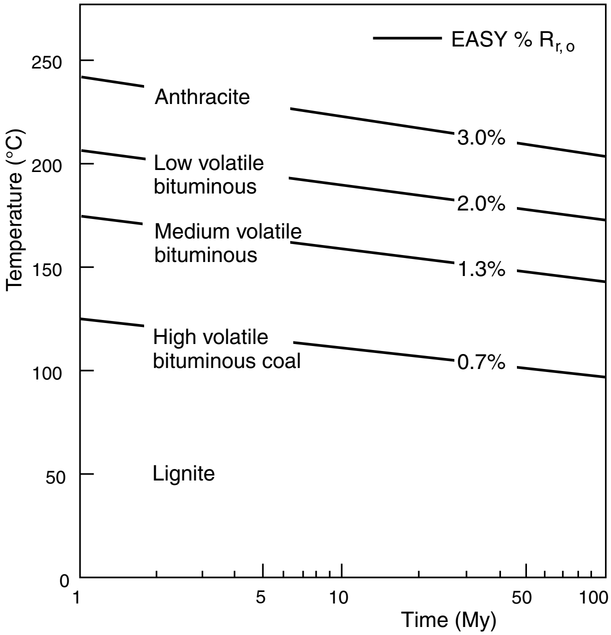

Figure 6.21 Vitrinite reflectance in a temperature-time diagram as calculated with the numeric coalification model EASY % from Sweeny & Burnham (1990). Comparison with coal rank is only indicative. AAPG [1990] reprinted by permission of the AAPG whose permission is required for further use.

Duration of coalification

Many investigations of coalification in geologically young sedimentary basins constrain the main parameters temperature, heat flow and duration of heating to narrow confidence limits. Results show that duration of coalification varies widely. For magmatic heating, coalification time is normally very short (<1 Ma). Long duration (25–35 Ma) was reported for anthracitization in eastern Pennsylvania (Daniels *et al.* 1994). The reaction rate of coalification is still not fully known, so that the effective heating time needed to reach equilibrium at a certain temperature cannot be predicted. The reverse is clearly displayed by observations: Rank once reached is hardly altered by lower temperatures, even if they act for a very long geological time. In this case, activation energy is the limiting factor. An example is the Ruhr District coals in Germany, where coalification patterns were imprinted during the Latest Carboniferous/Earliest Permian before the rocks were folded. In spite of elevated rock temperatures of >50 °C for the last 250 Ma, coal rank was not changed (Figure 6.22).

The role of lithostatic stress and fluid pressure

Considering the increase of coalification as a function of depth, lithostatic stress might play a role. This is certainly the case for lignite, which matures by compaction and dewatering. Bituminous coals attain higher rank mainly by chemical processes, but also by physical compaction such as decreasing porosity and this may be favoured by higher stress. High confining (fluid) pressure, however, may inhibit maturation (Carr 1999) by impeding expulsion of coalification by-products, such as H_2O, CO_2, CH_4, higher hydrocarbons and N.

Tectonic stress and strain

Many observations prove that folding of coal seams does not cause coalification (Figure 6.22). In fact, this was already documented by Petrascheck (1954) when he defined pre-, syn- and post-tectonic coalification based on microscopic investigations of the optical anisotropy of different folded coal seams (Figure 6.23). In the southern Ruhr District, where seams are most intensely folded, coalification is even lower than in less deformed regions (Nöth *et al.* 2001). Nevertheless, tectonic strain that favours permeability, such as pervasive shearing, advances maturation of bituminous coals and of anthracite, and graphitization (Ross & Bustin 1997). With shearing, graphite formation seems to be possible at temperatures little over 300 °C (Bustin *et al.* 1995). M. & R. Teichmüller (1966) observed a sharp coalification increase proximal to an overthrust fault in the Ruhr District. They suggested that friction heat may have been the agent. Heating by circulating hot hydrothermal fluids could be an alternative explanation (Golytsin *et al.* 1997).

Swamp facies

Seams that display marine influence on peat are of higher rank than close-by freshwater seams. This

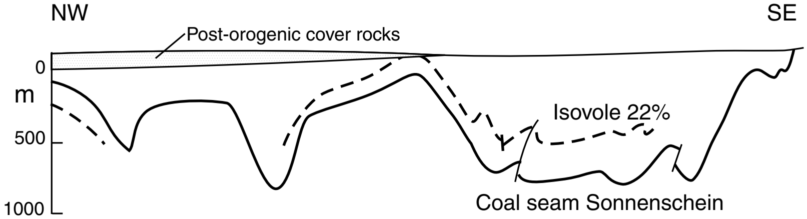

Figure 6.22 The parallel pattern of folded seam Sonnenschein in the Bochum synclinorium (Northern Germany) and the isovole 22% V.M. proves that coalification took place before deformation. Modified from M. & R. Teichmüller (1966, 1981) in Taylor *et al.* (1998). With permission from www.schweizerbart.de.

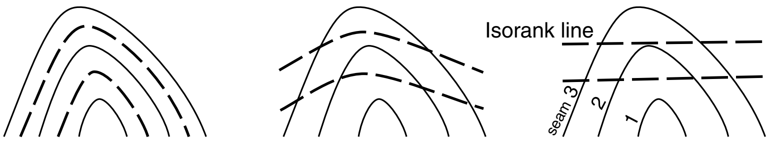

(a) Pre-orogenic coalification

(b) Syn-orogenic (or combined pre-/post-orogenic)

(c) Post-orogenic coalification

Figure 6.23 Pre-, syn- and post-tectonic relations between folded seams and the position of lines of equal coal rank (isovoles or isoreflectance limits). Modified from M. & R. Teichmüller (1966) and W.E. Petrascheck (1954) in Taylor *et al.* (1998). With permission from www.schweizerbart.de.

observation of coal miners was often verified, for example in the Netherlands, where Carboniferous coal rank decreases from deltaic to alluvial floodplain coal (Veld *et al.* 1996).

6.3.5 Coal maturity and diagenesis of country rocks

Studies of thermal evolution and burial history of sedimentary basins are not only based on vitrinite reflectance of coal and the maturation stage of dispersed kerogen in sediments. Detailed mineralogical investigations of pore cements, pore fluids and of pelitic rocks add another component. The field experience of the relations between coal rank and lithification grade of host rocks, such as lignite occurring in plastic clay and loose sand, black coal in hard shale and sandstone, and graphite in phyllite and quartzite, is resolved in numerous intricate details of diagenesis. Only one aspect is the chemical change and increasing crystallinity of clay minerals, from amorphous "clay" colloids and kaolin in the peat mire, to illite, chlorite and sericite near the transition to metamorphism (Bucher & Frey 2002).

Yet, the determination of coal rank and kerogen maturity provide a tool for highly accurate and high-resolution investigations of the thermal evolution of a basin and of the diagenetic grade of its components. Very low grade metamorphism begins approximately with the formation of meta-anthracite at $R_{max} > 4\%$, and the greenschist facies at $R_{max} > 5\%$ with semi-graphite and graphite.

Reflectance studies of disseminated coal particles and of kerogen in sediments are an important tool of petroleum and natural gas exploration. Already White (1935) had recognized that oil formation occurs mainly within a specific stage of diagenesis (the "oil window") that relates to coal rank. The oil window is confined between approximately 44 and 24% of volatile matter in coal, and 0.6 to 1.4% reflectance of vitrinite (Figure 6.4). Coal of higher rank is related to natural gas deposits (cf. Chapter 7.2 "The Origin of Petroleum and Natural Gas").

6.4 POST-DEPOSITIONAL CHANGES OF COAL SEAMS

After burial underneath siliciclastic sediments, peat is submitted to endogenetic alterations, foremost those of coalification. Meteoric and diagenetic fluids affect coal by epigenetic deposition of minerals in pores, joints (called cleats) and faults, raising ash content. Tectonic deformation of seams leaves structures that influence product quality and mining conditions. Exhumation and erosion expose coal to exogenetic alterations that reduce coal quality.

6.4.1 Tectonic deformation

Under tectonic strain, coal exhibits a more ductile response than its common siliciclastic host rocks. However, even peat and low-rank lignite may develop extensional fissures, which are intruded by liquefied mud and sand forming clastic dykes, probably caused by earthquakes. At higher rank, the ductility of coal promotes thinning and thickening of seams similar to marble bands in metamorphic rocks, and the injection of coal dykes into host rocks (Thomas 2002).

Brittle deformation of black coal at low temperature results in brecciation and mylonitization, yielding a fractured and powdery material. Shearing at elevated temperature causes structural adjustment, such as changes of the orientation of optical axes and locally increased coalification (Taylor *et al.* 1998).

Dense jointing (joints in coal are called *cleats*) is characteristic for black coal. Most lignites display no joints at all, just like their host rocks. In artifical outcrops (e.g. open pit walls), some intensely gelified lignites develop polygonal fractures soon after exposure, which are not tectonic but an effect of dehydration and shrinkage. Cleat systems of black coal form in response to tectonic stress. This is easily verified by the spatial and genetic relations to joints in host shales and sandstones. Spacing of joints depends on bed thickness and mechanical properties of rocks. The same is observed in coal, with a higher cleat density (lower spacing) in bright coal (vitrain) compared to dull coal (durain). Joints in siliceous wall rocks occur at even larger intervals. The orientation of cleats is skilfully exploited by miners for easier, that is less energy-consuming, extraction of the coal. Cleats (and many bedding planes in seams) are planes of mechanical separation. This is the reason why aperture and density of cleats (e.g. number per m) and the degree of penetration, or in other terms, their frequency, persistence and connectivity control properties such as gas flow, porosity, coal rock strength and grain size distribution of run-of-mine coal (Laubach *et al.* 1998). The careful documentation of cleat data is an important aspect of coal geological practice.

6.4.2 Epigenetic mineralization of coal seams

Coal cleats and other fractures may be coated by minerals such as carbonate, barite, clay, markasite, pyrite, galena, sphalerite (in the Illinois District), uraninite (in the western US) and quartz. This raises the ash content of coal. Rarely, exploitable veins were encountered. In the Ruhr District, Germany, veins with zinc and lead sulphides were commercially exploited until 1962. The base metal veins were hosted by faults cutting anticlines at right-angles, clearly indicating a late syntectonic (probably diagenetic) origin. Generally, hydrothermal ore deposits in coal are hardly ever of economic interest, although many mineralized coals are reported (Laznicka 1985). To the scientist, hydrothermal minerals in coal reveal properties of fluids, which migrated through the rock body, their relative and absolute timing, and the conditions of mineral precipitation (Daniels *et al.* 1994).

In contrast to black coal, peat and lignites are porous and reactive rocks that act as physicochemical traps for trace elements, which are transported with surface or groundwater. Potentially economic concentrations of vanadium, uranium and germanium were mentioned earlier. Laznicka (1985) reports coals anomalous in copper, gallium, molybdenum and nickel.

6.4.3 Exogenetic alteration of coal

Near-surface oxidation may induce self-ignition of seams and is the most common agent of reducing coal quality.

At the surface, sub-bituminous and bituminous coals alter to black, soot-like soft soil. Apart from solid residues of oxidation, reaction products include CO_2 and soluble organic matter (DOC – dissolved organic carbon: Chang & Berner 1999), which enters the groundwater. Lignites, however, rot and turn into humic soil constituents. The original thickness of the seam cannot be deduced from observations in the surface zone. In most settings, destructive weathering (supergene alteration zone I) only affects coal to a depth about equal to the saprolite zone of the regolith profile.

Below the first, a second zone of alteration leaves coal macroscopically intact. The seam displays its full thickness, and the coal is physically fresh. Only disseminated, or fracture-coating gypsum and other sulphates may be visible indicators of oxidation, but these often extend beyond degradation. The severe reduction of coal quality in this zone is only recognized by determination of calorific value and cokeability. Easily soluble sulphates are a nuisance for extraction and processing, and seepage water activates swelling clays in the seam, which cause additional problems. The vertical thickness of supergene alteration zone II is commonly several tens of metres.

Micropetrographical methods are not suited to map the extension of zone II, because vitrinite reflectance remains unchanged. Possible keys such as microfractures with higher reflecting rims occur only above an oxidation temperature of 150 °C (Taylor *et al.* 1998).

Meteoric seepage may reach hundreds of metres below the surface, as jointed seams behave as aquifers. This can be beneficial because infiltration initiates secondary microbial methanogenesis, enhancing gas production from Coal Bed Methane operations (c.f. Chapter 7.5 "Exploitation of Petroleum and Natural Gas Deposits").

Natural coal seam fires

Natural coal seam fires cause destruction of large panels of near-surface coal seams. In fact, the "fires" are rather smouldering sections with an activity that changes from hardly visible to quite dramatic. Ash and cinder are remains of burnt coal. Footwall rocks may be baked, but hanging wall shales are usually fired and sintered (cf. Chapter 3 "Clay and Clay Rocks"), and display attractive colours ranging from purple-violet through brick-red, orange, yellow to white. Very dense varieties are called *porcellanite* or *porcelain jasper*. Others resemble volcanic scoria. The fired clay rocks resist weathering and erosion so that long chains of hills mark the former presence of coal seams (Alberta, Colorado, North Dakota). Reduction of iron (by reaction with heated coal or with CO) causes widespread formation of magnetite (and some native iron), which facilitates aeromagnetic mapping of former seams, even under young cover.

Oxidation and self-ignition of coal is an exothermal process. The oxidation of pyrite produces 1546 kJ/mol and of coking coal 5176 kJ/mol (assuming a composition of $\sim C_{10}H_7O$), which results in heating. Coals rich in vitrinite and fusinite are especially vulnerable. Mylonitization multiplies the hazard, because a high internal surface favours reaction with oxygen. The thermal conductivity of coal is the smallest among all rocks (<0.50 [W/(m.K)] compared to 1.98 (shale) and 3.12 (sandstone) supporting heat accumulation. Usually, temperatures rise to 30–80 °C, but then drop off slowly, which may be due to: i) complete oxidation of all accessible surfaces; or ii) consumption of all available oxygen. Oxidizing coals with a high internal surface in contact with ample oxygen display continuing heating until self-ignition occurs at ~120–250 °C.

6.5 APPLICATIONS OF COAL GEOLOGY

> *An engineer, who has built a bridge, can strike you nearly dead with professional facts; the captain of a Ganges river steamer can, in one hour, tell legends sufficient to fill half a book, but a couple of days spent on, above and in a coal mine yields more mixed information than two engineers and three captains*
>
> Rudyard Kipling 1888

Practicians in the earth sciences serve the coal industry in the full cycle from exploration to extraction, environmental mitigation and mine closure, similar to other sectors of mining. However, some aspects of working in coal are specific, which is the motivation for this section.

6.5.1 Exploration

Exploration for buried coal seams is based on geological hypotheses that rely mainly on palaeogeography and facies distribution in space and time. Geophysical detection of coal at depth is only indirectly possible, for example by delineating bedding and structures utilizing methods such as seismic, gravity and magnetic surveys. At moderate depth, the low conductivity of coal may permit mapping by electrical methods. Oxidation of coal in the near-surface raises ground temperatures, allowing helicopter-mounted thermal (radiometric) mapping of coal seam outcrops. Soil gas analyses are a rarely used geochemical component of prospect exploration. Combined with geological outcrop mapping, facies models and geophysical data justify the design of a reconnaissance drilling grid. From the early planning stages through detailed exploration to coal extraction, geological, engineering and environmental perspectives must be equally considered (Bartlett *et al.* 2009).

Geological and geophysical indications allow no more than estimates of prognostic resources. Definition of identified resources requires quantitative data such as depth, thickness, structures and quality of coal. Defining measured resources implies drilling (Figure 6.24), supplemented by physical exposure and sampling of coal in deep trenches or underground exploration drifts. The distance between drilling sites may be based on geostatistics of nearby mining fields. If such data are unavailable, a relatively wide grid is initially chosen, which is filled in as the need arises. In the Latrobe Valley brown coal, initial drillholes were spaced at 1 to 2 km distance; mining reserves are defined by a 400 m drilling grid (Waghorne 2001). Continuous geostatistical control assures that an optimal solution is found as soon as possible (Figure 5.16; Saikia & Sarkar 2006).

In black coal regions with simple large-scale structure, such as the western margin of the Late Palaeozoic Bowen Basin, Queensland, Australia, drillhole spacings of 1 to 2 km are sufficient for the first phase of exploring underground mining resources. Reserve drilling at the Burton Downs Mine was initially laid out in the form of profiles

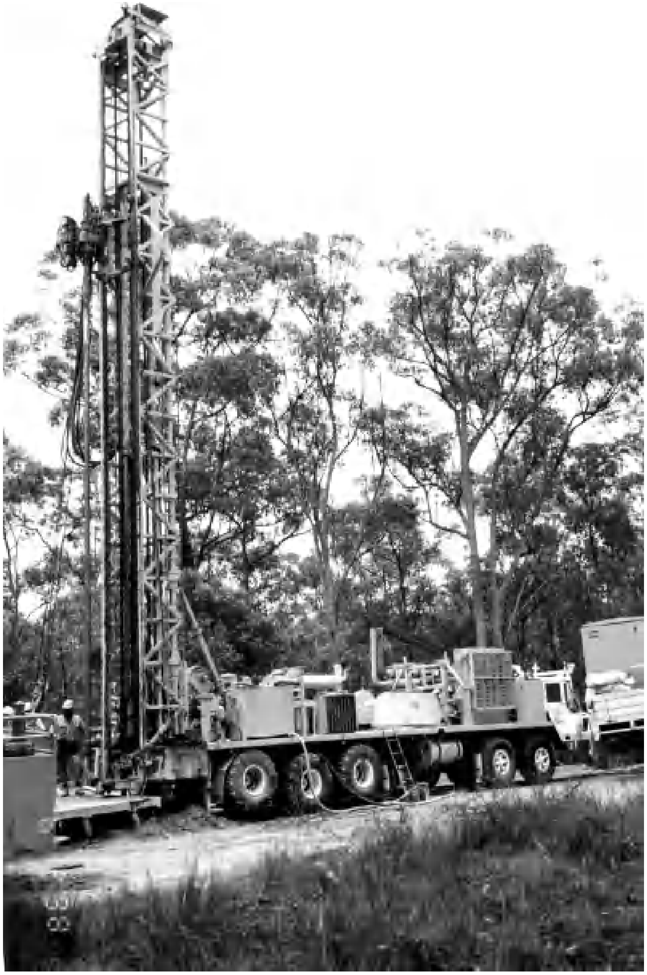

Figure 6.24 Truck-mounted drill rig, here employed in coal exploration in the Sydney basin, New South Wales, Australia. Courtesy of Keith Bartlett, Minarco-Mineconsult, Tuggerah, NSW.

across the strike of the seam at a 100 m distance, with intervals along the profiles of 50 m. Geostatistical variography soon demonstrated that the lateral homogeneity of the deposit allows a separation between profiles of 400 m. Considerable reduction of costs was the consequence. Note, however, that actual extraction of the coal at Burton (and elsewhere) is increasingly assisted by detailed three-dimensional seismic imaging of faults, unstable roof conditions and gas accumulations in advance of longwalls (Walton *et al.* 2000).

Core drilling (commonly using slimline 63.5 mm diameter) is advisable in all reconnaissance work, because the wealth of data that can be extracted from the core, such as lithology, stratigraphy, facies, spatial orientation, tectonic deformation, hydrogeological and geotechnical properties, justifies the higher costs (Figure 6.25). Subsequent infill drilling may employ down-the-hole hammers (DTH) or other percussion technologies through overburden, but should change to coring near the seam. A near 100% recovery of core in coal must be aspired. Because friable parts of the seam are easily lost during coring, triple-tube core barrels may be needed. Aluminium or plastic liners protect the samples from damages during removal from the barrel and later handling. After logging, e.g. brightness and inorganic partings, the containers are sealed in order to guard the coal from oxidation and desiccation, but allow X-ray radiography of the core samples with no additional manipulation. X-ray radiography is preferable to photographs, because it provides clear images of the distribution of minerals (ash) in the coal.

Geophysical borehole logging is commonly applied in order to provide *in-situ* control of seam boundaries and depth information reported by the drilling team, and data such as water and ash content. Frequently, radiometric, density and electrical methods are employed (Figure 5.8). Infill percussion (DTH) holes are routinely surveyed by geophysical borehole logs (Fullagar 2000). Recently, acoustic scanning technology emerged as an important wireline tool for investigating the orientation of joints, fractures and borehole breakout, which is a proxy revealing the horizontal stress direction (Bartlett & Edwards 2009). In mechanized underground mining and coal seam gas projects, for example, this is vital information.

Samples of coal, especially of lignite and brown coal are prone to desiccation and must be protected. Cool storage of low rank coals prevents the growth of fungi and bacterial attack. However, the only guarantee of long-term preservation of initial properties is coal sample storage under argon immersion. For petrographical and technological sampling, cores are split or sawed in half

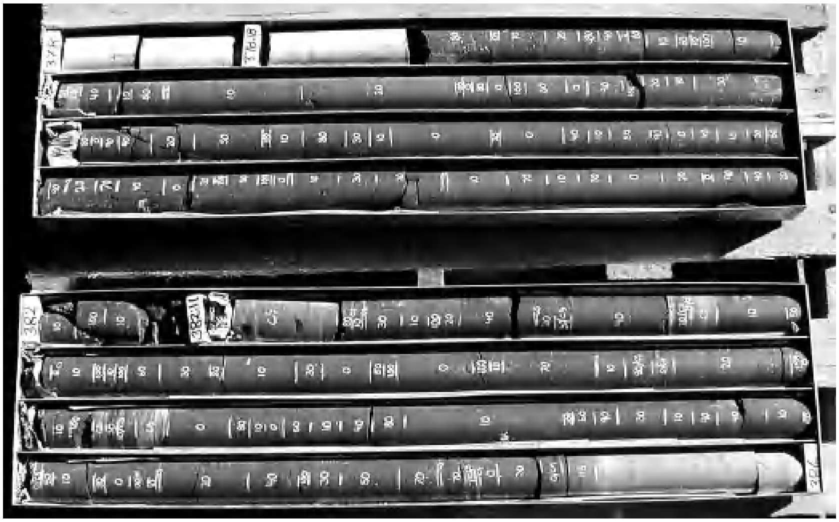

Figure 6.25 Slimline (HQ) drill core section of Permian Wallarah-Great Northern coal seam in the Sydney basin, New South Wales, Australia. Courtesy of Keith Bartlett, Minarco-Mineconsult, Tuggerah, NSW. Light shales in the footwall (foreground right) grade into bedded coal which is overlain by matrix-supported roof conglomerate (back, left). Figures marked in white on core denote brightness.

parallel to the core axis. One half is archived for eventual later requirements. Samples of the seam's immediate wall rocks are often needed for geomechanical investigations and must be as carefully preserved as the coal. In all cases, the needs of the hydrogeologist and the geotechnical engineer for data must be accounted for (cf. 5.2 "Trenching and Drilling").

Worldwide, **exploration for coal bed methane** (CBM), also called coal seam gas (CSG), is a rapidly growing field in the quest for energy. In principle, data on geology and volume of seams, and the properties of coal are required for an estimate of potential gas *in situ*. Rank, macerals, lithotype and moisture content are main controls on the methane adsorption capacity of coal and must be determined. In bituminous coals of the Pennsylvanian Weibei Coalfield, Ordos Basin, China, for example, the adsorption capacity (on a dry and ash-free basis) varies from 14 to 30 m^3/t but gas *in situ* is $<15\ m^3/t$ (Yanbin Yao *et al.* 2009). The permeability of these coals is between 0.1 and 10 mD and the porosity ranges from 2 to 7%. The authors combine regional data on seam thickness, gas content, coal rank, methane concentration, permeability, porosity, burial depth and deformation pattern to define targets for detailed investigations.

6.5.2 Reserve estimation

Geological coal resources and exploitable reserves are estimated and classified with the same methods that are stipulated for other solid minerals (e.g. JORC-Code: AusIMM 2004, cf. Chapter 5.3.2 "Ore Reserve Estimation and Determination of Grade"). Geological certainty and economic viability are the most important parameters.

The economic viability of a coal deposit is a function of: i) the geological situation; ii) coal quality; and iii) technical and economic conditions (the "modifying factors"). Geological situation and coal quality are objective determinants and independent of time. They include the geometry of the deposit, as well as geomechanical, hydrogeological, geochemical and geothermal parameters. The modifying factors are time-dependent and prone to change, for example by new technologies in mining, processing and utilization, and by new factors in economy, markets, law, environmental regulations, society and politics (Kininmonth & Baafi 2009, Waghorne 2001). Reserve estimates only conform to international standards if the modifying factors are accounted for. This is the main reason why coal reserves decrease consistently (Figure 6.1), whereas those of other minerals hardly change, as ever more coal producers adopt international bankable reporting standards.

Coal reserve estimation incorporates several distinct features. Unlike black coal, low rank coal (lignite and brown coal), for example, is hardly ever traded. Low energy (6–16 MJ/kg) and high water content (>30%) of run-of-mine coal preclude transport to any distance from the mine. Mines are usually linked to adjacent captive power stations, which are specifically designed for each deposit (Figure 5.18). In addition, low rank coal is hardly ever upgraded by processing. The consequence is that the feasibility of mining combined with electricity production must be demonstrated for a reserve. Utmost diligence must be used to determine the *in-situ* density, moisture and ash content, because this defines coal delivered to the power plant. Even then, small deviations are still to be expected: In the Latrobe Valley (Figure 6.12), run-of-mine coal is typically 1% higher in ash and 1% lower in moisture than indicated by drilling (Waghorne 2001). Certain variations of the coal quality, due to lateral or vertical facies change of the seam, may be unacceptable for the power station. If this cannot be mitigated by blending from different faces, such coal is not included in reserves. The overall economy of a lignite mine cannot be established by reference to a market. The only available economic measure is the price of electricity and its competitiveness. Resources and reserves need to be extensive, because amortization of power plants is measured in decades.

Higher-rank bituminous coal resource estimates are based on determination of the volume and *in-situ* bulk density at *in-situ* moisture of the coal (Lipton 2001). Large-diameter (100–200 mm) drilling provides advance samples for determination of additional important properties, such as washability and coal fragmentation (Figure 6.26). As soon as possible, semi-industrial scale bulk

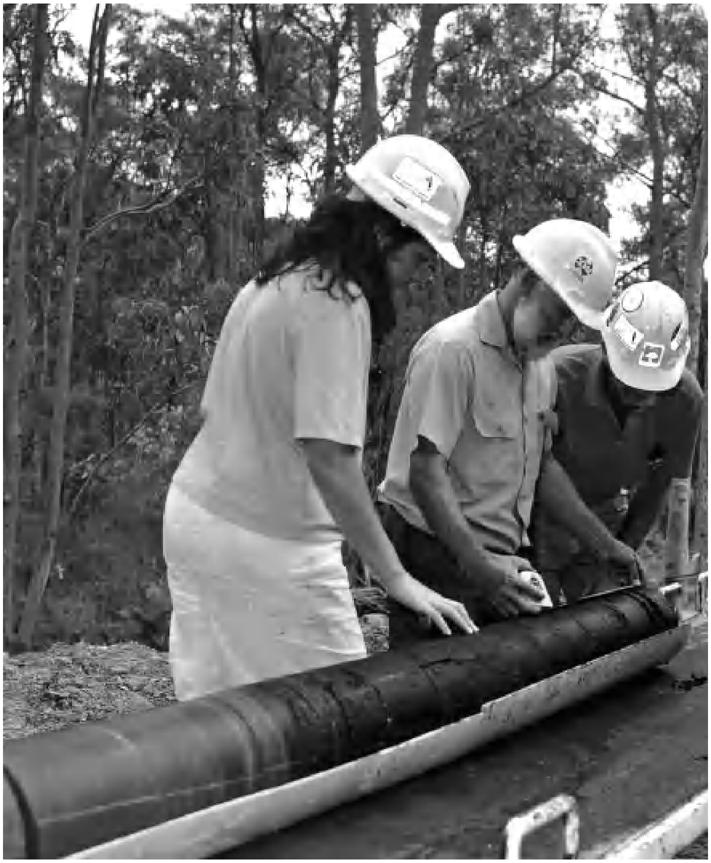

Figure 6.26 Large diameter core (200 mm diameter) is drilled for quantifying technological parameters of coal such as fragmentation and washability. Courtesy of Keith Bartlett, Minarco-Mineconsult, Tuggerah, NSW.

samples are acquired by trial box cuts and underground work. Oxidized parts must be outlined and clearly separated from unaltered coal. High-rank coal seams occur typically at an inclination to the horizontal. Therefore, the volume is best calculated from true thickness and true area of the seam. High ash plies or partings can be included or excluded, but consistency is vital. Dilution during mining (e.g. from hanging wall, footwall, partings, longwall edges) increases the tonnage, but mining losses decrease it. Black coal is typically crushed and washed, or submitted to density separation in order to lower ash content. Certain grain fractions of traded coal command higher prices. An optimum grain size distribution of the saleable product demands care from extraction and through processing. These are only some of the points that have to be considered when estimating *in-situ* tonnages and marketable products.

Present mining technologies pose a lower limit to the extractable thickness of black coal seams. Cut-off thickness may be ~50 cm in an opencast mine, and 100 cm for underground mining. Also, costs preclude coal mining at great depth. Northern Germany's indicated coal resources at <1500 m depth comprise ~25,000 Mt; extraction to this depth is technically feasible, although not economically competitive. Very deep coal (>1500 m) in Northern Germany is estimated to total ~350,000 Mt. Similar relations are known from many regions of the world.

Motivated by this situation, the potentially elegant method of ***in-situ*** **coal gasification** was examined by numerous research projects in the past, although with moderate success. The principle is to drill holes into a coal seam, pump in air and steam, ignite the coal so that gasification starts and extract the gas produced ("syngas"). Today, directional drilling is envisaged in order to divide a seam into panels (600 × 30 m) that allow better control of the process. The recovery of the energy inherent in coal is estimated as between 50 and 80%. Trial runs in the Surat Basin, Australia (2008), support hopes that this technology may finally reach profitability. Giant tonnages of deep, currently unmineable coal might be converted into profitable resources.

6.5.3 Coal mining geology

All available geological information is collected in a database, which is the foundation for a three-dimensional geological deposit model. Basic datasets include spatial information, coal rank, *in-situ* heat, moisture, ash and methane content, bulk density and the spatial orientation of cleats. Maps displaying contour lines of seam floors and isolines of seam thickness, and sections illustrating spatial geometry of stratigraphy, bedding planes and structures, assist in communicating the model. Hydrogeological and geomechanical information is integrated. Much of this work can be done in Geographic Information System (GIS) space, but dedicated specialized programmes allow integrated mine planning and scheduling. Note that the geological model must be validated by a competent person (cf. Chapter 5.3 "Ore Reserve Estimation and Determination of Grade").

In multi-seam deposits, the correlation of individual seams is crucial for the accuracy of the geological model. Only a correct correlation truly supports reserve estimates and mine planning. Modern underground mining technology and future automated mining methods require reasonably constant conditions. Severe production loss is hardly avoidable if longwall faces run unprepared into faults, erosion channels or magmatic dykes. Supporting geology, high-resolution seismic and tomographic methods are routinely employed to investigate and image the seam in front of the advancing face.

Methane and CO_2 content in coal and host rocks of a deposit are spatially varied. The gas distribution must be documented in order to assist mine planning. Gas is, of course, a security risk (Hargraves 1997), but also a major cost factor, because the necessary precautions such as higher air flow and gas drainage drillholes make extraction more expensive. Methane in mine return air should always be used, by burning in a power station or in a fuel cell unit. Apart from methane gas explosions, instantaneous coal outbursts are a deadly danger in many deep black coal mines. *Coal outbursts* are violent and spontaneous ejections of powdered coal and gas from the working coal face (Guan *et al*. 2009). They may be followed by methane explosions. The mechanism of coal outbursts is similar to other gas-driven solid eruptions (e.g. of magma, salt and other rocks) insofar as high internal gas pressure is released into expansion and fragmentation when external confining pressure is suddenly removed (Guan *et al*. 2009).

In most lignite and coal mining districts, **hydrogeological modelling** is an absolutely essential component of investigations, from prefeasibility studies to mine closure. Commonly, host rocks of coal include aquifers that enforce dewatering in order to avoid water inrushes and unstable ground conditions. Appropriate dewatering studies are highly critical (Brown 2010). Drawdown cones may be very wide and affect whole basins, with the consequence that regional water management is required (Kumar *et al*. 2010).

Geotechnical investigations of coal and host rocks (Hoek & Brown 2003, Terzaghi *et al*. 1996) are needed to design mine openings sufficiently safe but at lowest cost. In opencasts, this is mainly a question of pit slope angles. In underground mining, sections of rock mass quality below average must be identified in order to minimize the hazard for personnel, as well as costs. Often, seepage water raises fluid pressure (u) and reduces shear resistance (Figure 1.39; Brady & Brown 2004). Underground longwall operations should be oriented in a way as to minimize the hazard of spalling caused by joints, fractures and horizontal stress (Bartlett & Edwards 2009).

Underground extraction of coal causes subsidence that may induce lowering of the surface, open fractures and damage to buildings and infrastructure. Earth falls or slope instability can be triggered. Often, the pre-mining surface water regime is fundamentally changed. Abstraction of coal causes various reactions to the newly opened void (Figure 6.26). In the immediate hanging wall of the extracted coal, the rocks fracture and a loosened destressed zone develops to a certain height above the seam. Broken roof strata loosely fill the goaf (Zone 1). At a higher level, subsidence is enacted rather by bending than fracturing, and the rock mass is little disturbed (Zone 2). On the surface, extensional fracturing and faulting may occur. As the extraction front passes underneath buildings or infrastructure, induced strain is initially tensile followed by compressive deformation (Zone 3). For a stringent geomechanical analysis, refer to Brady & Brown (2004).

The total subsidence of the surface may reach 80% of the coal thickness extracted, mainly as a function of nature and thickness of the overburden. Duration of subsidence and surface extent of mining influence are controlled by several factors. which include the geomechanical properties of the overburden rock mass. The limits can be defined by an experimental angle α drawn from the edge of the underground void (Figure 6.27). Thick competent sandstones in the hanging wall above the seam may inhibit loosening and caving in zone (1). A possible consequence is the accumulation of stresses over a wider area, which are suddenly released when the strength of the rock mass is exceeded. The resulting shockwaves may cause damage in the surroundings (e.g. an earthquake of magnitude 4 in the Saar Province, Germany, in 2007). In mining practice, preventive counter measures such as filling the goaf with tailings are taken in order to minimize subsidence, hazard and damages.

6.5.4 Environmental aspects of coal mining

Black coal, green future…

Materials World 2003

Already during reconnaissance exploration, the influence of future mining on landscape, water and humans should be considered in order to avoid investing in sensitive areas. When entering the phase of detailed exploration, a preliminary environmental impact study should be done in order to design and install all required monitoring systems, such as groundwater wells and surface water discharge weirs. Studies of rare species are advisable. For the definition of reserves, large datasets must be acquired, including coal chemistry.

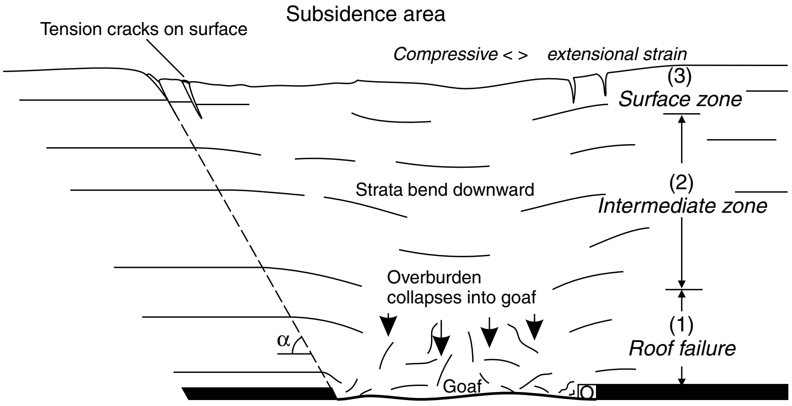

Figure 6.27 Underground longwall extraction of a coal seam panel causes surface subsidence (adapted from Ward 1984). Three affected depth zones are distinguished: (1) Loosened and destressed rock mass falls into the goaf, (2) zone of intermediate ductile deformation and (3) zone of surficial fracturing and damage by the "strain wave" passing from tension to compression. Angle α describes the width of mining influence. The square with the inscribed O is the longwall opening.

Standard coal quality is described by proximate analyses (ash, moisture, volatile matter and fixed carbon by difference), ultimate analyses (C, H, N, S, ash and O by difference), calorific values and sulphur forms. This allows estimating the potential atmospheric emissions of sulphur, carbon and nitrogen, and the potential contribution of these elements to environmental problems and global climate change. For environmental impact studies, properties including major, minor and trace element concentrations, modes of occurrence of environmentally sensitive elements, cleanability, mineralogy, organic chemistry, petrography and leachability, should be determined (Finkelman & Gross 1999). Trace element analyses of coal are the base for mitigation measures in the power station where the coal is combusted (Finkelman *et al.* 2002). Critical elements specified as hazardous air pollutants (HAPs) by the US Clean Air Act (1990) are As, Be, Cd, Cl, Cr, Co, F, Hg, Mn, Ni, Pb, Sb, Se and U. One example is mercury emissions from coal-fired power plants in the United States, which in 2004 amounted to 48 tonnes. Novel scrubber technologies similar to those used for SO_2 control are installed to alleviate this problem.

Operating coal mines

Lowering water tables by pumping, both in underground mines and in open pits (Figure 6.28), enforces discharge of large amounts of water into nearby streams. This may induce unwanted degradation of water quality (e.g. pH, total dissolved solids, iron, manganese, sulphate and trace metals such as Se). Treatment of the lifted groundwater is commonly required. Undisturbed coal seams normally act as weakly permeable aquitards; the permeability of host rocks depends on their nature, degree of consolidation and the characteristics of joint systems. Coal mine water is typically characterized by low pH and high content of Fe(II) or Fe(III), suspended particles, SO_4^{2-} (from pyrite oxidation), Cl^- (from formation or geothermal waters) and in the absence of sulphate, elevated content of Ba, Sr and Ra. When such water is mixed with common surface water, "radiobarite" is

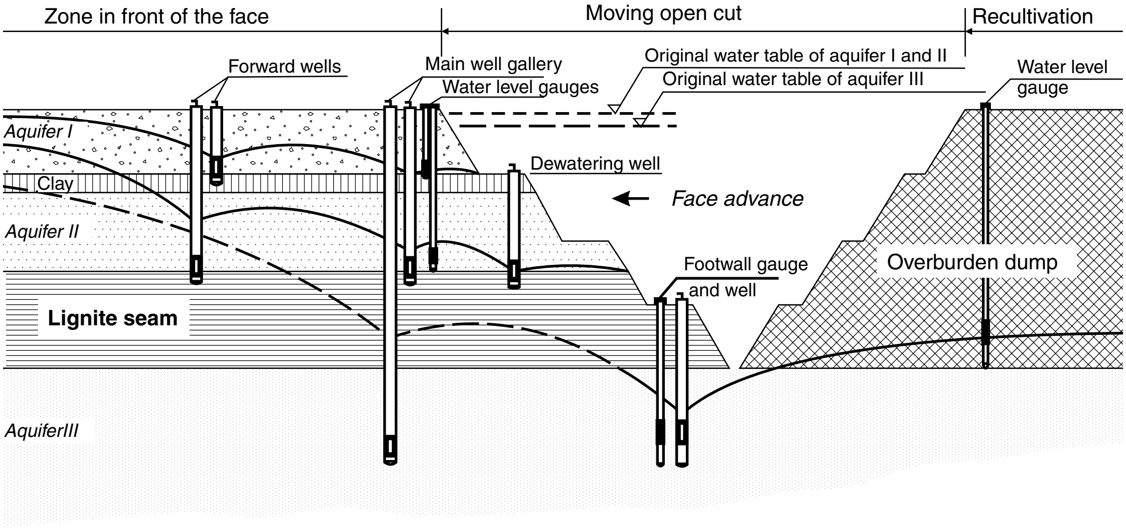
Zone in front of the face
Moving open cut
Recultivation
Forward wells
Main well gallery
Water level gauges
Original water table of aquifer I and II
Original water table of aquifer III
Water level gauge
Aquifer I
Clay
Dewatering well
Face advance
Aquifer II
Footwall gauge and well
Overburden dump
Lignite seam
AquiferIII

Figure 6.28 Schematic illustration of water management in a lignite open pit (not to scale). Aquifers I to III consist of poorly consolidated sand and gravels. In front of the advancing open cut, water tables are lowered by well screens, in order to minimize inflow into the pit and to stabilize pit slopes. Below the bottom of the pit, water pressure is reduced to avoid inrush of water or of liquefied sand. Water level gauges are for control, and alert in the case of rapid rise.

precipitated, which may be an environmental problem (Schmid & Wiegand 2003). In Silesia, Poland, radium concentrations reach a maximum of 390 kBq/m^3, but Ra is precipitated underground by reaction with phosphogypsum before the water is evacuated. The acid formation potential of waste rock and overburden destined for surface disposal must be investigated (Verburg *et al.* 2009). Any hazardous material is covered with standing water or with clay in order to prevent contact with oxygen.

As a greenhouse gas in the atmosphere, methane is 21 to 70 times more potent than CO_2 (depending on how the comparison is made). Conventionally, methane mixed with return ventilation air (VAM) was released into the atmosphere. In the recent past, VAM represented ~10% of all anthropogenic emissions of methane and 60 to 70% of all greenhouse gas emissions from underground mines. After agriculture, black coal mining was the largest human source of CH_4, followed by household refuse dumps. Today, the small concentrations of methane in ventilation air (0.2–1.2%) are combusted in mine-site power stations, for example in Australia, together with coal shale or with impure coal. Gasification of VAM with coal processing waste offers the greatest efficiency of energy production and the lowest environmental footprint (Clarke 2010). Mine methane that cannot be used must be burnt, because conversion to CO_2 lowers the greenhouse effect.

Nearly all coal mines move large masses (Figure 6.29) that must be transported, temporarily stored or ultimately disposed of, including coal, overburden, waste rock and processing sludges. This offers numerous possibilities to raise environmental compatibility, not least by well-planned recultivation (Richards *et al.* 1993). Landscaping and recultivation must be carried out as far as possible during mining when large earth-moving machinery is available. Of course, renaturation of artificial ponds, streams and barren land should also be considered, because spontaneous invasion of species often provides much higher ecological value.

The burning of coal produces a considerable mass of combustion residues, including fly-ash, boiler bottom ash and slag, and flue-gas desulphurization sludge including gypsum. Disposal of these materials requires well-planned strategies. Their possible environmental impact has to be carefully considered, not least because they concentrate potentially hazardous trace elements of the coal (Huggins & Goodarzi 2009). As far as feasible, the residues should be utilized, for example as cement raw materials and construction aggregates in the building industry (in America currently ~37% of the total coal mining waste). This preserves limited resources of sand and gravel, and saves energy. Combustion residues that cannot be marketed are buried in exhausted opencast mines and surface impoundments (58%), and only 5% are backfilled in underground coal mines. The latter procedure improves the stability of mine openings (Michalski & Gray 2001), reduces surface subsidence (Brady & Brown 2003) and is an important option in mine reclamation. Because coal ash is highly alkaline, it is

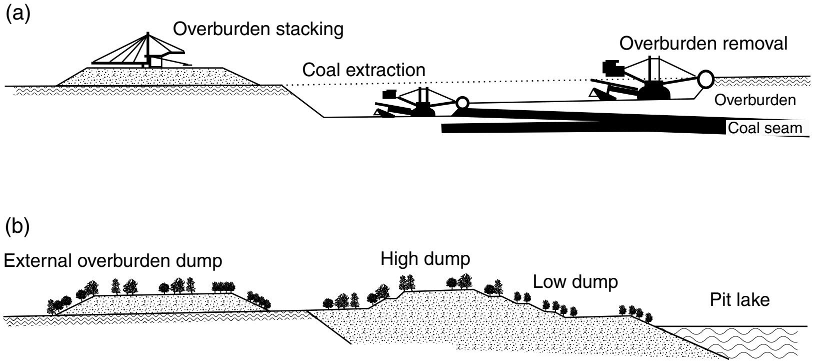

Figure 6.29 Lignite open pit in operation (upper section) and after landscaping, recultivation and rebound of groundwater levels (lower section).

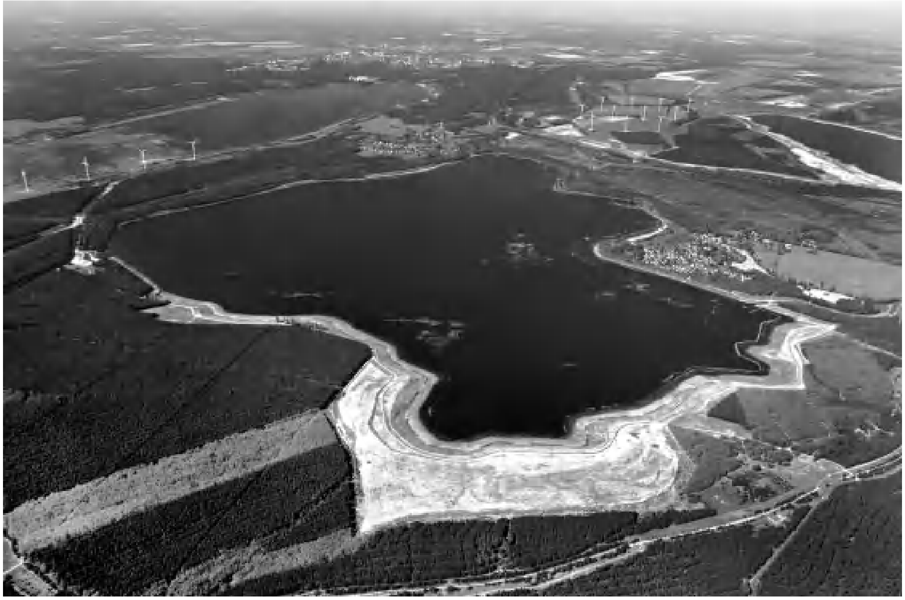

Figure 6.30 (Plate 6.30) Post-mining lignite open pit lakes in the Lausitz region, Germany, in the last stages of filling and rehabilitation. Courtesy of P. Radke, © LMBV, Lausitzer und Mitteldeutsche Bergbau-Verwaltungsgesellschaft mbH.

suitable for treatment or prevention of acid mine water generation (Canty & Everett 2006).

Closure of coal mines and remediation

Considerable investments are needed in order to avoid post-mining environmental damage. Main hazards include chemically (pyrite, markasite) or mechanically unstable overburden tips and processing sludge dams, coal fires in dumps or residual coal *in situ*, rising groundwater levels, outflow of methane and carbon dioxide, and of acid mine water with a high iron concentration (Younger 2002, Bell 1998). Best practices and technologies related to sulphide mineral oxidation, acid mine drainage and metal leaching are described in the online *GARD Guide* (Verburg *et al*. 2009). The severe reduction of coal mining in Europe within the last decades left many exemplarily remediated sites, but unfortunately, also a large number of brown fields, which still await action.

Underground openings of historic shallow mining can be prone to sudden collapse. Where maps are insufficient, ground geophysics or airborne remote sensing methods are used for localization. LIDAR (Light Detection And Ranging) is employed to create high-resolution digital elevation models (DEM), which illuminate slight depressions that develop above voids.

Rising groundwater levels after cessation of pumping might be considered a blessing, but in some coal mining districts surface subsidence accumulated to an extent that large areas were flooded, if nature would be allowed to take over. Although the resulting wetlands might be an ecologist's dream, densely populated countries cannot afford the loss of land and settlements. Water management by pumping may be the only long-term solution. Another potentially damaging effect of rising groundwater is uplift of land, which is mainly due to buoyancy forces (Terzaghi *et al*. 1996, Brady & Brown 2004).

Spoil heaps that have been built in the past from tailings of less efficient coal washing plants can today be a source of revenue by "tip washing" (i.e. recovery of remaining coal). Because this type of land cannot be developed before the coal is cleaned out (considering the threat of self-ignition) and the surface is levelled, tip washing by modern plants is an important step towards restoration.

Coal mine fires

Outcropping coal seams burned naturally in the geological past (e.g. in the Pliocene of the Powder River basin, USA: Heffern & Coates 2004). Today, thousands of coal mine fires are burning on abandoned mine lands throughout the world (Stracher 2004, 2007). They threaten the health and safety of local populations, destroy property values and consume a non-renewable resource. In abandoned mines, fires started by self-ignition or by human action may be unnoticed for many years, until fumes and collapse holes become a threat to nearby residents. In the Permian coal fields of Bihar in India, $\sim$2000 km^2 of land and one million people are endangered by underground fires (Michalski & Gray 2001). Some of the fires have been burning since 1916. Remediation would be possible, but the costs are prohibitive. Burning coal can only be extinguished by airtight sealing, whether in a mine, on coal dumps or in natural outcrops. Mitigation technologies include total excavation, trenching, flooding and quenching, bulk filling of mine workings, saturation grouting, surface seals, inert gas injection and chemical foams. Fubao Zhou *et al*. (2006) report successful extinction of a mine fire by borehole injection of a foam made of water, clay and nitrogen. Quenching with water alone is not possible.

Opencast lakes (Figure 6.29, Figure/Plate 6.30)

Closure involves cleaning up and shaping the interior of the pit, foremost the slopes. The stability safety margin acceptable for a mining operation is commonly not sufficient for post-mining use. In fact, the changing hydraulic regime may bring about large landslides. Many pits fill by natural groundwater inflow, which in others is supplemented with water from nearby streams. The latter is chosen in order to avoid a long period of slope weathering and acid formation, and to top up water quickly with inflow of an acceptable quality. Additional technical measures may be necessary, for example neutralization of low-pH lake water by coal ash (Loop *et al*. 2003). Well-planned pit lakes are often an enrichment of the landscape and provide refuges for nature as well as benefits to the people. Very instructive examples can be studied in all German lignite mining districts.

Post-closure uses

Recultivated land is assigned to forestry and agriculture. Brown fields may be valuable sites for other industries. Closed deep coal mines can be utilized for the storage of natural gas. Moderately toxic waste, such as fly and bottom ash from coal-fired power stations, is very suitable as a stabilizing fill of underground mine openings (Wendland & Himmelsbach 2002). CO_2 sequestration in deep coal mines is considered. Deep water-filled workings of former coal mines may provide abundant cheap geothermal energy (see below).

Gas seepage

(CH_4, CO_2) from closed coal mines is not rare, especially during the period of flooding after closure. The main hazard is accumulation of gas in buildings. Falling barometric air pressure causes expansion of gas in the mine, which can result in overflow. Mitigation methods include filling of near-surface mine openings and sealing by injections, if needed. Methane should never be released into the atmosphere but must be used. A pilot plant in Ohio, USA, demonstrates burning methane from a closed mine in a fuel cell for electricity production. Note that methane seepage (containing traces of ethane and propane) from the ground is a widespread natural process; with 42–64 Tg/year, geological sources such as petroleum and coal basins are second only after wetlands (Etiope & Ciccioli 2009).

Geothermal use of mine water

This is an economically alluring option for heating and cooling buildings based on heat pump systems (Watzlaf & Ackman 2006). Flooded coal mines are particularly suitable because of their broad-based accessibility. Coal seams are commonly mined over large areas, so that the warm water filling mine tunnels, collapsed longwall voids and loosened rock can be pumped from wide-spaced boreholes. The large contact surface between water and rocks increases the sustainability of heat exchange. Various designs of heat extraction are possible, for example closed loop systems (cycling a refrigerant fluid contained in thin-walled pipes through a water-filled shaft) and open-loop systems (pumping water from the mine and re-injecting it through a second well). Flooded parts of the Pittsburgh coal seam in the northern Appalachian coal basin of the United States might potentially heat and cool hundreds of thousands of homes (Watzlaf & Ackman 2006).

6.6 SUMMARY AND FURTHER READING

Coal supplies a third of the world's primary energy consumption, especially base load electricity, and is an important fuel and reductant in many industries. It is the foundation of the present rapid development of China, India and other nations. In that role it is a blessing, yet coal is highly controversial because most mines are very large and profoundly alter the land and adjacent communities. Burning coal contributes to anthropogenic carbon dioxide emissions (Box 6.1). Coal resources and reserves are very large and can support humanity for hundreds of years. Acceptance of continuing coal mining and combustion, however, depends on minimizing emissions and negative environmental effects. Progress is already made but critics expect faster action. Several elegant solutions are investigated, ranging from carbon dioxide capture and geological sequestration to *in-situ* gasification.

Coals are solid, combustible, fossil sedimentary rocks formed from land plants profusely growing in ancient wetlands. Early (biochemical) and late diagenetic (geochemical) processes enriched carbon and produced the coalification array, which reflects a continuous evolution of properties such as colour, transparency, reflectance, molecular structure, specific density, calorific value, organic chemistry, elemental composition, moisture content and many other parameters. Coal rank increases from lignite to bituminous coal and anthracite; the transition to graphite marks the boundary to metamorphism.

The chemical composition of coal is determined by its derivation from plants and comprises carbon, hydrogen and oxygen, with nitrogen and sulphur as minor components. Low-rank bituminous coal can be characterized by the "formula" $C_{10}H_7O$. During diagenesis, carbon increases from $\sim$60 to 90% C, whereas hydrogen decreases from 5.5 to <3%. This is due to the release of a large volume of methane (CH_4). Part of the methane remains absorbed in the coal, where it is a bane for underground miners as "fire damp", but a favourable resource for gas producers as coal bed methane (CBM). Most gas migrates towards the surface, acting as a powerful greenhouse gas in the atmosphere. A small part is trapped in the crust and forms many of the world's giant natural gas deposits.

Climate is an essential control on peat-forming plant communities and consequently, coal seams are terrestrial climate archives. At the same time, however, wetlands are prime factors of climate regulation by the fixation of carbon in peat and coal. The characteristic alternating dark and light bands of many lignites, and the repetitive sequences of host sediments that have been called "cyclothems" in black coal districts might be controlled by: i) eustatic forcing of sea levels; or ii) tectonic impulses. The first is probably the general background to occasional interference of the second. Presently, eustatic glacial forcing is attributed to orbital control of sea levels and climate, modulated by greenhouse gas control. With a better understanding of palaeoclimate, the influence of other climate-forcing processes will certainly be revealed.

At geological time-scales, coal formation is restricted to the last 10% of earth history. Earliest exploitable coal deposits date from the Late Devonian (ca. 370 Ma) of the Arctic realm, with fossils of genus *Archaeopteris* representing the first tall trees. In the Late Carboniferous (Pennsylvanian) of the Northern Hemisphere, coal was formed in extensive tropical coastal swamp forests of *Sigillaria* and *Lepidodendron*. The giant Permian coal deposits of the Southern Hemisphere with their boreal *Gangamopteris-Glossopteris* flora originated at high latitudes in a cool and humid climate. In both hemispheres, coal formation is intimately controlled by continental glaciation lasting from 326 to 267 Ma.

Coalification is preceded by humification of peat, which is a limited oxidation of lignin, cellulose and proteins by microbiota feeding on plant matter. Humins evolve during diagenetic coalification by increasing aromatization, condensation and clustering. Rank of lignites and sub-bituminous coals is measured by water content. Volatile matter yield differentiates between higher grade black coals. The standard method of precise rank determination is reflectance. Temperature, heat flow and duration of heating are controls of coalification. The process can be modelled applying the Arrhenius equation, which describes the kinetics of an endothermic chemical reaction. Results indicate that typical coalification temperatures are $\sim$50–200 °C (sub-bituminous and bituminous coal). Anthracite is formed at 200–300 °C.

Technologies in applied coal geology, coal mining and environmental mitigation are in a phase of revolutionary change. Because of the size of the industry, the impact of coal extraction and use affects large regions. Pioneers in the industry already approach the ideals of green mining but the bulk trails behind. Let us not forget that investments in green mining raise costs that have to be recovered from the electricity market. Clear national and international regulations are the precondition for industry to broadly invest in carbon capture and sequestration (Box 6.1), calling for governments to agree on actions. Let them act in such a way, however, as not to block human inventiveness in overcoming obstacles.

For a synopsis of the geological diversity of 13 world-scale coal mining districts, I recommend the volume edited by Cross (1993). As an insight into the present state of industrial practice, the book by Kininmonth & Baafi (2009) is singularly valuable. Beerling (2007), a climate scientist, recounts in a lively scientific style *How Plants Changed Earth's History*. Freese's (2003) *Coal, a Human History* is a very readable historical account of the significance of coal for economic development by fuelling the Industrial Revolution, which started in 18th-century England, its social impact and further fate until today's preoccupation with carbon dioxide.

CHAPTER 7

Petroleum and natural gas deposits

> *The Stone Age did not end because the world ran out of stones, and the oil age will end long before the world runs out of oil. The problem of oil is not its shortage but its concentration.*
>
> The Economist 2004

Synopsis

Petroleum and gas deposits are economically exploitable natural accumulations of hydrocarbons in the Earth's crust. Their most important role in our civilization is the supply of energy that is highly concentrated, easily distributed and versatile. Hydrocarbon products guarantee mobility. Public perception of oil and gas is marked by price fluctuations, disruption of society in producer regions, oil spills and occasional threats to stop delivery. Media announce depletion of resources for the middle of the current century.

The aim of this chapter is to provide a concise systematic survey of the economic geology of hydrocarbons. A short introduction presents published figures of production, reserves and resources. The scientific base is laid in the following section, with a presentation of hydrocarbon species and related compounds. Next we look at the preconditions of oil and gas formation, which start with the deposition of sedimentary source rocks with high content of organic matter, followed by diagenetic processes that induce exudation of oil and gas from the organic particles. The hydrocarbons are entrained by fluid flow in sedimentary basins and are usually dispersed in the shallow crust and in ocean water feeding microbes. A small part of generated hydrocarbons is trapped in a variety of geological structures, some of which develop into exploitable deposits. This chapter describes the nature and fluid fill of traps and their geological controls, and methods of exploration and exploitation that connect science with practice. In consideration of the crucial role of hydrocarbon availability, reserve and resource estimation methods are subsumed. Nature and the present role of unconventional petroleum and natural gas sources, such as tar sands, oil shale and tight gas shale, allow an outlook into a possible future. The chapter concludes with exposing typical environmental problems in the hydrocarbon industry and their prevention or mitigation.

Economic Geology Principles and Practice
Metals, Minerals, Coal and Hydrocarbons – Introduction to Formation and Sustainable Exploitation of Mineral Deposits, Walter L. Pohl
© 2011 Walter L. Pohl. Published 2011 by Blackwell Publishing Ltd.

Hydrocarbons are the base of liquid fuels supply. Also, they are important chemical raw materials for the production of numerous organic basic chemicals and final products, from plastics and pharmaceuticals to carbon fibres. With a share of only 3% of total crude oil sold, however, chemical uses pale in comparison. The large hydrocarbon provinces of the world occur in regions that are distant from the centres of consumption and a significant part of current production and resources is state-controlled. This is conceived as a possible risk concerning prices and availability, driving competitors to invest in hydrocarbon fields in lower-risk regions and in alternative fuel sources. Fuels that may replace natural gas and petroleum products include liquid hydrogen, methanol (CH_3OH) produced from carbon dioxide and water (Olah *et al.* 2006), liquids made by fermenting biomass ("biofuels", e.g. ethanol C_2H_5OH from cellulose or sugar), and hydrocarbon "synfuels" produced by Fischer-Tropsch synthesis from biomass and coal. At present, only ethanol and synfuels appear to be economically feasible. The environmental costs of biofuels may exceed those of fossil fuels (Scharlemann & Laurance 2008). Because of the generally high cost of crude oil, many coal-to-liquid synfuel plants are being constructed worldwide.

Much hope rests on a future "hydrogen economy", which implies that hydrogen replaces oil-based liquid fuels in vehicles and in stationary distributed applications. Hydrogen would be burned in fuel cells generating electric energy. Large challenges remain to be solved, however, concerning hydrogen production, distribution and onboard storage. In principle, hydrogen contains more energy on a weight-for-weight basis than any other liquid fuel, but has a very low energy-density per unit volume. Today, ~10 Mt/year of hydrogen are produced by steam reforming, from natural gas at ~800 °C and catalysed by nickel (eq. 7.1). This hydrogen is commonly contaminated with CO and CO_2, which poison the platinum catalysts of fuel cells.

Production of hydrogen by steam reforming:

$$CH_4 + 2H_2O \rightarrow CO_2 + 4H_2 \qquad (7.1)$$

Hydrogen produced according to eq. 7.1 is not climate-neutral, unless the waste CO_2 is stored in deep geological isolation. Alternatives of hydrogen production include biological or catalytic degradation of biomass and electrochemical or photochemical splitting of water (electrolysis). In all cases, the process is endothermic and requires a considerable energy input. Therefore, large-scale hydrogen production is only feasible if cheap electric energy can be provided. This appears to depend mainly on increasing the number of coal-fired and nuclear power stations (Jaccard 2006).

Petroleum and gas contain more hydrogen than coal and yield more energy per carbon unit than coal. Therefore, burning petroleum and gas releases relatively less CO_2 than coal. Of course, the sheer mass of hydrocarbons combusted is much higher than that of coal, so that total emissions from petroleum and gas are higher. Also, considering the typically dispersed use of oil products (e.g. in vehicles, buildings), it is very difficult to develop economically viable ways of carbon capture.

The world's measured (proved) reserves of economically exploitable petroleum at the end of 2009 were estimated at 1333 thousand million barrels or 181.7 thousand million tonnes. That was an increase of ~12.3% over the end 1999 figure, despite the large cumulative production during the intervening 10 years (*BP Statistical Review of World Energy* 2010). BP defines the term "proved reserves of oil" as those quantities that can be recovered in the future from known reservoirs under existing economic and operating conditions. Note that discovered resources (indicated and measured) are not reported. World production of oil in 2009 was 3820 Mt. Dividing the reserves by this figure gives an R/P-ratio of ~46, which is the highest for many years (before 1989, it was much lower, cf. Figure 6.1). In 2009, the largest oil producers were Russia, Saudi Arabia, USA, Iran, China, Canada and Mexico. Main consumers of oil were USA, China, Japan and Russia.

One barrel [bl] has a volume of 158.99 litres or 42 US gallons and contains 0.1364 tonnes of petroleum of average density. The barrel serves as a measure of volume since oil was transported to the market in wooden whisky containers from the world's first oilfield near Titusville, Pennsylvania, in the year 1870.

The term "conventional" petroleum (and natural gas) implies primary recovery by free flow from wells, by pumping, or by water and gas injection. Enhanced recovery methods can produce more oil and gas from the same deposit, but at higher costs. Of the total conventional reserves, ~57% occur in the Middle East, followed by Venezuela and Russia. Kazakhstan, Libya, Nigeria, Canada, USA and China share a notable part of the remaining reserves. Total historic production until 2009 is estimated at 160 Gt petroleum.

Additional undiscovered resources of conventionally recoverable petroleum are estimated by some at up to 400 Gt, with a geographical spread similar to present reserves. There is no agreed method by which to estimate undiscovered resources. Many scientists, the public and the media are fascinated by the so-called Hubbert Curve (Hubbert 1962), which was originally used for oilfield engineering. Hubbert first transferred its application to estimation of total oil production from single wells and fields to the whole of the United States. The production of oilfields typically rises to reach a peak ("depletion mid-point") and then falls to the point of exhaustion and closure. A plot of production over time produces a bell-shaped curve. The same method is used for estimating total world oil production and implicitly, total world oil resources. Results vary because of various factors and events that influenced past world production, such as war, nationalization and economic crises, which are differently weighted. A more problematic variable is the changing nature of oil production, from conventional to advanced technologies. Overall it seems that the Hubbert Curve method produces estimates that are decidedly too low.

The depletion mid-point of conventional oil ("peak oil"), the time when 50% of the total recoverable geological resources will have been exploited, is generally assumed to be reached around the year 2020 (Wellmer 2008). After the depletion mid-point, some forecasts presume a rapid decline of production. Already now, however, unconventional production is rapidly increasing. Generally, the availability of oil and gas is not only a function of resources, but also of political decisions, prices and advances in science and technology. This is why after the depletion midpoint, a plateau or a gradual decline of production is much more probable. Maugeri (2004) defended this view vividly, and points out that the future evolution of production and prices will be dominated by the market, politics and human inventiveness.

Today's proved economically exploitable natural gas reserves are estimated at $187.10^{12}\,m^3$ (normalized to a calorific value of 9500 kcal/m^3, this is ~168,000 Mt oil equivalent). Additional conventional resources are assessed at ~$240.10^{12}\,m^3$. Yearly consumption is rising (although with a dip in 2009 by −2.1% to 2940 billion m^3 or 2646 Mt oil equivalent) and total accumulated production is ~76,000 billion m^3. The largest proved reserves occur in the CIS (~30%, mainly Russia and Turkmenistan) and the Middle East (41%, Iran and Qatar). The European Union hosts no more than 3.2% of world reserves. Main consumers of gas are USA, Russia, Iran, Japan, Germany and Saudi Arabia (*BP Statistical Review of World Energy* 2010). For comparing the calorific value of different energy raw materials, conversion into oil equivalent mass is often used (Table 7.1).

Table 7.1 Average conversion factors for comparing mass of coal (t) and lignite (t), and volume of natural gas (m^3) and petroleum (m^3, barrels) with tonnes of oil equivalent (toe)

1 tonne of oil equivalent	→	~42 Gj (gigajoules) or 10 Gcal
1.5 metric tonnes of average bituminous coal	→	1 tonne of oil equivalent
3 tonnes of average lignite	→	1 tonne of oil equivalent
1 billion cubic metres natural gas	→	0.9 million tonnes of oil equivalent
1 tonne of average oil	→	1.165 m^3 or 7.33 barrels

A comparison based on toe units shows that proved reserves of fossil fuels at the end of 2009 amounted to 412 Gtoe of coal and lignite combined, and 182 plus 170 Gtoe of conventional oil and natural gas, respectively.

Conventional oil and gas can be economically exploited with today's technologies and at about present costs. It is estimated, however, that conventional oil and gas make up less than 5% of the total mass of hydrocarbons in sediments. Future technologies may generate giant exploitable resources from the total geological endowment. Less speculative unconventional resources are the Canadian oil sands that contain more recoverable oil ($50.10^9\,m^3$) than Saudi Arabia ($36.10^9\,m^3$). The Orinoko Belt in Venezuela hosts $\sim 186.10^9\,m^3$ of very heavy oil; serious development has not yet commenced. Gas hydrate deposits below permafrost land and beneath the oceans contain more than twice the mass of carbon of all known fossil fuels; industrial-scale trial production was successfully tested in 2008 in Arctic Canada. Submarine hydrates in sand reservoirs enclosed by mudrock represent substantial resources, which can be extracted by conventional technologies (Boswell 2009). In the USA, natural gas in "tight" (practically impermeable) sandstone, shale and in coal seams emerged as a giant new economic source. The world's potential for comparable deposits is enormous – global recoverable unconventional gas resources are estimated at $\sim 400.10^{12}$ (or T) m^3 (IEA 2009) compared to present annual consumption of 3 Tm^3. Oil shales may provide $\sim 500.10^9\,m^3$ of oil, compared to end 2009 proved world oil reserves of 212.10^9 m^3. Even conventional oil is far from finished – only a few percent of submarine sedimentary basins at more than 500 m water depth have been explored. The Circum-Arctic region contains large potential oil and gas resources (Gautier *et al.* 2009). Of course, much of the unconventional oil and gas will be more expensive. The reported observations confirm the introductory statement from *The Economist*. Our present dependence on hydrocarbons will not end because of exhaustion of geological resources, but because of new energy sources and technologies superior to oil and gas.

7.1 SPECIES OF NATURAL BITUMENS, GAS AND KEROGEN, AND THEIR PROPERTIES

Hydrocarbons may occur in gaseous, liquid, wax-like and solid phase. Most natural hydrocarbons are insoluble in water but soluble in alcohol and ether. Common species that form mineral deposits are:

- petroleum (liquid both at depth in the reservoir and on the surface);
- natural gas (free gas, not associated with oil or dissolved in water);
- natural gas hydrate (solid, currently first experimental exploitation);
- associated gas (dissolved in oil, or as a free gas cap above reservoir oil);
- tar (highly viscous, low-quality petroleum);
- earth wax (ozocerite; solid, soft to brittle, yellow to brown);
- pyrobitumen (solid, black, hard);
- asphalt (solid, black, brittle);
- kerogen (organic matter in oil schists that yields "synthetic" oil on retorting; in source rocks, kerogens are the generators of oil and gas).

7.1.1 Crude oil, or petroleum

Crude oil, or petroleum, is a liquid of yellowish-brown to black colour, with a green fluorescence under UV-light. Its odour is rarely aromatic but usually unpleasant due to traces of sulphur compounds. Petroleum consists predominantly of hydrocarbons, with a minor share of sulphur, oxygen and nitrogen compounds. The chemical differences between oil and black coal (high volatile bituminous A) are much higher hydrogen and lower oxygen contents of petroleum (Table 7.2).

The residue (ash) from burning oil contains a number of elements, some of which may be recoverable (e.g. vanadium). Trace elements include Si, Fe, Al, Ti, Ca, Mg, V, Mo, Ni, Ba, Sr, Mn, Pb, Cu, Cr, U (plus daughter nuclides) and noble metals. Some elements may foul up the catalysts in refineries (e.g. arsenic). Several of the trace elements (V, Ni, Mo) originate in organic substance, whereas others reflect geochemical

Table 7.2 Average elemental composition of fossil fuels, asphalt and kerogen (Hunt 1996, in wt. %)

	Gas	Petroleum	Asphalt	Black coal	Kerogen
C	76	84.5	84	83	79
H	24	13	10	5	6
S	0	1.5	3	1	5
N	0	0.5	1	1	2
O	0	0.5	2	10	8
Sum	100	100	100	100	100

characteristics of source rocks, and diagenetic reactions.

Petroleum is a mixture of hundreds of chemical compounds, which are investigated by ionization methods, liquid chromatography and mass spectrometry (Hunt 1996, Panda *et al.* 2009). Main groups are normal and branched-chain alkanes (paraffins), cyclo-alkanes (naphtenes), mono- and polyaromatic hydrocarbons and the rare olefins (Figure 7.1). All oils contain some asphaltics, or nitrogen-sulphur-oxygen (N-S-O) compounds. The latter give petroleum its colour and odour. Most petroleum components are products of decomposition, condensation and polymerization reactions after burial of organic substances. Their chemical diversity can be described as follows:

- Paraffins (C_nH_{2n+2}, alkanes, or aliphatic hydrocarbons) are economically most prominent, because they are easily transformed into the most valuable refinery products (gasoline, kerosine). Paraffins comprise gases at $n = 1 - 4$ (methane, ethane, propane, butane), liquids at $n = 5 - 15$ and solids at $n > 15$ (e.g. ozocerite). Paraffins are "saturated" hydrocarbons, because all available carbon bonds are saturated with hydrogen. Second only to naphthenes, they are the most common molecular structures in petroleum. Paraffins predominate in the oldest, most deeply buried reservoirs. Typical precursors are paraffinic waxes and lipids of plants.
- Cycloparaffins (C_nH_{2n}, cycloalkanes, or naphtenes) form ~50% of an average crude oil, with the percentage increasing in the heavier fractions. Naphtenes are built from carbon rings of 5 or 6 atoms. Like paraffins, they are saturated hydrocarbons.
- Aromatic hydrocarbons (C_nH_{2n-6}, benzenoids and arenes) amount rarely to more than 15% of crude oil. In distillation, they are concentrated in the heavy fraction. In spite of their name, aromatics have very little odour. The strong smell of crude oil is due to traces of non-hydrocarbons. All aromatic hydrocarbons contain at least one benzene ring, a flat 6-carbon ring (C_6H_6) in

Figure 7.1 Simplified classification of crude oil by compositional variation of paraffinic, naphtenic and aromatic hydrocarbon fractions. Position of average oil in important provinces after Miles (1994). This diagram was first proposed by Tissot & Welte (1984). By permission of Oxford University Press.

Publisher's Note:
Image not available
in the electronic edition

which the fourth bond of each carbon atom is shared. Aromatic hydrocarbons are unsaturated, i.e. they react by adding hydrogen or other elements to the ring.

- Asphaltics (non-hydrocarbon nitrogen, sulphur and oxygen compounds) predominate in the residual fraction of crude oil distillation. Typically, they contain very small amounts of N, S or O, in addition to C and H, in compounds such as thiol, phenol, pyridine and quinoline. The asphaltic residuum comprises resins, waxes and asphaltenes. The latter are the heaviest molecules of crude oil. A typical asphaltene molecule may comprise groups of condensed aromatic and naphtenic rings that are connected by paraffin chains and sulphur or oxygen bridges. The condensed aromatic structures of asphaltenes have free-radical sites that are capable of complexing metals (vanadium, nickel, etc.). Average contents of asphaltenes in ordinary crudes are ~3 wt. % and may reach 15%, but some Middle East oils are reported to contain >50%. Asphaltenes are part of the primary composition of crude petroleum, but are also a product of secondary bacterial degradation. They contain clues to the formation temperature of oil (Di Primio *et al.* 2000).

Biomarkers, or geochemical fossils are specific organic compounds found in petroleum and sediments, which can be useful biochemical indicators for the former presence of certain organisms (e.g. bacteria, diatoms, dinoflagellates). Biomarkers are derivatives from original substances of live organisms, such as haemoglobin and chlorophyll. These compounds (porphyrins) are extremely useful for reconstructing sedimentary conditions, for correlating oil to oil, or oil to source rock, and as indicators of oil maturity, because they change with rising temperature. Biomarkers can even be determined from oil in fluid inclusions, as at Elliott Lake, Canada, where pebbles of the uraniferous conglomerate with an age of ~2.4 Ga contain oil that is derived from cyanobacteria and eukaryotes (Dutkiewitz *et al.* 2006).

Sulphur concentration of petroleum rises with higher nitrogen contents and density. If reservoir rocks are limestone, dolomite or anhydrite, oil will be rich in sulphur. Petroleum may contain sulphur in elemental form, in organic compounds, or as dissolved H_2S gas (typically 5–14 wt. %). The source of sulphur can be organic precursors of oil or the host rocks. "Sweet" oil contains <0.5% S, but today this applies to <30% of well production. Oil with higher sulphur is "sour". In refinery products, sulphur is unwanted. Desulphurizing oil and natural gas, and the resulting by-product sulphur, provide a large part of world sulphur supply.

The technical characterization of crude oil is based on density and the yield on standardized fractional distillation. Most oils fall into a density range between 0.7 and 1.06 g/cm^3 (at 20 °C). In the industry, API degrees based on density at 15.6 °C are more commonly used (eq. 7.2).

Computation of API (American Petroleum Institute) gravity from density data:

$$\text{Degrees of API gravity} = \frac{141.5}{\text{Density at } 15.6\,^\circ\text{C } (60\,^\circ\text{F})} - 131.5 \tag{7.2}$$

10° API is the density of pure water. Increasing numbers indicate lower densities (e.g. 30° API equals D = 0.8762 g/cm^3).

Typical conventional crude oils have 22–35° API. Markets distinguish classes of extra heavy (<10° API), heavy (10–22.3° API), medium (22.3–31.1° API) and light oil (above 31.1° API). Condensates ("natural gasoline") have >55° API; they are gaseous in the reservoir and clear to straw-coloured liquids at surface conditions. Compared with average oil (1.5–1.9) the H/C-ratio of heavy oil is less than 1.5, which reduces the recovery of gasoline considerably.

Fractional distillation is the common processing technique for petroleum. In distillation towers of refineries, crude oil is separated into various molecular size fractions. The smallest molecule in petroleum is methane (CH_4), with a molecular weight of 16, and the largest molecules are asphaltenes that reach molecular sizes in the tens of thousands. Chemical processes such as cracking, polymerization and reforming are employed in order to improve output of the most valuable marketable products from crude oil. Gasoline, kerosine and diesel fuel are manufactured

Table 7.3 Example of products and boiling ranges for crude oil distillation (Hunt 1996)

Light gasoline	0–120 °C
Gasoline	120–190
Kerosine	190–260
Light gas oil (diesel fuel)	260–360
Heavy gas oil and lubricating oil	360–530
Asphaltic residuum	(not boiling)

from smaller or larger molecular fractions. Products and boiling range standards of refineries vary; the example in Table 7.3 is from a US Gulf Coast refinery.

Crude oil is classified as predominantly paraffinic, naphtenic or aromatic (Figure 7.1). Generally, the fraction of paraffins increases with depth as the density of oil decreases by thermal maturation. There is speculation that the autochthonous microflora (thermophilic bacteria and hyperthermophilic archaea) of deep oil pools may have a role in this (e.g. in the Paris Basin: Haridon *et al.* 1995). Even the conversion of long-chain alkanes into methane at great depth may be catalysed by anaerobe microbes (Zengler *et al.* 1999). Oil in older and more tectonized sediments also tends to be richer in paraffins, whereas younger and little deformed rocks are more likely to contain aromatic oil. This is probably caused by a different time of maturation. Exceptions from the general rule are common, however. From lacustrine source rocks, for example, paraffinic and high-wax oils are formed, even at low temperature. Contact with meteoric water and microbes causes enrichment of aromatics and N-S-O compounds and reduces the quality of oil (degradation).

Viscosity is a vital parameter for the extraction of oil from the reservoir, because it controls recovery. Viscosity is a function of temperature and pressure, and of the composition of the oil. Density of oil and viscosity are positively correlated. Accordingly, heavy and extra heavy oil have viscosities so high that flow is extremely slow and with conventional technology, commercial extraction is not possible (cf. Chapter 7.5 "Petroleum Mining").

Particular geochemical indices characterizing oil include the carbon preference index (CPI; chain length of certain paraffins), the pristane/phytane ratio, isotopic data and the V/Ni ratio. They assist, for example, source rock-oil correlation and determination of maturity, which are essential for understanding the petroleum system of an oilfield and of whole basins. Also, they allow differentiation of oil families that are derived from source rocks of similar sedimentary facies.

Isotopic characterization of petroleum is mainly based on the systems $^{12}C/^{13}C$, H/D, $^{32}S/^{34}S$ and $^{14}N/^{15}N$. The organic predecessors are marked by light $\delta^{13}C$ and δD, with lowest negative values in lipids. Kerogens that are derived from this biomass contain slightly changed isotope ratios, due to exchange with formation water (Schimmelmann *et al.* 1999). Petroleum that is derived from kerogen inherits its isotope characteristics, supporting source rock-oil and oil-oil correlations. ^{12}C in oil is somewhat enriched compared to kerogen. Accordingly, the wide spread of petroleum isotope data, with $\delta^{13}C$ from –20 to –32‰ and δD from −60 to −180‰, mainly reflects different biomass and sedimentary environments.

7.1.2 Natural gas

Natural gas is always a mixture of more than one gas. In addition to gaseous hydrocarbon compounds, CO_2, H_2S (toxic), N_2 and several noble gases are always present. With the exception of helium, these admixtures have no market value and at high percentages impede economic extraction. The hydrocarbons in natural gas are mainly methane and other low-molecular paraffins (C_1-C_4) and their isomers. Temperature and pressure determine the composition of the gas phase, because several higher hydrocarbons are gaseous in the reservoir but condense when the pressure is lowered (e.g. in the production well during the rise towards the surface). These condensates characterize "wet gas" with over 4 litres condensable liquids per 100 m^3. Dry gas consists mainly of methane (commonly ~90 mole %). The "dryness" of gas can be characterized by the percent methane/percent ethane ratio. "Sour gas" has elevated fractions of sulphur and CO_2, "sweet gas" contains less than 2% CO_2 and no H_2S. Only sweet gas can be directly used, sour gas must first be refined. In the recent past, by-product sulphur made the

Lacq gas deposit in southern France (methane with 15% H_2S and 10% CO_2) one of the largest sulphur producers in the world. Today, annual production of elemental sulphur from gas operations is ~25 Mt (mainly in Russia, Canada, the Middle East). In the future, much H_2S may be re-injected if a projected sulphur oversupply arrives. Natural gas can have trace contents of toxic metals such as mercury (e.g. in Northern Germany up to 1 mg/m^3) that must be removed before use.

High nitrogen or carbon dioxide contents of deep natural gas may be explained by different speed of flow: As methane (density of gas at surface pressure 0.72 g/L) migrates towards the surface, heavier nitrogen (N_2 1.25 g/L) and carbon dioxide (1.98 g/L) lag behind at depth. CO_2 may be derived from several sources, which include maturation of organic substance and degassing of deep magma bodies. $^3He/^4He$ and $CO_2/^3He$ ratios are employed to discern between the two variants (Ballentine *et al.* 2001). The Bravo Dome gasfield in New Mexico, USA, produces almost pure magmatic CO_2 from depths of 600–700 m. This gas is used for carbon dioxide injection to maximize oil recovery from oilfields in western Texas. Metamorphic devolatilization of carbonate rocks (e.g. calcsilicate formation) may also contribute CO_2 (Huang *et al.* 2003). Gas with higher nitrogen contents and almost pure nitrogen gas may be a product of organic matter maturation. Littke *et al.* (1995) demonstrated that after peak methane production, coal enters a stage of maximal nitrogen discharge. Alternatively, much nitrogen can be liberated by K^+ substitution from illite containing NH_4 and subsequent oxidation of ammonium (Friberg *et al.* 2000, Mingram *et al.* 2005). Less credibly, descending meteoric waters with dissolved atmospheric nitrogen may be a source. Determination of isotope ratios $^{14}N/^{15}N$ in gas can assist in identifying the origin of nitrogen (Gerling *et al.* 1997; Williams *et al.* 1995).

Nitrogen-rich natural gas may contain up to 2.5 vol. % helium, as in parts of the Hugoton-Panhandle gasfield (Kansas, Texas: Ballentine & Lollar 2002). Small, uneconomic concentrations of helium, neon, argon and xenon occur in all natural gas deposits. They are important genetic tracers. For example, relative contents of the stable isotopes ^4He and ^3He indicate the source of the gas. Radiogenic ^4He is a product of α-decay of various members of the U and Th nuclide series that are enriched in crustal rocks. The "primordial" ^3He, in contrast, originates predominantly from the Earth's mantle where it was captured during planetary accretion. Crustal helium has a ratio of $^3He/^4He$ of ~0.02 R_A (R_A is the $^3He/^4He$ ratio of air equal to 1.4×10^{-6}). Higher ratios reaching ~8 R_A show that degassing of the mantle contributes to He-contents in gas deposits, most frequently in tensional tectonic settings (Kennedy & van Soest 2007) and in volcanic provinces with a component of mantle magmas:

Helium (He) is the lightest (0.1785 kg/m^3 at standard pressure) of the six noble gases (helium, neon, argon, krypton, xenon, radon). All are chemically inert and serve many purposes, but helium is especially important. Apart from filling air ships and party balloons, it is employed in industrial processes such as extremely low-temperature cryogenic applications, or for flooding semiconductor fabrication tables in order to prevent contamination of the chips. Although noble gases can be produced from air, most of the traded helium is derived as a by-product from North American natural gasfields (e.g. Hugoton). Exploitable contents range from 0.3 to 1.5 vol %. In the near future, Qatar and Algeria are expected to become important producers.

Gas hosted in sulphate or carbonate rocks is usually enriched in hydrogen sulphide, sometimes to >90% H_2S. Most of this is a product of thermochemical sulphate (anhydrite) reduction by reaction with hydrocarbons at >100 °C (cf. TSR in Chapter 1.4 "Diagenetic Ore Formation Systems", eq. 1.21). The main field of microbial sulphate reduction lies below 100 °C. As native sulphur melts at 113–120 °C, many wells penetrating into deep carbonate-anhydrite rocks have encountered (and produced) liquid sulphur plus H_2S gas.

Natural gas is formed by several different processes from the Earth's surface down to great depths:

1 Near the surface and at low temperature, bacterial fermentation of organic substances produces very pure bacterial, or biogenic methane;

2 With increasing depth and elevated temperature, kerogen is partly converted to petroleum and associated, or primary petroleum gas;

3 Deep below the surface and at high temperature, oil breaks down into secondary wet gas (± condensates) and pyrobitumen.

Humic kerogen is transformed into dry gas. Parallel to (2) and (3), a large mass of methane is expulsed from coal seams.

Associated gas is dissolved in oil; only when saturation is reached, a free gas cap forms on top of the oil pool. Although one of the principles of reservoir management is always to conserve energy, oil cannot be extracted without some loss of gas pressure. The dissolved gas makes oil frothy as pressure decreases and at the surface, several 100 m^3 of gas may be separated per m^3 oil. Earlier, flaring-off petroleum gas was common industrial procedure, but is very rare now.

Many large and one giant gasfield (Groningen) in continental Europe have been formed from methane that originated in deeply buried Late Carboniferous (Westfalian) coals and older black shales below a Permo-Mesozoic cover blanket. Reservoirs include Carboniferous jointed hard rocks, Rotliegend dune sands, Zechstein (Ca2) carbonates and Buntsandstein. Of course, most of the methane formed during coalification dissipates towards the surface. Gas remaining absorbed in coal ("coal bed methane") is increasingly exploited and is of significant economic impact (Gayer & Harris 1996).

Isotopic geochemistry provides fundamental information on natural gas formation (Whiticar 1999, Schoell 1983; Figure 7.2). Bacterial/biogenic methane is characterized by very light carbon (low $\delta^{13}C$). Exceptionally heavy carbon was found in methane inclusions of German potassium salt, due to evaporation in the bittern brine (Potter *et al.* 2004). Gas produced by thermal maturation, including associated and dry gas, contains heavier carbon with increasing maturity. Because of different precursors, hydrogen isotopes of biogenic methane exhibit a wide spectrum. Similar to carbon, the D/H ratio increases with maturity. This conforms to the general observation that light isotopes are first mobilized. Of course, mixing of gases of different origin, later bacterial influence (e.g. bacterial methane oxidation) or migration may complicate this simple pattern.

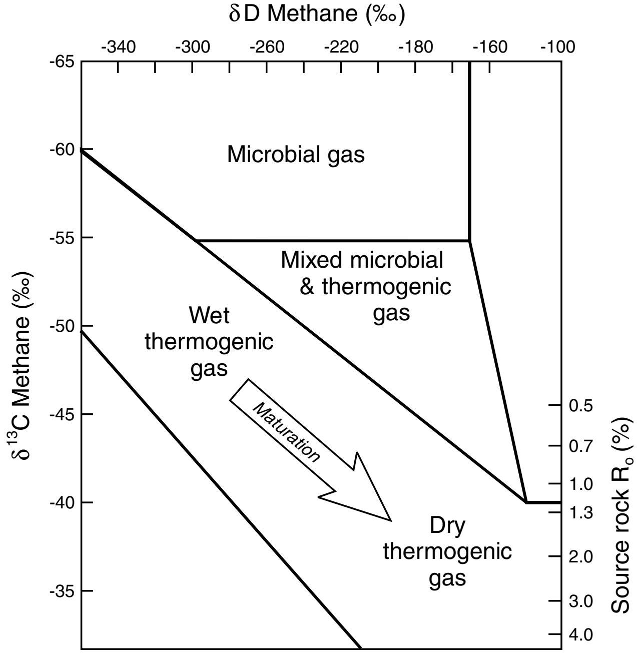

Figure 7.2 Isotopic differentiation of methane origin as a function of diagenetic grade (maturity) of source rocks. The scale on the right provides a measure of maturity (R_o = vitrinite reflectance in oil immersion). Modified from Schoell (1983). AAPG © [1983] reprinted by permission of AAPG whose permission is required for further use.

7.1.3 Natural gas hydrates (clathrates)

Natural gas hydrates (clathrates) are ice-like solids with determinate crystal structures that are characterized by cages of water molecules. The cages may contain methane or higher molecular hydrocarbons as "guest molecules". Complex gas hydrates with isobutane, propane and/or cyclopentane, in addition to methane, are more stable than simple methane hydrate (Hailong Lu *et al.* 2007), extending the P/T stability field of natural gas hydrates from a minimum of ~200 m water depth down into oceanic sediments. Generally, the bottom of hydrate stability depends on the local geothermal gradient, which causes temperature to rise above dissociation conditions as depth increases. This occurs commonly at 200–500 m below the sea floor (Pecher 2002). Pressure release (e.g. a sharp drop in sea level), or rising temperature liberate the occluded gas. Sudden melting of the Earth's gas hydrates increases greenhouse warming. Events of this kind were identified by strong spikes of atmospheric ^{12}C at the end-Triassic extinction (Beerling 2007) and in the early Tertiary (Dickens *et al.* 1997a), including the Palaeocene-Eocene thermal maximum. Giant beds of gas hydrates have been found in continental arctic sediments, in seafloor sediments worldwide and, less frequently, as exposed white "rocky mounds" on the sea floor (e.g. Gulf of Mexico: Max 2000). At some locations, hydrates occur in sea-floor gas vents, which have a diameter of hundreds to thousands of metres (Haacke *et al.* 2009). The methane in hydrates is derived from sediments beneath the hydrate layer. The source of the gas in hydrates can be narrowed down using (129) iodine age determination (Tomaru *et al.* 2007). Natural gas hydrates contain remarkable methane volumes, at normal (surface) pressure up to 164 times the hydrate volume. In spite of giant resources, experiments for economic recovery of hydrate gas were only recently initiated. Estimates range from 500 to 5000 Giga-tonnes (Gt) of carbon in methane, compared to ~140 Gt of carbon in natural gas and 700 Gt in coal reserves. The occurrence near Blake Ridge, off the southeastern coast of America (Figure 7.3), is thought to contain a volume of methane that could supply the total gas demand of the United States for over 100 years (Dickens *et al.* 1997b). In northern Canada, an ongoing large-scale pilot project aims at commercial production of gas from hydrates below the land surface (Mallik, Richards Bay Island, Beaufort Sea).

7.1.4 Tar

Tar is a term for heavy and extra heavy oils (6–12° API), that are highly viscous and sulphur-rich. Tar is a low quality and unconventional hydrocarbon resource. Only now, the exploitation of tar begins to reach a scale that is significant. Tar is the

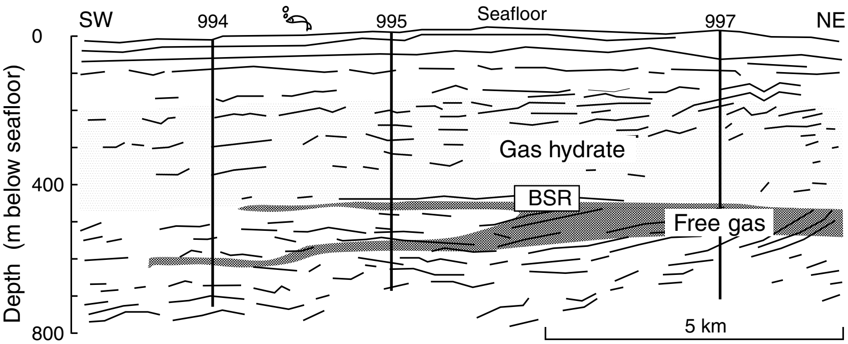

Figure 7.3 Seismic profile of the giant methane deposit at Blake Ridge, situated East of the North Carolina coast in the Atlantic Ocean, under ~2800 m of water (Fleming *et al.* 2003). Courtesy Geological Society of America. The remarkable feature is that trap and seal are formed by a layer of low permeability gas hydrates with a thickness of ~250 m. BSR = bottom simulating reflector, 994-997 are drill holes.

residuum of a degradation of normal petroleum. Degradation is essentially the loss of light hydrocarbons and an increase of N-S-O compounds. Several pathways of degradation are possible. The formation of the tar in the Canadian tar sand deposits, arguably the world's largest hydrocarbon resource after Russia, is due to biogenic processes (Head *et al.* 2003). At $T < 80\,^\circ C$, anaerobic microbes catabolize alkanes and produce organic acids. Metals, asphalthenes and resins are enriched in particles surrounded by liquid hydrocarbons, resulting in a colloidal suspension. An important co-product of oil degradation is biogenic methane that may form gas deposits if suitable traps are present.

7.1.5 Earth wax (ozocerite)

Earth wax (ozocerite) is essentially composed of high-molecular paraffins. Earth wax precipitating from paraffinic petroleum typically clogs pipes and drillholes. Its consistency ranges from a soft paste resembling medicinal salve to a brittle solid. Light yellowish to brown colour is common. The density of earth wax is between 0.84 and 0.93, melting occurs at 85–100 °C. It is soluble in petroleum, gasoline and organic solvents. Earth wax deposits are veins and stockwork bodies similar to hydrothermal ore deposits. Wax is concentrated in upflow channels of paraffinic oil, where pressure or temperature changed rapidly. Today, earth wax mining is hardly competitive with products extracted from petroleum.

7.1.6 Pyrobitumens

Pyrobitumens are black, hard, infusible (unlike ozocerite), insoluble, non-volatile hydrocarbon substances that occur in vein deposits. Pyrobitumens are commonly formed at high temperatures and pressures, which induce conversion of petroleum to dry gas and pyrobitumen. The term is, however, non-genetic and physically and chemically similar material formed by surface degradation of oil seeps is also called pyrobitumen (Hunt 1996). Thermal pyrobitumens originates from petroleum at $T > 150\,^\circ C$, by sudden pressure drop and loss of dissolved gas and condensate (cracking). Therefore, these substances are remains of former deep petroleum occurrences (Mossman & Nagy 1996, Stasiuk 1998).

7.1.7 Natural asphalt

Natural asphalt is a product of petroleum degradation similar to tar, but more advanced. It is formed at shallow depth or the surface under the influence of meteoric water and aerobic microbes. Note the increase in oxygen compared to oil (Table 7.2). Asphalt contains only a small fraction of hydrocarbons and is mainly composed of N-S-O compounds including asphaltenes. Asphaltene colloids with resins and waxes (micelles) form a solid, three-dimensional framework. The term asphalt is also used for the residual fraction of industrial oil distillation. Natural asphalt is a brown to black brittle solid with conchoidal fracture. Its density is 1–1.3 g/cm^3 and melting occurs at 100–140 °C. Natural asphalt capping oil seeps is commonly mixed with clay and sand.

7.1.8 Kerogen

Kerogen is that part of organic matter in a rock that is insoluble in organic solvents. This is the difference to bitumens (hydrocarbons) which are soluble, but in most rocks are only found in trace amounts. Kerogen originates from many different organisms. The main habitat of natural hydrocarbons – marine sediments as opposed to coal that is formed on land – implies that marine plankton should be the most common precursor of kerogen and petroleum. Marine plankton has a high percentage of lipids with elevated hydrogen contents, including fats, resins, waxes and oils. However, four types of kerogens are commonly differentiated according to different contents of C, O and H (Figure 7.4). The affinity with certain coal macerals (cf. Chapter 6.1 "The Substance of Coal") is indicated in Table 7.4.

Because kerogen types I and II have the highest hydrogen contents, they are prime sources of petroleum, although type I is relatively rare. Most oils are derived from type II kerogen, which is characterized by the "formula" $C_{515}H_{596}O_{72}$ (on the verge of generating oil; Helgeson *et al.* 2009). It

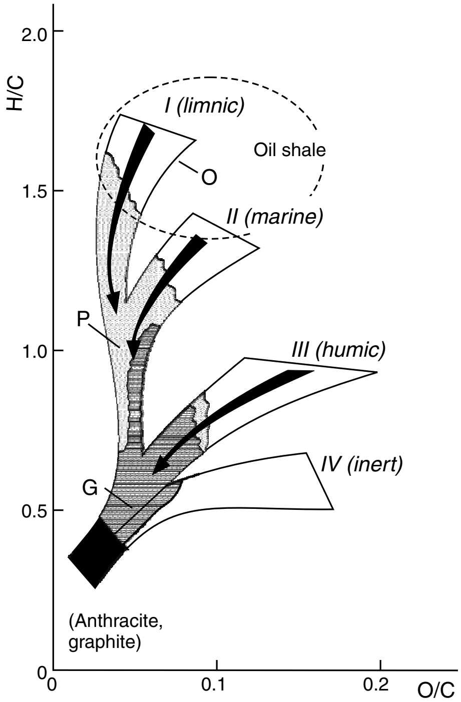

Figure 7.4 Progressive chemical changes of kerogen types with increasing temperature in the Van Krevelen diagram (modified from Tissot & Welte 1984). With permission from Springer Science + Business Media. Only kerogen types I and II produce important amounts of oil. Type III and IV are almost exclusively sources of natural gas. Arrows stress the direction of chemical evolution with increasing temperature (maturation). O = Early formation of oxygen-rich products (CO_2, H_2O); P = Generation of petroleum; G = Generation of natural gas. Note the field of typical oil shales.

is often labelled as representing "marine organic matter", but more precisely its dominating precursor is marine phytoplankton. Type III represents particles of higher plants similar to coal and is mainly a source of gas. Type IV contains very little hydrogen and is unable to generate oil, but may contribute some gas at high temperatures. Kerogens are investigated by coal petrographic methods (especially fluorescence microscopy: Taylor *et al.* 1998), infrared spectroscopy and various methods of organic chemistry (pyrolysis, gas chromatography, mass spectrometry, etc.). Industry standard determinations for rapid throughput of a large number of samples (e.g. drill cuttings) include vitrinite reflectance yielding a measure of kerogen maturity, and anhydrous or hydrous (Rock-Eval) pyrolysis (characterizing kerogen types and their potential for generating hydrocarbons: Espitalié *et al.* 1984; Figure 7.5). In addition, Rock-Eval pyrolysis provides an indication of the maximum temperature to which a sample of kerogen was equilibrated.

Table 7.4 Main types of kerogens, their atomic H/C ratio and common precursors

Type 1	H/C 1.9–1.0	algae and bacteria
Type 2	H/C 1.5–0.8	liptinite and marine plankton
Type 3	H/C 1.0–0.5	vitrinite
Type 4	H/C 0.6–0.1	inertinite

Publisher's Note:
Image not available
in the electronic edition

Figure 7.5 Petroleum and gas source rocks with different kerogen types in the hydrogen and oxygen index diagram as a result of Rock-Eval pyrolysis (after Miles 1994). By permission of Oxford University Press. Dots represent hydrocarbons and CO_2 generated from kerogen by cracking upon heating from ~350–550 °C.

During early diagenesis of sediments, dispersed organic matter is transformed into kerogens that generate CO_2, H_2O, oil and gas as they mature. At high pressure and temperature near the transition to low-grade metamorphism, kerogens approach the composition of graphite (Figure 7.4) and lose their hydrocarbon generation potential. Kerogens that are in the initial stages of maturation release hydrocarbons when heated. This motivated the term kerogen (Greek for "generating wax") and is the reason why rocks that have a high content of low maturity kerogen are considered to be significant future resources of hydrocarbons (cf. Chapter 7.7 "Oil Shales").

7.2 THE ORIGIN OF PETROLEUM AND NATURAL GAS

Nearly all deposits of crude oil and natural gas are derived from organic matter, which was buried with sediments. Sediments hosting the source organic matter are typically fine-grained and display low permeability. Siliciclastic source rocks (clay and silt) are most common, but carbonate pelite and algal mats in evaporites are also economically significant (Katz 1994). Early diagenesis near the surface in still unconsolidated sediments produces much microbial methane (Figure 7.2), but this is rarely conserved. At larger depths, increasing diagenesis releases petroleum and wet gas from lipid-rich kerogen. Kerogen "spent" after oil generation, dispersed humic kerogen and bituminous coal are sources of dry thermogenic gas:

However, there are exceptions and an abiotic origin of hydrocarbons was repeatedly proven, although hardly ever concentrated to economic significance. Recently, Fiebig *et al.* (2009) demonstrated the abiogenic origin of volcanic-hydrothermal methane in the Aegean island arc. Modelling the composition (H_2O, CO_2, CH_4, H_2, CO, O_2 and C_2H_6) of the C–O–H fluid system in the Earth's mantle clearly shows that generation of hydrocarbons such as methane and ethane is perfectly possible (Zhang & Duan 2008). Long ago, degassing of the mantle as a source of methane was proposed for natural gasfields in Miocene volcanoclastic rocks ("green tuffs") of Japan. Clear mantle signatures mark the geochemistry of several oil deposits in China (Bing-Quan *et al.* 2001). Many oceanic serpentinites and gabbros contain traces of methane and other low-molecular paraffins, which are formed abiotically by Fischer-Tropsch reduction of CO_2 dissolved in convecting seawater and oxidation of Fe^{2+} in host rocks. This process is a by-product of the serpentinization of ultramafics that liberates large amounts of H_2. The methane-forming reaction between dissolved HCO_3^- and H_2 is catalytically accelerated by Ni-Fe or Fe-Cr phases (Foustoukos & Seyfried 2004). $\delta^{13}C$ values of this "catalytic" methane resemble biogenic gas (Horita & Berndt 1999), but at the Lost City hydrothermal field, methane $\delta^{13}C$ is much heavier (−9 to −14‰: Proskurowski *et al.* 2008).

7.2.1 Petroleum source rocks

Petroleum source rocks include any rock that may generate crude oil. Commonly, marine and lacustrine source rocks are distinguished, but because terrestrial organic substance is carried far into the oceans, petroleum sources of a transitional mixed character are quite frequent. Although not exclusive, black shales are the most common hydrocarbon source rocks apart from their metallogenetic role (cf. Chapter 1.3 "Sedimentary Ore Formation"). Global source rock horizons (e.g. Jurassic Figure/Plate 7.6) are the product of major perturbations of carbon and climate cycles caused by orbital forcing, endogenetic (plate tectonic) and exogenetic processes (Emeis & Weissert 2009).

Marine source rocks

Modern oceans hold an estimated 700,000 Mt of carbon as dissolved organic matter (DOC), more than biomass on land and a little less than carbon in the atmosphere. Phytoplankton converts atmospheric CO_2 to ~60,000 Mt/y of organic carbon, equivalent to plant growth on land; 95% of marine DOC is refractory, i.e. hardly bio-digestible. Annually, dead organisms and DOC, such as complex polysaccharides and humic acids, deposit ~300 Mt carbon in seafloor sediments. This compares to ~5500 Mt/y C extracted in the form of oil and gas. Of course, ocean productivity was much higher during hothouse states of the Earth, when source rock formation peaked. As a

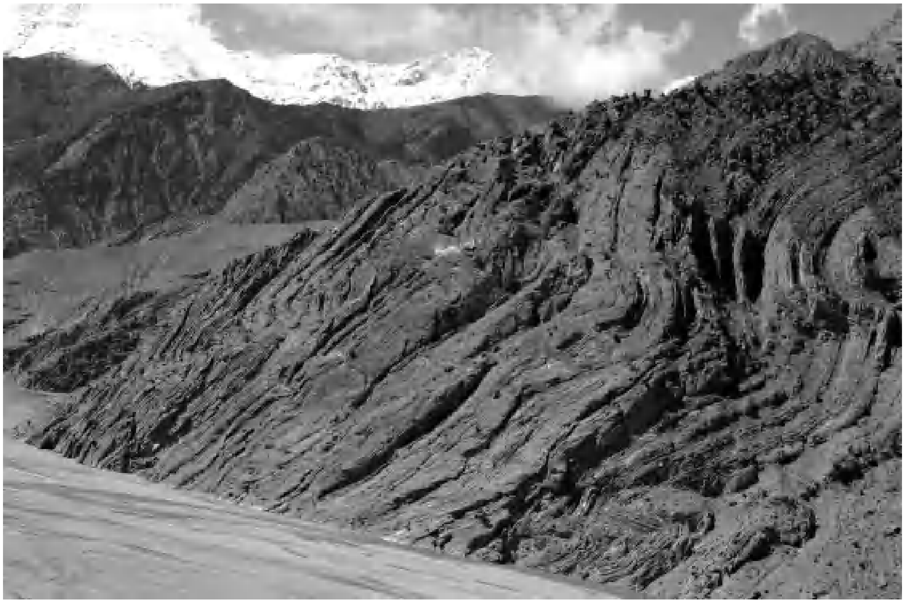

Figure 7.6 (Plate 7.6) Early Mesozoic bituminous rocks in the upper Kali Gandaki valley of the Annapurna-Dhaulagiri zone, western Nepal. This is part of the unmetamorphosed sediments of the Tethyan zone above the crystalline Greater Himalayan Sequence. Courtesy Krishna Karki, © Travel-to-Nature Asia. This image serves as a paradigm for hydrocarbon source rocks. Further up in the mountains, natural methane seepage feeds eternal flames in Jwala Mai temple.

consequence, all fine-grained marine sediments contain a fraction of organic matter. For its preservation, reducing conditions are required. A euxinic environment (i.e. H_2S dissolved in deep water) is not essential, but does promote high hydrogen contents. For the production of a good source rock, bottom sediments should certainly not be affected by oxidation. Low-energy seafloor areas provide favourable conditions. Marine clays display an average of 2.1% total organic carbon (TOC), carbonates 0.29%, but sandstone only 0.05%. Of course, sapropels (organic sludges) and comparable consolidated rocks include high TOC fractions and constitute important petroleum source rocks. In some regions (e.g. the Arabian Gulf), algal mats in evaporitic sediments such as dolomites, sulphates and salt generated much oil. Evaporites display typical lamination, which reflects periods of higher and lower salt concentration (cf. Chapter 4.2.2 "Environments of Evaporite Formation in the Geological Past"). At lower salinity, halotolerant organisms (mainly cyanobacteria and algae) flourish in surface water (Figure/Plate 4.12). The characteristic thermal and density stratification of brine pools favours anoxic conditions at depth and preservation of organic matter (Warren 2006).

A Holocene example of sapropel formation is the Black Sea. At ~7000 years BP, the previously dry basin was flooded with saline water through the Bosporus. The water inflow caused a burst in surface-water productivity, inducing anoxia and preservation of organic matter (Arthur & Dean 1998). This initiated deposition of finely laminated black mud, which contains 23–35% organic substance and a maximum of 10% soluble bitumen. Incidentally, this event is possibly the background to the Biblical flood narrative. Since ~5500 years BP, organic productivity is reduced but even today, black sapropel is laid down in two deep (>2000 m) basin centres around which marine currents revolve. Annual couplets comprise one clay and one TOC-rich varve. Generally in euxinic basins, higher organisms thrive in the upper, oxic seawater layer. Dead phyto- and zooplankton drifts to the seafloor, traversing the deep anoxic H_2S water layer. Remember that the term "euxinic" is derived from the Roman name of the Black Sea, *Pontus euxinus* (the hospitable sea).

Sedimentation of organic particles and refractory DOC is only one path of organic carbon (C_{org}) enrichment. During early diagenesis, dissolved C_{org} may be adsorbed to clay minerals and incorporated into interlayers of smectites and smectite-illite minerals (Kennedy *et al.* 2002). H_2S and HS^- in the pore fluids cause an early diagenetic "vulcanization" of the organic substance, preventing bacterial decomposition but increasing sulphur contents. Sapropels and sapropel rocks display a characteristic trace element composition (cf. Black Shales in Chapter 1.3 "Sedimentary Ore Formation Systems"). Vanadium and nickel have a special role, because these elements complex with porphyrins, which are transferred into crude oil. During oil generation and migration, the V/Ni ratio remains unchanged and allows correlation of the whole cycle from source rocks to petroleum, oil seeps and natural asphalt (Hunt 1996).

Petroleum source rocks are not restricted to confined marine basins. Upwelling of cold, phosphate-rich water in oceans causes a synergetic increase of life, which delivers a large mass of organic matter into bottom sediments (cf. Chapter 3 "Phosphates"). Fluvial import of nutrients into shallow warm epicontinental seas promotes organic production and deposition in platform sediments. Warming of the oceans in greenhouse periods of the Earth's past, for example in the Cretaceous with its much higher sea levels, may trigger ocean-wide mass production and associated anoxic conditions at the bottom. Resulting sediments with elevated organic matter fractions are termed "oceanic sapropels" in contrast to the confined euxinic facies. Even a rather ordinary TOC content of marine sediments of ~1.5% can be the source of oil deposits, although after the oil-generating stage, most good source rocks have residual TOC values between 2 and 3%. The loss of organic carbon in source rocks is correlated to increasing diagenesis, due to formation and expulsion of petroleum and gas. The loss is measurable by the C/S ratio, which decreases with increasing diagenesis. Source rock sulphur is immobilized early, mainly in pyrite, so that it constitutes a reference for the diagenetic mobilization of organic carbon. Oil from purely marine organic substance is typically sulphur-rich, low-wax, dominated by naphthenes, aromatics and short-chain (liquid) normal paraffins.

Lacustrine oil source rocks

Both saline and freshwater lakes often display stages of high organic production leading to formation and preservation of sapropelic sediments, supported by thermal and density stratification. Modern examples include the great lakes in Central and Eastern Africa (Johnson *et al.* 1996). Well-studied ancient equivalents are the Tertiary lakes of Colorado, Utah and Wyoming, with oil shales of the Green River Formation (Meyers 2008; cf. Chapter 3 "Sodium Carbonate"). Coals and coal measures can source petroleum, although restricted by the relatively low hydrogen content of most coals, and the relative rarity of sapropelic (hydrogen-rich) coal, which is estimated at <10% of world coal mass (Law & Rice 1993). In laboratory experiments, the quantity of expelled oil correlates directly with the hydrogen content of coal (Hunt 1996). In nature, liquid bitumen generated is largely retained in the coal (Taylor *et al.* 1998). However, several oilfields in the world are derived from coal, for example in northwestern China from Jurassic coal, which is not even especially rich in liptinite (Shao *et al.* 2003). Petroleum derivation from terrestrial organic matter in marine rocks is common, for example in the offshore Gippsland Basin of southeastern Australia. The source of Gippsland oil and gas is the Tertiary Latrobe Formation, which contains the giant onshore lignite deposits (Figure 6.12). Compare this with Amazon River, which exports 70 Mt carbon per year into the sea. Freshwater and brackish-water organic substance is prone to form low-sulphur and high-wax oil (containing pasty long-chain paraffins). Waxy paraffins are inherited from waxes that land plants use to protect their external surface. High-wax oil is very common and attests to the large share of land-derived organic matter in coastal marine sediments.

With sufficiently detailed geochemical data (Hunt 1996), nearly all oil deposits can be matched with specific source rocks. The world's largest petroleum deposit, Ghawar in Saudi Arabia, and many other accumulations in the Middle East are derived from Late Jurassic evaporitic-sapropelic strata (Kulke 1994). Oil of the Maracaibo Basin in Venezuela is sourced from the Late Cretaceous La Luna Formation (Mongenot *et al.* 1996) and the giant heavy oil belt (640 × 60 km) in east Venezuela from the Cretaceous Querecual series. In Europe, Early Jurassic Posidonia Shale (Toarcien), Late Jurassic Kimmeridge Shale (especially in the North Sea) and laminated Early Cretaceous mudstones are prominent source rocks that have been correlated with numerous oilfields (Littke 1993). Oils generated from lacustrine source rocks (e.g. Singliao and Bohai Basins) represent ~95% of all petroleum resources in terrestrial China.

7.2.2 Dry gas source rocks

Methane source rocks are mainly coal seams, clastic sediments with dispersed humic particles and so-called "post-mature" kerogen, which is beyond the stage of generating oil and wet gas (Rice & Schoell 1995). Deeply buried shales may produce gas from oil when heated above the stability boundary of petroleum (at ~160 °C) where it is thermally decomposed. This methane may remain *in situ* as in Barnett Shale or migrate away (Tian *et al.* 2008, Pollastro *et al.* 2007). The world's largest dry gas field, South Pars (Iran)– North Field (Qatar), is supposedly sourced from deeply buried Early Silurian marine shales rich in kerogen type II (Aali *et al.* 2006). The trap is a large arch trending northwards across the Arabian-Persian Gulf and the reservoir is formed of Permo-Triassic carbonates sealed by evaporites.

A remarkable number of gasfields in the world are derived from coal. Beginning at ~37% volatile matter or 0.8% vitrinite reflectance, profuse amounts of methane (with some ethane, propane, butane) are generated from coal as coalification progresses (Figure 7.7). Much of the gas moves away through pores, joints and faults of country rocks towards the surface and dissipates in the atmosphere. Some may be trapped in appropriate structures. Gas that remains adsorbed in coal is part of the important energy resource of *coal bed methane* (CBM).

Near-surface kerogen-rich rocks flooded by meteoric water may host considerable gas deposits, which are generated by microbes (McIntosh *et al.* 2004; cf. Antrim Shale). Shallow and deep "gas shales" are both source and reservoir. Because of recently developed novel extraction technologies, natural gas hosted in shale of low permeability emerges as a vast new resource.

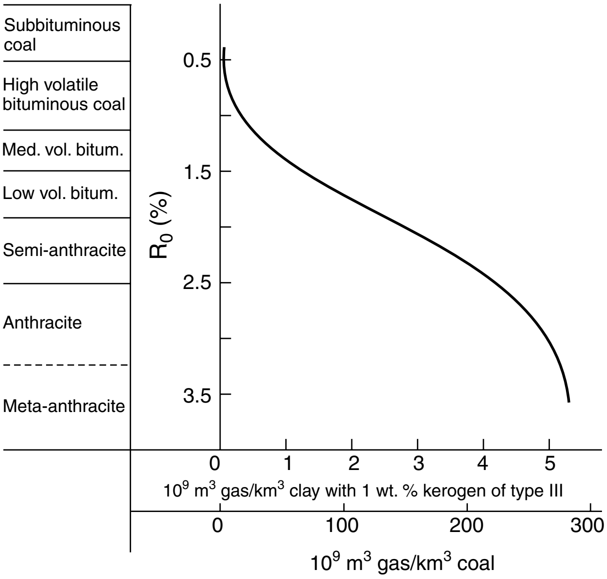

Figure 7.7 Cumulative methane production of a clay rock with 1% vitrinite or of massive coal (lower scale), as a function of increasing rank (modified after Glennie 1998). Data like this allow appraisal of total gas production of a basin provided that kerogen and coal mass can be estimated and maturity (rank) is known.

7.2.3 Eogenesis and catagenesis of kerogen

Eogenesis is the early and near-surface process system that includes biological, chemical and physical alteration of minerals and organic matter in rocks. It ends when the rock is heated to above ~50 °C and temperature takes over as the dominant driving force. Eogenetic processes include reduction, compaction, dehydration, some geochemical dissolution and reprecipitation, and biogenic gas generation. Organic matter in the rocks is transformed into kerogen. Note that the term "diagenesis of kerogens" (Tissot & Welte 1984) is sometimes used to describe the eogenetic stage. This usage can be misleading because diagenesis of sediments extends to ~220 °C. "Eogenesis" is preferable because it is clear without ambiguity.

Catagenesis comprises all processes that act on rock matrix and organic matter after considerable burial and that result in petroleum generation. Higher pressure and temperature (~50–200 °C) are essential factors of change. The main result of catagenesis is the generation of oil and wet gas (Figure 7.8) while kerogen "matures". At the same time, source rocks are altered, for example by darkening, disappearance of fine lamination and formation of a dense network of micro- and macro-cracks, which are filled by fluid-precipitated minerals and bitumen (Littke 1993). The morphological properties of kerogen macerals are increasingly lost. However, contents of typical source rock/black shale trace metals do not change measurably (Mongenot *et al.* 1996).

Eogenesis

Eogenesis, the early diagenesis of organic substance is essentially a biochemical process. Initially, anaerobe microbial fermentation produces methane (biogenic gas), water, CO_2 and kerogen (Figure 7.8). Two stages can be distinguished: i) an initial bacterial enzymatic conversion of easily digestible organic substance into H_2 and CO_2 is followed by ii) reduction of CO_2 that is dominated by methanogenic *archaea* (eq. 7.3).

Microbial methanogenesis by reduction of CO_2:

$$CO_2 + 4H_2 \rightarrow 2H_2O + CH_4 \qquad (7.3)$$

Isotope data suggest that much hydrogen of biogenic gas is derived from formation water (Martini *et al.* 1996). Economic deposits of eogenetic gas are rather rare because it is re-oxidized by synbiotic consortia of methane-oxidizing archaea and sulphate-reducing bacteria (Delong 2000). However, in low-sulphate environments, such as kerogen-rich rocks flooded by meteoric water (McIntosh *et al.* 2004), generation of considerable

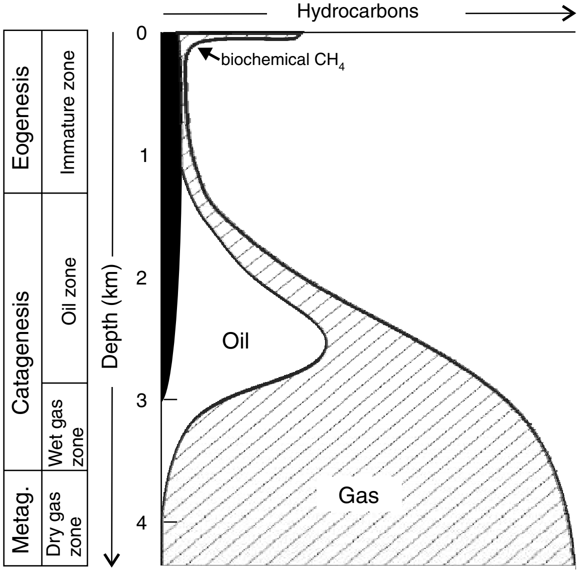

Figure 7.8 Formation of oil and gas during eogenesis (<50 °C), catagenesis (~50–160 °C) and metagenesis (~160–250 °C) of kerogens in sediments (modified from Tissot & Welte 1984). With permission from Springer Science + Business Media. Black area indicates the presence of "geochemical fossils", i.e. biological markers. Depth limits depend on the local geothermal gradient and other factors.

gas deposits is possible. About 20% of the world's gas resources may be of microbial origin:

> The Antrim Shale (Late Devonian, Michigan Basin, USA) is an outstanding example of biogenic methane formation long after sedimentation of the source rocks. The shale contains up to 20% of low-maturity organic substance derived from algae. Daily, >5000 wells pump $1.2 \times 10^7\,m^3$ gas from <600 m depth. The shale is both source and reservoir rock. Gas resources are estimated at $10^{12}\,m^3$ methane. Flooding of basin-marginal shale with meteoric water to ~200 m below the surface and consequent dilution of basinal brines favoured microbial degradation of kerogens and hydrocarbons in the shale (McIntosh *et al.* 2004). Pleistocene ice cover and increased hydrostatic head are thought to have acted as a seal retaining methane in the shale. ^{14}C dating implies a Late Pleistocene age of methanogenesis (<22,000 years; Martini *et al.* 1996).

Catagenesis

At ~50 °C (and ~1500 m overburden, the precise depth being a function of the local geothermal gradient), eogenesis changes without a break into catagenesis. Geochemical processes generate petroleum and thermogenic gas from kerogen. Catalysis by clay minerals, especially montmorillonite, may have a role. The mature, i.e. oil-generating kerogen loses its capacity to yield petroleum at ~160 °C (~5500 m depth). Only gas is generated at higher temperatures (Figure 7.8). This may not be simply due to continued heating of post-mature kerogen. Catalysis by transition metals (e.g. Ni, V) is assumed to amplify the action of heat (Mango *et al.* 1994). The stage of dry gas production between ~160 and 250 °C is called "metagenesis" (Tissot & Welte 1984). In it, the organic substance is increasingly transformed into pyrobitumen, graphite and gas. Organic metagenesis equals the highest grade of rock diagenesis and constitutes the bridge to metamorphism.

Like coalification, the generation of hydrocarbons from kerogen is described by the Arrhenius equation as a series of decomposition reactions (eq. 6.3, c.f. Chapter 6.3 "The Coalification Process"). Temperature constitutes an exponential factor and the kinetic factors E and A are measured in laboratory experiments by heating the source rock at various temperatures and recording the yield of hydrocarbons (Hunt 1996). Applying the method, it was soon recognized that the classical four kerogen types (Figure 7.4 and Figure 7.5) must be further subdivided for a correct simulation of burial, maturation and hydrocarbon yield in nature. Reaction rates of subtypes diverge widely. Also, other factors modify maturation, including elevated organic sulphur concentrations that lower the onset of oil generation (Lewan 1998), reactions with minerals of the source rocks and with pore fluids. The participation of ubiquitous pore water in the reactions is facilitated by disproportionation (eq. 7.4).

Disproportionation of water as a source of hydrogen for HC-generation from kerogen:

$$H_2O_{(liqu)} \leftrightarrow H_{2(aq)} + 0.5O_{2(aq)} \tag{7.4}$$

Diagenesis consumes oxygen, mainly by oxidation of Fe^{2+}, but also by formation of much CO_2 liberating hydrogen. The hydrogen may react with kerogen and generate hydrocarbons, even if the kerogen has already lost most of its inherent hydrogen. This "extraneous" hydrogen is thought to considerably enlarge the generation potential of kerogen (Seewald 1994).

Recently, a voluminous study based on thermodynamics presented a novel approach to the theory of petroleum generation (Helgeson *et al.* 2009): Kerogen maturation is modelled as a series of oxidation/reduction disproportionation reactions. Mature kerogen melts incongruently with increasing burial to produce crude oil, CO_2 gas and a kerogen with lower H/C. Depleted kerogen reacts with any water present by hydrolytic disproportionation to produce new kerogen with higher H/C and CO_2. The study is innovative and rigorous. It confirms part of the prevailing kinetic models and their application. Some conclusions of Helgeson *et al.* (2009) are thought-provoking, for example the suggestion that 75–80% of oil generated remains trapped in source rocks.

The characteristic temperature and depth ranges of hydrocarbon formation described in the preceding text (and in Figure 7.8 and Figure 7.9) are only indicative. The maturation of kerogen is

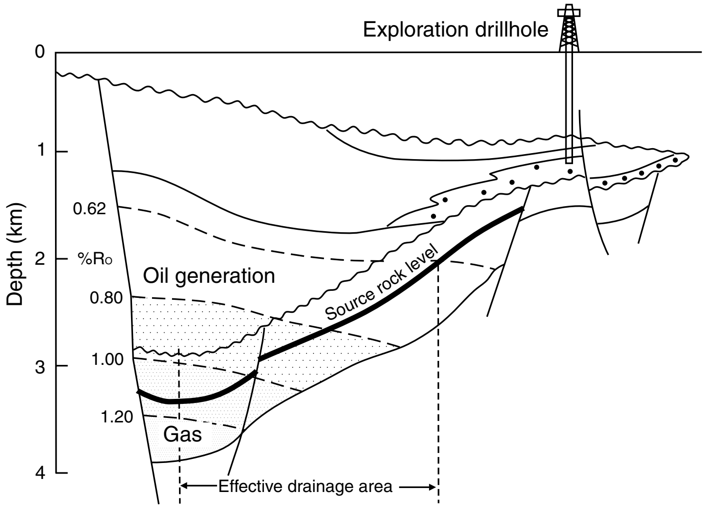

Figure 7.9 Profile of a simple petroleum system (time not shown): A hydrocarbon-producing depression, or "kitchen", displays a steeply dipping source rock layer that exhibits immature, mature and post-mature portions (modified from Hunt 1996). Maturity is depicted by vitrinite reflectance in oil immersion (R_o). Oil generation is thought to start at $R_O = 0.62\%$, and gas with condensate below $R_o = 1.0\%$. Hydrocarbons migrate upward and collect in a structural trap. The effective drainage area is delimited by sufficient maturation and geological constraints of fluid flow.

controlled by factors such as mentioned above, but also by physical criteria (e.g. overpressure delaying maturation; Carr 1999). The heating rate is a strong control on the evolution of vitrinite reflectance and hydrocarbon generation: Rapid heating accelerates petroleum formation compared to vitrinite reflectance and the reverse is observed for slow heating (Mukhopadhyay 1992). The consequences of the multiple controls are quite variable depths and temperatures of hydrocarbon formation in different provinces:

> Considerably higher heat flow is characteristic for marine rift basins compared with ordinary epicontinental sedimentary basins. A present example is the Gulf of California straddling the Pacific-North America plate boundary, where submarine hydrothermal vents produce abundant gas bubbles and drops of petroleum, which reach a diameter of 2 cm. Barite is precipitated around the vents, but the hydrocarbons are quickly dispersed Above a synrift metamorphic-igneous crust (Dorsey 2010), the basin contains young sediments with a total thickness of <500 m, which should exclude hydrocarbon generation. The sediments are, however, heated to >315 °C at a low pressure of only 200 bar. It is assumed that this setting is an exceptionally efficient environment of oil generation. Similar observations are reported by Svenson *et al.* (2007) from the nearby Salton Sea geothermal field and by Mark *et al.* (2010) for the UK Atlantic margin. The North Sea oil and gas province displays parallels to the Gulf of California: The Viking Graben, a major hydrocarbon kitchen in the province, was formed by extensional tectonic movements related to the opening of the Atlantic Ocean, which lasted throughout the Mesozoic. Higher heat flow between the Mid-Eocene and the Pliocene caused profuse hydrocarbon generation. The Ekofisk field was filled from an oil window at 3–5 km depth (Glennie 1998). Further to the North, in the Atlantic Ocean off Norway at about the latitude of Iceland, thousands of large fluid escape pipes occur that were probably formed at the dawn of the Eocene ($\sim$55 Ma). In this region, basaltic sills intruded TOC-rich Cretaceous-Palaeocene sediments at a depth of 1–3 km. The sudden heating of the sediments (<10,000 years) liberated giant amounts of methane, which possibly triggered the extreme global greenhouse climate of the Early Eocene (Svensen *et al.* 2004).
>
> With 6–12 km, the oil kitchen in the southern Caspian Basin (Azerbaijan) is unusually deep. The basin fill consists mainly ($\sim$10 km) of Pliocene and Pleistocene under-consolidated sediments and displays a very low geothermal gradient (Feizullayev *et al.* 1998).

7.2.4 The oil window

We have seen that oil generation may take place at shallow or at deep levels, and that the effect of temperature is exponential. The only true measure of kerogen maturity in reference to oil generation is its chemical composition determined by pyrolysis techniques such as Rock-Eval (Figure 7.5). Vitrinite reflectance and the fluorescence of liptinites provide an approximation. The oil window is the stage of maturation dominated by oil generation from kerogen ("catagenesis", Figure 7.8). The upper boundary of the oil window where petroleum generation begins varies between a vitrinite reflectance of 0.3 and 0.7% (Ro). The lower boundary of the oil window is usually between 1.0 and 1.3% Ro, where condensates and wet gas take over (Figure 7.9). The wide span of these figures is also due to the very different generation behaviour of kerogen types and subtypes.

The precise maturity of source rocks and their upper and lower oil window boundaries must be determined as a base for petroleum system analysis (cf. see below). In order to understand the relations of oil generation with migration and traps, the fate of the source rocks in geological time needs to be reconstructed and the generation time span fixed. The construction of the required time-temperature-generation history of a source rock comprises the combination of burial history ("geohistory") data with Arrhenius equation kinetics. The crucial input is thermal history. Time-temperature index graphs (Hunt 1996) and three-dimensional computer programs (Schneider & Wolf 2000) are based on quantitative burial models and Arrhenius parameters A and E determined by laboratory methods such as hydrous pyrolysis.

Some authors discuss the term oil window regarding the stability boundaries of petroleum. In this interpretation, the upper boundary is given by the many destructive processes, which affect oil near the Earth's surface (see below). The lower boundary is postulated at $\sim 160\,^{\circ}C$ where oil enters the field of thermal decomposition (cracking). In a first stage of cracking, C_{2-5} wet gases are produced. The second stage results in methane and pyrobitumen, and ends with dry gas, which may remain *in situ* or migrate away (Tian *et al.* 2008). Cracking generates vast amounts of methane that cause supralithostatic pressures and reservoir fracturing, confirmed by observations in pyrobitumen deposits. Increasing contents of diamondoids are a mark of deep thermal cracking of oil. Diamondoids reach a maximum concentration at about $R_o > 4.0\%$ and are decomposed at higher temperatures (Zhibin *et al.* 2006). Determination of diamondoids helps to predict the deepest oil deposits in a given district. This is, of course, of highest economic interest.

7.3 FORMATION OF PETROLEUM AND NATURAL GAS DEPOSITS

During maturation, the natural hydrocarbons exude from dispersed kerogen particles in source rocks. Tiny droplets move into nearest pores of the host sediment. Source rock-hosted oil is hardly ever exploitable but *in situ* gas was recently discovered as a giant new resource. Conventional deposits of hydrocarbons were formed by oil and gas moving out of the source rock, migrating some distance and collecting in the reservoir space of a trap structure. Fluid expulsion and migration are initiated and sustained by heating, compaction, maturation and dehydration of source and host rocks. Similar to coalification, the oil generation and migration phase is rather short, measuring in millions to tens of million years. An interesting aspect is the efficiency of the system, expressed by the ratio of known oil deposits to the estimated total generated petroleum. The efficiency factor is commonly not more than 0.1–1%, higher figures are rare (e.g. 5–6% in the Arabian Gulf, 10% in the Maracaibo Basin).

Clearly, the formation of oil and gas deposits is the product of favourable combinations of subsystems, including source rock formation, burial and heat flow, maturation, tectonic deformation, migration and the presence of reservoir rocks and traps. The subsystems combine to form complex master systems that have been called "oil play", or "petroleum system" (Magoon & Dow 1994, Figure 7.9). Once formed, petroleum deposits may be exposed to thermal, microbial or tectonic events, which often cause detrimental alteration or even total destruction of hydrocarbon accumulations (Figure 7.10).

7.3.1 Migration

Comprehension of hydrocarbon migration from the source rock into traps is enhanced by application of hydrogeological concepts and models (Verweij 1993). Geological and geochemical data

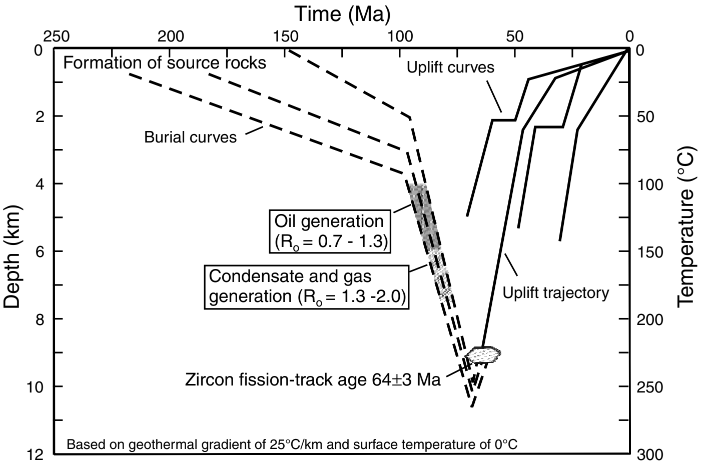

Figure 7.10 Sedimentation, burial, and hydrocarbon generation in the foreland of the Brooks Range, Alaska modelled in a temperature-depth-time diagram (modified from Parris *et al.* 2003). Oil and gas were generated before the source rocks reached peak temperature (250 °C at 10 km depth). The chance to find surviving oil and gas deposits is small, except if the hydrocarbons migrated away into shallower parts of the basin.

document that in some cases oil and gas migrated for horizontal distances of hundreds of kilometres and that other deposits originated by very short vertical migration. Compaction, heating, maturation and dehydration generate the fluid flow that is controlled by pressure (head) differences and rock permeability. Flow vectors generally point upwards and to basin margins. In the fluids, hydrocarbons are transported in dispersed and dissolved form. Apart from physical flow, diffusion acts on hydrocarbons. Because of its limited transport capacity, however, diffusion's role is insignificant, except for natural gas deposit formation.

Note that "hydrocarbon fluids" are a variant of diagenetic fluids and share most of the properties that are described in Chapter 1.4 "Diagenetic Ore Formation Systems". Fluids consist essentially of hot water with dissolved inorganic and organic matter. A hydrocarbon fluid may be dominated by an oil phase if very dense kerogen-rich rocks containing little water such as pelitic carbonates subside to oil generation depth. In this case, light hydrocarbons exuded from kerogen cause a rise of internal pressure (generation pressure) in the rocks. Oil and water in the pore fluids expand with heating. Liberation of CO_2 and organic acids from kerogen provokes dissolution and recrystallization of carbonate (Heydari & Wade 2002). All these processes create temporary permeability, which allows drainage of oil and gas.

Rock permeability is not only a function of intrinsic rock properties such as pore space and connectivity, but also of physical properties of the fluid (eq. 7.5). This has the consequence that light (low-viscosity) oil flows readily, whereas heavy (high-viscosity) oil in the same rock hardly moves. In the oil industry, permeability is usually expressed in Darcy units (1 Darcy equals an intrinsic permeability $k = 10^{-12}\,m^2$). Reservoir rocks in oil deposits typically have permeabilities in the range of tens to thousands of mD (millidarcy); the minimum permeability for conventional gas deposits is 0.1 mD. Halitites and very dense clayrocks display the lowest permeabilities of all rocks, down to about $k = 10^{-23}\,m^2$.

Permeability k_{fluid} of rocks for fluids of different density and viscosity:

$$k_{fluid} = (k \cdot \rho_f)/\mu \qquad (7.5)$$

k = intrinsic permeability of the rock (m^2), ρf = density of the fluid (g/cm^3), μ = dynamic viscosity of the fluid (water at 10 °C: $\mu = 1.31 \cdot 10^{-6}\,m^2/s$).

The migration of oil and gas from source rocks into permeable country rocks is called "primary migration" (Levorsen 1967). Early and late primary migration are distinguished:

1 The first occurs during the principle phase of compaction and dehydration (eogenesis), which mainly moves water out of the system, before the source rock reaches maturity. Oil or gas deposits hardly ever form at this stage.
2 Late primary migration takes place while oil and gas form from kerogen (catagenesis). At the

onset of catagenesis, water content in fine-grained rocks is already very low. Therefore, volume expansion of expelled hydrocarbons is probably the main driving force.

"Secondary migration" (Levorsen 1967) describes the flow of hydrocarbons in permeable country rocks. Because permeabilities vary, even within one bed, preferential flow paths evolve that may be envisaged as streams or rivulets. Subtle traces of the passage of hydrocarbon fluids are recorded, including residues of hydrocarbons in pores and in fluid inclusions of pore cement, thermal alteration (because deep fluids are hotter) and reduction of Fe^{3+} replacing haematite and goethite with magnetite. The hydrocarbon fluids themselves are altered by reactions with the host rocks, for example by loss of CO_2, which precipitates pore-cement calcite. Hydrocarbon fluids may be fractionated by density (because higher density causes lower flow velocity) or by degassing (evaporative fractionation). Fluid inclusions in diagenetic cements containing oil and gas provide evidence on timing and physical conditions of hydrocarbon migration (Mark *et al.* 2010). Oil saturation is estimated by counting the frequency of hydrocarbon inclusions (Lisk *et al.* 2002).

In some instances, petroleum migrated across layering in sedimentary basins. If beds of low permeability are present, this observation is counterintuitive and always requires careful investigations. Often, faults explain the connectivity, but faults may be either highly permeable fluid conduits (Haney *et al.* 2005) or impermeable barriers.

Migrating hydrocarbons are trapped when the fluid flow meets an adequate structure. Trap structures consist of a permeable reservoir rock, which is open to receive fluids but is semi-closed by impermeable seal rock. The best seals are gas hydrates, evaporites and shale, but dense sandstone or saline dolomite may suffice. The separation of hydrocarbons from an aqueous fluid flow can be envisaged as oil and gas bubbles floating up into a cupola-shaped trap and the water passing on underneath the base ("spill plane") of the cupola (remember that conventional crude oil is lighter than water).

Within the cupola of the trap structure, the components of the hydrocarbon fluids separate as a function of density, resulting in water at the bottom, overlain by layers of oil and gas. The boundaries of the density stratification are generally planar but not necessarily horizontal, as in Figure 7.11. Capillary forces and wetting

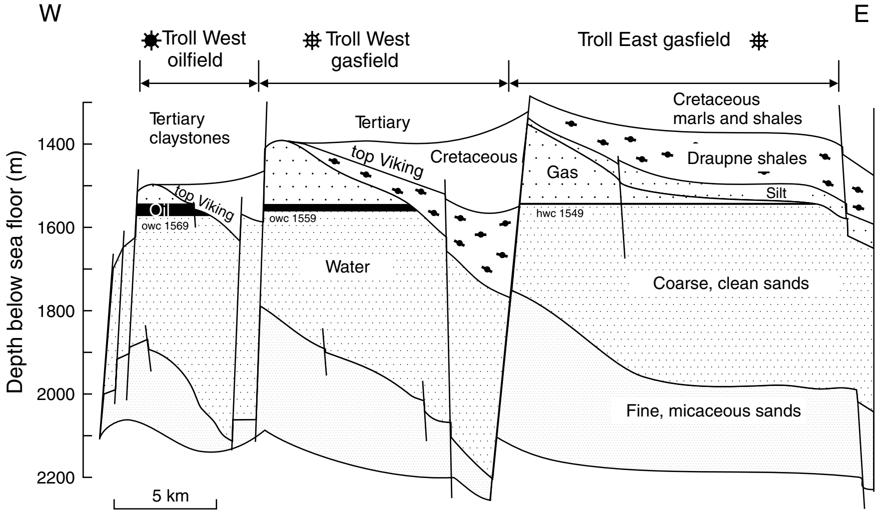

Figure 7.11 The offshore gas field Troll ca. 80 km northwest of Bergen, Norway contains giant gas reserves and considerable oil. Production is expected to last until about the year 2050 (Bolle 1992). The field lies on the eastern flank of the Jurassic Viking graben, in sandstones of the Middle to Late Jurassic Viking Group. Source rocks are Kimmeridgian Draupne shales in deeper parts of the graben in the West. owc = Oil/water contact, hcw = Gas/water contact with 0–4 m oil. Note that the horizontal scale is strongly shortened.

properties of the fluids often inhibit complete separation, resulting in gradual transition of relatively clean gas, oil and water through zones of mixed pore fluids.

$^{40}Ar/^{39}Ar$, Pb-Pb and ^{187}Re-^{187}Os dating assist to determine the time of migration and emplacement of hydrocarbons (Mark *et al.* 2010, Selby & Creaser 2005). Uranium, rhenium and osmium are enriched in organic matter of source rocks and are transferred into the hydrocarbon fluids. Geochemical markers provide estimates of the migration distance ("oedometers", Isaksen 1996).

The term "tertiary migration" is sometimes used for the flow of oil from a first into a second trap (Lisk *et al.* 2002) or its drainage to the surface, usually caused by tectonic events. In upflow channels, pressure release may lead to precipitation of pyrobitumen, ozocerite or asphalt. Rising light hydrocarbons, mostly methane, mixed with overpressured formation water erode the walls of flow paths and form mud volcanoes at the surface. Oil may reach the surface and form conspicuous oil seeps and asphalt lakes (e.g. Trinidad). Submarine seeps are ubiquitous, for example in the Gulf of Mexico. They are islands of rich life on the desert-like bare seafloor. In the Gulf, colonies of *Mytilus* and tube worms characterize the seep locations. Bubbles of gas and oil drops rise from the seeps, asphalt and gas hydrates occur nearby. On the surface of the sea, natural oilfilms produced by the seepage can be mapped in satellite images (MacDonald *et al.* 2004).

7.3.2 Reservoir rocks

Reservoir rocks of oil and gas deposits must be: i) porous (with a large volume for storing hydrocarbons); and ii) permeable in order to allow economic extraction. To be effective, porosity requires sufficient connectivity between pores. Porosity and permeability of rocks are measured *in situ* (by geophysical probes) and on core samples in the laboratory. In the laboratory, *in-situ* stress conditions are simulated because the samples expand during drilling and extraction. Generally, porosity and permeability decrease with increasing geological age and depth, as the grains are forced into a denser packing pattern. This is described by an exponential porosity reduction model; note, however, that there are exceptions to this rule (Davies 2005). The formation of pore cement is a frequent cause of lower than expected permeability and pore space. Typical petroleum reservoir rocks display porosities of 10–40 vol. % and permeabilities of tens to thousands mD. Exploitable gas deposits have a minimum porosity of 7 vol. % and a permeability >0.1 mD. Even lower permeabilities characterize so-called "unconventional" gas resources in tight sandstones and shales. Note that in this case, the gas is retained in its low-permeability source rock. Tight gas is increasingly redefined as a profuse and valuable resource. The key to this development are improved drilling and fracturing technologies.

The most frequent and economically important reservoir rocks are sand, sandstone, limestone and dolomite. Many other rock types have been found to host oil and gas deposits, such as fractured shale and chert (California), mafic intrusions (Texas), weathered granite regolith (Panhandle-Hugoton field in Texas) and Precambrian gneiss offshore of the Shetland Islands. Permian volcanics enclose gas in Northern Germany, as do the Miocene Green Tuffs in Japan. Worldwide, coal seams are economically significant gas reservoirs (CBM).

Porosity and permeability of sand are mainly determined by grain diameter and grain size spectrum, but also by grain shape and the packing of grains. Newly deposited sand has a porosity of 40–42%, which decreases during burial until at $\sim$2500 m depth a minimum of $\sim$26.5% is reached (Figure 7.12). Coarse sands often have higher porosities than finer sands. Well-sorted sands, such as aeolian dune deposits (e.g. Rotliegend sands hosting gas in Northern Germany, The Netherlands and the southern North Sea), display a higher porosity and permeability compared to sand with a broad grain size distribution. In the latter, small grains occupy pore space between the larger grains. The permeability depends on the diameter of connections between pores and on surface properties of the pore space. Reservoir sands of the giant Troll gasfield in the North Sea (Figure 7.11) for example, have 17–36% porosity and permeabilities of 0–10 Darcy.

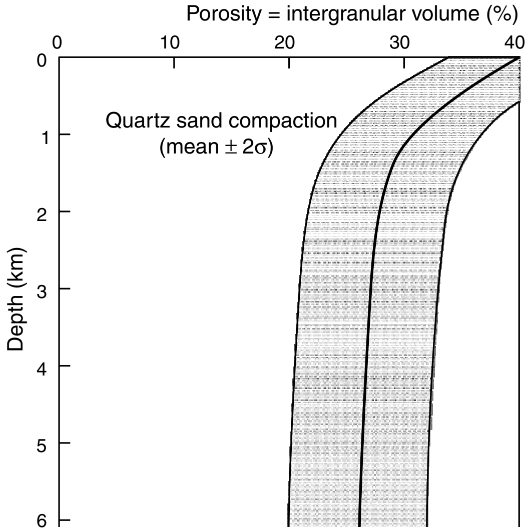

Figure 7.12 Compaction of quartz sand with increasing burial, in the absence of pore cement (Paxton *et al.* 2002). Curves depict the mean and ±2 standard deviations. Below ~2500 m depth, very little further compaction takes place.

Sandstones are characterized by partial or complete cementation of the pore space. Cements are usually quartz, K-feldspar, calcite or clay minerals. At very small porosities, the formation of oil or gas deposits is not possible. In certain regions of Northern Germany, illite cement in aeolian Rotliegend sands inhibited production of locked-in gas. In the southern North Sea, the same sands are impaired by anhydrite and barite cement, where faults allowed mixing of fluids derived from Zechstein evaporites and Carboniferous coal measures. When cement reduces permeability of pore throats but a sizeable pore space is filled with hydrocarbons, technical measures may enable extraction (e.g. acid treatment, hydraulic fracturing). Pore space filled with oil or gas is not accessible for later cement-forming fluids (e.g. in the Athabascan oil sands), in contrast to the water-filled reservoirs rocks beneath the oil. This explains cases of widely different permeability and porosity of the same rock in oil zones compared to aquifers below the oil-water contact.

Important aspects of sand and sandstone reservoirs include the original palaeogeographical and sedimentary setting, and depositional variations that need to be fully understood in order to determine the optimal pattern of drilling and extraction. These subjects are treated extensively in sedimentology books (Nichols 2009).

Carbonate reservoir rocks equal sand and sandstone in economic significance. Because calcite and dolomite are much more soluble than quartz, the diagenetic and petrophysical evolution of limestone and dolostone is more complex compared with sandstone. Reef rocks make outstanding reservoirs with primary porosities reaching 80%. Carbonate reefs are remarkable as one of the few sediments directly built as solid rock, not unconsolidated granular material. However, the high primary porosity and permeability of reefs favour the repeated passage of fluids (meteoric, marine, diagenetic and formation waters), which often leads to a complex history of solution and cementation events. The vuggy and fractured Oligocene-Miocene Asmari limestone of southern Iran, Permian reefs in Western Texas, Late Devonian reefs in Western Canada and the Ordovician Tazhong reef in the Tarim Basin, China (Zhou *et al.* 2009) are famous reservoirs. Karst cavities in limestone may be filled with oil, as in the submarine Rosso Mare field near the eastern coast of Italy. Pure and massive carbonates are normally too dense to be good reservoirs but there are exceptions such as the Late Cretaceous chalk in the central North Sea with the giant Ekofisk oilfield. Ekofisk chalk developed a dense network of microfractures when active diapirism of Permian salt at depth produced tensional domes (Glennie 1998). Elsewhere in the North Sea, Cretaceous chalk acts as a seal. Although primary porosity in carbonates is often lost by mineral precipitation, several diagenetic processes may produce secondary porosity. Calcite in dolomite, for example, is dissolved by CO_2 and carboxylic acid-rich hydrocarbon fluids (Seewald 2003), producing important reservoir horizons such as the upper portion of the Neogene Asmari Formation in the northern Arabian Gulf and southern Iran, and Late Cretaceous carbonates from Iraq to Qatar (Sadooni & Alsharhan 2003). Dolomitization of limestone reduces the volume of solids by 13%, increasing the porosity of the bulk rock mass. Secondary dolomites form metasomatic bodies of a friable crystalline (saccharoidal) nature near unconformities, faults and fractures. With porosities exceeding 30%, such rocks are world-class reservoirs, from the Middle East to Alberta, Canada.

Not unlike sand and sandstone reservoirs, the original palaeogeographical and sedimentary setting, and depositional variations of carbonate reservoirs must be investigated. At least as important, however, is the study of diagenetic evolution in time and space.

7.3.3 Petroleum and gas traps

Reservoir rocks allow flow of hydrocarbons by buoyancy and hydrodynamic forces. In order to halt flow and concentrate hydrocarbons from the dilute flow, the reservoir must be half-closed by rocks of low permeability (the "seal"). The efficiency of the seal is a function of its geometry, integrity and sealing capacity (controlled by capillary pressure: Vavra *et al.* 1992), or in different terms, its permeability (Luo & Vasseur 1997, Schlömer & Krooss 1998). The widely varying forms of hydrocarbon traps capped by a seal may be generalized as bell-shaped. In the context of "oil and gas traps", or structures, the word "structure" has no connotation of tectonic origin. Because closure of hydrocarbon structures must be upwards, it is common to use contour line maps (and sections) of the reservoir rock hanging wall boundary to characterize a structure (Figure 7.13). The comparison with a bell illustrates the finite volume of traps. Sealing capacity determines the height of the hydrocarbon column that a structure can hold, with excess oil escaping through a leaky seal. Once a well-sealed trap is filled, oil remains in the by-pass flow and may fill other traps

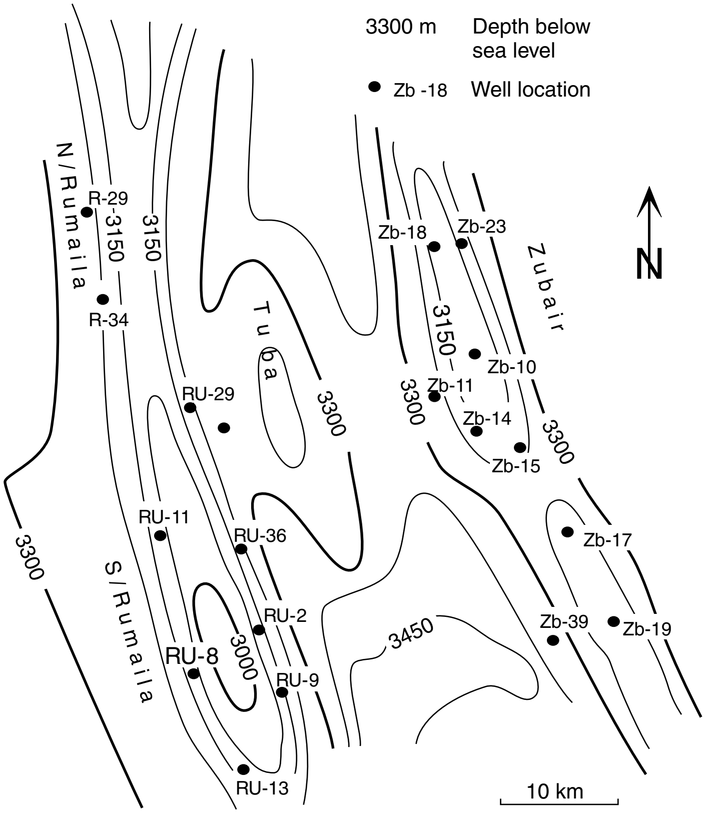

Figure 7.13 Contour lines of the hanging wall boundary of the Early Cretaceous reservoir horizon "Upper Sandstone Member" in the oil fields Zubair and Rumaila in southern Iraq as an example of a structure map (modified from company data). With permission from www.schweizerbart.de. S. Rumaila is Iraq's largest oil field and contains reserves of around 18,000 million barrels (2009). Note the relatively narrow NNW-striking anticlines and the broad depressions. Production wells (black dots) in the structurally high regions provide an indication of oil distribution.

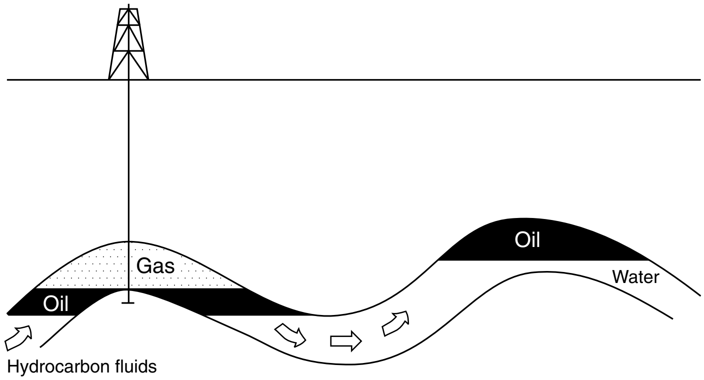
Gas
Oil
Oil
Water
Hydrocarbon fluids

Figure 7.14 The finite volume of a trap causes by-passing of hydrocarbon fluids which may form downstream deposits (Lisk *et al.* 2002). Gas is retained in the first trap where it displaces petroleum.

(Figure 7.14). Incoming gas, however, displaces oil and lowers the petroleum fraction of the upstream deposits. The time span of trap filling is probably between a few to tens of millions of years.

Because of its small molecule size (effective diameter 0.38 nm) and low density, methane is much more mobile in the subsurface than oil. Methane can flow or diffuse through seal rocks that are impermeable for oil, but is effectively retained by gas hydrates, salt and less efficiently, by shales. Many of the giant Siberian gasfields, for example, are sealed by permafrost-related near-surface gas hydrates.

In the pioneer times of petroleum geology, salt domes and anticlines were the only traps known and constituted the main target of exploration. Today, anticlines are still important (Figure 7.15), but a large diversity of traps is known. Classification of this diversity defies a simple approach and we shall here consider only the most important common classes and selected examples of special interest (Table 7.5).

Stratigraphical hydrocarbon traps

Stratigraphical hydrocarbon traps are the result of lateral or vertical changes in permeability, which are due to changes of lithology. Characteristic examples include vuggy reefs within marine mudrocks, sand bars or meandering fluvial channels, sand with laterally increasing clay contents and unconformities. As oil extraction moves out into deep water, buried delta sediments and masses, which flowed down continental slopes, gain

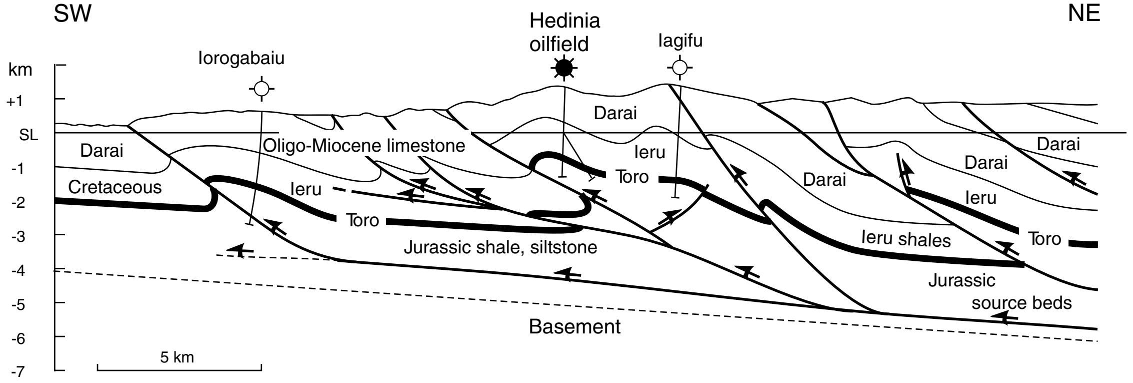
SW
NE
Hedinia oilfield
Iagifu
Iorogabaiu
km
+1
SL
-1
-2
-3
-4
-5
-6
-7
Darai
Cretaceous
Oligo-Miocene limestone
Ieru
Toro
Jurassic shale, siltstone
Darai
Ieru
Toro
Darai
Darai
Darai
Ieru
Ieru shales
Toro
Jurassic source beds
Basement
5 km

Figure 7.15 Hedinia oil field in the thin-skinned Cenozoic fold-and-thrust belt of Papua New Guinea was found by mapping geology and hydrocarbon seeps (after Matzke *et al.* 1992). Main reservoir rock is Early Cretaceous Toro sandstone with 12–15 % porosity and a permeability of several hundred mD. Source rocks are Jurassic shales in the internal zone of the orogen.

Table 7.5 A simple classification of hydrocarbon traps

1. Stratigraphical and diagenetic traps
2. Diapir-related traps
3. Tectonic traps
4. Impact-related traps
5. Hydrodynamic traps
6. Traps formed by self-sealing
7. Combination traps.

increasing importance (e.g. in the Gulf of Guinea sourced by rivers Niger and Congo).

Elongated sand bodies within pelite host rocks may be meandering channels of former deltas and tidal flats, or coastal barriers (bars; Figure 7.16) and dune belts. A broad Early Permian dune belt in Northern Germany and The Netherlands, for example, formed between a large playa lake in the north and a wide, graben-dissected land in the south, is an outstanding reservoir of gas. Today, with exploration moving to deeper and to offshore targets, elongate gravity flow channels and lateral slope fan deposits in deep axial parts of marine basins promise to provide large hydrocarbon reservoirs (Hubbard *et al.* 2005). Internal sedimentary structures, shape, spatial situation and genetic details are vital information required for exploration and exploitation.

Inclined sand horizons (sheets) between marine mudrocks may trap oil and gas where the bed passes updip into less permeable lagoonal and intertidal shales. Increase of pore fill by more intense cementing and consequent loss of permeability forms geometrically similar traps, but this characterizes diagenetic hydrocarbon traps. The thermal "chimney" effect of salt diapirs (Figure 4.26) induces substantial lateral temperature and cementation differences in the above-mentioned Rotliegend reservoir dune sands. Dolomitized porous bodies within tight calcite mudrocks are another illustration of diagenetic trap formation.

Unconformity traps contain a considerable share of world petroleum. The structural discordance between beds below and above an unconformity provides a large variety of spatial arrangements of reservoir and seal rocks. Two main groups are distinguished: i) reservoir rocks in the lower unit sealed by fine-grained sediments deposed above the discordancy plane; and ii) reservoir rock bodies above the unconformity forming traps where they pinch out between overlying shale and sub-unconformity impermeable rocks.

> The emersion of Cretaceous carbonates followed much later by sedimentation of Messinian (Miocene) evaporites and thick Pliocene mudrocks formed the sub-unconformity palaeokarst trap of the Rospo Mare field in the Adriatic Sea (Soudet *et al.* 1994), the largest offshore oil deposit of Southern Europe, with resources of 75 Mio t.

Reefs are frequently transgressed by marine shales, which may act as source rocks. Their high primary and secondary porosity (dolomitization, leaching, fracturing) provide excellent reservoir properties. Important reef oil occurs in Libya, the Arabian Gulf, western Canada and Mexico. From a Mid-Cretaceous barrier reef of 10 km length and 1 km width in southern Mexico, for example, more than one billion barrels (136 Mt) of oil was extracted. Pay zones occurred in the highest parts of

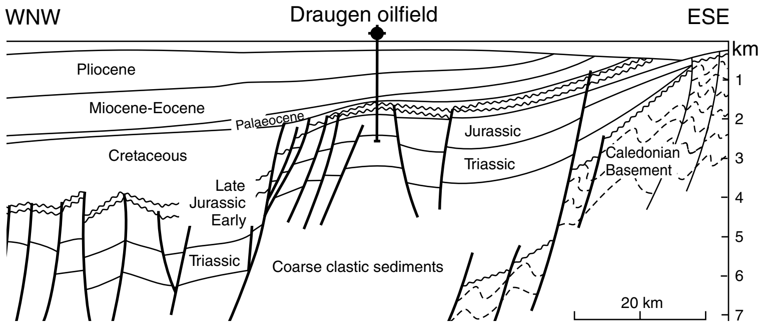

Figure 7.16 The offshore Draugen oil field ~150 km west of Trondhejm, Norway lies in a fault-bounded horst of the Viking graben at 240–280 m water depth (modified from Provan 1992). Reservoir is a sandbar that is enveloped by Late Jurassic shales. The shales are simultaneously source and seal rock. Reservoir sandstones display a porosity of 26–30% and a permeability of 700 mD to 10 Darcy.

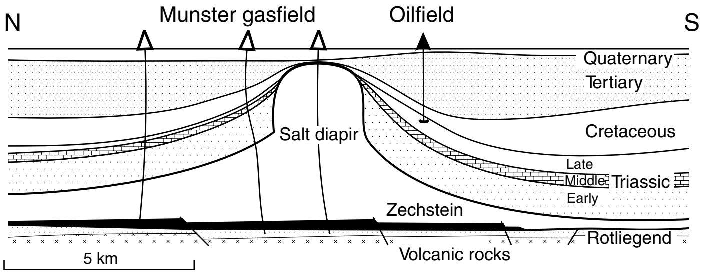

Figure 7.17 Schematic profile of a typical gas deposit in Northern Germany (after Kulke 1994). With permission from www.schweizerbart.de. Sealed by Zechstein salt, Rotliegend dune sands are faintly domed. Methane is sourced by Carboniferous coal at depth. Gas pay zone in black.

the reef. The same observation is reported from the Ordovician Tazhong reef in the Tarim Basin, China (Zhou *et al.* 2009), which is 220 km long and 5–10 km wide, but only 100–300 m thick.

The relations between the growth of reefs, submarine hydrothermal vents, cold seeps and hydrocarbon deposits in reefs are quite fascinating (Hovland 1990, Roberts & Carney 1997). Exploration of ocean floors resulted in the discovery of numerous fluid discharges with CH_4, CO_2 and heavier hydrocarbons of diagenetic origin. The vents are high-biodiversity islands of burgeoning micro- and macro-fauna on the bare seafloor (cf. Chapter 1.1.2 "Ore deposits at mid-oceanic ridges and in ophiolites"). This results in the build-up of organic mounds that may grow into reefs. If the flow of diagenetic fluids continues after the reef is covered by pelites, an early diagenetic formation of a hydrocarbon deposit is possible.

Diapir-related hydrocarbon traps

Oil and natural gas deposits occur trapped below little-deformed flat-lying salt formations, non-penetrating salt pillows, salt-cored anticlines and associated with intrusive salt diapirs (cf. Chapter 4.3.3 "Forms and structures of salt deposits"). Diapir-related traps are variegated and complex (Warren1793, 1792). These structures yield an important part of world oil production. Examples include the Arabian Gulf, parts of Iran, the Gulf of Mexico, Texas and the Pricaspian Basin in southern Russia (Volozh *et al.* 2003).

Oil and gas may be trapped in several positions relative to a diapir:

1 in the cap rock, which usually comprises anhydrite, gypsum, carbonates and collapse breccias; the last mentioned, and carbonates associated with biogenic sulphur formation (cf. Chapter 3 "Sulphur") are often the only good reservoir;
2 in updomed sediments above the top of diapiric salt;
3 in pierced country rocks, which are dragged upwards and ductilely bent; in this case, reservoirs are efficiently sealed by salt;Underneath the diapir in footwall rock (Figure 7.17).

Many salt structures in Northern Europe were deformed by compressional intraplate deformation ("inversion"), which is related to the Late Cretaceous-Early Palaeogene convergence of the European and African plates (Kley & Voigt 2008, Figure 7.18). Because of the high thermal conductivity of salt rocks, the maturation of organic matter in sediments surrounding salt diapirs at depth is retarded, extending to a distance of several kilometres (Figure 4.27).

Tectonic traps

Many of the Earth's giant hydrocarbon deposits are hosted in anticlinal tectonic structures. Their origin is due to various types of folding, reverse faults, overthrusts (Figure 7.15) and nappe tectonics. Others are tectonic highs within rifts (Figure 7.11 and Figure 7.16). Very rare are oil and gas deposits in a synclinal position, which seems to be due to dryness of reservoir rocks. Note that doming of reservoir rocks may be caused by several non-tectonic processes, such as buried hills of an ancient erosion surface, deep magmatic intrusions or halokinesis resulting in salt pillows and salt diapirs (Chapter 4.3.3 "Forms and structures of salt deposits").

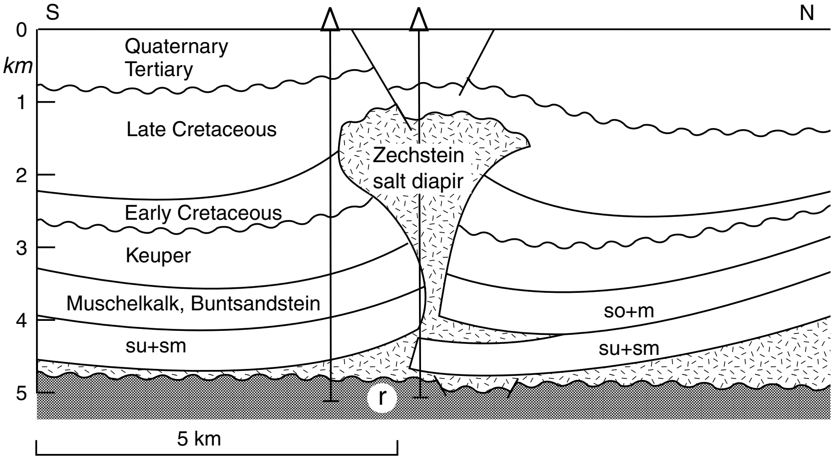

Figure 7.18 Inversion structure of the Taaken diapir in Northern Germany, with a gas deposit in Rotliegend aeolian sands underneath its base (modified from Baldschuhn *et al.* 1998). With permission from www.schweizerbart.de. The diapir formed in the Early Cretaceous. In the Late Cretaceous, it was deformed by compressive tectonics ("inversion") that is most clearly diagnosed by the overlap of Buntsandstein strata (su + sm). Very characteristic are also the narrow stem of the diapir and its wide overhang, which may have been amplified by submarine salt glaciers. Rotliegend (r); Zechstein (Z).

> The Earth's largest oilfield, with >70 billion barrels (9500 Mt) recoverable resources, is Ghawar in Saudi Arabia. It occupies an anticline with a length of 250 km and an area of 2300 km^2. The Iraqi field of Figure 7.13 is smaller but still impressive. Both discoveries are due to early geological and geophysical mapping. Some petroliferous anticlines are not only tectonic but also morphologic highs, such as the Island of Bahrain. The Qatar Peninsula is formed by a very flat arch trending northwards across the Arabian-Persian Gulf; the structure hosts the world's largest gasfield.

Faults are often flow channels that allow hydrocarbon fluids to vent into the sea or to discharge on land. This escape is probably the main reason for the low efficiency of petroleum systems. In contrast to common permeable faults, however, clay or shale fault gouge can transform faults into very effective seals for hydrocarbon reservoirs (Egholm *et al.* 2008). Truncated reservoir rock units sealed by impermeable clay rocks and fault gauge may contain sizeable hydrocarbon deposits. Exploration for this type of trap is expensive and the worldwide percentage of fault-trapped hydrocarbon reserves is small.

Impact-related traps

The supergiant (Table 7.6) Cantarell oilfield in the Gulf of Mexico is probably the largest deposit of this kind, produced by the Cretaceous-Palaeogene boundary Chicxulub impact (Grajales-Nishimura *et al.* 2000). The bolide shattered the submerged carbonate platform that crops out in the western Yucatan Peninsula. The resulting breccia is the reservoir for oil sourced by Late Jurassic rocks. It is sealed by overlying dolomitized ejecta. Obviously, extraterrestrial impacts may generate structures, seals and reservoir rocks that can host very large oil resources.

Table 7.6 Quantification of the terms giant and supergiant hydrocarbon deposits

	Giant	**Supergiant**
Petroleum	$>0.5 \times 10^9$ barrels (68 Mt)	$>5 \times 10^9$ barrels (682 Mt)
Natural gas	$>0.5 \times 10^9$ BOE (68 Mtoe)	$>5 \times 10^9$ BOE (682 Mtoe)

BOE = barrels of oil equivalent (calculated in thermal units, cf. Table 7.1)

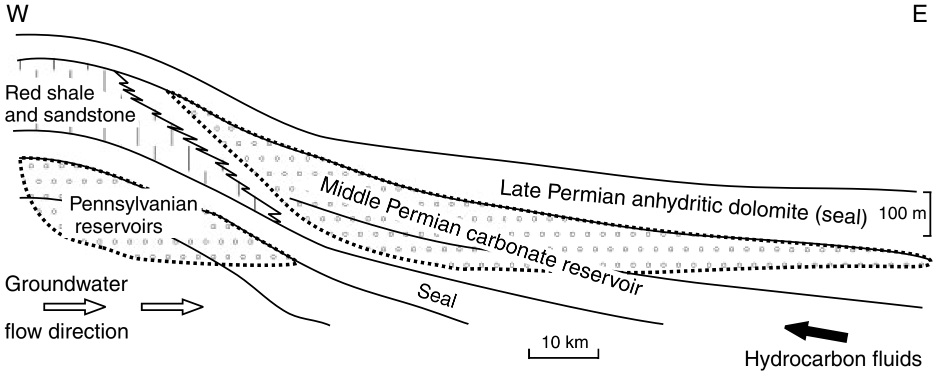
W
E
Red shale and sandstone
Pennsylvanian reservoirs
Middle Permian carbonate reservoir
Late Permian anhydritic dolomite (seal)
100 m
Seal
Groundwater flow direction
10 km
Hydrocarbon fluids

Figure 7.19 The gas field at Hugoton, Kansas is one of the world's giants (Ballentine & Lollar 2002). Copyright (2002) with permission from Elsevier. The field lies at the western border of the Palaeozoic Anadarko basin. Methane migrated from the East over a distance of about 250 km into a stratigraphic (or hydrodynamic?) trap. Nitrogen and helium were added by deep groundwater flowing from the West.

Hydrodynamic traps

Hydrodynamic traps occur where deep groundwater or formation waters move downdip against the updip flow of hydrocarbons. In this type of trap, there is no seal except the footwall and hanging wall of the aquifer bed. The hydrodynamic force of the water is sufficient "closure" if it surpasses the buoyancy force of the hydrocarbons. An inclined oil-water contact is thought to characterize hydrodynamic traps. The gasfield at Hugoton, Kansas (Figure 7.19) displays the typical setting and earlier was considered as a type locality of a hydrodynamic trap. This is now doubted because tilted (inclined) hydrocarbon-water contacts may be due to several causes, including:

- hydrodynamics as described, with an inclined potentiometric surface;
- oil and gas extraction;
- tectonic tilting of an oil-water contact with reduced permeability because of a tar mat or cemented pores in the water zone; and
- gradually changing capillary properties of a reservoir rock unit.

Self-sealing of oil reservoirs by tar or asphalt

Self-sealing of oil reservoirs by tar or asphalt is possible when permeable strata channel the hydrocarbon fluids to the near-surface, where meteoric water, oxygen and aerobic biodegradation (see below) affect the oil. Tar and asphalt clog the pores and diminish or arrest continuing discharge of the oil (e.g. Kern River Field, California: Coburn & Gillespie 2002). The giant tar resources of Athabasca probably have a similar origin as they were apparently emplaced before sedimentation of the mudrock seal (Selby & Creaser 2005).

Self-sealing of gas reservoirs by gas hydrates

Nearly all of the world's giant gasfields are sealed either by evaporites (in the Middle East) or by gas hydrates related to permafrost (in Russia). In the Messoyakha gasfield in western Siberia, the gas hydrate interval has been measured from ~350 to 870 m below the surface (Hunt 1996). Gas hydrates form from methane flowing towards the surface, where appropriate PT-conditions and water are encountered. In the Laptev Sea offshore of northeastern Siberia, permafrost apparently attains a depth of 500 m below the seafloor (Cramer & Franke 2006), which implies a wide distribution of gas hydrates at depth. Although economically less attractive, methane hydrates themselves will soon be exploited (cf. Chapter 7.1).

"Combination traps" result from the interaction of two or more of the trapping mechanisms described above.

7.3.4 Formation and reservoir waters

In hydrocarbon basins, the overwhelming part of pore fluids is water (formation water), and potential reservoirs are often found filled with water. Even within hydrocarbon deposits, water is an important component of pore fluids.

Formation waters reside in pores and joints. Usually they only move sluggishly and display the temperatures of surrounding rocks. If the flow is pronounced, the term "deep groundwater" is sometimes used. Flow may induce considerable temperature anomalies. In sedimentary basins with a mainly marine history, formation waters typically originated as enclosed seawater or evaporative brine. In other basins, meteoric water may have displaced primary seawater, or terrestrial surface water was the primary pore fluid. Water enclosed during sedimentation is "connate". However, water in sedimentary basins often has a complicated history, both concerning its origin and its further evolution by mixing and diagenetic reactions (cf. Chapter 1.4 "Diagenetic Ore Formation Systems"). Like other diagenetic basinal fluids, formation waters are characterized by Eh, pH, T, P, salinity (cf. Table 1.4), mole ratios of dissolved halogens and electrolytes (Botrell *et al.* 1988) and isotopic characteristics (^{14}C, H, O, ^{129}I, Sr, Li and other systems; Tomaru *et al.* 2007).

The pressure of formation water is essential information for a sufficient understanding of any basinal system. Usually, freely moving water at hydrostatic pressure predominates in the near surface zone. Deeper down, individual closed domains are found that display different pressure levels. Hydrostatic to moderate overpressure is most common. "Abnormal pressure" is defined as a pressure above the mean between hydrostatic and lithostatic values (cf. Section "The Exploitation of Petroleum and Natural Gas Deposits"). In extreme cases such as uncemented loose sand, which is totally enclosed by an impermeable formation, overpressure may reach lithostatic magnitude and the overburden weight is wholly carried by the pore fluid.

The precise *in-situ* chemical composition of formation and reservoir water is not easily established, because drilling always disturbs the system by inducing drilling fluids, cement or acids. Yet, water sampled from drillholes is routinely analysed for major cations and anions. Interpretation relies more on ratios, such as Na/Ca, Cl/Br and Na/Cl, than on absolute concentrations. Of course, technologies exist for sampling of nearly uncontaminated pore fluid through perforated borehole casing.

Elevated NaCl concentrations increasing with depth are common in formation and reservoir water. Concentrations vary from <1000 mg/L (freshwater: Table 1.4) to saturated brines, which are either evaporative or a product of halite dissolution. Common cations of formation water include Na^+, K^+, Ca^{2+}, Mg^{2+}, Fe^{2+} and $NH_4{}^{2+}$; important anions are Cl^-, I^-, Br^-, $HCO_3{}^-$ and $SO_4{}^{2-}$ in order of decreasing frequency. Elevated traces of Ba, Sr, B and V are always present. Compared with parental seawater and evaporitic brines, NaCl, Ca, N, Sr, Li, Br and I are typically enriched in reservoir water, whereas Mg and sulphate are depleted. Microbial sulphate reduction explains sulphate depletion. Magnesium is probably consumed by dolomitization or by formation of Mg-clay minerals releasing Ca and Sr. The reverse, higher Mg-concentration in pore fluids is brought about by precipitation of calcite cement (e.g. by microbial methanogenesis, McIntosh *et al.* 2004). Oilfield brines are usually moderately alkaline and reduced.

Routine water data from wells exploring or extracting hydrocarbon deposits provide valuable insight into an essential component of the hydrocarbon system. They assist interpretation of geophysical well logs and stratigraphical correlation. Hydraulic and genetic investigations of waters expose important features at all scales, from whole basins to single reservoirs.

7.3.5 Alteration of petroleum in reservoirs (degradation)

More than half of the world's crude oil resources are to some degree degraded. Much of the production from the next-generation deepwater fields on continental shelves will be biodegraded oil (Head *et al.* 2003). Biodegradation is principally a loss of value, but as it commonly includes the production of biogenic methane, the additional gas may be a limited compensation.

The quality of petroleum in reservoirs can be impaired throughout its existence, starting with the filling stage. The prime agents of degradation are water, oxygen and microbes. Aerobic biodegradation by bacteria and archaea is due to flow of oxygen- and nutrient-bearing meteoric water into shallow reservoirs. Degradation of shallow petroleum is ubiquitous. Similar processes affecting coal and kerogen-rich shales produce economically important microbial gas deposits (McIntosh *et al.* 2004). Associated reservoir waters are strikingly sulphate-depleted (Van Voast 2003). Aerobic biodegradation is the traditionally prevalent hypothesis to explain degraded oil but deeper and hotter oil pools are similarly degraded, although dissolved oxygen is unlikely to reach this environment and microbes found are anaerobes. Generally, biodegradation was assumed to end at 80 °C (Wilhelms *et al.* 2001), but hyperthermophilic methanogenic archaea are now known to thrive at 110 °C and to still be alive at 140 °C (Schippers *et al.* 2005). Obviously, anaerobic hydrocarbon degradation is more common in oil reservoirs than hitherto thought (Aitken *et al.* 2004) and may actually be the prevailing mode of petroleum degradation (Jones *et al.* 2008):

> Biodegradation of petroleum leads to the loss of n-alkanes (paraffins), isoprenoid alkanes, waxes and part of cycloalkanes, aromatics and biomarkers. Several anaerobic microbes reduce sulphate in order to satisfy their oxygen requirements (cf. Chapter "Sulphur"). The resulting reduced sulphur can be found in the form of native sulphur (e.g. in caprock of salt diapirs), H_2S, sulphides of iron, zinc, lead, etc., or in sulphur-enriched residual degraded petroleum. As a consequence of biodegradation, resins and asphaltenes prevail in the residual oil and contents of sulphur, nitrogen, vanadium and nickel increase. Also, density and viscosity rise. These changes handicap recovery and make processing more expensive. By-products of anaerobic biodegradation are methane and CO_2. Therefore, the process is also called "methanogenic biodegradation". Much of this carbon dioxide is probably converted to more methane. CO_2 is also produced by aerobic biogenic oxidation of methane (eq. 7.6), provoking the precipitation of carbonate cement in near-surface reservoir rocks.

Aerobic biogenic oxidation of methane:

$$CH_4 + 2O_2 \rightarrow 2H_2O + CO_2 \qquad (7.6)$$

Petroleum that is affected by large amounts of water or natural gas can be degraded by selective solution of light hydrocarbons ("water washing", "gas washing"). Typically, water washing removes water-soluble low molecular hydrocarbons such as benzene, toluene and xylene. At temperatures of 100–140 °C and in contact with anhydrite hosted by salt structures or by carbonate reservoir rocks, oil and gas are oxidized by abiotic thermochemical sulphate reduction (eq. 1.21 in Chapter 1.4 "Diagenetic Ore Formation Systems"). Magnetite and haematite, for example in sandstone, are also hydrocarbon-oxidizing agents (Seewald 2003).

7.3.6 Tectonic environments and age of hydrocarbon provinces

Hydrocarbon deposits are formed in all sedimentary basins on the Earth, which display: i) the presence of source rocks; ii) a total thickness of sediments and heat flow sufficient for kerogen maturation; and iii) adequate traps. Several geodynamic settings provide the suitable background:

- epicontinental platform and shelf basins (Saudi Arabia: Alsharhan & Nairn 1997; Sirte Basin, Libya, Western Siberia);
- continental or marine rift systems and aulacogens (Lambiase 1995; Nigeria, Gulf of Suez, North Sea: Glennie 1998, Sudan);
- back arc basins (Yellow Sea, Okhotsk Sea);
- passive continental margins (Arabian-Iranian Gulf: Konyuhov & Maleki 2006; the Campos Basin and the new deep-water supergiant Tupi field offshore of Rio de Janeiro; West Africa);
- orogenic thrust and fold belts (Zagros orogen in Iran, Alpine belts in Albania and Romania; Rocky Mountains, USA);
- foredeeps of orogenic belts (north of the Caucasus, south of the Zagros Belt in Iran: Alsharhan & Nairn 1997, eastern foreland of the Rocky Mountains in Canada);

- intramontane basins within orogens, often related to large transform or shear structures, transtensional, transpressional or pull-apart-basins (Southern California, Maracaibo in Venezuela).

Orogens may be both a location of oil and gas deposits and the source of migrating hydrocarbon fluids (Figure 7.15). Far-reaching horizontal fluid migration of "tectonic brines" including hydrocarbons may be induced by advancing nappe piles, such as depicted in Figure 1.74.

More than 75% of the world's conventional and heavy oils were generated from Jurassic and Cretaceous source rocks (Hunt 1996). Oil and gas deposits occur predominantly in geologically young positions (Jurassic to Neogene), because conservation of these delicate features through long geological periods is not favoured. Destruction is caused by uplift, faulting and erosion as well as by subsidence, deformation and metamorphism. Several graphite and pyrobitumen deposits bear evidence of representing former hydrocarbon deposits (cf. Chapters 3 "Graphite"; Section 7.5 "Pyrobitumen").

Geologically ancient remains of hydrocarbons are of high scientific interest. Although for most of the Earth's history, life was restricted to simple forms, potential source rocks such as black shales and stromatolites are common. Of course, most of the ancient organic substance is over-mature and oil and gas have been dissipated long ago. Archaean shales in the West Australian Pilbara craton, for example, display features pointing to pervasive petroleum generation (Rasmussen 2005). The earliest giant deposits of oil shale and (former) petroleum, called shungites, occur in the Palaeoproterozoic of the Onega basin (Northwest Russia; Melezhik *et al.* 2004). Similar rocks rich in over-mature organic matter were formed at ~2 Ga in North America, Greenland and West Africa (defining the worldwide "Shunga Event"). At the White Pine copper mine in Michigan, oil was actually found seeping from the 1.0 Ga Nonesuch Shale (Chapter 2.2 "Copper"). Oil traces of about the same age occur in the Roper Basin, Australia (Dutkiewicz *et al.* 2003).

The earliest economic oil and gas deposits, however, are extracted from Neoproterozoic rocks in Oman, China, Sudan, Australia's Amadeus Basin and in eastern Sibiria. With the explosion of oceanic multicellular life in the Ediacaran and Cambrian, and the conquest of land by higher plants in the Devonian, sources of organic matter multiplied and diversified at the same time.

7.4 EXPLORING FOR PETROLEUM AND NATURAL GAS DEPOSITS

An introduction into underlying principles and practice of exploration for ore and minerals is presented in Chapter 5.2 "The Search for Mineral Deposits". The principles are much the same, but the practice of exploration in the hydrocarbon industry is different. Prospective depths, scale of operations, available funds, financial risks and expected profits are all considerably larger.

The search for new oil and gas deposits increasingly extends into the seas and oceans of the world. In plate tectonic terms, these regions are mainly submerged rifts, passive continental margins and back arc basins. Offshore production is from ever deeper water, currently about 3000 m. Because present oceans are geologically young, Mesozoic and Cenozoic source and reservoir rocks have a dominant role. In the deep basins, mass flow sediments are important hosts and traps are mixed stratigraphic and structural. The marine environment poses new challenges that are met by developing adapted versions of exploration methods founded in terrestrial technology (Jahn *et al.* 1998).

Yet, even on land, new hydrocarbon discoveries are still being made. One example is TOC-rich Neoproterozoic-Cambrian stromatolites enclosed in Huqf (Hormuz) evaporites that host valuable light petroleum in Oman (Schröder *et al.* 2005). In the Sichuan Basin and the eastern Tarim Basin in China, considerable gas accumulations derived from cracked oil have been found beneath the oil window (Tian *et al.* 2008). New extraction technologies unlock vast gas resources in low-permeability shale, exemplified by the Barnett and Antrim shales in the USA (McIntosh *et al.* 2004).

The foundation of all hydrocarbon exploration is an understanding of the geological evolution of the target basin (Allen & Allen 2005). Without this base, even hydrocarbon seeps, which are "the best guide to oil", may be wrongly interpreted. Today, it is rare to locate new deposits by geological methods alone. One exception is the large oilfields in the tropical mountains of Papua New Guinea, which were discovered by mapping structures and oil seeps (Figure 7.15). Usually, geophysical and foremost seismic surveys are the most efficient discovery tool of the oil and gas industry, combined with geological, modelling and organic geochemistry methods. However, the geological synthesis of basin evolution with petroleum and gas systems in space and time (four-dimensional) is the overarching goal (cf. Figure 7.10, which shows part of the required data).

General search criteria in oil and gas exploration include:

- basins with sediments of >2000 m thickness (at average heat flow);
- presence of potential source and reservoir rocks;
- sufficient maturity of the organic substance in the source rocks (R_o ~0.7–1.3 for oil);
- presence of trap structures;
- favourable timing of oil and gas generation, migration and formation of traps;
- tight shale gas is sought in source rock matured to the thermogenic gas window (R_o ~1.3–2.0).

Hydrocarbon seeps and other pointers to oil, such as H_2S springs, bituminous rocks and mud volcanoes (Hovland *et al.* 1997, Hein *et al.* 2006), may be caused by ongoing secondary, or more likely tertiary migration from leaking oil and gas deposits. At the surface, oil loses light hydrocarbons ($<C_{15}$) within two weeks by evaporation and C_{15-24} in a few months. Water-soluble compounds are leached and microbial degradation sets in. Oxidation and polymerization harden the oil into tar, asphalt or pyrobitumen. However, carbon isotope and V/Ni ratios are well preserved and allow asphalt-oil correlations. Famous examples of active seeps with bubbling methane are the Tar Pits in Los Angeles (California), Lake Bermudez in Venezuela and La Brea asphalt lake of southwest Trinidad.

Fresh oil samples collected from seeps are analyzed for the hydrocarbon spectrum and biological markers. Already in the field, ultraviolet illumination distinguishes natural hydrocarbons from pollution with refined products. UV light of 302–366 nm wavelength (Figure 5.2) activates crude oil luminescence in yellow to brown colours, whereas fuels and lubricants appear white to violet. Remote determination of UV-spectra of oil films on the surface of the sea by laser fluorescence sensors allows correlation with known oil types and even with specific source rocks. Cold methane seeps on the sea floor (Figure 3.5), some of which are products of microbial methanogenesis (eq. 7.3), display vent towers or pockmarks built from carbonate and barite precipitates. Methane bubbling from the sea floor is detected during seismic surveys by sensors towed near the bottom ("sniffer", Figure 7.20). Asphalt-rich oil produces tar pits on land and asphalt flows on the sea floor (MacDonald *et al.* 2004). Paraffinic oil residue is earth wax. Submerged containers are used to sample gas bubbles in water. Isotopic characteristics help to distinguish shallow biogenic methane, coal seam gas and oil-associated gas (Figure 7.2). Fresh kerogen-rich rocks (potential source rocks) are brown, but ash-like white in weathered outcrops. Leaching in chloroform or boiling in water may yield a little oil that can be made visible by UV-light. Diffuse microseeps of hydrocarbons on land can be expressed by:

1. bleaching of red rocks (haematite → pyrite or siderite);
2. kaolinization (feldspar → illite → kaolinite);
3. formation of calcrete;
4. enrichment of uranium; and
5. sickly vegetation (Schumacher 1996).

All these guides are detected by remote sensing methods (Meer *et al.* 2002).

In little explored prospective basins, tectonic and salt-related traps are first sought. Regional magnetic and gravimetric surveys are able to map structural highs and lows, and to identify salt domes (Figure 4.29). Simple stratigraphic traps such as sandbars, channels and reefs are detected. In this early stage, recognition of complex stratigraphic, diagenetic, hydrodynamic and combination traps is not expected. With more data, foremost by a number of wells and seismic surveys, prospects of success are much better.

7.4.1 Geophysical methods

Geophysical methods in hydrocarbon exploration include first of all the relatively inexpensive and highly efficient reflection seismics (Gadallah & Fisher 2009). On land and offshore, airborne magnetic, magnetotelluric and gravimetric methods serve early reconnaissance (Gibson & Millegan 1998; cf. Chapter 5.2 "Geophysical Exploration Methods"). Seismic refraction is employed to investigate targets that do not respond well by seismic reflection.

On land, seismic reflection methods use signals created by detonating explosives in shallow drillholes or by vibrating a large mass (Figure 7.21, Figure/Plate 7.22 and Figure 7.23). Reflected signals are recorded by a chain of geophones. At sea, a boat produces sonar signals (e.g. by underwater air guns) and reflections are recorded by 8–10 towed streamers of hydrophones (Figure 7.20). The seismic signal is an elastic longitudinal compression sound wave (a P-wave). Reflections are due to lithological contrasts and depend on the difference of the acoustic impedance (density × seismic velocity, Table 7.7) of two adjacent rock units. By processing, depth and dip of lithological contrasts are imaged. Initially, seismic profiles are laid out crossing major structures. Tie lines and eventually, polygonal infill lines are added in order to produce a spatial image of the subsurface geology ("three-dimensional seismics"*)*. At this stage, tectonic and salt diapir- or salt pillow-related traps are confirmed. Less conspicuous traps can only be determined if a seismic stratigraphy frame can be established, which requires information from drilling. With special technology, very high-resolution three-dimensional images and models can be produced. Remember that seismic data interpretation was the foundation of global seismic stratigraphy, which is now called "sequence stratigraphy" (Miall 1997, 2000; Einsele 2000). This method allows advanced geological modelling with little well control. In response to the problems caused by salt bodies concealing sub-salt structures, marine seismic surveys increasingly rely on three-dimensional data acquisition such as "wide-azimuth" (several survey vessels moving in parallel) and "multi-azimuth" methods (repeat passes at different angles).

Seismic refraction methods are distinguished by using a specific path of seismic waves: Upon encountering a lithological interface between

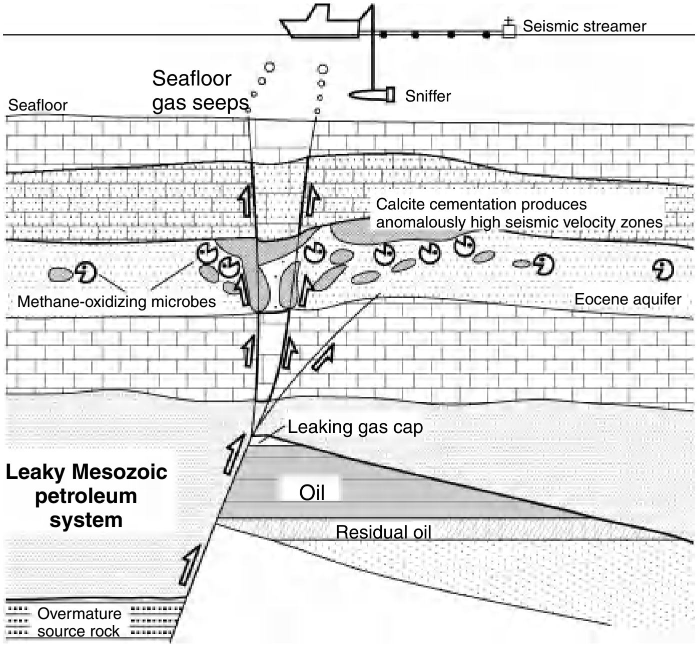
Seismic streamer
Seafloor gas seeps
Sniffer
Seafloor
Calcite cementation produces anomalously high seismic velocity zones
Methane-oxidizing microbes
Eocene aquifer
Leaking gas cap
Leaky Mesozoic petroleum system
Oil
Residual oil
Overmature source rock

Figure 7.20 Submarine gas seeps and seismic detection of calcite-cemented portions of Eocene sandstone in the Timor Sea facilitate localization of deep oil deposits which leak because of Miocene inversion tectonics (modified from AGSO Research Newsletter 21, 8–11, 1994). © Commonwealth of Australia (Geoscience Australia) 1994. The calcite-cementation is caused by methane-oxidizing microbes.

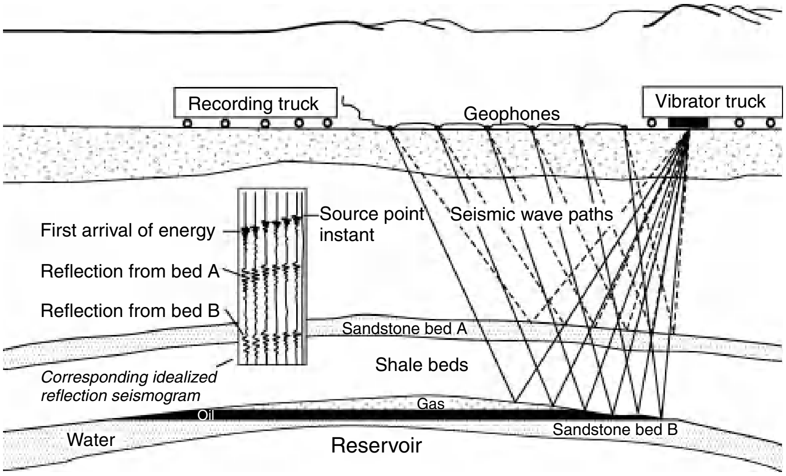

Figure 7.21 Principles of seismic reflection field work, the most common geophysical method in hydrocarbon exploration. The inset displays a typical time-distance graph resulting from one survey line.

a bed with low P-wave velocity above one with high V_p, impulses radiating downwards from the seismic source are refracted into a path parallel to the interface. From this travel path in the interface, some seismic energy returns to the surface. Nearly horizontal position of the interface is advantageous. The method is mainly used for the investigation of cover rocks and water table in engineering and hydrogeology. In oil and gas exploration, elucidation of relatively shallow salt structures is the main object. Salt has a high V_p of $\sim$5000 m/s, resembling hard rocks, whereas other sediments display lower velocities (Table 7.7).

Telluric currents in the lithosphere are induced by particle flow from the Earth's ionosphere. Telluric currents and the associated magnetic fields display pulsation of direction and strength. The magnetotelluric method (MT) measures the natural field variations at different frequencies. Lower frequency data provide information about deep conductors, such as graphite and sulphide rich rocks. MT cannot replace seismic and potential methods but provides additional constraints, especially concerning the presence of hydrocarbon source rocks in deep parts of sedimentary basins and in their basement.

Early distinction between barren and hydrocarbon-filled traps helps to avoid the expense of futile drilling. Specialized variations of geophysical methods have been developed to assist in this task. One approach is employing the higher resistivity of hydrocarbon pore fluids compared to saline waters. For the detection of such low-conductivity bodies, electromagnetic (EM) and magnetotelluric methods were adapted for submarine conditions. In seismic surveys, advanced analysis of P- and S-waves may differentiate hydrocarbon from brine pore fluid in reservoir rocks. This is the seismic "direct detection technique" (AVO = amplitude vs. offset).

7.4.2 Geochemical methods of hydrocarbon exploration

Geochemical methods of hydrocarbon exploration range from organic geochemistry of source rocks, oil and seeps (Hunt 1996) to regional reconnaissance targeting buried deposits on land (Peters & Fowler 2002). Past efforts to detect specific guides for surface prospecting included measuring hydrocarbon gas in soil and near-surface air (Klusman 1993), trace metal analyses and radiometric measurements. Detected hydrocarbon anomalies at the surface are, of course, just microseeps. which have the same probability to indicate the location of a hydrocarbon deposit as macroseeps. Considering that hundreds of dry wells have been drilled in the past near strong seeps (Hunt 1996). there is little reason to accept microseeps as stronger guides than the first. With due care and sufficient geological data, the significance of seeps can be evaluated and

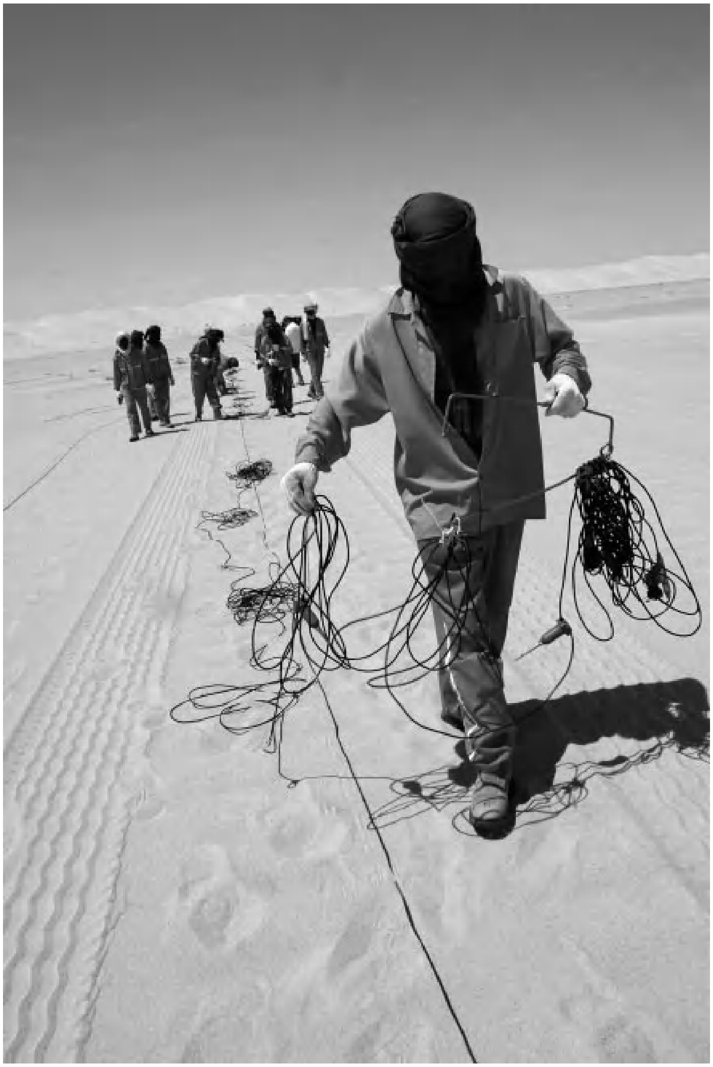

Figure 7.22 (Plate 7.22) Laying out a seismic reflection survey line of geophones in the desert of Cyrenaica, Libya. © Øyvind Hagen, Statoil.

mapping of light hydrocarbon (C_1 to C_4) distribution on the surface may help exploration (Zhang 2003). Only a clear understanding of the source of hydrocarbons seeps and the flow paths assists in directing drillholes to the right structure (Figure 7.20).

7.4.3 Exploration drilling

Data acquired by methods introduced above are the foundation for choosing the first drilling target. A "structure hole" provides a wealth of stratigraphical and lithological data and at the same time targets a seismically defined prospective trap structure. Seismic parameters measured *in situ* and petrophysical properties of the encountered rocks are invaluable information for refining the interpretation of seismic surveys and, of course, for an improved understanding of the investigated hydrocarbon system.

During drilling, all firms employ sophisticated data collection procedures. Lithology, fossils and

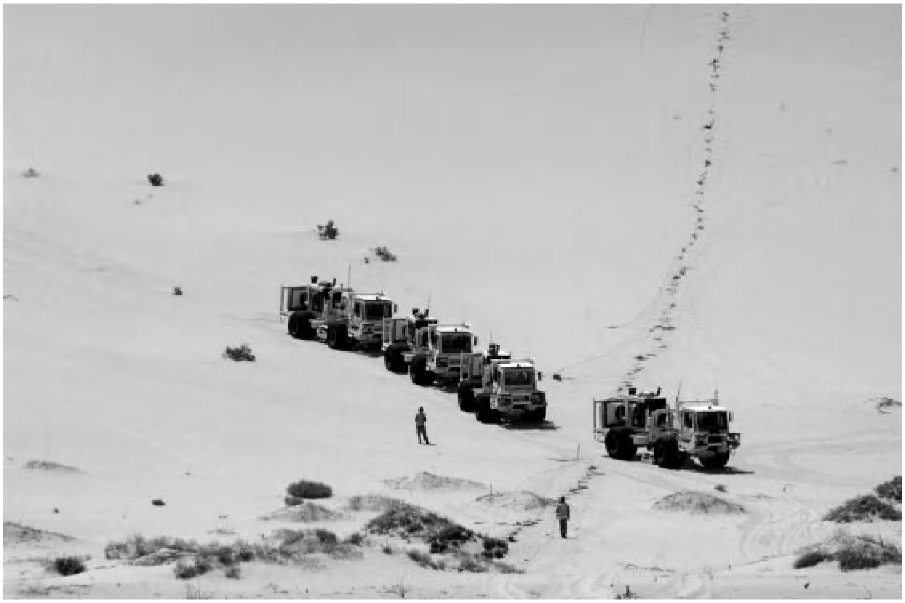

Figure 7.23 (Plate 7.23) A fleet of heavy vibrator trucks waiting for the deployment order. Cyrenaica, Libya. © Øyvind Hagen, Statoil.

hydrocarbon contents of drilling mud samples are recorded. Kerogen particles are separated and comprehensively analysed. Main parameters sought are kerogen type and maturity. Technical data such as the rate of penetration are recorded. Selective coring during drilling, or later by perforating borehole casing, provides little-disturbed samples for the determination of petrophysical properties, grain size spectrum, wetting characteristics, porosity and permeability of potential production horizons. *In-situ* fluid pressures are measured and oil (reservoir fluid) is sampled in order to study fluid behaviour under reservoir (and production) conditions. If oil or gas is found, flow rate and pressure are determined (Chierici 1994).

Table 7.7 Range of sonic P-wave velocity (m/s) of common rocks, water and air (gas)

Sand	200–2000	Clay	500–2500
Coal	1000–3000	Shale	2500–5000
Sandstone	2500–5000	Limestone	3000–7000
Salt	4500–5000	Anhydrite	4800–7000
Water	1500	Air	330

7.4.4 Geophysical borehole measurements

Geophysical borehole measurements are used in all wells drilled for hydrocarbon exploration. The technology was introduced by Conrad and Marcel Schlumberger when they opened an office in Paris (1920) offering geophysical surveys to the oil industry. A wide spectrum of methods is available, aimed at providing:

- data supporting geological description and analysis;
- petrochemical and petrophysical parameters, and;
- technical information, which is decisive for drilling and hydrocarbon production.

Well logging serves stratigraphical correlation, the distinction and localization of important single horizons (Figure 5.8), the identification of gas-oil and water-oil contacts, the determination of rock properties and the nature of pore fluids in a reservoir. Chapter 5.2 "Geophysical Exploration Methods" introduced borehole logging at a general level. Here, several methods are addressed in more detail. For professional information, consultation of works such as Ellis & Singer (2007) and Serra & Serra (2004) is recommended:

> Conventional resistivity logs measure the apparent electric resistivity of borehole wall rocks. Resistivity is the inverse of conductivity and is measured in Ohm metres (ohm/m). It is controlled by pore water content, salinity of the water and the presence of drilling fluid, oil, gas, sulphides or coal. Focused arrangement of electrodes (e.g. laterologs) renders bed boundary definition more precise. The main aim of resistivity surveys is to locate oil by its very low conductivity compared with formation water, but the data facilitate general formation correlation and evaluation. An example is the distinction between effective (macro-) and ineffective micro-porosity (Smith *et al*. 2003).
>
> Formation resistivity is also measured by inducing an alternating magnetic field and consequent current loops in the formation. The resulting signal is proportional to the conductivity and is recorded by a receiver coil. Application is typically related to formation of a non-conducting mudcake in the walls of the hole, or mud invasion in the wall rocks.
>
> Spontaneous potential logs display the natural difference in electrical potential (mV) between an electrode in the borehole and a fixed reference electrode on the surface. The SP potential results mainly from differing ion concentrations in drilling mud and formation water and the clay content of permeable beds. The logs are used to detect permeable beds, to estimate formation water salinity, formation clay content and, although data are not absolute values, for correlation with nearby drillholes.
>
> Dipmeter logs are indispensible for the geological interpretation of a borehole. Tools for this task are micro-resistivity devices with 3 or 4 electrodes set at angles of 120° or 90°. Another instrument (e.g. a magnetic compass) records the orientation of the probe as it is drawn up the hole. Data plots are evaluated in context with other information (e.g. seismic and sedimentological models).
>
> Borehole deviation logs are needed for technical control of the drillhole and especially in connection with directional drilling. Dip and azimuth of the borehole axis are recorded at predetermined depths. The orientation of the tool is given by a magnetic compass or by gyroscope-based instruments. Deviation and dipmeter surveys are typically performed in combination.
>
> Natural gamma radiation surveys can be run through casing (the steel tubes of wells). In open holes, gamma radiation is measured together with the hole diameter, which is recorded by a caliper logging device. This is needed because gamma readings are affected by missing mass in the wall, for example by wash-out or caving. Natural radioactivity is due to the radioactive decay of uranium, thorium and potassium (^{40}K). In hydrocarbon exploration, recognition of certain lithologies is the major aim, such as uranium-enriched phosphate, common shale, oil shale, source rocks and sapropelic coal, thorium lodged in heavy minerals concentrated in coastal sand bars, and potassium in potassium salts, feldspar, illite, mica and glauconite. Of course, using spectrometer detectors instead of scintillometers provides more meaningful data (cf. Chapter "Uranium").
>
> Bulk density logging (Gamma-Gamma, or GG method) is only run in uncased holes. Essentially, the reduction of the gamma ray flux in wall rocks due to Compton scattering between an emitting source, usually ^{137}Cs, and a detector is measured. Compton scattering reflects electron density and not bulk density, but calibration provides density logs, which apply to the majority of sedimentary rocks. Assuming that the instrument measures only that part of the wall rocks that is invaded by drilling fluid (of known density), porosity is easily calculated if the rock type and the densities of its dry and solid constituents are known (e.g. quartz grains of a sandstone, $D = 2.65\ g/cm^3$).
>
> Neutron-neutron porosity logs record the effect of wall rocks on fast neutrons emitted by a source in the hole. Slowing down and capturing of neutrons is most intensive on hitting hydrogen atoms. Because in carbonates and sandstone hydrogen occurs mainly in the pore fluid, the measured values of thermal or epithermal neutron detection correlate essentially with porosity. Clays and other hydrated minerals give relatively higher readings. Because of the low hydrogen density, natural gas as a pore fluid yields very low apparent porosity. This effect can be used to determine the hydrocarbon fluid composition in oil deposits ("geochemical reservoir analyser").
>
> Caliper logs display the measured diameter of a drillhole along depth. The instruments are commonly multifinger mechanical devices. Borehole wall irregularities (rugosity) assist lithological and geotechnical interpretation. The characteristic elliptic cross-section of open holes, for example, reflects the orientation of rock mass stress vectors. These data are of high scientific (Cloetingh *et al*. 2005) and practical interest, for example when high-pressure fracturing is planned for raising gas flow from a dense reservoir.

Temperature logs in boreholes are produced by determination of bottom hole temperatures (BHT) during drilling, or by logs run later. Circulating drilling fluid always induces cooling compared to the ambient temperature of surrounding rocks. Measured temperatures are corrected in order to establish the geothermal gradient in the well, which is essential information (e.g. for maturation modelling). Later temperature runs serve foremost the detection of anomalies, or departures, from the reference gradient. Anomalies are usually connected with outflow (of drilling fluid) or inflow (of pore fluid) into the hole. Cementing, acid stimulation and hydraulic fracturing induce transient anomalies that assist evaluation of these operations. Because most rocks and pore fluids have relatively low thermal conductivities, the temperature log records the behaviour of a well over a longer time period than other measurements.

Sonic, or acoustic velocity logs display velocity (or some other property) of acoustic P- and S-waves vs. depth. The instrument carries both an emitter of sound and several receivers. Data serve foremost to determine porosity, which is directly correlated with acoustic properties, because the solid components of rocks transfer most of the P-wave energy. With the rock type known (e.g. sandstone, limestone), the measured sound velocity is compared to the pure mineral at 0% porosity (e.g. quartz, calcite). Typical ranges of sonic velocity are listed in Table 7.7 (Milsom 1996). Sonic logs are also used for lithological correlation, the determination of permeability and potential gas zones, and for early recognition of overpressured zones. Other sonic tools have been developed, which produce borehole wall images that allow inspection of fracturing, breakouts and bed characteristics.

Measurement-while-drilling (MWD) is employed to determine pressure, temperature, electrical resistivity and mechanical rock parameters for real-time management of the drilling operation. Borehole seismic tools, which comprise seismic sources and receivers, are applied in order to refine spatial models derived from surface surveys.

Potentially economic hydrocarbon-bearing horizons in the well are investigated in great detail. This includes first flow tests (drill stem test, DST), although a full evaluation of production characteristics is only possible after well completion (installing hardware and technologies for extracting hydrocarbons from the reservoir). In both oil and gasfields, preliminary resource estimates can be based on only one well. However, reliable reserve determination is only possible when the full variation of reservoir properties and its fluids are known, requiring a number of wells. Even if the first exploration well located hydrocarbons, appraisal and development drilling will go on. Of course, all data acquired are integrated in qualitative, quantitative and dynamic analyses of the reservoir, the effective drainage area (Figure 7.9) and the whole basin (Miall 2000, Allen & Allen 2005). A model of the petroleum system generating the new field is assembled. The system's yield, efficiency and potential resources can be estimated. In mature basins such as the North Sea (Box 7.1), past production plus remaining measured resources are compared with estimated total generation (Balen *et al.* 2000). Strategies are developed to explore for "missing" amounts.

BOX 7.1 Discovery and Development of the North Sea Oil and Gas Province

The North Sea oil and gas province provides an illustrative tale of exploration and development (Glennie 1998).

For >100 years, small and medium-sized oil and gasfields had been exploited on both shores of the North Sea, in Germany (starting with Wietze, Hannover in 1859) and in England. The inducement for expanding exploration into the sea was the realization that the gasfield Groningen in the Netherlands was one of the world's largest deposits. In 1964, the first offshore drillhole was sunk by a German consortium (Nordsee B-1). The first large finds, however, were the gasfield Leman in the British sector (1965) and the oilfield Ekofisk (1969: 200×10^6 m^3 oil) in the Norwegian sector. The oil price spikes in the years around 1970 hastened developments. Exploration successes peaked in 1973–1979 and more than 50 giant oil and gasfields have been found. Until 2002, when annual production peaked at ~450 Mtoe, over 5.1 Gt of oil and 3.2 Tm^3 gas had been produced. Today, the North Sea province is mature, concerning both oil and gas. Production of oil is declining, whereas gas output is about equal to 2002 (*BP Statistical Review of World Energy* 2010). Few significant finds have been made for many years; recent discoveries average around 10 million barrels (1.4 Mt).

Prominent source rocks for oil and gas in the North Sea include:

- Late Carboniferous coal for gas in the southern sector;
- Early Jurassic shales for oil in the southern sector;
- Late Jurassic and Early Cretaceous shales (Kimmeridge Clay) in the northern sector; with 2 to >12% organic matter and elevated uranium contents, called "hot shale", because of a distinct signature in γ-logs.

Reservoir rocks display ages from the Devonian to the Eocene, but the largest oil deposits are hosted in Early and Middle Jurassic sandstones and in Late Cretaceous chalk. Formation and deposition of these sediments are controlled by a complex Mesozoic graben system with a width of >100 km. This is a failed rift related to the opening of the Atlantic Ocean. Source rock maturity sufficient for hydrocarbon generation is confined to more central parts of the rift. Oil and gas generation started in the Late Mesozoic. Hydrocarbons migrated mainly upwards and short distances to traps. In the southern sector, compressive tectonic overprint (inversion) destroyed a number of deposits formed. Most traps are stratigraphic, although influenced by a complex interplay of graben faults, halokinesis and palaeogeography.

Exploration and development of offshore oil and gas in the North Sea continue, although targeted traps are increasingly more complex and deposits found smaller (Figure 7.11 and Figure 7.16). An important part of future production is foreseen to result from field growth, for example by applying improved recovery technologies. Until recently, heavy oil and sour gas were hardly considered. This is expected to change with higher hydrocarbon prices on the market. Better sales revenues would considerably expand resources. Optimists believe that a paradigm shift in exploration concepts may yet end the decline and are supported by discovery of the Catcher fields (June 2010) with an estimated 300 Mb oil in place. In the future, deep aquifers in the North Sea province provide Britain and continental Europe with a huge volume for offshore geological sequestration of CO_2 (Figure/Plate 6.2; Haszeldine 2009).

7.5 THE EXPLOITATION OF PETROLEUM AND NATURAL GAS DEPOSITS

The rational exploitation of hydrocarbon deposits is the result of teamwork between petroleum engineering, geology, geochemistry and geophysics. The overall objective is not different from that of a mine operation (cf. Chapter 5.3 "Valuation of Mineral Deposits") and can be summarized by "optimization of the operation so that the investment is recovered and profits accrue". The recovery of hydrocarbons from a porous or fractured rock body at depth is based on geological input and managed by reservoir engineers (Chierici 1994, Dake 1994).

7.5.1 Reservoir conditions

Before the influence of drawing fluid from a reservoir can be evaluated, the initial conditions must be established. Integration of geometrical, physical and chemical data allows reservoir characterization and the application of numerical modelling.

Porosity and permeability are of overriding importance. Although they are determined by a number of other methods, investigations of reservoir rock core under simulated reservoir conditions such as P, T, fluid pressure and rock mass stresses are paramount. With these data, earlier wireline measurements can be calibrated and reinterpreted. The physical "intrinsic" permeability k (m^2) of reservoir rock is determined with an inert gas. "Effective" permeability of a rock depends on the composition of the hydrocarbon fluids (eq. 7.5). Wetting characteristics (water-wet or oil-wet grains) and capillary pressure related to different widths of pore throats are other factors that influence fluid flow. Permeability is greater parallel to bedding and smallest for fluid moving across bedding. This is especially important for today's trend to bedding-parallel production wells. Double porosity characterizes many hard rocks; the term describes the presence of both matrix and fracture/joint porosity. Fluid extraction reduces porosity because falling fluid pressure results in rising effective stresses (Figure 1.39). Grains are forced into a denser packing, fractures close and the solid framework takes up a higher share of total stress.

This is why hydrocarbon production induces compaction of the reservoir rock, which may result in seismic activity and subsidence of the land surface.

Petroleum reservoir fluids constitute a complex system of water, dissolved salt and hydrocarbon compounds, which may occur in liquid, gas and supercritical state (Danesh 1998). Subtle changes in T and P, which are unavoidable during extraction, may cause drastic changes such as foaming of fluids. Therefore, the fluids' behaviour is investigated in the laboratory at simulated reservoir and projected production conditions. At depth in the reservoir, fluids are compressed (more dense) and expand as they rise to the surface. Production volumes are measured at the surface, where oil and gas are separated and stored in tanks. For converting oil in place to tank oil (m^3), the "oil formation volume factor" is determined (oil plus dissolved gas volume at reservoir conditions divided by oil volume at surface conditions). Because of dissolved gas, oil formation volume factors are commonly >1 and reach >2 for volatile-rich oil and high gas/oil ratios. Similar rules are followed for natural gas deposits, but because of the high compressibility of gas, formation volume factors are <1. Gas at the surface is measured in standard cubic metres (Sm^3).

The viscosity of reservoir fluids is the principle property that controls flow through rocks of a given permeability to the well. Viscosity of crude oil is reduced by increasing amounts of dissolved gas and by rising temperature. Considering that the reservoir temperature changes little during production, it is mainly pressure and gas loss that cause gradually diminishing flow of oil from pore space to the well.

Saturation describes the relative amounts of water, oil and gas in pore space as a percentage of volume. Water saturation is the volume of water contained in a volume of pore space. It is essentially a measure for the boundary between the oil or gas zone and the water zone. Oil-water (OWC) or gas-water (GOC) contacts are always gradual and require a precise determination. Lithologically inhomogeneous reservoirs may display water-rich lenses within the oil or gas zone.

Reservoir pore fluid pressure is generally near hydrostatic conditions. Freshwater imparts an average pressure increase of 9.8 kPa/m. An increase in salinity of 0.01 g/cm^3 adds 0.098 kPa/m to the hydrostatic value. Vertical rock pressure (correctly "rock mass stress") is normally the upper bound of possible (abnormal) fluid pressures. In principle, the vertical, lithostatic stress at a depth z (m) from the surface is calculated by the weight of a rock column with a cross-section of 1 m^2 (eq. 7.7). For sandstone, this amounts to ~22 kPa/m, or in units of stress 22 kN/m.

Calculating lithostatic and hydrostatic stress:

$$\sigma_{(v)\ or\ (hyd)} = \gamma \cdot z(\mathrm{m}) \tag{7.7}$$

$\sigma_{(v)}$ is the lithostatic, $\sigma_{(hyd)}$ the hydrostatic stress, γ the rock unit weight calculated from density multiplied by gravitational acceleration (9.81 m/s^2, or rounded for estimates, 10 m/s^2). Inserting pore fluid unit weight for γ, hydrostatic stress (or pressure in kPa) will be the result.

In rock, the vertical stress induces smaller horizontal stresses, so that a complete stress field is defined by the three vectors σ (v), σ (H) and σ (h). The direction of the larger horizontal stress σ (H) is usually imposed by the regional plate tectonic stress field. However, the complex load path and geological history of most rock bodies cause frequent deviations from this idealized pattern (Brady & Brown 2004).

Average reservoir pressure is equal to a water column with the density of 1.1 (a brine with ~8 wt. % dissolved NaCl). Abnormal fluid overpressures are defined by a value above the mean of hydrostatic pressure and lithostatic stress. Even higher pressures are possible, but very rare. Overpressures typically occur in sand lenses enclosed by mudrock, but may also be a regional feature as in Late Cretaceous chalk in the North Sea (Mallon *et al.* 2005). In sand enclosed by clay, total vertical stress rests in part or fully on the pore fluid. In the latter case, the sand grains float in the fluid and have hardly any contact with each other. This is due to inhibited dewatering and compaction of the sand when it was rapidly buried (under-compaction or disequilibrium compaction). A second mechanism for creating overpressures is expansion by increasing fluid volume in a restricted pore space, for example conversion of kerogen to oil, gas and water (Swarbrick & Osborne 1998). Overpressures dissipate naturally by fluid flow out of the system. The required time is a function of permeability. Compressive tectonic stress fields favour longer conservation of high fluid pressures (Sibson 2003). Supralithostatic high-pressure fluids, such as gas generated by the decomposition of oil and kerogen in very deep (>3 km) compartments, may cause hydraulic fracturing and fluid flow in fractures (Grauls & Cassignol 1992). Transmission of high fluid pressure through fissures, or by uplift and inversion can cause unexpected overpressure at shallow depths (Tingay *et al.* 2007, Luo *et al.* 2003). Formations and reservoirs with unexpected overpressure endanger drilling because of the blowout risk. In spite of precautions, fatal accidents, high costs and environmental damages too often result from blowouts (Tingay *et al.* 2007, Fertit *et al.* 1994).

Abnormally low pressures (below hydrostatic conditions) are the result of over-consolidation, with dense packing and low pore volumes that were imprinted when the rocks were at greater depth than at present. Neuzil (2000) suggested that osmotic action may also induce abnormally low pressures. The retention of subhydrostatic pressure after erosion and uplift is evidence of very effective sealing against migrating fluids for geological time periods. Rock bodies with these characteristics are suitable hosts and barriers for toxic and radioactive waste (e.g. the Early Cretaceous shales, in Figure 5.30).

The subsurface temperature/depth profile reflects the local geothermal gradient but is modified by other factors. The average geothermal gradient in the crust approximates 25–30 °C/km. However, as a function of local heat flow and the thermal conductivity of rocks, it varies between extremes of 20 and 250 °C/km. As rock salt is an excellent conductor of heat, higher temperatures are measured on top of large salt bodies (e.g. diapirs). Locations with high temperature near the Earth's surface are prime targets for geothermal energy exploration.

7.5.2 Oil and gasfield development

After successful discovery of a new hydrocarbon field and its confirmation by a first well, resources and reserves must be established. This requires that the oil or gasfield is delineated and that spatial distribution and variation of essential parameters, such as porosity, permeability and hydrocarbon saturation, are known. These tasks necessitate drilling more wells. Apart from supporting reserve estimates, the new wells are later to serve production.

Development and production of a simple homogeneous oilfield is theoretically possible from only one well. In the case of gas drive and gravity flow, production would be from the base of the oil zone, and from the top with water drive. In good reservoir rocks, oil and gas may flow for considerable horizontal distances. In the Middle East, the first production wells were several kilometres apart (Figure 7.13). In practice, however, much smaller intervals are the rule, caused by changing reservoir properties, complex geometry and the need to support extraction by injection of gas or water. Similar conditions determine the development of a conventional gasfield.

Worldwide, coal bed methane (CBM) production is rapidly increasing (Figure/Plate 7.24). Because of porosity and jointing (cleats), most gas-bearing coals are moderately permeable aquifers. In order to facilitate gas flow to the wells, pressure is lowered by pumping water (Figure 7.25). Vertical production wells in the Powder River Basin are spaced in a grid, which allows degassing an area of ~160 ha. Production is often higher than original sampling indicated. This may be explained by flow from a greater distance than expected, or on-going microbial gas generation (Ayers 2002). Improved extraction technology incorporates in-seam, or horizontal wells with lengths of ~1000 m, drilled perpendicular to the fracture system of coal seams. This design maximizes drainage of the gas, resulting in many times greater flow rates than can be achieved from vertical, fracture-stimulated wells. Lowering pressure in permeable reservoirs by pumping is also the most promising technology for the development of gas hydrate deposits (Boswell 2009). Reduced pressure causes hydrate dissociation and releases methane.

Figure 7.24 (Plate 7.24) Drilling for CBM gas in the Rocky Mountains near Pinedale, Wyoming, USA (2008). Copyright Shell plc.

Tight shale gas development consists of drilling a pattern of parallel holes that run thousands of metres within beds, in order to enhance drainage. Shale in the thermogenic gas maturity stage (R_o ~1.3–2.0) is commonly lithified and fractured. If permeability should be too low, hydraulic fracturing is used to increase gas flow. The pioneering discovery and technological innovation took place in the Fort Worth region in Texas, where production started in 1999. The Mississippian (Early Carboniferous) Barnett Shale at Fort Worth is a thick organic-rich shale (TOC 3–5 wt. % of kerogen type II), which hosts giant recoverable gas resources (~$850 \times 10^9\,m^3$: Pollastro *et al.* 2007) and currently provides ~50% of US gas production. Although extraction is more expensive

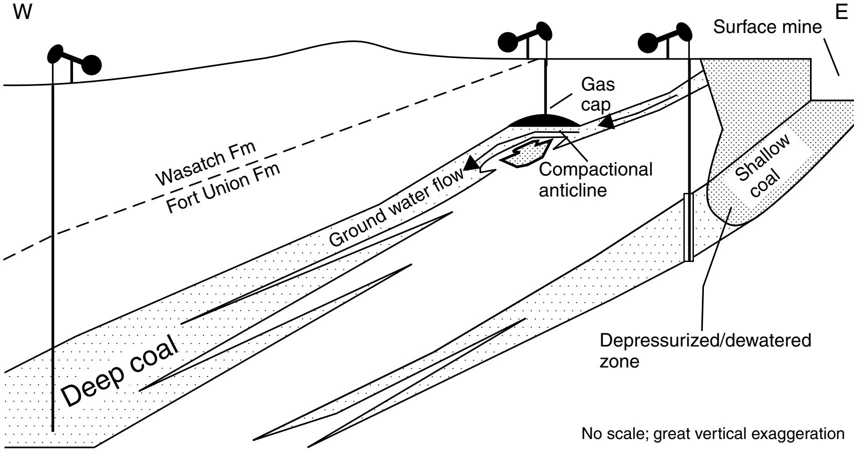
W
E
Surface mine
Gas cap
Wasatch Fm
Fort Union Fm
Ground water flow
Compactional anticline
Shallow coal
Deep coal
Depressurized/dewatered zone
No scale; great vertical exaggeration

Figure 7.25 Strategies of exploration and extraction of coal seam methane in the Palaeocene-Eocene Powder River Basin, Wyoming (Ayers 2002). Initially, production started in low-pressure zones near open pits and in shallow traps. Meanwhile, drill holes reach a depth of >1000 m. The coal is of low rank (<0.4% R_o), and the gas is of microbial origin. Because of well-developed cleats, the seams are aquifers with a permeability between 10 mD and several Darcy.

compared to conventional deposits, the economic success triggered a worldwide search for tight shale gas deposits:

> The giant gas play in the Barnett Shale occurs in an area of northwestern Texas where for >100 years conventional hydrocarbon deposits had been exploited, many of which were sourced from Barnett Shale. For some time now, the province was considered to be mature. Innovative thinking led to the recognition that source and reservoir may be one within this 300 m thick unit. Seals are provided by dense footwall and hanging wall limestones. The newly found gas resources are in shale with a maturity $R_o > 1.1\%$. Wet gas occurs in the maturity zone R_o 1.1–1.4%; near the Ouachita Structural Front at $R_o > 1.4\%$, only dry gas is found (Pollastro *et al.* 2007). The strong heat gradient may have been caused by fluids driven from the Ouachita orogen. *In-situ* gas was generated by cracking of oil and bitumen and is unassociated (no oil).

7.5.3 Oil and gas production

In many fields, initial oil production is by free flow from the well. The pressure in the reservoir is sufficient to drive the oil to the surface. Three main mechanisms cause a natural drive, and support primary production:

1. water drive (recharge of bottom water from an aquifer);
2. gas cap drive (expansion of the gas cap);
3. depletion, or dissolved gas drive (no gas cap, expansion of the oil and its dissolved gas).

Note that in practice these driving mechanisms are often combined. Gravity and compression of the pore space with decreasing fluid pressure have a secondary role:

> Water drive is more favourable than the other mechanisms, because oil and gas recovery is highest, with a range of 20–80% and an average of 50% of oil in place (Chierici 1994). Bottom water under a high hydraulic head forces the hydrocarbons upwards and to the wells. If the aquifer is continuously recharged, the original reservoir pressure may hardly change. With less effective recharge, the pressure drops. Heterogeneous reservoir rock may induce irregular rise of the water-oil or water-gas contact. If the natural water drive is insufficient or irregular, injection of water is a frequent corrective (Figure 7.26).

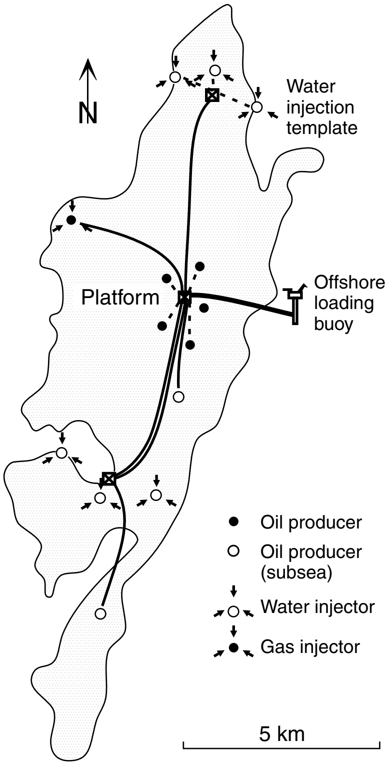

Figure 7.26 Development plan of offshore oil field Draugen (cf. Figure 7.16), with support of oil production by gas and water injection (Provan 1992). In this field, reservoir pressure is low and the oil is gas-undersaturated.

Gas cap drive occurs at oilfields with an important gas cap (Figure 7.14). Expansion of the gas displaces the oil downwards, where it is produced from wells near the bottom of the oil zone. Oil production and reservoir pressure fall steadily while the gas/oil ratio rises. Oil recovery is between 20 and 58%, with an average of 33%. Injection of gas (gas recycling) supports pressure and improves production and oil recovery.

Depletion gas drive characterizes oil deposits without a gas cap or a contact with an aquifer. This may be the case for a sand reservoir enclosed in tight shale. Oil and dissolved gas are lifted together so that pressure falls rapidly. Careful management must avoid effervescence of a gas phase in the reservoir, which drastically impairs oil production. Recovery by depletion gas drive is poor, with an average of 20% and a range of 13–30%. Secondary (e.g. gas injection) and tertiary production methods (see below) must be used at an early stage.

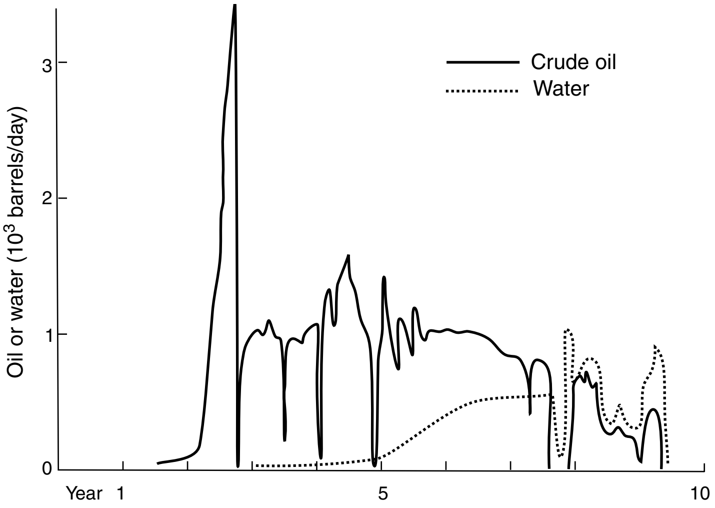

Figure 7.27 Production history of an oil well in North America showing change from dissolved gas drive to water drive. Note increase of co-produced water with time. Courtesy of Mobil Oil Germany.

At many oilfields, drive mechanisms change during production. Production vs. time diagrams characterize types and reveal the change. In Figure 7.27, initial drive by dissolved gas was quickly exhausted but replaced by water drive until depletion. If the reservoir pressure falls to a level too low for oil to flow to the surface, gravity may assist recovery by supporting a steady flow towards production holes. Gas injection and various stimulation methods, such as hydraulic fracturing, are often employed to assist oil flow. Pumping the oil is typical for many mature oilfields, often marked by hundreds of "nodding donkeys" (well-head pumps; Figure 7.28). The oilfield is depleted when the costs of pumping surpass earnings.

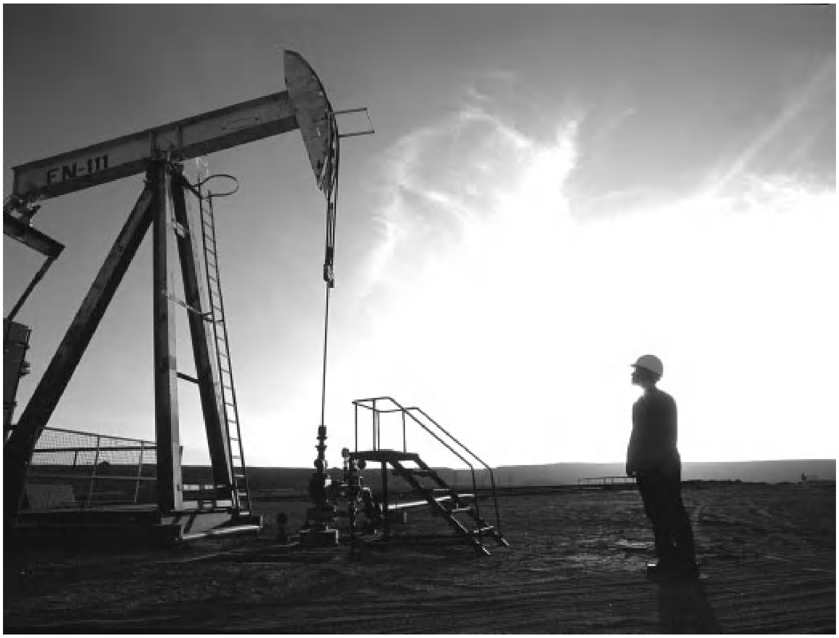

Figure 7.28 The symbol of mature oil fields: A nodding donkey in Oman. Copyright Shell plc.

Secondary, artificial lift methods

Secondary, artificial lift methods are employed to preserve reservoir energy, which is depleted during production. Primary oil recovery is usually low and injection of water and gas (predominantly CO_2, N_2) are widely utilized. Water "flooding" (injection) is very common. Wells for water injection are sited at oil zone margins or in the bottom aquifer. They support production and are also useful as a means to dispose of the saline water that is lifted with oil. The movement of injected water is controlled with tracers (Zemel 1995). Secondary production methods are essential but overall, average oil recovery still remains at unsatisfactory levels.

> Seawater for flooding is treated with biocides in order to prevent microbes from intruding the deposit. With untreated seawater, hyperthermophilic bacteria and archaea, some of which live at black smokers on the sea floor, are induced into the reservoir where they thrive in spite of high T and P, and reduce SO_4 to H_2S (Stetter *et al.* 1993). The result is simultaneous anaerobic biodegradation of the oil *in situ* and detrimental H_2S contents in the extracted oil. To avoid this, sulphate may be separated from seawater before injection, especially if barite precipitation in the reservoir is possible, which risks reducing porosity and permeability. Reactions of injected seawater in the reservoir are surprisingly rapid (Houston *et al.* 2007).

Flow management in the reservoir determines production rate and oil recovery. Important controls of production flow include the pressure gradient to the well, the viscosity of the pore fluid and the permeability of the reservoir rock. The latter is subject to geological inhomogeneity and anisotropy. Water-wet conditions (water films enclosing grains and narrowing pore throats) and free gas bubbles in the pores reduce permeability for oil. In the common water-oil systems, permeability for oil approaches zero when the share of oil in the pore space falls below 30–20%. A total recovery of oil in place with well-production methods is impossible. Compared with traditional fluid management and primary plus secondary methods, four-dimensional, or time-lapse seismic survey methods raise oil recovery by 10–15%. This is possible by close monitoring and improved management of the changing boundaries of gas, oil and water in the reservoir, comparing three-dimensional seismic data measured at time intervals (e.g. first during exploration, repeated during production). Time is the fourth dimension. Advanced visualization and modelling methods are the key to increased oil recovery.

Technical measures influence fluid flow in the immediate surroundings of a production well. They include "stimulation" by hydromechanical fracturing of the rocks or by injection of mixtures of hydrochloric and hydrofluoric acid creating dissolution voids. Frac methods (i.e. fracturing the rocks around a well) are important for the production from reservoir rocks with low permeability, for example tight shale and sandstone. For flow stimulation, a fluid (usually water) is injected under very high pressure. Induced fractures reach a length of 1000 m and a surface in the order of km^2. The fractures are kept open with co-injected sand or corundum pellets. By this method, the flow of gas and oil from "tight" formations to the well is dramatically improved.

Tertiary production, or improved oil recovery (IOR) Methods

Tertiary production, or improved oil recovery (IOR) methods raise the recovery by another 10–15% of initial oil in place, in addition to the advantage of 10–15% gained by four-dimensional seismics. This adds up to today's average oil recovery of ~50%. Enhanced recovery methods include (De Haan 1995):

- Chemical additives to flood water such as surfactants and polymer gels assist precise management of the oil-water boundary. Surfactants reduce the difference between the surface tension of oil and water, liberating oil trapped in narrow pores and improving flow. Polymers block preferential water flow through high permeability zones in the reservoir.
- Hydrocarbon gas-based recovery methods, especially the combination of hydrocarbon gas (typically propane and butane) and water injection, which are combined because water and gas displace oil from different parts of a reservoir. The technology is long proved and known as water-

alternating-gas method (WAG). Supercritical CO_2 liquid for IOR (Klusmann 2003) is expected to develop into an attractive alternative to hydrocarbon gas, once sequestration will be rewarded by carbon credits.
- Thermal flooding with hot water or water vapour (Coburn & Gillespie 2002) and *in-situ* combustion are extremely effective. Heating reduces the viscosity of oil and combustion creates a front of liquid hydrocarbons that are driven to production wells. Vapour flooding in Kern River oilfield, California, raised recovery of oil *in situ* to 75–80% (Coburn & Gillespie 2002).
- Microbially enhanced oil recovery (MEOR) works by injecting microbes or supporting oilfield-indigenous microbes in selective biodegradation of large molecules (reducing viscosity), production of surfactants (lowering interfacial tension) and increase of the driving force by biogenic methane production.

The economic significance of improved oil recovery methods rests in the increase of reserves ("field growth", see below). The methods are deployed in deposits that are mature (past peak production), well-known and fully developed. Additional investment for IOR is limited. Employing IOR methods is profitable and contributes to responsible management of natural resources.

7.5.4 Petroleum mining

Mining of near-surface petroleum is rapidly expanding (cf. tar sands). Future high prices and increasing shortage of oil may one day justify conventional mining of the giant amounts of oil, which are left behind in conventionally depleted deposits (George 1998). One version is to build a network of drainage galleries underneath reservoirs and to use vapour flooding to lower oil viscosity allowing seepage into collector adits. It is thought that reservoirs to a depth of 1000 m might be exploited by underground mining. Similar concepts exist for exploitation by means of horizontal drillholes, avoiding the costs of mining and the risks for workers. Alternatively, cost and risks might be alleviated by automated mining, which is already in development. *In-situ* steam-assisted gravity drainage based on boreholes is practised to recover oil from the Canadian tar sands situated below opencast depths. If this technology can be adapted for deep reservoirs, huge additional oil resources will be the result. In Germany, for example, estimated resources plus past production add up to 765 Mt of oil in place, but with present technologies 430 Mt are left in the ground.

7.5.5 Reserve and resource estimation

Reserve figures of oil and gas fields, provinces, countries and of the whole world are essential information for rational planning. Share values of large international companies are in part a function of their reserves. States controlling giant reserves and resources are sought as allies and are able to control markets. Oil and gas impart economic and political power. With so much at stake, it is hardly expected that published reserve figures can always be trusted.

In contrast to the political level, there is a highly developed professional standard of reserve estimation in the hydrocarbon industry. Refer to Chapter 5.3 "Ore Reserve Estimation and Determination of Grade" for general definitions and methods. There is little methodical difference between ore and hydrocarbons, including the extensive use of geostatistics. Only scale, complexity and financial risk are generally higher, compared with the average mine.

Here, allow me to point out some principles of reserve and resource estimation, which are specific to the oil and gas industry. Details are provided by Chierici (1994) and Dake (1994). Foremost, only proved and audited reserves may be published by companies whose shares are traded on the stock exchange (e.g. the Valmin code, AusIMM 2005). A large part of the figures reported in the introduction to Chapters 6 and 7, however, are not audited (BP Statistical Review of World Energy 2010), because controlling states allow no independent evaluation. The term "proved reserves" is defined by a high certainty of viable production under present economic conditions and with existing technology. Methods of reserve estimation in the hydrocarbon industry fall into the three categories: i) volumetric; ii) material balance; and iii) production performance methods.

Volumetric methods are the only way to estimate reserves in newly found hydrocarbon deposits, based on the geometry of the reservoir, its pore volume and oil (or gas) saturation. Because reserves are principally expressed in oil at surface conditions (tank oil), the volume change of oil from reservoir to the surface must be determined. Most critically, the overall recovery factor must be estimated. The principle of volumetric reserve calculation is illustrated by eq. 7.8.

Volumetric calculation of recoverable oil in place, measured at tank conditions:

$$N = A \cdot h \cdot \Phi \cdot (1 - S_w) \frac{\rho_o}{B_o} \cdot E_R \qquad (7.8)$$

N = recoverable oil (t), A = area of trap (m^2), h = average thickness of oil zone in reservoir rock (m), Φ = porosity of reservoir (−), S_w = share of water in pore fluid (−), ρ_o = density of oil (−), E_R = recovery factor for oil (−) and B_o = formation volume factor (−).

The material balance method works by carefully monitoring changes in the reservoir during exploitation. The extraction of hydrocarbon fluid imparts changes such as falling pressure, extension of the gas cap and a rising oil-water contact. Based on these data, a material balance is established for each of the phases in the reservoir. The material balance equation consists of a set of terms (eq. 7.9), which represent all physical changes that are balanced in such a way as to yield a very precise measure of extractable oil remaining in place (the reserves).

A simplified example of the term for oil in a material balance equation:

$$\text{Oil remaining } \textit{in situ} = (N - N_p)B_o \qquad (7.9)$$

N = initial volume of oil in the reservoir, in m^3 tank oil, N_p = cumulative tank volume (m^3) of oil produced, B_o oil formation volume factor.

During the productive lifetime of a field, the material balance calculation is regularly repeated and refined. The deposit is imaged by a numerical model, which consists of spatial elements (blocks). Measured dynamic changes are used to simulate the past and future behaviour of the system in every block of the model. Parameters that cannot be measured are derived by approximation or Monte Carlo simulations. History matching (adjusting model parameters in order to improve simulation of past behaviour) is employed to improve models. The results produce ever more precise figures for oil (or gas) in place. Yet, the validity of numerical simulation of a reservoir system is still limited to a near future.

Reserve estimation is very similar for an ideal, closed dry gas deposit within a homogeneous reservoir and without contact to water. A single borehole is sufficient: Initial production will cause a pressure drop. The extent of the fall in pressure is a function of the initial pressure, the volume of gas produced and the initial volume of gas *in situ* (the reserves). The results of preliminary calculations of this kind are normally insufficient for reserve declaration but may be critical for the decision to abandon the project or develop the field. With more wells and a better database for the reservoir, volumetric and material balance calculations are employed. Development of gas in tight (low-permeability) reservoirs relies on very close drillhole distances and reserves depend on highly efficient fracturing technology.

Production performance methods are a tool proved in oilfield engineering for estimates of remaining reserves. By definition, however, they are limited to projection of past performance into the future. This is the same principle as applied in constructing the Hubbert Curve (picturing production vs. time: Hubbert 1962). Utilization of the method must be guided by a deep understanding of the production history and its parameters. It is limited when different drive variants and production technologies were involved which, incidentally, produce rather plateaus than curves. Extrapolation of the Hubbert Curve is at best a measure of the most easily accessible resource, given technological, political and economic constraints (Cavallo 2004). Is it not thought-provoking that the Hubbert Curve and the Peak Production Method of resource estimation are little used in the non-hydrocarbon minerals community? The terms are not even mentioned in the remarkable volume on reserve and resource estimation by A.C. Edwards (2001). Also, the frequent occurrence of reserve growth in oil and gasfields falsifies blind acceptance of production history projections:

> Kern River oilfield in California was discovered in 1899. In 1942, after a production period of nearly 50 years, its remaining reserves were calculated at 54 Mbl. Production until 1986, however, amounted to 736 Mbl and remaining *in situ* reserves were declared at 970 Mbl (Maugeri 2004). Today, resources recoverable by steam flooding are estimated at >1000 million barrels.

Kern River is possibly exceptional. Yet, oil and gasfield reserve growth is widely observed. Causes of field growth include economic, technical and non-technical parameters (Attanasi & Root 1994). Steam flooding in Kern River field illustrates how the introduction of a new technology (human inventiveness) may change all apparently rational forecasts.

Estimates of undiscovered (prognostic) oil and gas resources are calculated with similar methods that have been described in Chapter 5.3 "Ore Reserve Estimation and Determination of Grade". An exemplary estimate of undiscovered oil and gas resources in the Arctic realm illustrates current best practice (Gautier *et al.* 2009).

7.5.6 Post-production uses of oil and gas fields

When an oil or gas field is abandoned because further production is an economic loss, all boreholes must be carefully sealed (Fuenkajorn & Daemen 1996) in order to minimize risks for humans, the biosphere and the geosphere (e.g. groundwater). Before taking the decision to close operations, companies will undoubtedly analyse the costs of preserving boreholes for later use against a possible future profit. In Chapter 5.3 "Valuation of Mineral Deposits", we have seen that future income, which accrues after a time of ~15 years, is nearly worthless. This is why the decision to dedicate drillholes to a different future utilization will rarely be positive. Some wells may be converted for CO_2 sequestration (Figure 6.3) and deep storage of fluid waste (Figure 5.27). In countries that have only limited resources of gas and oil (e.g. most of Europe), the underground storage of a strategic reserve of imported natural gas and oil (in salt caverns and depleted hydrocarbon reservoirs) is common practice. Transformation of deep oil and gas wells near large heat consumers such as industry and big cities, into geothermal energy producers may be economically attractive.

7.6 TAR SAND, ASPHALT, PYROBITUMEN AND SHUNGITE

Two totally different environments of petroleum degradation cause formation of the substances treated in this chapter:

1 oil reservoirs are heated beyond the stability of liquid hydrocarbons, usually caused by subsidence to great depth; and
2 deep, shallow or supergene biogenic degradation, oxidation, water washing and evaporation of volatile fractions increase the density of oil.

Compared to conventional crude oils with 22–35°API, the latter results in heavy (10–22.3° API) and extra heavy (<10° API) petroleum. Tar is a term for heavy and extra heavy oils with 6–12°API, whereas asphalt, pyrobitumen and shungite are the products of such severe alteration that any use resembling that of liquid hydrocarbons is precluded.

7.6.1 Tar sand

Tar is a highly viscous mixture of heavy and extra heavy petroleum. The chemical composition of tar is characterized by loss of aromatics and saturated hydrocarbons, whereas resins and asphaltenes are enriched. Tar is a source of valuable petroleum products but at a higher cost compared with oil. Therefore until recently, tar deposits have been shunned in favour of conventional oil. Giant tar deposits occur in Canada and Venezuela, and large resources are known in most oil provinces of the world.

The largest tar province known is the region around Athabasca, Peace River and Cold Lake in Alberta, Canada. Along the eastern margin of the Western Canada Sedimentary Basin east of the Rocky Mountains, an Early Cretaceous sandstone

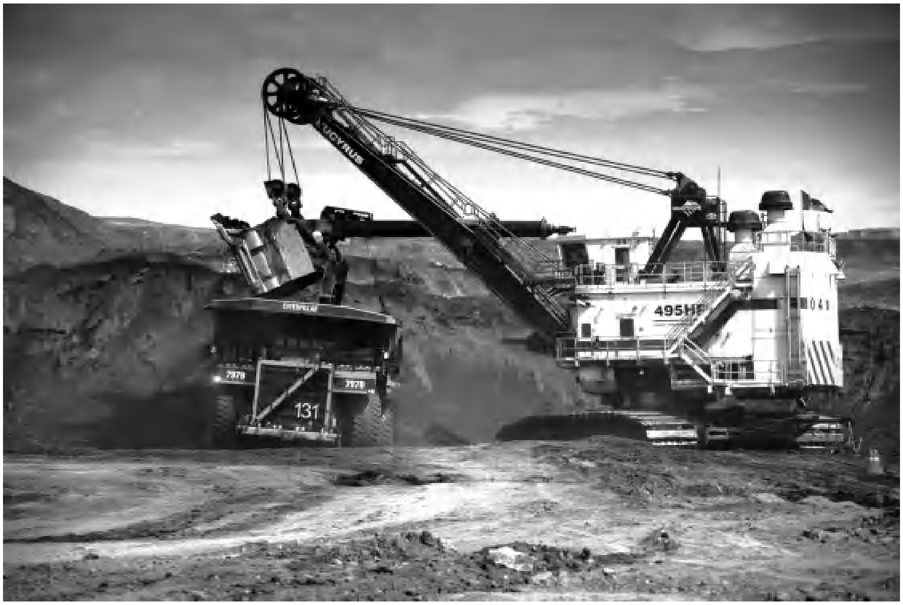

Figure 7.29 (Plate 7.29) Oil sand mining at Muskeg mine, Athabasca, Canada (2009). Copyright Shell plc.

unit (McMurray Formation) underlies an area of >140,000 km^2. In this area, channels and bars in the fluvial lower member of the McMurray Formation are impregnated with extra heavy oil (7° API gravity) and asphalt. The sandstone was deposited in a large coastal delta above Devonian limestones and covered by marine shales that later acted as the seal. Natural outcrops of the tar sands are known near Lake Mildred but the largest part is covered by 50 to >200 m thick glacial and fluviatile Quaternary sediments. The average thickness of tar sands is 50 m, but attains 275 m. The sand consists of quartz and clay, and up to 19% tar. The source rocks are buried beneath the Rocky Mountains and appear to include sediments of Devonian to Jurassic age. Earliest migration took place at 112 ± 5.3 Ma, synchronous with sedimentation of the Albian-Aptian host (Selby & Creaser 2005):

> The bitumen cements quartz grains of the sand, although pore space is mainly water-wetted. Leaching the bitumen leaves sand and a maximum of 30% clay. Various exploitation processes have been devised. At present, ca. 55% of oil is produced by excavating near-surface tar sand in large open pits (Figure/Plate 7.29). In extraction plants, the bitumen is separated from sand and clay by agitation in hot water with dissolved caustic soda, and flotation. The bitumen concentrate is cleaned, upgraded to crude oil and shipped to refineries. Deeper deposits are exploited by several *in-situ* technologies. Steam-assisted gravity drainage (SAGD) based on boreholes is the source of ~45% of oil from tar sands. The bitumen is liquefied *in situ* and pumped to the surface. This process consumes little water and its GHG footprint is comparable to conventional petroleum. In spite of high sulphur content of the bitumen, the final product is sweet light syncrude with ~40°API. Recovery is between 70% and 100%. In 2008, the combined production of three well-established mines reached ~1 Mbl/d (~160,000 m^3). With today's technology, the volume of total recoverable oil in the district is thought to surpass the conventional oil reserves of Saudi Arabia (George 1998). The *in-situ* volume is estimated at >1.7.10^{12} barrels (>270,000 Mm^3). At the end of 2009, proved reserves amounted to 23,300 Mt crude oil (143,000 Mbl: *BP Statistical Review of World Energy* 2010). Heavy minerals of the sand fraction, clay and trace metals (including V, Sc, Ni, Mo, Ga) in the ash of the residual bitumen are planned to be future by-products.

7.6.2 Asphalt

Asphalt (Abraham 1960, Yen & Chilingarian 1994, 2000) is a term used for the substance found in nature and the similar but not identical residual fraction of crude oil distillation. Natural asphalt contains less hydrogen but more nitrogen and oxygen than conventional oil (Table 7.2). High sulphur contents are characteristic. Asphalt is enriched in naphtenes, aromatic hydrocarbons and asphaltenes (N-S-O compounds). It is fusible and soluble in carbon disulphide. Asphalt is modelled as a suspension of asphaltene particles and micelles in liquid hydrocarbons. Structurally, asphalt is a gel. Many asphalts contain mineral substances, such as sand and clay, which is mainly due to flowage erosion. The distinction between tar and asphalt is based on rheological behaviour. At ambient temperature, asphalt is apparently solid but highly viscous, whereas tar is less viscous and liquid.

Asphalt originates where petroleum is subject to supergene alteration. It is a common product of oil seeps and oil-rich mud volcanoes. Oil at the surface loses light hydrocarbons ($<C_{15}$) within two weeks by evaporation and heavier HC up to about C_{24} in a few months. Water-soluble compounds are leached and microbial degradation sets in. Oxidation and polymerization harden the oil into asphalt and pyrobitumen.

Asphalt and the comparable residual fraction of petroleum distillation (sometimes referred to as "bitumen") are used in large amounts as a thermoplastic binder of aggregate materials in the construction of road surfaces and runways of airports. For manufacturing asphalt concrete, the material is heated to ~150 °C. Roofing, anti-corrosion pipe covering and the underbody protection of motor cars are a few examples of other uses. Properties that control asphalt use include the chemical and molecular composition, colloidal and physical characteristics. Road construction, for example, requires asphalt with a suitable thermal behaviour. At deep temperatures, asphalt should not harden to the state of easy fracturing, nor should it become plastic on hot summer days. Modifications of natural and artificial asphalt are employed in order to improve resistance against ageing, water, bacteria and UV-light, and to increase thermal and structural stability.

The earliest known use of asphalt occurred in the Middle East and in India. Mud volcanoes on Apsheron Peninsula, Azerbaijan produced profuse amounts of an asphalt-clay mixture. Industrial production was initated in the 19th century from the 1 km^2 asphalt lake near La Brea on the island of Trinidad and the larger Bermúdez lake in Venezuela. At Bermúdez, a thick layer of asphalt with ~25% H_2O and up to 50% of mineral substance floats on water. Although both sites continue to be worked, traded asphalt is dominated by oil residuum from refineries.

Asphalt limestones are not rare. Like oil in carbonate reservoir rocks, these limestones host asphalt in pores, and in fractures and veins. Asphaltic limestones may be regarded as exhumed oil reservoirs. Former mining areas in Europe include Dalmatia, Slovakia, the Jura Mountains of Switzerland, the Monte Abruzzi and Ragusa in Italy, and Lower Saxony in Germany. In the latter, Late Jurassic limestone with a thickness of 3.5–14 m and an average 2.5% asphalt is extracted by underground mining and manufactured into special floor tiles.

7.6.3 Pyrobitumens

Pyrobitumens are defined according to physical properties and uses, not by origin, maturity or chemical composition (Hunt 1996). Pyrobitumens are black, solid, non-volatile, infusible (unlike ozocerite) and insoluble in organic solvents including carbon disulphide. Pyrobitumens are chemical raw materials, sealing compounds, a component of control rods in nuclear reactors and of black pigments. Recent mining is reported from Utah, Argentina and China. Deposits are mostly veins and stratiform bodies (Parnell *et al.* 1996, Bing-Quan *et al.* 2001). Pyrobitumens form in at least two fundamentally different environments: i) Most pyrobitumen originates at a late stage of thermal oil cracking; and ii) physically similar material results from surface degradation of oil (Hunt 1996). Thermal pyrobitumen originates at $T > 150$ °C by sudden pressure drop and loss of dissolved gas and condensate (cf. "cracking equation" 7.10). This pyrobitumen is evidence of the former presence of petroleum (Mossman & Nagy 1996, Stasiuk 1998).

Schematic reaction describing the thermal conversion of oil to gas and pyrobitumen:

$$\underset{\text{(oil)}}{C_5H_9} \rightarrow \underset{\text{(gas)}}{2CH_4} + \underset{\text{(pyrobitumen)}}{C_3H} \qquad (7.10)$$

Under the microscope, thermal pyrobitumens exhibit characteristic features. In reservoir rocks, they mimic the shape of pores. Vein material is very homogeneous with a conchoidal fracture, displays flow textures and shrinkage cracks like coke and is partly vesicular. Small inclusions of authigenic pyrite, illite and carbonates have been reported. Trace metal contents are elevated and include V, Ni and Fe, but also Cd, Cr, Co, Cu and Zn. *In-situ* degassing is implied by many details. Flow-textures recall aspects of magmatic dykes, because the precursor oil is injected at high pressure and temperature into tectonic structures. As the rock yields, pressure drops, gas and condensate escape and the remainder freezes to pyrobitumen (or "migrabitumen", Jacob 1989). Under the name *impsonite*, pyrobitumens are quite common as a minor component of many hydrothermal vein deposits.

7.6.4 Shungite

Shungite is a non-crystalline, black, glassy and dense mineraloid, with a semi-metallic lustre reaching >98% C (with traces of N, O, S and H). With an age of ~2000 Ma, shungite deposits are the earliest giant accumulations of organic matter and of (former) petroleum. Hosted in a 1000 m thick volcano-sedimentary sequence, shungite formed in the brackish environment of an active continental rift. Shungite occurs in stratified beds (a former oil shale), in organosiliceous diapirs, or in redeposited clasts of migrated oil (Melezhik *et al.* 2004). It is remarkable that the organic matter was not graphitized, in spite of a Svekokarelian (~1.8 Ga) greenschist metamorphism. Shungite is exploited near Onega Lake in four large opencast mines. It is not combustible, but is used as a replacement for metallurgical coke, and as an absorber and filler.

7.7 OIL SHALES

The increasing depletion of conventional, cheap and easily accessible oil may intensify exploitation of oil shales. Like tar sand, oil shales contain giant potential energy resources that can be made available, although only with considerable technological and financial exertion (Russell 1990). The earliest industrial-scale oil retorting was founded by James Young at Bathgate, Midland Valley, Scotland, in 1847 (cf. torbanite in Chapter 6.1 "The Substance of Coal"). Raw materials were lacustrine and lagoonal oil shales interbedded with Early Carboniferous deltaic sandstones. Small artisanal operations, however, had provided humans with oil and pitch for medicinal purposes, water proofing and warfare since antiquity.

The designation "oil shale" is only used in order to communicate that a certain sedimentary rock may be useful to produce "synthetic" oil. The mineral matrix is irrelevant, but oil shale must contain organic substance (kerogen) that yields oil upon heating. Fine-grained sediments of almost any origin can contain high percentages of organic matter (cf. "Petroleum Source Rocks"). The petrographical range comprises siliciclastic pelites, carbonates and sapropelic coal, or coal shale. The presence of considerable amounts of authigenic pyrite is always an encumbrance. The organic substance is investigated with methods of organic chemistry and petrology (Taylor *et al.* 1998). Most oil shales are distinctly anomalous in uranium and in boreholes, can be detected by gamma ray logging.

Oil shale rarely contains oil or natural gas (cf. Antrim Shale). Most of the organic substance in oil shale occurs in the form of immature to low-maturity kerogen. Oil shale is a petroleum source rock that has not yet generated oil, or that retained a considerable potential of oil generation after going through a phase of partial catagenesis. Potentially economic total organic carbon (TOC) contents of oil shale range from 10 to 50 mass %. Oil yields vary from ~40 to 600 litres per tonne.

Because some of the energy contained must be spent on extraction and heating, mining and processing costs control the precise position of the lower boundary (the cut-off grade).

Kerogen rich rocks are commonly brown or black (Figure/Plate 7.6). When weathered, they stand out by whitish ash-like crusts that provoked, for example, the name "White Band" for an oil shale horizon in the Permo-Triassic Karroo of Southern Africa. Oil shales may be flammable with a simple pocket lighter, or at least release a strong aromatic odour. Fischer assay is the most common method of ranking oil shale in terms of potential oil produced (after Fischer-Schrader 1920). Conditions of the Fischer assay are similar to those of conventional pyrolysis under nitrogen. Also used are Rock-Eval pyrolysis (Espitalié *et al.* 1984; Figure 7.5) and the determination of whole-rock calorific values similar to coal. Because organic substances are considerably less dense than the minerals in shale, the determination of density is a shortcut whenever large numbers of samples are to be processed. Of course, a calibration curve for the project-specific correlation between TOC and density must be established.

Heated to ~500 °C, oil shale generates liquid and gaseous hydrocarbons that are raw materials for petroleum refineries, just like natural oil and gas. Technologies of oil extraction from shale include retorting, flushing with hot gas, and underground methods that were sketched in Chapter 7.5 "Mining of Petroleum". The largest current operations exist in China and Estonia. Estonian oil shale is mined in open pits and underground as a fuel for electric power stations. An increasing part of mine output, however, is the basis of synfuel production. Reserves amount to several thousand million tonnes. Across the border in Russia, mining the same shale bed recommenced in 2008. Depending on composition, the ash produced in power stations can also be used, for example as a hydraulic component of the cement formula (cf. Chapter 3 "Carbonate Rocks"). In many plants, oil shale is directly mixed with cement raw materials before sintering, saving fuel and replacing parts of clay or carbonate in the cement formula. Elevated metal contents may yield valuable by-products of oil shale processing (e.g. vanadium, uranium).

Petrologically, oil shales are organic matter-rich pelites or mineral matter-rich sapropelic coals. Oil shale formation is favoured by humid and hot climate. The frequency of oil shale beds (cycles/metre) in the Green River Basin, for example, is a function of orbital signals including precession, obliquity and eccentricity (cf. Chapter 3 "Sodium Carbonate"; Meyers 2008, Fischer & Roberts 1991). To be economically attractive, oil shale TOC needs to be higher compared with average hydrocarbon source rocks (e.g. 13% at Julia Creek: Lewis *et al.* 2010). Preservation of low-maturity kerogen is geologically more likely in settings that were not affected by deformation, subsidence and heating. This is typically realized in little deformed epicontinental platform sediments (e.g. Estonia) and in post-orogenic lake basins.

Characteristic depositional settings of important oil shales include:

- large inland lakes (the Eocene saline lakes of the Green River Basin in the western USA; Carboniferous lakes in New Brunswick, Canada; Triassic of the Congo Basin near Kisangani; the Songliao and Bohai basins of China); lacustrine oil shale typically displays low sulphur contents and yields a waxy, paraffinic oil (Hunt 1996);
- shallow epicontinental seas that deposit variegated sediments including shale, sandstone, carbonates and phosphates (the Ordovician kukersite of Estonia; Karroo of Brazil and Southern Africa; Middle Cretaceous in the Great Artesian Basin, Australia);
- paralic, coastal swamps where torbanite is associated with humic coal (Fushun, Manchuria, Figure 6.13; Liaoning, China; western margin of the Permian coking coal district of New South Wales, Australia);
- continental and marine rifts in a low heat flow setting (Carboniferous of the Midland Valley, Scotland).

Many oil shale occurrences are found in volcanic crater lake sediments (Neogene of Pula, Bakony in Hungary), in impact craters (Miocene Nördlinger Ries, Germany) and in maar lakes (Eocene at Messel, Germany).

The largest potential resources of oil shale occur in Brazil, China and USA. Many other countries such as Australia, Syria, Russia and Morocco have considerable volumes of oil shale. None of these states is a member of OPEC (Organization of Petroleum Exporting Countries). The world's prognostic oil shale resources are very large. Although estimates vary, extractable (synthetic) oil in place probably amounts to 500,000–700,000 Mm^3, counting oil shale with a minimum yield of 42 litres/tonne. This is about three times as much as conventional world oil reserves (212,000 Mm^3 in 2009) and might satisfy world consumption for >100 years. Because of relatively low current prices of conventional oil, the incentive to exploit oil shales as a source of liquid fuels is still moderate. Under changed conditions, exploration will expand and many new deposits will be discovered. Favourable economics are expected to encourage the development of new and better technologies, including extractive operations and environmental mitigation.

7.8 ENVIRONMENTAL ASPECTS OF OIL AND GAS PRODUCTION

The environmental disaster caused in 2010 by the offshore oil well blow-out in the Gulf of Mexico tragically demonstrated hazards and risks associated with oil production. Generally, however, the industry does not cause serious environmental problems. There are practically no emissions, no remaining waste and its footprint (e.g. land use) is minimal. Often, the lay person will not even notice the presence of producing fields. Sensitive landscapes, including permafrost tundra, or large cities, demand special precautions. In its own interest, the industry executes precautionary environmental management (Wilson & Richardson 1999, Orszulik 2008). Los Angeles is probably the city with the longest experience (since 1892) of oil and gas production within its perimeter. Its oil production is ~6.5 Mbl (2006) from 4000 onshore and offshore wells. The most critical problem encountered during the past was the seepage of methane and hydrogen sulphide into tunnels, basements and buildings (Bilodeau *et al.* 2007), caused by natural processes but also because formerly, oil wells were not properly plugged when abandoned. The city responded by publishing maps of risk zones and by enacting a Methane Mitigation Ordinance that prescribes building codes for proper venting, methane detection systems and automatic alarms when the methane concentration in air reaches 20% of the lower explosive limit (methane is only explosive between 5–15 vol. % concentration in air):

> One of the largest oil-contaminated landscapes in the world is Apsheron Peninsula in Azerbaijan, both by nature (mud volcanoes) and man. The peninsula is a ridge of the Caucasus Mountains plunging towards the southeast underneath the Caspian Sea. It was the site of the first major oil rush outside of the United States after oil had been found near Titusville, Pennsylvania, in 1870. When in the same year the Russian empire relinquished the oil monopoly, an explosion of entrepreneurship was released (Yergin 1991). Three years later, Robert Nobel, the oldest of the three famous brothers, visited Baku on Apsheron with the intention to buy walnut wood for army rifle stocks. He realized at once the business opportunity, bought petroleum wells and a distillery instead of wood, and launched a business that was in a short time closely competing with Rockefeller's American enterprise. Ludwig Nobel became the "Oil King of Baku"; brother Albert (the founder of the Nobel Price) helped with financing. In the 19th century, oil drilling was in its infancy and scientific understanding was limited, so that oil spills and outbreaks of oil ("gushers", or oil fountains) were lightly accepted. Baku was proudly called "the black town", because of spilled oil and the smoke of hundreds of distilleries. Apsheron was famous for producing many oil fountains, and the heritage from the pioneer days followed by 100 years of state management of the oil industry is quite impressive: Several thousand square kilometres of land and sea bottom are contaminated with oil, tar and asphalt. Abandoned industrial ruins, rusty derricks, oil pools, asphaltic soil and modern rubbish dumps serve as a paradigm of industrial pollution. It is a great achievement of free Azerbaijan that part of the present oil and gas income is invested in a giant land remediation project.
>
> More recently, in 1991, Saddam Hussein ordered the destruction and ignition of oil wells in Kuwait. For several months, 950,000 m^3/day of oil were lost by burning and flowing away over the desert. This

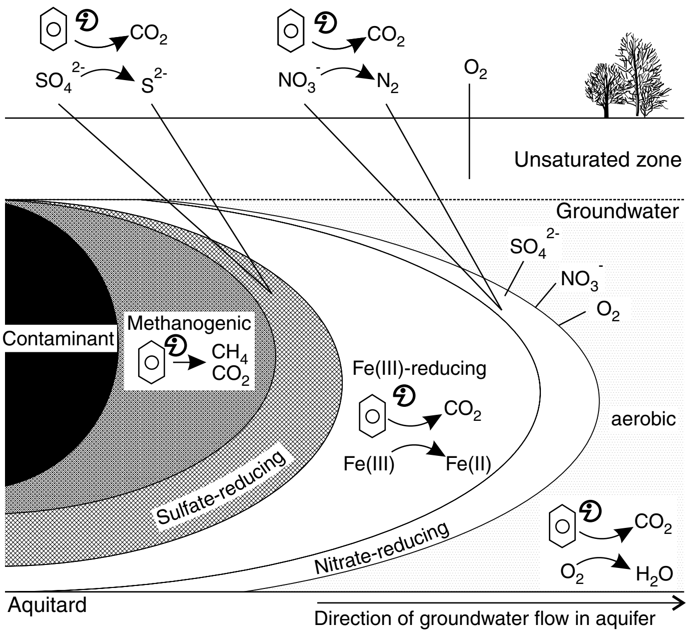

Figure 7.30 *In-situ* bioremediation of oil, gasoline or diesel fuel contaminated groundwater by supporting specialized anaerobe microbes that decompose hydrocarbons to harmless CO_2, N_2 and CH_4. Reprinted with permission from AAAS. Aerobe microbes are also capable of converting hydrocarbons (lower right), but it is difficult to inject enough oxygen into an oil-bearing aquifer (Lovley 2001).

bequeathed petroleum lakes, asphalt and soot covering ~6000 km^2. Because of the arid climate, natural biodegradation is virtually nil. Despite considerable mitigation work, negative impacts and hazards persist (Omar *et al.* 2009). Oil reaching the Gulf, however, was quickly decomposed by natural processes due to favourable conditions in a warm sea. Beaches are white as before, and life in the shallow sea is teeming.

Oil spills at production facilities, along pipelines and transport routes arouse public attention. Great care must be taken to avoid such accidents. The main problem is a sudden release of a large mass of petroleum; small diluted amounts are quickly decomposed by aerobic microbes (similar to eq. 7.6). This is confirmed by investigations of natural oil seeps. Every year, natural seeps introduce ~1.5 Mbl oil into the oceans and ~0.5 Mbl on land (Hunt 1996), with other sources suggesting a ten-fold upper bound (15 Mbl, 2.38 Mm^3 or 2 Mt). Biodegradation takes its course without human intervention. However, large concentrated quantities of oil defy microbes, because mineral nutrients are quickly depleted (especially phosphorous and nitrogen) and the contact surface is limited. Mechanical removal is therefore the first remedial action followed by application of mineral fertilizers. This was one of the lessons learned from the disaster of the Exon Valdez in the Prince William Sound, Alaska, in the year 1989. For oil in groundwater, anaerobic microbes are better qualified for biodegradation. They are assisted by injection of electron acceptors such as sulphate or nitrate (Figure 7.30).

Remarkable oil spills in the deep sea include IXTOC 1 in the southern Gulf of Mexico in 1979 (~560,000 m^3), Ekofisk in the North Sea in 1977 (32,000 m^3) and Santa Barbara off California in 1969 (16,000 m^3). At Macondo in the northern Gulf of Mexico in 2010, outflow amounted to ~4.4 Mbl (700,000±20% m^3; Crone & Tolstoy 2010) of oil within the 85 days until the well could be plugged. The composition of the oil determines much of the damage; the light paraffinic oil in the Gulf of Mexico, for example, evaporates in part and the remainder is more rapidly dispersed and biodegraded compared to heavy, asphaltene and NSO-rich oil. Natural seafloor vents of oil and gas support a specialized chemotrophic flora and fauna of high biodiversity. At a depth of 3000 m in the Gulf of Mexico, active oil seeps and tar flows ("asphalt volcanoes") have been discovered surrounding salt domes. Their species-rich fauna is comparable to the amazing ecology of black smokers at mid-oceanic ridges (MacDonald *et al.* 2004).

Oil slicks floating on water are removed with skimmers and booms. Applying dispersants, microbes and fertilizer may be considered. Several methods are available for the decontamination of soil and sediment:

- soil washing (soil is agitated in large containers, oil and asphalt are removed by hot water and steam; the oil recovered can pay for part of the costs; this technology is currently applied at an industrial scale for syncrude extraction from Canadian tar sands);
- incineration (destruction by burning);
- thermal energy recovery (using the inherent energy by combustion in cement works or power plants).

In the past, little attention was paid to the contents of natural radioactive substances in oil, gas and formation waters. Many source rocks and hydrocarbons are geochemically enriched in uranium and to a lesser extent, thorium. As both elements are insoluble at the reduced conditions of reservoirs, their daughter nuclides are of higher interest. Problematic are ^{226}Radium, ^{228}Radium and ^{210}Pb, which are dissolved in reservoir water and lifted together with oil. In pipes and settling ponds, they are concentrated in scales and muds. ^{222}Radon is dissolved in both hydrocarbons and reservoir water, and is concentrated in liquid gas during processing (Schmidt 2000).

7.8.1 Water resources protection

In the upstream oil and gas industry, formation water is carefully re-injected into deep aquifers in order to protect the environment and to support reservoir pressure. This is not possible when gas is produced from coal seams (coal bed methane = CBM operations), because much water has to be lifted before gas can be recovered. Water abstraction may affect the wider groundwater regime and entails problems of disposing of pumped water commonly rich in solutes. An average CBM-well in the USA is said to deliver ~20 t/y of salt.

7.8.2 Induced seismic activity

Oil and gas extraction at depth cause decreasing pore fluid pressures (Figure 7.31) and correspondingly, increasing effective stress (Brady & Brown 2004). This induces ductile consolidation or brittle fracturing, probably mainly along existing discontinuity planes. The subsidence of the centre above a field causes characteristic steep reverse (thrust) faults whose activity produces the earthquakes (Segal 1989). Subsidence can be predicted and mitigation measures can be planned, but timing and magnitude of earthquakes remain unpredictable.

The first and one of the largest gas production-related earthquakes to date occurred in 1951 at the Caviaga field (Northern Italy), with a magnitude of 5.5. Because seismic events at most oil and gas fields are very weak, good long-term records of seismic activity are rare. Excellent data exist on the seismicity of the Lacq field in the northern foreland of the Pyrenees (Maury 1997). At Lacq, a long suite of numerous micro-seismic signals was interspersed with a few earthquakes of magnitude 4.0 to 4.3. This is in a striking contrast to seismicity induced by injection of fluids (e.g. in geothermal frac-operations) or by large dams, which both raise fluid pressures in contrast to hydrocarbon production. Higher fluid pressures cause more frequent earthquakes that reach much higher magnitudes (the maximum measured until today was $M = 6.3$). In addition to the seismic risk, using former oil and gas fields for natural gas storage or CO_2-sequestration may lead to enhanced gas flow to the surface. This possibility must be carefully investigated as a potential hazard for people and environment.

7.8.3 Tar sand mining

Tar sand mining in the Fort McMurray region, Alberta, Canada, is rapidly expanding because of improved economic feasibility and the chance to diversify future petroleum supply. Oil shale mining shares a number of environmental aspects with the first: The useful substance in the rock is a very small fraction of the total volume, so that extraction and processing move very large masses indeed. Management of waste rock and tailings

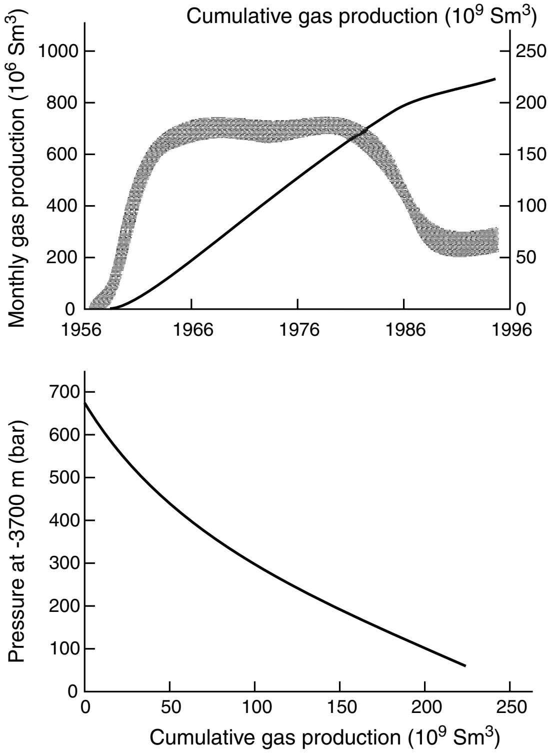

Figure 7.31 Production history (upper diagram) and concurrent pressure loss at 3700 m depth (lower diagram) in the French gas field Lacq Profond (modified from Maury 1997). Reproduced by kind permission of Total. Initially, the gas was highly overpressured (hydrostatic pressure should have been about 400 bar), promptly causing a gas outbreak when the discovery drill hole hit the reservoir. With declining pressure during production, earthquakes with a maximal magnitude of 4.3 first occurred in 1969. The surface above the field subsided 5–6 cm. Sm^3 is the methane volume measured at surface standard conditions. For location refer to Figure/Plate 1.89.

must consider possible self-ignition as with coal shale. Large masses moved translate into severe interference with the landscape. Recultivation and renaturalization are integral to all such operations. Tar sand processing uses large amounts of water. Both extraction and safe disposal of waste water have to be sustainable. Fossil organic substance is commonly associated with elevated contents of potentially toxic compounds, because organic matter-rich pelites are generally characterized by elevated contents of redox-sensitive elements, including Fe, Mn, U, V, Mo, Ni, Co, Cr, Cu, Pb, Zn, Cd and As (Morford & Emerson 1999). Dispersion of dangerous elements during processing, retorting and incineration must be avoided, preferably by recovering and selling these substances as a by-product. At present, the tar sand industry is changing very fast. Both the discovery of unforeseen environmental problems and of hitherto unknown solutions may be expected. One major advance is the newly established *in-situ* recovery of oil from tar sands by steam-assisted gravity drainage (SAGD) based on boreholes. SAGD results in lower production costs and a reduced environmental impact. Advantages include a lower carbon footprint and the elimination of large pits and tailings. One example of comprehensive oil shale use is a cement factory at Dotternhausen in southwestern Germany, where both the inherent energy and the mineral substance of Jurassic Posidonia shale are utilized for cement production.

7.8.4 Hydrocarbons and climate

As mentioned in the introduction to Chapter 6, climate is only one reason why the quest for a reduced dependence on oil and gas is rational. Hydrocarbons are considered less harmful for the climate, because they have a higher hydrogen content compared with coal. Yet, considerable efforts are under way to further minimize release of CO_2 from oil and gas power stations, for example by injecting it into depleted hydrocarbon reservoirs or into saline aquifers (cf. introduction to Chapter 6 "Coal"). The technology is executed since 1996 at the Sleipner Field in the North Sea off Norway (Figure/Plate 6.2), where nearly 1 Mt CO_2 per year is separated from natural gas and sequestered at depth (Bickle *et al*. 2007, Klusmann 2003). This is a paradigm for future deep geological storage of CO_2 captured from flue gas of coal, oil and gas-fired power plants or hydrogen production (eq. 7.1). Methane is the third largest contributor (after H_2O-vapour and CO_2) to radiative climate forcing, causing ~40% of the total anthropogenic change since pre-industrial times (Shine & Sturges 2007). Today, CH_4 is a valued product and is hardly ever wasted; unavoidable emission is converted by flaring. Liquid hydrocarbon fuels for traffic, however, remain a major source of CO_2 emissions, because no technology is foreseen that might capture the gas from a multitude of individual small sources. Immediate solutions include reduction of the fuel consumption of vehicles, ships and aeroplanes, and increasing the share of alternative fuels. Replacement of gas and oil in power stations and transport by sustainable fuels depends on technologies that themselves require a large variety and mass of mineral materials (e.g. metals, fertilizers, chemicals and energy). It appears that even if the role of individual mineral raw materials is certain to change in the future, geogenic resources will always be indispensable for the welfare of human societies.

7.9 SUMMARY AND FURTHER READING

Crude oil and gas are natural hydrocarbons occurring in the shallow crust. Processing of oil yields liquid fuels, which are the foundation of economic activities, most importantly of civilization's mobility. Reserves and resources of oil and gas are very large but not inexhaustible. Many experts agree that the depletion mid-point of conventional oil is not far in the future. Yet the latest (2009) reserves/production (R/P) ratio is ~45.7, little changed for the last 20 years; before 1989, it was even lower. This demonstrates vividly that the R/P ratio is not a measure of "the end of oil". Giant unconventional sources of oil are available, but will be more expensive and some may not gain society's consent. Global recoverable gas resources are enormous and promise to cover several hundred years of consumption. Overall, there is no reason to panic because of a geological oil and gas shortage. There are, however, good reasons to reduce our reliance on oil, which are not geological but strategic.

Oil and gas deposits are the result of hydrocarbon-forming systems consisting of many components that may be narrowed to source, hydrocarbon generation, fluid migration, reservoir and trap structure.

Source rocks of crude oil and natural gas are organic matter-rich sediments, which were formed in parts of oceans with proliferating life, typically during Earth's greenhouse states. Early diagenesis transformed organic particles into kerogens ("eogenesis" at <50 °C). Different organic matter converts into four main types of kerogen: (I) Alginite; (II) liptinite and marine plankton; (III) vitrinite; and (IV) inertinite. Like coal macerals, kerogens are amorphous and chemically indeterminate.

Hydrocarbon generation from kerogen starts when source rocks are heated by increasing burial. As they mature through "catagenesis" at temperatures of 50–160 °C, kerogens generate CO_2, H_2O, oil and gas. The main source of oil is type II kerogen, which at the onset of oil generation is characterized by the "formula" $C_{515}H_{596}O_{72}$. Gas is mainly derived from type III kerogen. At 160–250 °C during "metagenesis", oil is cracked to produce methane, pyrobitumen and condensates. This is also the domain of dry gas formation from vitrinite. Kerogens gradually lose their hydrocarbon generation potential and approach the composition of graphite.

Like coalification, the generation of hydrocarbons from kerogen is modelled as a series of decomposition reactions. Temperature constitutes an exponential factor. Kinetic factors are measured in laboratory experiments. The state of diagenetic alteration of kerogens ("maturity") is commonly measured by: i) vitrinite reflectance; and ii) Rock-Eval pyrolysis.

Fluid migration is initiated by exudation of droplets of water, oil and gas from kerogen. Compaction, heating, maturation and dehydration combine to support the resulting fluid flow that is controlled by pressure (head) differences and rock permeability. Preferential flow paths may be envisaged as streams and rivulets. Flow vectors generally point upwards and to basin margins.

Trap structures consist of a reservoir rock that is open to receive fluids but is semi-closed by impermeable seal rock. The best seals are gas hydrates, salt rocks and shale. The separation of hydrocarbons from a passing aqueous-HC fluid flow can be visualized as oil and gas bubbles floating up into a cupola-shaped trap, whereas the water passes on.

Economically significant reservoir rocks, such as sand, sandstone, limestone and dolomite, are characterized by high porosity and favourable permeability. Typical petroleum reservoir rocks display porosities of 10–40 vol. % and permeabilities of ten to several thousand milli-Darcy (mD). Conventional gas deposits have a minimum porosity of 7 vol. % and a permeability >0.1 mD.

Hydrocarbon trap structures occur in many variations. Major process systems of trap formation include sedimentation, diagenesis, salt diapirism, tectonic deformation and self-sealing. A curiosity are impact-related traps associated with the Cretaceous-Palaeogene boundary Chicxulub impact in the Gulf of Mexico, hosting the supergiant Cantarell oilfield. Most remarkable is the significance of self-sealing in the Russian North, where very large gas resources are trapped by gas hydrates formed in permafrost regions.

A large natural flow of oil and gas reaches the Earth's surface. Greenhouse gas methane dissipates in the atmosphere, whereas oil is degraded and decomposed by water, oxygen and microbes. In shallow reservoirs, much of the oil is aerobically biodegraded by preferential consumption of the more valuable hydrocarbon compounds. At oil seeps, tar and asphalt form as residues.

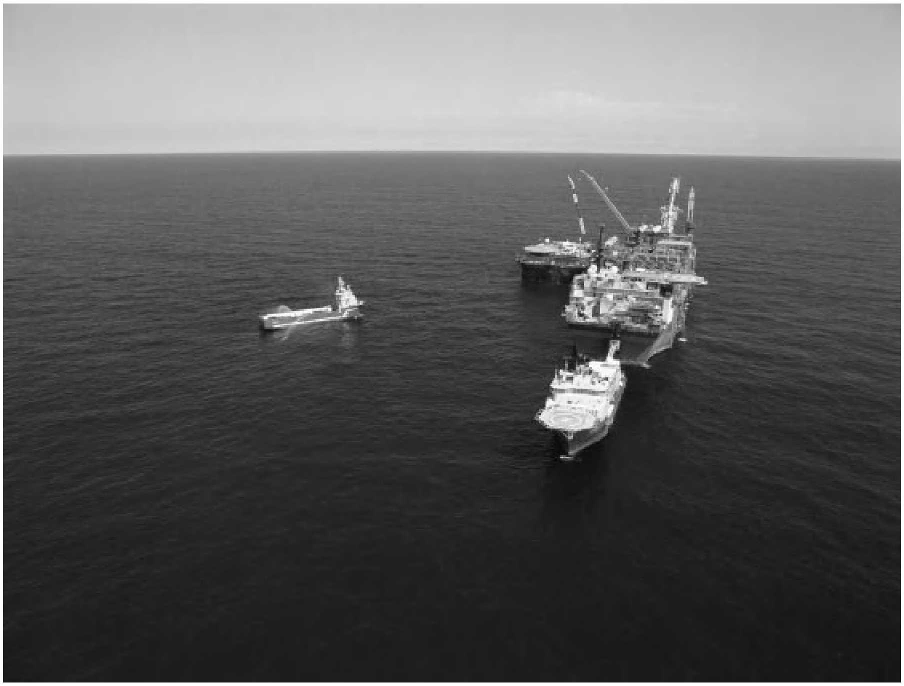

Figure 7.32 (Plate 7.32) Floating production storage and loading vessel in the Bonga field offshore Nigeria. The field lies 120 km from the River Niger mouth in water more than 1000 m deep. Copyright Shell plc.

The search for new hydrocarbon resources moves into ever deeper water of the world's oceans (Figure/Plate 7.32, Box 7.1). In this demanding setting, technologies of exploration, development, exploitation and environmental protection must be re-invented. Former poor practices bequeathed several seriously oil-contaminated landscapes that defy easy clean-up methods. Modern fields are unobtrusive and even blend into city areas. The Norwegian offshore gasfield Sleipner is a pioneering demonstration of deep geological storage of CO_2 captured from flue gas of coal, oil and gas-fired power plants, or from hydrogen production.

More details on petroleum science and its application are best sought in Selley's (1997) *Elements of Petroleum Geology* and Hunt's (1996) *Petroleum Geochemistry and Geology*. Relations between hydrocarbons and salt are analysed at depth in Warren (2006). Systematic short descriptions and illustrations of the world's oil and gas deposits are available in Kulke 1994, 1995). Valuable insights into regional petroleum geology are offered by Glennie (1998) for the North Sea and Alsharhan & Nairn (1997) for the Middle East. The world oil resource situation is lucidly analysed by Gorelick (2010). My favourite is Yergin (*The Prize*, 1991) who tells the story of oil in all its fascinating aspects, including outstanding players, technology, war, finance and the battles for supremacy.

Epilogue

Minerals support some of the most basic needs of humanity. Fertilizers, machines and fuels are essential for food production. Cement, rocks and aggregates are used to make dwellings, and a multitude of natural and processed substances is employed in building the infrastructure and manufacturing the tools, which help us to survive. Of course, minerals are also indispensable for advanced technologies to tap alternative energy sources, to make luxury goods and high-technology electronic devices.

The main groups of mineral raw materials include metal ores, industrial minerals and rocks, salt, coal and hydrocarbons. Energy is the most important natural resource of all. The extraction of minerals is only possible if all involved costs are recovered and value is added. These are the crucial conditions that determine the difference between terms such as "deposit", "reserve" and "ore", as opposed to "mineralization" and "resource".

Economic geology fulfils a central role in discovery, development and extraction of mineral raw materials, and – in partnership with environmental engineering – in the restoration of the land after mining. Economic geology is rooted in the natural sciences and in theory and practice includes many disciplines.

The core task of economic geology is the search for an ever greater understanding of the origin of mineral deposits. Typically, a certain substance such as gold must be concentrated in small rock volumes in order to be economically extractable. This concentration to exploitable ore results from dynamic interactions between the Earth's core, mantle and crust, of the hydro-, bio- and atmosphere. The key are energy gradients, which drive all of the Earth's processes, from the slow and inexorable movement of lithosphere plates to magmatic flare-ups and the migration of hot aqueous and hydrocarbon fluids in the crust, as well as climate and surface dynamics. The heat inherent in the Earth and the energy received as radiation from the sun are causative agents. Both result from nuclear processes, the first by radioactive decay and the second by nuclear fusion.

The formation of mineral deposits is an integral part of the Earth's major rock-forming process systems, such as magmatism, supergene alteration, erosion, sedimentation, diagenesis and metamorphism. Most mineral deposits, however, are uncommon rock bodies, which originated from complex combinations of several processes, boundary conditions and modifying factors that are subsumed as metallogenetic, or minerogenetic, systems. Full understanding of these systems, which operated millions of years ago in the geological past, is probably not achievable. Modern economic geology, however, does provide concepts, data and computational models, which considerably advance both theoretical comprehension and practical application. Successful search for hidden mineral deposits at ever greater depth is the critical test for progress.

The provision of metals, minerals and energy raw materials is the ultimate purpose of economic geology. The Earth's growing population and its constant struggle for higher living standards cause an ever-increasing consumption of natural

Economic Geology Principles and Practice
Metals, Minerals, Coal and Hydrocarbons – Introduction to Formation and Sustainable Exploitation of Mineral Deposits, Walter L. Pohl
© 2011 Walter L. Pohl. Published 2011 by Blackwell Publishing Ltd.

resources. As demand rises and the pace of extraction quickens, more deposits must be found, developed and exploited. Is this supported by a corresponding endowment with undiscovered resources?

The Earth is finite. Yet the mass of, for example, copper or reduced carbon in the accessible uppermost 10 km of the crust is immense. In the foreseeable future, however, only relatively high-grade new finds will be able to compete with deposits such as the Chilean copper porphyries or the Arabian oil fields. It is justly doubted that similarly rich provinces await discovery elsewhere. For many decades from now, a combination of mining, recycling and increasing the efficiency of mineral raw materials' use will have to guarantee sufficient availability. In the far future, supply will need to diversify to new, probably deep sources and new technologies such as automated mining and *in-situ* leaching. A key condition for this path is affordable energy. And the key to all of this is human inventiveness and adaptability.

Can an expanding extractive industry be reconciled with the aspirations of affected people and a sound environment? In this respect, the past performance of mining has certainly been poor. However, although impacts of large mining operations still affect communities, flora and fauna, land and water, there are best-practice performers that already implement the concepts of "green mining". Green mining contributes to communal and individual wealth of all stakeholders, minimizes the impact of operations on humankind and the environment, and restores sites at closure. Green mines achieve lower emissions of greenhouse gases and offset their unpreventable climate footprint by buying carbon credits. Deep geological sequestration of carbon dioxide in saline aquifers and depleted hydrocarbon reservoirs can buy the time needed for the transition to new energy technologies. Its broad application, however, is subject to national and international regulations that avoid drastically falling standards of living in countries rushing ahead. More of civilization's unavoidable waste will be buried in suitable mines. Specially engineered underground repositories are constructed for sustainably isolating hazardous waste from the biosphere. Future mining operations bequeath enriched landscapes, which provide a variety of ecosystem services (e.g. food and biomass production, flood and erosion control, areas for recreation and aesthetics, and clean water). All this is achievable if exploitation of the shallow geosphere is intelligently coordinated and diligently managed.

In conclusion, allow me to reiterate that well-managed extraction of minerals has every potential to contribute to communal wealth, a sustainable and vital social and natural environment, and peace.

References

Aali, J., Hossain Rahimpour-Bonaba, H. & Kamalib, M.R. (2006) Geochemistry and origin of the world's largest gas field from Persian Gulf, Iran. *J. Petroleum Sci. Engin.* **50**, 161–175.

Abed, A.M., Sadaqah, R. & Kuisi, M.A. (2008) Uranium and potentially toxic metals during the mining, beneficiation, and processing of phosphorite and their effects on ground water in Jordan. *Mine Water Environ* **27**, 171–182.

Abraham, A. (1960) *Asphalts and Allied Substances: Historical Review and Natural Raw Materials*. 6th edn. 370 pp. Van Nostrand.

Abu-Jaber, N.S. & Kimberley, M.M. (1992a) Origin of ultramafic-hosted magnesite on Margarita Island, Venezuela. *Miner. Deposita* **27**, 234–241.

Abu-Jaber, N.S. & Kimberley, M.M. (1992b) Origin of ultramafic-hosted vein magnesite deposits. *Ore Geol. Rev.* **7**, 155–191.

Abzalov, M.Z. & Bower, J. (2009) Optimisation of the drill grid at the Weipa bauxite deposit using conditional simulation. *Proc. 7th Int. Mining Geol. Conf. 2009*, pp. 247–251. AusIMM, Melbourne.

Ackman, T.E. (2003) An introduction to the use of airborne technologies for watershed characterization in mined areas. *Mine Water Environ* **22**, 62–68.

Adams, M.D. (ed.) (2005) *Advances in Gold Ore Processing*. 1076 pp. Elsevier.

Adams, R. & Younger, P.L. (2001) A strategy for modelling groundwater rebound in abandoned deep mine systems. *Groundwater* **39**, 249–261.

AGI (1999) *Dictionary of Mining, Mineral and Related Terms*. 2nd edn. 656 pp. American Geological Institute.

Agricola, G. (1556) *De re metallica libri XII*. 708 pp. Basel. Translated by Herbert Clark Hoover. 676 pp. Kessinger Publishing (2003).

Ahmed, A.H., Arai Shoji & Ikenne, M. (2009) Mineralogy and paragenesis of the Co-Ni arsenide ores of Bou Azzer, Anti-Atlas, Morocco. *Economic Geol.* **104**, 249–266.

Airo, M.-L. & Loukola-Ruskeeniemi, K. (2004) Characterization of sulfide deposits by airborne magnetic and gamma-ray responses in eastern Finland. *Ore Geol. Rev.* **24**, 67–84.

Aitken, C.M., Jones, D.M. & Larter, S.R. (2004) Anaerobic hydrocarbon biodegradation in deep subsurface oil reservoirs. *Nature* **431**, 291–294.

Alderton, D.H.M. & Fallick, A.E. (2000) The nature and genesis of gold-silver-tellurium mineralization in the Metaliferi Mountains of western Romania. *Economic Geol.* **95**, 495–516.

Alexandre, P., Kyser, K., Thomas, D., Polito, P. & Marlat, J. (2009) Geochronology of unconformity-related uranium deposits in the Athabasca Basin, Saskatchewan, Canada, and their integration in the evolution of the basin. *Miner. Deposita* **44**, 41–59.

Alexandre, P., Kyser, K., Polito, P. & Thomas, D. (2005) Alteration mineralogy and stable isotope geochemistry of Paleoproterozoic basement-hosted unconformity-type uranium deposits in the Athabasca basin, Canada. *Economic Geol.* **100**, 1547–1563.

Algeo, T.J. (2004) Can marine anoxic events draw down the trace element inventory of seawater? *Geology* **32**, 1057–1060.

Alibert, Ch. & McCulloch, M.T. (1993) Rare earth element and neodymium isotope compositions of the banded iron-formations and associated shales from Hamersley, Western Australia. *Geochim. Cosmochim. Acta* **57**, 187–204.

Allègre, C.J. (2008) *Isotope Geology*. 512 pp. Cambridge University Press.

Economic Geology Principles and Practice
Metals, Minerals, Coal and Hydrocarbons – Introduction to Formation and Sustainable Exploitation of Mineral Deposits, Walter L. Pohl

© 2011 Walter L. Pohl. Published 2011 by Blackwell Publishing Ltd.

Allen, P.A. & Allen, J.R. (2005) *Basin Analysis: Principles and Applications*, 2nd edn. 549 pp. Blackwell.

Allen, R.L., Weihed, P. and the Global VMS Research Project Team (2001) Global comparison of volcanic-associated massive sulfide districts. *Geol. Soc. Spec. Publ.* **204**, 13–37.

Allen, S.R. & McPhie, J. (2009) Products of neptunian eruptions. *Geology* **37**, 639–642.

Alloway, B.J. (1990) *Heavy Metals in Soils*. 339 pp. Blackie.

Alonso, R.N., Jordan, T.E., Tabutt, K.T. & Vandervoort, D.S. (1991) Giant evaporite belts of the Neogene central Andes. *Geology* **19**, 401–404.

Alpers, C.N. & Nordstrom, D.K. (1999) Geochemical modeling of water-rock interactions in mining environments. Pp 289–323 in Plumlee, G.S. & Logsdon, M.J. (Eds.), 1999a.

Alpers, C.N., Jambor, J.L. & Nordstrom, D.K. (eds) (2000) Sulfate minerals: crystallography, geochemistry and environmental significance. *Rev. Mineral. Geochem.* **40**, 531 pp.

Alsharhan, A.S. & Nairn, A.E.M. (eds) (1997) *Sedimentary Basins and Petroleum Geology of the Middle East*. 942 pp. Elsevier.

Alther, G. (2004) Some practical observations on the use of bentonite. *Env. Eng. Geoscience* **10**, 347–359.

Ames, D.E., Davidson, A. & Wodicka, N. (2008) Geology of the giant Sudbury polymetallic mining camp, Ontario, Canda. *Economic Geol.* **103**, 1057–1077.

Ames, D.E., Watkinson, D.H. & Parrish, R.R. (1998) Dating of a regional hydrothermal system induced by the 1850 Ma Sudbury impact event. *Geology* **26**, 447–450.

Anbar, A.D. (2008) Elements and evolution. *Science* **322**, 1481–1483.

Anbar, A.D., Yun Duan, Lyons, T.W., *et al.* (2007) A whiff of oxygen before the great oxidation event? *Science* **317**, 1903–1906.

Andersen, J.C.Ø., Thalhammer, O.A.R. & Schoenberg, R. (2006) Platinum-group element and Re-Os isotope variations of the high-grade Kilvenjärvi platinum group element deposit, Portimo layered igneous complex, Finland. *Economic Geol.* **101**, 159–177.

Andersen, J.C.Ø., Rasmussen, H., Nielsen, T.F.D., and Rønsbo, J.G. (1998) The Triple Group and the Platinova gold and palladium reefs in the Skaergaard intrusion: stratigraphic and petrographic relations. *Economic Geol.* **93**, 488–509.

Andersen, T. & Grorud, H.-F. (1998) Age and lead isotope systematics of uranium-enriched cobalt mineralization in the Modum complex, South Norway: Implications for Precambrian crustal evolution in the SW part of the Baltic Shield. *Precambrian Res.* **91**, 419–432.

Anderson, G.M. (1996) *Thermodynamics of Natural Systems*. 382 pp. Wiley.

André-Jehan, R. & Feraud, J. (2001) Dossier: Le radon. *Géochronique* **78**, 8–25.

Andreoli, M.A.G., Smith, C.B., Watkeys, M., Moore, J. M., Ashwal, L.D. & Hart, R.J. (1994) The geology of the Steenkampskraal monazite deposit, South Africa: Implications for REE-Th-Cu mineralization in charnockite-granulite terrains. *Economic Geol.* **89**, 994–1016.

Anhäusser, C.R. & Maske, S. (eds) (1986) *Mineral Deposits of Southern Africa*, 2 Vols. 2335 pp. Geol. Soc. S. Africa, Johannesburg.

Annels, A.E. (1991) *Mineral Deposit Evaluation – A Practical Approach*. 436 pp. Chapman & Hall.

Annels, A.E. & Dominy, S.C. (2003) Core recovery and quality: important factors in mineral resource estimation. *Applied Earth Sci.* **112**, 305–312.

Annels, A.E. & Simmonds, J.R. (1984) Cobalt in the Zambian Copperbelt. *Precambrian Res.* **25**, 75–98.

Anonymus (1972) Penrose field conference on ophiolites. *Geotimes* **17**, 24–25.

Anthony, E.Y. & Titley, S.R. (1994) Patterns of element mobility during hydrothermal alteration of the Sierrita porphyry copper deposit, Arizona. *Economic Geol.* **89**, 186–192.

Appleton, J.D. (2005) Radon in air and water. In: *Essentials of Medical Geology – Impacts of the Natural Environment on Public Health* (ed. O. Selinus *et al.*), pp 227–262. Elsevier Academic Press.

Arai, S. & Yurimoto, H. (1994) Podiform chromitites of the Tari-Misaka ultramafic complex, southwestern Japan, as mantle-melt interaction products. *Economic Geol.* **89**, 1279–1288.

Aral, H. & Bruckard, W.J. (2008) Characterisation of the Mt Weld (Western Australia) niobium ore. *Mineral Processing & Extractive Metallurgy* **117**, 4, 193–204.

Arbogast, B.F. (ed.) (1990) *Quality Assurance Manual for the Branch of Geochemistry*. US Geological Survey Open-File Report 90-688, 176 pp.

Archibald, S.M., Migdisov, A.A. & Williams-Jones, A.E. (2002) An experimental study of the stability of copper chloride complexes in water vapor at elevated temperatures and pressures. *Geochim. Cosmochim. Acta* **66**, 1611–1619.

Arif, M., Fallick, A.E. & Moon, C.J. (1996) The genesis of emeralds and their host rocks from Swat, northwestern Pakistan: a stable-isotope investigation. *Miner. Deposita* **31**, 255–268.

Armitage, P., McDonald, I. & Tredoux, M. (2007) A geological investigation of the Waterberg hydrothermal platinum deposit, Mookgophong, Limpopo Province, South Africa. *Applied Earth Sci.* **116**, 114–129.

Arndt, N., Lesher, C.M. & Barnes, S.J. (2008) *Komatiite*. 488 pp. Cambridge University Press.

Arndt, N.T., Czamanske, G.K., Walker, R.J., *et al.* (2003) Geochemistry and origin of the intrusive hosts of the Noril'sk-Talnakh Cu-Ni-PGE sulfide deposits. *Economic Geol.* **98**, 495–515.

Arnold, G.L., Anbar, A.D., Barling, J. & Lyons, T.W. (2004) Molybdenum isotope evidence for widespread anoxia in Mid-Proterozoic oceans. *Science* **304**, 87–90.

Arnould, M. (2006) Discontinuity networks in mudstones: a geological approach. *Bull. Eng. Geol. Environ.* **65**, 413–422.

Arrhenius, S. & Lachmann, R. (1912) Die physikalisch-chemischen Bedingungen bei der Bildung der Salzlagerstätten und ihre Anwendung auf geologische Probleme. *Geol. Rundschau* **3**, 139–157.

Arthur, M. A. & Dean, W.E. (1998) Organic-matter production and preservation and evolution of anoxia in the Holocene Black Sea, *Paleoceanography* **13**, 395–411.

Ashwal, L.D. (1993) *Anorthosites*. 422 pp. Springer.

Aston, R.L. (2001) *Surface Mining Law and Reclamation by Land Filling*. 512 pp. Imperial College Press, London.

Attanasi, E.D. & Root, D.H. (1994) The enigma of oil and gas field growth. *Amer. Assoc. Petrol. Geol. (AAPG) Bull.* **78**, 321–332.

Attia, O.E., Lowenstein, T.K. & Walp, A.M.A. (1995) Middle Miocene gypsum, Gulf of Suez: marine or non-marine? *J. Sedim. Research* **A65**, 614–626.

Aucamp, P. & Schalkwyk, A. van (2003) Trace element pollution of soils by abandoned gold mine tailings, near Potchefstroom, South Africa. *Bull Eng Geol Env* **62**, 123–134.

Audétat, A., Pettke, T., Heinrich, C.A. & Bodnar, R.J. (2008) The composition of magmatic-hydrothermal fluids in barren and mineralized intrusions. *Economic Geol.* **103**, 877–908.

Audétat, A. & Pettke, T. (2003) The magmatic-hydrothermal evolution of two barren granites: a melt and fluid inclusion study of the Rio del Medio and Canada Pinabete plutons in northern New Mexico (USA). *Geochim. Cosmochim. Acta* **67**, 97–121.

Audétat, A., Günther, D. & Heinrich, C.A. (2000) Causes for large-scale metal-zonation around mineralized plutons: fluid inclusion LA-ICP-MS evidence from the Mole granite, Australia. *Economic Geol.* **95**, 1563–1581.

Audétat, A., Günther, D. & Heinrich, C.A. (1998) Formation of a magmatic- hydrothermal ore deposit: insights with LA-ICP-MS analysis of fluid inclusions. *Science* **279**, 2091–2094.

Augé, T., Genna, A. & Legendre, O. (2005) Primary platinum mineralisation in the Nizhny Tagil and Kachkanar ultramafic complexes, Urals, Russia: a genetic model for PGE concentration in chromite-rich zones. *Economic Geol.* **100**, 707–732.

Australasian Institution of Mining and Metallurgy (AusIMM) (2005) *The VALMIN Code for the Technical Assessment and Valuation of Mineral and Petroleum Assets and Securities for Independent Expert Reports*. 23 pp. AusIMM, Melbourne.

AusIMM (2004) *Australasian Code for Reporting of Exploration Results, Mineral Resources and Ore Reserves (JORC-Code)*. 20 pp. AusIMM, Melbourne (http://www.jorc.org).

Austin, R.S. (1998) Origin of kaolin of the southeastern US. *Min. Eng.* **50**, 52–57.

Ayers, W.B. (2002) Coalbed gas systems, resources, and production, and a review of contrasting cases from the San Juan and Powder River basins. *AAPG Bull.* **86**, 1853–1890.

Bailey, D.K. (1993) Carbonate magmas. *J. Geol. Soc.* **150**, 637–651.

Bailly, L., Bouchot, V., Beny, C. & Milesi, J.-P. (2000) Fluid inclusion study of stibnite using infrared microscopy: an example from the Brouzils antimony deposit (Vendée, Armorican Massif, France). *Economic Geol.* **95**, 221–226.

Baker, D.R. & Vaillancourt, J. (1995) The low viscosities of F+ H_2O-bearing granitic melts and implications for melt extraction and transport. *Earth Planet. Sci. Lett.* **132**, 199–211.

Baker, E.M. & Andrew, A.S. (1991) Geologic, fluid inclusion, and stable isotope studies of the gold-bearing breccia pipe at Kidston, Queensland, Australia. *Economic Geol.* **86**, 810–830.

Baker, G.S. & Jol, H.M. (2007) Stratigraphic analyses using GPR. *Geol. Soc. America Special Paper 432*, 181 pp.

Baker, T., Mustard, R., Bin Fu, *et al.* (2008) Mixed messages in iron oxide-copper-gold systems of the Cloncurry district, Australia: insights from PIXE analysis of halogens and copper in fluid inclusions. *Miner. Deposita* **43**, 599–608.

Baker, T., Ebert, S., Rombach, C. & Ryan, C.G. (2006) Chemical compositions of fluid inclusions in intrusion-related gold systems, Alaska and Yukon, using PIXE microanalysis. *Economic Geol.* **101**, 311–327.

Baker, T., Pollard, P.J., Mustard, R. Mark, G. & Graham, J.L. (2005) A comparison of granite-related tin, tungsten, and gold-bismuth deposits: implications for exploration. *Soc. Economic Geol. Newsletter* **61**, 5–17.

Baker, T., Achterberg, E. van, Ryan, C.G. & Lang, J.R. (2004) Composition and evolution of ore fluids in a magmatic-hydrothermal skarn deposit. *Geology* **32**, 117–120.

Balci, N., Shanks, W.C., Mayer, B. & Mandernack, K. W. (2007) Oxygen and sulfur isotope systematics of sulfate produced by bacterial and abiotic oxidation of pyrite. *Geochim. Cosmochim. Acta* **71**, 3796–3811.

Baldschuhn, R., Frisch, U. & Kockel, F. (1998) Der Salzkeil, ein strukturelles Requisit der saxonischen Tektonik. *Z. dt. geol. Ges.* **149**, 59–69.

Balen, R.T. van, van Bergen, F., de Leeuw, C., *et al.* (2000) Modelling the hydrocarbon generation and migration in the West Netherlands Basin, the Netherlands. *Geologie en Mijnbouw* **79**, 29–44.

Ballentine, Ch.J. & Lollar, B.S. (2002) Regional groundwater focusing of nitrogen and noble gases into the Hugoton-Panhandle giant gas field, USA. *Geochim. Cosmochim. Acta* **66**, 2483–2497.

Ballentine, Ch.J., Schoell, M. Coleman, D. & Cain, B.A. (2001) 300-Myr-old CO_2 in natural gas reservoirs of the west Texas Permian basin. *Nature* **409**, 327–331.

Ballhaus, C. (1998) Origin of podiform chromite deposits by magma mingling. *Earth Planet. Sci. Lett.* **156**, 185–193.

Banfield, J.F. & Nealson, K.H. (eds) (1997) Geomicrobiology: interactions between microbes and minerals. *Min. Soc. America, Rev. in Mineral.* **35**, 448 pp.

Banks, D.A., Green, R., Cliff, R.A. & Yardley, W.D. (2000) Chlorine isotopes in fluid inclusions: Determinations of the origin of salinity in magmatic fluids. *Geochim. Cosmochim. Acta* **64**, 1785–1789.

Banks, D.A., Giuliani, G., Yardley, B.W.D. & Cheilleitz, A. (2000) Emerald mineralisation in Colombia: fluid chemistry and the role of brine mixing. *Miner. Deposita* **35**, 699–713.

Bao, Huiming, Fairchild, I.J., Wynn, P.M. & Spötl, C. (2009) Stretching the envelope of past surface environments: Neoproterozoic glacial lakes from Svalbard. *Science* **323**, 119–122.

Bardossy, G. & Aleva, G.J.J. (1990) *Lateritic Bauxites*. 624 pp. Elsevier.

Bardossy, G. (1982) *Karst Bauxites or Bauxite Deposits on Carbonate Rocks. Developments in Economic Geol.* **14**, 441 pp.

Barker, C.E., Bone, Y. & Lewan, M.D. (1998) Fluid inclusion and vitrinite reflectance geothermometry compared to heat-flow models of maximum paleotemperatures next to dykes, western onshore Gippsland Basin, Australia. *Int. J. Coal Geol.* **37**, 73–111.

Barker, S.L.L., Hickey, K.E., Cline, J.S., *et al.* (2009) Uncloaking invisible gold: Use of nanoSIMS to evaluate gold, trace elements, and sulfur isotopes in pyrite from Carlin-type gold deposits. *Economic Geol.* **104**, 897–904.

Barley, M.E., Pickard, A.L. & Sylvester, P.J. (1997) Emplacement of a large igneous province as a possible cause of banded iron formation 2.45 billion years ago. *Nature* **385**, 55–58.

Barley, M.E., Pickard, A.L., Hagemann, S.G. & Folkert, S. L. (1999) Hydrothermal origin for the 2 billion year old Mount Tom Price giant ore deposit, Hamersley Province, Western Australia. *Miner. Deposita* **34**, 784–789.

Barnes, H.L. & Seward, T.M. (1998) Geothermal systems and mercury deposits. In: *The Geochemistry of Hydrothermal Ore Deposits* (ed. H.L. Barnes), 3rd edn. pp 699–736. Wiley.

Barnes, H.L. (ed.) (1998) *The Geochemistry of Hydrothermal Ore Deposits*, 3rd. edn. 972 pp. Wiley.

Barnes, L.C. (1990) Gypsum deposits in South Australia and Western Australia. In: *Geology of the Mineral Deposits of Australia and Papua New Guinea* (ed. F. E. Hughes), pp. 1651–1654. AusIMM, Melbourne.

Barnes, S.J. (2004) Introduction to nickel sulfide orebodies and komatiites of the Black Swan area, Yilgran Craton, Western Australia. *Miner. Deposita* **39**, 679–683.

Barnes, S.J., Savard, D., Bédard, L.P. & Maier, W.D. (2009) Selenium and sulfur concentrations in the Bushveld Complex of South Africa and implications for formation of the platinum-group element deposits. *Miner. Deposita* **44**, 647–663.

Barnes, S.J., Lesher, C.M. & Sproule, R.A. (2007) Geochemistry of komatiites in the Eastern Goldfields Superterrane, Western Australia and the Abitibi Greenstone Belt, Canada, and implications for the distribution of associated Ni-Cu-PGE deposits. *Applied Earth Sci.* **116**, 167–187.

Barrie, C.D., Cook, N.J. & Boyle, A.P. (2010) Textural variation in the pyrite-rich ore deposits of the Røros district, Trondheim region, Norway: implications for pyrite deformation mechanisms. *Miner. Deposita* **45**, 51–68.

Barron, B.J., Barron, L.M. & Duncan, G. (2005) Eclogitic and ultrahigh-pressure crustal garnets and their relationship to Phanerozoic subduction diamonds, Bingara, area, New England fold belt, eastern Australia. *Economic Geol.* **100**, 65–1582.

Bartlett, K.E. & Edwards, J.L. (2009) The use of acoustic scanner results for mine design. *Proc. 7th Int. Mining Geol. Conf. 2009*. pp. 25–31. AusIMM, Melbourne.

Bartlett, K.E., Edwards, J.L., Hatherly, P. & Lea, J. (2009) Exploration of coal deposits. *Proc. 7th Int. Mining Geol. Conf. 2009*. pp. 33–40. AusIMM, Melbourne.

Barton, C.M., Gloe, C.S. & Holdgate, G.R. (1993) Latrobe Valley, Victoria, Australia: a world class brown coal deposit. *Int. J. Coal Geol.* **23**, 193–213.

Barton, M.D. & Johnson, D.A. (1996) Evaporitic source model for igneous related Fe oxide-(REE-Cu-Au-U) mineralization. *Geology* **24**, 259–262.

Bartos, P.J. (2000) The pallacos of Cerro Rico de Potosí, Bolivia: a new deposit type. *Economic Geol.* **95**, 645–654.

Batty, L.C. (2005) The potential importance of mine sites for biodiversity. *Mine Water Environ* **24**, 101–103.

Baumann, L., Kuschka, E. & Seifert, Th. (2000) *Lagerstätten des Erzgebirges*. 300 pp. Enke.

Baumgartner, R., Fontboté, L. & Vennemann, T. (2008) Mineral zoning and geochemistry of epithermal polymetallic Zn-Pb-Ag-Cu-Bi mineralisation at Cerro de Pasco, Peru. *Economic Geol.* **103**, 493–537.

Bawden, T.M., Einaudi, M.T., Bostick, B.C., *et al.* (2003) Extreme ^{34}S depletions in ZnS at the Mike gold deposit, Carlin Trend, Nevada: evidence for bacteriogenic supergene sphalerite. *Geology* **31**, 913–916.

Beal, E.J., House, C.H. & Orphan, V.J. (2009) Manganese and iron-dependent marine methane oxidation. *Science* **325**, 184–187.

Beard, B.L., Johnson, C.M., Von Damm, K.L. & Poulson, R.L. (2003) Iron isotope constraints on Fe cycling and mass balance in oxygenated Earth oceans. *Geology* **31**, 629–632.

Beaudoin, G. & Therrien, R. (1999) Sources and drains: major controls of hydrothermal fluid flow in the Kokanee Range, British Columbia, Canada. *Geology* **27**, 883–886.

Beaudoin, Y. & Scott, S.D. (2009) Pb in the Pacmanus seafloor hydrothermal system, eastern Manus Basin: Numerical modeling of a magmatic versus leached origin. *Economic Geol.* **104**, 749–758.

Bebout, G.E. & Fogel, M.L. (1992) Nitrogen-isotope compositions of metasedimentary rocks in the Catalina Schist, California: Implications for metamorphic devolatilization history. *Geochim. Cosmochim. Acta* **56**, 2839–2849.

Bechtel, A. & Hoernes, S. (1993) Stable isotope variations of clay minerals: A key to the understanding of Kupferschiefer-type mineralization, Germany. *Geochim. Cosmochim. Acta* **57**, 1799–1816.

Bechtel, A., Gruber, W., Sachsenhofer, R.F., Gratzer, R., Lucke, A. & Püttmann, W. (2003) Depositional environment of the Late Miocene Hausruck lignite (Alpine Foreland Basin): insights from petrography, organic geochemistry, and stable carbon isotopes. *Int. J. Coal Geology* **53**, 153–180.

Beer, Ch., Reichstein, M., Tomelleri, E., *et al.* (2010) Terrestrial gross carbon dioxide uptake: global distribution and covariation with climate. *Science* **329**, 834–838.

Beerling, D. (2007) *The Emerald Planet*. 288 pp. Oxford University Press.

Begossi, R. & Della Favera, J.C. (2002) Catastrophic floods as a possible cause of organic matter accumulation giving rise to coal, Parana Basin, Brazil. *Int. J. Coal Geol.* **52**, 83–89.

Bekker, A., Slack, J.F., Planavsky, N., *et al.* (2010) Iron formation: the sedimentary product of a complex interplay among mantle, tectonic, oceanic, and biospheric processes. *Economic Geol.* **105**, 467–508.

Bekker, A., Barley, M.E., Fiorentini, M.L., Rouxel, O.J., Rumble, D. & Beresford, S.W. (2009) Atmospheric sulfur in Archean komatiite-hosted nickel deposits. *Science* **326**, 1086–1089.

Bell, F.G. (1993) *Engineering Geology*. 359 pp. Blackwell Science.

Bell, F.G. (1998) *Environmental Geology – Principles and Practice*. 594 pp. Blackwell Science.

Bell, F.G. & Donelly, L.J. (2006) *Mining and its Impact on the Environment*. 547 pp. Taylor & Francis.

Bell, K. & Keller, J. (eds) (1995) *Carbonatite volcanism – Oldoinyo Lengai and the petrogenesis of natrocarbonatites*. 210 pp. Springer.

Bending, J.S. & Scales, W.G. (2001) New production in the Idaho Cobalt Belt: a unique metallogenic province. *Trans. Instn. Min. Metall. B* **110**, 81–87.

Bennet, P.C., Siegel, D.I., Hill, B.M. & Glaser, P.H. (1991) Fate of silicate minerals in a peat bog. *Geology* **19**, 328–331.

Berkman, D.A. (2001) *Field Geologist's Manual*, 4th edn. 430 pp. AusIMM, Parkville.

Bernard, A.J. (1973) Metallogenic processes of intrakarstic sedimentation. In: *Ores in Sediments* (eds G.C. Amstutz & A.J. Bernard). pp. 43–57. Springer.

Berner, E.K., Berner R.A. & Moulton, K.L. (2003) Plants and mineral weathering: present and past. *Treatise in Geochemistry* **5**, 169–188.

Berner, R.A. & Kothavala, Z. (2001) GEOCARB III: a revised model of atmospheric CO_2 over Phanerozoic time. *American J. Sci.* **301**, 182–204.

Berner, R.A. (1997) The rise of plants and their effect on weathering and atmospheric CO_2. *Science* **276**, 544–545.

Berning, J. (1986) The Rössing uranium deposit, South West Africa/Namibia. In: *Mineral Deposits of Southern Africa*, Vol. II (eds C.R. Anhäusser & S. Maske). Pp. 1819–1832. Geol. Soc. S. Africa, Johannesburg.

Bethke, C.M. (1996) *Geochemical Reaction Modelling: Concepts and Applications*. 397 pp. Oxford University Press.

Bettison-Varga, L., Varga, R.J. & Schiffman, P. (1992) Relation between ore-forming hydrothermal systems and extensional deformation in the Solea graben spreading center, Troodos ophiolite, Cyprus. *Geology* **20**, 987–990.

Betts, P.G., Giles, D. & Lister, G.S. (2003) Tectonic environment of shale-hosted massive sulfide Pb-Zn-Ag deposits of Proterozoic northeastern Australia. *Economic Geol.* **98**, 557–576.

Beukes, N.J. & Dreyer, C.J.B. (1986a) Amosite asbestos deposits of the Penge area. In: *Mineral Deposits of Southern Africa*, Vol. II (eds C.R. Anhäusser & S. Maske) pp. 901–910. Geol. Soc. S. Africa, Johannesburg.

Beukes, N.J. & Dreyer, C.J.B. (1986b) Crocidolite deposits of the Pomfret area, Griqualand West. In: *Mineral Deposits of Southern Africa*, Vol. II (eds C.R. Anhäusser & S. Maske) pp. 911–921. Geol. Soc. S. Africa, Johannesburg.

Beurlen, H., da Silva, M.R.R., Thomas, R., Soares, D.R. & Olivier, P. (2008) Nb-Ta-(Ti-Sn) oxide mineral chemistry as tracer of rare-element granitic pegmatite fractionation in the Borborema Province, Northeastern Brazil. *Miner. Deposita* **43**, 207–228.

Bevier, M.L. (2005) *Introduction to Field Geology*. 192 pp. McGraw-Hill Ryerson.

Bialecka, B. (2003) Assessment of phosphogypsum ultilisation in underground hard coal mines in Poland. *Mining Technology* **112**, A149–156.

Bickle, M., Chadwick, A., Huppert, H.E., Hallworth, M. & Lyle, S. (2007) Modelling carbon dioxide accumulation at Sleipner: Implications for underground carbon storage. *Earth Planet. Sci. Lett.* **255**, 164–176.

Biehler, D. & Falck, W.E. (1999) Simulation of the effects of geochemical reactions on groundwater quality during planned flooding of the Königstein uranium mine, Saxony, Germany. *Hydrogeol. J.* **7**, 284–293.

Bieniawski, Z.T. (1989) *Engineering Rock Mass Classifications*. 251 pp. Wiley.

Bierlein, F.P., Arne, D.C., McKnight, S., *et al.* (2000) Wall-rock petrology and geochemistry in alteration halos associated with mesothermal gold mineralization, Central Victoria, Australia. *Economic Geol.* **95**, 283–312.

Bilibin, Y.A. (1938) *Principles of Placer Geology*. 505 pp. Gonti, Moscow.

Bilodeau, W.L., Bilodeau, S.W., Gath, E.M., Oborne, M. & Proctor, R.J. (2007) Geology of Los Angeles, California, United States of America. *Env. Eng. Sci.* **13**, 99–160.

Bingen, B. & Stein, H. (2003) Molybdenite Re-Os dating of biotite dehydration melting in the Rogaland high-temperature granulites, S Norway. *Earth Planet. Sci. Lett.* **208**, 181–195.

Bing-Quan, Z., Jing-Lian, Z., Xiang-Yang, C., *et al.* (2001) Pb, Sr, and Nd isotopic features in organic matter from China and their implications for petroleum generation and migration. *Geochim. Cosmochim. Acta* **65**, 2555–2570.

Bish, D.L. & Ming, D.W. (eds) (2001) Natural zeolites: occurrence, properties, applications. *Rev. Mineral. & Geochem.* **45**, 654 pp, Mineral. Soc. America.

Blanc, G. & Anschutz, P. (1995) New stratification in the hydrothermal brine system of the Atlantis II Deep, Red Sea. *Geology* **23**, 543–546.

Blanc-Valleron, M.M. (1997) The salt basins of Alsace (Southern Rhine Graben). In: *Sedimentary Deposition in Rift and Foreland Basins in France and Spain (Paleogene and Lower Neogene)* (eds G. Brusson & B.C. Schreiber), pp 95–135. Columbia University Press.

Blanchard, R. (1968) Interpretation of leached outcrops. 196 pp, *Nevada Bureau of Mines, Bull.* 66.

Blevin, P.L. & Chappell, B.W. (1995) Chemistry, origin and evolution of mineralized granites in the Lachlan Fold Belt, Australia: the metallogeny of I- and S-type granites. *Economic Geol.* **90**, 1604–1619.

Blowes, D. (2002) Tracking hexavalent Cr in groundwater. *Science* **295**, 2024–2025.

Blundell, D., Arndt, N., Cobbold, P.R. & Heinrich, Ch. (eds) (2005) Geodynamics and ore deposit evolution in Europe. *Ore Geol. Rev.* **27**(1–4), 349.

Bodnar, R.J. (1993) Revised equation and table for determining the freezing point depression of H_2O-NaCl solutions. *Geochim. Cosmochim. Acta* **57**, 683–684.

Boetius, A. & Joye, S. (2009) Thriving in salt. *Science* **324**, 1523–1525.

Boettcher, A.L. (1967) The Rainy Creek alkaline-ultramafic igneous complex near Libby, Montana. *J. of Geology* **75**, 526–553.

Bolle, L. (1992) Troll field – Norway's giant offshore gas field. In: *Giant Oil and Gas Fields of the Decade 1978–1988* (ed. M.T. Halbouty), 526 pp. AAPG, Tulsa.

Bolton, B.R., Berents, H.W. & Frakes, L.A. (1990) Groote Eylandt manganese deposit. In: *Geology of the Mineral Deposits of Australia and Papua New Guinea* (ed. F.E. Hughes), pp 1575–1579. AusIMM, Melbourne.

Bolze, C.E., Malone, P.G. & Smith, M.J. (1974) Microbial mobilization of barite. *Chemical Geol.* **13**, 141–143.

Boni, M., Terracciano, R., Evans, N.J., Laukamp, C., Schneider, J. & Bechstädt, T. (2007) Genesis of vanadium ores in the Otavi Mountainland, Namibia. *Economic Geol.* **102**, 441–469.

Bopp, C.J., Lundstrom, C.C., Johnson, TM. & Glessner, J. J.G. (2009) Variations in $^{238}U/^{235}U$ in uranium ore deposits: Isotopic signatures of the U reduction process? *Geology* **37**, 611–614.

Borchert, H. (1960) Genesis of marine sedimentary iron ores. *Trans. Instn. Min. Metall. B* **69**, 261–279.

Border, S. & Butt, B. (2001) Evaluation of mineral resources and ore reserves of industrial minerals – the importance of markets. Pp 389–384 in Edwards (2001).

Borg, G., Karner, K., Buxton, M., Armstrong, R., van der Merwe, S.W. (2003) Geology of the Skorpion Supergene Zinc Deposit, Southern Namibia. *Economic Geol.* **98**, 749–771.

Bornemann, O., Behlau, J., Fischbeck, R., *et al.* (2008) Gorleben Site Description Part 3: Results of geological exploration of the salt structure. *Geol. Jahrbuch C* 73, 211 pp, Schweizerbart & BGR Hannover.

Borrok, D.M., Kesler, S.E., Boer, R.H. & Essene, E.J. (1998) The Vergenoeg magnetite-fluorite deposit, South Africa: support for a hydrothermal model for massive iron oxide deposits. *Economic Geol.* **93**, 564–586.

Boschker, H.T.S., Nold, S.C., Wellsbury, P., *et al.* (1998) Direct linking of microbial populations to specific biogeochemical processes by ^{13}C-labelling of biomarkers. *Nature* **392**, 801–805.

Boswell, R. (2009) Is gas hydrate energy within reach? *Science* **325**, 957–958.

Botrell, S.H., Yardley, B.W.D. & Buckley, F. (1988) A modified crush-leach method for the analysis of fluid inclusion electrolytes. *Bull. Mineral.* **111**, 279–290.

Botrell, S.H., Leosson, M.A. & Newton, R.J. (1996) Origin of brine flows at Boulby potash mine, Cleveland, England. *Trans. Instn. Min. Metall. B* **105**, 159–164.

Boudreau, A.E. & McCallum, I.S. (1992) Concentration of platinum-group elements by magmatic fluids in layered intrusions. *Economic Geol.* **87**, 1830–1848.

Bouzenoune, A. & Lecolle, P. (1997) Petrographic and geochemical arguments for hydrothermal formation of the Ouenza siderite deposit (NE Algeria). *Miner. Deposita* **32**, 189–196.

Bowden, R.A. & Shaw, R.P. (2007) The Kayelekera uranium deposit, Northern Malawi: past exploration activities, economic geology and decay series disequilibrium. *Applied Earth Sci.* **116**, 55–67.

Bowell, R.J. (2003) Pit lake systematics: a special issue. *Mine Water Environ* **22**, 167–169.

Bowell, R.J., Gize, A.P. & Foster, R.P. (1993) The role of fulvic acid in the supergene migration of gold in tropical rain forest soils. *Geochim. Cosmochim. Acta* **57**, 4179–4190.

Bowie, S.H.U., Kvalheim, A. & Haslam, H.W. (eds) (1979) *Mineral Deposits of Europe. I. Northwest Europe*. 362 pp, IMM London.

Boxer, G.L. & Jaques, A.L. (1990) Argyle (AK1) diamond deposit. In *: Geology of the mineral deposits of Australia and Papua New Guinea* (ed. F.E. Hughes), pp 697–706. AusIMM, Melbourne.

Boxer, G.L., Lorenz, V. & Smith, C.B. (1989) The geology and volcanology of the Argyle (AK1) lamproite diatreme, Western Australia. *Geol. Soc. Australia Spec. Publ.* **14**, 140–152.

Boyce, A.J., Little, C.T.S. & Russell, M.J. (2003) A new fossil vent biota in the Ballynoe barite deposit, Silvermines, Ireland: evidence for intracratonic sea-floor hydrothermal activity about 352 Ma. *Economic Geol.* **98**, 649–656.

Boyd, P.W. (2007) Biochemistry – iron findings. *Nature* **446**, 989–991.

BP Statistical Review of World Energy, June 2010. www.bp.com/ (accessed June 2010).

Brady, B.H.G. & Brown, E.T. (2004) *Rock Mechanics for Underground Mining*. 3rd edn. 626 pp. Springer.

Braithwaite, C.J.R. & Rizzi, G. (1997) The geometry and petrogenesis of hydrothermal dolomites at Navan, Ireland. *Sedimentology* **44**, 421–440.

Braithwaite, C.J.R. & Zedef, V. (1996) Hydromagnesite stromatolites and sediments in an alkaline lake, Salda Gölü, Turkey. *J. Sediment. Res.* **66**, 991–1002.

Braitsch, O. (1971) *Salt Deposits, Their Origin and Composition*. 297 pp, Springer.

Brannon, J.C., Podosek, F.A. & McLimans, R.K. (1992) Alleghenian age of the Upper Mississippi Valley zinc-lead deposit determined by Rb-Sr dating of sphalerite. *Nature* **356**, 509–511.

Brannon, J.C., Podosek, F.A., Viets, J.G., *et al.* (1991) Strontium isotopic constraints on the origin of ore forming fluids of the Viburnum trend, southeast Missouri. *Geochim. Cosmichim. Acta* **55**, 1407–1419.

Brathwaite, R.L., Simpson, M.P., Faure, K. & Skinner, D.N.B. (2001) Telescoped porphyry Cu-Mo-Au mineralisation, advanced argillic alteration and quartz-sulfide-gold-anhydrite veins in the Thames District, New Zealand. *Miner. Deposita* **36**, 623–640.

Breiter, K., Förster, H.-J. & Seltmann, R. (1999) Variscan silicic magmatism and related tin-tungsten mineralization in the Erzgebirge-Slavkovski les metallogenic province. *Miner. Deposita* **34**, 505–521.

Bristow, C.M. & Robson, J.L. (1994) Palaeogene basin development in Devon. *Trans. Instn. Min. Metall. B* **103**, 163–167.

Brooks, C.C. (2008) Uranium numbers alert: uncertainties associated with estimation of uranium resources. *Applied Earth Sci.* **117**, 29–36.

Brown, A. (2010) Reliable mine water technology. *Mine Water Environ* **29**, 85–91.

Brown, A.C. (2009) A process-based approach to estimating the copper derived from red beds in the sediment-hosted stratiform copper deposit model. *Economic Geol.* **104**, 857–868.

Brown, A.C. (2006) Genesis of native copper lodes in the Keweenaw district, northern Michigan: A hybrid evolved meteoric and metamorphogenic model. *Economic Geol.* **101**, 1437–1444.

Brown, M., Lazo, F., Carter, P., Goss, B. & Kirwin, D. (2010) The geology and discovery of the Merlin Mo-Re zone of the Mount Dore deposit, Mount Isa Inlier, NW Queensland, Australia. *SGA News* June 2010, p. 1, 9–15.

Brugger, J., McPhail, D.C., Wallace, M. & Waters, J. (2003) Formation of willemite in hydrothermal environments. *Economic Geol.* **98**, 819–836.

Brundtland, G.H. (1987) *Our common future. World Commission on Environment and Development*. 400 pp. Oxford University Press.

Bucci, L.A., McNaughton, N.J., Fletcher, I.R., *et al.* (2004) Timing and duration of high-temperature gold mineralization and spatially associated granitoid magmatism at Chalice, Yilgarn Craton, Western Australia. *Economic Geol.* **99**, 1123–1144.

Bucher, K. & Frey, M. (2002) *Petrogenesis of Metamorphic Rocks*, 7th edn, 341 pp. Springer.

Bucholz, C.E. & Ague, J.J. (2010) Fluid flow and Al transport during quartz-kyanite vein formation, Unst, Shetland Islands, Scotland. *J. Metamorphic Geology* **28**, 19–39.

Bühn, B. & Rankin, A.H. (1999) Composition of natural, volatile-rich Na-Ca-REE-Sr carbonatitic fluids trapped in fluid inclusions. *Geochim. Cosmochim. Acta* **63**, 3781–3797.

Burns, P.C. & Finch, R. (eds) (1999) Uranium: mineralogy, geochemistry and the environment. *Rev. Mineral. Geochem.* **38**, 439.

Burton, M., Allard, P. Muré, P., La Spina, A. (2007) Gas composition reveals the source depth of slug-driven Strombolian explosive activity. *Science* **317**, 227–230.

Bustin, R.M. & Clarkson, C.R. (1999) Geological controls on coalbed methane reservoir capacity and gas content. *Int. J. Coal Geol.* **38**, 3–26.

Bustin, R.M., Mastalerz, M. & Raudsepp, M. (1997) Electron-probe microanalysis of light elements in coal and other kerogen. *Int. J. Coal Geol.* **32**, 5–30.

Bustin, R.M., Ross, J.V. & Rouzaud, J.N. (1995) Mechanism of graphite formation from kerogen: experimental evidence. *Int. J. Coal Geol.* **28**, 1–36.

Butt, C.R.M., Lintern, M.J. & Anand, R.R. (2000) Evolution of regoliths and landscapes in deeply weathered terrain – implications for geochemical exploration. *Ore Geol. Rev.* **16**, 167–183.

Bychev, R.M., Petrova, G.I. & Bychev, M.I. (2004) Thermodynamic conditions of coalification. *J. Mining Science* **40**, 210–215.

Cabral, A.R., Beaudoin, G. & Taylor, B.E. (2009) The Transfiguration continental red-bed Cu-Pb-Zn-Ag deposit, Quebec Appalachians, Canada. *Miner. Deposita* **44**, 285–301.

Cabral, A.R., Lehmann, B., Kwitko, R. & Cravo Costa, C. H. (2002) The Serra Pelada Au-Pd-Pt deposit, Carajas Mineral Province, Northern Brazil. *Economic Geol.* **97**, 1127–1138.

Cabral, A.R., Lehmann, B., Sattler, C.D., *et al.* (2002) Hg-Tl-bearing manganese oxide from Conta Historia manganese deposit, Quadrilatero Ferrifero, Minas Gerais, Brazil. *Trans. Instn. Min. Metall. B* **111**, 123–127.

Cabri, L.J. (ed.) (2002) *The Geology, Geochemistry, Mineralogy And Mineral Beneficiation Of Platinum Group Minerals*. 852 pp. Can. IMMP, Calgary.

Cadle, A.B., Caircross, B., Christie, A.D.M. & Roberts, D. L. (1993) The Karoo Basin of South Africa: type basin for the coal-bearing deposits of southern Africa. *Int. J. Coal Geol.* **23**, 117–157.

Calmels, D., Gaillardet, J., Brenot, A., & France-Lanord, C. (2007) Sustained sulfide oxidation by physical erosion processes in the Mackenzie River basin: Climatic perspectives. *Geology* **35**, 1003–1006.

Cameron, E. (1990) Yeelirrie uranium deposit. Pp 1625–1629 in F.E. Hughes (ed.), *Geology of the Mineral Deposits of Australia and Papua New Guinea*. AusIMM, Melbourne.

Campbell, I.H. & Naldrett, A.J. (1979) The influence of silicate/sulfide ratios on the geochemistry of magmatic sulfides. *Economic Geol.* **74**, 1503–1506.

Campbell-McCuaig, T. & Kerrich, R. (1998) P-T-t-deformation-fluid characteristics of lode gold deposits: evidence of alteration systematics. *Ore Geol. Rev.* **12**, 381–453.

Canfield, D.E. & Teske, A. (1996) Late Proterozoic rise in atmospheric oxygen concentration inferred from phylogenetic and sulphur-isotope studies. *Nature* **382**, 127–132.

Canfield, D.E. & Thamdrup, B. (1994) The production of ^{34}S-depleted sulfide during bacterial disproportionation of elemental sulfur. *Science* **266**, 1973–1975.

Cannell, J., Cooke, D.R., Walshe, J.L. & Stein, H. (2005) Geology, mineralization, alteration, and structural evolution of the El Teniente porphyry Cu-Mo deposit. *Economic Geol.* **100**, 979–1003.

Canty, G.A. & Everett, J.W. (2006) Injection of fluidized bed combustion ash into mine workings for treatment of acid mine drainage. *Mine Water Environ* **25**, 45–55.

Carling, P.A. & Breakspear, R.M.D. (2006) Placer formation in gravel-bedded rivers: a review. *Ore Geol. Rev.* **28**, 377–401.

Carlowitz, H.C. von (1713) *Sylvicultura Oeconomica*. 432 pp. Braun, Leipzig.

Carr, A.D. (1999) A vitrinite reflectance kinetic model incorporating overpressure retardation. *Marine Petrol. Geol.* **16**, 355–377.

Carranza, E.J.M. (ed.) (2008) *Geochemical Anomaly and Mineral Prospectivity Mapping*. 368 pp, Elsevier.

Carter, L.J. & Pigford, T.H. (2005) Proof of safety at Yucca Mountain. *Science* **310**, 447–448.

Casas, E., Lowenstein, T.K., Spencer, R.J. & Zhang Pengxi (1992) Carnallite mineralization in the non-marine Qaidam basin, China: Evidence for the early diagenetic origin of potash evaporites. *J. Sediment. Petrol.* **62**, 881–898.

Castanier, S., Perthuisot, J.-P., Matrat, M. & Morvan, J.-Y. (1999) The salt ooids of Berre salt works (Bouches du Rhone, France): the role of bacteria in salt crystallisation. *Sediment. Geol.* **125**, 9–21.

Castor, S.B. & Henry, C.D. (2000) Geology, geochemistry, and origin of volcanic rock-hosted uranium deposits in northwestern Nevada and southeastern Oregon, USA. *Ore Geol. Rev.* **16**, 1–40.

Castor, S.B. & Nason, G.W. (2004) Mountain Pass rare earth deposit. *Nevada Bureau Min. Geol. Spec. Pub.* **33**, 68–81.

Castor, S.B. (2008) Rare earth deposits of North America. *Resource Geology* **58**, 337–347.

Cathless, L.M. (1993) A capless 350 °C flow zone model to explain megaplumes, salinity variations, and high-temperature veins in ridge axis hydrothermal systems. *Economic Geol.* **88**, 1977–1988.

Cathles, L.M., Erendei, A.H.J. & Barries, T. (1997) How long can a hydrothermal system be sustained by a single intrusive event? *Economic Geol.* **92**, 766–771.

Catigny, P., Harris, J.W. & Javoy, M. (1998) Eclogitic diamond formation at Jwaneng: no room for a recycled component. *Science* **280**, 1421–1424.

Cavallo, A.J. (2004) Hubbert's petroleum production model: an evaluation and implications for world oil production forecasts. *Natural Resources Research* **13**, 211–221.

Cawthorn, R.G. & Molyneux, T.G. (1986) Vanadiferous magnetite deposits of the Bushveld Complex. In: *Mineral Deposits of Southern Africa*. Vol. II (eds C.R. Anhäusser & S. Maske) pp 1251–1266. Geol. Soc. S. Africa, Johannesburg.

Cawthorn, R.G. (ed.) (1996) *Layered Intrusions*. 544 pp. Elsevier.

Cawthorn, R.G. (2005a) Contrasting sulphide contents of the Bushveld and Sudbury Igneous Complexes. *Miner. Deposita* **40**, 1–12.

Cawthorn, R.G. (2005b) Pressure fluctuations and the formation of the PGE-rich Merensky and chromitite reefs, Bushveld Complex. *Miner. Deposita* **40**, 231–235.

Cerny, P. (1991) Fertile granites of Precambrian rare-element pegmatite fields: is geochemistry controlled by tectonic setting or source lithologies? *Precambrian Res.* **51**, 429–468.

Ceuleneer, G. & Nicolas, A. (1985) Structures in podiform chromite from the Maqsad district (Sumail ophiolite, Oman). *Miner. Deposita* **20**, 177–184.

Ceuleneer, G., Monnereau, M. & Amri, I. (1996) Thermal structure of a fossil mantle diapir inferred from the distribution of mafic cumulates. *Nature* **379**, 149–153.

Chabiron, A., Cuney, M. & Poty, B. (2003) Possible uranium sources for the largest uranium district associated with volcanism: the Streltsovka caldera (Transbaikalia, Russia). *Miner. Deposita* **38**, 127–140.

Chan, L.-H., Starinski, A. & Katz, A. (2002) The behaviour of lithium and its isotopes in oilfield brines: evidence from the Heletz-Kokhav field, Israel. *Geochim. Cosmochim. Acta* **66**, 615–623.

Chang, Zhaoshan, Large, R.R. & Maslennikov, V. (2008) Sulfur isotopes in sediment-hosted orogenic gold deposits: evidence for an early timing and a seawater sulfur source. *Geology* **36**, 971–974.

Chang, Zhaoshan & Meinert, L.D. (2008) The Empire Cu-Zn mine, Idaho: exploration implications of unusual skarn features related to high fluorine activity. *Economic Geol.* **103**, 909–938.

Chang, S. & Berner, R.A. (1999) Coal weathering and the geochemical carbon cycle. *Geochim. Cosmochim. Acta* **63**, 3301–3310.

Chapman, L.H. (2004) Geology and mineralization styles of the George Fisher Zn-Pb-Ag deposit, Mount Isa, Australia. *Economic Geol.* **99**, 233–255.

Chapman, N. & McCombie, C. (2003) *Principles and Standards for the Disposal of Long-Lived Radioactive Wastes*. 277 pp, Pergamon.

Chappell, B.W. & Hine, R. (2006) The Cornubian batholith: an example of magmatic fractionation on a crustal scale. *Resource Geology* **56**, 203–244.

Chavez, W.X. (2000) Supergene oxidation of copper deposits: zoning and distribution of copper oxide minerals. *SEG-Newsletter* **41**(1), 10–21.

Chesley, J.T., Halliday, A.N., Snee, L.W., *et al.* (1993) Thermochronology of the Cornubian batholith in southwest England: Implications for pluton emplacement and protracted hydrothermal mineralization. *Geochim. Cosmochim. Acta* **57**, 1817–1835.

Chetti, D. & Frimmel, H.E. (2000) The role of evaporites in the genesis of base metal sulphide mineralisation in the northern platform of the Panafrican Damara belt, Namibia: geochemical and fluid inclusion evidence from carbonate wallrock alteration. *Miner. Deposita* **35**, 364–375.

Chi, G., Dubé, B., Williamson, K. & Williams-Jones, A.E. (2006) Formation of the Campbell-Red Lake gold deposit by H_2O-poor, CO_2-dominated fluids. *Miner. Deposita* **40**, 726–741.

Chi, G., Xue, C., Lai, J. & Qing, H. (2007) Sand injection and liquefaction structures in the Jinding Zn-Pb deposit, Yunnan, China: indicators of an overpressured fluid system and implications for mineralization. *Economic Geol.* **102**, 739–743.

Chiaradia, M. & Fontboté, L. (2003) Separate lead isotope analyses of leachate and residue rock fractions: implications for metal source tracing in ore deposit studies. *Miner. Deposita* **38**, 185–195.

Chierici, G.L. (1994) *Principles of Petroleum Reservoir Engineering*. 419 pp. Springer.

Childers, S.E., Ciufo, S. & Lovley, D.R. (2002) Geobacter metallireducens accesses insoluble Fe(III) oxide by chemotaxis. *Nature* **416**, 767–769.

Chopin, E.I.B. & Alloway, B.J. (2007) Distribution and mobility of trace elements in soils and vegetation around the mining and smelting areas of Tharsis, Ríotinto and Huelva, Iberian Pyrite Belt, SW Spain. *Water, Air & Soil Pollution* **182**, 245–261.

Chow, J., Kopp, R.J. & Portney, P.R. (2003) Energy resources and global development. *Science* **302**, 1528–1531.

Christidis, G.E. & Scott, P. (1996) Physical and chemical properties of bentonite deposits of Milos Island, Greece. *Trans. Instn. Min. Metall. B* **105**, 165–174.

Chyi, L.L. & Medlin, J.H. (1996) Characterizing coal beds in western Kentucky with the Al-La-Sc coherent triad. *Int. J. Coal Geol.* **30**, 349–359.

Cimon, J. & McCann, J. (2000) Le gite d'apatite-ilménite du complexe mafique lité d'age Cambrien de Sept-Iles, Québec. *Chron. Rech. Minière* **539**, 63–83.

Ciu, C.L., Cook, N.J. & Stein, H. (2002) Regional setting and geochronology of the Late Cretaceous banatitic magmatic and metallogenetic belt. *Miner. Deposita* **37**, 541–567.

Ciullo, P. (ed.) (1996) *Industrial Minerals and Their Uses – A Hand Book and Formulary*. 632 pp., Noyes Publication, USA.

Clark, A.H. & Kontak, D.J. (2004) Fe-Ti-P oxide melts generated through magma mixing in the Antauta subvolcanic center, Peru: implications for the origin of nelsonite and iron oxide-dominated hydrothermal deposits. *Economic Geol.* **99**, 377–395.

Clark, S.H.B., Gallagher, M.J. & Poole, F.G. (1990) World barite resources: a review of recent production patterns and a genetic classification. *Trans. Instn. Min. Metall. B* **99**, 125–132.

Clark, S.H.B., Poole, F.G. & Wang, Z. (2004) Comparison of some sediment-hosted, stratiform barite deposits in China, the United States, and India. *Ore Geol. Rev.* **24**, 85–101.

Clarke, M. (2010) Hybrid ventilation air methane (VAM) and coal waste fired power generation. *AusIMM Bulletin*, **June 2010**, 61–64.

Clarkson, R. (1998) A comparative evaluation of drilling techniques for deposits containing free gold using radioactive gold particles as tracers. *AusIMM Bulletin* **3**, 58–63.

Clauzon, G., Suc, J.-P., Gauthier, F., Berger, A. & Loutre, M.-F. (1996) Alternate interpretation of the Messinian salinity crisis: controversy resolved? *Geology* **24**, 363–366.

Clemens, J.D. (2003) S-type granitic magmas – petrogenetic issues, models and evidence. *Earth Science Rev.* **61**, 1–18.

Clement, C.R., Harris, J.W., Robinson, D.N. & Hawthorne, J.B. (1986) The De Beers kimberlite pipe – a historic South African diamond mine. In: *Mineral Deposits of Southern Africa*, Vols II (eds C.R. Anhäusser & S. Maske), pp 2193–2214. Geol. Soc. S. Africa, Johannesburg.

Clifford, T.N. (1966) Tectono-thermal units and metallogenic provinces of Africa. *Earth Planet. Sci. Lett.* **1**, 421–434.

Cloetingh S., Ziegler P.A., Beekman F., *et al.* (2005) Lithospheric memory, state of stress and rheology: neotectonic controls on Europe's intraplate continental topography. *Quat. Sci. Rev.* **24**, 241–304.

Clout, J.M.F. (2006) Iron formation-hosted iron ores in the Hamersley Province of Western Australia. *Applied Earth Sci.* **115**, 115–125.

Cobb, J.C. & Cecil, C.B. (eds) (1993) Modern and ancient coal-forming environments. *Geol. Soc. America Spec. Paper 286*, 189 pp.

Coburn, M.G. & Gillespie, J.M. (2002) A hydrologic study to optimize steamflood performance in a giant oil field: Kern River field, California. *AAPG Bull.* **86**, 1489–1505.

Coggon, R.M., Teagle, D.A.H., Smith-Duque, Ch.E., Alt, J.C. & Cooper, M.J. (2010) Reconstructing past seawater Mg/Ca and Sr/Ca from mid-ocean ridge flank calcium carbonate veins. *Science* **327**, 1114–1117.

Colpron, M. & Nelson, J.L. (eds) (2006) Paleozoic evolution and metallogeny of pericratonic terranes at the ancient Pacific margin of North America, Canadian and Alaskan Cordillera. Geol. Assoc. *Canada Spec. Paper 45*, 523 pp.

Combes, P.J. (1984) Regards sur la géologie des bauxites; aspects récents sur la genèse de quelques gisements à substratum carbonaté. *Bull. Rech. Explor. Prod. Elf-Aquitaine* **8**, 251–274.

Combs, G.F. (2005) Geological impacts on nutrition. In: *Essentials of Medical Geology – Impacts of the Natural Environment on Public Health* (ed. Selinus *et al.*) pp 161–177. Elsevier Academic Press.

Conrad, C.P. & Lithgow-Bertelloni, C. (2007) Faster seafloor spreading and lithosphere production during the mid-Cenozoic. *Geology* **35**, 29–32.

Coogan, L.A. & Cullen, J.T. (2009) Did natural reactors form as a consequence of the emergence of oxygenic photosynthesis during the Archean? *GSA Today* **19**, 4–10.

Cook, N.D.J. & Ashley, P.M. (1992) Meta-evaporite sequence, exhalative chemical sediments and associated rocks in the Proterozoic Willyama Supergroup, South Australia: implications for metallogenesis. *Precambrian Research* **56**, 211–226.

Cook, P.J. & Harris, P.M. (1998) Reserves, resources and the UK mining industry. *Intern. Mining & Minerals*, **1** (5), 120–135.

Cooke, D.R., Bull, S.W., Large, R.R. & McGoldrick, P.J. (2000) The importance of oxidized brines for the formation of Australian Proterozoic stratiform sediment-hosted Pb-Zn (Sedex) deposits. *Economic Geol.* **95**, 1–18.

Cooke, D.R., Hollings, P. & Walshe, J.L. (2005) Giant porphyry deposits: characteristics, distribution and tectonic control. *Economic Geol.* **100**, 801–818.

Coppin, N.J., Bryson, F.E. & Brown, C.W. (1996) Pyrometallurgy and the environment: at what cost? *Minerals Industry Intern.* **1030**, 23–32.

Cornell, D.H. & Schütte, S.S. (1995) A volcanic-exhalative origin for the world's largest (Kalahari) manganese field. *Miner. Deposita* **30**, 146–151.

Côte, C.M., Moran, C.J. & Hedemann, C.J. (2007) Evaluating the costs and benefits of salt management strategies at mine sites using a systems model. *Mine Water Environ* **26**, 229–236.

Counter Benison, K., Goldstein, R.H., Wopenka, B., *et al.* (1998) Extremely acid Permian lakes and ground waters in North America. *Nature* **392**, 911–914.

Courtney, R. G. & Timpson, J. P. (2005) Reclamation of fine fraction bauxite processing residue (Red Mud) amended with coarse fraction residue and gypsum. *Water, Air & Soil Pollution* **164**, 91–102.

Coveney, R.M. & Nansheng, C. (1991) Ni-Mo-PGE-Au-rich ores in Chinese black shales and speculations on possible analogues in the United States. *Miner. Deposita* **26**, 83–88.

Cox, R., Gutmann, E.D. & Hines, P.G. (2002) Diagenetic origin for quartz-pebble conglomerates. *Geology* **30**, 323–326.

Cox, D.P. & Singer, D.A. (2007) Descriptive and grade/tonnage models and data base for iron oxide Cu-Au deposits. *USGS Open-File Report 2007–1155*, 13 pp.

Cox, D.P. & Singer, D.A. (eds) (1986) Mineral deposit models. *USGS Bull.* **1693**, 379.

Craig, J.R. & Rimstidt, J.D. (1998) Gold production history of the United States. *Ore Geol. Rev.* **13**, 407–464.

Craig, J.R. & Vaughan, D.J. (1994) *Ore Microscopy and Ore Petrography*. 2nd ed., 434 pp, Wiley.

Craig, J.R. & Vokes, F.M. (1992) Ore mineralogy of the Appalachian–Caledonian stratabound sulfide deposits. *Ore Geol. Rev.* **7**, 77–123.

Craig, J.R., Vokes, F.M. & Solberg, T.N. (1998) Pyrite: physical and chemical textures. *Miner. Deposita* **34**, 82–101.

Cramer, B. & Franke, D. (2006) Indications for an active petroleum system in the Laptev Sea, NE Siberia. *J. Petroleum Geol.* **28**, 369–384.

Crandall, K.A. & Buhay, J.E. (2004) Genomic data bases and the Tree of Life. *Science* **306**, 1144–1145.

Cravotta, C.A. (2007) Passive aerobic treatment of net-alkaline, iron-laden drainage from a flooded underground anthracite mine, Pennsylvania, USA. *Mine Water Environ* **26**, 128–149.

Craw, D., Wilson, N. & Ashley, P.M. (2004) Geochemical controls on the environmental mobility of Sb and As at mesothermal antimony and gold deposits. *Applied Earth Sci.* **113**, B3–10.

Craw, D. & Chamberlain, C.P. (1996) Meteoric incursion and oxygen fronts in the Dalradian metamorphic belt, southwest Scotland: a new hypothesis for regional gold mobility. *Miner. Deposita* **31**, 365–373.

Craw, D., Koons, P.O., Horton, T. & Chamberlain, C.P. (2002) Tectonically driven fluid flow and gold mineralization in active collisional orogenic belts: Comparison between New Zealand and western Himalaya. *Tectonophysics* **348**, 135–153.

Creaser, R.A., Price, R.C. & Wormald, R.J. (1991) A-granites revisited: Assessment of a residual source model. *Geology* **19**, 163–166.

Crock, J.G., Arbogast, B.F. & Lamothe, P.J. (1999) Laboratory methods for the analysis of environmental samples. In: *The Environmental Geochemistry of Mineral Deposits* (eds G.S. Plumlee & M.J. Logsdon), pp 265–287.

Crone, T.J. & Tolstoy, M. (2010) Magnitude of the 2010 Gulf of Mexico oil leak. *Science* **330**, 634.

Cross, A.T. (ed.) (1993) World-class coal deposits: Proceedings of the 28th Int. Geol.Congress, Washington DC, July 1989. *Int. J. Coal Geol.* **23**, 1–321.

Crowe, D.E. (1994) Preservation of δ^{34}S values in greenschist to upper amphibolite volcanogenic massive sulfide deposits. *Geology* **22**, 873–876.

Crowe, D.E., Riciputi, L.R., Bezenek, S. & Ignatiev, A. (2001) Oxygen isotope and trace element zoning in hydrothermal garnets: windows into large-scale fluid-flow behaviour. *Geology* **29**, 479–482.

Cuney, M. (2009) The extreme diversity of uranium deposits. *Mineral. Deposita* **44**, 3–9.

Cuney, M. & Kyser, K. (2009) Recent and not-so-recent developments in uranium deposits and implications for exploration. *Mineral. Soc. Canada Short Course Series* **39**, 272.

Cunningham, C.G., Zartman, R.E., McKee, E.H., *et al.* (1996) The age and thermal history of Cerro Rico de Potosí, Bolivia. *Miner. Deposita* **31**, 374–385.

Czernichowski-Lauriol, I. & Fouillac, C. (1991) The chemistry of geothermal waters: its effect on exploitation. *Terra Nova* **3**, 477–491.

D'Argenio, B. & Mindszenty, A. (1995) Bauxites and related paleokarst: tectonic and climatic event markers at regional unconformities. *Eclogae geol. Helv.* **88**, 453–499.

Da Costa, M.L. & Moraes, E.L. (1998) Mineralogy, geochemistry and genesis of kaolins from the Amazon region. *Miner. Deposita* **33**, 283–297.

Dahanayake, K. & Krumbein, W.E. (1986) Microbial structures in oolitic iron formations. *Miner. Deposita* **21**, 85–94.

Dahlkamp, F.J. (1993) *Uranium Ore Deposits*. 460 pp. Springer.

Dahlkamp, F.J. (1978) Geologic appraisal of the Key Lake U-Ni deposits, northern Saskatchewan. *Economic Geol.* **73**, 1430–1449.

Dake, L.P. (1994) *The Practice Of Reservoir Engineering*. 556 pp. Elsevier.

Dalstra, H. & Guedes, S. (2004) Giant hydrothermal hematite deposits with Mg-Fe metasomatism: a comparison of the Carajas, Hamersley, and other iron ores. *Economic Geol.* **99**, 1793–1800.

Danesh, A. (1998) *PVT and Phase Behaviour of Petroleum Reservoir Fluids*. 400 pp. Elsevier.

Daniels, E.J., Aronson, J.L., Altaner, S.P. & Clauer, N. (1994) Late Permian age of NH_4-bearing illite in anthracite from eastern Pennsylvania: Temporal limits on coalification in the central Appalachians. *Geol. Soc. America Bull.* **106**, 760–766.

Daniels, L.R.M., Gurney, J.J. & Harte, B. (1996) A crustal mineral in a mantle diamond. *Nature* **379**, 153–156.

D'Ans, J. (1969) Bemerkungen zu Problemen der Kalisalzlagerstätten II. *Kali und Steinsalz* **5**, 152–157.

Daroussin, J.-l., Pfiffelmann, J.-P. & Ruhlmann, F. (1998) Réaménagement de sites miniers: l'exemple du site d'extraction et de traitement de minerai d'uranium de l'Ecarpière (COGEMA, France). *Chron. Rech. Minière* **533**, 31–41.

Darwin, Ch. 1968 (1859) *The Origin of Species by Means of Natural Selection*. 477 pp. Penguin.

Daubrée, A. (1887) *Les eaux souterraines, aux épOches anciennes et à l'épOche actuelle*. Vol. 3, Dunod, Paris.

Daudre, B. & Cloetingh, S. (1994) Numerical modelling of salt diapirism: influence of the tectonic regime. *Tectonophysics* **240**, 59–79.

Davies, A.G.S., Cooke, D.R., Gemmel, J.B. & Simpson, K.A. (2008) Diatreme breccias at the Kelian gold mine, Kalimantan, Indonesia: precursors to epithermal gold mineralisation. *Economic Geol.* **103**, 689–716.

Davies, G.R., Nixon, P.H., Pearson, D. G. & Obata, M. (1993) Tectonic implications of graphitized diamonds from the Ronda peridotite massif, southern Spain. *Geology* **21**, 471–474.

Davies, R.J. (2005) Differential compaction and subsidence in sedimentary basins due to silica diagenesis: a case study. *Geol. Soc. America Bulletin* **117**, 1146–1155.

Davis, A. (2003) A screening-level laboratory method to estimate pit lake chemistry. *Mine Water Environ* **22**, 194–205.

Davis, D.W. & Lin, S. (2003) Unraveling the geologic history of the Hemlo Archean gold deposit, Superior Province, Canada: a U-Pb geochronological study. *Economic Geol.* **98**, 51–67.

Davis, S.N. & DeWiest, R.J.M. (1966) *Hydrogeology*. 463 pp. Wiley.

Davis, T. (2004) Mine-scale structural controls on the Mount Isa Zn-Pb-Ag and Cu orebodies. *Economic Geol.* **90**, 543–559.

De Boorder, H., Spakman, W., White, S.H. & Wortel, M.J. R. (1998) Late Cenozoic mineralization, orogenic collapse and slab detachment in the European Alpine belt. *Earth Planet. Sci. Letters* **164**, 569–575.

Deelman, J.C. (2001) Breaking Ostwald's rule. *Chemie der Erde (Geochemistry)* **61**, 224–235.

De Haan, H.J. (ed.) (1995) New developments in improved oil recovery. *Geol. Soc. Spec. Publ.* **84**, 294.

De Wit, M.C.J. (1999) Post-Gondwana drainage and the development of diamond placers in western South Africa. *Economic Geol.* **94**, 721–740.

Deere, D.U. (1964) Technical description of rock cores for engineering purposes. *Rock Mech. Eng. Geol.* **1**, 17–22.

Dehmer, J. (1995) Petrological and organic geochemical investigation of recent peats with known environments of deposition. *Intern. J. Coal Geol.* **28**, 111–138.

Dejonghe, L. (1989) Le gisement de Fleurus (Belgique): une concentration de barytine sédimentaire en milieu lacustre piegée dans un paléokarst envahi par des sédiments wealdiens. *Chron. rech. min.* **494**, 25–42.

Delong, E.F. (2000) Resolving a methane mystery. *Nature* **407**, 577–578.

Demicco, R.V., Lowenstein, T.K., Hardie, L.A. & Spencer, R. J. (2005) Model of seawater composition for the Phanerozoic. *Geology* **33**, 877–880.

Dentith, M.C., Frankcombe, K.F., Ho, S.E., Shepherd, J. M., Groves, D.I. & Trench, A. (eds.) (1994) *Geophysical Signatures of Western Australian Mineral Deposits*. 454 pp. Publication 26, Geology Key Centre UWA.

Denton, J.S., Tuffen, H., Gilbert, J.S. & Odling, N. (2009) The hydration and alteration of perlite and rhyolite. *J. Geol. Soc.* **166**, 895–904.

Désindes, L., Durand, M., Bailly, L., *et al.* (2006) Genesis of the Dordogne (France) high-purity silica placers. *Int. J. Earth Sci.* **95**, 80–94.

Diaz, J., Ingall, E., Benitez-Nelson, C., *et al.* (2008) Marine polyphosphate: A key player in geologic phosphorus sequestration. *Science* **320**, 652–655.

Di Primio, R., Horsfield, B. & Guzman-Vega, M.A. (2000) Determining the temperature of petroleum formation from the kinetic properties of petroleum asphaltenes. *Nature* **406**, 173–176.

Dickens, G.R., Castillo, M.M. & Walker, J.C.G. (1997a) A blast of gas in the latest Paleocene: simulating first order effects of massive dissociation of oceanic methane hydrate. *Geology* **25**, 258–262.

Dickens, G.R., Pauli, C.K., Wallace, P. & ODP Leg 164 Scientific Party (1997b) Direct measurement of in situ methane quantities in a large gas-hydrate reservoir. *Nature* **385**, 426–428.

Dickin, A.P. (1995) *Radiogenic Isotope Geology*. 452 pp. Cambridge University Press.

Dickson, B.L. & Giblin, A.M. (2007) Effective exploration for uranium in South Australian paleochannels. *Applied Earth Sci.* **116**, 50–54.

Diessel, C.F.K. (1986) On the correlation between coal facies and depositional environments. Pp 11–22 in: *Advances in the Study of the Sydney Basin*, Proc. 20th Symp. Univ. of Newcastle, Australia.

Dietz, R.S. (1964) Sudbury structure as an astrobleme. *J. Geol.* **72**, 412–434.

Dilek, Y., Moores, E., Elthon, D. & Nicolas, A. (eds) (2001) *Ophiolites and Oceanic Crust*. 556 pp, Geol. Soc. America.

Dill, H.G. & Kantor, W. (1997) Depositional environment, geochemical facies, and a tentative classification system of selected types of phosphate occurrences. *Geol. Jb. D* **105**, 3–43.

Dill, H.G. (1998) Evolution of Sb mineralisation in modern fold belts: a comparison of the Sb mineralisation in the Central Andes (Bolivia) and the Western Carpathians (Slovakia). *Miner. Deposita* **33**, 359–378.

DiMichele, W.A., Falcon-Lang, H., Nelson, W.J., Elrick, S.D. & Ames, P.R. (2007) Ecological gradients within a Pennsylvanian mire forest. *Geology* **35**, 415–418.

Ding, K. & Seyfried, W.E. (1996) Direct pH measurement of NaCl-bearing fluid with an in situ sensor at 400 °C and 40 megapascals. *Science* **272**, 1634–1636.

Dissanayake, Ch. (2005) Of stones and health: medical geology in Sri Lanka. *Science* **309**, 883–885.

Distler, V.V., Kryachko, V.V., & Yudovskaya, M.A. (2008) Ore petrology of chromite-PGE mineralization in the Kempirsai ophiolite complex. *Min. Petrol.* **92**, 31–58 (Eugen F. Stumpfl Volume).

Distler, V.V., Yudovskaya, M.A., Mitrofanov, G.L. *et al.* (2004) Geology, composition, and genesis of the Sukhoi Log noble metals deposit, Russia. *Ore Geol. Rev.* **24**, 7–44.

Dolman, A.J. & de Jeu, R.A.M. (2010) Evaporation in focus. *Nature Geosci.* **3**, p. 296.

Dominy, S.C. & Camm, G.S. (1998) Geology and hydrothermal development of Bostraze-Balleswidden kaolin deposit, Cornwall, United Kingdom. *Trans. Instn. Min. Metall. B* **107**, 148–157.

Dominy, S.C. & Platten, I.M. (2007) Gold particle clustering: a new consideration in sampling applications. *Applied Earth Sci.* **116**, 130–142.

Dominy, S.C., Busell, M.A. & Camm, G.S. (1996) Development of complex, granite-hosted, tin-bearing fracture systems in southwest England: applications of fluid inclusion microfracture studies. *Trans. Instn. Min. Metall. B* **105**, 139–144.

Dong, G., Morrison, G. & Jaireth, S. (1995) Quartz textures in epithermal veins, Queensland – classification, origin, and implication. *Economic Geol.* **90**, 1841–1856.

Dorsey, R.J. (2010) Sedimentation and crustal recycling along an active oblique-rift margin: Salton Trough and northern Gulf of California. *Geology* **38**, 443–446.

Dreher, S.T., Macpherson, C.G., Pearson, D.G. & Davidson, J.P. (2005) Re-Os isotope studies of Mindanao adakites: implications for sources of metals and melts. *Geology* **33**, 957–960.

Driesner, T. (1997) The effect of pressure on deuterium-hydrogen fractionation in high-temperature water. *Science* **277**, 791–794.

Drozdzewski, G. (1993) The Ruhr coal basin (Germany): structural evolution of an autochthonous foreland basin. *Int. J. Coal Geol.* **23**, 231–250.

Drury, S.A. (2001) *Image Interpretation in Geology*. 3rd ed., 290 pp, Routledge.

Duane, M.J., Kruger, F.J., Roberts, P.J. & Smith, C.B. (1991) Pb and Sr isotopes and origin of Proterozoic base metal (fluorite) and gold deposits, Transvaal Sequence, South Africa. *Economic Geol.* **86**, 1491–1505.

Ducea, M.N. & Barton, M.D. (2007) Igniting flare-up events in Cordilleran arcs. *Geology* **35**, 1047–1050.

Duchesne, J.C., Liegois, J.P., Van Der Auwera, J. & Longhi, J. (1999) The crustal tongue melting model and the origin of massive anorthosites. *Terra Nova* **11**, 100–105.

Duk-Rodkin, A., Patyk-Kara, N. & Catto, N.R. (eds) (2001) *Quarternary Placer Deposits*. 127 pp, Quarternary International 82/1, Special Issue.

Duncan, R.K. & Willet, G.C. (1990) Mt Weld carbonatite. In: *Geology of Mineral Deposits of Australia and*

Papua New Guinea (ed. F.E. Hughes), pp 591–597. AusIMM, Melbourne.

Dunning, F.W. & Evans, A.M. (eds) (1986) *Mineral Deposits of Europe. III. Central Europe*. 355 pp. IMM, London.

Dunning, F.W., Garrard, D., Haslam, H.W. & Ixer, R.A. (eds) (1989) *Mineral Deposits of Europe. IV/V. Southwest and Eastern Europe, with Iceland*. 460 pp. IMM, London.

Dunning, F.W., Mykura, W. & Slater, D. (eds) (1982) *Mineral Deposits of Europe. II. Southeast Europe*. 304 pp. IMM, London.

Dutkiewicz, A., Volk, H., Ridley, J. & George, S. (2003) Biomarkers, brines, and oil in the Mesoproterozoic Roper Superbasin, Australia. *Geology* **31**, 981–984.

Dutkiewitz, A., Volk, H., George, S.C., Ridley, J. & Buick, R. (2006) Biomarkers from Huronian oil-bearing fluid inclusions: an uncontaminated record of life before the Great Oxidation Event. *Geology* **34**, 437–440.

Dyer, A. (1988) *An Introduction to Zeolite Molecular Sieves*. 149 pp. Wiley.

Dyni, J.R. (1996) Sodium carbonate resources of the Green River Formation. *USGS Open File Report 96–729*, 39 pp.

Eales, A. & Cawthorn, R.G. (1996) The Bushveld Complex. In: *Layered Intrusions* (ed. R.G. Cawthorn). 544 pp. Elsevier.

Eastoe, C.J. & Peryt, T. (1999) Stable chlorine isotope evidence for non-marine chloride in Badenian evaporites, Carpathian mountain region. *Terra Nova* **11**, 118–123.

Eastoe, C.J., Long, A. & Knauth, L.P. (1999) Stable chlorine isotopes in the Palo Duro basin, Texas: evidence for preservation of Permian evaporite brines. *Geochim. Cosmichim. Acta* **63**, 1375–1382.

Eaton, G.F., Criss, R.E., Fleck, R.J., *et al.* (1995) Oxygen, carbon, and strontium isotope geochemistry of the Sunshine mine, Coeur d'Alene mining district, Idaho. *Economic Geol.* **90**, 2274–2286.

Eble, C.F. & Greb, S.F. (1997) Channel-fill coal beds along the western margin of the Eastern Kentucky coal field. *Intern. J. Coal Geol.* **33**, 183–207.

Eby, G.N. (1992) Chemical subdivision of the A-type granitoids: Petrogenetic and tectonic implications. *Geology* **20**, 641–644.

Eckert, C.A., Knutson, B.L. & Debenetti, P.G. (1996) Supercritical fluids as solvents for chemical and materials processing. *Nature* **383**, 313–318.

Edmunds, M. & Smedley, P. (2005) Fluoride in natural waters. In: *Essentials of Medical Geology – Impacts of the Natural Environment on Public Health* (ed. O. Selinus *et al.*.), pp 301–329. Elsevier Academic Press.

Edwards, A.C. (ed.) (2001) Mineral resource and ore reserve estimation – the AusIMM guide to good practice. *AusIMM Monograph 23*, 719 pp. AusIMM, Melbourne.

Edwards, K.J., Bond, P.L., Gihring, T.M. & Banfield, J.F. (2000) An archeal iron-oxidising extreme acidophile important in acid mine drainage. *Science* **287**, 1796–1799.

Egholm, D.L., Clausen, O.R., Sandiford, M., Kristensen, M.B. & Kostgard, J.A. (2008) The mechanics of clay smearing along faults. *Geology* **36**, 787–790.

Eilu, P., Mikucki, E.J. & Dugdale, A.L. (2001) Alteration zoning and primary geochemical dispersion at the Bronzewing lode-gold deposit, Western Australia. *Miner. Deposita* **36**, 13–31.

Einsele, G. (2000) *Sedimentary Basins. Evolution, Facies, and Sediment Budget*, 2nd edn. 800 pp. Springer.

Eisenlohr, B.N., Tompkins, L.A., Cathles, L.M., *et al.* (1994) Mississippi Valley-type deposits: Products of brine expulsion by eustatically induced hydrocarbon generation? An example from northwestern Australia. *Geology* **22**, 315–318.

Elagami, N.L., Ibrahim, E.H. & Odah, H.H. (2000) Sedimentary origin of the Mn-Fe ore of Um Bogma, southwest Sinai: geochemical and paleomagnetic evidence. *Economic Geol.* **95**, 607–620.

Eldridge, C.S., Compston, W., Williams, C.S., *et al.* (1991) Isotope evidence for the involvement of recycled sediments in diamond formation. *Nature* **353**, 649–653.

Elick, J.M., Driese, S.G. & Mora, C.I. (1998) Very large plant and root traces from the Early to Middle Devonian: implications for early terrestrial ecosystems and atmospheric p(CO_2). *Geology* **26**, 143–146.

Eliopoulos, D.G. & Economou-Eliopoulos, M. (2000) Geochemical and mineralogical characteristics of Fe-Ni and bauxitic laterite deposits of Greece. *Ore Geol. Rev.* **16**, 41–58.

Ellis, A.S., Johnson, T.M. & Bullen, T.D. (2002) Chromium isotopes and the fate of hexavalent chromium in the environment. *Science* **295**, 2060–2062.

Ellis, D.V. & Singer, J.M. (2007) *Well Logging for Earth Scientists*. 2nd edn. 692 pp. Springer.

Ellmies, R., Voigtländer, G., Germann, K., *et al.* (1999) Origin of giant stratabound deposits of magnesite and siderite in Riphean carbonate rocks of the Bashkir mega-anticline, western Urals. *Geol. Rundschau* **87**, 589–602.

El Tabakh, M., Utha-Aroon, Ch. & Schreiber, Ch. (1999) Sedimentology of the Cretaceous Maha Sarakham evaporites in the Khorat Plateau of northeastern Thailand. *Sed. Geol.* **123**, 31–62.

Emberger, A. (1984) La carte métallogénique de l'Europe et des pays limitrophes 1:2 500 000. *Chron. Rech. Minière* **475**, 51–56.

Emeis, K.-C. & Weissert, H. (2009) Tethyan-Mediterranean organic carbon-rich sediments from Mesozoic black shales to sapropels. *Sedimentology* **56**, 247–266.

Enzel, Y., Agnon, A. & Stein, M. (2006) New frontiers in Dead Sea paleoenvironmental research. *Geol. Soc. America Spec. Paper 401*, 253 pp.

Eriksson, K.A. & Chuck, R.G. (1985) Aulacogens: sedimentological and tectonic evolution and associated mineralization. In: *Handbook of Strata-Bound and Stratiform Ore Deposits*, Vol. 12 (ed. K. H. Wolf), pp 461–529. Elsevier.

Espitalié, J., Marquis, F. & Barsony, I. (1984) Geochemical logging. In: *Analytical pyrolysis: Techniques and Applications* (ed. K.J. Voorhees), pp 276–304. Butterworth.

Esterle, J.S. & Ferm, J.C. (1994) Spatial variability in modern tropical peat deposits from Sarawak, Malaysia and Sumatra, Indonesia; analogues for coal. *Intern. J. Coal Geol.* **26**, 1–41.

Etiope, G. & Ciccioli, P. (2009) Earth's degassing: a missing ethane and propane source. *Science* **323**, 478.

Eugster, H.P. (1984) Geochemistry and sedimentology of marine and nonmarine evaporites. *Eclogae Geologicae Helvetiae* **77**, 237–248.

Eugster, H.P. & Hardie, L.A. (1978) Saline lakes. In: *Lakes: Chemistry, Geology, Physics* (ed. A. Lerman), pp 237–293. Springer.

Eugster, H.P. & Surdam, R. (1973) Depositional environment of the Green River Formation of Wyoming: a preliminary report. *GSA Bull.* **84**, 1115–1120.

Eugster, H.P. (1970) Chemistry and origin of the brines of Lake Magadi, Kenya. *SEPC Publ. Geol. Soc.* **3**, 215–235.

Eugster, H.P., Harvie, C.E. & Weare, J.H. (1980) Mineral equilibria in the six-component sea water system, $Na\text{-}K\text{-}Mg\text{-}Ca\text{-}SO_4\text{-}Cl\text{-}H_2O$, at 25 °C. *Geochim. Cosmochim. Acta* **44**, 1348–1355.

European Commission (EC) (2010) *Report of the Ad-hoc Working* Group on defining critical raw materials. European Commission Enterprise and Industry DG, http://ec.europa.eu/enterprise/policies/raw-materials/files/docs/report_en.pdf (accessed 17 June 2010).

Evans, A.M. (ed.) (1993) *Introduction to Mineral Exploration*. 408 pp. Blackwell Science.

Evans, A.M. (1998) *Introduction to Economic Geology and its Environmental Impact*. 376 pp. Blackwell Science.

Evans, D.A.D. (2006) Proterozoic low orbital obliquity and axial-dipolar geomagnetic field from evaporite latitudes. *Nature* **444**, 51–55.

Evensen, J.M. & London, D. (2002) Experimental mineral/melt partition coefficients for beryllium and the crustal Be cycle from migmatite to pegmatite. *Geochim. Cosmochim. Acta* **66**, 2239–2265.

Everett, C.E., Rye, D.M. & Ellam, R.M. (2003) Source or sink? An assessment of the role of the Old Red Sandstone in the genesis of the Irish Zn-Pb deposits. *Economic Geol.* **98**, 31–50.

Faccenda, M., Gerya, T.V. & Burlini, L. (2009) Deep slab hydration induced by bending-related variations in tectonic pressure. *Nature Geoscience* **2**, 790–793.

Falcon-Lang, H.J., Nelson, W.J., Elrick, S., *et al.* (2009) Incised channel fills containing conifers indicate that seasonally dry vegetation dominated Pennsylvanian tropical lowlands. *Geology* **37**, 923–926.

Falconer, D.M., Craw, D., Youngson, J.H. & Faure, K. (2005) Gold and sulphide minerals in Tertiary quartz pebble conglomerate gold placers, Southland, New Zealand. *Ore Geol. Rev.* **28**, 525–545.

Falkowski, P.G., Fenchel, T. & Delong, E.F. (2008) The microbial engines that drive Earth's biogeochemical cycles. *Science* **320**, 1034–1039.

Falkowski, P.G. & Isozaki, Y. (2008) The story of O_2. *Science* **322**, 540–542.

Fallick, A.E., Ashton, J.H., Boyce, A.J. *et al.* (2001) Bacteria were reponsible for the magnitude of the world-class hydrothermal base metal sulfide orebody at Navan, Ireland. *Economic Geol.* **96**, 885–890.

Fallick, A.E., Ilich, M. & Russell, M.J. (1991) A stable isotope study of the magnesite deposits associated with the alpine-type ultramafic rocks of Yugoslavia. *Economic Geol.* **86**, 847–861.

Fan, D., Zhang, T. & Ye, J. (2004b) The Xikuanshan Sb deposit hosted by the Upper Devonian black shale series, Hunan, China. *Ore Geol. Rev.* **24**, 121–133.

Fan, D., Zhang, T., Ye, J., *et al.* (2004a) Geochemistry and origin of tin-polymetallic sulfide deposits hosted by the Devonian black shale series near Dachang, Guangxi, China. *Ore Geol. Rev.* **24**, 103–120.

Fan, Hong-Rui, Xie, Yi-Han, Wang, Kai-Yi & Wilde, S.A. (2004) Methane-rich fluid inclusions in skarn near the giant REE-Nb-Fe deposit at Bayan Obo, Northern China. *Ore Geol. Rev.* **25**, 301–309.

Farquhar, J. & Chacko, Th. (1991) Isotopic evidence for involvement of CO_2-bearing magmas in granulite formation. *Nature* **354**, 61–63.

Farrow, C.E.G. & Watkinson, D.H. (1992) Alteration and the role of fluids in Ni, Cu and platinum-group element deposition, Sudbury Igneous Complex contact, Onaping-Levack area, Ontario. *Mineralogy & Petrology* **46**, 67–83.

Faure, G. & Mensing, T.M. (2004) *Isotopes: Principles and Applications*. 928 pp, Wiley-Blackwell.

Faure, K. (2003) δD values of fluid inclusion water in quartz and calcite ejecta from active geothermal systems: do values reflect those of original hydrothermal water? *Economic Geol.* **98**, 657–660.

Fayek, M., Janeczek, J. & Ewing, R.C. (1998) Mineral chemistry and oxygen isotopic analyses of uraninite, pitchblende and uranium alteration minerals from the Cigar Lake deposit, Saskatchewan, Canada. *Applied Geochem*. **12**, 549–565.

Feely, R.A., Gendron, J.F., Baker, E.T. & Lebon, G.T. (1994) Hydrothermal plumes along the East Pacific Rise, 8°40′ to 11°50′N: particle distribution and composition. *Earth Planet. Sci. Lett.* **128**, 19–36.

Fein, J.B. & William-Jones, A.E. (1997) The role of mercury-organic interactions in the hydrothermal transport of mercury. *Economic Geol.* **92**, 20–28.

Fein, J.B., Hemley, J.J., D'Angelo, W.M., *et al.* (1992) Experimental study of iron-chloride complexing in hydrothermal fluids. *Geochim. Cosmochim. Acta* **56**, 3179–3190.

Feizullayev, A.A., Guliev, I.S., Kuliev, K., *et al.* (1998) Deep petroleum occurrences in the Lower Kura depression, South Caspian basin, Azerbaijan: an organic geochemical and basin modelling study. *Marine Petroleum Geol.* **14**, 731–762.

Fendorf, S., Michael, H.A. & van Geen, A. (2010) Spatial and temporal variations of groundwater arsenic in South and Southeast Asia. *Science* **328**, 1123–1127.

Fergusson, J.E. (1990) *The Heavy Elements: Chemistry, Environmental Impact and Health Effects*. 614 pp. Pergamon.

Ferry, J.M. & Dipple, G.M. (1991) Fluid flow, mineral reactions, and metasomatism. *Geology* **19**, 211–214.

Fertit, W.H., Chapman, R.E. & Hotz, R.F. (eds) (1994) *Studies in Abnormal Pressures*. 472 pp. Elsevier.

Ficklin, W.H. & Mosier, E.L. (1999) Field methods for sampling and analysis of environmental samples for unstable and stable constitutents. In: *The Environmental Geochemistry of Mineral Deposits* (eds G.S. Plumlee & M.J. Logsdon), pp 249–264.

Fiebig, J., Woodland, A.B., D'Alessandro, W. & Püttmann, W. (2009) Excess methane in continental hydrothermal emissions is abiogenic. *Geology* **37**, 495–498.

Fielding, C.R., Allen, J.P., Alexander, J. & Gibling, M.R. (2009) Facies model for fluvial systems in the seasonal tropics and subtropics. *Geology* **37**, 623–626.

Fike, D.A., Grotzinger, J.P., Pratt, L.M. & Summons, R.E. (2006) Oxidation of the Ediacaran ocean. *Nature* **444**, 744–747.

Filipek, L.H. & Plumlee, G.S. (eds) (1999) The environmental geochemistry of mineral deposits. *Rev. Economic Geol.* **6B**, 583.

Filipelli, G.M., Laidlaw, M.A.S., Latimer, J.C. & Raftis, R. (2005) Urban lead poisoning and medical geology: an unfinished story. *GSA Today* **15**, 4–11.

Findlay, D. (1998) Boudinage – a key to an organizing principle for the formation of ore deposits. *Economic Geol.* **93**, 671–682.

Finkelman, R.B., Orem, W., Castranova, V., *et al.* (2002) Health impacts of coal and coal use: possible solutions. *Int. J. Coal Geol.* **50**, 425–443.

Finkelman, R.B. & Gross, P.M.K. (1999) The types of data needed for assessing the environmental and human health impacts of coal. *Int. J. Coal Geol.* **40**, 91–101.

Finlow-Bates, T. (1980) The chemical and physical controls on the genesis of submarine exhalative orebodies and their implications for formulating exploration concepts. A review. *Geol. Jb. D* **40**, 131–168.

Finlow-Bates, T. & Large, D. (1978) Water depth as major control on the formation of submarine exhalative ore deposits. *Geol. Jb. D* **30**, 27–39.

Finlow-Bates, T. & Stumpfl, E.F. (1979) The copper and lead-zinc-silver orebodies of Mt. Isa mine, Queensland: products of one hydrothermal system. *Ann. Soc. Géol. Belg.* **102**, 497–517.

Fiorentini, M.L., Rosengren, N., Beresford, S.W., Grguric, B. & Barley, M.E. (2007) Controls on the emplacement and genesis of the MKD5 and Sarah's Find Ni-Cu-PGE deposits, Mount Keith, Agnew-Wiluna greenstone belt, Western Australia. *Miner. Deposita* **42**, 847–877.

Fischer, A.G. & Roberts, L.T. (1991) Cyclicity in the Green River Formation (lacustrine Eocene) of Wyoming. *J. Sediment. Petrol.* **61**, 1146–1154.

Fisher, Ch.R. & Girguis, P. (2007) A proteomic snapshot of life at a vent. *Science* **315**, 198–199.

Fisher, L.A. & Kendrick, M.A. (2008) Metamorphic fluid origins in the Osborne Fe oxide-Cu-Au deposit, Australia: evidence from noble gases and halogens. *Miner. Deposita* **43**, 483–497.

Fleet, M.E. & Wu, Tsai-Way (1993) Volatile transport of platinum-group elements in sulfide-chloride assemblages at 1000 °C. *Geochim. Cosmochim. Acta* **57**, 3519–3531.

Fleming, P.B., Liu, X. & Winters, W.J. (2003) Critical pressure and multiphase flow in Blake Ridge gas hydrates. *Geology* **31**, 1057–1060.

Fletcher, R.C., Hudec, M.R. & Watson, I.A. (1995) Salt glacier and composite sediment-salt glacier models for the emplacement and early burial of allochthonous salt sheets. In: *Salt Tectonics: A Global Perspective* (eds M.P.A. Jackson, D.G. Roberts & S. Snelson), pp.87–108.AAPG Mem. 65.

Flood, P.G. (1991) Prospecting for natural zeolites: exploration model based on an occurrence in 300 m.y. old rocks near Werris Creek, New South Wales, Australia. *Trans. Instn. Min. Metall. B* **100**, 9–13.

Fontaine, R.C., Davis, A. & Fennemore, G.G. (2003) The comprehensive realistic yearly transient filling code CRYPTIC: a novel pit lake analytical solution. *Mine Water Environ* **22**, 187–193.

Force, E.C. & Maynard, J.B. (1991) Manganese: syngenetic deposits on margins of anoxic basins. *Rev. in Economic Geol.* **5**, 147–157.

Force, E.R. (1991) Geology of titanium-mineral deposits. *Geol. Soc. America Special Paper 259*, 112 pp.

Ford, D.C. & Williams, P. (2007) *Karst Hydrogeology and Geomorphology*. 576 pp. Wiley-Blackwell.

Fordyce, F. (2005) Selenium deficiency and toxicity in the environment. In: *Essentials of Medical Geology – Impacts of the Natural Environment on Public Health* (ed. O. Selinus *et al.*), pp 373–415. Elsevier Academic Press.

Förster, H.-J., Tischendorf, G., Trumbull, R.G. & Gottesmann, B. (1999) Late-collisional granites in the Variscan Erzgebirge, Germany. *J. Petrol.* **40**, 1613–1645.

Fortescue, J.A.C. (1992) Landscape geochemistry – retrospect and prospect. *Applied Geochemistry* **7**, 1–53.

Foster, K.R., Vecchia, P. & Repacholi, M.H. (2000) Science and the precautionary principle. *Science* **288**, 979–981.

Fouet, T., Riske, R., Morley, C., Cook, A., Conti, D. & Centofani, J. (2009) Standardising the reconciliation factors required in governance reporting. *Proc. 7th Int. Mining Geol. Conf. 2009*, 127–139, AusIMM Melbourne.

Foulger, G.R. & Natland, J.H. (2003) Is "hotspot" volcanism a consequence of plate tectonics? *Science* **300**, 921–922.

Fouquet, Y., Eissen, J-Ph., Ondreas, H., *et al.* (1999) Extensive volcaniclastic deposits at the Mid-Atlantic Ridge axis: results of deep water basaltic explosive volcanic activity? *Terra Nova* **10**, 280–286.

Fouquet, Y., Knott, R., Cambon, P., *et al.* (1996) Formation of large sulfide mineral deposits along fast spreading ridges. Example from off-axis deposits at 12°43′N on the East Pacific Rise. *Earth Planet. Sci. Lett.* **144**, 147–162.

Fournier, R.O. & Potter, R.W. (1982) A revised and expanded silica (quartz) geothermometer. *Geothermal Res. Council Bull.* **11**, 3–9.

Fournier, R.O. (1999) Hydrothermal processes related to movement of fluid from plastic into brittle rock in the magmatic-epithermal environment. *Economic Geol.* **94**, 1183–1211.

Foustoukos, D.I. & Seyfried, W.E. (2004) Hydrocarbons in hydrothermal vent fluids: the role of chromium-bearing catalysts. *Science* **304**, 1002–1005.

Fowler, A.D. & Anderson, M.T. (1991) Geopressure zones as proximal sources of hydrothermal fluids in sedimentary basins and the origin of Mississippi Valley-type deposits in shale rich sequences. *Trans. Instn. Min. Metall. B* **100**, 14–18.

Frakes, L. & Bolton, B. (1992) Effects of ocean chemistry, sea level, and climate on the formation of primary sedimentary manganese ore deposits. *Economic Geol.* **87**, 1207–1217.

Frank, T.D., Zi Gui & ANDRILL SMS Science Team (2010) Cryogenic origin for brine in the subsurface of southern McMurdo Sound, Antarctica. *Geology* **38**, 587–590.

Frank, T.D. & Fielding, C.R. (2003) Marine origin for Precambrian, carbonate-hosted magnesite? *Geology* **31**, 1101–1104.

Freeman, C., Fenner, N., Ostle, N.J., *et al.* (2004) Export of dissolved organic carbon from peatlands under elevated carbon dioxide levels. *Nature* **430**, 195–198.

Freese, B. (2003) *Coal, a Human History*. 336 pp. Heinemann, London.

Frey, P. & Church, M. (2009) How river beds move. *Science* **325**, 1509–1510.

Friberg, L., Poelchau, H.S., Kroos, B. & Littke, R. (2000) 3D-modelling of thermal history and simulation of methane and nitrogen migration along the Northeast German seismic Dekorp profile 9601. *J. Geochem. Explor.* **69–70**, 263–267.

Friend, T. (2007) *The Third Domain: The Untold Story of Archaea and the Future of Biotechnology*. 250 pp. Joseph Henry Press.

Frietsch, R., Tuisku, P., Martinsson, O. & Perdahl, J.-A. (1997) Early Proterozoic Cu-(Au) and Fe ore deposits associated with regional Na-Cl metasomatism in northern Fennoscandia. *Ore Geol. Rev.* **12**, 1–34.

Frimmel, H.E. & Gartz, V.H. (1997) Witwatersrand gold particle chemistry matches model of metamorphosed, hydrothermally altered placer deposits. *Miner. Deposita* **32**, 523–530.

Frisch, W. & Gawlick, H.-J. (2003) The nappe structure of the central Northern Calcareous Alps and ist disintegration during Miocene tectonic extrusion – a contribution to understanding the orogenic evolution of the Eastern Alps. *Int. J. Earth Sci.* **92**, 712–727.

Frost, B.R., Mavrogenes, J.A. & Tomkins, A.G. (2002) Partial melting of sulfide ore deposits during medium and high-grade metamorphism. *Canadian Mineralogist* **40**, 1–18.

Frost, B.R. (1979) Mineral equilibria involving mixed-volatiles in a C-O-H fluid phase; the stabilities of graphite and siderite. *American J. Sci.* **279**, 1033–1059.

Frost, D.J. & Wood, B. (1997) Experimental measurements of the fugacity of CO_2 and graphite/diamond stability from 36–77 kbar at 925 to 1650 °C. *Geochim. Cosmochim. Acta* **61**, 1565–1574.

Fubao Zhou, Wanxing Ren, Deming Wang, Tiliang Song, Xiang Li & Yuliang Zhang (2006) Application of three-phase foam to fight an extraordinarily serious coal mine fire. *Int. J. Coal Geol.* **67**, 95–100.

Fuenkajorn, F. & Daemen, J.J.K. (eds) (1996) *Sealing of Boreholes and Underground Excavations in Rock*. 329 pp. Chapman & Hall.

Fuenkajorn, F. & Daemen, J.J.K. (1997) Mine sealing: design guidelines and considerations. In: *Tailings and Mine Waste '97*. pp 59–68. Balkema.

Fullagar, P.K. (2000) The expanding role of mine geophysics. *In*: *Fourth International Mining Geology Conference 2000*. pp. 301–313. AusIMM, Carlton, Victoria.

Furnes, H., de Wit, M., Staudigel, H., Rosing, M. & Muehlenbachs, K. (2007) A vestige of Earth's oldest ophiolite. *Science* **315**, 1704–1707.

Fyfe, W.S., Price, N.J. & Thompson, A.B. (1978) *Fluids in the Earth's Crust*. 383 pp. Elsevier.

Gaal, G. (1990) Tectonic styles of early Proterozoic ore deposition in the Fennoscandian Shield. *Precambrian Res.* **46**, 83–114.

Gabet, E.J., Edelman, R. & Langner, H. (2006) Hydrological controls on chemical weathering rates at the soil-bedrock interface. *Geology* **34**, 1065–1068.

Gaboury, D. (2006) Geochemical approaches in the discrimination of synvolcanic intrusions as a guide for volcanogenic base metal exploration: an example from the Abitibi belt, Canada. *Applied Earth Sci.* **115**, 71–79.

Gabriel, G. & Rappsilber, I. (1999) Der Salzstock Arendsee bei Salzwedel – ein gravimetrischer Beitrag zur Klärung geologischer Fragestellungen. *Mitt. Geol. Sachsen-Anhalt* **5**, 5–17.

Gadallah, M.R. & Fisher, R.L. (2009) *Exploration Geophysics*. 262 pp. Springer.

Galan, E. & Caliani, J.C.F. (1997) Industrial properties and potential uses of some wollastonites from SW Spain. *Schriftenr. angew. Geowiss.* **1**, 35–39.

Galan, E. (1996) Properties and applications of palygorskite-sepiolite clays. *Clay Mineral.* **31**, 443–453.

Galeotti, S., von der Heydt, A., Huber, M., *et al.* (2010) Evidence for active El Niño Southern Oscillation variability in the Late Miocene greenhouse climate. *Geology* **38**, 419–422.

Gallup, D.L. (1998) Geochemistry of geothermal fluids and well scales, and potential for mineral recovery. *Ore Geology Rev.* **12**, 225–236.

Gandy, C.J. & Younger, P.L. (2007) Predicting groundwater rebound in the South Yorkshire coalfield, UK. *Mine Water Environ* **26**, 70–78.

Garcia-Veigas, J., Orti, F., Rosell, L. *et al.* (1995) The Messinian salt of the Mediterranean: geochemical study of the salt from the Central Sicily basin and comparison with the Lorca basin (Spain). *Bull. Soc. géol. France* **166**, 699–710.

Garfunkel, Z. & Ben-Avraham, Z. (1996) The structure of the Dead Sea. *Tectonophysics* **77**, 155–176.

Gargett, A., Wells, J., Tejada-Martinez, A.E. & Grosch, C.E. (2004) Langmuir supercells: a mechanism for sediment resuspension and transport in shallow seas. *Science* **306**, 1925–1928.

Garrels, R.M. & Christ, C.L. (1965) *Solutions, Minerals and Equilibria*. 450 pp. Harper & Row.

Garrels, R.M., Lerman, A. & Mackenzie, F.T. (1976) Controls of atmospheric O_2 and CO_2: past, present and future. *American Scientist* **64**, 306–315.

Garret, D.E. (1998) *Borates. Handbook of Deposits, Processing, Properties, and Uses*. 483 pp. Academic Press.

Garrett, D.E. (2004) *Handbook of Lithium and Calcium Chloride*. 488 pp. Academic Press.

Garuti, G., Pushkarev, E.V., Zaccarini, F., *et al.* (2003) Chromite composition and platinum-group mineral assemblage in the Uktus Uralian-Alaskan-type compex (Central Urals, Russia). *Miner. Deposita* **38**, 312–326.

Gass, I.G. (1980) The Troodos Massif: Its role in unravelling of the ophiolite problem and its significance in the understanding of constructive plate margin processes. In; Ophiolites (ed. A Panatiotou), pp 23–35. Geol. Survey Department, Cyprus.

Gautier, D.L., Bird, K.J., Charpentier, R.R., *et al.* (2009) Assessment of undiscovered oil and gas in the Arctic. *Science* **324**, 1175–1179.

Gayer, R. & Harris, I. (eds) (1996) Coalbed methane and coal geology. 344 pp, *Geol. Soc. London Spec. Publ. 109*.

Gayer, R. & Pesek, J. (eds) (1997) European coal geology and technology. *Geol. Soc. London Spec. Publ. 125*, 448 pp.

Gayer, R., Garven, G. & Rickard, D. (1998) Fluid migration and coal-rank development in foreland basins. *Geology* **26**, 679–682.

Gebre-Mariam, M., Hagemann, S.G. & Groves, D.I. (1995) A classification scheme for epigenetic Archean lode-gold deposits. *Miner. Deposita* **30**, 408–410.

Gemmell, J.B., Sharpe, R., Jonasson, I.R. & Herzig, P.M. (2004) Sulfur isotope evidence for magmatic contributions to submarine and subaerial gold mineralization: Conical Seamount and the Ladolam gold deposit, Papua New Guinea. *Economic Geol.* **99**, 1711–1725.

George, R.L. (1998) Mining for oil. *Sci. American* **278**, 66–67.

Gerdes, M.L. & Valley, J.W. (1994) Fluid flow and mass transport at the Valentine wollastonite deposit, Adirondack Mountains, New York State. *J. Metamorphic Geol.* **12**, 589–608.

Gerling, P., Idiz, E., Everlien, G. & Sohns, E. (1997) New aspects on the origin of nitrogen in natural gas in Northern Germany. *Geol. Jb. D* **103**, 65–84.

Germann, A., Lang, R., Werner, W. & Friedrich, G. (1994) Zur Mineralogie und Geochemie der Erzgänge im Bergbaurevier Freiamt-Sexau (Mittlerer Schwarzwald). *Abh. Geol. LA Baden-Württemberg* **14**, 119–154.

Gerst, M.D. (2008) Revisiting the cumulative grade-tonnage relationship for major copper ore types. *Economic Geol.* **103**, 615–628.

Gibb, F.G.F. & Attrill, P.G. (2003) Granite recrystallization: the key to the nuclear waste problem? *Geology* **31**, 657–660.

Gibbons, W. (2000) Amphibole asbestos in Africa and Australia; geology, health hazard and mining legacy. *J. Geol. Soc. London*, **157**, 851–858.

Gibowicz, S.J. & Kijko, A. (1994) *An Introduction to Mining Seismology*. 399 pp. Academic Press.

Gibson, R.I. & Millegan, P.S. (eds) (1998) *Geologic Applications of Gravity and Magnetics: Case Histories*. 162 pp. AAPG & SEG.

Giggenbach, W.F. (1995) Variations in the chemical and isotopic composition of fluids discharged from the Taupo Volcanic Zone, New Zealand. *J. Volcanology Geothermal Res.* **68**, 89–115.

Giles, A.D. & Marshall, B. (1994) Fluid inclusion studies on a multiply deformed, metamorphosed volcanic-associated massive sulfide deposit, Joma Mine, Norway. *Economic Geol.* **89**, 803–819.

Gilfillan, J.F. & Levy, I.W. (2001) Monitoring the reserve. Pp 537–544 in A.C. Edwards (Ed.), *Mineral Resource and Ore Reserve Estimation – the AusIMM Guide to Good Practice.* 719 pp. AusIMM, Melbourne.

Gilg, H.A. & Sheppard, S.M.F. (1996) Hydrogen isotope fractionation between kaolinite and water revisited. *Geochim. Cosmochim. Acta* **60**, 529–533.

Gilpin, A. (2000) *Environmental Economics: A Critical Overview*. 334 pp. Wiley.

Giuliani, G., Bourles, D., Massot, J. & Siame, L. (1999) Colombian emerald reserves inferred from leached beryllium of their host black shale. *Explor. & Mining Geol.* **8**, 109–116.

Givens, W.W. & Stromswold, D.C. (1989) Prompt fission neutron logging for uranium. *Nucl. Geophysics* **3**, 299–307.

Glasson, K.R. & Rattigan, J.H. (eds) (1990) Geological aspects of the discovery of some important mineral deposits in Australia. 503 pp, *Monograph 17*. AusIMM, Melbourne.

Glasspool, I.J. (2003) Hypautochthonous-allochthonous coal deposition in the Permian, South African, Witbank Basin no. 2 seam; a combined approach using sedimentology, coal petrology and palaeontology. *Int. J. Coal Geol.* **53**, 81–135.

Gleeson, S.A., Butt, C.R.M. & Elias, M. (2003) Nickel laterites: a review. *Soc. Econ. Geol. Newsletter* **54**(1), 12–17.

Glenn, C.R., Föllmi, K.B., Riggs, S.R. *et al.* (1994) Phosphorus and phosphorites: sedimentology and environments of formation. *Eclogae geol. Helv.* **87**, 747–788.

Glennie, K.W. (ed.) (1998) *Petroleum Geology of the North Sea*. 4th edn. 656 pp. Blackwell.

Gnandi, K., Tchangbedji, G., Killi, K., Baba, G. & Ouro Salim, A.I. (2005) Processing of phosphate mine tailings by coagulation flocculation to reduce marine pollution in Togo: laboratory tests. *Mine Water Environ* **24**, 215–221.

Goes, S., Spakman, W. & Bijwaard, H. (1999) A lower mantle source for Central European volcanism. *Science* **286**, 1928–1931.

Goetz, D., Roussel, V. & Tincelin, E. (1994) Cave-ins linked to mine flooding. *5th Intern. Mine Water Congress Nottingham*, 29–42.

Gokce, A. & Spiro, B. (1994) Stable isotope study of antimony deposits in the Muratdagi region, western Turkey. *Miner. Deposita* **29**, 361–365.

Goldfarb, R.J. (2002) Lode gold deposits through earth history – patterns in space and time. *Trans. Instn. Min. Metall. B* **111**, 141–142.

Goldfarb, R.J., Bradley, D. & Leach, D.L. (2010) Secular variation in economic geology. *Economic Geol.* **105**, 459–465.

Goldfarb, R.J., Baker, T., Dube, B., Groves, D.I., Hart, C.J.R. & Gosselin, P. (2005) Distribution, character and genesis of gold deposits in metamorphic terranes. *Economic Geol.* **100th Anniv. Vol.** 407–450.

Goldhaber, M.B., Church, S.E., Doe, B.R., *et al.* (1995) Lead and sulfur isotope investigation of Paleozoic sedimentary rocks from the southern midcontinent of the Unites States: implications for paleohydrology and ore genesis of the southeast Missouri lead belts. *Economic Geol.* **90**, 1875–1910.

Goldschmidt, V.M. (1958) *Geochemistry*. 730 pp. Oxford University Press (reprint).

Golytsin, A., Courel, L. & Debriette, P. (1997) A fault-related coalification anomaly in the Blanzy-Montceau coal basin (Massif Central, France). *Intern. J. Coal Geol.* **33**, 209–228.

Goodwin, A.M. (1973) Archaean iron formations and tectonic basins of the Canadian Shield. *Economic Geol.* **68**, 915–933.

Goncharenko, O.P. (2006) Potassic salts in Phanerozoic evaporite basins and specific features of salt deposition at the final stage of halogenesis. *Lithol. Mineral Res.* **41**, 378–388.

Gonzaga, M.I.S., Ma L.Q. & Santos, J.A.G. (2007) Effects of plant age on arsenic hyperaccumulation by *Pteris vittata* L. *Water, Air & Soil Pollution* **186**, 289–295.

González-Sánchez, F., Camprubí, A., González-Partida, E., *et al.* (2009) Regional stratigraphy and distribution of epigenetic stratabound celestine, fluorite, barite and Pb–Zn deposits in the MVT province of northeastern Mexico. *Miner. Deposita* **44**, 343–361.

Gorbachev, B.F., Sharapov, A.F., Lyaditskii, P.V. & Shmel'Kov, N.T. (2004) The south Ushkoty kaolin deposit in the southeastern Orenburg region. *Lithol. Mineral Res.* **39**, 412–424.

Gorbachev, B.F., Vasyanov, G.P., Kakorin, V.I. & Luzin, V.P. (2007) Kaolins and sericites of the Plast kaolin-bearing region, Chelyabinsk district, Russia. *Lithol. Mineral Res.* **42**, 168–179.

Gorelick, St M. (2010) *Oil Panic and the Global Crisis – Predictions and Myths*. 255 pp. Wiley-Blackwell.

Gracia, A., Meggiolaro, V., Baker, J. & Bitzios, D. (1999) Development of exploration and industrial technology to exploit new sources of wollastonite in Europe. *Trans. Instn. Min. Metall. B* **108**, 183–190.

Grajales-Nishimura, J.M., Cedillo-Pardo, E., Rosales-Domínguez, C., *et al.* (2000) Chicxulub impact: The origin of reservoir and seal facies in the southeastern Mexico oil fields. *Geology* **28**, 307–310.

Grammatikopoulos, T.A. & Clark, A.H. (2006) A comparative study of wollastonite skarn genesis in the Central Metasedimentary Belt, southeastern Ontario, Canada. *Ore Geol. Rev.* **29**, 146–161.

Grauls, D. & Cassignol, C. (1992) Fluid pressure-induced open fracture anomaly - characterization from well data and seismic velocities: mechanisms and major implications. *Bull. Centres Rech. Explor.-Prod. elf aquitaine* **16**, 275–284.

Graybeal, F.T., Smith, D.M. & Vikre, P.G. (1986) The geology of silver deposits. In: *Handbook of Strata-bound and Stratiform Ore Deposits*, Vol. 14 (ed. K. H. Wolff), pp. 1–184. Amsterdam.

Greb, S.F. & DiMichele, W.A. (eds) (2006) Wetlands through time. *Geol. Soc. America Spec. Paper 399*, 304 pp.

Gregory, M.J., Schaefer, B.F., Keays, R.R. & Wilde, A.R. (2008) Rhenium-osmium systematics of the Mt. Isa copper orebody and the Eastern Creek Volcanics, Queensland, Australia: implications for ore genesis. *Miner. Deposita* **43**, 553–573.

Greiling, R.O., Sabelfeld, A., Einarsson, Ö. & Sundqvist, E. (2005) Swedish feldspar. *Industrial Minerals* **454**, 49–51.

Grenne, T. & Slack, J.F. (2005) Geochemistry of jasper beds from the Ordovician Loekken ophiolite, Norway: origin of proximal and distal siliceous exhalites. *Economic Geol.* **100**, 1511–1527.

Grenne, T., Ihlen, P.M. & Vokes, F.M. (1999) Scandinavian Caledonide metallogeny in a plate tectonic perspective. *Miner. Deposita* **34**, 422–471.

Grew, E.S. (ed.) (2003) Beryllium: mineralogy, petrology, and geochemistry. *Rev. Mineral. Geochem.* **50**, 691.

Griffin, W.L. & Ryan, C.G. (1995) Trace elements in indicator minerals: area selection and target evaluation in diamond exploration. *J. Geochem. Explor.* **53**, 311–337.

Griffin, W.L., O'Reilley, S.Y. & Davies, R.M. (2002) Subduction-related diamond deposits? Constraints, possibilities, and new data from Eastern Australia. In: *Metamorphosed and Metamorphogenic Ore Deposits* (eds P.G. Spry, B. Marshall & F.M. Vokes), *Rev. Economic Geol.* **11**, 291–310.

Grimaldi, D. (2009) Pushing back amber production. *Science* **326**, 51–52.

Grishina, S., Dubessy, J., Kontorovich, A. & Pironon, J. (1992) Inclusions in salt beds resulting from thermal metamorphism by dolerite sills (eastern Siberia, Russia). *European J. Mineral.* **4**, 1187–1202.

Gromet, L.P., Dymek, R.F., Haskin, L.A. & Korotev, R.L. (1984) The "North American Shale Composite": its compilation, major and trace element characteristics. *Geochim. Cosmochim. Acta* **48**, 2469–2482.

Groves, D.I. (1993) The crustal continuum model for late Archean lode gold deposits of the Yilgarn Block, Western Australia. *Miner. Deposita* **28**, 366–374.

Groves, D.I. & Vielreicher, N.M. (2001) The Phalaborwa (Palabora) carbonatite-hosted magnetite-copper sulfide deposit, South Africa: an end member of the iron-oxide copper-gold-rare earth element deposit group? *Miner. Deposita* **36**, 189–194.

Groves, D.I., Bierlein, F.P., Meinert, L.D. & Hitzman, M. W. (2010) Iron oxide copper-gold (IOCG) deposits through earth history: implications for origin, lithospheric setting, and distinction from other epigenetic iron oxide deposits. *Economic Geol.* **105**, 641–654.

Groves, D.I., Goldfarb, R.J., Robert, F. & Hart, C.J.R. (2003) Gold deposits in metamorphic belts: overview of current understanding, outstanding problems, future research, and exploration significance. *Economic Geol.* **98**, 1–29.

Groves, D.I., Korkiakoski, E.A., McNaughton, N.J., Lesher, C. M. & Cowden, A. (1986) Thermal erosion by komatiites at Kambalda, Western Australia and the genesis of nickel ores. *Nature* **319**, 136–139.

Groves, I.M., Groves, D.I., Bierlein, F.P., Broome, J. & Penhall, J. (2008) Recognition of the hydrothermal feeder to the structurally inverted, giant broken Hill deposit, New South Wales, Australia. *Economic Geol.* **103**, 1389–1394.

Gruber, W. & Sachsenhofer, R.F. (2001) Coal deposition in the Noric depression (Eastern Alps): raised and low-lying mires in Miocene pull-apart basins. *Int. J. Coal Geol.* **48**, 89–114.

Guan, P., Wang, H., & Zhang, Y. (2009) Mechanism of instantaneous coal outbursts. *Geology* **37**, 915–918.

Guibal, D. (2001) Variography, a tool for the resource geologist. In: *Mineral Resource and Ore Reserve Estimation – the AusIMM Guide to Good Practice* (ed. A. C. Edwards), pp 85–90. AusIMM, Melbourne.

Guilbert, J.M. & Park, C.F. Jr., (1986) *The Geology of Ore Deposits*. 985 pp. Freeman.

Guliy, V.N. (1995) Main features of composition and origin of apatite deposits in metamorphic rocks of the Aldan Shield, Siberia, Russian Federation. *Trans. Instn. Min. Metall.* **104**, 171–178.

Gümbel, C.W. von (1883) Beiträge zur Kenntnis der Texturverhältnisse der Mineralkohlen. Sitz.-Ber. K. bayer. Akad. *Wiss. München* 111–211.

Guo, Qingjun, Strauss, H., Kaufman, A.J., *et al.* (2009) Reconstructing Earth's surface oxidation across the Archean-Proterozoic transition. *Geology* **37**, 399–402.

Guo, L., Andrews, J., Riding, R., Dennis, P. & Dresser, Q. (1996) Possible microbial effects on stable carbon isotopes in hot-spring travertines. *J. Sed. Res.* **66**, 468–473.

Guo, Y. & Bustin, R.M. (1998) FTIR spectroscopy and reflectance of modern charcoals and fungal decayed woods: implications for studies of inertinite in coals. *Int. J. Coal Geol.* **37**, 29–53.

Gurney, J.J., Helmstaedt, H.H., Richardson, S.H. & Shirey, S.B. (2010) Diamonds through time. *Economic Geol.* **105**, 689–712.

Gutzmer, J., Beukes, N.J., Bhalmi, M. & Mukhopadhyay, J. (2006) Cretaceous karstic cave-fill manganese-lead-barium deposits of Imini, Moroccco. *Economic Geol.* **101**, 385–405.

Gutzmer, J. & Beukes, N.J. (1995) Fault-controlled metasomatic alteration of early Proterozoic sedimentary manganese ores in the Kalahari manganese field, South Africa. *Economic Geol.* **90**, 823–844.

Gy, P.M. (1992) *Sampling of Heterogeneous and Dynamic Material Systems – Theories of Heterogeneity, Sampling and Homogenizing*. 653 pp, Elsevier.

Haack, U.K. & Zimmermann, H.D. (1996) Retrograde mineral reactions: a heat source in the continental crust? *Geol. Rundschau* **85**, 130–137.

Haacke, R.R., Hyndman, R.D., Park, K.P., Yoo, D.-G., Stoian, I. & Schmidt, U. (2009) Migration and venting of deep gases into the ocean through hydrate-choked chimneys offshore Korea. *Geology* **37**, 531–534.

Haas, J.L. (1971) The effect of salinity on the maximum thermal gradient of a hydrothermal system at hydrostatic pressure. *Economic Geol.* **66**, 940–946.

Haeberlin, Y., Moritz, R. & Fontboté, L. (2003) Paleozoic orogenic gold deposits in the eastern Central Andes and its foreland, South America. *Ore Geol. Rev.* **22**, 41–59.

Haest, M., Muchez, P., Dewaele, S., Franey, N. & Tyler, R. (2007) Structural control on the Dinkulushi Cu-Ag deposit, Katanga, Democratic Republic of Congo. *Economic Geol.* **102**, 1321–1333.

Haeussler, P.J., Bradley, D., Goldfarb, R., *et al.* (1995) Link between ridge subduction and gold mineralization in southern Alaska. *Geology* **23**, 995–998.

Hagemann, S.G. & Lüders, V. (2003) P-T-X conditions of hydrothermal fluids and precipitation mechanism of stibnite-gold mineralization at the Wiluna lode-gold deposits, Western Australia: conventional and infrared microthermometric constraints. *Miner. Deposita* **38**, 936–952.

Haggerty, S.E. (1999) A diamond trilogy: superplumes, supercontinents, and supernovae. *Science* **285**, 851–860.

Hailong Lu, Yu-taek Seo, Jong-won Lee, *et al.* (2007) Complex gas hydrate from the Cascadia margin. *Nature* **445**, 303–306.

Halbach, P.E., Fouquet, Y. & Herzig, P. (2003) Mineralization and compositional patterns in deep-sea hydrothermal systems. In: *Energy and Mass Transfer in Marine Hydrothermal Systems* (eds P.E. Halbach, V. Tunnicliffe & J.R. Hein), pp 85–122. *Dahlem Workshop Report 89.*

Hale, M. (ed.) (2000) *Geochemical Remote Sensing of yhe Subsurface*. 572 pp. Elsevier.

Hall, A. (ed.) (1996) Zeolite deposits. *Miner. Deposita* **31**, 451–596.

Hall, A. (1998) Zeolitisation of volcaniclastic sediments: the role of temperature and pH. *J. Sed. Res.* **68**, 739–745.

Hall, C.M., Higueras, P.L., Kesler, S.E., *et al.* (1997) Dating of alteration episodes related to mercury mineralization in the Almaden district, Spain. *Earth Planet. Sci. Lett.* **148**, 287–298.

Halls, C. & Zhao, R. (1995) Listvenite and related rocks: perspectives on terminology and mineralogy with reference to an occurrence at Cregganbaun, Co. Mayo, Republic of Ireland. *Miner. Deposita* **30**, 303–313.

Halter, W.E., Heinrich, C.A. & Pettke, T. (2005) Magma evolution and the formation of porphyry Cu-Au ore fluids: evidence from silicate and sulfide melt inclusions. *Miner. Deposita* **39**, 845–863.

Halter, W.E., Pettke, T. & Heinrich, C.A. (2002) The origin of Cu/Au ratios in porphyry-type ore deposits. *Science* **296**, 1844–1846.

Halter, W.E., Williams-Jones, A.E. & Kontak, D.J. (1996) The role of greisenization in cassiterite precipitation at the East Kemptville tin deposit, Nova Scotia. *Economic Geol.* **91**, 368–385.

Hamade, T., Konhauser, K.O., Raiswell, R., *et al.* (2003) Using Ge/Si ratios to decouple iron and silica fluxes in Precambrian banded iron formations. *Geology* **31**, 35–38.

Hamilton, S.J. & Buhl, K.J. (2004) Selenium in water, sediment, plants, invertebrates, and fish in the Blackfoot River drainage. *Water, Air & Soil Pollution* **159**, 3–34.

Hamilton, W.B. (1995) Subduction systems and magmatism. Pp 3–28 in J.L. Smellie (Ed.), Volcanism associated with extension at consuming plate margins. *Geol. Soc. London Spec. Pub. 81*.

Hammer, B. & Norskov, J.K. (1995) Why gold is the noblest of all the metals. *Nature* **376**, 238–240.

Hammerbeck, E.C.I. (1986) Andalusite in the metamorphic aureole of the Bushveld Complex. In: *Mineral Deposits of Southern Africa*. Vol.II (eds C.R. Anhaeusser, & S. Maske), pp. 993–1001. Geol.Soc.S.Africa, Johannesburg.

Hampson, G., Stollhoden, H. & Flint, S. (1999) A sequence stratigraphic model for the Lower Coal Measures (Upper Carboniferous) of the Ruhr District, north-west Germany. *Sedimentology* **46**, 1199–1231.

Hanchar, J.M. & Hoskin, P.W.O. (eds) (2003) Zircon. *Rev. Mineral. Geochem.* **53**, 500.

Haney, M.M., Snieder, R., Sheiman, J. & Losh, S. (2005) A moving fluid pulse in a fault zone. *Nature* **437**, 46.

Hannah, J.L., Stein, H.J., Wieser, M.E., de Laeter, J.R. and Varner, M.D. (2007) Molybdenum isotope variations in molybdenite: Vapor transport and Rayleigh fractionation of Mo. *Geology* **35**, 703–706.

Hannington, M.D. (1997) The porphyry-epithermal-VMS transition: lessons from the Iskut River area, British Columbia, and modern island arcs. *Soc. Econ. Geol. Newsletter* **29**, 12–13.

Hanson, R.B. (1997) Hydrodynamics of regional metamorphism due to continental collision. *Economic Geol.* **92**, 880–891.

Hardardóttir, V., Brown, K.L., Fridriksson, Th., Hedenquist, J.W., Hannington, M.D. & Thorhallsson, S. (2009) Metals in deep liquid of the Reykjanes geothermal system, southwest Iceland: Implications for the composition of seafloor black smoker fluids. *Geology* **37**, 1103–1106.

Hardie, L.A. (1996) Secular variation in seawater chemistry: An explanation for the coupled secular variations in the mineralogies of marine limestones and potash evaporites over the past 600 m.y. *Geology* **24**, 279–283.

Hardie, L.A. (1991) On the significance of evaporites. *Ann. Rev. Earth Planet. Sci.* **19**, 131–168.

Hardie, L.A. (1990) The roles of rifting and hydrothermal $CaCl_2$ brines in the origin of potash evaporites: an hypothesis. *American J. Sci.* **290**, 193–240.

Hargraves, A.J. (1997) International overview of seam gas emissions and instantaneous outbursts. *AusIMM Proceedings* **302**, 43–60.

Haridon, S.L., Reysenbach, A.-L., Glenat, P., *et al.* (1995) Hot subterranean biosphere in a continental oil reservoir. *Nature* **377**, 223–224.

Harlov, D.E., Andersson, U.B., Förster, H.-J., Nyström, J. O., Dulski, P. & Broman, C. (2002) Apatite–monazite relations in the Kiirunavaara magnetite-apatite ore, northern Sweden. *Chemical Geol.* **191**, 47–72.

Harper, D.D. & Borrok, D.M. (2007) Dolomite fronts and associated zinc-lead mineralization, USA. *Economic Geol.* **102**, 1345–1352.

Harris, A.C., Kamenetsky, V.S., White, N.C., *et al.* (2003) Melt inclusions in veins: linking magmas and porphyry Cu deposits. *Science* **302**, 2109–2111.

Harris, C., Compton, J.S. & Bevington, S.A. (1999) Oxygen and hydrogen isotope composition of kaolinite deposits, Cape Peninsula, South Africa: low-temperature, meteoric origin. *Economic Geol.* **94**, 1353–1366.

Hart, T.R., Gibson, H.L. & Lesher, C.M. (2004) Trace element geochemistry and petrogenesis of felsic volcanic rocks associated with volcanogenic massive Cu-Zn-Pb sulfide deposits. *Economic Geol.* **99**, 1003–1013.

Hartwig, T., Owor, M., Muwanga, A., Zachmann, D. & Pohl, W. (2005) Lake George as a sink for contaminants derived from Kilembe copper mining area, western Uganda. *Mine Water Environ* **24**(3), 114–123.

Harvie, C.E., Møller, N. and Weare, J.H. (1984) The prediction of mineral solubilities in natural waters - The $Na\text{-}K\text{-}Mg\text{-}Ca\text{-}H\text{-}Cl\text{-}SO_4\text{-}OH\text{-}HCO_3\text{-}CO_3\text{-}CO_2\text{-}H_2O$ system to high ionic strengths at 25 °C. *Geochim. Cosmochim. Acta* **48**, 723–751.

Haszeldine, R.S. (2009) Carbon capture and storage: How green can black be? *Science* **325**, 1647–1652.

Hatcher, M.I. & Clynick, G. (1990) Greenbushes tin-tantalum-lithium deposit. Pp 599–603 in F.E. Hughes (Ed.), *Geology of Mineral Deposits of Australia and Papua New Guinea*. AusIMM, Melbourne.

Hatcher, P.G. & Clifford, D.J. (1997) The organic geochemistry of coal: from plant materials to coal. *Organic Geochem.* **27**, 251–274.

Hattingh, J. & Rust, I.C. (1993) Flood transport and deposition of tracer heavy minerals in a gravel-bed meander bend channel. *J. Sediment. Petrology* **63**, 828–834.

Hattori, K.H. & Keith, J.D. (2001) Contribution of mafic melt to porphyry copper mineralization: evidence from Mt Pinatubo, Phillippines, and Bingham Canyon, Utah, USA. *Miner. Deposita* **36**, 799–806.

Hawkesworth, C., Cawood, P., Kemp, T., Storey, C. & Dhuime, B. (2009) A matter of preservation. *Science* **323**, 49–50.

Haymon, R.M. (1983) Growth history of hydrothermal black smoker chimneys. *Nature* **301**, 695–698.

Hayward, C.L., Reinmold, W.U., Robb, L.J. & Gibson, R. L. (2003) The Witwatersrand gold deposit, South Africa: an impact-modified metamorphosed placer. *Applied Earth Sci.* **112**, B147–149.

Head, I.M., Jones, D.M. & Larter, S.R. (2003) Biological activity in the deep subsurface and the origin of heavy oil. *Nature* **426**, 344–352.

Heaney, P.J. & Davis, A.M. (1995) Observation and origin of self-organized textures in agates. *Science* **269**, 1562–1565.

Heaney, P.J. (1995) Moganite as an indicator for vanished evaporites: a testament reborn? *J. Sediment. Research* **A65**, 633–638.

Hébert, R. & Bédard, J.H. (2000) Les ophiolites d'avant-arc et leur potentiel minéral: exemple des complexes ophiolitiques du sud du Québec. *Chron. Recherche Minière* **539**, 101–117.

Hecht, L. & Cuney, M. (2000) Hydrothermal alteration of monazite in the Precambrian crystalline basement of the Athabasca Basin (Saskatchewan, Canada):

implications for the formation of unconformity-related uranium deposits. *Miner. Deposita* **35**, 791–795.

Hecht, L., Freiberger, R., Gilg, H.A., Grundmann, G. & Kostitsyn, Y.A. (1999) Rare earth element and isotope (C, O, Sr) characteristics of hydrothermal carbonates: genetic implications for dolomite hosted talc mineralization at Göpfersgrün (Fichtelgebirge, Germany). *Chemical Geol.* **155**, 115–130.

Heckel, P.H. (1986) Sea level curve for Pennsylvanian eustatic-marine transgressive-regressive depositional cycles along mid-continent outcrop belt, North America. *Geology* **14**, 330–334.

Hedenquist, J.W., Thompson, J.F.H., Goldfarb, R.J. & Richards, J.P. (eds) (2005) *Economic Geology 100th Anniversary Volume*. 1146 pp, Society of Economic Geologists, Littleton.

Hedenquist, J.W., Simmons, S.F., Giggenbach, W.F. & Eldridge, C.S. (1993) White Island, New Zealand, volcanic-hydrothermal system represents the geochemical environment of high-sulfidation Cu and Au ore deposition. *Geology* **21**, 731–734.

Heffern, E.L. & Coates, D.A. (2004) Geological history of natural coal-bed fires, Powder River basin, USA. *Int. J. Coal Geol.* **59**, 25–47.

Heijlen, W., Banks, D.A., Muchez, P., Stensgard, B.M. & Yardley, B.W.D. (2008) The nature of mineralising fluids of the Kipushi Zn-Cu deposit, Katanga, DR Congo. *Economic Geol.* **103**, 1459–1482.

Heijlen, W., Muchez, P., Banks, D.A., *et al.* (2003) Carbonate-hosted Zn-Pb deposits in Upper Silesia, Poland: origin and evolution of mineralizing fluids and constraints on genetic models. *Economic Geol.* **98**, 911–932.

Heiken, G. (ed.) (2006) Tuffs – their properties, uses, hydrology, and resources. *Geol. Soc. America Spec. Paper 408*, 131 pp.

Heikoop, J.M., Tsujita, C.J., Risk, M.J. *et al.* (1996) Modern iron ooids from a shallow-marine volcanic setting: Mahengetang, Indonesia. *Geology* **24**, 759–762.

Heiligmann, M., Williams-Jones, A.E. & Clark, J.R. (2008) The role of sulfate-sulfide-oxide-silicate equilibria in the metamorphism of hydrothermal alteration at the Hemlo gold deposit, Ontario. *Economic Geol.* **103**, 335–351.

Hein, J.R. (ed.) (2004) *Life Cycle of the Phosphoria Formation – From Deposition to the Post-Mining Envrionment*. 635 pp, Elsevier.

Hein, J.R., Normark, W.R., McIntyre, B.R., Lorenson, T. D. & Powell II, C.L. (2006) Methanogenic calcite, ^{13}C-depleted bivalve shells, and gas hydrate from a mud volcano offshore Southern California. *Geology* **34**, 109–112.

Hein, J.R., Koschinsky, A., & McIntyre, B.B. (2005) Mercury and silver-rich ferromanganese oxides, southern California Borderland: deposit model and envionmental implications. *Economic Geol.* **100**, 1151–1167.

Heinrich, C.A. (2005) The physical and chemical evolution of low-salinity magmatic fluids at the porphyry to epithermal transition: a thermodynamic study. *Miner. Deposita* **39**, 864–889.

Heinrich, C.A. (1990) The chemistry of hydrothermal tin (-tungsten) ore deposition. *Economic Geol.* **85**, 457–481.

Heinrich, C.A., Driesner, T., Stefansson, A. & Seward, T. M. (2004) Magmatic vapor contraction and the transport of gold from the porphyry environment to epithermal ore deposits. *Geology* **32**, 761–764.

Heinrich, C.A. & Neubauer, F. (2002) Cu-Au-Pb-Zn-Ag metallogeny of the Alpine-Balkan-Carpathian-Dinaride geodynamic province. *Miner. Deposita* **37**, 533–540.

Heinrich, C.A., Andrew, A.S. & Knill, M.D. (2000) Regional metamorphism and ore formation: evidence from stable isotopes and other fluid tracers. Pp 97–117 in Spry et al. (Eds.).

Heinrich, C.A., Günther, D., Audétat, *et al.* (1999) Metal fractionation between magmatic brine and vapor, determined by microanalysis of fluid inclusions. *Geology* **27**, 755–758.

Heinrich, C.A., Ryan, Ch.G., Mernagh, P.T. & Eadington, P.J. (1992) Segregation of ore metals between magmatic brine and vapor: a fluid inclusion study using PIXE microanalysis. *Economic Geol.* **87**, 1566–1583.

Heinson, G.S., Direen, N.G., Gill, R.M. (2006) Magnetotelluric evidence for a deep-crustal mineralizing system beneath the Olympic Dam iron oxide copper-gold deposit, southern Australia. *Geology* **34**, 573–576.

Helba, H., Trumbull, R.B., Morteani, G., *et al.* (1997) Geochemical and petrographic studies of Ta mineralization in the Nuweibi albite granite complex, Eastern Desert, Egypt. *Miner. Deposita* **32**, 164–179.

Helgeson, H.C., Richard, L., McKenzie, W.F., Norton, D. L. & Schmitt, A. (2009) A chemical and thermodynamic model of oil generation in hydrocarbon source rocks. *Geochim. Cosmochim. Acta* **73**, 594–695.

Helliker, B.R. & Richter, S.B. (2008) Subtropical to boreal convergence of tree-leaf temperatures. *Nature* **453**, 956–958.

Helvaci, C. & Orti, F. (2004) Zoning in the Kirka deposit, western Turkey: Primary evaporitic fractionation or diagenetic modifications? *Canadian Mineralogist* **42**, 1179–1204.

Helvaci, C. & Orti, F. (1998) Sedimentology and diagenesis of Miocene colemanite-ulexite deposits (Western Anatolia, Turkey). *J. Sed. Res.* **68**, 1021–1033.

Helvaci, C. (1995) Stratigraphy, mineralogy, and genesis of the Bigadiç borate deposits, Western Turkey. *Economic Geol.* **90**, 1237–1260.

Henry, Ch. & Boden, D.R. (1998) Eocene magmatism: The heat source for Carlin-type gold deposits of northern Nevada. *Geology* **26**, 1067–1070.

Herbert, Ch. (1997) Relative sea level control of deposition in the Late Permian Newcastle coal measures of the Sydney basin, Australia. *Sed. Geol.* **107**, 167–187.

Hernandez, A., Jebrak, M., Higueras, P., *et al.* (1999) The Almadén mercury mining district, Spain. *Miner. Deposita* **34**, 539–548.

Herrmann, A.G. (1980) Bromide distribution between halite and NaCl-saturated seawater. *Chemical Geol.* **28**, 171–177.

Herrmann, A.G. & Knipping, B. (1993) *Waste Disposal and Evaporites*. 193 pp, Springer.

Herrmann, W., Green, G.R., Barton, M.D. & Davidson, G.J. (2009) Lithogeochemical and stable isotopic insights into submarine genesis of pyrophyllite-altered facies at the Boco prospect, Western Tasmania. *Economic Geol.* **104**, 775–792.

Herrington, R., Yakubchuk, A. & Puchkov, V. (2003) Uralide orogenic evolution through the Paleozoic and the link to metallogeny: an updated model. *Applied Earth Sci.* **112**, B118–120.

Herzig, P.M. & Hannington, M.D. (1995) Polymetallic massive sulfides at the modern seafloor: a review. *Ore Geology Rev.* **10**, 95–115.

Herzig, P.M., Hannington, M.D. & Arribas Jr, A. (1998) Sulfur isotopic composition of hydrothermal precipitates from the Lau back-arc: implications for magmatic contributions to seafloor hydrothermal systems. *Miner. Deposita* **33**, 226–237.

Hettler, J., Irion, G. & Lehmann, B. (1997) Environmental impact of mining waste disposal on a tropical lowland river system: a case study on the Ok Tedi mine, Papua New Guinea. *Miner. Deposita* **32**, 280–291.

Hewlett, P.C. (1997) *Lea's Chemistry of Cement and Concrete*. 4th edn. 1080 pp. Arnold Publishers.

Heydari, E. & Wade, W.J. (2002) Massive recrystallization of low-Mg calcite at high temperatures in hydrocarbon source rocks: implications for organic acids as factors in diagenesis. *AAPG Bull.* **86**, 1285–1303.

Higueras, P., Munha, J., Oyarzun, R. *et al.* (2005) First lead isotopic data for cinnabar in the Almadén district (Spain): implications for the genesis of the mercury deposits. *Miner. Deposita* **40**, 115–122.

Hildenbrand, T.G., Berger, B., Jachems, R.C. & Ludington, S. (2000) Regional crustal structures and their relationship to the distribution of ore deposits in the Western United States, based on magnetic and gravity data. *Economic Geol.* **95**, 1583–1603.

Hilt, C. (1873) Die Beziehungen zwischen der Zusammensetzung und den technischen Eigenschaften der Steinkohle. *Z. Ver. Dt. Ing.* **17**, 194–202.

Hinchey, J.G. & Hattori, K.H. (2007) Lead isotope study of the late Archean Lac des Iles palladium deposit, Canada: enrichment of platinum group elements by ponded sulfide melt. *Miner. Deposita* **42**, 601–611.

Hinckley, D.N. (1963) Variability in crystallinity values among the kaolin deposits of the Coastal Plain of Georgia & South Carolina. *Clay & Clay Minerals Monograph* **13**, 229–235.

Hitzman, M.W. & Valenta, R.K. (2005) Uranium in Iron Oxide-Copper-Gold (IOCG) systems. *Economic Geol.* **100**, 1657–1661.

Hitzman, M.W. (1999) Routine staining of drill core to determine carbonate mineralogy and distinguish carbonate alteration textures. *Miner. Deposita* **34**, 794–798.

Hitzman, M.W., Oreskes, N. & Einaudi, M.T. (1992) Geological characteristics and tectonic setting of Proterozoic iron oxide (Cu-U-Au-REE) deposits. *Precambrian Res.* **58**, 241–287.

Hoatson, D.M., Jaireth, S. & Jaques, A.L. (2006) Nickel sulfide deposits in Australia: characteristics, resources, and potential. *Ore Geol. Rev.* **29**, 177–241.

Hoefel, F. & Elgar, S. (2003) Wave-induced sediment transport and sandbar migration. *Science* **299**, 1885–1887.

Hoefs, J. (2009) *Stable Isotope Geochemistry*. 6th edn. 288 pp. Springer.

Hoek, E. & Bray, J.W. (1981) *Rock Slope Engineering*. 3rd edn. 358 pp. Instn. Min. Metall., London.

Hoek, E. & Brown, E.T. (2003) *Underground Excavations in Rock*. Revised 1st edn. 527 pp. Instn. Min. Metall., London.

Hoffman, P.F., Kaufman, A.J., Halverston, G.P. & Schrag, D.P. (1998) A Neoproterozoic Snowball Earth. *Science* **281**, 1342–1346.

Hofstra, A.H. & Cline, J.S. (2000) Characteristics and models for Carlin-type gold deposits. *Rev. Economic Geol.* **13**, 163–220.

Hofstra, A.H., John, D.A. & Theodore, T.G. (eds) (2003) A special issue devoted to gold deposits in northern Nevada: Part 2. Carlin-type deposits. *Economic Geol.* **98**, 6.

Holdaway, M.J. (1971) Stability of andalusite and the aluminum silicate phase diagram. *Am. J. Sci.* **271**, 97–131.

Holdgate, G.R., Cartwright, I., Blackburn, D.T., *et al.* (2007) The Middle Miocene Yallourn coal seam – The last coal in Australia. *Int. J. Coal Geol.* **70**, 95–115.

Holdgate, G.R. (2005) Geological processes that control lateral and vertical variability in coal seam moisture contents – Latrobe Valley (Gippsland Basin) Australia. *Int. J. Coal Geol.* **63**, 130–155.

Holk, G.J., Taylor, B.E. & Galley, A.G. (2008) Oxygen isotope mapping of the Archean Sturgeon Lake caldera complex and VMS-related hydrothermal system, Northwestern Ontario, Canada. *Miner. Deposita* **43**, 623–640.

Höll, R. & Eichhorn, R. (2000) Tungsten mineralization and metamorphic remobilization in the Felbertal scheelite deposit, Central Alps, Austria. Pp 233–264 in Spry et al. (2000).

Höll, R., Kling, M. & Schroll, E. (2007) Metallogenesis of germanium – a review. *Ore Geol. Rev.* **30**, 145–180.

Holland, H.D. (2005) Sedimentary mineral deposits and the evolution of the Earth's near-surface environment. *Economic Geol.* **100**, 1489–1509.

Holland, H.D. (2002) Volcanic gases, black smokers, and the great oxidation event. *Geochim. Cosmochim. Acta* **66**, 3811–3826.

Holland, H.D. & Turekian, K.K. (eds) (2003) *Treatise on Geochemistry*. 10 Vols. Elsevier.

Hollister, C.D. & Nadis, S. (1998) Burial of radioactive waste under the seabed. *Scientific American* **278**, 40–45.

Holmes, D.S. (1993) Brown coal in the Latrobe Valley. In: *Australasian Coal Mining Practice* (eds A.J. Hargraves & C.H. Martin), pp 243–259. AusIMM Monograph 12, Parkville.

Holser, W.T. (1979) Trace elements and isotopes in evaporites. *Mineral. Soc. America Short Course Notes* **6**, 295–346.

Holwell, D.A. & Jordaan, A. (2006) Three-dimensional mapping of the Platreef at the Zwartfontein South mine: implications for the timing of magmatic events in the northern limb of the Bushveld Complex, South Africa. *Applied Earth Sci.* **115**, 41–48.

Horita, J. & Berndt, M.E. (1999) Abiogenic methane formation and isotopic fractionation under hydrothermal conditions. *Science* **285**, 1055–1057.

Horita, J., Zimmermann, H. & Holland, H.D. (2002) Chemical evolution of seawater during the Phanerozoic: implications from the record of marine evaporites. *Geochim. Cosmochim. Acta* **66**, 3733–3756.

Horita, J., Driesner, Th. & Cole, D.R. (1999) Pressure effect on hydrogen isotope fractionation between brucite and water at elevated temperatures. *Science* **286**, 1545–1547.

Horita, J., Weinberg, A., Das, N. & Holland, H. (1996) Brine inclusions in halite and the origin of the Middle Devonian Prairie evaporites of Western Canada. *J. Sed. Res.* **66**, 956–964.

Horita, J., Wesolowski, D.J. & Cole, D.R. (1993) The acticity-composition relationship of oxygen and hydrogen isotopes in aqueous salt solutions: I. Vapor-liquid water equilibration of single salt solutions from 50–100 °C. *Geochim. Cosmochim. Acta* **57**, 2797–2817.

Horton, D.E. & Poulsen, C.J. (2009) Paradox of Late Paleozoic glacioeustasy. *Geology* **37**, 715–718.

Hostermann, J.W., Patterson, S.H. & Good, E.E. (1990) World non-bauxite aluminium resources excluding alunite. *USGS Prof. Paper 1076–C*, 73 pp.

Hough, M.A., Bierlein, F.P. & Wilde, A.R. (2007) A review of the metallogeny and tectonics of the Lachlan Orogen. *Miner. Deposita* **42**, 435–448.

Houston, S.J., Yardley, B.W.D., Smalley, P.C. & Collins, I. (2007) Rapid fluid-rock interaction in oilfield reservoirs. *Geology* **35**, 1143–1146.

Hovland, M. (1990) Do carbonate reefs form due to fluid seepage? *Terra Nova* **2**, 8–18.

Hovland, M., Hill, A. & Stokes, D. (1997) The structure and geomorphology of the Dashgil mud volcano, Azerbaijan. *Geomorphology* **21**, 1–15.

Howarth, R.J. (1983) Mapping. In: *Handbook of Exploration Geochemistry 2: Statistics and Data Analysis in Geochemical Prospecting* (ed. R.J. Howarth), pp 111–205. Elsevier.

Hower, J.C. & Gayer, R.A. (2002) Mechanisms of coal metamorphism: case studies from Paleozoic coalfields. *Int. J. Coal Geol.* **50**, 215–245.

Hsü, K.J. (1972) When the Mediterranean dried up. *Scientific American* **227**, 26–36.

Huang, B.J., Xiao, X.M. & Dong, W.L. (2003) Multiphase natural gas migration and accumulation and its relationship to diapir structures in the DF1-1 gas field, South China Sea. *Marine Petrol. Geol.* **19**, 861–872.

Huan-Zhang, L., Yimao, L., Changlie, W., *et al.* (2003) Mineralization and fluid inclusion study of the Shizhuyuan W-Sn-Bi-Mo-F skarn deposit, Hunan province, China. *Economic Geol.* **98**, 955–974.

Hubbard, S.M., de Ruig, M.J. & Graham, S.A. (2005) Utilizing outcrop analogs to improve subsurface mapping of natural gas-bearing strata in the Puchkirchen Formation, Molasse Basin, Upper Austria. *Austrian J. Earth Sci.* **98**, 52–66.

Hubbert, M.K. (1962) *Energy Resources. A Report to the Committee on Natural Resources, National Academy of Sciences*. Government Printing Office. Publication No. 1000-D.

Huggins, F. & Goodarzi, F. (2009) Environmental assessment of elements and polyaromatic hydrocarbons emitted from a Canadian coal-fired power plant. *Intern. J. Coal Geology* **77**, 282–288.

Hughes, F.E. (ed.) (1990) *Geology of the mineral deposits of Australia and Papua New Guinea*. 2 Vols, 1828 pp, AusIMM, Parkville.

Hunsche, U. & Hampel, A. (1999) Rock salt – the mechanical properties of the host rock material for a radioactive waste repository. *Engineering Geol.* **52**, 271–291.

Hunt, J.M. (1996) *Petroleum Geochemistry and Geology*. 743 pp. Freeman.

Huston, D.L., Pehrsson, S., Eglington, B.M. & Khin Zaw (2010) The geology and metallogeny of volcanic-hosted massive sulfide deposits: variations through geologic time and with tectonic setting. *Economic Geol.* **105**, 571–591.

Hutton, A.C. & Hower, J.C. (1999) Cannel coals: implications for classifications and terminology. *Intern. J. Coal Geology* **41**, 157–188.

Ihinger, P.D. & Zink, S.I., (2000) Determination of relative growth rates of natural quartz crystals. *Nature* **404**, 865–869.

Ihlen, P.M. (2000) Utilisation of sillimanite minerals, their geology, and potential occurrences in Norway – an overview. *Norg. Geol. Unders. Bull.* **436**, 113–128.

Iizasa, K., Fiske, R.S., Ishizuka, O., *et al.* (1999) A Kuroko-type polymetallic sulfide deposit in a submarine silicic caldera. *Science* **283**, 975–977.

Ingebritsen, S.E. & Manning, C.E. (1999) Geological implications of a permeability-depth curve for the continental crust. *Geology* **27**, 1107–1110.

Ings, St.J. & Beaumont, Ch. (2010) Shortening viscous pressure ridges, a solution to the enigma of initiating salt withdrawal minibasins. *Geology* **38**, 339–342.

International Energy Agency (IEA) (2010) *World Energy Outlook 2010*. 650 pp. IEA, Paris.

Inverno, C.M.C. & Hutchinson, R.W. (2006) Petrochemical discrimination of evolved granitic intrusions associated with Mount Pleasant deposits, New Brunswick, Canada. *Applied Earth Sci.* **115**, 23–39.

Ireland, T., Bull, S.W. & Large, R. (2004) Mass flow sedimentology within the HYC Zn-Pb-Ag deposit, Northern Territory, Australia: evidence for syn-sedimentary ore genesis. *Miner. Deposita* **39**, 143–158.

Irvine, T.N. (1965) Chromian spinel as a petrogenetic indicator. Part I: Theory. *Canadian J. Earth Sci.* **2**, 648–672.

Irvine, T.N. (1967) Chromian spinel as a petrogenetic indicator. Part II: Petrologic applications. *Canadian J. Earth Sci.* **4**, 71–104.

Irvine, T.N. (1982) Terminology for layered intrusions. *J. Petrol.* **23**, 127–162.

Isaaks, E.H. & Srivastava, R.M. (1990) *An Introduction to Applied Geostatistics*. 561 pp. Oxford University Press.

Isaksen, G.H. (1996) Oedometers for crude oil migration. *Nature* **383**, 573–574.

Ishihara, S. (1981) The granitoid series and mineralisation. Pp 458–484 in B.J. Skinner (ed.), *Economic Geol. 75th Anniversary Volume*, Economic Geol. Pub. Co.

Ishihara, S., Hua, R., Hoshino, M., Murakami, H. (2008) REE abundance and REE minerals in granitic rocks in the Nanling Range, Jiangxi Province, Southern China, and generation of the REE-rich weathered crust deposits. *Resource Geology* **58**, 355–372.

Jaccard, M. (2006) *Sustainable Fossil Fuels – The Unusual Suspect in the Quest for Clean and Enduring Energy*. 368 pp. Cambridge University Press.

Jackson, M.P.A., Cramez, C. & Fonck, J.-M. (2000) Role of subaerial volcanic rocks and mantle plumes in creation of South Atlantic margins: implications for salt tectonics and source rocks. *Marine & Petroleum Geol.* **17**, 477–498.

Jackson, M.P.A., Schultz-Ela, D.D., Hudec, M.R., *et al.* (1998) Structure and evolution of Upheaval Dome: A pinched-off salt diapir. *GSA Bull.* **110**, 1547–1573.

Jackson, M.P.A., Cornelius, R.R., Craig, C.H., Gansser, A., Stöcklin, J. & Talbot, C.J. (1991) Salt diapirs of the Great Kavir, Central Iran. *Geol. Soc. America Memoir 177*, 139 pp.

Jacob, H. (1989) Classification, structure, genesis and practical importance of natural solid oil bitumen ("migrabitumen"). *Intern. J. Coal Geol.* **11**, 65–79.

Jacob, J., Ward, J.D., Bluck, B.J., Scholz, R.A. & Frimmel, H.E. (2006) Some observations on diamondiferous bedrock gully trapsites on the Late Cainozoic, marine-cut platforms of the Sperrgebiet, Namibia. *Ore Geol. Rev.* **28**, 493–506.

Jaeger, J.C., Cook, N.G.W. & Zimmermann, R. (2007) *Fundamentals of Rock Mechanics*, 4th edn 488 pp Wiley-Blackwell.

Jahn, F., Cook, M. & Graham, M. (1998) *Hydrocarbon Exploration and Production*. 394 pp. Elsevier.

Jahren, A.H. & Sternberg, L.S.L. (2008) Annual patterns within tree rings of the Arctic middle Eocene (ca. 45 Ma): Isotopic signatures of precipitation, relative humidity, and deciduousness. *Geology* **36**, 99–102.

Jambour, J.L., Blowes, D.W. & Ritchie, A.I.M. (eds) (2003) Environmental aspects of mines wastes. *Mineral. Ass. Canada Short Course Series 31*, 430 pp.

James, C.S. & Minter, W.E.L. (1999) Experimental flume study of the deposition of heavy minerals in a simulated Witwatersrand sandstone unconformity. *Economic Geol.* **94**, 671–688.

James, D.E. & Sacks, I.S. (1999) Cenozoic formation of the Central Andes: a geophysical perspective. In: *Geology and Ore Deposits of the Central Andes. Spec. Pub. 7* (ed. B.J. Skinner), pp 1–25. Soc. Economic Geol, Boulder CO.

James, H.L. & Trendall, A.F. (1992) Banded iron formations: distribution in time and paleoenvironmental significance. In: *Mineral Deposits and the Evolution of the Biosphere* (eds H. D. Holland & M. Schidlowski), Dahlem Conferences, Berlin.

Jamieson, B.W. & Spross, J. (2000) The exploration and development of the high grade McArthur River uranium orebody. *Erzmetall* **53**, 457–469.

Jamveit, B. & Yardley, B.W.D. (eds) (1997) *Fluid Flow and Transport in Rocks: Mechanisms and Effects*. 319 pp. Chapman and Hall.

Jankovic, S. (1997) The Carpatho-Balkanides and adjacent area: a sector of the Tethyan Eurasian metallogenic belt. *Miner. Deposita* **32**, 426–433.

Jebrak, M. (1997) Hydrothermal breccias in vein-type ore deposits: a review of mechanisms, morphology and size distribution. *Ore Geol. Rev.* **12**, 114–134.

Jebrak, M., Higueras, P.L., Marcoux, E. & Lorenzo, S. (2002) Geology and geochemistry of high-grade, volcanic rock-hosted, mercury mineralisation in the Nuevo Entredicho deposit, Almaden district, Spain. *Miner. Deposita* **37**, 421–432.

Jennings, S.R., Dollhopf, D.J. & Inskeep, W.P. (2000) Acid production from sulfide minerals using hydrogen peroxide weathering. *Applied Geochem.* **15**, 247–255.

Jensen, K.A. & Ewing, R.C. (2001) The Okelobondo natural fission reactor, southeast Gabon: Geology, mineralogy, and retardation of nuclear-reaction products. *GSA Bull.* **113**, 32–62.

Jenyon, M.K. (2008) Identification of salt features in seismic data. *J. Petroleum Geol.* **31**, 409–417.

Jeremics, M.L. (1994) *Rock Mechanics in Salt Mining*. 544 pp., Balkema.

Jia, Y. & Kerrich, R. (1999) Nitrogen isotope systematics of mesothermal lode gold deposits: metamorphic, granitic, meteoric water, or mantle origin? *Geology* **27**, 1051–1054.

Jia, Y., Kerrich, R. & Goldfarb, R. (2003) Metamorphic origin of ore-forming fluids for orogenic gold-bearing quartz vein systems in the North American cordillera: constraints from a reconnaissance study of δ^{15}N, δD, and δ^{18}O. *Economic Geol.* **98**, 109–123.

Jia, Y., Li, X. & Kerrich, R. (2000) A fluid inclusion study of Au-bearing quartz vein systems in the Central and North Deborah deposits of the Bendigo gold field, Central Victoria, Australia. *Economic Geol.* **95**, 467–494.

Jochum, J. (2000) Variscan and post-Variscan lead-zinc mineralization, Rhenish Massif, Germany: evidence for sulfide precipitation via thermochemical sulfate reduction. *Miner. Deposita* **35**, 451–464.

Johansen, G.F. (2005) A solution to grade estimation in a high nugget environment – the Bendigo experience. *AusIMM Bull.* **2005/1**, 67–73.

John, D.A. (2001) Miocene and early Pliocene epithermal gold-silver deposits in the Northern Great Basin, Western United States: Characteristics, distribution, and relationship to magmatism. *Economic Geol.* **96**, 1827–1853.

Johnson, C., Beard, B. & Albarède, F. (eds) (2004) Non-traditional stable isotopes. *Rev. Mineral. Geochem.* **55**, 454.

Johnson, C.A., Kelley, K.D. & Leach, D.L. (2004) Sulfur and oxygen isotopes in barite deposits of the western Brooks Range, Alaska, and implications for the origin of the Red Dog massive sulfide deposits. *Economic Geol.* **99**, 1435–1448.

Johnson, C.M., Beard, B.L., Klein, C., Beukes, N.J. & Roden, E.E. (2008) Iron isotopes constrain biologic and abiologic processes in banded iron formation genesis. *Geochim. Cosmochim. Acta* **72**, 151–169.

Johnson, C.M. & Beard, B.L. (2005) Biogeochemical cycling of iron isotopes. *Science* **309**, 1025–1027.

Johnson, T.C., Odada, E.O. & Whittaker, K.T. (eds) (1996) *The Limnology, Climatology and Paleoclimatology of the East African Lakes*. 664 pp, CRC Press.

Johnston, J.D. (1999) Regional fluid flow and the genesis of Irish Carboniferous base metal deposits. *Miner. Deposita* **34**, 571–598.

Johnston, M.K., Thompson, T.B., Emmons, D.L. & Jones, K. (2008) Geology of the Cove Mine, Lander County, Nevada, and a genetic model for the McCoy-Cove hydrothermal system. *Economic Geol.* **103**, 759–782.

Jones, G. (2009) Mineral sands – an overview of the industry. *7th Int. Mining Geol. Conf. 009*, 213–222, AusIMM, Melbourne.

Jones, D.M., Head, I.M., Gray, N.D., *et al.* (2008) Crude-oil biodegradation via methanogenesis in subsurface petroleum reservoirs. *Nature* **451**, 176–180.

Jones, G.D., Whitaker, F.F., Smart, P.L. & Sanford, W.E. (2002) Fate of reflux brines in carbonate platforms. *Geology* **30**, 371–374.

Jowett, E.C. (1992) Role of organics and methane in sulfide ore formation, exemplified by Kupferschiefer Cu-Ag deposits, Poland. *Chemical Geol.* **99**, 51–63.

Jowett, E.C., Cathles, L.M. & Davis, B.W. (1993) Predicting depths of gypsum dehydration in evaporitic sedimentary basins. *AAPG Bull.* **77**, 402–413.

Jowett, E.C., Roth, T., Rydzewski, A. & Oszczepalski, S. (1991) "Background" δ^{34}S values of Kupferschiefer sulphides in Poland: pyrite-marcasite nodules. *Miner. Deposita* **26**, 89–98.

Jugo, P.J. (2009) Sulfur content at sulfur saturation in oxidised magmas. *Geology* **37**, 415–418.

Junlai Liu, Anjian Wang, Haoran Xia *et al.* (2010) Cracking mechanisms during galena mineralization in a sandstone-hosted lead-zinc ore deposit: case study of the Jinding giant sulfide deposit, Yunnan, SW China. *Miner. Deposita* **45**, 567–582.

Juve, G. & Storseth, L.R. (eds) (1997) *Europe and Neighbouring Countries. Sheet no. 9 of Mineral Atlas of the World at the Scale of 1:10 000 000*. Published by CGMW (Paris) and NGU (Trondheim).

Kah, L.C., Lyons, T.W. & Frank, T.D. (2004) Low marine sulphate and protracted oxygenation of the Proterozoic biosphere. *Nature* **431**, 834–838.

Kamenetsky, M.B., Sobolev, A.V., Kamenetsky, V.F., *et al.* (2004) Kimberlite melts rich in alkali chlorides and carbonates: A potent metasomatic agent in the mantle. *Geology* **32**, 845–848.

Kamo, S.L., Czamanske, G.K., Amelin, Y., *et al.* (2003) Rapid eruption of Siberian flood-volcanic rocks and evidence for coincidence with the Permian-Triassic boundary and mass extinction at 251 Ma. *Earth Planet. Sci. Lett.* **214**, 75–91.

Kane, A.B. (1993) Epidemiology and pathology of asbestos-related diseases. *Rev. Mineral.* **28**, 347–359.

Kappler, A., Pasquero, C., Konhauser, K.O. & Newman, D.K. (2005) Deposition of banded iron formations by anoxygenic phototrophic Fe(II)-oxidizing bacteria. *Geology* **33**, 865–868.

Kapral, R. & Showater, K. (eds) (1995) *Chemical Waves and Patterns*. 641 pp., Kluwer.

Kärkkäinen, N.K. & Bornhorst, T.J. (2003) The Svecofennian gabbro-hosted Koivusaarenneva magmatic ilmenite deposit, Kälviä, Finland. *Miner. Deposita* **38**, 169–184.

Kasprzyk, A. & Orti, F. (1998) Paleogeographic and burial controls on anhydrite genesis: the Badenian Basin in the Carpathian Foredeep (southern Poland, western Ukraine). *Sedimentology* **45**, 889–907.

Katz, B. (ed.) (1994) *Petroleum Source Rocks*. 327 pp. Springer.

Kaufhold, S. & Decher, A. (2003) Natural acidic bentonites from the island of Milos, Greece. *Z. Angew. Geol.* **49**(2), 7–12.

Kearey, P., Klepeis, K.A. & Vine, F. (2009) *Global Tectonics*, 3rd edn, 496 pp. Wiley-Blackwell.

Keary, P., Brooks, M. & Hill, I. (2002) *An Introduction to Geophysical Exploration*, 3rd edn. 280 pp. Blackwell.

Keays, R.R. (1995) The role of komatiitic and picritic magmatism and S-saturation in the formation of ore deposits. *Lithos* **34**, 1–18.

Kelley, D.L., Kelley, K.D., Coker, W.B. Caughlin, B. & Doherty, M.E. (2006) Beyond the obvious limits of ore deposits: the use of mineralogical, geochemical, and biological features for the remote detection of mineralisation. *Economic Geol.* **101**, 729–752.

Kelley, K.D. & Jennings, S. (2004) A special issue devoted to barite and Zn-Pb-Ag deposits in the Red Dog district, western Brooks Range, northern Alaska – Preface. *Economic Geol.* **99**, 1267–1280.

Kemp, A.I.S., Hawkesworth, C. J., Foster, G. L., *et al.* (2007) Magmatic and crustal differentiation history of granitic rocks from Hf-O isotopes in zircon. *Science* **315**, 980–983.

Kempe, U. & Wolf, D. (2005) Anomalously high Sc contents in ore minerals from Sn-W deposits: possible economic significance and genetic implications. *Ore Geol. Rev.* **28**, 103–122.

Kendall, A.C. (1979) Facies models: subaqueous evaporites. *Geoscience Canada* **5**, 124–139.

Kendall, T. (1996) Attapulgite. Absorbents and gellants. In: *Industrial Clays*, 2nd edn. pp. 36–37. Industrial Minerals, London.

Kendrick, M.A., Burgess, R., Leach, D. & Pattrick, R.A. D. (2002) Hydrothermal fluid origins in Mississippi Valley Type ore districts: Combined noble gas (He, Ar, Kr) and halogen (Cl, Br, I) analysis of fluid inclusions from the Illinois-Kentucky fluorspar district, Viburnum trend, and Tri-State districts, Midcontinent United States. *Economic Geol.* **97**, 453–469.

Kendrick, M.A., Burgess, R., Pattrick, R.A.D. & Turner, G. (2001) Noble gas and halogen evidence on the origin of Cu-porphyry mineralising fluids. *Geochim. Cosmochim. Acta* **65**, 2651–2668.

Kennedy, B.M. & van Soest, M.C. (2007) Flow of mantle fluids through the ductile lower crust: Helium isotope trends. *Science* **318**, 1433–1436.

Kennedy, C.S. & Kennedy, G.C. (1976) The equilibrium boundary between graphite and diamond. *J. Geophys. Res.* **81**, 2467–2470.

Kennedy, M.J., Pevear, D.R. & Hill, R.J. (2002) Mineral surface control of organic carbon in black shale. *Science* **295**, 657–660.

Kent, P.E. (1979) The emergent Hormuz salt plugs of southern Iran. *J. Petroleum Geol.* **2**, 117–144.

Keppler, H. & Wyllie, P.J. (1990) Role of fluids in transport and fractionation of uranium and thorium in magmatic processes. *Nature* **348**, 531–533.

Kerr, A. & Leitch, A.M. (2005) Self-destructive sulfide segregation systems and the formation of high-grade magmatic ore deposits. *Economic Geol.* **100**, 311–332.

Kerrich, R. (1999) Nature's gold factory. *Science* **284**, 2101–2102.

Kerrich, R. & Cassidy, K.F. (1994) Temporal relationships of lode gold mineralization to accretion, magmatism, metamorphism and deformation – Archean to present: A review. *Ore Geol. Rev.* **9**, 263–310.

Kesler, S.E. & Wilkinson, B.H. (2008) Earth's copper resources estimated from tectonic diffusion of porphyry copper deposits. *Geology* **36**, 255–258.

Kesler, S.E. & Wilkinson, B.H. (2006) The role of exhumation in the temporal distribution of ore deposits. *Economic Geol.* **101**, 919–922.

Kesler, S.E. & Ohmoto, H. (eds) (2006) Evolution of the early Earth's atmosphere, hydrosphere, and biosphere – constraints from ore deposits. *GSA Memoir 198*, 331 pp.

Kesler, S.E., Riciputi, L.C. & Ye, Z. (2005) Evidence of a magmatic origin for Carlin-type gold deposits: isotopic composition of sulfur in the Betze-Post-Screamer deposit, Nevada. *Miner. Deposita* **40**, 127–136.

Kesler, S.E., Campbell, I.H., Smith, C.N., Hall, C.M. & Allen, C.M. (2005) Age of the Pueblo Viejo gold-silver deposit and its significance to models for high-sulfidation epithermal mineralization. *Economic Geol.* **100**, 253–272.

Kesler, S.E., Russell, N. & McCurdy, K. (2003) Trace-metal content of the Pueblo Viejo precious metal deposits and their relation to other high-sulfidation epithermal systems. *Miner. Deposita* **38**, 668–682.

Kessel, R., Schmidt, M.W., Ulmer, P. & Pettke, T. (2005) Trace element signature of subduction-zone fluids, melts and supercritical liquids at 120–180 km depth. *Nature* **437**, 724–727.

Kharaka, Y.K. & Mariner, R.H. (1990) Chemical geothermometers and their application to formation waters from sedimentary basins. In: *Thermal History of Sedimentary Basins, Methods and Case Histories* (eds. N.D. Naeser & T.H. McCulloh), pp 99–117. Springer.

Kharin, G., Emelyanov, E.M. & Zagorodnich, V.A. (2004) Paleogene mineral resources of the SE Baltic Sea and Sambian Peninsula. *Zeitschrift f. Angewandte Geologie, Sonderheft* **2/2004**, 63–84.

Kholodov, V.N. & Butuzova, G.Y. (2004) Problems of siderite formation and iron ore epochs: Types of siderite-bearing iron ore deposits. *Lithology Mineral Resources* **39**, 389–411.

Khosrowshahi, S. & Shaw, W.J. (2001) Conditional simulation for resource characterisation and grade control – principles and practice. In: *Mineral Resource and Ore Reserve Estimation – the AusIMM Guide to Good Practice. Thermal History of Sedimentary Basins, Methods and Case Histories* (ed. A.C. Edwards), pp 285–292. AusIMM, Melbourne.

Kilias, S.P., Pozo, M., Bustillo, M., Stamatakis, M.G. & Calvo, J.P. (2006) Origin of the Rubian carbonate-hosted magnesite deposit, Galicia, Spain: mineralogical, REE, fluid inclusion and isotope evidence. *Miner. Deposita* **41**, 713–733.

Kim, J., Dong, H., Seabaugh, J., *et al.* (2004) Role of microbes in the smectite-to-illite reaction. *Science* **303**, 830–832.

Kimberley, M.M. (1994) Debate about ironstone: has solute supply been surficial weathering, hydrothermal convection, or exhalation of deep fluids? *Terra Nova* **6**, 116–132.

Kininmonth, R.J. & Baafi, E.Y. (eds) (2009) *Australasian Coal Mining Practice*. 1085 pp, 3rd ed., Monograph 12, AusIMM, Melbourne.

Kinnaird, J.A. & Nex, P.A.M. (2007) A review of geological controls on uranium mineralisation in sheeted leucogranites within the Damara Orogen, Namibia. *Applied Earth Sci.* **116**, 68–85.

Kinnaird, J.A. & Bowden, P. (1991) *Magmatism and mineralization associated with Phanerozoic anorogenic plutonic complexes of the African plate. In: Magmatism in Extensional Structural Settings* (eds A.B. Kampunzu & R.T. Lubala), 637 pp. Springer.

Kinnaird, J.A., Kruger, F.J., Nex, P.A.M. & Cawthorn, R. G. (2002) Chromitite formation – a key to understanding processes of platinum enrichment. *Trans. Instn. Min. Metall. B* **111**, 23–35. www.maney.co.uk/journals/aes and www.ingentaconnect.com/content/maney/aes.

Kirk, J., Ruiz, J., Chesley, J., *et al.* (2002) A major Archean, gold- and crust-forming event in the Kapvaal Craton, South Africa. *Science* **297**, 1856–1858.

Kirk, J., Ruiz, J., Chesley, J., Titley, S. & Walshe, J. (2001) A detrital model for the origin of gold and sulfides in the Witwatersrand basin based on Re-Os isotopes. *Geochim. Cosmochim. Acta* **65**, 2149–2159.

Kirkby, J. (2008) Cosmic rays and climate. *Surveys in Geophysics* **28**, 333–375.

Klammer, D. (1997) Mass change during extreme acid-sulphate hydrothermal alteration of a Tertiary latite, Styria, Austria. *Chem. Geol.* **141**, 33–48.

Klein C. & Hurlbut, C.S. (1999) *Manual of Mineralogy*, 21st edn. 681 pp. John Wiley.

Klein, C. & Ladeira, E.A. (2000) Geochemistry and petrology of some Proterozoic banded iron formations of the Quadrilatero Ferrifero, Minas Gerais, Brazil. *Economic Geol.* **95**, 405–428.

Klemm, L.M., Pettke, T. & Heinrich, C.A. (2008) Fluid and source magma evolution of the Questa porphyry Mo deposit, New Mexico, USA. *Miner. Deposita* **43**, 533–552.

Klemm, L.M., Pettke, T., Heinrich, C.A. & Campos, E. (2007) Hydrothermal evolution of the El Teniente deposit, Chile: porphyry Cu-Mo ore deposition from low-salinity magmatic fluids. *Economic Geol.* **102**, 1021–1045.

Kletzin, A. & Adams, M.W.W. (1996) Tungsten in biological systems. *FEMS Microbiology Rev.* **18**, 5–63.

Kley, J. & Voigt, T. (2008) Late Cretaceous intraplate thrusting in central Europe: Effect of Africa-Iberia-Europe convergence, not Alpine collision. *Geology* **36**, 839–842.

Klinge, H., Boehme, J., Grissemann, C., *et al.* (2007) Hydrogeology of the cover rocks of the Gorleben salt dome. *Geol. Jahrb*. C71, 147 pp. Hannover in German).

Klose, C.D. (2007) Mine water discharge and flooding: a cause of severe earthquakes. *Mine Water Environ* **26**, 172–180.

Klusmann, RW. (2003) A geochemical perspective and assessment of leakage potential for a mature carbon dioxide-enhanced oil recovery project and as a prototype for carbon dioxide sequestration; Rangely field, Colorado. *AAPG Bull.* **87**, 1485–1507.

Klusman, RW. (1993) *Soil Gas and Related Methods for Natural Resource Exploration*. 483 pp. Wiley.

Knauth, L.P. (1998) Salinity history of the Earth's early ocean. *Nature* **395**, 554–555.

Knight, J.A., Burger, K. & Bieg, G. (2000) The pyroclastic tonsteins of the Sabero Coalfield, north-western Spain, and their relationship to the stratigraphy and structural geology. *Int. J. Coal Geol.* **44**, 187–226.

Knight, J.B., Mortensen, J.K. & Morison, S.R. (1999) Lode and placer gold composition in the Klondike District, Yukon Territory, Canada: implications for the nature and genesis of Klondike placer and lode gold deposits. *Economic Geol.* **94**, 649–664.

Koch, J. (1997) Organic petrographic investigations of the Kupferschiefer in northern Germany. *Int. J. Coal Geol.* **33**, 301–316.

Kögel-Knabner, I. (1993) Biodegradation and humification processes in forest soils. Pp 101–135 in J.M. Bollag & G. Stotzky (Eds.), *Soil Biochemistry*. Marcel Dekker.

Kogel, J.E., Trivedi, N.C., Barker, J.M. & Krukowski, S.T. (eds) (2006) *Industrial Minerals & Rocks*, 7th edn, 1568 pp. Soc. Min. Met. Explor., Littleton CO.

Kohn, M.J., Rakovan, J. & Hughes, J. (eds) (2002) Phosphates: geochemical, geobiological, and materials importance. *Rev. Mineral. Geochem*. **48**, 742 pp.

Kojima, S., Takeda, S. & Kogita, S. (1994) Chemical factors controlling the solubility of uraninite and their significance in the genesis of unconformity-related uranium deposits. *Miner. Deposita* **29**, 353–360.

Komninou, A. & Sverjensky, D.A. (1996) Geochemical modelling of the formation of an unconformity-type uranium deposit. *Economic Geol.* **91**, 590–606.

Konhauser, K.O. (1998) Diversity of bacterial iron mineralization. *Earth Science Rev.* **43**, 91–121.

Kontak, D.J. & Clark, A.H. (2001) Genesis of the giant, bonanza San Rafael lode tin deposit, Peru: origin and significance of pervasive alteration. *Economic Geol.* **97**, 1741–1777.

Konyuhov, A. I. & Maleki, B. (2006) The Persian Gulf Basin: Geological history, sedimentary formations, and petroleum potential. *Lithology & Mineral Resources* **41**, 344–361.

Koons, P.O., Craw, D., Cox, S.C. *et al.* (1998) Fluid flow during active oblique convergence: a Southern Alps model from mechanical and geochemical observations. *Geology* **26**, 159–162.

Kopp, O.C., Bennet, M.E. & Clark, C.E. (2000) Volatiles lost during coalification. *Int. J. Coal Geol.* **44**, 69–84.

Koretsky, C.M., Havemann, M., Beuring, L., Cuellar, A., Shattuck, T. & Wagner, M. (2007) Spatial variation of redox and trace metal geochemistry in a minerotrophic fen. *Biochemistry* **86**, 33–62.

Korzhinskii, D.S. (1970) *Theory of Metasomatic Zoning*. Clarendon Press, Oxford, 162 pp

Korzhinsky, A.M., Tkachenko, S.I., Shmulovich, K.I., *et al.* (1994) Discovery of a pure rhenium mineral at Kudriavy volcano. *Nature* **369**, 51–52.

Koschinsky, A., Garbe-Schönberg, D., Sander, S., Schmidt, K., Gennerich, H.-H. & Strauss, H. (2008) Hydrothermal venting at pressure-temperature conditions above the critical point of seawater, 5°S on the Mid-Atlantic Ridge. *Geology* **36**, 615–618.

Kossow, D., Krawczyk, Ch., McCann, T., *et al.* (2000) Style and evolution of salt pillows and related structures in the northern part of the Northeast German Basin. *Int. J. Earth Sci.* **89**, 652–664.

Kostic, B., Süss, M.P. & Aigner, T. (2007) Three-dimensional sedimentary architecture of Quarternary sand and gravel resources: a case study of economic sedimentology (SW Germany). *Int. J. Earth Sci.* **96**, 743–767.

Köthe, A., Hoffmann, N., Krull, P., Zirngast, M. & Zwirner, R. (2007) The geology of the overburden and adjoining rocks of the Gorleben salt dome. *Geol. Jahrb. C72*, 201 pp Hannover in German).

Koyi, H.A. (2001) Modeling the influence of sinking anhydrite blocks on salt diapirs targeted for hazardous waste disposal. *Geology* **29**, 387–390.

Kretschmar, U. & Scott, S.D. (1976) Phase relations involving arsenopyrite in the system Fe-As-S and their application. *Canadian Mineralogist* **14**, 364–386.

Kreuzer, O.P., Etheridge, M.A., Guj, P., McMahon, M.E. & Holden, D.J. (2008) Linking mineral deposit models to quantitative risk analysis and decision-making in exploration. *Economic Geol.* **103**, 829–850.

Krige, D.G. (1981) *Lognormal De Wijsian Geostatistics for Ore Evaluation*, 2nd edn. 51 pp. South African Inst. Min. Metall., Johannesburg.

Krijgsman, W., Hilgen, F.J., Raffi, I., *et al.* (1999) Chronology, causes and progression of the Messinian salinity crisis. *Nature* **400**, 652–655.

Ku, T.L., Luo, S., Lowenstein, T.K., Li, J. & Spencer, R.J. (1998) U-series chronology of lacustrine deposits in Death Valley, California. *Quaternary Res.* **50**, 261–275.

Kühn, M. & Günther, A. (2007) Stratabound Rayleigh convection observed in a 4D hydrothermal reactive transport model based on the regional geological evolution of Allermöhe (Germany). *Geofluids* **7**, 301–312.

Kulke, H. (ed.) (1995) *Regional Petroleum Geology of the World: Africa, America, Australia And Antarctica.* 729 pp. Borntraeger.

Kulke, H. (ed.) (1994) *Regional Petroleum Geology of the World: Europe and Asia*. 931 pp. Borntraeger.

Kumar, V.R., Sahay, S. N. & Periasamy, N., Prasad, S.S. & Karthikeyan, S. (2010) Ground water basin management at the Neyveli Lignite Mines (India). *Mine Water Environ* **29**, 23–28.

Kump, L.R. (2008) The rise of atmospheric oxygen. *Nature* **451**, 277–278.

Kunzendorf, H. & Glasby, G.P. (1992) Tungsten accumulation in Pacific ferromanganese deposits. *Miner. Deposita* **27**, 147–152.

Kurlansky, M. (2002) *Salt, A World History*. 484 pp. Vintage.

Kurths, J., Spiering, Ch., Müller-Stoll, W. & Striegler, U. (1993) Search for solar periodicities in Miocene tree ring widths. *Terra Nova* **5**, 359–363.

Kus, J., Cramer, B. & Kockel, F. (2005) Effects of a Cretaceous structural inversion and a postulated high heat flow event on petroleum system of the western Lower Saxony Basin and the charge history of the Apeldorn gas field. *Netherlands J. Geosci.* **84**, 3–24.

Küster, D., Romer, R.L., Tolessa D., *et al.* (2009) The Kenticha rare-element pegmatite, Ethiopia: internal differentiation, U-Pb age and Ta mineralization. *Miner. Deposita* **44**, 723–750.

Küster, Y., Schramm, M., Bornemann, O. & Leiss, B. (2009) Bromide distribution characteristics of different Zechstein 2 rock salt sequences of the Southern Permian Basin: a comparison between bedded and domal salts. *Sedimentology* **56**, 1368–1391.

Kuznetsov, A.B., Krupenin, M.T., Ovchinnikova, G.V., *et al.* (2005) Diagenesis of carbonate and siderite deposits of the Lower Riphean Bakal Formation, the southern Urals: Sr isotope characteristics and Pb-Pb age. *Lithology and Mineral Resources* **40**, 195–215.

Kwiencinska, B. & Petersen, H.I. (2004) Graphite, semigraphite, natural coke, and natural char classification – ICCP-System. *Int. J. Coal Geol.* **57**, 99–116.

Kwon, S. & Kim, J. (2005) Effect of temperature variation on rock salt deformation – a case study. *Mining Technology (Trans. Inst. Min. Metall. A)* **114**, 89–98.

Kyle, J.R. & Ning, Li (2002) Jinding: A giant Tertiary sandstone-hosted Zn-Pb deposit, Yunnan, China. *SEG Newsletter* **50**(1), 9–16.

Kyle, J.R. & Price, P.E. (1986) Metallic sulfide mineralization in salt-dome cap-rocks, Gulf Coast, USA. *Trans. Instn. Min. Metall. B* **95**, 6–15.

Kyser, K. & Hiatt, E.E. (2003) Fluids in sedimentary basins: an introduction. *J. Geochemical Exploration* **80**, 139–149.

Labrenz, M., Druschel, G.K., Thomsen-Ebert, T., *et al.* (2000) Formation of sphalerite (ZnS) deposits in natural biofilms of sulfate-reducing bacteria. *Science* **290**, 1744–1747.

Lacis, A.A., Schmidt, G.A., Rind, D. & Ruedy, R.A. (2010) Atmospheric CO_2: Principal control knob governing Earth's temperature. *Science* **330**, 356–359.

Lackner, K.S. (2003) A guide to CO_2 sequestration. *Science* **300**, 1677–1678.

Lamberson, M.N., Bustin, R.M., Kalkreuth, W.D. & Pratt, K.C. (1996) The formation of inertinite-rich peats in the mid-Cretaceous Gates Formation: implications for the interpretation of mid-Albian history of paleowildfire. *Paleogeogr, Paleoclimatol. & Paleoecol.* **120**, 235–260.

Lambiase, J.J. (ed.) (1995) Hydrocarbon habitat in rift basins. *Geol. Soc. Spec. Publ.* **80**, 392.

Lane, K.F. (1997) *The Economic Definition of Ore*, 2nd edn. Mining Journal Books, London.

Lang, J.R. & Baker, T. (2001) Intrusion-related gold systems: the present level of understanding. *Miner. Deposita* **36**, 477–489.

Lange, G. (1995) Die Uranlagerstätte Ronneburg. *Z. geol. Wiss.* **23**, 517–526.

Lapointe, F., Fytas, K. & McConchie, D. (2006) Effiency of Bauxsol™ in permeable reactive barriers to treat acid rock drainage. *Mine Water Environ* **25**, 37–44.

Large, D. (2001) The geology of non-sulfide zinc deposits – an overview. *Erzmetall* **54**, 264–274.

Large, D. & Walcher, E. (1999) The Rammelsberg massive sulphide Cu-Zn-Pb-Ba-deposit, Germany: an example of sediment-hosted, massive sulphide mineralisation. *Miner. Deposita* **34**, 522–538.

Large, D.J., Jones, T.F., Briggs, J., *et al.* (2004) Orbital tuning and correlation of 1.7 m. y. of continuous carbon storage in an early Miocene peatland. *Geology* **32**, 873–876.

Large, D.J., Jones, T.F., Somerfield, C., *et al.* (2003) High-resolution record of orbital climate forcing in coal. *Geology* **31**, 303–306.

Large, R.R., Maslenikov, V.V., Robert, F., Danyushevsky, L.V. & Chang, Z. (2007) Multistage sedimentary and metamorphic origin of pyrite and gold in the giant Sukhoi Log deposit, Lena gold province, Russia. *Economic Geol.* **102**, 1233–1267.

Large, R.R. (1992) Australian volcanic-hosted massive sulfide deposits: Features, styles, and genetic models. *Economic Geol.* **87**, 471–510.

Lascelles, D.F. (2006) The genesis of the Hope Downs iron ore deposit, Hamersley Province, Western Australia. *Economic Geol.* **101**, 1359–1376.

Lasky, S.G. (1950) How tonnage and grade relations help predict ore reserves. *Eng. Mining J.* **151**, 81–85.

Latypov, R. (2007) Noril'sk- and Lower Talnakh-type intrusions are not conduits for overlying flood basalts: insights from residual gabbroic sequence of intrusions. *Applied Earth Sci.* **116**, 215–225.

Laubach, S.E., Marett, R.A., Olson, J.E. & Scott, A.R. (1998) Characteristics and origins of coal cleats: A review. *Int. J. Coal Geol.* **35**, 175–207.

Launay, L. de (1913) *Traité de Métallogénie*. 3 Vols. Paris.

Law, B.E. & Rice, D.D. (eds) (1993) *Hydrocarbons from Coal*. 400 pp. AAPG Studies in Geology 38.

Law, J.D.M. & Phillips, G.N. (2005) Hydrothermal replacement model for the Witwatersrand gold. *Economic Geol.* **100**, 799–811.

Lay, Th., Hernlund, J. & Buffett, B.A. (2008) Core–mantle boundary heat flow. *Nature Geoscience* **1**, 25–32.

Laznicka, P. (2006) *Giant Metallic Deposits – Future Sources of Industrial Metals*. 732 pp, Springer.

Laznicka, P. (1993) *Precambrian Empirical Metallogeny. Vol. 2: Precambrian Lithologic Associations And Ore Deposits*. 1622 pp. Elsevier.

Laznicka, P. (1985) *Empirical Metallogeny. Vol. 1: Phanerozoic Environments, Associations and Deposits*. 1002 pp. Elsevier.

Leach, D.L., Bradley, D.C., Huston, D., Pisarevsky, S.A., Taylor, R.D. & Gardoll, S.J. (2010) Sediment-hosted lead-zinc deposits in earth history. *Economic Geol.* **105**, 593–625.

Leach, D.L., Hofstra, A.H., Church, S.E. *et al.* (1998) Evidence for Proterozoic and late Cretaceous-early Tertiary ore-forming events in the Coeur d'Alene district, Idaho and Montana. *Economic Geol.* **93**, 347–359.

Leake, R.C., Bland, D.J. & Cooper, C. (1993) Source characterization of alluvial gold from mineral inclusions and internal compositional variation. *Trans. Instn. Min. Metall. B* **102**, 65–82.

Leblanc, M., Morales, J.A., Borrego, J. & Elbaz-Poulichet, F. (2000) 4500-year-old mining pollution in southwestern Spain: long-term implications for modern mining pollution. *Economic Geol.* **95**, 655–662.

Leca, X. (1990) Discovery of concealed massive sulfide bodies at Neves-Corvo, southern Portugal – a case history. *Transact. Instn. Min. Metall. B* **99**, 139–152.

Leckie, D.A., Kjarsgaard, B.A., Bloch, J., *et al.* (1997) Emplacement and reworking of Cretaceous, diamond-bearing, crater facies kimberlite of central Saskatchewan, Canada. *GSA Bull.* **109**, 1000–1020.

Ledin, M. & Pedersen, K. (1996) The environmental impact of mine wastes – roles of micro-organisms and their significance in treatment of mine wastes. *Earth Sci. Rev.* **41**, 67–108.

Lee, Ch.-H. & Farmer, I. (1993) *Fluid Flow in Discontinuous Rocks*. 169 pp. Chapman & Hall.

Lee, G. (2001) Mineral sands – some aspects of evaluation, resource estimation and reporting. In: *Mineral Resource and Ore Reserve Estimation – the AusIMM Guide to Good Practice* (ed. A.C. Edwards), pp 315–322. AusIMM, Melbourne.

Leeb-Du Toit, A. (1986) The Impala platinum mines. In: *Mineral Deposits of Southern Africa*. Vol.II (eds C.R. Anhäusser & S. Maske), pp. 1091–1106. Geol. Soc. S. Africa, Johannesburg.

Lefticariu, L., Perry, E.C., Fischer, M.P. & Banner, J.L. (2005) Evolution of fluid compartmentalization in a detachment fold complex. *Geology* **33**, 69–72.

Lehmann, B. (1990) *Metallogeny of Tin*. 211 pp. Springer.

Lehmann, B., Burgess, R., Frei, D., *et al.* (2010) Diamondiferous kimberlites in central India synchronous with Deccan flood basalts. *Earth Planet. Sci. Lett.* **290**, 142–149.

Lehmann, B., Nägler, T.F., Holland, H.D., *et al.* (2007) Highly metalliferous carbonaceous shale and Early Cambrian seawater. *Geology* **35**, 403–406.

Lehmann, J., Arndt, N., Windley, B., Zhou, M.F., Wang, C.Y. & Harris, C. (2007) Field relationships and geochemical constraints on the emplacement of the Jinchuan intrusion and its Ni-Cu-PGE sulfide deposit, Gansu, China. *Economic Geol.* **102**, 75–94.

Lehmann, B., Dietrich, A., Heinhorst, J., *et al.* (2000a) Boron in the Bolivian tin belt. *Miner. Deposita* **35**, 223–232.

Lehmann, B., Dietrich, A. & Wallianos, A. (2000b) From rocks to ore. *Int. J. Earth Sci.* **89**, 284–294.

Lengke, M.F. & Southam, G. (2007) The deposition of elemental gold from gold(I)-thiosulfate complexes mediated by sulfate-reducing bacterial conditions. *Economic Geol.* **102**, 109–126.

Lenoble, J.-P. (1996) Les nodules polymétalliques: bilan de 30 ans de travaux dans le monde. *Chronique recherche minière* **524**, 15–39.

Lentz, D.R. (ed.) (1998) Mineralized intrusion-related skarn systems. *Mineralog. Assoc. Canada Short Course* Vol. 26, 664 pp.

Lentz, D.R. (1998) Petrogenetic evolution of felsic volcanic sequences associated with Phanerozoic volcanic-hosted massive sulphide systems: the role of extensional geodynamics. *Ore Geol. Rev.* **12**, 289–327.

Lentz, D. (1996) U, Mo, and REE mineralization in late-tectonic granitic pegmatites, southwestern Grenville Province, Canada. *Ore Geol. Rev.* **11**, 197–227.

Lentz, D.R. (ed.) (1994) Alteration and alteration processes associated with ore forming systems. *Geol. Ass. Canada Short Course Notes 11*, 467 pp.

Lesher, C.M. & Campbell, I.H. (1993) Geochemical and fluid dynamic modelling of compositional variations in Archean komatiite-hosted nickel sulfide ores in Western Australia. *Economic Geol.* **88**, 804–816.

Lespade, P., Al-Jishi, R. & Dresselhaus, M.S. (1982) Model for Raman scattering from incompletely graphitised carbons. *Carbon* **20**, 427–431.

Leventhal, J. (1990) Comparative geochemistry of metals and rare earth elements from the Cambrian alum shale and kolm of Sweden. *Spec. Publs. Int. Ass. Sediment.* **11**, 203–216.

Levorsen, A.I. (1967) *Geology of Petroleum*, 2nd edn. Freeman.

Lewan, M.D. (1998) Sulphur-radical control on petroleum formation rates. *Nature* **391**, 164–166.

Lewis, R.W. (1990) The exploration and development of the Kidston gold deposit. In: *Geological Aspects of the Discovery of Some Important Mineral Deposits in Australia* (eds K.R. Glasson & J.H. Rattigan), pp. 83–89. *Monograph 17*. AusIMM, Melbourne.

Lewis, St. E., Henderson, R.A., Dickens, G.R., Shields, G. A. & Coxhell, S. (2010) The geochemistry of primary and weathered oil shale and coquina across the Julia Creek vanadium deposit (Queensland, Australia). *Miner. Deposita* **45**, 599–620.

Li, Chusi & Naldrett, A.J. (1999) Geology and petrology of the Voisey's Bay intrusion: reaction of olivine with sulfide and silicate liquids. *Lithos* **47**, 131.

Li, Chusi, Ripley, E.M. & Naldrett, A.J. (2009) A new genetic model for the giant Ni-Cu-PGE sulfide deposits associated with the Siberian flood basalts. *Economic Geol.* **104**, 291–301.

Li, Chusi, Xu, Z., de Waal, S.A. *et al.* (2004) Compositional variations of olivine from the Jinchuan Ni-Cu sulfide deposit, western China: implications for ore genesis. *Miner. Deposita* **39**, 159–172.

Li, J.-W., Vasconcelos, P., Zhang, W., *et al.* (2007) Timing and duration of supergene mineralization at the Xinrong manganese deposit, western Guandong Province, South China: cryptomelane ^{40}Ar/^{39}Ar dating. *Miner. Deposita* **42**, 361–383.

Li, Zheng-Xiang & Li, Xian-Hua (2007) Formation of the 1300-km-wide intracontinental orogen and postorogenic magmatic province in Mesozoic South China: a flat subduction model. *Geology* **35**, 179–182.

Liang, Hua-Ying, Sun, Weidong, Su, Wen-Chao & Zartman, R.E. (2009) Porphyry copper-gold mineralization at Yulong, China, promoted by decreasing redox potential during magnetite alteration. *Economic Geol.* **104**, 587–596.

Lichtervelde, M. van, Salvi, S. & Beziat, D. (2007) Textural features and chemical evolution in tantalum oxides: magmatic versus hydrothermal origins for Ta mineralization in the Tanco Lower Pegmatite, Manitoba, Canada. *Economic Geol.* **102**, 257–276.

Liebig, J. von (1842) *Die Chemie in ihrer Anwendung auf Agricultur und Physiologie*. 469 pp, Viehweg.

Liebig, E. & Althaus, E. (1998) Pozzolanic activity of volcanic tuff and suevite: Effects of calcination. *Cement & Concrete Res.* **28**, 567–575.

Lindgren, W. (1933) *Mineral Deposits*. *930 pp*. McGraw-Hill, New York.

Lindh, U. (2005) Biological functions of the elements. In: *Essentials of Medical Geology – Impacts of the Natural Environment on Public Health* (ed. O. Selinus *et al.*), pp 115–160. Elsevier Academic Press.

Lindsey, D.A. (1977) Epithermal beryllium deposits in water-laid tuff, western Utah. *Economic Geol.* **72**, 219–232.

Linnen, R.L. (1998) The solubility of Nb-Ta-Zr-Hf-W in granitic melts with Li and Li + F: constraints for mineralisation in rare metal granites and pegmatites. *Economic Geol.* **93**, 1013–1025.

Linnen, R.L. & Samson, I.M. (eds) (2005) Rare-element geochemistry and mineral deposits. *Geol. Ass. Canada Short Course Notes 17*, 341 pp.

Linnen, R.L., Pichavant, L. & Holtz, F. (1996) The combined effects of f_{O2} and melt composition on SnO_2 solubility and tin diffusivity in haplogranitic melts. *Geochim. Cosmochim. Acta* **60**, 4965–4976.

Lipton, I.T. (2001) Measuring of bulk density for resource estimation. In: *Mineral Resource and Ore Reserve Estimation – the AusIMM Guide to Good Practice* (ed. A.C. Edwards), pp. 57–66. AusIMM, Melbourne.

Lisk, M., O'Brien, G.W. & Eadington, P.J. (2002) Quantitative evaluation of the oil leg potential in the Oliver gas field, Timor Sea, Australia. *AAGP Bull.* **86**, 1531–1542.

Littke, R. (1993) *Deposition, Diagenesis and Weathering of Organic Matter-Rich Sediments*. 216 pp. Springer.

Littke, R., Kroos, B., Idiz, E. & Frielingsdorf, J. (1995) Molecular nitrogen in natural gas accumulations: generation from sedimentary organic matter at high temperatures. *Amer. Ass. Petrol. Geol. Bull.* **79**, 410–430.

Little, C.T.S., Cann, J.R., Herrington, R.J. & Morisseau, M. (1999) Late Cretaceous hydrothermal vent communities from the Troodos ophiolite, Cyprus. *Geology* **27**, 1027–1030.

Livaccari, R.F., Burke, K. & Şengör, A.M.C. (1981) Was the Laramide orogeny related to subduction of an oceanic plateau? *Nature* **289**, 276–278.

Locke, A. (1921) The profession of ore hunting. *Economic Geol.* **16**, 243–278.

Loen, J.S. (1992) Mass balance constraints on gold placers: possible solutions to "source area problems". *Economic Geol.* **87**, 1624–1634.

Logan, R.G., Murray, W.J. & Williams, N. (1990) HYC silver-lead-zinc deposit, McArthur River. In: *Geology of the mineral deposits of Australia and Papua New*

Guinea (ed. F.E. Hughes), pp. 907–911. AusIM, Melbourne.

Lombaard, A.F., Günzel, A., Innes, J. & Krüger, T.L. (1986) The Tsumeb lead-copper-zinc-silver deposit, South West Africa/Namibia. In: *Mineral Deposits of Southern Africa* (eds C.R. Anhäusser & S. Maske), pp 1761–1787. Geol. Soc. S. Africa, Johannesburg.

Lomborg, B. (2001) *The skeptical environmentalist*. 515 pp. Cambridge University Press.

London, D. (2008) Pegmatites. *Mineralogical Association of Canada Spec. Publ. 10*. 386 pp.

Long, D.G.F., McDonald, A.M., Yi Facheng, *et al.* (1997) Palygorskite in paleosols from the Miocene Xiacaowan Formation of Jiangsu and Anhui provinces, P. R. China. *Sediment. Geol.* **112**, 281–295.

Loop, C.M., Scheetz, B.E. & White, W.B. (2003) Geochemical evolution of a surface mine lake with alkaline ash addition: field observations vs. laboratory predictions. *Mine Water Environ* **22**, 206–213.

Lord, R.A. & Prichard, H.M. (1997) Exploration and origin of stratigraphically controlled platinum-group element mineralization in crustal-sequence ultramafics, Shetland ophiolite complex. *Trans. Instn. Min. Metall.* **B 106**, 179–193.

Lottermoser, B. (2007) *Mine Wastes – Characterization, Treatment and Environmental Impacts*, 2nd edn. 304 pp. Springer.

Lottermoser, B.G. (1995) Ore minerals of Mt Weld rare-earth element deposit. *Trans. Instn. Min. Metall. B* **104**, 203–209.

Lottermoser, B.G. (1992) Rare earth elements and hydrothermal ore formation processes. *Ore Geol. Rev.* **7**(1), 25–41.

Loukola-Ruskeeniemi, K. & Heino, T. (1996) Geochemistry and genesis of the black shale-hosted Ni-Cu-Zn deposit at Talvivaara, Finland. *Economic Geol.* **91**, 80–110.

Lovelock, J. (2006) *The Revenge of Gaia. Why the Earth is Fighting Back – And How We Can Still Save Humanity*. 222 pp. Penguin Books.

Lovley, D.R. (2001) Anaerobes to the rescue. *Science* **293**, 1444–1446.

Lovley, D.R., Phillips, E.J.P., Gorby, Y.A. & Landa, E.R. (1991) Microbial reduction of uranium. *Nature* **350**, 413–416.

Lowell, J.D. & Guilbert, J.M. (1970) Lateral and vertical alteration-mineralization zoning in porphyry ore deposits. *Economic Geol.* **65**, 373–408.

Lowenstein, T.K., Hardie, L.A., Timofeev, M.N. & Demicco, R.V. (2003) Secular variation in seawater chemistry and the origin of calcium chloride basinal brines. *Geology* **31**, 857–860.

Lowenstern, J.B. (2001) Carbon dioxide in magmas and implications for hydrothermal systems. *Miner. Deposita* **36**, 490–502.

Lowey, G.W. (2006) The origin and evolution of the Klondike goldfields, Yukon, Canada. *Ore Geol. Rev.* **28**, 431–450.

Lu, Jiemin, Wilkinson, M., Haszeldine, R.S. & Fallick, A. E. (2009) Long-term performance of a mudrock seal in natural CO_2 storage. *Geology* **37**, 35–38.

Lu, K. (2010) The Future of Metals. *Science* **328**, 319–320.

Lüders, V. (1996) Contribution of infrared microscopy to fluid inclusion studies in some opaque minerals (wolframite, stibnite, bournonite): Metallogenic implications. *Economic Geol.* **91**, 1462–1468.

Lüders, V., Ricker, K., Banks, D.A. & Meston, L. (2005) Fluid inclusion evidence for extreme element partitioning during subcritical phase separation. Abstracts 15th Annual Goldschmidt Conference. *Geochimica Cosmochimica Acta* **69**, A734.

Ludington, S., Folger, H., Kotlyar, B., Mossotti, V.G., Coombs, M.J. & Hildenbrand, T.G. (2006) Regional surficial geochemistry of the Northern Great Basin. *Economic Geol.* **101**, 33–57.

Lugli, S., Torres-Ruiz, J., Garuti, G. & Olmedo, F. (2000) Petrography and geochemistry of the Eugui magnesite deposit (Western Pyrenees, Spain): evidence for the development of a peculiar zebra banding by dolomite replacement. *Economic Geol.* **95**, 1775–1791.

Luo, X. & Vasseur, G. (1997) Sealing effiency of shales. *Terra Nova* **9**, 71–74.

Luo, X., Dong, W., Yang, J. & Yang, W. (2003) Overpressuring mechanisms in the Yinggehai basin, South China Sea. *AAPG Bull.* **87**, 629–645.

Luque, F.J., Pasteris, J.D., Wopenka, B., Rodas, M. & Barrenechea, J.F. (1998) Natural fluid-deposited graphite: mineralogical characteristics and mechanisms of formation. *Amer. J. Sci.* **298**, 471–498.

Luque, F.J., Rodas, M. & Galan, E. (1992) Graphite vein mineralization in the ultramafic rocks of southern Spain: mineralogy and genetic relationships. *Miner. Deposita* **27**, 226–233.

Lusk, J., Scott, S.D. & Ford, C.E. (1993) Phase relations in the Fe-Zn-S system to 5 kbars and temperatures between 325 and 150 °C. *Economic Geol.* **88**, 1880–1903.

Lynne, B.Y., Campbell, K.A., Perry, R.S., Browne, P.R.L. & Moore, J.N. (2006) Acceleration of sinter diagenesis in an active fumarole, Taupo volcanic zone, New Zealand. *Geology* **34**, 749–752.

Lyons, J.I. (1988) Volcanogenic iron oxide deposits, Cerro de Mercado and vicinity, Durango. *Economic Geol.* **83**, 1886–1906.

Lyons, P.C. (1991) Comment to: Hydrothermal alteration in anthracite from eastern Pennsylvania: Implications for mechanisms of anthracite formation. *Geology* **19**(2), 188.

Maas, R., Kamenetsky, M.B., Sobolev, A.V., Kamenetsky, V.S. & Sobolev, N.V. (2005) Sr, Nd, and Pb isotope evidence for a mantle origin of alkali chlorides and carbonates in the Udachnaya kimberlite, Siberia. *Geology* **33**, 549–552.

MacDonald, I.R., Bohrmann, G., Escobar, E., *et al.* (2004) Asphalt volcanism and chemosynthetic life in the Campeche Knolls, Gulf of Mexico. *Science* **304**, 999–1002.

Macfarlane, A.M. & Ewing, R.C. (eds.) (2006) *Uncertainty Underground: Yucca Mountain and the Nation's High-Level Nuclear Waste*. 416 pp. MIT Press.

MacLean, W.H., Bonavia, F.F. & Sanna, G. (1997) Argillite debris converted to bauxite during karst weathering: evidence from immobile element geochemistry at the Olmedo deposit, Sardinia. *Miner. Deposita* **32**, 607–616.

Madhukar, B.B.L. & Srivastava, S.N. (1995) *Mica and Mica Industry*. 212 pp. Balkema.

Magoon, L.B. & Dow, W.G. (eds) (1994) The petroleum system from source to trap. *AAPG Memoir* **60,** 655 pp.

Maier, W.D., Barnes, S.J., Campbell, I.H., *et al.* (2009) Progressive mixing of meteoritic veneer into the early Earth's deep mantle. *Nature* **460**, 620–623.

Maier, W.D., Barnes, S.-J., Gartz, V. & Andrews, G. (2003) Pt-Pd reefs in magnetites of the Stella layered intrusion, South Africa: a world of new exploration opportunities for platinum group elements. *Geology* **31**, 885–888.

Maier, W.D. & Eales, H.V. (1994) Facies model for the interval between UG2 and Merensky Reef, western Bushveld Complex, South Africa. *Trans. Instn. Min. Metall. B* **103**, 22–30.

Maineri, C., Benvenuti, M., Costagliola, P. *et al.* (2003) Sericitic alteration at the La Crocetta deposit (Elba island, Italy): interplay between magmatism, tectonics, and hydrothermal activity. *Miner. Deposita* **38**, 67–86.

Malkovets, V.G., Griffin, W.L., O'Reilly, S.Y. & Wood, B. J. (2007) Diamond, subcalcic garnet, and mantle metasomatism: kimberlite sampling patterns define the link. *Geology* **35**, 339–342.

Mallon, A.J., Swarbrick, R.E. & Katsube, T.J. (2005) Permeability of fine-grained rocks: new evidence from chalks. *Geology* **33**, 21–24.

Mameli, P., Mongelli, G., Oggiano, G & Dinelli, E. (2007) Geological, geochemical and mineralogical features of some bauxite deposits from Nurra (Western Sardinia, Italy): insights on conditions of formation and parental affinity. *Int. J. Earth Sci.* **96**, 887–902.

Mancktelow, N.S. (2006) How ductile are ductile shear zones? *Geology* **34**, 345–348.

Mandelbrot, B.B. (1982) *The Fractal Geometry of Nature*. 468 pp, Freeman, New York.

Mango, F.D., Hightower, J.W. & James, A.T. (1994) Role of transition-metal catalysis in the formation of natural gas. *Nature* **368**, 536–538.

Mango, H., Zantop, H. & Oreskes, N. (1991) A fluid inclusion and isotope study of the Rayas Ag-Au-Cu-Pb-Zn mine, Guanajuato, Mexico. *Economic Geol.* **86**, 1554–1561.

Manhenke, V. & Beer, H. (2004) Karten der Erdwärme des Landes Brandenburg (Maps of geothermal fields of Brandenburg, Germany). *Brandenburgische Geowiss. Beitr.* **11**, 1–10.

Marcillac, P. de, Coron, N., Dambier, G., *et al.* (2003) Experimental detection of α-particles from the radioactive decay of natural bismuth. *Nature* **422**, 876–878.

Marcoux, E. & Jebrak, M. (1999) Butte, Montana, Etats Unies: un exemple de télescopage et de district métallogénique stationnaire. *Chron. Rech. Minière* **535**, 45–58.

Marcuello, A., Gómez, P., Carrera, J. & Ayora, C. (2006) Multicomponent reactive transport modeling at the Ratones uranium mine, Cáceres, (Spain). *J. Iberian Geol.* **32**, 133–146.

Marignac, C. & Cuney, M. (1999) Ore deposits of the French Massif Central: insight into the metallogenesis of the Variscan collision belt. *Miner. Deposita* **34**, 472–504.

Marjoribanks, R. (1997) *Geological Methods in Mineral Exploration and Mining*. Chapman & Hall, 115 pp.

Mark, D.F., Parnell, J., Kelley, S.P., Lee, M.R. & Sherlock, S.C. (2010) ^{40}Ar/^{39}Ar dating of oil generation and migration at complex continental margins. *Geology* **38**, 75–78.

Mark, D.F., Parnell, J., Kelley, S.P. & Sherlock, S.C. (2007) Resolution of regional fluid flow related to successive orogenic events on the Laurentian margin. *Geology* **35**, 547–550.

Markl, G. & Bucher, K. (1998) Composition of fluids in the lower crust inferred from metamorphic salt in lower crustal rocks. *Nature* **391**, 781–783.

Marrett, R., Ortega, O.J. & Kelsey, C.M. (1999) Extent of power law scaling for natural fractures in rock. *Geology* **27**, 799–802.

Marshall, B., Vokes, F.M. & Larocque, A.C.L. (2000) Regional metamorphic remobilization: Upgrading and formation of ore deposits. pp 19–38 in Spry et al., 2000.

Marshall, C.P. & Fairbridge, R.W. (eds) (1999) *Encyclopedia of Geochemistry*. 768 pp, Springer (Kluwer).

Marshall, D.D., Diamond, L.W. & Skippen, G.B. (1993) Silver transport and deposition at Cobalt, Ontario, Canada: Fluid inclusion evidence. *Economic Geol.* **88**, 837–854.

Martin, R.F. & Cerny, P. (eds) (1992) Granitic Pegmatites. *Canadian Mineralogist* **30**(3), 499–954.

Martini, A.M., Budai, J.M., Walter, L.M. & Schoell, M. (1996) Microbial generation of economic accumulations of methane within a shallow organic-rich shale. *Nature* **383**, 155–157.

Marzoli, A., Renne, P.R. & Piccirillo, E.M., *et al.* (1999) Extensive 200-million-year-old continental flood basalts of the Central Atlantic Magmatic Province. *Science* **284**, 616–618.

Mastalerz, M., Drobniak, A. & Schimmelmann, A. (2009) Changes in optical properties, chemistry, and micropore and mesopore characteristics of bituminous coal at the contact with dikes in the Illinois Basin. *Int. J. Coal Geol.* **77**, 310–319.

Masters, R.L. & Ague, J.J. (2005) Regional-scale fluid flow and element mobility in Barrow's metamorphic zones, Stonehaven, Scotland. *Contrib. Mineralogy Petrology* **150**, 1–18.

Matheron, G. (1971) *The Theory of Regionalized Variables and its Applications*. Cahiers Centre Morph. Math. Fontainebleau 5, Ecole Nat. Sup. Mines, Paris.

Mathez, E.A. & Mey, J.L. (2005) Character of the UG2 chromitite and host rocks and petrogenesis of its pegmatoidal footwall, northeastern Bushveld Complex. *Economic Geol.* **100**, 1617–1630.

Matthäi, S.K., Heinrich, C.A., and Driesner, T. (2004) Is the Mount Isa copper deposit the product of forced brine convection in the footwall of a major reverse fault? *Geology* **32**, 357–360.

Matthäi, S.K., Henley, R.W. & Heinrich, C.A. (1995) Gold precipitation by fluid mixing in bedding-parallel fractures near carbonaceous slates at the Cosmopolitan Howley gold deposit, Northern Australia. *Economic Geol.* **90**, 2123–2142.

Matveev, S. & Ballhaus, C. (2002) Role of water in the origin of podiform chromitite deposits. *Earth Planet. Sci. Lett.* **203**, 235–243.

Matzke, R.H., Smith, J.G. & Foo, W.K. (1992) Iagifu/Hedinia field – first oil from the Papuan fold and thrust belt. In: *Giant Oil and Gas Fields of the Decade 1978–1988* (ed. M.T. Halbouty), pp. 471–482. AAPG, Tulsa.

Maucher, A. (1965) *Die Antimon-Wolfram-Quecksilber-Formation und ihre Beziehungen zu Magmatismus und Geotektonik*. Freiberger Forschungsh. **C186**, 173–187, Leipzig.

Mauger, A.J., Keeling, J.L. & Huntington, J.F. (2007) Alteration mapping of the Tarcoola goldfield (South Australia) using a suite of hyperspectral methods. *Applied Earth Sci.* **116**, 2–12.

Maugeri, L. (2004) Oil: never cry wolf – why the petroleum age is far from over. *Science* **304**, 1114–1115.

Mauk, J.L. & White, B.G. (2004) Stratigraphy of the Proterozoic Revett Formation and its control on Ag-Pb-Zn vein mineralization in the Coeur d'Alene district, Idaho. *Economic Geol.* **99**, 295–312.

Maury, V. (1997) Effets de la décompression du champs de Lacq – point recapitulatif à fin 1989 sur l'activité sismique et l'affaisement. Bull. *Centre Rech. Elf Explor. Prod.* **21**, 303–322.

Mavrogenes, J.A., Macintosh, I.W. & Ellis, D.J. (2001) Partial melting of the Broken Hill galena-sphalerite ore: experimental studies in the system PbS-FeS-ZnS-(Ag_2S). *Economic Geol.* **96**, 205–210.

Mavrogenes, J.A., Bodnar, R.J., Graney, J.R., *et al.* (1995) Comparison of decrepitation, microthermometric and compositional characteristics of fluid inclusions in barren and auriferous mesothermal quartz veins of the Cowra Creek gold district, New South Wales, Australia. *J. Geochem. Explor.* **54**, 167–175.

Max, M.D. (2000) *Natural Gas Hydrate in Oceanic and Permafrost Environments*. 432 pp. Kluwer.

Maynard, J.B. (2010) The chemistry of manganese ores through time: a signal of increasing diversity of earth-surface environments. *Economic Geol.* **105**, 535–552.

Maynard, J.B., Morton, J., Valdes-Nodarse, E.L. & Diaz-Carmona, A. (1995) Sr isotopes of bedded barites: guide to distinguishing basins with Pb-Zn mineralization. *Economic Geol.* **90**, 2058–2064.

Mazur, S. & Scheck-Wenderoth, M. (2005) Constraints on the tectonic evolution of the Central European Basin System revealed by seismic reflection profiles from Northern Germany. *Netherlands J. Geosciences* **84**, 389–401.

McCammon, C. (2001) Deep diamond mysteries. *Science* **293**, 813–814.

McClenaghan, M.B. (2005) Indicator mineral methods in mineral exploration. *Geochemistry: Exploration, Environment, Analysis* **5**, 233–245.

McClenaghan, S.H., Lentz, D.R., Martin, J. & Diegor, D.G. (2009) Gold in the Brunswick No. 12 volcanogenic massive sulfide deposit, Bathurst Mining Camp, Canada: Evidence from bulk ore analysis and laser ablation ICP-MS data on sulfide phases. *Miner. Deposita* **44**, 523–557.

McClung, C.R., Gutzmer, J., Beukes, N.J., Mezger, K., Strauss, H. & Gertloff, E. (2007) Geochemistry of bedded barite of the Mesoproterozoic Aggeneys-Gamsberg Broken Hill-type district, South Africa. *Miner. Deposita* **42**, 537–549.

McCready, A.J., Parnell, J. & Castro, L. (2003) Crystalline placer gold from the Rio Neuquen, Argentina: implications for the gold budget in placer gold formation. *Economic Geol.* **98**, 623–633.

McDonald, I. & Tredoux, M. (2005) The history of the Waterberg deposit: why South Africa's first platinum mine failed. *Applied Earth Sci.* **114**, 264–272.

McElroy, M.B., Xi Lu, Nielsen, C.P. & Yuxuan Wang (2009) Potential for wind-generated electricity in China. *Science* **325**, 1378–1380.

McGowan, R.R., Roberts, S. & Boyce, A.J. (2006) Origin of the Nchanga copper-cobalt deposits of the Zambian copperbelt. *Miner. Deposita* **40**, 617–638.

McGowan, R.R., Roberts, S., Foster, R.P., *et al.* (2003) Origin of the copper-cobalt deposits of the Zambian Copperbelt: an epigenetic view from Nchanga. *Geology* **31**, 497–500.

McInnes, B.I.A., McBride, J.S., Evans, N.J., *et al.* (1999) Osmium isotope constraints on ore metal recycling in subduction zones. *Science* **286**, 512–516.

McIntosh, J.C., Walter, L.M. & Martini, A.M. (2004) Extensive microbial modification of formation water geochemistry: case study from a Midcontinent sedimentary basin, United States. *GSA Bull.* **116**, 743–759.

McKelvey, V.E. (1973) *Mineral Resource Estimates and Public Policy*. Prof. Paper USGS 820.

McKenzie, J.A. & Vasconcelos, C. (2008) Dolomite Mountains and the origin of the dolomite rock of which they mainly consist: historical developments and new perspectives. *Sedimentology* **56**, 205–219.

McKibben, M.A., Williams, A.E. & Hall, G.E.M. (1990) Solubility and transport of platinum-group elements and Au in saline hydrothermal fluids: constraints from geothermal brine data. *Economic Geol.* **85**, 1926–1934.

McKinstry, H.E. (1948) *Mining Geology*. 680 pp. Prentice Hall.

McNaughton, N.J., Mueller, A.G. & Groves, D.I. (2005) The age of the giant Golden Mile deposit, Kalgoorlie, Western Australia: Ion-microprobe zircon and monazite U-Pb geochronology of a synmineralization lamprophyre dike. *Economic Geol.* **100**, 1427–1440.

Meadows, D. L. *et al.* (1974) *The Limits to Growth. A Report for the Club of Rome's Project on the Predicament of Mankind*, 2nd edn. 205 pp. Universe Books, New York.

Meccheri, M., Molli, G., Conti, P., Blasi, P. & Vaselli, L. (2007) The Carrara marbles (Alpi Apuane, Italy): a geological and economical updated review. *Z. dt. Ges. Geowiss.* **158**, 719–735.

Medwedev, P., Philippov, M., Romashkin, A. & Vavra, N. (2001) Primary organic matter and lithofacies of siliceous shungite rocks from Karelia. *N. Jb. Geol. Paläont. Mh.* **2001/11**, 641–658.

Meer, F. van der, van Dijk, P., van der Werff, H. & Yang, H. (2002) Remote sensing and petroleum seepage: a review and case study. *Terra Nova* **14**, 1–17.

Meier, D.L., Heinrich, C.A. & Watts, M.A. (2009) Mafic dikes displacing Witwatersrand gold reefs: Evidence against metamorphic-hydrothermal ore formation. *Geology* **37**, 607–610.

Melcher, F., Grum, W., Thalhammer, T.V. & Thalhammer, O.A.R. (1999) The giant chromite deposits at Kempirsai, Urals: constraints from trace element (PGE, REE) and isotope data. *Miner. Deposita* **34**, 250–272.

Melchiorre, E.B. & Enders, M.S. (2003) Stable isotope geochemistry of copper carbonates at the northwest extension deposit, Morenci district, Arizona: implications for conditions of supergene oxidation and related mineralization. *Economic Geol.* **98**, 607–62.

Melchiorre, E.B. & Williams, P.A. (2001) Stable isotope characterization of the thermal profile and subsurface biological activity during oxidation of the Great Australia deposit, Cloncurry, Queensland, Australia. *Economic Geol.* **96**, 1685–1693.

Melezhik, V.A., Filippov, M.M. & Romashkin, A.E. (2004) A giant Paleoproterozoic deposit of shungite in NW Russia: genesis and practical applications. *Ore Geol. Rev.* **24**, 135–154.

Melezhik, V.A., Fallick, A.E., Medvedev, P.V. & Makarikhin, V.V. (2001) Paleoproterozoic magnesite: lithological and isotopic evidence for playa/sabkha environments. *Sedimentology* **48**, 379–397.

Menard, J.-J. (1995) Relationship between altered pyroxene diorite and the magnetite mineralization in the Chilean Iron Belt, with emphasis on the El Algarrobo iron deposits (Atacama region, Chile). *Miner. Deposita* **30**, 268–274.

Merkel, B.J., Planer-Friedrich, B. & Wolkersdorfer, C. (eds) (2002) *Uranium in the Aquatic Environment*. 1112 pp + CD, Springer.

Meyers, S.R. (2008) Resolving Milankovitchian controversies: The Triassic Latemar limestone and the Eocene Green River Formation. *Geology* **36**, 319–322.

Mezeme, E.B., Faure, M., Chen, Y., Corcherie, A. & Talbot, J.-Y. (2007) Structural, AMS and geochronological study of a laccolith emplaced during Late Variscan orogenic extension: the Rocles pluton, (SE French Massif Central). *Int. J. Earth Sci.* **96**, 215–228.

Miall, A.D. (2000) *Principles of Sedimentary Basin Analysis*, 3rd edn. 490 pp. Springer.

Miall, A.D. (1997) *The Geology of Stratigraphic Sequences*. 433 pp. Springer.

Miall, A.D. (1996) *The Geology of Fluvial Deposits*. 586 pp. Springer.

Michalski, S.R. & Gray, R.E. (2001) Ash disposal – mine fires – environment: an Indian dilemma. *Bull. Eng. Env.* **60**, 23–29.

Michel, B., Thiébaut, J. & Wackenheim, C. (2003) Intérêt de la minéralogie des granulats dans la connaissance des risques de l'alcali-réaction. *Bull Eng Geol Env* **62**, 145–153.

Michel, J.-P. (1996) Guides et méthodes de l'exploration diamantifère. *Chronique rech. min.* **522**, 29–38.

Middelaar, van, W.T. & Keith, J.D. (1990) Mica chemistry as an indicator of oxygen and halogen fugacities in the CanTung and other W-related granitoids in the North American Cordillera. *GSA Spec. Paper* **246**, 205–220.

Migdisov, A.A., Williams-Jones, A.E. & Suleimenov, O.M. (1999) Solubility of chlorargyrite (AgCl) in water vapor at elevated temperatures and pressures. *Geochim. Cosmochim. Acta* **63**, 3817–3827.

Miguel, M.-C., Vespignani, A., Zapperi, S., *et al.* (2001) Intermittent dislocation flow in viscoplastic deformation. *Nature* **410**, 667–671.

Miles, J.A. (1994) *Illustrated Glossary of Petroleum Geochemistry*. 137 pp. Oxford University Press.

Milham, L. & Craw, D. (2009) Antimony mobilisation through two contrasting gold ore processing systems, New Zealand. *Mine Water Environ* **28**, 136–145.

Miller, W., Alexander, R., Chapman, N., McKinley, I. & Smellie, J. (2000) *Geological Disposal of Radioactive Wastes and Natural Analogues – Lessons from Nature and Archaeology*. 316 pp. Pergamon.

Milsom, J. (1996) *Field Geophysics*, 2nd edn, 187 pp. The Geological Field Guide Series, Wiley.

Min, M., XU, H. Chen, J. & Fayek, M. (2005) Evidence of uranium biomineralization in sandstone-hosted roll-front uranium deposits, northwestern China. *Ore Geol. Rev.* **26**, 198–206.

Minghai, Cai, Jingwen, Mao, Ting, Liang, Pirajno, F. & Huilan, Huang (2007) The origin of the Tongkeng-Changpo tin deposit, Dachang metal district, Guangxi, China: clues from fluid inclusions and He isotope systematics. *Miner. Deposita* **42**, 613–626.

Mingram, B., Hoth, P., Lüders, V. & Harlov, D. (2005) The significance of fixed ammonium in Paleozoic sediments for the generation of nitrogen-rich natural gases in the North German Basin. *Int. J. Earth Sci.* **94**, 1010–1022.

Minter, W.E.L., Hill, W.C.N., Kidger, R.J., *et al.* (1986) The Welkom gold field. Pp 497–539 in C.R. Anhäusser & S. Maske (Eds), *Mineral Deposits of Southern Africa*. Geol. Soc. S. Africa, Johannesburg.

Mintova, S., Olson, N.H., Valtchev, V. & Bein, Th. (1999) Mechanism of zeolite A nanocrystal growth from colloids at room temperature. *Science* **283**, 958–960.

Miranda-Gasca, M.A., Gomez-Caballero, J.A. & Eastoe, C.J. (1998) Borate deposits of northern Sonora, Mexico: stratigraphy, tectonics, stable isotopes, and fluid inclusions. *Economic Geol.* **93**, 510–523.

Mistry, M., Goetz, H. & Meyer, F.M. (1999) Compilation of Key Lake's ore reserve models during exploration, development and mining. *Erzmetall* **52**, 653–658.

Mitchell, R.H. (1991) Kimberlites and lamproites: primary sources of diamond. *Geosci. Canada* **18**, 1–16.

Mitchell, R.H. (1986) *Kimberlites: Mineralogy, Geochemistry and Petrology*. 442 pp. Plenum.

Mlynarczyk, M.S.J., Sherlock, R.L. & Williams-Jones, A.E. (2003) San Rafael, Peru: geology and structure of the worlds richest tin lode. *Miner. Deposita* **38**, 555–567.

Mohr, M., Warren, J.K., Kukla, P.A., Urai, J.L. & Irmen, A. (2007) Subsurface seismic record of salt glaciers in an extensional intracontinental setting (Late Triassic of northwestern Germany). *Geology* **35**, 963–966.

Moine, B., Fortune, J.P., Moreau, Ph. & Viguier, F. (1989) Comparative mineralogy, geochemistry, and conditions of formation of two metasomatic talc and chlorite deposits: Trimouns (Pyrenees, France) and Rabenwald (Eastern Alps, Austria). *Economic Geol.* **84**, 1398–1416.

Molina, J.A., Oyarzun, R., Esbrí, J.M. & Higueras, P. (2006) Mercury accumulation in soils and plants in the Almadén mining district, Spain: one of the most contaminated sites on Earth. *Environmental Geochemistry Health* **28**, 487–498.

Möller, P., Cerny, P. & Saupe, F. (eds) (1989) *Lanthanides, Tantalum and Niobium*. SGA Spec. Publ. 7, 380 pp, Springer.

Monecke, T., Gemmell, J.B. & Herzig, P.M. (2006) Geology and volcanic facies architecture of the Lower Ordovician Waterloo massive sulfide deposit, Australia. *Economic Geol.* **101**, 179–197.

Mongenot, T., Tribovillard, N.-P., Desprairies, A., *et al.* (1996) Trace elements as paleoenvironmental markers in strongly mature hydrocarbon source rocks: the Cretaceous La Luna formation of Venezuela. *Sediment. Geol.* **103**, 23–27.

Moon, C., Whateley, M. & Evans, A.M. (eds) (2006) *Introduction to Mineral Exploration*, 2nd edn. 498 pp. Wiley-Blackwell.

Moore, A.E. (2009) Type II diamonds: Flamboyant Megacrysts? *South African J. Geology* **112**, 23–38.

Moore, D.E. & Rymer, M.J. (2007) Talc-bearing serpentinite and the creeping section of the San Andreas fault. *Nature* **448**, 795–797.

Moore, J.N., Powell, Th.S., Heizler, M.T. & Norman, D.I. (2000) Mineralization and hydrothermal history of the Tiwi geothermal system, Philippines. *Economic Geol.* **95**, 1001–1023.

Moore, T.A. & Shearer, J.C. (2003) Peat/coal type and depositional environment – are they related? *Int. J. Coal Geol.* **56**, 233–252.

Moore, T.A., Shearer, J.C., & Miller, S.L. (1996) Fungal origin of oxidised plant material in the Palankaraya peat deposit, Kalimantan Tengah, Indonesia: Implications for "inertinite" formation in coal. *Int. J. Coal Geol.* **30**, 1–23.

Moores, E.M. & Fairbridge, R.W. (eds) (1997) *Encyclopedia of European and Asian Regional Geology*. 825 pp, Chapman & Hall/Springer.

Moosbrugger, V., Gee, C.T., Belz, G. & Ashraf, A.R. (1994) Three-dimensional reconstruction of an in-situ Miocene peat forest from the Lower Rhine embayment, northwestern Germany – new methods in paleovegetation analysis. *Paleogeography, Paleoclimatology, Paleoecology* **110**, 295–317.

Morelli, R., Creaser, R.A., Seltmann, R., Stuart, F.M., Selby, D. & Graupner, T. (2007) Age and source constraints for the giant Muruntau gold deposit, Uzbekistan, from coupled Re-Os-He isotopes in arsenopyrite. *Geology* **35**, 795–798.

Morey, G.B. (1992) Chemical composition of the Eastern Biwabik iron-formation (Early Proterozoic), Mesabi Range, Minnesota. *Economic Geol.* **87**, 1649–1658.

Morford, J.L. & Emerson, S.R. (1999) The geochemistry of redox sensitive trace metals in sediments. *Geochim. Cosmochim. Acta* **63**, 1735–1750.

Morozumi, H., Ishikawa, N. & Ishikawa, Y. (2007) Relationship between Kuroko mineralization and paleostress inferred from vein deposits and Tertiary granitic rocks in and around the Hokuroku District, northeast Japan. *Economic Geol.* **101**, 1345–1357.

Morris, R.C. (2003) Iron ore genesis and post-ore metasomatism at Mount Tom Price. *Applied Earth Sci.* **112**, 56–67.

Morris, R.C. (1993) Genetic modelling for banded iron-formation of the Hamersley Group, Pilbara Craton, Western Australia. *Prec. Research* **60**, 243–286.

Morris, R.C. (1985) Genesis of iron ore in banded iron-formation by supergene and supergene-metamorphic processes – a conceptual model. Pp 73–235 in K.H. Wolf (Ed.), *Handbook of Stratabound and Stratiform Ore Deposits*, Vol. 13, Elsevier.

Morrison, G.W., Rose, W.J. & Jaireth, S. (1991) Geological and geochemical controls on the silver content (fineness) of gold in gold-silver deposits. *Ore Geol. Rev.* **6**, 333–364.

Morteani, G., Preinfalk, C. & Horn, A.H. (2000) Classification and mineralization potential of the pegmatites of the Eastern Brazilian pegmatite province. *Miner. Deposita* **35**, 638–655.

Mossman, D.J., Minter, W.E.L., Dutkiewicz, A., *et al.* (2008) The indigenous origin of Witwatersrand "carbon". *Precambrian Research* **164**, 173–186.

Mossman, D.J. & Nagy, B. (1996) Solid bitumens: an assessment of their characteristics, genesis, and role in geological processes. *Terra Nova* **8**, 114–128.

Mountain, B.W. & Seward, T.M. (1999) The hydrosulfide/sulfide complexes of copper(I): Experimental determination of stoichiometry and stability at 22 °C and reassessment of high temperature data. *Geochim. Cosmochim. Acta* **63**, 11–29.

Moure, T. & Enami, M. (2008) Areal extent of eclogite facies metamorphism in the Sanbagawa belt, Japan: new evidence from a Raman microprobe study of quartz residual pressure. *Geology* **36**, 503–506.

Moyen, J.-F., Stevens, G. & Kisters, A. (2006) Record of mid-Archaean subduction from metamorphism in the Barberton terrain, South Africa. *Nature* **442**, 559–562.

Muchez, P. & Stassen, P. (2006) Multiple origin of the "Kniest feeder zone" of the stratiform Zn-Pb-Cu ore deposit of Rammelsberg, Germany. *Miner. Deposita* **41**, 46–51.

Muchez, P., Vanderhaeghen, P., El Desouky, H., *et al.* (2008) Anhydrite pseudomorphs and the origin of stratiform Cu-Co ores in the Catangan Copperbelt (Democratic Republic of Congo). *Miner. Deposita* **43**, 575–589.

Mücke, A. & Chaudhuri, J.N.B. (1991) The continuous alteration of ilmenite through pseudorutile to leukoxene. *Ore Geol. Rev.* **6**, 25–44.

Mücke, A. & Farshad, F. (2005) Whole rock and mineralogical composition of Phanerozoic ooidal ironstones: comparison and differentiation of types and subtypes. *Ore Geol. Rev.* **26**, 227–262.

Mücke, A., Dzigbodi-Adjimah, K. & Annor, A. (1999) Mineralogy, petrography, geochemistry and genesis of the Paleoproterozoic Birimian manganese formation of Nsuta/Ghana. *Miner. Deposita* **34**, 297–311.

Mueller, A.G., Hall, G.C., Nemchin, A.A. & O'Brien, D. (2008) Chronology of the Pueblo Viejo gold-silver deposit, Dominican Republic: formation in an Early Cretaceous intra-oceanic island arc and burial under ophiolite. *Miner. Deposita* **43**, 873–889.

Muggeridge, M.T. (1995) Pathfinder sampling techniques for locating primary sources of diamond: recovery of indicator minerals, diamonds, and geochemical signatures. *J. Geochem. Explor.* **53**, 182–204.

Mukhopadhyay, P.K. (1992) Maturation of organic matter as revealed by microscopic methods: applications and limitations of vitrinite reflectance, and continuous spectral and pulsed laser fluorescence spectroscopy. In: *Diagenesis III, Developments in Sedimentology* (eds K.H. Wolf & G.V. Chilingarian), **47**, 435–510.

Müller, A., Ihlen, P.M., Wanvik, J.E. & Flem, B. (2007) High-purity quartz mineralisation in kyanite quartzites, Norway. *Miner. Deposita* **42**, 523–535.

Müller, A.G., Nemchin, A.A. & Frei, R. (2004) The Nevoria gold skarn deposit, Southern Cross greenstone belt, Western Australia: II. Pressure-temperature-time path and relationship to postorogenic granites. *Economic Geol.* **99**, 453–478.

Müller, D., Kaminski, K., Uhlig, S., *et al.* (2002) The transition from porphyry to epithermal-style gold mineralization at Ladolam, Lihir island, Papua New Guinea: a reconnaissance study. *Miner. Deposita* **37**, 61–74.

Müller, S.G., Krapez, B., Barley, M.E. & Fletcher, I.R. (2005) Giant iron-ore deposits of the Hamersley province related to the breakup of Paleoproterozoic Australia: new insights from in situ SHRIMP dating of baddeleyite from mafic intrusions. *Geology* **33**, 577–580.

Mullis, J. (1996) P-T-t path of quartz formation in extensional veins of the Central Alps. Schweiz. *Mineral. Petrogr. Mitt.* **76**, 159–164.

Mungall, J.E. (2002) Roasting the mantle: slab melting and the genesis of major Au and Au-rich Cu deposits. *Geology* **30**, 915–918.

Munoz, M., Premo, W.R. & Courjault-Radé, P. (2005) Sm-Nd dating of fluorite from the worldclass Montroc fluorite deposit, southern Massif Central, France. *Miner. Deposita* **39**, 970–975.

Munoz, M., Courjault-Radé, P. & Tollon, P. (1992) The massive stibnite veins of the French Paleozoic basement: a metallogenic marker of Late Variscan brittle extension. *Terra Nova* **4**(2), 171–177.

Muntean, J.L. & Einaudi, M.T. (2000) Porphyry gold deposits of the Refugio district, Maricunga belt, northern Chile. *Economic Geol.* **95**, 1445–1472.

Mustard, R., Ulrich, Th., Kamenetsky, V.S. & Mernagh, T. (2006) Gold and metal enrichment in natural granitic melts during fractional crystallization. *Geology* **34**, 85–88.

Mutlu, H., Sariiz, K. & Kadir, S. (2005) Geochemistry and origin of the Saphane alunite deposit, Western Anatolia, Turkey. *Ore Geol. Rev.* **26**, 39–50.

Muzikar, P., Elmore, D. & Granger, D.E. (2003) Accelerator mass spectroscopy in geologic research. *GSA Bull.* **115**, 643–654.

Nabelek, P.I. (1997) Quartz-sillimanite leucosomes in high-grade schists, Black Hills, South Dakota: a perspective on the mobility of Al in high-grade metamorphic rocks. *Geology* **25**, 995–998.

Nabelek, P.I. (2007) Fluid evolution and kinetics of metamorphic reactions in calc-silicate contact aureoles – from H_2O to CO_2 and back. *Geology* **35**, 927–930.

Naden, J., Kilias, S.P. & Darbyshire, D.P.F. (2005) Active geothermal systems with entrained seawater as modern analogs for transitional volcanic-hosted massive sulfide and continental magmato-hydrothermal mineralization. The example of Milos Island, Greece. *Geology* **33**, 541–544.

Nadon, G.C. (1998) Magnitude and timing of peat-to-coal compaction. *Geology* **26**, 727–730.

Nagaseki, H. & Hayashi, K. (2008) Experimental study of the behavior of copper and zinc in a boiling hydrothermal system. *Geology* **36**, 27–30.

Nahnybida, T., Gleeson, S.A., Rusk, B.G. & Wassenaar, L.I. (2009) Cl/Br ratios and stable chlorine isotope analysis of magmatic-hydrothermal fluid inclusions from Butte, Montana and Bingham Canyon, Utah. *Miner. Deposita* **44**, 837–848.

Nakashima, S., Disnar, J.-R. & Perruchot, A. (1999) Precipitation kinetics of uranium by sedimentary organic matter under diagenetic and hydrothermal conditions. *Economic Geol.* **94**, 993–1006.

Naldrett, A.J. (2010) Secular variation of magmatic sulfide deposits and their source magmas. *Economic Geol.* **105**, 669–688.

Naldrett, A.J. (2004) *Magmatic Sulfide Deposits – Geology, Geochemistry and Exploration*. 728 pp. Springer.

Naldrett, A.J. (1999) World-class Ni-Cu-PGE deposits: key factors in their genesis. *Miner. Deposita* **34**, 227–240.

Naldrett, A.J. & Ch. Li (eds) (2000) A special issue on Voisey's Bay Ni-Cu-Co deposit. *Economic Geol.* **95**(4), 915.

Naldrett, A.J., Wilson, A., Kinnaird, J. & Chunnet, G. (2009) PGE tenor and metal ratios within and below the Merensky Reef, Bushveld Complex: Implications for its genesis. *J. of Petrology* **50**, 625–659.

Nalpas, T. & Brun, J.-P. (1993) Salt flow and diapirism related to extension at crustal scale. *Tectonophysics* **228**, 349–362.

Naslund, H.R. (1983) The effect of oxygen fugacity on liquid immiscibility in iron bearing silicate melts. *American J. Sci.* **283**, 1034–1059.

Nawrocki, J. (2000) Clay mineralogy, crystallinity, and K-Ar ages of illites within the Polish Zechstein basin: implications for the age of Kupferschiefer mineralization – a discussion. *Economic Geol.* **95**, 241–242.

Neng Jiang, Xuelei Chu, Toshio Misuta, Daizo Ishiyama & Jiguang Mi (2004) A magnetite-apatite deposit in the Fanshan alkaline ultramafic complex, northern China. *Economic Geol.* **99**, 397–408.

Nesbitt, H.W. (1979) Mobility and fractionation of rare earth elements during weathering of a granodiorite. *Nature* **279**, 206–210.

Neubauer, F., Lips, A., Kouzmanov, K., Lexa, J. & Ivascanu, P. (2005) Subduction, slab detachement and mineralization: the Neogene in the Apuseni Mountains and Carpathians. *Ore Geology Rev.* **27**, 13–44.

Neubauer, F., Genser, J. & Handler, R. (2000) The Eastern Alps: result of a two-stage collision process. *Mitteilungen Österr. Geol. Ges.* **92**, 117–134.

Neubert, N., Nägler, T.F. & Böttcher, M.E. (2008) Sulfidity controls molybdenum fractionation into euxinic sediments: evidence from the Black Sea. *Geology* **36**, 775–778.

Neuendorf, K.K.E., Mehl, J.P. & Jackson, J.A. (eds) (2005) *Glossary of Geology*, 5th edn. 779 pp. American Geological Institute.

Neuzil, C.E. (2000) Osmotic generation of "anomalous" fluid pressures in geological environments. *Nature* **403**, 182–184.

Newman, D.K. (2010) Feasting on minerals. *Science* **327**, 793–794.

Nichols, G. (2009) *Sedimentology and Stratigraphy*, 2nd edn. 432 pp. Wiley-Blackwell.

Nicholson, K. (1992) Contrasting mineralogical-geochemical signatures of manganese oxides: guides to metallogenesis. *Economic Geol.* **87**, 1253–1264.

Nicolescu, S., Cornell, D.H. & Bojar, A.-V. (1999) Age and tectonic setting of Bocsa and Ocna de Fier-Dognecea granodiorites (SW Romania) and of associated skarn mineralisation. *Miner. Deposita* **34**, 743–753.

Nieto, A. & Bascetin, A. (2006) Mining cutoff grade strategy to optimise NPV based on multiyear GRG iterative factor. *Mining Technology* **115**, 59–64.

Niggli, P. (1948) *Gesteine und Minerallagerstätten*. Bd. I, 540 pp, Birkhäuser.

Nironen, M. (1997) The Svecofennian orogen: a tectonic model. *Precambrian Res.* **86**, 21–44.

Noble, E.A. (1963) Formation of ore deposits by water of compaction. *Economic Geol.* **58**, 1145–1156.

Nordhaus, W. (2007) Critical assumptions in the Stern review on climate change. *Science* **317**, 201–202.

Nordstrom, D.K. (2002) Worldwide occurrences of arsenic in groundwater. *Science* **296**, 2143–2145.

Nordstrom, D.K. & Southam, G. (1997) *Geomicrobiology of Sulfide Mineral Oxidation.* In: *Geomicrobiology: Interactions between Microbes and Minerals* (eds J.F. Banfield & K.H. Nealson), pp. 361–390. Mineralogy Society of America.

Nordin, W. (2009) The effect of downhole uncertainty on modelled volume. *Proc. 7th Int. Mining Geol. Conf. 2009*. pp. 81–84. AusIMM, Melbourne.

Normile, D. (2009) Round and round: a guide to the carbon cycle. *Science* **325**, 1642–1643.

Nöth, S., Karg, H. & Littke, R. (2001) Reconstruction of Late Paleozoic heat flows and burial histories at the Rhenohercynian-Subvariscan boundary, Germany. *Int. J. Earth Sci.* **90**, 234–256.

Notholt, A.J.G., Highley, D.E. & Deans, T. (1990) Economic minerals in carbonatites and associated alkaline igneous rocks. *Transact. Instn. Min. Metall. B* **99**, 59–80.

Nozaki Tatsuo, Nakamura Kentaro, Awaji Shunsaku & Kato Yasuhiro (2008) Whole-rock geochemistry of basic schists from the Besshi Area, Central Shikoku: Implications for the tectonic setting of the Besshi sulfide deposit. *Resource Geology* **56**, 423–432.

Nriagou, J.O. & Nieboer, E. (1988) *Chromium in the Natural and Human Environments*. 496 pp. Wiley, New York.

Nyström, J.O. & Henriquez, F. (1994) Magmatic features of iron ores of the Kiruna type in Chile and Sweden: ore textures and magnetite geochemistry. *Economic Geol.* **89**, 820–839.

Oates, J.A.H. (1998) *Lime and Limestone: Chemistry znd Technology, Production and Uses*. 455 pp. Wiley-VCH.

Oberthür, T., Weiser, T.W. & Gast, L. (2003) Geochemistry and mineralogy of platinum-group elements at Hartley platinum mine, Zimbabwe. *Miner. Deposita* **38**, 344–355.

Obradovic, J., Stamatakis, M.G., Anicic, St. & Economou, G. (1992) Borate and borosilicate deposits in the Miocene Jarandol basin, Serbia, Yugoslavia. *Economic Geol.* **87**, 2169–2174.

Ochs, F.A. & Lange, R.A. (1999) The density of hydrous magmatic liquids. *Science* **283**, 1314–1317.

Ochsenius, C. (1877) *Die Bildung der Steinsalzlager und ihrer Mutterlaugensalze unter spezifischer Berücksichtigung der Flöze von Douglashall in der Egeln'schen Mulde*. 173 pp. Pfeffer, Halle.

Oelkers, E.H. & Helgeson, H.C. (1993) Calculation of dissociation constants and the relative stability of polynuclear clusters of 1:1 electrolytes in hydrothermal solutions at supercritical pressures and temperatures. *Geochim. Cosmochim. Acta* **57**, 2673–269.

Oen, I.S. & Lustenhouwer, W.J. (1992) Cl-rich biotite, Cl-K hornblende, and Cl-rich scapolite in meta-exhalites: Nora, Bergslagen, Sweden. *Economic Geol.* **87**, 1638–1648.

Oftedahl, C. (1958) A theory of exhalative-sedimentary ores. *Geol. Foren. Stockholm Forh.* **80**, 1–19.

Ogawa, Y., Shikazono, N., Ishiyama, D., Sato, H. & Mizuta, T. (2005) An experimental study on felsic rock-artificial seawater interaction: implications for hydrothermal alteration and sulfate formation in the Kuroko mining area of Japan. *Miner. Deposita* **39**, 813–821.

Okita, P.M. (1992) Manganese carbonate mineralization in the Molango District, Mexico. *Economic Geol.* **87**, 1345–1366.

Olah, G. A., Goeppert, A. & Surya Prakash, G.K. (2006) *Beyond Oil and Gas: The Methanol Economy*. 290 pp. Wiley-VCH.

Ohmoto, H. (2003a) Banded iron formations and the evolution of the atmosphere, hydrosphere, biosphere and lithosphere. *Applied Earth Sci.* **112**, B161–162.

Ohmoto, H. (2003b) Nonredox transformation of magnetite-hematite in hydrothermal systems. *Economic Geol.* **98**, 157–161.

Ohmoto, H. (1996) Formation of volcanogenic massive sulfide deposits: the Kuroko perspective. *Ore Geol. Rev.* **10**, 135–177.

Ohmoto, H., Watanabe, Y., Ikemi, H. Poulson, S.R. & Taylor, B.E. (2006) Sulphur evidence for an oxic Archean atmosphere. *Nature* **442**, 908–911.

Ohnenstetter, M., Johan, Z., Cocherie, A., *et al.* (1999) New exploration methods for platinum and rhodium deposits poor in base-metal sulphides – NEXTPRIM. *Trans. Instn. Min. Metall. B* **108**, 119–150.

Okamoto, A. & Tsuchiya, N. (2009) Velocity of vertical fluid ascent within vein-forming fractures. *Geology* **37**, 563–566.

Oliver, J. (1986) Fluids expelled tectonically from orogenic belts: their role in hydrocarbon migration and other geologic phenomena. *Geology* **14**, 99–102.

Oliver, N.H.S., McLellan, J.G., Hobbs, B.E., *et al.* (2006) Numerical models of extensional deformation, heat transfer, and fluid flow across basement-cover interfaces during basin-related mineralisation. *Economic Geol.* **101**, 1–31.

Ollas, M., Cerón, J.C., Fernández, I., Moral, F. & Rodriguez-Ramirez, A. (2005) State of contamination of the waters in the Guadiamar valley five years after the Aznalcollar spill. *Water Air Soil Pollution* **166**, 103–119.

Olsen, P.E. (1999) Giant lava flows, mass extinctions, and mantle plumes. *Science* **284**, 604–605.

Omar, S.A.S., Bhat, N.R. & Asem, A. (2009) Critical assessment of the environmental consequences of the invasion of Kuwait, the Gulf War, and the aftermath. Pp 141–170 in *Handbook of Environmental Chemistry*, Vol. U3, Springer.

Omichinski, J.G. (2007) Toward methylmercury bioremediation. *Science* **317**, 205–206.

Onasch, C.M. & Vennemann, T.W. (1995) Disequilibrium partitioning of oxygen isotopes associated with sector zoning in quartz. *Geology* **23**, 1103–1106.

Ondruš, P., Veselovsky, F., Gabašova, A., Hloušek, J. & Šrein, V. (2003) Geology and hydrothermal vein system of the Jachymov (Joachimsthal) ore district. *J. Czech Geol. Soc.* **48**, 3–18.

Oppliger, G.L., Murphy, J.B. & Brimhall, G.H. (1997) Is the ancestral Yellowstone hotspot responsible for the Tertiary "Carlin" mineralization in the Great Basin of Nevada? *Geology* **25**, 627–630.

Oremland, R.S. & Stolz, J.F. (2003) The ecology of arsenic. *Science* **300**, 939–943.

Oreskes, N., Shrader-Frechette, K., Belitz, K. (1994) Verification, validation, and confirmation of numerical models in the earth sciences. *Science* **263**, 641–646.

Osinski, G.R. (2005) Hydrothermal activity associated with the Ries impact event, Germany. *Geofluids* **5**, 202–220.

Orszulik, S.T. (ed.) (2008) *Environmental Technology in the Oil Industry*. 2nd ed., 408 pp, Springer.

Oszczepalski, S. (2000) Origin of the Kupferschiefer polymetallic mineralization in Poland. *Miner. Deposita* **34**, 599–613.

Owens, B.E. & Pasek, M.A. (2007) Kyanite quartzites in the Piedmont province of Virginia: evidence for a possible high-sulfidation system. *Economic Geol.* **102**, 495–509.

Oyarzun, R., Oyarzun, J., Menard, J.J. & Lillo, J. (2003) The Cretaceous iron belt of northern Chile: role of oceanic plates, a superplume vent, and a major shear zone. *Miner. Deposita* **38**, 640–646.

Ozdemir, E. (2009) Modeling of coal bed methane (CBM) production and CO_2 sequestration in coal seams. *Int. J. Coal Geology* **77**, 145–152.

Pagé, P. & Barnes, S.-J. (2009) Using trace elements in chromites to constrain the origin of podiform chromitites in the Thetford mines ophiolite, Québec, Canada. *Economic Geol.* **104**, 997–1018.

Page, B.W., Stevens, B.P.J. & Gibson, G.M. (2005) Geochronology of the sequence hosting the Broken Hill Pb-Zn-Ag orebody, Australia. *Economic Geol.* **100**, 633–661.

Palmer, C.A. & Lyons, P.C. (1997) Selected elements in major minerals from bituminous coal as determined by INAA: implications for removing environmentally sensitive elements from coal. *Int. J. Coal Geol.* **32**, 151–166.

Palmer, D.A.S. & Williams-Jones, A.E. (1996) Genesis of the carbonatite-hosted fluorite deposit at Amba Dongar, India: evidence from fluid inclusions, stable isotopes, and whole-rock-mineral geochemistry. *Economic Geol.* **91**, 934–950.

Palmer, M.A. & Filoso, S. (2009) Restoration of ecosystem services for environmental markets. *Science* **325**, 575–576.

Palmer, M.R. & Ernst, G.G.J. (1998) Generation of hydrothermal megaplumes by cooling of pillow basalts at mid-ocean ridges. *Nature* **393**, 643–647.

Pan, Y. & Dong, P. (1999) The Lower Changjiang (Yangzi/Yangtze River) metallogenic belt, east central China: intrusion and wall-rock hosted Cu-Fe-Au, Mo, Zn. Pb, Ag deposits. *Ore Geol. Rev.* **15**, 177–242.

Panda, S.K., Andersson, J.T. & Schrader, W. (2009) Characterization of supercomplex crude oil mixtures: What is really in there? *Angewandte Chemie Int. Ed.* **48**, 1788–1791.

Paquette, J.-L. & Cluzel, D. (2007) U-Pb zircon dating of post-obduction volcanic arc granotoids and a granulite-facies xenolith from New Caledonia. Inference on Southwest Pacific geodynamic models. *Int. J. Earth Sci.* **96**, 613–622.

Paradis, S. & Lavoie, D. (1996) Multiple-stage diagenetic alteration and fluid history of Ordovician carbonate-hosted barite mineralization, Southern Quebec Appalachians. *Sed. Geol.* **107**, 121–139.

Parafiniuk, J., Kowalski, W. & Halas, S. (1994) Stable isotope geochemistry and the genesis of the Polish native sulphur deposits – a review. *Geological Quarterly (Warsaw)* **38**, 473–496.

Parnell, J. (1996) Phanerozoic analogues for carbonaceous matter in Witwatersrand ore deposits. *Economic Geol.* **91**, 55–62.

Parnell, J., Ruffell, A.H., Monson, B. & Mutterlose, J. (1996) Petrography and origin of deposits at the Bentheim bitumen mine, northwestern Germany. *Miner. Deposita* **31**, 104–112.

Parr, J.M., Stevens, B.P.J., Carr, G.R. & Page, R.W. (2004) Subseafloor origin for Broken Hill Pb-Zn-Ag mineralization, New South Wales, Australia. *Geology* **32**, 589–592.

Parris, T.M., Burrus, R.C. & O'Sullivan, P.B. (2003) Deformation and the timing of gas generation and migration in the eastern Brooks Range foothills, Arctic National Wildlife Refuge, Alaska. *AAPG Bulletin* **87**, 1823–1846.

Parsons, M.B. & Percival, J.B. (eds) (2005) Mercury sources, cycles, and effects. *Mineral. Ass. Canada Short Course 34*. 297 pp.

Partey, F., Lev, S., Casey, R., Widom, E., Lueth, V.W. & Rakovan, J. (2009) Source of fluorine and petrogenesis of the Rio Grande Rift-type barite-fluorite-galena deposits. *Economic Geol.* **104**, 505–520.

Partington, G.A., McNaughton, N.J. & Williams, I.S. (1995) A review of the geology, mineralization, and geochronology of the Greenbushes pegmatite, Western Australia. *Economic Geol.* **90**, 616–635.

Pašava, J., Oszczepalski, S. & Du, A. (2010) Re-Os age of non-mineralized black shale from the Kupferschiefer, Poland, and implications for metal enrichment. *Miner. Deposita* **45**, 189–199.

Pašava, J., Kribek, B., Dobes, P. *et al.* (2003) Tin-polymetallic sulfide deposits in the eastern part of the Dachang tin field (South China) and the role of black shales in their origin. *Miner. Deposita* **38**, 39–66.

Paton, C., Hergt, J.M., Phillips, D., Woodhead, J.D. & Shee, S.R. (2007) New insights into the genesis of Indian kimberlites from the Dharwar Craton via in situ Sr isotope analysis of groundmass perovskite. *Geology* **35**, 1011–1014.

Patrier, P., Beaufort, D., Bril, H., *et al.* (1997) Alteration-mineralization at the Bernardan U deposit (Western Marche, France): the contribution of alteration petrology and crystal chemistry of secondary phases to a new genetic model. *Economic Geol.* **92**, 448–467.

Patterson, B.M., Robertson, B.S., Woodbury, R.J., Talbot, B. & Davis, G.B. (2006) Long-term evaluation of a composite cover overlaying a sulfidic tailings facility. *Mine Water Environ* **25**, 137–145.

Pavlov, A.L., Khomenko, A.V. & Gordeeva, A.O. (2005) Trappean magmatism as the basic cause of coal metamorphism and hydrocarbon generation in the Tungus Basin. *J. Mining Sci.* **41**, 558–565.

Paxton, S.T., Szabo, J.O., Adjukiewicz, J.M. & Klimentidis, R.E. (2002) Construction of an intragranular volume compaction curve for evaluating and predicting compaction and porosity loss in rigid-grain sandstone reservoirs. *AAPG Bull.* **86**, 2047–2067.

Paytan, A., Kastner, M., Campbell, D. & Thiemens, M.H. (2004) Seawater sulfur isotope fluctuations in the Cretaceous. *Science* **304**, 1636–1665.

Paytan, A., Mearon, S., Cobb, K. & Kastner, M. (2002) Origin of marine barite deposits: Sr and S isotope characterization. *Geology* **30**, 747–750.

Peabody, C.E. & Einaudi, M.T. (1992) Origin of petroleum and mercury in the Culver-Baer cinnabar deposit, Mayacmas District, California. *Economic Geol.* **87**, 1078–1103.

Peach, C.J. (1991) Influence of deformation on the fluid transport properties of salt rocks. *Geologica Ultraiectina* 77, 238 pp, Utrecht.

Peach, C.L., Mathez, E.A. & Keays, R.R. (1990) Sulfide melt – silicate melt distribution coefficients for noble metals and other chalcophile elements as deduced from MORB: implications for partial melting. *Geochim. Cosmochim. Acta* **54**, 3379–3389.

Pearce, J.A. (1982) Trace element characteristics of lavas from destructive plate boundaries. In: *Andesites* (ed. R.S. Thorpe), pp 525–548. Wiley.

Pearce, J.A., Harris, N.B.W. & Tindle, A.G. (1984) Trace element discrimination diagrams for the tectonic interpretation of granitic rocks. *J. Petrology* **25**, 956–983.

Pearton, T.N. & Viljoen, M.J. (1986) Antimony mineralization in the Murchison Greenstone Belt – an overview. In: *Mineral Deposits of Southern Africa*. Vol. I (eds C.R. Anhäusser & S. Maske), pp. 293–320. Geol. Soc. S. Africa, Johannesburg.

Peccerillo, A. (1992) Potassic and ultrapotassic rocks: Compositional characteristics, petrogenesis, and geological significance. *Episodes* **15**, 243–251.

Pecher, I.A. (2002) Gas hydrates on the brink. *Nature* **420**, 622–623.

Peltonen, P., Kontinen, A., Huhma, H. & Kuronen, U. (2008) Outokumpu revisited: New mineral deposit model for the mantle peridotite-associated Cu–Co–Zn–Ni–Ag–Au sulphide deposits. *Ore Geol. Rev.* **33**, 559–617.

Peng, Bo & Frei, R. (2004) Nd-Sr-Pb isotopic constraints on metal and fluid sources in W-Sb-Au mineralization at Woxi and Liaojiaping (Western Hunan, China). *Miner. Deposita* **39**, 313–327.

Peng, Q.M. & Palmer, M.R. (1995) The Paleoproterozoic boron deposits in eastern Liaoning, China: a metamorphosed evaporite. *Precambrian Res*. **72**, 185–197.

PERC – Pan-European Reserves and Resources Reporting Committee (2008) The PERC Reporting Code 2008. 38 pp, URL http://www.vmine.net/percreserves/index.htm accessed June 2010.

Perez Xavier, R., Wiedenbeck, M., Trumbull, R.B., *et al.* (2008) Tourmaline B-isotopes fingerprint marine evaporites as the source of high-salinity ore fluids in iron oxide copper-gold deposits, Carajás Mineral Province (Brazil). *Geology* **36**, 743–746.

Perthuisot, V. & Rouvier, H. (1992) Les diapirs du Maghreb central et oriental: des appareils variés, résultats d'une évolution structurale et pétrogénétique complexe. *Bull. Soc. géol. France* **163**, 751–760.

Peryt, T.M. (1996) Sedimentology of Badenian (middle Miocene) gypsum in eastern Galicia, Podolia and Bukovina (West Ukraine). *Sedimentology* **43**, 571–588.

Peters, E.K. (1991) Gold-bearing hot springs systems of the Northern Coast Ranges, California. *Economic Geol*. **86**, 1519–1528.

Peters, K.E. & Fowler, M.G. (2002) Applications of petroleum geochemistry to exploration and reservoir management. *Organic Geochem*. **33**, 5–36.

Petersen, S., Herzig, P.M. & Hannington, M.D. (2000) Third dimension of a presently forming VMS deposit: TAG hydrothermal mound, Mid-Atlantic Ridge, 26 °N. *Miner. Deposita* **35**, 233–259.

Petrascheck, W.E. (1965) Typical features of metallogenic provinces. *Economic Geol*. **60**, 1620–1634.

Petrascheck, W.E. (1954) Zur optischen Regelung tektonisch beanspruchter Kohlen. *Tschermaks Min. Petr. Mitt.* **4**, 232–239.

Petrov, N.N. (1998) Epigenetic stratified-infiltration uranium deposits of Kazakhstan (in Russian). *Geology of Kazakhstan* **2**(354), 22–39.

Petruk, W. (2000) *Applied Mineralogy in the Mining Industry*. 268 pp. Elsevier.

Pettke, T., Diamond, L.W. & Villa, I.M. (1999) Mesothermal gold veins and metamorphic devolatilization in the northwestern Alps: the temporal link. *Geology* **27**, 641–644.

Petts, G.E., Coats, J.S. & Hughes, N. (1991) Freeze-sampling method of collecting drainage sediments for gold exploration. *Trans. Instn. Min. Metall. B* **100**, 28–32.

Philippe, Y. (1994) Trasfer zone in the southern Jura thrust belt (eastern France): geometry, development and comparison with analogue modelling experiments. In: *Exploration and Petroleum Geology of France.*(ed. A. Mascle), pp. 327–346. EAPG Memoir 4.

Philippot, P., Van Zuilen, M., Lepot, K., Thomazo, C., Farquhar, J. & Van Kranendonk, M.J. (2007) Early Archean microorganisms preferred elemental sulfur, not sulfate. *Science* **317**, 1534–1537.

Phillips, G.H. & Evans, K.A. (2004) Role of CO_2 in the formation of gold deposits. *Nature* **429**, 860–863.

Phillips, G.N. & Hughes, M.J. (1996) The geology and gold deposits of the Victorian gold province. *Ore Geol. Rev.* **11**, 255–302.

Phillips, S., Bustin, R.M. & Lowe, R.E. (1994) Earthquake-induced flooding of a tropical coastal peat swamp: A modern analogue for high-sulfur coals? *Geology* **22**, 929–932.

Pi, T., Solé, J. & Taran, Y. (2005) (U-Th)/^{4}He dating of fluorite: application to the La Azul fluorspar deposit in the Taxco mining district, Mexico. *Miner. Deposita* **39**, 976–982.

Piestrzynski, A. (1990) Uranium and thorium in the Kupferschiefer formation, Lower Zechstein, Poland. *Miner. Deposita* **25**, 146–151.

Piestrzynski, A., Pieczonka, J. & Gluszek, A. (2002) Redbed type gold mineralisation, Kupferschiefer, southwest Poland. *Miner. Deposita* **37**, 512–528.

Pilet, S., Baker, M.B. & Stolper, E.M. (2008) Metasomatized lithosphere and the origin of alkaline lavas. *Science* **320**, 916–919.

Pine, R.J., Berger, E., Hammett, R.D. & Artigiani, E. (2006) Vitipeno mine, Italy – underground mining for marble. *Mining Technology* **113**, 142–152.

Piper, D.Z. & Link, P.K. (2002) An upwelling model for the Phosphoria sea: A Permian, ocean-margin sea in the northwest United States. *AAPG Bull.* **86**, 1217–1235.

Pitard, F.F. (1993) *Pierre Gy's Sampling Theory and Sampling Practice*, 2nd edn. 488 pp. RC Press.

Pitcairn, I.K., Teagle, D.A.H., Craw, D., Olivo, G.R., Kerrich, R. & Brewer, T.S. (2006) Sources of metals and fluids in orogenic gold deposits: insights from the Otago and Alpine Schists, New Zealand. *Economic Geol*. **101**, 1525–1546.

Pitcher, W.S. (1997) *The Nature and Origin of Granite*. 2nd Ed., 387 pp, Chapman & Hall.

Plant, J.A., Korre, A., Reeder, S., Smith, B. & Voulvoulis, N. (2005) Chemicals in the environment: implications for global sustainability. *Applied Earth Sci.* **114**, B65–97.

Plant, J.A., Stone, P., Flight, D.M.A. *et al.* (1997) Geochemistry of the British Caledonides: the setting for metallogeny. *Trans. Instn. Min. Metall. B* **106**, 67–78.

Plant, J.A., O'Brien, C., Tarney, J. & Hurdley, J. (1985) Geochemical criteria for the recognition of high heat production granites. Pp 87–98 in: C. Halls (ed.), *High Heat Production (HHP) Granites, Hydrothermal Circulation and Ore Genesis*. IMM London.

Plimer, I.R. (2009) Heaven + Earth – Global warming: The missing science. 503 pp, Connor Court.

Plimer, I.R. (1985) Broken Hill Pb-Zn-Ag deposit - a product of mantle metasomatism. *Miner. Deposita* **20**(3), 147–153.

Plumlee, G.S. & Logsdon, M.J. (eds) (1999a) The environmental geochemistry of mineral deposits. *Rev. Economic Geol.* 6A, 583 pp.

Plumlee, G.S. & Logsdon, M.J. (1999b) An earth-system science toolkit for environmentally friendly mineral resource development. In: The Environmental Geochemistry of Mineral Deposits (eds G.S. Plumlee and M.J. Logsdon), pp. 1–27. *Rev. Economic Geol.*

Plumlee, G.S., Goldhaber, M.B. & Rowan, E.L. (1995) The potential role of magmatic gases in the genesis of Illinois-Kentucky fluorspar deposits: implications from chemical reaction path modelling. *Economic Geol.* **90**, 999–1011.

Plumlee, G.S., Leach, D.L., Hofstra, A.H., *et al.* (1994) Chemical reaction path modeling of ore deposition in Mississippi Valley type Pb-Zn deposits of the Ozark region, US midcontinent. *Economic Geol.* **89**, 1361–1381.

Pogue, J.E. (1917) The emerald deposits of Muzo, Colombia. *Trans. Am. Inst. Mining Eng.* **55**, 1–43.

Pohl, W. (2005) *Mineralische und Energie-Rohstoffe: Eine Einführung zur Entstehung und nachhaltigen Nutzung von Lagerstätten*. 5th ed., 527 pp, Schweizerbart.

Pohl, W. (1994) Metallogeny of the northeastern Kibara belt, Central Africa – recent perspectives. *Ore Geol. Rev.* **9**, 105–130.

Pohl, W. (1992) Defining metamorphogenic mineral deposits – an introduction. *Mineralogy & Petrology* **45**, 145–152.

Pohl, W. (1990) Genesis of magnesite deposits – models and trends. *Geol. Rundschau* **79**(2), 291–299.

Pohl, W. (1968) *Zur Geologie und Paläogeographie der Kohlenmulden des Hausruck (Oberösterreich)*. 70 pp. Notring, Wien.

Pohl, W. & Belocky, R. (1994) Alpidic metamorphic fluids and metallogenesis in the Eastern Alps. *Mitt. Österr. Geol. Ges.* **86**, 141–152.

Pohl, W. & Belocky, R. (1999) Metamorphism and metallogeny in the Eastern Alps. *Miner. Deposita* **34**, 614–629.

Pohl, W. & Siegl, W. (1986) Sediment-hosted magnesite deposits. Pp 223–310 in K.H. Wolf (Ed.), *Handbook of Strata-Bound and Stratiform Ore Deposits*, Vol.14, Elsevier.

Pohl, W., Amouri, M., Kolli, O., *et al.* (1986) A new genetic model for the North African metasomatic siderite deposits. *Miner. Deposita* **21**, 228–233.

Pohl, W., Horkel, A., Neubauer, W., *et al.* (1980) Notes on the Geology and Mineral Resources of the Mtito Andei-Taita Area (Southern Kenya). *Mitt. Geol. Ges. Österr.* **73**, 135–152, 1 map 1:50,000, Vienna.

Pokrovski, G.S., Roux, J. & Harrichoury, J.-C. (2005) Fluid density control on vapor-liquid partitioning of metals in hydrothermal systems. *Geology* **33**, 657–660.

Pokrovski, G.S., Zakirov, I.V., Roux, J., *et al.* (2002) Experimental study of arsenic speciation in vapor phase to 500 °C: implications for As transport and fractionation in low-density crustal fluids and volcanic gases. *Geochim. Cosmochim. Acta* **66**, 3453–3480.

Polgari, M., Okita, P.M. & Hein, J.R. (1991) Stable isotope evidence for the origin of the Urkut manganese ore deposit, Hungary. *J. Sedim. Petrol.* **61**(3), 384–393.

Pollack, H.N. & Chapman, D.S. (1977) On the regional variation of heatflow, geotherms and lithospheric thickness. *Tectonophysics* **38**, 279–296.

Pollard, P.J. (2006) An intrusion-related origin for Cu-Au mineralization in iron oxide-copper-gold (IOCG) provinces. *Miner. Deposita* **41**, 179–187.

Pollastro, R.M., Jarvie, D.M., Hill, R.J. & Adams, C.W. (2007) Geologic framework of the Mississippian Barnett Shale, Barnett-Paleozoic total petroleum system, Bend Arch – Fort Worth Basin, Texas. *AAPG Bull.* **91**, 405–436.

Polya, D.A., Foxford, K.A., Stuart, F., Boyce, A. & Fallick, A.E. (2000) Evolution and paragenetic context of low δD hydrothermal fluids from the Panasqueira W-Sn deposit, Portugal: new evidence from microthermometric, stable isotope, noble gas and halogen analyses of primary fluid inclusions. *Geochim. Cosmochim. Acta* **64**, 3357–3371.

Polyak, V.J., McIntosh, W.C., Güven, N. & Provencio, P. (1998) Age and origin of Carlsbad cavern and related caves from ^{40}Ar/^{39}Ar of alunite. *Science* **279**, 1919–1921.

Porrenga, D.H. (1967) Glauconite and chamosite as depth indicators in the marine environment. *Marine Geol.* **5**, 495–501.

Posth, N.R., Hegler, F., Konhauser, K.O. & Kappler, A. (2008) Alternating Si and Fe deposition caused by temperature fluctuations in Precambrian oceans. *Nature Geosci.* **1**, 703–708.

Potma, W., Roberts, P.A., Schaubs, P.M., *et al.* (2008) Predictive targeting in Australianorogenic-gold systems at the deposit to district scale using numerical modelling. *Australian J. Earth Sci.* **55**, 101–122.

Potter, E.G. & Taylor, R.P. (2009) The lead isotope composition of ore minerals from precious metal-bearing, polymetallic vein systems in the Cobalt Embayment, Northern Ontarion: Metallogenetic implications. *Economic Geol.* **104**, 869–879.

Potter, J., Siemann, M.G. & Tsypukow. M. (2004) Large-scale carbon isotope fractionation in evaporites and the generation of extremely ^{13}C-enriched methane. *Geology* **32**, 533–536.

Potter, M. (2002) Palladium soil geochemistry, Baronskoye Pd-Au prospect, Sverdlowsk oblast, Russia. *Transact. IMM London* **111**, B58–64.

Potter, R.W.I., Clynne, M.A. & Brown, D.L. (1978) Freezing point depression of aqueous sodium chloride solutions. *Economic Geol.* **90**, 2156–2186.

Powell, W.G., Johnston, P.A., Collom, C.J. & Johnston, K.J. (2006) Middle Cambrian brine seeps on the Kicking Horse rim and their relationship to talc and magnesite mineralisation and associated dolomitization, British Columbia, Canada. *Economic Geol.* **101**, 431–451.

Prendergast, M.D. (2008) Archean komatiitic sill-hosted chromite deposits in the Zimbabwe Craton. *Economic Geol.* **103**, 981–1004.

Prendergast, M.D. (2003) The nickeliferous late Archean Reliance komatiitic event in the Zimbabwe craton – magmatic architecture, physical volcanology, and ore genesis. *Economic Geol.* **98**, 865–891.

Prendergast, M., Bennet, M. & Henicke, G. (1998) Platinum exploration in the Rinçon del Tigre Complex, eastern Bolivia. *Transactions IMM London* **107**, B39–47.

Prichard, H.M., Neary, C.R., Fisher, P.C. & O'Hara, M.J. (2008) PGE-rich podiform chromitites in the Al 'Ays ophiolite complex, Saudi Arabia: An example of critical mantle melting to extract and concentrate PGE. *Economic Geol.* **103**, 1507–1529.

Primel, L. & Tourenq, C. (2000) *Aggregates – Geology, Prospection, Environment, Testing, Extraction, Specifications, Processing Plants, Equipment, Quality*. 516 pp. Balkema.

Prochaska, W. (1989) Geochemistry and genesis of Austrian talc deposits. *Applied Geochem.* **4**, 511–525.

Prochaska, W., Huber, M. & Bechtel, A. (1997) Die alpidische Leukophyllitbildung am Alpenostrand. *Archiv Lagerstättenforschung Geol. B.-A. Wien* **20**, 37–52.

Proskurowski, G., Lilley, M.D., Seewald, J.S., *et al.* (2008) Abiogenic hydrocarbon production at Lost City hydrothermal field. *Science* **319**, 604–607.

Provan, D.M.J. (1992) Draugen oil field, Haltenbanken province, offshore Norway. In: *Giant Oil and Gas Fields of the Decade 1978–1988* (ed. M.T. Halbouty), pp. 371–382. AAPG, Tulsa.

Pueyo, J.J., Chong, G. & Jensen, A. (2001) Neogene evaporites in desert volcanic environments: Atacama desert, northern Chile. *Sedimentology* **48**, 1411–1431.

Querol. X., Whateley, M.K.G., Fernandez-Turiel, J.L. & Tuncali, E. (1997) Geological controls on the mineralogy and geochemistry of the Beypazari lignite, central Anatolia, Turkey. *Intern. J. Coal Geol.* **33**, 255–271.

Railsback, L.B. (2003) An earth scientist's periodic table of the elements and their ions. *Geology* **31**, 737–740.

Raimbault, L., Cuney, M., Azancott, C., *et al.* (1995) Geochemical evidence for a multistage magmatic genesis of Ta-Sn-Li mineralization in the granite at Beauvoir, French Massif Central. *Economic Geol.* **90**, 548–576.

Raith, J.G. & Stein, H.J. (2006) Variscan ore formation and metamorphism at the Felbertal scheelite deposit (Austria): constraining tungsten mineralisation from Re–Os dating of molybdenite. *Contrib. Miner. Petrol.* **152**, 505–521.

Ramdohr, P. (1980) *The Ore Minerals and Their Intergrowths*. 2nd ed., 1205 pp, Pergamon.

Ranville, J.F. & Schmiermund, R.L. (1999) General aspects of aquatic colloids in environmental geochemistry. In: *The Environmental Geochemistry of Mineral Deposits* (eds G.S. Plumlee & M.J. Logsdon), pp. 183–199. *Rev. Economic Geol. 6A*.

Rao, C.R.M., Sahuquillo, A. & Lopez Sanchez, J.F. (2008) A review of the different methods applied in environmental geochemistry for single and sequential extraction of trace elements in soils and related materials. *Water Air Soil Pollution* **189**, 291–333.

Rasmussen, B. (2005) Evidence for pervasive petroleum generation and migration in 3.2 and 2.63 Ga shales. *Geology* **33**, 497–500.

Rasmussen, B., Fletcher, I.R., Muhling, J.R., Mueller, A.G. & Hall, G.C. (2007) Bushveld-aged fluid flow, peak metamorphism, and gold mobilization in the Witwatersrand basin, South Africa: Constraints from in situ Shrimp U-Pb dating of monazite and xenotime. *Geology* **35**, 931–934.

Rasmussen, B., Fletcher, I.R. & Sheppard, S. (2005) Isotopic dating of the migration of a low-grade metamorphic front during orogenesis. *Geology* **33**, 773–776.

Ray, G.E., Webster, I.C.L. & Ettlinger, A.D. (1995) The distribution of skarns in British Columbia and the chemistry and ages of their related plutonic rocks. *Economic Geol.* **90**, 920–937.

Rayner, R.J. (1996) The paleoclimate of the Karroo: evidence from plant fossils. *Paleogeography, Paleoclimatology, Paleoecology* **119**, 385–394.

Reed, C.P. & Wallace, M.W. (2004) Zn-Pb mineralisation in the Silvermines district, Ireland: a product of burial diagenesis. *Miner. Deposita* **39**, 87–102.

Reich, M., Palacios, C., Vargas, G., *et al.* (2009) Supergene enrichment of copper deposits since the onset of modern hyperaridity in the Atacama Desert, Chile. *Miner. Deposita* **44**, 497–504.

Reich, M., Palacios, C., Parada, M.A., *et al.* (2008) Atacamite formation by deep saline waters in copper deposits from the Atacama Desert, Chile: evidence from fluid inclusions, groundwater geochemistry, TEM, and ^{36}Cl data. *Miner. Deposita* **43**, 663–675.

Reimann, C. & Caritat, P. de (1998) *Chemical Elements in the Environment: Factsheets for the Geochemist and Environmental Scientist*. 398 pp, Springer.

Reimann, C., Melezhig, V. & Niskavaara, H. (2007) Low-density regional geochemical mapping of gold and palladium highlighting the exploration potential of northernmost Europe. *Economic Geol.* **102**, 327–334.

Reinhard, Ch.T., Raiswell, R., Scott, C., Anbar, A.D. & Lyons, T.W. (2009) A Late Archean sulfidic sea stimulated by early oxidative weathering of the continents. *Science* **326**, 713–716.

Reith, F., Fairbrother, L., Nolze, G.,Wilhelmi, O., Clode, P.L., Gregg, A., Parsons, J.E., Wakelin, St. A., Pring, A., Hough, R., Southam, G. & Brugger, J. (2010) Nanoparticle factories: Biofilms hold the key to gold dispersion and nugget formation. *Geology* **38**, 843–846.

Relvas, J.M.R.S., Barriga, F.J.A.S., Ferreira, A., Noiva, P.C., Pacheco, N. & Barriga, G. (2006) Hydrothermal alteration and mineralization in the Neves-Corvo volcanic-hosted massive sulfide deposit, Portugal. I. Geology, mineralogy, and geochemistry. *Economic Geol.* **101**, 753–790.

Rempe, N.T. (ed.) (2008) Deep geologic repositories. *GSA Rev. Eng. Geol.* **19**, 119.

Rendu, J.-M. (2008) *An Introduction to Cut-Off Grade Estimation*. 112 pp, Society for Mining Metallurgy & Exploration (SME).

Rentzsch, J., Franzke, H.J., & Friedrich, G. (1997) Die laterale Verbreitung der Erzmineralassoziationen im deutschen Kupferschiefer. *Z. geol. Wiss.* **25**, 141–149.

Ressel, M.W. & Henry, C.D. (2006) Igneous geology of the Carlin Trend, Nevada: Development of the Eocene Plutonic Complex and significance for Carlin-type gold deposits. *Economic Geol.* **101**, 347–383.

Retallack, G.J. (2010) Lateritization and bauxitization events. *Economic Geol.* **105**, 655–667.

Retallack, G.J. (2001) A 300-million-year record of atmospheric carbon dioxide from fossil plant cuticles. *Nature* **411**, 287–290.

Reynolds, B.C., Wasserburg, G.J. & Baskaran, M. (2003) The transport of U- and Th-series nuclides in sandy confined aquifers. *Geochim. Cosmochim. Acta* **67**, 1955–1972.

Rice, A. & von Gruenewaldt, G. (1994) Convective scavenging and cascade enrichment in Bushveld Complex melts: possible mechanism for concentration of platinum-group elements and chromite in mineralized layers. *Trans. Instn. Min. Metall. B* **103**, 31–38.

Rice, D.D. & Schoell, M. (eds) (1995) Processes of natural gas formation. *Special Issue of Chemical Geology* **126**, 3–4.

Richards, F.C. & Bourg, A.C. (1991) Aqueous geochemistry of chromium: a review. *Water Research* **27**, 807–816.

Richards, I.G., Palmer, J.P. & Barrat, P.A. (1993) *The Reclamation of Former Coal Mines and Steel Works*. 718 pp, Elsevier.

Richards, J.P. (2009) Postsubduction porphyry Cu-Au and epithermal Au deposits: Products of remelting of subduction-modified lithosphere. *Geology* **37**, 247–250.

Richards, J.P. (2003) Tectono-magmatic precursors for porphyry Cu-(Mo-Au) deposit formation. *Economic Geol.* **98**, 1515–1533.

Richards, K.S. & Reddy, K.R. (2007) Critical appraisal of piping phenomena in earth dams. *Bull. Eng. Geol. Environ.* **66**, 381–402.

Richardson, S.H., Harris, J.W. & Gurney, J.J. (1993) Three generations of diamonds from old continental mantle. *Nature* **366**, 256–258.

Rickers, K., Thomas, R. & Heinrich, W. (2006) The behaviour of trace elements during the chemical evolution of the H_2O-, B-, and F-rich granite-pegmatite-hydrothermal system at Ehrenfriedersdorf, Germany: a SXRF study of melt and fluid inclusions. *Miner. Deposita* **41**, 229–245.

Ridge, J.D. (1990) *Annotated Bibliographies of Mineral Deposits in Europe, Including Selected Deposits in the USSR*. 2 Vols., 1285 pp, Pergamon.

Rimoldi, B., Alexander, J. & Morris, S. (1996) Experimental turbidity currents entering density-stratified water: analogues for turbidites in Mediterranean hypersaline basins. *Sedimentology* **43**, 527–540.

Rimstidt, J.D. & Vaughan, D.J. (2003) Pyrite oxidation: a state-of-the-art assessment of the reaction mechanism. *Geochim. Cosmochim. Acta* **67**, 873–880.

Ripley, E.M., Sarkar, A. & Li, C. (2005) Mineralogic and stable isotope studies of hydrothermal alteration at the Jinchuan Ni-Cu deposit, China. *Economic Geol.* **100**, 1349–1361.

Ritcey, G.M. (1990) *Tailings Management*. 1000 pp. Elsevier.

Robb, L.J. (2005) *Introduction o Ore-Forming Processes*. 373 pp. Blackwell.

Robb, L.J. & Meyer, F.M. (1995) The Witwatersrand Basin, South Africa: Geological framework and mineralization processes. *Ore Geol. Rev.* **10**, 67–94.

Robert, F. & Chaussidon, M. (2006) A paleotemperature curve for the Precambrian oceans based on silicon isotopes in cherts. *Nature* **443**, 969–972.

Roberts, H.H. & Carney, R.S. (1997) Evidence of episodic fluid, gas, and sediment venting on the northern Gulf of Mexico continental slope. *Economic Geol.* **92**, 863–879.

Roberts, M.D., Oliver, N.H.S., Fairclough, M.C., *et al.* (2003) Geochemical and oxygen isotope signature of seafloor alteration associated with a polydeformed and highly metamorphosed massive sulfide deposit, Ruostesuo, Central Finland. *Economic Geol.* **98**, 535–556.

Roberts, S., Sanderson, D.J. & Gumiel, P. (1998) Fractal analysis of Sn-W mineralization from Central Iberia: insights into the role of fracture connectivity in the formation of an ore deposit. *Economic Geol.* **93**, 360–365.

Roberts, S.M. & Spencer, R.J. (1995) Paleotemperatures preserved in fluid inclusions in halite. *Geochim. Cosmochim. Acta* **59**, 3929–3942.

Roedder, E. (1984) Fluid inclusions. *Rev. in Miner.* **12**, 644.

Rollinson, H. (1997) The Archean komatiite-related Inyala chromitite, Southern Zimbabwe. *Economic Geol.* **92**, 98–107.

Rombouts, L. (2003) Assessing the diamond potential of kimberlites from discovery to evaluation bulk sampling. *Miner. Deposita* **38**, 496–504.

Romer, R.L., Novaczyk, N. & Wirth, R. (2007) Secondary Fe-Mn-oxides in minerals heavily damaged by α-recoil: possible implications for paleomagnetism. *Int. J. Earth Sci.* **96**, 375–387.

Romer, R.L., Martinsson, O. & Perdahl, J.-A. (1994) Geochronology of Kiruna iron ores and hydrothermal alterations. *Economic Geol.* **89**, 1249–1261.

Rondenay, S., Abers, G.A. & van Keken, P.E. (2008) Seismic imaging of subduction zone metamorphism. *Geology* **36**, 275–278.

Rosière, C.A., Baars, F.J., Seoane, J.C.S., *et al.* (2006) Structure and iron mineralisation of the Carajás Province. *Applied Earth Sci.* **115**, 126–133.

Ross, J.V. & Bustin, R.M. (1997) Vitrinite anisotropy resulting from simple shear experiments at high temperature and high confining pressure. *Int. J. Coal Geol.* **33**, 153–168.

Ross, M. (1999) *The Health Effects of Mineral Dusts*. In: *The Environmental Geochemistry of Mineral Deposits* (eds G.S. Plumlee & M.J. Logsdon), pp. 339–356. *Rev. Economic Geol. 6A*.

Rouchy, J.-M. & Blanc-Valleron, M.M. (2006) *Les évaporites, matériaux singuliers, milieux extrêmes*. 216 pp, Vuibert & Société géologique de France.

Routhier, P. (1980) Oú sont les métaux pour l'avenir? Essai d'une métallogénie globale. *Mém. BRGM 105*, 408 pp. Orléans.

Routhier, P. (1963) *Les gisements métallifères. Géologie et principes de recherche*. 2 vols. 1282 pp. Masson.

Rouvier, H., Perthuisot, V. & Mansouri, A. (1985) Pb-Zn deposits and salt-bearing diapirs in Southern Europe and North Africa. *Economic Geol.* **80**, 666–687.

Rouxel, O.J., Bekker, A. & Edwards, K.J. (2005) Iron isotope constraints on the Archean and Paleoproterozoic ocean redox state. *Science* **307**, 1088–1091.

Rowan, E.L., Goldhaber, M.B. & Hatch, J.R. (2002) Regional fluid flow as a factor in the thermal history of the Illinois basin: constraints from fluid inclusions and the maturity of Pennsylvanian coals. *AAGP Bull.* **86**, 257–277.

Rowley, D.B., Raymond, A., Parrish, J.T., Scotese, C.R. & Ziegler, A.M. (1985) Carboniferous paleogeographic, phytogeographic, and paleoclimatic reconstructions. *Int. J. Coal Geology* **5**, 7–42.

Roy, P.S., Whitehouse, J., Cowell, P.J. & Oakes, G. (2000) Mineral sands occurrences in the Murray Basin, Southeastern Australia. *Economic Geol.* **95**, 1107–1128.

Roy, S. (1992) Environments and processes of manganese deposition. *Economic Geol.* **87**, 1218–1236.

Royer, D.L., Berner, R.A. & Park, J. (2007) Climate sensitivity constrained by CO_2 concentrations over the past 420 million years. *Nature* **446**, 530–532.

Royle, M. (2007) Giant Mine: identification of inflow water types and preliminary geochemical monitoring during reflooding. *Mine Water Environ* **26**, 102–109.

Rucker, D.F., Glaser, D.R., Osborne, T. & Maehl, W.C. (2009) Electrical resisitivity characterisation of a reclaimed gold mine to delineate acid rock drainage pathways. *Mine Water Environ* **28**, 146–157.

Ruckmick, J.C., Wimberly, B.H. & Edwards, A.F. (1979) Classification and genesis of biogenic sulfur deposits. *Economic Geol.* **74**, 469–474.

Rudenno, V. (1999) *The Mining Valuation Handbook*. 247 pp. Wrightbooks.

Ruffell, A.H., Moles, N.R. & Parnell, J. (1998) Characterisation and prediction of sediment-hosted ore deposits using sequence stratigraphy. *Ore Geol. Rev.* **12**, 207–223.

Ruitenbeek, F.J.A. van, Cudahy, T., Hale, M. & Meer, F. D. van der (2005) Tracing fluid pathways in fossil hydrothermal systems with near-infrared spectroscopy. *Geology* **33**, 597–600.

Rush, P.M. & Seegers, H.J. (1990) Ok Tedi copper-gold deposits. In: *Geology of the Mineral Deposits of Australia and Papua New Guinea*. 2 Vols (ed. F.E. Hughes), pp 1747–1754. AusIMM, Parkville.

Rusk, B. & Reed, M. (2002) Scanning electron microcope-cathodoluminescence analysis of quartz reveals complex growth histories in veins from the Butte porphyry copper deposit, Montana. *Geology* **30**, 727–730.

Rusk, B.G., Reed, M.H. & Dilles, J.H. (2008) Fluid inclusion evidence for magmatic-hydrothermal fluid evolution in the porphyry copper-molybdenum deposit at Butte, Montana. *Economic Geol.* **103**, 307–334.

Russell, M.J., Hall, A.J., Boyce, A.J. & Fallick, A.E. (2005) On hydrothermal convection systems and the emergence of life. *Economic Geol.* **100**, 419–438.

Russell, P.L. (1990) *Oil Shales of the World – Their Origin, Occurrence and Exploitation*. 753 pp. Pergamon.

Ryan, W.B.F. (2009) Decoding the Mediterranean salinity crisis. *Sedimentology* **56**, 95–136.

Sabins, F.F. (1999) Remote sensing for mineral exploration. *Ore Geol. Rev.* **14**, 157–183.

Sachsenhofer, R.F. (2000) Geodynamic controls on deposition and maturation of coal in the Eastern Alps. *Mitt. österr. geol. Ges.* **92**, 185–194.

Sadooni, F.N. & Alsharhan, A.S. (2003) Stratigraphy, microfacies, and petroleum potential of the Mauddud Formation (Albian-Cenomanian) in the Arabian Gulf basin. *AAPG Bull.* **87**, 1653–1680.

Saikia, K. & Sarkar, B.C. (2006) Exploration drilling optimisation using geostatistics: a case in Jharia coalfield, India. *Applied Earth Sci.* **115**, 13–22.

Saint John, D.A., Poole, A.B. & Sims, I. (1998) *Concrete Petrography*. 488 pp. Arnold Publishers.

Samson, I., Anderson, A. & Marshall, D. (eds) (2003) Fluid inclusions – analysis and interpretation. *Mineral. Assoc. Canada Short Course 32*, 374 pp.

Samson, I.M., Williams-Jones, A.E., Ault, K.M. Gagnon, J.E. & Fryer, B.J. (2008) Source of fluids forming distal Zn-Pb-Ag skarns: evidence from laser ablation-inductively coupled plasma-mass spectrometry analysis of fluid inclusions from El Mochito, Honduras. *Geology* **36**, 947–950.

Sanford, R.F. (1990) Hydrogeology of an ancient arid closed basin; implications for tabular sandstone-hosted uranium deposits. *Geology* **18**, 1099–1102.

Sangster, D.F. (2002) The role of dense brines in the formation of vent-distal sedimentary-exhalative (sedex) lead-zinc deposits: field and laboratory evidence. *Miner. Deposita* **37**, 149–157.

Sass-Gustkiewicz, M. (1996) Internal sediments as a key to understanding the hydrothermal karst origin of the Upper Silesian Zn-Pb ore deposits. *Economic Geol. Spec. Pub.* **4**, 171–181.

Sassier, C., Boulvais, P., Gapais, D. & Diot, H. (2006) From granitoid to kyanite-bearing micaschist during fluid-assisted shearing. *Int. J. Earth Sci.* **95**, 2–18.

Sato, M. (1992) Persistency-field Eh-pH diagrams for sulfides and their application to supergene oxidation and enrichement of sulfide ore bodies. *Geochim. Cosmochim. Acta* **56**, 3133–3156.

Sawkins, F.J. (1990a) Integrated tectonic-genetic model for volcanic-hosted massive sulfide deposits. *Geology* **18**, 1061–1064.

Sawkins, F.J. (1990b) *Metal Deposits in Relation to Plate Tectonics*, 2nd edn. 461 pp, Springer.

Saxton, J., Fralick, P., Panu, U. & Wallace, K. (2008) Density segregation of minerals during high-velocity transport over a rough bed: Implications for the formation of placers. *Economic Geol.* **103**, 1657–1664.

Schaad, W. (1995) Die Entstehung von Rauhwacken durch die Verkarstung von Gips. *Eclogae geol. Helv.* **88**, 59–90.

Schaap, A.D. (1990) Weipa kaolin and bauxite deposits. In: *Mineral Deposits of Australia and Papua New Guinea* (ed. F. E. Hughes), pp. 1699–1673. AusIMM, Melbourne.

Schäfer, A., Utescher, T., Klett, M., Valdivia-Manchego, M. (2005) The Cenozoic Lower Rhine Basin – rifting, sedimentation, and cyclic stratigraphy. *Int. J. Earth Sci.* **94**, 621–639.

Schärer, U., de Parseval, Ph., Polve, M. & de Saint Blanquat, M. (1999) Formation of the Trimouns talc-chlorite deposit (Pyrenees) from persistent hydrothermal activity between 112 and 97 Ma. *Terra Nova* **11**, 30–37.

Scharlemann, J.P.W. & Laurance, W.F. (2008) How green are biofuels? *Science* **319**, 43–44.

Schauberger, O. (1986) Bau und Bildung der Salzlagerstätten des ostalpinen Salinars. *Archiv Lagerstättenforschung Geol. B.-A.* **7**, 217–254.

Schellart, W.P., Freeman, J., Stegman, D.R., Moresi, L. & May, D. (2007) Evolution and diversity of subduction zones controlled by slab width. *Nature* **446**, 308–311.

Schimmelmann, A., Lewan, M.D. & Wintch, R.P. (1999) D/H isotope ratios of kerogen, bitumen, oil and water in hydrous pyrolysis of source rocks containing kerogen types I, II, IIS, and III. *Geochim. Cosmochim. Acta* **63**, 3751–3766.

Schippers, A., Neretin, L.N., Kallmeyer, J., *et al.* (2005) Prokaryotic cells of the deep sub-seafloor biosphere identified as living bacteria. *Nature* **433**, 861–864.

Schlepp, L., Landais, P., Elie M. & Faure, P. (2001) Influence of paleoenvironment and radiolytic alteration on the geochemistry of organic matter from Autunian shales of the Lodève uranium deposit, France. *Bull. Soc. géol. France* **172**, 99–109.

Schlömer, S. & Krooss, B.M. (1998) Experimental characterisation of the hydrocarbon sealing efficiency of cap rocks. *Marine Petrol. Geol.* **14**, 565–580.

Schmid, S. & Wiegand, J. (2003) Radionuclide contamination of surface waters, sediments, and soil caused by coal mining activities in the Ruhr District (Germany). *Mine Water Environ* **22**, 130–140.

Schmidt, A.P. (2000) Naturally occurring radioactive materials in the gas and oil industry. *Geologica Ultraiectina* **195**, 144 pp.

Schmidt-Mumm, A., Oberthür, T., Vetter, U. & Blenkinsop, T.G. (1997) High CO_2 content of fluid inclusions in gold mineralisations in the Ashanti Belt, Ghana: a new category of ore forming fluids? *Miner. Deposita* **32**, 107–118.

Schmincke, H.-U., Park, C. & Harms, E. (1999) Evolution and environmental impacts of the eruption of Laacher See Volcano (Germany) 12,900 a BP. *Quaternary Intern.* **61**, 61–72.

Schneider, F. & Wolf, J. (2000) Quantitative HC potential evaluation using 3D basin modelling: application to Franklin structure, Central Graben, North Sea, UK. *Marine Petroleum Geol.* **17**, 841–856.

Schneider, J., Haack, U. & Stedingk, K. (2003) Rb-Sr dating of epithermal vein mineralization stages in the eastern Harz Mountains (Germany) by paleomixing lines. *Geochim. Cosmochim. Acta* **67**, 1803–1819.

Schneider, J., Melcher, F. & Brauns, M. (2007) Concordant ages for the giant Kipushi base metal deposit (DR Congo) from direct Rb-Sr and Re-Os dating of sulfides. *Miner. Deposita* **42**, 791–797.

Schneiderhöhn, H. (1962) *Erzlagerstätten (Kurzvorlesungen)*. 4. Aufl., 371 pp. Fischer, Jena.

Schneiderhöhn, H. (1932) Die genetische Einteilung der Gesteine und Minerallagerstätten. *Z. Prakt. Geologie* **40**, 68–172.

Schoell, M. (1983) Genetic characterization of natural gases. *AAPG Bulletin* **67**, 2225–2238.

Scholz, C.H. & Contreras, J.C. (1998) Mechanics of continental rift architecture. *Geology* **26**, 967–970.

Schrag, D.P. (2009) Storage of carbon dioxide in offshore sediments. *Science* **325**, 1658–1659.

Schreiber, C. & Tabakh, M. (2000) Deposition and early alteration of evaporites. *Sedimentology* **47**, 215–238.

Schrenk, M.O., Edwards, K.J., Goodman, R.M. *et al.* (1998) Distribution of Thiobacillus ferrooxidans and Leptospirillum ferrooxidans: implications for generation of acid mine drainage. *Science* **279**, 1519–1521.

Schröder, S., Grotzinger, J.P., Amthor, J.E. & Matter, A. (2005) Carbonate deposition and hydrocarbon reservoir development at the Precambrian-Cambrian boundary: The Ara Group in South Oman. *Sed. Geol.* **180**, 1–28.

Schroll, E., Köppel, V. & Cerny, I. (2006) Pb and Sr isotope and geochemical data from the Pb–Zn deposit

Bleiberg (Austria): constraints on the age of mineralization. *Mineral. Petrol.* **86**, 129–156.

Schulz, H.N. & Schulz, H.D. (2005) Large sulfur bacteria and the formation of phosphorite. *Science* **307**, 416–418.

Schumacher, D. (1996) Hydrocarbon-induced alteration of soils and sediments, hydrocarbon migration and its near-surface expression. In: *Hydrocarbon Migration and its Near-Surface Expression* (eds D. Schumacher & M.A. Abrams), pp. 71–89. AAPG Memoir 66.

Schwartz, M.O. (1992) Geochemical criteria for distinguishing magmatic and metasomatic albite-enrichement in granitoids – examples from the Ta-Li granite Yichun (China) and the Sn-W deposit Tikus (Indonesia). *Miner. Deposita* **27**, 101–108.

Schwarz-Schampera, U. & Herzig, P. (1999) Indium: Geology, mineralogy and economics. *Z. Angew. Geol.* **45**, 164–169.

Scoates, J.S. & Mitchell, J.N. (2000) The evolution of troctolitic and high Al basaltic magmas in Proterozoic anorthosite plutonic suites and implications for the Voisey's Bay massive Ni-Cu deposit. *Economic Geol.* **95**, 677–701.

Scott, P.W. (1993) Distribution of flint and chert in Quarternary and recent gravel aggregates in the United Kingdom. *Instn. Min. Metall. (IMM) Transact.* **102**, 1–8.

Scrivener, R.C. & Shepherd, T.J. (1998) Mineralization. In: *The Geology of Cornwall* (eds E.B. Selwood, E.M. Durrance & C.M. Bristow) pp. 120–135. University of Exeter Press.

Seabrook, C.L., Cawthorn, R.G. & Kruger, F.J. (2005) The Merensky Reef, Bushveld Complex: mixing of minerals, not mixing of magmas. *Economic Geol.* **100**, 1191–1206.

Seewald, J.S. (2003) Organic-inorganic interactions in petroleum-producing sedimentary basins. *Nature* **426**, 327–333.

Seewald, J.S. (1994) Evidence for metastable equilibrium between hydrocarbons under hydrothermal conditions. *Nature* **370**, 285–287.

Segal, P. (1989) Earthquakes triggered by fluid extraction. *Geology* **17**, 942–946.

Selby, D. & Creaser, R.A. (2005) Direct radiometric dating of hydrocarbon deposits using rhenium-osmium isotopes. *Science* **308**, 1293–1295.

Selby, D. & Creaser, R.A. (2001) Re-Os geochronology and systematics in molybdenite from the Endako porphyry molybdenum deposit, British Columbia, Canada. *Economic Geol.* **96**, 197–204.

Selby, D., Creaser, R.A., Hart, C.G.R., *et al.* (2002) Absolute timing of sulfide and gold mineralization: a comparison of Re-Os molybdenite and Ar-Ar mica methods from the Tintina gold belt, Alaska. *Geology* **30**, 791–794.

Selby, D., Nesbitt, B.E., Muehlenbachs, K. & Prochaska, W. (2000) Hydrothermal alteration and fluid chemistry of the Endako porphyry molybdenum deposit, British Columbia. *Economic Geol.* **95**, 183–202.

Self, S., Blake, S., Sharma, K., Widdowson, M. & Sephton, S. (2008) Sulfur and chlorine in Late Cretaceous Deccan magmas and eruptive gas release. *Science* **319**, 1654–1657.

Selinus, O., Alloway, B., Centeno, J.A., *et al.* (eds) (2005) *Essentials of Medical Geology – Impacts of the Natural Environment on Public Health*. 812 pp. Elsevier Academic Press.

Selley, R. (1997) *Elements of Petroleum Geology*. 470 pp. Academic Press/Elsevier.

Seredin, V.V. & Finkelman, R.B. (2008) Metalliferous coals: A review of the main genetic and geochemical types. *Int. J. Coal Geol.* **76**, 253–289.

Seredin, V.V. (1996) Rare earth element-bearing coals from the Russian Far East deposits. *Int. J. Coal Geol.* **30**, 101–129.

Seredin, V.V., Danilcheva, Yu. A., Magazina, L.O., Sharova, I.G. (2006) Ge-bearing coals of the Luzanovka Graben, Pavlovka brown coal deposit, southern Primorye. *Lithology and Mineral Resources* **41**, 280–301.

Serra, O. & Serra, L. (2004) *Well Logging – Data Acquisition and Applications*. 674 pp. Editions Serralog, Mery-Corbon.

Seyfried, W.E. & Ding, K. (1993) The effect of redox on the relative solubilities of copper and iron in Cl-bearing aqueous fluids at elevated temperatures and pressures: An experimental study with application to subseafloor hydrothermal processes. *Geochim. Cosmochim. Acta* **57**, 1905–1917.

Seyfried, W.E., Foustoukos, D.I. & Qi Fu (2007) Redox evolution and mass transfer during serpentinization: An experimental and theoretical study at 200 °C, 500 bar with implications for ultramafic-hosted hydrothermal systems at Mid-Ocean Ridges. *Geochim. Cosmochim. Acta* **71**, 3872–3886.

Shackleton, N.J. (2000) The 100,000-year ice-age cycle identified and found to lag temperature, carbon dioxide, and orbital eccentricity. *Science* **289**, 1897–1902.

Shackley, D. & Allen, M.J. (1992) Perlite and the perlite industry. *Minerals Industry Intern.* 1008, 13–22, IMM London.

Shail, R.K., Stuart, F.M., Wilkinson, J.J. & Boyce, A.J. (2003) The role of post-Variscan extensional tectonics and mantle melting in the generation of the lower Permian granites and the giant W-As-Sn-Cu-Zn-Pb orefield of SW England. *Applied Earth Sci.* **112**, B127–129.

Shannon, J.R., Walker, B.M., Carter, R.B. & Geraghty, E. P. (1982) Unidirectional solidification textures and their significance in determining ages of intrusions at the Henderson mine, Colorado. *Geology* **10**, 293–297.

Shao, L., Zhang, P., Hilton, J., *et al.* (2003) Paleoenvironments and paleogeography of the Lower and lower Middle Jurassic coal measures in the Turpan-Hami oil-prone coal basin, northwestern China. *AAPG Bull.* **87**, 335–355.

Shao, L., Zhang, P., Ren, D. & Lei, J. (1998) Late Permian coal-bearing carbonate successions in southern China: coal accumulation on carbonate platforms. *Int. J. Coal Geol.* **37**, 235–256.

Shao-Yong Jiang, Yong-Quan Chen, Hong-Fei Ling, Jing-Hong Yang, Hong-Zhen Feng & Pei Ni (2006) Trace and rare-earth element geochemistry and Pb-Pb dating of black shales and intercalated Ni-Mo-PGE-Au sulfide ores in Lower Cambrian strata, Yangtze platform, South China. *Miner. Deposita* **41**, 453–467.

Shearer, Ch.K., Papike, J.J. & Jollif, B.L. (1992) Petrogenetic links among granites and pegmatites in the Harney Peak rare-element granite-pegmatite system, Black Hills, South Dakota. *Canadian Mineralogist* **30**, 785–809.

Sheldon, H.E. & Miklethwaite, S. (2007) Damage and permeability around faults: Implications for mineralization. *Geology* **35**, 903–906.

Shen, P., Shen, Y., Liu, T., Li, G. & Zeng, Q. (2008) Prediction of hidden Au and Cu-Ni ores from depleted mines in Northwestern China: four case studies of integrated geological and geophysical investigations. *Miner. Deposita* **43**, 499–517.

Sherlock, R.L. (2005) The relationship between the McLaughlin gold-mercury deposit and active hydrothermal systems in the Geysers-Clear Lake area, northern Coast Ranges, California. *Ore Geol. Rev.* **26**, 349–382.

Shin, D. & Lee, I. (2002) Carbonate-hosted talc deposits in the contact aureole of an igneous intrusion (Hwanggangri mineralized zone, South Korea): geochemistry, phase relationships, and stable isotope studies. *Ore Geol. Rev.* **22**, 17–39.

Shine, K.P. & Sturges, W.T. (2007) CO_2 is not the only gas. *Science* **315**, 1804–1805.

Shinohara, H., Kazhaya, K. & Lowenstern, J.B. (1995) Volatile transport in a convecting magma column: implications for porphyry Mo mineralization. *Geology* **23**, 1091–1094.

Shore, M. & Fowler, A.D. (1999) The origin of spinifex texture in komatiites. *Nature* **397**, 691–694.

Siame, L.L., Bourlès, D.L. & Brown, E.T. (eds) (2006) *In situ*-produced cosmogenic nuclides and quantification of geological processes. *GSA Spec. Paper 415*, 158 pp.

Sibson, R.H. (2003) Brittle-failure controls on maximum sustainable overpressure in different tectonic regimes. *AAPG Bull.* **87**, 901–908.

Sibson, R.H. (1990) Faulting and fluid flow. Pp 93–132 in B.E. Nesbitt (Ed.), Fluids in tectonically active regimes of the continental crust. *Mineral. Ass. Canada Short Course Handbook 18.*

Siefke, J.W. (1991) The Boron open pit mine at the Kramer borate deposit. Pp 4–15 in M.A. McKibben (ed.), The diversity of mineral and energy resources of Southern California. SEG Guidebook 12.

Siegers, A. & Lange, S.P. (1991) The Hoogenoeg mine in NE Transvaal/RSA – a producer of high grade andalusite. *Erzmetall* **44**, 384–391.

Siemann, M.G. & Schramm, M. (2002) Henry's and non-Henry's law behaviour of Br in simple marine systems. *Geochim. Cosmochim. Acta* **66**, 1387–1399.

Sikka, D.B., Petruk, W., Nehru, Ch.E. & Zhang, Z. (1991) Geochemistry of secondary copper minerals from Proterozoic porphyry copper deposit Malanjkhand, India. *Ore Geol. Rev.* **6**, 257–290.

Sillitoe, R.H. (2010) Porphyry copper systems. *Economic Geol.* **105**, 3–41.

Sillitoe, R.H. (2008) Major gold deposits and belts of the North and South American Cordillera: distribution, tectonomagmatic settings, and metallogenic considerations. *Economic Geol.* **103**, 663–687.

Sillitoe, R.H. (2003) Iron oxide-copper-gold deposits: an Andean view. *Miner. Deposita* **38**, 787–812.

Sillitoe, R.H. (1995) Exploration and discovery of base- and precious-metal deposits in the circum-Pacific region during the last 25 years. 119 pp, *Resource Geology Spec. Issue 19*, Tokyo.

Sillitoe, R.H. (1994) Erosion and collapse of volcanoes: causes of telescoping in intrusion-centered ore deposits. *Geology* **22**, 945–948.

Sillitoe, R.H. (1972) Relation of Metal Provinces in Western America to Subduction of Oceanic Lithosphere. *GSA Bulletin* **83**, 813–818.

Sillitoe, R.H. & Perelló, J. (2005) Andean copper province: tectonomagmatic settings, deposit types, metallogeny, exploration and discovery. *Economic Geol.* **100**, 845–890.

Sillitoe, R.H. & Burrows, D.R. (2003) New field evidence bearing on the origin of the El Laco magnetite deposit, Northern Chile – a reply. *Economic Geol.* **98**, 1501–1502.

Sillitoe, R.H., Steele, G.B., Thompson, J.F.H. & Lang, J.R. (1998) Advanced argillic lithocaps in the Bolivian tin-silver belt. *Miner. Deposita* **33**, 539–546.

Sillitoe, R.H., Folk, R.L. & Saric, N. (1996a) Bacteria as mediators of copper sulfide enrichment during weathering. *Science* **272**, 1153–1155.

Sillitoe, R.H., Hannington, M.D. & Thompson, J.F.H. (1996b) High sulfidation deposits in the volcanogenic massive sulfide environment. *Economic Geol.* **91**, 204–212.

Simandl, G.J. & Hancock, K.D. (1996) Magnesite in British Columbia, Canada: a neglected resource. *Minerals Industry Intern.* **1030**, 33–44.

Simmons, S.F. & Brown, K.L. (2007) The flux of gold and related metals through a volcanic arc, Taupo Volcanic Zone, New Zealand. *Geology* **35**, 1099–1102.

Simmons, S.F. & Brown, K.L. (2006) Gold in magmatic hydrothermal solutions and the rapid formation of a giant ore deposit. *Science* **314**, 288–291.

Simmons, S.F., White, N.C. & John, D.A. (2005) Geologic characteristics of epithermal precious and base metal deposits. *Economic Geol.* **100**, 485–522.

Simmons, S.F. & Browne, P.R.L. (2000) Hydrothermal minerals and precious metals in the Broadlands-Ohaaki geothermal system: implications for understanding low-sulfidation epithermal environments. *Economic Geol.* **95**, 971–999.

Simon, G., Kesler, S.E. & Essene, E.J. (1997) Phase relations among selenides, sulfides, tellurides and oxides: II. Applications to selenide-bearing ore deposits. *Economic Geol.* **92**, 468–484.

Sinclair, A.J. & Blackwell, G.H. (2002) *Applied Mineral Inventory Estimation*. 400 pp, Cambridge University Press.

Sinclair, W.D., Kooiman, G.J.A., Martin, D.A. & Kjarsgaard, I.M. (2006) Geology, geochemistry and mineralogy of indium resources at Mount Pleasant, New Brunswick, Canada. *Ore Geol. Rev.* **28**, 123–145.

Singer, D.A. & Menzie, W.D. (2010) *Quantitative Mineral Resource Assessments: An Integrated Appoach*. 232 pp, Oxford University Press.

Singer, D.A., Berger, V.I., Menzie, W.D. & Berger, B.B. (2005) Porphyry copper deposit density. *Economic Geol.* **100**, 491–514.

Sirkecioglu, A. & Erdem-Senatalar, A. (1996) Estimation of the zeolite contents of tuffaceous samples from the Bigadic clinoptilolite deposit, western Turkey. *Clays & Clay Minerals* **44**, 686–692.

Sivek, M., Čáslavský, M. & Jirásek, J. (2008) Applicability of Hilt's law to the Czech part of the Upper Silesian Coal Basin (Czech Republic). *Int. J. Coal Geology* **73**, 185–195.

Sizaret, S., Marcoux, E., Jébrak, M. & Touray, J.C. (2004) The Rossignol fluorite vein, Chaillac, France: multiphase hydrothermal activity and intravein sedimentation. *Economic Geol.* **99**, 1107–1122.

Skirrow, R.G., Bastrakov, E.N., Barovich, K. *et al.* (2007) Timing of iron oxide Cu-Au-(U) hydrothermal activity and Nd constraints on metal sources in the Gawler craton, South Australia. *Economic Geol.* **102**, 1441–1470.

Slack, J.F. & Cannon, W.F. (2009) Extraterrestrial demise of banded iron formations 1.85 billion years ago. *Geology* **37**, 1011–1014.

Slack, J.F., Turner, R.J.W. & Ware, P.L.G. (1998) Boron-rich mud volcanoes of the Black Sea region: Modern analogues to ancient sea-floor tourmalinites associated with Sullivan-type Pb-Zn deposits? *Geology* **26**, 439–442.

Sleep, N.H. (2001) Oxygenating the atmosphere. *Nature* **410**, 317–318.

Smedley, P. & Kinniburgh, D.G. (2005) Arsenic in groundwater and the environment. In: *Essentials of Medical Geology – Impacts of the Natural Environment on Public Health* (ed. O. Selinus *et al.*.), pp 263–299. Elsevier Academic Press.

Smil, V. (2003) *Energy at the Crossroads: Global Perspectives and Uncertainties*. 448 pp. MIT Press.

Smith, A. & Mudder, T. (1999) The environmental geochemistry of cyanide. In: *The Environmental Geochemistry of Mineral Deposits* (eds G.S. Plumlee & M.J. Logsdon), pp 229–248. *Rev. Economic Geol.* 6A.

Smith, C.G. (2001) Always the bridesmaid, never the bride: cobalt geology and resources. *Trans. Instn. Min. Metall.* **B 110**, 75–80.

Smith, C.N., Kesler, S.E., Klaue, B. & Blum, J.D. (2005) Mercury isotope fractionation in fossil hydrothermal systems. *Geology* **33**, 825–828.

Smith, G.I. (1979) Subsurface stratigraphy and geochemistry of Late Quarternary evaporites, Searles Lake, California. *USGS Prof. Paper 1043*, 130 pp.

Smith, K.S. & Huyck, H.L.O. (1999) *An Overview of the Abundance, Relative Mobility, and Human Toxicity of Metals. The Environmental Geochemistry of Mineral Deposits* (eds G.S. Plumlee & M.J. Logsdon), pp 29–79. *Rev. Economic Geol*. 6A.

Smith, L.B., Eberli, G.P., Masaferro, J.L. & Al-Dhahab, S. (2003) Discrimination of effective from ineffective porosity in heterogeneous Cretaceous carbonates, Al Ghubar field, Oman. *AAPG Bull*. **87**, 1509–1529.

Smith, M.P. & Henderson, P. (2000) Preliminary fluid inclusion constraints on fluid evolution in the Bayan Obo Fe-REE-Nb deposit, Inner Mongolia, China. *Economic Geol*. **95**, 1371–1388.

Smith, M.E., Carroll, A.R. & Mueller, E.R. (2008) Elevated weathering rates in the Rocky Mountains during the Early Eocene Climatic Optimum. *Nature Geoscience* **1**, 370–374.

Smith, R.E. & Singh, B. (2007) Recognising, in lateritic cover, detritus shed from the Archean Gossan Hill Cu-Zn-Au volcanic-hosted massive sulphide deposit, Western Australia. *Geochemistry: Exploration, Environment, Analysis* **7**, 71–86.

Smith, R.E., Anand, R.R. & Alley, N.F. (2000) Use and implications of paleoweathering surfaces in mineral exploration in Australia. *Ore Geol. Rev*. **16**, 185–204.

Snars, K. & Gilkes, R.J. (2009) Evaluation of bauxite residues (red muds) of different origins for environmental applications. *Applied Clay Science* **46**, 13–20.

Solomon, M., Tornos, F. & Gaspar, O.C. (2002) Explanation for many of the unusual features of the massive sulfide deposits of the Iberian pyrite belt. *Geology* **30**, 87–90.

Solomon, S., Rosenlof, K.H., Portmann, R.W., *et al.* (2010) Contributions of stratospheric water vapor to decadal changes in the rate of global warming. *Science* **327**, 1219–1223.

Sonnenfeld, P. (1995) The color of rock salt – a review. *Sedimentary Geol*. **94**, 267–276.

Sonnenfeld, P. (1991) Evaporite basin analysis. *Rev. Economic Geol.* **5**, 159–169.

Sorby, H.C. (1857) On the origin of the Cleveland Hill ironstone. *Geol. Polytechnic Soc. West Riding Yorkshire Proc.* **3**, 457–461.

Soudet, H.-J., Sorriaux, P. & Rolando, J.-P. (1994) Liaison fracturation-karstification. Le paléokarst petrolier de Rospo Mare (Italie). *Bull. Centres Rech. Explor.-Prod. Elf Aquitaine* **18**, 257–297.

Southam, G. & Saunders, J.A. (2005) The geomicrobiology of ore deposits. *Economic Geol*. **100**, 1067–1084.

Southam, G., Donald, R., Röstad, A. & Brock, C. (2001) Pyrite disks in coal: evidence for fossilized bacterial colonies. *Geology* **29**, 47–50.

Spaggiari, R.I., Bluck, B.J. & Ward, J.D. (2006) Characteristics of diamondiferous Plio-Pleistocene littoral deposits within the paleo-Orange River mouth, Namibia. *Ore Geol. Rev.* **28**, 475–492.

Spandler, C., Mavrogenes, J., Arculus, R. (2005) Origin of chromitites in layered intrusions: Evidence from chromite-hosted melt inclusions from the Stillwater Complex. *Geology* **33**, 893–896.

Sparks, H.A. & Mavrogenes, J.A. (2005) Sulfide melt inclusions as evidence for the existence of a sulfide partial melt at Broken Hill, Australia. *Economic Geol.* **100**, 773–779.

Sparks, R.S., Huppert, H.E., Koyaguchi, T. & Hallworth, M.A. (1993) Origin of modal and rhythmic layering by sedimentation in a convecting magma chamber. *Nature* **361**, 246–249.

Spera, F.J. (1984) Carbon dioxide in petrogenesis III: Role of volatiles in the ascent of alkaline magma with special reference to xenolith-bearing mafic lavas. *Contrib. Mineralogy Petrology* **88**, 217–232.

Spirakis, C.S. (1996) The roles of organic matter in the formation of uranium deposits in sedimentary rocks. *Ore Geol. Rev.* **11**, 53–69.

Spirakis, C.S. & Heyl, A.V. (1995) Evaluation of proposed precipitation mechanisms for Mississippi Valley-type ore deposits. *Ore Geology Rev*. **10**, 1–17.

Spötl, Ch. (1989) The Alpine Haselgebirge Formation, Northern Calcareous Alps (Austria): Permo-Skythian evaporites in an alpine thrust system. *Sedimentary Geol.* **65**, 113–125.

Spötl, Ch. & Pak, E. (1996) A strontium and sulfur isotopic study of Permo-Triassic evaporites in the Northern Calcareous Alps, Austria. *Chemical Geol.* **131**, 219–234.

Spötl, Ch., Longstaffe, F.J., Ramseyer, K., Kunk, M.J. & Wiesheu, R. (1998) Fluid-rock reactions in an evaporitic melange, Permian Haselgebirge, Austrian Alps. *Sedimentology* **45**, 1019–1044.

Spry, P.G., Marshall, B. & Vokes, F.M. (eds) (2000a) Metamorphosed and metamorphogenic ore deposits. *Rev. Economic Geol.* **11**, 310.

Spry, P.G., Peter, J.M. & Slack, J.F. (2000b) Meta-exhalites as exploration guides to ore? In: *Metamorphosed and Metamorphogenic Ore Deposits* (eds P.G. Spry, F.

J. Longstaff & F.M. Vokes), pp 163–201. *Rev. Economic Geol.* **11**.

Stach, E. (1935) *Lehrbuch der Kohlenpetrographie*. 293 pp. Borntraeger.

Stamatakis, M.G. (1995) Occurrence and genesis of huntite-hydromagnesite assemblages, Kozani, Greece – important new white fillers and extenders. *Trans. Instn. Min. Metall.* **104**, 179–186.

Standke, G., Rascher, J. & Strauss, C. (1993) Relative sea-level fluctuations and brown coal formation around the Early-Middle Miocene boundary in the Lusatian Brown Coal District. *Geol. Rundschau* **82**, 295–305.

Stan-Lotter, H., Radax, C., Gruber, C., *et al.* (2003) Astrobiology with haloarchaea from Permo-Triassic rock salt. *Int. J. Astrobiology (2002)*, **1**, 271–284.

Stanton, R.L. (1994) *Ore Elements in Arc Lavas*. 391 pp. Clarendon.

Stanton, R.L. (1972) *Ore Petrology*. 713 pp. McGraw-Hill.

Stasiuk, L.D. (1998) The origin of pyrobitumens in Upper Devonian Leduc Formation gas reservoirs, Alberta, Canada: an optical and EDS study of oil to gas transformation. *Marine Petroleum Geol.* **14**, 914–929.

Staub, J.R. & Esterle, J.S. (1994) Peat-accumulating depositional systems of Sarawak, East Malaysia. *Sedimentary Geology* **89**, 91–106.

Staubwasser, M., von Blanckenburg, F. & Schoenberg, R. (2006) Iron isotopes in the early marine diagenetic iron cycle. *Geology* **34**, 629–632.

Stefansson, A. & Seward, T.M. (2003) Experimental determination of the stability and stoichiometry of sulfide complexes of silver (I) in hydrothermal solutions to 400 °C. *Geochim. Cosmochim. Acta* **67**, 1395–1413.

Stein, H.J. (2006) Low-rhenium molybdenite by metamorphism in northern Sweden: recognition, genesis, and global implications. *Lithos* **87**, 300–327.

Stein, H.J., Markey, R.J., Morgan, J.W., *et al.* (2001) The remarkable Re-Os chronometer in molybdenite: how and why it works. *Terra Nova* **13**, 479–486.

Stein, H.J., Markey, R.J., Morgan, J.W., *et al.* (1997) Highly precise and accurate Re-Os ages for molybdenite from the East Qinling molybdenum belt, Shaanxi Province, China. *Economic Geol.* **92**, 827–835.

Stemprok, M. & Seltmann, R. (1994) The metallogeny of the Erzgebirge (Krusne Hory). In: *Metallogeny of Collisional Orogens* (eds Seltmann, Kämpf & Möllers), pp. 61–69. Czech Geol. Survey, Prag.

Stern, N. & Taylor, C. (2007) Climate change: risk, ethics, and the Stern review. *Science* **317**, 203–204.

Stetter, K.O., Huber, R., Blöchl, E., *et al.* (1993) Hyperthermophilic archaea are thriving in deep North Sea and Alaskan oil reservoirs. *Nature* **365**, 743–745.

Stevenson, R. (1999) Thoresby colliery outburst: a lesson learned. *Intern. Mining Minerals* **2**(2), 211–222.

Stix, J., Kennedy, B., Hanninton, H., *et al.* (2003) Caldera-forming processes and the origin of submarine volcanogenic massive sulfide deposits. *Geology* **31**, 375–378.

Stober, I. & Bucher, K. (1999) Origin of salinity in deep groundwater in crystalline rocks. *Terra Nova* **11**, 181–185.

Stoffers, P., Worthington, T.J., Schwarz-Schampera, U., *et al.* (2006) Submarine volcanoes and high-temperature hydrothermal venting on the Tonga arc, southwest Pacific. *Geology* **34**, 453–456.

Stoffers, P., Hannington, M., Wright, I., *et al.* (1999) Elemental mercury at submarine hydrothermal vents in the Bay of Plenty, Taupo volcanic zone, New Zealand. *Geology* **27**, 931–934.

Stone, M.S., George, A.D., Kneeshaw, M. & Barley, M.E. (2002) Stratigraphy and sedimentary features of the Tertiary Yandi channel iron deposits, Hamersley Province, Western Australia. *AusIMM Bull.* **6**(2002), 36–41.

Stopes, M.C. (1935) On the petrology of banded bituminous coals. *Fuel* **14**, 4–13.

Stowe, C.W. (1994) Compositions and tectonic settings of chromite deposits through time. *Economic Geol.* **89**, 528–546.

Stracher; G.B. (ed.) (2007) Geology of coal fires: Case studies from around the world. *GSA Rev. Eng. Geol.* **18**, 278.

Stracher; G.B. (ed.) (2004) Coal fires burning around the world: a global catastrophe. *Int. J. Coal Geol.* **59**, 1–151.

Streck, M.J. & Dilles, J.H. (1998) Sulfur evolution of oxidised arc magmas as recorded in apatite from a porphyry copper batholith. *Geology* **26**, 523–526.

Streckeisen, A.L. (1976) To each plutonic rock its proper name. *Earth Sci. Rev.* **12**, 1–33.

Strmić Palinkaš, S.S., Spangenberg, J.E. & Palinkaš, L.A. (2009) Organic and inorganic geochemistry of Ljubija siderite deposits, NW Bosnia and Herzegovina. *Miner. Deposita* **44**, 893–913.

Strohmenger, C., Antonini, M., Jäger, G., *et al.* (1996) Zechstein 2 carbonate reservoir facies distribution in relation to Zechstein sequence stratigraphy (Upper Permian, Northwest Germany): an integrated approach. *Bull. Centres Rech.Explor.-Prod. elf aquitaine* **20**(1), 1–35.

Stuckless, J.S. & Levich, R.A. (eds) (2007) The geology and climatology of Yucca Mountain and vicinity, Southern Nevada and California. *GSA Memoir* **199**, 205.

Stumpfl, E.F. (1986) Distribution, transport and concentration of platinum group elements. In: *Metallogeny of Basic and Ultrabasic Rocks*. pp 379–394 IMM London.

Stumpfl, E.F. (1979) Manganese haloes surrounding metamorphic stratabound base metal deposits. *Miner. Deposita* **14**, 207–217.

Sturesson, U., Heikoop, J.M. & Risk, M.J. (2000) Modern and Paleozoic iron ooids – a similar volcanic origin. *Sediment. Geol.* **136**, 137–146.

Sturt, B. A., Gautneb, H., Heldal, T. & Nilsson, L.P. (2002) Industrial minerals associated with ultramafic rocks in Norway. In: *Industrial Minerals and Extractive Industry Geology* (eds P. W. Scott P. W. & C. M. Bristow), pp. 43–58. Geological Society, London.

Su, Wenchao, Heinrich, C.A., Pettke, T., *et al.* (2009) Sediment-hosted gold deposits in Guizhou, China: Products of wallrock sulfidation by deep crustal fluids. *Economic Geol.* **104**, 73–93.

Suess, E. (1885) Das Antlitz der Erde. En: *The Face of the Earth* Vol. 1, Part 2, Die Gebirge der Erde. (eds F. Tempsky & G. Freytag), Prag und Leipzig (English edn 1906, Clarendon, London).

Sun, W., Arculus, R.J., Kamenetsky, V.S. & Binns, R.A. (2004) Release of gold-bearing fluids in convergent margin magmas prompted by magnetite crystallization. *Nature* **431**, 975–979.

Sun, Y. & Püttmann, W. (1998) Metal accumulation during and after deposition of the Kupferschiefer from the Sangerhausen basin, Germany. *Applied Geochem.* **12**, 577–592.

Sundblatt, K. (2003) Metallogeny of gold in the Precambrian of Northern Europe. *Economic Geol.* **98**, 1271–1290.

Sundblatt, K. & Parr, J.M. (eds) (1994) Swedish Svecofennian ore deposits. *Miner. Deposita* **29**, 109–205.

Süss, M.P., Drozdzewski; G. & Schäfer, A. (2000) Sequenzstratigraphie des kohleführenden Oberkarbons im Ruhrbecken. *Geol. Jb. A* **156**, 45–106.

Svensen, H., Planke, S., Malthe-Soerenssen, A. *et al.* (2004) Release of methane from a volcanic basin as a mechanism for initial Eocene global warming. *Nature* **429**, 542–545.

Svenson, H., Karlsen, D.A., Sturz, A., Backer-Owe, K., Banks, D.A. & Planke, S. (2007) Processes controlling water and hydrocarbon composition in seeps from the Salton Sea geothermal system, California, USA. *Geology* **35**, 85–88.

Swain, H.D. (1997) Due diligence – a proposal. *AusIMM Bulletin* **7**, 15–17.

Swaine, D.J. (1990) *Trace Elements in Coal*. 278 pp. Butterworths.

Swanson, E.R., Keizer, R.P., Lyons, J.L. & Clabough, S.E. (1978) Tertiary volcanism and caldera development near Durango City, Sierra Madre Occidental, Mexico. *Geol. Soc. America Bull.* **89**, 1000–1012.

Swarbrick, R.E. & Osborne, M.J. (1998) Mechanisms that generate abnormal pressures: An overview. In B.E. Law, G.F. Ulmishek and V.I. Slavin, (Eds.), Abnormal pressures in hydrocarbon environments. *AAPG Memoir* **70**, 13–34.

Swayze, G.A., Kokaly, R.F., Higgins, C.T., *et al.* (2009) Mapping potentially asbestos-bearing rocks using imaging spectroscopy. *Geology* **37**, 763–766.

Sweeny, M.A., Binda, P.L. & Vaughan, D.Y. (1991) Genesis of the ores of the Zambian Copperbelt. *Ore Geol. Rev.* **6**(1), 51–76.

Sweeny, J.J. & Burnham, A.K. (1990) Evaluation of a simple model of vitrinite reflectance based on chemical kinetics. *AAPG Bull.* **74**, 1559–1570.

Sweetapple, M.T. (2000) Characteristics of Sn-Ta-Be-Li-industrial mineral deposits of the Archean Pilbara craton, Western Australia. *AGSO Record 2000/44*, 54 pp.

Sweetapple, M.T. & Collins, P.L.F. (2002) Genetic framework for the classification and distribution of Archean rare metal pegmatites in the North Pilbara Craton, Western Australia. *Economic Geol.* **97**, 873–895.

Swenson, J.B. & Person, M. (2000) The role of basin-scale transgression and sediment compaction in stratiform copper mineralization: implications from White Pine, Michigan, USA. *J. Geochem. Explor.* **69–70**, 239–243.

Swift, G.M., Reddish, D.J., Lloyd, P.W. & Dunham, R.K. (2001) Numerical modelling of time-dependent deformation around an underground mine in rock salt. *Trans. Instn. Min. Metall. A* **110**, 107–113.

Swihart, G.H., McBay, E.H., Smith, D.H. & Siefke, J.W. (1996) A boron isotopic study of a mineralogically zoned lacustrine borate deposit: the Kramer deposit, California, USA. *Chemical Geology* **127**, 241–250.

Sykorova, I., Pickel, W., Christanis, K., Wolf, M., Taylor, G.H. & Flores, D. (2005) Classification of huminite (ICCP System 1994). *Int. J. Coal Geology* **62**, 85–106.

Sylvester, P.J. (ed.) (2008) Laser Ablation ICP–MS in the Earth Sciences: Current Practices and Outstanding Issues. *Mineral. Ass. Canada Short Course Vol. 40*, 356 pp.

Symons, D.T.A. (2007) Paleomagnetism of the HYC Zn-Pb sedex deposit, Australia: evidence of an epigenetic origin. *Economic Geol.* **102**, 1295–1310.

Symons, D.T.A., Pannalal, S.J., Coveney, B.M. & Sangster, D.F. (2005) Paleomagnetism of Late Paleozoic strata and mineralization in the Tri-State lead-zinc ore district. *Economic Geol.* **100**, 295–309.

Tachibana, Y., Kaneoka, I., Gaffney, A. & Upton, B. (2006) Ocean-island basalt-like source of kimberlite magmas from West Greenland revealed by high ^{3}He/^{4}He ratios. *Geology* **34**, 273–276.

Tackley, P.J. (2000) Mantle convection and plate tectonics: toward an integrated physical and chemical theory. *Science* **288**, 2002–2007.

Tafti, R., Mortensen, J.K., Lang, J.R., Rebagliati, M. & Oliver, J.L. (2009) Jurassic U-Pb and Re-Os ages for the newly discovered Xietongmen Cu-Au porphyry district, Tibet, PRC: Implications for metallogenic epochs in the southern Gangdese belt. *Economic Geol.* **104**, 127–136.

Tait, J.A., Bachtadse, V., Franke, W. & Soffel, H.C. (1997) Geodynamic evolution of the European Variscan fold belt: paleomagnetic and geological constraints. *Geol. Rundschau* **86**, 585–598.

Tal, M & Paola, C. (2007) Dynamic single-thread channels maintained by the interaction of flow and vegetation. *Geology* **35**, 347–350.

Talbot, C.J., Stanley, W., Soub, R. & Al-Sadoun, N. (1996) Epitaxial salt reefs and mushrooms in the southern Dead Sea. *Sedimentology* **43**, 1025–1047.

Tandon, S.K. & Gibling, M.R. (1997) Calcretes at sequence boundaries in Upper Carboniferous cyclothems of the Sydney basin, Atlantic Canada. *Sedim. Geol.* **112**, 43–67.

Tappert, R., Foden, J., Muehlenbachs, K., Tappert, M. & Wills, K. (2009) Deep mantle diamonds from South Australia: A record of Pacific subduction at the Gonwanan margin. *Geology* **37**, 43–46.

Tappert, R., Stachel, T., Harris, J.W., Muehlenbachs, K., Ludwig, T. & Brey, G.P. (2005) Subducting oceanic crust: the source of deep diamonds. *Geology* **33**, 565–568.

Tarkian, M. & Stribnry, B. (1999) Platinum-group elements in porphyry copper deposits: a reconnaissance study. *Mineral. Petrol.* **65**, 161–183.

Taylor, C.D. & Wirsen, C.O. (1997) Microbiology and ecology of filamentous sulfur formation. *Science* **277**, 1483–1485.

Taylor, D., Dalstra, H.J., Harding, A.E., Broadbent, G.C. & Barley, M.E. (2001) Genesis of high-grade hematite orebodies of the Hamersley Province, Western Australia. *Economic Geol.* **96**, 837–873.

Taylor, G. & Eggleton, T. (2004) "Little balls" – the origin of Weipa bauxite. In: *Regolith 2004* (ed. I.C. Roach), pp 350–354. CRC LEME Press.

Taylor, G.H., Teichmüller, M., Davis, A., Diessel, C.F. K., Littke, R. & Robert, P. (1998) *Organic Petrology*. 704 pp, Borntraeger.

Taylor, J.R. (1997) *Error Analysis*, 2nd edn, 327 pp. University Science Books.

Taylor, H.P. (1967) The zoned ultramafic complexes of southern Alaska. In: *Ultramafic and Related Rocks* (ed. P.J. Wyllie) pp 97–121. Wiley.

Taylor, J.R. & Wall, V.J. (1992) The behaviour of tin in granitoid magmas. *Economic Geol.* **87**, 403–420.

Taylor, R.P. & Fallick, A.E. (1997) The evolution of fluorine-rich felsic magmas: source dichotomy, magmatic convergence and the origins of topaz granite. *Terra Nova* **9**, 105–108.

Teagle, D.A.H. & Alt, J.C. (2004) Hydrothermal alteration of basalts beneath the Bent Hill massive sulfide deposit, Middle Valley, Juan de Fuca Ridge. *Economic Geol.* **99**, 561–584.

Teichmüller, M. (1991) *Rekonstruktionen verschiedener Moortypen des Hauptflözes der niederrheinischen Braunkohle.* 31 pp. Geol. LA Nordrhein-Westfalen.

Teichmüller, M. (1958) Rekonstruktion verschiedener Moortypen des Hauptflözes der Niederrheinischen Braunkohle. *Fortschr. Geol. Rheinld. Westf.* **2**, 599–612.

Teichmüller, M. & Teichmüller, R. (1981) The significance of coalification studies to geology – a review. *Bull. Centres Rech. Explor.-Prod. Elf-Aquitaine* **5**, 491–534.

Teichmüller, M. & Teichmüller, R. (1966) Geological causes of coalification. *Coal Sci. Adv. Chem. Ser.* **55**, 133–155.

Templeton, A.S., Chamberlain, C.P., Koons, P.O. & Craw, D. (1997) Stable isotopic evidence for mixing between metamorphic fluids and surface-derived waters during recent uplift of the Southern Alps, New Zealand. *Earth Planet. Sci. Lett.* **154**, 73–92.

Terzaghi, K., Peck, R.B. & Mesri, G. (1996) *Soil Mechanics in Engineering Practice*, 3rd edn. 729 pp. Wiley.

Thayer, T.P. (1969) Gravity differentiation and magmatic replacement of podiform chromite deposits. *Economic Geol. Monograph* **4**, 132–146.

Therriault, A.M., Fowler, A.D. & Grieve, R.A.F. (2002) The Sudbury Igneous Complex: a differentiated impact melt sheet. *Economic Geol.* **97**, 1521–1540.

Thom, J. & Anderson, G.M. (2008) The role of thermochemical sulfate reduction in the origin of Mississippi Valley-type deposits. I. Experimental results. *Geofluids* **8**, 16–26.

Thomas, L. (2002) *Coal Geology*. 396 pp. Wiley.

Thomas, R. & Webster, J.D. (2000) Strong tin enrichment in a pegmatite forming melt. *Miner. Deposita* **35**, 570–582.

Thomas, R., Webster, J.D. & Heinrich, W. (2000) Melt inclusions in pegmatite quartz: complete miscibility between silicate melts and hydrous fluids at low pressure. *Contrib. Mineral. Petrol.* **139**, 394–401.

Thomsen, R. (2004) Hydrogeological mapping as a basis for establishing site-specific groundwater protection zones in Denmark. *Hydrogeology J.* **12**, 550–562.

Thompson, A.J.B. & Thompson, J.F.H. (1997) *Atlas of Alteration – A Field and Petrographic Guide to Hydrothermal Alteration Minerals*. 119 pp. Geol. Assoc. Canada.

Thomson, R.O. & Lerche, I. (1991) Salt diapir velocity assessment from temperature and thermal indicator anomalies: application to Lulu-1, Danish North Sea. *Terra Nova* **3**, 500–509.

Thorne, W., Hagemann, S., Vennemann, T. & Oliver, N. (2009) Oxygen isotope compositions of iron oxides from high-grade BIF-hosted iron ore deposits of the central Hamersley Province, Western Australia: Constraints on the evolution of hydrothermal fluids. *Economic Geol.* **104**, 1019–1035.

Thorne, W.S., Hagemann, S.G. & Barley, M. (2004) Petrographic and geochemical evidence for hydrothermal evolution of the North Deposit, Mt. Tom Price, Western Australia. *Miner. Deposita* **39**, 766–783.

Thornton, J. (2000) *Pandora's Poison: On Chlorine, Health, and a New Environmental Strategy*. 611 pp. MIT Press.

Tian, Hui, Xiao, Xianming, Wilkins, R.W.T. & Tang, Yongchun (2008) New insights into the volume and pressure changes during the thermal cracking of oil to gas in reservoirs: Implications for the *in-situ* accumulation of gas cracked from oils. *AAPG Bulletin* **92**, 181–200.

Tingay, M.R.P., Hillis, R.R., Swarbrick, R.E., Morley, C. K. & Damit, A.R. (2007) Vertically transferred overpressures in Brunei: Evidence for a new mechanism for the formation of high-magnitude overpressure. *Geology* **35**, 1023–1026.

Tissot, B.P. & Welte, D.H. (1984) *Petroleum Formation and Occurrence: A New Approach to Oil and Gas Formation*. 2nd Edn, 699 pp, Springer.

Tistl, M. (1994) Geochemistry of platinum-group elements of the zoned ultramafic Alto Condoto complex, Northwest Colombia. *Economic Geol.* **89**, 158–167.

Tollo, R.P., Corriveau, L., McLelland, J. & Bartholomew, M.J. (eds) (2004) Proterozoic tectonic evolution of the Grenville orogen in North America. *GSA Memoir* **197**, 798 pp.

Tolstykh, N., Krivenko, A., Sidorov, E., Laajoki, K. & Podlipsky, M. (2002) Ore mineralogy of PGM placers in Siberia and the Russian Far East. *Ore Geol. Rev.* **20**, 1–25.

Tomaru, H., Lu, Z., Fehn, U., Muramatsu, Y. & Matsumoto, R. (2007) Age variation of pore water iodine in the eastern Nankai Trough, Japan: Evidence for different methane sources in a large gas hydrate field. *Geology* **35**, 1015–1018.

Tomkins, A.G. (2007) Three mechanisms of ore re-mobilisation during amphibolite facies metamorphism at the Montauban Zn-Pb-Au-Ag deposit. *Miner. Deposita* **42**, 627–637.

Tomkins, A.G. & Mavrogenes, J.A. (2003) Generation of metal-rich felsic magmas during crustal anatexis. *Geology* **31**, 765–768.

Tomkins, A.G. & Mavrogenes, J.A. (2002) Mobilization of gold as a polymetallic melt during pelite anatexis at the Challenger deposit, South Australia: a metamorphosed Archean gold deposit. *Economic Geol.* **97**, 1249–1272.

Tomkins, A.G., Weinberg, R.F. & McFarlane, C.R.M. (2009) Preferential magma extraction from K- and metal-enriched source regions in the crust. *Miner. Deposita* **44**, 171–181.

Tomkins, A.G., Pattison, D.R.M. & Zaleski, E. (2004) The Hemlo gold deposit, Ontario: an example of melting and mobilization of a precious metal-sulfosalt assemblage during amphibolite facies metamorphism and deformation. *Economic Geol.* **99**, 1063–1084.

Tooth, B., Brugger, J., Ciobanu, C. & Weihua Liu (2008) Modeling of gold scavenging by bismuth melts coexisting with hydrothermal fluids. *Geology* **36**, 815–818.

Tordoff, G. M., Baker, A. J. M., & Willis, A. J. (2000) Current approaches to the revegetation and reclamation of metalliferous wastes. *Chemosphere* **41**, 219–228.

Tornos, F. (2006) Environment of formation and styles of volcanogenic massive sulfides: the Iberian Pyrite Belt. *Ore Geol. Rev.* **28**, 259–307.

Tornos, F. & Spiro, B.F. (2000) The geology and isotope geochemistry of the talc deposits of Puebla de Lillo

(Cantabrian Zone, Northern Spain). *Economic Geol.* **95**, 1277–1296.

Torrealday, H.I., Hitzman, M.W., Stein, H.J. *et al.* (2000) Re-Os and U-Pb dating of the vein-hosted mineralization at the Kansanshi copper deposit, northern Zambia. *Economic Geol.* **95**, 1165–1170.

Torres, M.E., Bohrmann, G., Dube, T.E. & Poole, F.G. (2003) Formation of modern and Paleozoic stratiform barite at cold methane seeps on continental margins. *Geology* **31**, 897–900.

Torrez-Ruiz, J. (2006) Geochemical constraints on the genesis of the Marquesado iron ore deposits, Betic Cordillera, Spain: REE, C, O, and Sr isotope data. *Economic Geol.* **101**, 667–677.

Torsvik, T.H. (2003) The Rodinia jigsaw puzzle. *Science* **300**, 1379–1381.

Torsvik, T.H. & Cocks, R.M. (2004) Earth geography from 400 to 250 Ma: a palaeomagnetic, faunal and facies review. *J. Geol. Soc. London* **161**, 555–572.

Totsche, O., Fyson, A. & Steinberg, C.E.W. (2006) Microbial alkalinity production to prevent reacidification of neutralized mining lakes. *Mine Water Environ* **25**, 204–213.

Trenberth, K.E. & Fasullo, J.T. (2010) Tracking Earth's energy. *Science* **328**, 316–317.

Troesken, W. (2006) *The Great Lead Water Pipe Disaster*. 328 pp, MIT Press.

Trusheim, F. (1957) Über Halokinese und ihre Bedeutung für die strukturelle Entwicklung Norddeutschlands. *Z. dt. geol. Ges.* **109**, 111–159.

Tsikos, H. & Moore, J.M. (1997) Petrography and geochemistry of the Paleoproterozoic Hotazel iron formation, Kalahari manganese field, South Africa: implications for Precambrian manganese metallogeny. *Economic Geol.* **92**, 87–97.

Tsikos, H., Beukes, N.J., Moore, J.M. & Harris, C. (2003) Deposition, diagenesis, and secondary enrichment of metals in the Paleoproterozoic Hotazel Iron Formation, Kalahari manganese field, South Africa. *Economic Geol.* **98**, 1449–1462.

Turcotte, D.L. (1997) *Fractals znd Chaos in Geology and Geophysics*. 2nd ed., 398 pp., Cambridge University Press.

Turner, R.E., Baustian, J.J., Swenson, E.M. & Spicer, J.S. (2006) Wetland sedimentation from hurricanes Katrina and Rita. *Science* **314**, 449–452.

Turner, S., Sandford, M. & Foden, J. (1992) Some geodynamic and compositional constraints on "postorogenic" magmatism. *Geology* **20**, 931–934.

Uchida Etsuo, Endo Sho & Makino Mitsutoshi (2007) Relationship between solidification depth of granitic rocks and formation of hydrothermal ore deposits. *Resource Geology* **57**, 47–56.

Ulrich, T. & Mavrogenes, J. (2008) An experimental study of the solubility of molybdenum in H_2O and $KCl–H_2O$ solutions from 500 °C to 800 °C, and 150 to 300 MPa. *Geochim. Cosmochim. Acta* **72**, 2316–2330.

Ulrich, T., Günther, D. & Heinrich, C.A. (1999) Gold concentrations of magmatic brines and the metal budget of porphyry copper deposits. *Nature* **399**, 676–679.

UNDESA (United Nations Department of Economic and Social Affairs) & UNEP (United Nations Environment Programme) (2002) *Berlin II Guidelines for Mining and Sustainable Development.* 52 pp.

Unger, H.J., Fiest, W. & Niemeyer, A. (1990) Die Bentonite der ostbayerischen Molasse und ihre Beziehungen zu den Vulkaniten des Pannonischen Beckens. *Geol. Jb. D* **96**, 67–112.

United States Geological Survey (2010) *USGS minerals information webpages*. http://minerals.usgs.gov/minerals/; accessed in June 2010.

UN Conference on Environment and Development (1992) *The Rio de Janeiro Declaration on Environment and Development*. http://www.un.org/documents/ga/conf151/aconf15126-1annex1.htm, accessed September 2010.

Usiglio, J. (1849) Analyse de l'eau de la Méditerranée et études sur l'exploitation de sel qu'elle contient. *Annalen der Chemie* **27**, 172–191.

Vajda, V. & McLoughlin, S. (2004) Fungal profileration at the Cretaceous-Tertiary boundary, *Science* **303**, 1489.

Valenza, K., Moritz, R., Mouttaqi, A., *et al.* (2000) Vein and karst barite deposits in the western Jebilet of Morocco: fluid inclusion and isotope (S, O, Sr) evidence for regional fluid mixing related to Central Atlantic rifting. *Economic Geol.* **95**, 587–606.

Valeton, I. (1999) Saprolite-bauxite facies of ferralitic duricrusts on paleosurfaces of former Pangaea. *Spec. Pubs. intern. Assoc. Sediment.* **27**, 153–188.

Valley, J.W. & Cole, D.R. (eds) (2001) Stable isotope geochemistry. *Rev. in Mineral. Geochem. 43*, 570 pp. Mineral. Soc. America.

Van Dover, C.L. (2000) *The Ecology of Deep-Sea Hydrothermal Vents*. 444 pp. Princeton University Press.

van Geen, A., Adkins, J.F., Boyle, E.A. *et al.* (1997) A 120 yr record of widespread contamination from mining of the Iberian pyrite belt. *Geology* **25**, 291–294.

Van Gosen, B.S. (2007) The geology of asbestos in the United States and its practical applications. *Environmental Engineering Geosci.* **13**, 55–68.

Van Voast, W.A. (2003) Geochemical signature of formation waters associated with coalbed methane. *AAPG Bull.* **87**, 667–676.

Varekamp, J.C. & Buseck, P.R. (1984) The speciation of mercury in hydrothermal systems, with applications to ore deposition. *Geochim. Cosmochim. Acta* **48**, 177–185.

Varentsov, I.M. & Muzylev, N.G. (2001) Manganese ore giants of the eastern Paratethys; genesis in context of geological events at the Eocene-Oligocene boundary. *Doklady Earth Sci.* **376**, 118–122.

Varlamoff, N. (1972) Central and West African rare metal granitic pegmatites, related aplites, quartz veins and mineral deposits. *Miner. Deposita* **7**, 202–216.

Vasconselos, C. & McKenzie, J.A. (2000) Sulfate reducers – dominant players in a low-oxygen world? *Science* **290**, 1711–1712.

Vasconcelos, C., McKenzie, J.A., Bernasconi, S., Grujic, D. & Tien, A.J. (1995) Microbial mediation as a possible mechanism for natural dolomite formation at low temperatures. *Nature* **377**, 220–222.

Vavra, C.L., Kaldi, J.G. & Sneider, R.M. (1992) Geological applications of capillary pressure; a review. *AAPG Bulletin* **76**, 840–850.

Vearncombe, J.R. (1998) Shear zones, fault networks, and Archean gold. *Geology* **26**, 855–858.

Veld, H., Fermont, W.J.J., David, P. *et al.* (1996) Environmental influence on maturity parameters in Carboniferous coals of the Netherlands. *Int. J. Coal Geol.* **30**, 37–64.

Verburg, R., Bezuidenhout, N., Chatwin, T. & Ferguson, K. (2009) The global acid rock drainage guide (GARD Guide). *Mine Water Environ* **28**, 305–310 (www.gardguide.com).

Vermaak, C.F. & Van der Merwe, M.J. (2000) *The Platinum Mines and Deposits of the Bushveld Complex, South Africa*. 200 pp. Mintek.

Vermaak, C.F. & Von Gruenewaldt, G. (1986) Introduction to the Bushveld Complex. In: *Mineral Deposits of Southern Africa*, Vol II (eds C.R. Anhäusser & S. Maske), pp. 1021–1029. Geol. Soc. S. Africa, Johannesburg.

Vermaak, C.F. (1986) Summary aspects of the economics of chromium with special reference to Southern Africa. In C.R. Anhäusser & S. Maske (Eds), *Mineral Deposits of Southern Africa*, Vol. II, 1155–1181. Geol. Soc. S. Africa, Johannesburg.

Verweij, J.M. (1993) *Hydrocarbon Migration Systems Analysis*. 276 pp. Elsevier.

Verwoerd, W.J. (1986) Mineral deposits associated with carbonatites and alkaline rocks. In: *Mineral Deposits of Southern Africa*. Vol. II (eds C.R. Anhäusser & S. Maske), pp. 2173–2191. Geol. Soc. S. Africa, Johannesburg.

Vielreicher, N.M., Groves, D.I., Snee, L.W., Fletcher, I.R. & McNaughton, N.J. (2010) Broad synchroneity of three gold mineralization styles in the Kalgoorlie Gold Field: SHRIMP, U-Pb, and ^{40}Ar/^{39}Ar geochronological evidence. *Economic Geol.* **105**, 187–227.

Viets, J.G., Hopkins, R.T. & Miller, B.M. (1992) Variations in minor and trace metals in sphalerite from Mississippi Valley-type deposits of the Ozark Region: genetic implications. *Economic Geol.* **87**, 1897–1905.

Viljoen, M.J. (1999) The nature and origin of the Merensky Reef of the western Bushveld Complex based on geological facies and geophysical data. *S. African J. Geol.* **102**, 221–239.

Vokes, F.M. (2000) Ores and metamorphism: Introduction and historical perspectives. In: *Metamorphosed and Metamorphogenic Ore Deposits* (eds P.G. Spry *et al.*), pp. 1–18. *Rev. Economic Geol.* **11**.

Volkov, A.V., Serafimovski, T., Kochneva, N. T., Tomson, I. N. & Tasev, G. (2006) The Alshar epithermal Au-As-Sb-Tl deposit, southern Macedonia. *Geology of Ore Deposits* **48**, 175–192.

Volkov, V.N. (2003) Phenomenon of the formation of very thick coal beds. *Lith. Min. Res.* **38**, 223–232.

Volozh, Y., Talbot, C. & Ismail-Zadeh, A. (2003) Salt structures and hydrocarbons in the Pricaspian basin. *AAPG Bull.* **87**, 313–334.

Vreeland, R.H., Rosenzweig, W.D. & Powers, D.W. (2000) Isolation of a 250 million-year-old halotolerant bacterium from a primary salt crystal. *Nature* **407**, 897–900.

Waeser, B. (1923/1926) Verfahren zur Herstellung von Magnesiumcarbonat unter gleichzeitiger Gewinnung von Ammoniumsalzen. *Deutsches Reich Patentschrift* **431**, 618.

Wager, L.R., Vincent, E.A. & Smales, A.A. (1957) Sulfides in the Skaergaard intrusion, East Greenland. *Economic Geol.* **52**, 855–903.

Waghorne, E.P. (2001) Assessment of resources and reserves in low rank coals. In: *Mineral Resource and Ore Reserve Estimation – The Ausimm Guide to Good Practice* (ed A.C. Edwards), *p* p 347–354. AusIMM, Melbourne.

Wagner, G.A. & van den Haute, P. (1992) *Fission-track Dating*. 285 pp. Enke.

Wagner, T., Mlynarczyk, M.S.J., Williams-Jones, A.E. & Boyce, A.J. (2009) Stable isotope constraints on ore formation at the San Rafael tin-copper deposit, Southeast Peru. *Economic Geol.* **104**, 223–248.

Wagner, T., Klemd, R., Wenzel, T. & Mattsson, B. (2007) Gold upgrading in metamorphosed massive sulfide ore deposits: Direct evidence from laser-ablation-inductively coupled plasma-mass sprectrometry analysis of invisible gold. *Geology* **35**, 775–778.

Wagner, T., Jonsson, E. & Boyce, A.J. (2005) Metamorphic ore remobilization in the Hällefors district, Bergslagen, Sweden: constraints from mineralogical and small-scale sulphur isotope studies. *Miner. Deposita* **40**, 100–114.

Wagner, T. & Cook, N.J. (2000) Late Variscan antimony mineralisation in the Rheinisches Schiefergebirge, NW Germany: evidence for stibnite precipitation by drastic cooling of high temperature fluid systems. *Mineral. Deposita* **35**, 206–222.

Walde, D.H.G. & Steffen, S.G. (2007) The Neoproterozoic Fe and Mn deposits in W-Brazil/SE Bolivia: an assessment of ore deposit models. *Zeitschr.dt. Ges. Geowiss.* **158**, 45–55.

Walker, J.D. & Geissmann, J.W. (2009) The 2009 GSA Geologic Timescale. *GSA Today* **19**(4–5), 60–61.

Walker, J.D. & Cohen, H.A.(compilers) (2007) *The Geoscience Handbook – AGI Data Sheets*, 4th edn. 302 pp. American Geological Institute.

Wallier, S., Rey, R., Kouzmanov, K., *et al.* (2006) Magmatic fluids in the breccia-hosted epithermal Au-Ag deposit of Roş ia Montană, Romania. *Economic Geol.* **101**, 923–954.

Walters, S. G. & Bailey, A. (1998) Geology and mineralisation of the Cannington Ag-Pb-Zn deposit: an example of Broken Hill-type mineralisation in the Eastern Succession, Mount Isa Inlier, Australia. *Economic Geol.* **93**, 1307–1329.

Walther, H.W. (1983) The Alpidic metallogenetic epoch in Central Europe north of the Alps. In: *Mineral Deposits of the Alps* (ed. H.-J. Schneider), pp. 313–328. Springer.

Walton, C., Evans, B. & Urosevic, M. (2000) Imaging coal seam structure using 3-D seismic methods. *Exploration Geophysics* **31**, 509–514.

Walvoord, M.A., Phillips, F.M., Stonestrom, D.A., *et al.* (2003) A reservoir of nitrate beneath desert soils. *Science* **302**, 1021–1024.

Wanless, H.R. & Weller, J.M. (1932) Correlation and extent of Pennsylvanian cyclothems. *Geol. Soc. America Bull.* **43**, 1003–1016.

Wanty, R.B. & Goldhaber, M.B. (1992) Thermodynamics and kinetics involving vanadium in natural systems: accumulation of vanadium in sedimentary rocks. *Geochim. Cosmochim. Acta* **56**, 1771–1784.

Ward, C.R. (2002) Analysis and significance of mineral matter in coal seams. *Int. J. Coal Geol.* **50**, 135–168.

Ward, C.R. (1984) *Coal geology and coal technology*. 345 pp. Blackwell.

Ward, C.R., Corcoran, J.F., Saxby, J.D. & Read, H.W. (1996) Occurrence of phosphorus minerals in Australian coal seams. *Int. J. Coal Geol.* **30**, 185–210.

Warhurst, A. & Noronha, L. (2000) *Ecological Management of Mining*. 513 pp. Lewis Publishers.

Warren, J.K. (2006) *Evaporites: Sediments, Resources and Hydrocarbons*. 1035 pp. Springer.

Warren, J.K. (1999) *Evaporites – Their Evolution and Economics*. 432 pp. Blackwell.

Watanabe, M., Hoshino, K., Kagami, H. *et al.* (1998) Rb-Sr, Sm-Nd and K-Ar systematics of metamorphosed pillowed basalts and associated Besshi-type deposits in the Sanbagawa Belt, Japan. *Miner. Deposita* **34**, 113–120.

Watson, E.B., Wark, D.A. & Thomas, J.B. (2006) Crystallization thermometers for zircon and rutile. *Contr. Mineral. Petrol.* **151**, 413–433.

Watterson, J.R. (1992) Preliminary evidence for the involvement of budding bacteria in the origin of Alaskan placer gold. *Geology* **20**, 315–318.

Watzlaf, G.R. & Ackman, T.E. (2006) Underground mine water for heating and cooling using geothermal heat pump systems. *Mine Water Environ* **25**, 1–14.

Wavra, C.S., Bond, W.D. & Reid, R.R. (1994) Evidence from the Sunshine Mine for dip-slip movement during Coeur d'Alene district mineralization. *Economic Geol.* **89**, 515–527.

Weatherstone, N. (2005) The role of the mineral reserve estimator in promoting sustainable development in the mining industry. *Applied Earth Sci. B* **114**, 14–22.

Wedepohl, K.H. (1995) The composition of the continental crust. *Geochim. Cosmochim. Acta* **59**, 1217–1232.

Wedepohl, K. H. & Rentzsch, J. (2006) The composition of brines in the early diagenetic mineralization of the Permian Kupferschiefer in Germany. *Contrib. Mineralogy Petrology* **152**, 323–333.

Wegener, A. (transl. J.G.A. Skerl) (1924) *Origin of Continents and Oceans*. Methuen, London.

Weibel, C.P. (2004) Stratal order in Pennsylvanian cyclothems: Discussion. *GSA Bull.* **116**, 1545–1550.

Weihed, P. & Williams, P.J. (2005) Metallogeny of the northern Fennoscandian Shield: a set of papers on Cu-Au and VMS deposits of northern Sweden. *Miner. Deposita* **40**, 347–350.

Weinberg, R.F. (2006) Melt segregation structures in granitic plutons. *Geology* **34**, 305–308.

Weinberg, R.F., Hodkiewicz, P.F. & Groves, D.I. (2004) What controls gold distribution in Archean terranes? *Geology* **32**, 545–548.

Weinstein, P. & Cook, A. (2004) Volcanic emissions and health. In: *Essentials of Medical Geology – Impacts of the Natural Environment on Public Health* (ed. O. Selinus *et al.*), pp 203–226. Elsevier Academic Press.

Welch, B.K., Soufoulis, J. & Fitzgerald, A.J.F. (1975) Mineral sand deposits of the Capel area W.A. Pp 1070–1088 in C.L.Knight (Ed.), *Economic Geology of Australia and Papua New Guinea. 1. Metals*. AusIMM, Parkville.

Welland, M. (2009) *Sand – The Never-ending Story*. 374 pp. University of California Press.

Wellmer, F.-W. (2008) Reserves and resources of the geosphere, terms so often misunderstood. Is the life index of reserves of natural resources a guide to the future? *Z .dt. geol. Ges.* **159**, 575–590.

Wellmer, F.-W., Dahlheimer, M. & Wagner, M. (2007) *Economic Evaluations in Exploration*. 250 pp. Springer.

Wendland, E. & Himmelsbach, Th. (2002) Underground waste repositories in exhausted coal mines – recent developments. *Mine Water Environ* **21**, 160–167.

Whalen, J.B., Currie, K.L. & Chappel, B.W. (1987) A-type granites: geochemical characteristics, discrimination and petrogenesis. *Contrib. Miner. Petrol.* **95**, 407–419.

White, D. (1935) Metamorphism of organic sediments and derived oils. *Bull. Amer. Assoc. Petrol. Geol.* **18**, 589–617.

White, N.C. & Hedenquist, J.W. (1995) Epithermal gold deposits: styles, characteristics and exploration. *SEG Newsletter* **23**, 1, 9–13.

Whitehouse, M.J. & Fedo, C.M. (2007) Microscale heterogeneity of Fe-isotopes in >3.71 Ga banded iron formation from the Isua greenstone belt, southwest Greenland. *Geology* **35**, 719–722.

Whiticar, M.J. (1999) Carbon and hydrogen isotope systematics of bacterial formation and oxidation of methane. *Chem. Geol.* **161**, 291–314.

Whiticar, M.J. (1997) Stable isotope geochemistry of coals, humic kerogens and related natural gases. *Int. J. Coal Geol.* **32**, 191–215.

Whiting, S.N., Reeves, R.D. & Baker, A.J.M. (2002) Conserving biodiversity – mining metallophytes and land reclamation. *Mining Env. Management* **10**, 11–16.

Whittaker, J.M., Müller, R.D., Leitchenkov, G., *et al.* (2007) Major Australian-Antarctic plate reorganization at Hawaiian-Emperor bend time. *Science* **318**, 83–86.

Whitworth, D. (2009) Geology, grade control and reconciliation at the Douglas mineral sands deposit, Murray Basin, western Victoria. *Proc. 7th Int. Mining Geol. Conf. 2009*, 155–168, AusIMM, Melbourne.

WHO (World Health Organization) (2006) *Guidelines for Drinking-Water Quality*, 3rd edn. Geneva. URL http://www.who.int/water_sanitation_health/dwq/gdwq3rev/en/index.html; accessed June 2010.

Widera, M., Jachna-Filipczuk, G., Kozula, R. & Mazurek, S. (2007) From peat bog to lignite seam: a new method to calculate the consolidation coefficient of lignite seams, Wielkopolska region in central Poland. *Int. J. Earth Sci.* **96**, 947–955.

Wiesheu, R., Lenczowski, B. & Morteani, G. (1997) Scandium – a current review of its deposits, production and technical use. *Erzmetall* **50**, 631–639.

Wigley, T.M.L. (2006) A combined mitigation/geoengineering approach to climate stabilization. *Science* **314**, 453–454.

Wilcock, S. (2000) Kunwarara magnesite deposit. In: *4th Int. Mining Geol. Conf. Proc.*, pp. 129–133, AusIMM, Carlton, Victoria.

Wilhelms, A., Larter, S.R., Head, I., *et al.* (2001) Biodegradation of oil in uplifted basins prevented by deep-burial sterilization. *Nature* **411**, 1034–1037.

Wilkins, R.W.T. & George, S.C. (2002) Coal as a source rock for oil: a review. *Int. J. Coal Geol.* **50**, 317–361.

Wilkinson, B.H. & Kesler, S.E. (2009) Quantitative identification of metallogenic epochs and provinces: Application to Phanerozoic porphyry copper deposits. *Economic Geol.* **104**, 607–622.

Wilkinson, B.H., Merrill, G.K. & Kivett, S.J. (2003) Stratal order in Pensylvanian cyclothems. *Geol. Soc. America Bull.* **115**, 1068–1087.

Wilkinson, J.J. (2010) A review of fluid inclusions constraint on mineralization in the Irish Ore Field and implications for the genesis of sediment-hosted Zn-Pb deposits. *Economic Geol.* **105**, 417–442.

Wilkinson, J.J., Stoffell, B., Wilkinson, C.C., Jeffries, T.E. & Appold, M.S. (2009) Anomalously metal-rich fluids form hydrothermal ore deposits. *Science* **323**, 764–767.

Wilkinson, J.J., Everett, C.E., Boyce, A.J., Gleeson, S.A. & Rye, D.M. (2005) Intracratonic crustal seawater circulation and the genesis of sub-seafloor zinc-lead mineralization in the Irish ore field. *Geology* **33**, 805–808.

Wilkinson, J.J., Nolan, J. & Rankin, A.H. (1996) Silicothermal fluid: a novel medium for mass transport in the lithosphere. *Geology* **24**, 1059–1062.

Wille, M., Nägler, T.F., Lehmann, B., Schröder, S. & Kramers, J.D. (2008) Hydrogen sulphide release to surface waters at the Precambrian/Cambrian boundary. *Nature* **453**, 767–769.

Williams, L.B., Ferrel, R.E., Hutcheon, I., *et al.* (1995) Nitrogen isotope geochemistry of organic matter and minerals during diagenesis and hydrocarbon migration. *Geochim. Cosmochim. Acta* **54**, 765–799.

Williams, P.J. (1998) An introduction to the metallogeny of the McArthur River-Mt Isa-Cloncurry minerals province. *Economic Geol.* **93**, 1120–1131.

Williams-Jones, A.E. & Heinrich, C.A. (2005) Vapor transport of metals and the formation of magmatic-hydrothermal ore deposits. *Economic Geol.* **100**, 1287–1312.

Williams-Jones, A.E., Samson, I.M. & Olivo, G.R. (2000) The genesis of hydrothermal fluorite-REE deposits in the Gallinas Mountains, New Mexico. *Economic Geol.* **95**, 327–342.

Willman, C. E., Korsch, R. J., Moore, D. H., Cayley, R. A., Lisitsin, V. A., Rawling, T. J., Morand, V. J. & O'Shea, P. J. (2010) Crustal-scale fluid pathways and source rocks in the Victorian Gold Province, Australia: Insights from deep seismic reflection profiles. *Economic Geology* **105**, 895–915.

Wilson, A.H., Lee, C.A. & Brown, R.T. (1999) Geochemistry of the Merensky Reef, Rustenburg Section, Bushveld Complex: controls on the silicate framework and distribution of trace elements. *Miner. Deposita* **34**, 657–672.

Wilson, A.J., Cooke, D.R. & Harper, B.J. (2003) The Ridgeway gold-copper deposit: A high-grade alkalic porphyry deposit in the Lachlan Fold Belt, New South Wales, Australia. *Economic Geol.* **98**, 1637–1666.

Wilson, A.M., Sanford, W., Whitaker, F. & Smart, P. (2000) Geothermal convection: a mechanism for dolomitization at Enewetak Atoll? *J. Geochem. Explor.* **69–70**, 41–45.

Wilson, L. & Head, J.W. (2007) An integrated model of kimberlite ascent and eruption. *Nature* **447**, 53–57.

Wilson, M.G.C., MacKenna, N. & Lynn, M.D. (2007) The occurrence of diamonds in South Africa. 105 pp, South Africa Council for Geoscience, *Mineral Resources Series 1*.

Wilson, M.J. & J.D.F. Richardson (eds) (1999) Evironmental engineering for exploration and production facilities. *Monograph 18*, 114 pp. Society of Petroleum Engineers.

Wilson, P.D. (ed.) (1996) *The Nuclear Fuel Cycle*. 323 pp. Oxford University Press.

Wilson, S.A., Dipple, G.M., Power, I.M., *et al.* (2009) Carbon dioxide fixation within mine wastes of ultramafic-hosted ore deposits: Examples from the Clinton Creek and Cassiar chrysotile deposits, Canada. *Economic Geol.* **104**, 95–112.

Winchester, J.A. & Floyd, P.A. (1977) Geochemical discrimination of different magma series and their differentiation products using immobile elements. *Chem. Geol.* **20**, 325–343.

Windh, J. (1995) Saddle reef and related gold mineralization, Hill End gold field, Australia: evolution of an auriferous vein system during progressive deformation. *Economic Geol.* **90**, 1764–1775.

Windley, B.F. (1995) *The Evolving Continents*, 3rd edn. 526 pp. Wiley.

Wise, D.U., Belt, E.S. & Lyons, P.C. (1991) Clastic diversion by fold salients and blind thrust ridges in coal-swamp development. *Geology* **19**, 514–517.

Wise, M.A. (1995) *Trace* element chemistry of lithium-rich micas from rare-element granitic pegmatites. *Mineralogy Petrology* **55**, 203–215.

Wittke, W. (1990) *Rock Mechanics*. 1075 pp. Springer.

Wodzicki, A. & Piestrzynski, A. (1994) An ore genetic model for the Lubin-Sieroszowice mining district, Poland. *Miner. Deposita* **29**, 30–43.

Wolkersdorfer, C. (2009) An apostil from the secretary general. *Mine Water Environ* **28**, 245–246.

Wolkersdorfer, C. (2008) *Water Management at Abandoned Flooded Underground Mines*. 465 pp, Springer.

Wood, S.A. (1996) The role of humic substances in the transport and fixation of metals of economic interest (Au, Pt, Pd, U, V). *Ore Geol. Rev.* **11**, 1–31.

Wood, S.A. & Samson, I.M. (2005) The aqueous geochemistry of gallium, germanium, indium and scandium. *Ore Geol. Rev.* **28**, 57–102.

Wood, S.A. & Samson, I.M. (2000) The hydrothermal geochemistry of tungsten in granitoid environments. I. Relative solubilities of ferberite and scheelite as a function of T, P, pH, and m_{NaCl}. *Economic Geol.* **95**, 143–182.

Wood, W.W., Sanford, W.E. & Al Habshi, A.R. (2002) Source of solutes to the coastal sabkha of Abu Dhabi. *GSA Bulletin* **114**, 259–268.

Wortmann, U.G. & Chernyavsky, B.M. (2007) Effect of evaporite deposition on Early Cretaceous carbon and sulphur cycling. *Nature* **446**, 654–656.

Wu, C.Y., Bai, G. & Xu, L.M. (1993) Types and distribution of silver ore deposits in China. *Miner. Deposita* **28**, 223–239.

Wu, Chengyu (2008) Bayan Obo controversy: Carbonatites versus Iron Oxide-Cu-Au-(REE-U). *Resource Geology* **58**, 348–354.

Xiandong Liu, Xiancai Lu, Rucheng Wang, Huiqun Zhou & Shijin Xu (2011) Speciation of gold in hydrosulphide-rich ore-forming fluids: Insights from first-priciples molecular dynamic simulations. *Geochim. Cosmochim. Acta* **75**, 185–194.

Xiao, Wenjiao, Kröner, A. & Windley, B. (2009) Geodynamic evolution of Central Asia in the Paleozoic and Mesozoic. *Int. J. Earth Sci.* **98**, 1185–1188.

Xiong, Y. & Wood, S.A. (2000) Experimental quantification of hydrothermal solubility of platinum-group elements with special reference to porphyry copper systems. *Mineral. Petrol.* **68**, 1–28.

Xiong, Y. (2003) Predicted equilibrium constants for solid and aqueous selenium species to 300 °C: applications to selenium-rich mineral deposits. *Ore Geol. Rev.* **23**, 259–276.

Yagmurlu, F. & Helvaci, C. (1994) Sedimentological characteristics and facies of the evaporite-bearing Kirmir Formation (Neogene), Beypazari basin, central Anatolia, Turkey. *Sedimentology* **41**, 847–860.

Yakubchuk, A. & Nikishin, A. (2004) Noril'sk-Talnakh Cu-Ni-PGE deposits: a revised tectonic model. *Miner. Deposita* **39**, 125–142.

Yanbin Yao, Dameng Liu, Dazhen Tang, Shuheng Tang, Yao Che & Wenhui Huang (2009) Preliminary evaluation of the coalbed methane production potential and its geological controls in the Weibei Coalfield, Southeastern Ordos Basin, China. *Int. J. Coal Geology* **78**, 1–15.

Yang, Xiao-Yong, Sun, Wei-Dong, Zhang, Yu-Xu & Zheng, Yong-Fei (2008) Geochemical constraints on the genesis of the Bayan Obo Fe–Nb–REE deposit in Inner Mongolia, China. *Geochim. Cosmochim. Acta* **73**, 1417–1435.

Yang, K. & Scott, S.D. (2005) Vigorous exsolution of volatiles in the magma chamber beneath a hydrothermal system on the modern sea floor of the eastern Manus back-arc basin, Western Pacific: Evidence from melt inclusions. *Economic Geol.* **100**, 1085–1096.

Yang, K. & Scott, S.D. (1996) Possible contribution of a metal-rich magmatic fluid to a sea-floor hydrothermal system. *Nature* **383**, 420–423.

Yardley, B.W.D. (2005) Metal concentrations in crustal fluids and their relationship to ore formation. *Economic Geol.* **100**, 613–632.

Yardley, B.W.D., Gleeson, S., Bruce, S. & Banks, D. (2000) Origin of retrograde fluids in metamorphic rocks. *J. Geochem. Explor.* **69–70**, 281–285.

Yardley, B.W.D. & Lloyd, G.E. (1995) Why metasomatic fronts are really metasomatic sides. *Geology* **23**, 53–56.

Yen, T.F. & Chilingarian, G.V. (eds) (2000) *Asphaltenes and Asphalts*, Vol. 2. 450 pp, Elsevier.

Yen, T.F. & Chilingarian, G.V. (eds) (1994) *Asphaltenes and Asphalts*, Vol. 1. 476 pp. Elsevier.

Yergin, D. (1991) *The Prize*. 876 pp. Simon & Schuster.

Yin, L., Pollard, P.J., Shouxi, H. & Taylor, R.G. (1995) Geologic and geochemical characteristics of the Yichun Ta-Nb-Li deposit, Jiangxi Province, South China. *Economic Geol.* **90**, 577–585.

Young, T.P. (1992) Ooidal ironstones from Ordovician Gondwana: a review. *Palaeogeography, Palaeoclimatology, Palaeoecology* **99**, 321–347.

Younger, P.L. (2006) *Groundwater in the Environment: an Introduction*. 312 pp. Wiley-Blackwell.

Younger, P.L. (2002) Coalfield closure and the water environment in Europe. *Trans. Instn. Min. Metall. A* **111**, 201–209.

Younger, P.L. (2000) The adoption and adaptation of passive treatment technologies for mine waters in the United Kingdom. *Mine Water Environ* **19**, 84–97.

Younger, P.L. & Wolkersdorfer, Ch. (eds) (2004) Mining impact on the fresh water environment: technical and managerial guidelines for catchment scale management. *Mine Water Environ* **23**, Supplement 1, 2–80.

Younger, P.L. & Robins, N.S. (ed.) (2002) *Mine Water Hydrology and Geochemistry*. 408 pp, Geol. Soc. London.

Youngson, J.H. & Craw, D. (1993) Gold nugget growth during tectonically induced sedimentary recycling, Otago, New Zealand. *Sedimentary Geol.* **84**, 71–88.

Yudovich, Y.E. & Ketris, M.P. (2006a) Chlorine in coal. *Int. J. Coal Geol.* **67**, 127–144.

Yudovich, Y.E. & Ketris, M.P. (2006b) Selenium in coal. *Int. J. Coal Geol.* **67**, 112–126.

Zartman, R.E. & Doe, B.R. (1981) Plumbotectonics – the model. *Tectonophysics* **75**, 135–162.

Zaw, K. & Singoyi, B. (2000) Formation of magnetite-scheelite skarn mineralization at Kara, northwestern Tasmania: evidence from mineral chemistry and stable isotopes. *Economic Geol.* **95**, 1215–1230.

Zedef, V., Russell, M.J., Fallick, A.E. & Hall, A.J. (2000) Genesis of vein stockwork and sedimentary magnesite and *hydromagnesite* deposits in the ultramafic terranes of southwestern Turkey: a stable isotope study. *Economic Geol.* **95**, 429–446.

Zemel, B. (1995) *Tracers in the Oil Field*. 514 pp. Elsevier.

Zengler, K., Richnow, H.H., Rosello-Mora, R., *et al.* (1999) Methane formation from long-chain alkanes by anaerobic microorganisms. *Nature* **401**, 266–269.

Zhang, L. (2003) Vacuum desorption of light hydrocarbons adsorbed on soil particles: a new method in geochemical exploration for petroleum. *AAPG Bull.* **87**, 89–97.

Zhang, Chi & Duan, Zhenhao (2008) A model for C–O–H fluid in the Earth's mantle. *Geochim. Cosmochim. Acta* **73**, 2089–2102.

Zhao, Y., Dong, Y., Li, D. & Bi, Ch. (2003) Geology, mineralogy, geochemistry, and zonation of the Bajiazi dolostone-hosted Zn-Pb-Ag skarn deposit, Liaoning Province, China. *Ore Geol. Rev.* **23**, 153–182.

Zhao, Zi-Fu, Zheng, Yong-Fei, Wei, Chun-Sheng & Gong, Bing (2004) Temporal relationship between granite cooling and hydrothermal uranium mineralization at Dalongshan in China: a combined radiometric and oxygen isotope study. *Ore Geol. Rev.* **25**, 221–236.

Zheng, Y.-F. (1991) Sulphur isotopic fractionation between sulphate and sulphide in hydrothermal ore deposits: disequilibrium vs. equilibrium processes. *Terra Nova* **3**, 510–516.

Zhibin Wei, Moldowan, J.M., Jarvie, D.M. & Hill, R. (2006) The fate of diamondoids in coals and sedimentary rocks. *Geology* **34**, 1013–1016.

Zhou, M.-F. & Robinson, P.T. (1997) Origin and tectonic environment of podiform chromite deposits. *Economic Geol.* **92**, 259–262.

Zhou, Xinyuan, Wang, Zhaoming, Yang, Haijun, Zhang, Lijuan, Han, Jianfa & Wang, Zhenyu (2009) Large-scale Tazhong Ordovician reef-flat oil-gas field in the Tarim Basin of China. *Acta Geologica Sinica* **83**, 179–188 (engl. ed.).

Zhu, J.-Ch., Li, R.-K., Li, F.-Ch., Xiong, X.-L., et al. (2001) Topaz-albite granites and rare-metal mineralization in the Limu District, Guangxi Province, southeast China. *Miner. Deposita* **36**, 393–405.

Zhu, Y., Merkel, B.J., Stober, I. & Bucher, K. (2003) The hydrochemistry of arsenic in the Clara mine, Germany. *Mine Water Environ* **22**, 110–117.

Zieg, M.J. & Marsh, B.D. (2005) The Sudbury Igneous Complex: Viscous emulsion differentiation of a superheated impact melt sheet. *Geol. Soc. America Bull.* **117**, 1427–1450.

Ziegler, A.M., Hulver, M.L. & Rowley, D.B. (1997) Permian world topography and climate. In: *Late Glacial and Postglacial Environmental Changes: Quaternary, Carboniferous–Permian and Proterozoic* (ed. I.P. Martini), pp. 111–146. Oxford University Press.

Ziegler, P.A. (1982) *Geological Atlas of Western and Central Europe*. 130 pp, 40 enclosures. Shell International/Elsevier.

Ziehrenberg, R.A., Fouquet, Y., Miller, D.J., *et al.* (1998) The deep structure of a sea-floor hydrothermal deposit. *Nature* **392**, 485–488.

Zimmermann, H. (2001) On the origin of fluids included in Phanerozoic marine halite – basic interpretation strategies. *Geochim. Cosmochim. Acta* **65**, 35–46.

Zirngast, M. (1991) Die Entwicklungsgeschichte des Salzstocks Gorleben – Ergebnis einer strukturgeologischen Bearbeitung. *Geol. Jb. A* **132**, 31 pp

Ziserman, A. (1980) Les gisements de Chaillac (Indre): la barytine des Redoutières, la fluorine du Rossignol. Association d'un gite stratiforme de couverture et d'un gite filonien du socle. *26th Intern. Geol. Congr. Paris*, E3, 46 pp.

Zuffardi, P. (1976) Karst and economic mineral deposits. Pp 175–211 in K.H. Wolf (Ed.), *Handbook of Stratabound and Stratiform Ore Deposits*, Vol. **3**, Elsevier.

Zuffardi, P. (1989) Italy. In: *Mineral Deposits of Europe* (eds F.W. Dunning, D. Garrard, H.W. Haslam & R.A. Ixer), pp. 221–277. IMM London.

Zweibel, K. (2010) The impact of tellurium supply on cadmium telluride photovoltaics. *Science* **328**, 699–701.

Index

Bold numbers point to colour plates

Abu Dabbab Sn-Ta, Egypt 204, 264, **2.18**
acidity 75ff, 85, 90, 93, 455, 541
acid rock or mine drainage (ARD, AMD) 187, 450, 453, 456, 516, **5.24, 5.25**
adularia 76
Agricola 419
Åheim olivine, Norway 342, **3.26, 3.27**
albitization 53
alkaline igneous complexes 23ff, 255, 262
Almadén Hg, Spain 242
Alpine type Pb-Zn 199
Alquife Fe, Spain 62
Altaussee salt, Austria 394, **4.3**
alum salts 355
aluminium 233ff
alunite 53, 76, 80, 233
andalusite 288ff
anhydrite 57ff, 71, 73, 112, 114, 327ff, 383, 394
anomaly 422ff, 429
anorthosite-ferrodiorite complexes 16
antimony 243ff
Antrim Shale gas, Michigan 538
apatite 80, 260, 342ff
Araxa Nb, Brazil 261, 262, 346
archaea *see* microbes
argillic alteration 53
Argyle diamonds, W.A. 25, 314, 315, **3.13**
Arrhenius-equation (modelling coalification) 503, 538
arsenic 245ff
asbestos 291ff
asphalt 572
Aswan Fe, Egypt 104
Athabasca District U, Canada 276–277
atmospheric carbon dioxide evolution 493
atmospheric emissions 30, 272, 469, 494, 514
aulacogen 134

background (geochemical) 422, 429
bacterial sulphate reduction (BSR) *see* microbes
Bad Aussee salt, Austria 394, **4.3**
Bajiazi Zn-Pb-Ag, China 223, 224, 225
Bakal siderite, Russia 154
banded iron formation (BIF) 81–82, 87, 100ff, 123
  Algoma type 100–101
  Rapitan type 100, 103
  Superior type 101ff, **1.67**
banded sulphide ore **1.72, 1.81**
barite 38, 293ff
Barnett Shale gas, Texas 564–565
bauxite 8, 9, 81, 233ff, **1.1**
Bayan Obo REE, China 24, 259
Beauvoir kaolin-Ta, France 29, 264
bentonite 299ff, **3.8**
Bergslagen Cu-Au, Sweden 124
beryllium 268ff
Besshi Cu 73
Bingham Cu, Utah 188
biodegradation of oil 552, 567
biodiversity 20, 21, 458, 577
biofuels 522
bismuth 250
bituminous coal 473ff, **6.20**
black shales 93–94, polymetallic 169–170, 179
black smoker 19ff, **1.11, 1.12**
Bleiberg Pb-Zn, Austria 44, 91
Boddington Au, W. A. 81
boiling 38, 42, 49, 71, 72, 75, 222, 240, 321
  first b. 31
  second b. 31

Economic Geology Principles and Practice
Metals, Minerals, Coal and Hydrocarbons – Introduction to Formation and Sustainable Exploitation of Mineral Deposits, Walter L. Pohl

© 2011 Walter L. Pohl. Published 2011 by Blackwell Publishing Ltd.

borehole deviation 435
borehole geophysics 432–433, 509, 558ff
boron 302ff, **3.9**
Bougainville Cu-Au, Papua New Guinea 87
breccia ore 64, 71, 73, **1.33, 1.76**
brine 16, 22, 30, 32, 36, 37–38, 46–47, 59, 71, 75, 110ff, 118, 119–120, 128, 266–267, 274, 280, 334, 338, 408, 551
brittle 65, 124, 130
Broken Hill Pb-Zn, Australia 110, 121, 122, 124, 197–198
bromine 111, 373, 374, 551
Brunswick Cu, Canada 124
Bugarama W, Rwanda 67
Bushveld Pt-Cr, South Africa (S.A.) 13, 32, 121, 133, 166, 185, 230ff, 290, 322

cadmium 195ff, 247ff
caesium 265
calorific value (coal) 486
CanTung W, Canada 56
cap rock 404–405
carbon 43, 310 ff, 325ff, 465ff
carbon capture and storage (CCS) 469–471, 517, 561, 579, **6.2**
carbon dioxide 24, 31, 36, 38, 43, 46, 55, 60, 77, 85, 90, 93, 112, 113, 128, 135, 138, 203, 241, 258, 273, 305, 312, 326, 335, 359, 364, 373, 408, 453, 454, 459, 469–471, 483–484, 517, 528, 533, 537
carbonatites 23–25, 80, 260, 322, 339, 341, 344ff
carbonatization 54
Carlin type Au, Nevada 212
Carlsbad cave, New Mexico, USA 90
Caroline Pb-Ag, Germany 50
catagenesis 538
celestite 293ff, 328, **3.3**
cement 307, 328
cementation 86–87
Central African Cu-Co Belt 192–193
Central Andes profile 136
Cerro de Mercado Fe, Mexico 17
Cerro Rico de Potosí Ag-Sn, Bolivia 224, 225, 226, **2.30**
Challenger Au, S. Australia 125
Chicxulub impact, Gulf of Mexico 133, 549
chromium 14, 19, 163ff, 231, **2.9**
Chuquicamata Cu-Mo, Chile 57, 58, **1.31, 1.33**
clay 308ff
  refractory 308
  ceramic 309
  expanding 310
  sealing 310
climate 78, 380, 389, 492–494
  engineering 356
  greenhouse 78, 535
Climax Mo, Colorado 178
coal 467ff, 536
coal bed methane (CBM) *see* methane
coalification 500–505
coal lithotypes 475
coal macerals 475–479
coal rank 472
coal seam 487ff, **6.20**
coal seam fires 507, 517
cobalt 173ff
Cobalt District Ag-Ni-Co, Canada, 175
Coeur d'Alene Ag, Idaho 227
collapse structures *see* earth falls
colloform *see* gels
colloids 37, 50–51, 71, 273
Colorado Plateau U, USA 89
combustion residues 484–485, 515, 516
Conolly diagram 67
constructed wetlands 455–456
contact metamorphism 121, 327, 396, 502
copper 15, 21ff, 24, 56ff, 70, 76, 85, 114ff, 185ff
Copper Shale 114ff, 232
core logging 436, 509, 511
Cornwall, England 69–70, 332–333
cosmogenic ^{10}Be-dating 269
Coulomb-Mohr stress diagram 65
Cowra Au, NSW, Australia 48
cut-off grade 444
cyanide 454
cyclothem 494, 495
Cyprus Cu 23, 74, 189–190

Dachang Sn-Zn, China 206
Dalnegorsk boron, Russia 305
Dampier salt, W.A. 376, **4.6**
Dead Sea Mg-salt 239
De Beers diamonds, S. Africa 313
dehydration *see* devolatilization
devolatilization 125, 121, 127–128, 136, 138
diagenetic 110–121
diagenetic crystallization rhythmites (DCR) *see* zebra textures
diamond 25, 32, 310ff, **3.13, 3.14**
diamond core drilling 434
diatomite 317ff
differentiation of magmas 29
dolomite 305ff
dolomitization 54
Draugen oil field, offhore Norway 547, 565

drilling 406, 432ff, 508–509, **7.24**
ductile (plastic) 122, 124, 130, 397–398, **1.81**
Dwars River Cr, S.Africa 14

earth falls, sinkholes 329, 404, 407, 409, 512, **4.30**
earthquakes, induced 408, 513, 577
Earth systems 132ff
economic 414ff, 441
ecosystem services 457, 584
effervescence 38
Ekati diamonds, Canada 313, **3.14**
elements
  chalcophile 29, 186
  compatible, incompatible 29
  essential to human health 151, 370
  essential trace elements 177
  granophile 29
  halogens 40
  hazardous air pollutants (HAPs) 514
  high field strength (HFSE) 29, 30
  immobile 125, 255
  large ion lithophile (LILE) 29, 30
  lithophile, or oxyphile 30
  major e., essential for all life 344, 356, 465
  native 86, 208
  noble 38, 86, 209
  redox-sensitive 93
  siderophile 150
  volatile 213–214
El Romeral Fe, Chile 153
El Teniente Cu, Chile 57
emerald 270
endogenetic 10
endothermic 128, 503, 538
environment 428, 437, 448ff, 513ff
Environmental Impact Assessment (EIA) 450ff
eogenesis 537
epigenetic 10
epithermal (volcanogenic) 74ff, **2.30**
epizonal 48–49
Erzberg Fe, Austria 61
Erzgebirge, Germany 29, 141, Ni 170, Sn 205, U 281
euxinic 93, 107, 114, 534
evaluation 419, 437ff
evaporation 376ff, **4.6, 4.12a**
evaporites 369ff
exhalative *see* submarine exhalative
exhalite 70, 123
exogenetic 10
exothermic 128, 130
exotic oxide ore 86

exploration 416ff
extinction 493
extraterrestrial 10, 15, 133, 228, 549

fahlband 74
feasibility study 448
Felbertal W, Austria 182
feldspar 319ff
fenitization 25
fluid inclusions 45–48, 372–373
fluorite 320ff, **3.16**
foam textures 121
fossil fuels 465ff
fractional crystallization 10, 29, 34–35
fracturing 65
fracture-stimulation of wells 567
framboidal 71, 93, 109
fusain 475
fusinite 478
Fushun bituminous coal, China 488

gallium 247ff
Ganges plains mass poisoning 247
garnierite 83, 84
gas hydrates (clathrates) 530
gas phase 30, 32, 38, 186, 356
Gash Emir W, Sudan 52
Gatumba Sn-Ta, Rwanda 97, 264
Gebeit Au, Sudan 458
gels 37, 50–51, 116
geochemical exploration 422ff
geological exploration 417ff
geological carbon sequestration *see* carbon capture and storage
geometallurgy 440
geophysical exploration 428ff
geostatistics 445
geothermal gradient 138, 401–402, 502–503
geothermal systems 32, 35–37, 40, 74, 75, 241, **1.21**
germanium 247ff
Gifurwe W, Rwanda 66
glaciation 103, 389, 493–495, 499
gold 26, 27, 56–59, 66, 76, 81, 98, 207ff
  orogenic 125, 129, 139, 140, 213
Golden Mile Au, W. A. 39, **2.25**
gondite 82
Gondwana 134, 389, 493
Gora Magnitnaja Fe, Russia 153
Gorleben waste repository, Germany 401, 402, 460, **5.29**
gossan 85, 418, **1.56**
granites 25ff, high heat production 28, 273

granitoids *see* granite
graphite 325ff
gravitational settling 11, 50
gravity 406
Great Oxidation Event 77, 102
Greenbushes Sn-Ta-Li, W.A. 263, 266
greenhouse climate 78, 535
greenhouse gas (GHG) 454, 515, 578
greisenization 54
Grimsel Alpine veins, Switzerland 126
Groote Eylandt Mn, 162
Guanajuato Ag-Au, Mexico 223–224
Guaymas Basin vents, Gulf of California 38
gypsum 327ff, 383, 394, 506

haematite, high-grade 81–82, 157
hafnium 251
halite 369ff
halokinesis 403
Hamersley Fe-province, W.A. 101, 156
Harz Mts. Pb-Ag-Zn veins, Germany 68, 201
Haselgebirge salt 392ff, **4.3**
Hausruck lignite, Austria 498, 490
hazard 450
hazardous air pollutants (HAP) 514
heavy minerals 96
Hedinia oil field, Papua New Guinea 546
helium 528
Hemlo Au, Canada 66, 123, 124
Herfa-Neurode K-salt & waste repository, Germany 399
Hohentauern magnesite, Austria 337
hot spots *see* rifting
Hubbert Curve 523
Hugoton gas field, Kansas 550
humic substances 480
huminite 475, 477, **6.7, 6.8**
Huntley bauxite, W.A. 8, 9, **1.1, 1.2**
HYC-McArthur River Pb-Zn, Australia 107
hydraulic equivalence 97–98
hydrocarbons 524ff
  in hydrothermal fluids 38
  hydrocarbon fluids 541
  seeps 554
hydrogen fuel 522
hydrothermal alteration 34, 51ff, 57, 123, 421, 436
hydrothermal systems 35–54
hydrothermal water 31, 40
  liquid, gaseous (vapour) and fluid state (supercritical "gas" or "liquid") 37
hypogene 10
hypozonal 48–49

Iberian pyrite belt Cu 76, 190–191
immiscibility
  hydrothermal fluids 38
  melts 11, 16, 34
impact, *see* extraterrestrial
Inagli Pt, Russia 230, 232
indicator minerals 316, 427
indium 247ff
infiltration 88–91
Ingessana Hills Cr, Sudan 167, **2.9**
in-situ leaching 271, 279
inversion 549
Irish type Pb-Zn-Ag 199
iron 60–62, 81, 87–88, 100–103, 120, 149ff
  oolitic 103–105
iron oxide-copper-gold (-U-REE) deposits (IOCG) 16, 138, 140, 188, 277
isotope geochemistry 41ff
  boron 374
  carbon 43, 311, 325, 357, 483, 529
  chlorine 374
  dating 41–42, 79–80, 269, 329, 375
  helium 271, 528
  lead 44
  strontium 43–44, 294
  sulphur 43, 296, 329, 357, 374
  uranium 272
  water 42–43, 329, 374–375
Itabira Fe, Brazil 156

Jinchuan Ni-Cu-PGM, China 172
Jinding Zn-Pb, China 200
Joachimsthal Ag-U, CZ 281
Joma Cu, Norway 122
JORC Code 442, 443
Julia Creek oilshale-Mo-V, Australia 184

Kambalda Ni, W.A. 12, 172
kaolin 79, 330ff, 350, **1.50**
karst 89ff, 236, 329
Kenticha Ta-Li, Ethiopia 33, 264
Kerio Valley F, Kenya 323
Kern River oilfield, California 570
kerogen 114, 531ff
Key Lake U, Canada 276–277
Khibini apatite, Russia 24, 346, 347
kimberlites 23–25, 312ff
Kipushi Zn-Cu-Ge, DR Congo 200
Kirka boron, Turkey 304, **3.9**
Kiruna-Malmberget Fe, Sweden 16–17, 152, 450
Kiya-Shaltyr nepheline, Russia 237
komatiites 12, 172

Königstein U, Germany 278, 279
Kongsberg Ag, Norway 38, 39, 65, 175
Konrad waste repository, Germany 460, 461
Kramer boron, California 303
Kunwarara magnesite, Australia 336
Kuroko Cu-Pb-Zn 72–73
kyanite 288ff

Lafatsch Zn, Tyrol, Austria 117, **1.76**
Laisvall Pb, Sweden 200
Lake Assal salt, Djibouti 383
lamproites 314
Lacq Profond gas, France 578
Lake Katwe salt, Uganda 382, **4.12a**
lateral secretion 10, 126–127
laterite 78, 79, 235–236
lateritic ores 81, 163, 172, 230, 235, 248, 260
Latrobe Valley brown coal, Australia 487
layered mafic intrusions 13
lead 44, 50, 61, 68, 70, 90, 91, 116ff, 195ff
Les Redoutières barite, France 298
Liaoning boron, China 305
Libby vermiculite, Montana 341
life 77–78
lignite 472ff, 515, **5.18**
Lihir Au, Papua New Guinea 59, 137, 214, 215
limestone 305ff
liptinite 475, 478, **6.9**
lithium 265ff, **2.43, 2.44**
lithosphere 134, 311
Luzenac talc, France 360–361, **3.34**

macerals 475ff
magma
  oxidized 26–27, 30–31, 59
  reduced 26–27, 30–31,
magmatic brine, fluid, gas, vapour 30ff, 303, 356
magmatic flare-up 138
magmatic-hydrothermal 25, 30–32, 47, 177–178, 180, 187–188, 205, 210ff, 364
magnesite 84, 333ff
magnesium 238ff, 338
Mammoth Cu, Queensland, Australia 64
manganese 71, 80, 82, 103, 109, 123, 159ff
  oolitic 105–106
  nodules 106–107
Manono Sn-Ta, D.R.Congo 33, 267, **2.43**
mantle
  diamonds 310ff
  fluids 110, 135, 321
  melts 12, 13, 19, 23, 26, 27, 59, 60, 135, 138, 181
  plume 93, 116, 135, 144
mapping 416ff, 420ff, 439
marble 305ff
Marillana Creek Fe, W.A. 155
marlstone 305ff
mass extinction 391
massive ore 70
Mawatwan Mn, S.Africa 163
McArthur River U, Canada 276–277
mercury 239ff, 454
Merensky Reef Pt 14, 32, 231–232, **2.32**
mesozonal 48–49
metallogeny 132ff, Europe 140ff, **1.89**
metal zonation
  Copper Shale 115
  hydrothermal systems 67–68, 69–70
  MVT deposits 117
  pegmatites 33ff
  porphyry 57ff
  sedex 93, 109
  skarn 56
  volcanogenic massive sulphides (VMS) 70
  epithermal 74
metamorphic 121ff, 127, 215
metamorphogenic 125ff, 216–219
metamorphosed 121ff
metasomatism 60–62, 138
methane 483–484, 510, 515, 527ff, 563–565, **7.24**
methane seepage (natural) 517
microbes
  chemolithotrophic 21, 84
  deep 111
  extremophile 84
  gold-reducing 209
  hyperthermophilic, in hydrothermal systems 38, 75
  sulphate-reducing 90, 92, 273, 357
  sulphur-oxidizing 22, 84, 86, 345
  thermophilic 84, 86
microthermometry 45
mid-ocean ridge 18–23
migration (oil) 540ff
mine closure and ecosystems restoration 9, 457, 458, **6.30**
mining 438
mirabilite 355
Mississippi Valley type (MVT) Pb-Zn 116–119, **1.76**
mixing and mingling
  fluids 38, 40, 118
  melts 18, 55, 231, 233
mobilization 124
modelling 417, 445–446, 457, 512
Molango Mn, Mexico 161
molybdenum 56–59, 175ff

Mount Tom Price Fe, W. A. 157, 158, **2.4**
Mountain Pass REE, California 24, 259
Mt. Isa Cu-Pb-Zn, Australia 128, 193–195, 197, 418
Mt. Oxide Cu, Australia 87
Mt. Weld REE, W.A. 260
Munster gas field, Germany 548
Murray Basin Zr, Australia 252–253
muscovite 339ff
Muskeg oil sand, Canada 571, **7.29**
Muzo emerald, Colombia 270

natural gas *see* methane
natural nuclear reactors 275
Nchanga Cu-Co, Zambia 193
nelsonite 347
Neves Corvo Cu-Zn-Sn, Portugal 191, 431
Ngara Sn-Ta, Rwanda 96
nickel 12, 15, 81, 168ff
  lateritic 82–84
Nikopol Mn, Ukraine 105
niobium 24, 261ff
Noril'sk-Talnakh Cu-Pd, Sibiria 14, 171
North Sea oil and gas 560–561
Nsuta Mn, Ghana 163
nugget 446
Nuweibi quartz, Egypt 349

ocean floor hydrothermal vents, *see* black smoker
ocean floor metamorphism 19
oceanic spreading 18ff
offshore oil **7.32**
oil *see* petroleum
oil sand 570, **7.29**
oil seeps, submarine 543, 555
oil shale 573ff
oil spills 575–576
oil spill remediation 576, 577
oil window 539–540
Oklo U, Gabon 275
Ok Tedi Cu-Au, Papua-New Guinea 455
Oldoinyo Lengai volcano, Tanzania 24
olivine 342–343, **3.26, 3.27**
Olympic Dam Cu-U, S. Australia 188–189, 277–278, 418
oolitic ore 103–1054, 157–159, 161, **1.68**
open pit (lignite) 449, **5.18, 5.19, 6.30**
ophiolite 18ff, 74, 83, 293, 359
orbital cycles 495, 574
ore, ore deposit 1–2, **1.33**
ore grade 414
ore microscopy 49, **13**
ore processing 415
ore reserves *see* reserves
organic matter 93–94
orogenic gold *see* gold
orthomagmatic 11ff
Ouenza Fe, Algeria 61, 119–120
Outokumpu Cu-Zn-Co, Finland 190
overpressure 562–563
oxidation 84–86, 121
oxidized fluids 110, 112, 115

Pacific "ring of fire" 137
Palabora Cu, S.A. 24, 187–188, vermiculite 341, apatite 346
Panasqueira W, Portugal 48, 183
Pangaea 116, 119, 139, 161, 390, 493
paragenesis 49, 66
passive mine water treatment 453, 455, 456, **5.24, 5.25**
pathfinder elements 221, 423
peat 487ff, 499–500
pegmatites 32ff, 204, 263ff, 269
perlite 362
permeability 64, 375, 541
petroleum 524ff, 539, **7.32**
  conventional 523
  unconventional 524
  degraded 551–552
petroleum system 539
Phanerozoic carbon dioxide evolution 493
phlogopite 339ff, **3.24**
phosphate *see* apatite
phosphogypsum 330, 344
Pine Point Pb-Zn, Canada 38
pit lakes 516, 517, **6.30**
photosynthesis 479
placers
  aeolian 95, **1.61**
  alluvial 96–97, 256, 265, **1.64**
  coastal 98–100, 252, 256, **2.39**
  minerals 96
  residual 81, **1.62**
plant expansion 499
plate tectonics 134ff
platinum group metals (PGM) 14, 228ff, **2.32**
pneumatogenic 31
porosity and permeability 561ff
porphyry deposits 56ff, 136ff, 188
potassium 369ff
prefeasibility study 437
propylitization 53
prospecting 418
protore 84
Pueblo Viejo Au-Ag, Dominican Rep. 213–214

pumice 362
pyrobitumen 572, 573
pyrophyllite 361

quartz 347
quartzite 349–350
quartz sand & gravel 350

Rabenwald talc, Austria 361
radioactive decay 41, 44, 271, 272, 282
radioactive waste 275, 283, 458ff, **5.29**
radioactivity in exploration 282, 347, 431
radiobarite 514
radium 271, 330, 577
radon 271, 577
Rammelsberg Zn-Pb-Cu, Germany 108, 123, 191–192, **1.72, 1.81**
rare earth elements (REE) 24, 257ff
Rayleigh distillation 129
reclamation (mine) 457, 516, **5.19, 6.30**
reconnaissance 419
Red Dog Pb-Zn, Alaska 107, 109, 110
red mud 234, 271
reduced fluids 110, 112, 118, 295, 541
reduction 39, 121
reforestation **1.2**
regolith 78, 83
remediation *see* reclamation
remote sensing 420ff
reserves 440ff, 510–512, 568ff
reserve growth 570
reserves/production ratio 468
reservoir rocks 543ff
resources 440ff, 510–512, 570, 575
residual 80–82
reverse circulation drilling 434
rhenium 176
Riecke's principle 124
rifting 134–5
risk 450
rock salt *see* halite
Rodinia 139, 264
Rössing U, Namibia
Rossignol F, France 50, 324
Rutongo Sn, Rwanda 26, 63

sabkha 383
Salar de Atacama Li, Chile 267
Salar de Uyuni Li, Bolivia 268, **2.44**
saline 42, 110, 405, 469
salinity 37, 46–47, 110, 111, 376
salt diapirs 119–121, 400ff
salt giants 387
salt lagoons 383, 387
salt lakes 380ff
Salton Sea, California 36, 229
sampling 220–221, 353, 424ff, 439, 509, **5.6**
San Rafael Sn-Cu, Peru 205
saprolite 84
sapropel 534
Sarbai Fe, Kazakhstan 153
scandium 261
scheelite 182, **2.12**
seals (oil and gas) 454 ff
Searles Lake boron-sodium, California 303, 354
seawater
  convection 19
  evaporation 111, 376ff, **4.6**
  modern 42, 93, 151, 274, 345, 376–377, 533
  past 151, 384–385
sedex *see* submarine exhalative
sedimentary exhalative *see* sedex
segregation 11, 31, 34
seismic pumping 38, 65
seismic reflection geophysics 555–556, 557, 558, **7.22, 7.23**
selenium 247ff
Sempaya hot springs, NW Uganda 36
Sept-Îles Complex Ti-apatite, Canada 347
sericite 340
sericitization 54
Shizhuyuan W-Sn-Bi-Mo, China 181, 250
Shuiximiao Sn-Ta, SE China 26
shungite 573
Siilinjärvi carbonatite, Finland 339, **3.24**
silicification 53
silicon 247ff, 347–348
silicothermal fluids 51
sillimanite 288ff
silver 39, 50, 65, 68, 76, 115, 221ff
Silvermines Zn-Pb-Ag, Ireland 109, 199
Skaergaard Au-Pt, Greenland 418
skarn 54ff, 71, 153, 181, 364, 366
slab rollback 73
Sleipner gas, offshore Norway 469, 579, **6.2**
Snowball Earth 103
sodium 369ff
sonic P-wave velocity in rocks 558
Southern Cross Au, W.A. 55
source rocks (oil and gas) 533ff
Spor Mountain Be, Utah 269
Sri Lanka (Ceylon) graphite 327
Steyn Au, West Rand, S.A. 99
stockwork ore 63

Stoke's law 50, 97
stream sediments 425, **5.6**
strontium 43–44, 294ff, 328, **3.3**
subduction 136ff
submarine exhalative 70
  volcanic-exhalative 70
  sedimentary-exhalative (sedex) 70, 107ff, **1.72**
subrosion 403, 404
subsidence 110, 403ff, 494, 513
Sudbury Igneous Complex (SIC) Ni-Cu, Canada 15, 103, 133, 170–171, 428
sulphate reduction
  microbial 90, 92, 116, 118
  thermochemical (TSR) 112, 118, 528, 552
sulphidation, desulphidation 39, 75, 76, 121, 124
sulphide melt 12, 66, 124, 169, 229
sulphur 43, 76, 121, 124, 138, 296, 355ff, 481
Sulphur Bank Hg, California 241
supercontinents 139
supercritical fluid 31, 37–38, 138, 347, 470
supergene 10, 76ff
  alteration of salt 405
  degradation of coal 506
  enrichment 84–88, **1.56**
  vertical zonation 85, 86
Superior type BIF 100ff, **1.67**
sustainability 3, 463, 466, 579, 584
synfuels 486, 522, 571, 573–574
syngenetic 10

Taaken gas field, Germany 549
Tabba Tabba Ta, NW Australia 34
tailings 415, 451ff, 458
talc 358ff, **3.34**
Talvivaara Ni-Cu-Co-Zn, Finland 179
tantalum 26, 29, 34, 261ff, **2.18**
tar (heavy and extra-heavy oil) 570, **7.29**
Taupo Volcanic Zone, New Zealand 36
tectonic control 65ff, 71, 73, 137
telescoping 74
Tellnes Ti, Norway 253
tellurium 247ff
thorium 270ff
Tikhvin bauxite, Russia 263
tin 26, 27, 63, 202ff
tin granite 27, 52, 202–203, 204
titanium 16, 29, 254, **2.39**
Tongkeng-Changpo Sn, S-China 63
Torres del Paine fluids, Chile 46
tourmalinization 54, 427
trap 130, 542, 545–550, 454 ff
trap basalt 14, 135, 141, 502
trass 363
Trepča (Trepcë) Pb-Zn-Ag, Kosovo 201
tripoli 319
Tri-State Pb-Zn, USA 44, 61, 118
Troll gas field, offshore Norway 542
trona 354
Tsumeb Pb-Ge, Namibia 87, 135
tungsten 26, 27, 48, 52, 56, 66, 67, 179ff, **2.12**
Tungus coal, Siberia 502
Tyndrum Au, Scotland 131

Uhry quartz sand, Germany 352, **3.30**
underground mining 438
underground waste disposal 399, 402, 458ff
unidirectional solidification textures (USTs) 34, 178
uranium 28, 88–89, 270ff
Uston bauxite, France 237

valuation 437ff, 447ff
vanadium 14, 183ff
vapour *see* boiling
veins 62–68
  hydraulic permeability 64
  sheeted 64
vermiculite 339ff
Viburnum Pb-Zn, Missouri 61, 117–118
vitrinite 475, 476,
vitrinite reflectance 501
Voisey's Bay Ni-Cu-Co, Canada 171, 418
volatiles 30ff, 75, 122, 176
volcanogenic deposits 70–76

Wackersdorf U, Germany 274
Wadi Essel celestite, Egypt 294, **3.3**
waste repositories 458ff, **5.29**
water connate 111
  critical density and temperature 31
  diagenetic 111ff, 395, 551
  formation and reservoir 42, 111, 551
  geothermal 35–37, 40, 75, 240
  stable isotopes 42, 80, 111, 374–375
  juvenile 40
  magmatic 30, 42, 47, 55, 75
  metamorphic 127ff
  meteoric 42
  mine 450ff, 514
  saline 110, 405
  surface 42, 77, 274
  volcanic 42
water management (coal mines) 514
weighting 444
Weipa Al, Australia 235

Western Australia (W.A.) 12
wetlands 493ff
White Pine Cu, USA 192
white smokers 20ff
Willis Mountain kyanite, Virginia 290
Wilson cycle 139
Witwatersrand Au-U, S.A. 98, 99, 219–220, 278, **2.26**
wolfram *see* tungsten
wollastonite 364ff
Woxi Au-Sb-W, China 244

Xikuanshan Sb, China 244

Yanshanian granites 181
Yeelirrie U, W.A. 280
Yichun Ta, China 262

zebra textures 51, 113
Zechstein salt 389ff
zeolites 365ff
zink 61, 70, 90, 113, 116ff, 195ff
zirconium, zircon 251ff, **2.39**
zonation *see* metal zonation
zone refining 70